

Special Issue Reprint

---

# Sustainable Biopolymer- Based Composites

Processing, Characterization, and Application

---

Edited by  
Raffaella Striani

[mdpi.com/journal/polymers](https://mdpi.com/journal/polymers)

# **Sustainable Biopolymer-Based Composites: Processing, Characterization, and Application**





# **Sustainable Biopolymer-Based Composites: Processing, Characterization, and Application**

Editor

**Raffaella Striani**



Basel • Beijing • Wuhan • Barcelona • Belgrade • Novi Sad • Cluj • Manchester

*Editor*

Raffaella Striani  
Engineering for Innovation  
University of Salento  
Lecce, Italy

*Editorial Office*

MDPI  
St. Alban-Anlage 66  
4052 Basel, Switzerland

This is a reprint of articles from the Special Issue published online in the open access journal *Polymers* (ISSN 2073-4360) (available at: <https://www.mdpi.com/journal/polymers/special.issues/4P2ZXQ04IP>).

For citation purposes, cite each article independently as indicated on the article page online and as indicated below:

Lastname, A.A.; Lastname, B.B. Article Title. <i>Journal Name</i> <b>Year</b> , <i>Volume Number</i> , Page Range.
--

**ISBN 978-3-0365-9537-5 (Hbk)**

**ISBN 978-3-0365-9536-8 (PDF)**

**[doi.org/10.3390/books978-3-0365-9536-8](https://doi.org/10.3390/books978-3-0365-9536-8)**

© 2023 by the authors. Articles in this book are Open Access and distributed under the Creative Commons Attribution (CC BY) license. The book as a whole is distributed by MDPI under the terms and conditions of the Creative Commons Attribution-NonCommercial-NoDerivs (CC BY-NC-ND) license.

# Contents

Preface . . . . .	ix
<b>Marwan A. Ibrahim, Mona H. Alhalafi, El-Amir M. Emam, Hassan Ibrahim and Rehab M. Mosaad</b> A Review of Chitosan and Chitosan Nanofiber: Preparation, Characterization, and Its Potential Applications Reprinted from: <i>Polymers</i> <b>2023</b> , <i>15</i> , 2820, doi:10.3390/polym15132820 . . . . .	1
<b>Francesca Ferrari, Raffaella Striani, Daniela Fico, Mohammad Mahbubul Alam, Antonio Greco and Carola Esposito Corcione</b> An Overview on Wood Waste Valorization as Biopolymers and Biocomposites: Definition, Classification, Production, Properties and Applications Reprinted from: <i>Polymers</i> <b>2022</b> , <i>14</i> , 5519, doi:10.3390/polym14245519 . . . . .	37
<b>Ngoc-Thang Nguyen, Tien-Hieu Vu and Van-Huan Bui</b> Antibacterial and Antifungal Fabrication of Natural Lining Leather Using Bio-Synthesized Silver Nanoparticles from <i>Piper Betle</i> L. Leaf Extract Reprinted from: <i>Polymers</i> <b>2023</b> , <i>15</i> , 2634, doi:10.3390/polym15122634 . . . . .	75
<b>Nurul Syazwanie Fatiroi, Abdul Aziz Jaziri, Rossita Shapawi, Ruzaidi Azli Mohd Mokhtar, Wan Norhana Md. Noordin and Nurul Huda</b> Biochemical and Microstructural Characteristics of Collagen Biopolymer from Unicornfish ( <i>Naso reticulatus</i> Randall, 2001) Bone Prepared with Various Acid Types Reprinted from: <i>Polymers</i> <b>2023</b> , <i>15</i> , 1054, doi:10.3390/polym15041054 . . . . .	93
<b>Yueting Wu, Xing Gao, Jie Wu, Tongxi Zhou, Tat Thang Nguyen and Yutong Wang</b> Biodegradable Polylactic Acid and Its Composites: Characteristics, Processing, and Sustainable Applications in Sports Reprinted from: <i>Polymers</i> <b>2023</b> , <i>15</i> , 3096, doi:10.3390/polym15143096 . . . . .	109
<b>Ana Costa, Telma Encarnação, Rafael Tavares, Tiago Todo Bom and Artur Mateus</b> Bioplastics: Innovation for Green Transition Reprinted from: <i>Polymers</i> <b>2023</b> , <i>15</i> , 517, doi:10.3390/polym15030517 . . . . .	127
<b>Jijo Thomas Koshy, Devipriya Vasudevan, Dhanaraj Sangeetha and Arun Anand Prabu</b> Biopolymer Based Multifunctional Films Loaded with Anthocyanin Rich Floral Extract and ZnO Nano Particles for Smart Packaging and Wound Healing Applications Reprinted from: <i>Polymers</i> <b>2023</b> , <i>15</i> , 2372, doi:10.3390/polym15102372 . . . . .	161
<b>Aqsa Zafar, Muhammad Kaleem Khosa, Awal Noor, Sadaf Qayyum and Muhammad Jawwad Saif</b> Carboxymethyl Cellulose/Gelatin Hydrogel Films Loaded with Zinc Oxide Nanoparticles for Sustainable Food Packaging Applications Reprinted from: <i>Polymers</i> <b>2022</b> , <i>14</i> , 5201, doi:10.3390/polym14235201 . . . . .	179
<b>Chenxin Yan, Mengzhen Xing, Suohui Zhang and Yunhua Gao</b> Clinical Development and Evaluation of a Multi-Component Dissolving Microneedle Patch for Skin Pigmentation Disorders Reprinted from: <i>Polymers</i> <b>2023</b> , <i>15</i> , 3296, doi:10.3390/polym15153296 . . . . .	191
<b>Zahra Rajabimashhadi, Nunzia Gallo, Luca Salvatore and Francesca Lionetto</b> Collagen Derived from Fish Industry Waste: Progresses and Challenges Reprinted from: <i>Polymers</i> <b>2023</b> , <i>15</i> , 544, doi:10.3390/polym15030544 . . . . .	207

<b>Taweechai Amornsakchai, Sorn Duangsuwan, Karine Mouglin and Kheng Lim Goh</b> Comparative Study of Flax and Pineapple Leaf Fiber Reinforced Poly(butylene succinate): Effect of Fiber Content on Mechanical Properties Reprinted from: <i>Polymers</i> <b>2023</b> , <i>15</i> , 3691, doi:10.3390/polym15183691 . . . . .	<b>235</b>
<b>Antonio Soldo and Marta Miletic</b> Durability against Wetting-Drying Cycles of Sustainable Biopolymer-Treated Soil Reprinted from: <i>Polymers</i> <b>2022</b> , <i>14</i> , 4247, doi:10.3390/polym14194247 . . . . .	<b>251</b>
<b>Pouyan Bagheri, Ivan Gratchev, Suwon Son and Maksym Rybachuk</b> Durability, Strength, and Erosion Resistance Assessment of Lignin Biopolymer Treated Soil Reprinted from: <i>Polymers</i> <b>2023</b> , <i>15</i> , 1556, doi:10.3390/polym15061556 . . . . .	<b>265</b>
<b>Anne Shayene Campos de Bomfim, Daniel Magalhães de Oliveira, Kelly Cristina Coelho de Carvalho Benini, Maria Odila Hilário Cioffi, Herman Jacobus Cornelis Voorwald and Denis Rodrigue</b> Effect of Spent Coffee Grounds on the Crystallinity and Viscoelastic Behavior of Polylactic Acid Composites Reprinted from: <i>Polymers</i> <b>2023</b> , <i>15</i> , 2719, doi:10.3390/polym15122719 . . . . .	<b>277</b>
<b>Ashoka Gamage, Punniamoorthy Thiviya, Sudhagar Mani, Prabaharan Graceraj Ponnusamy, Asanga Manamperi, Philippe Evon, et al.</b> Environmental Properties and Applications of Biodegradable Starch-Based Nanocomposites Reprinted from: <i>Polymers</i> <b>2022</b> , <i>14</i> , 4578, doi:10.3390/polym14214578 . . . . .	<b>293</b>
<b>Sherif S. Hindi and Mona Othman I. Albureikan</b> Fabrication, Characterization, and Microbial Biodegradation of Transparent Nanodehydrated Bioplastic (NDB) Membranes Using Novel Casting, Dehydration, and Peeling Techniques Reprinted from: <i>Polymers</i> <b>2023</b> , <i>15</i> , 3303, doi:10.3390/polym15153303 . . . . .	<b>323</b>
<b>Antonio Veloso-Fernández, Leire Ruiz-Rubio, Imanol Yugueros, M. Isabel Moreno-Benítez, José Manuel Laza and José Luis Vilas-Vilela</b> Improving the Recyclability of an Epoxy Resin through the Addition of New Biobased Vitrimers Reprinted from: <i>Polymers</i> <b>2023</b> , <i>15</i> , 3737, doi:10.3390/polym15183737 . . . . .	<b>359</b>
<b>Abisha Mohan, Retnam Krishna Priya, Krishna Prakash Arunachalam, Siva Avudaiappan, Nelson Maureira-Carsalade and Angel Roco-Videla</b> Investigating the Mechanical, Thermal, and Crystalline Properties of Raw and Potassium Hydroxide Treated <i>Butea Parviflora</i> Fibers for Green Polymer Composites Reprinted from: <i>Polymers</i> <b>2023</b> , <i>15</i> , 3522, doi:10.3390/polym15173522 . . . . .	<b>373</b>
<b>Morakot Piemjai, Onusa Waleepitackdej and Franklin Garcia-Godoy</b> Marginal Micro-Seal and Tensile Bond Strength of a Biopolymer Hybrid Layer Coupled with Dental Prosthesis Using a Primerless-Wet System Reprinted from: <i>Polymers</i> <b>2023</b> , <i>15</i> , 283, doi:10.3390/polym15020283 . . . . .	<b>391</b>
<b>Edy Subroto, Yana Cahyana, Rossi Indiaranto and Tiara Aray Rahmah</b> Modification of Starches and Flours by Acetylation and Its Dual Modifications: A Review of Impact on Physicochemical Properties and Their Applications Reprinted from: <i>Polymers</i> <b>2023</b> , <i>15</i> , 2990, doi:10.3390/polym15142990 . . . . .	<b>403</b>
<b>Siti Shazra Shazleen, Fatimah Athiyah Sabaruddin, Yoshito Ando and Hidayah Ariffin</b> Optimization of Cellulose Nanofiber Loading and Processing Conditions during Melt Extrusion of Poly(3-hydroxybutyrate-co-3-hydroxyhexanoate) Bionanocomposites Reprinted from: <i>Polymers</i> <b>2023</b> , <i>15</i> , 671, doi:10.3390/polym15030671 . . . . .	<b>437</b>

<b>Nour Houda M'sakni and Taghreed Alsufyani</b> Part B: Improvement of the Optical Properties of Cellulose Nanocrystals Reinforced Thermoplastic Starch Bio-Composite Films by Ex Situ Incorporation of Green Silver Nanoparticles from <i>Chaetomorpha linum</i> Reprinted from: <i>Polymers</i> <b>2023</b> , <i>15</i> , 2148, doi:10.3390/polym15092148 . . . . .	453
<b>Seiko Jose, Puthenpurackal Shajimon Shanumon, Annmi Paul, Jessen Mathew and Sabu Thomas</b> Physico-Mechanical, Thermal, Morphological, and Aging Characteristics of Green Hybrid Composites Prepared from Wool-Sisal and Wool-Palf with Natural Rubber Reprinted from: <i>Polymers</i> <b>2022</b> , <i>14</i> , 4882, doi:10.3390/polym14224882 . . . . .	473
<b>Supitcha Yaisun and Tatiya Trongsatitkul</b> PLA-Based Hybrid Biocomposites: Effects of Fiber Type, Fiber Content, and Annealing on Thermal and Mechanical Properties Reprinted from: <i>Polymers</i> <b>2023</b> , <i>15</i> , 4106, doi:10.3390/polym15204106 . . . . .	491
<b>Siti Nor Najihah Yasin, Zulfahmi Said, Nadia Halib, Zulaiha A Rahman and Noor Izzati Mokhzani</b> Polymer-Based Hydrogel Loaded with Honey in Drug Delivery System for Wound Healing Applications Reprinted from: <i>Polymers</i> <b>2023</b> , <i>15</i> , 3085, doi:10.3390/polym15143085 . . . . .	505
<b>Ada Pacheco, Arian Evangelista-Osorio, Katherine Gabriela Muchaypiña-Flores, Luis Alejandro Marzano-Barreda, Perla Paredes-Concepción, Heidy Palacin-Baldeón, et al.</b> Polymeric Materials Obtained by Extrusion and Injection Molding from Lignocellulosic Agroindustrial Biomass Reprinted from: <i>Polymers</i> <b>2023</b> , <i>15</i> , 4046, doi:10.3390/polym15204046 . . . . .	529
<b>Vinna K. Sugiaman, Jeffrey, Silvia Naliani, Natallia Pranata, Rudy Djuanda and Rosalina Intan Saputri</b> Polymeric Scaffolds Used in Dental Pulp Regeneration by Tissue Engineering Approach Reprinted from: <i>Polymers</i> <b>2023</b> , <i>15</i> , 1082, doi:10.3390/polym15051082 . . . . .	557
<b>Zinnia Mansoor, Fideline Tchuenbou-Magaia, Marek Kowalczyk, Grazyna Adamus, Georgina Manning, Mattia Parati, et al.</b> Polymers Use as Mulch Films in Agriculture—A Review of History, Problems and Current Trends Reprinted from: <i>Polymers</i> <b>2022</b> , <i>14</i> , 5062, doi:10.3390/polym14235062 . . . . .	575
<b>Namthip Bureewong, Preeyaporn Injorhor, Saifa Krasaekun, Pawida Munchan, Oatsaraphan Waengdongbang, Jatuporn Wittayakun, et al.</b> Preparation and Characterization of Acrylonitrile Butadiene Rubber Reinforced with Bio-Hydroxyapatite from Fish Scale Reprinted from: <i>Polymers</i> <b>2023</b> , <i>15</i> , 729, doi:10.3390/polym15030729 . . . . .	605
<b>Laila A. Damiati, Marwa El-Yaagoubi, Safa A. Damiati, Rimantas Kodzius, Farshid Sefat and Samar Damiati</b> Role of Polymers in Microfluidic Devices Reprinted from: <i>Polymers</i> <b>2022</b> , <i>14</i> , 5132, doi:10.3390/polym14235132 . . . . .	619
<b>Herlina Marta, Ari Rismawati, Giffary Pramafisi Soeherman, Yana Cahyana, Mohamad Djali, Tri Yuliana and Dewi Sondari</b> The Effect of Dual-Modification by Heat-Moisture Treatment and Octenylsuccinylation on Physicochemical and Pasting Properties of Arrowroot Starch Reprinted from: <i>Polymers</i> <b>2023</b> , <i>15</i> , 3215, doi:10.3390/polym15153215 . . . . .	639

**Chanaporn Thongphang, Atitiya Namphonsane, Sombat Thanawan, Chin Hua Chia,  
Rungtiwa Wongsagonsup, Siwaporn Meejoo Smith and Taweechai Amornsakchai**  
Toward a Circular Bioeconomy: Development of Pineapple Stem Starch Composite as a  
Plastic-Sheet Substitute for Single-Use Applications  
Reprinted from: *Polymers* **2023**, *15*, 2388, doi:10.3390/polym15102388 . . . . . **655**

# Preface

In the last several years, issues related to environmental pollution, health, and safety have pushed the global research community to address new challenges in order to find valid solutions able to substitute petroleum-based materials, providing advantages for the environment and humans. In this scenario, bio-polymers have gradually caught on in several application fields in materials science, such as manufacturing, biomedical engineering, the food industry, packaging, cosmetic and pharmaceutical industries, agriculture, the energy sector, green nanotechnology, and recycling by attracting the interest of the industrial world, which is increasingly forced to comply with restrictions for environmental and health protection. This reprint collects 32 scientific works of scholars that contributed their own expertise, passion, and science to expand the boundaries of knowledge by addressing new challenges. The topic of new biopolymer-based composite materials is addressed from several aspects, from the development to characterization and application, in several fields of scientific interest.

**Raffaella Striani**

*Editor*





Review

# A Review of Chitosan and Chitosan Nanofiber: Preparation, Characterization, and Its Potential Applications

Marwan A. Ibrahim <sup>1,2</sup>, Mona H. Alhalafi <sup>3,\*</sup>, El-Amir M. Emam <sup>4</sup>, Hassan Ibrahim <sup>5,\*</sup> and Rehab M. Mosaad <sup>1,2</sup><sup>1</sup> Department of Biology, College of Science, Majmaah University, Al-Majmaah 11952, Saudi Arabia<sup>2</sup> Faculty of Women for Arts, Science and Education, Ain Shams University, Cairo 11566, Egypt<sup>3</sup> Department of Chemistry, College of Science, Majmaah University, Al-Majmaah 11952, Saudi Arabia<sup>4</sup> Faculty of Applied Arts, Textile Printing, Dyeing and Finishing Department, Helwan University, Cairo 11795, Egypt<sup>5</sup> Pretreatment and Finishing of Cellulosic Fibers Department, Textile Research and Technology Institute, National Research Centre, Cairo 12622, Egypt

\* Correspondence: m.alhalafi@mu.edu.sa (M.H.A.); hmaibrahim@gmail.com (H.I.)

**Abstract:** Chitosan is produced by deacetylating the abundant natural chitin polymer. It has been employed in a variety of applications due to its unique solubility as well as its chemical and biological properties. In addition to being biodegradable and biocompatible, it also possesses a lot of reactive amino side groups that allow for chemical modification and the creation of a wide range of useful derivatives. The physical and chemical characteristics of chitosan, as well as how it is used in the food, environmental, and medical industries, have all been covered in a number of academic publications. Chitosan offers a wide range of possibilities in environmentally friendly textile processes because of its superior absorption and biological characteristics. Chitosan has the ability to give textile fibers and fabrics antibacterial, antiviral, anti-odor, and other biological functions. One of the most well-known and frequently used methods to create nanofibers is electrospinning. This technique is adaptable and effective for creating continuous nanofibers. In the field of biomaterials, new materials include nanofibers made of chitosan. Numerous medications, including antibiotics, chemotherapeutic agents, proteins, and analgesics for inflammatory pain, have been successfully loaded onto electro-spun nanofibers, according to recent investigations. Chitosan nanofibers have several exceptional qualities that make them ideal for use in important pharmaceutical applications, such as tissue engineering, drug delivery systems, wound dressing, and enzyme immobilization. The preparation of chitosan nanofibers, followed by a discussion of the biocompatibility and degradation of chitosan nanofibers, followed by a description of how to load the drug into the nanofibers, are the first issues highlighted by this review of chitosan nanofibers in drug delivery applications. The main uses of chitosan nanofibers in drug delivery systems will be discussed last.

**Keywords:** chitosan; nanofiber; preparation; characterization; applications; wound dressing

**Citation:** Ibrahim, M.A.; Alhalafi, M.H.; Emam, E.-A.M.; Ibrahim, H.; Mosaad, R.M. A Review of Chitosan and Chitosan Nanofiber: Preparation, Characterization, and Its Potential Applications. *Polymers* **2023**, *15*, 2820. <https://doi.org/10.3390/polym15132820>

Academic Editor: Raffaella Striani

Received: 25 April 2023

Revised: 13 June 2023

Accepted: 15 June 2023

Published: 26 June 2023



**Copyright:** © 2023 by the authors. Licensee MDPI, Basel, Switzerland. This article is an open access article distributed under the terms and conditions of the Creative Commons Attribution (CC BY) license (<https://creativecommons.org/licenses/by/4.0/>).

## 1. Introduction

Henry Braconot (1780–1855) isolated chitin from mushrooms in 1811. Chitin was the second carbohydrate discovered in 1859 [1]. It was hydrolyzed in an alkaline medium in 1894 to produce a new carbohydrate soluble in dilute acids called chitosan. Chitosan and its oligomers drew a lot of attention because of their unique properties [2–4]. Chitin represents the second natural polysaccharide in nature, after cellulose. Its chemical name is poly *N*-acetamido-2-decoxy- $\beta$ -D-glucose [5]. Figure 1 shows the chemical structure and some sources of chitin and chitosan [6–9].

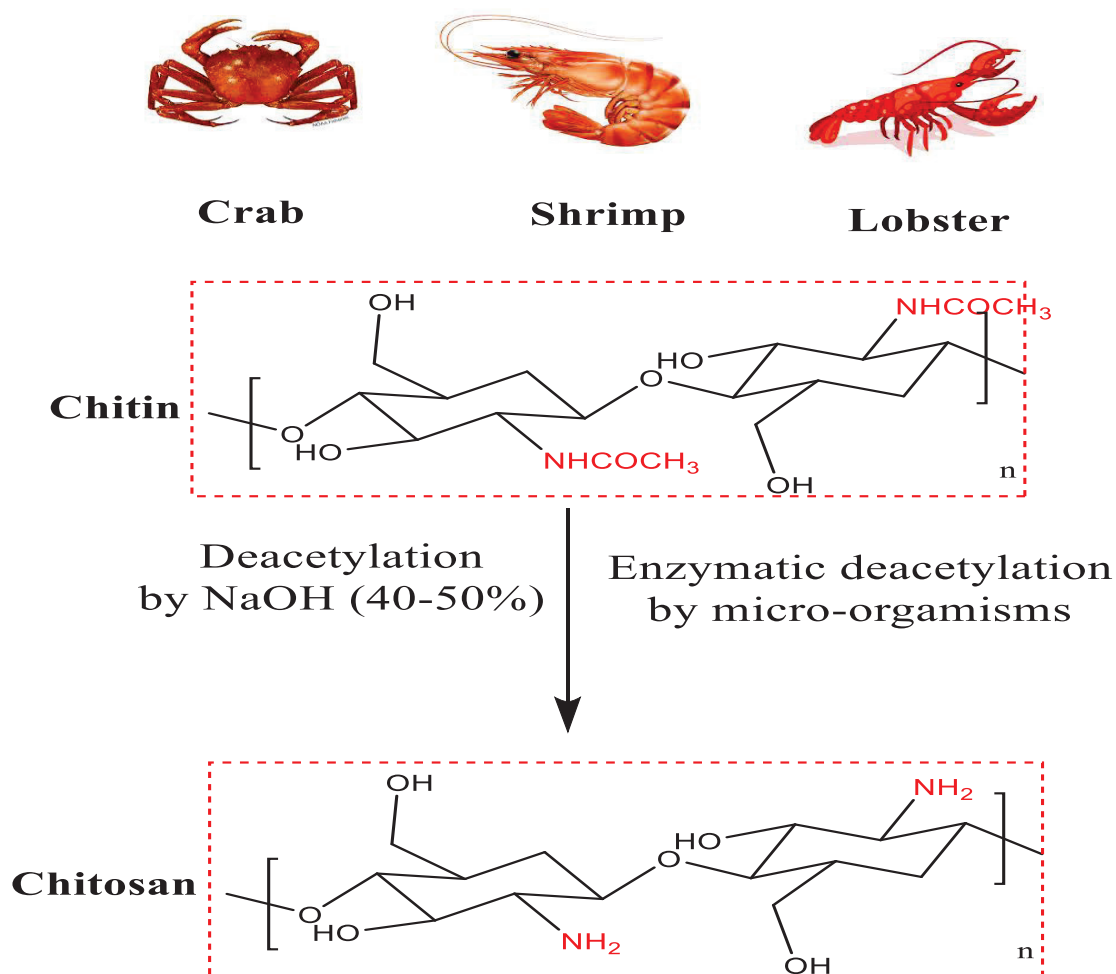


Figure 1. Chemical Structure and some sources of chitin and chitosan [5].

## 2. Structure of Chitin and Chitosan

Chitosan, a white polymer found in crabs, is a nitrogenous polysaccharide that is rigid inelastic and found both inside and outside the exoskeleton of invertebrates. The primary distinction is the solubility of chitosan in diluted acid (at PH = 7). The ocean, lakes, and seas are the sources of chitosan products [10]. Chitosan has potential applications in various fields, such as biomedical applications and the fabrication of protective clothes [10].

Chitin and chitosan, as natural renewable biopolymers, have unique properties, as they are biocompatible, biodegradable, and non-toxic [11]. Because of the  $\text{NH}_2$  groups that open the structure of chitosan, it is easier to modify than cellulose. As a result, it can be converted into a variety of chitosan derivatives [12]. The main purpose of this modification is to improve its solubility and chemical reactivity [13,14].

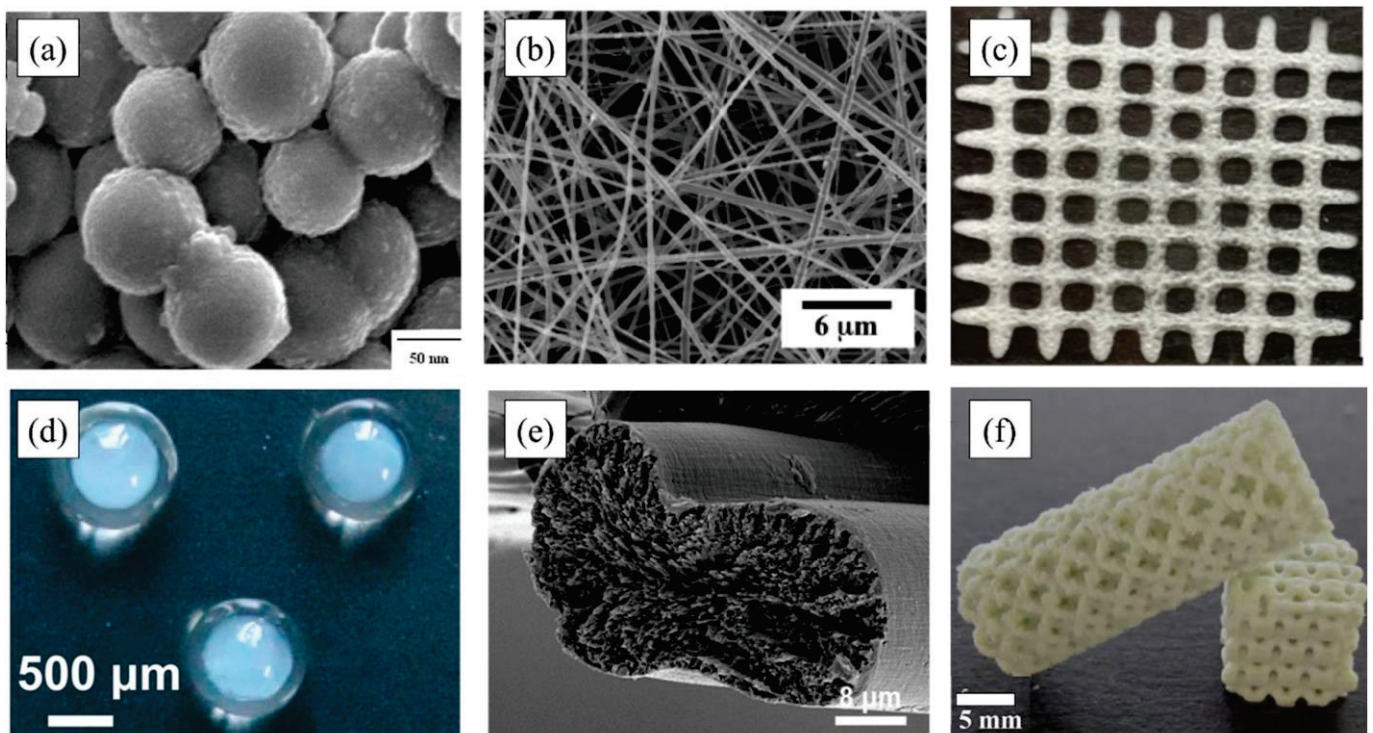
Acetylation degree is the presence of acetyl glucose amine to glucose amine in the chitin structure. Which determines the solubility of chitin and chitosan? Chitosan is more accepted than chitin due to its high degree of solubility in dilute acetic acid [15,16].

The presence of acetyl groups in chitin and chitosan makes their solubility problematic, although M.W.T. represents an important later component for chitin and chitosan properties. There are several methods used to estimate the molecular weight (M.W.T.) of chitin and chitosan, such as light scattering and viscosity [15,16].

Chitin is hydrophobic material insoluble in water and most organic solvents. Its solvent is a mixture of 1,2-dichloroethane and trichloroacetic acid (35:65), fresh saturated solution of lithium thiocyanate, chloroalcohols in conjugation with aqueous solutions of mineral acids and Dimethylacetamide containing 5% lithium chloride [10,17].

Chitin and chitosan are biocompatible, biodegradable, and non-toxic. Because they are amino polysaccharides, they exhibit interesting properties in biology, pharmacology, and physiology and have numerous applications such as wound healing, wound dressing, hemostatic agency, and antimicrobial activity, requiring them to be used as a biomedical material [17].

Figure 2 shows chitosan-based materials with different shapes and sizes: chitosan nanoparticles, chitosan nanofibers fabricated by electrostatic spinning technology, chitosan–pectin hydrogel grid scaffold prepared by 3D printing technology, chitosan core–alginate shell microspheres, chitosan-based fibers fabricated by solvent spinning technology, and 3D-printed chitosan porous structures [18].



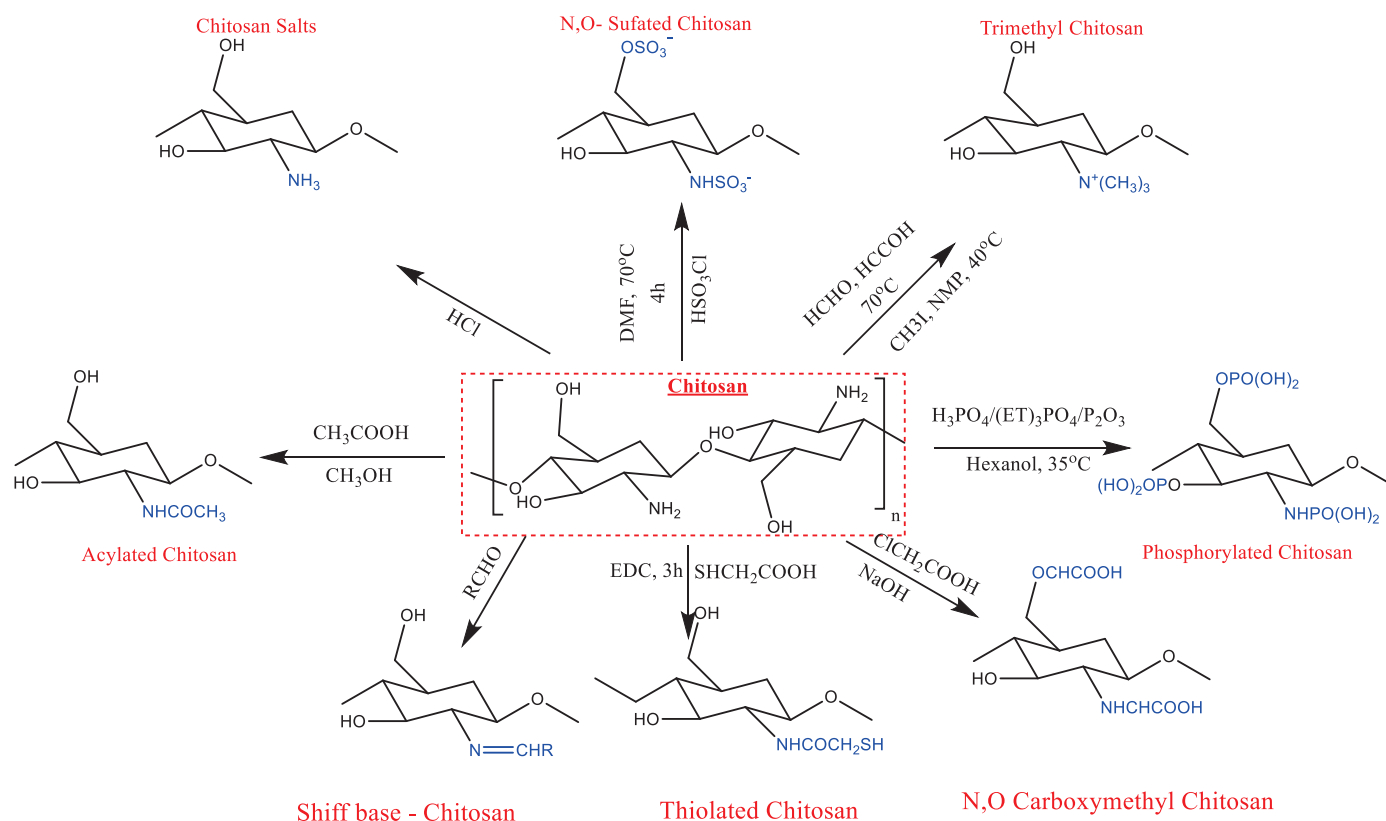
**Figure 2.** Chitosan-based materials with different shapes and sizes: (a) chitosan nanoparticles; (b) chitosan nanofibers fabricated by electrostatic spinning technology; (c) chitosan–pectin hydrogel grid scaffold prepared by 3D printing technology; (d) chitosan core–alginate shell microspheres (e) chitosan-based fibers fabricated by solvent spinning technology; and (f) 3D-printed chitosan porous structures. Copyright 2023. Reproduced with permission from Elsevier Science Ltd. [18].

### 3. Modification of Chitin and Chitosan

Although chitin and chitosan possess several useful qualities, their application is constrained by their poor solubility, small surface area, and porous makeup. To modify chitin and chitosan physically or chemically, various researchers have tested their theories. The two main benefits of modifying chitin and chitosan are to increase their solubility and improve their ability to absorb metals. The OH at the C3, C6, and NH<sub>2</sub> at the C2 groups in chitosan undergo substitution reactions. These changes also improve the capacity of the membrane to swell in water [19–21].

In the molecular structure of chitosan, there are three types of active groups: amino groups, and primary and secondary hydroxyl groups at the C-3 and C-6 positions, which allow for chemical modification of chitosan. C6-OH is a main hydroxyl group with little steric hindrance, whereas C3-OH is a secondary hydroxyl group with a lot. As a result, the main hydroxyl group could freely rotate while the secondary hydroxyl group could not. The amino group is usually more reactive than the primary hydroxyl group, and the primary hydroxyl group is usually more reactive than the secondary hydroxyl group [22–24]. Chitosan

can be chemically modified on the amino, hydroxyl, or both amino and hydroxyl groups to generate N-modified, O-modified, or N, O-modified chitosan derivatives [25] (Figure 3).



**Figure 3.** Chemical modification of chitosan.

The proposed mechanism of chitosan modification can pass through one of the following four mechanisms: (a) free radical-induced conjugation to form a polyphenol chitosan conjugation; (b) carbodiimide chemical mechanism to form Schiff base compounds; (c) functional group conversion strategy, which converts the amino group of chitosan into an azide group, substituted carboxyl group, substituted mercapto group, and where the hydroxyl group can be azidate, aminated, oxidized to an aldehyde or carbonyl group, or further oxidized to a carboxyl group; or (d) conjugation of chitosan with polyphenol via enzymatic assisted coupling reaction, as shown in Figure 4a–d [26].

Chitosan has a low specific surface area ( $2\text{--}30\text{ m}^2\cdot\text{g}^{-1}$ ) [27] and is present in flake, which is unsuitable for many applications, so that it has been modified into beads to increase its value in different fields of application [19–21]. Due to the open structure and pores of chitosan, which has poor mechanical properties, shrinkage, and deformation in dry form and is only soluble in weak acids, numerous modifications have been made to it to improve its properties [28]. Chitosan contains amino and hydroxyl groups, so it is a poly-nucleophilic polymer. Nucleophilic substitution occurs. Protonation in  $\text{NH}_2$  groups results in the formation of  $\text{NH}_3^+$  [29,30], such as N-alkylated chitosan prepared from Schiff base reactions followed by imine reduction by sodium borohydride. Furthermore, positive chitosan charges interacted with polyanion polymers such as alginate, carrageen, and pectin between the  $\text{COOH}$  and  $\text{NH}_3^+$  groups [31]. Chitosan produce new functionalized derivatives via a grafting reaction [32]. The properties of grafted chitosan are determined by the side chains and the cross-linking agent [33]. Chitin threads are prepared to be used in absorbable suture fabrication, dressing, and biodegradable materials for human skin fiber growth [34].

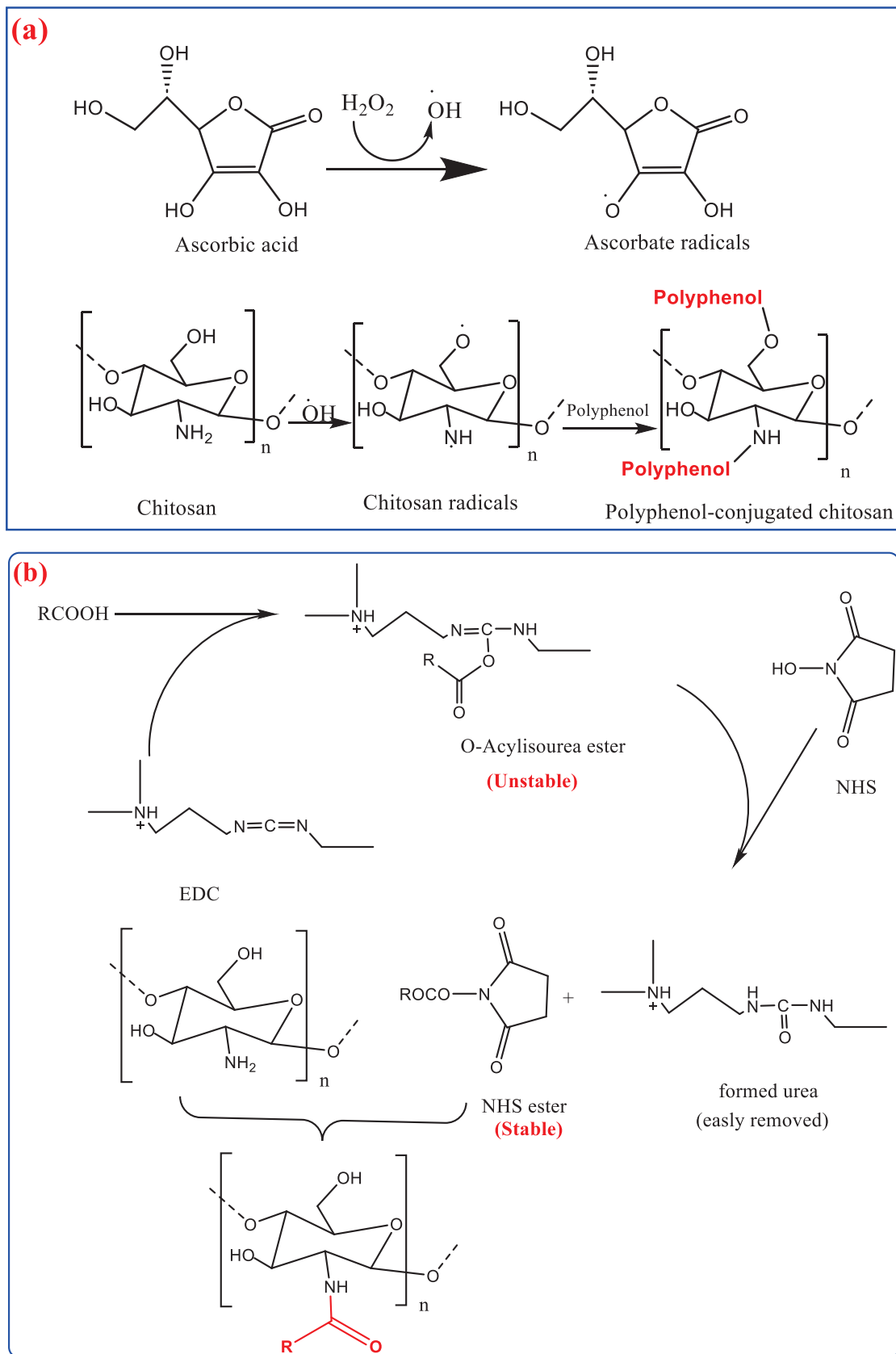
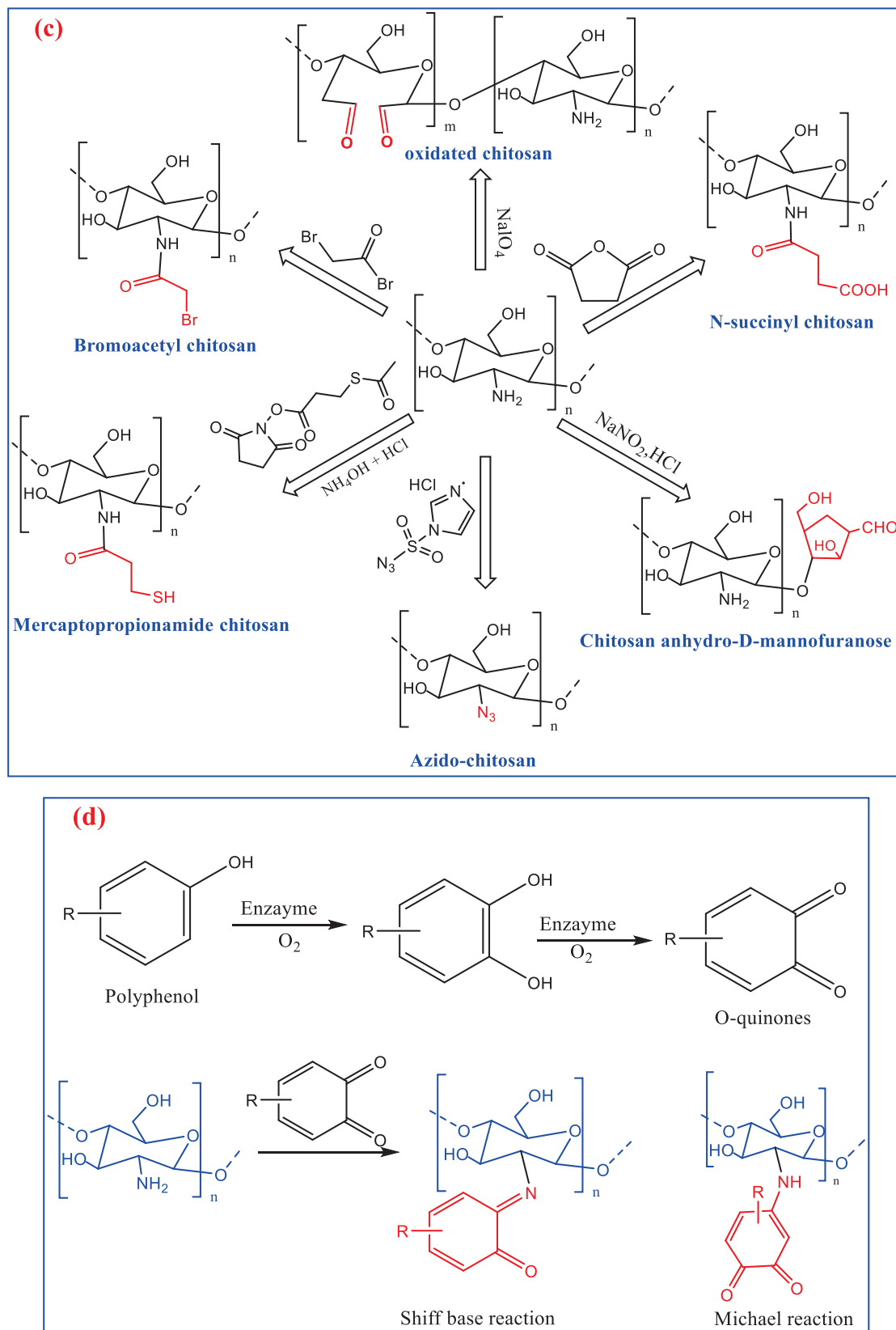


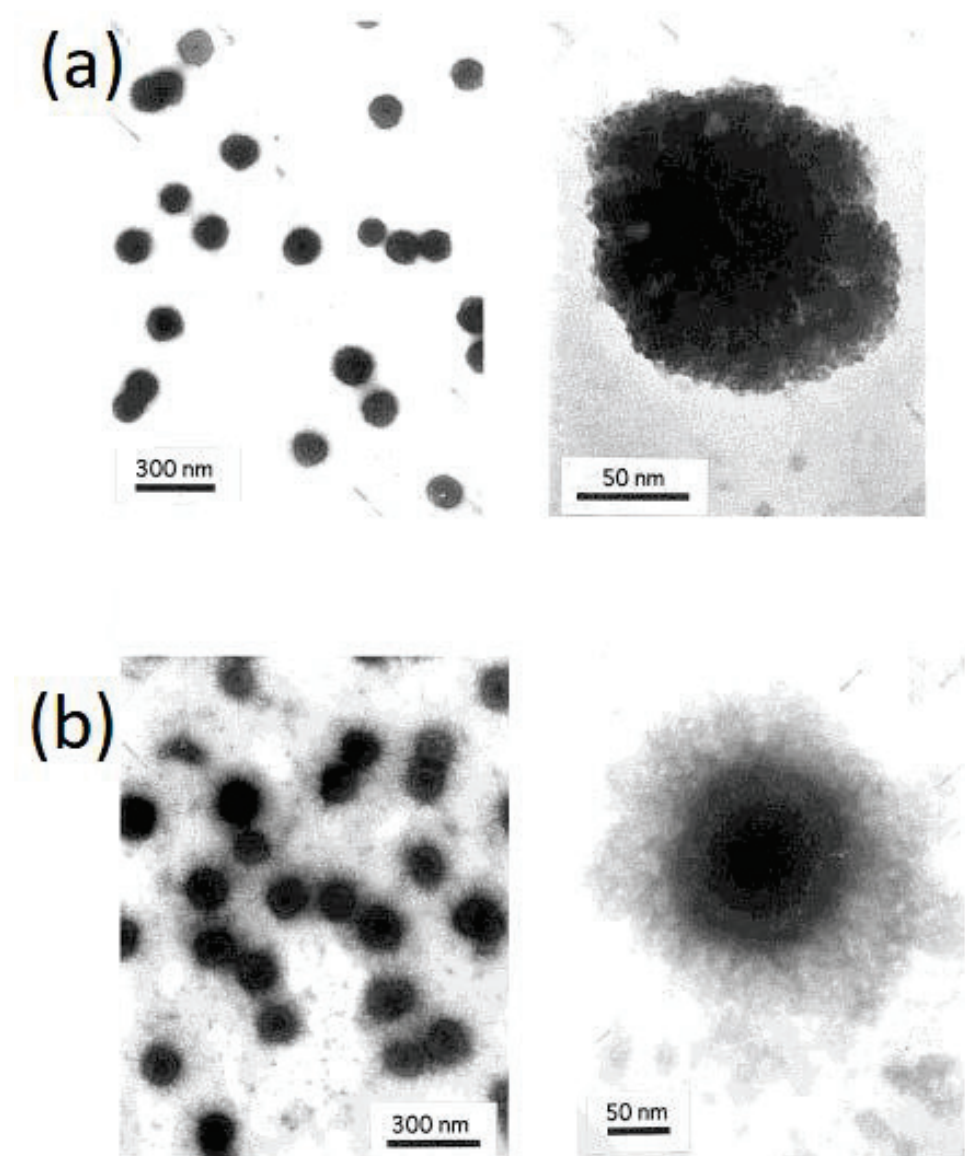
Figure 4. Cont.





**Figure 4.** Proposed mechanisms (pathway) for chemical modification of chitosan via conjugation (a) free radical-induced conjugation to form a polyphenol chitosan conjugation; (b) carbodiimide chemical mechanism to form Schiff base compounds; (c) functional group conversion strategy, or (d) conjugation of chitosan with polyphenol via enzymatic assisted coupling reaction.

Chitosan is a hydrophilic material used to impart hydrophilicity to some other polymer in its composites, such as polyacrylonitrile (PAN) [35]. Hydrophilic polymer nanoparticles were prepared by ionic gelation in mild conditions at room temperature, via two phases; one is for polymers such as chitosan polysaccharide (CS) and polyethylene oxide (PEO), and the other phase contains sodium tripolyphosphate (TPP). Calvo et al. prepared chitosan nanoparticles with high protein loading capacity, which were released within a week [36]. The morphology of these nanoparticles is spherical, as shown in Figure 5.



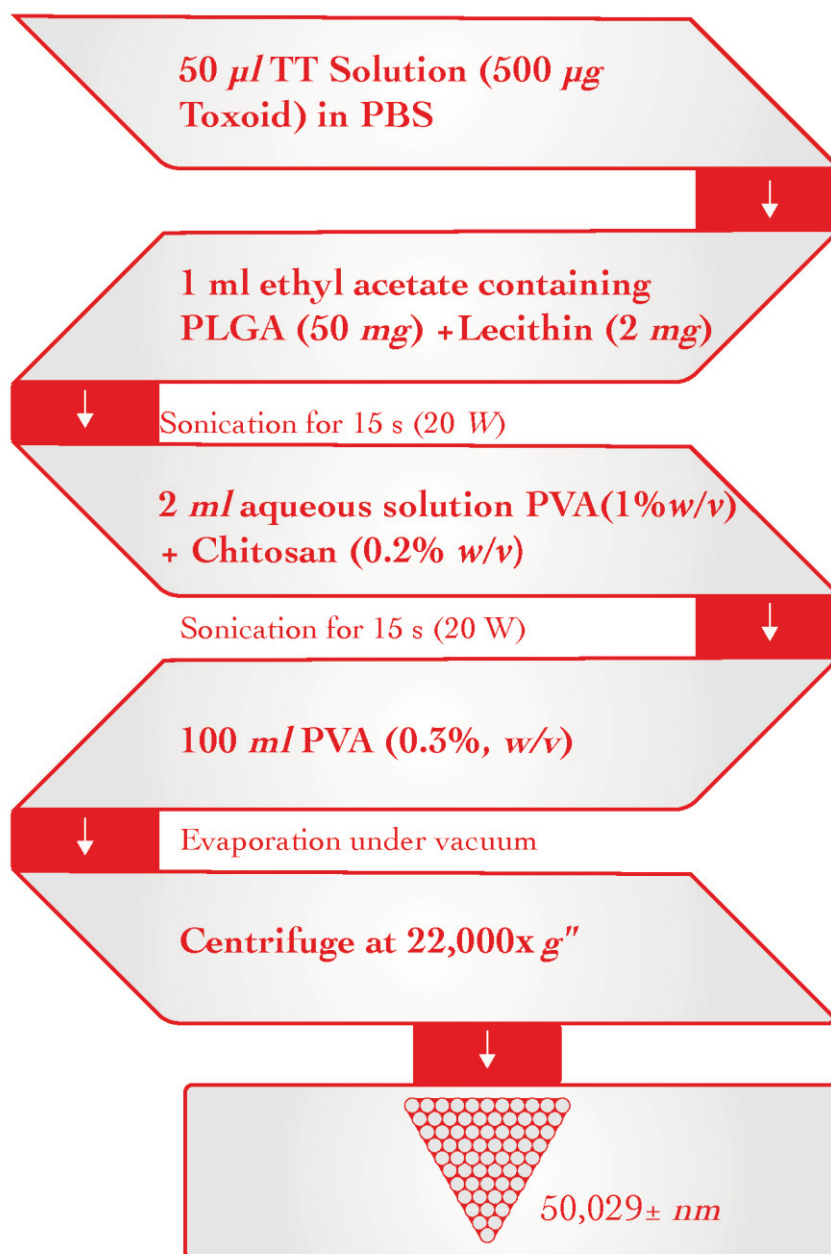
**Figure 5.** Electron transmission microphotography of: (a) CS nanoparticles; (b) CS/PEO-PPO nanoparticles (concentration of PEO-PPO in the chitosan solution: 10 mg/mL) prepared by Calvo et al. [36], reproduced with permission from John Wiley and Sons.

Nanoparticles of chitosan by using a variety of agents, the freeze-drying method increases shelf life. Chitosan nanoparticles of two different types were prepared by Alonso et al. in 1999 [37]. The prepared nanoparticles ranged in size from 300 to 400 nm, had a positive surface charge, and were efficient. These nanoparticles are used to address the nasal absorption of insulin. In addition, chitosan nanoparticles were used as a poly load of the anthracycline drug doxorubicin (DOX) [38,39]. In addition, these nanoparticles were used to load dextran sulphate to enhance its drug loading [40]. With cyclosporine serving



as the model drug, chitosan nanoparticles (CSNP) were used to enhance the drug at the ocular surface. The size of these nanoparticles was 29 nm [41].

Chitosan-coated PLGA–Lecithin nanoparticles were prepared by the modified double emulsion method; these nanoparticles were used through the oral or nasal administration route. Figure 6 depicts the process of preparing CS–PLGA nanoparticles, and Table 1 summarizes the properties of the prepared nanoparticles [41].



**Figure 6.** Flowchart showing the creation of chitosan–PLGA particles step-by-step.

Chitosan nanoparticles loaded by *Mycobacterium uaceae aerivatiuem* antineoplastic proteoglycans exhibit wide antimicrobial activity, as repeated by Tian and Groves (1999) [42]. The researchers prepared chitosan nanoparticles with particle sizes of 600–700 nm without using organic solvents and discovered that the two reactants affected the absorption and release of bovine, as well as that the initial Nanoparticles of chitosan by using a variety of agents, the freeze-drying method increases shelf life. Chitosan nanoparticles of two different

types were prepared by Alonso et al. in 1999 release was followed by a steady release for 4 h in water [43].

**Table 1.** Particle size zeta potential theoretical loading, and encapsulation efficiency values of CS [41].

Polymer	Protein Loaded	Size (nm)	Potential (mV)	Theoretical Lading (%)	Encapsulation Efficiency (%)
PLA	Tetanus Toxoid	192 ± 12	−47.9 ± 1.5	1	36.7 ± 0.3
PEG-PLA	Tetanus Toxoid	196 ± 20	−23.9 ± 1.2	1	31.1 ± 0.5
CS-PLGA	Tetanus Toxoid	500 ± 29	−21.8 ± 1.1	1	90.0 ± 3.6
CS	Tetanus Toxoid	354 ± 27	−37.1 ± 5.9	10	55.1 ± 3.4
CS	Insulin	337 ± 14	−36.9 ± 0.3	40	94.7 ± 2.1

Using self-aggregates of chitosan modified by deoxycholic acid, there is a novel and straightforward method of delivering adriamycin [44].

Deoxycholic acid and chitosan are covalently conjugated through an EDC-mediated reaction, resulting in self-aggregating chitosan nanoparticles. The Adriamycin active ingredient was physically trapped in nanoparticles, and the resulting self-aggregates were assessed using a variety of methods, including spectroscopy, which shows that these self-aggregates are spherical and that the drug concentration affects the shape of the particles [44].

These self-aggregates of chitosan modified by deoxycholic acid were used as DNA carriers by Kim et al. in 2001 [45]. Chitosan is used to overcome the side effects of drugs such as their solubility and hydrophobicity so that it can be used as a drug carrier. For example, commercial chitosan can be used to control body weight.

#### 4. Chitosan as Biomaterial

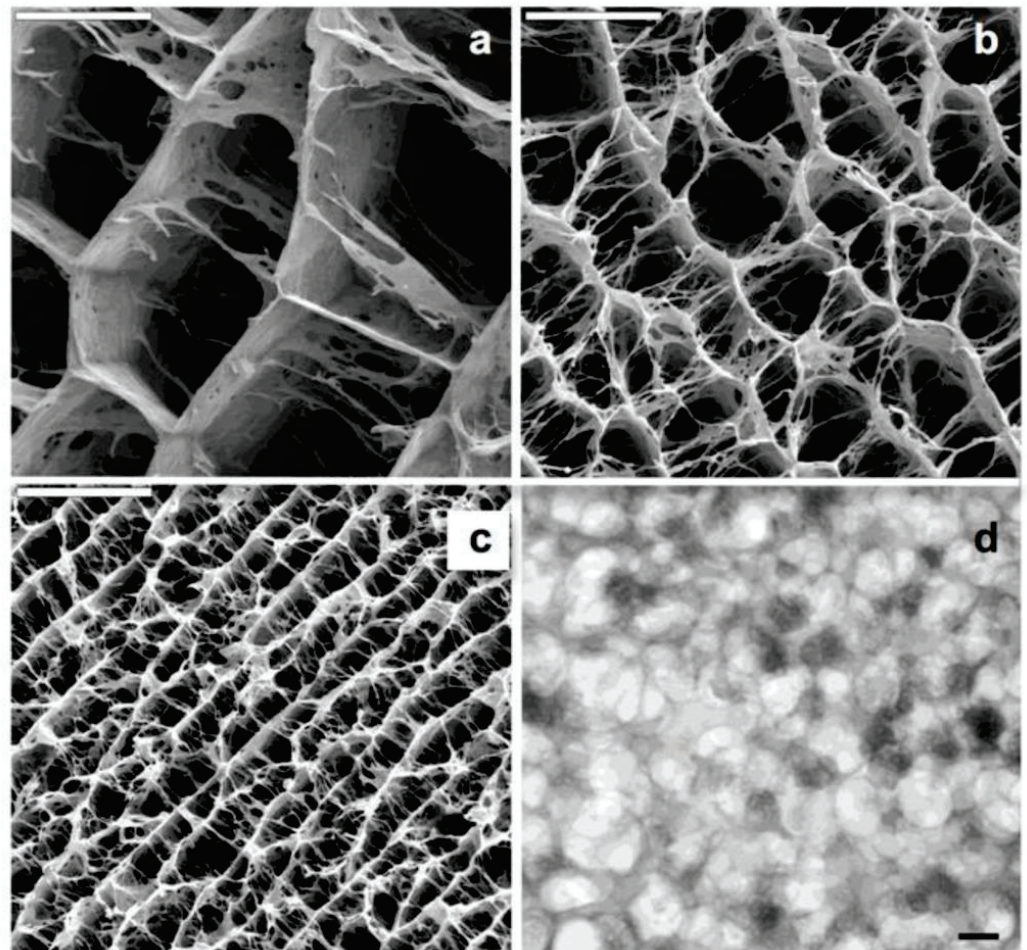
Chitosan is a semi-crystalline polymer that is partially deacetylated chitin, and the degree of crystallinity is correlated with the degree of deacetylation. Chitin and fully deacetylated chitosan have the highest crystallinity, while intermediate levels of deacetylation have the lowest crystallinity [12]. Chitosan is stable, crystalline, and soluble in aqueous solutions at PH 7, but it is insoluble in weak acids due to the protonation of amino groups. Chitosan solutions could be extruded at higher PH values or in non-solvent baths, e.g., methyl alcohol. Chitosan polymer is used for industrial applications in such forms as fiber or film [46]. Chitosan solution's cationic nature and high charge density make it potentially useful as a biomaterial. Chitosan forms soluble ionic complexes or complexes with water soluble anionic polymers such as alginates and synthetic polymers such as poly (acrylic acid) due to its charge density [21]. When used for local delivery of biologically active poly anions like GAGs and DNA, for example, ionic complexes release heparin to increase the efficacy of growth factor secreted by inflammatory cells [21,47–51].

Chitosan DNA complex is used to facilitate cellular transfection and prevent plasmid degradation by nucleases. Chitosan can become porous through freezing and lyophilization, making it useful for both tissue regeneration and cell transplantation [52]. Figure 7 illustrates how ice crystals form in the freezing process from a solution, grow from the ice crystal phase, and are then removed by lyophilization from a general porous mother.

Pore size and pore orientation affect the mechanical properties of scaffold-based chitosan, with porous chitosan membranes having less elasticity (0.1–0.5 MPa) than non-porous membranes (5–7 MPa).

The maximum strain of the porous membrane of chitosan is greater than that of the non-porous membrane, and the 100% chemical modification of chitosan introduces new biological activity with modified mechanical properties. The chitosan NH<sub>2</sub> group is reactive and capable of introducing side group attachment with several reactions that affect primarily crystallinity disruption with lower stiffness and alter soluble derivatives feasible in chemical reactions, such as alkyl derivatives of chitosan, which have lower solubility than chitosan itself and give aggregates miscible for  $c > 5$ . In addition, the basic

properties of chitosan are hemostatic, cationic, and insoluble at pH 7, which are completely reversed by the solvation process to give ionic, water-soluble derivatives, and anticoagulant properties, so that chitosan can attack with unlimited side groups and be chosen according to specific needed functions, e.g., biological activity or modified properties, etc.



**Figure 7.** SEM micrographs of different hybrid hierarchical structures resulting from freezing hydrogel nanocomposites, with identical CHI and calcium phosphate composition (93.25 and 6.75 wt.%, respectively) at different rates of freezing: (a) 0.7 mm/min; (b) 2.7 mm/min, and (c) 5.7 mm/min. Scale bars are 50  $\mu\text{m}$ . TEM (d) micrographs of ACP nanoclusters forming the ACP/CHI hierarchical structure. Ref. [52] Reproduced with permission from MDPI.

## 5. Applications of Chitosan and Chitosan Derivatives

Chitosan is a biodegradable, biocompatible, and non-toxic biomaterial; therefore, it has many applications in areas such as medicine, agriculture, food processing, cosmetics, and treatment of water.

### 5.1. Agricultural Application

Chitosan can be used safely in agricultural applications because it does not pollute the environment or harm consumers; it is used as a leaf coating, fertilizer, and sea coating [10,53]. The use of chitosan in agricultural fields has increased exponentially, especially for germination improvement, leaf growth, retention of moisture, and fungal and disease reduction [53]. Chitosan boosts photosynthetic efficiency while enhancing plant tolerance to salinity, high temperatures, and drought [54]. Chitosan's hydrophilic properties encourage water absorption while reducing transpiration [55]. To encourage plant development, chitosan can be employed as an additional carbon source in plant synthesis [56]. In com-

parison to the control group, seedlings treated with Cu-chitosan nanoparticles (NPs) at concentrations of 0.04 percent and 0.12 percent had greater rates of germination, seedling length, root length, and root number [57]. To encourage the mobilization of protein and starch to boost seedling growth, Cu-chitosan NPs can increase protease and -amylase activities [58].

### 5.2. Wastewater Treatment Applications

Chitosan contains both OH and NH<sub>2</sub> groups as chelating agent groups, which allow it to be used in water treatments from wastes due to the high-power effect of these functional groups to bind with heavy dissolved metals present in wastewater such as Cu, Pb, Hg, and Ur [59]. Furthermore, chitosan can be used to break down food particles, particularly food proteins, as well as remove dyes from wastewater [60].

Cu (II) ion-containing wastewater was examined by Qin et al. [61] using sodium alginate and chitosan as treatment agents. They investigated how various parameters affected this ion removal. According to the findings, chitosan and sodium alginate worked better together than they did separately. Pesticide removal from wastewater was explored by Dwivedi et al. [61] using hydrogel beads made of chitosan and gold nanoparticles. The data obtained indicated that the synthetic sorbent has good pesticide removal capacity.

Heterogeneous catalysis is one technique that heavily relies on adsorption. Purification is one of the earliest documented uses of adsorption. Adsorbents are still used to clarify water [62]. Numerous adsorbents, including activated carbon, low-cost biomass adsorbents, waste sludge, rice husk, sugarcane bagasse, lignite, and chitosan, were used in the adsorption tests. Heavy metal contamination clean-up frequently employs chitosan. In order to study the adsorptions of three metal ions—Cu (II), Zn (II), and Pb (II) ions—in an aqueous solution, cross-linked chitosan was created by the homogeneous reaction of chitosan in an aqueous acetic acid solution with epichlorohydrin [63].

### 5.3. Food Industry Applications

Because of the high potential for toxicity of chitosan as a chelating agent and its high functional properties, as previously stated, chitosan is used in a variety of applications in the food industry, such as removing specific elements, particles, and undesirable materials, such as dyes and fats. In addition, it is widely used as a natural, safe preservative in the United States to store food [64,65].

There has been an increase in interest in recent years in studying the potential applications of chitosan as films or coatings in food packaging. This is due to their film-forming, antioxidant, and antibacterial properties, as well as their mechanical and barrier properties, which were studied as films. In order to extend the storability and shelf life of perishable commodities, these experiments sought to develop active packaging based on chitosan, either on its own or in combination with other materials. By combining chitosan with other natural antimicrobial agents, it is also possible to make food products that guarantee food safety against a variety of mutating and pathogenic bacteria [66–68].

An edible coating or thin edible film made of chitosan can be applied to food to act as active food packaging. The edible coating is a thin layer that is added to a food item and is generated by dipping the item in a chitosan solution or spraying, in which case, the film-forming solution is crushed up using an aerosol spray coating. Even though the chitosan film is a thin, prefabricated layer, once it is produced, it can be deposited on the surface of or in between food ingredients [66,67,69]. Studies using chitosan films and coatings on food products are shown in Table 2 [66].



**Table 2.** Chitosan-based films have been used in a wide variety of food products.

Chitosan Film/Coated	Food	References
Chitosan	Citrus fruit	[70,71]
Chitosan	Logan fruit	[72]
Chitosan	Green coffee beans	[73]
Chitosan	Frozen salmon	[74]
Chitosan	Tankan citrus fruit	[75]
Chitosan	Apples	[76,77]
Chitosan	Mushroom	[78]
Chitosan	Mangoes	[70,71,79]
Chitosan	Litchi fruit	[80,81]
Chitosan	Salmon fillets	[82]
Chitosan	Tomatoes	[83]
Chitosan	Strawberries	[83]
Chitosan	Peach fruit	[72]
Chitosan	Fresh-cut Chinese water chestnut L.T.	[84]
Chitosan	Silver carp	[85]

#### 5.4. Medical Applications

Chitosan is applicable in several medical industries, especially periodontal and orthopedic drug delivery, wound healing, and tissue engineering applications [86]. Surgical sutures, contact lenses, eye fluids, artificial skin, artificial blood vessels, bandages, sponges, burn dressings, blood cholesterol vessels, antitumor, antibacterial, antiviral, bone regenerator, antimicrobial, and hemostatic agents are the most well-known examples of these applications [86–91].

Chitosan inhibits tumor cell proliferation, and Liu et al. demonstrated that chitosan induces apoptosis in tumor cells by decreasing Bcl-2 and increasing Caspase-3 expression [92,93]. Carboxymethyl chitosan (CMCS) increases macrophage viability, deeply penetrates the tumor microenvironment, generates cytokines like TNF and IL-1, improves phagocytosis, and increases NO levels. Notably, CM-COS is not significantly toxic to normal liver cells but inhibits the growth of BEL-7402 and sarcoma cells in vivo [94,95]. Additionally, chitosan inhibits the invasion and metastasis of tumor cells. During tumor invasion and metastasis, matrix metalloenzymes (MMP) are involved in the breakdown of extracellular matrix, and MMP-2 can encode an enzyme that breaks down type IV collagen [96].

Chitosan is a great material for creating wound dressings because it can promote wound healing. It exhibits good antibacterial activity due to its alkaline amino groups, which cause the destruction of bacterial cells and protect the wound surface from microbial infection [97]. To improve the antibacterial and coagulation capabilities, Zhang et al. created a nanocomposite hydrogel utilizing zinc oxide (ZnO), chitosan, and aldehydic sodium alginate (SA) [98]. It significantly inhibited the growth of *Escherichia coli* and *Staphylococcus aureus*. I-sexual collagen hydrogels sulphated chitosan-doped by Shen et al. improved macrophage polarization from M1 to M2. The IL-4 and TGF-1 secreted by macrophages were stimulated, which resulted in an increase in collagen synthesis, regeneration epithelialization, and neovascularization [99].

Tissue engineering is an emerging interdisciplinary discipline combining material science, engineering mechanics, and biomedicine. The structure and function of damaged tissues and organs are repaired or replaced by cell transplantation combined with bioactive molecules and 3D scaffolds. Chitosan is similar to mucopolysaccharides of the extracellular matrix and is used as a scaffolding material for cartilage tissue engineering [100].

Kaviani et al. used the cryogel approach to construct nano porous scaffolds from chitosan, collagen, and nanohydroxyapatite, which lowered the rate of biodegradation, increased mechanical characteristics, and enabled cell proliferation and adhesion [58]. Porous scaffolds made from chitosan, gelatin, and silk proteins have higher compressive strength and modulus, whereas incidental chondrocytes can produce seed scaffolds and

stimulate cartilage tissue regeneration [58]. By mixing gelatin, chitosan, and polyvinyl alcohol with nano-hydroxyapatite, Martino et al. created porous composite scaffolds [58]. Table 3 summarizes the biological application of chitosan and its derivatives.

**Table 3.** Biological applications of chitosan and its derivatives.

Composite/Properties	Stimulatory Effects	References
Environmental purposes		
Flocculation	Removes a variety of contaminants from wastewater in an efficient manner	[101]
Metals and organic compounds adsorption	Removes pathogens, radioactive materials, heavy metals, colors, organic chemicals, and inorganic nutrients (nitrates and phosphates)	[101]
Agricultural purposes		
Biocontrol agent	Safe alternative to the use of pesticides and agrochemicals as a biocontrol material against many pathogenic microorganisms	[102]
Enhance crop production	- Effectively raises the productivity of various agricultural plants - Effectively encourages plant development in a variety of crops	[103]
Aquafeed additives	Positively impacts the growth, digestive enzymes, body composition, intestinal bacterial count, immunological response, and hematological and liver health of commercial freshwater fish	[104,105]
Biomedical purposes		
Chitosan microspheres	- Used as a carrier for targeted and prolonged delivery of drugs - Increases the bioavailability of degradable substances such as protein - Increases uptake of hydrophilic substances across the epithelial layers	[106]
Chitosan mesh membrane	Decreases wound healing time and increases the recovery of the granular layer	[107]
Chitosan collagen blend membrane	Increases the antibacterial activity against <i>E. coli</i> and <i>S. aureus</i> and decreases the excessive dehydration of the wound	[108]
Alginate/carboxymethyl chitosan blend fibers	Increased water-retention and increased antibacterial activity against <i>S. aureus</i>	[109]
Composite nanofibrous membranes (NFM) of collagen and chitosan	Increased wound-healing and increased tissue regeneration	[110]
Electro spun chitosan fiber with polyethylene oxide	Used effectively as surface layers on the wound site in periodontal disease	[111]
Chitosan membranes loaded with Tetracycline hydrochloride or silver sulfadiazine	Increased wettability, decreased swelling rate, water vapor permeability, and tensile strength, and increased antimicrobial activity against <i>E. coli</i> and <i>S. aureus</i>	[112]
Chitosan titanium dioxide composite membranes	Increased antimicrobial activity against <i>S. aureus</i> , decreased oxidative stress and apoptosis of fibroblast cell sand, increased proliferation in L929 fibroblast cells	[113]
Chitosan nano silver dressing	Increased wound-healing using the non-invasive dressing	[114]
Chitosan sponges loaded with norfloxacin	The dressing can conduct the role of normal skin and the antibiotic release is swelling-controlled	[115]
Chitosan-gelatin sponge	Increased antimicrobial activity against <i>E. coli</i> K88 over penicillin Increased antimicrobial activity against <i>S. aureus</i> over cefradine	[116]
Photo cross linkable chitosan hydrogel containing fibroblast growth factor-2	Increased wound healing in diabetic and normal mice	[117]
Carboxymethyl chitosan alginate hydrogel	Increases Bactericidal properties toward <i>S. aureus</i> and <i>E. coli</i> , and antibiotic continues to be released from the hydrogel	[118]

## 6. Electro-Spun Nanofibers: Process and Application

### 6.1. History of Electrospinning

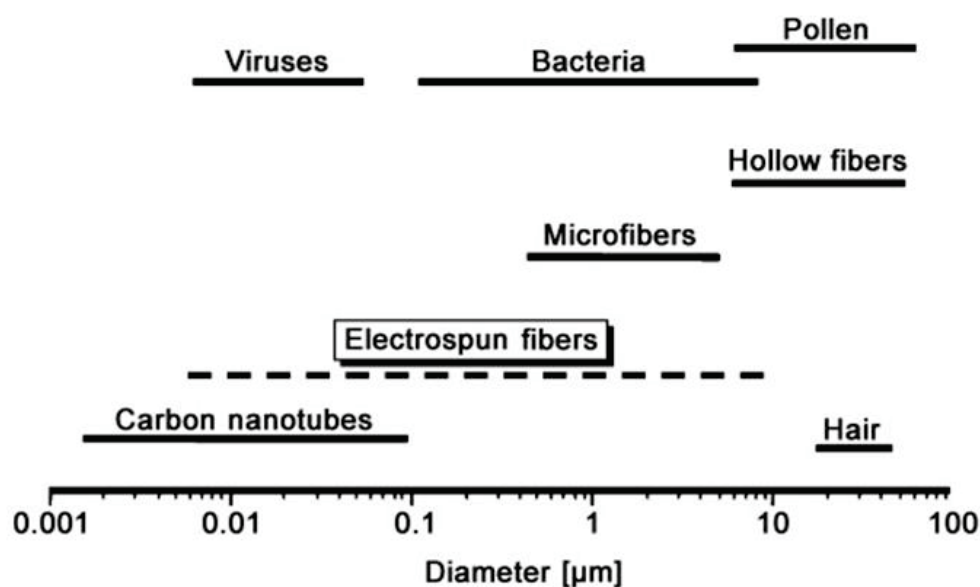
In 1897, Rayleigh discovered electrospinning. The early 1700s saw the discovery of electrostatic effects on water behavior and their impact on the dielectric values of liquid excitation. Around the turn of the twentieth century, Cooley and Morton developed elec-

trospinning technology. The rotatory electrode was then incorporated into electrospinning by Cooley. Formhals created yarns using electrospinning in 1930 without the use of a spinneret, and his technique and apparatus granted him a patent for his creation [119–121].

After that, Formhals submitted a patent for a different method of creating electrostatic polymer fibers: composite fibers made of several polymers. In 1969, Taylor conducted research on the composition of the polymer droplet formed at the needle tip by a strong electric field. This proved that the droplet assumed a cone-like shape, with jets emerging from vortices. The “Taylor cone” is the final name given to this cone. Additionally, factors affecting fiber stability, such as the electric field, flow rate, and experimental settings, were examined [122,123].

Compared to conventional spinning, electrospinning produces fibers at a much slower rate. Electrospinning produces yarn at a rate of 30 m per minute, compared to conventional spinning’s 200–1500 m per minute [119,120,124]. So, before 1990, melt spinning was the preferred method for creating fibers from natural and synthetic polymers, and only a small number of businesses were interested in electrospinning for fiber production. Nanometer-scale fibers cannot be produced through melt spinning [120,124].

For the purpose of removing harmful solvents and for use in tissue engineering applications, Dalton et al. applied an electro spun nanofiber web to tissue cells [125]. The use of electro-spun nanofibers today spans a wide range of potential uses [119,124,126]. Surface nanostructures may produce extraordinary phenomena, such as the lotus effect (self-cleaning effect). Since proteins, viruses, and bacteria all have dimensions in this range, the nanoscale is particularly important for biological systems. Electro spun fibers display a strikingly broad range of sizes when compared to the diameters of these things. Figure 8 depicts the dimensions of bacterial cells, proteins, viruses, and nanofibers [119,124,126,127].



**Figure 8.** Position of nanofibers between protein, bacteria, and viruses [126]. reproduced with permission from John Wiley and Sons.

### 6.2. Electrospinning Process

A high electric field (kV) is used to create micro or nanofibers from polymer solutions while maintaining ambient temperature and pressure. There are two primary setups for electrospinning devices: vertical and horizontal [119,124,128].

The major components of the electrospinning device are the power supply (high voltage), the syringe (spinneret), and the collector (electrode) [119,123,129].

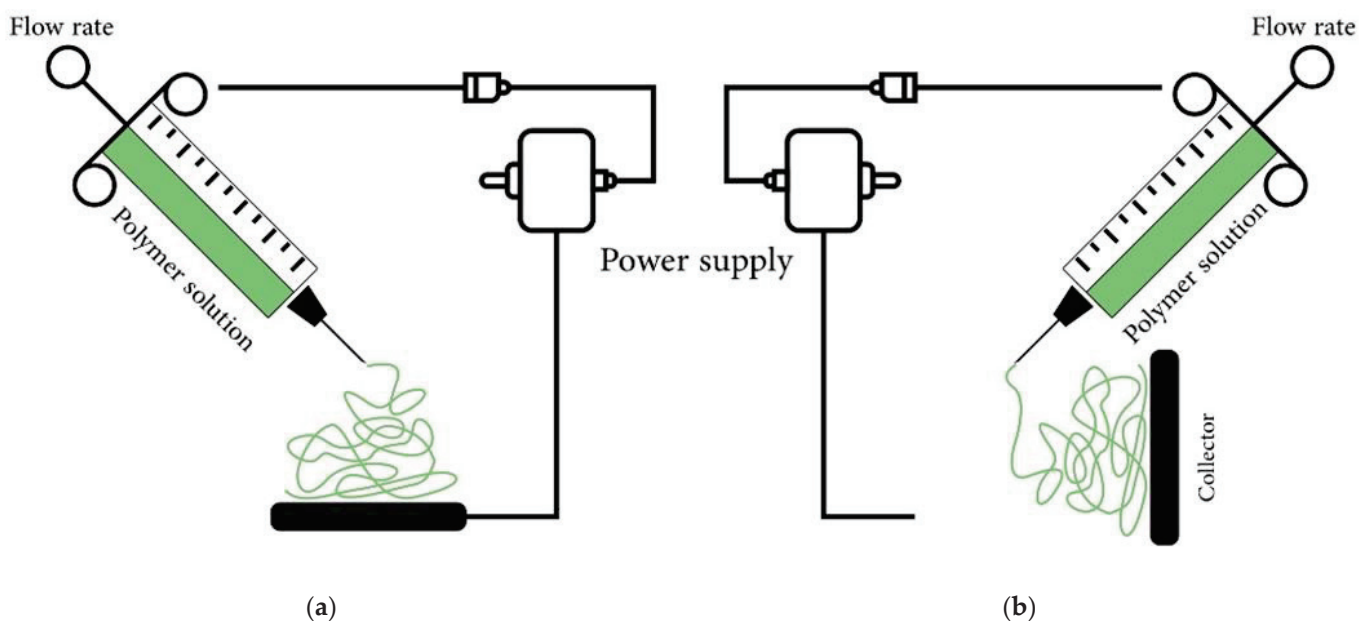
High voltage creates electric charges on the surface of the polymer solution during the electrospinning process, and these charges build up on the surface. These charges possess

repelling forces in a critical electric field that can dissipate the surface tension of the solution and the unstable charges. A Taylor cone-tip jet ejects a solvent-causing jet [119,123,124,130].

A stable jet created at the spinneret needle then changes into an unstable jet to create electro-spun fibers using a straightforward process. When the applied electric field reaches a critical value, jets shoot out of the cone tip, and the tensile force is transferred to the polymer, creating bending instability in that polymer. After that, a jet moves from the cone's apex to a collector with opposing charges, which has the power to draw charged fibers to it. Jet travel causes the solvent to evaporate, leaving the dry fiber on the collector [119,122–124,131,132].

A typical electrospinning device can be created using a power supply with high voltage power, a syringe, and a collector electrode alone, as demonstrated in the experimental part. Polymeric materials can be electro spun to create continuous nanofibers, and there are a number of variables that affect the nanofibers' properties. These variables are either processing variables (electric field) or polymer properties (concentration, viscosity, surface tension, and conductivity) (extrusion rate: distance from needle tip to collector) [119,123,124,129,133].

The definition of the electrospinning technique is the use of a strong electric field to spin polymer solutions into micro- to nanofibers at room temperature and atmospheric pressure (kV). Electrospinning devices can be set up in either a vertical or horizontal orientation [119,124,134–136], (Figure 9).



**Figure 9.** A diagram of electrospinning equipment with a syringe injecting polymer solution into an electric field generated by a high voltage power source between the spinneret and the grounded collector; a high voltage is applied. (a) A typical vertical arrangement of an electrospinning apparatus. (b) A typical horizontal setup of an electrospinning apparatus [119].

The three primary components of an electrospinning device are the power supply (high voltage), the syringe (spinneret), and the collector (electrode) [119,123,137,138]. When a polymer solution is subjected to a high voltage, electric charges accumulate on its surface. These charges repel one another so strongly that they can overcome the surface tension of the solution and form a Taylor cone in a critical electric field. When the electric field stretches the Taylor cone tip further, a charged jet is ejected. The jet eventually transforms into solid fibers due to solvent evaporation [123,139–141].

Using a simple process, a stable jet at the spinneret needle is converted to an unstable jet to generate electro-spun fibers. When the applied electric field reaches a critical magnitude, the surface tension is overcome by the charge repulsion force, and jets erupt from the cone tip, transferring the tensile force to the polymer and causing it to bend. The



charged fibers are then attracted by jets, with opposing charges moving from the cone apex to the collector. As the solvent evaporates through the jet, it leaves dry fiber on the collector [119,124,131,139,141].

A high-voltage power source, a syringe, and a collector electrode may be used to construct a standard electrospinning apparatus that can be configured vertically or horizontally, as illustrated in Figure 7. Continuous nanofibers may be generated by electrospinning polymeric materials, and the quality of electro-spun nanofibers is determined by some criteria. Polymer physical properties (concentration, viscosity, surface tension, and conductivity) or processing factors (electric field, flow rate, needle tip to collector distance) are examples [119,124,139,141].

Prior to electrospinning, most polymers are dissolved in a range of solvents; when fully dissolved, they create a polymer solution. The polymer solution is then poured into the capillary tube in preparation for electrospinning. However, because some polymers emit unpleasant or even dangerous odors, the procedures should be done in well-ventilated areas [142]. In the electrospinning process, a polymer solution at the capillary tube's end is exposed to an electric field, which causes an electric charge to form on the liquid's surface. The repelling electrical forces outweigh the surface tension forces when the applied electric field is strong enough. The solvent evaporates, and a polymer is formed when a charged jet of the solution is eventually released from the Taylor cone's tip. The jet is unstable and whips quickly in the area between the capillary tip and collector. Just past the spinneret's tip, where the jet is stable, instability sets in. Consequently, the electrospinning technology makes the process of making a fiber simpler [143].

Solution parameters, process parameters, and environmental or "ambient" parameters are the three main groups into which factors that have an impact on the electrospinning process are divided [119,144]. These factors are gathered in order to produce smooth fibers without beads, so a thorough understanding of these factors is required in order to obtain electro-spun nanofibers that are bead-free.

### 6.3. Application of Electro-Spun Nanofibers

Nanofiber membranes are created using electrospinning and used in a variety of applications, including biomedicine, security, clothing, and nano-sensors. Nanofibers are used in the biomedical field to focus on tissue engineering, wound dressing, drug delivery systems, and enzyme immobilization because they resemble the majority of organs and tissues, including skin, collagen, cartilage, and bone [145].

Electro-spun nanofibers are unique in that they have a consistent morphology, a high surface area to volume ratio, and inter- and inner porosity. These characteristics make them promising as scaffold biomaterials [146,147]. Additionally, nanofibers improve protein absorption, cell growth, cell differentiation, and cell adhesion [148,149].

Due to their pores, nanofibers are also used in filtration as micro and nano filters based on membrane design and construction, allowing liquids and small particles to pass while arresting larger particle sizes (contaminants), similar to how paper coffee filters prevent undissolved particles from passing through their pores while allowing dissolved ones to do so [150–153].

Affinity membranes, which have numerous uses in the biomedical and environmental fields, were also developed to select immobilized targets and remove contaminant targets [146,147,152–154]. Although electro-spun nanofibers have many uses, including those for tissue engineering, drug delivery, enzyme immobilization, wound dressing, antibacterial properties, filtration, desalination, and protective clothing, the focus of this article will be on biomedical uses.

#### 6.3.1. Tissue Engineering Applications

Electro-spun nanofibers are used in tissue engineering scaffold construction [155]. The use of biodegradable and biocompatible nanofibers to provide target tissues has increased daily [156]. Due to the similarities between these fibers and the natural extracellular matrix,

these fiber scaffolds had an impact on both cell-to-cell and cell-to-matrix communication and produced excellent growth factors [157].

### 6.3.2. Drug Delivery Applications

Based on the observation that the drug's rate of dissolution increased as the surface area of both the drug and the carrier increased, nanofibers were used to coat the drug and deliver it to the target site [158,159]. Anticancer medications, antibiotics, proteins, ribonucleic acid (RNA), and deoxyribonucleic acid are all delivered by electro-spun nanofibers (DNA) [160].

Recently, Yang et al. created a composite scaffold using nanofibers made of gelatin and polyvinyl alcohol (PVA) to transport raspberry ketone [161,162]. Additionally, to transport the growth factor calcium hydroxyapatite, Haider et al. prepared PLGA nanofibers [146,147].

### 6.3.3. Enzymes Immobilization Applications

Immobilization of enzymes onto insoluble material is essential to improve durability and maintain the enzyme properties such as bioprocessing and long duration controls [163]. The immunized material essentials are biocompatible, durable and hydrophobic or hydrophilic [164].

Recently, electro-spun nanofiber prepared from the dual electrospinning process increased the enzyme immobilization [165]. Yet, there are some limitations that hinder this technique, and enzymes encapsulation and the enzyme immobilized on the fibers surface are limited [166], so that some chemical modification of the surface needs to overcome these limitations [167,168].

### 6.3.4. Wound Dressing Applications

Inhibiting microorganisms, removing exudate, and protecting the wound site are all important functions of wound dressing. In addition to having antimicrobial properties, wound dressings provide a pleasant, moist environment to speed up the healing process [169–171]. Consequently, electro-spun wound dressings have more benefits than those made using traditional techniques [172]. These benefits include fiber pores, a large surface area, and the ability to stimulate fibroblast cells, making it suitable for use in cosmetic masks for skin cleansing and healing [142,173]. The electro spun nanofiber matrix incorporates various skin-treatment components [174].

Due to its capacity to create cationic clusters that can bind with anions on red blood cells, chitosan nanofibers have amazing hemostatic capabilities that can speed up platelet and red blood cell aggregation and ultimately reduce blood loss [175]. Additionally, this technique is successful even in individuals with coagulation abnormalities and is independent of the patient's own clotting system [176]. By electrospinning, Ren and colleagues [177] created a medicinal dressing made of a composite of silk fibroin, chitosan, and halloysite nanotubes. Aluminum silicate-based halloysite nanotubes have a hollow tubular structure, can efficiently bind antibacterial medications, and can provide delayed, sustained drug release [177]. The findings showed that using halloysite nanotubes caused the loaded-drug release time to increase by about 8 days. Additionally, the electro-spun chitosan composite membrane demonstrated a better blood coagulation rate, improved tensile property, and antibacterial activity, all of which support its potential value as a medical dressing.

An anti-fibrinolytic medication known as tranexamic acid (TXA) is frequently used during trauma surgery and has been found to improve wound healing [178]. For hemorrhage control applications, Sasmal and colleagues [178] created TXA-loaded chitosan/PVA electro-spun nanofibers. The findings support the role of chitosan in hemostasis by demonstrating that the total blood clotting time of pure chitosan/PVA nanofibrous membranes decreased from 21,010 s to 1676 s as the amount of chitosan increased. Additionally, clotting time and plasma recalcification time were dramatically shortened after TXA was added to chitosan nanofibers, demonstrating the enormous potential of TXA-loaded chitosan

nanofibers for managing civil and military hemostasis. Additionally, by fabricating chitosan within a hydrogel carrier template produced from cyclodextrin through proton exchange and complexation, Leonhardt and colleagues [179] observed the development of nanoscale features in chitosan mats. With nanofiber diameters of 9.23.7 nm and a macroscopic shape resembling a honeycomb, the assembled chitosan was highly entangled. When compared to commercially available absorbable hemostatic dressings, the chitosan-based composite hydrogels result in much less blood loss and faster timeframes for hemostasis.

#### 6.3.5. Antibacterial Applications

Many antibacterial hybrid electro-spun nanofiber scaffolds, including polyacrylonitrile/silver PAN and Ag nanofiber scaffolds, prepared by various research groups, have antibacterial activity against both gram-positive and gram-negative bacteria. Therefore, a wide variety of antimicrobial amidoxime was immobilized using PAN nanofibers. Amidoxime's antibacterial action is caused by its binding to the  $Mg^{2+}$  and  $Ca^{2+}$  ions, which upset the balance of the bacteria and result in bacterial death [180].

#### 6.4. Electrospinning of Chitosan

Template synthesis, drawing, phase separation, electrospinning, self-assembly, and other techniques have all been used to create nanofibers [181]. For the creation of micro- and nanofibers, electrospinning is one of these techniques that is particularly adaptable [182]. With their high surface area to volume ratio, oxygen permeable porosity, and variety of pore sizes, electro-spun nanofibers act as a wound dressing material by promoting fibroblast growth [183]. Chitosan has a low electro spinnability and needs a strong applied electric field to work properly because of its polycationic nature, which is brought on by the amino groups on its backbone [184,185]. A strong electric field is necessary because the polycationic nature of chitosan results in very viscous solutions with high surface tension. Additionally, the chitosan's strong hydrogen bond network minimizes molecule exposure to the applied voltage [184,185].

Chitosan, like the majority of other polysaccharides, needs a strong acidic environment to dissolve properly, but this can be dangerous and prevent the use of chitosan fibers in some circumstances. Furthermore, when it comes to the creation of pure chitosan fibers, chitosan with a low molecular weight and low biological activity frequently produces better results. This has a negative impact on the biological functioning of the electro-spun chitosan [184–186]. As in all electrospinning techniques, changing parameters cause morphological changes in the spun fibers. The correlations between parameters and morphology are generally as follows: The diameter and length of the end fiber are decreased as the applied voltage is increased. Low chitosan concentrations can lead to fiber formation and breakdown, which increases fiber diameter and leads to morphological flaws [184,187].

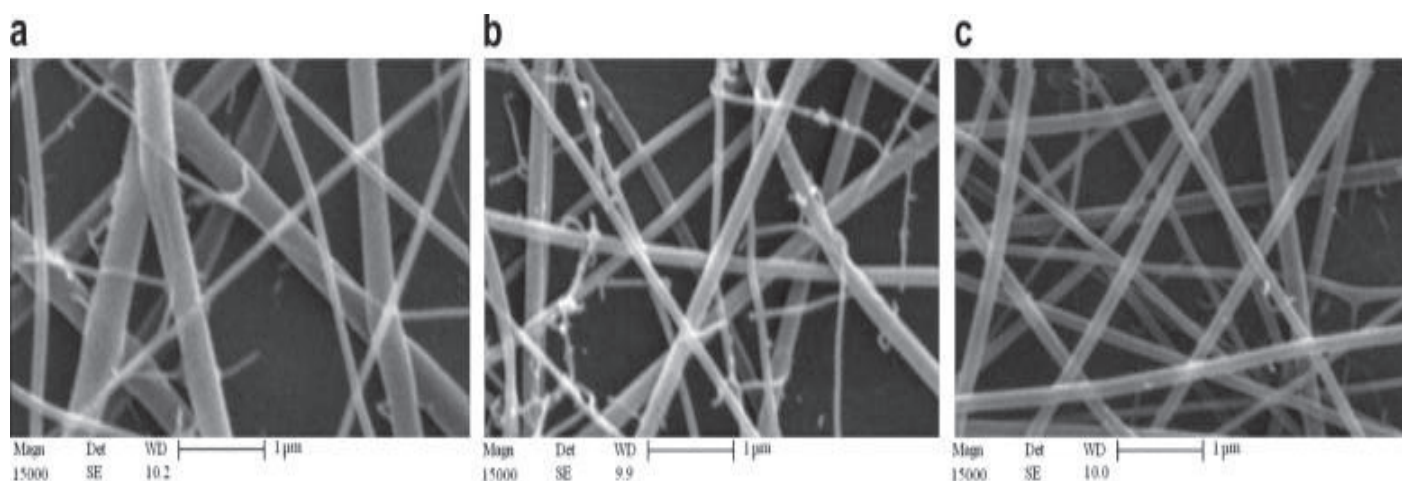
Chitosan's electro spinnability may be improved by using co-spinning polymers, either natural or synthetic. Frequently, chitosan is employed in the following fields: collagen, zein, silk fibroin, PEO, PVA, PLA, and zein [185,188]. Another method for resolving the issues with electrospinning chitosan is to chemically modify it to produce derivatives that are suitable for electrospinning, as with what was done with cellulose. More often than not, these derivatives have improved solubility and electro spinnability. Chitosan derivatives that have been investigated for this purpose include quarternized chitosan, hexanoyl chitosan, N-carboxyethyl chitosan, and others [189].

Chitosan is soluble in diluted aqueous formic, acetic, and lactic acids but insoluble in most mineral acidic media, alkalis, and water solutions. Chitosan dissolves when a small amount of acid is added to mixtures of water, ethanol, methanol, and acetone. Chitosan is a positively charged polyelectrolyte with a pH range of 2–6, which results in its greater solubility when compared to chitin. This characteristic makes chitosan solutions extremely viscous, making electrospinning difficult [190,191]. In addition, the three-dimensional network created by the potent hydrogen bonds prevents the polymeric chains from moving when they are exposed to an electrical field [192,193].

The unique properties of the polymer in solution, such as its polycationic nature, high molecular weight, and broad molecular weight dispersion, make chitosan electrospinning a challenging process. The inner tip–collector gap, the electric field voltage, the molecular weight, and the input velocity are just a few of the variables that have an impact on the quality of the electrospinning process and the finished product. When the electrostatic force in a solution is greater than the solution’s surface tension, the electrospinning process starts. When an electric field is applied, the surface of the polymer solution charges up. A strong electrical charge encourages jet extension and increases the volume of solution the needle can draw. On the other hand, a higher voltage leads to a longer stretch of the solution. This has a significant impact on electro-spun fiber morphology, frequently reducing their diameter, and raising the possibility of bead formation [190,194].

The feed rate, which regulates the number of solutions available, is another crucial component. A solution’s jet velocity and transfer rate are also impacted by its feed rate. For the evaporation of the solvent and the production of solid nanofibers, lower feed rates are preferred [119]. The solution must be removed from the tip at a rate that is substantially higher than the feed rate. Low feeding rates may prevent electrospinning, and high feeding rates may cause beaded large diameter fibers because sufficient solvent evaporation time must pass before the collector is reached [195].

SEM images of Figures 10 and 11 show the effect of tip–collector distance and electrical field voltage, respectively, on the structure of electro-spun nanofibers. As shown in these figures, increasing gap distance and voltage not only decreases and refines nanofibers diameters, but also improves the quality of electro-spun nanofibers.



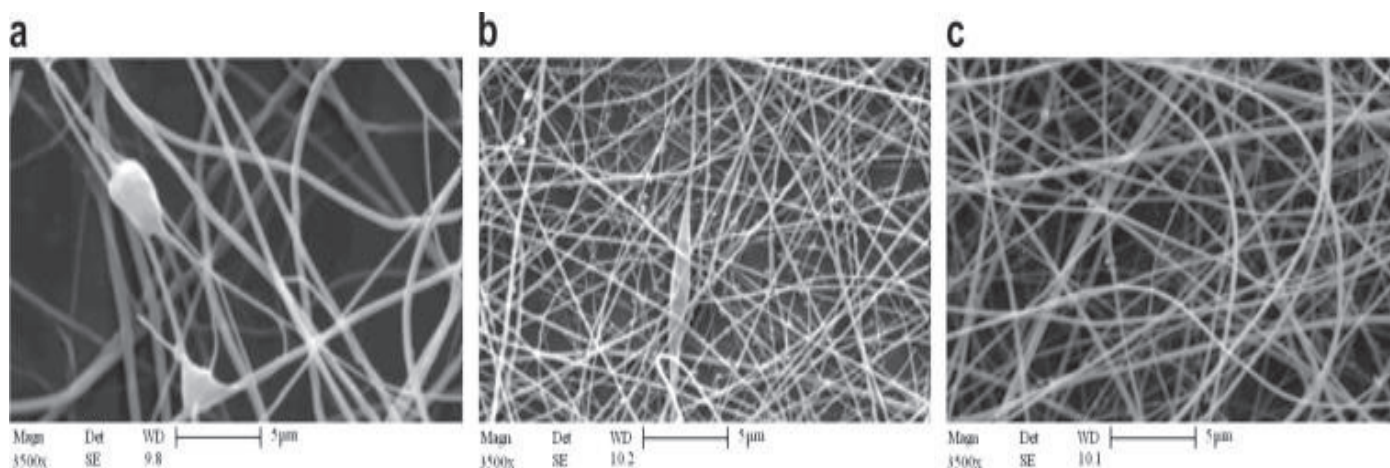
**Figure 10.** SEM images of 5 wt.% chitosan hydrolyzed 48 h nanofibers in aqueous acetic acid 90%, tip needle–collector distance: 14 cm (a), 15 cm (b), 16 cm (c). [119] Copyright 2023. Reproduced with permission from Elsevier Science Ltd.

Another factor that affects the sizes and shapes of the nanofibers is the separation between the tip and the collector. In order to give the fibers enough time to dry before reaching the collector, a minimum distance is necessary; otherwise, beads have been observed when distances are either too close or too far apart [119]. This variable directly affects the strength of the electric field and the duration of the jet’s flight. The reduced tip–collector distance has a nearly identical effect on the circuit as increased voltage [196].

Additionally, rheological and electrical properties like viscosity, surface tension, conductivity, and dielectric strength are significantly influenced by molecular weight. High molecular weight nanofiber solutions produce fibers with a larger average diameter while too low a molecular weight solution tends to produce beads instead of fibers [197]. Polymer molecular weight, which is important to the electrospinning process, reveals how many polymer chains condense in a solution. It has been suggested that if there are sufficient interactions between molecules to compensate for chain entanglements, high molecular



weights may not always be required for the electrospinning process. High molecular weight solutions typically result in the production of very long fibers. When a low molecular weight solution is employed, beads rather than fibers are produced [198].



**Figure 11.** SEM images of 5 wt.% chitosan hydrolyzed 48 h nanofibers in aqueous acetic acid 90%, electric field voltage: 14 kV (a), 16 kV (b), 17 kV (c). [196] Copyright 2023. Reproduced with permission from Elsevier Science Ltd.

## 6.5. Applications of Chitosan Nanofibers

### 6.5.1. Chitosan Nanofibers in Tissue Engineering

Tissue-engineered scaffolds should be biocompatible and capable of mimicking the extracellular matrix to create a microenvironment conducive to cell growth. Natural bone extracellular matrix, for example, has a complex microstructure of multi-layered collagen fibers and calcium deposits with fiber sizes in the nano meter range [199].

Nanofibrous scaffolds, as nanostructured scaffolds, have the distinct characteristics of large surface area, high porosity, and mechanical strength, resulting in extraordinary biological properties such as mimicking the nanoscale properties of the extracellular matrix, promoting cell adhesion and migration, transporting nutrients, and discharging waste [200].

Among these properties are the functional groups of nanofibrous polymers, which can coordinate with other components to promote cell adhesion, proliferation, differentiation, and, eventually, tissue regeneration [201]. Nanofibrous scaffolds may be a viable solution for the synthesis of extracellular matrix substitutes with the required biological functions [201].

Chitosans are polysaccharide polymers that are similar to extracellular matrix components, so they can be metabolized and their degradation products can be stored as proteoglycans in vivo [202]. Because of their excellent biological properties, chitosan nanofibers are popular in tissue engineering research [202].

Nanofibrous scaffolds based on chitosan are widely used in a variety of applications, including nerve, bone, and cartilage engineering, cardiac and vascular tissue engineering, tendon, ligament, and skeletal muscle regeneration, and wound healing (Table 4). Because of their chemical properties, chitin and chitosan can be dissolved in solvents such as acetic acid, trifluoroacetic acid, formic acid, succinic acid, and 1,1,1,3,3,3-Hexafluoroisopropanol (HFIP) [203].

Electrospinning, self-polymerization, and thermally induced phase separation can all be used to create chitin/chitosan nanofibrous scaffolds [204]. Furthermore, chitin/chitosan nanofibers derived from polymer blending can alter the biological and mechanical properties of composite scaffolds [205]. To meet the requirements of tissue engineering, these composite nanofibrous scaffolds can mimic the nanoscale structure and porosity of the extracellular matrix [206,207].

**Table 4.** Tissue engineering applications of chitosan nanofibers.

Composition	Nanofiber Diameter	Cells	Application	Reference
Chitosan/montmorillonite/PVA nanofiber composite mesh	60–140 nm	Human dental pulp stem cells	Nerve tissue engineering	[208]
PVA/chitosan nanofiber composite scaffolds	94–410 nm	PC12 nerve cells	Nerve tissue engineering and repair	[209]
Polycaprolactone/chitosan nanofibers composite	110–240 nm	Schwann cell (SC)	Nerve tissue engineering	[210]
Chitosan/PVA/graphene oxide nanofibers composite	123–160 nm	ATDC5 cells	Cartilage tissue engineering	[211]
Chitosan/polyethylene oxide nanofiber composite	140 ± 41 nm	C2C12 myoblast cells	Tendon tissue engineering	[212]
Chitosan nanofiber scaffolds	50–450 nm	Primary ventricular cardiomyocytes	Cardiac tissue engineering	[213]
Polycaprolactone/chitosan nanofibers	150 ± 2 nm	Mouse model and sheep	Vascular tissue engineering	[214]
Chitosan/poly (vinyl alcohol) nanofibrous composite scaffold	137 nm	rMSC	Skeletal muscle regeneration	[215]
Chitosan nano-/micro fibrous double-layered composite	20–300 nm	Bovine chondrocytes	Cartilage tissue engineering	[216]

### 6.5.2. Chitosan Nanofibers in Enzyme Immobilization

Nanofibers, in contrast to other nanomaterials, have recently attracted attention for enzyme immobilization not only due to their higher surface-area-to-volume ratio and greater enzyme-loading capacity, but also due to their higher chemical and mechanical protection, which is crucial to ensure physical resistance for the support. The disadvantages of nanoparticles, such as the behavior of aggregation, which affects the stability and activity of enzymes, are not present in nanofibers. They also do not need an additional procedure (such as centrifugation or membranes) to separate nano capsules. The gathered nanofibers form a macrostructure of nanofibers that is simple to separate and repurpose [217–220]. Therefore, chitosan has been used as a support for enzyme immobilization because of its benefits [221–224]. In fact, it is important to note that chitosan-based nanofibers should be further investigated as a support for enzyme immobilization due to the characteristics of chitosan combined with the benefits of nanofibrous structures. The use of chitosan-based nanofibers in enzyme immobilization is summarized in Table 5.

**Table 5.** Chitosan-based nanofibers in enzyme immobilization.

Composition	Component's Ratio	Enzyme	References
Chitosan/poly (vinyl alcohol) composite in 0.1 M Sodium acetate	1:5,4	Phytase by entrapment	[225]
Chitosan/poly (vinyl alcohol) composite in 1% acetic acid	1:1	B-D-galactosidase by entrapment	[226]
Chitosan/poly (vinyl alcohol) composite in water	1:6	Urease by Cross-linking	[227]
Chitosan/poly (vinyl alcohol) composite in 0.5% acetic acid	1:10	Lysozyme by Cross-linking	[228]
Chitosan/poly (vinyl alcohol) composite in 2% acetic acid	1:4	Laccase by Cross-linking	[229]
Chitosan/polyethylene oxide composite in 1% acetic acid	22:1	Trypsin by Adsorption/Covalent	[230]
Chitosan/poly (ethylene oxide) composite in 90% acetic acid	95:5	Glucose oxidase by Cross-linking	[219]
Chitosan/polyamide 6 composite in Formic acid and Acetic acid (2:1 v/v)	1:9	Laccase by Cross-linking	[231]
Chitosan/Cellulose monoacetate composite in acetone 99%	1:5, 2:5, 1:1, 7:5	Protease by Adsorption/ Cross linking	[232]
Chitosan/gelatin composite in 60% acetic acid	4:6	Peroxidase by Cross-linking	[233]

### 6.5.3. Chitosan Nanofibers in Cancer Treatment

There are numerous anticancer medications, including Doxorubicin, Paclitaxel, Berberine, Methotrexate, Adriamycin, Curcumin, Vincristine, Mercaptopurine, Indomethacin, Ibuprofen, Ketoprofen, Dexamethasone, Tetracycline, Gemifloxacin, Tetanus Toxoid, and Folic acid. The quantity of these anticancer medications is loaded onto the carriers of fibers during in vitro and in vivo cancer treatment. The polycationic nature of chitosan makes it a good candidate in this field among other fiber carriers. Table 6 lists several anticancer drug-loaded chitosan fiber systems along with information on how they affected cancer tissues in vitro.

**Table 6.** The chitosan nanofibers as anticancer drug delivery in vitro conditions.

Composition	Anticancer Drug	Cancer Type	References
Chitosan	Fe <sub>3</sub> O <sub>4</sub> /under magnetic field	HFL1	[234]
Chitosan	Fe <sup>2+</sup> /under magnetic field	HFL1	[234]
Chitosan	Glutaraldehyde/under magnetic field	HFL1	[234]
Chitosan/poly(ε-caprolactone) composite	5-Fluorouracil	B16F10	[235]
Chitosan/polyvinyl alcohol-g-C <sub>3</sub> N <sub>4</sub> -g-C <sub>3</sub> N <sub>4</sub> composite	5-Fluorouracil, Doxorubicin, Paclitaxel	MCF-7	[236]
Chitosan/polycaprolactone composite	Resveratrol, ferulic acid	HaCat, A431	[237]
Chitosan/polyethylene oxide composite	Berberine	HeLa, BT474, MCF-7, MDA-MB-468	[237]
Polyethylene oxide/chitosan/graphene oxide composite	Doxorubicin	A549	[238]
Chitosan/gelatin composite	Resveratrol	HT29	[239]
Polyvinyl alcohol/chitosan/Au composite	Doxorubicin	SKOV3	[240]
Polycaprolactone/chitosan composite	Cisplatin	Erlich ascites carcinoma	[241]
Chitosan/polyethylene oxide/hyaluronic acid composite	Paclitaxel	DU145	[242]
Chitosan/cobalt ferrite/TiO <sub>2</sub> composite	Doxorubicin	B16F10	[234]
Chitosan/poly (lactic acid)/TiO <sub>2</sub> /graphene oxide	Doxorubicin	A549	[243]
Chitosan/PVA/graphene oxide/Si composite	Curcumin	MCF-7	[244]
Poly (ε-caprolactone diol)/polyurethane/chitosan/Au TiO <sub>2</sub>	Temozolomide	U-87 MG	[245]
Graphene oxide/chitosan composite	Curcumin	MCF-7, HepG2, L929	[244]
Poly (lactic-co-glycolic acid)/chitosan/SiO <sub>2</sub> composite	Doxorubicin	HeLa	[246]
Chitosan/polyvinyl alcohol/MoS <sub>2</sub> composite	Doxorubicin	HT29, HT29 cell lines	[247]
Chitosan	Cupric oxide	A549	[248]

### 6.5.4. Chitosan Nanofibers in Food Technology

Chitosan's polycationic nature, biodegradability, nontoxicity, antimicrobial, chelating, mucoadhesive, and gelling properties set it apart. All these properties, combined with the high surface area: volume ratio of nanofibrous structures, make chitosan-based nanofibers suitable for a wide range of applications in food technology that have yet to be fully explored. As a result, the following sessions highlight some plausible studies in this field.

Food waste poses a problem for the food industry. According to the Food and Agriculture Organization of the United Nations [249], one-third of the world's food is wasted,

causing economic and environmental problems. Indeed, food packaging has emerged as a viable option for improving the quality and safety of food products by increasing their biological, physical, and chemical stability. It is necessary to avoid chemical contaminants, oxygen, microorganisms, light, and moisture to achieve these properties. As a result, active packaging with antimicrobial properties has received a lot of attention [250–252].

Nanofibers made of chitosan have enormous potential for use in active food packaging. It has been widely reported that chitosan is effective against bacteria, viruses, and fungi [253–257]. In addition, chitosan, a renewable and biodegradable polymer, presents an intriguing real alternative to petroleum-based polymers in the development of green packaging materials.

Arkoun et al. [258] prepared chitosan/poly(ethylene oxide) (PEO) and tested its antibacterial activity against pathogenic microorganisms such as *E. coli*, *Salmonella enterica* serovar *Typhimurium*, *Staphylococcus aureus*, and *Listeria innocuous*.

The nanofibers had an irreversible antibacterial effect, resulting in a bactericidal rather than bacteriostatic mechanism, according to the authors. Furthermore, bacterial growth was reduced at pH 5.8, which is lower than the pKa of amine groups on chitosan, and as a result, the authors proposed that the nanofibers could be applied to foods such as yoghurt, milk, cheese, meat, and fish, where lactic acid is liberated during the storage period.

Cui et al. [259] formed chitosan/poly(ethylene oxide) loaded with tea tree oil and tested it against *Salmonella enteric* subsp. *enteric* serovar *Enteritidis* and *Salmonella typhimurium*, two food pathogenic microorganisms. When the concentration of tea tree liposome was increased to 50%, the tensile strength increased by around 350%. Tea tree liposomes improved the antibacterial effect of the chitosan/poly(ethylene oxide) nanofiber as well. Furthermore, the chitosan/poly(ethylene oxide) loaded with liposomes tea tree demonstrated a four-day stable antibiofilm activity in chicken meat samples.

To prevent microbial spoilage of fish fillets, Ceylan et al. [260] created electro spun chitosan/thymol/liquid smoke nanofibers. The electro spun chitosan/thymol/liquid smoke nanofibers effectively reduced nearly 60% of total mesophilic bacteria. Furthermore, the authors stated that the nanofibers were thermostable until 150 °C, which is within the temperature range used in traditional food preservation methods.

The field of food packaging is a developing one that will most likely expand in the coming years. There are still numerous opportunities to investigate the role of chitosan-based nanofibers in other pathogenic microorganisms and different food types. Furthermore, the effect of other biopolymers and bioactive compounds on food packaging properties, such as mechanical properties and water vapor permeability, can be evaluated. Chitosan-based nanofibers could also be used to control food quality by monitoring external and internal conditions.

The majority of bioactive substances, volatile molecules, antioxidants, and flavors are unstable or even degradable [261].

Therefore, in addition to increasing bioavailability, chitosan-based nanofibers could improve the stability of functional food compounds. Chitosan's mucoadhesive property can be used to deliver bioactive molecules to the body in a manner similar to how drugs are delivered; the mucoadhesion of the functional compounds increases their absorption through the gastrointestinal tract [262,263]. These qualities have increased interest in using chitosan-based nanofibers as a drug delivery vehicle in addition to their non-toxic and biocompatibility benefits [264,265]. Although some research has been done using various nanomaterials as food carriers [266,267], chitosan-based nanofibers have not yet been sufficiently investigated in this regard.

As a delivery vehicle for curcumin, Shekarforoush et al. [268] created electro spun chitosan/xanthan gum nanofiber. The authors discovered that pH 2.2 had a lower release of curcumin from nanofibers than other studied pH values at 6.5 and 7.4. According to one theory, there were stronger electrostatic interactions between chitosan and xanthan at pH levels below the pKa of the amine groups on chitosan, such as pH 2.2, which decreased the swelling behavior of the nanofiber and, as a result, the diffusion of curcumin. As a result,



curcumin was able to be transported using the electro spun chitosan/xanthan gum, which improved its stability and bioavailability.

Biocatalysts called enzymes are essential in the food industry. However, due to their poor operational stability, short shelf life, and challenging recovery and reuse, their green chemistry and substrate specificity are compromised [269,270]. These issues might be solved by the enzyme immobilization on chitosan-based nanofibers, though. Due to their high pore-interconnectivity, which improves mass transfer between the substrate and the enzyme and, as a result, the enzyme activity, they stand out as promising supports.

Chitosan's functional groups can be used to functionalize surfaces, which can then be used to adsorb controlled-release enzymes. Lactose is hydrolyzed using chitosan/poly (vinyl alcohol) nanofibers. According to the authors, at 50 °C, the immobilized enzyme was more thermostable than the free enzyme. Additionally, after 28 days of storage at 4 °C and 25 °C, the immobilized -D-galactosidase retained 77% and 42%, respectively, of its activity. As a result, the thermal and storage stability was increased by immobilizing -D-galactosidase in chitosan/poly (vinyl alcohol) nanofibers.

Nanofibers made of chitosan have been developed for the immobilization of enzymes.

Indeed, they offer promising resources for the creation of hypoallergenic foods as well as a number of dairy products (baking, jam, jellies, wine, beer and juices). The application of chitosan-based nanofibers on the immobilization of enzymes in food processing, including amylase, trypsin, pectinase, protease, tyrosinase, lipase, pectin lyase, pectin, laccase, among many others, should therefore receive significant attention.

## 7. Limitations and Future Perspectives for Chitosan Application

The use of chitosan has several restrictions in addition to its many benefits. Chitosan's low solubility at a neutral pH is its most significant drawback. Numerous chemical and physical procedures have been employed to increase its solubility in order to get around this drawback. Chitosan has three types of functional groups: an amino group at C-2, a primary hydroxyl group at C-6, and a secondary hydroxyl group at C-3. Recent research has attempted to modify the three reactive functional groups in order to improve antimicrobial properties as well as solubility. For example, adding CH<sub>3</sub> to chitosan increased its solubility and allowed it to be used in a wider pH range. The addition of disaccharides and N-alkylation increased its solubility and antimicrobial activity against *E. coli* across a wider pH range.

These findings collectively appear to suggest that chitosan can be modified in a variety of ways to increase its solubility and antimicrobial activity. Chitosan and its derivatives have received a lot of attention in recent decades due to their numerous applications in various fields. Several studies have shown that chitosan's antimicrobial properties are affected by a variety of factors, including pH, temperature, Mw, metal chelation, and microorganism type. In vivo studies have also shown that chitosan and its derivatives can be used to treat microbial infections with no side effects. More research is needed, however, to determine the optimal chitosan conditions.

Chitosan's nontoxic, biocompatible, biodegradable, and antimicrobial properties indicate that this compound and its derivatives have a wide range of applications, which have been discussed in this review. In the future, chitosan may be used as an alternative to synthetic bactericides for crops because it has already been shown to be effective against the treatment of bacterial infections in animals. In the food industry, it can be used in food packaging materials to extend the shelf-life of food products, as well as in dressings that treat wounds in the pharmaceutical industry.

However, more research is required to determine its mode of action. A more standardized and comprehensive description of procedures, on the other hand, is required to match the results of different investigators. More research is needed to understand the molecular events that underpin chitosan's antimicrobial action. Finally, more research should be focused on improving chitosan's antimicrobial activity while maintaining its low toxicity and biodegradability.

## 8. Conclusions

Chitosan-based polymers can be used in a variety of biological applications. Chitosan is a biomaterial that is both biocompatible and biodegradable. Chemistry increases the utility of chitosan. Chitosan and its derivatives are employed as nano-delivery systems in biotechnology. Electrospinning includes preparation, fiber configuration, material selection, intended applications, and the spinning method. Foundation polymers based on chitosan are anticipated to be used in biological applications more frequently.

The development of biodiversity materials with applications in biomedicine (tissue engineering, wound treatment, drug delivery), as well as environmental protection (air and water filters), is a promising field. Because of the difficulties, the most common method for electrospinning clean chitosan fibers is blending with a co-spinning agent, which has the advantages of easier electrospinning and complementary qualities for specific applications. The result is that chitosan has been combined with a wide range of synthetic polymers, such as poly (ethylene oxide), polyvinyl alcohol, poly (lactic acid), polycaprolactone, polyurethanes, polyamides, polyacrylates, polyethylene terephthalate, polyacrylonitrile, polyaniline, and natural polyproteins (collagen, gelatin, silk fibroin, sericin), as well as polyanionic polysaccharides (hybrid). The systematic analysis of the properties of these blend nanofibers revealed the advantages and disadvantages of each method, the main rules that should be followed when aiming for a specific morphology, and the impact of the co-spinning agents on the fiber properties, which further directs their use. All this foundational knowledge in chitosan electrospinning is useful for the design of materials for real-world applications, which appear to be focused on the fabrication of complex chitosan-based nanofiber blends or composites in order to meet the need for multifunctionality.

**Author Contributions:** Conceptualization, all authors; methodology, all authors; software, all authors; validation, all authors; formal analysis, all authors; investigation, all authors; resources, all authors; data curation, all authors; writing—original draft preparation, all authors; writing—review and editing, all authors; visualization, all authors; supervision, all authors; project administration, all authors; funding acquisition, all authors. All authors have read and agreed to the published version of the manuscript.

**Funding:** This research received no external funding.

**Institutional Review Board Statement:** Not applicable.

**Informed Consent Statement:** Not applicable.

**Data Availability Statement:** Data is contained within the article.

**Acknowledgments:** The authors extend their appreciation to the Deanship of scientific research Majmaah university, Saudi Arabia, for funding this research work through the Project No: R-2023-495.

**Conflicts of Interest:** The authors declare no conflict of interest.

## References

1. Brück, W.M.; Slater, J.W.; Carney, B.F. Chitin and chitosan from marine organisms. In *Chitin, Chitosan, Oligosaccharides and Their Derivatives: Biological Activities and Applications*; Taylor & Francis: Boca Raton, FL, USA, 2010; pp. 11–19.
2. Zhou, A.; Wei, Y.; Wu, B.; Chen, Q.; Xing, D. Pyropheophorbide A and c (RGDyK) comodified chitosan-wrapped upconversion nanoparticle for targeted near-infrared photodynamic therapy. *Mol. Pharm.* **2012**, *9*, 1580–1589. [CrossRef] [PubMed]
3. Vinsova, J.; Vavrikova, E. Chitosan derivatives with antimicrobial, antitumour and antioxidant activities—A review. *Curr. Pharm. Des.* **2011**, *17*, 3596–3607. [CrossRef] [PubMed]
4. Philippova, O.; Korchagina, E. Chitosan and its hydrophobic derivatives: Preparation and aggregation in dilute aqueous solutions. *Polym. Sci. Ser. A* **2012**, *54*, 552–572. [CrossRef]
5. Dutta, P.K.; Ravikumar, M.; Dutta, J. Chitin and chitosan for versatile applications. *J. Macromol. Sci. Part C Polym. Rev.* **2002**, *42*, 307–354. [CrossRef]
6. Salama, R.; Osman, H.; Ibrahim, H.M. Preparation of biocompatible chitosan nanoparticles loaded with Aloe vera extract for use as a novel drug delivery mechanism to improve the antibacterial characteristics of cellulose-based fabrics. *Egypt. J. Chem.* **2022**, *65*, 581–595. [CrossRef]

7. Mosaad, R.M.; Alhalafi, M.H.; Emam, E.A.M.; Ibrahim, M.A.; Ibrahim, H. Enhancement of Antimicrobial and Dyeing Properties of Cellulosic Fabrics via Chitosan Nanoparticles. *Polymers* **2022**, *14*, 4211. [CrossRef]
8. Mohamed, F.A.; Sheier, M.B.; Reda, M.M.; Ibrahim, H.M. Synthesis, Application, and Antibacterial Activity of New Direct Dyes based on Chromene Derivatives. *Curr. Org. Synth.* **2022**, *19*, 757–766. [CrossRef]
9. Ali, M.A.; Bydoon, E.A.; Ibrahim, H.M. Bioactive Composite Nonwoven Surgical Dressing based on Cellulose Coated with Nanofiber Membrane using the layer-by-layer technique. *Egypt. J. Chem.* **2022**, *65*, 525–542. [CrossRef]
10. Madni, A.; Kousar, R.; Naem, N.; Wahid, F. Recent advancements in applications of chitosan-based biomaterials for skin tissue engineering. *J. Bioresour. Bioprod.* **2021**, *6*, 11–25. [CrossRef]
11. Hamed, I.; Özogul, F.; Regenstein, J.M. Industrial applications of crustacean by-products (chitin, chitosan, and chitooligosaccharides): A review. *Trends Food Sci. Technol.* **2016**, *48*, 40–50. [CrossRef]
12. Wang, J.; Chen, C. Chitosan-based biosorbents: Modification and application for biosorption of heavy metals and radionuclides. *Bioresour. Technol.* **2014**, *160*, 129–141. [CrossRef]
13. Zappino, M.; Cacciotti, I.; Benucci, I.; Nanni, F.; Liburdi, K.; Valentini, F.; Esti, M. Bromelain immobilization on microbial and animal source chitosan films, plasticized with glycerol, for application in wine-like medium: Microstructural, mechanical and catalytic characterisations. *Food Hydrocoll.* **2015**, *45*, 41–47. [CrossRef]
14. Salmon, S.; Hudson, S.M. Crystal morphology, biosynthesis, and physical assembly of cellulose, chitin, and chitosan. *J. Macromol. Sci. Part C Polym. Rev.* **1997**, *37*, 199–276. [CrossRef]
15. Aranaz, I.; Mengibar, M.; Harris, R.; Paños, I.; Miralles, B.; Acosta, N.; Galed, G.; Heras, Á. Functional characterization of chitin and chitosan. *Curr. Chem. Biol.* **2009**, *3*, 203–230.
16. Gupta, K.; Kumar, M.N.R. pH dependent hydrolysis and drug release behavior of chitosan/poly (ethylene glycol) polymer network microspheres. *J. Mater. Sci. Mater. Med.* **2001**, *12*, 753–759. [CrossRef] [PubMed]
17. Jayakumar, R.; Menon, D.; Manzoor, K.; Nair, S.; Tamura, H. Biomedical applications of chitin and chitosan based nanomaterials—A short review. *Carbohydr. Polym.* **2010**, *82*, 227–232. [CrossRef]
18. Wang, J.; Zhuang, S. Chitosan-based materials: Preparation, modification and application. *J. Clean. Prod.* **2022**, *355*, 131825. [CrossRef]
19. Mourya, V.; Inamdar, N.N.; Tiwari, A. Carboxymethyl chitosan and its applications. *Adv. Mat. Lett.* **2010**, *1*, 11–33. [CrossRef]
20. Peniche, C.; Argüelles-Monal, W.; Goycoolea, F. Chitin and chitosan: Major sources, properties and applications. *Monomers Polym. Compos. Renew. Resour.* **2008**, *1*, 517–542.
21. Aranaz, I.; Harris, R.; Heras, A. Chitosan amphiphilic derivatives. Chemistry and applications. *Curr. Org. Chem.* **2010**, *14*, 308. [CrossRef]
22. Wang, W.; Xue, C.; Mao, X. Chitosan: Structural modification, biological activity and application. *Int. J. Biol. Macromol.* **2020**, *164*, 4532–4546. [CrossRef]
23. Ahmed, F.; Soliman, F.M.; Adly, M.A.; Soliman, H.A.M.; El-Matbouli, M.; Saleh, M. Recent progress in biomedical applications of chitosan and its nanocomposites in aquaculture: A review. *Res. Vet. Sci.* **2019**, *126*, 68–82. [CrossRef]
24. Zhao, D.; Yu, S.; Sun, B.; Gao, S.; Guo, S.; Zhao, K. Biomedical Applications of Chitosan and Its Derivative Nanoparticles. *Polymers* **2018**, *10*, 462. [CrossRef]
25. Ibrahim, H.M.; Klingner, A. A review on electrospun polymeric nanofibers: Production parameters and potential applications. *Polym. Test.* **2020**, *90*, 106647. [CrossRef]
26. Qin, Y.; Li, P. Antimicrobial Chitosan Conjugates: Current Synthetic Strategies and Potential Applications. *Int. J. Mol. Sci.* **2020**, *21*, 499. [CrossRef]
27. Crini, G. Recent developments in polysaccharide-based materials used as adsorbents in wastewater treatment. *Prog. Polym. Sci.* **2005**, *30*, 38–70. [CrossRef]
28. Liu, H.; Du, Y.; Wang, X.; Sun, L. Chitosan kills bacteria through cell membrane damage. *Int. J. Food Microbiol.* **2004**, *95*, 147–155. [CrossRef] [PubMed]
29. Kenawy, E.; Abdel-Hay, F.; Mohy Eldin, M.; Tamer, T.; Ibrahim, E. Novel Aminated Chitosan-Aromatic Aldehydes Schiff Bases: Synthesis, Characterization and Bio-evaluation. *Int. J. Adv. Res.* **2015**, *3*, 563–572.
30. Sashiwa, H.; Shigemasa, Y. Chemical modification of chitin and chitosan 2: Preparation and water soluble property of N-acylated or N-alkylated partially deacetylated chitins. *Carbohydr. Polym.* **1999**, *39*, 127–138. [CrossRef]
31. Martău, G.A.; Mihai, M.; Vodnar, D.C. The use of chitosan, alginate, and pectin in the biomedical and food sector—biocompatibility, bioadhesiveness, and biodegradability. *Polymers* **2019**, *11*, 1837. [CrossRef]
32. Di Martino, A.; Sedlarik, V. Amphiphilic chitosan-grafted-functionalized polylactic acid based nanoparticles as a delivery system for doxorubicin and temozolomide co-therapy. *Int. J. Pharm.* **2014**, *474*, 134–145. [CrossRef] [PubMed]
33. Bosquez-Molina, E.; Zavaleta-Avejar, L. New Bioactive Biomaterials Based on Chitosan. In *Chitosan in the Preservation of Agricultural Commodities*; Academic Press: Cambridge, MA, USA, 2016; pp. 33–64.
34. Furuike, T.; Komoto, D.; Hashimoto, H.; Tamura, H. Preparation of chitosan hydrogel and its solubility in organic acids. *Int. J. Biol. Macromol.* **2017**, *104*, 1620–1625. [CrossRef] [PubMed]
35. Schügerl, K. Integrated processing of biotechnology products. *Biotechnol. Adv.* **2000**, *18*, 581–599. [CrossRef]
36. Calvo, P.; Remunan-Lopez, C.; Vila-Jato, J.L.; Alonso, M.J. Novel hydrophilic chitosan-polyethylene oxide nanoparticles as protein carriers. *J. Appl. Polym. Sci.* **1997**, *63*, 125–132. [CrossRef]

37. Sathiyabama, M.; Parthasarathy, R. Biological preparation of chitosan nanoparticles and its in vitro antifungal efficacy against some phytopathogenic fungi. *Carbohydr. Polym.* **2016**, *151*, 321–325. [CrossRef]
38. Ramezani, Z.; Zarei, M.; Raminnejad, N. Comparing the effectiveness of chitosan and nanochitosan coatings on the quality of refrigerated silver carp filets. *Food Control* **2015**, *51*, 43–48. [CrossRef]
39. Janes, K.A.; Fresneau, M.P.; Marazuela, A.; Fabra, A.; Alonso, M.A.J. Chitosan nanoparticles as delivery systems for doxorubicin. *J. Control. Release* **2001**, *73*, 255–267. [CrossRef]
40. De Campos, A.M.; Sánchez, A.; Alonso, M.A.J. Chitosan nanoparticles: A new vehicle for the improvement of the delivery of drugs to the ocular surface. Application to cyclosporin A. *Int. J. Pharm.* **2001**, *224*, 159–168. [CrossRef]
41. Pan, Y.; Li, Y.-J.; Zhao, H.-Y.; Zheng, J.-M.; Xu, H.; Wei, G.; Hao, J.-S. Bioadhesive polysaccharide in protein delivery system: Chitosan nanoparticles improve the intestinal absorption of insulin in vivo. *Int. J. Pharm.* **2002**, *249*, 139–147. [CrossRef]
42. Tian, X.X.; Groves, M.J. Formulation and biological activity of antineoplastic proteoglycans derived from *Mycobacterium vaccae* in chitosan nanoparticles. *J. Pharm. Pharmacol.* **1999**, *51*, 151–157. [CrossRef]
43. Hassan, E.A.; Hassan, M.L.; Abou-Zeid, R.E.; El-Wakil, N.A. Novel nanofibrillated cellulose/chitosan nanoparticles nanocomposites films and their use for paper coating. *Ind. Crops Prod.* **2016**, *93*, 219–226. [CrossRef]
44. Lee, Y.-M.; Park, Y.-J.; Lee, S.-J.; Ku, Y.; Han, S.-B.; Klokkevold, P.R.; Choi, S.-M.; Chung, C.-P. Tissue engineered bone formation using chitosan/tricalcium phosphate sponges. *J. Periodontol.* **2000**, *71*, 410–417. [CrossRef] [PubMed]
45. Kim, Y.H.; Gihm, S.H.; Park, C.R.; Lee, K.Y.; Kim, T.W.; Kwon, I.C.; Chung, H.; Jeong, S.Y. Structural characteristics of size-controlled self-aggregates of deoxycholic acid-modified chitosan and their application as a DNA delivery carrier. *Bioconjugate Chem.* **2001**, *12*, 932–938. [CrossRef]
46. Duan, B.; Dong, C.; Yuan, X.; Yao, K. Electrospinning of chitosan solutions in acetic acid with poly(ethylene oxide). *J. Biomater. Sci. Polym. Ed.* **2004**, *15*, 797–811. [CrossRef] [PubMed]
47. Abou-Okeil, A.; Refaei, R.; Khalil, E.M.; Refaei, R.; Moustafa, S.E.; Ibrahim, H.M. Fabrication of novel green magnetic electrospun nanofibers based on Fe<sub>3</sub>O<sub>4</sub> nanoparticles/PVA/chitosan/collagen. *Egypt. J. Chem.* **2022**, *65*, 283–299. [CrossRef]
48. Bakr, M.M.; Taha, M.A.; Osman, H.; Ibrahim, H.M. Novel green printing of cotton, wool and polyester fabrics with natural safflower dye nanoparticles. *Egypt. J. Chem.* **2021**, *64*, 6221–6230. [CrossRef]
49. Abou-Okeil, A.; Fahmy, H.M.; Fouda, M.M.G.; Aly, A.A.; Ibrahim, H.M. Hyaluronic Acid/Oxidized K-Carrageenan Electrospun Nanofibers Synthesis and Antibacterial Properties. *BioNanoScience* **2021**, *11*, 687–695. [CrossRef]
50. Ibrahim, H.M.; Mostafa, M.; Kandile, N.G. Potential use of N-carboxyethylchitosan in biomedical applications: Preparation, characterization, biological properties. *Int. J. Biol. Macromol.* **2020**, *149*, 664–671. [CrossRef]
51. Ibrahim, H.; El-Zairy, E.M.R.; Emam, E.A.M.; Adel, E. Combined antimicrobial finishing dyeing properties of cotton, polyester fabrics and their blends with acid and disperse dyes. *Egypt. J. Chem.* **2019**, *62*, 965–976. [CrossRef]
52. Aranaz, I.; Gutiérrez, M.C.; Ferrer, M.L.; Del Monte, F. Preparation of chitosan nanocomposites with a macroporous structure by unidirectional freezing and subsequent freeze-drying. *Mar. Drugs* **2014**, *12*, 5619–5642. [CrossRef]
53. de Oliveira, J.L.; Campos, E.V.R.; Bakshi, M.; Abhilash, P.; Fraceto, L.F. Application of nanotechnology for the encapsulation of botanical insecticides for sustainable agriculture: Prospects and promises. *Biotechnol. Adv.* **2014**, *32*, 1550–1561. [CrossRef] [PubMed]
54. Pichyangkura, R.; Chadchawan, S. Biostimulant activity of chitosan in horticulture. *Sci. Hortic.* **2015**, *196*, 49–65. [CrossRef]
55. Shahrajabian, M.H.; Chaski, C.; Polyzos, N.; Tzortzakis, N.; Petropoulos, S.A. Sustainable Agriculture Systems in Vegetable Production Using Chitin and Chitosan as Plant Biostimulants. *Biomolecules* **2021**, *11*, 819. [CrossRef] [PubMed]
56. Ghasemi Pirbalouti, A.; Malekpoor, F.; Salimi, A.; Golparvar, A. Exogenous application of chitosan on biochemical and physiological characteristics, phenolic content and antioxidant activity of two species of basil (*Ocimum ciliatum* and *Ocimum basilicum*) under reduced irrigation. *Sci. Hortic.* **2017**, *217*, 114–122. [CrossRef]
57. Saharan, V.; Kumaraswamy, R.V.; Choudhary, R.C.; Kumari, S.; Pal, A.; Raliya, R.; Biswas, P. Cu-Chitosan Nanoparticle Mediated Sustainable Approach To Enhance Seedling Growth in Maize by Mobilizing Reserved Food. *J. Agric. Food Chem.* **2016**, *64*, 6148–6155. [CrossRef]
58. Zhang, M.; Zhang, F.; Li, C.; An, H.; Wan, T.; Zhang, P. Application of Chitosan and Its Derivative Polymers in Clinical Medicine and Agriculture. *Polymers* **2022**, *14*, 958. [CrossRef]
59. Vakili, M.; Rafatullah, M.; Salamatinia, B.; Abdullah, A.Z.; Ibrahim, M.H.; Tan, K.B.; Gholami, Z.; Amouzgar, P. Application of chitosan and its derivatives as adsorbents for dye removal from water and wastewater: A review. *Carbohydr. Polym.* **2014**, *113*, 115–130. [CrossRef]
60. Lodhi, G.; Kim, Y.-S.; Hwang, J.-W.; Kim, S.-K.; Jeon, Y.-J.; Je, J.-Y.; Ahn, C.-B.; Moon, S.-H.; Jeon, B.-T.; Park, P.-J. Chitoooligosaccharide and its derivatives: Preparation and biological applications. *BioMed Res. Int.* **2014**, *2014*, 654913. [CrossRef]
61. Dwivedi, C.; Gupta, A.; Chaudhary, A.; Nandi, C.K. Gold nanoparticle chitosan composite hydrogel beads show efficient removal of methyl parathion from waste water. *RSC Adv.* **2014**, *4*, 39830–39838. [CrossRef]
62. Yadla, S.V.; Sridevi, V.; Lakshmi, M.V.V.C. A review on adsorption of heavy metals from aqueous solution. *J. Chem. Biol. Phys. Sci.* **2012**, *2*, 1585.
63. Chen, A.-H.; Yang, C.-Y.; Chen, C.-Y.; Chen, C.-Y.; Chen, C.-W. The chemically crosslinked metal-complexed chitosans for comparative adsorptions of Cu (II), Zn (II), Ni (II) and Pb (II) ions in aqueous medium. *J. Hazard. Mater.* **2009**, *163*, 1068–1075. [CrossRef]



64. Younes, I.; Rinaudo, M. Chitin and chitosan preparation from marine sources. Structure, properties and applications. *Mar. Drugs* **2015**, *13*, 1133–1174. [CrossRef]
65. Kyzas, G.Z.; Bikiaris, D.N. Recent modifications of chitosan for adsorption applications: A critical and systematic review. *Mar. Drugs* **2015**, *13*, 312–337. [CrossRef] [PubMed]
66. Cazón, P.; Vázquez, M. Applications of chitosan as food packaging materials. In *Sustainable Agriculture Reviews 36*; Springer: Berlin/Heidelberg, Germany, 2019; pp. 81–123.
67. Falguera, V.; Ceron, J.P.Q.; Jiménez, A.; Muñoz, A. Películas y recubrimientos comestibles: Estructuras, funciones activas y tendencias en su uso. *Tend. Cienc. Tecnol. Los Aliment.* **2011**, *22*, 292–303.
68. Aider, M. Chitosan application for active bio-based films production and potential in the food industry. *LWT-Food Sci. Technol.* **2010**, *43*, 837–842. [CrossRef]
69. Muxika, A.; Etxabide, A.; Uranga, J.; Guerrero, P.; De La Caba, K. Chitosan as a bioactive polymer: Processing, properties and applications. *Int. J. Biol. Macromol.* **2017**, *105*, 1358–1368. [CrossRef] [PubMed]
70. Chien, P.-J.; Sheu, F.; Lin, H.-R. Coating citrus (*Murcott tangor*) fruit with low molecular weight chitosan increases postharvest quality and shelf life. *Food Chem.* **2007**, *100*, 1160–1164. [CrossRef]
71. Chien, P.-J.; Sheu, F.; Yang, F.-H. Effects of edible chitosan coating on quality and shelf life of sliced mango fruit. *J. Food Eng.* **2007**, *78*, 225–229. [CrossRef]
72. Jiang, Y.; Li, Y. Effects of chitosan coating on postharvest life and quality of longan fruit. *Food Chem.* **2001**, *73*, 139–143. [CrossRef]
73. Ferreira, L.F.; de Abreu, G.F.; Lago, A.M.T.; Figueiredo, L.P.; Borém, F.M.; Martins, M.A.; Borges, S.V.; Dias, M.V. Development and application of biopolymer coatings to specialty green coffee beans: Influence on water content, color and sensory quality. *LWT* **2018**, *96*, 274–280. [CrossRef]
74. Soares, N.M.; Mendes, T.S.; Vicente, A.A. Effect of chitosan-based solutions applied as edible coatings and water glazing on frozen salmon preservation—A pilot-scale study. *J. Food Eng.* **2013**, *119*, 316–323. [CrossRef]
75. Chien, P.J.; Chou, C.C. Antifungal activity of chitosan and its application to control post-harvest quality and fungal rotting of Tankan citrus fruit (*Citrus tankan Hayata*). *J. Sci. Food Agric.* **2006**, *86*, 1964–1969. [CrossRef]
76. Choi, W.Y.; Park, H.J.; Ahn, D.J.; Lee, J.; Lee, C.Y. Wettability of chitosan coating solution on ‘Fuji’ apple skin. *J. Food Sci.* **2002**, *67*, 2668–2672. [CrossRef]
77. Shao, X.F.; Tu, K.; Tu, S.; Tu, J. A combination of heat treatment and chitosan coating delays ripening and reduces decay in “Gala” apple fruit. *J. Food Qual.* **2012**, *35*, 83–92. [CrossRef]
78. Eissa, H.A.A. Effect of chitosan coating on shelf life and quality of fresh-cut mushroom. *J. Food Qual.* **2007**, *30*, 623–645. [CrossRef]
79. Djioua, T.; Charles, F.; Freire, M., Jr.; Filgueiras, H.; Ducamp-Collin, M.N.; Sallanon, H. Combined effects of postharvest heat treatment and chitosan coating on quality of fresh-cut mangoes (*Mangifera indica* L.). *Int. J. Food Sci. Technol.* **2010**, *45*, 849–855. [CrossRef]
80. Jiang, Y.; Li, J.; Jiang, W. Effects of chitosan coating on shelf life of cold-stored litchi fruit at ambient temperature. *LWT-Food Sci. Technol.* **2005**, *38*, 757–761. [CrossRef]
81. Dong, C.; Chen, W.; Liu, C. Flocculation of algal cells by amphoteric chitosan-based flocculant. *Bioresour. Technol.* **2014**, *170*, 239–247. [CrossRef]
82. Souza, C.P.; Almeida, B.C.; Colwell, R.R.; Rivera, I.N.G. The Importance of Chitin in the Marine Environment. *Mar. Biotechnol.* **2011**, *13*, 823–830. [CrossRef]
83. Ahmed, K.B.M.; Khan, M.M.A.; Siddiqui, H.; Jahan, A. Chitosan and its oligosaccharides, a promising option for sustainable crop production—A review. *Carbohydr. Polym.* **2020**, *227*, 115331. [CrossRef]
84. Pen, L.T.; Jiang, Y.M. Effects of chitosan coating on shelf life and quality of fresh-cut Chinese water chestnut. *LWT-Food Sci. Technol.* **2003**, *36*, 359–364. [CrossRef]
85. Fan, M.; Hu, Q. Chitosan-LiOH-urea aqueous solution—A novel water-based system for chitosan processing. *Carbohydr. Res.* **2009**, *344*, 944–947. [CrossRef]
86. Patrúlea, V.; Ostafe, V.; Borchard, G.; Jordan, O. Chitosan as a starting material for wound healing applications. *Eur. J. Pharm. Biopharm.* **2015**, *97*, 417–426. [CrossRef]
87. Farag, S.; Ibrahim, H.M.; Amr, A.; Asker, M.S.; El-Shafai, A. Preparation and characterization of ion exchanger based on bacterial cellulose for heavy metal cation removal. *Egypt. J. Chem.* **2019**, *62*, 457–466. [CrossRef]
88. Mohamed, F.A.; Ibrahim, H.M.; Aly, A.A.; El-Alfy, E.A. Improvement of dyeability and antibacterial properties of gelatin treated cotton fabrics with synthesized reactive dye. *Biosci. Res.* **2018**, *15*, 4403–4408.
89. Mohamed, F.A.; Abd El-Megied, S.A.; Bashandy, M.S.; Ibrahim, H.M. Synthesis, application and antibacterial activity of new reactive dyes based on thiazole moiety. *Pigment Resin Technol.* **2018**, *47*, 246–254. [CrossRef]
90. Ibrahim, H.M.; Farid, O.A.; Samir, A.; Mosaad, R.M. Preparation of chitosan antioxidant nanoparticles as drug delivery system for enhancing of anti-cancer drug. In *Key Engineering Materials*; Trans Tech Publications Ltd.: Wollerau, Switzerland, 2018; Volume 759, pp. 92–97.
91. Mosaad, R.M.; Samir, A.; Ibrahim, H.M. Median lethal dose (LD50) and cytotoxicity of Adriamycin in female albino mice. *J. Appl. Pharm. Sci.* **2017**, *7*, 77–80. [CrossRef]
92. Liu, L.; Xin, Y.; Liu, J.; Zhang, E.; Li, W. Inhibitory effect of chitosan oligosaccharide on human hepatoma cells in vitro. *Afr. J. Tradit. Complement. Altern. Med.* **2017**, *14*, 272–277. [CrossRef] [PubMed]

93. Ngo, D.H.; Ngo, D.N.; Kim, S.-K.; Vo, T.S. Antiproliferative effect of aminoethyl-chitooligosaccharide on human lung A549 cancer cells. *Biomolecules* **2019**, *9*, 195. [CrossRef]
94. Jiang, Z.; Wang, S.; Hou, J.; Chi, J.; Wang, S.; Shao, K.; Liu, W.; Sun, R.; Han, B. Effects of carboxymethyl chitosan oligosaccharide on regulating immunologic function and inhibiting tumor growth. *Carbohydr. Polym.* **2020**, *250*, 116994. [CrossRef]
95. Zhai, X.; Li, C.; Ren, D.; Wang, J.; Ma, C.; Abd El-Aty, A.M. The impact of chitooligosaccharides and their derivatives on the in vitro and in vivo antitumor activity: A comprehensive review. *Carbohydr. Polym.* **2021**, *266*, 118132. [CrossRef]
96. Muanprasat, C.; Chatsudthipong, V. Chitosan oligosaccharide: Biological activities and potential therapeutic applications. *Pharmacol. Ther.* **2017**, *170*, 80–97. [CrossRef] [PubMed]
97. Wang, C.-H.; Cherng, J.-H.; Liu, C.-C.; Fang, T.-J.; Hong, Z.-J.; Chang, S.-J.; Fan, G.-Y.; Hsu, S.-D. Procoagulant and antimicrobial effects of chitosan in wound healing. *Int. J. Mol. Sci.* **2021**, *22*, 7067. [CrossRef]
98. Zhang, M.; Qiao, X.; Han, W.; Jiang, T.; Liu, F.; Zhao, X. Alginate-chitosan oligosaccharide-ZnO composite hydrogel for accelerating wound healing. *Carbohydr. Polym.* **2021**, *266*, 118100. [CrossRef] [PubMed]
99. Shen, T.; Dai, K.; Yu, Y.; Wang, J.; Liu, C. Sulfated chitosan rescues dysfunctional macrophages and accelerates wound healing in diabetic mice. *Acta Biomater.* **2020**, *117*, 192–203. [CrossRef] [PubMed]
100. Di Martino, A.; Sittinger, M.; Risbud, M.V. Chitosan: A versatile biopolymer for orthopaedic tissue-engineering. *Biomaterials* **2005**, *26*, 5983–5990. [CrossRef]
101. Kaur, S.; Dhillon, G.S. The versatile biopolymer chitosan: Potential sources, evaluation of extraction methods and applications. *Crit. Rev. Microbiol.* **2014**, *40*, 155–175. [CrossRef]
102. Wu, L.; Liu, M. Preparation and properties of chitosan-coated NPK compound fertilizer with controlled-release and water-retention. *Carbohydr. Polym.* **2008**, *72*, 240–247. [CrossRef]
103. Malerba, M.; Cerana, R. Chitosan Effects on Plant Systems. *Int. J. Mol. Sci.* **2016**, *17*, 996. [CrossRef]
104. Abd El-Naby, F.S.; Naiel, M.A.E.; Al-Sagheer, A.A.; Negm, S.S. Dietary chitosan nanoparticles enhance the growth, production performance, and immunity in *Oreochromis niloticus*. *Aquaculture* **2019**, *501*, 82–89. [CrossRef]
105. Abd El-Naby, A.S.; Al-Sagheer, A.A.; Negm, S.S.; Naiel, M.A.E. Dietary combination of chitosan nanoparticle and thymol affects feed utilization, digestive enzymes, antioxidant status, and intestinal morphology of *Oreochromis niloticus*. *Aquaculture* **2020**, *515*, 734577. [CrossRef]
106. Sinha, V.R.; Singla, A.K.; Wadhawan, S.; Kaushik, R.; Kumria, R.; Bansal, K.; Dhawan, S. Chitosan microspheres as a potential carrier for drugs. *Int. J. Pharm.* **2004**, *274*, 1–33. [CrossRef]
107. Azad, A.K.; Sermsintham, N.; Chandkrachang, S.; Stevens, W.F. Chitosan Membrane as a Wound-Healing Dressing: Characterization and Clinical Application. *J. Biomed. Mater. Res. Part B Appl. Biomater.* **2004**, *69*, 216–222. [CrossRef] [PubMed]
108. Wu, Y.-B.; Yu, S.-H.; Mi, F.-L.; Wu, C.-W.; Shyu, S.-S.; Peng, C.-K.; Chao, A.-C. Preparation and characterization on mechanical and antibacterial properties of chitsoan/cellulose blends. *Carbohydr. Polym.* **2004**, *57*, 435–440. [CrossRef]
109. Fan, L.; Du, Y.; Zhang, B.; Yang, J.; Zhou, J.; Kennedy, J.F. Preparation and properties of alginate/carboxymethyl chitosan blend fibers. *Carbohydr. Polym.* **2006**, *65*, 447–452. [CrossRef]
110. Chen, J.-P.; Chang, G.-Y.; Chen, J.-K. Electrospun collagen/chitosan nanofibrous membrane as wound dressing. *Colloids Surf. A Physicochem. Eng. Asp.* **2008**, *313–314*, 183–188. [CrossRef]
111. Qasim, S.B.; Najeeb, S.; Delaine-Smith, R.M.; Rawlinson, A.; Ur Rehman, I. Potential of electrospun chitosan fibers as a surface layer in functionally graded GTR membrane for periodontal regeneration. *Dent. Mater.* **2017**, *33*, 71–83. [CrossRef]
112. Ma, Y.; Xin, L.; Tan, H.; Fan, M.; Li, J.; Jia, Y.; Ling, Z.; Chen, Y.; Hu, X. Chitosan membrane dressings toughened by glycerol to load antibacterial drugs for wound healing. *Mater. Sci. Eng. C* **2017**, *81*, 522–531. [CrossRef]
113. Behera, S.S.; Das, U.; Kumar, A.; Bissoyi, A.; Singh, A.K. Chitosan/TiO<sub>2</sub> composite membrane improves proliferation and survival of L929 fibroblast cells: Application in wound dressing and skin regeneration. *Int. J. Biol. Macromol.* **2017**, *98*, 329–340. [CrossRef] [PubMed]
114. Ghannam, S.F.; Korayem, H.E.; Farghaly, L.M.; Hosny, S. The effect of chitosan nanosilver dressing versus mesenchymal stem cells on wound healing. *J. Afr. Assoc. Physiol. Sci.* **2018**, *6*, 23–31.
115. Denkbaş, E.B.; Öztürk, E.; Özdemir, N.; Keçeci, K.; Agalar, C. Norfloxacin-loaded chitosan sponges as wound dressing material. *J. Biomater. Appl.* **2004**, *18*, 291–303. [CrossRef] [PubMed]
116. Deng, C.-M.; He, L.-Z.; Zhao, M.; Yang, D.; Liu, Y. Biological properties of the chitosan-gelatin sponge wound dressing. *Carbohydr. Polym.* **2007**, *69*, 583–589. [CrossRef]
117. Obara, K.; Ishihara, M.; Ishizuka, T.; Fujita, M.; Ozeki, Y.; Maehara, T.; Saito, Y.; Yura, H.; Matsui, T.; Hattori, H.; et al. Photocrosslinkable chitosan hydrogel containing fibroblast growth factor-2 stimulates wound healing in healing-impaired db/db mice. *Biomaterials* **2003**, *24*, 3437–3444. [CrossRef] [PubMed]
118. Chen, H.; Xing, X.; Tan, H.; Jia, Y.; Zhou, T.; Chen, Y.; Ling, Z.; Hu, X. Covalently antibacterial alginate-chitosan hydrogel dressing integrated gelatin microspheres containing tetracycline hydrochloride for wound healing. *Mater. Sci. Eng. C* **2017**, *70*, 287–295. [CrossRef] [PubMed]
119. Bhardwaj, N.; Kundu, S.C. Electrospinning: A fascinating fiber fabrication technique. *Biotechnol. Adv.* **2010**, *28*, 325–347. [CrossRef]
120. Teo, W.E.; Ramakrishna, S. A review on electrospinning design and nanofibre assemblies. *Nanotechnology* **2006**, *17*, R89. [CrossRef]
121. Celebioglu, A.; Uyar, T. Electrospinning of nanofibers from non-polymeric systems: Electrospun nanofibers from native cyclodextrins. *J. Colloid Interface Sci.* **2013**, *404*, 1–7. [CrossRef]

122. Subbiah, T.; Bhat, G.; Tock, R.; Parameswaran, S.; Ramkumar, S. Electrospinning of nanofibers. *J. Appl. Polym. Sci.* **2005**, *96*, 557–569. [CrossRef]
123. Ghorani, B.; Tucker, N. Fundamentals of electrospinning as a novel delivery vehicle for bioactive compounds in food nanotechnology. *Food Hydrocoll.* **2015**, *51*, 227–240. [CrossRef]
124. Pillay, V.; Dott, C.; Choonara, Y.E.; Tyagi, C.; Tomar, L.; Kumar, P.; du Toit, L.C.; Ndesendo, V.M. A review of the effect of processing variables on the fabrication of electrospun nanofibers for drug delivery applications. *J. Nanomater.* **2013**, *2013*, 789289. [CrossRef]
125. Dalton, P.D.; Klinkhammer, K.; Salber, J.; Klee, D.; Möller, M. Direct in vitro electrospinning with polymer melts. *Biomacromolecules* **2006**, *7*, 686–690. [CrossRef]
126. Greiner, A.; Wendorff, J.H. Electrospinning: A fascinating method for the preparation of ultrathin fibers. *Angew. Chem. Int. Ed.* **2007**, *46*, 5670–5703. [CrossRef]
127. Agarwal, S.; Greiner, A.; Wendorff, J.H. Functional materials by electrospinning of polymers. *Prog. Polym. Sci.* **2013**, *38*, 963–991. [CrossRef]
128. Haider, A.; Haider, S.; Kang, I.-K. A comprehensive review summarizing the effect of electrospinning parameters and potential applications of nanofibers in biomedical and biotechnology. *Arab. J. Chem.* **2018**, *11*, 1165–1188. [CrossRef]
129. Liang, D.; Hsiao, B.S.; Chu, B. Functional electrospun nanofibrous scaffolds for biomedical applications. *Adv. Drug Deliv. Rev.* **2007**, *59*, 1392–1412. [CrossRef] [PubMed]
130. Adomavičiūtė, E.; Milašius, R. The influence of applied voltage on poly (vinyl alcohol)(PVA) nanofiber diameter. *Fibres Text. East. Eur.* **2007**, *15*, 63.
131. Reneker, D.; Yarin, A.; Zussman, E.; Xu, H. Electrospinning of nanofibers from polymer solutions and melts. *Adv. Appl. Mech.* **2007**, *41*, 43–346.
132. Shin, Y.; Hohman, M.; Brenner, M.; Rutledge, G. Electrospinning: A whipping fluid jet generates submicron polymer fibers. *Appl. Phys. Lett.* **2001**, *78*, 1149–1151. [CrossRef]
133. Ramakrishna, S.; Fujihara, K.; Teo, W.-E.; Lim, T.-C.; Ma, Z. *An Introduction to Electrospinning and Nanofibers*; World Scientific: Singapore, 2005; Volume 90.
134. Kidoaki, S.; Kwon, I.K.; Matsuda, T. Mesoscopic spatial designs of nano- and microfiber meshes for tissue-engineering matrix and scaffold based on newly devised multilayering and mixing electrospinning techniques. *Biomaterials* **2005**, *26*, 37–46. [CrossRef]
135. Stankus, J.J.; Freytes, D.O.; Badylak, S.F.; Wagner, W.R. Hybrid nanofibrous scaffolds from electrospinning of a synthetic biodegradable elastomer and urinary bladder matrix. *J. Biomater. Sci. Polym. Ed.* **2008**, *19*, 635–652. [CrossRef]
136. El-Alfy, E.A.; El-Bisi, M.K.; Taha, G.M.; Ibrahim, H.M. Preparation of biocompatible chitosan nanoparticles loaded by tetracycline, gentamycin and ciprofloxacin as novel drug delivery system for improvement the antibacterial properties of cellulose based fabrics. *Int. J. Biol. Macromol.* **2020**, *161*, 1247–1260. [CrossRef]
137. Xue, J.; Wu, T.; Dai, Y.; Xia, Y. Electrospinning and electrospun nanofibers: Methods, materials, and applications. *Chem. Rev.* **2019**, *119*, 5298–5415. [CrossRef]
138. Liao, Y.; Loh, C.-H.; Tian, M.; Wang, R.; Fane, A.G. Progress in electrospun polymeric nanofibrous membranes for water treatment: Fabrication, modification and applications. *Prog. Polym. Sci.* **2018**, *77*, 69–94. [CrossRef]
139. Senthil, T.; George, G.; Srinivasan, A. Electrospinning: From Fundamentals to Applications. In *Advances in Polymer Materials and Technology*; CRC Press: Boca Raton, FL, USA, 2016; pp. 171–240.
140. Zagho, M.M.; Elzatahry, A. Recent trends in electrospinning of polymer nanofibers and their applications as templates for metal oxide nanofibers preparation. In *Electrospinning: Material, Techniques, and Biomedical Applications*; IntechOpen: London, UK, 2016.
141. Bode-Aluko, C.A.; Laatikainen, K.; Perea, O.; Nechaev, A.; Kochnev, I.; Rossouw, A.; Dobretsov, S.; Branger, C.; Sarbu, A.; Petrik, L. Fabrication and characterisation of novel nanofiltration polymeric membrane. *Mater. Today Commun.* **2019**, *20*, 100580. [CrossRef]
142. Huang, Z.-M.; Zhang, Y.-Z.; Kotaki, M.; Ramakrishna, S. A review on polymer nanofibers by electrospinning and their applications in nanocomposites. *Compos. Sci. Technol.* **2003**, *63*, 2223–2253. [CrossRef]
143. Mohamed, F.A.; Reda, M.M.; Ibrahim, H. Enhancement of Dyeing and Antimicrobial Properties of Chitosan and Chitosan Nanoparticles-Treated Cotton and Viscose Fabrics with Acid Dyes. *Egypt. J. Chem.* **2022**, *65*, 339–344.
144. Teo, W.-E.; Inai, R.; Ramakrishna, S. Technological advances in electrospinning of nanofibers. *Sci. Technol. Adv. Mater.* **2016**, *12*, 013002. [CrossRef]
145. Metreveli, G.; Wågberg, L.; Emmoth, E.; Belák, S.; Strømme, M.; Mihranyan, A. A Size-Exclusion Nanocellulose Filter Paper for Virus Removal. *Adv. Healthc. Mater.* **2014**, *3*, 1546–1550. [CrossRef]
146. Haider, A.; Gupta, K.C.; Kang, I.-K. Morphological effects of HA on the cell compatibility of electrospun HA/PLGA composite nanofiber scaffolds. *BioMed Res. Int.* **2014**, *2014*, 308306. [CrossRef]
147. Haider, A.; Gupta, K.C.; Kang, I.-K. PLGA/nHA hybrid nanofiber scaffold as a nanocargo carrier of insulin for accelerating bone tissue regeneration. *Nanoscale Res. Lett.* **2014**, *9*, 314. [CrossRef] [PubMed]
148. Tysseling-Mattiace, V.M.; Sahni, V.; Niece, K.L.; Birch, D.; Czeisler, C.; Fehlings, M.G.; Stupp, S.I.; Kessler, J.A. Self-assembling nanofibers inhibit glial scar formation and promote axon elongation after spinal cord injury. *J. Neurosci.* **2008**, *28*, 3814–3823. [CrossRef]



149. Woo, K.M.; Chen, V.J.; Ma, P.X. Nano-fibrous scaffolding architecture selectively enhances protein adsorption contributing to cell attachment. *J. Biomed. Mater. Res. Part A* **2003**, *67*, 531–537. [CrossRef]
150. Gupta, K.C.; Haider, A.; Choi, Y.-R.; Kang, I.-K. Nanofibrous scaffolds in biomedical applications. *Biomater. Res.* **2014**, *18*, 5. [CrossRef]
151. Haider, S.; Binagag, F.F.; Haider, A.; Mahmood, A.; Shah, N.; Al-Masry, W.A.; Khan, S.U.-D.; Ramay, S.M. Adsorption kinetic and isotherm of methylene blue, safranin T and rhodamine B onto electrospun ethylenediamine-grafted-polyacrylonitrile nanofibers membrane. *Desalination Water Treat.* **2015**, *55*, 1609–1619. [CrossRef]
152. Haider, S.; Binagag, F.F.; Haider, A.; Mahmood, A.; Al Masry, W.A.; Alhoshan, M.; Khan, S.U.-D. Fabrication of the Diethylenetriamine Grafted Polyacrylonitrile Electrospun Nanofibers Membrane for the Aqueous Removal of Cationic Dyes. *Sci. Adv. Mater.* **2015**, *7*, 309–318. [CrossRef]
153. Haider, S.; Haider, A.; Ahmad, A.; Khan, S.U.-D.; Almasry, W.A.; Sarfarz, M. Electrospun nanofibers affinity membranes for water hazards remediation. *Nanotechnol. Res. J.* **2015**, *8*, 511.
154. Haider, S.; Al-Zeghayer, Y.; Ali, F.A.A.; Haider, A.; Mahmood, A.; Al-Masry, W.A.; Imran, M.; Aijaz, M.O. Highly aligned narrow diameter chitosan electrospun nanofibers. *J. Polym. Res.* **2013**, *20*, 105. [CrossRef]
155. Vasita, R.; Katti, D.S. Nanofibers and their applications in tissue engineering. *Int. J. Nanomed.* **2006**, *1*, 15. [CrossRef]
156. Sun, B.; Long, Y.; Zhang, H.; Li, M.; Duvail, J.; Jiang, X.; Yin, H. Advances in three-dimensional nanofibrous macrostructures via electrospinning. *Prog. Polym. Sci.* **2014**, *39*, 862–890. [CrossRef]
157. Li, W.J.; Laurencin, C.T.; Caterson, E.J.; Tuan, R.S.; Ko, F.K. Electrospun nanofibrous structure: A novel scaffold for tissue engineering. *J. Biomed. Mater. Res.* **2002**, *60*, 613–621. [CrossRef]
158. Kenawy, E.-R.; Bowlin, G.L.; Mansfield, K.; Layman, J.; Simpson, D.G.; Sanders, E.H.; Wnek, G.E. Release of tetracycline hydrochloride from electrospun poly (ethylene-co-vinylacetate), poly (lactic acid), and a blend. *J. Control. Release* **2002**, *81*, 57–64. [CrossRef] [PubMed]
159. Liu, W.; Thomopoulos, S.; Xia, Y. Electrospun nanofibers for regenerative medicine. *Adv. Healthc. Mater.* **2012**, *1*, 10–25. [CrossRef] [PubMed]
160. Hu, X.; Liu, S.; Zhou, G.; Huang, Y.; Xie, Z.; Jing, X. Electrospinning of polymeric nanofibers for drug delivery applications. *J. Control. Release* **2014**, *185*, 12–21. [CrossRef] [PubMed]
161. Kanani, A.G.; Bahrami, S.H. Effect of changing solvents on poly ( $\epsilon$ -caprolactone) nanofibrous webs morphology. *J. Nanomater.* **2011**, *2011*, 31.
162. Yang, D.; Li, Y.; Nie, J. Preparation of gelatin/PVA nanofibers and their potential application in controlled release of drugs. *Carbohydr. Polym.* **2007**, *69*, 538–543. [CrossRef]
163. Xie, J.; Hsieh, Y.-L. Ultra-high surface fibrous membranes from electrospinning of natural proteins: Casein and lipase enzyme. *J. Mater. Sci.* **2003**, *38*, 2125–2133. [CrossRef]
164. Ye, P.; Xu, Z.-K.; Che, A.-F.; Wu, J.; Seta, P. Chitosan-tethered poly (acrylonitrile-co-maleic acid) hollow fiber membrane for lipase immobilization. *Biomaterials* **2005**, *26*, 6394–6403. [CrossRef]
165. Huang, X.J.; Xu, Z.K.; Wan, L.S.; Innocent, C.; Seta, P. Electrospun nanofibers modified with phospholipid moieties for enzyme immobilization. *Macromol. Rapid Commun.* **2006**, *27*, 1341–1345. [CrossRef]
166. Kim, H.S.; Yoo, H.S. MMPs-responsive release of DNA from electrospun nanofibrous matrix for local gene therapy: In vitro and in vivo evaluation. *J. Control. Release* **2010**, *145*, 264–271. [CrossRef]
167. Im, J.S.; Yun, J.; Lim, Y.-M.; Kim, H.-I.; Lee, Y.-S. Fluorination of electrospun hydrogel fibers for a controlled release drug delivery system. *Acta Biomater.* **2010**, *6*, 102–109. [CrossRef]
168. Theron, S.; Yarin, A.; Zussman, E.; Kroll, E. Multiple jets in electrospinning: Experiment and modeling. *Polymer* **2005**, *46*, 2889–2899. [CrossRef]
169. Gallant-Behm, C.L.; Yin, H.Q.; Liu, S.; Hegggers, J.P.; Langford, R.E.; Olson, M.E.; Hart, D.A.; Burrell, R.E. Comparison of in vitro disc diffusion and time kill-kinetic assays for the evaluation of antimicrobial wound dressing efficacy. *Wound Repair Regen.* **2005**, *13*, 412–421. [CrossRef] [PubMed]
170. Jones, S.A.; Bowler, P.G.; Walker, M.; Parsons, D. Controlling wound bioburden with a novel silver-containing Hydrofiber<sup>®</sup> dressing. *Wound Repair Regen.* **2004**, *12*, 288–294. [CrossRef]
171. Rim, N.G.; Shin, C.S.; Shin, H. Current approaches to electrospun nanofibers for tissue engineering. *Biomed. Mater.* **2013**, *8*, 014102. [CrossRef]
172. Gao, Y.; Bach Truong, Y.; Zhu, Y.; Louis Kyratzis, I. Electrospun antibacterial nanofibers: Production, activity, and in vivo applications. *J. Appl. Polym. Sci.* **2014**, *131*. [CrossRef]
173. Smith, D.J.; Reneker, D.H.; McManus, A.T.; Schreuder-Gibson, H.L.; Mello, C.; Sennett, M.S. Electrospun Fibers and an Apparatus Therefor. U.S. Patent 6,753,454, 22 June 2004.
174. Si, Y.; Tang, X.; Yu, J.; Ding, B. Electrospun Nanofibers: Solving Global Issues. In *Electrospun Nanofibers for Energy and Environmental Applications*; Springer: Berlin/Heidelberg, Germany, 2014; pp. 3–38.
175. Nakielski, P.; Pierini, F. Blood interactions with nano- and microfibers: Recent advances, challenges and applications in nano- and microfibrous hemostatic agents. *Acta Biomater.* **2019**, *84*, 63–76. [CrossRef]
176. Huang, J.; Cheng, Y.; Wu, Y.; Shi, X.; Du, Y.; Deng, H. Chitosan/tannic acid bilayers layer-by-layer deposited cellulose nanofibrous mats for antibacterial application. *Int. J. Biol. Macromol.* **2019**, *139*, 191–198. [CrossRef]



177. Ren, X.; Xu, Z.; Wang, L.; Meng, K.; Wang, H.; Zhao, H. Silk fibroin/chitosan/halloysite composite medical dressing with antibacterial and rapid haemostatic properties. *Mater. Res. Express* **2019**, *6*, 125409. [CrossRef]
178. Sasmal, P.; Datta, P. Tranexamic acid-loaded chitosan electrospun nanofibers as drug delivery system for hemorrhage control applications. *J. Drug Deliv. Sci. Technol.* **2019**, *52*, 559–567. [CrossRef]
179. Leonhardt, E.E.; Kang, N.; Hamad, M.A.; Wooley, K.L.; Elsabahy, M. Absorbable hemostatic hydrogels comprising composites of sacrificial templates and honeycomb-like nanofibrous mats of chitosan. *Nat. Commun.* **2019**, *10*, 2307. [CrossRef] [PubMed]
180. Zhang, L.; Luo, J.; Menkhaus, T.J.; Varadaraju, H.; Sun, Y.; Fong, H. Antimicrobial nano-fibrous membranes developed from electrospun polyacrylonitrile nanofibers. *J. Membr. Sci.* **2011**, *369*, 499–505. [CrossRef]
181. Subramanian, A.; Krishnan, U.M.; Sethuraman, S. Fabrication of uniaxially aligned 3D electrospun scaffolds for neural regeneration. *Biomed. Mater.* **2011**, *6*, 025004. [CrossRef] [PubMed]
182. Jayakumar, R.; Prabakaran, M.; Sudheesh Kumar, P.T.; Nair, S.V.; Tamura, H. Biomaterials based on chitin and chitosan in wound dressing applications. *Biotechnol. Adv.* **2011**, *29*, 322–337. [CrossRef] [PubMed]
183. Reneker, D.H.; Yarin, A.L. Electrospinning jets and polymer nanofibers. *Polymer* **2008**, *49*, 2387–2425. [CrossRef]
184. Augustine, R.; Rehman, S.R.U.; Ahmed, R.; Zahid, A.A.; Sharifi, M.; Falahati, M.; Hasan, A. Electrospun chitosan membranes containing bioactive and therapeutic agents for enhanced wound healing. *Int. J. Biol. Macromol.* **2020**, *156*, 153–170. [CrossRef]
185. Ranjith, R.; Balraj, S.; Ganesh, J.; Milton, M.C.J. Therapeutic agents loaded chitosan-based nanofibrous mats as potential wound dressings: A review. *Mater. Today Chem.* **2019**, *12*, 386–395. [CrossRef]
186. Yang, X.; Wang, J.; Guo, H.; Liu, L.; Xu, W.; Duan, G. Structural design toward functional materials by electrospinning: A review. *e-Polymers* **2020**, *20*, 682–712. [CrossRef]
187. Guo, H.; Chen, Y.; Li, Y.; Zhou, W.; Xu, W.; Pang, L.; Fan, X.; Jiang, S. Electrospun fibrous materials and their applications for electromagnetic interference shielding: A review. *Compos. Part A Appl. Sci. Manuf.* **2021**, *143*, 106309. [CrossRef]
188. Zhao, L.; Duan, G.; Zhang, G.; Yang, H.; He, S.; Jiang, S. Electrospun Functional Materials toward Food Packaging Applications: A Review. *Nanomaterials* **2020**, *10*, 150. [CrossRef]
189. Tao, F.; Cheng, Y.; Shi, X.; Zheng, H.; Du, Y.; Xiang, W.; Deng, H. Applications of chitin and chitosan nanofibers in bone regenerative engineering. *Carbohydr. Polym.* **2020**, *230*, 115658. [CrossRef] [PubMed]
190. Homayoni, H.; Ravandi, S.A.H.; Valizadeh, M. Electrospinning of chitosan nanofibers: Processing optimization. *Carbohydr. Polym.* **2009**, *77*, 656–661. [CrossRef]
191. Liu, L.; Xu, W.; Ding, Y.; Agarwal, S.; Greiner, A.; Duan, G. A review of smart electrospun fibers toward textiles. *Compos. Commun.* **2020**, *22*, 100506. [CrossRef]
192. Neamark, A.; Rujiravanit, R.; Supaphol, P. Electrospinning of hexanoyl chitosan. *Carbohydr. Polym.* **2006**, *66*, 298–305. [CrossRef]
193. Li, S.; Guo, H.; He, S.; Yang, H.; Liu, K.; Duan, G.; Jiang, S. Advanced electrospun nanofibers as bifunctional electrocatalysts for flexible metal-air (O<sub>2</sub>) batteries: Opportunities and challenges. *Mater. Des.* **2022**, *214*, 110406. [CrossRef]
194. Geng, X.; Kwon, O.-H.; Jang, J. Electrospinning of chitosan dissolved in concentrated acetic acid solution. *Biomaterials* **2005**, *26*, 5427–5432. [CrossRef]
195. Okutan, N.; Terzi, P.; Altay, F. Affecting parameters on electrospinning process and characterization of electrospun gelatin nanofibers. *Food Hydrocoll.* **2014**, *39*, 19–26. [CrossRef]
196. Frenot, A.; Chronakis, I.S. Polymer nanofibers assembled by electrospinning. *Curr. Opin. Colloid Interface Sci.* **2003**, *8*, 64–75. [CrossRef]
197. Haggi, A.K.; Akbari, M. Trends in electrospinning of natural nanofibers. *Phys. Status Solidi (A)* **2007**, *204*, 1830–1834. [CrossRef]
198. Burger, C.; Hsiao, B.S.; Chu, B. NANOFIBROUS MATERIALS AND THEIR APPLICATIONS. *Annu. Rev. Mater. Res.* **2006**, *36*, 333–368. [CrossRef]
199. Su, H.; Liu, K.-Y.; Karydis, A.; Abebe, D.G.; Wu, C.; Anderson, K.M.; Ghadri, N.; Adatrow, P.; Fujiwara, T.; Bumgardner, J.D. In vitro and in vivo evaluations of a novel post-electrospinning treatment to improve the fibrous structure of chitosan membranes for guided bone regeneration. *Biomed. Mater.* **2016**, *12*, 015003. [CrossRef]
200. Rasouli, R.; Barhoum, A.; Bechelany, M.; Dufresne, A. Nanofibers for biomedical and healthcare applications. *Macromol. Biosci.* **2019**, *19*, 1800256. [CrossRef]
201. Singh, B.N.; Pramanik, K. Development of novel silk fibroin/polyvinyl alcohol/sol-gel bioactive glass composite matrix by modified layer by layer electrospinning method for bone tissue construct generation. *Biofabrication* **2017**, *9*, 015028. [CrossRef]
202. Kean, T.; Thanou, M. Biodegradation, biodistribution and toxicity of chitosan. *Adv. Drug Deliv. Rev.* **2010**, *62*, 3–11. [CrossRef] [PubMed]
203. Pagon, A.; Saesoo, S.; Saengkrit, N.; Ruktanonchai, U.; Intasanta, V. Hydroxyapatite-hybridized chitosan/chitin whisker bionanocomposite fibers for bone tissue engineering applications. *Carbohydr. Polym.* **2016**, *144*, 419–427. [CrossRef] [PubMed]
204. Ding, F.; Deng, H.; Du, Y.; Shi, X.; Wang, Q. Emerging chitin and chitosan nanofibrous materials for biomedical applications. *Nanoscale* **2014**, *6*, 9477–9493. [CrossRef] [PubMed]
205. Kalantari, K.; Afifi, A.M.; Jahangirian, H.; Webster, T.J. Biomedical applications of chitosan electrospun nanofibers as a green polymer—Review. *Carbohydr. Polym.* **2019**, *207*, 588–600. [CrossRef]
206. Hokmabad, V.R.; Davaran, S.; Aghazadeh, M.; Alizadeh, E.; Salehi, R.; Ramazani, A. A Comparison of the Effects of Silica and Hydroxyapatite Nanoparticles on Poly( $\epsilon$ -caprolactone)-Poly(ethylene glycol)-Poly( $\epsilon$ -caprolactone)/Chitosan Nanofibrous Scaffolds for Bone Tissue Engineering. *Tissue Eng. Regen. Med.* **2018**, *15*, 735–750. [CrossRef]

207. Lastra, M.L.; Molinuevo, M.S.; Blaszczyk-Lezak, I.; Mijangos, C.; Cortizo, M.S. Nanostructured fumarate copolymer-chitosan crosslinked scaffold: An in vitro osteochondrogenesis regeneration study. *J. Biomed. Mater. Res. Part A* **2018**, *106*, 570–579. [CrossRef]
208. Ghasemi Hamidabadi, H.; Rezvani, Z.; Nazm Bojnordi, M.; Shirinzadeh, H.; Seifalian, A.M.; Joghataei, M.T.; Razaghpour, M.; Alibakhshi, A.; Yazdanpanah, A.; Salimi, M.; et al. Chitosan-Intercalated Montmorillonite/Poly(vinyl alcohol) Nanofibers as a Platform to Guide Neuronlike Differentiation of Human Dental Pulp Stem Cells. *ACS Appl. Mater. Interfaces* **2017**, *9*, 11392–11404. [CrossRef]
209. Alhosseini, S.N.; Moztarzadeh, F.; Mozafari, M.; Asgari, S.; Dodel, M.; Samadikuchaksaraei, A.; Kargozar, S.; Jalali, N. Synthesis and characterization of electrospun polyvinyl alcohol nanofibrous scaffolds modified by blending with chitosan for neural tissue engineering. *Int. J. Nanomed.* **2012**, *25*–34.
210. Bolaina-Lorenzo, E.; Martínez-Ramos, C.; Monleón-Pradas, M.; Herrera-Kao, W.; Cauich-Rodríguez, J.V.; Cervantes-Uc, J.M. Electrospun polycaprolactone/chitosan scaffolds for nerve tissue engineering: Physicochemical characterization and Schwann cell biocompatibility. *Biomed. Mater.* **2016**, *12*, 015008. [CrossRef] [PubMed]
211. Cao, L.; Zhang, F.; Wang, Q.; Wu, X. Fabrication of chitosan/graphene oxide polymer nanofiber and its biocompatibility for cartilage tissue engineering. *Mater. Sci. Eng. C* **2017**, *79*, 697–701. [CrossRef] [PubMed]
212. Tonda-Turo, C.; Ruini, F.; Ramella, M.; Boccafoschi, F.; Gentile, P.; Gioffredi, E.; Falvo D’Urso Labate, G.; Ciardelli, G. Non-covalently crosslinked chitosan nanofibrous mats prepared by electrospinning as substrates for soft tissue regeneration. *Carbohydr. Polym.* **2017**, *162*, 82–92. [CrossRef] [PubMed]
213. Hussain, A.; Collins, G.; Yip, D.; Cho, C.H. Functional 3-D cardiac co-culture model using bioactive chitosan nanofiber scaffolds. *Biotechnol. Bioeng.* **2013**, *110*, 637–647. [CrossRef] [PubMed]
214. Fukunishi, T.; Best, C.A.; Sugiura, T.; Shoji, T.; Yi, T.; Udelsman, B.; Ohst, D.; Ong, C.S.; Zhang, H.; Shinoka, T. Tissue-engineered small diameter arterial vascular grafts from cell-free nanofiber PCL/chitosan scaffolds in a sheep model. *PLoS ONE* **2016**, *11*, e0158555. [CrossRef] [PubMed]
215. Kheradmandi, M.; Vasheghani-Farahani, E.; Ghiaseddin, A.; Ganji, F. Skeletal muscle regeneration via engineered tissue culture over electrospun nanofibrous chitosan/PVA scaffold. *J. Biomed. Mater. Res. Part A* **2016**, *104*, 1720–1727. [CrossRef]
216. Shim, I.K.; Suh, W.H.; Lee, S.Y.; Lee, S.H.; Heo, S.J.; Lee, M.C.; Lee, S.J. Chitosan nano-/microfibrous double-layered membrane with rolled-up three-dimensional structures for chondrocyte cultivation. *J. Biomed. Mater. Res. Part A* **2009**, *90A*, 595–602. [CrossRef]
217. De Farias, B.S.; Sant’Anna Cadaval, T.R., Jr.; de Almeida Pinto, L.A. Chitosan-functionalized nanofibers: A comprehensive review on challenges and prospects for food applications. *Int. J. Biol. Macromol.* **2019**, *123*, 210–220. [CrossRef]
218. Sharifi, M.; Sohrabi, M.J.; Hosseinali, S.H.; Hasan, A.; Kani, P.H.; Talaei, A.J.; Karim, A.Y.; Nanakali, N.M.Q.; Salihi, A.; Aziz, F.M.; et al. Enzyme immobilization onto the nanomaterials: Application in enzyme stability and prodrug-activated cancer therapy. *Int. J. Biol. Macromol.* **2020**, *143*, 665–676. [CrossRef]
219. Bösiger, P.; Tegl, G.; Richard, I.M.T.; Le Gat, L.; Huber, L.; Stagl, V.; Mensah, A.; Guebitz, G.M.; Rossi, R.M.; Fortunato, G. Enzyme functionalized electrospun chitosan mats for antimicrobial treatment. *Carbohydr. Polym.* **2018**, *181*, 551–559. [CrossRef]
220. Ismail, A.R.; Baek, K.-H. Lipase immobilization with support materials, preparation techniques, and applications: Present and future aspects. *Int. J. Biol. Macromol.* **2020**, *163*, 1624–1639. [CrossRef]
221. Srivastava, B.; Singh, H.; Khatri, M.; Singh, G.; Arya, S.K. Immobilization of keratinase on chitosan grafted- $\beta$ -cyclodextrin for the improvement of the enzyme properties and application of free keratinase in the textile industry. *Int. J. Biol. Macromol.* **2020**, *165*, 1099–1110. [CrossRef]
222. de Oliveira, R.L.; da Silva, M.F.; da Silva, S.P.; de Araújo, A.C.V.; Cavalcanti, J.V.F.L.; Converti, A.; Porto, T.S. Fructooligosaccharides production by an *Aspergillus aculeatus* commercial enzyme preparation with fructosyltransferase activity covalently immobilized on Fe<sub>3</sub>O<sub>4</sub>-chitosan-magnetic nanoparticles. *Int. J. Biol. Macromol.* **2020**, *150*, 922–929. [CrossRef] [PubMed]
223. Soares, A.M.B.F.; Gonçalves, L.M.O.; Ferreira, R.D.S.; de Souza, J.M.; Fangueiro, R.; Alves, M.M.M.; Carvalho, F.A.A.; Mendes, A.N.; Cantanhêde, W. Immobilization of papain enzyme on a hybrid support containing zinc oxide nanoparticles and chitosan for clinical applications. *Carbohydr. Polym.* **2020**, *243*, 116498. [CrossRef] [PubMed]
224. Tavernini, L.; Ottone, C.; Illanes, A.; Wilson, L. Entrapment of enzyme aggregates in chitosan beads for aroma release in white wines. *Int. J. Biol. Macromol.* **2020**, *154*, 1082–1090. [CrossRef] [PubMed]
225. Duru Kamaci, U.; Peksel, A. Fabrication of PVA-chitosan-based nanofibers for phytase immobilization to enhance enzymatic activity. *Int. J. Biol. Macromol.* **2020**, *164*, 3315–3322. [CrossRef]
226. Haghju, S.; Bari, M.R.; Khaled-Abad, M.A. Affecting parameters on fabrication of  $\beta$ -D-galactosidase immobilized chitosan/poly(vinyl alcohol) electrospun nanofibers. *Carbohydr. Polym.* **2018**, *200*, 137–143. [CrossRef]
227. Kutlu, N.; İspirli Doğaç, Y.; Deveci, İ.; Teke, M. Urease immobilized electrospun PVA/chitosan nanofibers with improved stability and reusability characteristics: An application for removal of urea from artificial blood serum. *Prep. Biochem. Biotechnol.* **2020**, *50*, 425–437. [CrossRef]
228. Park, J.-M.; Kim, M.; Park, H.-S.; Jang, A.; Min, J.; Kim, Y.-H. Immobilization of lysozyme-CLEA onto electrospun chitosan nanofiber for effective antibacterial applications. *Int. J. Biol. Macromol.* **2013**, *54*, 37–43. [CrossRef]

229. Jhuang, J.-R.; Lou, S.-N.; Lin, S.-B.; Chen, S.H.; Chen, L.-C.; Chen, H.-H. Immobilizing laccase on electrospun chitosan fiber to prepare time-temperature indicator for food quality monitoring. *Innov. Food Sci. Emerg. Technol.* **2020**, *63*, 102370. [CrossRef]
230. Srbová, J.; Slováková, M.; Křípalová, Z.; Žárská, M.; Špačková, M.; Stránská, D.; Bílková, Z. Covalent biofunctionalization of chitosan nanofibers with trypsin for high enzyme stability. *React. Funct. Polym.* **2016**, *104*, 38–44. [CrossRef]
231. Maryšková, M.; Ardao, I.; García-González, C.A.; Martinová, L.; Rotková, J.; Ševců, A. Polyamide 6/chitosan nanofibers as support for the immobilization of *Trametes versicolor* laccase for the elimination of endocrine disrupting chemicals. *Enzym. Microb. Technol.* **2016**, *89*, 31–38. [CrossRef] [PubMed]
232. Demirkan, E.; Avci, T.; Aykut, Y. Protease immobilization on cellulose monoacetate/chitosan-blended nanofibers. *J. Ind. Text.* **2017**, *47*, 2092–2111. [CrossRef]
233. Teepoo, S.; Dawan, P.; Barnthip, N. Electrospun Chitosan-Gelatin Biopolymer Composite Nanofibers for Horseradish Peroxidase Immobilization in a Hydrogen Peroxide Biosensor. *Biosensors* **2017**, *7*, 47. [CrossRef] [PubMed]
234. Radmansouri, M.; Bahmani, E.; Sarikhani, E.; Rahmani, K.; Sharifianjazi, F.; Irani, M. Doxorubicin hydrochloride-Loaded electrospun chitosan/cobalt ferrite/titanium oxide nanofibers for hyperthermic tumor cell treatment and controlled drug release. *Int. J. Biol. Macromol.* **2018**, *116*, 378–384. [CrossRef]
235. Lu, L.; Cao, X.; Shen, Z.; Li, L.; Huo, J.; Chen, W.; Liu, C.; Liu, H. Electrospun nitrogen-doped carbon nanofibers for electrocatalysis. *Sustain. Mater. Technol.* **2020**, *26*, e00221. [CrossRef]
236. Jouybari, M.H.; Hosseini, S.; Mahboobnia, K.; Boloursaz, L.A.; Moradi, M.; Irani, M. Simultaneous controlled release of 5-FU, DOX and PTX from chitosan/PLA/5-FU/g-C<sub>3</sub>N<sub>4</sub>-DOX/g-C<sub>3</sub>N<sub>4</sub>-PTX triaxial nanofibers for breast cancer treatment in vitro. *Colloids Surf. B Biointerfaces* **2019**, *179*, 495–504. [CrossRef]
237. Balan, P.; Indrakumar, J.; Murali, P.; Korrapati, P.S. Bi-faceted delivery of phytochemicals through chitosan nanoparticles impregnated nanofibers for cancer therapeutics. *Int. J. Biol. Macromol.* **2020**, *142*, 201–211. [CrossRef]
238. Ardeshirzadeh, B.; Anaraki, N.A.; Irani, M.; Rad, L.R.; Shamshiri, S. Controlled release of doxorubicin from electrospun PEO/chitosan/graphene oxide nanocomposite nanofibrous scaffolds. *Mater. Sci. Eng. C* **2015**, *48*, 384–390. [CrossRef] [PubMed]
239. Rostami, M.; Ghorbani, M.; Aman Mohammadi, M.; Delavar, M.; Tabibiazar, M.; Ramezani, S. Development of resveratrol loaded chitosan-gellan nanofiber as a novel gastrointestinal delivery system. *Int. J. Biol. Macromol.* **2019**, *135*, 698–705. [CrossRef]
240. Yan, E.; Cao, M.; Wang, Y.; Hao, X.; Pei, S.; Gao, J.; Wang, Y.; Zhang, Z.; Zhang, D. Gold nanorods contained polyvinyl alcohol/chitosan nanofiber matrix for cell imaging and drug delivery. *Mater. Sci. Eng. C* **2016**, *58*, 1090–1097. [CrossRef] [PubMed]
241. Aggarwal, U.; Goyal, A.K.; Rath, G. Development and characterization of the cisplatin loaded nanofibers for the treatment of cervical cancer. *Mater. Sci. Eng. C* **2017**, *75*, 125–132. [CrossRef] [PubMed]
242. Ma, G.; Liu, Y.; Peng, C.; Fang, D.; He, B.; Nie, J. Paclitaxel loaded electrospun porous nanofibers as mat potential application for chemotherapy against prostate cancer. *Carbohydr. Polym.* **2011**, *86*, 505–512. [CrossRef]
243. Samadi, S.; Moradkhani, M.; Beheshti, H.; Irani, M.; Aliabadi, M. Fabrication of chitosan/poly(lactic acid)/graphene oxide/TiO<sub>2</sub> composite nanofibrous scaffolds for sustained delivery of doxorubicin and treatment of lung cancer. *Int. J. Biol. Macromol.* **2018**, *110*, 416–424. [CrossRef]
244. Sedghi, R.; Shaabani, A.; Mohammadi, Z.; Samadi, F.Y.; Isaei, E. Biocompatible electrospinning chitosan nanofibers: A novel delivery system with superior local cancer therapy. *Carbohydr. Polym.* **2017**, *159*, 1–10. [CrossRef] [PubMed]
245. Irani, M.; Mir Mohamad Sadeghi, G.; Haririan, I. A novel biocompatible drug delivery system of chitosan/temozolomide nanoparticles loaded PCL-PU nanofibers for sustained delivery of temozolomide. *Int. J. Biol. Macromol.* **2017**, *97*, 744–751. [CrossRef]
246. Zhou, X.; Chen, L.; Wang, W.; Jia, Y.; Chang, A.; Mo, X.; Wang, H.; He, C. Electrospun nanofibers incorporating self-decomposable silica nanoparticles as carriers for controlled delivery of anticancer drug. *RSC Adv.* **2015**, *5*, 65897–65904. [CrossRef]
247. Zhao, J.; Zhu, Y.; Ye, C.; Chen, Y.; Wang, S.; Zou, D.; Li, Z. Photothermal transforming agent and chemotherapeutic co-loaded electrospun nanofibers for tumor treatment. *Int. J. Nanomed.* **2019**, 3893–3909. [CrossRef] [PubMed]
248. Bharathi, D.; Ranjithkumar, R.; Chandarshekar, B.; Bhuvaneshwari, V. Bio-inspired synthesis of chitosan/copper oxide nanocomposite using rutin and their anti-proliferative activity in human lung cancer cells. *Int. J. Biol. Macromol.* **2019**, *141*, 476–483. [CrossRef]
249. Ibrahim, H.M.; Reda, M.M.; Klingner, A. Preparation and characterization of green carboxymethylchitosan (CMCS) – Polyvinyl alcohol (PVA) electrospun nanofibers containing gold nanoparticles (AuNPs) and its potential use as biomaterials. *Int. J. Biol. Macromol.* **2020**, *151*, 821–829. [CrossRef]
250. Farhoodi, M. Nanocomposite Materials for Food Packaging Applications: Characterization and Safety Evaluation. *Food Eng. Rev.* **2016**, *8*, 35–51. [CrossRef]
251. Mousavi Khaneghah, A.; Hashemi, S.M.B.; Limbo, S. Antimicrobial agents and packaging systems in antimicrobial active food packaging: An overview of approaches and interactions. *Food Bioprod. Process.* **2018**, *111*, 1–19. [CrossRef]
252. Youssef, A.M.; El-Sayed, S.M. Bionanocomposites materials for food packaging applications: Concepts and future outlook. *Carbohydr. Polym.* **2018**, *193*, 19–27. [CrossRef] [PubMed]
253. Calderón, L.; Harris, R.; Cordoba-Diaz, M.; Elorza, M.; Elorza, B.; Lenoir, J.; Adriaens, E.; Remon, J.P.; Heras, A.; Cordoba-Diaz, D. Nano and microparticulate chitosan-based systems for antiviral topical delivery. *Eur. J. Pharm. Sci.* **2013**, *48*, 216–222. [CrossRef]
254. Helander, I.M.; Nurmiaho-Lassila, E.L.; Ahvenainen, R.; Rhoades, J.; Roller, S. Chitosan disrupts the barrier properties of the outer membrane of Gram-negative bacteria. *Int. J. Food Microbiol.* **2001**, *71*, 235–244. [CrossRef]



255. Ing, L.Y.; Zin, N.M.; Sarwar, A.; Katas, H. Antifungal Activity of Chitosan Nanoparticles and Correlation with Their Physical Properties. *Int. J. Biomater.* **2012**, *2012*, 632698. [CrossRef]
256. Jaime, M.D.L.A.; Lopez-Llorca, L.V.; Conesa, A.; Lee, A.Y.; Proctor, M.; Heisler, L.E.; Gebbia, M.; Giaever, G.; Westwood, J.T.; Nislow, C. Identification of yeast genes that confer resistance to chitosan oligosaccharide (COS) using chemogenomics. *BMC Genom.* **2012**, *13*, 267. [CrossRef] [PubMed]
257. Abdul Khalil, H.P.S.; Banerjee, A.; Saurabh, C.K.; Tye, Y.Y.; Suriani, A.B.; Mohamed, A.; Karim, A.A.; Rizal, S.; Paridah, M.T. Biodegradable Films for Fruits and Vegetables Packaging Application: Preparation and Properties. *Food Eng. Rev.* **2018**, *10*, 139–153. [CrossRef]
258. Arkoun, M.; Daigle, F.; Heuzey, M.-C.; Aji, A. Mechanism of action of electrospun chitosan-based nanofibers against meat spoilage and pathogenic bacteria. *Molecules* **2017**, *22*, 585. [CrossRef]
259. Cui, H.; Bai, M.; Li, C.; Liu, R.; Lin, L. Fabrication of chitosan nanofibers containing tea tree oil liposomes against *Salmonella* spp. in chicken. *LWT* **2018**, *96*, 671–678. [CrossRef]
260. Ceylan, Z.; Unal Sengor, G.F.; Yilmaz, M.T. Nanoencapsulation of liquid smoke/thymol combination in chitosan nanofibers to delay microbiological spoilage of sea bass (*Dicentrarchus labrax*) filets. *J. Food Eng.* **2018**, *229*, 43–49. [CrossRef]
261. He, X.; Hwang, H.-M. Nanotechnology in food science: Functionality, applicability, and safety assessment. *J. Food Drug Anal.* **2016**, *24*, 671–681. [CrossRef] [PubMed]
262. Cook, S.L.; Bull, S.P.; Methven, L.; Parker, J.K.; Khutoryanskiy, V.V. Mucoadhesion: A food perspective. *Food Hydrocoll.* **2017**, *72*, 281–296. [CrossRef]
263. Martins, J.T.; Ramos, Ó.L.; Pinheiro, A.C.; Bourbon, A.I.; Silva, H.D.; Rivera, M.C.; Cerqueira, M.A.; Pastrana, L.; Malcata, F.X.; González-Fernández, Á.; et al. Edible Bio-Based Nanostructures: Delivery, Absorption and Potential Toxicity. *Food Eng. Rev.* **2015**, *7*, 491–513. [CrossRef]
264. Ali, A.; Ahmed, S. A review on chitosan and its nanocomposites in drug delivery. *Int. J. Biol. Macromol.* **2018**, *109*, 273–286. [CrossRef]
265. Darbasizadeh, B.; Motasadizadeh, H.; Foroughi-Nia, B.; Farhadnejad, H. Tripolyphosphate-crosslinked chitosan/poly (ethylene oxide) electrospun nanofibrous mats as a floating gastro-retentive delivery system for ranitidine hydrochloride. *J. Pharm. Biomed. Anal.* **2018**, *153*, 63–75. [CrossRef]
266. Hasani, S.; Ojagh, S.M.; Ghorbani, M. Nanoencapsulation of lemon essential oil in Chitosan-Hicap system. Part 1: Study on its physical and structural characteristics. *Int. J. Biol. Macromol.* **2018**, *115*, 143–151. [CrossRef]
267. Omwenga, E.O.; Hensel, A.; Shitandi, A.; Goycoolea, F.M. Chitosan nanoencapsulation of flavonoids enhances their quorum sensing and biofilm formation inhibitory activities against an *E.coli* Top 10 biosensor. *Colloids Surf. B Biointerfaces* **2018**, *164*, 125–133. [CrossRef]
268. Shekarforoush, E.; Ajallouei, F.; Zeng, G.; Mendes, A.C.; Chronakis, I.S. Electrospun xanthan gum-chitosan nanofibers as delivery carrier of hydrophobic bioactives. *Mater. Lett.* **2018**, *228*, 322–326. [CrossRef]
269. Kuddus, M. *Enzymes in Food Biotechnology: Production, Applications, and Future Prospects*; Elsevier Inc.: Amsterdam, The Netherlands, 2018.
270. Wang, Z.-G.; Wan, L.-S.; Liu, Z.-M.; Huang, X.-J.; Xu, Z.-K. Enzyme immobilization on electrospun polymer nanofibers: An overview. *J. Mol. Catal. B Enzym.* **2009**, *56*, 189–195. [CrossRef]

**Disclaimer/Publisher’s Note:** The statements, opinions and data contained in all publications are solely those of the individual author(s) and contributor(s) and not of MDPI and/or the editor(s). MDPI and/or the editor(s) disclaim responsibility for any injury to people or property resulting from any ideas, methods, instructions or products referred to in the content.



Review

# An Overview on Wood Waste Valorization as Biopolymers and Biocomposites: Definition, Classification, Production, Properties and Applications

Francesca Ferrari, Raffaella Striani \*, Daniela Fico, Mohammad Mahbubul Alam, Antonio Greco and Carola Esposito Corcione

Department of Engineering for Innovation, University of Salento, Via Arnesano, 73100 Lecce, Italy

\* Correspondence: raffaella.striani@unisalento.it

**Abstract:** Bio-based polymers, obtained from natural biomass, are nowadays considered good candidates for the replacement of traditional fossil-derived plastics. The need for substituting traditional synthetic plastics is mainly driven by many concerns about their detrimental effects on the environment and human health. The most innovative way to produce bioplastics involves the use of raw materials derived from wastes. Raw materials are of vital importance for human and animal health and due to their economic and environmental benefits. Among these, wood waste is gaining popularity as an innovative raw material for biopolymer manufacturing. On the other hand, the use of wastes as a source to produce biopolymers and biocomposites is still under development and the processing methods are currently being studied in order to reach a high reproducibility and thus increase the yield of production. This study therefore aimed to cover the current developments in the classification, manufacturing, performances and fields of application of bio-based polymers, especially focusing on wood waste sources. The work was carried out using both a descriptive and an analytical methodology: first, a description of the state of art as it exists at present was reported, then the available information was analyzed to make a critical evaluation of the results. A second way to employ wood scraps involves their use as bio-reinforcements for composites; therefore, the increase in the mechanical response obtained by the addition of wood waste in different bio-based matrices was explored in this work. Results showed an increase in Young's modulus up to 9 GPa for wood-reinforced PLA and up to 6 GPa for wood-reinforced PHA.

**Keywords:** biopolymers; biocomposites; renewable sources; wood waste; waste valorization

**Citation:** Ferrari, F.; Striani, R.; Fico, D.; Alam, M.M.; Greco, A.; Esposito Corcione, C. An Overview on Wood Waste Valorization as Biopolymers and Biocomposites: Definition, Classification, Production, Properties and Applications. *Polymers* **2022**, *14*, 5519. <https://doi.org/10.3390/polym14245519>

Academic Editor: Antonios N. Papadopoulos

Received: 3 December 2022

Accepted: 13 December 2022

Published: 16 December 2022



**Copyright:** © 2022 by the authors. Licensee MDPI, Basel, Switzerland. This article is an open access article distributed under the terms and conditions of the Creative Commons Attribution (CC BY) license (<https://creativecommons.org/licenses/by/4.0/>).

## 1. Introduction

Nowadays, the manufacturing of bio-based polymers is characterized by a strong development. Because of the present rapid expansion in the manufacture of these polymers, the use of plastic items created from them is also expanding, according to the European Environment Agency (EEA) [1]. However, they even correspond to a very modest portion of the market, since they are around one percent of the more than 368 million tons of plastic produced yearly. The total amount of biopolymers is going to increase up to 2.11 million tons [2]. The main challenge in the next few years will be to significantly reduce production costs. Economies of scale are vital for competitive pricing. However, because bio-based supply chains are often extensive, scaling them up is difficult, especially since many of the essential technologies have not been validated [3,4].

Today, growing attention is paid to the manufacturing of bio-based materials, starting from scraps. The circular economy has, in fact, grown in importance in academic study over the previous decade. A key development goal of the circular economy is the reuse of different kinds of wastes, particularly wastes from industrial operations [5]. The increase in population and the usage of polymers for disposable items and packaging generate uncontrolled waste, posing severe management and disposal issues. The unrestricted



waste stream from many sources poses a major challenge to waste management [6]. Several researchers have been studying the potential and valorization of the organic component in a circular economy scenario. The valorization technique has numerous benefits over conventional organic fraction collecting and treatment technologies. These treatments use the organic portion as an energy source by burning or composting it [7,8].

The organic fraction of municipal scraps includes a huge quantity of carbohydrate and wood derivatives [9]. In today's world, the increase in population and the continuous usage of throwaway materials for lots of applications causes significant problems in waste management [2].

Among the different kinds of organic wastes, agro-industrial and forestry wastes present an unsustainable environmental and economic scenario [10]. Therefore, the valorization of this class of wastes represents one of the main issues in terms of disposal management. Many studies are currently being carried out to develop new procedures to produce biopolymers and biocomposites, starting with agro-industrial wastes. Due to the innovation of the topic, a summary of the last developments in the production of biopolymers and biocomposites can be useful to help carry out future research.

This work reports the current developments in the classification, production, properties and application of biopolymers, particularly those obtained from the valorization of wood wastes. Among the different application fields, the possibility to use wood scraps as a reinforcement for the production of biocomposites is also reported and the improvements in the performances obtained by the use of wood waste fillers are analyzed.

## 2. General Definition of Biopolymers and Biocomposites

### 2.1. Biopolymers: Difference between Biodegradable and Bio-Based

A polymer can be defined as a bioplastic when the material exhibits biodegradability, or it comes from bio-based or raw materials, or both [11,12]. Other researchers define a bioplastic as a material that can be decomposed into CO<sub>2</sub>, H<sub>2</sub>O and non-organic particles or biomass, generally thanks to the enzymatic decomposition carried out by microorganisms. Nevertheless, a bio-based polymer could be not biodegradable and vice versa. A bio-based polymer is derived from natural sources obtained from biomass, which can be partially or totally renewable. There are three basic methods for creating bio-based polymers. To achieve the performance criteria, one option is to partially change polymers derived from green sources, for example, cellulose, and lipids, using extraction, separation and filtration [13].

Depending on the type of synthesis and source, biopolymers can be classified into three groups (Table 1) [14]. Natural sources, such as carbohydrates and proteins, or monomers, such as lactic acid, can be the raw materials for biopolymers. Furthermore, other biopolymers such as polyhydroxyalkanoate (PHA) can be obtained from microorganisms [15]. Commercially accessible biopolymers are divided into the categories which follow: polyhydroxyalkanoates (PHAs/PHBs), polylactic acid (PLA) polyamides, polyols, bio-PET, butyl rubber and cellulose acetate; these are some of the materials used [16]. For practical usage in plastics or as water-soluble polymers, polysaccharides are mostly confined to starch and cellulose derivatives. Both of these compounds are made up of D-glycopyranoside-repeating units, which result in molecular weights in the thousands [14].

**Table 1.** A brief definition and classification of bio-based polymers.

Types	Chemical Group	Example	References
Biomass-based polymers	Polysaccharides Proteins and lipids	<ul style="list-style-type: none"> <li>• Carbohydrates (wheat, potatoes, maize);</li> <li>• Products made from cellulosic and ligno-cellulosic materials (wood, straws, etc.);</li> <li>• Pectins (chitosan/chitin, gums, etc.);</li> <li>• Casein, whey, collagen/gelatin from animals;</li> <li>• Plants which are a type of living thing (zein, soya, gluten).</li> </ul>	[16–18]
Polymers derived via microbial fermentation	Polyhydroxyalkanoates (PHA)	<ul style="list-style-type: none"> <li>• Poly(hydroxybutyrate) (PHB)</li> <li>• Poly(hydroxybutyrate-cohydroxyvalerate) (PHBV)</li> </ul>	[19–21]
Agro-resource monomers are used to chemically manufacture polymers	Poly(hydroxyacid)	<ul style="list-style-type: none"> <li>• Poly(lactic acid) (PLA)</li> <li>• Polyglycolic acid (PGA)</li> </ul>	[22–24]

### 2.1.1. Biodegradable Polymers

Biodegradability is an important property of biopolymers, which does not refer to the raw materials used for the production. A biodegradable polymer could, in fact, be derived from fossil sources. Biodegradation is a biological process that occurs during composting, which involves the release of carbon dioxide, water, non-organic particles and biomass. In order to be defined as biodegradable, the biopolymer should degrade with a similar rate of certified compostable materials, without leaving hazardous residue [25]. If the plastic is able to decompose, but it doesn't follow the established standards, even if it is biodegradable, it must be classified as non-compostable. Finally, degradable materials should also not be derived from natural sources; for example, oxo-biodegradation is a phenomenon that occurs with some polyolefins through an oxidative process, which implies the breakage of the plastics into small pieces making them easier to biodegrade. Nevertheless, oxo-degradation is not currently classified as biodegradable or compostable, as its decomposition does not occur following established standards [26].

Table 2 shows the biodegradability of the most-used bioplastics in different fields. Biopolymer degradation depends on the physical and chemical structure of the biomaterial [27]. Furthermore, pH, temperature, moisture and oxygen must be considered.

**Table 2.** Definition of compostability and biodegradability of some bioplastics in different environments.

Bioplastic	Biodegradability					Ref.
	Environment	Condition	Biodegradability (%)	Biodegradability/Degradability Method	Testing Period (Day)	
Starch-based	Compost (starch, thermoplastic)	58 °C	73.1	CO <sub>2</sub> produced	56	[11,27–29]
	Soil (wheat, starch-derived plastic)	20 °C, 60% RH	14.2	CO <sub>2</sub> produced	110	
	Marine (neat starch)	26 °C	100	Weight loss	50	
Cellulose-based	Compost (cellulose acetate)	53 °C	100	CO <sub>2</sub> produced	18	[11,27,28]
	Soil (bacterial and vegetable cellulose)	25 °C	100	Weight loss	180	
	Simulated marine environment (neat cellulose)	Room temperature	75	Oxygen consumed	150	

Table 2. Cont.

Bioplastic	Biodegradability					Ref.
	Environment	Condition	Biodegradability (%)	Biodegradability/Degradability Method	Testing Period (Day)	
PLA	Compost	58 °C, 60% RH	60–70	CO <sub>2</sub> produced	30	[11,12,27,30]
	Soil	10–25 °C	0	CO <sub>2</sub> produced	120	
	Simulated marine environment	25 °C	3–4	CO <sub>2</sub> produced	180	
PHB	Compost	55 °C, 70% RH	80	CO <sub>2</sub> produced	28	[11,27,28]
	Soil	20 °C, 60% RH	48.5	CO <sub>2</sub> produced	280	
	Simulated marine environment	25 °C	38–45	CO <sub>2</sub> produced	180	

### 2.1.2. Bio-Based Polymers

The greatest part of bioplastics currently available on the market are obtained from biomasses of the first generation, for example, corn, potatoes, sugar cane, palm oil and straw. All these sources have a high amount of carbohydrates and can be eaten by people and animals. Feedstocks of the first generation have a high efficiency for the production of biopolymers, since they need less land to grow and have a high yield of production compared to the other feedstocks. The technical maturity of these feedstocks is then very high [25], although the subtraction of sources to the food chain poses important issues.

The second generation of feedstocks is related to those raw materials which cannot be eaten by animals, such as non-edible harvests (e.g., cellulose) or derivatives of raw materials of the first generation, for example, sugarcane bagasse. Although second-generation feedstocks are commercially available, the use is not so widespread due to a relatively high cost.

Finally, the third-generation feedstock, obtained from food scraps, algae biomass and industrial or municipal waste, is the most innovative and can solve the problems related to the consumption of sources from the food chain. Several studies are underway in order to develop new biopolymers from food wastes [31].

Figure 1 shows a summary of the three generations of feedstocks.

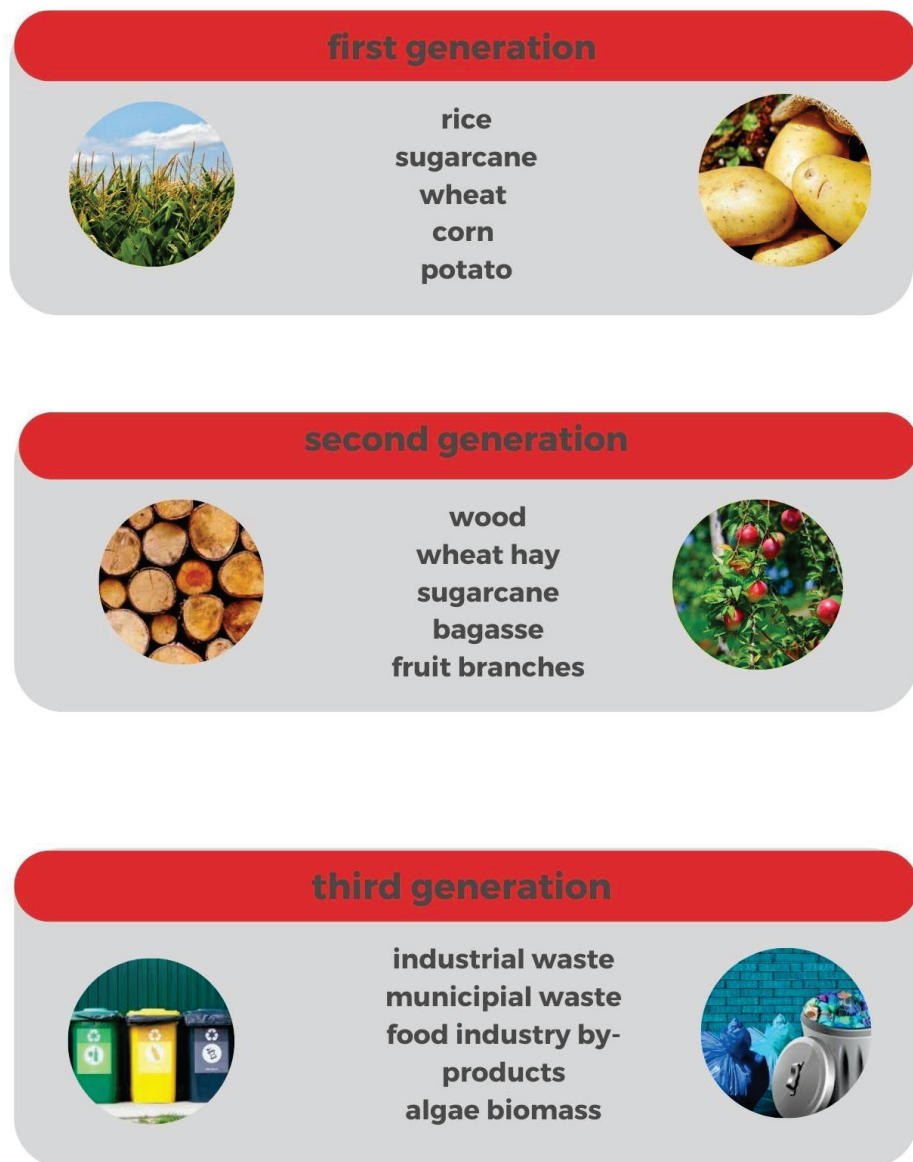
This review is focused on a special class of the third-generation biopolymers, i.e., those obtained from the reuse and valorization of wood-based waste. The following paragraphs, hence, refer to the description of the main production methods, properties and applications of biopolymers from wood sources, with a special focus on wood scraps, such as agricultural waste.

### 2.2. Biocomposites

The tendency to substitute the petroleum-based polymers with biopolymers has also made its way into the field of composite materials. In the last decade, it has become a possibility to combine biopolymers with natural fillers in developing new materials, i.e., biocomposites. They have attracted the interest of the research community all over the world, as well as the industrial sector, for a wide spectrum of applications that these new materials can offer, such as aerospace parts, automotive components, consumer goods, sporting goods and their use in the marine and oil industries [32]. Biocomposites are defined as composite materials composed of biodegradable natural fibers used as reinforcement and biodegradable (or non-biodegradable) polymers in a matrix. Starch, cellulose, soya, polylactic acid and polyhydroxyalkanoates are the most commonly available biopolymers [33]. Natural fibers are largely divided into two categories: plant-based and animal-based. In general, plant-based fibers are lignocellulosic in nature, and they are composed of cellulose, hemicellulose and lignin; animal-based fibers consist of proteins, for example, silk and wool [34]. In fact, the great advantage offered by biocomposites with respect to traditional composites is related to low energy and low CO<sub>2</sub> emission during their processing, biodegradability, renewability, low specific weight, higher specific

strength, and stiffness, high electrical resistance, low cost and good thermal and acoustic insulating properties [35]. Despite some drawbacks that affect biocomposites, mostly due to their high sensitivity to moisture, low durability and low adhesion between matrix and fiber [36], natural fillers play an important role in order to develop fully biodegradable green composites as a possible solution for contemporary environmental difficulties.

## Classification of biopolymers



**Figure 1.** An overview of the classification of biopolymers.

### 3. Production of the Main Biopolymers from Bio-Based Sources

#### 3.1. Cellulose Traditional Sources

Cellulose is constituted of anhydroglucose units linked by a  $\beta$ -(1,4) glycosidic bond. The repeating unit of cellulose is the glucose dimer known as cellobiose. In the condensation process, glycosidic oxygen bridges the sugar rings which are formed and the cellulose chains reach a degree of polymerization (DP) around 15,000 in native cellulose

cotton and 10,000 glucose units in wood cellulose. Each monomer has three hydroxyl groups that allow the creation of hydrogen bonds by influencing the crystalline packing and, consequentially, the cellulosic physical characteristics. The van der Waals and intermolecular hydrogen interactions allow numerous cellulose chains to stack in parallel and self-assemble into microfibrils, constituted of crystalline sections in which the cellulose chains are organized in a highly ordered form, and amorphous regions, which are less ordered than the former [37,38]. For such a reason, cellulose is a semi-crystalline substance whose crystallinity is determined by its source, extraction technique and treatments. The degree of crystallinity of wood-based and plant-based cellulose is typically 40–60% [39].

Cellulose is a nearly limitless polymeric raw material since it is the most abundant component in most plants. The availability, renewability and biodegradability of this material, as well as its low cost, are the major benefits, but it has two major drawbacks when compared to synthetic polymers: high hygroscopicity, owing to hydroxyl groups, and limited processing due to rapid disintegration [40]. Cellulose can be extracted from several natural sources, such as wood (lignocellulosic biomass), agricultural scraps, cotton, flax, hemp, sisal and especially vegetable byproducts [40]. Wood pulp is the most widespread raw material for cellulose processing, especially for paper and cardboard manufacture [31,41–43].

It is well known that cellulose, which is extracted from wood such as spruce, pine and many other trees, is being used to produce regenerated fibers such as viscose, lyocell, modal, cellulose acetate and cellulose triacetate. Cellulose esters and ethers are the principal industrially used cellulose derivatives, with the former being used in molding, extrusion and films, and the latter in a varied range of application fields (building materials, food, personal care products, paints and pharmaceuticals). However, until solvent methods for dissolving cellulose became available, the processability and application of this type of cellulose in biodegradable plastic films were limited. In order to modify the mechanical and chemical properties of cellulose, plasticization and blending with other polymers are used [44]. There have been a number of recent developments in the field of polymeric thermoplastic film and functional polymeric materials such as composite and composite films [45]. Cellulose-based biocomposite systems use cellulose as a reinforcement and/or matrix (host material) [45]. Cellulose fibers and derivatives are currently being used to make biopolymeric materials such as fillers and polymer matrices in biopolymer composites. Recent biocomposite research has enabled the replacement of petroleum-based polymers (PE and PP) with naturally generated biopolymers, such as cellulose and starch, and glass fibers with cellulose fibers.

Cellulose could also be used in wastewater treatment because it is naturally hydrophilic, it has been employed as an antifouling hydrophilic coating on membranes in order to increase the flow of the membranes and also the adsorption capability of cellulose-based functional materials is excellent for water treatment applications. It has been found that cellulose has a high adsorption capacity for pollutants after being subjected to appropriate chemical alteration on its surface, with the goal being the absorption of molecules with basic groups, particularly those containing significant concentrations of nitrogen, sulfur and oxygen [45]. In fact, as reported by Li et al. [46], cellulose, as well as other biopolymers such as lignocellulose, chitosan, chitin and lignin, shows a good absorption capability of heavy metal ions from aqueous solutions. Li et al. [46] collected the main studies related to cellulose properties, in particular, the capability of a cellulose-based copolymer to adsorb chromium (VI) and convert it in Cr (III) by means of the ultrasonication method [47]; the capability of cellulose aerogels to encapsulate iron oxides [48] and the employment of carboxylated cellulose derivatives for absorbing  $\text{Co}^{2+}$ ,  $\text{Cu}^{2+}$  and  $\text{Ni}^{2+}$  in aqueous solutions [49]. Dassanayake et al. [50] reported the use of cellulose-based materials and derivative (chitin and chitosan)-based materials in specific applications in which their absorption properties are employed, such as the removal of organic dyes and heavy metals, oil and solvent spillage cleanup and  $\text{CO}_2$  adsorption. Furthermore, cellulose-based functional materials are widely employed in biomedical fields such as drug delivery systems [51–53]; in cancer



therapy [54]; in bone regeneration [55,56] and in tissue engineering [57]. Demitri et al. [58], in fact, developed an innovative method for producing cellulose-based (CMCNa) foams, demonstrating an excellent biocompatibility profile with a good cell proliferation rate. When cellulose is linked with conductive polymers, it can form nanocomposites with high conductivity [59,60]. Shahbazi et al. [61] demonstrated that CMC modified by both photo and chemical cross-linking can improve surface hydrophobicity, the water barrier and mechanical properties of food packaging materials.

The applications of cellulose in the field of sensing material was also studied, including employing cellulose as a membrane for inkjet printing [62]; as CNT–cellulose composites on ammonia sensors [63]; as hybrid cellulose hydrogel used in release systems [64]; and as active mesoporous cellulosic materials with potential applications in optics, tissue engineering, chiral separation, functional membranes and biosensing [65]. Li et al. [46] also reported the employment of cellulose nanocrystal (CNC)–polymer nanocomposites as reinforcing material [66] or RGO–cellulose composites employed in storage energy filed as supercapacitors [67]. Furthermore, in the field of solar cells, cellulose-based composites were found to have a collocation, as studied by Bisconti et al. [68], that realized semi-transparent perovskite–polymer composites by employing hydroxyethyl cellulose and obtaining advantages in terms of ease of processing; improvement of visible transmittance; and enhancement of thermal stability, by preserving the photovoltaic performances of semi-transparent perovskite solar cells.

### 3.2. Lignin Traditional Sources

After cellulose, lignin is the second most predominant sustainable bioresource and it is found in abundance in wood, which is the world's primary supply. It is considered as a waste product in a number of industrial processes [69–71]. Because lignin is found in biomass combined with cellulose and hemicellulose, it serves as a restrictive issue in the bioconversion of wood, which is now under investigation [72,73]. Lignin is a naturally occurring component of wood and plant cell walls. Its polyphenolic chemical structure has been studied for industrial applications. Various delignification chemical procedures can extract lignin from wood, which has a structure and qualities unique to each plant species. In recent years, however, the chemical industry has concentrated on using lignin as a feasible renewable source for the production of innovative and ecological biomaterials. Its organization is complicated and hard to describe, making it difficult to blend into polymers, fibers and other materials [74]. Its hydrophilicity, polyanionic structure and nontoxicity make it an ideal choice for modifying membrane bulk and surface properties. Various lignin derivatives have been studied extensively for bulk modification of polymeric membranes. A preliminary material, such as the wood from which the pulp is made, is normally required for the extraction of lignin from several types of biomass. Lignin yield is influenced by numerous factors, including extraction process, reaction time, medium and temperature. The extraction of lignin from cellulosic pulp can be conducted via enzymatic, chemical and physical techniques. Acid hydrolysis, the kraft process, the lignosulphonate process and organo solvolysis are just a few of the chemical processes used to extract lignin. Acid hydrolysis is a process in which the lignin in wood pulp is dissolved using a mixture of argon and concentrated hydrochloric acid (HCl) [75]. The lignosulphonate procedure includes heating wood with sodium sulfite (aqueous) in acidic conditions to extract lignin. Functions include surfactants, additives, dispersants and flocculants [76].

Lignin is another cheap, renewable, biodegradable plastic preference, which improves matrix polymer compatibility and UV stability. Functional groups in matrix and lignin interact to create positive compatibility with both natural and manufactured polymers. The reinforcing activity and thermal stability of lignin have resulted in a high modulus value. Additionally, thermal insulation ratings are a bit higher than those of other materials [77].

Lignin has been extensively explored for its possible use as a sustainable alternative to petroleum derivatives and chemicals. Its polyphenolic structure makes it suitable for usage in phenolic monomers, polyurethane foams, polyolefins, adhesive resins, packaging



materials, unsaturated polyester, epoxy resins and material filler. Lignin can be chemically modified or incorporated into a matrix to provide it with new qualities. Banu et al. [78] selected several pretreatment methods (mechanical, chemical, biological, physical and physiochemical) able to extract lignin from diverse kinds of lignocellulosic biomass and reported the influence on medium and short chains of PHA yield for producing packaging materials, such as films, coatings, bags and bottles [78]. They also reported case studies concerning an increase in the production of PHA using genetically modified and engineered bacteria grown in lignin substrate. Furthermore, Banu et al. reported several synthesis processes aimed at producing lignin nanoparticles and their application in biocide systems [79], drug storage and delivery [80] and coatings [81].

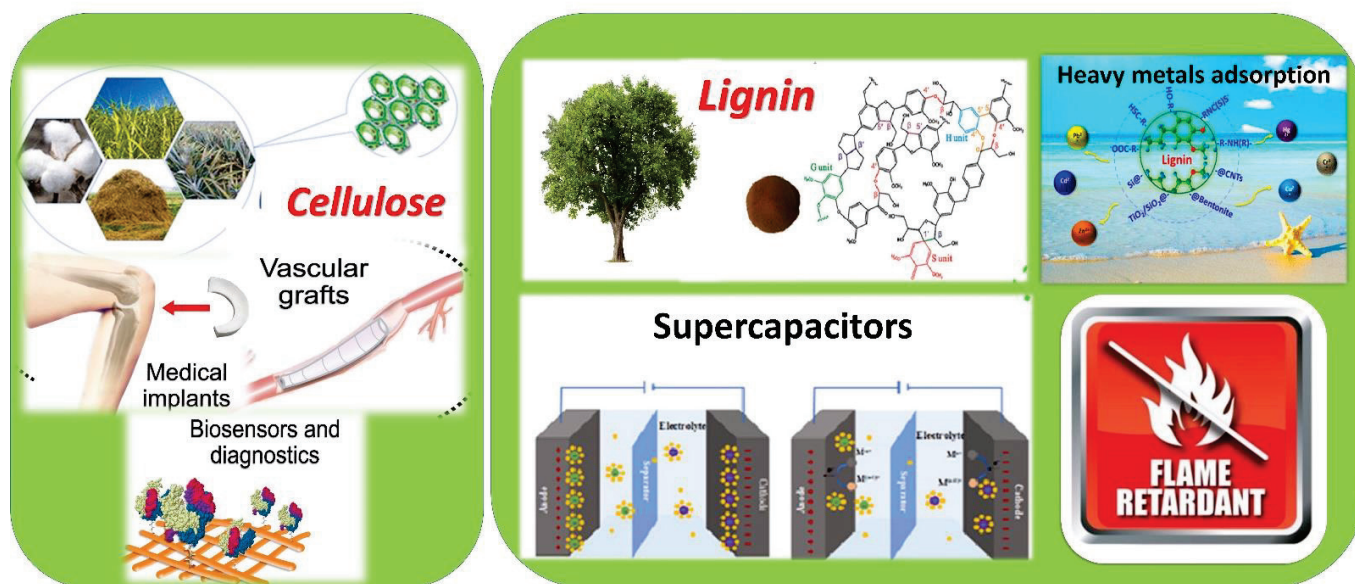
Lignin conversion to high quality products is critical to a biorefinery's economic success. These studies have established catalytic pathways for the production of aromatic chemical reagents and bio-based compounds, epoxy resins, carbon fibers, phenolic adhesive resins, hydrogels, 3D-printed biocomposite and polyurethane foams [74]. To make polymer matrix composites, the amorphous polyphenolic macromolecule Lignin is utilized as a filler. The composite's characteristics are enhanced by the inclusion of lignin. Antioxidant properties of lignin make it a good stabilizer for polymers. Because char inhibits the combustion and the heat release rate of polymeric materials, lignin can produce a significant quantity of carbonize residue when heated at a high temperature in an inert atmosphere. This property is fundamental to flame-retardant additives. Lignin can also influence the structure of thermoplastic polymers by acting as a nucleating agent during the crystallization process [82]. A potential alternative to inorganic fillers is represented by lignin-based nanoparticles due to phenolic groups and their UV resistance and antioxidant properties. Furthermore, it was demonstrated that lignin-based nanoparticles are able to improve the mechanical and physical properties of the final nanocomposite. Banu et al. [78] reported the main lignin nanoparticle synthesis processes. Thanks to the several reaction sites of lignin (hydroxyl, carboxylic acid, phenolic clusters) it is possible to cross-link it with the polymeric monomers (polyesters and polyurethanes; phenol-formaldehyde resins). For such a reason, the development of different lignin-based biopolymers is possible. What has been studied, in fact, is how a lignin presence minimizes the biodegradation of polyhydroxyalkanoates (PHA), increasing the resistance towards the microbial activity [83]; how lignin enhances the biodegradability of polyester, increasing the photoreactivity and the glass transition temperature [84]; how lignin is blended to polylactic acid (PLA) in order to obtain higher flame resistance [85]; and how lignin can substitute 30–50% of petroleum-derived polyols for the synthesis process of polyurethane, etc. [86,87].

Figure 2 reports a schematic overview of the main bio-based polymers from traditional wood sources.

### 3.3. Cellulose and Lignin Biopolymers from Wood Waste

One of the most promising challenges is the possibility of exploiting biomasses from wood as biosources of hemicellulose, cellulose and lignin. Lignocellulosic biomass represents, in fact, the highest amount of unused global biomass [88] and it is mostly composed of dry matter with the addition of oils, minerals and other components, which account for less than 10% [89]. Biomasses from wood wastes can be obtained by using different raw materials, such as forest and crop scraps, municipal solid waste, wood and paper wastes [89,90], which influence the quantity of each constituent of the biomass. Lignocellulosic material shows different amounts of each component, in terms of chemical composition, since they are usually altered by the environment [91]. In particular, based on the amount of biomass, woods can be classified into hardwoods and softwoods which contain, respectively, higher (78.8%) and lower (70.3%) amounts of cellulose and emicellulose and, reversely, there is lower lignin content in hardwoods (21.7%) than in softwoods (29.2%) [89]. Since the cellulose, lignin and hemicellulose amount depends on the kind of wood biomass, a suitable material should be chosen for the fermentation.

# Biopolymers: sources and purposes



**Figure 2.** Sources and purposes of biopolymers from traditional wood sources.

Plant biomass can, therefore, be used to produce high-performance functionalized polymers. Large-scale lignocellulosic biomass production will provide plentiful renewable feedstock for biomaterials with physical and chemical performances that are equal to or higher than those of petroleum-based mixtures, including lignin, cellulose and hemicellulosic polysaccharides [92].

Agro-waste recycling by composting and fertilizer manufacturing boosts global carbon emissions, according to data collected in Italy. Wastes from olives (OWC) and anaerobic digester-based compost (ADC), respectively, yielded 64 and 67 kg of CO<sub>2</sub> equivalent per milligram. Furthermore, each milligram of compost produced by re-composting and co-composting, ranging from 8 to 31 kg of CO<sub>2</sub>, was released [93].

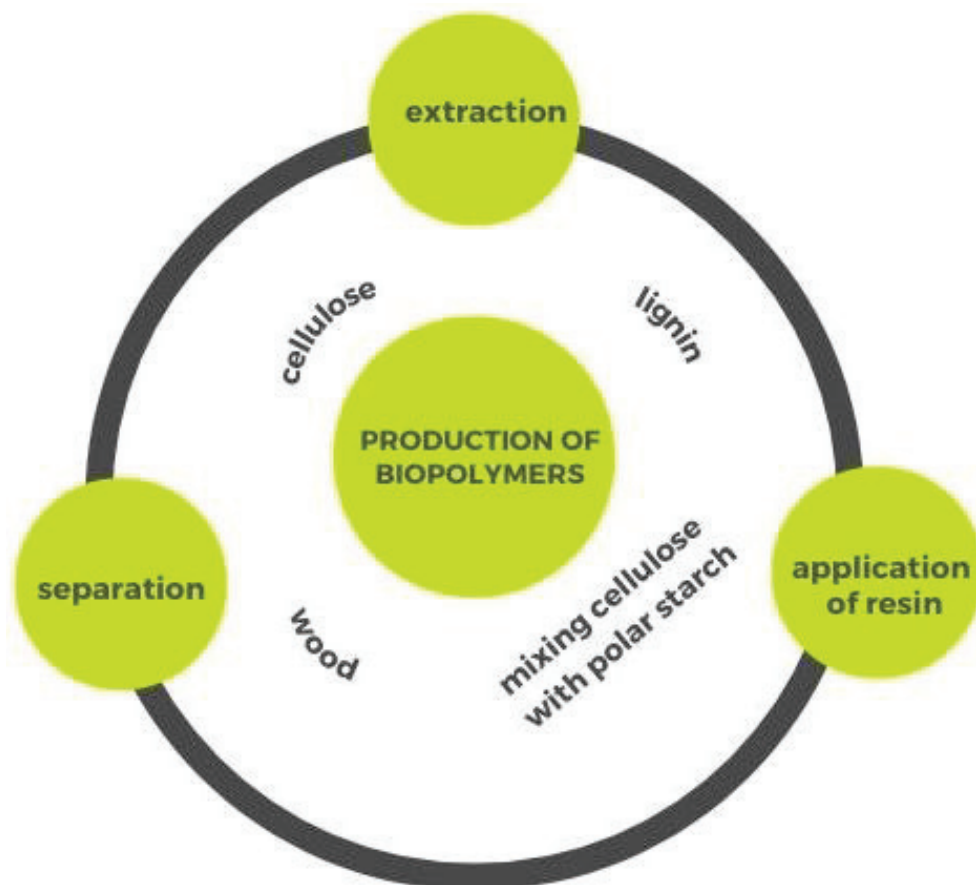
Particular attention was given to agro-waste cellulose for producing biopolymers in a critical review by Motaung et al. [94]. As discussed by the authors, even if several studies on the chemical modification of cellulose fibers were well known, very few discuss agricultural cellulose waste fibers. Sundarraj et al. [95] focused their study on the cellulose derived from agro-industrial residues as effective reinforcement for the building construction material industry. Lately, Urbina et al. [96] collected in their review the main case studies about the production of bacteria cellulose by employing agro-wastes (residues of agricultural products), focusing on the applications of this kind of biopolymer for environmental applications, optoelectronic and conductive devices, food ingredients and packaging, biomedicine and 3D-printing technology. El Achaby et al. [97] studied the employment of red algae waste as a natural resource for producing superior cellulose nanocrystals and their capability to act as strengthening filler.

The extraction of lignocellulose from waste materials represents a great environmental advantage since it avoids the problem that agro-waste can become a source of contamination.

Lignin can also be derived from wood waste. In fact, as demonstrated by Zikeli et al. [98], a lignin fraction was isolated from the wood wastes of a wood house producer for the production of lignin nanoparticles and then used for wood surface treatment. The developed coatings showed significant results after an artificial weathering test. Nevertheless, the extraction of lignin from wood waste is an open research question due to the difficulty of processing and the consideration of lignin as a waste material, i.e., an undesirable component in the manufacture of ethanol and paper, as reported by Parvathy et al. [99]. Thanks to its high thermal stability, biodegradability, antioxidant property, cross-linked

structure and UV absorption characteristics, lignin could be effectively employed in several applications to produce valuable materials.

Figure 3 reports a flow production of bio-based polymers from wood waste.



**Figure 3.** Flow production of bio-based polymers from wood waste.

### 3.4. PHAs' Traditional Sources

Microbial manufacturing techniques are used to produce polyhydroxyalkanoates (PHAs). PHAs are a class of aliphatic polyester which are naturally obtained in a sugar-based media by bacteria and operate as carbon and energy storage materials. They were the first biodegradable polyesters used in the plastics industry. Aliphatic polyesters are the easiest synthetic polymers to biodegrade [14].

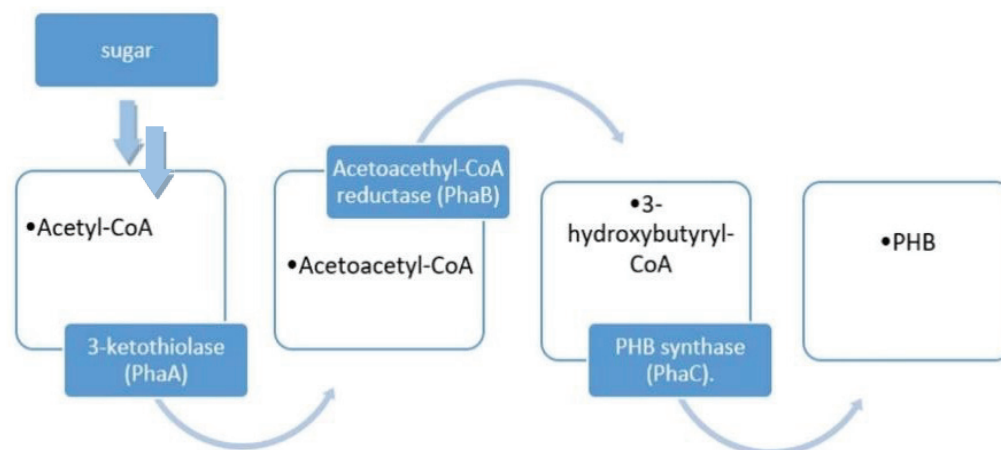
Synthesis of PHAs requires the use of different organisms, especially plants and bacteria, often employed for a large-scale production [100]. On the other hand, plants allow the producing of only small amounts (<10% (*w/w*) of dry weight) of PHA, since higher quantities of storage PHAs inside the plants lead to negative effects on the plants' growth [101]. Therefore, synthesis of PHA is actually carried out by bacteria, which naturally accumulate more than 90% *w/w* of PHAs in order to store carbon and energy during the metabolism of nutrients [102]. In particular, the accumulation of PHAs only occurs if bacteria grow with a reduction in oxygen, nitrogen and phosphorous, and an increase in carbon sources [103].

Once the soluble nutrients and intermediates are converted into insoluble PHA polymers, PHAs are stored in intracellular granules inside the cell. In this way, the osmotic state of the cell is preserved, which in turn means a secure storage of the nutrients without any losses through the cell membrane [104].

After the production, the PHA pellets are coated with a layer of proteins and phospholipids. This layer, mainly composed of a particular class of proteins, the phasins, changes both the size and the amount of PHA pellets [105].

Among PHAs, PHB is the first and commonly used, obtained by *Alcaligenes Eutrophorus* bacteria through the conversion of acetyl-CoA in the following three steps [106], reported in Figure 4:

1. First, starting with sugar, two molecules of acetyl-CoA are combined with 3-ketothiolase (PhaA) and acetoacetyl-CoA is obtained.
2. In the second step, acetoacetyl-CoA is reduced using Acetoacetyl-CoA reductase (PhaB) to obtain 3-hydroxybutyryl-CoA.
3. In the third step, PHB is obtained after the conversion of 3-hydroxybutyryl-CoA using PHB synthase (PhaC).



**Figure 4.** Synthesis pathway of PHB.

PHB is characterized by high hydrophobicity and can be produced at low temperatures. However, PHB is thermally instable when heated close to the melting of the material. The polymer exhibits essential thermoplasticity and degradability qualities in decomposition and other settings including sea water and, as a result, it has gained a lot of industrial attention [107–109]. PHB, a commercially accessible biopolymer, is one of the most attractive members of the polyhydroxyalkanoates family for the packaging of food. PHB is a polymer which should be modified using standard industrial polymer processing facilities. It also has strong mechanical qualities, such as strength and stiffness, that are equivalent to or better than some of the products (such as PP), as well as good barrier properties (similar to PET). PHB degrades in decomposition situations and in other conditions, such as in seawater [109]. Even though PHB is a good choice for green applications such as packaging, it has significant flaws that prevent it from being widely used in the packaging industry. Owing to room temperature crystallization and physiological ageing phenomena, PHB has a relatively high instability which increases over time. PHB also has a small processing range which makes it difficult to treat in some typical packaging applications, such as heat treating [110]. Another major impediment to its application in the packaging industry is its expensive cost, which continues to surpass EUR 5/kg. In this regard, the inclusion of a long-lasting, low-cost or hard filler might help mitigate the raw price rise by (a) minimizing the overall packaging cost and/or (b) decreasing the thicknesses required in standard packaging [110].

### 3.5. PHA from Wood Wastes

A particular problem that limits the use of PHAs is related to its cost of production, starting from the raw materials to the recovery process [111]. In particular, the price of PHA raw materials is strongly attributable to the carbon contribution; therefore, many efforts are currently made in order to replace traditional sources with derivatives of wood scraps [112]. A potential way to replace traditional sources was studied by Kumar [113], who used wood hydrolysates obtained using enzymatic hydrolysis of hemicellulose and



cellulose fermentable sugars. To use substrates of wood hydrolysates, the appropriate bacteria must be selected. In his study, Kumar [113] tested various colonies of different morphologies of bacteria for the production of PHA, using biomass substrates obtained from wood wastes. Results obtained allowed the production of PHA from paper paste and tannery effluent water samples with both using gram-positive and gram-negative bacteria, even if gram-negative bacteria were predominant.

PHA properties are mostly related to the length of the polymer chain. Long-chain (PHAs with  $C \geq 15$ ), medium-chain (PHAs with  $6 \leq C \leq 14$ ) and short-chain (PHAs with  $C \leq 5$ ) polymers are the three types of PHAs, considering the amount of carbons in the monomer units [114]. Short-chain polymers cannot be used if a high strength is required, because they are too brittle, high-crystalline and stiff. Medium chains have higher elastic modulus and, therefore, show lower brittleness, higher elongation at break and low-crystalline zones. On the other hand, these PHAs are less suited to high-temperature applications [115,116]. Films, fibers [117,118], foams, food additives, medical implants [119], medication delivery carriers, control release material, medical scaffolds for tissue regeneration [120], biofuels [121] and animal feeds all include PHA. PHA can be converted into chiral hydroxyalkanoic acids (HAs). PHA is a renewable substance that should be approved by the market [122]. The high manufacturing costs of PHA, which are at least three times higher than those of traditional materials, e.g., polypropylene (PP), polyethylene (PE) and related biopolymer polylactic acid, have contributed to their limited success [123]; therefore, as explained in previous paragraphs, alternative sources derived from wastes are currently under investigation, which allow for a strong decrease in the production costs.

PHAs showed a higher barrier and mechanical properties than PLA. Nevertheless, they only account for 1.4 percent of the biopolymer industry, even if their manufacturing is expected to double by 2023. PHA has comparable brittleness constraints to PLA, and its fragility can be reduced by the addition of a specific plasticizer. Though PHA has higher barrier properties than other biomaterials, the disadvantages in manufacturing costs are higher and its recycling process is still under development [109,124]. While PET recycling methods are well known and commonly employed [6], there are few studies of the mechanical and chemical recycling of PHA due to the high production costs and low yields of the recycling process [125]. PHAs can then be manufactured and processed for use in many applications, including packaging, thermoplastic products, protective coatings, nonwoven textiles, resins, sheets and activity enhancers, to name a few. PHAs, in contrast to other biomaterials, have a lot of promise for applications such as packaging because of their superior thermal-mechanical and protective qualities [109].

### 3.6. PLA's Traditional Sources

PLA is obtained from lactic acid precursors, which are produced from renewable sources such as sugar feedstock, straw maize, corn and food or agricultural waste products via fermentation [31,126].

Nowadays, fermentation represents the most common way to produce lactic acid, particularly if pure optical isomers are needed.

To obtain lactic acid, three main steps are required:

- In the first one, mono- and disaccharides are produced by the hydrolysis of carbohydrate sources.
- Then, lactic acid is attained by the fermentation of saccharides through lactic acid bacteria (LAB).
- Finally, the purity of lactic acid is obtained using further purification processes.

The main sources of starch which can be used in the first step are as follows: corn (maize), straw, tapioca (cassava), potatoes and other raw materials which, after hydrolysis, are transformed into mono- and disaccharides (Figure 5). The hydrolysis of starch was first carried out by using chemicals, but nowadays enzymatic methods are preferred. On the

other hand, only few bacteria are suitable for fermentation, because maltose results in the key product of enzymatic hydrolysis.

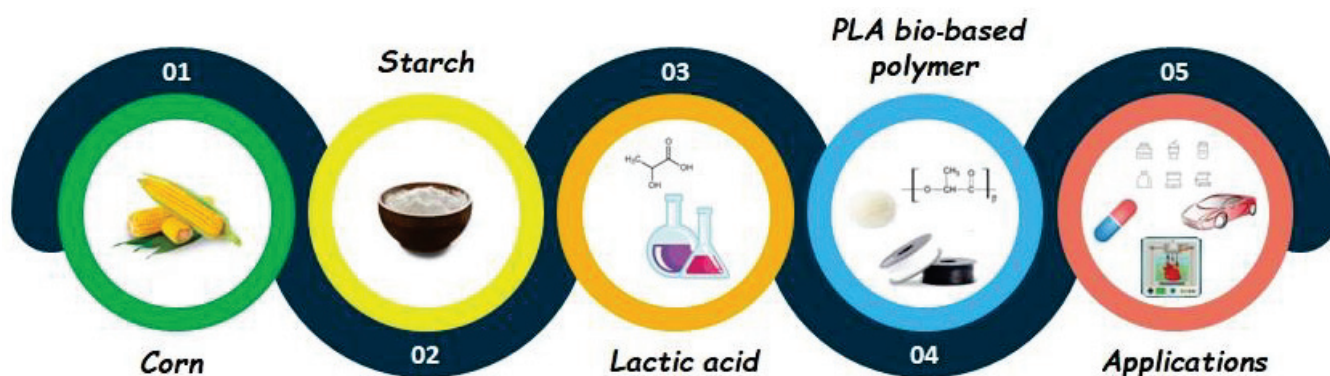


Figure 5. PLA from feedstocks to the final product.

Furthermore, sucrose-derived raw materials can be used for the fermentation of lactic acid. Conversely, lactose has a limited use because of the low quantities which can be found in readily available whey, and it also requires a high purification of whey [127,128].

Afterwards, to produce lactic acid, different families of bacteria (LAB) can be used (e.g., *Lactobacillus*, *Streptococcus* and *Pediococcus*), which are characterized by high productivity in very narrow pH ranges [114] and allow the producing not only of lactic acid, but also of other organic acids during fermentation. Therefore, in order to focalize the production to lactic acid, decreasing as much as possible the number of other byproducts, the pH is kept between 5.5 and 6.5, thanks to particular bases such as hydroxides or carbonates.

To select the right raw material for the fermentation, some parameters must be considered, such as the availability, the price and, above all, the purity, which influence the field of application of PLA. Mono- and disaccharide traditionally employed mainly derive from the conversion of different substrates and are:

- Glucose and glucose syrups deriving from the conversion of starch with enzymes such as glucoamylases;
- Maltose, derived from the starch enzymatic conversion with amylases of malt;
- Sucrose, obtained as a byproduct or intermediate of cane sugar;
- Lactose, derived from mil whey, a natural substrate of several lactic acid bacteria.

### 3.7. PLA from Wood Wastes Sources

Lactic acid, traditionally used in several fields (chemical, cosmetic, food industries and pharmaceutical), is a hydroxycarboxylic acid characterized by two optical isomers [129–131].

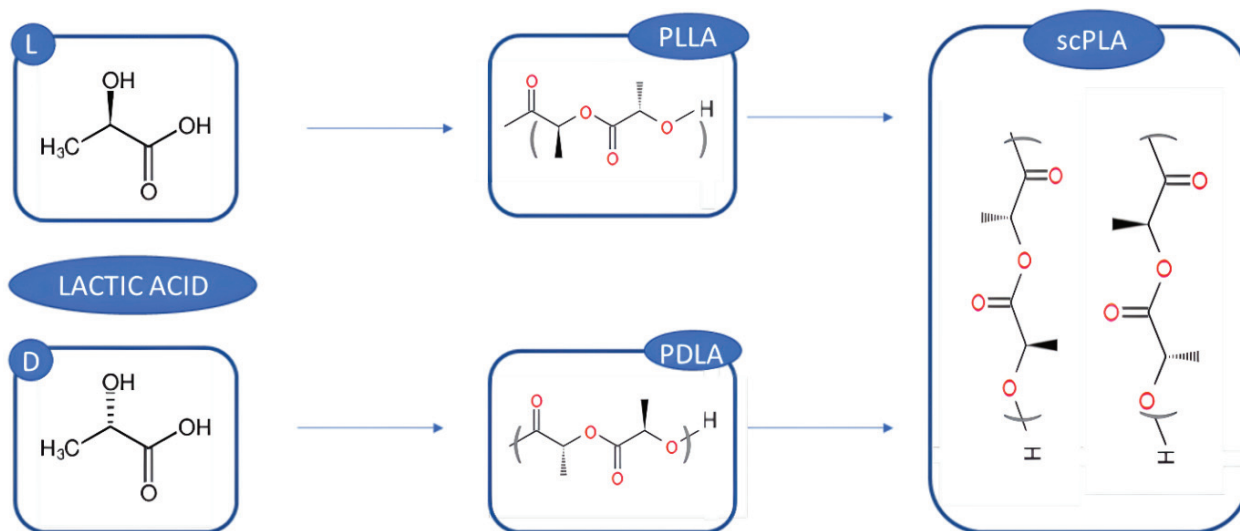
Recently, the use of optically pure lactic acid (l- or d-isomer) was studied as a building block for the polylactic acid (PLA: PLLA and PDLA). As already mentioned, PLA is one of the most eco-friendly biomaterials and can be used as a green alternative to traditional fossil polymers [132,133]. Nevertheless, the traditional ways to produce PLA cause the subtraction of important sources from the food chain; therefore, many efforts are currently made to obtain PLA from scraps, thus producing a biopolymer of the third generation.

An innovative way to optimize PLA mechanical properties, using optically pure lactic acid isomers, involves the mixture of pure PLLA and PDLA, thus obtaining Sc-PLA, a stable stereo-complex with good mechanical properties, higher hydrolysis resistance compared to the use of a single enantiomer [134], a melting point  $\sim 50$  °C higher than the pure materials and higher biodegradability [135].

The pure isomers can be obtained through microbial fermentation [136,137], although there are many issues which hinder the scale-up of the production from laboratory to industries, such as the high cost, the raw materials and the nutrient sources [136,138]. In order to solve these problems, second-generation feedstocks, which involve lignocellulosic



biomass from agro-industrial or forest sources, are nowadays studied as inexpensive renewable sources for lactic acid production and the consequent microbial fermentation to produce PLA isomers [139,140] (Figure 6).



**Figure 6.** Synthesis pathway of PLA.

Lignocellulosic feedstocks, although seemingly a promising way to replace traditional sources for PLA production, are characterized by a complex structure; therefore, their conversion in optically pure lactic acid is still a challenge [141]. Furthermore, all the feedstocks must be pretreated in order to remove the lignin, thus allowing the enzymes to access the cellulose. Furthermore, inhibitions of the enzymatic catalysis can occur due to the pretreatment of the material; the inhibition mainly consists of the slowdown of both cellulose hydrolysis of lignocellulosic biomass and of the microbial growth [142].

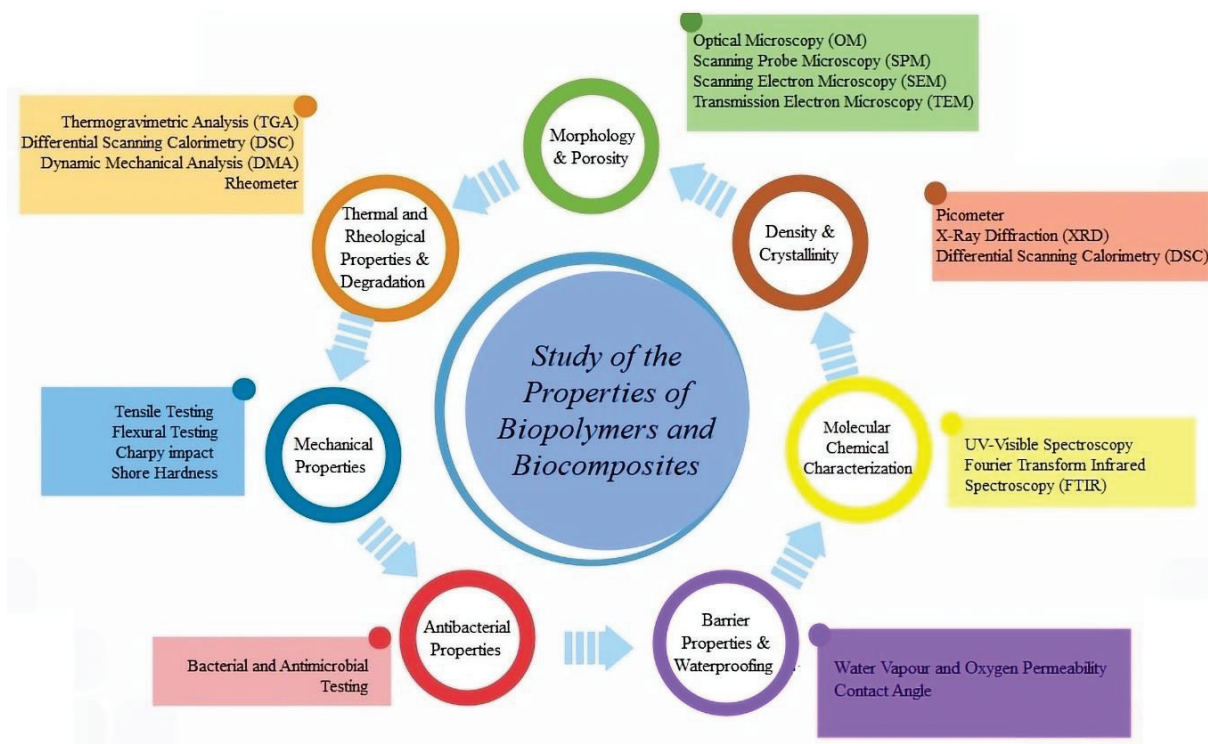
Another drawback which occurs with the use of lignocellulosic scraps is that they are composed of a heterogeneous mixture of sugars, which cannot be easily used at the same time.

The main bacteria often used to produce lactic acid are lactic acid bacteria (LAB). Nevertheless, their use is still not widespread due to many factors, such as the requirement of specific nutrients, the low resistance to acid and the difficulties with co-utilizing glucose and xylose [143]. Recent improvements in bacterial D-lactic acid involve a genetic modification [144,145]. Some of the recent advanced processes, aiming to increase D-lactic production, include fed-batch fermentation, continuous fermentation with cell recycling and integrated membrane fermentation [146].

The industrial and commercial employment of lignocellulose to produce lactic acid is still an issue. In fact, various processing steps are necessary to convert the lignocellulosic biomass to monomeric sugars that are then fermented to obtain lactic acid. The conventional processes used to produce lactic acid from wood biomass involve four main steps: First, the lignocellulosic raw material needs to be pretreated, to break the structure of the biomass; after pretreatment, enzymatic hydrolysis occurs, thus obtaining fermentative sugars through hydrolytic enzymes. The third step consists of fermentation, which allows the metabolization of sugars to lactic acid, usually via LAB. Finally, in the fourth step, the lactic acid is collected and purified. It is worth highlighting the important role of the pretreatment of lignocellulosic biomass, since the native lignocellulose has a low enzymatic susceptibility due to the association of cellulose and hemicellulose with lignin [147,148]; therefore, the efficiency of the pretreatment plays a key role for the subsequent saccharification via hydrolytic enzymes. Finally, if the pretreatment is too strong, toxic materials can be released with a consequent inhibition of the microbial metabolism and growth [149].

#### 4. Main Properties of Bio-Based Polymers and Biocomposites

Generally, the most investigated features for newly developed biofilms and biocomposites are morphological, thermal, mechanical, rheological, water absorption and antibacterial properties [40,150–153]. Their characterization involves the use of specific analytical techniques, some of which are discussed in this section and shown in Figure 7. Specifically, microscopy (Scanning Probe Microscopy SPM, Scanning Electron Microscopy SEM and Transmission Electron Microscopy TEM) is utilized for the measurement of morphology and porosity, the picometer is useful for density measurement, X-ray Diffraction (XRD) allows one to determine crystallinity, spectroscopy (UV-Visible and Fourier Transform Infrared Spectroscopy FTIR) is employed for molecular chemical characterization, thermal analysis (Thermogravimetric Analysis TGA, Differential Scanning Calorimetry DSC and Dynamic Mechanical Analysis DMA) is employed for the measurement of thermal properties and the study of thermomechanical degradation, water and oxygen adsorption is considered for the evaluation of barrier properties and Tensile and Flexural Testing, the Charpy impact test and Shore Hardness are utilized for the measurements of mechanical properties, etc. [40,150–155]. Usually, the environmental impact and biodegradability of biopolymers and biocomposites are evaluated according to American Society for Testing and Materials (ASTM) standards [153].



**Figure 7.** Some of the characterization methods commonly used to study the main properties of biopolymers and biocomposites.

The mechanical qualities of biopolymers include strength [15], ductility [156], deformability [157], stress [158] and durability [159]. Mechanical properties are usually detected using a dynamometer and by choosing the geometry, the load cell and the test speed according to the appropriate standard test method. Six replicates for each measurement are usually performed, in order to obtain statistically relevant results. Durability tests are carried out on a climate chamber, following the ageing procedure described in the standard test method. The degradation in the flexural modulus, in the strength of the composites and in the interlaminar strength are evaluated after the ageing.

The intrinsic qualities of a polymer are determined by its structure and/or chemical composition [160]. Density is a fundamental feature of polymers, varying between classes

and constituents [160] and often measured using a pycnometer. In comparison to petroleum-derived polymers, most biodegradable polymers have higher densities.

Though crystallinity isn't considered a self-reflective feature, it affects many other qualities. High-crystalline biopolymers are more resistant to dissolution than low-crystalline biopolymers. A single biopolymer's crystallization degree affects its melting and glass transition temperatures [160], as well as affects solubility; with greater compactness of the structure, there is a lower chance of dissolution [160]. In order to evaluate the crystallinity of the material, both X-Ray diffraction and Differential Scanning Calorimetry are used.

Scientific studies show that the tensile strength, and thus the crystallinity and solubility of biopolymers, can be increased by inserting different kinds of fillers into the polymer matrix, obtaining biocomposites [161]. For example, both PLA and polyolefin-based composites containing wood fillers have similar mechanical properties [161]. Generally, the addition of wood filler to the polymer matrix has different effects on tensile strength. In fact, the measured values arise from the wood species used as fillers and the amount added, the composites' processing methods and the quality of the PLA [161–163]; an additional cause of the reduced mechanical properties of the polymer composites with wood filler is also due to the poor adhesion at the interface between the filler and polymer matrix [154]. This phenomenon is especially evident from high-magnification images obtained using scanning electron microscopy (SEM) on both biofilms and biocomposites and/or biofilaments for 3D printing. For example, some authors report that the transparent films produced have pores and cracks that facilitate the passage of water vapor and gases [150]. Alternatively, other works highlight in SEM images of composites in general, or composite filaments for 3D printing, an irregular, rough, outer surface with several points of discontinuity due to the addition of wood filler, which is often non-homogeneously distributed in the polymer matrix, with the formation of particle aggregates [154,164]. Furthermore, the presence of voids and poor interfacial adhesion between layers (observable in composite sections and often on 3D prints as defects between layers) are attributed to the different polarity between the biopolymer (which has a non-polar surface) and the wood fillers (which have a polar surface) [154,164]. Instead, SEM results often indicate correct dispersion of the filler in the polymer matrix and an improved hydrophobic nature compared to the neat polymer film [151]. Overall, the results depend on the physical and mechanical properties of the polymers and fillers, concentration of the parts, filler geometry, polarity, compatibility, addition of plasticizers and type [151,152,154,165,166]. However, most studies show that, overall, the stiffness of polymeric composites with wood fillers increases, as does the crystallinity compared to pure polymer, and scientific research has focused on improving structural properties, such as through the use of plasticizers [161]. XRD and DSC analyses are useful in order to evaluate the effect of the addition of a plasticizer to different kinds of biopolymers. As reported by Greco et al. [155], the mechanical properties of PLA can be tailored by the addition of different green plasticizers. The plasticization of PLA can be carried out via the extrusion of the polymer with a specific amount of different bio-based plasticizers (e.g., neat cardanol, epoxidized cardanol acetate (ECA) and poly(ethylene glycol) (PEG 400)). Results evidenced the plasticization effectiveness of the different additives in terms of the reduction in glass transition temperature: compared to neat PLA, which showed a T<sub>g</sub> of 60 °C, the addition of PEG 400, cardanol and epoxidized cardanol involved a decrease in the T<sub>g</sub> to 17.5 °C, 16.9 °C and 22.3 °C, respectively. On the other hand, the addition of the plasticizer can influence the degree of crystallinity of the polymer: faster crystallization and an increase in the degree of crystallinity was found for PLA plasticized by PEG, compared to PLA plasticized by cardanol derivatives. Furthermore, mechanical properties were influenced after plasticization, which involves a decrease in the stiffness of the polymer. In particular, as reported in Table 3, different results were obtained if the plasticized polymer was amorphous or semicrystalline; neat amorphous PLA had a Young modulus of 1740 MPa. When PLA was plasticized with cardanol derivatives and an amorphous structure was detected after plasticization, a good efficiency occurred;

however, the thicker crystals formed during crystallization of PLA with PEG and cardanol derivatives led to a high increase in the stiffness of the material.

**Table 3.** Young's modulus (MPa) in relation to the added plasticizer and the initial polymer structure.

Plasticizer	Young's Modulus	Amorphous Plasticized PLA (MPa)	Semicrystalline Plasticized PLA (MPa)
PEG 400		581	962
Cardanol		691	1156
Epoxidized cardanol		353	961

Xie et al. [167] studied the influence of plasticizing agents (glycerol and tributyl citrate, TBC) on the stability and water absorption of samples based on poplar wood flour and PLA for 3D printing. Two different weight concentrations were tested for each plasticizer agent, 2% and 4% wt. Good compatibility between filler and polymer, good interfacial adhesion and good mechanical properties were obtained using TBC at 4% wt. [167]. In contrast, Zhang et al. [168] developed high-yield esterified lignocellulose nanofibers (LC-NFs) from lignocellulose (LCs) by swelling with a deep eutectic solvent lactic acid/choline chloride (LA/ChCl DES) (100 °C for 3 h), followed by mechanical colloidal grinding. LC-NFs/PLA composites were obtained via direct mixing, and the morphological, structural and mechanical properties were studied. The authors showed a significant improvement in compatibility at the LCNF/PLA interface highlighting the potential of natural wood-derived nanofibers for making bio-based composites [168]. However, there is an impact of plasticizers on tensile strength up to a threshold value, because the tensile strength decreases with an increase in the amount of plasticizer, particularly in the case of films produced from starch [169]. Mechanical properties are lower for wood-PHA polymers, and even more so for starch. Young's modulus, tensile strength and stiffness decrease for wood-PHA composites, while strain at break is higher [161,170]. Scientific interest in PHA polymers with wood is growing due precisely to their sustainability and interesting and modular mechanical properties [161,170]. For example, Mehrpouya et al. [171], in their work focused on 3D printing, report some examples where the combination of PHAs and natural wood-derived additives (i.e., fibers, lignin, fibrillated nanocellulose, cellulose nanocrystals, etc.) makes remarkable improvements to the strength and microstructural features of pure PHAs. Wu et al. [172] achieved 20% higher parameters of tensile strength at break (7%) and Young's modulus (65 MPa) than pure PHAs by developing a wood-PHA composite (PHA-g-MA/TPF) with polyhydroxyalkanoate engaged with maleic anhydride (PHA-g-MA) and palm fiber treated with coupling agents (TPF) [172]. In addition, the use of wood-PHA composites also offers the possibility of reducing costs compared to pure PHA, while still using a sustainable material [170,172].

Thermoplastic starch (TPS) is the least-used material for the development of wood plastic composites (WPCs), compared to materials such as PLA and PHAs; it has poor mechanical and water barrier properties, and difficult processability [31,161]. Yet, wood filling to the polymer-based specimen results in improvements in tensile strength at break, elastic modulus and elongation at break, and these changes are even more pronounced than with other biodegradable polyesters, due to greater compatibility between the two materials (starch and wood) due to the hydrogen bonding of OH groups [161,173]. Zeng et al. [174] investigated the consequences of three additives (plasticizer, cross-linking agent and blowing agent) on the mechanical properties of a foamed composite made of starch, wood fibers and polyvinyl alcohol (PVA), using a predictive model. The work shows how using the appropriate amount of plasticizer (glycerin/NaOH) can reduce the crystallinity of starch and increase the compatibility between the different components and the tensile strength of the ultimate material (maximum range of 5.91–6.12 MPa) [174].

Dorigato et al. [175] improved the final mechanical properties of fully biodegradable composites laminated with starch and beech wood by impregnating them with



poly(ethylene glycol) (PEG) and consolidating via hot pressing [175]. Alternatively, Harusani et al. [169] analyzed various quantities of two plasticizers (sorbitol and glycerol) in different concentrations by weight (30%, 45% and 60%) on cornstarch-based composites, obtaining better mechanical performance with the use of 30% sorbitol: increased tensile strength (13.61 MPa) by 46% and unchanged elastic modulus [169].

Unlike PLA and PHAs, research on starch-based bio-based composites has focused more on understanding the increase in mechanical performance due to different types of wood fillers, and not on increasing the adhesion of the interface and material compatibilities through the use of plasticizing agents [161,174]. For example, Curvelo et al. [176] measured a 100% increase in tensile strength and 50% increase in elastic modulus, compared to pure thermoplastic starch, after the addition of *Eucalyptus urograndis* pulp fibers to the composite in 16% wt. concentration [176].

Until today, the use of polymeric degradable matrices for the production of composites has also sometimes been reduced due to their poor moisture and gas barrier properties and limited stability [161]. Barrier, rheological and thermal properties are in fact also of great importance, and are closely related to the structural and mechanical properties already mentioned. For example, the glass transition temperature ( $T_g$ ) of different pure materials exhibits great differences (i.e., Starch 31–98 °C, PLA 45–60 °C, PHA –4–8 °C) [161], and the addition of wood fillers makes different changes to this and to the viscosity and processability of wood–bioplastic composites [154,169].

Polymer barrier qualities are strongly linked to their capability to allow the interchange molecules that have small size. The form, orientation and crystalline nature of the diffusing molecule, as well as the degree of polymerization and polymer chains, influence the barrier qualities. No material is totally resistant to ambient gasses, water vapor or to other generic natural compounds. In terms of ability of the biopolymer to permeate water or oxygen molecules, generically it is possible to identify three classes: permeable to both water vapor and oxygen; low ability to permeate water vapor but high barrier against oxygen; or contrastingly, less permeable to oxygen but very permeable to water vapor [161]. Among all bioplastics, starch-based composites usually exhibit higher hydrophobicity and low water resistance [31,161,174]. For this reason, several scientific studies have also been conducted to improve the barrier features of starch-based materials by modifying the structural properties through natural fillers of different origins. Curvelo et al. [176], in their starch-based composites developed by the addition of wood pulp (*Eucalyptus urograndis* at 16% wt.), also measured a significant improvement in water absorption properties. The new composites were conditioned by maintaining relative humidity values of 43 and 100%, and a temperature of 25 °C, and the water absorption values were found to be almost halved, unlike the values of neat starch [176]. Miranda et al. [177] studied changes in the structural and absorption properties of flexible thermoplastic films of corn starch, following the addition of cellulose nanocrystals (CNC) as reinforcement, and measured a significant improvement in the stability and barrier properties of pure starch [173]. Alternatively, Chen et al. [178] investigated the addition of nanoscale cellulose particles of different types (bamboo, cotton linter and sisal) to starch samples, using different content (0–10 wt%), and obtained better water vapor barrier properties with the use of bamboo nanocellulose, among others [178].

PLA and PHA-based composites, on the other hand, have higher intrinsic water resistance properties than starch [161]; however, the water barrier properties of biocomposites, to which a wood filler is added, decrease as the percentage content of wood particles/fibers increases and improvements are needed [178]. Da Silva et al. [178] studied the reaction of Struktol used as an adjuvant on the final features of wood–PHB biocomposites, showing a slight improvement in water absorption properties only for the sample containing 20% of wood filler [178]. Wu et al. [172] showed lower water absorption of the developed wood–PHA composite (PHA-g-MA/TPF) with polyhydroxyalkanoate grafted with maleic anhydride (PHA-g-MA) and palm fiber treated with coupling agents (TPF), compared to the corresponding PHA/PF composite [172]. In addition, Song et al. [179] focused their work



on increasing the water vapor barrier characteristics of PLA films by using nano-cellulose fibers (NCFs) modified by adding hydrophobic molecules onto the NCFs to increase the compatibility between NCFs and PLA during mixing. Paper water vapor transmission rate (WVTR) tests were conducted following different operating parameters and with different weight coatings showed that the coating of NCF/PLA innovative samples reduced the WVTR (up to 34 g/m<sup>2</sup>/d) [179].

Some important properties of the main types of bio-based wood composites are reported in Table 4.

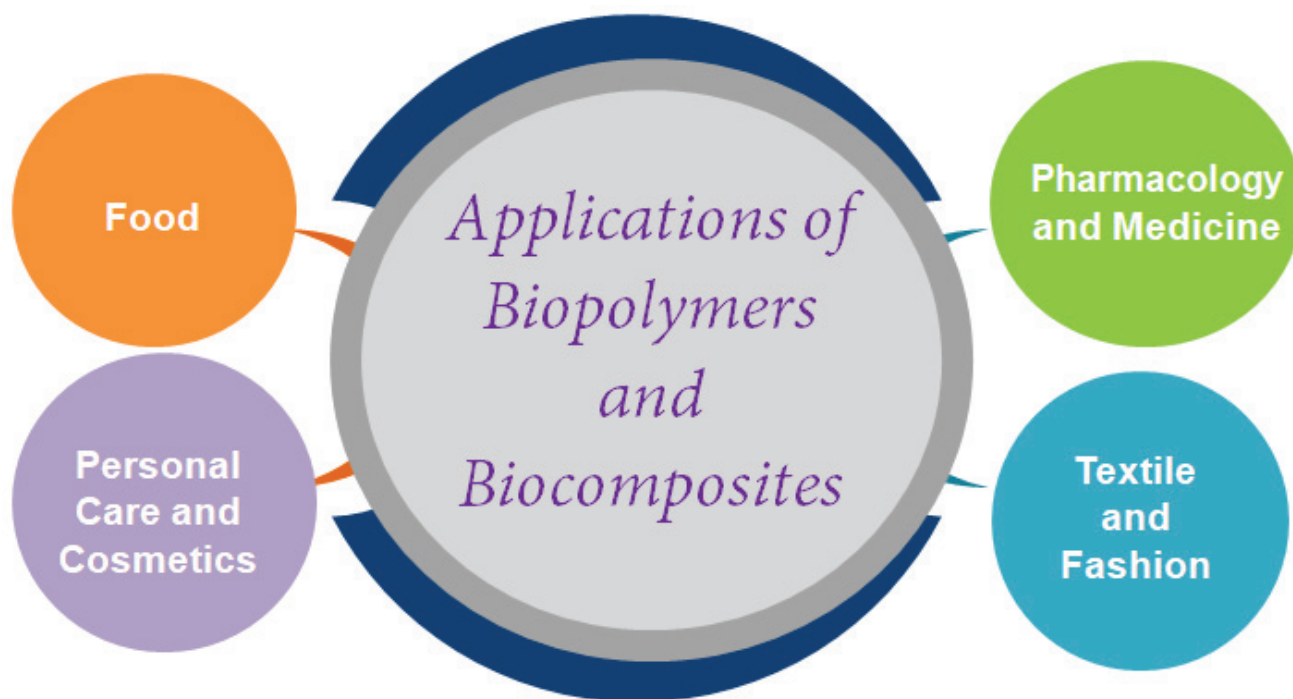
**Table 4.** Some features of the main types of bio-based wood composites.

Bio-based Polymers	Density (g/cm <sup>3</sup> )	Tensile Strength (MPa)	Young's Modulus (GPa)	Elongation at Break (%)	Tg (°C)	Tm (°C)	Ref.
Wood–starch	1.29–1.41	14–36	0.7–4.8	1.1–2.9	−33–−26	83.1–130.3	[161,169,176,177,180–184]
Wood–PLA	1.26–1.41	30–71	1.2–8.9	1.0–3.1	52.0–60.8	143.4–169.0	[12,154,161–163,181,185–189]
Wood–PHA	1.23	13–65	0.4–6.1	0.5–7	−2.2–−6.0	56.8–158.7	[161,170,172,190,191]

## 5. Market Scenarios and Applications of Biopolymers and Biocomposites

The global bioplastics market is growing significantly due to an increased focus of manufacturers and users on the use of sustainable products, social and economic factors and the more restrictive legislation implemented in recent years [192]. For example, the United Kingdom (UK) introduced a new tax from April 2022 on plastic packaging (called “Plastic Packaging Tax, PPT”), locally produced or imported, containing less than 30% reused plastic by weight, to increase the use of biopolymers, recycling and sustainable development. Aside from this, the tax in Italy has been postponed to the year 2023 [193]. Overall, estimates report a likely increase in bioplastics production from the current USD 9.2 billion to USD billion by the year 2026 [194]. Among different geographic areas, Asia is the largest production center (producing 46% compared to total bio-based polymers produced worldwide), followed by Europe (26%) and North (17%) and South America (10%) [27,194]. Europe is the geographic area where research activities on bioplastic development are most concentrated, and biopolymers are especially used in food packaging (60%) followed by other industries such as agriculture (13%), consumer goods (9%), coatings and adhesives (9%), textiles (5%), automotive (1%) and all others (3%) [27,192]. Several elements influence the market scenarios of bio-based polymers, and consequently also the application areas: the availability of raw materials and renewable sources, the ease of scalability and the production process, the biodegradability features (i.e., durability, degradation conditions and end-of-life treatment) and costs [27]. By cost it is not only meant that which is associated with the recovery of the raw material, but also that of its processing which must be suitable for market demands so that users prefer biopolymers to traditional polymers of petrochemical origin, which usually possess good mechanical and structural properties and often low costs [192,195]. Cost becomes a significant factor, especially in areas known for the development of single-use plastics for food packaging or low performance. Usually, bioplastics are more expensive than petroleum-based plastics. In addition, bioplastics also often have a higher density, causing further cost increases. However, there are exceptions when prices are compared at the product level; redesign and specific material properties can result in raw material savings, for example, due to the higher stiffness of PLA compared to PS, rigid PLA products can be reduced in thickness or the use of additive techniques, which involve adding natural or recycled fillers to the polymer matrix, can further reduce the initial cost of the biopolymer [12,154,196,197]. For example, in the European market, Nylon 6 (virgin polymer, PA6) costs around EUR 2.5–4.0/kg, while low-density polyethylene (LDPE) costs EUR 1.1–2.7/kg and PET costs around EUR 1.60–5.0/kg [193,198]. The price of petroleum-derived plastics is likely to rise further, due to rising raw material and energy costs in recent months. However, the cost per EUR of bioplastics has decreased significantly in recent years; for example, PLA, which had a cost of EUR 7/kg in the 1990s has dropped to

about EUR 1.6–2.5/kg in 2022 [198]. Rising oil prices have thus made the cost of bio-based plastics similar to that of thermoplastics of synthetic derivation; moreover, recent progress in the development of biopolymers has caused an increase in demand in different industrial sectors, such as food [110,199–201], pharmaceutical and medical [45,202–205], personal care [206,207], cosmetics [206,208] and textile and fashion [12,209,210] (Figure 8).



**Figure 8.** Main application of biopolymers and biocomposites.

### 5.1. Biopolymers in Food Industry

Generally, several applications of biopolymers sintered and extracted from animals, plants or marine organisms are known in the literature in the food field. Among these, extracts from plant species, such as cellulose, lignin, polyphenols and essential oils have been extensively used for different aims [211]. For example, they are used for the fabrication of edible films and coatings [212]; these constitute a thin layer of soluble bioactive compounds that is applied to the surface of foods or between layers for different purposes such as extending food shelf life, improving quality or acting as a barrier for oxygen, water and solutes [153,213]. Specifically, these compounds are extracted using conventional or innovative methods for the development of edible films and coatings [214]. Improved mechanical and barrier properties of these films have been achieved through the use of composites (derived by combining multiple biopolymers and layers or by adding fibers and fillers to the biopolymer, such as laponite, montmorillonite, sepiolite, palygorskite, etc.) or biopolymer nanocomposites (i.e., by the addition of nano  $\text{SiO}_2$ -x, nano ZnO, nano oxide and nano  $\text{TiO}_2$ , etc., to the polymer) [214]. Typically, these biopolymer-based coatings, in addition to being biodegradable and nontoxic, may have a natural microbial action; others can serve as a carrier for antioxidant or antimicrobial biopolymers [215]. In fact, better antibacterial, antifungal or antioxidant properties of edible films have been achieved by incorporating active compounds (i.e., antimicrobials, antioxidants, dyes, flavors and nutraceuticals) into filmogenic solutions [216]. For example, organic acids and essential oils (EOs), which have intrinsic antimicrobial and antioxidant properties, have been added to biopolymers derived from cellulose and derivatives [217], i.e., thyme, clove, rosemary, oregano, cinnamon and tea oils [211]. Polyphenols (i.e., phenolic acids, flavonoids and proanthocyanidins) are other important active compounds added to polymeric edible films for their antioxidant, aromatic and antimicrobial properties [211]. Scientific studies have shown that nanoma-

materials can also be used to control the release of bioactive agents incorporated into edible packaging, improving its durability [212]. Several reviews have been written in recent years highlighting the progress made by research in the development of new biopolymer-based edible films/coatings [212,214,216]. For example, Das et al. [214] emphasized in their work the use of non-thermal techniques (such as cold plasma, ultrasound, UV irradiation, high-pressure homogenization) and the addition of nanomaterials (nanoparticles of silver, zinc oxide, titanium dioxide, montmorillonite) to improve the structural (color, thickness, intermolecular bonds, particle size), water and oxygen barrier properties and mechanical features of edible films. Kumar et al. [212] reported the different natural materials used for either pure or composites and, for each, reported the preparation techniques of edible films/coatings and the antimicrobial, antioxidant, physical and sensory properties, also highlighting any critical issues, recent applications and commercial products. In the last few years, the growth of concern for the environment has led to a preference for the use of agricultural and industrial scraps for the development of edible films/coatings that provide a feasible alternative to the use of plastics or bio-based materials of natural origin or from biomass, in favor of sustainable development and the circular economy [212,216,218,219].

Biopolymers are mainly used in food packaging [110,153,220]. The causes mainly can be attributed to the problems that have emerged from the disposal of traditional petroleum-derived materials and the mandatory regulations now existing and increasingly developed in recent years in food packaging, as well as the significant increase in the cost of petroleum products, due to various reasons [213]. Food packaging is supposed to extend the conservation life of all sorts of foods by storing and protecting them from oxidative and microbiological degradation. Next-generation food packaging must have certain durability and good mechanical and barrier properties, as well as aesthetic functions related to marketing [219]. Among the natural polymers most commonly used for food packaging, cellulose and derivatives are usually treated, processed, melted and dried. Chitosan, for example, is an antibacterial biopolymer. The encapsulation of chitosan has an important place in obtaining food and packaging with a long shelf life, as demonstrated in a recent study by Baysal et al. [221]. Other biopolymers used for food packaging are PLA, PHA, PBAT or blends of biopolymers, such as a starch-based blend with PLA, PHB, PHAs, PVAs, PCL, PVOH, etc. [149]. Torres-Giner et al. [222], after a classification of polymers used extensively in food packaging (divided into petroleum materials, and into non-biodegradable and biodegradable products), focused the paper on materials such as PLA, PHAs, PBAT, PBS, bio-based PET, cellulose and derivatives of different origins. Similarly, as for edible films, for food packaging the best mechanical, physical and antimicrobial barrier properties have been achieved through the use of multilayers [223] and by adding active ingredients (usually in the form of a sachet or covering on the packaging material embedded in the surface of the material itself) [211] or even nanometer fillers to biopolymers (nanofillers) [224]. In the former case, traditional multilayer packaging comprising polymeric layers (i.e., PE, PET, HDPE, PP, EVO, EVOH, PA, etc.) and inorganic layers (i.e., Al, SiO<sub>x</sub>, etc.) [223] is being replaced by biocompostable packaging called “active” packaging, which has a reduced environmental impact. Wang et al. [200] report several advanced examples of biodegradable active multilayer packaging composed of sandwich-like substances. These are based on polymer matrices of different natures (among them, methylcellulose has often been used) and active components, such as polyphenols, potassium sorbate, lysozymes, etc. [200]. The authors in the paper examine different production techniques, focusing on a mathematical pattern for release control of the active component of the packaging [200]. In the second case, nanofillers (classified into nanoplatelets, nanofibers and nanoparticles), having nanometric structures and antibacterial properties, are added to biodegradable and environmentally friendly polymers in so-called “smart” packaging (which allows the freshness of the food to be checked in real time), which has recently been added to “active” packaging (in which the added substances protect the food from UV rays, oxygen and microbes interacting directly with the food) on the market. The addition of nanofillers to green polymers produces a number of benefits, such as reduced risk of spreading pathogens,

improved food quality, reduced material waste and sustainability [224,225]. Among these, the most widely used nanofillers are antibacterial nanoparticles (such as Ag, ZnO, Cu/CuO, TiO<sub>2</sub>, Fe<sub>2</sub>O<sub>3</sub>, Fe<sub>3</sub>O<sub>4</sub> and MgO), mesoporous particles, graphene and carbon dots, added in green polymers [224,225]. However, recent research highlights the importance of prior evaluation of the safety of metal oxide nanoparticle additives (through migration testing), and biocompatibility with polymers to minimize the risk of toxicity [225].

The scientific literature has developed several studies on natural fiber-based biopolymers too. Different lignocellulosic fibers, such as wheat straw, linen fibers, jute, coconut, kenaf and olive pomace, have been investigated for their usefulness as fillers [110]. Even if there is an increasing awareness of environmentally friendly packaging, it is necessary to use bio-based and sustainable packaging solutions. Next-generation packaging (often called 4G) combines all these properties with environmental friendliness, through the use of innovative materials [226]. The commercial and technological potential of industrial by-products for the production of next-generation (active and smart) food packaging to support zero waste activities has been known for some years now. For example, Bhat et al. [227] used lignin derived from oil palm black liquor scrap added to sago palm (*Metroxylon sagu*) films for the development of food packaging. After extraction and solubilization in DMSO, the lignin was added in several percentages (from 1 to 5% *v/w*) to the starting solution to form the packaging films. The authors in their work demonstrated an increase in the mechanical properties, resistance to thermal sealing, water vapor permeability, solubility and thermal stability of the films obtained using lignin produced from waste [227]. Sánchez-Safont et al. [110] tested the use of local lignocellulosic scraps (rice husk, almond shell and sea grass) as additives for the development of PHB/fiber composites for use in food packaging. Improved mechanical and permeability properties of the composites were obtained, as well as improved thermoforming ability of the films. Tumwesigye et al. [228] used bitter cassava waste to develop a low-cost food packaging film, turning environmental waste into a sustainable resource. Specifically, two different transparent films were produced and tested by the authors, from intact and decorticated bitter cassava; among these, the former were shown to have the best mechanical qualities and structural and higher thermal stability, while leading to a higher yield with a 16% reduction in waste [228].

### 5.2. Biopolymers in Pharmacology and Medicine

Biopolymers and their composites are also used in the pharmacological and medical fields due to their biodegradability, cost-effectiveness, wide availability, processability and especially biocompatibility with human organs and tissues [153,205,229]. For all of these qualities, they are used, for example, as materials for transporting pharmaceutical molecules and substances (such as enzymes, antibiotics and antineoplastic drugs, etc.), in ocular, dental, nasal and other systems [153,229,230]. Biopolymers from different sources and that have pharmaceutically active ingredients (capable of influencing the drug delivery process), are used for the production of Drug Delivery Systems (DDS), usually in the form of microcapsules, microspheres, nanospheres, hydrogels, nanogels and liposomes [153,229]. In this area, polysaccharides have been exploited for years mainly for their properties that can form linkages with proteins and lipids. Among the polysaccharides, cellulose (together with starch) is the most widely used in pharmacology and medicine, in general [203,231]. The use of cellulose (and its derivatives) for the development of DDS has expanded due to its exceptional properties, such as its ability to absorb and retain water, its biocompostability and its structural characteristics that allow the loading of specific molecules [203]; in addition, the possibility of producing nanocellulose from wood pulp, along with the use of advanced technologies (such as 3D printing), has opened up an opportunity for the development of innovative materials for pharmacological applications in recent years [231]. For example, Yu et al. [231] used ethylcellulose and hydroxypropyl methylcellulose for the development of a drug delivery device, prepared automatically using 3D printing, that was capable of providing a linear release profile of acetaminophen. Specifically, hydrophobic ethyl cellulose delays the initial rapid release of the drug, while hydroxypropyl



methylcellulose swells into a gel after contact with the dissolution medium, releasing the drug for an extended period [231]. Biopolymers are also used in the medical field for the production of hydrogels and nanogels, materials suitable for wound healing [203,232,233]. Several hydrogels and biopolymer-based formulations have emerged from the addition of therapeutic and bioactive agents such as antimicrobials, growth factors, antioxidants, antiseptics, etc., that facilitate the skin healing process [203,232,233]. Wound-healing materials use hydrocolloids such as foam, gel or spray [153,203,232]. Many researchers have invented several methods for the development of cellulose, hemicellulose and lignin from agricultural wastes, such as from sugar beet, cashew nuts, sago waste, waste from the cotton ginning industry, etc., using a variety of techniques [234,235]. Among them, Cui et al. [236] tested aqueous-based hydrogels from cellulose derived from industrial durian rind waste, fortified with glycerol to obtain organohydrogels, which proved to be suitable for antimicrobial wound dressing, even under extreme thermal conditions (for example,  $-30\text{ }^{\circ}\text{C}$ ). In their work, Amores-Monge et al. [237] investigated the opportunity to build a high-profit market that focuses on the production of products (i.e., cellulose, hemicellulose, lignin and enzymes) with biomedical applications from waste obtained from pineapple (*Bromeliaceae family*); among them, the proteolytic enzyme bromelain was found to have an essential application in skin reconstitution [237].

Properties such as biocompatibility, biodegradation and noncytotoxicity also make biopolymers excellent candidates for use in implantable medical materials and scaffolds [153,238,239]. Implantable medical devices are predominantly used to simulate and replace a human structure that has been damaged, or to support normal body function or control trunk posture [239,240]; scaffolds, on the other hand, are used to facilitate hard and soft tissue regeneration in tissue engineering [153,238,241,242]. Bones, heart, eyes, ears, knees, hips, etc. constitute the anatomical parts that are undergoing integration and replacement with polymeric medical implants the most [153]. Teeth, bones and the cartilage of humans, in contrast, are the human parts most concerned with the application of scaffolds [243,244]. Today, traditional materials such as metals and ceramics have been almost completely replaced by biopolymers, due to the immunological rejection by the body that they can cause; biopolymers, on the other hand, exhibit biocompatibility, good degradability, renewability, anti-toxicity and antibacteriability throughout their life cycle [202,238,239]. For the fabrication of medical devices, the materials usually used are polylactic acid (PLA), polyglycolic acid (PGA), poly(lactic-co-glycolic acid) (PGLA) and polycaprolactone (PCL) [153,243], also known as nanocomposites (nanotubes, nanoparticles and nanofibers) [12]. These polymers have also been combined to produce implants. For example, copolymers of PLA and PGA have often been used in place of their respective homopolymers in orthopedic applications (e.g., for the creation of plates or screws for the treatment of fractures and the filling of bone defects) [153]. Alternatively, PLA and PET have been combined to produce prostheses for vascular surgery [153]. The development of Additive Manufacturing (AM) techniques has also affected the biomedical and tissue engineering fields: 3D printing of tissues, organs and body parts using biopolymer nanocomposites has been made possible by the spread of some easy and low-cost 3D-printing techniques, which also have the advantage of printing complex geometries [12,202,240]. For example, S. Bartlett [245] reports on the 3D printing of a bioresorbable tracheal splint that was successfully implanted in the patient and was produced by combining TC images of the airway with the 3D printer. Gross et al. [246] report that 3D printing has also been used for the reproduction of anatomic parts needed for the preliminary study of surgical procedures, for example, to create a calcified aorta with 3D printing for the study of plaque removal surgery, to optimize the removal of bony outgrowths on a shoulder and for the study of drug delivery into the lungs of a premature infant [246]. The fabrication of scaffolds for bone tissue regeneration requires good biomimetic and bioactive properties; therefore, micro- or nanoparticles, comparable to the natural mineral components of bone, are often added to traditional polymers, such as tricalcium phosphate (TP), hydroxyapatite (HA), calcium phosphate cements (CPC), monetite or brushite [246]. For example, in their work,



Corcione et al. (2017, 2018, 2019) [242,243,247] explored the possibility of using FFF printing to develop an osteogenic bone graft based on hydroxyapatite (HA) and polylactic acid (PLA). PLA, PGA, PCL, etc. have also been used together with other biopolymers, such as hyaluronic acid, cellulose, collagen, gelatin, elastin and fibroin, for the synthesis of tissues such as adipose, ligaments, blood vessels, liver, cartilage, pancreas, spinal cord and bone regeneration [153,244]. For example, collagen was often mixed with PLA, PGA, PCL, etc., to improve wettability and interaction with biological substrates [248,249].

### 5.3. Biopolymers in Personal Care and Cosmetics

Biopolymers are also used for the production of personal care products and cosmetics [207,250]. The first group includes sanitary napkins, panty liners, feminine hygiene pads, baby diapers and adult incontinence items, which are aimed at improving peoples' lifestyles [239]. These are products that possess multiple layers, each with specific functions, and are composed of different types of synthetic or natural raw materials [239]. So-called "Superabsorbent polymers" (SAPs) constitute the main absorbent component of the layered structure of a personal care product (such as diapers or sanitary napkins for babies and adults). SAPs are a group of cross-linked hydrophilic polymers that are suitable for absorbing aqueous solutions, such as blood and urine, in a short time while keeping the skin dry and limiting infection or irritation [239]. For example, the most well-known SAPs used in personal care are polysaccharide SAPs (such as cellulose, hemicelluloses, bamboo, etc.), in addition to protein SAPs [250]. The demand for hygiene and personal care products will increase in years to come; conversely, environmental concerns over the use of products that are not fully biodegradable are growing, and there is an increasing need to instigate research activities aimed at producing non-toxic and eco-friendly products. Vivicot (Sanicot s.r.l., Prato, Italy) was the first line of compostable pads marketed in Italy (2011), made of pure organic cotton and certified by Certiquality [251]. Subsequently, the company Intimaluna (Borgo San Giovanni, Lodi, Italy) marketed fully compostable "Ecoluna line" feminine hygiene pads made of mater-bi and 100 percent organic cotton, menstrual cups and other washable feminine products [252]. Also in this area, scientific research is focusing on the recycling of raw materials for the production of new materials. For example, Lacoste et al. [253] produced a bio-based superabsorbent (bio-SAP) polymer for nappies from recycled cellulose. The authors demonstrated that they can recover and reuse waste packaging cellulose through a chlorine-free process, which transforms it into carboxymethylcellulose (CMC) that is cross-linked with citric acid afterwards [249]. In recent years, biopolymers have also been used in cosmetics due to their low cost, durability, versatility and biodegradability, and especially after the discovery of the presence of microplastics in aquatic ecosystems released from facial masks and scrubs, mascaras and lipsticks, shampoo, etc. [254].

Cellulose and derivatives, polyhydroxyalkanoates, etc., are used in cosmetics for different purposes: for nanoparticle preparation or fragrance delivery, hair care, skin care and make-up [207]. Generally, biopolymers such as collagen, keratin and chitin are mostly used in this sector. For example, the major application of collagen hydrogels in cosmetics is to act as fillers for wrinkles and correctors of other skin defects [206]. Chitosan, on the other hand, is used more for hair care, and is included in shampoos, hair dyes, styling lotions, hair sprays and gels, or it is included in oral hygiene products, for the purpose of preventing tooth and gum disease [206]. Keratin, on the other hand, is mainly used for hair conditioning [206]. However, these substances are often used in combination with other polymers or biopolymers (such as cellulose and hydroxyethyl cellulose) or collagen hydrogel can be cross-linked with starch dialdehyde, tannic acid, squaric acid, PEG and other substances [206]. Examples of cosmetic actives derived from fish, meat, dairy and agro-industrial waste exist in the literature; products obtained from waste are a viable alternative to the usual plant extracts commonly used in cosmetic formulations, as they are effective, inexpensive and biosustainable [208,255]. In the area of industrial-waste-derived biopolymers, Meyabadi et al. [256] studied the reuse of waste cotton fibers

and their conversion to cellulose powder for various applications, including cosmetics. The authors showed that spherical cellulose nanoparticles (less than 100 nm), produced through enzymatic hydrolysis followed by ultrasonic treatment, do not undergo significant changes in structure and major properties, providing a viable sustainable alternative [256]. In their work, Bongao et al. [257] highlighted the potential of micro- and nanocellulose extracted using conventional methods and synthesized from Pili pulp waste to replace the mineral ingredients used in cosmetics. Innovative research in the field of green chemistry and sustainable production now involves many companies. For example, the company Anomera (Montreal, Canada) has been awarded a 1.7 million grant to carry out in its research labs research into the replacement of environmentally harmful plastic microbeads with biodegradable, environmentally friendly, high-performance ingredients for cosmetics and skin care, made with cellulose derived from wood waste from the paper industry [258].

#### 5.4. Biopolymers in Textile and Fashion

Biodegradable polymers also support the textile and fashion industry, by reducing raw material processing energy, materials and costs of sourcing, production and disposal [209]. In fact, the textile industry is one of the world's most contaminating sectors, after petroleum; the greatest environmental damage comes from the production, processing and dyeing of the textiles [210]. This sector therefore needs alternative raw materials more than others; biopolymers are a responsible choice. Bio-based textiles, which must contain at least 20% renewable carbon, include natural materials and natural, synthetic or regenerated fibers [209,210]. Natural biopolymers are produced from polysaccharides (i.e., cellulose, lignin, etc.), as well as proteins and lipids of plant or animal origin [30]. In fact, natural fibers also come from plant sources (i.e., hemp, wool, cotton, etc.) [30,209,210]. Of these, cotton (together with silk and wool) is the most widely used in clothing production, as it meets aesthetic and wearability standards [30]. Synthetic and regenerated fibers used in textiles come from bacterial activities (such as polyhydroxyalkanoates, PHA) and from the synthesis of natural raw materials (e.g., polylactides, polyglycols, polycaprolactones, etc.) [30]. In recent years, the need for sustainable production has shifted the textile industry's attention not only to materials such as organic cotton (grown without the use of pesticides, fertilizers or other chemical products), but also to the production of synthetic biodegradable textile fibers, referred to as "biodegradable nonwovens." Among them, the biopolymers that find the most applications used in fiber spinning in the modern biodegradable textile industry are in fact polylactic acid (PLA), butyric acid (PHB), valeric acid (PHV), caprolactone (PCL), etc. [12,209].

Other examples of biodegradable nonwovens include those made of natural cellulosic fiber, cotton (cotton/cellulose or biodegradable cotton/co-polyester), the biodegradable nonwovens mentioned above and laminates (composites in which a layer includes a nonwoven fabric) [30]. In fact, composite materials derived from the addition of natural source fibers (such as hemp, flax, cellulose acetate, jute, pineapple, kenaf and many others) to synthetic biopolymers are often used [30]. For example, Gabryś et al. [259] transformed viscous, commercial, nonwoven fabrics by adding PLA (in addition to potassium nitrate,  $\text{KNO}_3$ ) to impart fertilizing properties to fabrics used in modern agricultural mulching. Many technologies are being developed to manufacture biosynthetic fibers from biomass and waste materials derived from agriculture, forestry and even food [30,201,209,260,261]. Several examples of biodegradable synthetic fibers are already commercially available, such as the biodegradable PLA thermoplastic Ingeo (company NatureWorks LLC, Blair, NE, USA) or Modal biofilters and Tencel/Lyocell products produced from beech and eucalyptus wood pulp (Lenzing Aktiengesellschaft, Lenzing, Austria) [209]. Commercial biodegradable products are often enriched with innovative antimicrobial agents to produce workwear, home wear, sportswear, etc. [209]. Early instances of biosynthetics using novel feedstocks such as algae, fungi, enzymes and bacteria are also available [30]. For example, the use of bacterial cellulose (produced by microorganisms) is growing in the textile sector, compared to the traditional use of plant cellulose, because it is sustainable, is biodegradable,

does not pollute and can also be dyed, resulting in an attractive textile surface that meets current market research [210]. In addition, Patti et al. [30] report on several bio-based and sustainable textiles produced by large known companies from microbes, algae and bacteria for the production of jackets, shoes and other garments. The search for new biodegradable materials and the continuing evolution of traditional textile production methods, which usually involve the use of chemicals, have also led to the emergence of 3D-printing techniques [12]. Additive Manufacturing (AM) techniques enable the development of innovative and sustainable models for the textile industry and are being employed recently by major brands to shift the production of shoes, clothing, jewelry and other accessories to environmentally friendly and green materials [12,30]. Companies using 3D-printing techniques and biopolymers such as PLA and softened PLA (along with other materials such as, e.g., Ninjaflex, BendLay, TPE [262,263]), have resulted in nonwoven fabrics with improved morphological and structural properties compared to traditional polymers. For example, Loh et al. [264] developed and studied three different polymer composites for the textile world morphologically and mechanically, using a different combination of PLA, nylon and polyesters, and direct extrusion of the materials.

Table 5 reports the main properties and applications of bio-based polymers and biocomposites.

**Table 5.** Main properties and applications of some bio-based polymers and biocomposites.

Bio-Based Polymers and Biocomposites	Properties	Applications	Source	Ref.
Starch-based	Low toxicity, biocompatibility and equivalent mechanical and degrading qualities.	Packaging applications, wound-healing materials, drug delivery system, agricultural foils, textiles, automobiles and transportation, construction and building materials, etc.	Plants	[215,261,265–267]
Cellulose-based	Microbial characteristics, exceptionally crystalline, chemically and thermally stable.	Packaging applications, edible films and coatings, hydrogels for personal care products, medical device, biosensors, drug delivery system, electronic and energy devices, cosmetics, textiles and nonwovens etc.	Plants	[45,250,256,259]
Lignin-based	Biodegradability, hydrophilicity, low-cost, nontoxicity, thermal and mechanical stability	Food packaging, applications in biocide systems, adhesive resins and foams, filling materials, construction and building materials, biomedical applications	Plants	[154,205,227,231,268]
PLA-based	Higher mechanical strength, degradation in nature either through reduction or by M, excellent barrier and permeability properties.	Packaging applications, 3D printing, biomedical applications, scaffolds and medical implants, textiles and nonwoven fabrics, agricultural applications, etc.	Fermentation/ conventional chemistry followed by polymerization	[12,226,238,264,269]

Table 5. Cont.

Bio-Based Polymers and Biocomposites	Properties	Applications	Source	Ref.
PHA-based	Biocompatible, biodegradable, considerable elastomeric with excellent elongation at break.	Food packaging and coatings, scaffolds and medical implants, textile industry, etc.	Bacterial fermentation	[205,207,270,271]

## 6. Conclusions

During the last decade, the production of bioplastics has mainly increased with the intention of decreasing the harmful effects of synthetic polymers on the environment. This study summarizes the current developments in the definition, classification, production, properties and applications of bio-based materials, particularly focusing on wood-waste derivatives. The third-generation feedstock, obtained from food scraps, algae biomass and industrial or municipal waste, is the most promising category. It represents an innovative solution to the questions related to the consumption of sources from the food chain, according to the circular economy approach. Among the numerous varieties of organic wastes, agro-industrial and forestry wastes, which are generated in massive quantities each year, represent an unjustifiable environmental and economic scenario. The production of the main classes of biopolymers, starting from wood scraps, was reported in this work. Although lab-scale experiments showed promising ways to produce biopolymers from lignocellulosic wastes, the industrial production is still not sufficiently profitable, due to the high cost of the processes. Nevertheless, thanks to the relevant benefits obtained by the use of wood scraps, several studies regarding the development of genetically modified bacteria for the hydrolytic fermentation are under development, in order to overcome all the issues related to the high cost of the production processes.

Finally, in this work it was reported that wood waste can be used not only as a source for the production of third-generation biopolymers, but it can also be employed as a reinforcement for bio-based matrices, thus obtaining biocomposites with improved mechanical performances, as well as enhanced antibacterial, gas barrier and migration properties. Therefore, following both a descriptive and an analytical methodology, the main properties of bio-based polymers and biocomposites were discussed in this review and a comparison of thermal and mechanical properties of polymer matrices and wood biocomposites was reported.

**Author Contributions:** Conceptualization, C.E.C.; investigation and writing—original draft preparation, F.F., R.S., D.F., M.M.A. and C.E.C.; review, editing and supervision, C.E.C. and A.G. All authors have read and agreed to the published version of the manuscript.

**Funding:** Innovative doctoral scholarship from the Development and Cohesion Fund (FSC)—Extract Plan Research and innovation 2015–2017.

**Institutional Review Board Statement:** Not applicable.

**Informed Consent Statement:** Not applicable.

**Data Availability Statement:** The data presented in this study are available on request from the corresponding author.

**Conflicts of Interest:** The authors declare no conflict of interest.

## References

- Sikorska, W.; Musioł, M.; Zawidlak-Węgrzyńska, B.; Rydz, J. End-of-Life Options for (Bio)Degradable Polymers in the Circular Economy. *Adv. Polym. Technol.* **2021**, *2021*, 6695140. [CrossRef]
- Lionetto, F.; Esposito Corcione, C. An Overview of the Sorption Studies of Contaminants on Poly(Ethylene Terephthalate) Microplastics in the Marine Environment. *J. Mar. Sci. Eng.* **2021**, *9*, 445. [CrossRef]



3. Storz, H.; Vorlop, K.D. Bio-Based Plastics: Status, Challenges and Trends. *Landbauforsch. Volkenrode* **2013**, *63*, 321–332. [CrossRef]
4. González-Barreiro, C.; Rial-Otero, R.; Simal-Gándara, J.; Astray, G.; Cid, A.; Mejuto, J.C.; Morales, J. Starch-Derived Cyclodextrins and Their Future in the Food Biopolymer Industry. In *Starch-Based Polymeric Materials and Nanocomposites Chemistry, Processing, and Applications*; CRC Press: Boca Raton, FL, USA, 2012; pp. 167–182.
5. Striani, R.; Stasi, E.; Giuri, A.; Seiti, M.; Ferraris, E.; Esposito Corcione, C. Development of an Innovative and Green Method to Obtain Nanoparticles from Carbon-Based Waste Ashes. *Nanomaterials* **2021**, *11*, 577. [CrossRef] [PubMed]
6. Ferrari, F.; Esposito Corcione, C.; Montagna, F.; Maffezzoli, A. 3D Printing of Polymer Waste for Improving People’s Awareness about Marine Litter. *Polymers* **2020**, *12*, 1738. [CrossRef] [PubMed]
7. Ferrari, F.; Striani, R.; Minosi, S.; de Fazio, R.; Visconti, P.; Patrono, L.; Catarinucci, L.; Esposito Corcione, C.; Greco, A. An Innovative IoT-Oriented Prototype Platform for the Management and Valorization of the Organic Fraction of Municipal Solid Waste. *J. Clean. Prod.* **2020**, *247*, 119618. [CrossRef]
8. Sánchez-Gutiérrez, M.; Espinosa, E.; Bascón-Villegas, I.; Pérez-Rodríguez, F.; Carrasco, E.; Rodríguez, A. Production of Cellulose Nanofibers from Olive Tree Harvest—A Residue with Wide Applications. *Agronomy* **2020**, *10*, 696. [CrossRef]
9. Esposito Corcione, C.; Ferrari, F.; Striani, R.; Visconti, P.; Greco, A. Recycling of Organic Fraction of Municipal Solid Waste as an Innovative Precursor for the Production of Bio-Based Epoxy Monomers. *Waste Manag.* **2020**, *109*, 212–221. [CrossRef]
10. Ballinas-Casarrubias, L.; Camacho-Davila, A.; Gutierrez-Méndez, N.; Ramos-Sánchez, V.H.; Chávez-Flores, D.; Manjarrez-Nevárez, L.; González-Sánchez, G. Biopolymers from Waste Biomass—Extraction, Modification and Ulterior Uses. In *Recent Advances in Biopolymers*; Intechopen: London, UK, 2016; pp. 3–18.
11. Ibrahim, N.I.; Shahar, F.S.; Sultan, M.T.H.; Md Shan, A.U.; Safri, S.N.A.; Yazik, M.H.M. Overview of Bioplastic Introduction and Its Applications in Product Packaging. *Coatings* **2021**, *11*, 1423. [CrossRef]
12. Fico, D.; Rizzo, D.; Casciaro, R.; Esposito Corcione, C. A Review of Polymer-Based Materials for Fused Filament Fabrication (FFF): Focus on Sustainability and Recycled Materials. *Polymers* **2022**, *14*, 465. [CrossRef]
13. Chan, J.X.; Wong, J.F.; Hassan, A.; Zakaria, Z. *Bioplastics from Agricultural Waste*; Matthew Deans: Oxford, UK, 2021.
14. Elsayy, M.A.; Kim, K.H.; Park, J.W.; Deep, A. Hydrolytic Degradation of Polylactic Acid (PLA) and Its Composites. *Renew. Sustain. Energy Rev.* **2017**, *79*, 1346–1352. [CrossRef]
15. Reichert, C.L.; Bugnicourt, E.; Coltelli, M.B.; Cinelli, P.; Lazzeri, A.; Canesi, I.; Braca, F.; Martínez, B.M.; Alonso, R.; Agostinis, L.; et al. Bio-Based Packaging: Materials, Modifications, Industrial Applications and Sustainability. *Polymers* **2020**, *12*, 1558. [CrossRef] [PubMed]
16. Gontard, N.; Sonesson, U.; Birkved, M.; Majone, M.; Bolzonella, D.; Celli, A.; Angellier-Coussy, H.; Jang, G.W.; Verniquet, A.; Broeze, J.; et al. A Research Challenge Vision Regarding Management of Agricultural Waste in a Circular Bio-Based Economy. *Crit. Rev. Environ. Sci. Technol.* **2018**, *48*, 614–654. [CrossRef]
17. Ghanbarzadeh, B.; Almasi, H. Biodegradable Polymers. In *Biodegradation-Life of Science*; Intechopen: London, UK, 2013; pp. 141–185.
18. Raza, S.; Zhang, J.; Ali, I.; Li, X.; Liu, C. Recent Trends in the Development of Biomass-Based Polymers from Renewable Resources and Their Environmental Applications. *J. Taiwan Inst. Chem. Eng.* **2020**, *115*, 293–303. [CrossRef]
19. Shah, T.V.; Vasava, D.V. A Glimpse of Biodegradable Polymers and Their Biomedical Applications. *E-Polymers* **2019**, *19*, 385–410. [CrossRef]
20. Karande, R.D.; Abitha, V.K.; Rane, A.V.; Mishra, R.K. Preparation of Polylactide From Synthesized Lactic Acid and Preparation of Polylactide From Synthesized Lactic Acid and Effect of Reaction Parameters on Conversion. *J. Mater. Sci. Eng. Adv. Technol.* **2015**, *12*, 1–37. [CrossRef]
21. Hernández-García, E.; Vargas, M.; González-Martínez, C.; Chiralt, A. Biodegradable Antimicrobial Films for Food Packaging: Effect of Antimicrobials on Degradation. *Foods* **2021**, *10*, 1256. [CrossRef]
22. Tan, B.H.; Muiruri, J.K.; Li, Z.; He, C. Recent Progress in Using Stereocomplexation for Enhancement of Thermal and Mechanical Property of Polylactide. *ACS Sustain. Chem. Eng.* **2016**, *4*, 5370–5391. [CrossRef]
23. Rosen, T.; Goldberg, I.; Venditto, V.; Kol, M. Tailor-Made Stereoblock Copolymers of Poly(Lactic Acid) by a Truly Living Polymerization Catalyst. *J. Am. Chem. Soc.* **2016**, *138*, 12041–12044. [CrossRef]
24. Nakajima, H.; Dijkstra, P.; Loos, K. The Recent Developments in Biobased Polymers toward General and Engineering Applications: Polymers That Are Upgraded from Biodegradable Polymers, Analogous to Petroleum-Derived Polymers, and Newly Developed. *Polymers* **2017**, *9*, 523. [CrossRef] [PubMed]
25. Brizga, J.; Hubacek, K.; Feng, K. The Unintended Side Effects of Bioplastics: Carbon, Land, and Water Footprints. *One Earth* **2020**, *3*, 45–53. [CrossRef]
26. A Straightforward Explanation of Biodegradable vs. Compostable vs. Oxo-Degradable Plastics. Available online: <https://www.greendotbioplastics.com/biodegradable-vs-compostable-vs-oxo-1479degradable-plastics-a-straightforward-explanation/> (accessed on 10 October 2022).
27. Zhao, X.; Cornish, K.; Vodovotz, Y. Narrowing the Gap for Bioplastic Use in Food Packaging: An Update. *Environ. Sci. Technol.* **2020**, *54*, 4712–4732. [CrossRef]
28. Emadian, S.M.; Onay, T.T.; Demirel, B. Biodegradation of Bioplastics in Natural Environments. *Waste Manag.* **2017**, *59*, 526–536. [CrossRef] [PubMed]



29. Imam, S.H.; Gordon, S.H.; Shogren, R.L.; Tosteson, T.R.; Govind, N.S.; Greene, R.V. Degradation of starch-poly(beta-hydroxybutyrate-co-beta-hydroxyvalerate) bioplastic in tropical coastal waters. *Appl. Environ. Microbiol.* **1999**, *65*, 431–437. [CrossRef]
30. Patti, A.; Acierno, D. Towards the Sustainability of the Plastic Industry through Biopolymers: Properties and Potential Applications to the Textiles World. *Polymers* **2022**, *14*, 692. [CrossRef] [PubMed]
31. Corcione, C.E.; Striani, R.; Ferrari, F.; Visconti, P.; Rizzo, D.; Greco, A. An Innovative Method for the Recycling of Waste Carbohydrate-Based Flours. *Polymers* **2020**, *12*, 1414. [CrossRef] [PubMed]
32. Rangappa, S.M.; Siengchin, S.; Parameswaranpillai, J.; Jawaid, M.; Ozbakkaloglu, T. Lignocellulosic Fiber Reinforced Composites: Progress, Performance, Properties, Applications, and Future Perspectives. *Polym. Compos.* **2022**, *43*, 645–691. [CrossRef]
33. Lomelí-Ramírez, M.G.; Kestur, S.G.; Manríquez-González, R.; Iwakiri, S.; De Muniz, G.B.; Flores-Sahagun, T.S. Bio-Composites of Cassava Starch-Green Coconut Fiber: Part II—Structure and Properties. *Carbohydr. Polym.* **2014**, *102*, 576–583. [CrossRef]
34. Cheung, H.Y.; Ho, M.P.; Lau, K.T.; Cardona, F.; Hui, D. Natural Fibre-Reinforced Composites for Bioengineering and Environmental Engineering Applications. *Compos. Part B Eng.* **2009**, *40*, 655–663. [CrossRef]
35. Jawaid, M.; Abdul Khalil, H.P.S. Cellulosic/Synthetic Fibre Reinforced Polymer Hybrid Composites: A Review. *Carbohydr. Polym.* **2011**, *86*, 1–18. [CrossRef]
36. Thakur, V.K.; Thakur, M.K.; Gupta, R.K. Review: Raw Natural Fiber-Based Polymer Composites. *Int. J. Polym. Anal. Charact.* **2014**, *19*, 256–271. [CrossRef]
37. Couret, L.; Irle, M.; Belloncle, C.; Cathala, B. Extraction and Characterization of Cellulose Nanocrystals from Post-Consumer Wood Fiberboard Waste. *Cellulose* **2017**, *24*, 2125–2137. [CrossRef]
38. Hassan, I.F. Nanocellulose for Sustainable Future Applications. In *Handbook of Nanomaterials and Nanocomposites for Energy and Environmental Applications*; Springer: Cham, Switzerland, 2020; pp. 1–12, ISBN 9783030111557.
39. Seddiqi, H.; Oliaei, E.; Honarkar, H.; Jin, J.; Geonzon, L.C.; Bacabac, R.G.; Klein-Nulend, J. *Cellulose and Its Derivatives: Towards Biomedical Applications*; Springer: Dordrecht, The Netherlands, 2021; Volume 28, ISBN 1057002003.
40. Balart, R.; Garcia-Garcia, D.; Fombuena, V.; Quiles-Carrillo, L.; Arrieta, M.P. Biopolymers from Natural Resources. *Polymers* **2021**, *13*, 2532. [CrossRef] [PubMed]
41. Poletto, M.; Ornaghi Júnior, H.L.; Zattera, A.J. Native Cellulose: Structure, Characterization and Thermal Properties. *Materials* **2014**, *7*, 6105–6119. [CrossRef] [PubMed]
42. Darie, R.N.; Lack, E.; Lang Jr, F.; Sova, M.; Nistor, A.; Spiridon, I. Wastes from Wood Extraction Used in Composite Materials: Behavior after Accelerated Weathering. *Int. J. Polym. Anal. Charact.* **2014**, *19*, 453–467. [CrossRef]
43. Yokoi, H.; Nakase, T.; Goto, K.; Ishida, Y.; Ohtani, H.; Tsuge, S.; Sonoda, T.; Ona, T. Rapid Characterization of Wood Extractives in Wood by Thermal Desorption-Gas Chromatography in the Presence of Tetramethylammonium Acetate. *J. Anal. Appl. Pyrolysis* **2003**, *67*, 191–200. [CrossRef]
44. Ferreira, A.R.V.; Alves, V.D.; Coelho, I.M. Polysaccharide-Based Membranes in Food Packaging Applications. *Membranes* **2016**, *6*, 22. [CrossRef]
45. Shaghaleh, H.; Xu, X.; Wang, S. Current Progress in Production of Biopolymeric Materials Based on Cellulose, Cellulose Nanofibers, and Cellulose Derivatives. *RSC Adv.* **2018**, *8*, 825–842. [CrossRef]
46. Li, Y.Y.; Wang, B.; Ma, M.G.; Wang, B. Review of Recent Development on Preparation, Properties, and Applications of Cellulose-Based Functional Materials. *Int. J. Polym. Sci.* **2018**, *2018*, 8973643. [CrossRef]
47. Kalidhasan, S.; Santhana KrishnaKumar, A.; Rajesh, V.; Rajesh, N. Ultrasound-Assisted Preparation and Characterization of Crystalline Cellulose-Ionic Liquid Blend Polymeric Material: A Prelude to the Study of Its Application toward the Effective Adsorption of Chromium. *J. Colloid Interface Sci.* **2012**, *367*, 398–408. [CrossRef]
48. Wan, C.; Li, J. Facile Synthesis of Well-Dispersed Superparamagnetic  $\gamma$ -Fe<sub>2</sub>O<sub>3</sub> Nanoparticles Encapsulated in Three-Dimensional Architectures of Cellulose Aerogels and Their Applications for Cr(VI) Removal from Contaminated Water. *ACS Sustain. Chem. Eng.* **2015**, *3*, 2142–2152. [CrossRef]
49. Teodoro, F.S.; Ramos, S.N.D.C.; Elias, M.M.C.; Mageste, A.B.; Ferreira, G.M.D.; da Silva, L.H.M.; Gil, L.F.; Gurgel, L.V.A. Synthesis and Application of a New Carboxylated Cellulose Derivative. Part I: Removal of Co<sup>2+</sup>, Cu<sup>2+</sup> and Ni<sup>2+</sup> from Monocomponent Spiked Aqueous Solution. *J. Colloid Interface Sci.* **2016**, *483*, 185–200. [CrossRef]
50. Dassanayake, R.S.; Acharya, S.; Abidi, N. Biopolymer-Based Materials from Polysaccharides: Properties, Processing, Characterization and Sorption Applications. In *Advanced Sorption Process Applications*; Intech Open: London, UK, 2018; pp. 1–24.
51. Akhlaghi, S.P.; Berry, R.C.; Tam, K.C. Surface Modification of Cellulose Nanocrystal with Chitosan Oligosaccharide for Drug Delivery Applications. *Cellulose* **2013**, *20*, 1747–1764. [CrossRef]
52. Brown, E.E.; Hu, D.; Abu Lail, N.; Zhang, X. Potential of Nanocrystalline Cellulose-Fibrin Nanocomposites for Artificial Vascular Graft Applications. *Biomacromolecules* **2013**, *14*, 1063–1071. [CrossRef]
53. Dammak, A.; Moreau, C.; Beury, N.; Schwikal, K.; Winter, H.; Bonnin, E.; Saake, B.; Cathala, B. Elaboration of Multilayered Thin Films Based on Cellulose Nanocrystals and Cationic Xylans: Application to Xylanase Activity Detection. *Holzforschung* **2013**, *67*, 579–586. [CrossRef]
54. Jian, C.; Gong, C.; Wang, S.; Wang, S.; Xie, X.; Wei, Y.; Yuan, J. Multifunctional Comb Copolymer Ethyl Cellulose-g-Poly( $\epsilon$ -Caprolactone)-Rhodamine B/Folate: Synthesis, Characterization and Targeted Bonding Application. *Eur. Polym. J.* **2014**, *55*, 235–244. [CrossRef]

55. Voicu, S.I.; Condruz, R.M.; Mitran, V.; Cimpean, A.; Miculescu, F.; Andronescu, C.; Miculescu, M.; Thakur, V.K. Sericin Covalent Immobilization onto Cellulose Acetate Membrane for Biomedical Applications. *ACS Sustain. Chem. Eng.* **2016**, *4*, 1765–1774. [CrossRef]
56. He, J.X.; Tan, W.L.; Han, Q.M.; Cui, S.Z.; Shao, W.; Sang, F. Fabrication of Silk Fibroin/Cellulose Whiskers–Chitosan Composite Porous Scaffolds by Layer-by-Layer Assembly for Application in Bone Tissue Engineering. *J. Mater. Sci.* **2016**, *51*, 4399–4410. [CrossRef]
57. Liu, S.; Jin, M.; Chen, Y.; Gao, H.; Shi, X.; Cheng, W.; Wang, Y. High Internal Phase Emulsions Stabilised by Supramolecular Cellulose Nanocrystals and Their Application as Cell-Adhesive Macroporous Hydrogel Monoliths. *J. Mater. Chem. B* **2017**, *5*, 2671–2678. [CrossRef]
58. Demitri, C.; Giuri, A.; Raucci, M.G.; Giugliano, D.; Madaghiele, M.; Sannino, A.; Ambrosio, L. Preparation and Characterization of Cellulose-Based Foams via Microwave Curing. *Interface Focus* **2014**, *4*, 20130053. [CrossRef]
59. Fu, J.; Pang, Z.; Yang, J.; Huang, F.; Cai, Y.; Wei, Q. Fabrication of Polyaniline/Carboxymethyl Cellulose/Cellulose Nanofibrous Mats and Their Biosensing Application. *Appl. Surf. Sci.* **2015**, *349*, 35–42. [CrossRef]
60. Xu, D.; Fan, L.; Gao, L.; Xiong, Y.; Wang, Y.; Ye, Q.; Yu, A.; Dai, H.; Yin, Y.; Cai, J.; et al. Micro-Nanostructured Polyaniline Assembled in Cellulose Matrix via Interfacial Polymerization for Applications in Nerve Regeneration. *ACS Appl. Mater. Interfaces* **2016**, *8*, 17090–17097. [CrossRef] [PubMed]
61. Shahbazi, M.; Ahmadi, S.J.; Seif, A.; Rajabzadeh, G. Carboxymethyl Cellulose Film Modification through Surface Photo-Crosslinking and Chemical Crosslinking for Food Packaging Applications. *Food Hydrocoll.* **2016**, *61*, 378–389. [CrossRef]
62. Hu, C.; Bai, X.; Wang, Y.; Jin, W.; Zhang, X.; Hu, S. Inkjet Printing of Nanoporous Gold Electrode Arrays on Cellulose Membranes for High-Sensitive Paper-like Electrochemical Oxygen Sensors Using Ionic Liquid Electrolytes. *Anal. Chem.* **2012**, *84*, 3745–3750. [CrossRef]
63. Han, J.W.; Kim, B.; Li, J.; Meyyappan, M. A Carbon Nanotube Based Ammonia Sensor on Cellulose Paper. *RSC Adv.* **2014**, *4*, 549–553. [CrossRef]
64. Shi, X.; Zheng, Y.; Wang, G.; Lin, Q.; Fan, J. PH- and Electro-Response Characteristics of Bacterial Cellulose Nanofiber/Sodium Alginate Hybrid Hydrogels for Dual Controlled Drug Delivery. *RSC Adv.* **2014**, *4*, 47056–47065. [CrossRef]
65. Giese, M.; Blusch, L.K.; Khan, M.K.; Hamad, W.Y.; MacLachlan, M.J. Responsive Mesoporous Photonic Cellulose Films by Supramolecular Cotemplating. *Angew. Chem.* **2014**, *126*, 9026–9030. [CrossRef]
66. Fox, D.M.; Rodriguez, R.S.; Devillbiss, M.N.; Woodcock, J.; Davis, C.S.; Sinko, R.; Keten, S.; Gilman, J.W. Simultaneously Tailoring Surface Energies and Thermal Stabilities of Cellulose Nanocrystals Using Ion Exchange: Effects on Polymer Composite Properties for Transportation, Infrastructure, and Renewable Energy Applications. *ACS Appl. Mater. Interfaces* **2016**, *8*, 27270–27281. [CrossRef]
67. Ouyang, W.; Sun, J.; Memon, J.; Wang, C.; Geng, J.; Huang, Y. Scalable Preparation of Three-Dimensional Porous Structures of Reduced Graphene Oxide/Cellulose Composites and Their Application in Supercapacitors. *Carbon N. Y.* **2013**, *62*, 501–509. [CrossRef]
68. Bisconti, F.; Giuri, A.; Dominici, L.; Carallo, S.; Quadrivi, E.; Po', R.; Biagini, P.; Listorti, A.; Corcione, C.E.; Colella, S.; et al. Managing Transparency through Polymer/Perovskite Blending: A Route toward Thermostable and Highly Efficient, Semi-Transparent Solar Cells. *Nano Energy* **2021**, *89*, 106406. [CrossRef]
69. Tanase-Opedal, M.; Espinosa, E.; Rodríguez, A.; Chinga-Carrasco, G. Lignin: A Biopolymer from Forestry Biomass for Biocomposites and 3D Printing. *Materials* **2019**, *12*, 3006. [CrossRef] [PubMed]
70. Tribot, A.; Amer, G.; Abdou Alio, M.; de Baynast, H.; Delattre, C.; Pons, A.; Mathias, J.D.; Callois, J.M.; Vial, C.; Michaud, P.; et al. Wood-Lignin: Supply, Extraction Processes and Use as Bio-Based Material. *Eur. Polym. J.* **2019**, *112*, 228–240. [CrossRef]
71. Mazurchevici, S.N.; Vaideanu, D.; Rapp, D.; Varganici, C.D.; Cărăușu, C.; Boca, M.; Nedelcu, D. Dynamic Mechanical Analysis and Thermal Expansion of Lignin-Based Biopolymers. *Polymers* **2021**, *13*, 2953. [CrossRef]
72. Kun, D.; Pukánszky, B. Polymer/Lignin Blends: Interactions, Properties, Applications. *Eur. Polym. J.* **2017**, *93*, 618–641. [CrossRef]
73. Borrero-l, A.M.; Valencia, C.; Franco, J.M. Lignocellulosic Materials for the Production of Biofuels, Biochemicals and Biomaterials and Applications of Lignocellulose-Based Polyurethanes: A Review. *Polymers* **2022**, *14*, 881. [CrossRef] [PubMed]
74. Vásquez-Garay, F.; Carrillo-Varela, I.; Vidal, C.; Reyes-Contreras, P.; Faccini, M.; Mendonça, R.T. A Review on the Lignin Biopolymer and Its Integration in the Elaboration of Sustainable Materials. *Sustainability* **2021**, *13*, 2697. [CrossRef]
75. Sharma, S.; Sharma, A.; Mulla, S.I.; Pant, D.; Sharma, T.; Kumar, A. Lignin as Potent Industrial Biopolymer: An Introduction. In *Lignin*; Springer: Cham, Switzerland, 2020; pp. 1–15.
76. Aro, T.; Fatehi, P. Production and Application of Lignosulfonates and Sulfonated Lignin. *ChemSusChem* **2017**, *10*, 1861–1877. [CrossRef]
77. Silva, N.; Blumberga, D. Why Biopolymer Packaging Materials Are Better. *Environ. Clim. Technol.* **2019**, *23*, 366–384. [CrossRef]
78. Rajesh Banu, J.; Kavitha, S.; Yukesh Kannah, R.; Poornima Devi, T.; Gunasekaran, M.; Kim, S.H.; Kumar, G. A Review on Biopolymer Production via Lignin Valorization. *Bioresour. Technol.* **2019**, *290*, 121790. [CrossRef]
79. Gilca, I.A.; Popa, V.I.; Crestini, C. Obtaining Lignin Nanoparticles by Sonication. *Ultrason. Sonochem* **2015**, *23*, 369–375. [CrossRef]
80. Li, H.; Deng, Y.; Liang, J.; Dai, Y.; Li, B.; Ren, Y.; Li, C. Direct Preparation of Hollow Nanospheres with Kraft Lignin: A Facile Strategy for Effective Utilization of Biomass Waste. *BioResources* **2016**, *11*, 3073–3083. [CrossRef]

81. Lievonen, M.; Valle-Delgado, J.J.; Mattinen, M.L.; Hult, E.L.; Lintinen, K.; Kostianen, M.A.; Paananen, A.; Szilvay, G.R.; Setälä, H.; Österberg, M. A Simple Process for Lignin Nanoparticle Preparation. *Green Chem.* **2016**, *18*, 1416–1422. [CrossRef]
82. Bertini, F.; Canetti, M.; Cacciamani, A.; Elegir, G.; Orlandi, M.; Zoia, L. Effect of Ligno-Derivatives on Thermal Properties and Degradation Behavior of Poly(3-Hydroxybutyrate)-Based Biocomposites. *Polym. Degrad. Stab.* **2012**, *97*, 1979–1987. [CrossRef]
83. Mousavioun, P.; George, G.A.; Doherty, W.O.S. Environmental Degradation of Lignin/Poly(Hydroxybutyrate) Blends. *Polym. Degrad. Stab.* **2012**, *97*, 1114–1122. [CrossRef]
84. Kaneko, T.; Thi, T.H.; Shi, D.J.; Akashi, M. Environmentally Degradable, High-Performance Thermoplastics from Phenolic Phytomonomers. *Nat. Mater.* **2006**, *5*, 966–970. [CrossRef] [PubMed]
85. Ouyang, W.; Huang, Y.; Luo, H.; Wang, D. Poly(Lactic Acid) Blended with Cellulolytic Enzyme Lignin: Mechanical and Thermal Properties and Morphology Evaluation. *J. Polym. Environ.* **2012**, *20*, 1–9. [CrossRef]
86. Cateto, C.A.; Barreiro, M.F.; Rodrigues, A.E. Monitoring of Lignin-Based Polyurethane Synthesis by FTIR-ATR. *Ind. Crop. Prod.* **2008**, *27*, 168–174. [CrossRef]
87. Mahmood, N.; Yuan, Z.; Schmidt, J.; Xu, C. Depolymerization of Lignins and Their Applications for the Preparation of Polyols and Rigid Polyurethane Foams: A Review. *Renew. Sustain. Energy Rev.* **2016**, *60*, 317–329. [CrossRef]
88. Lin, Y.; Tanaka, S. Ethanol Fermentation from Biomass Resources: Current State and Prospects. *Appl. Microbiol. Biotechnol.* **2006**, *69*, 627–642. [CrossRef]
89. Balat, M. Production of Bioethanol from Lignocellulosic Materials via the Biochemical Pathway: A Review. *Energy Convers. Manag.* **2011**, *52*, 858–875. [CrossRef]
90. John, R.P.; Nampoothiri, K.M.; Pandey, A. Fermentative Production of Lactic Acid from Biomass: An Overview on Process Developments and Future Perspectives. *Appl. Microbiol. Biotechnol.* **2007**, *74*, 524–534. [CrossRef] [PubMed]
91. Demirbas, A. Potential Applications of Renewable Energy Sources, Biomass Combustion Problems in Boiler Power Systems and Combustion Related Environmental Issues. *Prog. Energy Combust. Sci.* **2005**, *31*, 171–192. [CrossRef]
92. Ten, E.; Vermerris, W.J.P. Functionalized Polymers from Lignocellulosic Biomass: State of the Art. *Polymers* **2013**, *5*, 600–642. [CrossRef]
93. Diacono, M.; Persiani, A.; Testani, E.; Montemurro, F.; Ciaccia, C. Recycling Agricultural Wastes and By-Products in Organic Farming: Biofertilizer Production, Yield Performance and Carbon Footprint Analysis. *Sustainability* **2019**, *11*, 3824. [CrossRef]
94. Motaung, T.E.; Liganiso, L.Z. *Critical Review on Agrowaste Cellulose Applications for Biopolymers*; Springer: New Delhi, India, 2018; Volume 22, ISBN 1258801892.
95. Sundarraj, A.A.; Ranganathan, T.V. A Review on Cellulose and Its Utilization from Agro-Industrial Waste. *Drug Invent. Today* **2018**, *10*, 89–94.
96. Urbina, L.; Corcuera, M.Á.; Gabilondo, N.; Eceiza, A.; Retegi, A. A Review of Bacterial Cellulose: Sustainable Production from Agricultural Waste and Applications in Various Fields. *Cellulose* **2021**, *28*, 8229–8253. [CrossRef]
97. El Achaby, M.; Kassab, Z.; Aboukhas, A.; Gaillard, C.; Barakat, A. Reuse of Red Algae Waste for the Production of Cellulose Nanocrystals and Its Application in Polymer Nanocomposites. *Int. J. Biol. Macromol.* **2018**, *106*, 681–691. [CrossRef] [PubMed]
98. Zikeli, F.; Vinciguerra, V.; D’Annibale, A.; Capitani, D.; Romagnoli, M.; Mugnozza, G.S. Preparation of Lignin Nanoparticles from Wood Waste for Wood Surface Treatment. *Nanomaterials* **2019**, *9*, 281. [CrossRef]
99. Parvathy, G.; Sethulekshmi, A.S.; Jayan, J.S.; Raman, A.; Saritha, A. Lignin Based Nano-Composites: Synthesis and Applications. *Process Saf. Environ. Prot.* **2021**, *145*, 395–410. [CrossRef]
100. Verlinden, R.A.J.; Hill, D.J.; Kenward, M.A.; Williams, C.D.; Radecka, I. Bacterial Synthesis of Biodegradable Polyhydroxyalkanoates. *J. Appl. Microbiol.* **2007**, *102*, 1437–1449. [CrossRef]
101. Bohmert, K.; Balbo, I.; Steinbüchel, A.; Tischendorf, G.; Willmitzer, L. Constitutive Expression of the  $\beta$ -Ketothiolase Gene in Transgenic Plants. A Major Obstacle for Obtaining Polyhydroxybutyrate-Producing Plants. *Plant Physiol.* **2002**, *128*, 1282–1290. [CrossRef] [PubMed]
102. Steinbüchel, A.; Lütke-Eversloh, T. Metabolic Engineering and Pathway Construction for Biotechnological Production of Relevant Polyhydroxyalkanoates in Microorganisms. *Biochem. Eng. J.* **2003**, *16*, 81–96. [CrossRef]
103. Shang, L.; Jiang, M.; Chang, H.N. Poly(3-Hydroxybutyrate) Synthesis in Fed-Batch Culture of *Ralstonia Eutropha* with Phosphate Limitation under Different Glucose Concentrations. *Biotechnol. Lett.* **2003**, *25*, 1415–1419. [CrossRef] [PubMed]
104. Peters, V.; Rehm, B.H.A. In Vivo Monitoring of PHA Granule Formation Using GFP-Labeled PHA Synthases. *FEMS Microbiol. Lett.* **2005**, *248*, 93–100. [CrossRef]
105. Pötter, M.; Steinbüchel, A. Poly(3-Hydroxybutyrate) Granule-Associated Proteins: Impacts on Poly(3-Hydroxybutyrate) Synthesis and Degradation. *Biomacromolecules* **2005**, *6*, 552–560. [CrossRef]
106. Tsuge, T. Metabolic Improvements and Use of Inexpensive Carbon Sources in Microbial Production of Polyhydroxyalkanoates. *J. Biosci. Bioeng.* **2002**, *94*, 579–584. [CrossRef]
107. Stasi, E.; Giuri, A.; Ferrari, F.; Armenise, V.; Colella, S.; Listorti, A.; Rizzo, A.; Ferraris, E.; Corcione, C.E. Biodegradable Carbon-Based Ashes/Maize Starch Composite Films for Agricultural Applications. *Polymers* **2020**, *12*, 524. [CrossRef]
108. Katiyar, V.; Gaur, S.S.; Pal, A.K.; Kumar, A. Properties of Plastics for Packaging Applications. In *Polymers for Packaging Applications*; CRC Press: Boca Raton, FL, USA, 2014; pp. 3–39.
109. Bugnicourt, E.; Cinelli, P.; Lazzeri, A.; Alvarez, V.A. Polyhydroxyalkanoate (PHA): Review of Synthesis, Characteristics, Processing and Potential Applications in Packaging. *eXPRESS Polym. Lett.* **2014**, *8*, 791–808. [CrossRef]



110. Sánchez-Safont, E.L.; Aldureid, A.; Lagarón, J.M.; Gámez-Pérez, J.; Cabedo, L. Biocomposites of Different Lignocellulosic Wastes for Sustainable Food Packaging Applications. *Compos. Part B Eng.* **2018**, *145*, 215–225. [CrossRef]
111. Chen, G.Q.; Zhang, G.; Park, S.J.; Lee, S.Y. Industrial Scale Production of Poly(3-Hydroxybutyrate-Co-3-Hydroxyhexanoate). *Appl. Microbiol. Biotechnol.* **2001**, *57*, 50–55. [CrossRef]
112. Godbole, S.; Gote, S.; Latkar, M.; Chakrabarti, T. Preparation and Characterization of Biodegradable Poly-3-Hydroxybutyrate-Starch Blend Films. *Bioresour. Technol.* **2003**, *86*, 33–37. [CrossRef] [PubMed]
113. Kumar, A.M. Wood Waste—Carbon Source for Polyhydroxyalkanoates (PHAs) Production. *Int. J. For. Wood Sci.* **2017**, *4*, 36–40.
114. Vaidya, A.N.; Pandey, R.A.; Mudliar, S.; Kumar, M.S.; Chakrabarti, T.; Devotta, S. Production and Recovery of Lactic Acid for Polylactide—An Overview. *Crit. Rev. Environ. Sci. Technol.* **2005**, *35*, 429–467. [CrossRef]
115. Anjum, A.; Zuber, M.; Zia, K.M.; Noreen, A.; Anjum, M.N.; Tabasum, S. Microbial Production of Polyhydroxyalkanoates (PHAs) and Its Copolymers: A Review of Recent Advancements. *Int. J. Biol. Macromol.* **2016**, *89*, 161–174. [CrossRef] [PubMed]
116. Ntaikou, I.; Valencia Peroni, C.; Kourmentza, C.; Ilieva, V.I.; Morelli, A.; Chiellini, E.; Lyberatos, G. Microbial Bio-Based Plastics from Olive-Mill Wastewater: Generation and Properties of Polyhydroxyalkanoates from Mixed Cultures in a Two-Stage Pilot Scale System. *J. Biotechnol.* **2014**, *188*, 138–147. [CrossRef] [PubMed]
117. Hinchliffe, J.D.; Madappura, A.P.; Mohammad, S.; Syed, D.; Roy, I. Biomedical Applications of Bacteria-Derived Polymers. *Polymers* **2021**, *13*, 1081. [CrossRef]
118. Khosravi-Darani, K.; Bucci, D.Z. Application of Poly (Hydroxyalkanoate) in Food Packaging: Improvements by Nanotechnology. *Chem. Biochem. Eng. Q.* **2015**, *29*, 275–285. [CrossRef]
119. Ilyas, R.A.; Zuhri, M.Y.M.; Norrrahim, M.N.F.; Misenan, M.S.M.; Jenol, M.A.; Samsudin, S.A.; Nurazzi, N.M.; Asyraf, M.R.M.; Supian, A.B.M.; Bangar, S.P.; et al. Natural Fiber-Reinforced Polycaprolactone Green and Hybrid Biocomposites for Various Advanced Applications. *Polymers* **2022**, *14*, 182. [CrossRef]
120. Lim, J.; You, M.; Li, J.; Li, Z. Emerging Bone Tissue Engineering via Polyhydroxyalkanoate (PHA)-Based Scaffolds. *Mater. Sci. Eng. C* **2017**, *79*, 917–929. [CrossRef]
121. Ortega, F.; Versino, F.; López, O.V.; García, M.A. Biobased Composites from Agro-Industrial Wastes and by-Products. In *Emergent Materials*; Springer International Publishing: New York, NY, USA, 2022; Volume 5, pp. 873–921, ISBN 0123456789.
122. Zheng, Y.; Chen, J.C.; Ma, Y.M.; Chen, G.Q. Engineering Biosynthesis of Polyhydroxyalkanoates (PHA) for Diversity and Cost Reduction. *Metab. Eng.* **2020**, *58*, 82–93. [CrossRef]
123. Singh, A.K.; Srivastava, J.K.; Chandel, A.K.; Sharma, L.; Mallick, N.; Singh, S.P. Biomedical Applications of Microbially Engineered Polyhydroxyalkanoates: An Insight into Recent Advances, Bottlenecks, and Solutions. *Appl. Microbiol. Biotechnol.* **2019**, *103*, 2007–2032. [CrossRef]
124. Lamberti, F.M.; Román-Ramírez, L.A.; Wood, J. Recycling of Bioplastics: Routes and Benefits. *J. Polym. Environ.* **2020**, *28*, 2551–2571. [CrossRef]
125. Rivas, L.F.; Casarin, S.A.; Nepomuceno, N.C.; Alencar, M.I.; Agnelli, J.A.M.; De Medeiros, E.S.; De Oliveira Wanderley Neto, A.; De Oliveira, M.P.; De Medeiros, A.M.; Ferreira Santos, A.S. Reprocessability of PHB in Extrusion: ATR-FTIR, Tensile Tests and Thermal Studies. *Polimeros* **2017**, *27*, 122–128. [CrossRef]
126. Alavi, S.; Thomas, S.; Sandeep, K.P.; Kalarikkal, N.; Varghese, J.; Yaragalla, S. *Polymers for Packaging Applications*; CRC Press: Boca Raton, FL, USA, 2014.
127. Chiarini, L.; Mara, L.; Tabacchioni, S. Influence of Growth Supplements on Lactic Acid Production in Whey Ultrafiltrate by *Lactobacillus Helveticus*. *Appl. Microbiol. Biotechnol.* **1992**, *36*, 461–464. [CrossRef]
128. Boergardts, P.; Krischke, W.; Chmiel, H.; Troesch, W. Development of an Integrated Process for the Production of Lactic Acid from Whey Permeate. *Prog. Biotechnol.* **1994**, *9*, 905–908.
129. Abdel-Rahman, M.A.; Tashiro, Y.; Sonomoto, K. Recent Advances in Lactic Acid Production by Microbial Fermentation Processes. *Biotechnol. Adv.* **2013**, *31*, 877–902. [CrossRef]
130. Cubas-Cano, E.; Venus, J.; González-Fernández, C.; Tomás-Pejó, E. Assessment of Different *Bacillus Coagulans* Strains for L-Lactic Acid Production from Defined Media and Gardening Hydrolysates: Effect of Lignocellulosic Inhibitors. *J. Biotechnol.* **2020**, *323*, 9–16. [CrossRef]
131. Tan, J.; Abdel-Rahman, M.A.; Sonomoto, K. Biorefinery-Based Lactic Acid Fermentation: Microbial Production of Pure Monomer Product. *Adv. Polym. Sci.* **2018**, *279*, 27–66. [CrossRef]
132. Chai, C.Y.; Tan, I.S.; Foo, H.C.Y.; Lam, M.K.; Tong, K.T.X.; Lee, K.T. Sustainable and Green Pretreatment Strategy of *Eucheuma Denticulatum* Residues for Third-Generation L-Lactic Acid Production. *Bioresour. Technol.* **2021**, *330*, 124930. [CrossRef]
133. Wang, Y.; Cao, W.; Luo, J.; Qi, B.; Wan, Y. One Step Open Fermentation for Lactic Acid Production from Inedible Starchy Biomass by Thermophilic *Bacillus Coagulans* IPE22. *Bioresour. Technol.* **2019**, *272*, 398–406. [CrossRef]
134. Sawai, H.; Na, K.; Sasaki, N.; Mimitsuka, T.; Minegishi, S.I.; Henmi, M.; Yamada, K.; Shimizu, Y.S.; Yonehara, T. Membrane-Integrated Fermentation System for Improving the Optical Purity of D-Lactic Acid Produced during Continuous Fermentation. *Biosci. Biotechnol. Biochem.* **2011**, *75*, 2326–2332. [CrossRef] [PubMed]
135. Ikada, Y.; Jamshidi, K.; Tsuji, H.; Hyon, S.H. Stereocomplex Formation between Enantiomeric Poly(Lactides). *Macromolecules* **1987**, *20*, 904–906. [CrossRef]
136. de la Torre, I.; Ladero, M.; Santos, V.E. Production of D-Lactic Acid by *Lactobacillus Delbrueckii* Ssp. *Delbrueckii* from Orange Peel Waste: Techno-Economical Assessment of Nitrogen Sources. *Appl. Microbiol. Biotechnol.* **2018**, *102*, 10511–10521. [CrossRef]

137. Ma, K.; Hu, G.; Pan, L.; Wang, Z.; Zhou, Y.; Wang, Y.; Ruan, Z.; He, M. Highly Efficient Production of Optically Pure L-Lactic Acid from Corn Stover Hydrolysate by Thermophilic *Bacillus Coagulans*. *Bioresour. Technol.* **2016**, *219*, 114–122. [CrossRef] [PubMed]
138. Nwamba, M.C.; Sun, F.; Mukasekuru, M.R.; Song, G.; Harindintwali, J.D.; Boyi, S.A.; Sun, H. Trends and Hassles in the Microbial Production of Lactic Acid from Lignocellulosic Biomass. *Environ. Technol. Innov.* **2021**, *21*, 101337. [CrossRef]
139. Abdel-Rahman, M.A.; Tashiro, Y.; Sonomoto, K. Lactic Acid Production from Lignocellulose-Derived Sugars Using Lactic Acid Bacteria: Overview and Limits. *J. Biotechnol.* **2011**, *156*, 286–301. [CrossRef] [PubMed]
140. Wang, Y.; Cao, W.; Luo, J.; Wan, Y. Exploring the Potential of Lactic Acid Production from Lignocellulosic Hydrolysates with Various Ratios of Hexose versus Pentose by *Bacillus Coagulans* IPE22. *Bioresour. Technol.* **2018**, *261*, 342–349. [CrossRef]
141. Yadav, A.K.; Chaudhari, A.B.; Kothari, R.M. Bioconversion of Renewable Resources into Lactic Acid: An Industrial View. *Crit. Rev. Biotechnol.* **2011**, *31*, 1–19. [CrossRef]
142. Mussatto, S.I.; Roberto, I.C. Alternatives for Detoxification of Diluted-Acid Lignocellulosic Hydrolyzates for Use in Fermentative Processes: A Review. *Bioresour. Technol.* **2004**, *93*, 1–10. [CrossRef]
143. Vijayakumar, J.; Aravindan, R.; Viruthagiri, T. Recent Trends in the Production, Purification and Application of Lactic Acid. *Chem. Biochem. Eng. Q.* **2008**, *22*, 245–264.
144. Zhou, S.; Causey, T.B.; Hasona, A.; Shanmugam, K.T.; Ingram, L.O. Production of Optically Pure D-Lactic Acid in Mineral Salts Medium by Metabolically Engineered *Escherichia Coli* W3110. *Appl. Environ. Microbiol.* **2003**, *69*, 399–407. [CrossRef] [PubMed]
145. Baek, S.H.; Kwon, E.Y.; Kim, Y.H.; Hahn, J.S. Metabolic Engineering and Adaptive Evolution for Efficient Production of D-Lactic Acid in *Saccharomyces Cerevisiae*. *Appl. Microbiol. Biotechnol.* **2016**, *100*, 2737–2748. [CrossRef] [PubMed]
146. Eş, I.; Mousavi Khaneghah, A.; Barba, F.J.; Saraiva, J.A.; Sant’Ana, A.S.; Hashemi, S.M.B. Recent Advancements in Lactic Acid Production—A Review. *Food Res. Int.* **2018**, *107*, 763–770. [CrossRef] [PubMed]
147. Schmidt, A.S.; Thomsen, A.B. Optimization of Wet Oxidation Pretreatment of Wheat Straw. *Bioresour. Technol.* **1998**, *64*, 139–151. [CrossRef]
148. Chandel, A.K.; ES, C.; Rudravaram, R.; Narasu, L.; Rao, V.; Ravindra, P. Economics and Environmental Impact of Bioethanol Production Technologies: An Appraisal. *Biotechnol. Mol. Biol. Rev.* **2007**, *2*, 14–32.
149. Kodali, B.; Pogaku, R. Pretreatment Studies of Ricebran for the Effective Production of Cellulose. *Electr. J. Environ. Agric. Food Chem.* **2006**, *5*, 1253–1264.
150. Mohammed, A.A.B.A.; Omran, A.A.B.; Hasan, Z.; Ilyas, R.A.; Sapuan, S.M. Wheat Biocomposite Extraction, Structure, Properties and Characterization: A Review. *Polymers* **2021**, *13*, 3624. [CrossRef]
151. Shahavi, M.H.; Selakjani, P.P.; Abatari, M.N.; Antov, P.; Savov, V. Novel Biodegradable Poly (Lactic Acid)/Wood Leachate Composites: Investigation of Antibacterial, Mechanical, Morphological, and Thermal Properties. *Polymers* **2022**, *14*, 1227. [CrossRef]
152. Khan, M.Z.R.; Srivastava, S.K.; Gupta, M.K. A State-of-the-Art Review on Particulate Wood Polymer Composites: Processing, Properties and Applications. *Polym. Test.* **2020**, *89*, 106721. [CrossRef]
153. Udayakumar, G.P.; Muthusamy, S.; Selvaganesh, B.; Sivarajasekar, N.; Rambabu, K.; Banat, F.; Sivamani, S.; Sivakumar, N.; Hosseini-Bandegharaei, A.; Show, P.L. Biopolymers and Composites: Properties, Characterization and Their Applications in Food, Medical and Pharmaceutical Industries. *J. Environ. Chem. Eng.* **2021**, *9*, 105322. [CrossRef]
154. Fico, D.; Rizzo, D.; De Carolis, V.; Montagna, F.; Palumbo, E.; Corcione, C.E. Development and Characterization of Sustainable PLA/Olive Wood Waste Composites for Rehabilitation Applications Using Fused Filament Fabrication (FFF). *J. Build. Eng.* **2022**, *56*, 104673. [CrossRef]
155. Greco, A.; Ferrari, F. Thermal Behavior of PLA Plasticized by Commercial and Cardanol-Derived Plasticizers and the Effect on the Mechanical Properties. *J. Therm. Anal. Calorim.* **2021**, *146*, 131–141. [CrossRef]
156. Reddy, M.S.B.; Ponnamma, D.; Choudhary, R.; Sadasivuni, K.K. A Comparative Review of Natural and Synthetic Biopolymer Composite Scaffolds. *Polymers* **2021**, *13*, 1105. [CrossRef] [PubMed]
157. Imre, B.; Pukánszky, B. Compatibilization in Bio-Based and Biodegradable Polymer Blends. *Eur. Polym. J.* **2013**, *49*, 1215–1233. [CrossRef]
158. Shesan, O.J.; Stephen, A.C.; Chioma, A.G.; Neerish, R.; Rotimi, S.E. Improving the Mechanical Properties of Natural Fiber Composites for Structural and Biomedical Applications. In *Renewable and Sustainable Composites*; IntechOpen: London, UK, 2019; pp. 1–27.
159. Meng, L.; Xie, F.; Zhang, B.; Wang, D.K.; Yu, L. Natural Biopolymer Alloys with Superior Mechanical Properties. *ACS Sustain. Chem. Eng.* **2019**, *7*, 2792–2802. [CrossRef]
160. George, A.; Sanjay, M.R.; Srisuk, R.; Parameswaranpillai, J.; Siengchin, S. A Comprehensive Review on Chemical Properties and Applications of Biopolymers and Their Composites. *Int. J. Biol. Macromol.* **2020**, *154*, 329–338. [CrossRef]
161. Chan, C.M.; Vandi, L.J.; Pratt, S.; Halley, P.; Richardson, D.; Werker, A.; Laycock, B. Composites of Wood and Biodegradable Thermoplastics: A Review. *Polym. Rev.* **2018**, *58*, 444–494. [CrossRef]
162. Liu, R.; Chen, Y.; Cao, J. Effects of Modifier Type on Properties of in Situ Organo-Montmorillonite Modified Wood Flour/Poly(Lactic Acid) Composites. *ACS Appl. Mater. Interfaces* **2016**, *8*, 161–168. [CrossRef]
163. Febrianto, F.; Yoshioka, M.; Nagai, Y.; Tahir, P.M.D.; Syafii, W.; Shiraiishi, N. The Morphological, Mechanical and Physical Properties of Wood Flour-Poly Lactic Acid Composites under Various Filler Types. *J. Biol. Sci.* **2006**, *6*, 555–563.



164. Tao, Y.; Wang, H.; Li, Z.; Li, P.; Shi, S.Q. Development and Application Of wood Flour-Filled Polylactic Acid Composite Filament for 3d Printing. *Materials* **2017**, *10*, 339. [CrossRef]
165. Le Duigou, A.; Castro, M.; Bevan, R.; Martin, N. 3D Printing of Wood Fibre Biocomposites: From Mechanical to Actuation Functionality. *Mater. Des.* **2016**, *96*, 106–114. [CrossRef]
166. Das, A.K.; Agar, D.A.; Rudolfsson, M.; Larsson, S.H. A Review on Wood Powders in 3D Printing: Processes, Properties and Potential Applications. *J. Mater. Res. Technol.* **2021**, *15*, 241–255. [CrossRef]
167. Xie, G.; Zhang, Y.; Lin, W. Plasticizer Combinations and Performance of Wood Flour-Poly(Lactic Acid) 3D Printing Filaments. *BioResources* **2017**, *12*, 6736–6748. [CrossRef]
168. Zhang, Q.; Ma, R.; Ma, L.; Zhang, L.; Fan, Y.; Wang, Z. Contribution of Lignin in Esterified Lignocellulose Nanofibers (LCNFs) Prepared by Deep Eutectic Solvent Treatment to the Interface Compatibility of LCNF/PLA Composites. *Ind. Crop. Prod.* **2021**, *166*, 113460. [CrossRef]
169. Harussani, M.M.; Sapuan, S.M.; Firdaus, A.H.M.; El-Badry, Y.A.; Hussein, E.E.; El-Bahy, Z.M. Determination of the Tensile Properties and Biodegradability of Cornstarch-Based Biopolymers Plasticized with Sorbitol and Glycerol. *Polymers* **2021**, *13*, 3709. [CrossRef]
170. Vandi, L.J.; Chan, C.M.; Werker, A.; Richardson, D.; Laycock, B.; Pratt, S. Wood-PHA Composites: Mapping Opportunities. *Polymers* **2018**, *10*, 751. [CrossRef]
171. Sliwa, F.; El Bounia, N.E.; Charrier, F.; Marin, G.; Malet, F. Mechanical and Interfacial Properties of Wood and Bio-Based Thermoplastic Composite. *Compos. Sci. Technol.* **2012**, *72*, 1733–1740. [CrossRef]
172. Wu, C.S.; Liao, H.T.; Cai, Y.X. Characterisation, Biodegradability and Application of Palm Fibre-Reinforced Polyhydroxyalkanoate Composites. *Polym. Degrad. Stab.* **2017**, *140*, 55–63. [CrossRef]
173. Peidayesh, H.; Mosnáčková, K.; Špitalský, Z.; Heydari, A.; Šišková, A.O.; Chodák, I. Thermoplastic Starch-Based Composite Reinforced by Conductive Filler Networks: Physical Properties and Electrical Conductivity Changes during Cyclic Deformation. *Polymers* **2021**, *13*, 3819. [CrossRef]
174. Zeng, G.S.; Hu, C.; Zou, S.; Zhang, L.; Sun, G. BP Neural Network Model for Predicting the Mechanical Performance of a Foamed Wood-Fiber Reinforced Thermoplastic Starch Composite. *Polym. Compos.* **2019**, *40*, 3923–3928. [CrossRef]
175. Dorigato, A.; Fredi, G.; Pegoretti, A. Thermo-Mechanical Behavior of Novel Wood Laminae-Thermoplastic Starch Biodegradable Composites with Thermal Energy Storage/Release Capability. *Front. Mater.* **2019**, *6*, 76. [CrossRef]
176. Curvelo, A.A.S.; De Carvalho, A.J.F.; Agnelli, J.A.M. Thermoplastic Starch-Cellulosic Fibers Composites: Preliminary Results. *Carbohydr. Polym.* **2001**, *45*, 183–188. [CrossRef]
177. Miranda, C.S.; Ferreira, M.S.; Magalhães, M.T.; Santos, W.J.; Oliveira, J.C.; Silva, J.B.A.; José, N.M. Mechanical, Thermal and Barrier Properties of Starch-Based Films Plasticized with Glycerol and Lignin and Reinforced with Cellulose Nanocrystals. *Mater. Today Proc.* **2015**, *2*, 63–69. [CrossRef]
178. Da Silva, V.; Batista, K.C.; Zattera, A.J.; Silva, D.; Pezzin, A. Poly(3-Hydroxybutyrate-Co-3-Hydroxyvalerate)/Wood Powder Biocomposites: Thermal and Mechanical Properties and Water Absorption Profile. *J. Reinf. Plast. Compos.* **2014**, *33*, 741–748. [CrossRef]
179. Song, Z.; Xiao, H.; Zhao, Y. Hydrophobic-Modified Nano-Cellulose Fiber/PLA Biodegradable Composites for Lowering Water Vapor Transmission Rate (WVTR) of Paper. *Carbohydr. Polym.* **2014**, *111*, 442–448. [CrossRef]
180. Souza, A.G.; Ferreira, R.R.; Paula, L.C.; Mitra, S.K.; Rosa, D.S. Starch-Based Films Enriched with Nanocellulose-Stabilized Pickering Emulsions Containing Different Essential Oils for Possible Applications in Food Packaging. *Food Packag. Shelf Life* **2021**, *27*, 100615. [CrossRef]
181. Nazrin, A.; Sapuan, S.M.; Zuhri, M.Y.M. Mechanical, Physical and Thermal Properties of Sugar Palm Nanocellulose Reinforced Thermoplastic Starch (TPS)/Poly (Lactic Acid) (PLA) Blend Bionanocomposites. *Polymers* **2020**, *12*, 2216. [CrossRef]
182. Pérez-Pacheco, E.; Canto-Pinto, J.C.; Moo-Huchin, V.M.; Estrada-Mota, I.A.; Estrada-León, R.J.; Chel-Guerrero, L. Thermoplastic Starch (TPS)-Cellulosic Fibers Composites: Mechanical Properties and Water Vapor Barrier: A Review. In *Composites from Renewable and Sustainable Materials*; InTechOpen: London, UK, 2016.
183. Aila-Suárez, S.; Palma-Rodríguez, H.M.; Rodríguez-Hernández, A.I.; Hernández-Urbe, J.P.; Bello-Pérez, L.A.; Vargas-Torres, A. Characterization of Films Made with Chayote Tuber and Potato Starches Blending with Cellulose Nanoparticles. *Carbohydr. Polym.* **2013**, *98*, 102–107. [CrossRef]
184. Li, M.; Jia, Y.; Shen, X.; Shen, T.; Tan, Z.; Zhuang, W.; Zhao, G.; Zhu, C.; Ying, H. Investigation into Lignin Modified PBAT/Thermoplastic Starch Composites: Thermal, Mechanical, Rheological and Water Absorption Properties. *Ind. Crop. Prod.* **2021**, *171*, 113916. [CrossRef]
185. Karkhanis, S.S.; Stark, N.M.; Sabo, R.C.; Matuana, L.M. Water Vapor and Oxygen Barrier Properties of Extrusion-Blown Poly(Lactic Acid)/Cellulose Nanocrystals Nanocomposite Films. *Compos. Part A Appl. Sci. Manuf.* **2018**, *114*, 204–211. [CrossRef]
186. Harmaen, A.S.; Khalina, A.; Azowa, I.; Hassan, M.A.; Tarmian, A. Thermal and Biodegradation Properties of Poly (Lactic Acid)/Fertilizer/Oil Palm Fibers Blends Biocomposites. *Polym. Compos.* **2014**, *36*, 576–583. [CrossRef]
187. Ruz-Cruz, M.A.; Herrera-Franco, P.J.; Flores-Johnson, E.A.; Moreno-Chulim, M.V.; Galera-Manzano, L.M.; Valadez-González, A. Thermal and Mechanical Properties of PLA-Based Multiscale Cellulosic Biocomposites. *J. Mater. Res. Technol.* **2022**, *18*, 485–495. [CrossRef]

188. Sanchez-Garcia, M.D.; Gimenez, E.; Lagaron, J.M. Morphology and Barrier Properties of Solvent Cast Composites of Thermoplastic Biopolymers and Purified Cellulose Fibers. *Carbohydr. Polym.* **2008**, *71*, 235–244. [CrossRef]
189. Espino-Pérez, E.; Bras, J.; Ducruet, V.; Guinault, A.; Dufresne, A.; Domenek, S. Influence of Chemical Surface Modification of Cellulose Nanowhiskers on Thermal, Mechanical, and Barrier Properties of Poly(Lactide) Based Bionanocomposites. *Eur. Polym. J.* **2013**, *49*, 3144–3154. [CrossRef]
190. Martínez-Sanz, M.; Villano, M.; Oliveira, C.; Albuquerque, M.G.E.; Majone, M.; Reis, M.; Lopez-Rubio, A.; Lagaron, J.M. Characterization of Polyhydroxyalkanoates Synthesized from Microbial Mixed Cultures and of Their Nanobiocomposites with Bacterial Cellulose Nanowhiskers. *N. Biotechnol.* **2014**, *31*, 364–376. [CrossRef]
191. Torres-Giner, A.S. *Development of PHA/Fiber-Based Composites with Antimicrobial Performance for Active Food Packaging Applications*; University of Minho: Braga, Portugal, 2017.
192. Döhler, N.; Wellenreuther, C.; Wolf, A. Market Dynamics of Biodegradable Bio-Based Plastics: Projections and Linkages to European Policies. *EFB Bioecon. J.* **2022**, *2*, 100028. [CrossRef]
193. ICIS Independent Commodity Intelligence Service. Available online: <https://www.icis.com/explore/> (accessed on 16 September 2022).
194. Nanda, S.; Patra, B.R.; Patel, R.; Bakos, J.; Dalai, A.K. Innovations in Applications and Prospects of Bioplastics and Biopolymers: A Review. *Environ. Chem. Lett.* **2022**, *20*, 379–395. [CrossRef]
195. van den Oever, M.; Molenveld, K.; van der Zee, M.; Bos, H. *Biobased and Biodegradable Plastics—Facts and Figures. Focus on Food Packaging in the Netherlands*; Springer: Berlin/Heidelberg, Germany, 2017; Volume 4, ISBN 9783319682556.
196. Fico, D.; Rizzo, D.; De Carolis, V.; Montagna, F.; Esposito Corcione, C. Sustainable Polymer Composites Manufacturing through 3D Printing Technologies by Using Recycled Polymer and Filler. *Polymers* **2022**, *14*, 3756. [CrossRef]
197. Díez-Pascual, A.M. Synthesis and Applications of Biopolymer Composites. *Int. J. Mol. Sci.* **2019**, *20*, 2321. [CrossRef]
198. Plastic Finder. Available online: <https://www.plasticfinder.it/> (accessed on 16 September 2022).
199. Dawson, P.L. Packaging. In *Poultry Meat Processing*; CRC Press: Boca Raton, FL, USA, 2000; pp. 83–106, ISBN 9781420042177.
200. Wang, Q.; Chen, W.; Zhu, W.; McClements, D.J.; Liu, X.; Liu, F. A Review of Multilayer and Composite Films and Coatings for Active Biodegradable Packaging. *npj Sci. Food* **2022**, *6*, 18. [CrossRef]
201. Provin, A.P.; de Aguiar Dutra, A.R.; de Sousa e Silva Gouveia, I.C.A.; Cubas, e.A.L.V. Circular Economy for Fashion Industry: Use of Waste from the Food Industry for the Production of Biotextiles. *Technol. Forecast. Soc. Chang.* **2021**, *169*, 120858. [CrossRef]
202. Kumar, S.S. Biopolymers in Medical Applications. In *Technical Textile*; CRC Press: Boca Raton, FL, USA, 2007; pp. 1–9.
203. Bayón, B.; Berti, I.R.; Gagnetten, A.M.; Castro, G.R. Biopolymers from Wastes to High-Value Products in Biomedicine. In *Waste to Wealth. Energy, Environment, and Sustainability*; Springer Nature: Singapore; Singapore Pte Ltd.: Singapore, 2018; pp. 1–44, ISBN 9789811074318.
204. Jacob, J.; Haponiuk, J.T.; Thomas, S.; Gopi, S. Biopolymer Based Nanomaterials in Drug Delivery Systems: A Review. *Mater. Today Chem.* **2018**, *9*, 43–55. [CrossRef]
205. Abdelhak, M. A Review: Application of Biopolymers in the Pharmaceutical Formulation. *J. Adv. Bio-Pharm.* **2019**, *1*, 15–25. [CrossRef]
206. Mitura, S.; Sionkowska, A.; Jaiswal, A. Biopolymers for Hydrogels in Cosmetics: Review. *J. Mater. Sci. Mater. Med.* **2020**, *31*, 50. [CrossRef] [PubMed]
207. Gupta, S.; Sharma, S.; Kumar Nadda, A.; Saad Bala Husain, M.; Gupta, A. Biopolymers from Waste Biomass and Its Applications in the Cosmetic Industry: A Review. *Mater. Today Proc.* **2022**, *68*, 873–879. [CrossRef]
208. Barbulova, A.; Colucci, G.; Apone, F. New Trends in Cosmetics: By-Products of Plant Origin and Their Potential Use as Cosmetic Active Ingredients. *Cosmetics* **2015**, *2*, 82–92. [CrossRef]
209. Younes, B. Classification, Characterization, and the Production Processes of Biopolymers Used in the Textiles Industry. *J. Text. Inst.* **2016**, *108*, 674–682. [CrossRef]
210. de Silva, C.J.G., Jr.; de Medeiros, A.D.M.; de Amorim, J.D.P.; do Nascimento, H.A.; Converti, A.; Costa, A.F.S.; Sarubbo, L.A. Bacterial Cellulose Biotextiles for the Future of Sustainable Fashion: A Review. *Environ. Chem. Lett.* **2021**, *19*, 2967–2980. [CrossRef]
211. Sivakanthan, S.; Rajendran, S.; Gamage, A.; Madhujith, T.; Mani, S. Antioxidant and Antimicrobial Applications of Biopolymers: A Review. *Food Res. Int.* **2020**, *136*, 109327. [CrossRef]
212. Kumar, L.; Ramakanth, D.; Akhila, K.; Gaikwad, K.K. Edible Films and Coatings for Food Packaging Applications: A Review. *Environ. Chem. Lett.* **2022**, *20*, 875–900. [CrossRef]
213. Khalid, M.Y.; Arif, Z.U. Novel Biopolymer-Based Sustainable Composites for Food Packaging Applications: A Narrative Review. *Food Packag. Shelf Life* **2022**, *33*, 100892. [CrossRef]
214. Das, D.; Panesar, P.S.; Saini, C.S.; Kennedy, J.F. Improvement in Properties of Edible Film through Non-Thermal Treatments and Nanocomposite Materials: A Review. *Food Packag. Shelf Life* **2022**, *32*, 100843. [CrossRef]
215. Feng, M.; Yu, L.; Zhu, P.; Zhou, X.; Liu, H.; Yang, Y.; Zhou, J.; Gao, C.; Bao, X.; Chen, P. Development and Preparation of Active Starch Films Carrying Tea Polyphenol. *Carbohydr. Polym.* **2018**, *196*, 162–167. [CrossRef]
216. Galus, S.; Kibar, E.A.A.; Gniewosz, M.; Kraśniewska, K. Novel Materials in the Preparation of Edible Films and Coatings—A Review. *Coatings* **2020**, *10*, 674. [CrossRef]
217. Perumal, A.B.; Huang, L.; Nambiar, R.B.; He, Y.; Li, X.; Sellamuthu, P.S. Application of Essential Oils in Packaging Films for the Preservation of Fruits and Vegetables: A Review. *Food Chem.* **2022**, *375*, 131810. [CrossRef] [PubMed]

218. Bayram, B.; Ozkan, G.; Kostka, T.; Capanoglu, E.; Esatbeyoglu, T. Valorization and Application of Fruit and Vegetable Wastes and By-Products for Food Packaging Materials. *Molecules* **2021**, *26*, 4031. [CrossRef] [PubMed]
219. Lionetto, F.; Esposito Corcione, C. Recent Applications of Biopolymers Derived from Fish Industry Waste in Food Packaging. *Polymers* **2021**, *13*, 2337. [CrossRef]
220. Elhussieny, A.; Faisal, M.; D'Angelo, G.; Aboulkhair, N.T.; Everitt, N.M.; Fahim, I.S. Valorisation of Shrimp and Rice Straw Waste into Food Packaging Applications. *Ain Shams Eng. J.* **2020**, *11*, 1219–1226. [CrossRef]
221. Baysal, G.; Olcay, H.S.; Keresteci, B.; Özpınar, H. The Antioxidant and Antibacterial Properties of Chitosan Encapsulated with the Bee Pollen and the Apple Cider Vinegar. *J. Biomater. Sci.* **2022**, *33*, 995–1011. [CrossRef]
222. Torres-giner, S.; Figueroa-lopez, K.J.; Melendez-rodriguez, B.; Prieto, C.; Pardo-figueres, M.; Lagaron, J.M. Emerging Trends in Biopolymers for Food Packaging 1. 1 Introduction to Polymers in Packaging. In *Emerging Trends in Biopolymers for Food Packaging*; Woodhead Publishing: Sawston, UK, 2021.
223. Schmidt, J.; Grau, L.; Auer, M.; Maletz, R.; Woidasky, J. Multilayer Packaging in a Circular Economy. *Polymers* **2022**, *14*, 1825. [CrossRef]
224. Omerović, N.; Djisalov, M.; Živojević, K.; Mladenović, M.; Vunduk, J.; Milenković, I.; Knežević, N.; Gadjanski, I.; Vidić, J. Antimicrobial Nanoparticles and Biodegradable Polymer Composites for Active Food Packaging Applications. *Compr. Rev. Food Sci. Food Saf.* **2021**, *20*, 2428–2454. [CrossRef] [PubMed]
225. Nikolic, M.V.; Vasiljevic, Z.Z.; Auger, S.; Vidic, J. Metal Oxide Nanoparticles for Safe Active and Intelligent Food Packaging. *Trends Food Sci. Technol.* **2021**, *116*, 655–668. [CrossRef]
226. Shershneva, E.G. Biodegradable Food Packaging: Benefits and Adverse Effects. In *IOP Conference Series: Earth and Environmental Science*; IOP Publishing: Bristol, UK, 2022; Volume 988.
227. Bhat, R.; Abdullah, N.; Din, R.H.; Tay, G.S. Producing Novel Sago Starch Based Food Packaging Films by Incorporating Lignin Isolated from Oil Palm Black Liquor Waste. *J. Food Eng.* **2013**, *119*, 707–713. [CrossRef]
228. Tumwesigye, K.S.; Oliveira, J.C.; Sousa-Gallagher, M.J. New Sustainable Approach to Reduce Cassava Borne Environmental Waste and Develop Biodegradable Materials for Food Packaging Applications. *Food Packag. Shelf Life* **2016**, *7*, 8–19. [CrossRef]
229. Gheorghita, R.; Anchidin-Norocel, L.; Filip, R.; Dimian, M.; Covasa, M. Applications of Biopolymers for Drugs and Probiotics Delivery. *Polymers* **2021**, *13*, 2729. [CrossRef] [PubMed]
230. Silva, S.S.; Rodrigues, L.C.; Fernandes, E.M.; Reis, R.L. Biopolymer Membranes in Tissue Engineering. In *Biopolymer Membranes and Films*; Elsevier: Amsterdam, The Netherlands, 2020; pp. 141–163, ISBN 9780128181348.
231. Xu, W.; Wang, X.; Sandler, N.; Willför, S.; Xu, C. Three-Dimensional Printing of Wood-Derived Biopolymers: A Review Focused on Biomedical Applications. *ACS Sustain. Chem. Eng.* **2018**, *6*, 5663–5680. [CrossRef] [PubMed]
232. de Souza, R.F.B.; de Souza, F.C.B.; Bierhalz, A.C.K.; Pires, A.L.R.; Moraes, A.M. Biopolymer-Based Films and Membranes as Wound Dressings Renata. In *Biopolymers Membranes and Films*; Elsevier: Amsterdam, The Netherlands, 2020; pp. 165–194, ISBN 9780128181348.
233. Bibire, T.; Yilmaz, O.; Ghiciuc, C.M.; Bibire, N.; Radu, D. Biopolymers for Surgical Applications. *Coatings* **2022**, *12*, 211. [CrossRef]
234. Haleem, N.; Arshad, M.; Shahid, M.; Tahir, M.A. Synthesis of Carboxymethyl Cellulose from Waste of Cotton Ginning Industry. *Carbohydr. Polym.* **2014**, *113*, 249–255. [CrossRef]
235. Zainal, S.H.; Mohd, N.H.; Suhaili, N.; Anuar, F.H.; Lazim, A.M.; Othaman, R. Preparation of Cellulose-Based Hydrogel: A Review. *J. Mater. Res. Technol.* **2021**, *10*, 935–952. [CrossRef]
236. Cui, X.; Lee, J.; Ng, K.R.; Chen, W.N. Food Waste Durian Rind-Derived Cellulose Organohydrogels: Toward Anti-Freezing and Antimicrobial Wound Dressing. *ACS Sustain. Chem. Eng.* **2021**, *9*, 1304–1312. [CrossRef]
237. Amores-Monge, V.; Goyanes, S.; Ribba, L.; Lopretti, M.; Sandoval-Barrantes, M.; Camacho, M.; Corrales-Ureña, Y.; Vega-Baudrit, J.R. Pineapple Agro-Industrial Wastes to Produce Biomedical Applications Post-COVID-19 Pandemic: Biorefinery and the Circular Economy. *Preprints* **2022**, 2022040192. [CrossRef]
238. Rebelo, R.; Fernandes, M.; Figueiro, R. Biopolymers in Medical Implants: A Brief Review. *Procedia Eng.* **2017**, *200*, 236–243. [CrossRef]
239. Shirvan, A.R.; Nouri, A. Medical Textiles. In *Advances in Functional and Protective Textiles*; Butola, B.S., Ed.; Elsevier: Chennai, India, 2020; pp. 291–333, ISBN 9780128202579.
240. Calcagnile, P.; Cacciatore, G.; Demitri, C.; Montagna, F.; Corcione, C.E. A Feasibility Study of Processing Polydimethylsiloxane-Sodium Carboxymethylcellulose Composites by a Low-Cost Fused Deposition Modeling 3D Printer. *Materials* **2018**, *11*, 1578. [CrossRef] [PubMed]
241. Corcione, C.E.; Gervaso, F.; Scalera, F.; Montagna, F.; Maiullaro, T.; Sannino, A.; Maffezzoli, A. 3D Printing of Hydroxyapatite Polymer-Based Composites for Bone Tissue Engineering. *J. Polym. Eng.* **2017**, *37*, 741–746. [CrossRef]
242. Esposito Corcione, C.; Scalera, F.; Gervaso, F.; Montagna, F.; Sannino, A.; Maffezzoli, A. One-Step Solvent-Free Process for the Fabrication of High Loaded PLA/HA Composite Filament for 3D Printing. *J. Therm. Anal. Calorim.* **2018**, *134*, 575–582. [CrossRef]
243. Esposito Corcione, C.; Gervaso, F.; Scalera, F.; Padmanabhan, S.K.; Madaghiele, M.; Montagna, F.; Sannino, A.; Licciulli, A.; Maffezzoli, A. Highly Loaded Hydroxyapatite Microsphere/PLA Porous Scaffolds Obtained by Fused Deposition Modelling. *Ceram. Int.* **2019**, *45*, 2803–2810. [CrossRef]



244. Veeman, D.; Sai, M.S.; Sureshkumar, P.; Jagadeesha, T.; Natrayan, L.; Ravichandran, M.; Mammo, W.D. Additive Manufacturing of Biopolymers for Tissue Engineering and Regenerative Medicine: An Overview, Potential Applications, Advancements, and Trends. *Int. J. Polym. Sci.* **2021**, *2021*, 4907027. [CrossRef]
245. Bartlett, S. Printing Organs on Demand. *Lancet Respir. Med.* **2013**, *1*, 684. [CrossRef]
246. Gross, B.C.; Erkal, J.L.; Lockwood, S.Y.; Chen, C.; Spence, D.M. Evaluation of 3D Printing and Its Potential Impact on Biotechnology and the Chemical Sciences. *Anal. Chem.* **2014**, *86*, 3240–3253. [CrossRef]
247. Esposito Corcione, C.; Gervaso, F.; Scalera, F.; Montagna, F.; Sannino, A.; Maffezzoli, A. The Feasibility of Printing Polylactic Acid–Nanohydroxyapatite Composites Using a Low-Cost Fused Deposition Modeling 3D Printer. *J. Appl. Polym. Sci.* **2017**, *134*, 44656. [CrossRef]
248. Bonferoni, M.C.; Caramella, C.; Catenacci, L.; Conti, B.; Dorati, R.; Ferrari, F.; Genta, I.; Modena, T.; Perteghella, S.; Rossi, S.; et al. Biomaterials for Soft Tissue Repair and Regeneration: A Focus on Italian Research in the Field. *Pharmaceutics* **2021**, *13*, 1341. [CrossRef] [PubMed]
249. Gregor, A.; Filová, E.; Novák, M.; Kronek, J.; Chlup, H.; Buzgo, M.; Blahnová, V.; Lukášová, V.; Bartoš, M.; Nečas, A.; et al. Designing of PLA Scaffolds for Bone Tissue Replacement Fabricated by Ordinary Commercial 3D Printer. *J. Biol. Eng.* **2017**, *11*, 31. [CrossRef] [PubMed]
250. Bashari, A.; Rouhani Shirvan, A.; Shakeri, M. Cellulose-Based Hydrogels for Personal Care Products. *Polym. Adv. Technol.* **2018**, *29*, 2853–2867. [CrossRef]
251. SANICOT. Available online: <https://www.sanicot.com/contatti-assorbenti-cotone/> (accessed on 10 September 2022).
252. Intima Luna. Available online: <https://www.intimaluna.it/ecoluna/> (accessed on 10 September 2022).
253. Lacoste, C.; Lopez-Cuesta, J.M.; Bergeret, A. Development of a Biobased Superabsorbent Polymer from Recycled Cellulose for Diapers Applications. *Eur. Polym. J.* **2019**, *116*, 38–44. [CrossRef]
254. Bhattacharya, P. Aa Review on the Impacts of Microplastic Beads Used in Cosmetics. *Acta Biomed. Sci.* **2016**, *3*, 47–52.
255. Jang, J.H.; So, B.R.; Yeo, H.J.; Kang, H.J.; Kim, M.J.; Lee, J.J.; Jung, S.K.; Jung, Y.H. Preparation of Cellulose Microfibril (CMF) from Gelidium Amansii and Feasibility of CMF as a Cosmetic Ingredient. *Carbohydr. Polym.* **2021**, *257*, 117569. [CrossRef]
256. Meyabadi, T.F.; Dadashian, F.; Sadeghi, G.M.M.; Asl, H.E.Z. Spherical Cellulose Nanoparticles Preparation from Waste Cotton Using a Green Method. *Powder Technol.* **2014**, *261*, 232–240. [CrossRef]
257. Bongao, H.; Gabatino, R.; Arias, C.F.H.; Magdaluyo, E.R., Jr. Micro/Nanocellulose from Waste Pili (Canarium Ovatum) Pulp as a Potential Anti-Ageing Ingredient for Cosmetic Formulations. *Mater. Today Proc.* **2020**, *22*, 275–280. [CrossRef]
258. ANOMERA. Available online: <https://www.anomera.ca/> (accessed on 10 September 2022).
259. Gabryś, T.; Fryczkowska, B.; Grzybowska-Pietras, J.; Biniś, D. Modification and Properties of Cellulose Nonwoven Fabric—Multifunctional Mulching Material for Agricultural Applications. *Materials* **2021**, *14*, 4335. [CrossRef]
260. Tesfaye, T.; Ayele, M.; Ferede, E.; Gibril, M.; Kong, F.; Sithole, B. A Techno-economic Feasibility of a Process for Extraction of Starch from Waste Avocado Seeds. *Clean Technol. Environ. Policy* **2020**, *23*, 581–595. [CrossRef]
261. Tesfaye, T.; Gibril, M.; Sithole, B.; Ramjugernath, D.; Chavan, R.; Chunilall, V. Valorisation of Avocado Seeds: Extraction and Characterisation of Starch for Textile Applications. *Clean Technol. Environ. Policy* **2018**, *20*, 2135–2154. [CrossRef]
262. Cano-Vicent, A.; Tambuwala, M.M.; Hassan, S.S.; Barh, D.; Aljabali, A.A.A.; Birkett, M.; Arjunan, A.; Serrano-Aroca, Á. Fused Deposition Modelling: Current Status, Methodology, Applications and Future Prospects. *Addit. Manuf.* **2021**, *47*, 102378. [CrossRef]
263. Biswas, M.C. Fused Deposition Modeling 3D Printing Technology in Textile and Fashion Industry: Materials and Innovation. *Mod. Concepts Mater. Sci.* **2019**, *2*, 1–5. [CrossRef]
264. Loh, G.H.; Sotayo, A.; Pei, E. Development and Testing of Material Extrusion Additive Manufactured Polymer–Textile Composites. *Fash. Text.* **2021**, *8*, 2. [CrossRef]
265. Jiang, T.; Duan, Q.; Zhu, J.; Liu, H.; Yu, L. Starch-Based Biodegradable Materials: Challenges and Opportunities. *Adv. Ind. Eng. Polym. Res.* **2018**, *39*, 245–258. [CrossRef]
266. Kenawy, E.R.; Kamoun, E.A.; Mohy Eldin, M.S.; El-Meligy, M.A. Physically Crosslinked Poly(Vinyl Alcohol)-Hydroxyethyl Starch Blend Hydrogel Membranes: Synthesis and Characterization for Biomedical Applications. *Arab. J. Chem.* **2014**, *7*, 372–380. [CrossRef]
267. Encalada, K.; Aldás, M.B.; Proaño, E.; Valle, V. *An Overview of Starch-Based Biopolymers and Their Biodegradability*; Ciencia e Ingeniería, Universidad de los Andes: Mérida, Venezuela, 2018; Volume 39.
268. Solihat, N.N.; Sari, F.P.; Falah, F.; Ismayati, M.; Lubis, M.A.R.; Fatriasari, W.; Santoso, E.B.; Syafii, W. Lignin as an Active Biomaterial: A Review. *J. Sylva Lestari* **2021**, *9*, 1. [CrossRef]
269. Ilyas, R.A.; Sapuan, S.M.; Harussani, M.M.; Hakimi, M.Y.A.Y.; Haziq, M.M.; Atikah, M.S.N.; Asyraf, M.R.M.; Ishak, M.R.; Razman, M.R.; Nurazzi, N.M.; et al. Polylactic Acid (Pla) Biocomposite: Processing, Additive Manufacturing and Advanced Applications. *Polymers* **2021**, *13*, 1326. [CrossRef]
270. Ilyas, R.A.; Sapuan, S.M.; Kadier, A.; Kalil, M.S.; Ibrahim, R.; Atikah, M.S.N.; Nurazzi, N.M.; Nazrin, A.; Lee, C.H.; Faiz Norrrahim, M.N.; et al. *Properties and Characterization of PLA, PHA, and Other Types of Biopolymer Composites*; Elsevier Inc.: Amsterdam, The Netherlands, 2020; ISBN 9780128196618.
271. Rodriguez-Contreras, A. Recent Advances in the Use of Polyhydroxyalkanoates in Biomedicine. *Bioengineering* **2019**, *6*, 82. [CrossRef]





## Article

# Antibacterial and Antifungal Fabrication of Natural Lining Leather Using Bio-Synthesized Silver Nanoparticles from *Piper Betle* L. Leaf Extract

Ngoc-Thang Nguyen <sup>1,\*</sup>, Tien-Hieu Vu <sup>1,2</sup> and Van-Huan Bui <sup>1</sup>

<sup>1</sup> Department of Textile Material and Chemical Processing, School of Textile-Leather and Fashion, Hanoi University of Science and Technology, 1 Dai Co Viet, Hanoi 11615, Vietnam; huan.buivan@hust.edu.vn (V.-H.B.)

<sup>2</sup> Department of Leather and Footwear Technology, Ho Chi Minh City Industry and Trade College, 20 Tang Nhon Phu, Ho Chi Minh 71210, Vietnam; vutienhieu@hitu.edu.vn (T.-H.V.)

\* Correspondence: thang.nguyenngoc@hust.edu.vn; Tel.: +84-904309930

**Abstract:** Leather is often used to make comfortable shoes due to its soft and breathable nature. However, its innate ability to retain moisture, oxygen and nutrients renders it a suitable medium for the adsorption, growth, and survival of potentially pathogenic microorganisms. Consequently, the intimate contact between the foot skin and the leather lining surface in shoes, which are subject to prolonged periods of sweating, may result in the transmission of pathogenic microorganisms and cause discomfort for the wearer. To address such issues, we modified pig leather with silver nanoparticles (AgPBL) that were bio-synthesized from *Piper betle* L. leaf extract as an antimicrobial agent via the padding method. The evidence of AgPBL embedded into the leather matrix, leather surface morphology and element profile of AgPBL-modified leather samples (pLeAg) was investigated using colorimetry, SEM, EDX, AAS and FTIR analyses. The colorimetric data confirmed that the pLeAg samples changed to a more brown color with higher wet pickup and AgPBL concentration, owing to the higher quantity of AgPBL uptake onto the leather surfaces. The antibacterial and antifungal activities of the pLeAg samples were both qualitatively and quantitatively evaluated using AATCC TM90, AATCC TM30 and ISO 16187:2013 test methods, approving a good synergistic antimicrobial efficiency of the modified leather against *Escherichia coli* and *Staphylococcus aureus* bacteria, a yeast *Candida albicans* and a mold *Aspergillus niger*. Additionally, the antimicrobial treatments of pig leather did not negatively impact its physico-mechanical properties, including tear strength, abrasion resistance, flex resistance, water vapour permeability and absorption, water absorption and desorption. These findings affirmed that the AgPBL-modified leather met all the requirements of upper lining according to the standard ISO 20882:2007 for making hygienic shoes.

**Keywords:** silver nanoparticles; green synthesis; *Piper betle* L. leaf; pig lining leather; antibacterial activity; antifungal activity

**Citation:** Nguyen, N.-T.; Vu, T.-H.; Bui, V.-H. Antibacterial and Antifungal Fabrication of Natural Lining Leather Using Bio-Synthesized Silver Nanoparticles from *Piper Betle* L. Leaf Extract. *Polymers* **2023**, *15*, 2634. <https://doi.org/10.3390/polym15122634>

Academic Editor: Raffaella Striani

Received: 11 May 2023

Revised: 3 June 2023

Accepted: 5 June 2023

Published: 9 June 2023



**Copyright:** © 2023 by the authors. Licensee MDPI, Basel, Switzerland. This article is an open access article distributed under the terms and conditions of the Creative Commons Attribution (CC BY) license (<https://creativecommons.org/licenses/by/4.0/>).

## 1. Introduction

Leather is a natural material obtained through the tanning process of a hide of an animal, bird or reptile. Leather has been extensively employed for making various items, such as footwear, clothing, bags, wallets and other accessories. Owing to its softness, breathability and high moisture-absorbing properties, leather provides comfort to the wearer [1–4]. However, due to its good moisture absorption, sweat-containing proteins may serve as a nutrient source that supports the growth of bacteria and fungi on leather goods, particularly within shoes where the foot skin is in close contact with the lining surface [5–8]. In addition, the collagen fiber network within the leather structure provides suitable conditions of moisture, temperature and oxygen for microorganism growth. Moreover, leather footwear products are commonly not washed during use, leading to the accumulation

and proliferation of microorganisms, resulting in unpleasant odors, discoloration, reduced mechanical strength and skin diseases in wearers [9–11]. The hot and humid climate in Vietnam provides proper conditions for bacterial and fungal growth on leather goods during storage, transportation and use. Hence, the antimicrobial characteristics of leather footwear products are concerns among both consumers and enterprises.

To overcome such issues, antimicrobial finishing of leather footwear products using various antimicrobial agents and treatment methods is often employed [2,3,8–11]. Many antibacterial and antifungal agents have been investigated for their effectiveness in leather treatment, including silver nanoparticles, zinc oxide nanoparticles, polymer compounds containing quaternary ammonium, chitosan and its derivatives [12–16]. These agents work through contact mechanisms and cell membrane disruption of microorganisms [17–19]. Although some chemical antimicrobial agents are used in the tanning process, their main function is to prevent the biodegradation of the leather rather than providing antimicrobial properties [2,12]. Furthermore, the use of some antibacterial and antifungal agents has been limited due to health and environmental concerns [20,21]. Therefore, developing high-performance antimicrobial agents that are effective against broad-spectrum bacterial and mold strains and environmentally friendly for leather material is imperative [20–22].

Thus, the appropriate selection of antimicrobial agents and treatment methods is important for creating durable antimicrobial leather materials that effectively prevent undesirable microbial growth while minimizing negative impacts on the material properties and the environment. To address these concerns, bio-synthesized silver nanoparticles (AgNPs) treated on leather have attracted significant attention from scientists due to their broad antimicrobial activity and durability to microorganisms [17,21,23,24]. The synthesis of green AgNPs involves the utilization of bio-reductants derived from natural resources such as plants, algae and microorganisms. Incorporating AgNPs into the collagen fiber matrix of leather enhances the material's long-lasting antimicrobial effects and exhibits low toxicity towards mammalian cells, making them suitable for producing high-quality leather goods [2,3].

Recently, we reported on a green approach to fabricating silver nanoparticles using *Piper betle* L. leaf extract (PBL) as bio-reductants to reduce Ag<sup>+</sup> ions into silver metal, which adheres fully to the principles of green chemistry [25]. The spherical shape and narrow size distribution of the obtained silver nanoparticles (AgPBL) showed good synergistic antibacterial activity against three common bacterial strains, including *Escherichia coli*, *Pseudomonas aeruginosa* and *Staphylococcus aureus*. In this work, we further evaluated the antifungal activity of AgPBL against one mold strain (*Aspergillus niger*) and one yeast strain (*Candida albicans*). We then investigated a simple approach to apply AgPBL onto tanned pig leather utilized for shoe lining (Le) by a padding method. The padding method was selected to apply antimicrobial treatment to the pig leather because it is suitable for use during the wet finishing stage of leather production. The presence and distribution of AgPBL on the pig leather surface were evaluated using various analytical techniques, namely colorimetry, scanning electron microscopy (SEM), energy-dispersive X-ray spectroscopy (EDX), atomic absorption spectroscopy (AAS) and Fourier-transform infrared spectroscopy (FTIR). The antibacterial and antifungal efficacy of the modified leather was assessed qualitatively and quantitatively using established protocols for antimicrobial testing of textile and leather materials in accordance with AATCC TM90, AATCC TM30 and ISO 16187:2013 against two bacterial strains (*Escherichia coli* and *Staphylococcus aureus*) and two fungal strains (*Aspergillus niger* and *Candida albicans*). To the best of our knowledge, there is no report available on the antibacterial and antifungal treatment of pig leather using bio-synthesized AgPBL for shoe lining application.

## 2. Materials and Methods

### 2.1. Materials

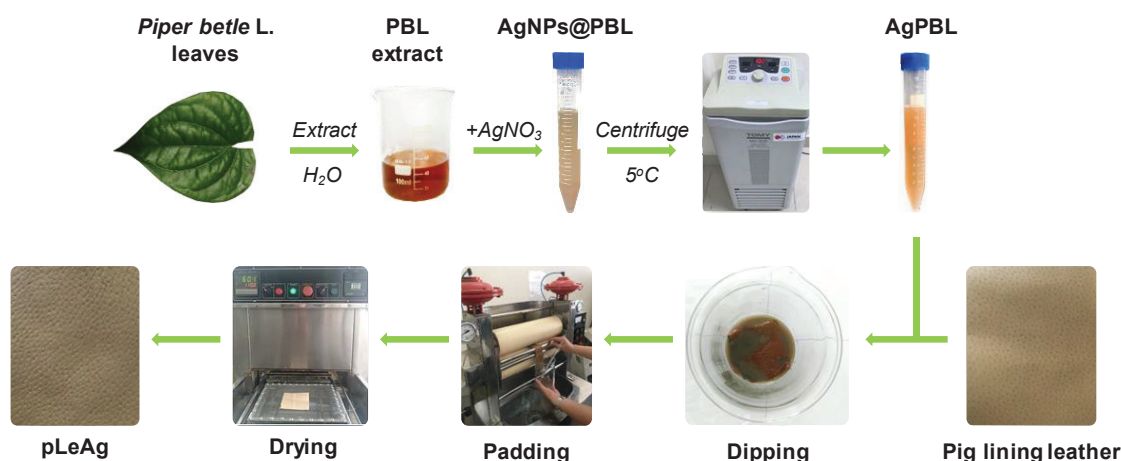
Analytical grade silver nitrate (Ag(NO)<sub>3</sub> 99.99%, Aladdin Biochemical Technology Co., Ltd., Shanghai, China) and *Piper betle* L. leaves (PBL, Hai Duong Province, Vietnam)

were used for the preparation of the silver nanoparticles (AgPBL) under optimal conditions according to our published research [25]. The samples of pristine pig leather (Le) in the wet-blue tanning form were obtained from Hung Thai Brothers Tannery Co., Ltd., Ho Chi Minh, Vietnam. The leather was then split in our laboratory using a DS818-420L leather splitter (Wenzhou Dashun Machinery Manufacture Co., Ltd., Zhejiang, China) to obtain a uniform thickness of  $1 \pm 0.1$  mm, which is proper for use as shoe lining material. The pig lining leather was further cut into small pieces ( $100 \times 100$  mm) and dried in a Mesdan M250-RH conditioning chamber (Brescia, Italy) at 65% RH and 25 °C for 24 h before being stored in a plastic bag for further study. In all experiments, double distilled water from an EYELA Still Ace SA-2100E (Tokyo Rikakikai Co., Ltd., Tokyo, Japan) was employed as the solvent. The dedicated medium (SCDLP), Luria-Bertani (LB) agar and Sabouraud dextrose agar (SDA) were supplied by Oxoid (Thermo Fisher Scientific Inc., Waltham, MA, USA). All microbial strains, including two bacterial strains *Escherichia coli* (*E. coli*, ATCC 25922) and *Staphylococcus aureus* (*S. aureus*, ATCC 29213, ATCC, Manassas, VA, USA), a mold strain *Aspergillus niger* (*A. niger*, ATCC 16404) and a yeast strain *Candida albicans* (*C. albicans*, ATCC 10231) were provided from the School of Biotechnology—International University, NTT Hi-Tech Institute—Nguyen Tat Thanh University, Institute of Tropical Biology—Vietnamese Academy of Science and Technology.

## 2.2. Synthesis and Application of AgPBL to Pig Lining Leather

We have previously described the bio-synthesis of the silver nanoparticles using *Piper betle* L. leaf extract as bio-reductants [25]. Briefly, dried PBL leaves were boiled with double distilled water at a ratio of 1:40 for 15 min. The mixture was then filtered through Whatman No. 1 filter paper. Subsequently, the resulting PBL filtrate underwent centrifugation at 10,000 rpm for 20 min to eliminate any insoluble residues. Prior to the nanosilver synthesis, the PBL supernatant was further diluted 20 times with double distilled water. For the AgPBL synthesis, 1 mL of 10 mM AgNO<sub>3</sub> solution was reduced with 10 mL of the diluted PBL extract and allowed to stand for 4 h at room temperature in the dark to avoid any unnecessary photochemical reactions. The mixtures containing silver nanoparticles were purified by centrifugation at 16,000 rpm, 5 °C for 30 min, followed by washing with double distilled water in a UT-106H Ultrasonic Cleaner (Sharp Corporation, Osaka, Japan). The purification process was repeated twice to remove residual reagents, and the AgPBL was collected and re-dispersed in double distilled water to achieve various concentrations for further investigation.

In the next step, the pig lining leather samples were treated with the bio-synthesized AgPBL solutions using the padding method. The leather samples were dipped in AgPBL solutions with various concentrations (160, 80, 40 and 20 µg/mL) for 30 min at a liquor-to-leather ratio of 5:1 (*w/w*). The wet pickups were set at 70%, 80% and 90%, and the padded samples were then dried at  $105 \pm 3$  °C for 3 min using SDL mini-drier 398 laboratory thermostatisation (SDL Atlas China, Shenzhen, China). The dipping–padding–drying processes of the leather samples were repeated two times. All processed leather samples were conditioned at 65% RH and 25 °C in a Mesdan M250-RH (Mesdan SpA, Brescia, Italy) conditioning chamber for 24 h before storage in plastic bags for microbiological analysis. The processes of synthesizing AgPBL and applying it onto pig lining leather are depicted in Figure 1.



**Figure 1.** Schematic illustration of the processes of AgPBL synthesis and its application onto pig lining leather, namely pLeAg.

### 2.3. Analytical Methods

#### 2.3.1. Characterization of the AgPBL

The UV-vis absorption spectrum of the AgPBL was acquired employing a UV-1800 spectrophotometer (Shimadzu, Kyoto, Japan) with a quartz cuvette in the range of 300–700 nm and with a resolution of 1 nm.

The diameters of AgPBL nanoparticles were recorded by transmission electron microscopy (JEOL JEM-1400, JEOL, Tokyo, Japan). A suspension of AgPBL in double distilled water was sonicated for 2 min and dropped onto a Cu-grid for TEM analysis.

#### 2.3.2. Characterization of the Modified Pig Leather

The morphology and chemical content of the control and AgPBL-modified leather samples after platinum sputtering were inspected using SM-6510LV JEOL (JEOL, Tokyo, Japan) scanning electron microscope (SEM) coupled to Oxford EDS Microanalysis System (Oxford Instruments NanoAnalysis, High Wycombe, UK).

A PinAAcle 900T atomic absorption spectrometer (AAS, PerkinElmer, Waltham, MA, USA) was employed to record silver content in the AgPBL-modified leather sample.

A Nicolet 6700 spectrometer (Thermo Scientific, Waltham, MA, USA) was utilized to record the FTIR spectra of the control and modified leather samples within the  $4000\text{--}500\text{ cm}^{-1}$  range.

Ci4200 spectrophotometer (X-rite, Grandville, MI, USA) was employed to report both colorimetric data ( $L^*$ ,  $a^*$  and  $b^*$ ) and color differences ( $\Delta E^*$ ) of the leather samples before and after treatment with the AgPBL solutions. In the CIELab color space,  $L^*$  is lightness from brightest white (100) to darkest black (0);  $a^*$  is the color ratio from red (+) to green (−) and  $b^*$  is the color ratio from yellow (+) to blue (−). The total color difference was determined using Equation (1):

$$\Delta E = \sqrt{\Delta L^{*2} + \Delta a^{*2} + \Delta b^{*2}} \quad (1)$$

where  $\Delta L^*$ ,  $\Delta a^*$  and  $\Delta b^*$  represent the colorimetric differences in  $L^*$ ,  $a^*$  and  $b^*$  values, respectively, of the blank and modified leather samples.

#### 2.3.3. Physico-Mechanical Characterization

The AgPBL-modified leather was evaluated for its physico-mechanical properties, which are essential requirements for shoe lining materials, in accordance with the standard ISO 20882:2007 [26]. These properties include tear strength (ISO 17696), abrasion resistance (ISO 17704), flex resistance (ISO 17694), lining water vapour permeability and absorption (ISO 17699), and lining water absorption and desorption (ISO 22649). The physico-mechanical tests were carried out at the Institute of Footwear Research, Vietnam.



## 2.4. Antibacterial and Antifungal Activities

### 2.4.1. Bio-Synthesized Silver Nanoparticles (AgPBL)

The antifungal activities of the AgPBL against yeast *C. albicans* and mold *A. niger* were studied by well diffusion method and disk diffusion method, respectively, following the Clinical Laboratory Standard Institute guidelines [27]. For the anti-yeast test, a suspension of *C. albicans* strain (0.1 mL,  $10^6$  CFU/mL) was spread uniformly on plates containing Sabouraud dextrose agar (SDA). Next, five 6 mm diameter holes were made using a sterile cork borer. Then, 60  $\mu$ L of AgPBL solutions at various concentrations (100, 50 and 25  $\mu$ g/mL), a standard antibiotic (Streptomycin, 80  $\mu$ g/mL) as positive control and double distilled water as negative control were poured into their respective wells. The zone of inhibition (ZOI) produced by *C. albicans* was recorded after 24 h of incubation at 37 °C.

For the anti-mold test of *A. niger*, the disk diffusion method was performed using sterile 6 mm paper discs loaded with AgPBL solutions (100, 50 and 25  $\mu$ g/mL) and double distilled water as the negative control. Aliquots of 0.1 mL of *A. niger* strain (approximately  $10^6$  CFU/mL) were spread on SDA agar plates, followed by the placement of the prepared paper discs on their surface. The zone of inhibition against *A. niger* was measured after 7 and 14 days of growth at 28 °C. The results were expressed as the mean  $\pm$  standard deviation (SD) of three independent tests.

The zone of inhibition (ZOI) was calculated based on Equation (2):

$$W = (T - D)/2 \quad (2)$$

where

W is the width of clear zone of inhibition, mm;

T is the total diameter of the test specimen and clear zone, mm;

D is the diameter of the test specimen, mm.

### 2.4.2. The Modified Pig Leather

The antibacterial and antifungal activities of the control and AgPBL-modified leather samples against *E. coli*, *S. aureus*, *C. albicans* and *A. niger* were investigated qualitatively and quantitatively using established protocols for testing the antimicrobial activity of textile and leather materials, including AATCC TM90, AATCC TM30 and ISO 16187:2013 test methods [28–30].

For qualitative tests (AATCC TM90 and AATCC TM30), the disk diffusion method was used to determine the zone of inhibition. A volume of 0.1 mL of each organism strain (approximately  $10^6$  CFU/mL) was spread on Luria-Bertani (LB) agar plates for bacteria and SDA agar plates for fungi. Next, the control and AgPBL-modified leather samples were positioned on the surface of agar plates, which were subsequently incubated at 37 °C for 24 h for bacteria and *C. albicans*, and at 28 °C for 7 and 14 days for *A. niger*. Zones of inhibition around and on the leather samples were visually examined.

For quantitative tests (ISO 16187:2013), the static challenge protocol was performed to determine the percentage reduction of bacteria. Six control samples (pristine leather, Le) and six modified leather samples (pLeAg) at each AgPBL concentration were prepared with dimensions of 25  $\times$  25  $\times$  1 mm and placed in individual sterile glass flasks. To each flask, 1 mL of bacterial suspension with a concentration of  $5.0 \times 10^5$  CFU/mL was added. At the initial time (zero contact time), three control samples and three modified leather samples were collected and washed out with 20 mL of dedicated medium (SCDLP). The remaining six flasks were incubated for 24 h at 37 °C (24 h contact time) and then washed out with 20 mL of the SCDLP medium. All flasks were tightly capped and shaken in an incubator shaker at 120 rpm and 37 °C for 30 s. A series of ten-fold dilutions of the bacterial sample solutions were made using NaCl 0.85% aqueous solution, and 100  $\mu$ L of each diluted bacterial solution was spread over LB agar plates. After incubating the plates



at 37 °C for 24 h, the surviving bacteria were enumerated by counting their colonies. The bacterial reduction percentage was measured using Equation (3):

$$R = (C_t - T_t) \times 100\% / C_t \quad (3)$$

where

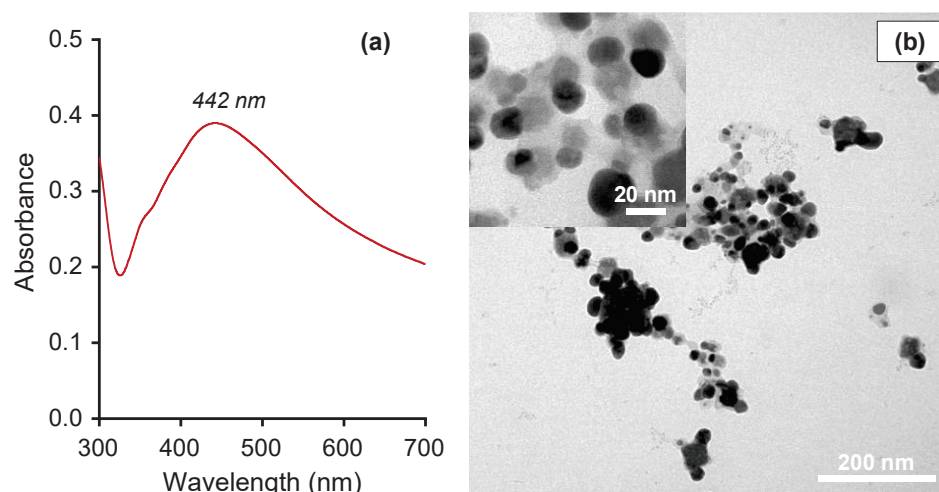
R is the bacterial reduction percentage, %;

$C_t$  and  $T_t$  are the average number of colonies of three control samples and three test samples after 24 h, respectively, CFU/mL.

### 3. Results and Discussion

#### 3.1. Synthesis and Antimicrobial Activity of AgPBL

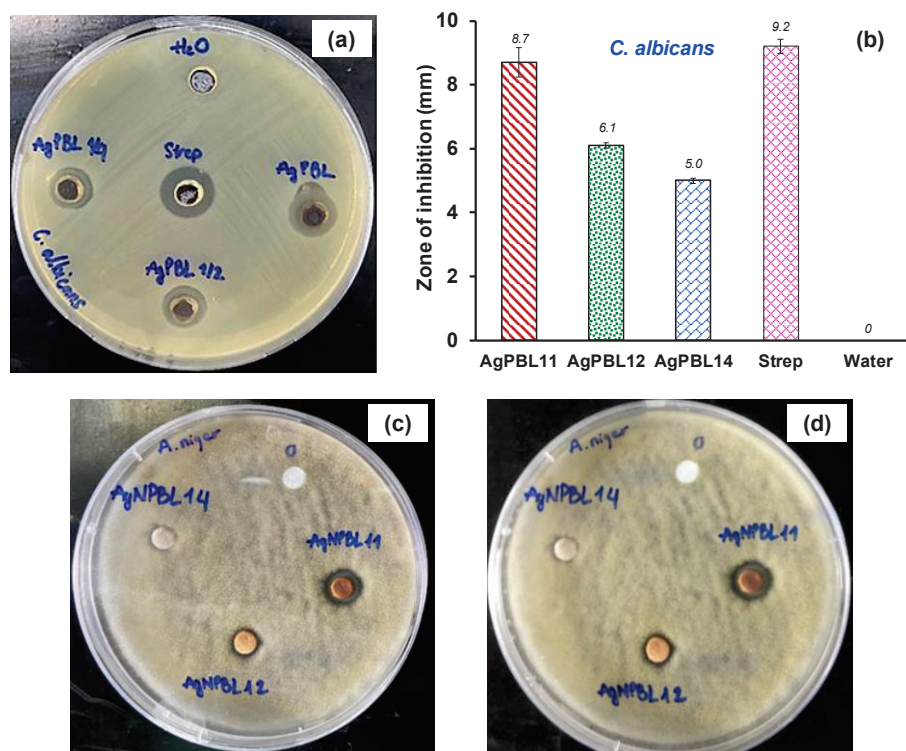
In previous research, we optimized the conditions for the bio-synthesis of silver nanoparticles from PBL leaf extract and evaluated their antibacterial activities against three bacterial strains, including *E. coli*, *P. aeruginosa* and *S. aureus* [25]. In the current work, we re-fabricated AgPBL under the optimized conditions and characterized its properties using UV-vis, TEM and antifungal activity analyses. The UV-Vis spectrum in Figure 2a indicated a maximum absorption peak at 442 nm due to the surface plasmon resonance (SPR) of spherical silver nanoparticles [21,22,25]. The TEM image in Figure 2b confirmed well-dispersed, spherical-shaped nanoparticles with a fairly uniform size of about 20 nm. The well-dispersion of AgPBL was attributed to the bio-constituents in the PBL extract, which effectively prevented nanoparticle agglomeration and stabilized them.



**Figure 2.** (a) UV-vis spectrum and (b) TEM micrographs of AgPBL with different magnification  $\times 30$  k and  $\times 200$  k (inset).

To assess the antifungal activity of the AgPBL, one mold strain (*A. niger*) and one yeast strain (*C. albicans*) were exposed to various AgPBL concentrations (100, 50 and 25  $\mu\text{g}/\text{mL}$ ) via the plate diffusion method. As shown in Figure 3a–d, the double distilled water (a negative control) exhibited no antifungal activity in terms of inhibition zone, while the AgPBL and the Streptomycin (Strep) obviously revealed ZOI. It was evident that AgPBL showed promising antifungal activity against both tested fungi. A comparison of the ZOI size for each fungal strain indicated a tendency for decreased antifungal action with decreasing AgPBL concentration, although this tendency was not proportional to the change in AgPBL concentration. For instance, reducing the AgPBL concentration by 50% and 75% resulted in a ZOI reduction for *C. albicans* of 29.9% and 42.5%, respectively. The results observed from Figure 3c,d after 7 and 14 days of the antifungal tests against *A. niger* revealed clearly that mold spores could not grow on the AgPBL-impregnated paper disks at any concentration. However, the paper disk impregnated with 25  $\mu\text{g}/\text{mL}$  AgPBL solution did not exhibit a clear inhibition zone, indicating that the antifungal activity of AgPBL against *C. albicans* was better than against *A. niger*. The

antifungal properties exhibited by bio-synthesized AgNPs were consistent with the findings of previous studies [31,32].



**Figure 3.** Antifungal activities of the AgPBL: (a) Well diffusion method displaying the anti-*C. albicans* action of AgPBL11 (AgPBL 100  $\mu\text{g}/\text{mL}$ ), AgPBL12 (AgPBL 50  $\mu\text{g}/\text{mL}$ ), AgPBL14 (AgPBL 25  $\mu\text{g}/\text{mL}$ ), Streptomycin (80  $\mu\text{g}/\text{mL}$ , positive control) and H<sub>2</sub>O (negative control); (b) Mean zone of inhibition of AgPBL against *C. albicans* ( $\pm\text{SD}$ ,  $n = 3$ ); Disk diffusion method displaying the anti-*A. niger* action of AgPBL after (c) 7 days and (d) 14 days of incubation.




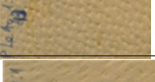




### 3.2. Coloration and Characteristics of the AgPBL-Modified Pig Leather

The presence of AgPBL on pig lining leather was visually observed through the color change of the sample during the treatment of the leather with bio-synthesized AgPBL solutions using the padding method. Indeed, the color of the leather was changed significantly from bright yellow to light brownish color. To illustrate the effect of the wet pickup and AgPBL concentration on the coloration of the leather surface, the colorimetric data ( $L^*$ ,  $a^*$ ,  $b^*$ ) and color differences ( $\Delta E^*$ ) of the leather samples were evaluated, as shown in Table 1. The color of the blank leather was bright yellow with relatively high  $L^*$ ,  $a^*$  and  $b^*$  values of 62.42, 9.77 and 23.86, respectively. To compare with the blank leather, the AgPBL-modified leather samples showed smaller  $L^*$ ,  $a^*$  and  $b^*$  values, indicating a browning effect of the AgPBL on the leather samples. The  $\Delta E^*$  of the modified samples increased with higher wet pickup and AgPBL concentration, owing to the higher quantity of AgPBL uptake onto the leather surfaces.

To get visual evidence of the AgPBL embedded onto the leather, leather surface morphologies and element profile of the blank and modified leather samples were investigated. As shown in Figure 4, the blank and modified leather revealed a distinctive hierarchically suprafibrillar structure of the collagen fiber strands. The micrographs of modified leather samples (Figure 4) revealed the occurrence of nanoparticles loosely attached to the leather surface. In dark-field SEM images, nano metals usually appear as bright spots due to their strong light scattering [22,33]. However, the silver nanoparticles employed in this work were about 20 nm in size and could impregnate deeply into the collagen fiber strands of the leather matrix. As a result, they could be challenging to detect in SEM images, which only provide information on the surface morphology of the sample. Therefore, EDX analytical

technique was performed to validate the presence of nanosilver on the leather sample after treatment.

**Table 1.** Colorimetric data, color differences and images of the AgPBL-modified leather samples in comparison with the blank pig leather.

Sample	Wet Pickup (%)	AgPBL ( $\mu\text{g/mL}$ )	L*	a*	b*	$\Delta E^*$	Real Images
Le	-	-	62.42	9.77	23.86	0	
pLeAg11	70		57.94	9.13	21.38	2.33	
pLeAg12	80	160	57.97	9.75	21.12	2.41	
pLeAg13	90		57.01	9.27	21.38	2.66	
pLeAg12		160	57.97	9.75	21.12	2.41	
pLeAg22	80	80	59.85	9.29	22.27	1.39	
pLeAg32		40	59.94	9.79	23.07	1.15	
pLeAg42		20	60.01	9.54	23.74	1.04	

The EDX spectrum of the blank leather in Figure 4 revealed no Ag signal, but the occurrence of a Cr signal confirming that the pig leather was chrome-tanned leather. In contrast, the EDX spectra of the AgPBL-modified leather sample via the padding treatment (pLeAg) clearly showed a strong signal of elemental silver at 3 keV which authenticated the existence of AgPBL on the leather surface [9,12]. The EDX spectra of those modified samples confirmed again that the bright points in the SEM images were AgPBL.

To evaluate the amount of AgPBL adhered to the pig leather after padding treatment, the AAS analysis was performed, and the result was presented in Table 2. The data indicates that the total silver content in the padded sample was around 380 mg/kg, whereas the blank leather sample did not contain any silver.

**Table 2.** Total silver content of the leather samples.

Sample	Wet Pickup (%)	AgPBL ( $\mu\text{g/mL}$ )	Total Silver Content (mg/kg)
Le	-	-	0
pLeAg12	80	160	379.0 $\pm$ 4.6

In order to determine the possible interaction between AgPBL and the functional groups of collagen proteins on the modified leather, the FTIR analyses of Le and pLeAg samples were carried out, and the spectra were given in Figure 5. The characteristic peaks corresponding to the functional groups of the collagen proteins in the Le sample at 3304.5, 2921.1, 2852.3, 1633.5, 1547.8, 1236.6 and 1030.9  $\text{cm}^{-1}$  were assigned to  $-\text{NH}$ ,  $-\text{CH}_3$ ,  $=\text{CH}_2$ ,  $-\text{C}=\text{O}$ ,  $-\text{NH}$ ,  $-\text{C}=\text{O}$  (in amide III) and  $\text{C}-\text{N}$  (in amine) groups, respectively [10,13,34]. Compared to the blank leather, the pLeAg spectrum exhibited similarity in their characteristic peaks, except for the stronger peak intensities, suggesting the chemical structure of the leather was mostly unchanged. The collagen proteins of leather contain polar groups on the side chains of their constituent amino acid residues, and as such, the amide and carboxylate functional groups of these residues have a tendency to bind with metal atoms [10,12]. Thus, AgPBL could be

absorbed onto the leather surface through the electrostatic interaction of  $\text{Ag}^+$  ions with the negative charge of  $\text{RCOO}^-$  or lone-pair electrons of N atoms of amino acids. In addition, the formation of hydrogen bonding between the amide and carboxylate groups of the collagen proteins with the appropriate functional groups of the organic layer existing on the AgPBL surface also contributes to these binding interactions. The shifted peaks of the functional groups in the modified leather samples could be attributed to the interaction of heavy silver atoms with the amino and amide groups of collagen protein molecules, resulting in an increase in peak intensity [12]. The results of coloration, SEM, EDX, AAS and FTIR measurements for both blank and modified leather samples were consistent with each other, providing strong evidence for the incorporation of AgPBL into the leather matrix.

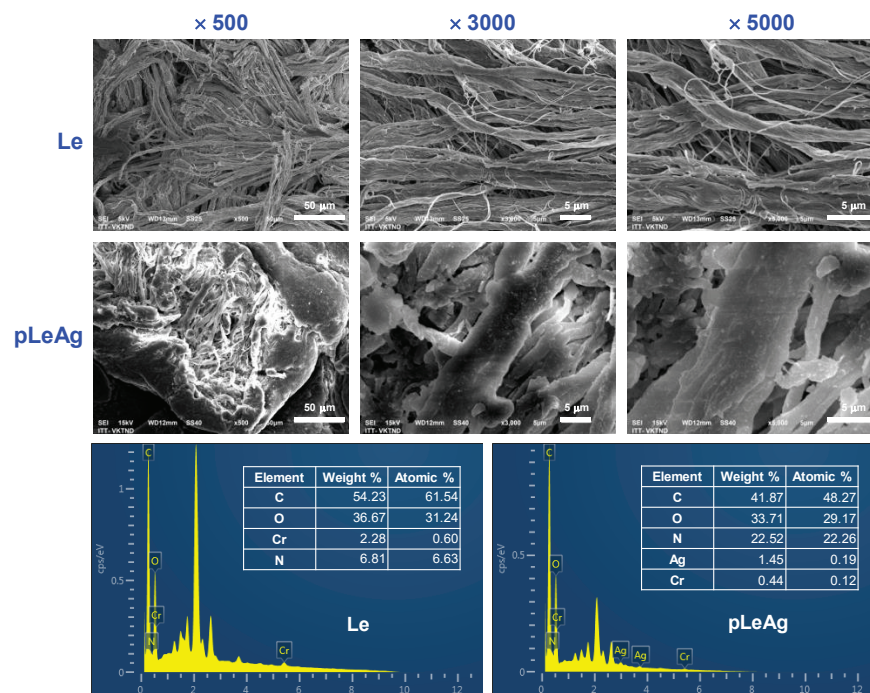


Figure 4. The SEM micrographs at different magnifications of  $\times 500$ ,  $\times 3000$  and  $\times 5000$ , and EDX spectra of the blank leather (Le) and the AgPBL-modified leather sample (pLeAg).

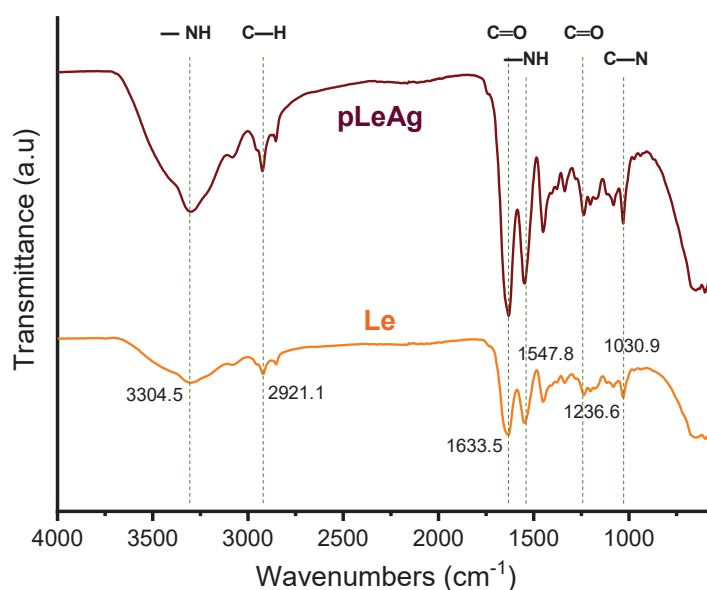


Figure 5. The FTIR spectra of the Le and pLeAg samples.



### 3.3. Antibacterial and Antifungal Efficacy of the AgPBL-Modified Pig Leather

Leather is a naturally hydrophilic material that offers a potential medium for the growth of microorganisms such as bacteria, yeasts and molds. The utilization of silver nanoparticles on the lining of leather could avoid the risk of infection and extend the lifetime of leather products by inhibiting microorganism growth. In this research, we investigated the antibacterial and antifungal efficacy of AgPBL-modified leather against *E. coli*, *S. aureus*, *C. albicans* and *A. niger*. Both qualitative (the disk diffusion method) and quantitative (the static challenge protocol of dynamic contact method) tests were employed to determine the antimicrobial activities of the modified leather.

#### 3.3.1. Antibacterial Efficacy

The AgPBL-modified leather samples obtained via the padding method were evaluated for their antibacterial activities against a gram-negative bacterium *E. coli* and a gram-positive bacterium *S. aureus*. The effect of the wet pickup and AgPBL concentration on the antibacterial efficacy of the modified leather was examined, and results were shown in Figure 6 and Table 3.

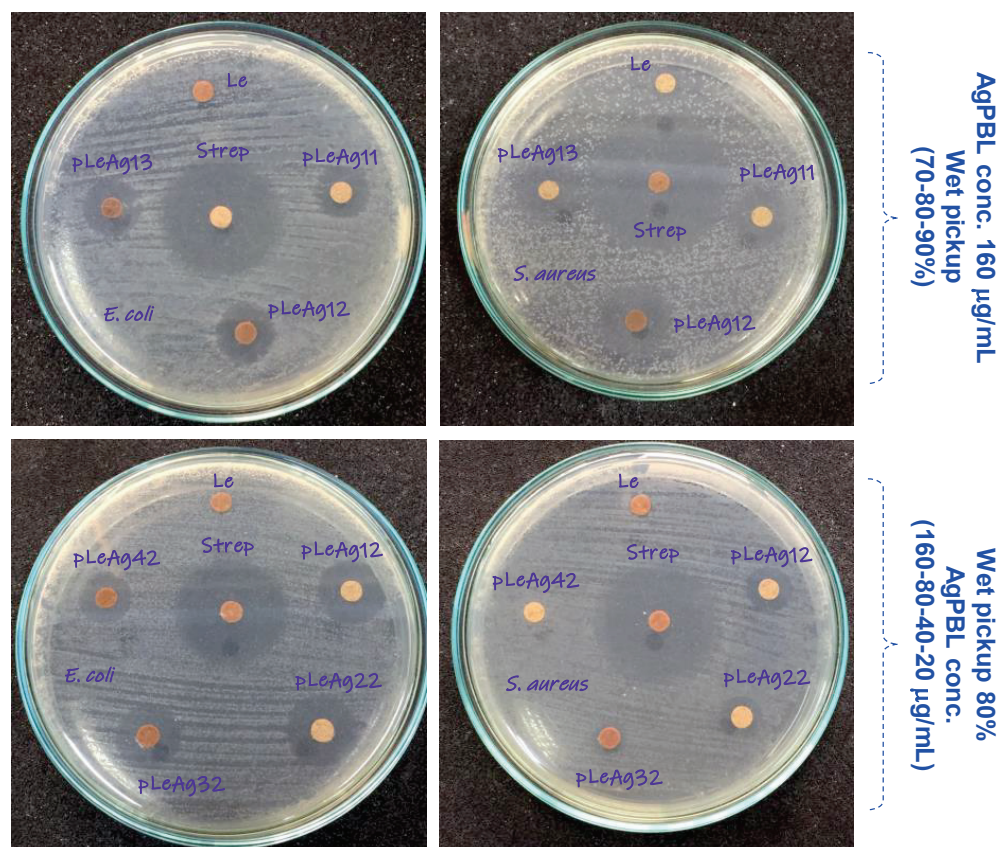
**Table 3.** The ZOI of AgPBL-modified leather samples against *E. coli* and *S. aureus* ( $\pm$ SD,  $n = 3$ ).

Sample	Wet Pickup (%)	AgPBL ( $\mu$ g/mL)	<i>E. coli</i>	<i>S. aureus</i>
Vis	-	-	0	0
Strep	-	-	21.10 $\pm$ 1.10	29.00 $\pm$ 0.73
pLeAg11	70		8.40 $\pm$ 0.37	9.60 $\pm$ 0.33
pLeAg12	80	160	8.70 $\pm$ 0.21	10.20 $\pm$ 0.24
pLeAg13	90		8.20 $\pm$ 0.22	9.10 $\pm$ 0.36
Strep'	-	-	23.30 $\pm$ 0.92	24.00 $\pm$ 1.02
pLeAg12		160	11.40 $\pm$ 1.10	8.40 $\pm$ 0.33
pLeAg22	80	80	11.20 $\pm$ 0.24	7.30 $\pm$ 0.22
pLeAg32		40	10.50 $\pm$ 1.00	2.10 $\pm$ 0.08
pLeAg42		20	8.40 $\pm$ 0.37	-

A quick survey across Figure 6 evidences that all the AgPBL-modified leather samples and the Strep-treated leather exhibited obviously ZOI against *E. coli* and *S. aureus*, whereas the pristine leather (Le) showed no activity at all. These findings demonstrate the antibacterial efficacy of the AgPBL-modified leather in this work. As shown in Figure 6, the ZOI of the modified leather samples did not change significantly with varying wet pickups. The pLeAg12 sample with a wet pickup of 80% exhibited the highest ZOI of 8.7  $\pm$  0.21 and 10.2  $\pm$  0.24 mm against *E. coli* and *S. aureus*, respectively. Accordingly, the wet pickup of 80% was selected for further evaluation of the antibacterial activity.

Table 3 presents the results of the antibacterial tests of the padded leather samples, which showed that higher AgPBL concentrations led to larger inhibition zones. However, the relationship between AgPBL concentration and inhibition zone was not proportional. Indeed, as compared to the pLeAg12 sample, when the AgPBL concentrations were decreased by 50% and 75%, the ZOI of pLeAg22 and pLeAg32 samples against *E. coli* decreased by 0.9% and 42.0%, respectively. Additionally, there was a slight difference in the inhibition zone between leather samples treated with AgPBL concentrations of 160 and 80  $\mu$ g/mL. Moreover, the antibacterial results in terms of inhibition zone clearly demonstrated that the AgPBL-modified leather samples exhibited higher effectiveness against gram-negative bacteria than gram-positive bacteria, which is in line with previous findings regarding the bactericidal properties of bio-synthesized silver nanoparticles [25,35].





**Figure 6.** The photographs showing zone of inhibition of the Le, pLeAg and Streptomycin (80 µg/mL) treated leather samples against *E. coli* and *S. aureus*, with change in the wet pickup and AgPBL concentration.

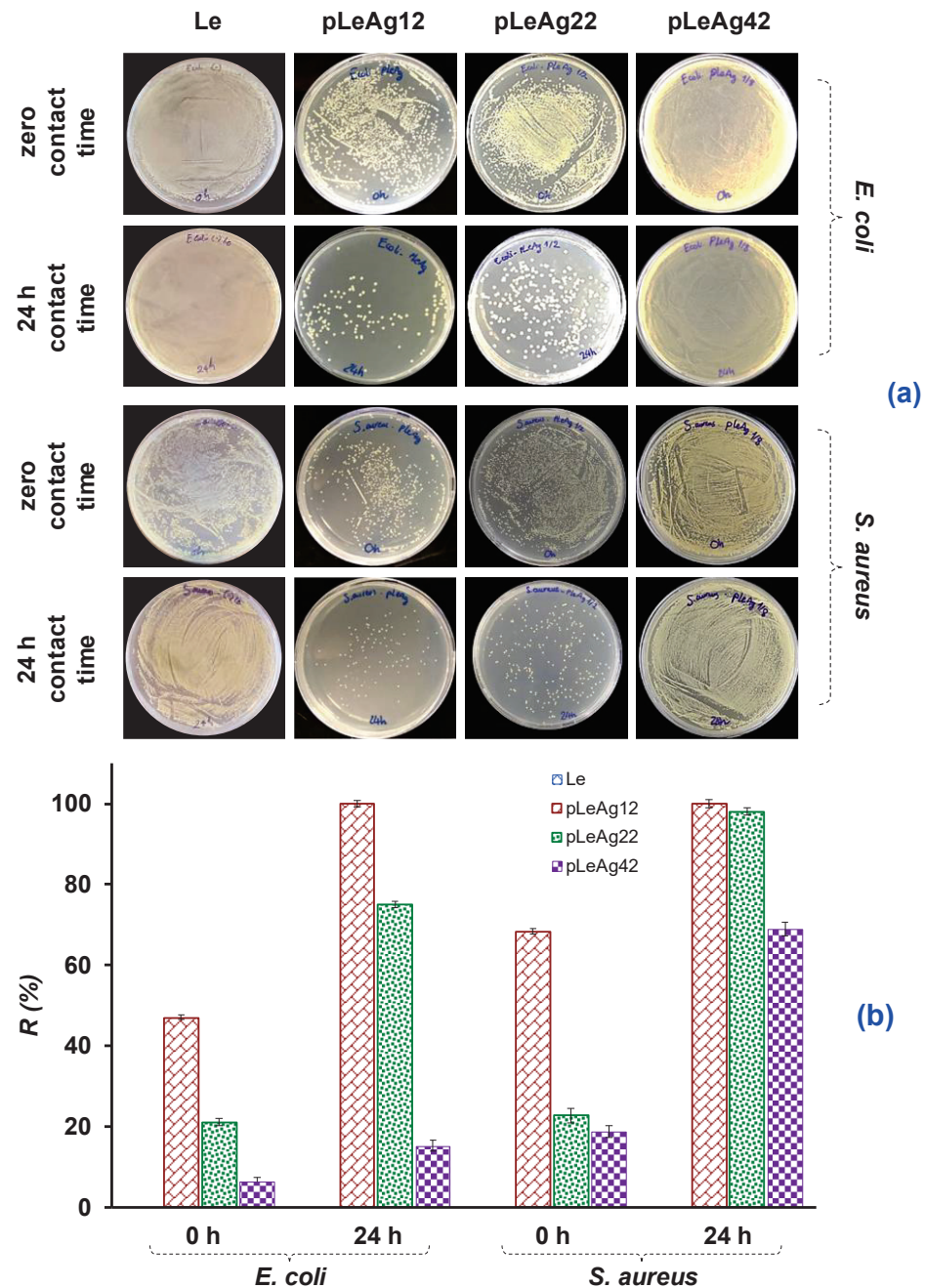
The leather samples treated with various AgPBL concentrations at the wet pickup of 80% were subjected to the quantitative test to determine the bacterial reduction percentage. This test was performed at 0 h and 24 h contact times between the sample and the test bacteria inoculate. As shown in Figure 7a, the Petri dishes for 24 h contact time revealed that both tested bacteria grew well on the Petri dishes of blank leather, indicating that Le did not possess bacterial inhibition. Based on the agar's turbidity, the pLeAg12 samples showed the highest antibacterial activity, while the pLeAg42 samples exhibited the lowest.

By counting the number of colonies of tested bacteria on agar dishes, the bacterial reduction percentage of the treated leather samples with different concentrations of AgPBL was plotted in Figure 7b. The results showed that the pLeAg12 samples treated with 160 µg/mL AgPBL exhibited the highest antibacterial efficiency against both *E. coli* and *S. aureus* after 0 h contact time, with bacterial reduction percentages of 47.02% and 68.43%, respectively. Moreover, both achieved a 100% antibacterial rate after a 24 h contact time.

The antibacterial activity of pLeAg22 samples treated with 80 µg/mL AgPBL decreased significantly against *E. coli* after both 0 h and 24 h contact time. In comparison to pLeAg12 samples, the bactericidal rates of pLeAg22 samples against *E. coli* and *S. aureus* decreased by 24.8% and 1.88%, respectively, after 24 h contact time. Similarly, pLeAg42 samples treated with 20 µg/mL AgPBL exhibited a sharp decrease in antibacterial activity against both tested bacteria. Compared to the pLeAg12 samples, the bactericidal rates of the pLeAg42 samples against *E. coli* and *S. aureus* after 24 h contact time declined by 84.93% and 31.13%, respectively. Despite the lack of a zone of inhibition in the AgPBL-modified leather sample at a low concentration (20 µg/mL AgPBL) observed by the qualitative antibacterial method, the sample still possessed a weak antibacterial ability.

Based on the obtained antibacterial results, the quantitative antibacterial efficiency of the modified leather samples is strongly influenced by the initial AgPBL concentration

in the treated solutions. The antibacterial efficiency also depends on the tested bacteria and is not proportional to the change in AgPBL concentration. The findings are consistent with the qualitative antibacterial evaluation of the modified leather samples. The suitable concentration of AgPBL for pig lining leather treatment was 160 µg/mL to achieve 100% antibacterial efficiency after 24 h contact time.

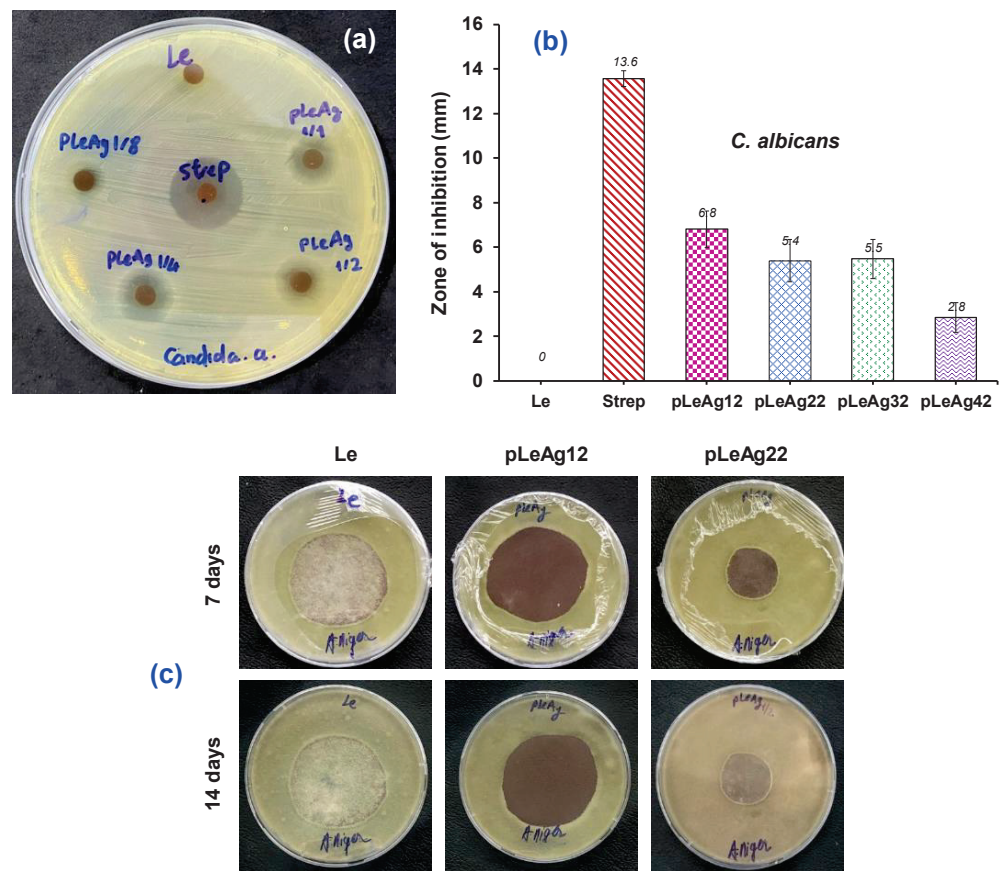


**Figure 7.** (a) The photographs of bacterial growth in the nutrient agar plates and (b) The bacterial reduction percentage (%R) of the Le and AgPBL-modified leather samples against *E. coli* and *S. aureus*.

### 3.3.2. Antifungal Efficacy

The AgPBL-modified leather samples were evaluated for their antifungal activities against one yeast strain (*C. albicans*) and one mold strain (*A. niger*) according to AATCC TM30. Figure 8 depicted that the blank leather revealed no antifungal activity, whereas both AgPBL-modified leather samples and the Strep-treated leather exhibited considerable antifungal efficiency against the tested fungi. Figure 8a,b confirmed that a decrease in the treated

AgPBL concentration resulted in a reduction of antifungal efficacy against the *C. albicans* strain, as evidenced by a decrease in the ZOI value by 20.6% and 19.6% when the treated AgPBL concentration was reduced by 50% and 75%, respectively. As shown in Figure 8c, the antifungal tests against *A. niger* after 7 and 14 days revealed that the pLeAg12 sample padded with 160 µg/mL AgPBL solution did not show any mold spore germination or growth. However, the pLeAg22 sample padded with 80 µg/mL AgPBL solution exhibited mold spore growth on its surface after 7 days, which was obviously seen after 14 days of incubation. These findings confirm once again the strong dependence of the antimicrobial effectiveness of the AgPBL-modified samples on the AgPBL concentration in the antimicrobial-treated solution. Consequently, pig leather treated with 160 µg/mL solution at a wet pickup of 80% was selected for further evaluation of its physico-mechanical properties.



**Figure 8.** (a) Antifungal activities of the Le, pLeAg and Strep-treated leather samples against *C. albicans* with change in the AgPBL concentration; (b) Mean zone of inhibition against *C. albicans* ( $\pm$ SD,  $n = 3$ ); (c) Antifungal activities of the Le, pLeAg12 and pLeAg22 samples against *A. niger* after 7 and 14 days of incubation.

### 3.4. The Physico-Mechanical Properties of the AgPBL-Modified Pig Leather

The blank leather and AgPBL-modified leather samples were subjected to various tests following standard specifications to evaluate their physico-mechanical properties. The experimental data were compared with the requirements of the shoe lining material according to the standard ISO 20882:2007. As presented in Table 4, the mechanical properties of the AgPBL-modified leather including tear strength, abrasion resistance and flex resistance were nearly identical to those of pristine leather. This is because the antimicrobial treatment process used in this research did not alter the chemical structure of pig leather, and nanosilver adheres to the leather matrix solely through physical bonds. The mechanical data of the modified samples met all the standard requirements for shoe lining, and the tear strength was even over 200% of the standard requirement.



Similarly, the antimicrobial treatment of leather with AgPBL did not affect its water absorption and water desorption. The water absorption of the leather samples before and after treatment was around 90% of the standard requirements for the lining. However, this lining layer is typically combined with a porous layer in the shoe upper structure, resulting in an enhancement of its water absorption capacity. The water desorption of the leather samples was excellent, reaching over 160% of the standard requirement. The water vapour permeability and water vapour absorption of the leather samples were very good, exceeding 150% of the standard requirements for upper lining material. Pore expansion on the modified leather surface after the padding process led to an increase in its water vapour permeability. The leather material swells when it absorbs water and then shrinks during the drying process. However, the collagen fiber strands' shrinkage is greater than that of the pores, leading to pore expansion.

**Table 4.** The physico-mechanical properties of the pristine leather and AgPBL-modified pig leather.

No	Properties	Unit	Le	pLeAg	ISO 20882:2007 Requirements
1	<b>Tear strength</b> (ISO 17696)	N	32	32.5	lining $\geq$ 15 N
	<i>Compare to the pristine leather (Le)</i>	%	100.0	101.6	
	<i>Compare to ISO 20882:2007</i>	%	213.3	216.7	
2	<b>Abrasion resistance</b> (ISO 17704)	cycles	Without hole through the thickness of the material component		25,600 cycles dry 12,800 cycles wet
3	<b>Flex resistance</b> (ISO 17694)	cycles	15,000 cycles dry without visible damage		Dry 15,000 cycles without visible damage
4	<b>Lining water vapour permeability</b> (ISO 17699)	mg/cm <sup>2</sup> .h	3.13	3.62	WVP of lining $\geq$ 2.0 mg/cm <sup>2</sup> .h
	<i>Compare to the pristine leather (Le)</i>	%	100.0	115.7	
	<i>Compare to ISO 20882:2007</i>	%	156.0	181.0	
5	<b>Lining water vapour absorption</b> (ISO 17699)	mg/cm <sup>2</sup>	21.0	20.8	WVA of lining $\geq$ 8.0 mg/cm <sup>2</sup>
	<i>Compare to the pristine leather (Le)</i>	%	100.0	99.0	
	<i>Compare to ISO 20882:2007</i>	%	263.0	260.0	
6	<b>Lining water absorption</b> (ISO 22649)	mg/cm <sup>2</sup>	54.1	53.9	absorption $\geq$ 70 mg/cm <sup>2</sup>
	<i>Compare to the pristine leather (Le)</i>	%	100.0	99.6	
	<i>Compare to ISO 20882:2007</i>	%	90.1	89.3	
7	<b>Lining water desorption</b> (ISO 22649)	%	97.1	97.2	desorption $\geq$ 60 %
	<i>Compare to the pristine leather (Le)</i>	%	100.0	100.1	
	<i>Compare to ISO 20882:2007</i>	%	161.8	162	

In general, the antimicrobial treatments of pig leather did not negatively impact its physico-mechanical properties. The AgPBL-modified leather met all the requirements according to the standard ISO 20882:2007 for making shoe linings. The padding method is suitable for tanneries, which is carried out at the wet finishing stage (dyeing, oiling, etc.) in a rotary drum, then padded and transferred to the drying finishing stage in a drying chamber.

#### 4. Conclusions

This research provided a simple approach for the fabrication of highly effective antimicrobial pig leather modified with bio-synthesized silver nanoparticles as an antimicrobial agent via the dipping–padding–drying processes. The effect of the wet pickup and AgPBL concentration on the coloration, antimicrobial activity and physico-mechanical properties of the modified leather were investigated according to standard methods. The experiment data validated that the higher wet pickup and AgPBL concentration led to a browner color and enhanced antimicrobial efficacy of the AgPBL-modified leather against both bacteria (*E. coli* and *S. aureus*) and fungi (a yeast *C. albicans* and a mold *A. niger*). These observed results could be attributed to the increased uptake of AgPBL into the leather matrix, which was verified through SEM, EDX, AAS, and FTIR analyses. However, the antimicrobial treatment of pig leather using the padding method did not have any adverse effect on its physico-mechanical properties, and it met the ISO 20882:2007 standard’s requirements for the upper lining. Therefore, based on the efficient antimicrobial and suitable physico-mechanical properties, the AgPBL-modified pig leather meets the criteria for making upper lining in hygienic shoe production.

**Author Contributions:** Conceptualization, N.-T.N. and V.-H.B.; methodology, N.-T.N., V.-H.B. and T.-H.V.; formal analysis, T.-H.V.; investigation, N.-T.N., V.-H.B. and T.-H.V.; data curation, N.-T.N. and V.-H.B.; writing—original draft preparation, T.-H.V.; writing—review and editing, N.-T.N. and V.-H.B.; visualization, N.-T.N. and T.-H.V.; supervision, N.-T.N. and V.-H.B.; project administration, N.-T.N.; funding acquisition, N.-T.N. All authors have read and agreed to the published version of the manuscript.

**Funding:** This work was funded by the Vietnam Ministry of Education and Training under Grant No. B2022-BKA-23.

**Institutional Review Board Statement:** Not applicable.

**Data Availability Statement:** The data presented in this study are available on request from the corresponding author.

**Acknowledgments:** The authors also would like to thank colleagues from School of Textile—Leather and Fashion, Hanoi University of Science and Technology for their efforts in supporting this work.

**Conflicts of Interest:** The authors declare no conflict of interest.

#### References

- Bai, Z.; Wang, X.; Zheng, M.; Yue, O.; Xie, L.; Zha, S.; Dong, S.; Li, T.; Song, Y.; Huang, M.; et al. Leather for flexible multifunctional bio-based materials: A review. *J. Leather Sci. Eng.* **2022**, *4*, 16. [CrossRef]
- Xia, Q.; Yang, L.; Hu, K.; Li, K.; Xiang, J.; Liu, G.; Wang, Y. Chromium Cross-Linking Based Immobilization of Silver Nanoparticle Coating on Leather Surface with Broad-Spectrum Antimicrobial Activity and Durability. *ACS Appl. Mater. Interface* **2019**, *11*, 2352–2363. [CrossRef]
- Wu, X.; Wu, J.; Mu, C.; Wang, C.; Lin, W. Advances in Antimicrobial Polymer Coatings in the Leather Industry: A Comprehensive Review. *Ind. Eng. Chem. Res.* **2021**, *60*, 15004–15018. [CrossRef]
- Fan, Q.; Ma, J.; Xu, Q. Insights into functional polymer-based organic-inorganic nanocomposites as leather finishes. *J. Leather Sci. Eng.* **2019**, *1*, 3. [CrossRef]
- Liu, G.; Haiqi, G.; Li, K.; Xiang, J.; Lan, T.; Zhang, Z. Fabrication of silver nanoparticle sponge leather with durable antibacterial property. *J. Colloid Interface Sci.* **2018**, *514*, 338–348. [CrossRef]
- Lkhagvajav, N.; Koizhaiganova, M.; Yasa, I.; Çelik, E.; Sari, Ö. Characterization and antimicrobial performance of nano silver coatings on leather materials. *Braz. J. Microbiol.* **2015**, *46*, 41–48. [CrossRef]



7. Sportelli, M.C.; Picca, R.A.; Paladini, F.; Mangone, A.; Giannossa, L.C.; Di Franco, C.; Gallo, A.L.; Valentini, A.; Sannino, A.; Pollini, M. Spectroscopic characterization and nanosafety of Ag-modified antibacterial leather and leatherette. *Nanomaterials* **2017**, *7*, 203. [CrossRef]
8. Abou Elmaaty, T.; Sayed-Ahmed, K.; Mohamed Ali, R.; El-Khodary, K.; Abdeldayem, S.A. Simultaneous sonochemical coloration and antibacterial functionalization of leather with selenium nanoparticles (SeNPs). *Polymers* **2022**, *14*, 74. [CrossRef]
9. Velmurugan, P.; Lee, S.-M.; Cho, M.; Park, J.-H.; Seo, S.-K.; Myung, H.; Bang, K.-S.; Oh, B.-T. Antibacterial activity of silver nanoparticle-coated fabric and leather against odor and skin infection causing bacteria. *Appl. Microbiol. Biotechnol.* **2014**, *98*, 8179–8189. [CrossRef]
10. Elsayed, H.; Hasanin, M.; Rehan, M. Enhancement of multifunctional properties of leather surface decorated with silver nanoparticles (Ag NPs). *J. Mol. Struct.* **2021**, *1234*, 130130. [CrossRef]
11. Xiang, J.; Ma, L.; Su, H.; Xiong, J.; Li, K.; Xia, Q.; Liu, G. Layer-by-layer assembly of antibacterial composite coating for leather with cross-link enhanced durability against laundry and abrasion. *Appl. Surf. Sci.* **2018**, *458*, 978–987. [CrossRef]
12. Velmurugan, P.; Cho, M.; Lee, S.-M.; Park, J.-H.; Bae, S.; Oh, B.-T. Antimicrobial fabrication of cotton fabric and leather using green-synthesized nanosilver. *Carbohydr. Polym.* **2014**, *106*, 319–325. [CrossRef] [PubMed]
13. Koizhaiganova, M.; Yaşa, I.; Gülümser, G. Assessment of antibacterial activity of lining leather treated with silver doped hydroxyapatite. *Int. Biodeterior. Biodegrad.* **2015**, *105*, 262–267. [CrossRef]
14. Velmurugan, P.; Shim, J.; Bang, K.-S.; Oh, B.-T. Gold nanoparticles mediated coloring of fabrics and leather for antibacterial activity. *J. Photochem. Photobiol. B* **2016**, *160*, 102–109. [CrossRef]
15. Kate, S.; Sahasrabudhe, M.; Pethe, A. Biogenic Silver Nanoparticle Synthesis, Characterization and its Antibacterial activity against Leather Deteriorates. *Jordan J. Biol. Sci.* **2020**, *13*, 493–498.
16. Rohaeti, E.; Kasmudjiastuti, E.; Murti, R.; Dodi, I. Enhancement of antibacterial activity of suede leather through coating silver nanoparticles synthesized using piper betle. *Rasayan J. Chem.* **2020**, *13*, 628–635. [CrossRef]
17. Abdelghany, T.M.; Al-Rajhi, A.M.H.; Al Abboud, M.A.; Alawlaqi, M.M.; Ganash Magdah, A.; Helmy, E.A.M.; Mabrouk, A.S. Recent Advances in Green Synthesis of Silver Nanoparticles and Their Applications: About Future Directions. A Review. *BioNanoScience* **2018**, *8*, 5–16. [CrossRef]
18. Sharma, V.K.; Yngard, R.A.; Lin, Y. Silver nanoparticles: Green synthesis and their antimicrobial activities. *Adv. Colloid Interface Sci.* **2009**, *145*, 83–96. [CrossRef]
19. Thi Lan Huong, V.; Nguyen, N.T. Green synthesis, characterization and antibacterial activity of silver nanoparticles using *Sapindus mukorossi* fruit pericarp extract. *Mater. Today Proc.* **2021**, *42*, 88–93. [CrossRef]
20. Ahmad, S.; Munir, S.; Zeb, N.; Ullah, A.; Khan, B.; Ali, J.; Bilal, M.; Omer, M.; Alamzeb, M.; Salman, S.M.; et al. Green nanotechnology: A review on green synthesis of silver nanoparticles—An ecofriendly approach. *Int. J. Nanomed.* **2019**, *14*, 5087–5107. [CrossRef]
21. Jadoun, S.; Arif, R.; Jangid, N.K.; Meena, R.K. Green synthesis of nanoparticles using plant extracts: A review. *Environ. Chem. Lett.* **2021**, *19*, 355–374. [CrossRef]
22. Nguyen, N.-T.; Vo, T.-L.-H. Fabrication of Silver Nanoparticles Using *Cordyline fruticosa* L. Leave Extract Endowing Silk Fibroin Modified Viscose Fabric with Durable Antibacterial Property. *Polymers* **2022**, *14*, 2409. [CrossRef] [PubMed]
23. Gour, A.; Jain, N.K. Advances in green synthesis of nanoparticles. *Artif. Cells Nanomed., Biotechnol.* **2019**, *47*, 844–851. [CrossRef]
24. Sharma, D.; Kanchi, S.; Bisetty, K. Biogenic synthesis of nanoparticles: A review. *Arabian J. Chem.* **2019**, *12*, 3576–3600. [CrossRef]
25. Vu, T.H.; Bui, V.H.; Nguyen, N.T. Antibacterial Properties of Silver Nanoparticles Synthesized Using Piper betle L. Leaf Extract. *Mater. Sci. Forum* **2021**, *1020*, 236–242. [CrossRef]
26. ISO 20882:2007; Footwear—Performance Requirements for Components for Footwear—Lining and Insocks. ISO: Geneva, Switzerland, 2007.
27. The Clinical and Laboratory Standards Institute (CLSI). *Approved Standard M7-A7; Methods for Dilution Antimicrobial Susceptibility Tests for Bacteria that Grow Aerobically*; The Clinical and Laboratory Standards Institute (CLSI): Wayne, PA, USA, 2006; Volume 26.
28. AATCC TM90; Test Method for Antibacterial Activity of Textile Materials: Agar Plate. AATCC: Research Triangle Park, NC, USA, 2016.
29. AATCC TM30; Test Method for Antifungal Activity, Assessment on Textile Materials: Mildew and Rot Resistance of Textile Materials. AATCC: Research Triangle Park, NC, USA, 2017.
30. ISO 16187:2013; Footwear and Footwear Components—Test Method to Assess Antibacterial Activity. ISO: Geneva, Switzerland, 2013.
31. Vijay, R.; Drisya, V.M.; Selta, D.R.F.; Rathi, M.A.; Gopalakrishnan, V.K.; Alkhalifah, D.H.M.; Hozzein, W.N. Synthesis and characterization of silver nanomaterial from aqueous extract of *Commelina forskaolii* and its potential antimicrobial activity against Gram negative pathogens. *J. King Saud Univ. Sci.* **2023**, *35*, 102373. [CrossRef]
32. Biswas, A.; Vanlalveni, C.; Adhikari, P.P.; Lalfakzuala, R.; Rokhum, L. Green biosynthesis, characterisation and antimicrobial activities of silver nanoparticles using fruit extract of *Solanum viarum*. *IET Nanobiotechnol.* **2018**, *12*, 933–938. [CrossRef]
33. Shaheen, T.I.; Abd El Aty, A.A. In-situ green myco-synthesis of silver nanoparticles onto cotton fabrics for broad spectrum antimicrobial activity. *Int. J. Biol. Macromol.* **2018**, *118*, 2121–2130. [CrossRef]

34. Carvalho, I.; Lima, M.J.; Nobre, D.; Marques, S.M.; Castro, D.; Leite, T.R.; Henriques, M.; Duarte, F.; Ramalho, A.; Carvalho, S. Silver oxide coatings deposited on leathers to prevent diabetic foot infections. *Surf. Coat. Technol.* **2022**, *442*, 128338. [CrossRef]
35. Zhang, X.; Wang, W.; Yu, D. Synthesis of waterborne polyurethane–silver nanoparticle antibacterial coating for synthetic leather. *J. Coat. Technol. Res.* **2018**, *15*, 415–423. [CrossRef]

**Disclaimer/Publisher’s Note:** The statements, opinions and data contained in all publications are solely those of the individual author(s) and contributor(s) and not of MDPI and/or the editor(s). MDPI and/or the editor(s) disclaim responsibility for any injury to people or property resulting from any ideas, methods, instructions or products referred to in the content.



## Article

# Biochemical and Microstructural Characteristics of Collagen Biopolymer from Unicornfish (*Naso reticulatus* Randall, 2001) Bone Prepared with Various Acid Types

Nurul Syazwanie Fatiroi<sup>1</sup>, Abdul Aziz Jaziri<sup>1,2</sup>, Rossita Shapawi<sup>3</sup>, Ruzaidi Azli Mohd Mokhtar<sup>4</sup>, Wan Norhana Md. Noordin<sup>5</sup> and Nurul Huda<sup>6,\*</sup>

<sup>1</sup> Faculty of Food Science and Nutrition, Universiti Malaysia Sabah, Kota Kinabalu 88400, Sabah, Malaysia

<sup>2</sup> Faculty of Fisheries and Marine Science, Universitas Brawijaya, Malang 65145, East Java, Indonesia

<sup>3</sup> Borneo Marine Research Institute, Universiti Malaysia Sabah, Kota Kinabalu 88400, Sabah, Malaysia

<sup>4</sup> Biotechnology Research Institute, Universiti Malaysia Sabah, Kota Kinabalu 88400, Sabah, Malaysia

<sup>5</sup> Fisheries Research Institute, Batu Maung 11960, Penang, Malaysia

<sup>6</sup> Faculty of Sustainable Agriculture, Universiti Malaysia Sabah, Sandakan 90509, Sabah, Malaysia

\* Correspondence: drnurulhuda@ums.edu.my; Tel.: +60-124-843-144

**Abstract:** Biopolymer-like collagen has great industrial potential in terms of its excellent properties, such as strong biocompatibility, high degradability, and low antigenicity. Collagen derived from fish by-products is preferable as it is safer (free from transmittable diseases) and acceptable to most religious beliefs. This study aimed to characterize the unicornfish (*Naso reticulatus* Randall, 2001) bone collagens prepared with different type of acids, i.e., acetic acid, lactic acid, and citric acid. A higher yield (Y) ( $p < 0.05$ ) was obtained in the citric-acid-soluble collagen (CASC) (Y = 1.36%), followed by the lactic-acid-soluble collagen (LASC) (Y = 1.08%) and acetic-acid-soluble collagen (AASC) (Y = 0.40%). All extracted collagens were classified as type I due to the presence of 2-alpha chains ( $\alpha 1$  and  $\alpha 2$ ). Their prominent absorption spectra were located at the wavelengths of 229.83 nm to 231.17 nm. This is similar to wavelengths reported for other fish collagens. The X-ray diffraction (XRD) and infrared (IR) data demonstrated that the triple-helical structure of type I collagens was still preserved after the acid-extraction process. In terms of thermal stability, all samples had similar maximum transition temperatures ( $T_{max} = 33.34\text{--}33.51$  °C). A higher relative solubility (RS) of the unicornfish bone collagens was observed at low salt concentration (0–10 g/L) (RS > 80%) and at acidic condition (pH 1.0 to pH 3.0) (RS > 75%). The extracted collagen samples had an irregular and dense flake structure with random coiled filaments. Overall, bones of unicornfish may be used as a substitute source of collagen.

**Keywords:** collagen biopolymer; unicornfish bone; acid extraction; characterization

**Citation:** Fatiroi, N.S.; Jaziri, A.A.; Shapawi, R.; Mokhtar, R.A.M.; Noordin, W.N.M.; Huda, N. Biochemical and Microstructural Characteristics of Collagen Biopolymer from Unicornfish (*Naso reticulatus* Randall, 2001) Bone Prepared with Various Acid Types. *Polymers* **2023**, *15*, 1054. <https://doi.org/10.3390/polym15041054>

Academic Editor: Raffaella Striani

Received: 1 December 2022

Revised: 10 February 2023

Accepted: 13 February 2023

Published: 20 February 2023



**Copyright:** © 2023 by the authors. Licensee MDPI, Basel, Switzerland. This article is an open access article distributed under the terms and conditions of the Creative Commons Attribution (CC BY) license (<https://creativecommons.org/licenses/by/4.0/>).

## 1. Introduction

Biopolymer collagen, a fibrillar protein, is one of the main structural components in the connective tissues of mammals and makes up almost 30% of total protein composition [1]. It is characterized by the unique right-handed triple-helical structure, composed of three left-handed polyproline-like helices, each with a (Gly-Xa-Ya) repeating sequence where Xa and Ya are often proline and hydroxyproline [2]. At least 29 types (I–XXIX) of collagens with different structures of polypeptides, amino acid motifs, and molecular characteristics have been studied [3]. Type I collagen has been intensively explored by researchers because of its special traits (i.e., strong biocompatibility, high biodegradability, and lack of antigenicity) [4]. Collagen has great potential in various industrial sectors such as medical, pharmaceutical, nutraceutical, and cosmetic. It has been approved for use in tissue engineering due to its ability to stimulate cellular migration, tissue matrix interaction, and tissue regeneration [5,6]. It is also applicable in developing drug-delivery systems and



in treating hypertension, obesity, and diabetes [7]. In addition, it is an important cosmetic ingredient that serves as a natural humectant and moisturizer, preventing aging of the skin [8]. In food manufacturing, collagen is often used as a colloidal stabilizer, emulsifier, and foaming agent [9]. Collagens are mostly derived from the skins and bones of land vertebrates, especially bovine and porcine vertebrates. However, use of these animals raises consumer apprehension due to reported infectious diseases such as bovine spongiform encephalopathy, transmissible spongiform encephalopathy, and foot-and-mouth disease. Another constraint is associated with religious belief. For instance, Muslims and Jews are prohibited to consume or use porcine-derivative products, while cows and beef derivatives are forbidden in Hinduism [10]. To deal with these issues, alternative sources of collagen are necessary.

Over the last decade, fish collagen has gained considerable attention amongst scientists. This is evidenced by the large number of publications related to the extraction of fish collagens. Sources of the collagens include tiger grouper (*Epinephelus fuscoguttatus*) skin [11], bigeye tuna (*Thunnus obesus*) skin, bone, and scale [12], lizardfish (*Saurida tumbil*) skin, bone, and scale [13–15], grass carp (*Ctenopharyngodon idellus*) skin, bone, and scale [16], golden pompano (*Trachinotus blochii*) skin and bone [17], Spanish mackerel (*Scomberomorus niphonius*) skin and bone [18], sturgeon (*Huso huso*) skin [19], puffer fish (*Lagocephalus inermis*) skin [20], red stingray (*Dasyatis akajei*) skin [21], Siberian sturgeon (*Acipenser baerii*) cartilage [22], leather jacket (*Odonus niger*) bone [23], tilapia (*Oreochromis mossambicus*) bone [24], grey mullet (*Mugil cephalus*) scale [25], and yellow tuna (*thunnus albacore*) swim bladders [26]. Fish collagens are mostly categorized as type I and their physicochemical properties, including thermal stability, solubility, and triple-helical structures, have also been evaluated. Interestingly, few studies have demonstrated that modification of the extraction process could increase the thermostability of fish collagen [27].

Unicornfish (*Naso reticulatus* Randall, 2001) belongs to the family Acanthuridae. It has a convex head with slight angularity before its eye, no horn on the forehead, and an emarginated caudal fin. This fish mainly lives in tandem with coral reefs, feeds on algae, and has tight skin-like jacket [28]. It is popularly served grilled in restaurants. By-products from *N. reticulatus* are usually discarded after processing, resulting in loss of a valuable biological resource. Therefore, converting the by-products into high-end product such as collagen is highly beneficial. Moreover, there is little information regarding extraction of collagen from this fish. Hence, this work aimed to compare the extractability of collagen from unicornfish bone using different acids (i.e., acetic acid, lactic acid, and citric acid), and determine the physicochemical and structural properties of the collagens.

## 2. Results and Discussion

### 2.1. Yield and Hydroxyproline Content of Acid-Soluble Collagens

Table 1 shows the yields (%) of acid-soluble collagens derived from unicornfish bone. The highest yield (Y) was recorded in CASC (Y = 1.36%) ( $p < 0.05$ ) compared to AASC (Y = 0.40%) and LASC (Y = 1.08%) suggesting that citric acid may be the most effective acid for extracting collagen from fish bones. This finding was in agreement with the previous report on collagen from lizardfish (*S. tumbil*) bone [13]. The results in the present study were also comparable to those for other acid-soluble fish bone collagens such as bigeye tuna (*T. obesus*) (Y = 0.1%) [12], tilapia (*O. niloticus*) (Y = 0.5%) [24], grass carp (*C. idellus*) (Y = 0.7%) [16], carp (*C. carpio*) (Y = 1.06%) [25], and golden pompano (*T. blochii*) (Y = 1.25%) [17]. Logically different fish species, acids, and extraction procedures might influence the collagen yields [14,15]. There was no significant difference in hydroxyproline (Hyp) content ( $p > 0.05$ ) between AASC and LASC. However, the Hyp content in CASC was significantly lower ( $p < 0.05$ ). The Hyp contents recorded in the present study were lower than those for bigeye tuna (*T. obesus*) (82–87 mg/g) [12], cobia (*Rachycentron canadum*) (84–99 mg/g) [29], and marine eel (*Evencheslys macrura*) (94–98 mg/g) [30] bone collagens. These differences could be attributed to several factors including type of species, size, age, structure, and composition of fish tissue, as well as the extraction process [31]. Collagen

with high Hyp content could help to improve the structural stability of its molecules. Kittiphattanabawon et al. [32] stated that Hyp is a prominent component of amino acids and plays an essential role in stabilizing the triple-helical structure of collagen.

**Table 1.** Yield, Hyp composition, and color parameters of the acid soluble unicornfish (*N. reticulatus*) bone collagen.

Sample	Yield (%)	Hyp (mg/g)	$L^*$	Color Parameters		WI
				$a^*$	$b^*$	
AASC	$0.40 \pm 0.15^c$	$81.41 \pm 0.11^a$	$81.44 \pm 5.25^a$	$-0.19 \pm 0.10^b$	$0.79 \pm 1.27^c$	$81.37 \pm 5.21^a$
LASC	$1.08 \pm 0.12^b$	$81.32 \pm 0.02^a$	$82.55 \pm 2.45^a$	$0.40 \pm 0.38^a$	$6.51 \pm 2.59^a$	$81.28 \pm 3.09^a$
CASC	$1.36 \pm 0.21^a$	$80.17 \pm 0.10^b$	$79.35 \pm 0.92^a$	$0.04 \pm 0.18^b$	$3.26 \pm 2.29^b$	$78.97 \pm 0.99^a$

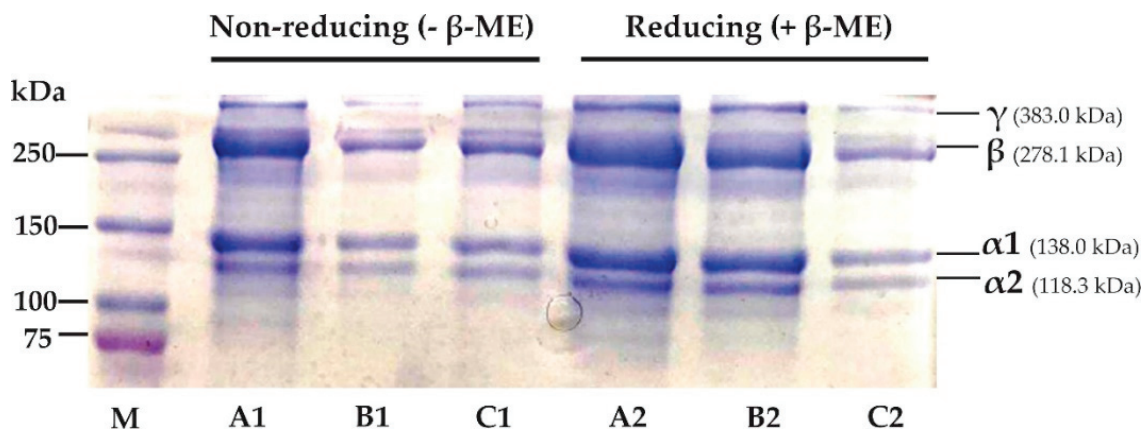
AASC: acetic acid soluble unicornfish (*N. reticulatus*) bone collagen; LASC: lactic acid soluble unicornfish bone collagen; CASC: citric acid soluble unicornfish bone collagen.  $L^*$  = lightness;  $a^*$  = redness;  $b^*$  = yellowness; blue to yellow; and WI = whiteness index. Different lowercase superscripts in the same column indicate significant difference ( $p < 0.05$ ).

## 2.2. Color Attributes

Color attributes of the AASC, LASC, and CASC are presented in Table 1. Sadowska et al. [33] pointed out that a lighter-color collagen is more preferable for developing new products in food, nutraceutical, or medical applications because it does not alter the original color of a product. There were no significant differences ( $p > 0.05$ ) in the lightness ( $L^*$ ) and whiteness (WI) values of all extracted collagens in the present study. However, significantly higher  $L^*$  values ranging from 79.25 to 82.55 was noted in the unicornfish bone collagens compared to lizardfish (*S. tumbil*) (72.76) [15] and barramundi (*Lates calcalifer*) (44.76–65.41) skin collagens [34]. Addition of hydrogen peroxide ( $H_2O_2$ ) could increase the lightness of acid extracted collagens, as reported in lizardfish (*S. tumbil*) bone (88.54) [13] and snakehead fish (*Channa argus*) skin (89.49) [35] collagens so there is potential for further experimentation with different  $H_2O_2$  concentrations. Moreover, the  $a^*$  and  $b^*$  values of LASC were significantly higher ( $p < 0.05$ ) than those of AASC and CASC.

## 2.3. SDS-PAGE Profile

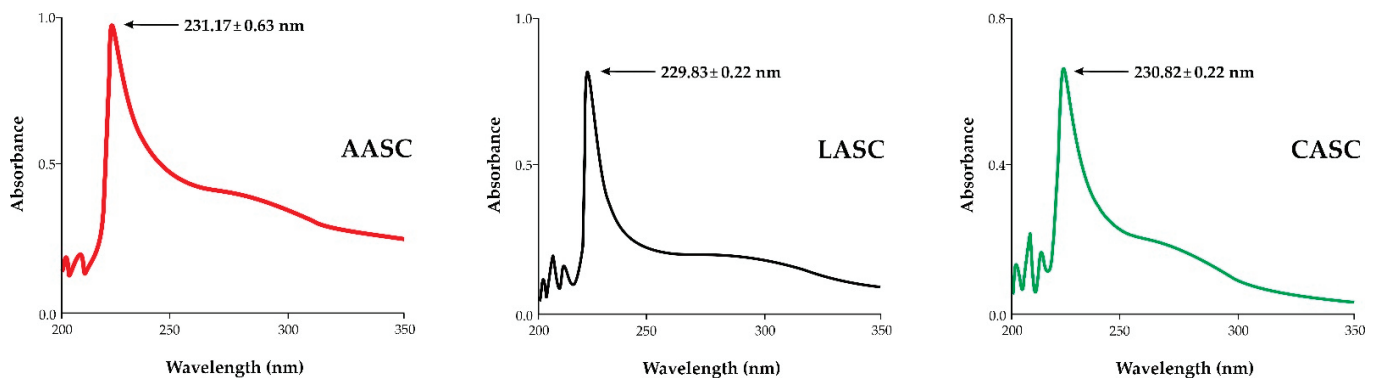
An SDS-PAGE image of the unicornfish bone collagens is presented in Figure 1. The electrophoretic pattern of each sample was almost similar, with two alpha ( $\alpha_1$  and  $\alpha_2$ ), one beta ( $\beta$ ), and one gamma ( $\gamma$ ) chains. The molecular weight (MW) of each alpha chain was estimated as 138.0 kDa and 118.3 kDa, respectively. Benjakul et al. [36] suggested that type I collagen was characterized by the presence of two alpha chains ( $\alpha_1$  and  $\alpha_2$ ). Based on this, unicornfish bone collagens were also categorized as type I. All acid-soluble collagens assessed in this study were comparable to previous literature on type I collagen fish collagen from seabass (*L. calcarifer*) ( $\alpha_1 = 118$  kDa and  $\alpha_2 = 105$  kDa) [37], loach (*M. anguillicaudatus*) ( $\alpha_1 = 127$  kDa and  $\alpha_2 = 115$  kDa) [38], golden pompano (*T. blochii*) ( $\alpha_1 = 120$  kDa and  $\alpha_2 = 100$  kDa) [17], and Nile tilapia (*O. niloticus*) ( $\alpha_1 = 125$  kDa and  $\alpha_2 = 114$  kDa) [39]. Other electrophoretic chains found in all extracted collagens (i.e.,  $\beta = 278.1$  kDa and  $\gamma = 383.0$  kDa), indicate dimer and trimer bands as observed in our previous findings on lizardfish (*S. tumbil*) fish collagens [13–15]. Further analysis with addition of  $\beta$ -ME (reducing) and without  $\beta$ -ME (non-reducing), showed no differences in electrophoretic patterns of AASC, LASC, or CASC, and absence of disulfide bonds, as mentioned in previous literature [13–15].



**Figure 1.** SDS-PAGE image of acid soluble unicornfish bone collagen. M: protein marker; A1 and A2: acetic acid soluble collagen (AASC); B1 and B2: lactic acid soluble collagen (LASC); C1 and C2: citric acid soluble collagen (CASC).

#### 2.4. UV Absorption Spectra

Figure 2 presents the UV absorption spectra of the AASC, LASC, and CASC. In general, a prominent spectrum of fish collagen was located at the wavelengths of 210 nm to 240 nm [40]. All acid-soluble collagens from the bone of unicornfish were within the maximum spectral ranges proposed by previous works, with no significant differences ( $p > 0.05$ ) among the samples. The highest peak observed in this study was in accordance with other fish collagens, such as Siberian sturgeon (*A. baerii*) [22], red drum (*Sciaenops ocellatus*) [41], lizardfish (*S. tumbil*) [13], and puffer fish (*L. inermis*) [20]. The spectra observed were associated with the functional groups of carboxyl ( $-\text{COOH}$ ), carbonyl ( $\text{C}=\text{O}$ ), and amides ( $\text{CONH}_2$ ), which belong to the polypeptide chains of fish collagen, as proposed by Jaziri et al. [13]. Other low absorption peaks (300 nm to 250 nm) were also observed in all extracted collagens and were likely related to the aromatic amino acids, such as phenylalanine, tryptophan, and tyrosine. It is therefore assumed that collagens extracted from the bone of unicornfish contain low composition of aromatic amino acids.

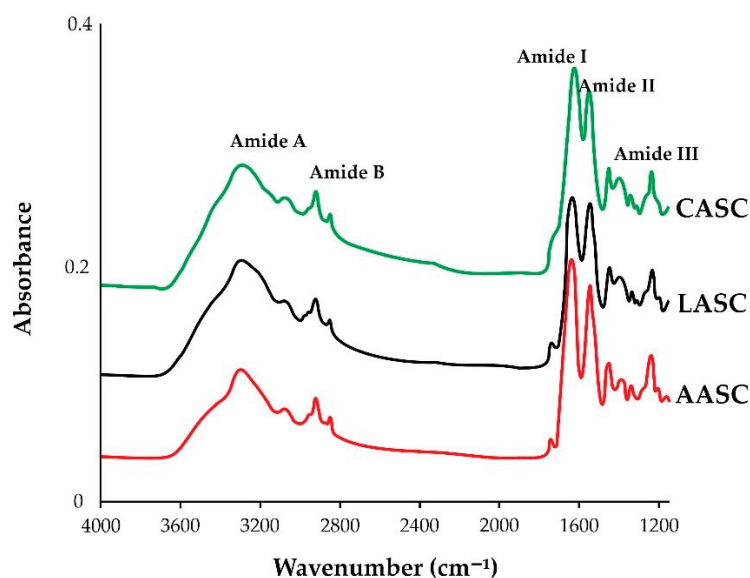


**Figure 2.** UV absorption spectra of acid soluble unicornfish (*N. reticulatus*) bone collagen. AASC: acetic acid soluble collagen; LASC: lactic acid- soluble collagen; CASC: citric acid soluble collagen.

#### 2.5. Attenuated Total Reflection–Fourier Transform Infrared Spectroscopy (ATR–FTIR)

FTIR spectra of AASC, LASC, and CASC are shown in Figure 3. Five significant peaks (Amides: A, B, I, II, and III) were clearly identified in all samples. As described in Table 2, Amide A represents the N-H stretching vibrations with hydrogen bonds which represents the protein molecules and is usually located at  $3200\text{--}3440\text{ cm}^{-1}$  region [42], as observed in the present study. For Amide B, it described an asymmetric stretching of  $\text{CH}_2$  vibrations [21], and the higher wavenumber region of Amide B was observed in the

LASC and CASC samples. Meanwhile, Amide I is often related to the secondary structure of proteins, with wavenumbers ranging from 1600 to 1700  $\text{cm}^{-1}$  [43] and represents the stretching vibration of the backbone carbonyl group (C=O) in polypeptides. The strong bands of Amide I in all acid-soluble collagens in the present study were in accordance with other literature [23]. On the other hand, Amides II and III have been widely used for the identification of triple-helical structure of collagen [44]. Amide II, typically located at the wavenumbers from 1500  $\text{cm}^{-1}$  to 1600  $\text{cm}^{-1}$  [45], which correspond to the N–H bending vibrations combined with the C–N stretching vibrations. The CASC showed lower wavenumbers compared to the AASC and LASC, indicating more H bonds in the CASC. Meanwhile, Amide III reflected the peak combination between C–N stretching and N–H remodeling, resulting in amide linkages which generally occur between 1200  $\text{cm}^{-1}$  and 1350  $\text{cm}^{-1}$  [41]. Similar peaks were also noted in other fish collagens, such as Nile tilapia (*O. niloticus*) [39], lizardfish (*S. tumbil*) [13–15], purple spotted bigeye snapper (*P. tayanus*) [46], sturgeon fish (*H. huso*) [19], barramundi (*L. calcarifer*) [37], and loach (*M. anguillicaudatus*) [38].



**Figure 3.** IR spectra of acid soluble unicornfish (*N. reticulatus*) bone collagen. AASC: acetic acid soluble collagen; LASC: lactic acid soluble collagen; CASC: citric acid soluble collagen.

**Table 2.** The peak area and the description for the acid soluble unicornfish (*N. reticulatus*) bone collagen.

AASC	Peak Location LASC	CASC	Peak Annotation
3308.10 $\text{cm}^{-1}$	3278.28 $\text{cm}^{-1}$	3278.28 $\text{cm}^{-1}$	Amide A, N-H stretching coupled with H bond
2920.44 $\text{cm}^{-1}$	2924.17 $\text{cm}^{-1}$	2924.17 $\text{cm}^{-1}$	Amide B, CH <sub>2</sub> asymmetric stretching
1638.21 $\text{cm}^{-1}$	1638.21 $\text{cm}^{-1}$	1617.71 $\text{cm}^{-1}$	Amide I, C=O stretching/H bond coupled with COO-
1543.16 $\text{cm}^{-1}$	1545.02 $\text{cm}^{-1}$	1541.29 $\text{cm}^{-1}$	Amide II, N-H bend coupled with C-N stretching
1237.51 $\text{cm}^{-1}$	1237.51 $\text{cm}^{-1}$	1235.64 $\text{cm}^{-1}$	Amide III, N-H bend coupled with C-H stretching

AASC: acetic acid soluble unicornfish (*N. reticulatus*) bone collagen; LASC: lactic acid soluble unicornfish bone collagen; CASC: citric acid soluble unicornfish bone collagen.

In terms of stability of the triple-helical structures, Benjakul et al. [36] suggested that the triple-helical structure was preserved if the difference in wavenumber between Amides I and II ( $\Delta v = v_I - v_{II}$ ) was less than 100  $\text{cm}^{-1}$  [47]. Based on this guideline, our results confirmed that the triple-helical structure of all extracted collagens from unicornfish bone were maintained because  $\Delta v$  of the AASC, LASC, and CASC were 95.05  $\text{cm}^{-1}$ , 93.19  $\text{cm}^{-1}$ , and 76.42  $\text{cm}^{-1}$ , respectively. Another approach is through the ratio of the Amide III and



1450  $\text{cm}^{-1}$  band (AIII/A1450), as proposed by Doyle et al. [48]. After validation, the triple-helical structures of extracted collagens did not change during the extraction process as described from their absorption ratio values ( $\sim 1.0$ ), suggesting that the use of acetic, citric, and lactic acids during the extraction process could solubilize collagens without damaging the structures.

## 2.6. Evaluation of X-ray Diffraction (XRD)

Table 3 presents the diffraction data of the AASC, LASC, and CASC. Generally, two significant peaks were observed. The first peak was sharp, and second peak was broader. The obtained diffraction data were comparable to the triple-helical structure of calf-skin collagen (standard) [15]. Similar diffraction motifs were also noted in tilapia (*O. niloticus*) skin [49], carp fish (*C. carpio*) scale [24], golden pompano (*T. blochii*) skin and bone [27] and lizardfish (*S. tumbil*) skin, scale, and bone [13–15] collagens. In order to predict the minimum value of repeated spacings  $d$  ( $\text{\AA}$ ), the Bragg formula by Zhang et al. [25]. was used with  $d(\text{\AA}) = \lambda/2\sin \theta$  (where  $\lambda$  is the X-ray wavelength of 1.54  $\text{\AA}$  and  $\theta$  is the Bragg diffraction angle). As shown in Table 3, the first peak ( $d = 1.13$ – $1.14$  nm) reflects the distance between the molecular chains of triple-helical structure found in fish collagen, with higher  $d$  values being detected in the AASC and LASC samples. Meanwhile, the  $d$  value of AASC, LASC, and CASC samples in the second highest peak ranged from 0.33 nm to 0.34 nm, with the lowest observed in the CASC. This peak denotes the distance between skeletons of fish-collagen structure. The diameter ( $d$ ) of a collagen molecule with a single left-handed helix chain and a triple-helical structure was consistent with the diameter of collagen from the barracuda skin prepared by solubilizing with different acids [13]. Overall, our extracted collagens showed no denaturation in the triple-helical structures and were in their native conformations.

**Table 3.** XRD and DSC analyses of the acid soluble unicornfish (*N. reticulatus*) bone collagen.

Sample	XRD Evaluation				DSC Data	
	1st Peak (Sharp Peak) $2\theta$	1st Peak (Sharp Peak) $d$ Value (nm)	2nd Peak (Broad Peak) $2\theta$	2nd Peak (Broad Peak) $d$ Value (nm)	$T_{max}$ ( $^{\circ}\text{C}$ )	$\Delta H$ (mJ/g)
AASC	7.22	1.13	21.33	0.34	33.51	3.9
LASC	7.24	1.13	21.74	0.33	33.39	7.7
CASC	6.66	1.14	20.11	0.33	33.34	5.7

AASC: acetic acid soluble unicornfish (*N. reticulatus*) bone collagen; LASC: lactic acid soluble unicornfish bone collagen; CASC: citric acid soluble unicornfish bone collagen.

## 2.7. Thermostability of Acid-Soluble Collagen

Thermostability, as determined by  $T_{max}$  value of the AASC, LASC, and CASC, is listed in Table 3. A higher thermostability was demonstrated in the AASC ( $T_{max} = 33.51$   $^{\circ}\text{C}$ ), followed by LASC ( $T_{max} = 33.39$   $^{\circ}\text{C}$ ) and CASC ( $T_{max} = 33.34$   $^{\circ}\text{C}$ ). According to Benjakul et al. [36], thermostability of collagen was related to the presence of amino acids (proline and hydroxyproline), particularly at pyrrolidine rings that are governed by the H bonding via the hydroxyl group of Hyp. In addition, Hyp served as stabilizer of the triple-helical structure through H bonding in coil-coiled alpha chains [50]. Our  $T_{max}$  results (around 33  $^{\circ}\text{C}$ ) were comparable to other fish bone collagens, such as purple-spotted bigeye (*P. taylori*) (30.80–31.48  $^{\circ}\text{C}$ ) [32], Siberian sturgeon (*A. baerii*) skin (28.30  $^{\circ}\text{C}$ ) [22], grass carp (*C. idellus*) (36  $^{\circ}\text{C}$ ) [16], and golden pompano (*T. blochii*) skin (38.23  $^{\circ}\text{C}$ ) [17]. Interestingly, fish from tropical waters showed higher thermostability compared to temperate fish such as Spanish mackerel (*S. niphonius*) (18.02  $^{\circ}\text{C}$ ) [18]. The delta H value ( $\Delta H$ ) was defined as the area located under the thermogram peaks, which reflects the energy required to uncouple the alpha chains of collagen and convert them into random coils. The  $\Delta H$  of the AASC sample was lower than of the LASC and CASC samples, indicating a lower energy used in AASC. The differences in the  $T_{max}$  and  $\Delta H$  values of fish collagen were likely influenced by



many factors, such as the composition of amino acids, extraction process, fish species, and other factors, particularly water temperature and habitat [32].

### 2.8. Microstructure Profile

The AASC, LASC, and CASC were scanned under a scanning electron microscope (SEM), and the morphological structures were appraised. As illustrated in Figure 4, the extracted collagens of unicornfish bones showed fibril-forming structures, multi-layered forms, and irregular sheet-like films linked by random-coiled filaments. In addition, the wrinkled and porous structures were also clearly visible at magnification of  $500\times$ , indicating the samples were dehydrated during the lyophilization process, as documented by Schuetz et al. [51]. According to Lim et al. [7], fish collagen with fibrillary, interconnectivity, and sheet-like film structures could be a potential source of biomaterials for nutraceutical, pharmaceutical, and biomedical products to be used in wound dressing, skin and bone tissue formation, cell migration, and coating material. The microstructure profiles of Lizardfish (*S. tumbil*) skin, bone, and scale [13–15], miiuy croaker (*M. miiuy*) scale [52], black ruff (*Centrolophus niger*) skin [53], and marine eel (*E. macrura*) skin [30] collagens were in agreement with this recent work.

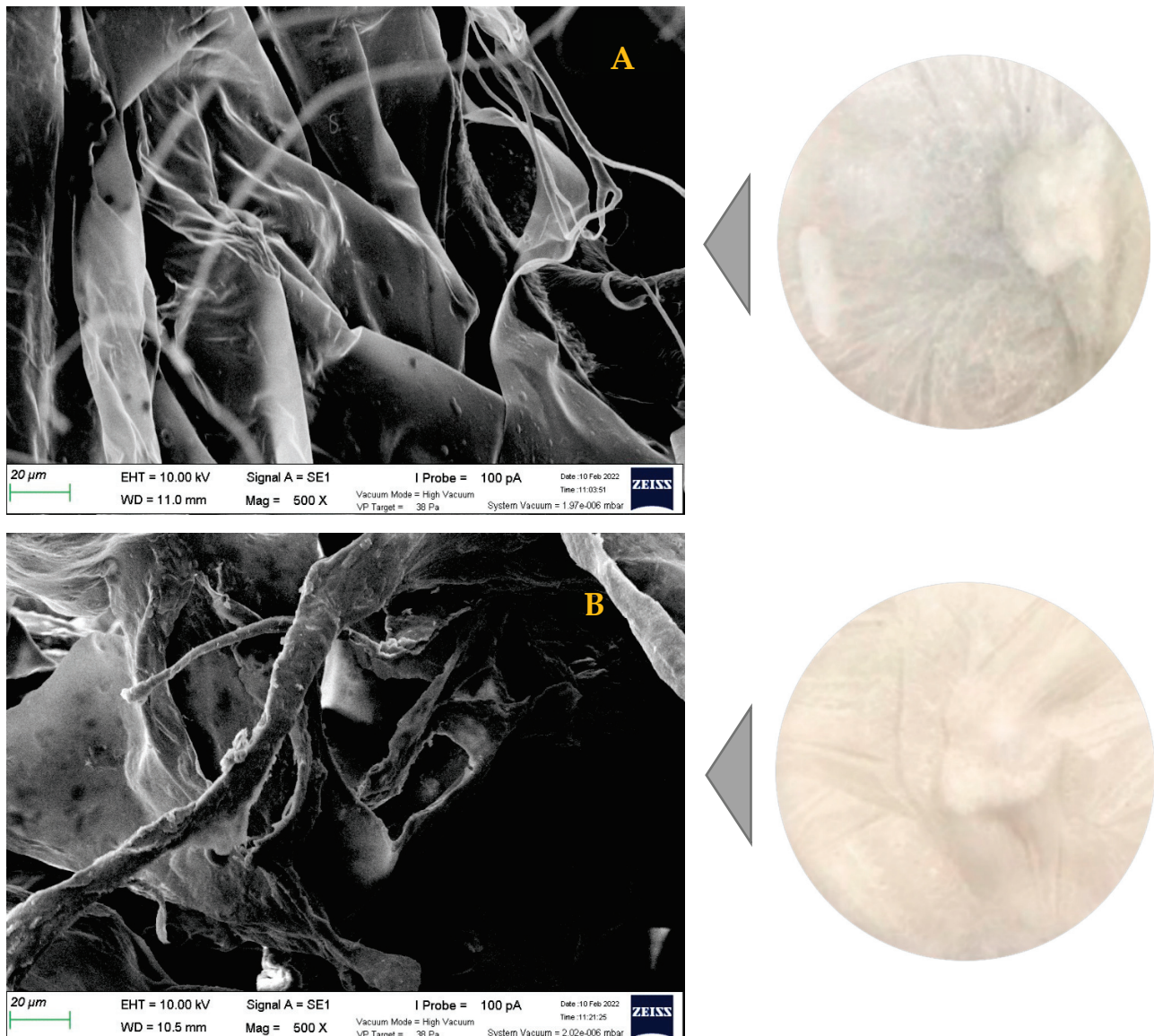
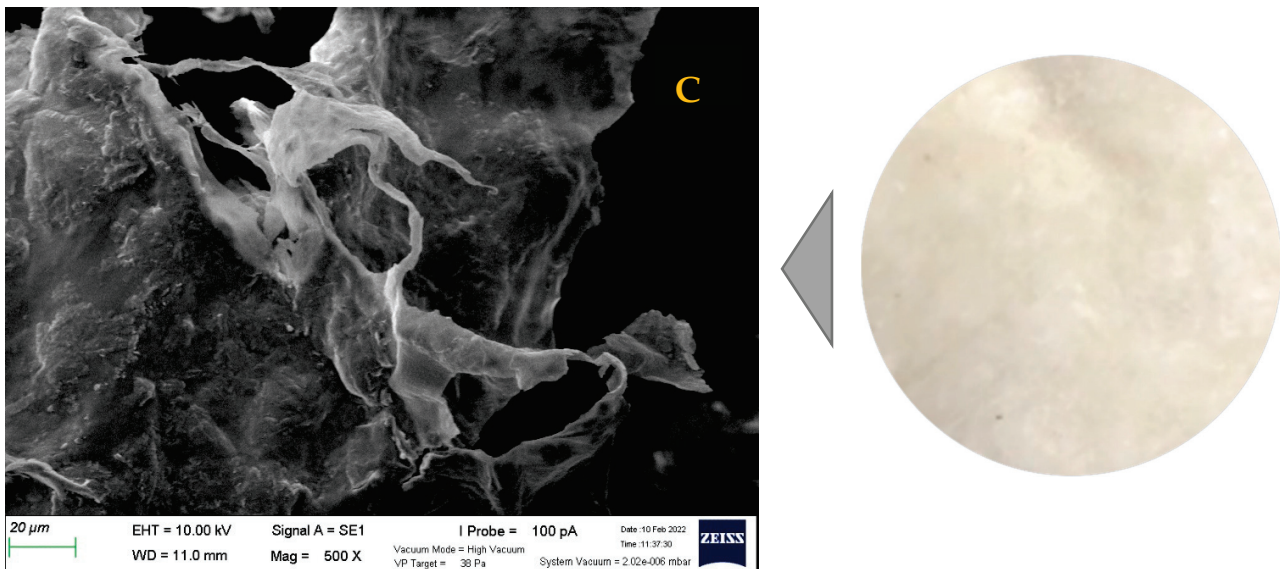


Figure 4. Cont.

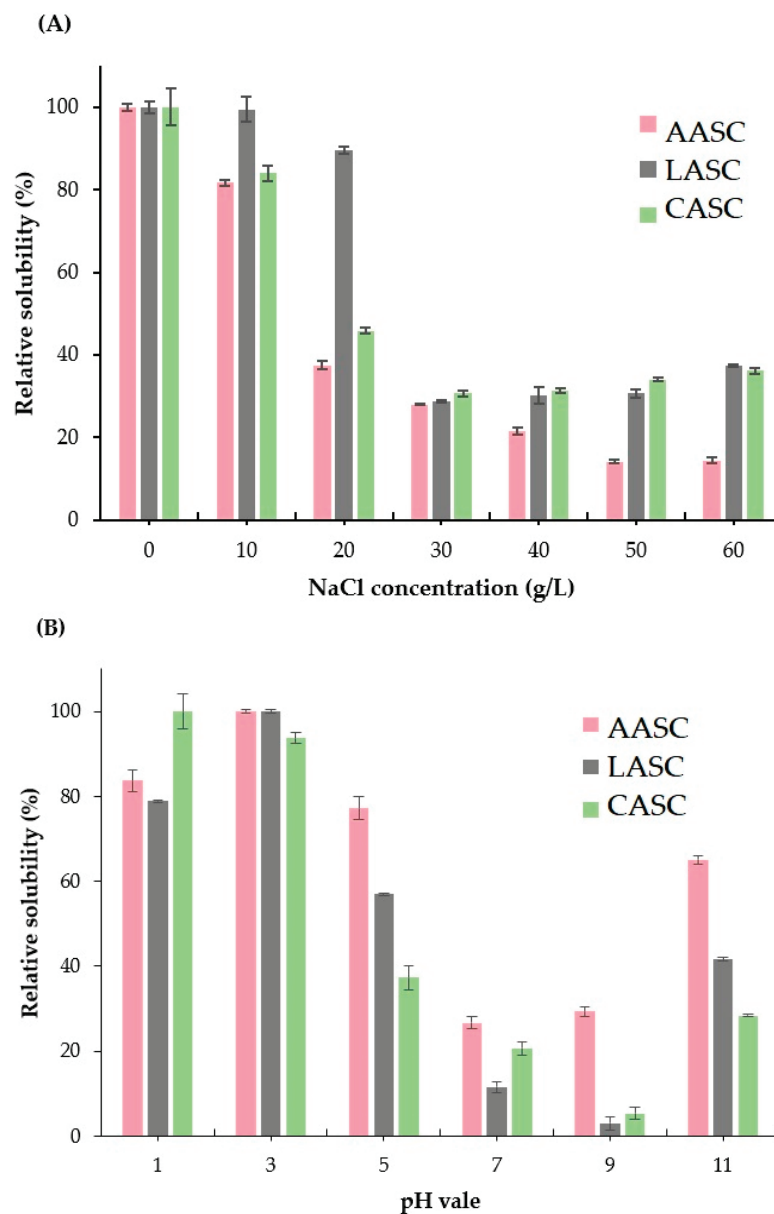


**Figure 4.** SEM image (magnification 500×) of the acid-soluble unicornfish (*N. reticulatus*) bone collagen. (A) acetic acid soluble collagen (AASC); (B) lactic acid soluble collagen (LASC); and (C) citric acid soluble collagen (CASC).

### 2.9. Solubility Studies

Solubility of the AASC, LASC, and CASC samples was evaluated at different sodium chloride (NaCl) concentrations and various pH conditions. Higher solubility (more than 80% of relative solubility (RS)) was observed in all extracted collagens when treated with low NaCl concentration (0–10%). RS of >85% was recorded in the LASC sample (Figure 5A). This might have been due to the effect of the dialysis process in LASC that completely removed the remaining salt after being salted out during the precipitation process. As a result, no salt was detected in the lyophilized collagen. However, at high concentrations of NaCl (30 g/L to 60 g/L), the RS decreased sharply to less than 40% in all extracted collagens. Chen et al. [41] suggested that at high salt concentration, the hydrophobic–hydrophobic interactions in the polypeptide chain were escalated. The competition for water with salt ions was also increased, resulting in protein precipitation. These results were in accordance with collagens isolated from the skin and bone of Spanish mackerel (*S. niphonius*) [18], the skin of lizardfish (*S. tumbil*) [13], the skin and bone of golden pompano (*T. blochii*) [17], and the cartilage of Siberian sturgeon (*A. baerii*) [22].

In the context of pH, the solubility was increased in acidic acid conditions, especially at pH 1.0 and pH 5.0 (Figure 5B). The highest RS value (>90%) was noted in all extracted collagens treated at pH 3.0. In contrast, the solubility decreased at pH 7.0 and alkaline (pH 9.0) conditions. The increase in the hydrophobic–hydrophobic interactions among the collagen molecules might have resulted in the total net charge becoming zero, particularly at the isoelectric point which commonly occurs at slightly acidic and neutral conditions [54]. However, at pH 11.0, the RS were slightly increased to around 25–60%. This could be due to the effect of electrostatic repulsion between collagen molecules and hydration of charged residues at pH values above the isoelectric point (pI) [22]. Chuaychan et al. [22] stated that differences in the solubility of collagen treated with various pH were related to the difference in the molecular properties and conformations of collagen. Our findings were equivalent to those for the collagens extracted from the skin and bone of Spanish mackerel (*S. niphonius*) [18], skin of lizardfish (*S. tumbil*) [13], skin and bone of golden pompano (*T. blochii*) [17], and cartilage of Siberian sturgeon (*A. baerii*) [22].



**Figure 5.** Relative solubility (RS) of acid soluble collagens from the unicornfish (*N. reticulatus*) bone at (A) different NaCl concentrations and (B) various pH levels. AASC: acetic acid soluble collagen; LASC: lactic acid soluble collagen; CASC: citric acid soluble collagen.

### 3. Conclusions

Unicornfish (*N. reticulatus*) bone collagens extracted with the aid of various organic-acid solutions (i.e., acetic, lactic, and citric acids) were evaluated. The highest collagen yield ( $p < 0.05$ ) was recorded for the citric-acid-soluble collagen (CASC) compared to that of acetic-acid-soluble collagen (AASC) and lactic-acid-soluble collagen (LASC). The triple-helical structures of type I extracted collagens were still maintained, indicating no denaturation of all samples during the acid-extraction process as confirmed by FTIR and XRD analysis. Although LASC had a lower collagen yield than CASC, other characteristics (i.e., thermostability, hydroxyproline content, color attributes, and solubility) were found to be preferable in the LASC sample. Thus, lactic-acid-soluble collagen (LASC) could be used as an alternative collagen for further research.



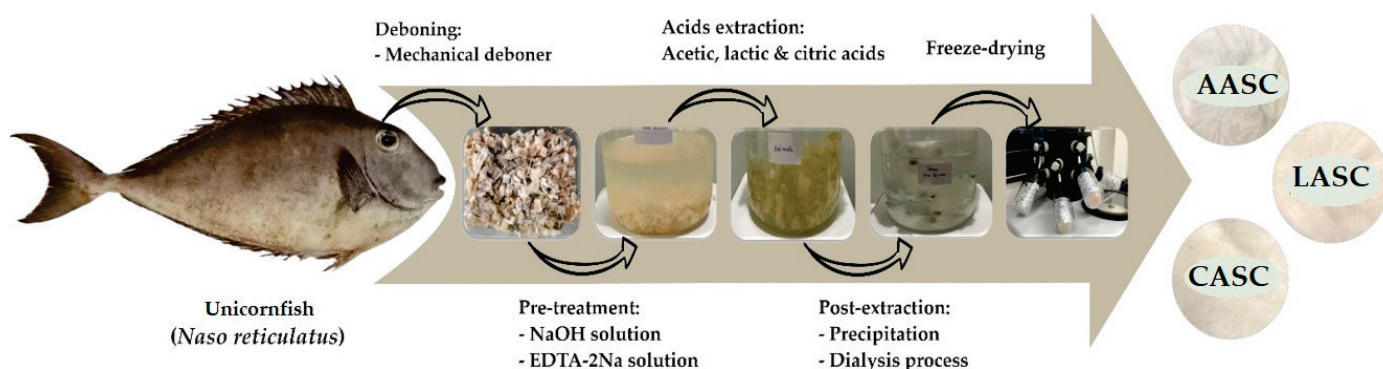
## 4. Materials and Method

### 4.1. Materials

Fifteen kilograms of fresh unicornfish (*N. reticulatus*) were obtained from a local supplier in Kota Kinabalu, Sabah, Malaysia. Samples were placed in an ice-cooled insulating box (ratio of fish to ice was 1:2 (*w/w*)) to maintain their freshness during transportation. Upon arrival, fish were subjected to species identification and weight ( $521.58 \pm 32.27$  g) and length ( $30.52 \pm 4.28$  cm) measurement. The prepared samples were separated automatically using a mechanical deboner machine (SFD-8 type, Taiwan). The fish bones were subsequently cut into small portions ( $1.0 \times 1.0$  cm<sup>2</sup>) with a stainless-steel knife (Brisscoes, Malaysia), and washed with running tap water. The washed samples were packed in a polyethylene bag and then stored in a freezer ( $-20$  °C) for further analyses. Sodium dodecyl sulphate (SDS), acrylamide powder, Coomassie Blue R-250, *N,N,N',N'*-tetramethyl ethylene diamine (TEMED), and Folin–Ciocalteu’s phenol reagent acetic acid (glacial) were purchased from Merck (Darmstadt, Germany). Precision Plus Protein Dual Color standards (markers) was purchased from Bio-Rad Laboratories (Hercules, CA, USA). Bovine serum albumin (BSA) and Lowry reagent were supplied from Sigma Chemical Co., (St. Louis, MO, USA). Citric acid and lactic acid solution were supplied from System (Selangor Darul Ehsan, Malaysia) and Bendosen (Selangor, Malaysia), respectively. Other chemicals used in this research were of analytical grade.

### 4.2. Preparation of Acid-Soluble Collagen

Extraction of unicornfish bone collagens with different acid solutions was carried out according to Jaziri et al. [13] with slight modification. All steps were strictly performed in a chiller ( $4$  °C), and the extraction process is depicted in Figure 6. A total of 100 g fish bones was soaked in ten volumes of 0.1 M sodium hydroxide solution for 6 h (the solution was changed every 3 h) with continuous stirring. The pretreated samples were washed with distilled water to achieve neutral condition (pH 7.0). This step aimed to remove non-collagenous protein and pigmentation. Next, the neutralized samples were demineralized by dissolving in ten volumes of 0.5 M ethylenediaminetetraacetic acid disodium salt solution (pH 7.4) for 24 h with continuous stirring, and the solution was changed every 12 h. The demineralized samples were then washed with cold distilled water for 30 min and the distilled water was replaced every 10 min. After the pre-treatment step, the fish-bone samples were subjected to extraction by adding 15 volumes of 0.5 M organic-acid solutions (i.e., acetic acid, lactic acid, and citric acid) for 72 h. The extracted samples were then filtered through two layers of cheesecloth, and the filtrates were salted-out by dissolving in 2.5 M sodium chloride, followed by 0.05 M Tris (hydroxymethyl) aminomethane hydrochloride at a neutral pH (7.0). After that, the precipitates were centrifuged (Eppendorf Centrifuge 5810R, Hamburg, Germany) at  $15,000 \times g$  for 15 min. The pellets were subsequently dissolved in acid solution (based on each acid used during extraction) at a ratio of 1:1 (*w/v*). The solutions were prepared for dialysis by transferring into a cellulose-membrane tubing (average flat width 43 mm, 1.7 in.) (Sigma-Aldrich, St. Louis, MO, USA) and then put in 15 volumes of 0.1 M acid solution for 24 h, followed by a distilled water for 48 h (the distilled water was changed every 24 h). The dialyzed samples were dried using a freeze-dryer machine (Labconco, Kansas City, MO, USA). After freeze drying, all dried samples were stored at a  $-20$  °C. The dried collagens were labeled acetic-acid-soluble bone collagen (AASC), lactic-acid-soluble bone collagen (LASC), and citric-acid-soluble bone collagen (CASC).



**Figure 6.** The procedure of acid-soluble unicornfish (*N. reticulatus*) bone collagen. AASC: acetic-acid-collagen; LASC: lactic-acid-soluble collagen; CASC: citric-acid-soluble collagen.

#### 4.3. Analyses

##### 4.3.1. Yield and Hydroxyproline (Hyp) Measurement

The yields of collagens (AASC, LASC, and CASC) were measured according to the formula developed by Jongjareonrak et al. [54], as noted below:

$$\text{Yield (\%)} = \frac{\text{Weight of dried collagen}}{\text{Initial weight of unicornfish bone}} \times 100 \quad (1)$$

The Hyp content (mg/g) of extracted collagens was determined using an established procedure [55]. The lyophilized collagens were subjected to hydrolysis by adding a strong acid solution (6 M of HCl) at high temperature (110 °C) for 24 h. Afterwards, the hydrolysates were filtered through a Whatman filter paper No. 4 (Sigma-Aldrich, St. Louis, MO, USA). The filtrates were subsequently adjusted with 2.5 M NaOH solution to achieve pH of 6.5–7.0. Approximately 0.2 mL of hydrolysates was transferred into prepared test tubes and 0.4 mL isopropyl alcohol added. Subsequently, 0.2 mL of oxidant solution was added to the solutions and they were allowed to stand at room temperature for 5 min. After that, a total of 2.3 mL Ehrlich's reagent solution was dropped in and mixed thoroughly. The mixtures were then heated in a water bath (Memmert, Schwabach, Germany) at 60 °C for 25 min. After heating, the treated samples were cooled for 10 min at room temperature. The cooled samples were further diluted with an isopropyl alcohol (up to 10 mL). Absorbance against distilled water was determined at a wavelength of 558 nm using a spectrophotometer (Agilent Cary 60, Santa Clara, CA, USA). Hyp standard solution (10 to 70 ppm) was also prepared in this current study.

##### 4.3.2. Color Attributes

Color attributes of AASC, LASC, and CASC samples were determined as described by Ismail et al. [56] using a colorimeter (ColorFlex CX2379, HunterLab, Reston, VA, USA). The attributes examined were  $L^*$  (lightness),  $a^*$  (redness: green to red), and  $b^*$  (yellowness: blue to yellow). The whiteness index (WI) of the extracted collagens was calculated using the following formula [57].

$$\text{WI} = 100 - \left[ (100 - L^*)^2 + (a^*)^2 + (b^*)^2 \right]^{0.5} \quad (2)$$

##### 4.3.3. Sodium Dodecyl Sulfate-Polyacrylamide Gel Electrophoresis (SDS-PAGE)

SDS-PAGE analysis of unicornfish bone collagens was conducted using a Mini-PROTEAN electrophoresis system (Bio-Rad Laboratories, Hercules, CA, USA). We used the established method from Laemmli [58] with minor amendments. Each dried collagen (around 2.5 mg) was dissolved in SDS solution (5%) and mixed thoroughly. The mixture was treated with high thermal condition (85 °C) using a water bath (Memmert, Schwabach, Germany) for 1 h. After heating, the mixtures were prepared by centrifuging at 8500 ×  $g$  for 5 min to



remove undissolved matter. Around 15  $\mu\text{L}$  of supernatants was transferred into a mini centrifuge tube and subsequently, 15  $\mu\text{L}$  sample buffer in the presence and absence of 10%  $\beta$ -mercaptoethanol ( $\beta$ -ME) was added. After that, the mixtures were reheated at the same temperature for 5 min and then loaded into polyacrylamide gel composed of 4% stacking gel and 7.5% resolving gel. The acrylamide gel was electrophoresed with a constant voltage of 120 volts for 90 min. When electrophoresis ended, the gel was immersed in the staining solution containing 0.1% ( $v/v$ ) Coomassie Blue R-250, 30% ( $v/v$ ) methanol and 10% ( $v/v$ ) acetic acid for approximately 30 min. Next, the stained acrylamide gel was destained with 10% ( $v/v$ ) acetic acid and 30% ( $v/v$ ) methanol solutions. The electrophoretic bands of AASC, LASC, and CASC were compared to the protein marker (Precision Plus Protein Dual Color Standards).

#### 4.3.4. Ultraviolet–Visible Absorption Spectra

Ultraviolet–visible (UV–vis) absorption spectra of all extracted collagens were determined using a UV–vis spectrophotometer (Agilent Cary 60, Santa Clara, CA, USA). A total of 5 mg of lyophilized collagens was dissolved with acetic acid solution (0.5 M), and well mixed. Next, the mixtures were centrifuged at  $8500\times g$  for 15 min to separate solubilized and insolubilized matters. The solubilized samples were then placed into a quartz cell (its optical path length was of 10 mm). The spectral wavelengths used in the present study were arranged from 400 nm to 200 nm with a baseline of acetic acid solution [14].

#### 4.3.5. Attenuated Total Reflectance–Fourier Transform Infrared Spectroscopy (ATR–FTIR)

ATR–FTIR data of the AASC, LASC, and CASC were obtained from FTIR spectrometer (Agilent Cary 630, Santa Clara, CA, USA) as described from our previous study [15]. A total of 10 mg dried fish bone collagens was placed onto the crystal cell of FTIR spectrometer. Spectral data were prepared with a resolution of  $2\text{ cm}^{-1}$  throughout a wavenumber range of  $4000\text{--}1000\text{ cm}^{-1}$  for 32 scans against a background spectrum found from clean empty cells at ambient temperature. The obtained data were then analyzed using a software of Agilent Microlab.

#### 4.3.6. X-ray Diffraction (XRD) Data

Dried samples (AASC, LASC, and CASC) were scanned using a XRD instrument (Rigaku Smart Lab<sup>®</sup>, Tokyo, Japan), with copper  $K\alpha$  applied as an x-ray source. The tube voltage and current were set up at 40 kV and 50 mA, respectively. The scanning range in all acid-soluble collagens was prepared by adjusting from  $10^\circ$  to  $40^\circ$  ( $2\theta$ ) with a speed of  $0.06^\circ$  per second. The obtained data were recorded and analyzed by comparing to another previous research. XRD was carried out using the method of Chen et al. [21].

#### 4.3.7. Differential Scanning Calorimetry (DSC)

A DSC machine (Perkin-Elmer, Model DSC7, Norwalk, CA, USA) was used to obtain the thermostability value of the extracted collagens from the unicornfish bones. First, the prepared samples were hydrated by adding deionized water at a ratio of 1:40 ( $w/v$ ) for 48 h in a chiller. The hydrates were then weighed from 5 mg to 10 mg into an aluminum pan (Perkin-Elmer, Norwalk, CA, USA), and tightly sealed. The DSC instrument was previously calibrated using an indium as a standard, and the sealed samples were subsequently scanned, ranging from  $20^\circ\text{C}$  to  $50^\circ\text{C}$  at a rate of  $1^\circ\text{C}$  per minute. An empty pan was used as a reference. Thermostability in all samples was determined using the maximum transition temperature ( $T_{max}$ ), which was collected from the endothermic peak of thermogram, and the total denaturation enthalpy ( $\Delta H$ ) was recorded from the area of thermogram [59].

#### 4.3.8. Scanning Electron Microscopy (SEM)

Morphological evaluation of the AASC, LASC, and CASC samples was carried out using a scanning electron microscopy (Carl Zeiss, model MA 10, Germany). Prior to scanning, all acid-extracted collagens were sputter-coated with the gold for 5 min using a

coater device (JEOL JFC-1200, Tokyo Rikakikai Co., Ltd., Tokyo, Japan). Next, all coated samples were imaged with a magnification (500×) [52].

#### 4.3.9. Solubility Study

Solubility of acid-soluble collagen was assessed at different sodium chloride (NaCl) concentrations and pH conditions. The procedure used was as described by Matmaroh et al. [59]. For solubility in NaCl, different NaCl concentrations (0–60 g/L) were used. Approximately 5 mL of solubilized collagens was prepared and transferred into 5 mL of different NaCl concentrations. The mixtures were then stirred continuously using a magnetic stirrer (ST0707V2, Selangor, Malaysia) for 30 min in a chiller. The mixtures were centrifuged (8500× g) for 10 min after being dissolved. For pH treatment, the dried collagens were added to 0.5 M of acetic acid solution. Afterwards, the dissolved samples were adjusted with different pH, from pH 1.0 to pH 11.0. The 2.5 N HCl and 2.5 N NaOH solutions were used for pH adjustment. The pH-adjusted samples were stirred for 2 h and subsequently centrifuged at 8500 × g for 10 min. To determine percentage of relative solubility (% RS), all solubilized collagens (treated by different NaCl or pH) were subjected to protein measurement using the method of Lowry et al. [60], with bovine serum albumin (BSA) used as a standard. The RS (%) of all samples was measured using the following equation:

$$\text{Relative solubility (\%)} = \frac{\text{Current concentration of protein at current NaCl or pH}}{\text{The highest concentration of protein}} \times 100 \quad (3)$$

#### 4.4. Statistical Analysis

Experiment in this study was carried out in triplicate, and collected data are presented as means with standard deviation. One-way ANOVA was applied, and Duncan's multiple range test was used to compare means with a significant effect signed in  $p < 0.05$  under a SPSS Statistics version 28.0 (IBM Corp., Armonk, NY, USA).

**Author Contributions:** Conceptualization, N.H.; methodology, A.A.J. and N.H.; software, N.S.F. and A.A.J.; validation, R.S., R.A.M.M., W.N.M.N. and N.H.; formal analysis, N.S.F.; investigation, N.S.F. and A.A.J.; resources, A.A.J. and N.H.; data curation, R.S., R.A.M.M., W.N.M.N. and N.H.; writing—original draft, N.S.F. and A.A.J.; writing—review and editing, R.S., R.A.M.M., W.N.M.N. and N.H.; visualization, A.A.J.; supervision, N.H.; project administration, N.H.; funding acquisition, N.H. All authors have read and agreed to the published version of the manuscript.

**Funding:** This work was supported by the Ministry of Higher Education Malaysia (FRGS/1/2019/STG03/UMS/02/5) and Universiti Malaysia Sabah (UMS) for the payment of APC.

**Institutional Review Board Statement:** Not applicable.

**Informed Consent Statement:** Not applicable.

**Data Availability Statement:** The data presented in this study are available upon request from the corresponding author.

**Acknowledgments:** The authors are grateful to the Ministry of Higher Education Malaysia for the funds provided through the Fundamental Research Grant Scheme (FRGS) with a grant number FRGS/1/2019/STG03/UMS/02/5 and to Universiti Malaysia Sabah (UMS) for their support in completing this research article.

**Conflicts of Interest:** The authors declare no conflict of interest.

## References

1. Jaziri, A.A.; Shapawi, R.; Mokhtar, R.A.M.; Noordin, W.N.M.; Huda, N. Physicochemical and Microstructural Analyses of Pepsin-Soluble Collagens Derived from Lizardfish (*Saurida tumbil* Bloch, 1795) Skin, Bone and Scales. *Gels* **2022**, *8*, 471. [CrossRef]
2. Sorushanova, A.; Delgado, L.M.; Wu, Z.; Shologu, N.; Kshirsagar, A.; Raghunath, R.; Mullen, A.M.; Bayon, Y.; Pandit, A.; Raghunath, M.; et al. The Collagen Suprafamily: From Biosynthesis to Advanced Biomaterial Development. *Adv. Mater.* **2019**, *31*, e1801651. [CrossRef] [PubMed]

3. Shoulders, M.D.; Raines, R.T. Collagen structure and stability. *Annu. Rev. Biochem.* **2009**, *78*, 929–958. [CrossRef] [PubMed]
4. Lim, Y.-S.; Ok, Y.-J.; Hwang, S.-Y.; Kwak, J.-Y.; Yoon, S. Marine Collagen as a Promising Biomaterial for Biomedical Applications. *Mar. Drugs* **2019**, *17*, 467. [CrossRef]
5. Gajbhiye, S.; Wairkar, S. Collagen Fabricated Delivery Systems for Wound Healing: A New Roadmap. *Biomater. Adv.* **2022**, *142*, 213152. [CrossRef] [PubMed]
6. Yakaew, P.; Phetchara, T.; Kampeerapappun, P.; Srikulkit, K. Chitosan-Coated Bacterial Cellulose (BC)/Hydrolyzed Collagen Films and Their Ascorbic Acid Loading/Releasing Performance: A Utilization of BC Waste from Kombucha Tea Fermentation. *Polymers* **2022**, *14*, 4544. [CrossRef] [PubMed]
7. Wang, H. A Review of the Effects of Collagen Treatment in Clinical Studies. *Polymers* **2021**, *13*, 3868. [CrossRef] [PubMed]
8. Sionkowska, A.; Adamiak, K.; Musiał, K.; Gadomska, M. Collagen Based Materials in Cosmetic Applications: A Review. *Materials* **2020**, *13*, 4217. [CrossRef]
9. Jaziri, A.A.; Shapawi, R.; Mokhtar, R.A.M.; Noordin, W.N.M.; Huda, N. Tropical Marine Fish Surimi By-products: Utilisation and Potential as Functional Food Application. *Food Rev. Int.* **2021**, *37*, 1–26. [CrossRef]
10. Chen, L.; Cheng, G.; Meng, S.; Ding, Y. Collagen Membranes Derived from Fish Scales of Application in Bone Tissue Engineering. *Polymers* **2022**, *14*, 2532. [CrossRef]
11. Prihanto, A.A.; Jaziri, A.A.; Pratomo, M.D.; Putri, S.E.; Fajriati, C.; Nurdiani, R.; Firdaus, M. Characteristics of Collagen from Parrotfish (*Chlorurus sordidus*), Tiger Grouper (*Epinephelus fuscoguttatus*) and Pink Ear Emperor (*Lethrinus lentjan*): Effect of Acetic Acid Concentration and Extraction Time. *Online J. Biol. Sci.* **2022**, *22*, 26–35. [CrossRef]
12. Ahmed, R.; Haq, M.; Chun, B.-S. Characterization of Marine Derived Collagen Extracted from the By-products of Bigeye Tuna (*Thunnus obesus*). *Int. J. Biol. Macromol.* **2019**, *135*, 668–676. [CrossRef] [PubMed]
13. Jaziri, A.A.; Shapawi, R.; Mokhtar, R.A.M.; Noordin, W.N.M.; Huda, N. Biochemical Analysis of Collagens from the Bone of Lizardfish (*Saurida tumbil* Bloch, 1795) Extracted with Different Acids. *PeerJ* **2022**, *10*, e13103. [CrossRef]
14. Jaziri, A.A.; Shapawi, R.; Mokhtar, R.A.M.; Noordin, W.N.M.; Huda, N. Microstructural and Physicochemical Analysis of Collagens from the Skin of Lizardfish (*Saurida tumbil* Bloch, 1795) Extracted with Different Organic Acids. *Molecules* **2022**, *27*, 2452. [CrossRef] [PubMed]
15. Jaziri, A.A.; Shapawi, R.; Mokhtar, R.A.M.; Noordin, W.N.M.; Huda, N. Biochemical and Microstructural Properties of Lizardfish (*Saurida tumbil*) Scale Collagen Extracted with Various Organic Acids. *Gels* **2022**, *8*, 266. [CrossRef] [PubMed]
16. Wang, H.; Liang, Y.; Wang, H.; Zhang, H.; Wang, M.; Liu, L. Physical-Chemical Properties of Collagens from Skin, Scale, and Bone of grass carp (*Ctenopharyngodon idellus*). *J. Aquat. Food Prod. Technol.* **2014**, *23*, 264–277. [CrossRef]
17. Cao, J.; Duan, Q.; Liu, X.; Shen, X.; Li, C. Extraction and Physicochemical Characterization of Pepsin Soluble Collagens from Golden Pompano (*Trachinotus blochii*) Skin and Bone. *J. Aquat. Food Prod. Technol.* **2019**, *28*, 837–847. [CrossRef]
18. Li, Z.-R.; Wang, B.; Chi, C.-F.; Zhang, Q.-H.; Gong, Y.-D.; Tang, J.-J.; Luo, H.Y.; Ding, G.-F. Isolation and Characterization of Acid Soluble Collagens and Pepsin Soluble Collagens from the Skin and Bone of Spanish Mackerel (*Scomberomorus niphonius*). *Food Hydrocoll.* **2013**, *31*, 103–113. [CrossRef]
19. Atef, M.; Ojagh, S.M.; Latifi, A.M.; Esmaeili, M.; Udenigwe, C.C. Biochemical and Structural Characterization of Sturgeon Fish Skin Collagen (*Huso huso*). *J. Food Biochem.* **2020**, *44*, e13256. [CrossRef]
20. Iswariya, S.; Velswamy, P.; Uma, T.S. Isolation and Characterization of Biocompatible Collagen from the Skin of Puffer Fish (*Lagocephalus inermis*). *J. Polym. Environ.* **2018**, *26*, 2086–2095. [CrossRef]
21. Chen, J.; Li, J.; Li, Z.; Yi, R.; Shi, S.; Wu, K.; Wu, S. Physicochemical and Functional Properties of Type I Collagens in Red Stingray (*Dasyatis akajei*) Skin. *Mar. Drugs* **2019**, *17*, 558. [CrossRef] [PubMed]
22. Luo, Q.B.; Chi, C.F.; Yang, F.; Zhao, Y.Q.; Wang, B. Physicochemical properties of acid- and pepsin-soluble collagens from the cartilage of Siberian sturgeon. *Environ. Sci. Pollut. Res. Int.* **2018**, *25*, 31427–31438. [CrossRef] [PubMed]
23. Muralidharan, N.; Shakila, M.; Sukumar, R.J.; Jeyasekaran, D. Skin, Bone and Muscle Collagen Extraction from the Trash Fish, Leather Jacket (*Odonus niger*) and Their Characterization. *J. Food Sci. Technol.* **2013**, *50*, 1106–1113. [CrossRef] [PubMed]
24. Liu, H.; Huang, K. Structural Characteristics of Extracted Collagen from Tilapia (*Oreochromis mossambicus*) Bone: Effects of Ethylenediaminetetraacetic Acid Solution and Hydrochloric Acid Treatment. *Int. J. Food Prop.* **2016**, *19*, 63–75. [CrossRef]
25. Thuy, L.T.M.; Okazaki, E.; Osako, K. Isolation and characterization of acid-soluble collagen from the scales of marine fishes from Japan and Vietnam. *Food Chem.* **2014**, *149*, 264–270. [CrossRef] [PubMed]
26. Kaewdang, O.; Benjakul, S.; Kaewmanee, T.; Kishimura, H. Characteristic of Collagens from the Swim Bladders of Yellowfin Tuna (*Thunnus albacares*). *Food Chem.* **2014**, *155*, 264–270. [CrossRef]
27. Zhang, X.; Xu, S.; Shen, L.; Li, G. Factors Affecting Thermal Stability of Collagen from the Aspects of Extraction, Processing and Modification. *J. Leather Sci. Eng.* **2020**, *2*, 19. [CrossRef]
28. Randall, J.E. *Naso reticulatus*, a New Unicornfish (Perciformes: Acanthuridae) from Taiwan and Indonesia, with a Key to the Species of *Naso*. *Zool. Stud.* **2001**, *40*, 170–176.
29. Zeng, S.; Yin, J.; Zhang, C.; Yang, P.; Wu, W. Structure and Characteristics of Acid and Pepsin-solubilized Collagens from the Skin of Cobia (*Rachycentron canadum*). *Food Chem.* **2012**, *135*, 1975–1984. [CrossRef]
30. Veeruraj, A.; Arumugam, M.; Balasubramanian, T. Isolation and Characterization of Thermostable Collagen from the Marine Eel Fish (*Evenchelys macrura*). *Process Biochem.* **2013**, *48*, 1592–1602. [CrossRef]

31. Regenstein, J.; Zhou, P. Collagen and Gelatin from Marine By-products. In *Maximising the Value of Marine By-Products*, 1st ed.; Shahidi, F., Ed.; Woodhead Publishing Limited: Cambridge, UK; CRC Press LLC: Boca Raton, FL, USA, 2006; pp. 273–303.
32. Kittiphattanabawon, P.; Benjakul, S.; Visessanguan, W.; Nagai, T.; Tanaka, M. Characterisation of Acid-soluble Collagen from Skin and Bone of Bigeye Snapper (*Priacanthus tayenus*). *Food Chem.* **2005**, *89*, 363–372. [CrossRef]
33. Sadowska, M.; Kołodziejska, I.; Niecikowska, C. Isolation of Collagen from the Skins of Baltic Cod (*Gadus morhua*). *Food Chem.* **2003**, *81*, 257–262. [CrossRef]
34. Bakar, J.; Hartina, U.M.R.; Hashim, M.D.; Sazili, A.Q. Properties of Collagen from Barramundi (*Lates calcarifer*) Skin. *Int. Food. Res. J.* **2013**, *20*, 835–884.
35. Liua, W.; Zhanga, Y.; Cuic, N.; Wang, T. Extraction and Characterization of Pepsin-solubilized Collagen from Snakehead (*Channa argus*) Skin: Effects of Hydrogen Peroxide Pretreatments and Pepsin Hydrolysis Strategies. *Process Biochem.* **2019**, *76*, 194–202. [CrossRef]
36. Benjakul, S.; Thiansilakul, Y.; Visessanguan, W.; Roytrakul, S.; Kishimura, H.; Prodpran, T. Extraction and Characterisation of Pepsin Solubilised Collagens from the Skin of Bigeye Snapper (*Priacanthus tayenus* and *Priacanthus macracanthus*). *J. Sci. Food Agric.* **2010**, *90*, 132–138. [CrossRef]
37. Chuaychan, S.; Benjakul, S.; Kishimura, H. Characteristics of Acid- and Pepsin-soluble Collagens from Scale of Seabass (*Lates calcarifer*). *LWT Food Sci. Technol.* **2015**, *63*, 71–76. [CrossRef]
38. Wang, J.; Pei, X.; Liu, H.; Zhou, D. Extraction and Characterization of Acid-soluble and Pepsin-soluble Collagen from Skin of Loach (*Misgurnus anguillicaudatus*). *Int. J. Biol. Macromol.* **2018**, *106*, 544–550. [CrossRef] [PubMed]
39. Kittiphattanabawon, P.; Sriket, C.; Kishimura, H.; Benjakul, S. Characteristics of Acid and Pepsin Solubilized Collagens from Nile Tilapia (*Oreochromis niloticus*) scale. *Emir. J. Food Agric.* **2019**, *31*, 95–101. [CrossRef]
40. Wu, Q.-Q.; Li, T.; Wang, B.; Ding, G.-F. Preparation and Characterization of Acid and Pepsin-soluble Collagens from Scales of croceine and redlip croakers. *Food Sci. Biotechnol.* **2015**, *24*, 2003–2010. [CrossRef]
41. Chen, S.; Chen, H.; Xie, Q.; Hong, B.; Chen, J.; Hua, F.; Bai, K.; He, J.; Yi, R.; Wu, H. Rapid Isolation of High Purity Pepsin-soluble Type I Collagen from Scales of Red Drum Fish (*Sciaenops ocellatus*). *Food Hydrocoll.* **2016**, *52*, 468–477. [CrossRef]
42. Tamilmozhi, S.; Veeruraj, A.; Arumugam, M. Isolation and Characterization of Acid and Pepsin-solubilized Collagen from the Skin of Sailfish (*Istiophorus platypterus*). *Food Res. Int.* **2013**, *54*, 1499–1505. [CrossRef]
43. Jeong, H.S.; Venkatesan, J.; Kim, S.K. Isolation and Characterization of Collagen from Marine Fish (*Thunnus obesus*). *Biotechnol. Bioprocess. Eng.* **2013**, *18*, 1185–1191. [CrossRef]
44. Plepis, A.M.D.; Goissis, G.; DasGupta, D.K. Dielectric and Pyroelectric Characterization of Anionic and Native Collagen. *Polym. Eng. Sci.* **1996**, *36*, 2932–2938. [CrossRef]
45. Abedin, M.Z.; Karim, A.A.; Ahmed, F.; Latiff, A.A.; Gan, C.-Y.; Ghazali, F.C.; Sarker, M.Z.I. Isolation and Characterization of Pepsin-solubilized Collagen from the Integument of Sea Cucumber (*Stichopus vastus*). *J. Sci. Food Agric.* **2013**, *93*, 1083–1088. [CrossRef]
46. Oslan, S.N.H.; Shapawi, R.; Mokhtar, R.A.M.; Noordin, W.N.M.; Huda, N. Characterization of Acid- and Pepsin-soluble Collagen Extracted from the Skin of Purple-spotted Bigeye Snapper. *Gels* **2022**, *8*, 665. [CrossRef]
47. Nikoo, M.; Benjakul, S.; Ocen, D.; Yang, N.; Xu, B.; Zhang, L.; Xu, X. Physical and Chemical Properties of Gelatin from the Skin of Cultured Amur Sturgeon (*Acipenser schrenckii*). *J. Appl. Ichthyol.* **2013**, *29*, 943–950. [CrossRef]
48. Doyle, B.B.; Bendit, E.G.; Blout, E.R. Infrared Spectroscopy of Collagen and Collagen-like Polypeptides. *Biopolymers* **1975**, *14*, 937–957. [CrossRef] [PubMed]
49. Reátegui-Pinedo, N.; Salirrosas, D.; Sánchez-Tuesta, L.; Quiñones, C.; Jáuregui-Rosas, S.R.; Barraza, G.; Cabrera, A.; Ayala-Jara, C.; Martinez, R.M.; Baby, A.R.; et al. Characterization of Collagen from Three Genetic Lines (Gray, Red and F1) of *Oreochromis niloticus* (tilapia) Skin in Young and Old Adults. *Molecules* **2022**, *27*, 1123. [CrossRef]
50. Bae, I.; Osatomi, K.; Yoshida, A.; Osako, K.; Yamaguchi, A.; Hara, K. Biochemical Properties of Acid-soluble Collagens Extracted from the Skins of Underutilised Fishes. *Food Chem.* **2008**, *108*, 49–54. [CrossRef]
51. Schuetz, T.; Richmond, N.; Harmon, M.E.; Schuetz, J.; Castaneda, L.; Slowinska, K. The Microstructure of Collagen Type I Gel Cross-linked with Gold Nanoparticles. *Colloids Surf. B Biointerfaces* **2012**, *101*, 118–125. [CrossRef] [PubMed]
52. Li, L.-Y.; Zhao, Y.-Q.; He, Y.; Chi, C.-F.; Wang, B. Physicochemical and Antioxidant Properties of Acid- and Pepsin-Soluble Collagens from the Scales of Miiuy Croaker (*Miichthys miiuy*). *Mar. Drugs* **2018**, *16*, 394. [CrossRef] [PubMed]
53. Bhuimbar, M.V.; Bhagwat, P.K.; Dandge, P.B. Extraction and Characterization of Acid Soluble Collagen from Fish Waste: Development of Collagen-chitosan Blend as Food Packaging Film. *J. Environ. Chem. Eng.* **2019**, *7*, 102983. [CrossRef]
54. Jongjareonrak, A.; Benjakul, S.; Visessanguan, W.; Nagai, T.; Tanaka, M. Isolation and Characterisation of Acid and Pepsin-solubilised Collagens from the Skin of Brownstripe Red Snapper (*Lutjanus vitta*). *Food Chem.* **2005**, *93*, 475–484. [CrossRef]
55. Bergman, I.; Loxley, R. Two Improved and Simplified Methods for the Spectrophotometric Determination of Hydroxyproline. *Anal. Chem.* **1963**, *35*, 1961–1965. [CrossRef]
56. Ismail, I.; Huda, N.; Ariffin, F.; Ismail, N. Effects of Washing on the Functional Properties of Duck Meat. *Int. J. Poult. Sci.* **2010**, *9*, 556–561. [CrossRef]
57. Briones, V.; Aguilera, J.M. Image Analysis of Changes in Surface Color of Chocolate. *Food Res. Int.* **2005**, *38*, 87–94. [CrossRef]
58. Laemmli, U.K. Cleavage of Structural Proteins during the Assembly of the Head of Bacteriophage T4. *Nature* **1970**, *227*, 680–685. [CrossRef]



59. Matmaroh, K.; Benjakul, S.; Prodpran, T.; Encarnacion, A.B.; Kishimura, H. Characteristics of Acid Soluble Collagen and Pepsin Soluble Collagen from Scale of Spotted Golden Goatfish (*Parupeneus heptacanthus*). *Food Chem.* **2011**, *129*, 1179–1186. [CrossRef]
60. Lowry, O.H.; Rosebrough, N.J.; Farr, A.L.; Randall, R.J. Protein Measurement with the Folin Phenol Reagent. *J. Biol. Chem.* **1951**, *193*, 265–275. [CrossRef]

**Disclaimer/Publisher’s Note:** The statements, opinions and data contained in all publications are solely those of the individual author(s) and contributor(s) and not of MDPI and/or the editor(s). MDPI and/or the editor(s) disclaim responsibility for any injury to people or property resulting from any ideas, methods, instructions or products referred to in the content.

Review

# Biodegradable Polylactic Acid and Its Composites: Characteristics, Processing, and Sustainable Applications in Sports

Yueting Wu <sup>1</sup>, Xing Gao <sup>1,\*</sup>, Jie Wu <sup>1</sup>, Tongxi Zhou <sup>1</sup>, Tat Thang Nguyen <sup>2</sup> and Yutong Wang <sup>1</sup>

- <sup>1</sup> Graduate School, College of Sports and Human Sciences, Post-Doctoral Mobile Research Station, Harbin Sport University, Harbin 150008, China; wuyueting@hrbipe.edu.cn (Y.W.); wujie@hrbipe.edu.cn (J.W.); zhoutongxi@hrbipe.edu.cn (T.Z.); wangyutong@hrbipe.edu.cn (Y.W.)
- <sup>2</sup> College of Wood Industry and Interior Design, Vietnam National University of Forestry, Xuan Mai, Hanoi 13417, Vietnam; thangnt@vnuf.edu.vn
- \* Correspondence: gaoping@hrbipe.edu.cn

**Abstract:** Polylactic acid (PLA) is a biodegradable polyester polymer that is produced from renewable resources, such as corn or other carbohydrate sources. However, its poor toughness limits its commercialization. PLA composites can meet the growing performance needs of various fields, but limited research has focused on their sustainable applications in sports. This paper reviews the latest research on PLA and its composites by describing the characteristics, production, degradation process, and the latest modification methods of PLA. Then, it discusses the inherent advantages of PLA composites and expounds on different biodegradable materials and their relationship with the properties of PLA composites. Finally, the importance and application prospects of PLA composites in the field of sports are emphasized. Although PLA composites mixed with natural biomass materials have not been mass produced, they are expected to be sustainable materials used in various industries because of their simple process, nontoxicity, biodegradability, and low cost.

**Keywords:** PLA; biocomposites; biodegradation; sports equipment manufacturing

**Citation:** Wu, Y.; Gao, X.; Wu, J.; Zhou, T.; Nguyen, T.T.; Wang, Y. Biodegradable Polylactic Acid and Its Composites: Characteristics, Processing, and Sustainable Applications in Sports. *Polymers* **2023**, *15*, 3096. <https://doi.org/10.3390/polym15143096>

Academic Editor: Raffaella Striani

Received: 16 June 2023

Revised: 16 July 2023

Accepted: 17 July 2023

Published: 19 July 2023



**Copyright:** © 2023 by the authors. Licensee MDPI, Basel, Switzerland. This article is an open access article distributed under the terms and conditions of the Creative Commons Attribution (CC BY) license (<https://creativecommons.org/licenses/by/4.0/>).

## 1. Introduction

The continuous advancement of science and technology has increased the global demand for natural resources, leading to frequent problems, such as material shortages and environmental pollution. Rapidly depleting oil reserves, greenhouse gas emissions, and the large-scale use of oil-based products have resulted in a lack of biodegradable products, prompting researchers to explore biodegradable, renewable, and recyclable materials. Polylactic acid (PLA) is a biodegradable bio-based aliphatic polyester that can be extracted from 100% renewable resources, such as corn, potatoes, and sugarcane [1]. Compared with traditional petroleum-based composite materials, PLA has a low density, low cost, good plasticity, and rigidity. PLA possesses excellent workability, making it an ideal choice for 3D printing sports equipment. 3D printing can be used to adjust the density and structure of a material according to specific requirements, allowing for personalized customization and innovative designs based on individual measurements and particular needs. This can achieve an ideal combination of lightweight and high strength to ensure that PLA sports equipment does not impose excessive burdens on athletes, enhances athletic performance, and protects different individuals. Although PLA possesses many characteristics suitable for the fabrication of sports equipment, more research is needed. Figure 1 compares the characteristics of bioplastics and petroplastics, showing that PLA occupies a crucial position in the biopolymer market and plays a vital role in various fields, such as in automotive, aerospace, construction, defense, food packaging, and sports equipment applications [2–5].

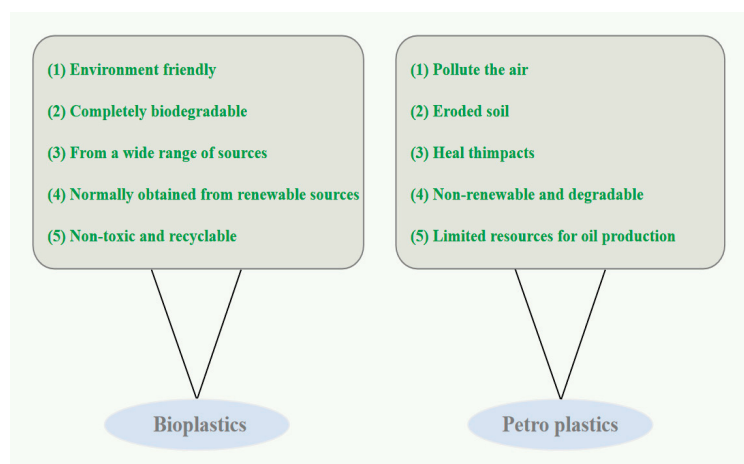


Figure 1. Properties of bioplastics and petro plastics (adapted from Refs. [6,7]).

PLA is an extracted thermoplastic that is suitable for manufacturing composite materials using various methods, such as injection molding, extrusion molding, and compression molding [8]. Increases in the annual supply of PLA (Figure 2) and competitive petroleum costs are key factors driving researchers to develop new PLA-based biocomposites. PLA can biodegrade and bioaccumulate, which helps reduce production and waste disposal costs. PLA can also be treated by landfilling, incineration, or pyrolysis. More than 50% (2.8 kg CO<sub>2</sub>/kg PLA) of the released CO<sub>2</sub> in the PLA life cycle is released during its conversion. By optimizing the conversion process of PLA, there is tremendous potential for PLA to become a low-carbon material [9].

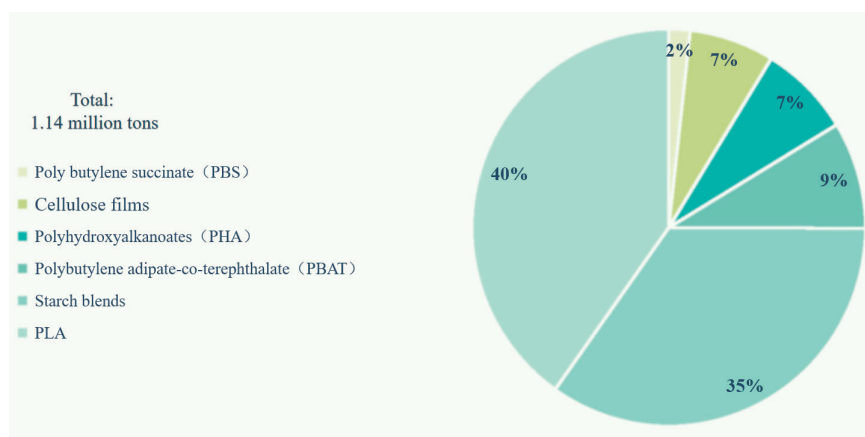


Figure 2. Global production capacity of PLA (adapted from Ref. [10]).

This report discusses the latest developments in the research and development of PLA and its composites. It first outlines the basic structure, characteristics, production, degradation process, and latest modification methods of PLA, and it discusses the inherent advantages of selecting PLA composite materials and focuses on the relationship between different biodegradable materials and their performance in the final PLA composite materials. Then, it introduces the application prospects of PLA composite materials in the field of sports. Finally, it discusses the challenges faced by PLA composite materials and competing materials.

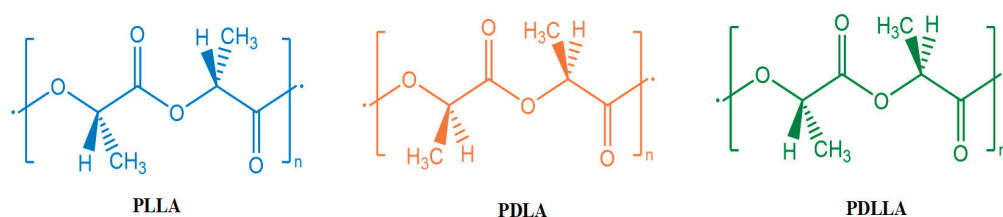
## 2. Overview of PLA

PLA is an entirely biodegradable polymer hailed as one of the most promising bio-based polymers because of its biocompatibility, biodegradability, high mechanical strength, nontoxicity, nonirritation, and processability. PLA can be synthesized by low-energy processes, and it is independent of petroleum resources. Microorganisms can decompose

waste PLA into  $H_2O$  and  $CO_2$ . After photosynthesis,  $CO_2$  and water are converted back into substances such as starch, which can be used as raw materials to resynthesize PLA, thereby realizing a carbon cycle process [11] that does not pollute the environment.

### 2.1. PLA Structure

Lactic acid molecules contain a chiral asymmetric  $\alpha$ -carbon atom and exhibit optical activity that can be divided into two configurations: left-handed (L) and right-handed (D). The dehydration of two lactic acid molecules forms three optical isomers of lactide: L-lactide, D-lactide, and meso-lactide. L-lactide is cheaper because it is naturally occurring. The content of D-lactic acid changes the crystallization behavior of PLA, including different crystallization rates, multiple crystal types, different scales, and layer thicknesses. The crystal morphology is closely related to the mechanical properties of the polymer: the larger the PLA crystal, the more defects in the interior and on the surface of the crystal, and the poorer the mechanical properties of the resulting material [12]. Like L-lactide, meso-lactide is a cyclic diester with two chiral carbon atoms that are not optically active. PLA synthesized via lactide ring-opening polymerization (ROP) has three different stereo configurations: left-handed polylactic acid (PLLA), right-handed polylactic acid (PDLA), and racemic polylactic acid (PDLLA) [13]. Figure 3 shows the three stereo configurations of PLA. The properties and applications of these PLA stereo configurations depend on the molecular weight, molecular weight distribution, crystal structure, and melt rheological behavior.



**Figure 3.** Three-dimensional configuration of PLA (adapted from Ref. [13]).

### 2.2. Properties of PLA

PLA is a member of the family of aliphatic polyesters and has the essential characteristics of universal polymer materials. PLA has a tensile strength similar to that of polyethylene terephthalate (PET), approximately 54 MPa, while its tensile modulus is 3.4 GPa, which is slightly higher than that of PET [14,15]. The mechanical properties of PLA are greatly affected by its molecular weight ( $M_w$ ). When the molecular weight doubles from 50 kDa to 100 kDa, the PLA's tensile strength and elastic modulus also double [16]. The mechanical properties of PLA depend on its semicrystalline structure, amorphous structure, and crystallinity. Semicrystalline PLA shows greater mechanical properties than amorphous PLA. Upon increasing the PLA crystallinity and decreasing the molecular chain mobility, the elongation at the break of the material decreases, while the tensile strength and modulus increase. Table 1 shows the properties of PLA and its different stereo configurations. In addition, the stereochemical structure of lactic acid-based polymers can be controlled by copolymerizing L-lactide, D-lactide, D, L-lactide, and meso-lactide to slow the crystallization rate, which significantly impacts the mechanical properties [17,18].

The environmental degradation process of PLA occurs in two steps: hydrolysis and microbial degradation. PLA first undergoes the hydrolytic cleavage of ester bonds, degrading into PLA oligomers (OLAs) [19]. The hydrolysis of PLA can be catalyzed by acid or alkali and is also affected by temperature and humidity [20,21]. As hydrolysis proceeds, the number of  $-COOH$  groups in the system gradually increases, which plays a catalytic role in the cleavage of PLA ester bonds [22]. This makes the degradation of PLA a self-catalytic process. When the molecular weight of PLA decreases to below 10,000 g/mol, microorganisms can participate in the degradation process of PLA and eventually degrade it into  $H_2O$  and  $CO_2$ .

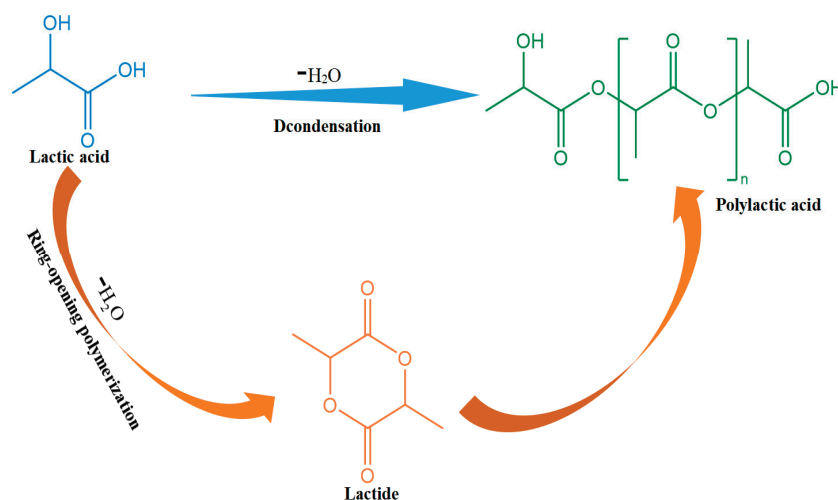


**Table 1.** Properties of PLA and PLA stereo configurations.

Polymer	Density (g/cm <sup>3</sup> )	Glass Transition Temperature (°C)	Melting Point (°C)	Molecular Weight (g/mol)	Tensile Strength (MPa)	Solubility	Refs.
PLA	1.25	54–56	120–170	66,000	21–60	Trimethylsilyl	[23–25]
PLLA	1.290	55–80	173–178	<350,000	15.5–150	Chloroform, furan, dioxane, and dioxole	[25–29]
PDLA	1.248	40–50	120–150	21,000–67,000	15.5–150	PLLA solvents, plus acetone	[26–28, 30,31]
PDLLA	1.25	43–53	230–240	<350,000	27.6–50	Tetrahydrofuran, ethyl acetate, dimethyl sulfoxide, and dimethyl formamide	[25–29]

### 2.3. PLA Production

Figure 4 shows the synthetic route of PLA. Researchers extract starch from renewable natural resources, such as corn and potatoes, and ferment it to produce PLA. Traditional lactic acid fermentation uses starchy raw materials, and some countries have developed the use of agricultural and sideline products as raw materials for this process. The two main methods for synthesizing PLA are direct condensation and lactide ROP [32].

**Figure 4.** PLA synthetic pathways (adapted from Ref. [32]).

#### 2.3.1. Direct Polycondensation

In the late 1980s, the advancement of direct condensation technology significantly increased the global production of PLA and greatly reduced its costs. Direct condensation involves preparing PLA by dehydrating and condensing lactic acid molecules. The disadvantage of this method is that the reaction system is in a dynamic equilibrium between condensation and depolymerization, and the high viscosity of the system makes it difficult to remove the water by-product. The unremoved water causes the depolymerization reaction to proceed, even under vacuum conditions, making it difficult to extract water and increasing the molecular weight of the PLA. Under a high temperature (>200 °C), the PLA will undergo depolymerization, discoloration, and racemization accompanied by a series of side reactions, such as ester exchange, which may form differently sized cyclic products. This results in reduced product properties and poor mechanical properties, which limit their industrial applications. However, the use of direct condensation to produce PLA is a short

and inexpensive method. Chen et al. used a combination of direct condensation and melt polymerization using tetra butyl titanate as a catalyst. They used different vacuum periods, esterification, and condensation reactions. The results showed that this method reduced the system's viscosity, thus helping to remove water and increase the molecular weight [33].

### 2.3.2. Ring-Opening Polymerization (ROP)

In the early 1990s, Cargill Inc. applied for a patent for a solvent-free process and new distillation technology based on ROP to convert lactic acid into high-molecular-weight polymers. This made PLA the second-highest volume bioplastic after starch-based materials. By utilizing specific microbial strains, natural agricultural materials can undergo fermentation to produce lactic acid (LA), which is a precursor for PLA [34,35]. The mature ROP process can make high-molecular-weight and chemically controllable PLA samples with good mechanical properties by controlling lactide's purity and reaction conditions. This is currently the most common method for the industrial production of high-molecular-weight PLA. The technical difficulties of ROP production lie in the synthesis and purification of lactide. Lactide ROP, first, generates oligomers via the dehydration–condensation of lactic acid, and then oligomers are cracked into lactide using initiators, and the lactide, finally, undergoes ROP to generate PLA. Only high-purity lactide can be used to synthesize high-molecular-weight PLA with the desirable physical properties. Depending on the initiator used, lactide ROP can be divided into anionic, cationic, or coordination ROP. Among them, cationic ROP uses a smaller amount of catalyst, while anionic ROP has high reactivity and a fast speed [36].

## 2.4. Modified PLA

According to Refs. [37–39], the low flexibility, elongation, impact resistance, and heat distortion temperature of PLA results in problems such as low crystallinity, long injection molding cycle, high moisture sensitivity, and low hydrolysis resistance. Researchers have used different modification techniques to improve the performance of PLA, such as copolymers and blending with nanocomposites or other polymers.

### 2.4.1. Copolymers

PLA is a thermoplastic polymer whose processing temperature is generally between 170 and 230 °C. In recent years, researchers have produced self-reinforcing PLA through techniques such as melt extrusion, stretching, and injection molding without the need for additives, which retain the biocompatibility and biodegradability of PLA. This method can also solve the trade-off between the toughness and strength and compatibility of blends. In addition, Cao et al. [40] designed a new modification process. After isothermal crystallization, blow molding was carried out below the melting point of crystalline PLA. A crystal network was formed through stretching and blow-molding to prepare a self-reinforcing PLA film. The elongation at the break of this film increased by approximately 67.50% and 104.83% in the transverse and longitudinal directions, respectively, and the tensile strength increased by approximately 45.4 MPa and 78.0 MPa in the transverse and longitudinal directions. This overcame the trade-off between the toughness and strength.

### 2.4.2. Blending with Nanocomposites

Chrissafis et al. [41] added 2.5% oxidized multiwalled carbon nanotubes into PLA and found that the thermal stability of the modified PLA material was greater than that of pure PLA, and the thermal conductivity increased by about 60%. The hexagonal mesh structure and stable chemical bonds of oxidized multiwalled carbon nanotubes made them highly durable, with a decomposition temperature above 1000 °C. Since oxidized multiwalled carbon nanotubes disperse the heat absorbed by PLA, the modified PLA's thermal conductivity and thermal stability were enhanced. In addition, oxidized multiwalled carbon nanotubes acted as heterogeneous nucleating agents in the PLA matrix. The growth of PLA crystals around the oxidized multiwalled carbon nanotubes shortened the

induction process of PLA nucleation, accelerated the PLA crystallization, and reduced the spherulite size. Seligra et al. [42] grafted modified carbon nanotubes onto PLA, which significantly increased the conductivity of the modified PLA material to 4000 S/m. The added carbon nanotubes formed an electron-conducting network that lowered the percolation threshold, thereby transforming PLA into a conductive polymer. A small amount of carbon nanotubes was sufficient to increase the conductivity without affecting the material's mechanical properties.

#### 2.4.3. Blending with Other Polymers

Researchers can improve the mechanical properties of polymers by changing the structure and composition of copolymers. Adjusting the ratio of lactic acid and other monomers in the copolymer system can produce copolymers with the desired mechanical strength to improve the mechanical properties of PLA. By utilizing the hydroxyl and carboxyl groups on the lactic acid segment, different monomers, such as caprolactone (CL), ethylene oxide (EO), ethylene glycol (EG), and trimethylene carbonate (TMC), can be used to synthesize PLA copolymers with improved mechanical properties, especially toughness. Li et al. [43] prepared alternating and random polyurethane copolymers using PLA and polyethylene glycol (PEG). The alternating polyurethane copolymer had a more controllable structure than the random polyurethane copolymer and, therefore, showed higher crystallinity and mechanical properties. Huang et al. [44] developed an electrochemically controlled switchable copolymer system and used it to quickly synthesize multisegment copolymers of PLA and polycarbonate propylene (PPC) without adding external oxidants or reducing agents. In this way, they exploited the complementary advantages of PPC (toughness) and PLA (mechanical strength).

#### 2.5. PLA Degradation

PLA is a biopolymer that can also undergo biodegradation under certain conditions without producing environmental pollution [45,46]. Polymer degradation can be divided into heterogeneous and homogeneous degradation, also known as surface and intramolecular polymer degradation, which can occur through three different chemical reactions: (a) main-chain cleavage, (b) side-chain cleavage, and (c) cross-link cleavage. PLA degradation mainly occurs through ester bond cleavage, which splits long polymer chains into shorter oligomers, dimers, or even monomers. Specifically, the ester bonds of PLA are cleaved via chemical hydrolysis, and under the action of salicylic acid, they are split into carboxylic acids and alcohols. These shorter units are small enough to pass through the cell walls of microorganisms, where they serve as substrates for their biochemical processes and are degraded by microbial enzymes. PLA can be composted to produce CO<sub>2</sub> and H<sub>2</sub>O, requiring temperatures near the  $T_g$  (60 °C) of the polymer and a high relative humidity [47]. The CO<sub>2</sub> emissions are offset by the initial absorption during PLA production. Under such conditions, the degradation time can be as short as 30 days.

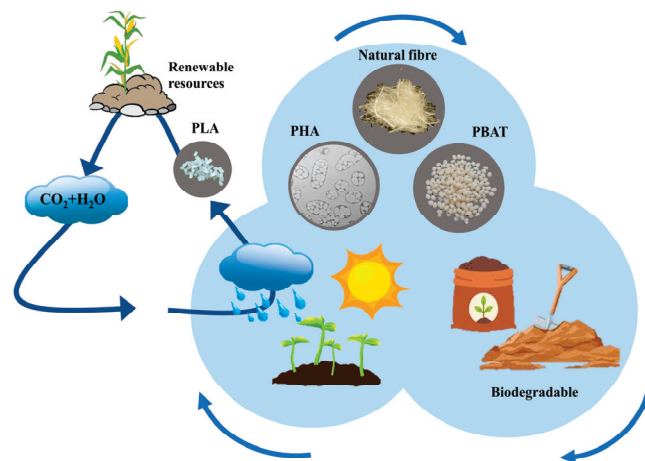
Piedmont and Gironi [48] studied the hydrolytic degradation kinetics of PLA at concentrations of 5–50 wt% between temperatures of 140 °C and 180 °C. The results showed that the reaction kinetics did not depend on the concentration of PLA, and the collected data indicated two different reaction mechanisms. The first mechanism was related to a biphasic reaction ( $E_a = 53.2 \text{ kJ mol}^{-1}$ ), and the second mechanism was associated with a self-catalytic effect of increasing carboxylic acid groups during the depolymerization process ( $E_a = 36.9 \text{ kJ mol}^{-1}$ ). This effect was previously noted in PLA hydrolysis and lowered the solution pH. The group's further work modeled the hydrolysis of PLA at higher temperatures (170–200 °C). The kinetic model described the batch erosion of PLA and subsequent hydrolysis of oligomers, and the model accurately predicted the conversion and concentration of oligomers. Under these conditions, PLA could be completely transformed within 90 min.

### 3. PLA Composite Materials

Although PLA has excellent mechanical properties, renewability, biodegradability, and low costs [49], Figure 5 shows PLA composite degradation process, it is also brittle and has low heat resistance [50]. Researchers have explored various reinforcement materials to develop PLA composite materials to overcome these drawbacks [51], such as cellulose, lignin, silk, PBAT, and PHA. Table 2 compares the mechanical properties of different PLA composite materials.

**Table 2.** Comparison of the mechanical properties of different PLA composites.

Reinforcement	Addition of Fiber (wt.%)	Best Combination (wt.%)	Tensile Strength (MPa)	Tensile Modulus (GPa)	Ref.
Cellulose	30	-	62.3	4.1	[52]
Wood flour	20–40	30	63.3	5.3	[53]
Silk	1–7	5	62.08	2.54	[54]
PBAT	20	-	66.1	1.078	[55]
PHA	20	-	25.4	1.2	[56]



**Figure 5.** PLA composite degradation process (adapted from Refs. [46,47,57]).

#### 3.1. Natural Fibers

Natural fibers can be divided into plant and animal fibers according to their sources [58]. Generally, combining natural fibers with PLA significantly improves the tensile strength, flexural strength, elastic modulus, heat distortion temperature, and other properties of PLA composites. This also enhances their impact resistance and dimensional stability [59,60] while reducing costs. Therefore, natural fibers are an ideal choice for preparing PLA composite materials.

##### 3.1.1. Cellulose Nanocrystals

Cellulose nanocrystals (CNCs) are rod-shaped nanoparticles extracted from cellulose through acid hydrolysis. A wide range of sources, including bleached wood pulp, cotton, and hemp fibers, can be used to produce CNCs [61,62]. Because of their high specific surface area, high reactivity, high strength, and low density, CNCs are an attractive reinforcement material.

Since Favier et al. [63] first attempted to use cellulose whiskers to reinforce polymers in 1995, nano cellulose products have been commercialized, which has prompted researchers to develop PLA/CNCs composite materials. Most studies have shown that CNCs can be well dispersed in PLA and act as a heterogeneous nucleating agent that affects the crystallization of PLA [64]. During isothermal or nonisothermal bulk crystallization, the presence of CNCs reduces the activation energy of PLA crystallization and increases



the crystallization rate of PLA. Kamal et al. [65] prepared CNCs/PLA composites by melt blending and found that CNCs acted as a heterogeneous nucleating agent that promoted the formation of PLA crystals, increased the crystallization rate, and improved the crystallinity. Karkhanis et al. [66] used CNCs to prepare packaging film with PLA composites. Compared with a PLA film, the water vapor permeability of the composite film decreased by 40%. The oxygen permeability decreased by 75%, thus significantly improving the barrier properties of the thin film. The presence of numerous hydroxyl groups on the surface of CNCs controlled the degradation performance of the material and enhanced the hydrophilicity of PLA composites. Shuai et al. [67] introduced CNCs into a laser-sintered PLA scaffold and found that CNCs, as a heterogeneous nucleating agent, caused the ordered arrangement of PLLA chains by forming hydrogen bonds between the surface hydroxyl groups of CNCs and PLLA, thereby increasing the crystallization rate and crystallinity. In addition, since the mechanical strength of polymers is closely related to their crystallinity, the addition of 3 wt% CNCs to the PLA scaffold increased its compressive strength, compressive modulus, tensile strength, tensile modulus, and Vickers hardness by 191%, 351%, 34%, 83.5%, and 56%, respectively. Adding hydrophilic CNCs also improved the hydrophilicity and degradation performance of PLLA.

### 3.1.2. Lignin

Lignin is the most abundant aromatic biomass in nature, accounting for 20–30% of the weight of wood [57,68]. Most natural lignin (approximately 98%) is currently unused as a value-added product and is discarded as industrial waste because its chemical structure in its raw form is fragile and lacks resistance to heat, chemicals, external loads, and other factors. When lignin is mixed with organic polymers, acetylation reactions reduce the strength of the hydrogen bonds in lignin molecules, thereby reducing the size of the structural domains when polymerized lignin is mixed with organic polymers [69]. Interactions between the hydroxyl groups of lignin and the carboxyl groups of PLA underpin the production of PLA/lignin composite materials [70].

Spiridon et al. [71] obtained PLA/lignin biocomposites by melt blending, and a study of the impact of their physicochemical parameters showed that adding different concentrations of lignin increased the Young's modulus and tensile strength of the material. PLA/lignin biocomposites showed excellent mechanical resistance, remained stable during a 30-day degradation process, and maintained their dimensional stability in fluid environments. In addition, lignin did not cause cytotoxicity, demonstrating that PLA/lignin biocomposites have good biocompatibility. Tanase-Opedal et al. [72] studied the 3D printing of PLA/lignin biocomposites. Because of the antioxidant activity of lignin, PLA/lignin biocomposites showed incredibly high antioxidant activity, good extrudability, and excellent flowability, making them a promising renewable substitute for traditional 3D printing materials.

### 3.1.3. Silk Fiber

Silk fiber is a natural animal protein fiber with a higher crystallinity, toughness, and tensile strength than plant fibers [73]. In addition to having good mechanical properties and biocompatibility, silk fiber is also easier to process. However, its softness may limit its applications in fields that require high hardness and rigidity. Therefore, it is necessary to optimize the properties of silk fiber for specific applications, including by mixing it with other materials such as PLA to produce tough and rigid materials [74] with improved mechanical properties. Silk/PLA composites may also show greater biocompatibility, making them suitable for various sports medicine and bioengineering applications.

Zhao et al. [75] prepared silk/PLA biocomposites by melt blending and found that adding silk fiber improved the dimensional stability. The presence of silk fiber also enhanced the enzymatic degradation of the PLA matrix, thereby controlling its susceptibility to hydrolysis. Cheung et al. [76] studied the mechanical properties and thermal behavior of silk/PLA biocomposites and found that their tensile performance was superior to that of

pure PLA. Therefore, adding silk fiber improved the thermal and physical properties of the composite, making it suitable for use in medical scaffolds.

### 3.2. PHA

As a new bio-based polymer material, PHA has diverse structures, various sources, and biodegradability, biocompatibility, optical activity, piezoelectricity, and gas barrier properties. They can be naturally biodegraded into CO<sub>2</sub> and H<sub>2</sub>O and are nontoxic to the soil and air [77,78]. Currently, over 150 different PHA monomers have been discovered and produced by other bacteria and growth conditions of which PHB, PHBV, PHBHHx, and P34HB are the four main types. The discovery of these different PHA monomers has dramatically increased the development of PHA into commercial plastic products [79,80].

Zembouai et al. [81] studied PHBV/PLA blends with different mass ratios and found that PHBV acted as a nucleating agent for PLA, thus improving the crystallization of PLA, and the tensile strength and elongation at the break of PHBV/PLA blends were higher than those of pure PHBV. ePHA is a PHA belonging to the polyhydroxy fatty acid family with the same chemical structure, biodegradability, and renewability. Takagi et al. [82] prepared PLA/PHA blends with different compositions by mixing PLA with PHA and functionalized ePHA containing 30% epoxy groups in the side chains. They found that the Charpy impact strength of the PLA/PHA and PLA/ePHA blends increased with the PHA or ePHA content and was higher than that of pure PLA. Functionalizing ePHA with epoxy side groups enhanced the compatibility of the mix, thereby increasing the tensile strength and Charpy impact strength of the PLA/ePHA mixture. The blending of PHA and PLA improved the properties of PHA and also guaranteed the degradability of the composite material.

### 3.3. PBAT

PBAT is a biodegradable material produced on large scales and widely used in packaging materials and biomedical fields. PBAT has good processability and can toughen and modify other polyesters [83], but commercially available PBAT/PLA blends often exhibit macroscale phase separation and show two glass transition temperatures ( $T_g$ ), indicating the poor compatibility of unmodified PBAT/PLA blends. In experimental studies, the preparation of PBAT/PLA blends usually involves melt blending. At high temperatures and sufficient time, ester exchange reactions occur between the two polyesters, thereby improving their compatibility [84]. By increasing the PBAT content within a specific range, the mechanical properties of PLA/PBAT composites, such as impact strength and elongation at break, can be improved [85].

Arruda et al. [86] prepared PLA/PBAT blends using an epoxy-functionalized chain extender and investigated the effect of 0.3% and 0.6% chain extenders on the mechanical properties, thermal properties, and microstructure of PLA/PBAT blends with ratios of 40/60 and 60/40. In the blend containing 40% PLA and no chain extender, the microstructure was significantly affected by the chain extender. PLA exhibited a fibrous dispersed phase, appearing elongated in the film stretching direction. In the mixture containing 60% PLA and no chain extender, PBAT displayed a large, belt-like structure in the middle of the film, with an overall skin-core design. The chain extender increased the crystallization temperature of PLA in both blends with different ratios and reduced the crystallinity of PBAT.

### 3.4. Methods for Manufacturing PLA-Based Composites

#### 3.4.1. Microcellular Injection Molding

Microcellular injection molding was first proposed in the 1980s by Nam et al. [87]. The formation of pores in microcellular foams proceeds via four main stages: construction of a polymer/supercritical fluid homogeneous system, bubble nucleation, bubble expansion, and cooling and solidification [88–91]. Microcellular foam injection molding can be used to produce microcellular foam products with micropores, with millions of pores per unit

volume. Compared with nonfoamed substrates, microcellular foam materials exhibit at least a four-fold higher fracture toughness and impact resistance [92].

#### 3.4.2. Extrusion Molding

Extrusion molding can be divided into continuous and intermittent types based on the different pressures used during extrusion. Continuous extrusion applies pressure with the rotation of a screw to uniformly plasticize the material inside the barrel. The material undergoes mixing and heating through the action of the screw during the extrusion process, resulting in good material uniformity [93]. Intermittent extrusion applies pressure to the material through a plunger. While this provides a higher pressure than screw extruders, its ability to generate significant shear action is limited, and its operation is discontinuous, which limits its application range [94].

#### 3.4.3. Compression Molding

Compression molding is a standard processing method for PLA. During compression molding, PLA particles are placed in a heated mold, and pressure is applied to liquefy and flow the material at high temperatures [95]. As the material cools, it resolidifies and shapes the mold. The final product's body, size, and performance can be controlled by adjusting the temperature, pressure, and holding time. Compared with other molding methods, compression molding has lower mold fabrication costs [96].

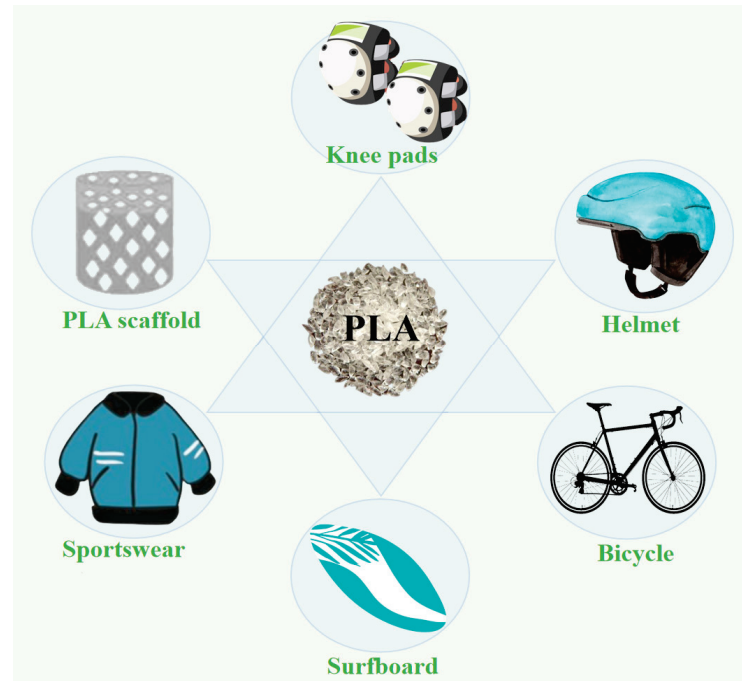
### 4. PLA Composites for Sports Applications

The global production capacity of all biodegradable plastics, including PLA, is expected to increase rapidly to approximately 1.33 million in 2024 [6], with primary applications in the automotive industry, electronic components, and sports equipment. In the automotive industry, 3D printing has had a revolutionary impact by enabling the rapid fabrication of lighter and more complex structures. For instance, in 2014, Local Motors manufactured the first electric car using 3D printing. The automotive industry utilizes 3D printing during the improvement stage to explore various alternative solutions to promote ideal and efficient car design. 3D printing can also reduce material waste and consumption [97]. Because of the ability of 3D printing to create highly integrated three-dimensional multifunctional structures, many researchers have actively explored this emerging technology to fabricate geometrically complex and biocompatible devices and scaffolds. These include biosensors, electrically stimulated tissue-regenerating scaffolds and microelectrodes [98,99]. New technologies for producing high-molecular-weight PLA have expanded their applications in recent years. PLA is becoming a popular substitute for petroleum-based synthetic polymers (PETs, polystyrene (PS), polyethylene (PE), etc.) in various fields, particularly the sports industry [100,101], as shown in Figure 6.

#### 4.1. Sportswear

PLA fiber is a biodegradable synthetic fiber that is refined and fermented from starch sugar in corn, beets, or wheat. It is a new type of polyester fiber in the textile industry. PLA fiber is 100% compostable and reduces the Earth's carbon dioxide levels throughout its entire life cycle. The cross-section of PLA fiber is generally circular with a smooth surface. Its load–elongation curve is similar to that of wool, while its toughness is lower than that of cotton. PLA fiber has good core absorbency and fast moisture management. Therefore, by blending PLA fiber with cotton, the moisture transmission properties of cotton fabrics can be improved. Guruprasad et al. [102] developed a sports textile by combining cotton and PLA at a ratio of 65:35. Then, they tested the moisture management performance, moisture vapor transmission rate, and thermal performance of the cotton/PLA blended fabric. Experiments showed that the mixture of PLA fiber and cotton provided improved moisture management performance. The liquid transfer rate of cotton/PLA blended fabric was faster than that of 100% cotton fabric. The cotton/PLA composite fabric had a high unidirectional transmission capacity, spreading speed, and bottom absorption rate, giving

it a higher OMMC value and allowing it to transfer sweat to the other side faster. The moisture vapor transmission rate of the cotton/PLA blended fabric was 14% higher than that of the 100% cotton fabric, which helped liquid moisture diffuse quicker, making it an ideal material for sportswear.



**Figure 6.** PLA applications in the sports industry.

#### 4.2. Helmets

Raykar et al. [103] used PLA plastic to manufacture a bicycle helmet through a combination of fused deposition modeling (FDM) and 3D printing. PLA plastic filaments were used and melted and deposited using layer-by-layer heat extrusion onto the building platform of the 3D model until the entire exterior of the helmet was covered in PLA plastic. After cleaning and trimming, a PLA bicycle sports helmet was produced. Experiments proved that the 3D printed PLA bicycle sports helmet had high safety, good breathability, and lighter weight, thus balancing the safety and comfort of the athlete.

#### 4.3. Protective Sports Gear

Traditional protective sports gear has a structure consisting of a hard outer shell made of a thermoplastic material and an inner soft foam padding. Currently, there are new “soft shell” technologies for sports protectors based on the use of soft polymer foams typically made of polyurethane or polyacrylate with good cushioning properties. During the manufacturing process of sports protectors, soft polymer foams can be combined with PLA. Soft polymer foams are used as the internal cushioning material. In contrast, PLA can be used as the outer shell material to improve sports knee protectors’ lightweight, breathability, and comfort properties, thus achieving better protection results. Yang et al. [104] used tensile materials (PLA and thermoplastic polyurethane (TPU)). They tested them through 3D printing prototyping and compared the results with calculated predictions to evaluate the possibility of using tensile materials in sports protectors. The results showed that the tensile material had a high fracture toughness, high shear modulus, superior specific strength, compressive indentation resistance, strong energy dissipation, and a controllable strain penetration rate, making it suitable for protective sports gear to reduce the risk of injuries.



#### 4.4. Surfboards

The source of power for a surfboard comes from the movement of waves, and the significant impact force generated by an impact wave can often break a surfboard, mainly when materials such as fiberglass are used in its production. In recent years, researchers have turned their attention to biodegradable materials. Soltani et al. [105] used the finite element method (FEM) and 3D printing to manufacture a surfboard with a uniform honeycomb core structure based on a PLA composite material. They then conducted three-point bending experiments and used accurate finite element tools to simulate surfboards with different core structures. The PLA composite material surfboard passed the three-point bending test, and the overall volume of the surfboard remained unchanged.

#### 4.5. Sports Medicine Tools

Because of the biocompatibility and biodegradability of PLA when in contact with mammalian bodies, it has been widely used in the biomedical and pharmaceutical fields [106] to manufacture screws, pins, surgical sutures, stents, etc. [107,108]. The unique properties of PLA make it suitable for reinforcing rotator cuff repairs and can help heal tendon tissues in various body parts. PLA and its copolymers are often used in orthopedic surgery to manufacture artificial bones and joints, providing a temporary structure for tissue growth, which eventually decomposes. Koh et al. [109] used PLA-reinforced suture anchors to suture and repair tendons separated from the bone. The tensile strength of PLA is approximately 1200 N, and it can be manufactured to the required size. The experiment showed that adding a PLA scaffold to the bone bridge increased the fixation strength by 1.3 times. The use of PLA scaffolds showed significant advantages when used to fix the rotator cuff.

#### 4.6. 3D Printed Sports Equipment

Compared with traditional printing materials, PLA produces almost no harmful gases and has a lower shrinkage rate, making it ideal for 3D printing sports equipment. Protective gear, such as mouthguards, helmets, and shin guards [110], can be 3D printed using PLA, providing athletes with customizable, comfortable, and lightweight equipment. Because of its biocompatibility, PLA is the preferred material for 3D printing protective gear, as it can be safely used in contact sports without causing harm to athletes. In addition to protective gear, PLA can be used to 3D print bicycle frames, kayak paddles, and skis [111]. PLA's mechanical properties and biodegradability make it an attractive alternative to durable materials, such as plastics, metals, and other traditional materials for sports applications.

#### 4.7. Limitations of PLA Composites in Sports Applications

Compared with traditional petroleum-based plastic sports equipment, the green disposal of idle sports equipment meets the requirements of sustainable development. Sports equipment made of PLA composites can be used safely and decomposes after being discarded, which can prevent environmental pollution. In addition, PLA has a lower density, allowing for the production of relatively lightweight sports equipment. Through 3D printing, PLA enables personalized customization, offering more possibilities for the innovative design of sports equipment. However, as a linear thermoplastic polyester, PLA's strength may not meet the requirements of certain sporting equipment in specific environments. For example, because of PLA's high brittleness and low elongation at break [25], sports equipment made from PLA composite materials are more susceptible to rupturing during contact sports. Additionally, prolonged exposure to sunlight can cause a decrease in the molecular weight of PLA composite materials [112], potentially impacting the mechanical performance of outdoor sports equipment.

### 5. Conclusions

PLA is a natural, renewable, and low-cost biodegradable material, but its inherently poor toughness limits its broader applications. By adding reinforcement materials to de-

velop PLA composites, it can adapt to the increasing performance requirements of various fields. Compared with most inorganic and synthetic fibers, natural fibers have abundant sources, low prices, complete degradability, low energy consumption, and environmental friendliness. In the future, appropriate additives, modifications to polymerization conditions, and reinforcement techniques will be employed to enhance the strength of PLA and meet specific needs. At the same time, by developing low-cost reinforcement materials and optimizing formulations and processing methods, the manufacturing costs of PLA composites can be reduced. Their performance can be improved to meet various environmentally friendly applications, including sports equipment manufacturing. Currently, the application of PLA composites in the sports field is expanding. Compared with petroleum-based materials, the mechanical properties of PLA composites still need to be improved. However, as biodegradable alternatives to petroleum-based plastics, they still have tremendous potential.

**Author Contributions:** Conceptualization, writing—original draft, Y.W. (Yueting Wu); conceptualization, writing—review and editing, project administration, and funding acquisition, X.G.; investigation and formal analysis, J.W.; investigation and formal analysis, T.Z.; software and visualization, T.T.N.; investigation and formal analysis, Y.W. (Yutong Wang). All authors have read and agreed to the published version of the manuscript.

**Funding:** This research was funded by the Heilongjiang Natural Science Foundation Joint Guidance Project of China, grant number: LH2022E097.

**Institutional Review Board Statement:** Not applicable.

**Data Availability Statement:** Not applicable.

**Conflicts of Interest:** The authors declare no conflict of interest.

## References

1. Yusoff, N.H.; Pal, K.; Narayanan, T.; de Souza, F.G. Recent trends on bioplastics synthesis and characterizations: Polylactic acid (PLA) incorporated with tapioca starch for packaging applications. *J. Mol. Struct.* **2021**, *1232*, 129954. [CrossRef]
2. Pan, G.W.; Xu, H.L.; Mu, B.B.; Ma, B.M.; Yang, J.; Yang, Y.Q. Complete stereo-complexation of enantiomeric poly lactides for scalable continuous production. *Chem. Eng. J.* **2017**, *328*, 759–767. [CrossRef]
3. Yu, H.Y.; Wang, C.; Abdalkarim, S.Y.H. Cellulose nanocrystals/polyethylene glycol as bifunctional reinforcing/compatibilizing agents in poly(lactic acid) nanofibers for controlling long-term in vitro drug release. *Cellulose* **2017**, *24*, 4461–4477. [CrossRef]
4. Yang, C.; Vora, H.D.; Chang, Y.B. Evaluation of auxetic polymeric structures for use in protective pads. In Proceedings of the ASME International Mechanical Engineering Congress and Exposition (IMECE2016), Phoenix, AZ, USA, 11–17 November 2016.
5. Bartolucci, L.; Cordiner, S.; De Maina, E.; Kumar, G.; Mele, P.; Mulone, V.; Igliński, B.; Piechota, G. Sustainable Valorization of Bioplastic Waste: A Review on Effective Recycling Routes for the Most Widely Used Biopolymers. *Int. J. Mol. Sci.* **2023**, *24*, 7696. [CrossRef]
6. Naser, A.Z.; Deiab, I.; Darras, B.M. Poly(lactic acid) (PLA) and polyhydroxyalkanoates (PHAs), green alternatives to petroleum-based plastics: A review. *RSC Adv.* **2021**, *11*, 17151–17196. [CrossRef] [PubMed]
7. Sarkingobir, Y.; Lawal, A.A. Bioplastics: Their advantages and concerns. *Mater. Metallurg. Eng.* **2021**, *11*, 13–18.
8. Naser, A.Z.; Deiab, I.; Defersha, F.; Yang, S. Expanding poly(lactic acid) (PLA) and polyhydroxyalkanoates (PHAs) applications: A review on modifications and effects. *Polymers* **2021**, *13*, 4271. [CrossRef]
9. Rezvani, G.E.; Khosravi, F.; Saedi, A.A.; Dai, Y.; Neisiyany, R.E.; Foroughi, F.; Wu, M.; Das, O.; Ramakrishna, S. The Life Cycle Assessment for Polylactic Acid (PLA) to Make It a Low-Carbon Material. *Polymers* **2021**, *13*, 1854. [CrossRef]
10. European Bioplastics. Bioplastics: Facts and Figures. Available online: <https://www.european-bioplastics.org/bioplastics-facts-figures/> (accessed on 21 May 2023).
11. Williams, C.K.; Hillmyer, M.A. Polymers from Renewable Resources: A Perspective for a Special Issue of Polymer Reviews. *Polym. Rev.* **2008**, *48*, 1–10. [CrossRef]
12. Chen, Y.J.; Han, L.J.; Ju, D.D.; Liu, T.T.; Dong, L.S. Disentanglement induced by uniaxial pre-stretching as a key factor for toughening poly(L)-lactic acid sheets. *Polymer* **2018**, *140*, 47–55. [CrossRef]
13. Zhou, L.; Ke, K.; Yang, M.B.; Yang, W. Recent progress on chemical modification of cellulose for high mechanical-performance poly(lactic acid)/cellulose composite: A review. *Compos. Commun.* **2021**, *23*, 100548. [CrossRef]
14. Henton, D.E.; Gruber, P.; Lunt, J.; Randall, J. *Natural Fibers, Biopolymers, and Biocomposites*; CRC Press: Boca Raton, FL, USA, 2005; pp. 527–577.
15. Scaffaro, R.; Lopresti, F.; Botta, L. PLA based biocomposites reinforced with *Posidonia oceanica* leaves. *Compos. Part B Eng.* **2018**, *139*, 1–11. [CrossRef]

16. Saeidlou, S.; Huneault, M.A.; Li, H.; Park, C.B. Poly(lactic acid) crystallization. *Prog. Polym. Sci.* **2012**, *37*, 1657–1677. [CrossRef]
17. Jin, F.-L.; Hu, R.-R.; Park, S.-J. Improvement of thermal behaviors of biodegradable poly(lactic acid) polymer: A review. *Compos. Part B Eng.* **2019**, *164*, 287–296. [CrossRef]
18. Tsuji, H.; Kondoh, F. Synthesis of meso-lactide by thermal configurational inversion and depolymerization of poly(l-lactide) and thermal configurational inversion of lactides. *Polym. Degrad. Stab.* **2017**, *141*, 77–83. [CrossRef]
19. Lunt, J. Large-scale production, properties and commercial applications of polylactic acid polymers. *Polym. Degrad. Stab.* **1998**, *59*, 145–152. [CrossRef]
20. Mooninta, S.; Poompradub, S.; Prasassarakich, P. Packaging Film of PP/LDPE/PLA/Clay Composite: Physical, Barrier and Degradable Properties. *J. Polym. Environ.* **2020**, *28*, 3116–3128. [CrossRef]
21. Vasile, C.; Tudorachi, N.; Zaharescu, T.; Darie-Nita, R.N.; Cheaburu-Yilmaz, C.N. Study on Thermal Behavior of Some Biocompatible and Biodegradable Materials Based on Plasticized PLA, Chitosan, and Rosemary Ethanolic Extract. *Int. J. Polym. Sci.* **2020**, *2020*, 4269792. [CrossRef]
22. Paul, M.-A.; Delcourt, C.; Alexandre, M.; Degée, P.; Monteverde, F.; Dubois, P. Polylactide/montmorillonite nanocomposites: Study of the hydrolytic degradation. *Polym. Degrad. Stab.* **2005**, *87*, 535–542. [CrossRef]
23. Cai, Q.; Yang, J.; Bei, J.; Wang, S. A novel porous cells scaffold made of polylactide–dextran blend by combining phase-separation and particle-leaching techniques. *Biomaterials* **2002**, *23*, 4483–4492. [CrossRef]
24. Haleem, A.; Kumar, V.; Kumar, L. Mathematical Modelling & Pressure Drop Analysis of Fused Deposition Modelling Feed Wire. *Int. J. Eng. Technol.* **2017**, *9*, 2885–2894. [CrossRef]
25. Farah, S.; Anderson, D.G.; Langer, R. Physical and mechanical properties of PLA, and their functions in widespread applications—A comprehensive review. *Adv. Drug Deliv. Rev.* **2016**, *107*, 367–392. [CrossRef] [PubMed]
26. Basu, A.; Kunduru, K.R.; Doppalapudi, S.; Domb, A.J.; Khan, W. Poly(lactic acid) based hydrogels. *Adv. Drug Deliv. Rev.* **2016**, *107*, 192–205. [CrossRef] [PubMed]
27. Lopes, M.S.; Jardini, A.; Filho, R.M. Poly (Lactic Acid) Production for Tissue Engineering Applications. *Procedia Eng.* **2012**, *42*, 1402–1413. [CrossRef]
28. Södergård, A.; Stolt, M. Properties of lactic acid based polymers and their correlation with composition. *Prog. Polym. Sci.* **2002**, *27*, 1123–1163. [CrossRef]
29. Korhonen, H.; Helminen, A.; Seppälä, J.V. Synthesis of polylactides in the presence of coinitiators with different numbers of hydroxyl groups. *Polymer* **2001**, *42*, 7541–7549. [CrossRef]
30. Zaaba, N.F.; Jaafar, M. A review on degradation mechanisms of polylactic acid: Hydrolytic, photodegradative, microbial, and enzymatic degradation. *Polym. Eng. Sci.* **2020**, *60*, 2061–2075. [CrossRef]
31. Shao, J.; Liu, Y.-L.; Xiang, S.; Bian, X.-C.; Sun, J.-R.; Li, G.; Chen, X.-S.; Hou, H.-Q. The stereocomplex formation and phase separation of PLLA/PDLA blends with different optical purities and molecular weights. *Chin. J. Polym. Sci.* **2015**, *33*, 1713–1720. [CrossRef]
32. Murariu, M.; Dubois, P. PLA composites: From production to properties. *Adv. Drug Deliv. Rev.* **2016**, *107*, 17–46. [CrossRef]
33. Chen, G.-X.; Kim, H.-S.; Kim, E.-S.; Yoon, J.-S. Synthesis of high-molecular-weight poly(l-lactic acid) through the direct condensation polymerization of l-lactic acid in bulk state. *Eur. Polym. J.* **2006**, *42*, 468–472. [CrossRef]
34. Huang, S.; Xue, Y.; Yu, B.; Wang, L.; Zhou, C.; Ma, Y. A Review of the Recent Developments in the Bioproduction of Polylactic Acid and Its Precursors Optically Pure Lactic Acids. *Molecules* **2021**, *26*, 6446. [CrossRef] [PubMed]
35. Djukić-Vuković, A.; Mladenović, D.; Ivanović, J.; Pejin, J.; Mojović, L. Towards sustainability of lactic acid and poly-lactic acid polymers production. *Renew. Energy Rev.* **2019**, *108*, 238–252.
36. Kalia, S.; Avérous, L. *Biopolymers: Biomedical and Environmental Applications*; John Wiley & Sons: Hoboken, NJ, USA, 2011; pp. 173–180.
37. Zengwen, C.; Lu, Z.; Pan, H.; Bian, J.; Han, L.; Zhang, H.; Dong, L.; Yang, Y. Structuring poly (lactic acid) film with excellent tensile toughness through extrusion blow molding. *Polymer* **2020**, *187*, 122091. [CrossRef]
38. Rapa, M.; Nita, R.N.D.; Vasile, C. Influence of plasticizers over some physico-chemical properties of PLA. *Mater. Plast.* **2017**, *54*, 73–78. [CrossRef]
39. Mofokeng, J.P.; Luyt, A.S. Dynamic mechanical properties of PLA/PHBV, PLA/PCL, PHBV/PCL blends and their nanocomposites with TiO<sub>2</sub> as nanofiller. *Thermochim. Acta* **2015**, *613*, 41–53. [CrossRef]
40. Cao, Z.W.; Pan, H.W.; Chen, Y.J.; Bian, J.J.; Han, L.J.; Zhang, H.L.; Dong, L.S.; Yang, Y.M. Transform poly (lactic acid) packaging film from brittleness to toughness using traditional industrial equipments. *Polymer* **2019**, *180*, 121728. [CrossRef]
41. Chrissafis, K. Detail kinetic analysis of the thermal decomposition of PLA with oxidized multi-walled carbon nanotubes. *Thermochim. Acta* **2010**, *511*, 163–167. [CrossRef]
42. Seligra, P.G.; Nuevo, F.; Lamanna, M.; Fama, L. Covalent grafting of carbon nanotubes to PLA in order to improve compatibility. *Compos. Part B Eng.* **2013**, *46*, 61–68. [CrossRef]
43. Li, L.; Liu, X.; Niu, Y.; Ye, J.; Huang, S.; Liu, C.; Xu, K. Synthesis and wound healing of alternating block polyurethanes based on poly(lactic acid) (PLA) and poly(ethylene glycol) (PEG). *J. Biomed. Mater. Res. Part B Appl. Biomater.* **2017**, *105*, 1200–1209. [CrossRef]
44. Huang, Y.; Hu, C.; Pang, X.; Zhou, Y.; Duan, R.; Sun, Z.; Chen, X. Electrochemically Controlled Switchable Copolymerization of Lactide, Carbon Dioxide, and Epoxides. *Angew. Chem. Int. Ed.* **2022**, *61*, e202202660. [CrossRef]

45. Dornburg, V.; Faaij, A.; Patel, M.; Turkenburg, W. Economics and GHG emission reduction of a PLA bio-refinery system—Combining bottom-up analysis with price elasticity effects. *Resour. Conserv. Recycl.* **2006**, *46*, 377–409. [CrossRef]
46. Armentano, I.; Bitinis, N.; Fortunati, E.; Mattioli, S.; Rescignano, N.; Verdejo, R.; Lopez-Manchado, M.; Kenny, J. Multifunctional nanostructured PLA materials for packaging and tissue engineering. *Prog. Polym. Sci.* **2013**, *38*, 1720–1747. [CrossRef]
47. McKeown, P.; Jones, M.D. The Chemical Recycling of PLA: A Review. *Sustain. Chem.* **2020**, *1*, 1. [CrossRef]
48. Piemonte, V.; Gironi, F. Kinetics of Hydrolytic Degradation of PLA. *J. Polym. Environ.* **2013**, *21*, 313–318. [CrossRef]
49. Raquez, J.-M.; Habibi, Y.; Murariu, M.; Dubois, P. Polylactide (PLA)-based nanocomposites. *Prog. Polym. Sci.* **2013**, *38*, 1504–1542. [CrossRef]
50. Li, X.R.; Lin, Y.; Liu, M.L.; Meng, L.P.; Li, C.F. A review of research and application of polylactic acid composites. *J. Appl. Polym. Sci.* **2022**, *140*, e53477. [CrossRef]
51. Arif, Z.U.; Khalid, M.Y.; Noroozi, R.; Sadeghianmaryan, A.; Jalalvand, M.; Hossain, M. Recent advances in 3D-printed polylactide and polycaprolactone-based biomaterials for tissue engineering applications. *Int. J. Biol. Macromol.* **2022**, *218*, 930–968. [CrossRef]
52. Spiridon, I.; Darie, R.N.; Kangas, H. Influence of fiber modifications on PLA/fiber composites. Behavior to accelerated weathering. *Compos. Part B Eng.* **2016**, *92*, 19–27. [CrossRef]
53. Huda, M.S.; Drzal, L.T.; Misra, M.; Mohanty, A.K. Wood-fiber-reinforced poly(lactic acid) composites: Evaluation of the physicomechanical and morphological properties. *J. Appl. Polym. Sci.* **2006**, *102*, 4856–4869. [CrossRef]
54. Cheung, H.-Y.; Lau, K.-T.; Tao, X.-M.; Hui, D. A potential material for tissue engineering: Silkworm silk/PLA biocomposite. *Compos. Part B Eng.* **2008**, *39*, 1026–1033. [CrossRef]
55. Hongdilokkul, P.; Keeratipinit, K.; Chawthai, S.; Hararak, B.; Seadan, M.; Suttiruengwong, S. A study on properties of PLA/PBAT from blown film process. In Proceedings of the Global Conference on Polymer and Composite Materials (PCM), Beijing, China, 16–19 May 2015.
56. Injorhor, P.; Trongsatitkul, T.; Wittayakun, J.; Ruksakulpiwat, C.; Ruksakulpiwat, Y. Biodegradable polylactic acid-polyhydroxyalkanoate-based nanocomposites with bio-hydroxyapatite: Preparation and characterization. *Polymers* **2023**, *15*, 1261. [CrossRef] [PubMed]
57. Margellou, A.G.; Lazaridis, P.A.; Charisteidis, I.D.; Nitsos, C.K.; Pappa, C.P.; Fotopoulos, A.P.; Van den Bosch, S.; Sels, B.F.; Triantafyllidis, K.S. Catalytic fast pyrolysis of beech wood lignin isolated by different biomass (pre) treatment processes: Organosolv, hydrothermal and enzymatic hydrolysis. *Appl. Catal. A-Gen.* **2021**, *623*, 118298. [CrossRef]
58. Ramamoorthy, S.K.; Skrifvars, M.; Persson, A. A Review of Natural Fibers Used in Biocomposites: Plant, Animal and Regenerated Cellulose Fibers. *Polym. Rev.* **2015**, *55*, 107–162. [CrossRef]
59. Sanivada, U.K.; Marmol, G.; Brito, F.P.; Figueiro, R. PLA composites reinforced with flax and jute fibers—A review of recent trends, processing parameters and mechanical properties. *Polymers* **2020**, *12*, 2373. [CrossRef]
60. Costa, C.S.M.F.; Fonseca, A.C.; Serra, A.C.; Coelho, J.F.J. Dynamic Mechanical Thermal Analysis of Polymer Composites Reinforced with Natural Fibers. *Polym. Rev.* **2016**, *56*, 362–383. [CrossRef]
61. Kusmono; Listyanda, R.F.; Wildan, M.W.; Ilman, M.N. Preparation and characterization of cellulose nanocrystal extracted from ramie fibers by sulfuric acid hydrolysis. *Heliyon* **2020**, *6*, e05486. [CrossRef]
62. Dufresne, A. Nanocellulose: A new ageless bionanomaterial. *Mater. Today* **2013**, *16*, 220–227. [CrossRef]
63. Favier, V.; Chanzy, H.; Cavaille, J.Y. Polymer Nanocomposites Reinforced by Cellulose Whiskers. *Macromolecules* **1995**, *28*, 6365–6367. [CrossRef]
64. Shi, Q.F.; Zhou, C.J.; Yue, Y.Y.; Guo, W.H.; Wu, Y.Q.; Wu, Q.L. Mechanical properties and in vitro degradation of electrospun bio-nanocomposite mats from PLA and cellulose nanocrystals. *Carbohydr. Polym.* **2012**, *90*, 301–308. [CrossRef]
65. Kamal, A.; Ashmawy, M.; Shanmugan, S.; Algazzar, A.M.; Elsheikh, A.H. Fabrication techniques of polymeric nanocomposites: A comprehensive review. *Proc. Inst. Mech. Eng. Part C J. Mech. Eng. Sci.* **2022**, *236*, 4843–4861. [CrossRef]
66. Karkhanis, S.S.; Stark, N.M.; Sabo, R.C.; Matuana, L.M. Water vapor and oxygen barrier properties of extrusion-blown poly(lactic acid)/cellulose nanocrystals nanocomposite films. *Compos. Part A-Appl. Sci. Manuf.* **2018**, *114*, 204–211. [CrossRef]
67. Shuai, C.J.; Yuan, X.; Yang, W.J.; Peng, S.P.; He, C.X.; Feng, P.; Qi, F.W.; Wang, G.Y. Cellulose nanocrystals as biobased nucleation agents in poly-L-lactide scaffold: Crystallization behavior and mechanical properties. *Polym. Test.* **2020**, *85*, 106458. [CrossRef]
68. Beluns, S.; Platnieks, O.; Gaidukovs, S.; Starkova, O.; Sabalina, A.; Grase, L.; Thakur, V.K.; Gaidukova, G. Lignin and Xylan as Interface Engineering Additives for Improved Environmental Durability of Sustainable Cellulose Nanopapers. *Int. J. Mol. Sci.* **2021**, *22*, 12939. [CrossRef] [PubMed]
69. Kim, Y.; Suhr, J.; Seo, H.-W.; Sun, H.; Kim, S.; Park, I.-K.; Kim, S.-H.; Lee, Y.; Kim, K.-J.; Nam, J.-D. All Biomass and UV Protective Composite Composed of Compatibilized Lignin and Poly (Lactic-acid). *Sci. Rep.* **2017**, *7*, 43596. [CrossRef]
70. Thakur, V.K.; Thakur, M.K.; Raghavan, P.; Kessler, M.R. Progress in green polymer composites from lignin for multi-functional applications: A review. *ACS Sustain. Chem. Eng.* **2014**, *2*, 1072–1092. [CrossRef]
71. Spiridon, I.; Tanase, C.E. Design, characterization and preliminary biological evaluation of new lignin-PLA biocomposites. *Int. J. Biol. Macromol.* **2018**, *114*, 855–863. [CrossRef]
72. Tanase-Opedal, M.; Espinosa, E.; Rodriguez, A.; Chinga-Carrasco, G. Lignin: A Biopolymer from forestry biomass for biocomposites and 3D Printing. *Materials* **2019**, *12*, 3006. [CrossRef]
73. Shah, D.U.; Porter, D.; Vollrath, F. Can silk become an effective reinforcing fibre? A property comparison with flax and glass reinforced composites. *Compos. Sci. Technol.* **2014**, *101*, 173–183. [CrossRef]



74. Luzi, F.; Puglia, D.; Torre, L. *Natural Fiber Biodegradable Composites and Nanocomposites: A Biomedical Application*; Woodhead Publishing Ltd.: Cambridge, UK, 2019; pp. 179–201.
75. Zhao, Y.-Q.; Cheung, H.-Y.; Lau, K.-T.; Xu, C.-L.; Zhao, D.-D.; Li, H.-L. Silk worm silk/poly(lactic acid) biocomposites: Dynamic mechanical, thermal and biodegradable properties. *Polym. Degrad. Stab.* **2010**, *95*, 1978–1987. [CrossRef]
76. Cheung, H.Y.; Dean, J.; Stearn, B.; Clyne, T.W. Characterisation on PLA–silk fibre composites for prosthetic applications. In Proceedings of the 15th European Conference on Composite Materials, Venice, Italy, 24–28 June 2012.
77. Insomphun, C.; Chuah, J.-A.; Kobayashi, S.; Fujiki, T.; Numata, K. Influence of Hydroxyl Groups on the Cell Viability of Polyhydroxyalkanoate (PHA) Scaffolds for Tissue Engineering. *ACS Biomater. Sci. Eng.* **2017**, *3*, 3064–3075. [CrossRef]
78. Khare, A.; Deshmukh, S. Studies toward producing eco-friendly plastics. *J. Plast Film Sheet.* **2006**, *22*, 193–211. [CrossRef]
79. Sun, J.Y.; Shen, J.J.; Chen, S.K.; Cooper, M.A.; Fu, H.B.; Wu, D.M.; Yang, Z.G. Nanofiller Reinforced Biodegradable PLA/PHA Composites: Current Status and Future Trends. *Polymers* **2018**, *10*, 505. [CrossRef]
80. Lee, C.H.; Sapuan, S.M.; Ilyas, R.A.; Lee, S.H.; Khalina, A. *Advanced Processing, Properties, and Applications of Starch and Other Bio-Based Polymers*; Elsevier: Amsterdam, The Netherlands, 2020; pp. 47–63.
81. Zembouai, I.; Kaci, M.; Bruzard, S.; Benhamida, A.; Corre, Y.M.; Grohens, Y. A study of morphological, thermal, rheo-logical and barrier properties of Poly (3-hydroxybutyrate-Co-3-Hydroxyvalerate)/polylactide blends prepared by melt mixing. *Polym. Test* **2013**, *32*, 842–851. [CrossRef]
82. Takagi, Y.; Yasuda, R.; Yamaoka, M.; Yamane, T. Morphologies and mechanical properties of polylactide blends with medium chain length poly(3-hydroxyalkanoate) and chemically modified poly(3-hydroxyalkanoate). *J. Appl. Polym. Sci.* **2004**, *93*, 2363–2369. [CrossRef]
83. Su, S. Prediction of the Miscibility of PBAT/PLA Blends. *Polymers* **2021**, *13*, 2339. [CrossRef]
84. Lins, L.C.; Livi, S.; Duchet-Rumeau, J.; Gerard, J.F. Phosphonium ionic liquids as new compatibilizing agents of biopolymer blends composed of poly(butylene-adipate-co-terephthalate)/poly(lactic acid) (PBAT/PLA). *RSC Adv.* **2015**, *5*, 59082–59092. [CrossRef]
85. Zhang, T.; Han, W.; Zhang, C.; Weng, Y. Effect of chain extender and light stabilizer on the weathering resistance of PBAT/PLA blend films prepared by extrusion blowing. *Polym. Degrad. Stab.* **2021**, *183*, 109455. [CrossRef]
86. Arruda, L.C.; Magaton, M.; Bretas, R.E.S.; Ueki, M.M. Influence of chain extender on mechanical, thermal and morpho-logical properties of blown films of PLA/PBAT blends. *Polym. Test* **2015**, *43*, 27–37. [CrossRef]
87. Colton, J.S.; Suh, N.P. The nucleation of microcellular thermoplastic foam with additives: Part I: Theoretical considerations. *Polym. Eng. Sci.* **1987**, *27*, 485–492. [CrossRef]
88. Suh, N.P. Impact of microcellular plastics on industrial practice and academic research. *Macromol. Symp.* **2003**, *201*, 187–202. [CrossRef]
89. Colton, J.S.; Suh, N.P. Nucleation of microcellular foam: Theory and practice. *Polym. Eng. Sci.* **1987**, *27*, 500–503. [CrossRef]
90. Colton, J.; Suh, N. The nucleation of microcellular thermoplastic foam with additives: Part II: Experimental results and discussion. *Polym. Eng. Sci.* **1987**, *27*, 493–499. [CrossRef]
91. Ding, Y.; Hassan, M.H.; Bakker, O.; Hinduja, S.; Bártolo, P. A Review on Microcellular Injection Moulding. *Materials* **2021**, *14*, 4209. [CrossRef]
92. Okolieocha, C.; Raps, D.; Subramaniam, K.; Altstädt, V. Microcellular to nanocellular polymer foams: Progress (2004–2015) and future directions—A review. *Eur. Polym. J.* **2015**, *73*, 500–519. [CrossRef]
93. Ji, S.; Fan, Z.; Bevis, M. Semi-solid processing of engineering alloys by a twin-screw rheomoulding process. *Mater. Sci. Eng. A* **2001**, *299*, 210–217. [CrossRef]
94. Li, S.; Jones, D.S.; Andrews, G.P. *Hot Melt Extrusion: A Process Overview and Use in Manufacturing Solid Dispersions of Poorly Water-Soluble Drugs*; Wiley: Hoboken, NJ, USA, 2013; pp. 325–358. [CrossRef]
95. Jiang, J.; Liu, F.; Yang, X.; Xiong, Z.; Liu, H.; Xu, D.; Zhai, W. Evolution of ordered structure of TPU in high-elastic state and their influences on the autoclave foaming of TPU and inter-bead bonding of expanded TPU beads. *Polymer* **2021**, *228*, 123872. [CrossRef]
96. Tatara, R.A. Compression molding. In *Applied Plastics Engineering Handbook*; Elsevier: Amsterdam, The Netherlands, 2017; pp. 291–320.
97. Shahrudin, N.; Lee, T.; Ramlan, R. An Overview on 3D Printing Technology: Technological, Materials, and Applications. *Procedia Manuf.* **2019**, *35*, 1286–1296. [CrossRef]
98. Hales, S.; Tokita, E.; Neupane, R.; Ghosh, U.; Elder, B.; Wirthlin, D.S.; Kong, Y.L. 3D printed nanomaterial-based electronic, biomedical, and bioelectronic devices. *Nanotechnology* **2020**, *31*, 172001. [CrossRef]
99. Khan, Y.; Pavinatto, F.J.; Lin, M.C.; Liao, A.; Swisher, S.L.; Mann, K.; Subramanian, V.; Maharbiz, M.M.; Arias, A.C. Inkjet-Printed Flexible Gold Electrode Arrays for Bioelectronic Interfaces. *Adv. Funct. Mater.* **2016**, *26*, 1004–1013. [CrossRef]
100. Morales, A.P.; Guemes, A.; Fernandez-Lopez, A.; Valero, V.C.; Llano, S.D. Bamboo-poly(lactic acid) (PLA) composite material for structural applications. *Materials* **2017**, *10*, 1286. [CrossRef]
101. Battagazzore, D.; Abt, T.; Maspoch, M.L.; Frache, A. Multilayer cotton fabric bio-composites based on PLA and PHB co-polymer for industrial load carrying applications. *Compos. Part B-Eng.* **2019**, *163*, 761–768. [CrossRef]
102. Guruprasad, R.; Vivekanandan, M.V.; Arputharaj, A.; Saxena, S.; Chattopadhyay, S.K. Development of cotton-rich/poly(lactic acid) fiber blend knitted fabrics for sports textiles. *J. Ind. Text* **2015**, *45*, 405–415. [CrossRef]

103. Raykar, S.J.; Narke, M.M.; Desai, S.B.; Warke, S.S. Manufacturing of 3D printed sports Helmet. In *Techno-Societal 2018: Proceedings of the 2nd International Conference on Advanced Technologies for Societal Applications-Volume 2*; Springer: Berlin/Heidelberg, Germany, 2018.
104. Yang, C.; Vora, H.D.; Chang, Y. Behavior of auxetic structures under compression and impact forces. *Smart Mater. Struct.* **2018**, *27*, 025012. [CrossRef]
105. Soltani, A.; Noroozi, R.; Bodaghi, M.; Zolfagharian, A.; Hedayati, R. 3D Printing On-Water Sports Boards with Bio-Inspired Core Designs. *Polymers* **2020**, *12*, 250. [CrossRef] [PubMed]
106. Kim, G.-J.; Lee, K.-J.; Choi, J.-W.; An, J.H. Modified Industrial Three-Dimensional Polylactic Acid Scaffold Cell Chip Promotes the Proliferation and Differentiation of Human Neural Stem Cells. *Int. J. Mol. Sci.* **2022**, *23*, 2204. [CrossRef]
107. Chen, C.H.; Cheng, Y.H.; Chen, S.H.; Chuang, A.D.C.; Chen, J.P. Functional hyaluronic acid-poly(lactic acid)/silver nanoparticles core-sheath nanofiber membranes for prevention of post-operative tendon adhesion. *Int. J. Mol. Sci.* **2021**, *22*, 8781. [CrossRef]
108. Grottkau, B.E.; Hui, Z.; Yao, Y.; Pang, Y. Rapid Fabrication of Anatomically-Shaped Bone Scaffolds Using Indirect 3D Printing and Perfusion Techniques. *Int. J. Mol. Sci.* **2020**, *21*, 315. [CrossRef]
109. Koh, J.L.; Szomor, Z.; Murrell, G.A.C.; Warren, R.F. Supplementation of Rotator Cuff Repair with a Bioresorbable Scaffold. *Am. J. Sports Med.* **2002**, *30*, 410–413. [CrossRef]
110. Colonna, M.; Zingerle, B.; Parisi, M.F.; Gioia, C.; Speranzoni, A.; Pisaneschi, G.; Prosdocimo, S. A Novel Approach for a Faster Prototyping of Winter Sport Equipment Using Digital Image Correlation and 3D Printing. *Proceedings* **2020**, *49*, 125. [CrossRef]
111. Beigbeder, J.; Soccalingame, L.; Perrin, D.; Benezet, J.C.; Bergeret, A. How to manage biocomposites wastes end of life? A life cycle assessment approach (LCA) focused on polypropylene (PP)/wood flour and poly(lactic acid) (PLA)/flax fibres biocomposites. *Waste Manag.* **2019**, *83*, 184–193. [CrossRef]
112. Mosnáčková, K.; Danko, M.; Šišková, A.; Falco, L.M.; Janigová, I.; Chmela, Š.; Vanovčanová, Z.; Omaníková, L.; Chodák, L.; Mosnáček, J. Complex study of the physical properties of a poly(lactic acid)/poly(3-hydroxybutyrate) blend and its carbon black composite during various outdoor and laboratory ageing conditions. *RSC Adv.* **2017**, *7*, 47132–47142. [CrossRef]

**Disclaimer/Publisher's Note:** The statements, opinions and data contained in all publications are solely those of the individual author(s) and contributor(s) and not of MDPI and/or the editor(s). MDPI and/or the editor(s) disclaim responsibility for any injury to people or property resulting from any ideas, methods, instructions or products referred to in the content.



# Bioplastics: Innovation for Green Transition

Ana Costa <sup>1</sup>, Telma Encarnação <sup>1,2,3</sup>, Rafael Tavares <sup>1</sup>, Tiago Todo Bom <sup>4</sup> and Artur Mateus <sup>1,\*</sup>

<sup>1</sup> CDRSP-IPL, Centre for Rapid and Sustainable Product Development, Polytechnic Institute of Leiria, 2430-028 Marinha Grande, Portugal

<sup>2</sup> CQC-IMS, Department of Chemistry, University of Coimbra, 3004-535 Coimbra, Portugal

<sup>3</sup> PTScience, Avenida do Atlântico, N<sup>o</sup> 16, Office 5.07, Parque das Nações, 1990-019 Lisboa, Portugal

<sup>4</sup> Complexo Industrial VANGEST—Edifício 2, Rua de Leiria 210, 2430-527 Marinha Grande, Portugal

\* Correspondence: artur.mateus@ipleiria.pt

**Abstract:** Bioplastics are one of the possible alternative solutions to the polymers of petrochemical origins. Bioplastics have several advantages over traditional plastics in terms of low carbon footprint, energy efficiency, biodegradability and versatility. Although they have numerous benefits and are revolutionizing many application fields, they also have several weaknesses, such as brittleness, high-water absorption, low crystallization ability and low thermal degradation temperature. These drawbacks can be a limiting factor that prevents their use in many applications. Nonetheless, reinforcements and plasticizers can be added to bioplastic production as a way to overcome such limitations. Bioplastics materials are not yet studied in depth, but it is with great optimism that their industrial use and market scenarios are increasing; such growth can be a positive driver for more research in this field. National and international investments in the bioplastics industry can also promote the green transition. International projects, such as EcoPlast and Animpol, aim to study and develop new polymeric materials made from alternative sources. One of their biggest problems is their waste management; there is no separation process yet to recycle the nonbiodegradable bioplastics, and they are considered contaminants when mixed with other polymers. Some materials use additives, and their impact on the microplastics they leave after breaking apart is subject to debate. For this reason, it is important to consider their life cycle analysis and assess their environmental viability. These are materials that can possibly be processed in various ways, including conventional processes used for petrochemical ones. Those include injection moulding and extrusion, as well as digital manufacturing. This and the possibility to use these materials in several applications is one of their greatest strengths. All these aspects will be discussed in this review.

**Keywords:** bioplastics; biopolymers; conventional polymers; biodegradability; renewable resources; LCA

**Citation:** Costa, A.; Encarnação, T.; Tavares, R.; Todo Bom, T.; Mateus, A. Bioplastics: Innovation for Green Transition. *Polymers* **2023**, *15*, 517. <https://doi.org/10.3390/polym15030517>

Academic Editor: Raffaella Striani

Received: 7 November 2022

Revised: 16 December 2022

Accepted: 25 December 2022

Published: 18 January 2023



**Copyright:** © 2023 by the authors. Licensee MDPI, Basel, Switzerland. This article is an open access article distributed under the terms and conditions of the Creative Commons Attribution (CC BY) license (<https://creativecommons.org/licenses/by/4.0/>).

## 1. Introduction

The use of polymeric materials is widely spread around the world. These materials have significant advantages compared with other, more conventional materials, such as metals and wood, mainly because of their properties and performance.

It is estimated that 99% of these polymeric materials come from fossil fuels. These plastics entail several issues since their primary raw material is a hazard to environment conservation [1].

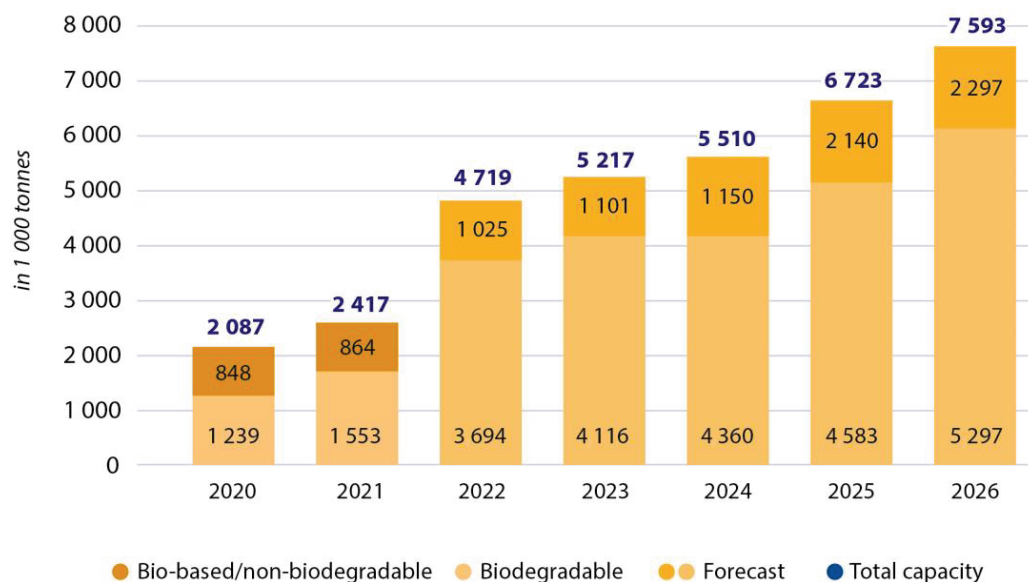
The durability and degradability of these materials are two contradictory topics. For most applications, it is favourable that the material maintains specific properties throughout time, but it is also desirable to discard them easily after their use. There are some alternative processes usually used to manage this kind of waste: recycling (one of the most sustainable waste management processes but requires a controlled process to have a final product with good properties) and energy recovery (allows the production of energy by burning the waste but ends up producing toxic emissions and greenhouse gases) [2,3]. However, a massive quantity of material ends up in landfills or even abandoned, and some of it reaches



the ocean. A long-term study took place on the North Atlantic Sea, where it was observed a seawater sample contained 580,000 pieces of plastic per square kilometre. This waste management has created a crisis, since landfills have a limited capacity, high costs and strict legislation [4].

The remaining percentage of plastics is produced from natural raw materials and are denominated bio-based plastics or bioplastics [1]. The use of bioplastics dates centuries ago. In 1500 BCE, Mesoamerican cultures (Maya, Aztecs) used natural rubber and latex to make containers and waterproof their clothes. However, only in 1862 was the first manmade bioplastic produced (Parkesine, a bioplastic made from cellulose), created by Alexander Parkes. The first company to produce bioplastics was Marlborough Biopolymers in 1983. They produced strips, filaments, chips, panels and powders of bacteria called Biopol. More recently, in 2018, Project Effective was launched with the goal of replacing nylon with bio-nylon, and it created the first bioplastic made from the fruit [5].

Although investigations regarding bioplastics have been done for over a century, their implementation and extensive production is not yet developed. Figure 1 presents a chart of the last few years' production and the forecast for the years to come. In 2019, 1.95 Mt of bioplastic was produced, corresponding to about 0.6% of all plastic production worldwide.

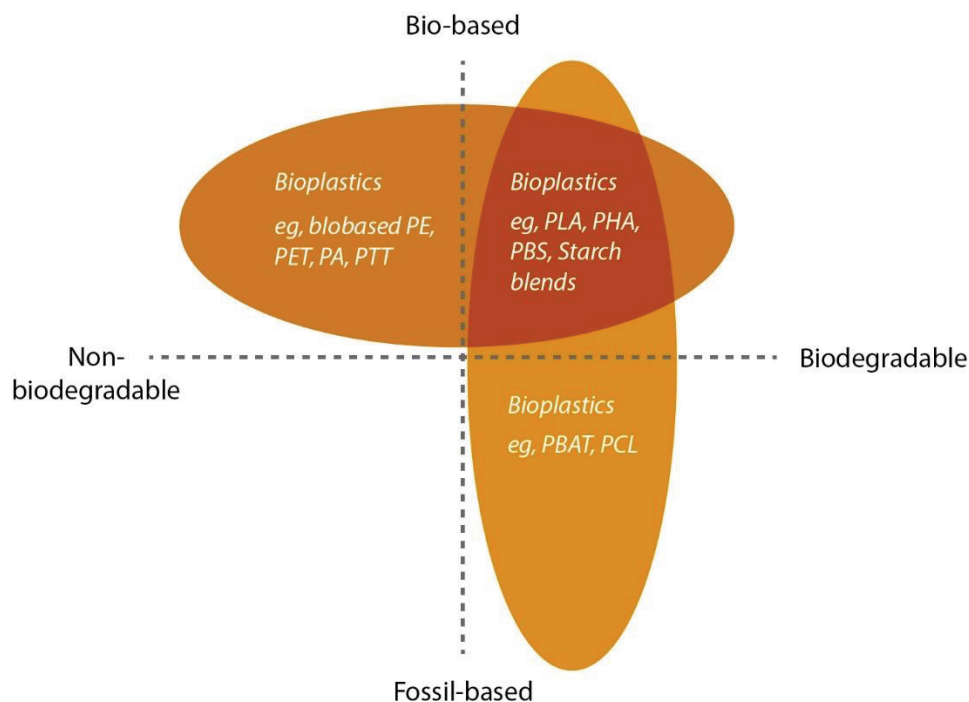


**Figure 1.** Global production capacities of bioplastics 2021–2026. Adapted from European Bioplastics, “Bioplastics Market Development Update 2021”. [https://docs.european-bioplastics.org/publications/market\\_data/Report\\_Bioplastics\\_Market\\_Data\\_2021\\_short\\_version.pdf](https://docs.european-bioplastics.org/publications/market_data/Report_Bioplastics_Market_Data_2021_short_version.pdf) (accessed on 29 December 2022) [6].

The small production of these plastics is mainly due to their more expensive manufacturing and generally inferior mechanical properties compared to fossil-based polymers. However, it is necessary to develop these materials to have a sustainable alternative to petrochemical materials [7]. This paper will discuss current scenarios and the inherent production limitations and present the pros and cons of producing and using bioplastics to replace some petrochemical-based polymers. While several reviews on biopolymers have been extensively published [8–11], the contribution of this review is to gather current knowledge in several aspects and present the latest discoveries in this topic. We have selected the most representative biopolymers and composites and present new ones. Several applications are described, and processing techniques are discussed. Moreover, some fundamental approaches to bioplastic waste management are presented. Lastly, we highlight legislation and policies that can contribute to promising future perspectives for innovation for the green transition.

## 2. Materials

The European Bioplastics organization classifies bioplastics as “plastics based on renewable resources or as plastics which are biodegradable and/or compostable”. When it is possible to decompose a polymer into carbon dioxide (CO<sub>2</sub>), methane, water, inorganic compounds or biomass through an enzymatic process using microorganisms, the polymer is considered biodegradable. It is possible to compost some of these materials under controlled conditions [12]. Based on this definition, it is possible to organize this classification in a simple graph represented in Figure 2.

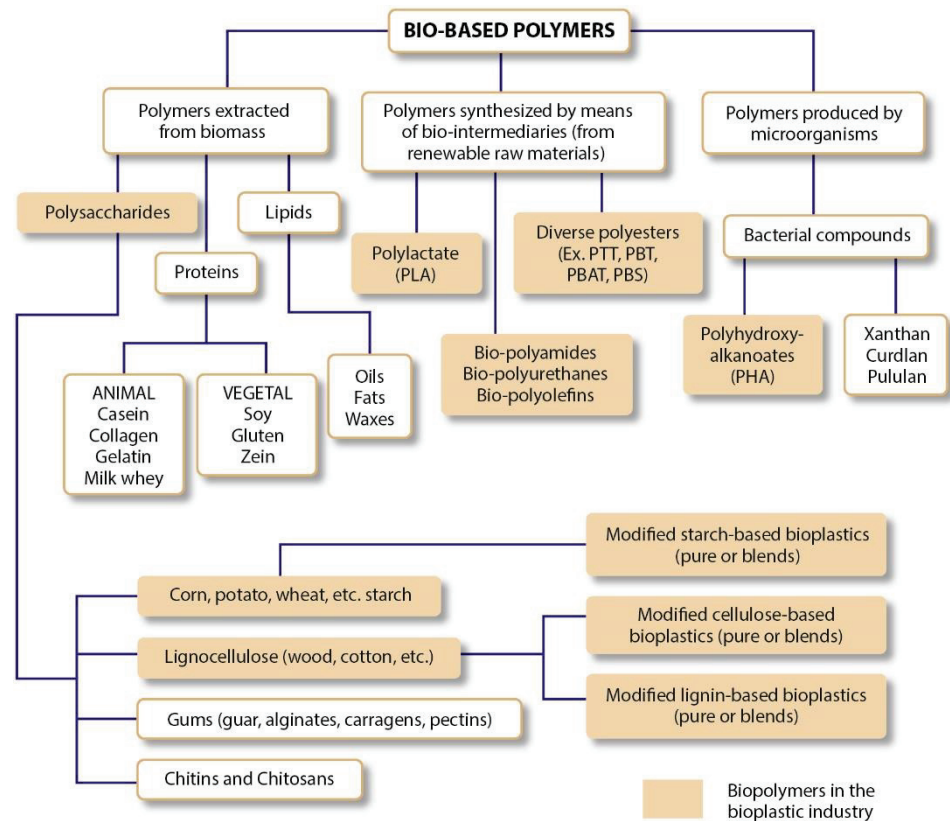


**Figure 2.** Classification of bioplastics according to The European Bioplastics Organization. Adapted from European Bioplastics, “What are bioplastics?”. [https://docs.european-bioplastics.org/publications/fs/EuBP\\_FS\\_What\\_are\\_bioplastics.pdf](https://docs.european-bioplastics.org/publications/fs/EuBP_FS_What_are_bioplastics.pdf) (accessed on 29 December 2022) [13].

In the bioplastic group, they can be classified under three different classes, as shown in Figure 2: (1) polymers originated from biomass materials, and they can be either modified or not; (2) polymers extracted from natural or genetically modified microorganism production and (3) and polymers produced from renewable raw materials with the involvement of bio-intermediaries. Although only some of these materials are available on a commercial scale, the most used bioplastics are based on cellulosic esters, starch, polyhydroxy butyrate (PHB), polylactic acid (PLA) and polycaprolactone (PCL). Figure 3 shows some of the most used bio-based polymers according to their base of production and raw material [14–16].

Some biopolymers have properties comparable with conventional plastics, such as LDPE (low-density polyethylene), PS (polystyrene) and PET (polyethylene terephthalate); some of these properties are important to predict the behaviour of the material during use and the proper conditions to process it. Some of these characteristics, listed in Table 1, are the glass transition temperature (T<sub>g</sub>), melting temperature (T<sub>m</sub>), tensile strength, tensile modulus and elongation break [2].

Another characteristic important to consider is the rate of crystallinity of the polymer. It influences a vast quantity of essential properties such as hardness, modulus, tensile strength, stiffness, crease point and the melting point, making it important to pay special attention to this property [2].



**Figure 3.** Types of bioplastics according to their raw material. Adapted from “Innovation and industrial trends in bioplastics”, Polymer Reviews vol. 49, no. 2, pp. 65–78, April 2009 [14].

**Table 1.** Comparison of typical biodegradable polymer physical properties with LDPE, PS and PET. [2,17–26].

	Tg (°C)	Tm (°C)	MFR (g/10 min)	Tensile Strength (MPa)	Tensile Modulus (MPa)	Elongation Break (%)	Flexural Strength (MPa)	Flexural Modulus (GPa)	Izod Impact Strength (J/cm)
LDPE	−100	98 to 115	0.25 to 2300	8 to 20	300 to 500	100 to 1000	9.03 to 932	0.0248 to 1.45	0.343 to 5340
PCL	−60	59 to 64	-	4 to 28	390 to 470	700 to 1000	-	-	-
Starch	-	110 to 115	1.98	35 to 80	600 to 850	580 to 820	-	-	-
PBAT	−30	110 to 115	-	34 to 40	-	500 to 800	-	-	-
PTMAT	−30	108 to 110	-	22	100	700	-	-	-
PS	70 to 115	100	1.2 to 100	34 to 50	2300 to 3300	1.2 to 2.5	28 to 106	0.894 to 3.60	0.107 to 2.14
Cellulose	-	-	-	55 to 120	3000 to 5000	18 to 55	-	-	-
PLA	40 to 70	130 to 180	0.20 to 92.8	48 to 53	3500	30 to 240	0.170 to 159	0.167 to 13.8	0.105 to 8.54
PHB	0	140 to 180	17 to 20	25 to 40	3500	5 to 8	18	16	-
PHA	−30 to 10	70 to 170	-	18 to 24	700 to 1800	3 to 25	40	2	0.260
PHB—PHV	0 to 30	100 to 190	-	25 to 30	600 to 1000	7 to 15	-	-	1
PVA	58 to 85	180 to 230	17 to 21	28 to 46	380 to 530	-	-	-	-
Cellulose Acetate	-	115	-	10	460	13 to 15	27 to 72	0.08 to 2.62	0.480 to 4.50
PET	73 to 80	245 to 265	3.5 to 65	48 to 72	200 to 4100	30 to 300	55.3 to 135	0.138 to 3.50	0.139 to 100
PGA	35 to 40	225 to 230	-	890	7000 to 8400	30	-	-	-
PEA	−20	125 to 190	-	25	180 to 220	400	-	-	-

Another characteristic important to consider is the rate of crystallinity of the polymer. It influences a vast quantity of essential properties such as hardness, modulus, tensile

strength, stiffness, crease point and the melting point, making it important to pay special attention to this property [2].

The values in Table 1 are generic, since it is possible to obtain materials with different properties with different combinations of monomers or through chemical derivatization or introduction of additives such as plasticizers, stabilizers, fillers, processing aid and colourants.

Table 2 summarizes some characteristics that may be important for specific applications listed as guidelines. Some typical applications and the degradability of the discussed bioplastics are also included in Table 2 [27].

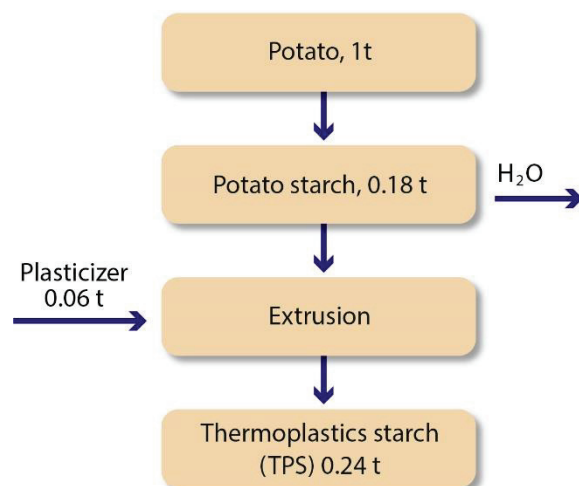
**Table 2.** Major bioplastic classes, some properties and average degradation time in different environments [27–29]. (✓/✗: present/absent).

Bioplastic	Manufacturer	Properties	Applications	Degradable	Degradation Time (Days)
Starch—TPS	Novamont (Italy) Livan (Canada) Ever Corn (Japan) Plaststar (USA)	✓ Thermoplastic	Packaging; Food trays; Trash bags; Flowerpots	✓ In Water	72–236
		✓ Gas Barrier			
		✗ UV-Resistant		✓ In Soil	
		✓ Biocompatible			
		✗ Thermostable		✓ Industrial Compost	
		✓ Elastic			
		✓ Rigid			
✗ Hydrophobic					
Polyhydroxyalkanoates—PHA, PHB and PHV	Minerv (Italy) Biogreen (Japan) Biocycle (Brazil) Green Bio (China)	✓ Thermoplastic	Packaging; Adhesives; Fibers; Medical implants	✓ In Water	15–280
		✓ Gas Barrier			
		✓ UV-Resistant		✓ In Soil	
		✓ Biocompatible			
		✗ Thermostable		✓ Industrial Compost	
		✓ Elastic			
		✓ Rigid			
✓ Hydrophobic					
Polylactide—PLA	Nature Works (USA) Biofoam (The Netherlands) Ingeo (USA) Hisun (China) Biofront (Japan)	✓ Thermoplastic	Packaging; Textiles; Medical implants; Films	✗ In Water	28–98
		✓ Gas Barrier			
		✓ UV-Resistant		✓ In Soil	
		✓ Biocompatible			
		✗ Thermostable		✓ Industrial Compost	
		✓ Elastic			
		✓ Rigid			
✓ Hydrophobic					
Cellulose-Based Polymers	Natural flex (UK) Tenite (USA) Biograde (Germany) Sateri (China)	✗ Thermoplastic	Wound dress; Textiles; Air filters; Coatings	✓ In Water	14–154
		✗ Gas Barrier			
		✗ UV-Resistant		✓ In Soil	
		✓ Biocompatible			
		✓ Thermostable		✓ Industrial Compost	
		✗ Elastic			
		✓ Rigid			
✗ Hydrophobic					
Protein-Based Polymers		✓ Thermoplastic	Cast film; Injection moulding; Extrusion sheets; Compression moulding	✓ In Water	36–50
		✗ Gas Barrier			
		✓ UV-Resistant		✓ In Soil	
		✓ Biocompatible			
		✓ Thermostable		✓ Industrial Compost	
		✓ Elastic			
		✓ Rigid			
✓ Hydrophobic					



### 2.1. Starch

The synthesis of this bioplastic began in the 1970s and is now produced worldwide by companies such as Futerro, Novamont, Biome and Biotec [26,27]. Starch is one of the common names for carbohydrates, along with sugars, saccharides and polysaccharides. They are formed by photosynthesis when  $\text{CO}_2$  reacts with water. The chemical symbol is generically represented as  $\text{C}_x(\text{H}_2\text{O})_y$ , where  $x$  and  $y$  are numbers between 3 and 12. Starch is a type of polysaccharide obtained from floral sources [28]. The production of polymeric film from starch requires a significant quantity of water or plasticizers (glycerol, sorbitol). They are used widely worldwide as a substitute for PS in several thermal and mechanical applications. There are a lot of different possible sources of starch, but the main ones used are corn, wheat, cassava and potatoes, with 82%, 8%, 5% and 5% starch, respectively. The raw material is prevalent, and the production process allows obtaining large quantities of a biodegradable thermoplastic-like material (TPS) with a fair ease of management. Although starch is not a thermoplastic, starch-based bioplastics melt at high temperatures (91–180 °C) and tend to be fluid under shearing. The use of plasticizers helps to achieve this behaviour, making it possible to process the material with injection moulding, extrusion and blow moulding. Plasticizers work embedded between polymer chains, which soften the material and lowers the glass transition temperature by spacing the polymer chains apart. There are several processes involved in the conversion of starch into thermoplastic, such as gelatinization, melting, water diffusion, granule expansion, decomposition and crystallization. The thermoplastic material forms in the presence of heat and shearing forces. The energy absorbed melts the original structure and creates new bonds between the starch and the plasticizer. When the mixture cools down to room temperature and the granules reswell, a new granule structure is formed, and the thermoplastic material is produced. The final material has both amorphous and crystalline regions. Cereplast is a producer of TPS that collects starch from tapioca, corn, wheat and potatoes. Out of 1 t of potatoes, they are capable of gathering 0.18 t of starch, which produces 0.24 t of TPS when adding 0.06 t of plasticizer, a process summarized in Figure 4 [12,30–35].



**Figure 4.** Production flow chart of thermoplastic starch (TPS). Adapted from “Bioplastics: Development, Possibilities and Difficulties”, Environmental Research, Engineering and Management, vol. 68, no. 2, July 2014 [36].

Since water has a plasticizer effect on starch, one of the problems of the use of starch is the effect water and humidity have on it, creating, for example, variations in its mechanical properties and low resistance to impact. Some derivatives of starch have high permeability to moisture and degrade rapidly in specific applications; solutions used to avoid these problems might make the final material expensive. Throughout time, the material’s properties change even when temperature and moisture are controlled, lowering the elongation break and increasing the rigidity [30].

Examples of products made of starch bioplastic are grocery bags and trays (rigid or foamed) used to pack fruits and vegetables. One important material widely used is paper foam, used to pack items where product protection is essential, for example, in egg boxes and the packaging of electronic devices [37,38].

## 2.2. Cellulose

This polymer is a biodegradable polysaccharide made from wood pulp or cotton linters. Cellophane film starts by dissolving the raw material in a mixture of sodium hydroxide and carbon disulphide and recast the obtained product into an acid solution (sulfuric acid) [12,32].

Pure cellulose bioplastic is very hard to be produced; it is not possible to make it in an industrial environment with standard processes such as thermoforming or dissolution due to its strong and highly structured intermolecular hydrogen bonding network. For this reason, it is usually produced industrially as cellulose derivatives, such as cellulose esters or ethers, which requires extra time and costly chemical purification steps [39]. Some of these derivatives are cellulose nanocrystals (CNC), nano-fibre cellulose (NFC), cellulose acetate butyrate, cellulose acetate and bio-PE, and they are produced by the esterification or etherification of hydroxyl groups. A lot of derivatives need additives to produce thermoplastics, and some of them are water-soluble [12,40].

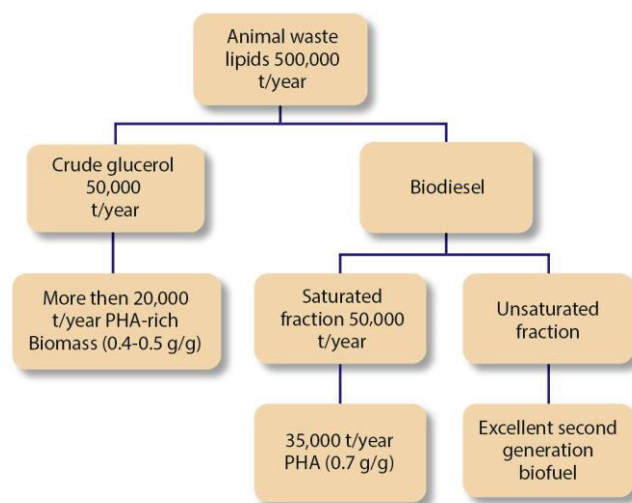
Cellophane is transparent, and it can be pigmented. It is common to use it as candy wrappings, laminates, flower wrapping and pack products ranging from cheese to coffee and chocolate [33].

## 2.3. Polyhydroxyalkanoates (PHA)

PHA is a family of biodegradable thermoplastic polymers where more than 160 different monomeric units were identified. The most common one is polyhydroxybutyrate (PHB). PHA is a material regularly used to replace conventional polymers due to their similar chemical and physical properties. This biopolymer is produced by the fermentation process in microbial cells (such as *Cupriavidus necator*, *Bacillus* sp., *Alcaligenes* sp., *Pseudomonas* spp., *Aeromonas hydrophila*, *Rhodospseudomonas palustris*, *Escherichia coli*, *Burkholderia sacchari* and *Halomonas boliviensis*), and the polymeric material is then recovered using solvents (chloroform, methylene chloride or propylene chloride) [8,33]. Corn, whey, wheat and rice bran, starch and starchy wastewaters, effluents from olive and palm oil mills, activated sludge and swine waste are some examples of material sources for the fermentation process. Although the conditions of the fermentation process depend on the demands of the microbes, temperatures of 30 °C to 37 °C, along with low stirrer speeds (resulting in low dissolved oxygen tension), are the conditions used.

Several national and international programmes foster the development and advancement for a green transition. That can be expressed in several projects' results. In 2010, the "Animpol" project was developed by the European Commission with the goal of developing an efficient process that could convert waste streams from slaughterhouses into improved biodiesel and biodegradable high-value polymeric materials, such as PHA. The Consortium was able to produce 35,000 t per year of PHA from 500,000 yearly t of animal waste on an industrial level, as represented in Figure 5. The introduction of this process in the bioplastic production industry would mean that some of the solvents used in the production of bioplastics would be eliminated, and the slaughterhouse waste could be useful to produce added-value products, while nowadays, this waste material is simply burned [8,32,33,38].

PHB is produced by bacteria, algae and genetically modified plants through enzymatic processes. The process starts with the condensation of two molecules of acetyl-CoA into acetoacetyl-CoA, which is then reduced by acetoacetyl-CoA reductase to produce  $\beta$ -hydroxybutyryl-CoA. PHB is obtained by the polymerization of  $\beta$ -hydroxybutyryl-CoA. To harvest the PHB, it is necessary to destroy the cell, since it is present as cysts within the cytoplasm of the cell [33,39,40].



**Figure 5.** Production flow chart of PHA from waste streams from slaughterhouses. Adapted from “Bioplastics: Development, Possibilities and Difficulties”, Environmental Research, Engineering and Management, vol. 68, no. 2, July 2014 [32].

Due to its characteristics, PHA is extensively used in medical fields, especially in tissue engineering. For example, PHA is used in long-term dosage of drugs, medicines, hormones, insecticides and herbicides, as osteosynthetic materials in the stimulation of bone growth owing to their piezoelectric properties in bone plates, surgical sutures and blood vessel replacements. Other products made of this biopolymer are composting bags, food packaging, diapers and fishing nets [33]. Tianan Biopolymer, BASF, Tephra and Biocycle are some examples of companies that produce this type of bioplastics [41].

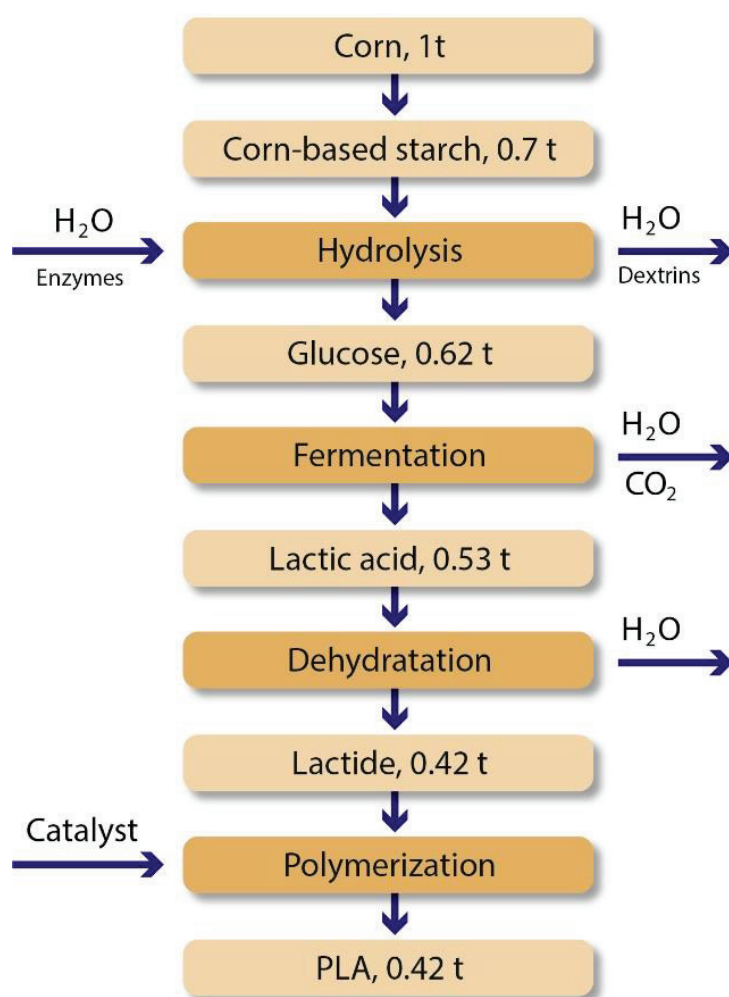
#### 2.4. Polylactide (PLA)

PLA was initially used in combination with polyglycolic acid (PGA) under the name Vicryl during the 1970s, but its discovery goes back to 1932 when it was discovered by Carother. At the time, he produced a low molecular weight polylactide by heating lactic acid under vacuum while removing the condensed water. Nowadays, most of the PLA produced is used in packaging (about 70%), although its application in other fields has been increasing, especially in fibres and fabrics. The leading producer of PLA in the world is NatureWorks® (USA), but other companies stand out, such as Ingeo, Toyobo, Dai Nippon Printing Co., Mitsui Chemicals, Shimadzu, NEC, Toyota, Biofront (Japan), PURAC Biomaterials, Hycail, Biofoam (The Netherlands), Galactic (Belgium), Cereplast, FkuR, Biomer, Stanelco, Inventa-Fischer (Germany) and Snamprogetti, Hisun (China) [2,30,42].

Similar to PHA, PLA is one of the bioplastics considered to have significant potential to be widely used as a replacement to several fossil fuel-based polymers, such as LDPE and high-density polyethylene (HDPE), PS and PET [8].

PLA involves different types of sciences to be produced: agriculture, for the growth of the crops; biological, during the fermentation process; and chemical, for polymerization. The PLA monomer is called lactic acid (2-hydroxy propionic acid), and it has two configurations, L(+) and D(−) stereoisomers, produced by the bacterial fermentation of carbohydrates (homofermentative and heterofermentative). Lactic acid is produced using one of two processes, fermentation or chemical synthesis. The first one is usually used industrially, since it does not depend on other processes’ by-products, it produces L-lactic acid stereoisomer easier and the manufacturing costs are not as high as the synthesis process. The homofermentative method is also preferable, since it creates less by-products and lactic acid with greater yields, and pure L-lactic acid is used to produce PLA. The production procedure uses *Lactobacillus* genera such as *L. delbrueckii*, *L. amylophilus*, *L. bulgaricus* and *L. leichmanii* under specific conditions (a pH range of 5.4 to 6.4, a temperature range of 38 to 42 °C and a low oxygen concentration).

After the production of lactic acid, it is then polymerized into PLA. There are three possible processes to do the polymerization: direct condensation polymerization, direct polycondensation in an azeotropic solution and polymerization through lactide formation. High molecular weight PLA with good mechanical properties is not easily achieved using the direct condensation polymerization method. It involves the esterification of lactic acid with some solvents under progressive vacuum and high temperatures, where water is removed. The second process is a more feasible way to produce PLA with high molecular weight. The azeotropic solution reduces the distillation pressure, and using molecular sieves helps the separation of the PLA and the solvent. Lastly, polymerization through lactide formation is also used in the industrial environment to produce high-weight PLA. Lactide is a cyclic dimer formed by removing water under mild conditions and without solvent. As shown in Figure 6, it is possible to produce 0.42 tons of PLA from 1 ton of corn using processes such as hydrolysis, fermentation, dehydration and polymerization [32,33,43–45].



**Figure 6.** Production flow chart of PLA by synthesizing corn-based starch. Adapted from “Bioplastics: Development, Possibilities and Difficulties”, Environmental Research, Engineering and Management, vol. 68, no. 2, July 2014 [32].

PLA is widely used in the food packaging industry for short and long shelf-life products. This bioplastic and its blends are also used to make implants, plates, nails and screws for medical surgery. The application fields are expanding to textile, cosmetic, automobile industries and the household [33].

### 2.5. Polycaprolactone (PCL)

PCL is a synthetic polyester that is produced from crude oil. Since it is a biodegradable polymer, it is considered a biopolymer.

PCL is regularly used in tissue engineering and biomedical applications due to its blend compatibility, absorbability, good solubility and low melting point. This is a hydrophobic and semi-crystalline material; its crystallinity depends on its molecular weight (high molecular weight means low crystallinity), which is possible to control using low molecular weight alcohols. This biopolymer is characterized by its ease to manufacture and shaping, tailorable degradation kinetics and mechanical properties, making PCL distinguish itself from other bioplastics.

Initially, when it was studied in the 1930s, this polymer was relatively popular, but soon, its use decreased significantly for a long time due to its weak mechanical properties in comparison to other resorbable polymers such as polylactides and polyglycolide. Recently, this material has regained great interest because of its application in the field of tissue engineering widely developed in the 1990s. It not only possesses superior rheological and viscoelastic properties when compared to other polymers, but its ease of processing also stands out.

Although PCL is a bioplastic biodegraded by specific bacteria and fungi present in outdoor environments, this polymer is not degradable in animal or human bodies due to the lack of those organisms. This particularity makes PCL an excellent material to be used in medicine and tissue engineering fields of study; its degradability is relatively slow when compared to PLA, PGA and other resorbable polymers, making it an excellent material to be used “for long-term degradation applications delivery of encapsulated molecules extending over a period of more than 1 year”. The rate at which this drug release is achieved may be manipulated by combining PLC with cellulose propionate, cellulose acetate butyrate, PLA or polylactic acid-co-glycolic acid [46].

### 2.6. Protein-Based

Protein is a heteropolymer of amino acids with a fibrous and globular structure arranged by hydrogen, covalent and ionic bonds. Protein-based materials have great mechanical and barrier to gas and aroma properties than lipids and polysaccharides. By incorporating keratin, the material produced has thermal stability, mechanical properties and flame resistance. Due to their abundance, biodegradability, nutritional value and better film development capability, packaging is one of this material’s main applications [47]. Other applications include matrices for enzyme immobilization or controlled-release devices and in fields where water absorbency and retention are important, such as water-absorbent materials in healthcare, agriculture and horticulture. With further technological development, packaging technology, natural fibre reinforcements, nanotechnology and innovative product design could be fields to be developed using this type of bioplastic.

To produce products with this material, there are two possible processes, the casting method (or physicochemical method) and the mechanical method (or thermoplastic processing). The first process divides itself into three different steps, starting with using chemical or physical rupturing agents to break the intermolecular bonds that stabilize polymers in their native forms; next, the mobile polymer chains are rearranged and oriented to the intended shape. Finally, the three-dimensional network is stabilized by allowing the formation of new intermolecular bonds and interactions. The second method involves mixing proteins and plasticizers to obtain a dough-like material [31,47]. Techniques that can be used to observe the molecular reorganization and orientation are based on time-resolved small-angle X-ray scattering (SAXS) that allows analysing of the anisotropy. Usually, these techniques are available in research facilities that allow in situ observation. It is possible to, through in situ experiments, observe the molecular rearrangement and reorganization that impose levels of preferential orientations [48]. The time-resolved SAXS allows monitoring the evolution (in time) of changes in the morphological organization.



### 2.7. Polyamide 11 (PA 11)

PA 11 or nylon 11 is a nonbiodegradable bioplastic produced from renewable material, such as castor oil. The polymer is obtained by the polymerization of 11-aminoundecanoic acid. Although it is nonbiodegradable, PA11 and its composites can be recycled. Due to its nonbiodegradability, the PA11 has greater longevity than most bioplastics. This characteristic, along with the high melting point (200 °C) and mechanical and chemical stability, makes it possible to apply it as reinforcement material in the manufacturing of natural gas piping, water tubing, electrical cables, clips and wires in aerospace and automobile industries, metal coatings, footwear, badminton racket strings and shuttlecocks. Other important characteristics are its good resistance to oil and water, high resistance to ionization radiation, strong resistance to different chemicals, fuels and salt solutions and its resistance to abrasion and cracking. It has low heat resistance and rigidity, low resistance to ultraviolet radiation and weak resistance to acetic acid and phenols, and its electrical properties are highly dependent on the moisture content. However, the market price is relatively higher than other polyamides. One of the main PA11 producers is Arkema [47,49,50].

### 2.8. Spidroin—Spider Silk

Spiders can, in a fraction of a second, under ambient conditions and from renewable resources, create a material which mechanical properties outperform any manufactured material: spider silk. It has the potential to be used in a wide variety of fields, for example, for making high-performance textiles and sports goods, durable components for robotics, ropes and reinforcements of composite materials and for applications in medicine (spider silk enhances wound healing and has successfully been used to bridge critical size nerve defects and as fascia replacements in animal models) [39,51,52]. However, it is currently not possible to farm spider silk efficiently on large scales because of spiders' cannibalistic nature, the difficulty of breeding, the low production rate in captivity and the collection of silk from spider webs is very time-consuming and not efficient enough for production. Genetic engineering is the most promising way to produce this material. The plan is to express the spider silk protein (spidroin) into different kinds of hosts, such as bacteria, yeast, plant and in the milk of transgenic mammals [40,51,52]. This technique was widely researched using *Escherichia coli*, a well-established host for the industrial-scale production of proteins. Yet, these materials produced do not have as good mechanical properties as spider silk, so new methods need to be developed. Although spider silk always looks the same to the naked eye, there are several different types of thread; the same spider can produce up to seven different types of silk, each one with different mechanical properties. The strength of these natural threads ranges from 0.02 to 1.7 GPa, and its extensibility varies between 10 and 500%. Additionally, using the same natural fibres, those spun technically show different properties than the natural fibres created by the spider, which shows that this is an important process and is done differently than the technology usually used. Despite a biomimetic spinning process to process the silk not existing, there are other alternatives to use this material since recombinant spider silks can self-assemble into non-natural shapes such as spheres, capsules, films, non-wovens or hydrogels. There are other concerns regarding solubility, storage and assembly of the underlying spider silk proteins [53].

## 3. Bioplastics Composites

The synthetic assembly of two or more materials, a matrix binder and selected reinforcing agents, is used for various applications. The goal is to overcome the weaknesses and increase versatility. The most common fibres exercised in recent times are glass fibres, carbon fibres, aramid fibres, natural fibres, nylon and polyester fibres. There is a clear advantage to using natural-based fibres; for example, they are biodegradable, renewable, available in bulk, cheaper and lighter [54–56].

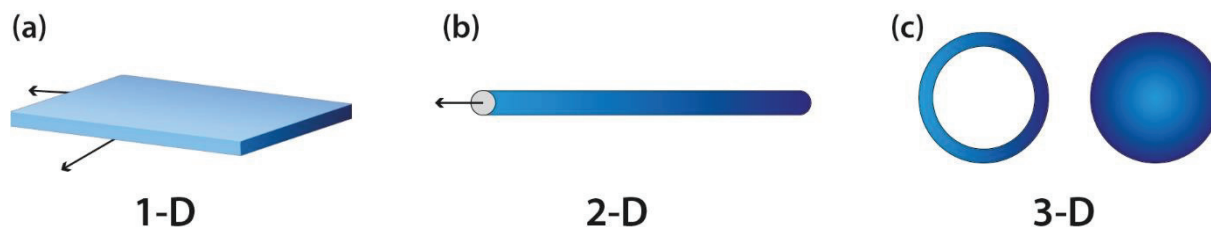
### 3.1. Coating

Coating bioplastics is an excellent technique to improve some of the properties of these materials; it is specially used to enhance the barrier properties. By applying a thin layer of other polymers on top of the bioplastic, the tensile strength and elasticity can be improved, as well as increasing oxygen and water vapour permeability and resistance. Some examples of usually used coatings are listed below:

- PLA barrier properties (oxygen and water vapour) can be improved by applying a PLA-Si/SiO<sub>x</sub>, AlO<sub>x</sub> (aluminium oxide), PCL-Si/SiO<sub>x</sub> or PEO-Si/SiO<sub>x</sub> (polyethylene oxide) coating.
- When coated with PLA, SPI (soy protein isolate) films tensile strength increases from 2.8 to 17.4 MPa, and the elongation went from 165.7% to 203.4%. However, the water vapor permeability decreases 20- to 60-fold, depending on the PLA concentration in the coating solution.
- Nitrocellulose or PVdC (polyvinylidene chloride) coating on cellophane is also used to improve oxygen and water vapour barrier properties.
- Coating acetylated cellulose film with PHB increases elastic modulus and tensile strength for films containing 10% or more PHB and a better strain at break for films containing 15% or more PHB while lowering the water vapour permeability values [8].

### 3.2. Nanocomposites

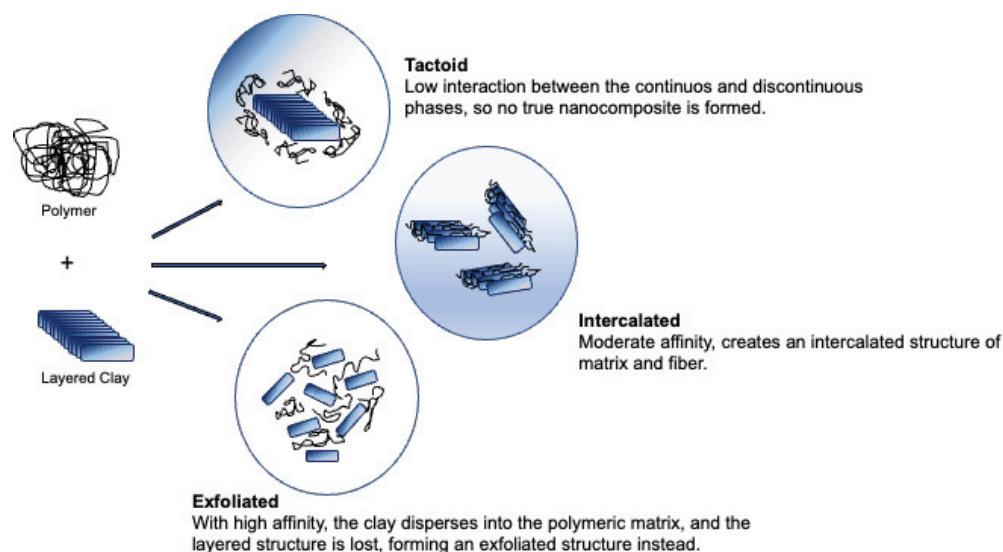
For a composite to be considered a nanocomposite, it must have at least one of its types of particles with dimensions in the nano range. The composite can be classified as polymer layered crystal nanocomposites (Figure 7a), nanotubes or whiskers (Figure 7b) and isodimensional nanoparticles (Figure 7c), according to the number of dimensions it has: three, two or one, respectively [2].



**Figure 7.** Nanoparticle geometries: (a) layered particles (1D), (b) acicular or fibrous ones (2D) and (c) isodimensional nanoparticles (3D). Adapted from “Block copolymer nanocomposites” [57].

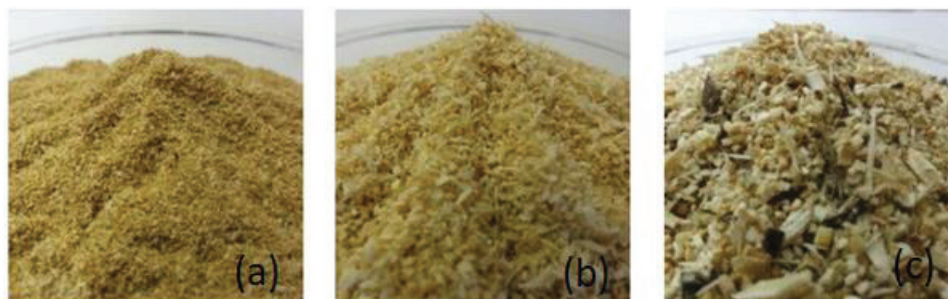
The use of these materials as reinforcement to other polymers depends on the capacity of the matrix (continuous phase) to interact with the fibre (discontinuous phase). There are several ways to mix the phases of the composite; one of them is situ polymerization, which involves the dissolution of the nanoparticles in the monomer solution before polymerization; the addition of the nanoparticles during the extrusion process, a process called melt intercalation; or solvent intercalation (use of a solvent to enhance the affinity between the nanoparticles and the matrix). These processes help change some of the composite properties according to the intention.

Nanoclays are one of the most used fibres as reinforcement of bioplastics. They are usually used as layered particles of 1  $\mu\text{m}$ . Different affinities between the matrix and the nanofibers create different interactions: tactoid, intercalated and exfoliated. The first case occurs when the interaction between the continuous and discontinuous phases is low; this happens because the clay interlayer does not expand within the matrix, so no true nanocomposite is formed. When the affinity is moderate, it is possible for a part of the polymer to penetrate the clay interlayer, since there was some level of expansion of the fibre; this creates an intercalated structure of matrix and fibre. The last situation entails a high affinity, the clay disperses into the polymeric matrix, and the layered structure is lost, forming an exfoliated structure instead [8] (Figure 8).



**Figure 8.** Structures of polymer nanoclay composite.

It is also possible to create composites using bigger particles as reinforcement. The project EcoPlast works with melt intercalation using natural fibres (sawdust, cellulose and cork) and biodegradable polymers as matrices (such as PLA, PBS (polybutylene succinate), starch, cellulose and PCL) in several different combinations. The materials used are represented in Figure 9. They are within different ranges of dimensions and densities, where (a) (less than 0.7 mm) and (b) (between 0.7 and 1.4 mm) are quite homogeneous. At the same time, (c) (between 1.4 and 2.8 mm) has very different particles in shape, size and colouring.



**Figure 9.** Different batches of sawdust used (a) (less than 0.7 mm), (b) (between 0.7 and 1.4 mm) and (c) (between 1.4 and 2.8 mm). From the project EcoPlast.

The dispersion of the fibres is affected by the hydrophobic/hydrophilic character of the polymer and the clay; this can be adapted with chemical modifications such as cationic exchange, ionomers, block copolymers adsorption and organosilane grafting. Since a high surface-to-volume ratio leads to better polymer properties, the exfoliated structure is preferred.

Some of the properties affected are the elongation at break (especially when using PLA film as matrix); barrier properties, explained by the confinement effect (the molecules of the polymeric matrix penetrate the dispersed nanoparticles, creating a denser material and creating a more tortuous path for the water and gas molecules to travel through) and thermal stability [8].

### 3.3. Cellulose

Adding cellulose to the bioplastic is another way to influence some properties of the final material. It is possible to have good adhesion between the fibre and the matrix due to the chemical similarity between starch and natural fibres. The main effect this addition has

on the composite is the reduction of water vapour permeability due to the fibres' highly crystalline and hydrophobic character, also affecting the Young's modulus, tensile strength and the elongation break [8].

#### 4. Processing

To achieve the maximum possible benefits of bioplastics, the processing of these materials is well established for each one of them, differing between them according to the characteristics of the specific bioplastic [2].

When processing bioplastics, the technologies used are the same as conventional polymers; it is only necessary to adapt the parameters used for the specific material intended to use [58]. Depending on the material, some processes might not be efficient, sustainable or economically reasonable. That is why it is essential to further research the processability of biopolymers to make their range of applications wider [59]. Table 3 summarizes some of the most common processes where bioplastics might be modified.

**Table 3.** Processing possibilities of typical commercial biopolymers. Adapted from "Poly-Lactic Acid: Production, applications, nanocomposites, and release studies", *Comprehensive Reviews in Food Science and Food Safety*, vol. 9, no. 5, pp. 552–571, September 2010 [2].

	Injection Moulding	Extrusion	Extrusion Blow Moulding	Cast Film Extrusion	Blow Moulding	Fibre Spinning	Thermo-Forming
Starch	x	x	x	x			
Cellulose	x	x			x		
PHB	x	x	x	x	x		x
PHB-PHV	x	x	x	x	x	x	x
PLA	x	x		x	x	x	x
PBS	x	x					
PCL	x	x	x		x	x	x
PBST	x	x		x			x
PBAT		x	x	x			
PTMAT		x	x	x		x	
PVA	x		x	x		x	x
PP, PE + additives	x	x		x	x	x	x
Starch + PVA	x	x		x	x	x	
Starch + cellulose acetate	x	x	x		x		x

##### 4.1. Injection Moulding and Extrusion

The possibility of processing bioplastics via injection moulding or extrusion is not very different compared to processing conventional polymers. Each type of bioplastic has its own chemical structure, so each material will have different parameters, the same as happens with conventional plastics. Only a few conditions require some attention; for example, some bioplastics are sensitive to moisture or heat exposure; therefore, it is essential to control the drying process of the bioplastics and the long-time cycles in the case of injection moulding. Thus, it is important to consider these characteristics when choosing materials, equipment, and resources [60].

##### 4.2. Digital Manufacturing

Several research studies have been developed in the past years with the goal of evaluating the possibility of integrating new bioplastics into production processes usually used to transform conventional polymers. One in specific was conducted by Sneha Gokhale [61]. The objectives were to "Understanding sustainable 3DP (3D printing) in the context of bioplastic filaments; Testing commercial bioplastic filaments for sustainability and material properties; Guiding users in the industry towards green 3DP material and process choices".

To achieve this, several polymeric materials were tested in three different phases, evaluating their energy consumption when processed by FDM (Fused Deposition Modelling); comparing their printability and dimensional accuracy and rating their mechanical properties (tensile modulus, ultimate tensile strength and elongation). The materials chosen to test were three Ultimaker standard materials (from the FDM machine used): UM-PLA, UM-TPLA (talc-injected PLA) and UM-CPE (chlorinated polyethylene), and five materials available on the online market: ALGA (PLA + Algae), OMNI (PLA based blend), PLAPHA (PLA + PHA from 3DPrintLife), PLAPHA (PLA + PHA from Colorfabb) and BioPETG (bio-polyethylene terephthalate glycol). The obtained results are summarized in Figure 10 (about mechanical properties), Figure 11 (print quality) and Figure 12 (regarding the energy consumption and some material characteristics) [61].

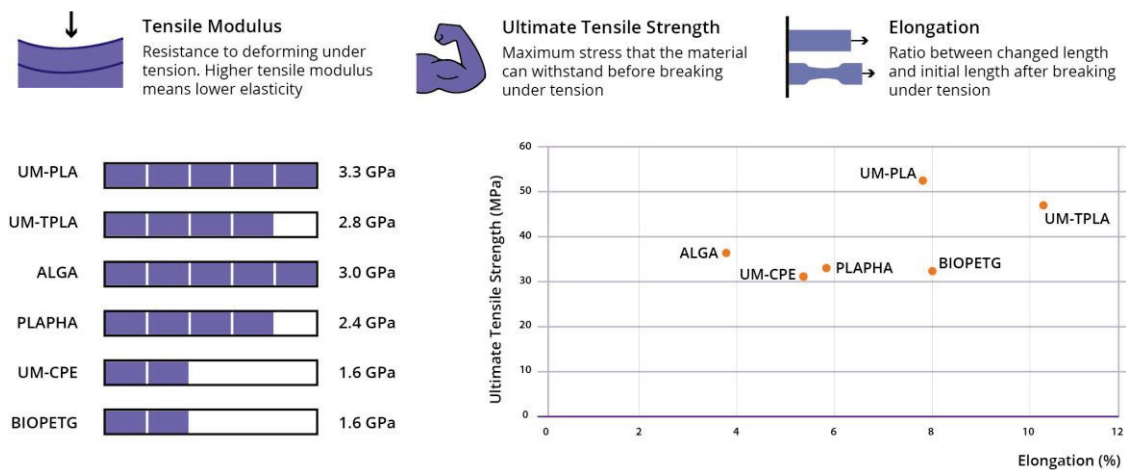


Figure 10. Material Guide for Green 3D printing: mechanical properties. Adapted from “3D Printing with Bioplastics”, 2020 [61]. Mechanical properties for materials PLAYPHAB and QMNI are estimated to be similar to PLAPHA and UM-TPLA respectively.

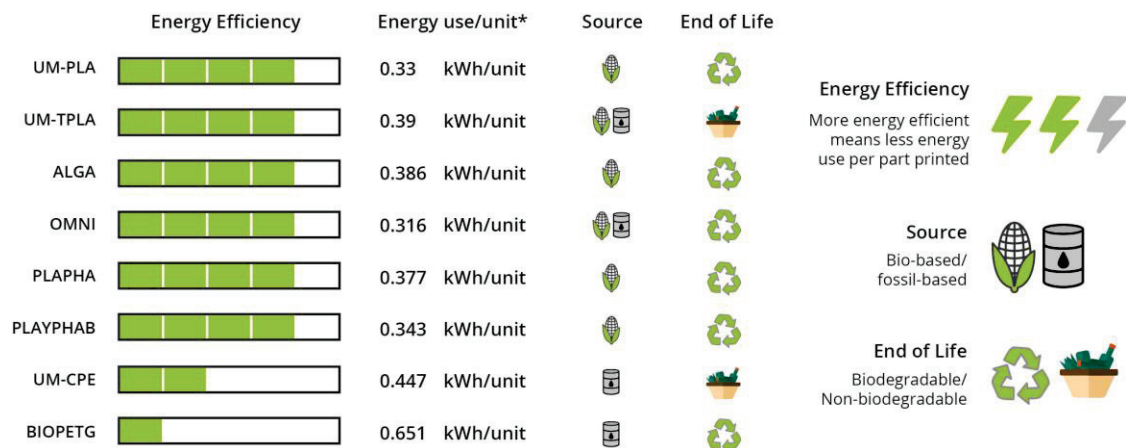
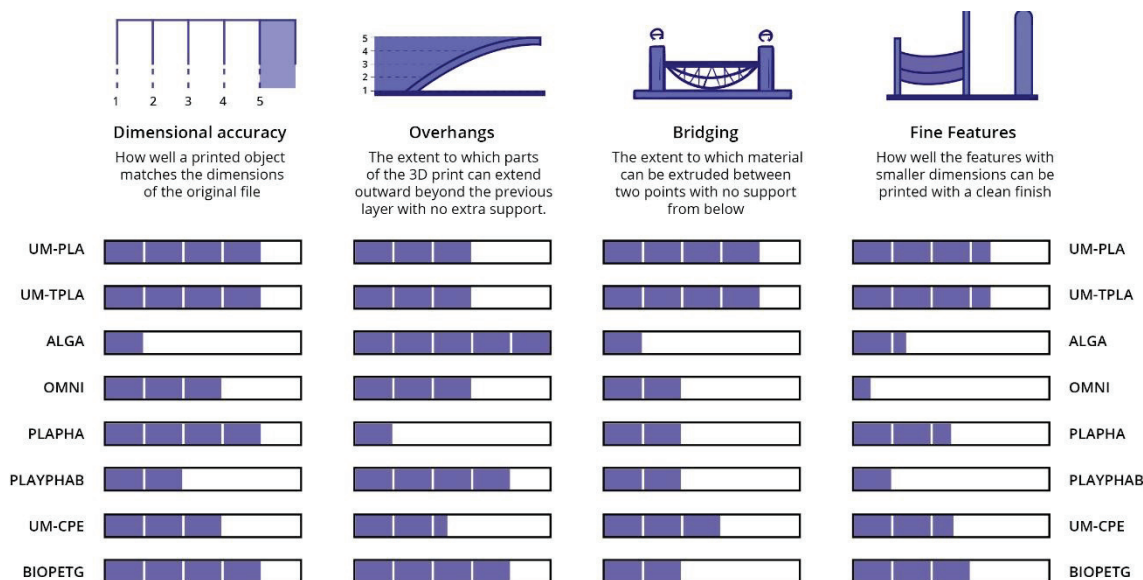


Figure 11. Material Guide for Green 3D printing: energy consumption and some material characteristics. Adapted from “3D Printing with Bioplastics”, 2020 [61]. \* One unit refers to this reference part used for universal comparisons.

PLA-based materials bought scored similarly to the standard Ultimaker PLA for print quality and tensile properties. Although the print quality is likely to improve when building simpler parts. While BIOPETG, the material used to compare with UM-CPE behaved slightly better. During the tests, it was verified that the heating of the build plate of the printer was the parameter that consumed the most energy. With this information, it was possible to say that materials that require lower building plate temperatures consume less energy, making them more eco-friendly. It was possible to conclude that new biomaterials



have characteristics similar to conventional materials, making it possible to substitute these with greener materials [62]. This technique is widely used to produce a variety of biomedical devices, such as orthopaedic implants, thanks to the possibility to build manufacturing customized, low-volume and complex implants. Some filaments are already made from biological sources and may utilize waste material from producing beer or coffee grounds as filling. This makes the process eco-friendlier [63].



**Figure 12.** Material Guide for Green 3D printing: print quality. Adapted from “3D Printing with Bioplastics”, 2020 [61].

### 4.3. Electrospinning

Electrospinning is a relatively inexpensive process used since the 1930s to produce fibres on the micro and nano scales using a high voltage (20 kV) as an electrostatic field on a polymeric solution. The polymeric solution becomes electrified and stretches, becoming a thin fibre. Although it has been under development for a long time, it is still in its relative developmental infancy in industrial application.

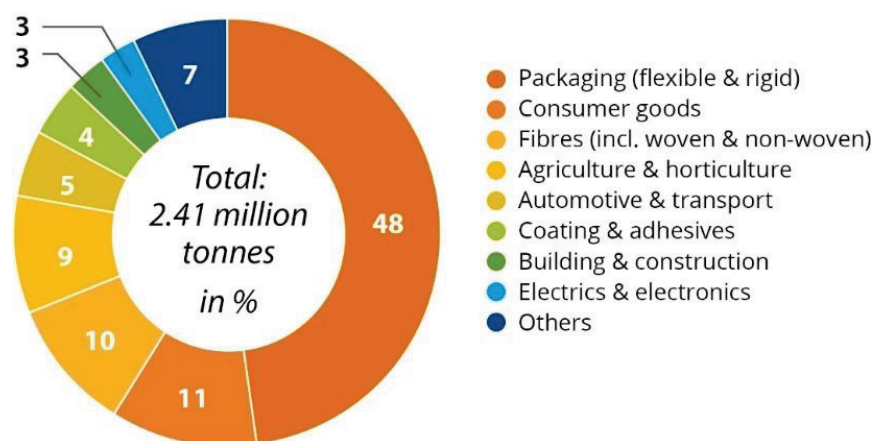
An electrospun mat is usually made with a carrying polymer, ensuring that the mat is stable and able to incorporate other components. Bioplastics are widely used in biomedical applications since some materials are required to be biodegradable or biocompatible; PLA is one of the most commonly used biopolymers [46,64].

## 5. Applications

The applications of bioplastics are several (Figure 13), for example, food packaging (with 48% or 1.15 Mt of the total bioplastics market in 2021), consumer goods (11%), fibres (10%), agriculture (9%), automotive (5%), coating and adhesives (4%), construction (3%), electronics (3%) and other sectors (7%). It is expected that bioplastics will grow and the fields of application expand [6].

### 5.1. Medical Industry

Bioplastics are an excellent replacement for conventional polymer, as they may cause less allergies than the chemical-based products usually used. They are a sustainable material for the large amounts of one-time-use products used. Since some bioplastics may be breathable and allow water vapour to permeate and be waterproof at the same time; they can be used as sanitary products such as diaper foils, bed underlay and disposable gloves [33].



**Figure 13.** Global production capacities of bioplastics in 2021 (by market segment). Adapted from European Bioplastics “Global production capacities of bioplastics in 2021 (by market segment)”. [https://www.european-bioplastics.org/wp-content/uploads/2021/11/Global\\_Prod\\_Market\\_Segment\\_circle\\_2021.jpg](https://www.european-bioplastics.org/wp-content/uploads/2021/11/Global_Prod_Market_Segment_circle_2021.jpg) (accessed on 29 December 2022) [65].

### 5.2. Food Packaging Industry

The use of bioplastics in the food packaging industry has been increasing rapidly. The materials used in these types of applications require some specific characteristics to achieve the product’s intended shelf-life time and respect the food safety regulations. The mainly used bioplastics are PLA, starch and cellulose-based [33].

### 5.3. Agriculture

Some crops require using blankets of biodegradable plastic on part of their fields to increase their product yield. Usually, petroleum-based polymers are used, but bioplastics can achieve the same objective and do not leave residues, unlike conventional polymers. This makes it possible to reduce labour and disposal costs [33].

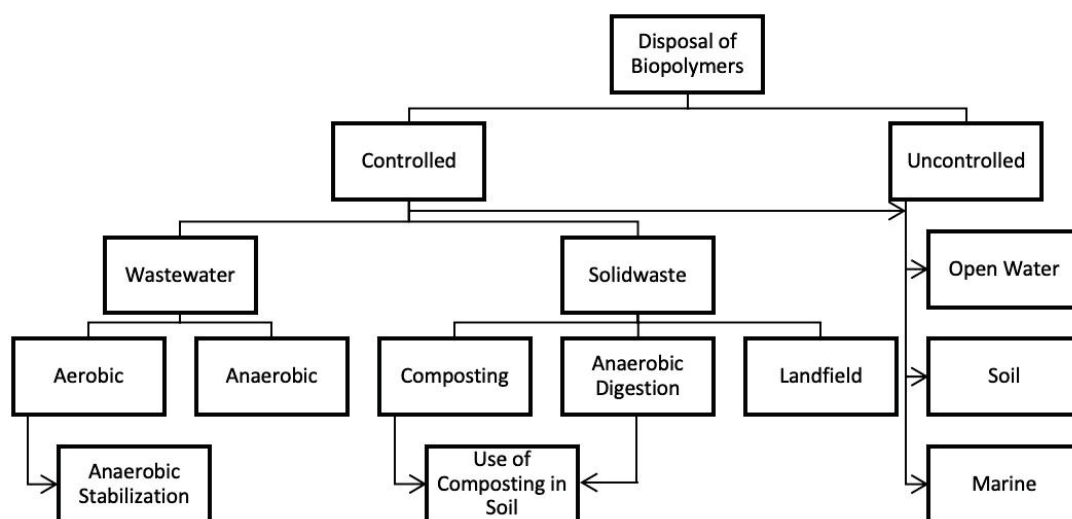
## 6. Bioplastic Waste Management

The waste management process of bioplastics is not as simple as it may seem. Although some of the process’s parameters are similar to the ones used for conventional plastics, it is not possible to mix these two types of materials without contaminating either the material itself or the environment. Another big misconception is the idea that there is no harm in dumping bioplastics anywhere with degradation assured. This only applies to some biopolymers, such as those made from seaweed.

The proper way to treat bioplastics is to recycle them mechanically, chemically, or organically, depending on the material’s capacity to compost or biodegrade (Figure 14). If a material is compostable, it is possible to obtain enriched compost (a valuable material) under industrial composting conditions. If the material is not compostable, the ideal process to use is chemical or mechanical recycling [31,66,67].

### 6.1. Mechanical and Chemical Recycling

Physical or mechanical recycling is already an established technology. The main problem with the mechanical recycling of bioplastics is that it is not possible to obtain a good quality material if more than one type of material is mixed; for example, PLA is a material widely used in packaging, and it is possible to recycle it mechanically; however it is difficult to distinguish it from materials such as PET by mere appearance, and this means that it would be necessary to add additional labelling to enable a correct separation by the consumers, but before that, it is needed to create a separate PLA recycling stream.



**Figure 14.** Waste management process of biopolymers. Adapted from “Bioplastics: A boon or bane?” *Renewable and Sustainable Energy Reviews*, vol. 147. Elsevier Ltd., 1 September 2021 [31].

In chemical recycling, unlike the mechanical process, the aim is to reuse carbon and biogenic substances obtained from waste material to synthesize new plastic materials through treatments that can involve hydrolysis/solvolytic, hydrothermal depolymerization and enzymatic depolymerization. Some of the advantages of chemical recycling are related to the simplicity of the overall process, and it does not require sorting or thermomechanical degradation, and it is not a process sensitive to material impurities [31,67].

### 6.2. Composting

Some materials are specifically designed to be compostable or organically recyclable; the final product is an enhancer to the soil, providing nitrogen, potassium, phosphorus and organic matter to the soil. This is an aerobic process divided into three stages, mesophilic, thermophilic and maturation. The application of these materials in single-use objects, such as bags, food packaging and cutlery strengthens their industrial utilization. Mechanical processing is necessary to separate missorted materials, reduce particle sizes for better bioavailability and mix different organic substrates for optimal dry matter content and C/N-ratio. It is possible to obtain high-value products that can be used as a soil amendment (due to the high capacity to hold water because of its organic matter content), biogas, hydrogen, ethanol and biodiesel.

The composting process at home is very difficult to control, which may result in the formation of methane gas. This process is more variable and less optimized than industrial composting, and the temperature achieved is rarely more than a few degrees Celsius above the ambient temperature [66,67].

### 6.3. Anaerobic Digestion

Anaerobic digestion aims to degrade organic wastes to biogas and digestate through four successive phases: hydrolysis, acidogenesis, acetogenesis and methanogenesis. The process can be operated at psychrophilic (18–20 °C), mesophilic (35–40 °C) and thermophilic (50–60 °C) temperature regimes, although the last two conditions are more efficient for the degradation of the bioplastics [67].

### 6.4. Waste-to-Energy (WTE)

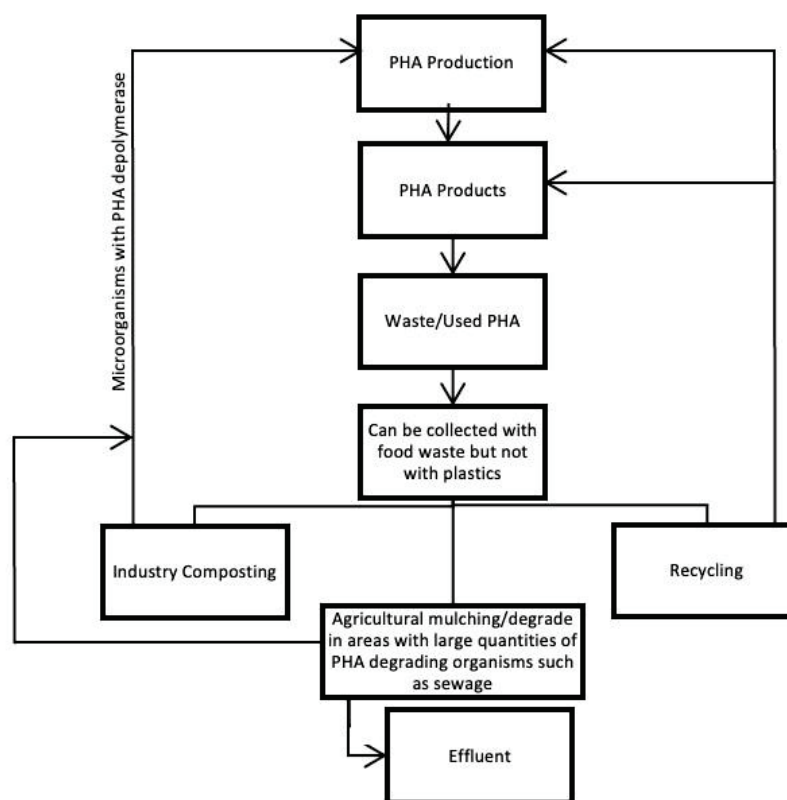
The waste-to-energy process, also known as incineration, is highly influenced by the capacity of the polymer to degrade in terms of its sustainability, and 56% of the energy comes from the incineration of biogenic organic MSW (municipal solid waste), which means that at least half of the process products does not contribute to an increase of CO<sub>2</sub> in the biosphere;

in other words, “incineration of bio-based waste emits CO<sub>2</sub> which was recently captured and will be captured again when new bio-based products are produced, whereas incineration of fossil plastics emits CO<sub>2</sub> that had been sequestered for millions of years” [66].

## 6.5. Materials

### 6.5.1. Disposal of PHA

The types of microorganisms capable of degrading PHA are numerous, which makes this biopolymer easily compostable under industrial and nonindustrial conditions. Home composting is possible in this case, since the degradation of the polymer may start at 30 °C. PHA is known to improve the soil in which it decomposes, since it increases the diversity of microbes present in the soil; in turn, this also increases the composting efficiency, as well as the variety of materials able to be degraded. This means that the separation process of these materials does not need to be so stringent, saving time and money. The waste management process of this material is summarized in Figure 15. Industrial decomposition of PHA takes  $124 \pm 83$  days; under anaerobic digestion, it takes about  $31 \pm 20$  days, while improperly abandoning this type of material on the soil takes 1–2 years.



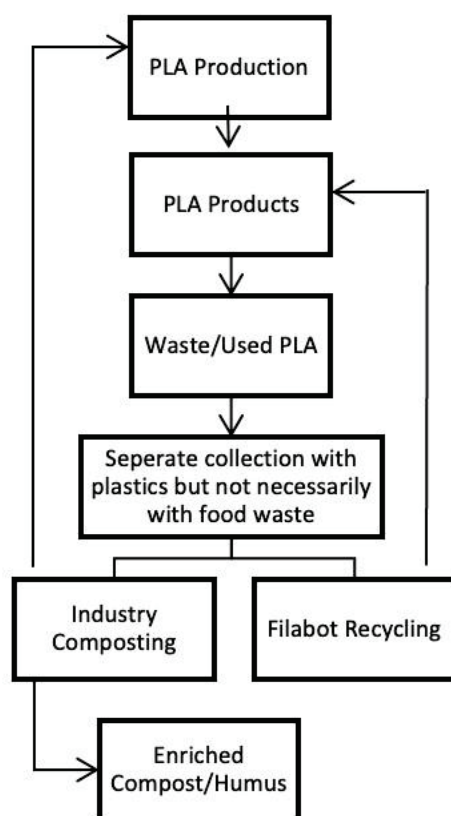
**Figure 15.** Waste management process of PHA. Adapted from “Bioplastics: A boon or bane?”, *Renewable and Sustainable Energy Reviews*, vol. 147. Elsevier Ltd., 1 September 2021 [31].

PHA is also degradable in aerobic lagoon water treatment systems, which house a wide variety of microorganisms. This process is even more efficient than the one occurring on the soil. It is also possible to degrade these materials in landfills, although a lot slower and not ideal [31,67].

Although it is possible, it is not feasible to recycle PHA since its properties at high temperatures are very unstable and, if not isolated from other materials, it might contaminate the final polymer. Chemical recycling is still a method under study; some materials such as herbicides and plasticizers, among others, can be made from products of the chemical recycling of PHA [31].

### 6.5.2. Disposal of PLA

Initially, the objective of using PLA on single-use plastic items was to transit from petrochemical plastics to biodegradable bioplastics. However, currently, the disposal process of these materials is not any different from the conventional plastics, which is not the most effective method to use. Some manufacturers, such as NatureWorks, have clearly stated that the materials they produce PLA are to be industrially composted and have even explained how the process works. PLA is commonly used as a 3D printing filament, and there are several machines that convert used filament into a new one, making it possible to recycle these materials more efficiently. The waste management process of this material is summarized in Figure 16 [31].



**Figure 16.** Waste management process of PLA. Adapted from “Bioplastics: A boon or bane?”, *Renewable and Sustainable Energy Reviews*, vol. 147. Elsevier Ltd., 1 September 2021 [31].

It is hard to determine if a material is truly biodegradable; for example, in the case of PLA, the enzymes needed to degrade this biopolymer are not present in the natural environment. This means that to biodegrade PLA efficiently, the environment in which this process occurs must be controlled, especially its temperature and moisture. PLA needs to be at least 60 °C and with a lot of moisture to catalyse self-hydrolysis of the material. It is hard to achieve these conditions in home composting, which might lead to the production of inert materials. The conversion of the polymer to lactic acid is aided by the temperature and moisture available; this element is then used as a source of nutrients by several types of microorganisms. Under controlled industrial composting conditions, it takes  $84 \pm 47$  days for the complete degradation of PLA; using anaerobic digestion takes about  $423 \pm 76$  and  $116 \pm 48$  days in mesophilic and thermophilic conditions, respectively, while in soil, 4–5 years are necessary for PLA to disappear.

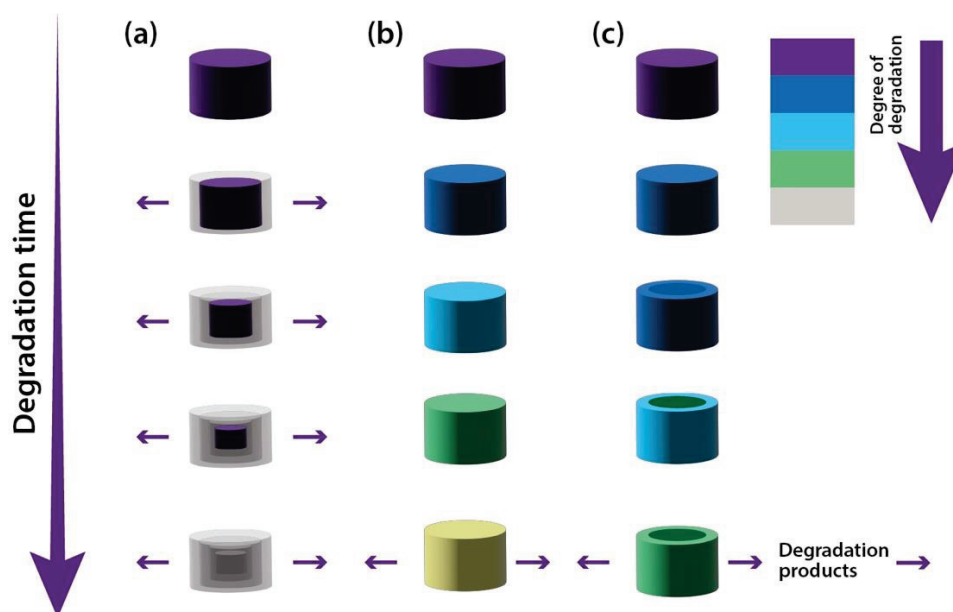
The end product of the process should be a mix of humus, water and CO<sub>2</sub>. If not processed, the remaining lactic acid reduces the soil’s pH, affecting the development of microorganisms and their activity [31].



## 7. Degradation Process

This process may be anaerobic or aerobic, and according to the type of product obtained from the process, biomass or gas and minerals, it can be called complete biodegradation or mineralization, respectively. Both processes are influenced by endogenous (such as molecular weight, crystallinity and flexibility of the molecule) and exogenous (temperature, humidity, pH, availability of oxygen and enzymatic activity) factors, which may directly affect the entire process. The best outcome regarding the degradation of bioplastics is composting, since the final products of the process are a soil-like substance called humus, CO<sub>2</sub>, water and inorganic compounds, leaving no toxic residues (if no additives were used). However, it is important to consider that this is only achievable if the right conditions are met: precisely controlled temperature, humidity, oxygen, etc. Studies show that composting PLA under natural conditions equals approximately 10–20% efficiency when compared to the process under a controlled environment [68].

Various degradation mechanisms degrade PHA and PLA; those include physical, chemical, oxidative, hydrolytic, enzymatic, microbial, photodegradation and thermodegradation mechanisms and have been studied by many researchers [69]. The different mechanisms in which the polymer degradation may occur are linked to the type of diffusion-reaction phenomenon taking place. When the absorption of water into the polymer is slower than the hydrolytic chain scission and the diffusion of the monomers into the surroundings of the plastic, it is said that the degradation is called surface erosion. As represented in Figure 17a, over time, a thinning of the plastic piece occurs without decreasing the internal molecular weight of the polymer.



**Figure 17.** Degradation modes for degradable polymers: surface erosion (a), bulk degradation (b) and bulk degradation with autocatalysis (c). Adapted from [46].

Bulk degradation, on the other hand, happens when water penetrates the entire volume of the polymer, resulting in its molecular weight decrease throughout the piece matrix (Figure 17b). If this process does not occur in equilibrium, the erosion does not occur gradually (water does not penetrate the polymer to hydrolyse the chains, making it impossible for the monomers to diffuse out). In that case, it is possible that internal autocatalysis could take place via the carboxyl and hydroxyl end group by-products. The internal concentration of this autocatalysis may create an acidic gradient, resulting in a nucleus with a faster degradation rate than the polymer's surface. The process evolves with the outer layer with a higher molecular weight than the piece's interior, as shown

in Figure 17c. Thus, this polymer is denominated as having a bimodal molecular weight distribution. In time, with the continuous diffusion of the inner polymer through the outer layer, the piece turns into a hollowed-out structure [46].

There is, however, an important notion to consider when referring to the degradation of plastics, which is the possibility of mixing additives with conventional plastics (such as PE, PP (polypropylene), PS, PET or PVC (polyvinylchloride)) to mimic the biodegradation process. These materials are called “oxo-biodegradable” or “oxo-degradable” plastics, and the additives used are usually transition metals such as nickel, iron, manganese and cobalt. Their main function is to make it easier for the polymer to break down into smaller pieces. The idea is to allow microorganisms to process the material and convert it into CO<sub>2</sub> and the biomass. This degradation process is called oxo-degradation and is divided into two different stages: the first is related to the fragmentation of the polymer itself, which is an abiotic process where the prooxidant actions create an oxidative degradation of the polymer; in the second stage occurs in the biotic process where microorganisms convert the products of the previous stage into CO<sub>2</sub> and the biomass. However, this process is hard to predict concerning the time frame in which it takes place, since it depends on the climate factors such as temperature and intensity of solar radiation.

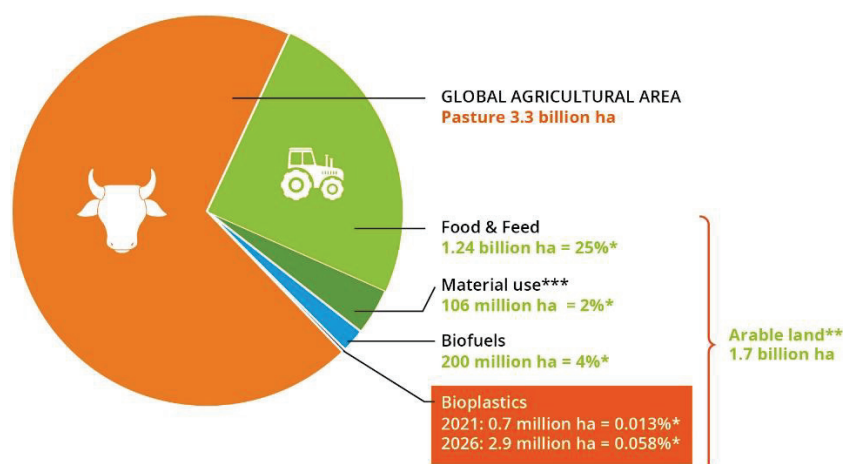
Oxo-degradable materials, however, are not considered as compostable or recyclable, as defined according to the standards accepted by the industry (ASTM D6400—Standard Specification for Labelling of Plastics Designed to be Aerobically Composted in Municipal or Industrial Facilities; ASTM D6868—Standard Specification for Labelling of End Items that Incorporate Plastics and Polymers as Coatings or Additives with Paper and Other Substrates Designed to be Aerobically Composted in Municipal or Industrial Facilities; EN 13432—Requirements for packaging recoverable through composting and biodegradation—Test scheme and evaluation criteria for the final acceptance of packaging; ISO 17088—Specifications for compostable plastics; ASTM D5338—Standard Test Method for Determining Aerobic Biodegradation of Plastic Materials Under Controlled Composting Conditions, Incorporating Thermophilic Temperatures and ASTM D5929—Standard Test Method for Determining Biodegradability of Materials Exposed to Source-Separated Organic Municipal Solid Waste Mesophilic Composting Conditions by Respirometry); after the first stage of the process, the fragmented materials, although invisible, are still present in the environment as microplastics, and there is no guarantee that the entirety of the material will biodegrade or how long it takes.

In 2019, the European Parliament banned the use of oxo-degradable plastics. Until then, companies such as Pizza Hut, Nescafe, KFC, Tiger Brands, Tesco Barclay and Walmart usually used oxo-degradable materials in their products. On the other hand, countries such as the United States of Emirates, Saudi Arabia, Bahrain and Jordan regularly use oxo-biodegradable plastics. In Saudi Arabia, since April 2017, many single-use plastics have been made of these types of materials, and the intention is to expand this utilization. The available literature is divided regarding the eco-friendliness of these materials, and the companies that produce these polymers strongly defend their biodegradability [32,70–72].

## 8. Environmental Viability Assessment

Although bioplastics are known as a green alternative to conventional polymers, some drawbacks are making it a questionable choice. There are some bioplastics that only break down in specific conditions or when treated in municipal composters or digesters. When decomposed in composts, they release methane and CO<sub>2</sub> into the atmosphere.

The production of bioplastics is also controversial, because some of them are made from plants which production requires the occupation of land that could be used to plant food. Statistics revealed that 0.7 million ha of agricultural land are used to produce bioplastics (Figure 18). This situation has consequences on food prices and in the economy of some countries [6,39].



**Figure 18.** Land use estimation for bioplastics 2021 and 2026. Adapted from European Bioplastics, “BIOPLASTICS MARKET DEVELOPMENT UPDATE 2021”, \* in relation to global agricultural area, \*\* including approx. 1% fallow land, \*\*\* land-use for bioplastics is part of the 2% material use. [https://docs.european-bioplastics.org/publications/market\\_data/Report\\_Bioplastics\\_Market\\_Data\\_2021\\_short\\_version.pdf](https://docs.european-bioplastics.org/publications/market_data/Report_Bioplastics_Market_Data_2021_short_version.pdf) (accessed on 29 December 2022) [6].

Recently, some studies revealed that, when comparing the production of traditional plastics and bioplastics, the bioplastics production created more pollutants due to the use of pesticides and fertilizers when growing the crops, and bioplastics contribute more to ozone depletion than conventional plastics.

However, recent studies reveal that not only the production of PLA saves two-thirds of energy when compared to traditional plastics production, but also, the disintegration of this material does not increase CO<sub>2</sub> in the atmosphere. This is possible, because the plant used as raw material to produce PLA absorbed the same quantity of CO<sub>2</sub> as the quantity released during the degradation of this polymer. Plus, the degradation of PLA in landfills emits 70% less greenhouse effect gases than conventional plastics. The use of renewable energies also helps to make the final products greener.

The problem regarding using food sources as raw materials to produce bioplastics is easily avoided by using crop residues as the base production material, such as stems, straws, husks and leaves. By using alternative carbohydrate sources, this problem is averted. It is also possible to use kitchen waste, fish meal wastes and paper sludge as a source of carbohydrates to produce PLA, making it possible to help the waste management in big cities.

To correctly evaluate the environmental impact and viability of bioplastics, it is necessary to assess all the processes from initial production to the final disposal. An LCA (life cycle assessment) is usually used to do this. A cradle-to-grave analysis, for example, helps determine the impact of the use of certain materials and compare them with other ones, making it possible to evaluate the whole life of products from beginning to end and in each stage of utilization. Several scenarios are studied, for example, if it is better to recycle or compost the material, to determine the best possible solution. Recent studies revealed that incineration or landfilling of bioplastics is not a useful option. It was also concluded that using PLA and TPS reduces greenhouse emissions by 50 to 70%. PTT (polytrimethylene terephthalate) and bio-urethanes release 36 and 44% less greenhouse gases, respectively. Studies have shown that the issues observed during the production of bioplastics are still less harmful than the use of conventional plastics, and it is possible to address them verified during the production of bioplastics [2,31,39,73].

There are several factors important to consider when performing an LCA; environmentally, some of the most relevant ones are:

### 8.1. Abiotic Depletion

Minerals and fossil fuels are some of the system's inputs that are important to consider, since the extraction of these materials affects the health of humans and the environment. For each extraction of these materials, the abiotic depletion factor is determined. This factor is measured based on kg of antimony (Sb) equivalents per kg of extracted mineral.

### 8.2. Global Warming

This is related to the amount of greenhouse gas emissions. Global warming is a hazard that severely affects the ecosystem, human health and material welfare. The absorption of infrared radiation changes the climatic patterns and increases the global average temperatures. This factor is measured based on its kg of CO<sub>2</sub> equivalents per kg of emission.

### 8.3. Human Toxicity

This category does not include health risks in the work environment; the main concerns are related to toxic substances' effects on the human environment. The purpose is to measure the human toxicity potentials, which may include the fate, exposure and effects of toxic substances for an infinite time. This factor is measured based on its kg of 1,4-DB (1,4-Dichlorobenzene) equivalents per kg of emission.

### 8.4. Freshwater Aquatic Ecotoxicity

Similar to human toxicity, the goal is to determine the fate, exposure and effects of toxic substances in the air, water and soil on fresh water. This factor is measured based on its kg of 1,4-DB equivalents per kg of emission.

### 8.5. Marine Aquatic Ecotoxicology

The logic used to determine this factor is the same as the human toxicity and the freshwater aquatic ecotoxicity; the characterization factor is the potential of marine aquatic toxicity of each substance emitted into the air, water or/and soil. This factor is measured based on its kg of 1,4-DB equivalents per kg of emission.

### 8.6. Terrestrial Ecotoxicity

Once again, the characterization factor is the potential of terrestrial toxicity of each substance emitted into the air, water or/and soil. This factor is measured based on its kg of 1,4-DB equivalents per kg of emission.

### 8.7. Photochemical Oxidation

Reactions between NO<sub>x</sub> (nitrogen oxides) and VOCs (volatile organic compounds) when in contact with UV (ultraviolet) light create photochemical oxidant smog, leading to the formation of ozone in the troposphere. This phenomenon depends on the metrological conditions and the background concentrations of pollutants. This factor is measured based on its kg of C<sub>2</sub>H<sub>4</sub> (Ethylene) equivalents per kg of emission.

### 8.8. Acidification

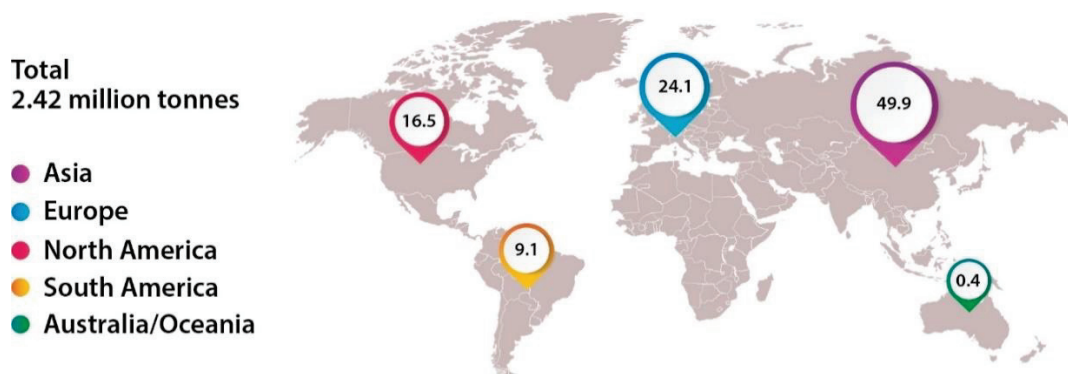
Refers to the increase of potentially toxic elements or the decrease of pH by the deposition of pollutants such as SO<sub>2</sub> (sulphur dioxide), NO<sub>x</sub>, HCl (hydrochloric acid), CO<sub>2</sub> and NH<sub>3</sub> (ammonia), which may affect soil, groundwater, surface water, organisms, ecosystems and materials. This factor is measured based on its kg of SO<sub>2</sub> equivalents per kg of emission.

### 8.9. Eutrophication

The deposition of excessive nutrients in a soil or water system, especially phosphates and nitrates, usually leads to excessive algae growth, potentially damaging life forms in the system by affecting the ecosystem equilibrium. This factor is measured based on its kg of PO<sub>4</sub><sup>3-</sup> (Phosphate) equivalents per kg of emission [68,74,75].

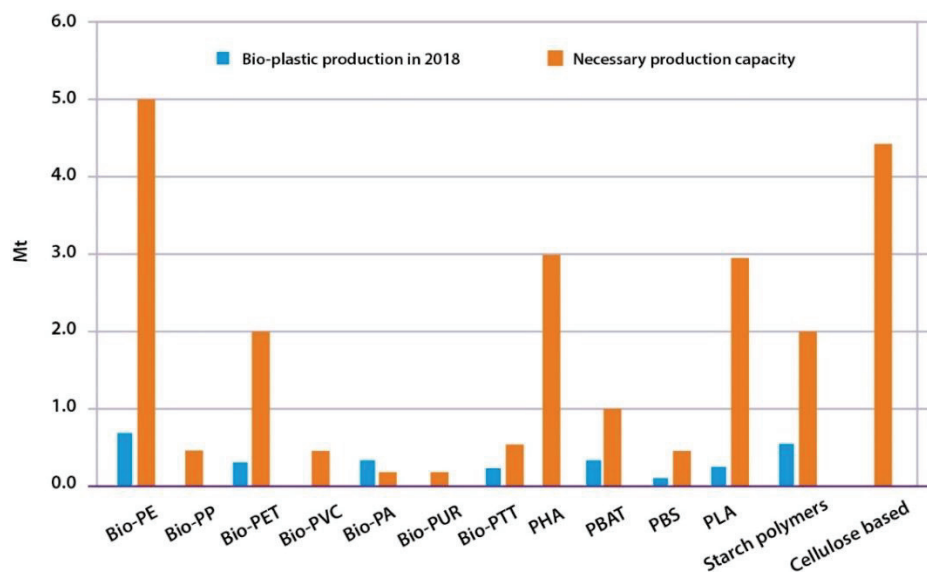
### 9. Statistics of Bioplastics

According to European Bioplastics, the production of bioplastics represents only 1% (2.42 Mt) of all plastic production, and the vast majority was produced in Asia, about 50%. Europe is the second continent with a greater capacity to produce bioplastics, as shown in Figure 19. The growth of the last few years is greatly influenced by the incentives of the European Commission to decrease the dependency on fossil fuels and transition to a circular economy [33,75].



**Figure 19.** Global production capacities of bioplastics in 2021 (world map). Adapted from “Global production capacities of bioplastics in 2021 (world map)”, [https://www.european-bioplastics.org/wp-content/uploads/2021/11/Global\\_Prod\\_Capacity2021\\_map.jpg](https://www.european-bioplastics.org/wp-content/uploads/2021/11/Global_Prod_Capacity2021_map.jpg) (accessed on 29 December 2022) [76].

However, this growth is not yet sufficient to consider it possible to replace the use of petrochemical plastics with biopolymers. A study developed by Janis Brizga et al. (2020) revealed that, to achieve this on packaging application alone, it would be necessary to increase by 8.4 times some of the bioplastics production (Figure 20). Other bioplastics would even need to increase production by 100 times. Although these values are only theoretical and no economic feasibility and resource availability are considered, it is possible to observe that the production of bioplastics is still very far from what it would be necessary to replace petrochemical polymers [77].



**Figure 20.** Current Bioplastic Packaging Production versus Necessary Production Capacity Source. Adapted from “The Unintended Side Effects of Bioplastics: Carbon, Land, and Water Footprints”, *One Earth*, vol. 3, no. 1. Cell Press, pp. 45–53, 24 July 2020 [77].



Another study by F. Klein, A. Emberger-Klein, K. Menrad et al. (2019) evaluated the possible motives influencing the intention to purchase bioplastic products on the German market. The study concluded that green consumer values, attitudes towards bioplastic, product experience and interest in information are crucial factors influencing the community to buy bioplastic products. This means that information and communication are key aspects for people to choose to use bioplastics. To reinforce this, it was mentioned that “the purchase intention for bioplastic products measured for all German citizens is moderate at about 56%. In contrast, about 95% of the consumers with product experience intend to buy bioplastic products”. This means that, by increasing the promotion of bioplastics, the community becomes more aware of the importance of using these materials. One good starting point would be to set standards regarding the end-of-life usage of bioplastics, eliminating the confusion of some companies and consumers. Therefore, it is useful to consider the LCA analysis to support the choices made [78].

Numerous analyses can be done regarding the use of bioplastics and the consequences it has on important issues, such as fossil fuel consumption, economics, pollution, energy consumption and health.

### 9.1. Fossil Fuel Consumption

Using bioplastics instead of petrochemical ones can reduce fossil fuel consumption, since its production does not depend on them. Although it is not yet possible if all the petrochemical polymers were replaced by bioplastics and considering the energy used for its production as renewable, the consumption of fossil fuels would decrease 4% (3.49 million barrels a day). This value surpasses the daily consumption of every country except the United States, China and Japan. This simplified case reveals that the savings in oil consumption would be significant [79].

### 9.2. Economics

Generally, bioplastics are more expensive to produce than petrochemical polymers, but with the development of production techniques and the instability of oil prices, this reality tends to shift. For example, Mirel bioplastic made by Metabolix is about double the price of a petrochemical equivalent. The potential price stability is another benefit bioplastics have, and with the industry’s growth, the production prices of bioplastics should decrease [79]. To put it in perspective, Table 4 contains a list of typical market prices for common bioplastics inputs and polymers.

**Table 4.** Bioplastics and raw material prices (2018). Adapted from “Green Bioplastics as Part of a Circular Bioeconomy”, Trends in Plant Science, vol. 24, no. 3. Elsevier Ltd., pp. 237–249, 1 March 2019 [23].

Bioplastic	Approximate Price (EUR/kg)
Corn starch	0.34
Lactic acid	1.14
Unbleached dissolving pulp	1.26
Soybean protein isolate	2.02
PLA	1.72
PHA	2.49
Cellulose acetate	21.50

### 9.3. Energy Consumption

Several examples prove that the energy required to produce petrochemical polymers is higher than bioplastics. The total life cycle of HDPE requires 73.7 MJ kg<sup>-1</sup> of plastic produced, LDPE uses 81.8 MJ kg<sup>-1</sup> and PP 85.9 MJ kg<sup>-1</sup>. On the other hand, PHB requires 44.7 MJ kg<sup>-1</sup> of plastic produced, PLA uses 54.1 MJ kg<sup>-1</sup> and TPS 25.4 MJ kg<sup>-1</sup>. This represents significant consumption savings, and these values might have even greater

differences due to the development of the techniques used to produce bioplastics. PLA energy requirement might reach values as low as  $7.4 \text{ MJ kg}^{-1}$ .

Hypothetically, if all the PP used in the United States were replaced by PHB, PLA or TPS, the annual energy savings would be 363, 280 and 529 PJ, respectively. Considering that it is necessary to use 31,250 metric t of coal to produce 1PJ of energy, the savings would be enormous [79].

#### 9.4. Pollution

Less pollution is produced by the production of bioplastics when compared with petrochemical polymers, not only by requiring less energy to be produced and emitting less  $\text{CO}_2$  but also by the possibility of recycling these materials. Bioplastics need to have their own recycling process, but they are not yet produced in enough quantities for that to happen; for this reason, they are considered a contaminant to the process. In perspective, if 0.1% of bioplastic material mixes with PET during its recycling process, the entire batch would become useless. It is important, however, to notice that bioplastics are as easily recyclable as petrochemical ones; they just need to be processed separately [79].

#### 9.5. Health

So far, bioplastics have not been linked to any type of health problem. However, it is important to consider that the bioplastic industry is still under development, which means that further studies could reveal some issues with the use of these materials. It is essential to consider the use of pesticides, used during crop growth, and plasticizers. The problem with plasticizers is better understood than the bioplastics themselves. Nevertheless, bioplasticizers with low toxicity can be used in bioplastics [79].

### 10. Advantages and Disadvantages

Petrochemical-based polymers are a type of material in the process of extinction for several motives, such as the environmental hazard they usually provoke; their waste management difficulties; the risk of toxicity for other materials, animals and plants; the limited oil and gas resources and their increasing prices. However, these disadvantages are balanced by the low cost and high-speed production of pieces made of these materials, their high mechanical performance, good barrier properties and good heat stability.

Based on those disadvantages, the utilization of bioplastics works as an alternative. Bioplastics have a much lower carbon footprint, although if the polymer is biodegradable, the  $\text{CO}_2$  stored during the formation of the raw material will be released when it degrades, unlike the permanent bioplastics, which can be recycled many times while still storing the  $\text{CO}_2$  absorbed, but this released  $\text{CO}_2$  is compensated for by the fact that, during the growth of some types of bioplastics raw materials (plants), they absorbed the same quantity of this gas from the atmosphere. For example, 1 kg of bioplastic resin produces about 0.49 kg of  $\text{CO}_2$ , while petrochemical-based polymers produce 2 to 3 kg of  $\text{CO}_2$ . They make it possible for every country to produce polymeric materials without depending on countries with petroleum reserves. The production of bioplastics also takes less energy than conventional plastics.

However, the overall costs to produce bioplastics are higher than the petroleum-based polymers; nevertheless, it is important to consider the possibility of implementing several cost reduction mechanisms. Currently, bioplastics are considered to contaminate the recycling process of other plastics, but this problem is easily overcome by separating it from conventional plastic from the beginning of the process. The production of bioplastics might also reduce the available resource reserves usually used as food by-products. The composting possibility of some bioplastics might create some confusion. These materials are not compostable in the same way as conventional food waste, as it might be interpreted. The process requires controlled conditions that can only be achieved under an industrial composting site. The production, usage and waste management of bioplastics are not yet under any specific legislation in some countries [2,4,33,80].

### 11. Regulation

Currently, bioplastics and biodegradable plastics are identified by the ASTM International Resin Identification Coding System as part of group 7 or ‘other’ (Figure 21b), an identification system developed by the Society of the Plastics Industry in 1988 and administered by ASTM International since 2008. This means that the polymers included in this category do not have specified characteristics, and their management process is not defined. A solution to this problem would be to globalize a symbol easily identifiable identifying polymers classified as compostable or biodegradable according to proper standards, such as ASTM D6400, ASTM D6868, EN 13432, ISO 17088, ASTM D5338 and ASTM D5929. For example, the European Bioplastics created the Seeding logo (Figure 21a) as a label to identify compostable polymers according to the EN 13432 standard. Usually, this label goes along with one other created by Vinçotte (taken over by TÜV AUSTRIA Group), the “OK compost home”, “OK compost industrial”, “OK marine biodegradable”, “OK soil biodegradable”, “OK water biodegradable” and “OK biobased” (Figure 21c), because these should guarantee complete biodegradability in the light of specific requirements [31,39,73].

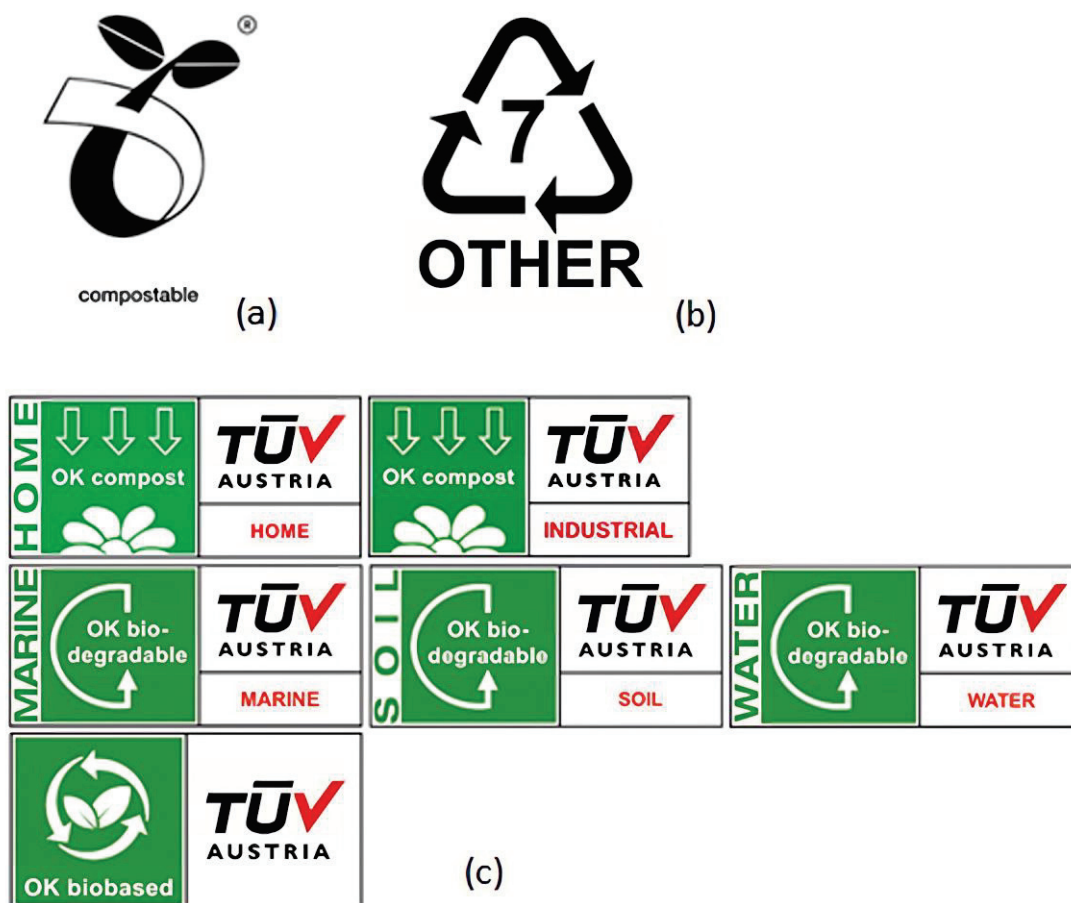


Figure 21. Labels currently used as compost, biobased and biodegradable polymers by European Bioplastics (a), ASTM International (b) and the Vinçotte/TÜV AUSTRIA Group (c) [32,73,81].

Some companies already use bioplastics in their products; for example, Coca-Cola uses bioplastics in its packaging. Recently, Coca-Cola revealed that they are launching their first 100% biobased bottle (excluding the cap and label), made of bio-PX (plant-based paraxylene) converted to bio-PTA (plant-based terephthalic acid) and using a new process, commercially viable developed by Virent. PTA is one of the main components of PET (70%); the remaining 30% is MEG (monoethylene glycol), which was already being produced from sugarcane. Since then, Coca-Cola has allowed non-competitive companies to use the technology and brand in their products, from Heinz Ketchup to the fabric interior in

Ford Fusion hybrid cars. This, however, is done by their own initiative. To incentive the implementation of bioplastics as a substitute for conventional plastics, it is important to encourage companies with certain promotion and support mechanisms, such as regulations and monetary inducement. Financial profit is one of the main reasons a company invests in something. However, this principle is not yet applicable to the industry of bioplastic production. This is due to the fact that consumers are not expected to buy bioplastic goods more expensive than conventional plastics just because they might be more eco-friendly. Cereplast, a TPS producer, estimated that when the oil price reaches around 95 USD per barrel, the company’s production costs will be lower than petrochemical plastics, and the demand for bioplastics will increase. According to European Bioplastics, the packaging is still the main application of bioplastics, 48% (1.15 million t) of the total bioplastics market in 2021 (Figure 22) [32,82].

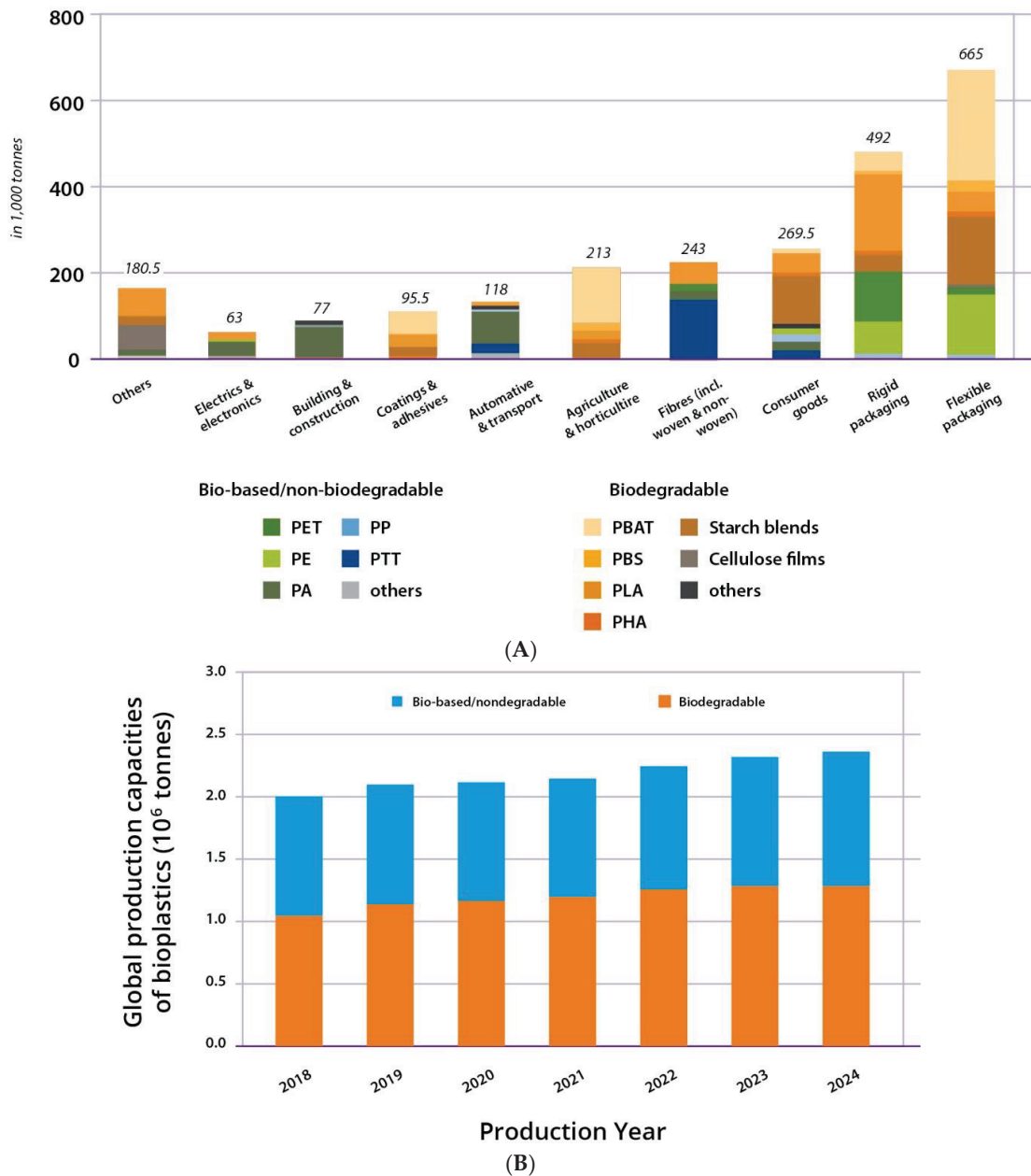


Figure 22. Global production capacities of bioplastics 2021 (by market segment) (A) and growth of bioplastic production in recent years (B). Adapted from European Bioplastics, “Bioplastics market data”, <https://www.european-bioplastics.org/market/> (accessed on 29 December 2022) [82].

With the objective of creating a simple tool for companies to select the best possible solution when selecting a good bioplastic material for food packaging, the Association of Organic Food Producers in Germany, created an Internet tool called the “Biokunststoff-Tool”. This program evaluates areas such as ecology, social acceptability, safety, quality and technology of several bioplastics, which makes it possible to select environmentally and socially responsible production methods and materials.

To make the transition to bioplastics easier, some legal changes should be applied. For example, create a strict separation between biobased and biodegradable plastics using marks and labels as in the previous examples. This facilitates the implementation of waste treatment processes specialized in these materials. However, before that, the labelling information should be spread through consumers and waste management companies [32,83].

## 12. Conclusions

Bioplastics are materials with great potential for development. Although it is not yet used industrially on a large scale, the ecological advantages of using this material compared with other plastics are enormous. Less chemical pollution, less energy consumption and less CO<sub>2</sub> emissions are some of the major drivers of a transition to a circular economy using bioplastics. On the other hand, its production is costly, and they do not have a proper recycling process. The limitations derived from the mechanical characteristics may be overcome and adapted to the intended application using additives. The disadvantages will be gradually overcome with the development of new technology and further research, over time, regarding these materials. To speed up the process, it is essential to spread the information about bioplastics to companies and consumers to convince the consumers that these materials are an excellent alternative to petrochemical-based polymers. In fact, global production capacities have been increasing and show strong growth trends; as such, new applications can be foreseen when large amounts of biopolymers are available for large-scale productions. However, biopolymers and bioplastics are not exempt from sustainability issues. Recycling these materials is a controversial debate because of their biodegradability-specific conditions, their potential methane emissions with a negative climate impact when discarded in landfills and potential contamination of the petroleum-based recycling stream. Other issues are related to land use due to ethical reasons about the potential competition with food resources. These and other concerns are all essential aspects to debate, at the academic, civil, economic and political levels. Laws, norms and regulations related to the environment have the potential to reduce the impacts on the environment. The LCA analysis can be used as a universal tool to assess those impacts and to support political decisions, therefore paving the way for a green transition.

**Author Contributions:** Conceptualization, A.C., T.E. and A.M.; investigation, A.C., T.E. and A.M.; supervision, A.M. and T.E.; writing, review and editing A.C., T.E. and A.M.; images editing, A.C., R.T. and T.E.; funding acquisition, A.M., T.E. and T.T.B. All authors have read and agreed to the published version of the manuscript.

**Funding:** The authors acknowledge the Fundação para a Ciência e a Tecnologia (FCT) through the projects UIDB/04044/2020 and UIDP/04044/2020, Associate Laboratory ARISE LA/P/0112/2020, and PTDC/BTA-GES/2740/2020\_NABIA. The Coimbra Chemistry Centre (CQC) is supported by the FCT through the projects UIDB/00313/2020 and UIDP/00313/2020. PAMI—ROTEIRO/0328/2013 (No. 022158), EcoPlast, Materiais compósitos eco-sustentáveis para substituição dos plásticos convencionais, ref POCI-01-0247-FEDER-069002, funded by the National Agency of Innovation (ANI). We are grateful for funding from PTScience, which is supported through the programs CENTRO-05-4740-FSE-001526 and FEDER.

**Conflicts of Interest:** The authors declare no conflict of interest.



## Nomenclature

1,4-DB	1,4-Dichlorobenzene	3DP	3D printing
Bio-PETG	Bio Polyethylene Terephthalate Glycol	Bio-PTA	Plant-based Terephthalic Acid
Bio-PX	Plant-based Paraxylene	CNC	Cellulose Nano Crystals
C <sub>2</sub> H <sub>4</sub>	Ethylene	CO <sub>2</sub>	Carbone Dioxide
CPE	Chlorinated Polyethylene	FDM	Fused Deposition Modeling
H <sub>2</sub> O	Water	HCl	Hydrochloric Acid
HDPE	High-Density Polyethylene	LCA	Life Cycle Assessment
LDPE	Low-Density Polyethylene	MEG	Monoethylene Glycol
NFC	Nano Fiber Cellulose	NH <sub>3</sub>	Ammonia
NOx	Nitrogen Oxides	MSW	Municipal Solid Waste
PA	Polyamide	PBAT	Polybutylene Adipate Terephthalate
PBS	Polybutylene Succinate	PBST	Polybutylene Succinate
PBT	Polybutylene Terephthalate	PCL	Polycaprolactone
PE	Polyethylene	PEA	Polyethylene Adipate
PET	Polyethyleneterephthalate	PGA	Polyglycolic Acid
PHA	Polyhydroxyalkanoates	PHB	Polyhydroxy Butyrate
PHV	Polyhydroxybutyrate	PLA	Poly lactide
PO <sub>4</sub> <sup>3-</sup>	Phosphate	PP	Polypropylene
PS	Polystyrene	PTMAT	Polytetramethylene Adipate Terephthalate
PTT	Polytrimethylene Terephthalate	PVA	Polyvinyl Alcohol
PVC	Polyvinylchloride	PVdC	Polyvinylidene Chloride
SO <sub>2</sub>	Sulfur Dioxide	SPI	Soy Protein Isolate
Tg	Transition Temperature	Tm	Melting Temperature
TPLA	Talc-Injected PLA	TPS	Thermoplastic Starch
UV	Ultraviolet	VOC	Volatile Organic Compound

## References

1. Plastic Soup. What Are Bioplastics? Available online: <https://www.plasticsoupfoundation.org/en/plastic-problem/what-is-plastic/bioplastics/> (accessed on 2 October 2021).
2. Jamshidian, M.; Tehrani, E.A.; Imran, M.; Jacquot, M.; Desobry, S. Poly-Lactic Acid: Production, applications, nanocomposites, and release studies. *Compr. Rev. Food Sci. Food Saf.* **2010**, *9*, 552–571. [CrossRef] [PubMed]
3. Rebeiz, K.S.; Craft, A.P. Plastic waste management in construction: Technological and institutional issues. *Resour. Conserv. Recycl.* **1995**, *15*, 245–257. [CrossRef]
4. Arikan, E.B.; Ozsoy, H.D. A Review: Investigation of Bioplastics. *J. Civ. Eng. Arch.* **2015**, *9*, 188–192. [CrossRef]
5. Bioplasticsnews. The History of Bioplastics. Available online: <https://bioplasticsnews.com/2018/07/05/history-of-bioplastics/> (accessed on 15 October 2021).
6. European Bioplastics. Bioplastics Market Development Update 2021. Available online: [https://docs.european-bioplastics.org/publications/market\\_data/Report\\_Bioplastics\\_Market\\_Data\\_2021\\_short\\_version.pdf](https://docs.european-bioplastics.org/publications/market_data/Report_Bioplastics_Market_Data_2021_short_version.pdf) (accessed on 4 January 2022).
7. Fredi, G.; Dorigato, A. Recycling of bioplastic waste: A review. *Adv. Ind. Eng. Polym. Res.* **2021**, *4*, 159–177. [CrossRef]
8. Peelman, N.; Ragaert, R.; De Meulenaer, B.; Adons, D.; Peeters, R.; Cardon, L.; Van Impe, F.; Devlieghere, F. Application of bioplastics for food packaging. *Trends Food Sci. Technol.* **2013**, *32*, 128–141. [CrossRef]
9. European Bioplastics. What Are Bioplastics? Available online: [https://docs.european-bioplastics.org/publications/fs/EuBP\\_FS\\_What\\_are\\_bioplastics.pdf](https://docs.european-bioplastics.org/publications/fs/EuBP_FS_What_are_bioplastics.pdf) (accessed on 4 January 2022).
10. Queiroz, A.U.B.; Collares-Queiroz, F.P. Innovation and industrial trends in bioplastics. *Polym. Rev.* **2009**, *49*, 65–78. [CrossRef]
11. Ashter, S.A. *Introduction to Bioplastics Engineering*; Elsevier: Merrimack, NH, USA, 2016. [CrossRef]
12. Lackner, M. Bioplastics. In *Kirk-Othmer Encyclopedia of Chemical Technology*; John Wiley & Sons, Inc.: Hoboken, NJ, USA, 2015; pp. 1–41. [CrossRef]
13. MatWeb. Biomer P209 PHB Biodegradable Polymer. Available online: <https://www.matweb.com/search/DataSheet.aspx?MatGUID=4149f34f7f9a4d4c86455a175168c77a> (accessed on 24 November 2022).
14. MatWeb. Telles MirelTM P1003 Injection Molding Grade PHA Bioplastic. Available online: <https://www.matweb.com/search/DataSheet.aspx?MatGUID=0119b247cb5646cdb12c211943d2b48a> (accessed on 24 November 2022).
15. MatWeb. Goodfellow Polyhydroxybutyrate/Polyhydroxyvalerate (PHB 92/PHV 8). Available online: <https://www.matweb.com/search/DataSheet.aspx?MatGUID=cde9552270de441eb2ca0cf54f7135cc> (accessed on 24 November 2022).

16. MatWeb. Ultimaker PVA Filament. Available online: <https://www.matweb.com/search/DataSheet.aspx?MatGUID=caec4fe134c44e148568374997657fc4> (accessed on 24 November 2022).
17. MatWeb. Overview of Materials for Polyethylene Terephthalate (PET), Unreinforced Overview of Materials for Polyethylene Terephthalate (PET), Unreinforced. Available online: <https://www.matweb.com/search/DataSheet.aspx?MatGUID=a696bdcdf6f41dd98f8eec3599eaa20> (accessed on 24 November 2022).
18. MatWeb. Overview of Materials for Polylactic Acid (PLA) Biopolymer. Available online: <https://www.matweb.com/search/DataSheet.aspx?MatGUID=ab96a4c0655c4018a8785ac4031b9278> (accessed on 24 November 2022).
19. MatWeb. Overview of Materials for Cellulose Acetate, Molded. Available online: <https://www.matweb.com/search/DataSheet.aspx?MatGUID=dc5eaa98a96498889cb7292165523a8> (accessed on 24 November 2022).
20. MatWeb. Overview of Materials for Polystyrene, Molded, Unreinforced. Available online: <https://www.matweb.com/search/DataSheet.aspx?MatGUID=df6b1ef50ce84e7995bdd1f6fd1b04c9> (accessed on 24 November 2022).
21. MatWeb. BiologiQ EcoStarch GS270 Thermoplastic Starch. Available online: <https://www.matweb.com/search/DataSheet.aspx?MatGUID=add0ac47758b439b88965f6de3061ab1> (accessed on 24 November 2022).
22. MatWeb. Overview of Materials for Low Density Polyethylene (LDPE), Molded. Available online: <https://www.matweb.com/search/DataSheet.aspx?MatGUID=557b96c10e0843dbb1e830ceedeb35b0> (accessed on 24 November 2022).
23. Karan, H.; Funk, C.; Grabert, M.; Oey, M.; Hankamer, B. Green Bioplastics as Part of a Circular Bioeconomy. *Trends Plant Sci.* **2019**, *24*, 237–249. [CrossRef] [PubMed]
24. Emadian, S.M.; Onay, T.T.; Demirel, B. Biodegradation of bioplastics in natural environments. *Waste Manag.* **2017**, *59*, 526–536. [CrossRef]
25. Domenek, S.; Feuilleley, P.; Graud, J.; Morel, M.H.; Guilbert, S. Biodegradability of wheat gluten based bioplastics. *Chemosphere* **2004**, *54*, 551–559. [CrossRef]
26. Vilpoux, O.; Avérous, L. *Starch-Based Plastics, Technology, Use and Potentialities of Latin American Starchy Tubers*; Book 3, Chapter 18; NGO Raízes and Cargill Foundation: São Paulo, Brazil, 2002.
27. Polymer Database. Starch Based Bioplastics. Available online: <https://polymerdatabase.com/Polymer%20Brands/Starch.html> (accessed on 15 February 2022).
28. Shafqat, A.; Tahir, A.; Mahmood, A.; Tabinda, A.B.; Yasar, A.; Pugazhendhi, A. A review on environmental significance carbon foot prints of starch based bio-plastic: A substitute of conventional plastics. *Biocatal. Agric. Biotechnol.* **2020**, *27*, 101540. [CrossRef]
29. Ashok, A.; Abhijith, R.; Rejeesh, C.R. Material Characterization of Starch Derived Bio Degradable Plastics and Its Mechanical Property Estimation. 2018. Available online: [www.sciencedirect.com/www.materialstoday.com/proceedings2214-7853](http://www.sciencedirect.com/www.materialstoday.com/proceedings2214-7853) (accessed on 15 February 2022).
30. Ashok, A.; Mathew, M.; Rejeesh, C.R. Innovative Value Chain Development of Modified Starch for a Sustainable Environment: A Review. 2016. Available online: [www.journalspub.com](http://www.journalspub.com) (accessed on 15 February 2022).
31. Nandakumar, A.; Chuah, J.A.; Sudesh, K. Bioplastics: A boon or bane? *Renew. Sustain. Energy Rev.* **2021**, *147*, 111237. [CrossRef]
32. Karpušenkaitė, A.; Varžinskas, V. Bioplastics: Development, Possibilities and Difficulties. *Environ. Res. Eng. Manag.* **2014**, *68*. [CrossRef]
33. Venkatachalam, H.; Palaniswamy, R. Bioplastic World: A Review. 2020. Available online: <http://www.sciensage.info> (accessed on 15 February 2022).
34. van Soest, J.J.; Hulleman, S.; de Wit, D.; Vliegthart, J. Crystallinity in starch bioplastics. *Ind. Crop. Prod.* **1996**, *5*, 11–22. [CrossRef]
35. Jabeen, N.; Majid, I.; Nayik, G.A. Bioplastics and food packaging: A review. *Cogent Food Agric.* **2015**, *1*, 1117749. [CrossRef]
36. Bayer, I.S.; Guzman-Puyol, S.; Heredia-Guerrero, J.A.; Ceseracciu, L.; Pignatelli, F.; Ruffilli, R.; Cingolani, R.; Athanassiou, A. Direct transformation of edible vegetable waste into bioplastics. *Macromolecules* **2014**, *47*, 5135–5143. [CrossRef]
37. Isroi; Cifriadi, A.; Panji, T.; Wibowo, N.A.; Syamsu, K. Bioplastic production from cellulose of oil palm empty fruit bunch. *IOP Conf. Ser. Earth Environ. Sci.* **2017**, *65*, 012011. [CrossRef]
38. El-malek, F.A.; Khairy, H.; Farag, A.; Omar, S. The sustainability of microbial bioplastics, production and applications. *Int. J. Biol. Macromol.* **2020**, *157*, 319–328. [CrossRef]
39. Atiwesh, G.; Mikhael, A.; Parrish, C.C.; Banoub, J.; Le, T.-A.T. Environmental impact of bioplastic use: A review. *Heliyon* **2021**, *7*, e07918. [CrossRef]
40. Luengo, J.M.; García, B.; Sandoval, A.; Naharro, G.; Olivera, E.R. Bioplastics from microorganisms. *Curr. Opin. Microbiol.* **2003**, *6*, 251–260. [CrossRef]
41. Polymer Database. Polyhydroxyalkanoates (PHAs). Available online: <https://polymerdatabase.com/Polymer%20Brands/PHA.html> (accessed on 15 February 2022).
42. Polymer Database. Polylactic Acid or Polylactide (PLA). Available online: <https://polymerdatabase.com/Polymer%20Brands/PLA.html> (accessed on 16 February 2022).
43. DeStefano, V.; Khan, S.; Tabada, A. Applications of PLA in modern medicine. *Eng. Regen.* **2020**, *1*, 76–87. [CrossRef]
44. Inkinen, S.; Hakkarainen, M.; Albertsson, A.C.; Södergård, A. From lactic acid to poly(lactic acid) (PLA): Characterization and analysis of PLA and its precursors. *Biomacromolecules* **2011**, *12*, 523–532. [CrossRef]
45. Vink, E.T.H.; Rábago, K.R.; Glassner, D.A.; Gruber, P.R. Applications of life cycle assessment to NatureWorks™ polylactide (PLA) production. *Polym. Degrad. Stab.* **2003**, *80*, 403–419. [CrossRef]

46. Woodruff, M.A.; Hutmacher, D.W. The return of a forgotten polymer—Polycaprolactone in the 21st century. *Prog. Polym. Sci. (Oxford)* **2010**, *35*, 1217–1256. [CrossRef]
47. Nanda, S.; Patra, B.R.; Patel, R.; Bakos, J.; Dalai, A.K. Innovations in applications and prospects of bioplastics and biopolymers: A review. *Environ. Chem. Lett.* **2022**, *20*, 379–395. [CrossRef]
48. Jerez, A.; Partal, P.; Martínez, I.; Gallegos, C.; Guerrero, A. Protein-based bioplastics: Effect of thermo-mechanical processing. *Rheol. Acta* **2007**, *46*, 711–720. [CrossRef]
49. Costa, A.A.; Gameiro, F.; Potêncio, A.; Silva, D.P.d.; Carreira, P.; Martinez, J.C.; Pascoal-Faria, P.; Mateus, A.; Mitchell, G.R. Evaluating the Injection Moulding of Plastic Parts Using In Situ Time-Resolved Small-Angle X-ray Scattering Techniques. *Polymers* **2022**, *14*, 4745. [CrossRef]
50. Polymer Database. Biopolyamides (Polyalkylene Sebacamides). Available online: <https://polymerdatabase.com/Polymer%20Brands/Biopolyamides.html> (accessed on 25 February 2022).
51. Johansson, J.; Rising, A. Doing what spiders cannot—a road map to supreme artificial silk fibers. *ACS Nano* **2021**, *15*, 1952–1959. [CrossRef]
52. Qiao, X.; Qian, Z.; Li, J.; Sun, H.; Han, Y.; Xia, X.; Zhou, J.; Wang, C.; Wang, Y.; Wang, C. Synthetic Engineering of Spider Silk Fiber as Implantable Optical Waveguides for Low-Loss Light Guiding. *ACS Appl. Mater. Interfaces* **2017**, *9*, 14665–14676. [CrossRef] [PubMed]
53. Eisoldt, L.; Smith, A.; Scheibel, T. Decoding the secrets of spider silk. *Materialstoday* **2011**, *14*, 80–86. [CrossRef]
54. Lubin, G. *Handbook of Composites*; Springer Science & Business Media: Berlin/Heidelberg, Germany, 2013.
55. Prashanth, S.; Subbaya, K.M.; Nithin, K.; Sachhidananda, S. Fiber Reinforced Composites—A Review. *J. Mater. Sci. Eng.* **2017**, *6*, 3. [CrossRef]
56. Chong, T.Y.; Law, M.C.; Chan, Y.S. The Potentials of Corn Waste Lignocellulosic Fibre as an Improved Reinforced Bioplastic Composites. *J. Polym. Environ.* **2021**, *29*, 363–381. [CrossRef]
57. Kortaberria, G.; Tercjak, A. *Block Copolymer Nanocomposites*, 1st ed.; Jenny Stanford Publishing: New York, NY, USA, 2016.
58. European Bioplastics. Processing Technology. Available online: <https://www.european-bioplastics.org/about-us/> (accessed on 22 October 2021).
59. Bioplastics Magazine. Processing of Bioplastics—What Is Feasible? Available online: [https://www.bioplasticsmagazine.com/en/news/meldungen/20140925\\_ifbb.php](https://www.bioplasticsmagazine.com/en/news/meldungen/20140925_ifbb.php) (accessed on 22 October 2021).
60. NaturePlast. Transformation of Bioplastic Materials. Available online: <http://natureplast.eu/en/the-bioplastics-market/transformation-of-bioplastic-materials/> (accessed on 5 November 2021).
61. Gokhale, S. 3D Printing with Bioplastics. Master Thesis, Delft University of Technology, Delft, The Netherlands, 2020.
62. Gokhale, M.T.S.; Tempelman, E.; Faludi, T.D.J.; Rijnaarts, T.D.T.; van Deursen, U.B. 3D printing of biomaterials. *MRS Bull.* **2015**, *40*, 108–115. [CrossRef]
63. Schulze, C.; Juraschek, M.; Herrmann, C.; Thiede, S. Energy Analysis of Bioplastics Processing. *Procedia CIRP* **2017**, *61*, 600–605. [CrossRef]
64. Bioplastics Magazine. Scientists Successfully Produce PLA/Protein Electrospun Mats for Future Biomedical Applications. Available online: <https://www.bioplasticsmagazine.com/en/news/meldungen/20200408-Scientists-successfully-produce-PLA-protein-electrospun-mats-for-future-biomedical-applications.php> (accessed on 15 November 2021).
65. European Bioplastics. Global Production Capacities of Bioplastics in 2021 (by Market Segment). Available online: [https://www.european-bioplastics.org/wp-content/uploads/2021/11/Global\\_Prod\\_Market\\_Segment\\_circle\\_2021.jpg](https://www.european-bioplastics.org/wp-content/uploads/2021/11/Global_Prod_Market_Segment_circle_2021.jpg) (accessed on 24 January 2022).
66. Wojnowska-Baryła, I.; Kulikowska, D.; Bernat, K. Effect of bio-based products on waste management. *Sustainability* **2020**, *12*, 2088. [CrossRef]
67. Cucina, M.; de Nisi, P.; Tambone, F.; Adani, F. The role of waste management in reducing bioplastics' leakage into the environment: A review. *Bioresour. Technol.* **2021**, *337*, 125459. [CrossRef]
68. Gironi, F.; Piemonte, V. Bioplastics and petroleum-based plastics: Strengths and weaknesses. *Energy Sources Part A Recovery Util. Environ. Effects* **2011**, *33*, 1949–1959. [CrossRef]
69. Chamas, A.; Moon, H.; Zheng, J.; Qiu, Y.; Tabassum, T.; Jang, J.H.; Abu-Omar, N.; Scott, S.L.; Suh, S. Degradation Rates of Plastics in the Environment. *ACS Sustain. Chem. Eng.* **2020**, *8*, 3494–3511. [CrossRef]
70. European Bioplastics. EU Takes Action against Oxo-Degradable Plastics. Available online: <https://www.european-bioplastics.org/eu-takes-action-against-oxo-degradable-plastics/> (accessed on 24 February 2022).
71. The Guardian. European Parliament Votes to Ban Single-Use Plastics. 2019. Available online: <https://www.theguardian.com/environment/2019/mar/27/the-last-straw-european-parliament-votes-to-ban-single-use-plastics> (accessed on 24 February 2022).
72. European Bioplastics. 'Oxo-Biodegradable' Plastics and Other Plastics with Additives for Degradation. Available online: [www.european-bioplastics.org](http://www.european-bioplastics.org) (accessed on 24 February 2022).
73. Rezvani Ghomi, E.; Khosravi, F.; Saedi Ardahaei, A.; Dai, Y.; Neisiany, R.E.; Foroughi, F.; Wu, M.; Das, O.; Ramakrishna, S. The Life Cycle Assessment for Polylactic Acid (PLA) to Make It a Low-Carbon Material. *Polymers* **2021**, *13*, 1854. [CrossRef]
74. Biron, M. EcoDesign. In *Material Selection for Thermoplastic Parts*; Elsevier: Amsterdam, The Netherlands, 2016; pp. 603–653. [CrossRef]

75. Singh, V.; Dincer, I.; Rosen, M.A. Life Cycle Assessment of Ammonia Production Methods. In *Exergetic, Energetic and Environmental Dimensions*; Elsevier Inc.: Amsterdam, The Netherlands, 2018; pp. 935–959. [CrossRef]
76. European Bioplastics. Global Production Capacities of Bioplastics in 2021 (World Map). Available online: [https://www.european-bioplastics.org/wp-content/uploads/2021/11/Global\\_Prod\\_Capacity2021\\_map.jpg](https://www.european-bioplastics.org/wp-content/uploads/2021/11/Global_Prod_Capacity2021_map.jpg) (accessed on 24 January 2022).
77. Brizga, J.; Hubacek, K.; Feng, K. The Unintended Side Effects of Bioplastics: Carbon, Land, and Water Footprints. *One Earth* **2020**, *3*, 45–53. [CrossRef]
78. Klein, F.; Emberger-Klein, A.; Menrad, K.; Möhring, W.; Blesin, J.M. Influencing factors for the purchase intention of consumers choosing bioplastic products in Germany. *Sustain. Prod. Consum.* **2019**, *19*, 33–43. [CrossRef]
79. Momani, B.L. Digital WPI Interactive Qualifying Projects (All Years) Interactive Qualifying Projects Assessment of the Impacts of Bioplastics: Energy Usage, Fossil Fuel Usage, Pollution, Health Effects, Effects on the Food Supply, and Economic Effects Compared to Petroleum Based Plastics. 2009. Available online: <https://digitalcommons.wpi.edu/iqp-all> (accessed on 24 February 2022).
80. Sidek, I.S.; Draman, S.F.S.; Abdullah, S.R.S.; Anuar, N. CURRENT DEVELOPMENT ON BIOPLASTICS AND ITS FUTURE PROSPECTS: AN INTRODUCTORY REVIEW. *INWASCON Technol. Mag.* **2019**, *1*, 03–08. [CrossRef]
81. TÜV AUSTRIA, EN13432? Compostability? Biodegradability? Biobased? Certified by TÜV AUSTRIA. Available online: <https://www.tuv-at.be/green-marks/> (accessed on 14 February 2022).
82. European Bioplastics. Bioplastics Market Data. Available online: <https://www.european-bioplastics.org/market/> (accessed on 17 February 2022).
83. Yeh, C.-H.; Lücke, F.-K.; Janssen, J. Bioplastics: Acceptable for the Packaging of Organic Food? A Policy Analysis. *J. Agric. Food Syst. Community Dev.* **2015**, *6*, 95–105. [CrossRef]

**Disclaimer/Publisher’s Note:** The statements, opinions and data contained in all publications are solely those of the individual author(s) and contributor(s) and not of MDPI and/or the editor(s). MDPI and/or the editor(s) disclaim responsibility for any injury to people or property resulting from any ideas, methods, instructions or products referred to in the content.



## Article

# Biopolymer Based Multifunctional Films Loaded with Anthocyanin Rich Floral Extract and ZnO Nano Particles for Smart Packaging and Wound Healing Applications

Jijo Thomas Koshy, Devipriya Vasudevan, Dhanaraj Sangeetha \* and Arun Anand Prabu \*

Department of Chemistry, School of Advanced Sciences, Vellore Institute of Technology, Vellore 632014, Tamil Nadu, India

\* Correspondence: dsangeetha@vit.ac.in (D.S.); anandprabu@vit.ac.in (A.A.P.)

**Abstract:** There are significant societal repercussions from our excessive use of plastic products derived from petroleum. In response to the increasing environmental implications of plastic wastes, biodegradable materials have been proven to be an effective means of mitigating environmental issues. Therefore, protein- and polysaccharide-based polymers have gained widespread attention recently. In our study, for increasing the strength of a biopolymer (Starch), we used ZnO dispersed nanoparticles (NPs), which resulted in the enhancement of other functional properties of the polymer. The synthesized NPs were characterized using SEM, XRD, and Zeta potential values. The preparation techniques are completely green, with no hazardous chemicals employed. The floral extract employed in this study is *Torenia fournieri* (TFE), which is prepared using a mixture of ethanol and water and possesses diverse bioactive features and pH-sensitive characteristics. The prepared films were characterized using SEM, XRD, FTIR, contact angle and TGA. The incorporation of TFE and ZnO (SEZ) NPs was found to increase the overall nature of the control film. The results obtained from this study confirmed that the developed material is suitable for wound healing and can also be used as a smart packaging material.

**Citation:** Koshy, J.T.; Vasudevan, D.; Sangeetha, D.; Prabu, A.A.

Biopolymer Based Multifunctional Films Loaded with Anthocyanin Rich Floral Extract and ZnO Nano Particles for Smart Packaging and Wound Healing Applications. *Polymers* **2023**, *15*, 2372. <https://doi.org/10.3390/polym15102372>

Academic Editor: Raffaella Striani

Received: 21 February 2023

Revised: 9 March 2023

Accepted: 13 March 2023

Published: 19 May 2023

**Keywords:** starch; *Torenia fournieri*; zinc oxide nanoparticle; smart packaging sensors; wound healing

## 1. Introduction

In contrast to biodegradable materials, natural compounds in any environment accessible to humans are incapable of decomposing quickly. In engineering, automotive, packaging, and electrical applications, synthetic plastics serve as the primary material for a wide variety of equipment [1]. Biopolymers with numerous applications have established a new path for societal implication in both packaging and wound care sectors. The use of proteins and polysaccharides with diverse applications is ushering in a new era of escalating environmental consequences. With the aim of improving the effectiveness of treatment, a paradigm change in healthcare towards individualized wound care management is steadily taking place. It is essential to develop dressings that are non-toxic, have good adhesion, and excellent mechanical and hemostasis qualities (for sealing wounds) [2].

Active packaging has garnered substantial attention in the food packaging industry over the past decade due to its capacity to increase shelf life or improve safety or sensory attributes while retaining the food's quality by integrating active compounds and components into packaging materials [3,4]. In order to prevent microbiological contamination and food oxidation, the food industry uses antibacterial and antioxidant components as innovative technology. Additionally, new packaging solutions with active and intelligent features have been launched as a result of recent advancements in food packaging. As a potential pathogen intervention method for a variety of foods, antimicrobial packaging is a promising variant of active packaging. This packaging is able to kill or inhibit pathogenic



**Copyright:** © 2023 by the authors. Licensee MDPI, Basel, Switzerland. This article is an open access article distributed under the terms and conditions of the Creative Commons Attribution (CC BY) license (<https://creativecommons.org/licenses/by/4.0/>).



microorganisms that are contaminating food products and causing deterioration [5,6]. “Active and intelligent packaging” is a cutting-edge innovation in the packaging industry that combines the benefits of active (antimicrobial and antioxidant) and intelligent (product freshness, temperature, safety, etc.) materials to create a synergistic impact [7].

In terms of sustainability, safety, biodegradability, and environmental friendliness, bio-based polymers (polysaccharides, proteins, polyacids, etc.) surpass synthetic polymers derived from petroleum in the manufacturing of active packaging films. To create biopolymer-based functionally active packaging films, there is growing interest in creating binary composite films employing a combination of polysaccharides and proteins. This has always been interesting among scientists since it may help to lessen environmental contamination [8]. Starch is commonly employed as a biopolymer matrix due to its abundance, low cost, renewability, and biodegradability [9,10]. However, the starch film’s weak mechanical characteristics, high brittleness, and low water sensitivity limit its applications [11,12]. Generally, the incorporation of other macromolecular compounds into starch can improve the physicochemical properties of the films [13]. Starch, comparatively a simple polymer, is made up of glucose molecules connected in two distinct ways. The most prevalent form of carbohydrate storage in plants is starch. Corn starch is one of the biopolymers that has hydrocolloid components and can be used to create a nanocomposite film matrix. Since corn starch has a high amylose content of about 25% (*w/w*), it can create a robust film [14]. It may be possible to use a corn starch variety (Paragon) as a film matrix polymer. However, the stiffness, brittleness and high hygroscopic qualities of this maize starch-based biodegradable film lead to poor physical and mechanical properties. Additionally, the moisture barrier capabilities of films based on starch are poor. Typically, natural polymers are blended with synthetic polymers or nanomaterials (NMs) to expand their applications [15].

In the fabrication of antibacterial packaging films, numerous NMs made of metals and metal oxides have already been utilised as antibacterial agents, these NMs include Ag, Cu, CuO, ZnO and TiO<sub>2</sub> nanoparticles (NPs), amongst others [16]. Zinc oxide is one of the oxide group chemicals that is widely used as a source of NPs. Typical applications for ZnO NPs include biosensors, packaging, cosmetics, pharmaceuticals and colour degradation [17]. ZnO NPs have gained prominence as a filler nanocomposite in bioplastic films due to their exceptional ability to interact with polymer matrices to create nanocomposite films (NCFs) with enhanced physical, mechanical, chemical and biological properties compared to the bulk form. One of the five zinc compounds now generally recognised and designated as safe (GRAS) materials is ZnO [18]. The NCFs formed from corn starch and ZnO NPs still have a hard and brittle film quality in spite of their remarkable properties, and so it is required to add chemicals that function as plasticizers to strengthen the film’s plastic qualities.

Recent studies have demonstrated that adding ZnO NPs to biopolymers can improve the mechanical and film permeability while reducing the hydrophilic characteristics [19]. It is known that edible flowers are sources of a variety of bioactive substances, primarily phenolics, but also vitamins and carotenoids. *Torenia fournieri*, often known as the wish-bone flower, is one of these edible flowers. It is safe to eat and non-toxic to consume. *Torenia fournieri* is combined with ethanol and water to prepare an extract. This extract is a better substitute for chemical additions because it has strong biological properties and pH sensitive characteristics [20]. From the detailed literature survey carried out, our study is the first to report on the *Torenia Fournieri*’s pH sensitive behaviour, the novelty of the work is implied from the incorporation of a floral extract into the starch matrix and the application studies. To ensure that the active ingredient is released from the food packaging film during storage and distribution, the active ingredient is added to the film. The functional packaging film regulates the active ingredient’s rate of release and enables its storage at an effective dose throughout the storage times. The goal of this work is to assess the properties of NCFs included with ZnO NPs and *Torenia fournieri* with corn starch as the polymer foundation. The current effort involves producing ZnO NPs in biopolymer

systems mixed with *Torenia fournieri* [21,22]. The objective of this research was to develop high-performance, biodegradable starch-based films that may be utilised for wound treatment and food packaging.

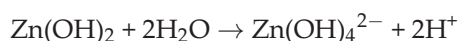
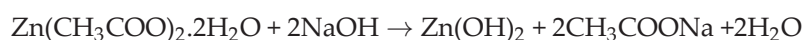
## 2. Materials and Methods

Corn starch, Glycerol, Zinc Acetate dihydrate, NaOH, and ethanol were purchased from S.D.Fine, India. Dulbecco's Modified Eagles Medium was obtained from Himedia. The remaining reagents were of analytical quality. For all sample preparations, double-distilled water was used.

The extract was prepared from *Torenia fournieri* flower, which was plucked from the neighbourhood places in Kerala. Kerala Forest Research Institute in Thrissur, Kerala, India, authorized the plant *Torenia fournieri* Lind. Ex. Fourn. (KFRI Accession number: 19347) and issued the authentication certificate. Scratch wound healing assay was performed with L929 cell line. The L929 cell line (Murine fibroblast cells) was procured from National Centre for cell science (NCSS), Pune, India.

### 2.1. Preparation of ZnO NPs

The ZnO NPs were prepared by using a co-precipitation method with some modifications. A 0.1 M 50 mL  $\text{Zn}(\text{CH}_3\text{COO})_2 \cdot 2\text{H}_2\text{O}$  solution was stirred for 2 h and 2M NaOH added drop by drop until the pH reached 12. After stirring further for 2 h, the solution is aged for settling down the precipitate. The resultant solution was centrifuged with 3000 rpm for 20 min, and pH was adjusted using distilled water to attain neutral pH. After drying at 100 °C for 2 h, the remaining powder was calcined for 4 h at 500 °C. The obtained powders (As-synthesized and Calcined) were used for further characterization. The chemical reactions of ZnO NPs under the co-precipitation method mentioned are as follows:



### 2.2. Extraction of *Torenia Fournieri*

About 100 g of *Torenia fournieri* flower was weighed and crushed with ethanol:water mixture in a ratio of 1:3. The extract was then centrifuged at 5000 rpm for 20 min and filtered. The supernatant solution of TFE was collected and kept in a dark (refrigerated) place, and the calculated weight % of the samples was measured and used for further incorporation of TFE in polymer matrix.

### 2.3. Preparation of SEZ Composite Film

SEZ film were developed by using solution-casting method. About 5 gm of starch was weighed and mixed with 50 mL of distilled water and TFE extract 8.4 mL (0.5%) with 0.025 g of dispersed ZnO NPs (41.1 mL water containing 0.025 g ZnO NPs, sonicated for 20 min) were added with a total volume of 100 mL. Then, 30 wt.-% glycerol (on starch dry basis) was added as plasticiser. At 85 °C, the solution is magnetically agitated for 30 min. The film-forming solution was casted and oven-dried at 50 °C. Using the same procedure, different sets of starch films with ZnO NPs (SZ), extract (SE), and control (S) films were prepared.

### 2.4. Characterization of ZnO NPs

X-ray powder diffractometer (XRD, Bruker D8 Advance, Germany) with Cu k radiation ( $\lambda = 1.5405 \text{ \AA}$ ) in a wide  $2\theta(^{\circ})$  (Bragg angle) range ( $10^{\circ}$  to  $90^{\circ}$ ) was utilised to analyse the structural properties of the modified ZnO NPs. The optical characteristics of ZnO NPs will become increasingly noticeable when their size decreases into the nano-domain. The morphology of ZnO NPs was analysed using scanning electron microscope (SEM, Oxford

Instruments, Zeiss EVO 18) with an electron voltage of 10 KV. Zeta potential and particle size were measured using a zeta potential analyser. Initially, ZnO powder was dispersed in double-distilled water in the ratio of 1:9 and sonicated for 5 min and filtered. The filtrate solution again sonicated to convert ZnO to nanoscale range.

### 2.5. Test for Anthocyanin and Its Colour Response

The anthocyanin test was carried out by utilizing acidic and alkaline pH using buffers, and the anthocyanin pigment extracted from *Torenia fournieri*. The solution was then combined with acids and bases of varying strengths, and its colour was observed during the process. As a preliminary investigation, we investigated whether or not there was a change in colour between the extract when we used acid and alkaline buffer. Under 12 distinct pH conditions, the colour intensity of the TFE anthocyanin extract was analysed, and photographs were taken of the resulting solutions. Utilizing phosphate buffer, a range of 1 to 12 pH buffer solutions were prepared and tested using a digital pH meter. The colour variations were taken using a digital camera after 9 mL of buffer solution was added to 1 mL of TFE.

### Determination of Total Anthocyanins Concentration

Briefly, a 0.2 mL of anthocyanin extract was combined with 7 mL of buffer at pH 1.0 and another with 7 mL of a buffer at pH 4.5. The difference in absorbance at 530 nm and 700 nm between both buffers is related to the anthocyanin content [23]. Measurements were performed on a UV-Vis spectrometer.

Anthocyanin pigment (cyanidin-3-glucoside equivalents, mg/L) = (1)

$$\frac{A \times MW \times DF \times 1000}{\epsilon \times L} \quad (1)$$

where  $A = (A_{520\text{nm}} - A_{700\text{nm}}) \text{ pH } 1.0 - (A_{520\text{nm}} - A_{700\text{nm}}) \text{ pH } 4.5$ ;  $MW$  (molecular weight) = 449.2 g/mol for cyanidin-3-glucoside;  $DF$  = dilution factor;  $L$  = pathlength (10 mm) in cm; ( $\epsilon = 26,900$  molar extinction coefficient, in  $\text{L mol}^{-1} \text{cm}^{-1}$ , for cyanidin-3-glucoside; and 1000 = factor for conversion from g to mg).

### 2.6. Morphology of Film

SEM measurements were carried out using  $3 \times 3$  mm samples coated with a thin layer of gold under 10 kV electron voltage.

### 2.7. Physical Properties of Film

Physical properties such as water solubility, swelling analysis, water vapour permeability, thickness, mechanical properties such as tensile strength (TS) and elongation at break % (E) were analysed. Water solubility was determined following the method proposed by Rekha et al. with slight modifications [7]. The film samples cut into  $2 \times 2$  cm and dried in  $80^\circ\text{C}$  for 24 h and weighed to obtain  $W_1$ . After drying, each film sample was soaked for 2 h in 50 mL of distilled water and then dried using filter paper. Again, the film was dried to constant weight in an air oven for 24 h and then weighed  $W_2$ . There were three measures taken. Using the formula, solubility % was calculated.

$$\text{Solubility \%} = \frac{(W_1 - W_2)}{W_1} \times 100 \quad (2)$$

A tensile analysis with a Tinius Olsen device determined the material's ( $12.5 \times 1.5$  cm) tensile characteristics. The speed of the crosshead was set to 50 mm/min. Utilizing Horizon software, the ultimate tensile strength and elongation at break were calculated. The Dial Thickness Gauge 7301 Micrometer was used to measure the film's thickness with an accuracy of 0.01 mm. For each, an average of 3 measurements were calculated [7]. The surface wettability of the film has been systematically analysed by SEO Phoenix 300T. Liq-

uid contact angle analysis accurately measures the film surface's proclivity to be wetted by liquids.

### 2.8. Structural Characterization

XRD measurements were carried out at room temperature to record the crystalline diffraction patterns of all the film samples. ATR-FTIR (ALPHA-T, Bruker) was utilised to detect functional groups within a range of 4000–400  $\text{cm}^{-1}$  and was employed in ATR mode for the study.

### 2.9. Thermal Stability of Polymers

Samples of the films were tested for their thermal stability using a SETARAM Labsys Evo thermogravimetric analyser for evaluating the mass loss of different polymers. Specifically, samples were heated in an environment containing nitrogen at a rate of 10  $^{\circ}\text{C}/\text{min}$  from ambient temperature to 800  $^{\circ}\text{C}$ .

### 2.10. Film Colour and Light Transmittance

The colour and transparency of the composite films with various AP concentrations on a white background plate were assessed using a colorimeter (Nix mini 2 colour sensor). Three points were chosen at random to repeat the experiment after each film was cut into squares ( $2 \times 2$  cm).  $L^*$  (lightness/brightness),  $a^*$  (redness/greenness), and  $b^*$  (yellowness/blueness) are used to describe the parameters [24]. The following formula is used to determine the total chromatic aberration:

$$\Delta E^* = \sqrt{(\Delta L^*)^2 + (\Delta a^*)^2 + (\Delta b^*)^2} \quad (3)$$

where  $\Delta L^*$ ,  $\Delta a^*$  and  $\Delta b^*$  are the differences in the sample and control values for the respective colour parameters ( $L^* = 81.78$ ,  $a^* = 0.30$ ,  $b^* = -4.59$ ).

### 2.11. Sensitivity to Ammonia and Spoilage Analysis

According to the method proposed by Rekha et al., the ability of the indicators to detect ammonia vapours was examined [7]. SEZ film used to differentiate the colour change of absorbing ammonia vapours with different concentrations. The indicators were placed one cm above 80 mL of an aq. solution containing 0.8 M and 1.4 M ammonia for the duration of 24 min. Using a Nix Pro 2 colour sensor, colour parameters (values for R, G, and B) were measured every 4 min. The sensitivity percentage (SRGB) of indicator films to volatile ammonia was calculated as follows:

$$SRGB = \frac{(R1 - R2) + (G1 - G2) + (B1 - B2)}{R1 + G1 + B1} \times 100\% \quad (4)$$

where, R1 = red, G1 = green and B1 = blue were the initial colour parameters of the indicators and R2, G2, B2 were the colour parameters after exposing to ammonia.

In order to check on the freshness of chicken samples while they were being stored, colorimetric films containing TFE were utilized. This was accomplished by affixing film samples ( $1 \times 1$  cm) to the inner surface of a plastic packaging containing fresh chicken samples, taking care to avoid direct contact with the chicken samples. The container was kept at 4  $^{\circ}\text{C}$  and analysed to check the spoilage of chicken samples. The colour change of the film was captured to monitor the freshness of chicken.

### 2.12. In-Vitro Wound Healing Studies

Wound healing studies were carried out using L929 cells (1 million cells/well), seeded on 6 well plates and allowed to acclimatize to the culture conditions such as 37  $^{\circ}\text{C}$  and 5%  $\text{CO}_2$  environment in the incubator for 24 h. The test samples were prepared in cell culture grade DMSO (10 mg/mL) and filter sterilized using 0.2  $\mu\text{m}$  Millipore syringe filter. The samples were further diluted in DMEM (Dulbecco's Modified Eagle Medium) media and

added to the wells containing cultured cells of at least 80 = % confluency at final concentrations of 25, 50 and 100  $\mu\text{g}/\text{mL}$ , respectively. Untreated wells were kept as control. The cell monolayer was scraped in a straight line to create a “scratch” with a 200  $\mu\text{L}$  pipette tip. Remove the debris and smoothen the edge of the scratch by washing the cells once with 1 mL of the growth medium and then replace with 5 mL of fresh medium.

It is important to create scratches of approximately similar size in the assessed cells and control cells to minimize any possible variation caused by the difference in the width of the scratches. To obtain the same field during the image acquisition, create markings to be used as reference points close to the scratch. The reference points can be made by etching the well plate lightly with a razor blade on the outer bottom of the dish or with an ultrafine tip marker. After the reference points are made, place the dish under a phase-contrast microscope, and leave the reference mark outside the capture image field, but within the eye-piece field of view. Acquire the first image of the scratch.

The well plate is placed in a tissue culture incubator at 37 °C. Photomicrographs were taken for varying durations (0, 12, 24 and 36 h). The time frame for incubation should be determined empirically for the particular cell type used. The well plates can be taken out of the incubator to be examined periodically and then returned to resume incubation. Choose a time frame of incubation that allows the cells under the fastest migrating condition to just achieve the complete closure of the scratch. After the incubation, place the dish under a phase-contrast microscope, match the reference point, align the photographed region acquired in Step 6 and acquire a second image. Likewise, images should be taken until the complete closure of the wound.

### 2.13. Statistical Analysis

Data were analysed statistically with SPSS 20. Results from three independent studies, including their means and standard deviations (SD). Duncan’s multiple range test and one-way analysis of variance (ANOVA) were employed to determine whether or not the data showed statistically significant differences between the groups ( $p < 0.05$ ).

## 3. Results and Discussions

### 3.1. Characterization of ZnO NPs

#### 3.1.1. Structural Characterization of ZnO NPs

Figure 1 shows the different set of data as synthesized and calcined. From the data, it is evident that XRD data of the prepared nanoparticle are almost similar to the JCPDS data. As per the results, we compared different XRD data of calcined and without calcined NPs. From calcined, we obtained sharp peaks compared with as-synthesized ZnO NPs. For further studies, we used calcined ZnO NP for integrating with the polymer matrix.

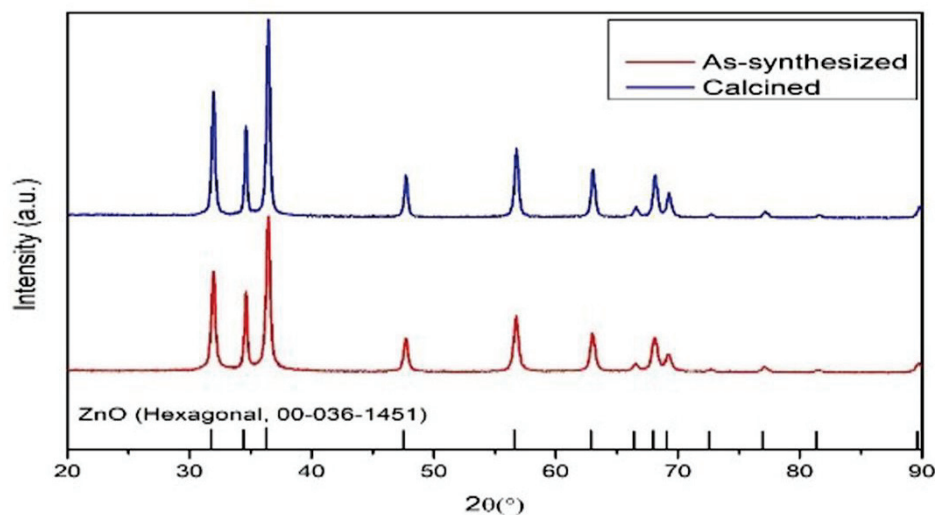
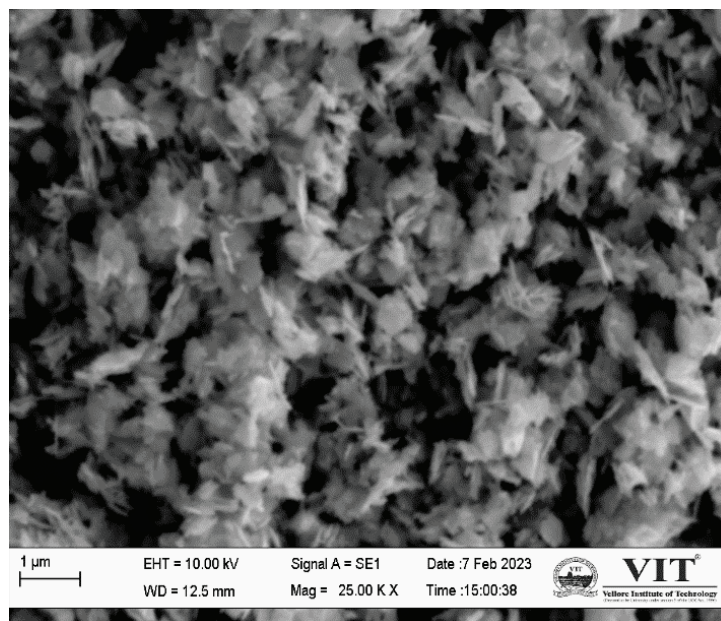


Figure 1. XRD image of ZnO NPs before and after calcined.



### 3.1.2. Morphology of ZnO NPs

The morphology of ZnO NPs was analysed using SEM. The obtained image is similar to a ZnO nanoflower (NF)-like structure. According to the SEM image displayed in Figure 2, nano-flowers aggregate into clusters. Many researchers have demonstrated the therapeutic potential of ZnO NPs in the medical field. An evaluation of cell proliferation was carried out on endothelial cells that contained ZnO NFs. The proangiogenic properties of the ZnO NFs were demonstrated by the fact that they were able to stimulate the endothelial cells [25]. Similar-shaped ZnO NFs were prepared using a chemical method as reported by Saif et al. [26].



**Figure 2.** SEM morphology of ZnO NPs.

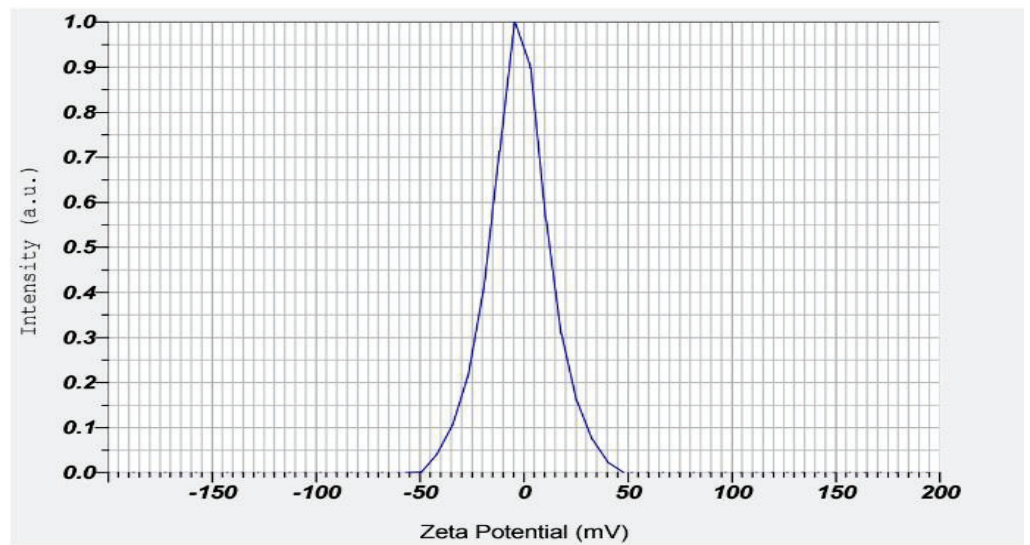
### 3.2. Zeta Potential

Zeta potential analyses were conducted to assess the surface charges obtained by all of the manufactured NPs. The results of the zeta potentials indicate the samples' stability. If the particles in suspension have substantial amounts of either negative or positive zeta potential values, it is common knowledge that the particles will repulse each other and inhibit the aggregation of NPs [27].

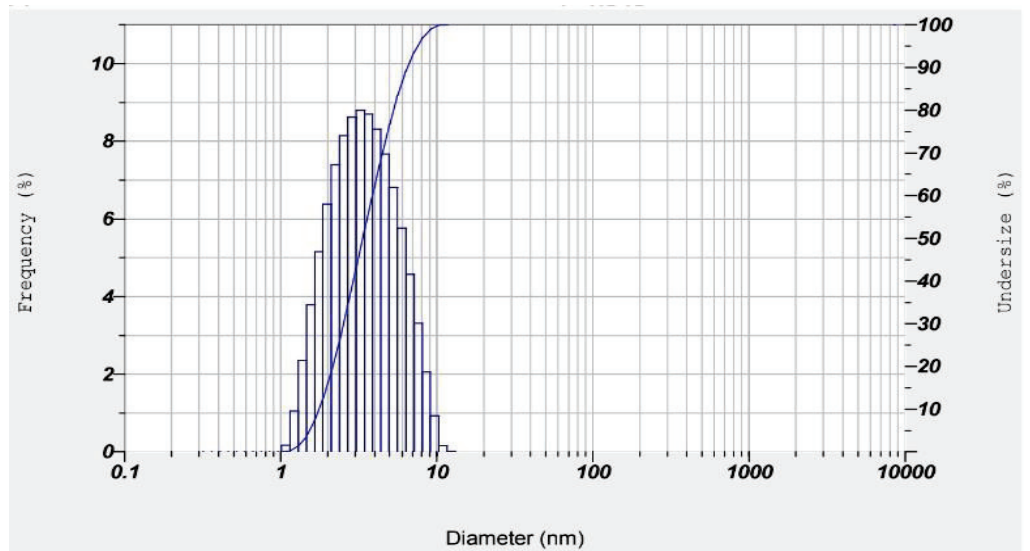
It is generally accepted that NPs with a zeta potential ranging from  $-10$  mV to  $+10$  mV are close to neutral. From the results, the prepared NP had  $-2.3$  mV with a particle size of  $4.2$  nm. Figure 3 shows the zeta potential graph and DLS curve of the prepared material.

### 3.3. Anthocyanin Colour Changes with pH

TFE was extracted using an acidic alcoholic aqueous solution to obtain phenolic compounds. As shown by pH differential assays (Figure 4), the total anthocyanin concentration in BPE was  $18.26$  mg cyanidin-3-glucoside equivalent per litre of extract. By using different pH buffers, the colour changes were monitored. From red to green, the colour changed as per the range of pH 1 to 12. According to different pH buffers, the colour ranges from red to green. The red colour was first present in the acid medium, then it gradually faded to orange, yellow and finally green. This is just a fundamental study reporting the behaviour of pH sensitivity of *Torenia fournieri* flower extract. In addition to anthocyanin, the flower extract contains a variety of natural antioxidants, including as flavonoids, phenolic acids, etc., according to previous literature [28].



(A)



(B)

Figure 3. (A) Zeta potential of ZnO NP; and (B) DLS curve of ZnO NP.

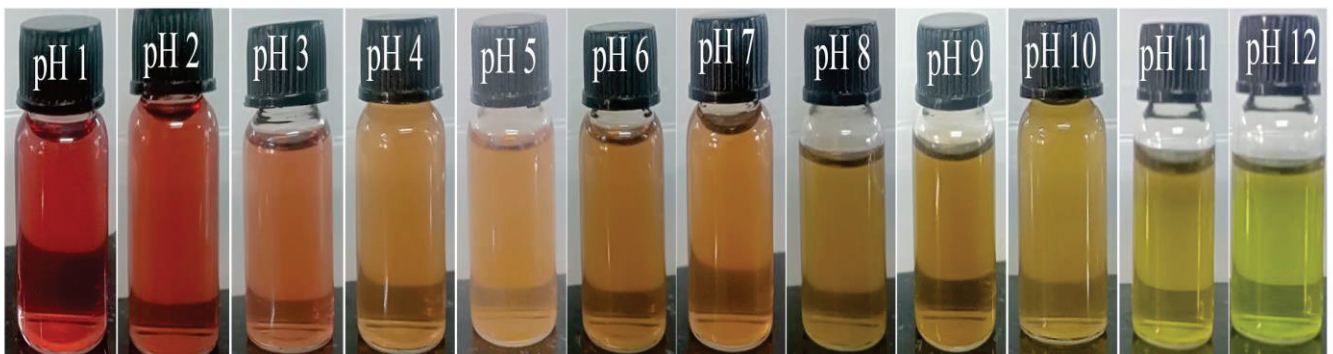
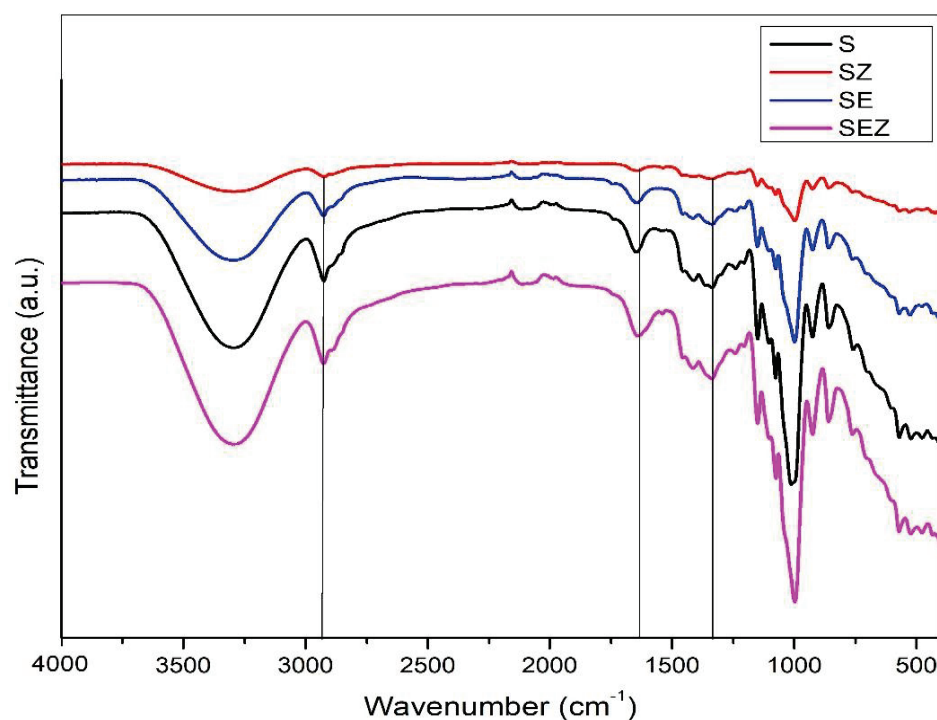


Figure 4. Colour difference of TFE extract in pH 1 to pH 12.

### 3.4. Characterization of Films

#### 3.4.1. Chemical Characterization of Film Samples

The FTIR spectra of various starch-based films are depicted in Figure 5. The fundamental stretching modes of hydroxyl groups (OH) that are caused by water and carbohydrates can be found in the broad range between 3100 and 3600  $\text{cm}^{-1}$  [29]. Starch film FTIR spectra revealed typical characteristic peaks at 918, 993, 1146  $\text{cm}^{-1}$  (C-O stretching), 1424  $\text{cm}^{-1}$  (glycerol), and 1634  $\text{cm}^{-1}$  (bound water). The same results were found in the scientific literature. There is not much of a difference between the FTIR spectra of synthesized SEZ composite films and the control S film; only minor variations in intensity and peak position are found in composite films. The addition of ZnO nano in control film causes some minor changes in the spectrum. There was no shift in the adsorption peaks, confirming the high compatibility of starch molecules with ZnO.

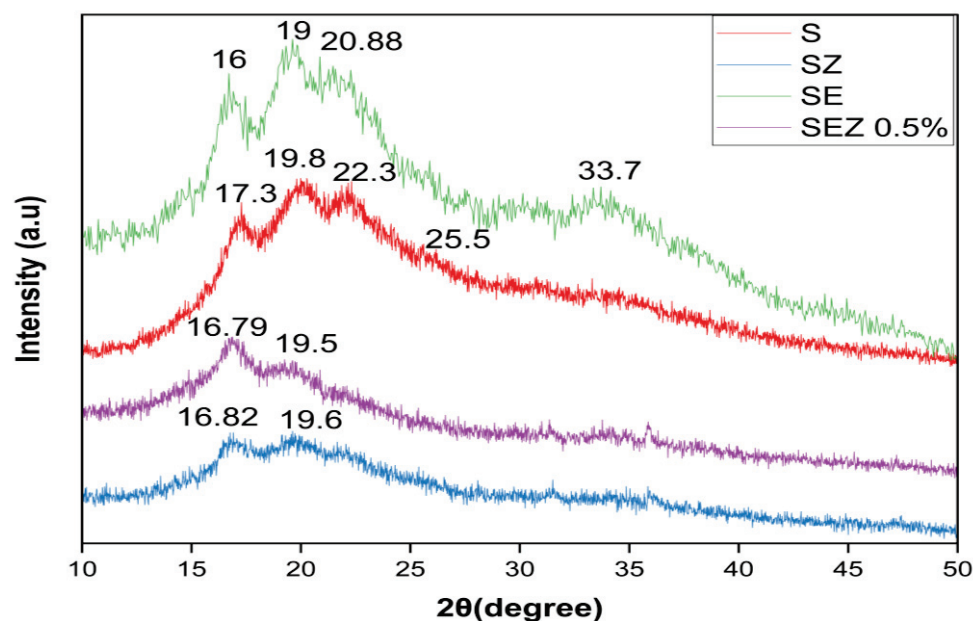


**Figure 5.** FTIR spectrum of S, SE, SZ and SEZ.

#### 3.4.2. Structural Characterization

The XRD patterns of the films with TFE extract contents were examined and are shown in Figure 6. In order to analyse the change in the structure of different starch-based films, the intermolecular attraction between starch (mentioned as “S” in Figures), glycerol, TFE and ZnO in different starch films can be studied with the help of XRD. The control starch film shows diffraction peaks at 17.3, 19.8, and 22.1 with weak intensity. The XRD data reveal that despite the presence of ZnO (mentioned as “Z” in Figures), in the starch film, no ZnO signal peaks were detected. The weakened peak at  $2\theta$  values of 17° and 22.1° illustrates the essentially amorphous characteristics of the starch film. The incorporation of ZnO nano dispersed in the starch matrix improved the overall distribution.

The addition of TFE extract shows significant changes in the control and SZ film. One peak that appeared in 33.7° represents the concentration of extract incorporated in the base matrix. This is demonstrated by the fact that the weak peaks visible in the S and SZ films remain the same and that the peak intensity increases.



**Figure 6.** XRD image of film samples S, SZ, SE and SEZ.

#### 3.4.3. Microstructure

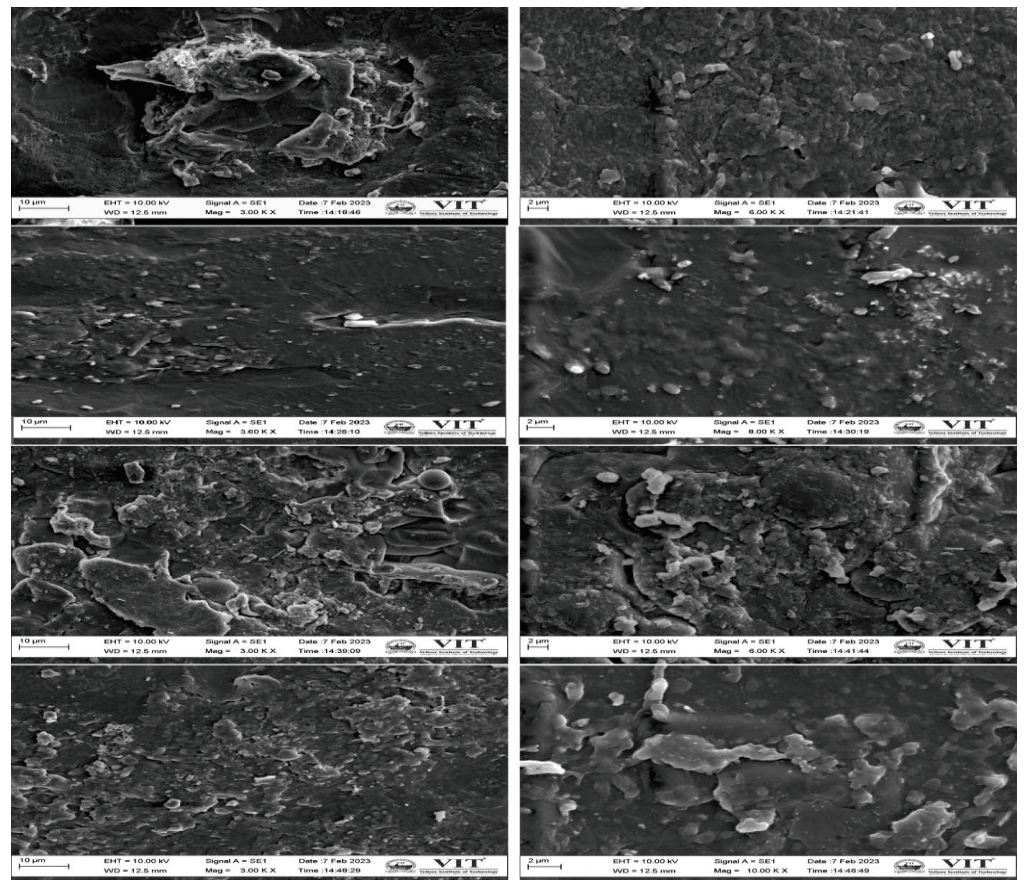
Figure 7 shows the surface morphology of different sets of films. The aggregation of ZnO NPs can be seen as bright spots on the surface of the material when it is viewed under SEM.

The control film displays starch dispersion, and the property of the ZnO NPs caused the nanostructures to disperse well in the solution, thereby preventing the ZnO NPs from aggregating in the film samples. From Figure 7b, it is evident that how much concentration we added into the starch film. The percentage composition of ZnO nano is around 2%. This indicates that the added ZnO nano is very little and the usage of prepared nanoparticles in the polymer matrix is safe for both applications. There were also apparent voids on the broken surface, which contributed to the poor impact and tensile strengths. Amin et al. reported that TiO<sub>2</sub> NPs increased the roughness of the surface of starch bioplastic while decreasing its homogeneity. From this image, it is clear that the NPs agglomerated in the surface creating a rough surface nature. The composite bioplastic has a higher concentration of residual starch particles and non-gelatinized NP granules than starch bioplastic [30]. The surface morphology is altered slightly by the addition of the extract. The ZnO on the surface interacts with the extract and exhibits a similar structure.

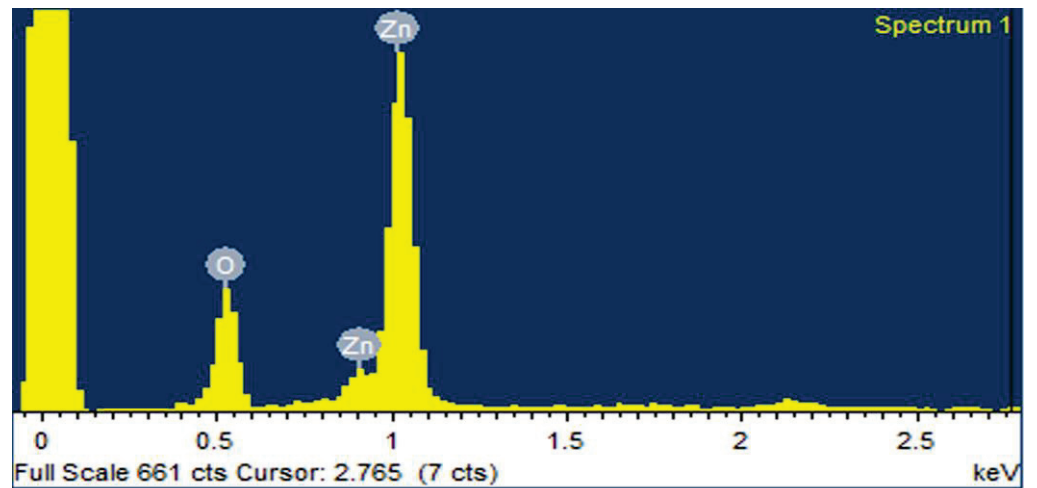
#### 3.4.4. Physical Properties of Film

In order to keep the food's prior form and properties intact, the composite films must be able to withstand the regular pressures that occur during shipping, storage, and application. It is usual practise to utilise tensile strength (TS) and elongation at break (E) to describe the mechanical qualities of the film. These parameters, which represent the strength and flexibility of the film, are strongly related to the physicochemical structure of the film [31,32]. Figure 8 represents the tensile and elongation graph of different films. As per the results, it is evident that the NP addition causes significant changes in the control film. Comparing all the films, the SZ film has high tensile strength. The film solubility value is also depicted in Figure 8. It is evident that the control film has a high percentage of solubility compared to other films. The thickness of the film increased by the addition of ZnO nano is also mentioned in Table 1.





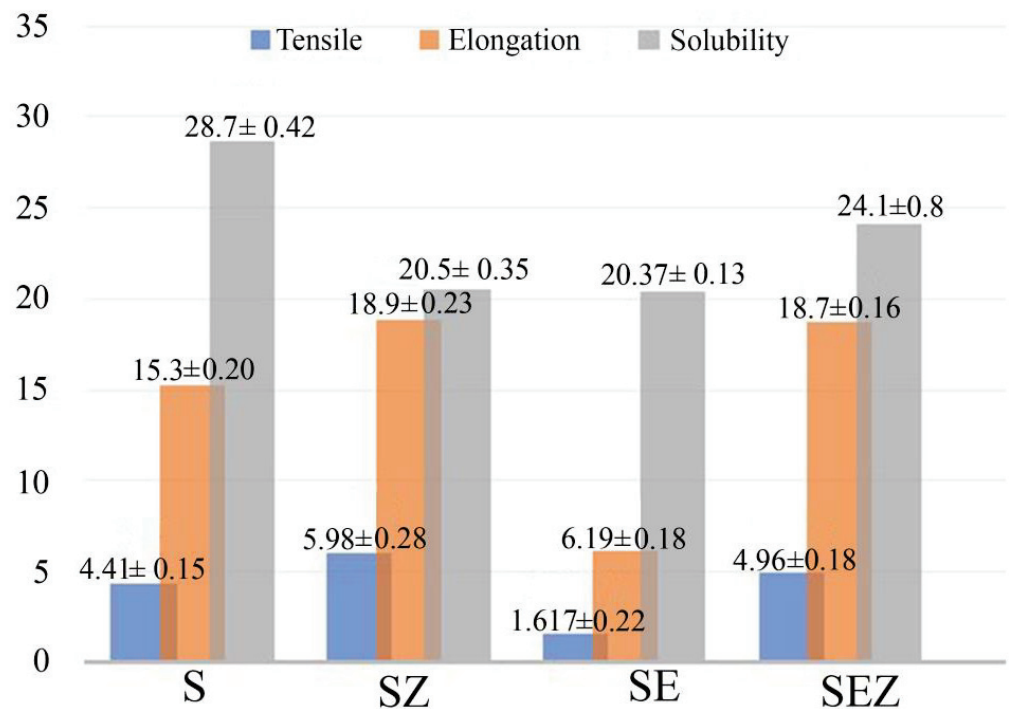
(A)



(B)

Figure 7. (A). SEM image of S, SZ, SE, and SEZ films at 10 μm and 2 μm (B). EDX compositional spectrum of sample SEZ.





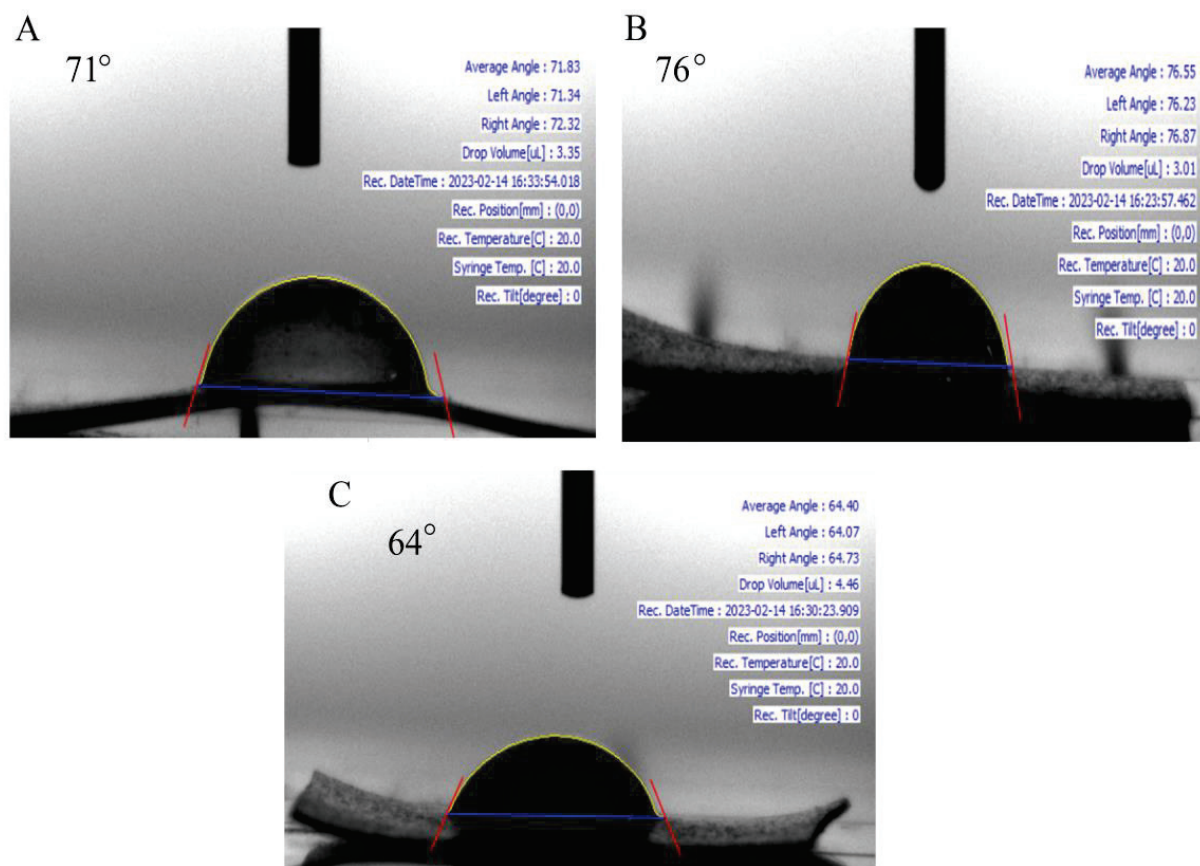
**Figure 8.** Bar graph distinguishing the characteristic features of various films' tensile, elongation of break and water solubility.

**Table 1.** Physical properties of film.

Film	Thickness (mm)	Water Contact Angle ( $\theta$ )
S	0.12 ± 0.15 <sup>c</sup>	71°
SZ	0.24 ± 0.28 <sup>b</sup>	76°
SE	0.18 ± 0.22 <sup>c</sup>	43°
SEZ	0.22 ± 0.18 <sup>b</sup>	64°

### 3.4.5. Water Contact Angle

For measuring the water holding capacity of the prepared polymeric material, the water contact angle were used. Contact angle measurement is used to determine whether the film surface is hydrophilic or hydrophobic in nature. The contact angle ( $\theta$ ) was used to determine where the liquid/vapor interface met the film's surface. In order to take a measurement, some deionized water was introduced to a platform that had a piece of film on it while the temperature was kept at room temperature. The droplets (3–5  $\mu$ L) shown on the surface of the film were generated using a micro-syringe. Wettability requires the biomaterial to possess all of its properties, including the ability to take up water, interact with cells, degrade in vitro and in vivo, etc. When the water contact angle is less than 90°, the solid surface is said to be hydrophilic; whereas, when it is greater than 90°, the surface is said to be hydrophobic [33]. Figure 9 shows the contact angle images of the film specimen. It is found that starch itself has near hydrophobic behaviour and a value of 71°. By adding the extract, the hydrophilic character increased rapidly and the surface of the film bent into a concave shape. It is evident that the addition of nanoparticles increases the overall hydrophobic nature, which corresponds with the value 76°.



**Figure 9.** Contact angle measurement of films (A) S, (B) SZ and (C) SEZ.

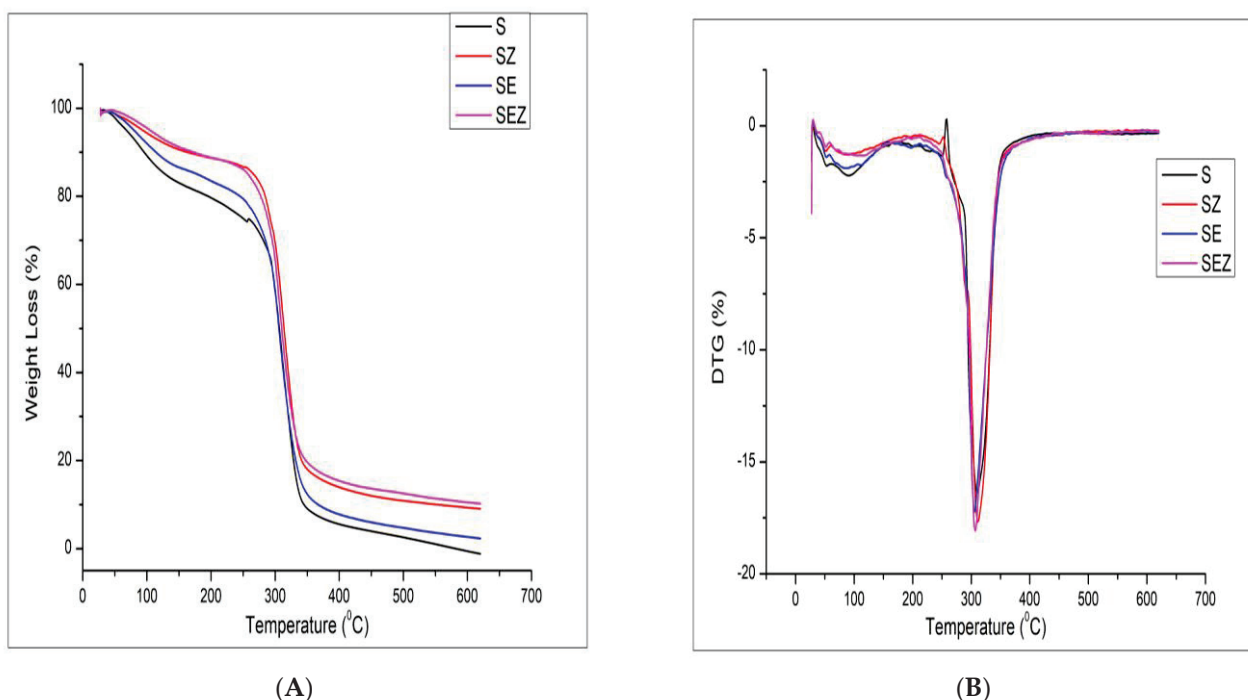
#### 3.4.6. Thermal Decomposition of Polymer Samples

A thermal study of polymers was analysed using a thermogravimetric analyser for evaluating the thermal stabilities and degradation profiles of the starch film. Figure 10 shows the TG and DTG curve of S, SZ, SE and SEZ composites. Starch-based composites exhibit similar weight degradation stages with different residues. The reported results available from the literature say that the TGA curve of thermoplastic starch films exhibited a three-step degradation pattern. The weight loss started from 40 °C due to the evaporation of water and glycerol [34]. The second stage of thermal degradation started at 255 °C, 260 °C, 248 °C and 245 °C for S, SZ, SE and SEZ films, respectively. However, the addition of ZnO enhanced the thermal stability of the starch films to a significant extent. Additionally, the weight loss initially starts with the SE and SEZ films. The DTG curve showed that the maximum weight loss rate of the films occurred at this stage, appearing around 315 °C. Corn starch completely decomposed when the temperature reached 600 °C. The thermal decomposition residue of corn starch was –16.60%.

#### 3.4.7. Colour Values of Film

The colour value of nanocomposites plays an important role in packaged products. Table 2 displays the L, a and b values of S, SZ, SE, and SEZ films. The L\* value of the control film significantly decreases by the addition of nanoparticles and TFE extract (SEZ). By adding glycerol as a plasticizer, the value of L\* lowered. This is due to the fact that the nanoparticle in the film matrix impacts the film's brightness level. Light reflected in minuscule amounts from the NPs surfaces, rendering the film opaque. The a\* value of the control film decreases ( $p < 0.05$ ) by the addition of NP and increases the value by adding 0.5% concentration of TFE extract. The value b\* shows an increase in colour by the addition of ZnO nano. By adding 0.5% extract, the value of a\* increased significantly. The colour

value increased above 17, which means that adding extract and incorporating NPs also affected the yellowness of the film.



**Figure 10.** (A) TGA and (B) DTG (dm/dt) curve of S, SZ, SE, and SEZ films.

**Table 2.** Colour values of S, SZ, SE and SEZ films.

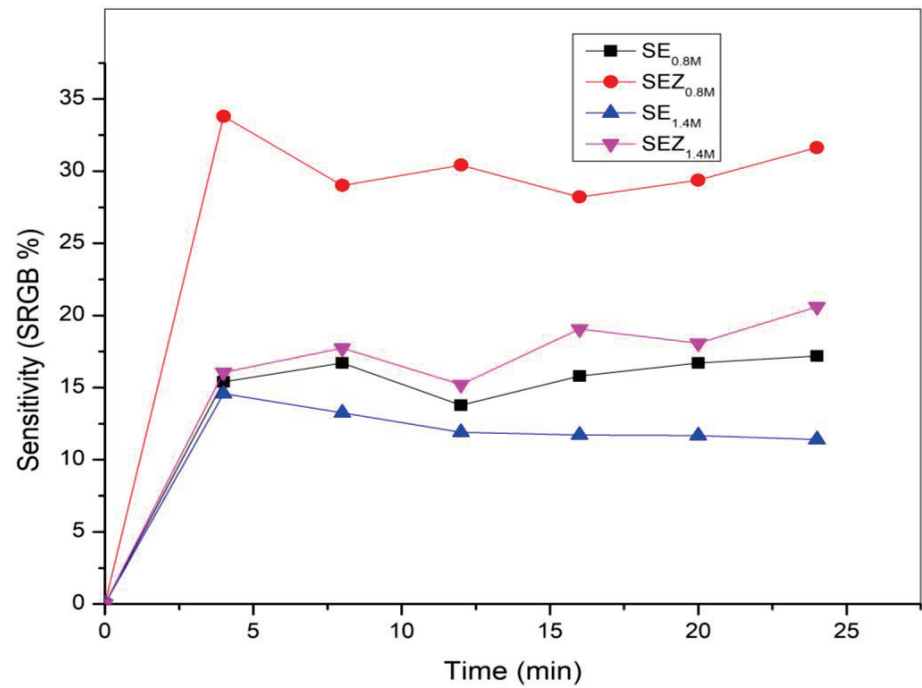
Film	L	a	b	$\Delta E$
S	81.9033 $\pm$ 0.11 <sup>c</sup>	0.13 $\pm$ 0.157 <sup>a</sup>	−4.42 $\pm$ 0.286 <sup>de</sup>	0.303 $\pm$ 0.286 <sup>f</sup>
SZ	80.7033 $\pm$ 0.19 <sup>c</sup>	−0.303 $\pm$ 0.15 <sup>b</sup>	−2.59 $\pm$ 0.026 <sup>ef</sup>	2.367 $\pm$ 0.152 <sup>g</sup>
SE	76.2333 $\pm$ 0.99 <sup>ab</sup>	1.406 $\pm$ 0.306 <sup>c</sup>	2.59 $\pm$ 0.94 <sup>f</sup>	9.196 $\pm$ 0.647 <sup>h</sup>
SEZ	70.680 $\pm$ 1.7 <sup>ab</sup>	0.3667 $\pm$ 0.295 <sup>d</sup>	17.01 $\pm$ 1.37 <sup>b</sup>	24.298 $\pm$ 2.01 <sup>e</sup>

<sup>a–h</sup> Values are displayed as a function of standard deviation divided by mean. Any two means that are separated by the same letter in the same column have no statistically significant difference between them ( $p > 0.05$ ).

#### 3.4.8. Ammonia Sensitivity and Freshness Indicators for Film Samples

Figure 11A displays the SRGB value of different films taken every 4 min. Figure 11C shows the colour change of films after immersing into a bottle containing ammonia vapour with two different concentrations.

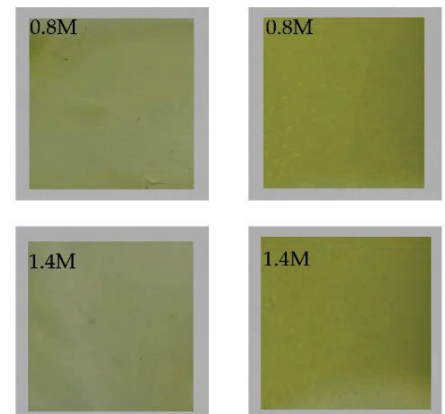
As expected, after exposing, the colour of the film changes to green. The SRGB value of SEZ film in 0.8 M increases up to 33.8% and declined slightly and maintained 31.63% after 24 min. Comparing with 1.4 M concentration, the SRGB value of the SEZ film colour slightly reduced. This indicates that, at a high concentration, the SRGB value shows some difference in colour parameters. It is evident that, without NPs, the SRGB value of the functional film (SE0.8M and SE1.4M) is low.



(A)



(B)



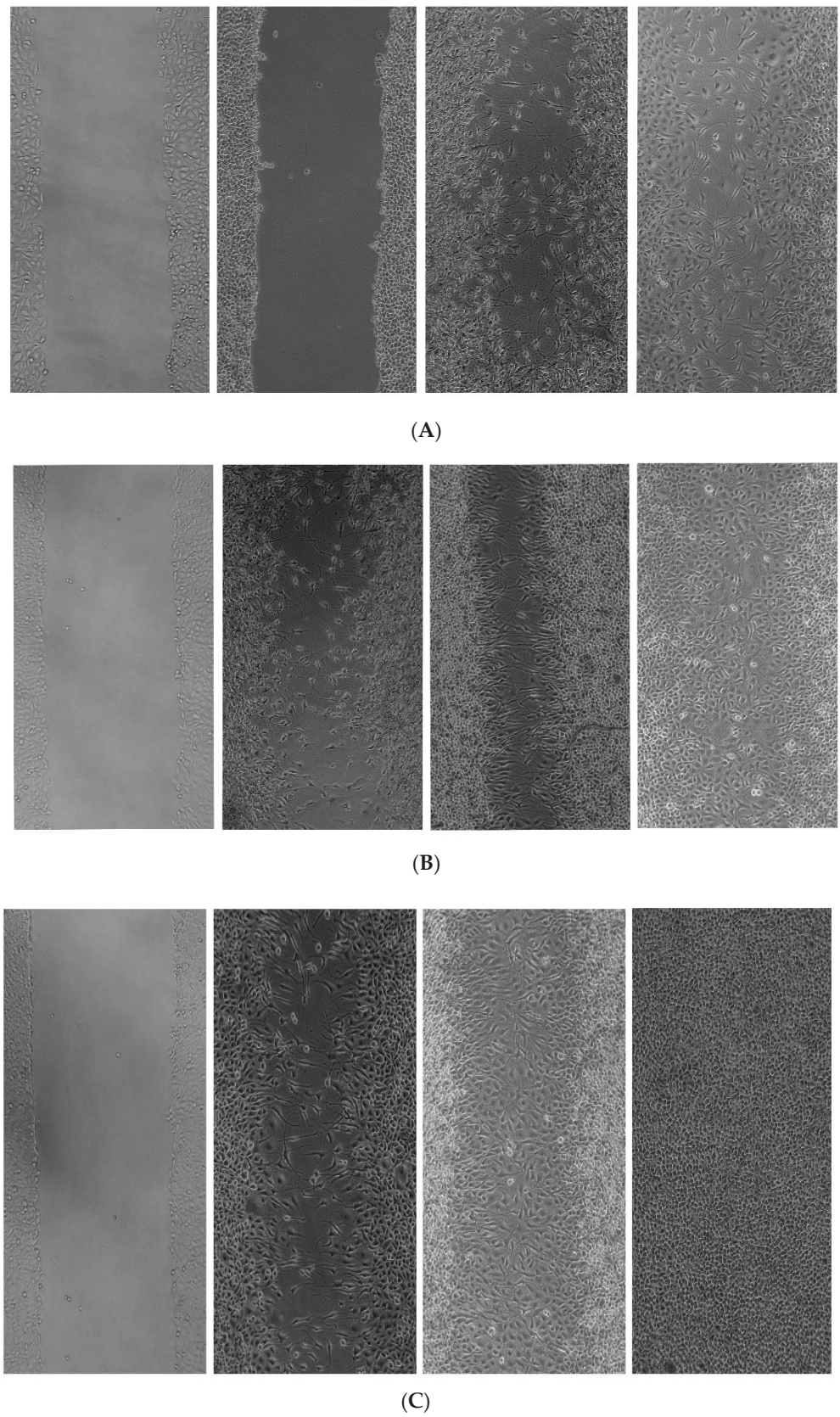
(C)

**Figure 11.** (A) Ammonia sensitivity at two different concentrations. (B) Spoilage analysis of chicken sample with film as freshness indicator. (C) Colour change of films after immersing into ammonia vapour with two different concentrations.

### 3.4.9. In Vitro Scratch Wound Healing Assay

Figure 12 shows the in vitro wound healing activity of SEZ composite film. As shown by the photomicrographs, the sample SEZ was discovered to possess a significant wound healing efficacy, which was confirmed by the observations. It was revealed that the efficacy of wound healing was dependent on both the concentration and the amount of time. At a concentration of 100 g/mL and for a period of time lasting 36 h, the medication's effectiveness was found to be at its highest. This is a sign that the sample has the potential to be successfully developed therapeutically as a wound healing agent, or that it can be applied to human cells even when there are scratches or wounds present.





**Figure 12.** Scratch wound healing activity of SEZ film with three different concentration 25, 50, and 100 µg/mL at (A) 12 h, (B) 24 h and (C) 36 h.



#### 4. Conclusions

By integrating anthocyanin derived from *Torenia Fourieni* with ZnO, this research was able to successfully construct intelligent pH-sensitive starch-based films. It was noticed that the incorporation of TFE and ZnO into the films could result in a significant shift in the films' physical properties (colour, thickness, tensile strength). Hydrophobic antioxidant species can be added to films without sacrificing mechanical qualities and while boosting barrier properties if they are adequately disseminated throughout the film matrix, which requires good hydrogen-bonding with starch or encapsulation in a hydrophilic species. The prepared material is effectively useful for wound care applications. The trial for using the SEZ film (S/TFE/ZnO) as a freshness monitor showed that the colour changes noticeably from a light yellowish colour (the fresh stage) to a bright green colour (beginning of spoilage). We could distinguish the colour with the naked eye. The change in colour is caused by basic compounds that form as the food goes bad and raise the pH of the sample. Therefore, these smart films can be used to make pH indicator films that are safe and good for the environment. This is a promising alternative for society, but each sector needs to put in more effort to separate out these many applications and uses of the material.

**Author Contributions:** Conceptualization, investigation and supervision, D.S.; visualization and supervision, A.A.P.; writing—original draft preparation, methodology and validation, J.T.K.; software and validation, D.V. All authors have read and agreed to the published version of the manuscript.

**Funding:** This research received no external funding.

**Institutional Review Board Statement:** This investigation was conducted in accordance with the guidelines. Dr. Sreekumar V B, Head of the Department, Forest of Botany, KSCSTE-Kerala Forest Research Institute in Thrissur, Kerala, India, authorized the plant *Torenia fournieri* Lind. Ex. Fourn.(KFRI Accession number: 19347) and issued the authentication certificate. Scratch wound healing assay performed with L929 cell line. The L929 cell line (Murine fibroblast cells) was procured from National Centre for cell science (NCSS), Pune, India. Details regarding Plant Authentication documents have been included in the manuscript.

**Data Availability Statement:** Not applicable.

**Acknowledgments:** The authors gratefully acknowledge Vellore Institute of Technology, India for research facilities.

**Conflicts of Interest:** The authors declare no conflict of interest.

#### References

1. Harussani, M.M.; Sapuan, S.M.; Firdaus, A.H.M.; El-Badry, Y.A.; Hussein, E.E.; El-Bahy, Z.M. Determination of the Tensile Properties and Biodegradability of Cornstarch-Based Biopolymers Plasticized with Sorbitol and Glycerol. *Polymers* **2021**, *13*, 3709. [CrossRef] [PubMed]
2. Kumar, M.; Hilles, A.R.; Ge, Y.; Bhatia, A.; Mahmood, S. A Review on Polysaccharides Mediated Electrospun Nanofibers for Diabetic Wound Healing: Their Current Status with Regulatory Perspective. *Int. J. Biol. Macromol.* **2023**, *234*, 123696. [CrossRef]
3. Suppakul, P.; Miltz, J.; Sonneveld, K.; Bigger, S.W. Active Packaging Technologies with an Emphasis on Antimicrobial Packaging and Its Applications. *J. Food Sci.* **2003**, *68*, 408–420. [CrossRef]
4. Mahieu, A.; Terrié, C.; Youssef, B. Thermoplastic Starch Films and Thermoplastic Starch/Polycaprolactone Blends with Oxygen-Scavenging Properties: Influence of Water Content. *Ind. Crop. Prod.* **2015**, *72*, 192–199. [CrossRef]
5. Aider, M. Chitosan Application for Active Bio-Based Films Production and Potential in the Food Industry: Review. *LWT* **2010**, *43*, 837–842. [CrossRef]
6. Dutta, P.K.; Tripathi, S.; Mehrotra, G.K.; Dutta, J. Perspectives for Chitosan Based Antimicrobial Films in Food Applications. *Food Chem.* **2009**, *114*, 1173–1182. [CrossRef]
7. Koshy, R.R.; Koshy, J.T.; Mary, S.K.; Sadanandan, S.; Jisha, S.; Pothan, L.A. Preparation of PH Sensitive Film Based on Starch/Carbon Nano Dots Incorporating Anthocyanin for Monitoring Spoilage of Pork. *Food Control.* **2021**, *126*, 108039. [CrossRef]
8. Roy, S.; Ezati, P.; Rhim, J.-W. Gelatin/Carrageenan-Based Functional Films with Carbon Dots from Enoki Mushroom for Active Food Packaging Applications. *ACS Appl. Polym. Mater.* **2021**, *3*, 6437–6445. [CrossRef]
9. Shah, U.; Naqash, F.; Gani, A.; Masoodi, F.A. Art and Science behind Modified Starch Edible Films and Coatings: A Review. *Compr. Rev. Food Sci. Food Saf.* **2016**, *15*, 568–580. [CrossRef]

10. Garcia, N.L.; Fama, L.; Accorso, N.B.D.; Goyanes, S. *Biodegradable Starch Nanocomposites*; Springer: New Delhi, India, 2015; pp. 17–77.
11. Santacruz, S.; Rivadeneira, C.; Castro, M. Edible Films Based on Starch and Chitosan. Effect of Starch Source and Concentration, Plasticizer, Surfactant's Hydrophobic Tail and Mechanical Treatment. *Food Hydrocoll.* **2015**, *49*, 89–94. [CrossRef]
12. Pinzon, M.I.; Sanchez, L.T.; Garcia, O.R.; Gutierrez, R.; Luna, J.C.; Villa, C.C. Increasing Shelf Life of Strawberries (*Fragaria Ssp*) by Using a Banana Starch-chitosan-Aloe Vera Gel Composite Edible Coating. *Int. J. Food Sci. Technol.* **2020**, *55*, 92–98. [CrossRef]
13. Tabatabaei, R.H.; Jafari, S.M.; Mirzaei, H.; Nafchi, A.M.; Dehnad, D. Preparation and Characterization of Nano-SiO<sub>2</sub> Reinforced Gelatin-κ-Carrageenan Biocomposites. *Int. J. Biol. Macromol.* **2018**, *111*, 1091–1099. [CrossRef] [PubMed]
14. Ghizdareanu, A.-I.; Pasarin, D.; Banu, A.; Afilipoaei, I.; Enascuta, C.E.; Vlaicu, A. Accelerated Shelf-Life and Stability Testing of Hydrolyzed Corn Starch Films. *Polymers* **2023**, *15*, 889. [CrossRef]
15. Shankar, S.; Teng, X.; Li, G.; Rhim, J.-W. Preparation, Characterization, and Antimicrobial Activity of Gelatin/ZnO Nanocomposite Films. *Food Hydrocoll.* **2015**, *45*, 264–271. [CrossRef]
16. Roy, S.; Rhim, J.-W. Carboxymethyl Cellulose-Based Antioxidant and Antimicrobial Active Packaging Film Incorporated with Curcumin and Zinc Oxide. *Int. J. Biol. Macromol.* **2020**, *148*, 666–676. [CrossRef]
17. Díez-Pascual, A.M.; Díez-Vicente, A.L. ZnO-Reinforced Poly(3-Hydroxybutyrate-Co-3-Hydroxyvalerate) Bionanocomposites with Antimicrobial Function for Food Packaging. *ACS Appl. Mater. Interfaces* **2014**, *6*, 9822–9834. [CrossRef]
18. Espitia, P.J.P.; de Fátima Ferreira Soares, N.; dos Reis Coimbra, J.S.; De Andrade, N.J.; Cruz, R.S.; Medeiros, E.A.A. Zinc Oxide Nanoparticles: Synthesis, Antimicrobial Activity and Food Packaging Applications. *Food Bioproc. Technol.* **2012**, *5*, 1447–1464. [CrossRef]
19. Arifin, H.R.; Djali, M.; Nurhadi, B.; Azlin-Hasim, S.; Masruchin, N.; Vania, P.A.; Hilmi, A. Corn Starch-Based Bionanocomposite Film Reinforced with ZnO Nanoparticles and Different Types of Plasticizers. *Front. Sustain. Food Syst.* **2022**, *6*, 248. [CrossRef]
20. Shindo, K.; Saito, E.; Sekiya, M.; Matsui, T.; Koike, Y. Antioxidative Activity of the Flower of *Torenia Fournieri*. *J. Nat. Med.* **2008**, *62*, 247–248. [CrossRef] [PubMed]
21. Xie, F.; Pollet, E.; Halley, P.J.; Avérous, L. Starch-Based Nano-Biocomposites. *Prog. Polym. Sci.* **2013**, *38*, 1590–1628. [CrossRef]
22. Lan, C.; Yu, L.; Chen, P.; Chen, L.; Zou, W.; Simon, G.; Zhang, X. Design, Preparation and Characterization of Self-Reinforced Starch Films through Chemical Modification. *Macromol. Mater. Eng.* **2010**, *295*, 1025–1030. [CrossRef]
23. Liu, Y.; Qin, Y.; Bai, R.; Zhang, X.; Yuan, L.; Liu, J. Preparation of PH-Sensitive and Antioxidant Packaging Films Based on κ-Carrageenan and Mulberry Polyphenolic Extract. *Int. J. Biol. Macromol.* **2019**, *134*, 993–1001. [CrossRef] [PubMed]
24. Lin, L.; Peng, S.; Shi, C.; Li, C.; Hua, Z.; Cui, H. Preparation and Characterization of Cassava Starch/Sodium Carboxymethyl Cellulose Edible Film Incorporating Apple Polyphenols. *Int. J. Biol. Macromol.* **2022**, *212*, 155–164. [CrossRef] [PubMed]
25. Raj, V.J.; Ghosh, R.; Girigoswami, A.; Girigoswami, K. Application of Zinc Oxide Nanoflowers in Environmental and Biomedical Science. *BBA Adv.* **2022**, *2*, 100051. [CrossRef]
26. Saif, M.S.; Zafar, A.; Waqas, M.; Hassan, S.G.; Haq, A.U.; Tariq, T.; Batool, S.; Dilshad, M.; Hasan, M.; Shu, X. Phyto-Reflexive Zinc Oxide Nano-Flowers Synthesis: An Advanced Photocatalytic Degradation and Infectious Therapy. *J. Mater. Res. Technol.* **2021**, *13*, 2375–2391. [CrossRef]
27. Elsayed, M.S.; Ahmed, I.A.; Bader, D.M.D.; Hassan, A.F. Green Synthesis of Nano Zinc Oxide/Nanohydroxyapatite Composites Using Date Palm Pits Extract and Eggshells: Adsorption and Photocatalytic Degradation of Methylene Blue. *Nanomaterials* **2021**, *12*, 49. [CrossRef]
28. Nishihara, M.; Higuchi, A.; Watanabe, A.; Tasaki, K. Application of the CRISPR/Cas9 System for Modification of Flower Color in *Torenia Fournieri*. *BMC Plant Biol.* **2018**, *18*, 331. [CrossRef]
29. Shahabi-Ghahfarrokhi, I.; Babaei-Ghazvini, A. Using Photo-Modification to Compatibilize Nano-ZnO in Development of Starch-Kefiran-ZnO Green Nanocomposite as Food Packaging Material. *Int. J. Biol. Macromol.* **2019**, *124*, 922–930. [CrossRef]
30. Amin, R.; Chowdhury, M.A.; Kowser, A. Characterization and Performance Analysis of Composite Bioplastics Synthesized Using Titanium Dioxide Nanoparticles with Corn Starch. *Heliyon* **2019**, *5*, e02009. [CrossRef]
31. Acevedo-Fani, A.; Salvia-Trujillo, L.; Rojas-Graü, M.A.; Martín-Belloso, O. Edible Films from Essential-Oil-Loaded Nanoemulsions: Physicochemical Characterization and Antimicrobial Properties. *Food Hydrocoll.* **2015**, *47*, 168–177. [CrossRef]
32. Talón, E.; Trifkovic, K.T.; Nedovic, V.A.; Bugarski, B.M.; Vargas, M.; Chiralt, A.; González-Martínez, C. Antioxidant Edible Films Based on Chitosan and Starch Containing Polyphenols from Thyme Extracts. *Carbohydr. Polym.* **2017**, *157*, 1153–1161. [CrossRef] [PubMed]
33. Koshy, J.; Sangeetha, D. Hemigraphis Alternata Leaf Extract Incorporated Agar/Pectin-Based Bio-Engineered Wound Dressing Materials for Effective Skin Cancer Wound Care Therapy. *Polymers* **2022**, *15*, 115. [CrossRef] [PubMed]
34. Mary, S.K.; Koshy, R.R.; Daniel, J.; Koshy, J.T.; Pothen, L.A.; Thomas, S. Development of Starch Based Intelligent Films by Incorporating Anthocyanins of Butterfly Pea Flower and TiO<sub>2</sub> and Their Applicability as Freshness Sensors for Prawns during Storage. *RSC Adv.* **2020**, *10*, 39822–39830. [CrossRef] [PubMed]

**Disclaimer/Publisher's Note:** The statements, opinions and data contained in all publications are solely those of the individual author(s) and contributor(s) and not of MDPI and/or the editor(s). MDPI and/or the editor(s) disclaim responsibility for any injury to people or property resulting from any ideas, methods, instructions or products referred to in the content.

## Article

# Carboxymethyl Cellulose/Gelatin Hydrogel Films Loaded with Zinc Oxide Nanoparticles for Sustainable Food Packaging Applications

Aqsa Zafar <sup>1</sup>, Muhammad Kaleem Khosa <sup>1,\*</sup>, Awal Noor <sup>2,\*</sup>, Sadaf Qayyum <sup>2</sup> and Muhammad Jawwad Saif <sup>3</sup><sup>1</sup> Department of Chemistry, Government College University, Faisalabad 38000, Pakistan<sup>2</sup> Department of Basic Sciences, Preparatory Year Deanship, King Faisal University, Al-Hassa 31982, Saudi Arabia<sup>3</sup> Department of Applied Chemistry, Government College University, Faisalabad 38000, Pakistan

\* Correspondence: mkhosapk@yahoo.com (M.K.K.); anoor@kfu.edu.sa (A.N.)

**Abstract:** The current research work presented the synthesis of carboxymethyl cellulose–gelatin (CMC/GEL) blend and CMC/GEL/ZnO-Nps hydrogel films which were characterized by FT-IR and XRD, and applied to antibacterial and antioxidant activities for food preservation as well as for biomedical applications. ZnO-Nps were incorporated into the carboxymethyl cellulose (CMC) and gelatin (GEL) film-forming solution by solution casting followed by sonication. Homogenous mixing of ZnO-Nps with CMC/GEL blend improved thermal stability, mechanical properties, and moisture content of the neat CMC/GEL films. Further, a significant improvement was observed in the antibacterial activity and antioxidant properties of CMC/GEL/ZnO films against two food pathogens, *Staphylococcus aureus* and *Escherichia coli*. Overall, CMC/GEL/ZnO films are eco-friendly and can be applied in sustainable food packaging materials.

**Keywords:** hydrogel films; gelatin; antimicrobial activity; food packaging; TGA

**Citation:** Zafar, A.; Khosa, M.K.; Noor, A.; Qayyum, S.; Saif, M.J. Carboxymethyl Cellulose/Gelatin Hydrogel Films Loaded with Zinc Oxide Nanoparticles for Sustainable Food Packaging Applications. *Polymers* **2022**, *14*, 5201. <https://doi.org/10.3390/polym14235201>

Academic Editor: Raffaella Striani

Received: 23 October 2022

Accepted: 25 November 2022

Published: 29 November 2022



**Copyright:** © 2022 by the authors. Licensee MDPI, Basel, Switzerland. This article is an open access article distributed under the terms and conditions of the Creative Commons Attribution (CC BY) license (<https://creativecommons.org/licenses/by/4.0/>).

## 1. Introduction

Today, food packaging is a growing technology because of rapid advancements in the fields of biopolymers and materials science. They are being used as new modes of food coatings. Encapsulation of biopolymers matrices, and food packaging materials for functional foods, proteins and polysaccharides have gained a lot of attention recently [1–3]. Active packaging is thought to be the best way to increase the safety and shelf life of food [4]. The presence of antimicrobial agents and antioxidants in active packaging plays a vital role in stopping biological or chemical changes and microbial growth in packaged foods [5]. In addition to antimicrobial agents, antioxidants, essential oils, natural pigments, and plant extracts have also been used in packaging materials [6]. Inorganic materials such as nano-sized metals, metal salts, and metal oxides seem promising for this purpose and are frequently used as antibacterial agents [7,8]. The incorporation of metal nanoparticles (ZnO, TiO<sub>2</sub> and silica) into composite films has resulted in nanocomposites that are light in weight, stronger in thermomechanical performance, fire resistant, and less permeable to gases. They also reduce the flow of oxygen inside packaging containers when added to plastic films. To keep food fresh for a very long time, they serve as a barrier against gases and moisture [9]. The many properties of packaging materials are greatly enhanced by nanomaterials, which have a significant impact on the food packaging industry. One of the most significant categories of nanomaterials is zinc oxide nanoparticles to improve thermomechanical and antimicrobial properties [10]. Zinc oxide nanoparticles are now widely available commercially and are easy to be used directly due to their outstanding antibacterial properties, high thermal stability, excellent mechanical properties, and heat resistivity [11–13]. Tetrapod-shaped ZnO nanomaterials have recently been reported to

inhibit herpes simplex virus (HSV) infection. It exhibits adjuvant-like properties, improves viral presentation to dendritic cells, and boosts humoral and cell-mediated immunity. ZnO-Nps have been evaluated for their antiviral properties against HSV-1, HSV-2, and influenza. This is primarily because ZnO nanoparticles have the ability to modulate the immune system [14,15]. As packaging materials and coating agents, natural polymers have numerous other uses. In the pharmaceutical sector, gelatin is commonly employed as an absorbent sheet, a wound dressing, an adhesive, and as an excipient in controlled drug delivery [16]. Several studies have shown that combining gelatin with polysaccharides, including alginate, chitosan, hyaluronic acid and other proteins, can enhance its properties due to their permeability and self-adhesiveness, as well as their capacity to form chemical and physical hydrogel films. They also serve as drug delivery and tissue regeneration support matrices. Cellulose is another biopolymer that is plentiful, renewable, and biodegradable and has been used to prepare biocompatible composite films [17]. Carboxymethyl cellulose (CMC), a cellulose derivative, has been extensively applied in cellular growth, food processing, food packaging, the pharmaceutical industry, and medical fields because of its good hydrophilicity, biocompatibility, and film formability [18,19]. The basic requirements for materials used in packaging are that they have good mechanical and thermal performance, protection against gases, and transparency. Therefore, the aim of the current research was to fabricate carboxymethyl cellulose and gelatin-based films using ZnO nanoparticles as a functional material. After characterization by FT-IR and XRD, CMC/GEL/ZnO composite films were investigated for the water vapor permeability (WVP), moisture contents, thermal and mechanical stability, antimicrobial activity, and free radical inhibition activity.

## 2. Materials and Methods

### 2.1. Chemicals

Gelatin powder (Food grade; Halal), carboxymethyl cellulose (CMC: pKa =3.5, with medium viscosity; Mw. 90,000), glutaraldehyde (GTA), sodium azide, zinc nitrate hexahydrate ( $\text{Zn}(\text{NO}_3)_2 \cdot 6\text{H}_2\text{O}$ ), 2,2-diphenyl-1-picrylhydrazyl (DPPH), iron sulphate ( $\text{FeSO}_4$ ), 2,2-azino-bis-(3-ethylbenzothiazoline-6-sulfonic acid) (ABTS) and ferric chloride ( $\text{FeCl}_3$ ) were used as received. All chemicals were procured from Sigma-Aldrich Pakistan.

### 2.2. Chemical Characterization

For major functional groups and shifting of absorption bands in synthesized CMC/GEL/ZnO-nanocomposite films, IR spectrophotometer (Bruker) was used, and spectra were recorded in  $4000\text{--}400\text{ cm}^{-1}$ . TGA was determined, under nitrogen from room temperature to  $700\text{ }^\circ\text{C}$ , using Netzsch and Perkin Elmer TGA-7. Tensile strength and % elongation were determined by DMA Q800 V21.3 Build 96. Surface morphology was examined (FEI-NOVA Nano SEM-450, Hillsboro, OR, USA) by using Chroma meter (Konica Minolta, CR-400, Tokyo, Japan) with white standard colour plate ( $L_o = 92.15$ ,  $a_o = -0.41$ , and  $b_o = 4.55$ ) as a background, of surface colour (Hunter L, a, and b-values).

### 2.3. Green Synthesis of ZnO-Nps

Green chemistry is extensively used in research and is considered eco-friendly because it uses plant phytochemicals to prepare nanoparticles. Keeping this in mind, ZnO-Nps (<50 nm) were prepared using mint (*Mentha longifolia*) leaf extract. Fresh mint leaves were cleaned by washing with distilled water and were ground until very fine particle sizes were obtained, and were then air dried. About 10 g of fine powdered mint leaves in distilled water (250 mL) were heated at  $70\text{ }^\circ\text{C}$ . After cooling at room temperature for about 30–40 min, the heavy biomaterial that settled down after centrifugation at 4000 rpm was removed by filtration. The clear solution of mint extract was then stored at  $4\text{ }^\circ\text{C}$  and used for the preparation of nanoparticles. Following that, zinc oxide nanoparticles (50 nm) were prepared using mint leaves extract as an oxidizing agent as per the literature with slight modifications [20]. A mixture of 100 mL zinc nitrate Solution (0.01 M) and



30 mL of mint leave extract was heated at 60 °C with constant stirring until the bio-reduced ZnO nanoparticles settled down as white precipitates. The resulting, white-colored precipitates were dried at 80 °C for approximately six hours before being calcined at 600 °C for approximately two hours.

#### 2.4. Fabrication of Carboxymethyl Cellulose-Gelatin-ZnO Composite Films

To prepare carboxymethyl cellulose-gelatin-ZnO (CMC/GEL/ZnO) hydrogel films, the process of solution casting was employed for CMC/GEL (75:25). Briefly, CMC and GEL solutions (2% *w/v*) were mixed at 40 °C for 4 h along with 1 mL of glutaraldehyde as a crosslinking agent and 0.02% sodium azide to stop the bacterial growth. The CMC/GEL solutions were then slowly mixed with ZnO nanoparticles (1, 1.5, 2, 2.5 *w/w*) by sonication for two hours to obtain a clear solution. Then 10 mL of CMC/GEL/ZnO composite solution was poured into Teflon-made boats and dried at 25 °C. The films were peeled then off after drying in an oven at 70 °C for about twelve hours [21].

#### 2.5. Moisture Contents and Water Vapor Permeability

To determine the moisture contents (MC), each CMC/GEL/ZnO nanocomposite film was cut into 2.5 × 2.5 cm square sizes and dried in an oven at 70 °C for about twelve hours. The difference in final and initial weight of film was noted as a moisture content. Whereas water vapor permeability (WVP) was determined gravimetrically. For this purpose, square-shaped pieces (6 × 6 cm) of the film were mounted on top of water vapor permeability measuring cups horizontally, having water (20 mL) and placed in the oven at 50 °C. The weight of the cups was noted at regular intervals of 30 min during twelve hours. [22]. After that WVP was calculated as:

$$WVP = \frac{(WVTR \times L)}{\Delta p} \quad (1)$$

Here, WVTR: rate of water vapor transmission ( $\text{g}/\text{m}^2 \cdot \text{s}$ ),

L: film thickness (m),  $\Delta p$ : partial water vapor pressure differential across the film.

#### 2.6. Antimicrobial Assay

Six pathogens were tested using neat CMC, GEL, CMC/GEL, and CMC/GEL/ZnO nanocomposite films. Three of which were gram-positive: *Staphylococcus aureus* (ATCC 6538), *Bacillus subtilis* (ATCC 6633), and *Listeria monocytogenes* (ATCC 19111), and three of which were gram-negative: *Enterobacter aerogenase* (ATCC 13048), *Escherichia coli* (ATCC 15224), and *Bordetella bronchiseptica* (ATCC 4617). Briefly, bacterial strains were cultured for about 24 h in agar-agar nutrient broth at 37 °C. 1.5 mL of the broth culture of bacterial strains  $10^4$ – $10^6$  (CFU/mL). In Petri dishes that had been sterilized, strains were added to an agar-agar medium and allowed to set at 45 °C. The solutions of CMC, GEL, CMC/GEL, and CMC/GEL/ZnO nanocomposite films in DMSO (10 mg/mL) were then added to each well. Each bacterial strain was prepared in triplicate and was incubated for about 24 h at 37 °C. By measuring the size of the inhibition zone, antibacterial activity was calculated (mm). Cefixime (1 mg/mL), a standard antibiotic, was used as a positive control [23,24].

#### 2.7. Antioxidant Assays

The DPPH method was used to measure activity that scavenges free radicals of neat CMC, neat GEL, CMC/GEL, and CMC/GEL/ZnO nanocomposite films [25]. Stock solutions (5 mg/mL) of neat CMC, GEL, and nanocomposite films were made in DMSO. Serial dilutions of 5, 10, 20, 40, 100, and 200 g/mL were performed. In glass vials, 15  $\mu\text{L}$  of each film solution and solution of DPPH (0.1 mM) were mixed together and diluted to 3 mL with methanol. For about 45 min, the reaction mixture was incubated at 37 °C in a dark chamber; this caused the DPPH solution's color to change from deep violet to light yellow. At 517 nm, absorbance was noted by using a spectrophotometer. A standard, butylated hydroxyanisole, was used for each experiment, which was carried out in triplicate (BHA,



5 mg/mL). The decreased absorbance of the mixture indicated higher radical inhibition activity. The % age of scavenging activity was calculated as:

$$\% \text{ scavenging activity} = \frac{\text{absorbance of control} - \text{absorbance of test sample}}{\text{absorbance of control}} \times 100$$

### 3. Statistical Analysis

The obtained data were verified statistically by applying ANOVA using Minitab Software. Each experiment was carried out in triplicate. The statistical significance value was tested at  $p < 0.05$ .

## 4. Results and Discussion

### 4.1. IR Investigation

The FT-IR absorption spectra of neat carboxymethyl cellulose, gelatin, CMC/GEL/glutaraldehyde, and CMC/GEL/ZnO nanocomposites are shown in Figure 1. Peak positions and modes of interaction are presented in Table 1. The crosslinking between CMC/GEL and ZnO-Nps was responsible for the majority of the changes in absorption frequencies that were seen. The bands at 2910, 1600, and 1440  $\text{cm}^{-1}$  in CMC are due to stretching vibrations of aliphatic C-H,  $(-\text{COO})_{\text{asy}}$ , and  $(-\text{COO})_{\text{sym}}$ , respectively (Figure 1a). The absorption bands of glucosidic units (C-O-C) appeared at 1160 and 1070  $\text{cm}^{-1}$ . A broad absorption band at 3390  $\text{cm}^{-1}$  was attributed to the hydrogen bonding of OH groups of absorbed water and secondary alcohols (CMC) [26,27]. Absorption bands at 3390 and 3315  $\text{cm}^{-1}$  correspond to the hydroxyl and amino groups of gelatin film, respectively (Figure 1b). The absorption bands at 1649 and 1551  $\text{cm}^{-1}$  are due to the (C=O) and (C-N) absorption bands of amide I and amide II in the gelatin structure. The interaction of CMC's anionic groups with the gelatin's cationic groups was confirmed by the shifting of peaks from 3315, 1450 to 3328, 1460  $\text{cm}^{-1}$  (Figure 1c). The absorption band of the C-H group has been shifted from 2910 to 2955  $\text{cm}^{-1}$  in CMC/Gel/GTA (Figure 1d). The reaction of GTA with CMC/GEL was confirmed by an absorption band below 1210  $\text{cm}^{-1}$  forming a hemiacetal structure. Similarly, homogenous mixing of ZnO-Nps with CMC/GEL film (Figure 1e) was confirmed by an absorption peak at 470  $\text{cm}^{-1}$  [28].

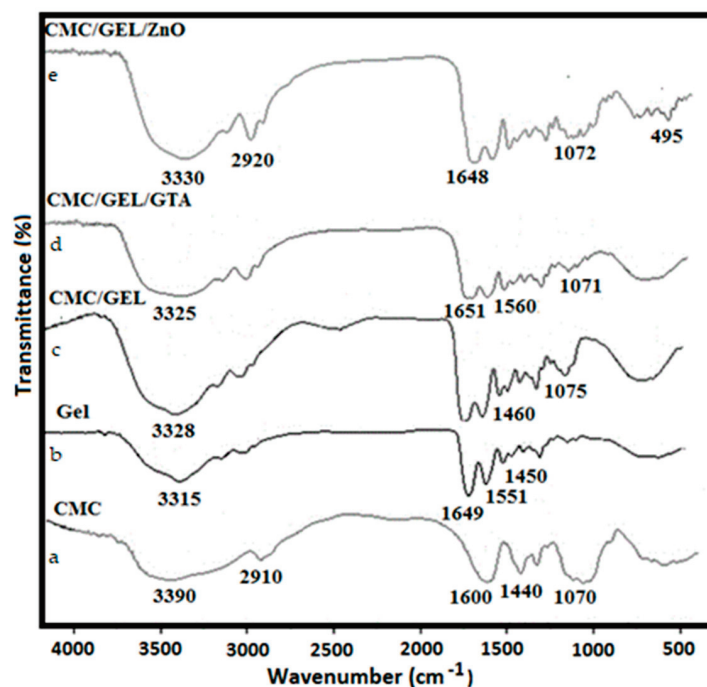


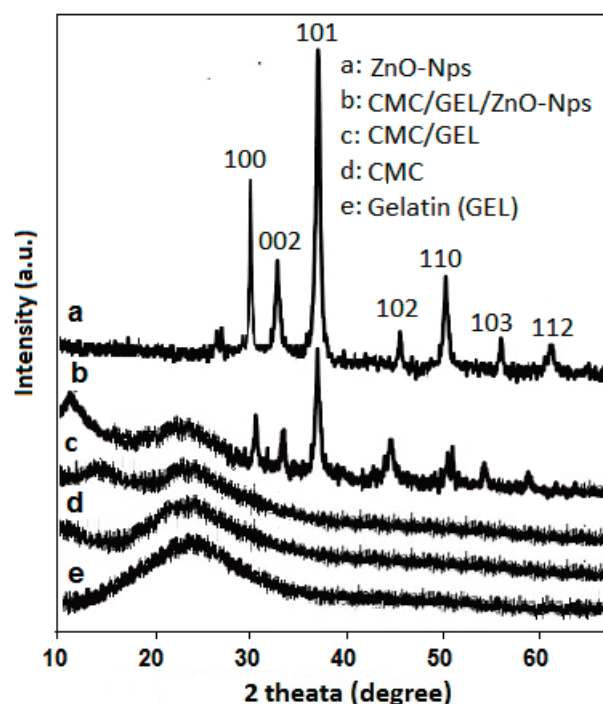
Figure 1. FT-IR Spectra of CMC/Gel/ZnO-Nps hydrogel films: (a) CMC, (b) Gel, (c) CMC/GEL, (d) CMC/GEL/GTA, (e) CMC/GEL/ZnO.

**Table 1.** Peak positions and vibration modes in CMC/GEL/ZnO nanocomposites hydrogels.

Wavenumber (cm <sup>-1</sup> )	Assignment	Ref.	Wavenumber (cm <sup>-1</sup> )	Assignment	Ref.
3350–3390	Stretching vibration of -OH group	[22]	1400–1460	(COO) <sub>sym</sub>	[24]
2910–2920	Asym. -CH <sub>2</sub> stretching	[23,24]	1160–1165	(C-O-C) Ether stretching	[24]
1600–1649	(COO) <sub>asy</sub>	[22,24]	1070–1075	Stretching CH-O-CH <sub>2</sub>	[24,25]
1551–1560	C-N group	[23,24]	839–860	Asymmetric rocking	[26]

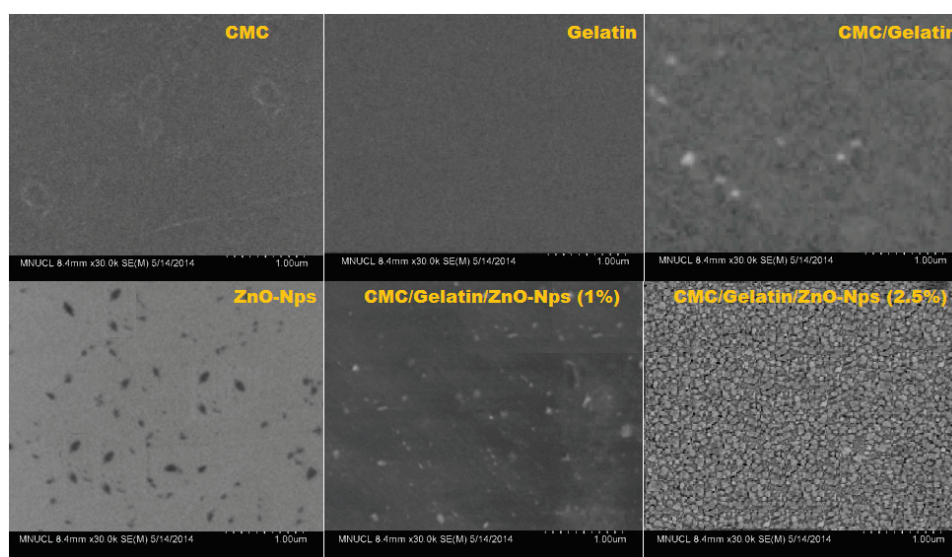
#### 4.2. XRD Analysis

The homogenous mixing of ZnO nanoparticles in the CMC/GEL film was confirmed by the X-ray diffraction pattern, which also quantified the changes from an amorphous to crystalline structure. The XRD pattern of ZnO-Nps (a), CMC/Gel/ZnO (b), CMC/Gelatin (c), CMC (d), and Gelatin (e) is shown in Figure 2. The sharp peaks of the ZnO nanoparticle (Figure 2a) that correspond with the data in JCPDS No. 36-1451, confirmed the wurtzite crystal structure with a hexagonal phase [29]. The diffraction pattern of CMC/GEL/ZnO composite film revealed a characteristic peak of ZnO at  $2\theta$ ; 32.130, 34.620, 36.460, 46.930, 53.740, 56.460, and 61.350 with low intensity, which indicated the homogenous mixing of ZnO-Nps in CMC/GEL film (Figure 2b). The CMC has an amorphous structure, while gelatin is partially crystalline with peaks at  $2\theta = 7.6^\circ$  and  $22.31^\circ$ , Figure 2d,e. In Figure 2c–e, there is no sharp diffraction peak, and an increased diameter of the interreticular triple helix with increased intensity is observed due to the mixing of CMC and gelatin. The interaction between CMC and gelatin has been confirmed by the absence of X-peaks. This phenomenon shows the reduction of hydrogen bonding between the hydroxyls of gelatin and the cellulose groups of CMC. The cross-linking between CMC and gelatin films by GTA exhibited a negligible triple helix approaching 0.8% are in close agreement with the literature [30].

**Figure 2.** XRD pattern of CMC/Gel/ZnO nanocomposites hydrogels.

#### 4.3. Morphological Studies

All the prepared CMC/gelatin/ZnO nanocomposites were mechanically flexible and self-standing. SEM was used to examine the surface morphology of CMC, gelatin, and ZnO-nanocomposite films and images are shown in Figure 3. The interaction of zinc oxide nanoparticles with CMC and gelatin controls the networked microstructure. Without ZnO nanoparticles, neat CMC, gelatin biopolymer, and CMC/gelatin blend films showed a uniform surface, demonstrating that the film-forming polymers were mostly amorphous and had little crystallization. While the CMC/gelatin film with zinc oxide-Nps additions had a heterogeneous rough surface, with the zinc nanoparticles being uniformly distributed throughout the films and preventing particle separation. It explained that how metal nanoparticles prevented particle aggregation and created high-viscosity CMC/gelatin films, thus a highly stable CMC/gelatin mixture was used [31].



**Figure 3.** Scanning microscopy images of neat CMC, gelatin, CMC/gelatin and CMC/gelatin/ZnO-Nps.

#### 4.4. Optical Properties

Optical properties of CMC/GEL-based films loaded with various weight ratios (2.5% *w/w*) of ZnO-Nps were studied, and data is shown in Table 2 and in Figure 4. Neat gelatin film had two peaks for typical CMC and gelatin peaks at 230–240 nm and 265–280 nm. The nanocomposite films containing ZnO nanoparticles, on the other hand, revealed an additional peak for the ZnO-nps near 370 nm. The peak intensity increased with increasing ZnO nanoparticle contents in CMC/gelatin matrices from 1% to 2.5% [32].

**Table 2.** Optical data of CMC/gelatin/ZnO composite films loaded with different contents of ZnO-Nps.

Sample	L	a	b	$\Delta E$	$T_{280nm}$ (%)	$T_{660nm}$ (%)
Neat CMC	91.45 ± 0.15	−0.30 ± 0.15	5.3 ± 0.1	1.12	58.3 ± 1.25	87.2 ± 0.50
Neat Gelatin	91.31 ± 0.15	−0.50 ± 0.25	6.2 ± 0.50	1.89	30.4 ± 1.50	90.7 ± 0.15
CMC/Gelatin	91.20 ± 0.15	−0.80 ± 0.15	6.7 ± 0.15	2.40	25.6 ± 0.25	88.4 ± 1.25
CMC/Gelatin/ZnO <sup>1</sup>	90.44 ± 0.25	−1.24 ± 0.15	6.9 ± 0.50	3.06	14.5 ± 1.50	85.3 ± 0.25
CMC/Gelatin/ZnO <sup>1.5</sup>	90.27 ± 1.50	−1.31 ± 0.50	7.3 ± 0.25	3.26	2.4 ± 0.50	81.7 ± 1.15
CMC/Gelatin/ZnO <sup>2</sup>	90.64 ± 1.25	−1.38 ± 0.50	7.1 ± 0.15	3.15	1.5 ± 0.15	72.5 ± 1.50
CMC/Gelatin/ZnO <sup>2.5</sup>	90.85 ± 1.50	−1.46 ± 0.25	7.6 ± 0.15	3.50	0.9 ± 0.25	68.5 ± 0.15

± standard deviation. ( $p < 0.05$ ).

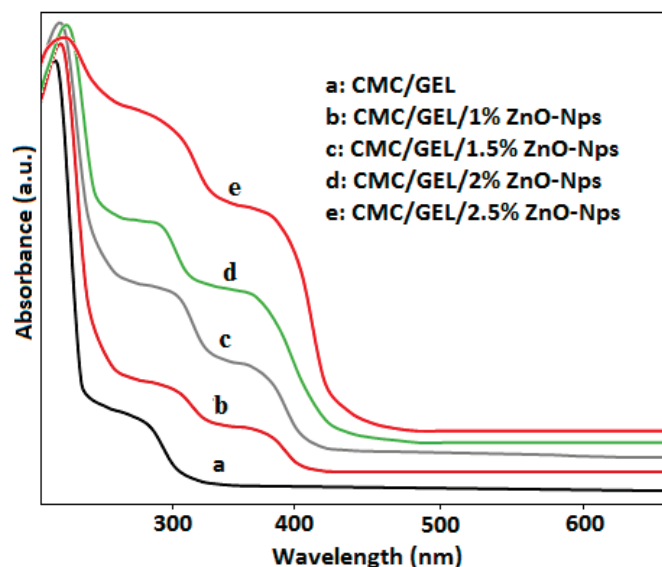


Figure 4. Optical studies of CMC/gelatin/ZnO-Nps.

The L-values of the CMC, gelatin, and CMC/gelatin films exceeded 91, and the a and b parameters ranged from 0.8 to 0.3 and 5.3 to 6.7, respectively, making the films highly transparent. By incorporating ZnO nanoparticles, L and a values were significantly shifted to the lower end, while b values increased. As a result of these changes, the total colour difference between the films increased significantly ( $\Delta E$ ) [33]. The  $\Delta E$  was calculated by:

$$\Delta E = ((\Delta L)^2 + (\Delta a)^2 + (\Delta b)^2)^{0.5}$$

where  $\Delta L$ ,  $\Delta a$ , and  $\Delta b$  are the differences between value of standard colour plate and composite films. In the presence of UV rays, food ingredients oxidise, destroying nutrients and bioactive compounds. Film transparency and UV protection are essential optical properties for applications in food packaging. For the sake of food safety and quality, oxidation reactions that result in toxic substances, off flavours, discoloration, or rancidity are not allowed [34].

Furthermore, the % transmittance of light was measured at  $T_{280}$  and  $T_{660}$  nm. At  $T_{660}$  nm and  $T_{280}$  nm, the neat CMC and gelatin films had transmittance values of  $87.2 \pm 0.50$ ,  $90.7 \pm 0.15$ ,  $58.3 \pm 1.25$ , and  $30.4 \pm 1.50$ , respectively. When ZnO-Nps was added to CMC/gelatin blend, the percentage transmittance of films at 280 nm was drastically reduced, falling to just 0.3%, whereas the percentage transmittance values at 660 nm only slightly decreased as ZnO-Nps concentrations were increased [35]. The amount of ZnO-Nps present had a significant impact on the transmittance value of the nanocomposite films.

#### 4.5. Thermal Stability

The TGA technique was used to study the thermal properties of pure biopolymer films as well as films containing ZnO-Nps, and thermograms are shown in Figure 5, which demonstrate the degradation patterns of neat CMC/GEL films and CMC/GEL/ZnO-Nps. All films showed multiple steps of thermal degradation. The first step of degradation started around 95 to 100 °C, with a percentage weight loss ranging from 10 to 20% because of the evaporation of loosely bound gases from films. The second stage of degradation of amino groups in CMC/GEL film was observed at 290–360 °C with 84% weight loss. The other loss in weight was observed at 415 and 75 °C, which were considered the third and fourth steps of degradation in weight, respectively [33]. Compared to neat CMC/GEL films, the degradation curves of prepared nanocomposites films are shifted towards higher temperatures because biopolymers and ZnO-Nps have a strong interaction and are thoroughly mixed [36].



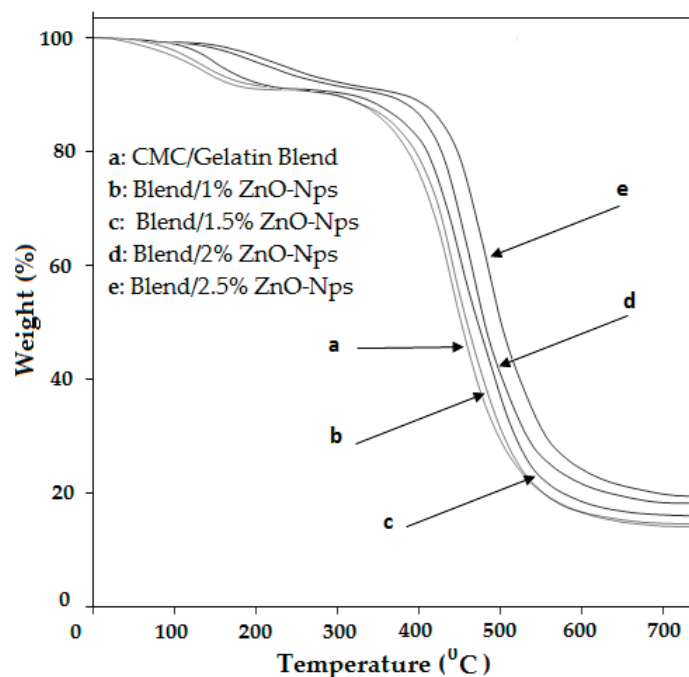


Figure 5. TGA of CMC/Gel/ZnO-nanocomposite hydrogels.

#### 4.6. Mechanical Properties

Tensile strength, percent elongation at break (EB), and elastic modulus, which are key factors in determining the strength and flexibility of the film, were studied as mechanical properties. The effect of ZnO-Nps on EB, tensile strength, and elastic modulus of CMC/GEL films was determined, and the data is presented in Table 3. The addition of ZnO-Nps to the CMC/GEL films has significantly improved the flexibility (EB) and strengthened the CMC/GEL film. Initially, the CMC/GEL (75:25) film had tensile strength and elongation at break values of 39.25 MPa and 4.41 0.23%, respectively. The incorporation of ZnO nanoparticles has increased the elongation at break, and tensile strength values for the CMC/GEL films to 44.6 MPa and 10%, respectively. The increased tensile strength of CMC/gelatin films may be attributed to the incorporation of the proper amount of nanoparticles as well as the bonding between hydroxy groups of gelatin and the hydrophilic groups of CMC, resulting in the formation of a mechanically stable nanocomposite between CMC, gelatin, and zinc oxide nanoparticles [35].

Table 3. Mechanical properties and Physical Data of CMC/GEL/ZnO nanocomposite films.

Components	Tensile Strength ± SD, (MPa)	Young's Modulus ± SD, (MPa)	Elongation at Break ± SD, (%)	Moister Contents	Water Vapor Permeability (g m <sup>-1</sup> day <sup>-1</sup> atm <sup>-1</sup> )
Neat CMC	35.15 ± 1.25	1186 ± 0.06	14.18 ± 0.06	12.5 ± 1.15	1.15 ± 0.15
Neat GEL	37.25 ± 1.5	1390 ± 2.5	2.34 ± 0.06	10.25 ± 0.5	1.25 ± 1.5
75 CMC: 25 GEL Blend	39.25 ± 2.0	1255 ± 5.6	4.41 ± 0.23	11.5 ± 0.5	2.15 ± 0.5
Blend: 1 ZnO	40.15 ± 6.4	1050 ± 2.8	6.5 ± 2.5	13.5 ± 1.5	2.55 ± 0.05
Blend: 1.5 ZnO	41.9 ± 1.25	970 ± 1.86	8.2 ± 1.5	13.8 ± 0.5	2.84 ± 1.25
Blend: 2 ZnO	42.5 ± 1.4	895 ± 7.25	8.58 ± 2.25	14.1 ± 0.0	2.92 ± 1.5
Blend: 2.5 ZnO	44.6 ± 2.5	765 ± 9.5	10.0 ± 1.25	14.5 ± 0.5	3.11 ± 0.05

#### 4.7. Moisture Content and Water Vapor Permeability

The moisture contents (MC) and water vapour permeability (WVP) of neat CMC, neat GEL, CMC/GEL, and MCM/GE/ZnO- films were determined and the data are

presented in Table 1. CMC/GEL films had slightly lower moisture contents and water vapour permeability, whereas CMC/GEL/ZnO-Nps films had higher values and these values increased with higher zinc oxide nanoparticle concentration. ZnO nanoparticles in the CMC/GEL film matrix make the films porous, increasing water vapour permeability.

#### 4.8. Antibacterial Results

The antimicrobial screening data of CMC, GEL, and ZnO films are presented in Table 4. As per the literature and experiments, the CMC/GEL film had no antibacterial action against both types of tested microorganisms; however, the composite films incorporating ZnO-Nps had marked antibacterial activity. The antimicrobial activity of composites depends on the nature and type of inorganic fillers and the type of bacterial strains used. On both types of tested bacterial strains, the CMC/GEL hydrogel films had a bacteriostatic effect due to the presence of ZnO-Nps, which delayed the growth of the germs because the structure of their cell walls was different. Generally, gram-negative bacteria have a complex cell wall made of a thin layer of peptidoglycan protected by an extra outer membrane, in contrast to gram-positive pathogens that have a thick cell wall with many layers of peptidoglycan. The size and shape of zinc oxide nanoparticles in CMC/GEL/ZnO composite films mainly increased the antibacterial activity of tested bacterial strains. Though the antibacterial mechanism of ZnO is unknown, it is thought that zinc oxide nanoparticles increased the permeability of the membrane around the bacteria, allowing metal nanoparticles to readily pass through the bacterium's cell wall. Various reactive oxygen species (ROS) such as hydroxyl radicals ( $\text{OH}^-$ ), hydrogen peroxide ( $\text{H}_2\text{O}_2$ ), superoxide anions ( $\text{O}_2^-$ ), and organic hydroperoxides are produced inside the cell during this process. When ROS overcomes the cellular antioxidant defense mechanism, oxidative stress occurs, which is linked to damage of several critical macromolecules that ultimately leads to cell death [34].

**Table 4.** Antibacterial activity of CMC/GEL/ZnO-Nps hydrogel films.

Compound No.	Zone of Inhibition (mm) + St. Dev.					
	<i>Staphylococcus aureus</i>	<i>Bacillus subtilis</i>	<i>Listeria monocytogenes</i>	<i>Enterobacter aerogenase</i>	<i>Escherichia coli</i>	<i>Bordetella bronchiseptica</i>
Neat CMC	-	-	-	-	-	-
Neat GEL	-	-	-	-	-	-
75 CMC: 25 GEL Blend	12 ± 1.0	14 ± 1.25	-	-	13 ± 1.15	-
Blend: 1% ZnO	18 ± 1.05	22 ± 1.5	20 ± 1.15	15 ± 2.0	17 ± 1.15	14 ± 1.25
Blend: 1.5% ZnO	22 ± 1.0	25 ± 1.25	23 ± 1.5	19 ± 1.75	20 ± 1.5	19 ± 1.5
Blend: 2% ZnO	28 ± 2.0	26 ± 1.5	27 ± 1.0	22 ± 1.5	24 ± 1.5	21 ± 1.25
Blend: 2.5% ZnO	30 ± 1.03	29 ± 2.0	32 ± 1.0	26 ± 1.25	31 ± 1.25	24 ± 2.0
Cefixime	33 ± 1.5	31 ± 1.0	35 ± 1	29 ± 0.5	36 ± 1	31 ± 2

± = SD, standard deviation, ( $p < 0.05$  vs. control); 5–10 mm zone of inhibition (Activity present); 11–25 mm zone of inhibition (Moderate activity); 26–40 mm zone of inhibition (Strong activity).

#### 4.9. Antioxidant Activity

The antioxidant activity of neat CMC, GEL, CMC/GEL and CMC/GEL/ZnO nanocomposite films was evaluated by their DPPH (1,1-diphenyl-2-picrylhydrazyl) free radical scavenging activity. The effect of tested nanocomposite materials on generation of free radical of DPPH or radical scavenging activity is measured at 517 nm by decrease in molar absorptivity of DPPH. The degree of discoloration reveals the antioxidant compounds' scavenging capacity in terms of H-donating capacity. Furthermore, the ability of antioxidant compounds to scavenge free radicals depends on their concentration. The radical-scavenging activity rises with antioxidant compound concentration, and a low  $IC_{50}$  value (i.e., 50% inhibitory concentration) indicates a high antioxidant activity. The obtained results are shown in Table 5. Synthesized composite films containing ZnO-Nps showed free radical

scavenging activity with  $IC_{50}$  in the range of 39 to 85  $\mu\text{g}/\text{mL}$  while their respective matrix polymers (CMC/GEL) showed activity more than 100  $\mu\text{g}/\text{mL}$ . On comparison of  $IC_{50}$  values of CMC, GEL and their composite films with different wt ratio of ZnO-Nps, it was observed that such CMC/GEL/ZnO-nanocomposites are more active for DPPH activity than their parent polymers [35,36].

**Table 5.** Antioxidant results of CMC/GEL films loaded with different concentration of ZnO-Nps.

Compound	% Scavenging $\pm$ sd Concentration $\mu\text{g}/\text{mL}$						$IC_{50}$ $\mu\text{g}/\text{mL}$
	200	100	40	20	10	5	
Neat CMC	65 $\pm$ 1	58 $\pm$ 1	47 $\pm$ 1	38 $\pm$ 2	29 $\pm$ 1	15 $\pm$ 1	>200
Neat GEL	61 $\pm$ 1	56 $\pm$ 1	49 $\pm$ 1	33 $\pm$ 1	26 $\pm$ 1	18 $\pm$ 1	>150
75 CMC: 25 GEL Blend	68 $\pm$ 1	59 $\pm$ 2	52 $\pm$ 2	44 $\pm$ 2	38 $\pm$ 1	22 $\pm$ 1	>100 $\pm$ 1
Blend: 1 ZnO	71 $\pm$ 1	66 $\pm$ 2	59 $\pm$ 1	38 $\pm$ 1	29 $\pm$ 1	24 $\pm$ 1	85 $\pm$ 1
Blend: 1.5 ZnO	74 $\pm$ 2	65 $\pm$ 1	54 $\pm$ 1	42 $\pm$ 1	35 $\pm$ 2	20 $\pm$ 1	62 $\pm$ 1
Blend: 2 ZnO	79 $\pm$ 1	66 $\pm$ 1	58 $\pm$ 1	43 $\pm$ 2	33 $\pm$ 1	18 $\pm$ 1	54 $\pm$ 1
Blend: 2.5 ZnO	84 $\pm$ 1	69 $\pm$ 1	65 $\pm$ 2	52 $\pm$ 1	48 $\pm$ 1	22 $\pm$ 1	42 $\pm$ 1
Butylated hydroxyanisole (BHA)	89 $\pm$ 0.5	85 $\pm$ 1	76 $\pm$ 0.25	68 $\pm$ 0.5	45 $\pm$ 1	15 $\pm$ 1	8 $\pm$ 0.05

$\pm$  = SD, standard deviation, ( $p < 0.05$  vs. control); Antioxidant activity:  $IC_{50}$  0–10  $\text{mg}/\text{mL}^{-1}$ , very strongly active; 10–50  $\text{mg}/\text{mL}^{-1}$ , strongly active; 50–100  $\text{mg}/\text{mL}^{-1}$ , moderately active; 100–250  $\text{mg}/\text{mL}^{-1}$ , weakly active; >250  $\text{mg}/\text{mL}^{-1}$ , inactive.

## 5. Conclusions

Owing to the versatile nature of biopolymer composites, ZnO nanoparticles have drawn a lot of attention in the field of food packaging. The purpose of this research was to synthesize zinc oxide nanoparticles (<50 nm) by using plant extract as a reducing agent, and to incorporate this in CMC/gelatin matrices to assess the optical, thermal, mechanical and microbial properties. ZnO-based multifunctional CMC/GEL nanocomposites were prepared. ZnO-Nps affected the bio-functional and physical properties of CMC/gelatin composite films. The FTIR and XRD results confirmed the uniform dispersion of ZnO-Nps in the CMC/GEL, matrix to prepare compatible films. The addition of ZnO-Nps (1–2.5 wt. %) to CMC/GEL improved the thermal stability, mechanical properties, moisture contents, and water vapor permeability. CMC/GEL/ZnO-2.5% composite film showed good thermal stability and mechanical properties. CMC/GEL/ZnO 2.5% composite film showed strong antibacterial activity against foodborne pathogenic bacteria, *E. coli*, and *L. monocytogenes* and had high antioxidant activity. CMC-based composite films, such as CMC/GEL/ZnO 2.5%, showed improved thermo-mechanical properties with higher antioxidant and antibacterial activity as compared to CMC/GEL blend films. On the basis of the obtained results, CMC/GEL/ZnO nanocomposite films can be used to prevent photooxidation, ensure food safety, and increase the shelf life of packaged goods in active food packaging applications.

**Author Contributions:** Conceptualization, M.K.K.; methodology, A.Z.; formal analysis, M.K.K.; writing—original draft preparation, A.Z. and M.K.K.; writing—review and editing, A.N. and S.Q. supervision, M.K.K.; Characterization and discussion, M.J.S.; funding acquisition, writing—review and editing, A.N. and S.Q. All authors have read and agreed to the published version of the manuscript.

**Funding:** This work was supported by the Deanship of Scientific Research, Vice Presidency for Graduate Studies and Scientific Research, King Faisal University, Saudi Arabia (grant no. Grant1974).

**Institutional Review Board Statement:** Not applicable.

**Informed Consent Statement:** Not applicable.

**Data Availability Statement:** The authors declare that data supporting the findings of this study are available within the article entitled: “Carboxymethyl cellulose/gelatin hydrogel films loaded with Zinc Oxide nanoparticles for sustainable food packaging applications”.

**Acknowledgments:** This work was supported by the Deanship of Scientific Research, Vice Presidency for Graduate Studies and Scientific Research, King Faisal University, Saudi Arabia (grant no. Grant 1974).

**Conflicts of Interest:** There is no conflict of interest regarding this publication entitled, Carboxymethyl cellulose/gelatin hydrogel films loaded with Zinc Oxide nanoparticles for sustainable food packaging applications.

## References

- Sohail, M.; Sun, D.W.; Zhu, Z. Recent developments in intelligent packaging for enhancing food quality and safety. *Crit. Rev. Food Sci. Nutr.* **2018**, *58*, 2650–2662. [CrossRef]
- Atta, O.M.; Manan, S.; Ahmed, A.A.Q.; Awad, M.F.; Ul-Islam, M.; Subhan, F.; Ullah, M.W.; Yang, G. Development and characterization of plant oil-incorporated carboxymethyl cellulose/bacterial cellulose/glycerol-based antimicrobial edible films for food packaging applications. *Adv. Compos. Mater.* **2022**, *5*, 973–990. [CrossRef]
- Pernas-Pleite, C.; Conejo-Martínez, A.M.; Marín, I.; Abad, J.P. Green extracellular synthesis of silver nanoparticles by *Pseudomonas allopuntida*, their growth and biofilm-formation inhibitory activities and synergic behavior with three classical antibiotics. *Molecules* **2022**, *27*, 7589. [CrossRef]
- Balasubramaniam, S.P.L.; Patel, A.S.; Nayak, B. Surface modification of cellulose nanofiber film with fatty acids for developing renewable hydrophobic food packaging. *Food Packag. Shelf Life* **2020**, *26*, 100587–100591. [CrossRef]
- Atta, O.M.; Manan, S.; Ahmed, A.A.Q.; Awad, M.F.; Ul-Islam, M.; Subhan, F.; Ullah, M.W.; Yang, G. Development and Characterization of Yeast-Incorporated Antimicrobial Cellulose Biofilms for Edible Food Packaging Application. *Polymers* **2021**, *13*, 2310. [CrossRef]
- Atta, O.M.; Manan, S.; Ahmed, A.A.Q.; Awad, M.F.; Ul-Islam, M.; Subhan, F.; Ullah, M.W.; Yang, G. Silver decorated bacterial cellulose nanocomposites as antimicrobial food packaging materials. *ES Food Agrofor.* **2021**, *6*, 12–26. [CrossRef]
- Yildirim, S.; Röcker, B.; Pettersen, M.K.; Nilsen-Nygaard, J.; Ayhan, Z.; Rutkaite, R.; Radusin, T.; Suminska, P.; Marcos, B.; Coma, V. Active packaging applications for food. *Compr. Rev. Food Sci. Food Saf.* **2018**, *17*, 165–199.
- Roy, S.; Rhim, J.W. Preparation of carrageenan-based functional nanocomposite films incorporated with melanin nanoparticles. *Colloids Surf. B-Biointerfaces* **2019**, *176*, 317–324. [CrossRef]
- Zia, J.; Paul, U.C.; Heredia-Guerrero, J.A.; Athanassiou, A.; Fragouli, D. Low-density polyethylene/curcumin melt extruded composites with enhanced vapor barrier and antioxidant properties for active food packaging. *Polymers* **2019**, *175*, 137–143. [CrossRef]
- Mazeyer, P.G.; Naeemeh, D. Gel diffusion-inspired biomimetic calcium iodate/gelatin composite particles: Structural characterization and antibacterial activity. *J. Solid State Chem.* **2020**, *285*, 121262–121274.
- Huang, Y.; Mei, L.; Chen, X.; Wang, Q. Recent developments in food packaging based on nanomaterials. *Nanomaterials* **2018**, *8*, 830. [CrossRef]
- Suo, B.; Li, H.; Wang, Y.; Li, Z.; Pan, Z.; Ai, Z. Effects of ZnO nanoparticle-coated packaging film on pork meat quality during cold storage. *J. Sci. Food Agri.* **2017**, *971*, 2023–2029. [CrossRef]
- Lishchynskiy, O.; Shymborska, Y.; Stetsyshyn, Y.; Raczowska, Y.; Skirtach, A.G.; Peretiatchko, T.; Budkowski, A. Passive antifouling and active self-disinfecting antiviral surfaces. *Rev. Chem. Eng. J.* **2022**, *446*, 137048–137064. [CrossRef]
- Ting, T.; Shuangfei, D.; Xiaotong, Z.; Liurong, F.; Jiangong, L.; Shaobo, X. Inhibitory effect and mechanism of gelatin stabilized ferrous sulfide nanoparticles on porcine reproductive and respiratory syndrome virus. *J. Nanobiotech.* **2022**, *20*, 70–82. [CrossRef]
- Gupta, J.; Irfan, M.; Ramgir, N.; Muthe, K.P.; Debnath, A.K.; Ansari, S.; Gandhi, J.; Ranjith, K.C.T.; Surjit, M. Antiviral Activity of Zinc Oxide Nanoparticles and Tetrapods Against the Hepatitis E and Hepatitis C Viruses. *Front. Microbiol.* **2022**, *13*, 881595–881608. [CrossRef]
- Shi, W.; Sun, M.; Hu, X. Structurally and functionally optimized silk fibroin-gelatin scaffold using 3D printing to repair cartilage injury in vitro and in vivo. *Adv. Mater.* **2017**, *29*, 1701089–1701096. [CrossRef]
- Sun, M.; Sun, X.; Wang, Z. Synthesis and properties of gelatin methacryloyl (GelMA) hydrogels and their recent applications in load-bearing tissue. *Polymers* **2018**, *10*, 1290. [CrossRef]
- Xu, Q.; Chen, C.; Rosswurm, K.; Yao, T.; Janaswamy, S. A facile route to prepare cellulose-based films. *Carbohydr. Polym.* **2016**, *149*, 274–281. [CrossRef]
- Yang, W.; Wang, J.; Yang, Q.; Pei, H.; Hu, N.; Suo, Y.; Li, Z.; Zhang, D.; Wang, J. Facile fabrication of robust MOF membranes on cloth via a CMC macromolecule bridge for highly efficient Pb(II) removal. *Chem. Eng. J.* **2018**, *339*, 230–239. [CrossRef]
- Jayachandran, A.; Aswathy, T.R.; Nair, A.S. Green synthesis and characterization of zinc oxide nanoparticles using Cayratia pedata leaf extract. *Biochem. Biophys. Rep.* **2021**, *26*, 100995–101005. [CrossRef]
- Swarup, R.; Rhim, J.W. Carboxymethyl cellulose-based antioxidant and antimicrobial active packaging film incorporated with curcumin and zinc oxide. *Int. J. Biol. Macromol.* **2020**, *148*, 666–676.



22. Kowalczyk, D.; Szymanowska, U.; Skrzypek, T.; Basiura-Cembala, M.; Łupina, K.; Biendl, M. Edible films based on gelatin, carboxymethyl cellulose, and their blends as carriers of potassium salts of iso- $\alpha$ -acids: Structural, physicochemical and antioxidant properties. *Food Hydrocoll.* **2021**, *115*, 106574–106579. [CrossRef]
23. Rehman, A.; Choudhary, M.I.; Thomsen, W.J. *Bioassay Techniques for Drug Development*; Harwood Academic Publishers: Amsterdam, The Netherlands, 2001.
24. Khoushika, R.; Brindha, D. Polymeric materials as platforms for topical drug delivery: A review. *Int. J. Appl. Pharm.* **2017**, *9*, 116–120.
25. Thanyacharoen, T. The chemical composition and antioxidant and release properties of a black rice (*Oryza sativa* L.)-loaded chitosan and polyvinyl alcohol composite. *J. Mol. Liq.* **2017**, *248*, 1065–1070. [CrossRef]
26. Abdelghany, A.M.; Abdelrazek, E.M.; Badr, S.I.; Morsi, M.A. Effect of gamma-irradiation on (PEO/PVP)/Au nanocomposite: Materials for electrochemical and optical applications. *Mater. Des.* **2016**, *97*, 532. [CrossRef]
27. Abdelrazek, E.M.; Abdelghany, A.M.; Badr, S.I.; Morsi, M.A. Structural, optical, morphological and thermal properties of PEO/PVP blend containing different concentrations of biosynthesized Au nanoparticles. *J. Mater. Res. Technol.* **2018**, *7*, 419. [CrossRef]
28. Bella, G.R.; Jeevitha, R.S.J.; Booshan, S.A.T. Polyvinyl alcohol/starch carboxymethyl cellulose ternary polymer blends: Synthesis, characterization and thermal properties. *Int. J. Curr. Res. Chem. Pharm. Sci.* **2016**, *3*, 43–50.
29. Samsi, M.S.; Kamari, A.; Din, S.M. Synthesis, characterization and application of gelatin–carboxymethyl cellulose blend films for preservation of cherry tomatoes and grapes. *J. Food Sci. Technol.* **2019**, *56*, 3099–3108. [CrossRef]
30. Raghunath, A.; Perumal, E. Metal oxide nanoparticles as antimicrobial agents: A promise for the future. *Int. J. Antimicrob. Agents.* **2017**, *49*, 137–152. [CrossRef]
31. Mohammadalinejad, S.; Almasi, H.; Moradi, M. Immobilization of Echiium Amoenum Anthocyanins into Bacterial Cellulose Film: A Novel Colorimetric pH Indicator for Freshness/Spoilage Monitoring of Shrimp. *Food Control.* **2020**, *113*, 107169–107181. [CrossRef]
32. Kim, D.; Jeon, K.; Lee, Y.; Seo, J.; Seo, K.; Han, H.; Khan, S.B. Preparation and characterization of UV cured polyurethane acrylate/ZnO nanocomposite films based on surface modified ZnO. *Prog. Org. Coat.* **2012**, *74*, 435–442. [CrossRef]
33. Bai, R.; Zhang, X.; Yong, H.; Wang, X.; Liu, Y.; Liu, J. Development and Characterization of Antioxidant Active Packaging and Intelligent Al<sup>3+</sup>-Sensing Films Based on Carboxymethyl Chitosan and Quercetin. *Int. J. Biol. Macromol.* **2019**, *126*, 1074–1084. [CrossRef] [PubMed]
34. Ezati, P.; Bang, Y.-J.; Rhim, J.W. Preparation of a Shikonin-Based pH-Sensitive Color Indicator for Monitoring the Freshness of Fish and Pork. *Food Chem.* **2021**, *337*, 127995–128006. [CrossRef] [PubMed]
35. Albert, J.; D'Andrea, L.; Granell, J.; Pla-Vilanova, P.; Quirante, J.; Khosa, M.K.; Calvis, C.; Messeguer, R.; Badía, J.; Baldomà, L.; et al. Cyclopalladated and cycloplatinated benzophenone imines: Antitumor, antibacterial and antioxidant activities, DNA interaction and cathepsin B inhibition. *J. Inorg. Biochem.* **2014**, *140*, 80–88. [CrossRef] [PubMed]
36. Zia, M.A.; Khosa, M.K.; Noor, A.; Qayyum, S.; Shakir, M.S. PMMA/ABS/CoCl<sub>2</sub> Composites for Pharmaceutical Applications: Thermal, Antimicrobial, Antibiofilm, and Antioxidant Studies. *Molecules* **2022**, *27*, 7669. [CrossRef] [PubMed]

## Article

# Clinical Development and Evaluation of a Multi-Component Dissolving Microneedle Patch for Skin Pigmentation Disorders

Chenxin Yan <sup>1,2</sup>, Mengzhen Xing <sup>3</sup>, Suohui Zhang <sup>1,4,\*</sup> and Yunhua Gao <sup>1,2,4,\*</sup>

<sup>1</sup> Key Laboratory of Photochemical Conversion and Optoelectronic Materials, Technical Institute of Physics and Chemistry, Chinese Academy of Sciences, Beijing 100190, China; yanchenxin20@mails.u.ac.cn

<sup>2</sup> University of Chinese Academy of Sciences, Beijing 100049, China

<sup>3</sup> Key Laboratory of New Material Research Institute, Department of Acupuncture-Moxibustion and Tuina, Shandong University of Traditional Chinese Medicine, Jinan 250355, China; mengzhen@mail.ipc.ac.cn

<sup>4</sup> Beijing CAS Microneedle Technology Ltd., Beijing 102609, China

\* Correspondence: suohuizhang@mail.ipc.ac.cn (S.Z.); yhgao@mail.ipc.ac.cn (Y.G.);  
Tel.: +86-010-8254-3582 (S.Z.); +86-010-8254-3581 (Y.G.)

**Abstract:** Excessive melanin deposition in the skin leads to various skin pigmentation diseases, such as chloasma and age spots. The deposition is induced by several factors, including tyrosinase activities and ultraviolet-induced oxidative stress. Herein, we propose a multi-component, multi-pathway drug combination, with glabridin, 3-O-ethyl-L-ascorbic acid, and tranexamic acid employed as, respectively, a tyrosinase inhibitor, an antioxidant, and a melanin transmission inhibitor. Considering the poor skin permeability associated with topical application, dissolving microneedles (MNs) prepared with hyaluronic acid/poly(vinyl alcohol)/poly(vinylpyrrolidone) were developed to load the drug combination. The drug-loaded microneedles (DMNs) presented outstanding skin insertion, dissolution, and drug delivery properties. In vitro experiments confirmed that DMNs loaded with active ingredients had significant antioxidant and inhibitory effects on tyrosinase activity. Furthermore, the production of melanin both in melanoma cells (B16-F10) and in zebrafish was directly reduced after using DMNs. Clinical studies demonstrated the DMNs' safety and showed that they have the ability to effectively reduce chloasma and age spots. This study indicated that a complex DMN based on a multifunctional combination is a valuable depigmentation product worthy of clinical application.

**Keywords:** glabridin; 3-O-Ethyl-L-ascorbic acid; tranexamic acid; microneedles; pigmentation; multifunctional drug

**Citation:** Yan, C.; Xing, M.; Zhang, S.; Gao, Y. Clinical Development and Evaluation of a Multi-Component Dissolving Microneedle Patch for Skin Pigmentation Disorders. *Polymers* **2023**, *15*, 3296. <https://doi.org/10.3390/polym15153296>

Academic Editors: Dimitrios Bikiaris and Raffaella Striani

Received: 27 June 2023

Revised: 24 July 2023

Accepted: 28 July 2023

Published: 4 August 2023



**Copyright:** © 2023 by the authors. Licensee MDPI, Basel, Switzerland. This article is an open access article distributed under the terms and conditions of the Creative Commons Attribution (CC BY) license (<https://creativecommons.org/licenses/by/4.0/>).

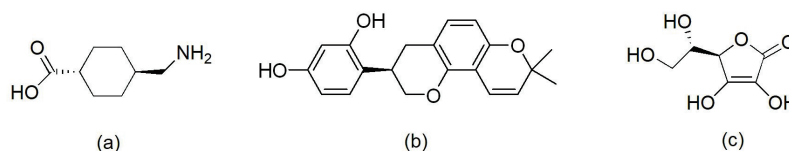
## 1. Introduction

The normal deposition of melanin in the basal layer of the skin results in the pigmentation of human skin and hair. Aside from conferring protection against ultraviolet (UV) rays, excessive melanin deposition leads to melasma [1] and age spots [2]. Specifically, melasma occurs because of inducing factors such as UV radiation, hormone levels, and family history [1,3]. However, the exact mechanism of age spot formation is currently unclear, and it is widely believed that UV radiation is the main cause of its formation [4].

Melanin production is governed by the rate-limiting enzyme tyrosinase [5]. UV radiation indirectly stimulates tyrosinase, thus increasing melanin production. Recently, several tyrosinase inhibitors intended for skin whitening have been developed, including hydroquinone [6], kojic acid [7], arbutin [8], and aloesin [9]. However, these agents can cause significant side effects, including skin irritation, inflammation, and potential teratogenicity [10]. Furthermore, UV radiation can induce oxidative stress [11], which leads to the formation of oxidants such as nitric oxide [12] and which indirectly stimulates skin pigmentation. Therefore, certain antioxidants can decrease melanin production, such as glutathione [13], ascorbic acid (ASA) [14], and ferulic acid [15]. Recently, researchers

have combined tyrosinase inhibitors and antioxidants, to treat pigmented lesions. For instance, Yu et al. [16] showed that combining the tyrosinase inhibitor azelaic acid with the antioxidant taurine significantly improved melanin inhibition compared to using azelaic acid alone.

Tranexamic acid (TXA) (seen in Figure 1a), which is a derivative of lysine, was initially proven to be an anti-fibrinolytic agent [17]. It was discovered that TXA has great whitening effects, and it is commonly used to treat melasma through oral administration, injection, or local application [18,19]. However, the systemic administration of TXA usually leads to adverse effects in patients, such as gastrointestinal discomfort and skin rash [20]. Glabridin (GLA) (seen in Figure 1b), which comes from the flavonoid group of compounds in the root of *glycyrrhiza glabra*, is an excellent tyrosinase inhibitor. It can effectively reduce the transformation of tyrosine to melanin in melanocytes [21–23]. Additionally, 3-O-Ethyl-L-ascorbic acid (EAA) (seen in Figure 1c), a derivative of vitamin C (VC), has better stability and hydrophilic–lipophilic balance than VC [24]. Simultaneously, EAA retains the apparent antioxidant effects of VC. The combined use of three effective components is expected to ameliorate stubborn, hard-to-treat skin hyperpigmentation, lengthy treatment, and high recurrence rates. However, because of the protective barrier function of the stratum corneum, drug absorption through the skin is challenging. Therefore, the key to the drug’s intended efficacy lies in achieving efficient transdermal drug delivery.



**Figure 1.** The chemical structural formula of (a) TXA; (b) GLA; and (c) EAA.

Microneedles (MNs) are a recent drug delivery innovation [25]. These needle tips, measuring several hundred micrometers in length, can create micrometer-sized pores on the skin, allowing drugs to bypass the skin barrier and to reach the site of the disease. Their small size ensures that they do not come into contact with blood vessels and nerves, which improves patient compliance and comfort, while reducing usage burden. The use of hyaluronic acid (HA) as a matrix for MNs is preferred, due to its excellent biocompatibility. The hyaluronic acid microneedle delivery system has been successfully applied to transport a variety of drugs, including vaccines [26], exenatide [27], proteins [28], and anesthetics [29]. To fabricate microneedle arrays, a mixture of three polymers with biocompatibility and flexibility was used: Polyvinyl alcohol (PVA), polyvinyl pyrrolidone (PVP) [30], and hyaluronic acid (HA).

In this study, we employed MNs as drug delivery carriers to combine GLA, TXA, and EAA, aiming to synergistically inhibit melanin production from multiple perspectives. Through performing a series of experiments—including *in vitro* antioxidant assays, tyrosinase inhibition assays, melanin generation inhibition evaluations, zebrafish assays, and clinical trials—we examined the efficacy of the newly developed drug-loaded microneedles (DMNs). Moreover, the effectiveness of DMNs in decolorization was confirmed by *in vitro* and *ex vivo* experiments.

## 2. Materials and Methods

### 2.1. Materials

Tranexamic acid and Glabridin were purchased from Linkebe Technology Co., Ltd. (Hangzhou, China). 3-O-Ethyl-L-ascorbic acid was procured from Dezhou Anglida Biotechnology Co., Ltd. (Dezhou, China). The hyaluronic acid (HA, Mw: 240,000) was procured from Bloomage Biotech (Beijing, China). Poly(vinylpyrrolidone) (PVP) was bought from Boai Nky Pharma Co., Ltd. (Beijing, China). Poly(vinyl alcohol) (PVA) was purchased from Alpha Hi-Tech Pharm Co., Ltd. (Pingxiang, China). The 2-Phenyl-4,4,5,5-tetramethylimidazole-1-oxyl-3-oxide (PTIO) was bought from Santa Cruz Biotechnology,

Inc. (Santa Cruz, CA, USA), while 1,1-diphenyl-2-picrylhydrazyl (DPPH) was bought from Aladdin Biochemical Technology Co., Ltd. (Shanghai, China), and L-DOPA from Sigma-Aldrich (St. Louis, MO, USA). Dulbecco's Modified Eagle's Medium (DMEM low glucose), RPMI 1640 medium, fetal bovine serum (FBS), phosphate-buffered saline (pH = 7.0–7.4), penicillin–streptomycin (P/S), and 0.25% trypsin (1×) were procured from Gibco (Rockville, MD, USA). The Cell Counting Kit-8 assay kit was provided by Dojindo (Kumamoto Prefecture, Japan). Non-tissue/cell lysate was ordered from Solarbio Tech Co., Ltd. (Beijing, China), while RIPA buffer was bought from Beyotime Biotechnology (Shanghai, China). Sodium hydroxide and dimethyl sulfoxide were obtained from InnoChem (Beijing, China) and Beijing Chemical Works (Beijing, China), respectively. PBS (50 mM, pH = 6.8) was purchased from Regen Biotechnology Co., Ltd. (Beijing, China).

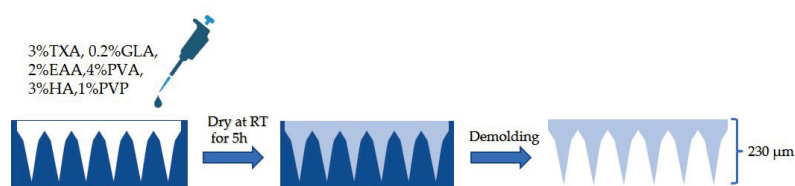
Sprague Dawley (SD) rats (male, 8 weeks old,  $220 \pm 20$  g) were obtained from SPF Biotech Co., Ltd. (Beijing, China). Procedures for animal studies were approved by the Institutional Animal Care and Utilisation Committee of the Technical Institute of Physics and Chemistry, CAS (approval number, LHDW-23025 and IACUCIPC-23025). The animal experiments followed the Guide for the Care and Use of Laboratory Animals (Eighth Edition, 2011). B16-F10 cells were purchased from Shanghai Enzyme Research Biotechnology Co., Ltd. (Shanghai, China). The wild-type AB strain of zebrafish was obtained from China Zebrafish Resource Center (Wuhan, China), and their breeding and propagation followed the requirements of the international AAALAC certification (certification number: 001458). The animal experimentation procedures were executed according to The Standard Operating Procedures for Evaluating the Whitening Efficacy of Zebrafish.

## 2.2. Volunteers

For the safety evaluation of DMNs, we recruited 30 participants, comprising 6 males and 24 females, aged between 20 and 58 years old. To assess the efficacy of DMNs in reducing facial pigmentation, 6 eligible female participants, aged from 18 to 60 years old, with noticeable facial pigmentation were chosen based on a predetermined set of criteria. The recruitment of volunteers was carried out following the medical and ethical principles outlined in the Helsinki Declaration. Before participation, all volunteers had to provide their informed consent to be involved in the study by signing a written consent form. All aspects of the study, including but not limited to conducting the experiment, analyzing data, and compiling the report, adhered to the principles of Good Clinical Practice.

## 2.3. Preparation of DMNs

HA, PVA, and PVP were chosen as the primary matrix for MNs fabrication due to their outstanding biocompatibility [31]. When preparing the drug-containing solution, 3% TXA, 0.2% GLA, 2% EAA, 4% PVA, 3% HA, and 1% PVP were dissolved in deionized water. The pH of the solution was then adjusted to 5.5–6 and filtered through a 220 nm filter. PVA was dissolved in deionized water at 80 °C while HA and PVP were dissolved at room temperature. The three polymers were then mixed to form a homogeneous solution containing 4% PVA, 3% HA, and 1% PVP. After sterilizing the high-molecular-weight mixed solution with high pressure, it was combined with the drug-containing solution to obtain the DMN solution. The DMN solution was then applied onto a polydimethylsiloxane (PDMS) mold using vacuum suction to fill the holes with the solution. Finally, the DMNs were left to dry for more than 5 h in an environment with a relative humidity of not more than 30% (Figure 2).



**Figure 2.** The manufacturing process of DMNs.



#### 2.4. Characterizations of DMNs

DMNs were fabricated by employing PDMS molds that were designed to have a needle height of 230  $\mu\text{m}$ . We then evaluated the DMNs' morphology and actual height by utilizing fluorescence microscopy (BX51, Olympus, Tokyo, Japan). Additionally, the dissolution characteristics of DMNs were investigated using detached piglet pig skin. DMNs were affixed to a hydrogel backing, and a microneedle applicator (20  $\text{N}/\text{cm}^2$ ) was employed to exert pressure for 20 s, followed by a 40 min waiting period before the removal of DMNs. Finally, the needle height of the remaining DMNs was analyzed. According to a previous study [32], Parafilm sealing film was employed to evaluate the penetration performance of DMNs. DMNs were applied with a pressure of 20  $\text{N}/\text{cm}^2$  for 20 s on an 8-layer sealing film. The DMNs were then removed to observe the puncture holes and maximum puncture depth formed on the sealing film. To further validate the puncture performance of DMNs, a needle injector (20  $\text{N}/\text{cm}^2$ ) was used to facilitate the insertion of DMNs into excised porcine skin. Subsequently, the DMNs were removed and stained with a 4  $\text{mg}/\text{mL}$  trypan blue dye solution for 30 min. Following the staining process, the dye was wiped off, and photographs were taken to document the array of needle punctures. Additionally, DMNs were also applied on the skin of SD rats, and the array formed on the rat's skin was recorded.

#### 2.5. The PTIO Antioxidant Activity of DMNs

The PTIO antioxidant test was adapted from a study by Li et al. [33]. Firstly, dissolve a single piece of DMN dry film in 1 mL of PBS buffer solution to obtain a 100% active solution. Next, prepare a solution with a concentration of 0.5  $\text{mg}/\text{mL}$  each for PTIO and ASA. Distribute 1, 5, and 20  $\mu\text{L}$  of the 100% active solution to the wells of a 96-well plate, adding PBS to all wells with less than 20  $\mu\text{L}$  and setting up three replicates for each group. Use PBS as a blank control and ASA as a positive control. Finally, introduce 80  $\mu\text{L}$  of PTIO solution into each well and incubate the plate in an incubator set at a constant temperature of 37  $^{\circ}\text{C}$  for 2 h. Next, complete processing by measuring absorbance at 570 nm using an enzyme-linked immunosorbent assay (ELISA) reader (Epoch2, BioTek). Compute the PTIO• scavenging rate using the formula:

$$\text{PTIO}\bullet \text{ scavenging rate}\% = (A_0 - A) \times 100\% / A_0 \quad (1)$$

where  $A$  and  $A_0$  represent the absorbance values of the sample group and the control group, respectively.

#### 2.6. DPPH• Scavenging Efficiency of DMNs

Antioxidant assays were performed according to the procedure described by Kim et al. [34], with appropriate modifications. A 100% DMN water solution was prepared as outlined in Section 2.5 and then diluted into concentrations of 40% and 10% with PBS solutions. Subsequently, 2 mg of DPPH powder was weighed and added to a 5 mL centrifuge tube, followed by the addition of 2 mL anhydrous ethanol to make a 1  $\text{mg}/\text{mL}$  solution. The solution was sonicated in the dark for 5 min, shaken in the dark for 10 min, and then left undisturbed in the dark for 30 min until it was stable. The solution was further diluted to a concentration of 0.1  $\text{mg}/\text{mL}$ . Positive control ASA was prepared in water to a concentration of 0.2  $\text{mg}/\text{mL}$ . A 96-well plate was arranged with 100  $\mu\text{L}$  of the different concentrations of the test solution, the positive control, and the negative control in each well. Each group was replicated three times. Then, 100  $\mu\text{L}$  of DPPH solution was applied to each well. The plate was kept in the dark while it was agitated for 30 min. After this time, the absorbance was measured at 517 nm using an ELISA reader. The scavenging effect of DPPH radicals was measured using the formula:

$$\text{DPPH}\bullet \text{ clearance rate}\% = (A_0 - A) \times 100\% / A_0 \quad (2)$$

where  $A$  and  $A_0$  represent the absorbance values of the sample group and the control group, respectively.

### 2.7. Safety on B16-F10 Cells

First, prepare the DMN extract. Sterilize the dry film with UV light for 24 h, then add a low-sugar DMEM culture medium in a ratio of one sheet per milliliter to obtain 100% extract. Next, prepare four concentration gradients of extract at 50%, 20%, 5%, and 1%. Seed B16-F10 cells in 96-well plates, with each well containing 8000 cells, and incubate for 24 h at 37 °C, 5% CO<sub>2</sub>, and saturated humidity in a culture box. Then, add 100 µL of different concentrations of DMN extract to each well, with four parallel groups set for each concentration and blank controls established at the same time. After administration, continue incubating for 24 h. After processing, wash the cells with PBS and add 100 µL of 10% Cell Counting Kit-8 (CCK-8) solution to each well, then continue incubation for 50 min. Finally, use an ELISA reader to measure the absorbance at 450 nm, and calculate cell vitality using the following formula:

$$\text{Cell viability \%} = (A_0/A) \times 100\% \quad (3)$$

where  $A$  and  $A_0$  represent the absorbance values of the sample group and the control group, respectively.

### 2.8. Effects of Cellular Tyrosinase Activity

The method developed by No et al. [35] was modified. Firstly, B16-F10 cells were seeded into 96-well plates at a density of 8000 cells/well and cultured for 48 h. The 100% concentration extraction solution was prepared following the method from Section 2.7. Then, it was diluted into three concentration gradients of 20%, 5%, and 1%. The test solution was added after 48 h, and each group was set up with 4 parallel experiments and a blank control. The cells were further incubated for 24 h after drug administration. After treatment, the cells were washed with PBS, and then 40 µL of cell lysis buffer containing 1 mM Phenylmethanesulfonyl fluoride was added to each well. The plate was incubated at 4 °C for 30 min, followed by incubation at 37 °C for 5 min. Subsequently, 100 µL of 1 mg/mL L-DOPA solution was added to each well and incubated in a 37 °C incubator for 2 h. After incubation, the activity of cellular tyrosinase was measured by obtaining the absorbance at 475 nm using an ELISA reader according to the following formula:

$$\text{Tyrosinase activity \%} = (A_0/A) \times 100\% \quad (4)$$

where  $A$  and  $A_0$  represent the absorbance values of the sample group and the control group, respectively.

### 2.9. Melanin Measurement

According to the methods described in a previous study [36], with appropriate modifications, B16-F10 cells were seeded at a density of 200,000 cells per well in a 6-well plate and incubated for 48 h. The extraction method for the solution was performed as described in Section 2.8. Following the incubation period, each well was treated with 2 mL of extraction solution at varying concentrations with a blank control and further incubated for 48 h. The cells were processed by washing with PBS twice and treated with 500 µL of cell lysis solution in each well, followed by incubation at room temperature for two hours for lysis. The melanin component was collected in a 1.5 mL centrifuge tube and centrifuged at a speed of 8000 rpm for 5 min. Then, the supernatant was discarded, and 200 µL of 1 M NaOH solution containing 10% DMSO was added to the samples. The samples were incubated in a 70–80 °C water bath for 4 h to dissolve the melanin. The solution was placed

in a 96-well plate and the absorbance was measured at 405 nm using an ELISA reader. The melanin contents are calculated as follows:

$$\text{Melanin contents \%} = (A_0/A) \times 100\% \quad (5)$$

where  $A$  and  $A_0$  represent the absorbance values of the sample group and the control group, respectively.

#### 2.10. Zebrafish Experiment

Fifteen zebrafish from the wild-type AB strain, exhibiting typical developmental characteristics after six hours of fertilization, were selected and assigned to each well of a six-well plate. Caution should be exercised while removing deionized water from the wells to avoid causing harm to the embryos. Following this, 3 mL of 0.5% DMN solution was rapidly added to each well, and a negative control group (adding 3 mL of deionized water) was established. The plate was wrapped in aluminum foil and incubated in a biochemical incubator at 28.5 °C for 45 h. Subsequently, ten zebrafish were randomly selected from each group for photography and observation. ImageJ software (version 1.53t) was employed to analyze the strength of the melanin signal present in their heads. Whitening efficacy was calculated using the formula below:

$$\text{Whitening effect \%} = (S_0 - S) \times 100\%/S_0 \quad (6)$$

where  $S$  and  $S_0$  represent the signal intensity of melanin in the head of the zebrafish in the sample group and the control group, respectively.

#### 2.11. Clinical Research in DMNs

We recruited a total of 30 participants, consisting of 6 males and 24 females, with ages ranging from 20 to 58 years. Each participant applied DMNs for a duration of 24 h. At the conclusion of the application, the DMNs were removed, and the participants' skin conditions were observed at 0.5, 24, and 48 h.

To study the clinical whitening efficacy of DMNs, six subjects were selected, two with facial freckles, three with melasma, and one with age spots. Prior to starting the trial, the 6 participants were required to undergo a standardized cleansing process. Following the cleansing process, the participants were instructed to sit in a room with standard conditions (temperature: 20–24 °C, humidity: 40–60%) for a minimum of 30 min. This was to ensure that the skin could naturally dry. Subsequently, a DMN patch was placed on the area of pigmentation beneath the right eye and left in place for one full night, a minimum of 8 h, before being removed. The DMN patch was applied every 48 h, totaling 28 applications. The use of any other products (such as cosmetics or topical medications) in the treated area was avoided during DMN application. The participants underwent facial imaging using a VISIA (a commercial skin imaging analyzer) before the trial and at weeks 2 (W2), 4 (W4), 6 (W6), and 8 (W8) to obtain pre- and post-treatment comparative data. The measured data comprised the water content of the stratum corneum at the application site, values of trans-epidermal water loss (TEWL), melanin, hematochrome, individual type angle (ITA), and a photograph of the subject's facial area at the site of pigmentation. Tests on the same subject were completed by the same measurer.

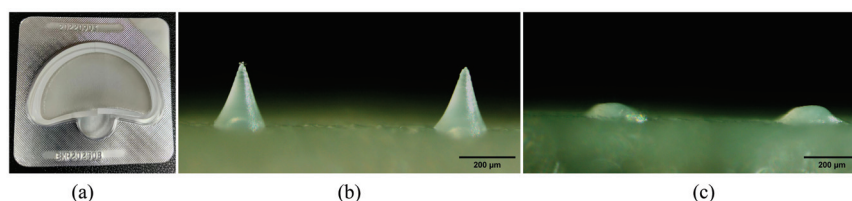
#### 2.12. Statistical Analysis

The quantitative data were analyzed through the IBM SPSS Statistics application, version 23.0, provided by IBM SPSS Inc. located in Chicago, IL, USA. Paired  $t$ -tests were used to analyze statistical differences in data that followed a normal distribution, either for within-group comparisons or for comparisons between the experimental and control groups. Significance levels of  $p < 0.05$ ,  $p < 0.01$ , and  $p < 0.001$  are indicated by asterisks: \*, \*\*, and \*\*\*, respectively.

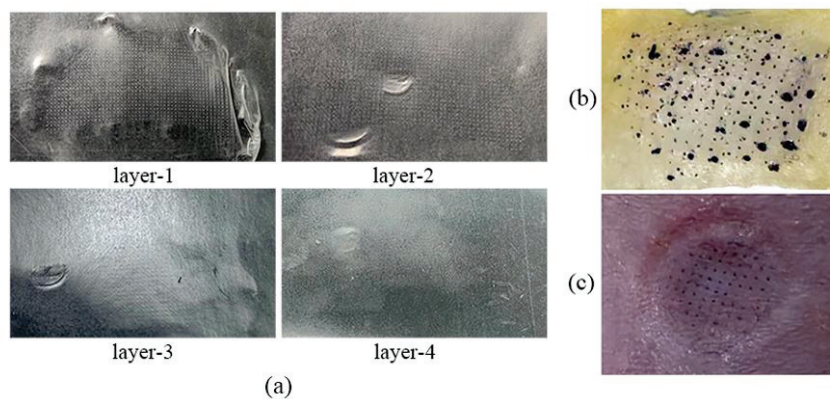
### 3. Results and Discussion

#### 3.1. Preparation and Characterization of DMNs

DMNs were manufactured in a clean room with a classification of ten thousand and packed with an aluminum–plastic foam cover, as illustrated in Figure 3a. A fluorescence microscope (BX51, Olympus, Tokyo, Japan) was used to capture images and observations, revealing that DMNs possess a complete needle tip structure. The needle height of the DMNs measures approximately  $224.4 \pm 4.4 \mu\text{m}$  (Figure 3b). In addition, after 40 min of skin (detached pigskin) treatment, the DMNs almost completely dissolved (Figure 3c). This indicates that DMNs have good dissolution ability, which can promote the rapid penetration of drugs into the skin. We conducted the puncture experiment for the DMNs using a sealant film with an average thickness of  $126 \mu\text{m}$  per layer [32]. As illustrated in Figure 4a, the DMNs created a needle hole array on the first and second layers of the sealant film, but not on the third and fourth layers. Moreover, DMNs have the capability to create distinct arrays of needle punctures on both isolated pig skin and SD rat skin as illustrated in Figure 4b,c. These findings suggest that DMNs perform well in puncture tests.



**Figure 3.** (a) DMNs prepared in a tens of thousands level clean room and packaged in aluminum and plastic; (b) DMN image captured after fabrication using a fluorescence microscope; (c) the needle tip that remains after inserting into pig skin and being dissolved in DMNs for 40 min.



**Figure 4.** (a) Results of puncturing 1–4 layers of sealing film; the needle hole array obtained by applying DMNs to (b) pig skin and (c) the SD rat.

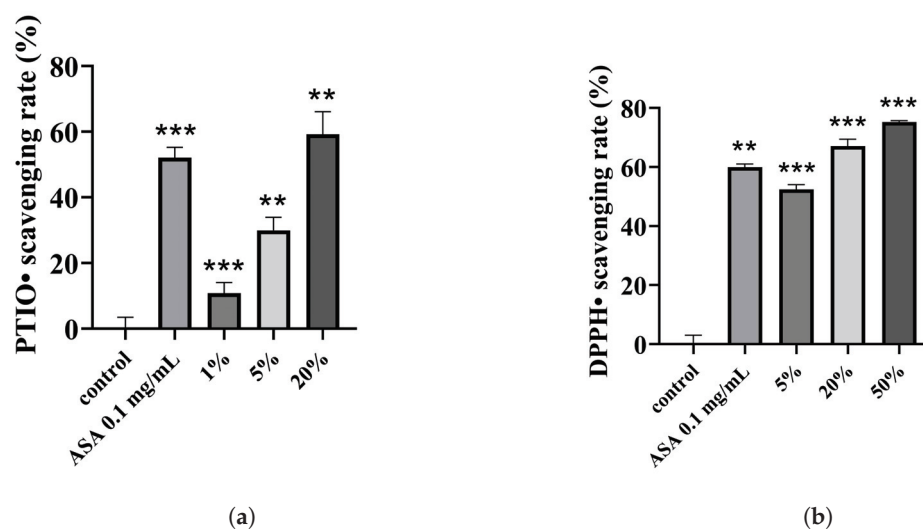
The height of the MN tips ranges between 50 and 900  $\mu\text{m}$ , allowing the MN to penetrate the stratum corneum [37]. However, an excessive needle height can cause skin damage. Xing et al. [38] assessed the impact of three various heights of MNs (230  $\mu\text{m}$ , 500  $\mu\text{m}$ , and 700  $\mu\text{m}$ ) on penetration depth and skin recovery. Among them, the depth of penetration of the 230  $\mu\text{m}$  MNs into the skin was  $85 \pm 12 \mu\text{m}$ , and the skin could recover within 30 min. The stratum corneum has a thickness of approximately 10–20  $\mu\text{m}$ . Consequently, a 230  $\mu\text{m}$  needle can pierce through the stratum corneum, reaching the epidermis or shallow dermis, resulting in swiftly healing small wounds on the skin. As a result, we have selected a 230  $\mu\text{m}$  needle height for the DMNs. Simultaneously, we selected HA, PVP, and PVA as matrix materials for the preparation of MNs. HA can hydrate and quickly absorb moisture, thereby accelerating the dissolution process of the DMNs [39]. The basal part of the DMNs, which is not inserted into the skin, will gradually dissolve and penetrate the skin through the pores created by the DMNs. Additionally, we utilized a PVA/PVP hybrid form to



effectively address the lack of mechanical strength in PVA when used alone. PVA is widely used due to its excellent biocompatibility and ability to form films, yet its inability to provide sufficient mechanical strength can be solved by mixing with PVP [40].

### 3.2. Antioxidant Results of DMNs

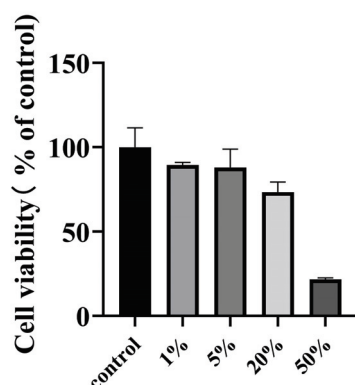
We conducted two studies to assess the antioxidant capacity of the combination using the DPPH assay [41] and PTIO radical scavenging assay [42]. Results from the PTIO experiment indicate that the 5% DMN extract possesses modest antioxidant activity, with a PTIO• scavenging rate of approximately 30%, while the scavenging rate of the 20% extract surpasses that of the positive control (0.1 mg/mL ASA). Furthermore, the combination's free radical scavenging efficacy positively correlates with the extract concentration (Figure 5a). Additionally, DMNs exhibit superior DPPH• clearing properties, with a 50% clearance rate at a 5% concentration and a higher clearance efficiency at a 20% concentration compared to the positive control (Figure 5b). Oxidative stress reactions arise from reactive oxygen species (ROS) accumulation [43] and may cause acquired melanin pigmentation. This can be countered by activating the cell's antioxidant defense system [44] or by introducing antioxidants [45,46]. Therefore, we introduced the VC derivative EAA to the combination, and the experimental results confirm that the inclusion of EAA enhances the combination's antioxidant effects.



**Figure 5.** (a) PTIO• scavenging rate and (b) DPPH• scavenging rate of different concentrations of DMNs and positive control group (0.1 mg/mL ASA). Significance levels of  $p < 0.01$ , and  $p < 0.001$  are indicated by asterisks: \*\*, and \*\*\*, respectively.

### 3.3. Cytotoxicity Results of DMNs

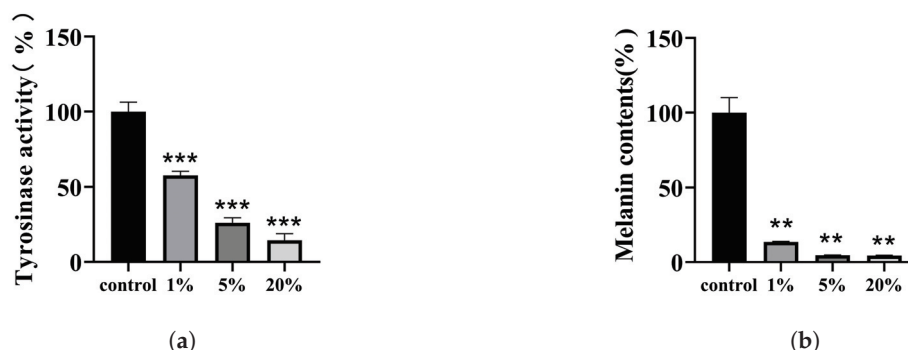
The objective of this section is to evaluate the potential cytotoxicity of the DMN extract. We exposed the B16-F10 cells to different concentrations of DMN extract solution for 24 h. Then, we performed CCK-8 experiments to analyze their individual cytotoxic activities. The findings indicated that concentrations of 5% and below did not exhibit any cytotoxicity. Similarly, cellular viability at 20% concentration was approximately 75%, indicating non-cytotoxicity. In contrast, the 50% concentration showed higher cytotoxicity, as shown in Figure 6. This experiment provides a basis for our subsequent experiments on anti-melanogenesis and cellular tyrosinase activity.



**Figure 6.** Cell viability of B16-F10 melanoma cells. Cells (8000) were seeded for 24 h, followed by treatment with different concentrations (1%, 5%, 20%, or 50%) of DMN extract for another 24 h. Untreated cells were used as controls.

#### 3.4. Effect of DMNs on The Activity of Tyrosinase in B16-F10 Cells

Tyrosinase is a crucial enzyme in the melanogenesis process [47]. To enhance the melanin inhibitory effect of the combination, we supplemented the tyrosinase inhibitor GLA. The tyrosinase inhibition effect of the combination was tested with B16-F10 cells. The outcomes demonstrated that at 1% concentration, about 42% of the enzyme activity was inhibited; at 5% concentration, around 74% was inhibited; and the inhibition rate at 20% concentration was over 80% (Figure 7a). It can be observed that the inhibition ability of the combination exhibited a direct correlation with the concentration. As a result, these findings suggest that DMNs have a greater tyrosinase inhibition efficiency.



**Figure 7.** (a) Detection of tyrosinase activity in B16-F10 cells using L-DOPA. Cells were treated with various concentrations (1%, 5%, or 20%) of DMNs for 24 h. Controls were untreated. (b) Melanin contents of B16-F10 cells. Cells were treated with various concentrations of DMNs for 24 h. Controls were untreated. Significance levels of  $p < 0.01$ , and  $p < 0.001$  are indicated by asterisks: \*\*, and \*\*\*, respectively.

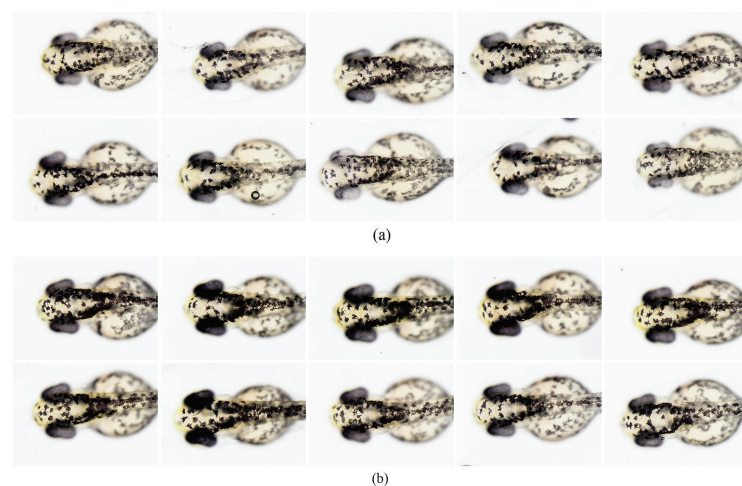
#### 3.5. Effect of DMNs on Melanin Production in B16-F10 Cells

For better visualization of the DMNs' depigmentation effect, we quantitatively analyzed melanin using B16-F10 cells. As shown in Figure 7b, the DMNs' effect on cellular melanogenesis was dose-dependent, inhibiting at rates of 86.43%, 95.35%, and 95.62% at concentrations of 1%, 5%, and 20% respectively. Previous tyrosinase experiments revealed that the tyrosinase inhibition rate for a 1% DMN extract was approximately 42%, whereas the melanin inhibition rate was 86%. Therefore, the combination of EAA, a potent antioxidant, and TXA, a melanin transfer inhibiting component, work synergistically with GLA to enhance its decolorization ability.

### 3.6. Effect of DMNs on Melanin Pigmentation of Zebrafish Embryos

Considering the prolonged duration and intricate procedures associated with guinea pig experiments, we therefore chose zebrafish as an animal model to evaluate the discoloration capacity of DMNs [48,49].

Ten zebrafish were selected randomly for each group to observe the back discoloration. The chromatophores on the backs of treated zebrafish were lighter than those in the control group (Figure 8a,b). Next, we used ImageJ software to evaluate the melanin on the backs of both groups of zebrafish quantitatively, and the decolorization rate in the treatment group rose to 32%, as shown in Figure 9a. The qualitative and quantitative results of the zebrafish experiment preliminarily verified that DMNs have decolorization potential. However, the depigmentation effect of the drug combination on zebrafish is relatively poor compared to its effects on B16-F10 cells. One possible reason is that the GLA in the combination does not exert a depigmentation effect on zebrafish and has a certain teratogenicity on zebrafish embryos [23]. The toxicity of GLA reduces the overall drug concentration of the combination. However, DMNs can achieve a depigmentation rate of 32% even at low administration concentrations and in the absence of GLA's effectiveness, indicating DMNs' whitening potential. In Figure 9b, the red dashed box delineates the region where we employed ImageJ software to quantify the concentration of melanin in the head of the zebrafish.



**Figure 8.** Representative photographs of zebrafish embryos at 51 h post fertilization (hpf). Embryos were treated with (a) 0.5% DMNs from 6 to 51 hpf; (b) Controls were untreated.

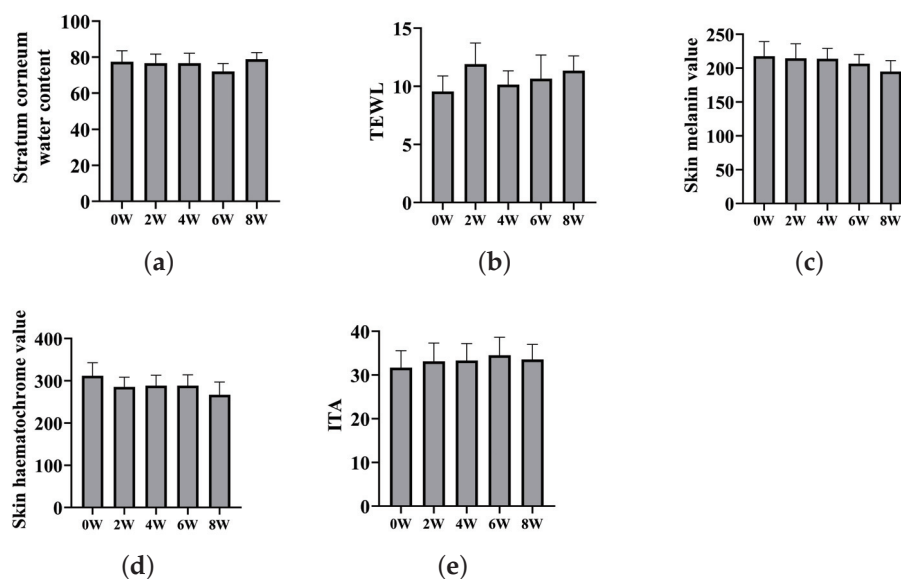


**Figure 9.** (a) Whitening efficacy evaluation of 0.5% DMNs and blank control. All groups were quantitatively analyzed for zebrafish head melanin using ImageJ software, and the results are expressed as mean  $\pm$  SD ( $n = 10$ ). (b) The melanin content is determined by analyzing the region enclosed by the red dashed box. The significance level of  $p < 0.001$  is indicated by asterisk \*\*\*.

### 3.7. The Clinical Trial of DMNs

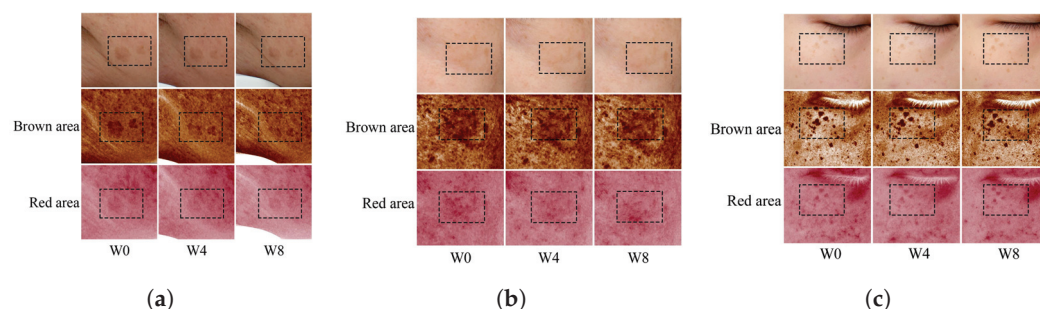
Thirty volunteers were recruited to assess the irritability of DMNs. Low-sensitivity adhesive tape was utilized to apply DMNs to the participants' backs for 24 h, followed by removal. The participants' skin reactions were observed at 0.5 h, 24 h, and 48 h, respectively. The results were recorded based on the skin reaction grading standards outlined in the Cosmetic Safety Technical Specifications (2015 version). The results indicated no occurrence of adverse reactions among these 30 volunteers, thus confirming the safety of DMN usage.

Due to its assured safety, we enlisted various volunteers exhibiting visible freckles, melasma, and age spots on their faces for an eight-week efficacy test of DMNs for skin whitening. During the procedure, there were no noticeable changes observed in the moisture content of the stratum corneum and the TEWL of all individuals (Figure 10a,b). This suggests that DMN application does not result in moisture loss in the stratum corneum. The primary component of DMNs, HA, exhibits potent hydrating properties and is extensively utilized in cosmetics to improve skin moisture retention [50], which might be the reason for there being no observed loss of moisture. The skin's melanin and red pigment at the site of drug administration both decreased. Melanin decreased by 10.49% and red pigment decreased by 14.40% (Figure 10c,d). ITA (ITA is used to represent the chromatic individual type angle, with a higher value indicating a brighter skin color) value slightly increased by approximately 5.97% (Figure 10e), signifying that DMNs can reasonably lighten spots and whiten skin. We captured the participants' facial images using VISIA (a commercial skin imaging analyzer) every four weeks. Patients with age spots exhibited a reduction in pigmentation in the brown and red regions (Figure 11a), while patients with melasma showed slight a reduction in the pigment in their faces (Figure 11b), but it was less than that of age spots. Nonetheless, the treatment effect of DMNs on freckles was not significant (Figure 11c). The reason for the different efficacies of DMNs on melasma, age spots, and freckles may be due to the reality that freckles are primarily determined by genetic and congenital factors, whereas melasma and age spots are primarily caused by postnatal factors such as UV exposure and hormone levels [51]. Meanwhile, most drugs are more effective in treating postnatal diseases rather than congenital diseases. In conclusion, clinical trials have validated the safety of DMNs for topical application and have shown that it does not cause any loss of skin moisture. Moreover, DMNs exhibit selective efficacy in treating both age spots and melasma.



**Figure 10.** All subjects were tested at 0 W, 2 W, 4 W, 6 W, and 8 W for (a) skin stratum corneum water content, (b) TEWL, (c) skin melanin, (d) skin hematochrome, and (e) ITA.





**Figure 11.** Subjects with (a) age spots, (b) melasma, and (c) freckles on the face were taken at 0 W, 4 W, and 8 W using VISIA (a commercial skin imaging analyzer) to capture facial images. The dashed box highlights the area of pigment reduction.

#### 4. Conclusions

UV radiation triggers oxidative stress, which leads to an increase in intracellular ROS levels in human epidermal melanocytes [52]. Additionally, UV exposure increases the activity of intracellular tyrosinase, accelerating melanin production in the epidermis [53]. In this study, a polymer matrix containing GLA, EAA, and TXA was loaded onto MNs, and the antioxidant effects of DMNs were confirmed. DMNs inhibit intracellular tyrosinase and melanin production, as demonstrated in B16-F10 cells and zebrafish models. DMNs were found safe in clinical trials and selectively lightened chloasma and age spots. Future research will determine the optimal ratios of the three-drug components. In conclusion, the DMNs, which consist of various components and exhibit multiple effects, have the potential for whitening.

**Author Contributions:** Conceptualization, Y.G. and S.Z.; Data curation, C.Y. and M.X.; Supervision, S.Z.; Writing—original draft, C.Y.; Writing—review and editing, C.Y., M.X. and Y.G. All authors have read and agreed to the published version of the manuscript.

**Funding:** This research was funded by the Director’s Fund of the Technical Institute of Physics and Chemistry, Chinese Academy of Sciences (grant number: E0AK076M12).

**Institutional Review Board Statement:** The clinical safety test was supported by Suzhou Guochen Bio-tech Co., Ltd., on human subjects. Procedures for animal studies were approved by the Institutional Animal Care and Utilisation Committee of the Technical Institute of Physics and Chemistry, CAS (approval number, LHDW-23025, and IACUCIPC-23025). The animal experiments followed the Guide for the Care and Use of Laboratory Animals (Eighth Edition, 2011). The human efficacy evaluation experiment of DMNs was carried out at the Cosmetics Testing Center under the Medical Biotechnology Research and Development Center at Jinan University in Guangzhou. All clinical studies conducted adhered to the Helsinki Declaration guidelines. However, an ethics review was not carried out at the Jinan University Testing Center due to the small sample size. Additionally, Guochen Bio-tech Co., Ltd., could not provide an ethics number as a result of the confidentiality of their data.

**Data Availability Statement:** Data are available on request due to restrictions, e.g., privacy or ethics; the data presented in this study are available on request from the corresponding author.

**Conflicts of Interest:** The authors declare no conflict of interest.

#### Abbreviations

MNs, microneedles; DMNs, drug-loaded microneedles; ASA, ascorbic acid; TXA, Tranexamic acid; GLA, Glabridin; EAA, 3-O-Ethyl-L-ascorbic acid; VC, vitamin C; HA, hyaluronic acid; PVA, Poly(vinyl alcohol); PVP, poly(vinylpyrrolidone); PDMS, polydimethylsiloxane; ELISA, enzyme-linked immunosorbent assay; CCK-8, Cell Counting Kit-8; TEWL, trans-epidermal water loss; ITA, individual type angle; ROS, reactive oxygen species; PTIO, 2-Phenyl-4,4,5,5-tetramethylimidazoline-1-oxyl-3-oxide; DPPH, 1,1-diphenyl-2-picrylhydrazyl.

## References

- Khalili, M.; Amiri, R.; Iranmanesh, B.; Zartab, H.; Aflatoonian, M. Safety and efficacy of mesotherapy in the treatment of melasma: A review article. *J. Cosmet. Dermatol.* **2022**, *21*, 118–129. [CrossRef] [PubMed]
- Kang, H.Y.; Lee, J.W.; Papaccio, F.; Bellei, B.; Picardo, M. Alterations of the pigmentation system in the aging process. *Pigment. Cell Melanoma Res.* **2021**, *34*, 800–813. [CrossRef] [PubMed]
- Phansuk, K.; Vachiramon, V.; Jurairattanaporn, N.; Chanprapaph, K.; Rattananukrom, T. Dermal pathology in melasma: An update review. *Clin. Cosmet. Investig. Dermatol.* **2022**, *15*, 11–19. [CrossRef]
- Choi, W.; Yin, L.; Smuda, C.; Batzer, J.; Hearing, V.J.; Kolbe, L. Molecular and histological characterization of age spots. *Exp. Dermatol.* **2017**, *26*, 242–248. [CrossRef]
- Burestedt, E.; Narvaez, A.; Ruzgas, T.; Gorton, L.; Emnéus, J.; Domínguez, E.; Marko-Varga, G. Rate-limiting steps of tyrosinase-modified electrodes for the detection of catechol. *Anal. Chem.* **1996**, *68*, 1605–1611. [CrossRef]
- Searle, T.; Al-Niaimi, F.; Ali, F. Hydroquinone: Myths and reality. *Clin. Exp. Dermatol.* **2021**, *46*, 636–640. [CrossRef]
- Wang, W.; Gao, Y.; Wang, W.; Zhang, J.; Yin, J.; Le, T.; Xue, J.; Engelhardt, U.H.; Jiang, H. Kojic acid showed consistent inhibitory activity on tyrosinase from mushroom and in cultured B16F10 cells compared with arbutins. *Antioxidants* **2022**, *11*, 502. [CrossRef]
- Xu, H.; Li, X.; Xin, X.; Mo, L.; Zou, Y.; Zhao, G.; Yu, Y.; Chen, K. Antityrosinase mechanism and antimelanogenic effect of arbutin esters synthesis catalyzed by whole-cell biocatalyst. *J. Agric. Food Chem.* **2021**, *69*, 4243–4252. [CrossRef]
- Kim, J.H.; Yoon, J.Y.; Yang, S.Y.; Choi, S.K.; Kwon, S.J.; Cho, I.S.; Jeong, M.H.; Ho Kim, Y.; Choi, G.S. Tyrosinase inhibitory components from Aloe vera and their antiviral activity. *J. Enzym. Inhib. Med. Chem.* **2017**, *32*, 78–83. [CrossRef]
- Draeos, Z.D. Skin lightening preparations and the hydroquinone controversy. *Dermatol. Ther.* **2007**, *20*, 308–313. [CrossRef]
- Hseu, Y.C.; Chang, C.T.; Gowrisankar, Y.V.; Chen, X.Z.; Lin, H.C.; Yen, H.R.; Yang, H.L. Zerumbone exhibits antiphotodamage and dermatoprotective properties in ultraviolet A-irradiated human skin fibroblast cells via the activation of Nrf2/ARE defensive pathway. *Oxidative Med. Cell. Longev.* **2019**, *2019*, 4098674. [CrossRef]
- Panich, U.; Tangsupa-a nan, V.; Onkoksoong, T.; Kongtaphan, K.; Kasetsinsombat, K.; Akarasereenont, P.; Wongkajornsilp, A. Inhibition of UVA-mediated melanogenesis by ascorbic acid through modulation of antioxidant defense and nitric oxide system. *Arch. Pharmacol. Res.* **2011**, *34*, 811–820. [CrossRef]
- Dilokthornsakul, W.; Dhipayom, T.; Dilokthornsakul, P. The clinical effect of glutathione on skin color and other related skin conditions: A systematic review. *J. Cosmet. Dermatol.* **2019**, *18*, 728–737. [CrossRef]
- Zduńska-Pęciak, K.; Kołodziejczak, A.; Rotsztejn, H. Two superior antioxidants: Ferulic acid and ascorbic acid in reducing signs of photoaging—A split-face comparative study. *Dermatol. Ther.* **2022**, *35*, e15254. [CrossRef]
- Park, H.J.; Cho, J.H.; Hong, S.H.; Kim, D.H.; Jung, H.Y.; Kang, I.K.; Cho, Y.J. Whitening and anti-wrinkle activities of ferulic acid isolated from *Tetragonia tetragonioides* in B16F10 melanoma and CCD-986sk fibroblast cells. *J. Nat. Med.* **2018**, *72*, 127–135. [CrossRef]
- Yu, J.S.; Kim, A.K. Effect of combination of taurine and azelaic acid on antimelanogenesis in murine melanoma cells. *J. Biomed. Sci.* **2010**, *17*, 1–5. [CrossRef]
- Keragala, C.B.; Medcalf, R.L. Plasminogen: An enigmatic zymogen. *Blood* **2021**, *137*, 2881–2889. [CrossRef] [PubMed]
- Na, J.; Choi, S.; Yang, S.; Choi, H.; Kang, H.; Park, K.C. Effect of tranexamic acid on melasma: A clinical trial with histological evaluation. *J. Eur. Acad. Dermatol. Venereol.* **2013**, *27*, 1035–1039. [CrossRef] [PubMed]
- Kanechorn Na Ayuthaya, P.; Niumphradit, N.; Manosroi, A.; Nakakes, A. Topical 5% tranexamic acid for the treatment of melasma in Asians: A double-blind randomized controlled clinical trial. *J. Cosmet. Laser Ther.* **2012**, *14*, 150–154. [CrossRef]
- Litaiem, N.; Daadaa, N.; Karray, M.; Chamli, A.; Zeglaoui, F. Hypopigmentation as a side effect of melasma treatment with tranexamic acid intradermal microinjections. *Dermatol. Ther.* **2020**, *33*, e13503. [CrossRef]
- Simmler, C.; Pauli, G.F.; Chen, S.N. Phytochemistry and biological properties of glabridin. *Fitoterapia* **2013**, *90*, 160–184. [CrossRef]
- Pan, C.; Liu, X.; Zheng, Y.; Zhang, Z.; Li, Y.; Che, B.; Liu, G.; Zhang, L.; Dong, C.; Aisa, H.A.; et al. The mechanisms of melanogenesis inhibition by glabridin: Molecular docking, PKA/MITF and MAPK/MITF pathways. *Food Sci. Hum. Wellness* **2023**, *12*, 212–222. [CrossRef]
- Chen, J.; Yu, X.; Huang, Y. Inhibitory mechanisms of glabridin on tyrosinase. *Spectrochim. Acta Part Mol. Biomol. Spectrosc.* **2016**, *168*, 111–117. [CrossRef]
- Chen, S.J.; Hseu, Y.C.; Gowrisankar, Y.V.; Chung, Y.T.; Zhang, Y.Z.; Way, T.D.; Yang, H.L. The anti-melanogenic effects of 3-O-ethyl ascorbic acid via Nrf2-mediated  $\alpha$ -MSH inhibition in UVA-irradiated keratinocytes and autophagy induction in melanocytes. *Free Radic. Biol. Med.* **2021**, *173*, 151–169. [CrossRef]
- Le, Z.; Yu, J.; Quek, Y.J.; Bai, B.; Li, X.; Shou, Y.; Myint, B.; Xu, C.; Tay, A. Design principles of microneedles for drug delivery and sampling applications. *Mater. Today* **2022**, *63*, 137–169. [CrossRef]
- Nguyen, T.T.; Oh, Y.; Kim, Y.; Shin, Y.; Baek, S.K.; Park, J.H. Progress in microneedle array patch (MAP) for vaccine delivery. *Hum. Vaccines Immunother.* **2021**, *17*, 316–327. [CrossRef] [PubMed]
- Liu, H.; Wang, B.; Xing, M.; Meng, F.; Zhang, S.; Yang, G.; Cheng, A.; Yan, C.; Xu, B.; Gao, Y. Thermal stability of exenatide encapsulated in stratified dissolving microneedles during storage. *Int. J. Pharm.* **2023**, *636*, 122863. [CrossRef] [PubMed]

28. Mönkäre, J.; Nejadnik, M.R.; Baccouche, K.; Romeijn, S.; Jiskoot, W.; Bouwstra, J.A. IgG-loaded hyaluronan-based dissolving microneedles for intradermal protein delivery. *J. Control. Release* **2015**, *218*, 53–62. [CrossRef] [PubMed]
29. Chiu, Y.H.; Chen, M.C.; Wan, S.W. Sodium hyaluronate/chitosan composite microneedles as a single-dose intradermal immunization system. *Biomacromolecules* **2018**, *19*, 2278–2285. [CrossRef]
30. Teodorescu, M.; Bercea, M.; Morariu, S. Biomaterials of PVA and PVP in medical and pharmaceutical applications: Perspectives and challenges. *Biotechnol. Adv.* **2019**, *37*, 109–131. [CrossRef]
31. Saha, I.; Rai, V.K. Hyaluronic acid based microneedle array: Recent applications in drug delivery and cosmetology. *Carbohydr. Polym.* **2021**, *267*, 118168. [CrossRef] [PubMed]
32. Enggi, C.K.; Sulistiawati, S.; Stephanie, S.; Tangdilintin, F.; Achmad, A.A.; Putri, R.A.; Burhanuddin, H.; Arjuna, A.; Manggau, M.A.; Permana, A.D. Development of probiotic loaded multilayer microcapsules incorporated into dissolving microneedles for potential improvement treatment of vulvovaginal candidiasis: A proof of concept study. *J. Colloid Interface Sci.* **2023**. [CrossRef]
33. Li, X.; Lin, J.; Chen, B.; Xie, H.; Chen, D. Antioxidant and cytoprotective effects of kukoamines A and B: Comparison and positional isomeric effect. *Molecules* **2018**, *23*, 973. [CrossRef] [PubMed]
34. Kim, D.E.; Chang, B.Y.; Ham, S.O.; Kim, Y.C.; Kim, S.Y. Neobavaisoflavone inhibits melanogenesis through the regulation of Akt/GSK-3 $\beta$  and MEK/ERK pathways in B16F10 cells and a reconstructed human 3D skin model. *Molecules* **2020**, *25*, 2683. [CrossRef]
35. Ullah, S.; Kang, D.; Lee, S.; Ikram, M.; Park, C.; Park, Y.; Yoon, S.; Chun, P.; Moon, H.R. Synthesis of cinnamic amide derivatives and their anti-melanogenic effect in  $\alpha$ -MSH-stimulated B16F10 melanoma cells. *Eur. J. Med. Chem.* **2019**, *161*, 78–92. [CrossRef] [PubMed]
36. Wolnicka-Glubisz, A.; Nogal, K.; Żądło, A.; Płonka, P.M. Curcumin does not switch melanin synthesis towards pheomelanin in B16F10 cells. *Arch. Dermatol. Res.* **2015**, *307*, 89–98. [CrossRef]
37. Bariya, S.H.; Gohel, M.C.; Mehta, T.A.; Sharma, O.P. Microneedles: An emerging transdermal drug delivery system. *J. Pharm. Pharmacol.* **2012**, *64*, 11–29. [CrossRef]
38. Xing, M.; Liu, H.; Meng, F.; Ma, Y.; Zhang, S.; Gao, Y. Design and Evaluation of Complex Polypeptide-Loaded Dissolving Microneedles for Improving Facial Wrinkles in Different Areas. *Polymers* **2022**, *14*, 4475. [CrossRef]
39. Oh, E.J.; Park, K.; Kim, K.S.; Kim, J.; Yang, J.A.; Kong, J.H.; Lee, M.Y.; Hoffman, A.S.; Hahn, S.K. Target specific and long-acting delivery of protein, peptide, and nucleotide therapeutics using hyaluronic acid derivatives. *J. Control. Release* **2010**, *141*, 2–12. [CrossRef]
40. Wei, Q.; Wang, Y.; Chai, W.; Wang, T.; Zhang, Y. Effects of composition ratio on the properties of poly (vinyl alcohol)/poly (acrylic acid) blend membrane: A molecular dynamics simulation study. *Mater. Des.* **2016**, *89*, 848–855. [CrossRef]
41. Li, X. Comparative Study of 1, 1-Diphenyl-2-picryl-hydrazyl Radical (DPPH $\bullet$ ) Scavenging Capacity of the Antioxidant Xanthenes Family. *ChemistrySelect* **2018**, *3*, 13081–13086. [CrossRef]
42. Li, X. 2-Phenyl-4, 4, 5, 5-tetramethylimidazoline-1-oxyl 3-Oxide (PTIO $\bullet$ ) radical scavenging: A new and simple antioxidant assay in vitro. *J. Agric. Food Chem.* **2017**, *65*, 6288–6297. [CrossRef]
43. Trouba, K.J.; Hamadeh, H.K.; Amin, R.P.; Germolec, D.R. Oxidative stress and its role in skin disease. *Antioxidants Redox Signal.* **2002**, *4*, 665–673. [CrossRef]
44. Onkoksoong, T.; Jeayeng, S.; Pongvarin, N.; Limsaengurai, S.; Thamsermsang, O.; Tripatara, P.; Akarasereenont, P.; Panich, U. Thai herbal antipyretic 22 formula (APF22) inhibits UVA-mediated melanogenesis through activation of Nrf2-regulated antioxidant defense. *Phytother. Res.* **2018**, *32*, 1546–1554. [CrossRef]
45. Nahhas, A.F.; Abdel-Malek, Z.A.; Kohli, I.; Braunberger, T.L.; Lim, H.W.; Hamzavi, I.H. The potential role of antioxidants in mitigating skin hyperpigmentation resulting from ultraviolet and visible light-induced oxidative stress. *Photodermatol. Photoimmunol. Photomed.* **2019**, *35*, 420–428. [CrossRef] [PubMed]
46. Babbush, K.M.; Babbush, R.A.; Khachemoune, A. The therapeutic use of antioxidants for melasma. *J. Drugs Dermatol.* **2020**, *19*, 788–792. [CrossRef]
47. Hseu, Y.C.; Cheng, K.C.; Lin, Y.C.; Chen, C.Y.; Chou, H.Y.; Ma, D.L.; Leung, C.H.; Wen, Z.H.; D Wang, H.M. Synergistic effects of linderanolide B combined with arbutin, PTU or kojic acid on tyrosinase inhibition. *Curr. Pharm. Biotechnol.* **2015**, *16*, 1120–1126. [CrossRef]
48. Lajis, A.F.B. A zebrafish embryo as an animal model for the treatment of hyperpigmentation in cosmetic dermatology medicine. *Med. Lith.* **2018**, *54*, 35. [CrossRef] [PubMed]
49. Sturm, R.A. A golden age of human pigmentation genetics. *Trends Genet.* **2006**, *22*, 464–468. [CrossRef]
50. Juncan, A.M.; Moisă, D.G.; Santini, A.; Morgovan, C.; Rus, L.L.; Vonica-Țincu, A.L.; Loghin, F. Advantages of hyaluronic acid and its combination with other bioactive ingredients in cosmeceuticals. *Molecules* **2021**, *26*, 4429. [CrossRef]
51. Praetorius, C.; Sturm, R.A.; Steingrimsson, E. Sun-induced freckling: Ephelides and solar lentigines. *Pigment. Cell Melanoma Res.* **2014**, *27*, 339–350. [CrossRef] [PubMed]

52. Jiang, Y.; Zhao, D.; Sun, J.; Luo, X.; Li, H.; Sun, X.; Zheng, F. Analysis of antioxidant effect of two tripeptides isolated from fermented grains (Jiupei) and the antioxidative interaction with 4-methylguaiacol, 4-ethylguaiacol, and vanillin. *Food Sci. Nutr.* **2019**, *7*, 2391–2403. [CrossRef] [PubMed]
53. Fu, W.; Wu, Z.; Zheng, R.; Yin, N.; Han, F.; Zhao, Z.; Dai, M.; Han, D.; Wang, W.; Niu, L. Inhibition mechanism of melanin formation based on antioxidant scavenging of reactive oxygen species. *Analyst* **2022**, *147*, 2703–2711. [CrossRef] [PubMed]

**Disclaimer/Publisher’s Note:** The statements, opinions and data contained in all publications are solely those of the individual author(s) and contributor(s) and not of MDPI and/or the editor(s). MDPI and/or the editor(s) disclaim responsibility for any injury to people or property resulting from any ideas, methods, instructions or products referred to in the content.





Review

# Collagen Derived from Fish Industry Waste: Progresses and Challenges

Zahra Rajabimashhadi <sup>1</sup>, Nunzia Gallo <sup>1</sup>, Luca Salvatore <sup>2</sup> and Francesca Lionetto <sup>1,\*</sup><sup>1</sup> Department of Engineering for Innovation, University of Salento, Ecotekne Center, 73100 Lecce, Italy<sup>2</sup> Typeone Srl, Muro Leccese (LE), 73100 Lecce, Italy

\* Correspondence: francesca.lionetto@unisalento.it

**Abstract:** Fish collagen garnered significant academic and commercial focus in the last decades featuring prospective applications in a variety of health-related industries, including food, medicine, pharmaceuticals, and cosmetics. Due to its distinct advantages over mammalian-based collagen, including the reduced zoonosis transmission risk, the absence of cultural-religious limitations, the cost-effectiveness of manufacturing process, and its superior bioavailability, the use of collagen derived from fish wastes (i.e., skin, scales) quickly expanded. Moreover, by-products are low cost and the need to minimize fish industry waste's environmental impact paved the way for the use of discards in the development of collagen-based products with remarkable added value. This review summarizes the recent advances in the valorization of fish industry wastes for the extraction of collagen used in several applications. Issues related to processing and characterization of collagen were presented. Moreover, an overview of the most relevant applications in food industry, nutraceutical, cosmetics, tissue engineering, and food packaging of the last three years was introduced. Lastly, the fish-collagen market and the open technological challenges to a reliable recovery and exploitation of this biopolymer were discussed.

**Keywords:** fish collagen; fish industry waste; collagen extraction; nano collagen; sustainability

**Citation:** Rajabimashhadi, Z.; Gallo, N.; Salvatore, L.; Lionetto, F. Collagen Derived from Fish Industry Waste: Progresses and Challenges. *Polymers* **2023**, *15*, 544. <https://doi.org/10.3390/polym15030544>

Academic Editor: George Z. Papageorgiou

Received: 15 November 2022

Revised: 11 January 2023

Accepted: 13 January 2023

Published: 20 January 2023



**Copyright:** © 2023 by the authors. Licensee MDPI, Basel, Switzerland. This article is an open access article distributed under the terms and conditions of the Creative Commons Attribution (CC BY) license (<https://creativecommons.org/licenses/by/4.0/>).

## 1. Introduction

In order to exploit natural resources as much as possible, a long-term plan titled “Blue Growth” was approved by the European Commission and has been implemented to pay particular attention to fish resources in order to preserve the environment from industrial pollution. The enormous amount of valuable protein that could be extracted [1–5] (about 30–40% of the total weight), is one of the most appealing aspects of seafood by-products. More than 20 million tons of them are produced annually from the fish tissues that are discarded as waste, including fins, heads, skin, and viscera [6–8]. Because of their elevated protein content, absence of disease transmission risks, high bioactivity, and less considerable religious and ethical restrictions, the use of fish by-products as a new source of collagen has drawn increasing attention [9–11].

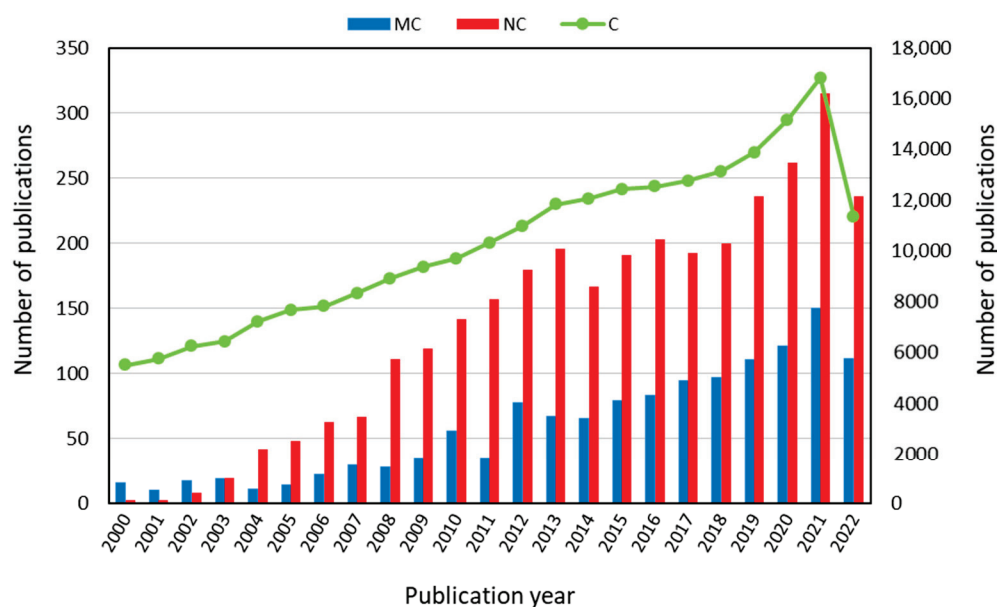
The importance of both aquaculture and fishing to food security is expanding continuously, particularly in light of the rising global fish production and the United Nations' 2030 program of sustainable development [12]. Approximately 70% of fish and other seafood are processed before being sold, resulting in enormous amounts of solid waste from processes such as beheading, de-shelling, degutting, separating fin and scales, and filleting [13,14]. More than half of the weight of fresh fish becomes by-products of the fish industry. Most of these by-products are buried or burned, causing environmental, health, and economic issues. A minor portion are employed as inexpensive ingredients in animal feeds. Fish waste is a rising problem that requires quick, creative methods and solutions. Numerous initiatives and programs have been performed globally to prevent food waste. In addition to reducing the cost of waste disposal, investing in waste from the fish industry can offer

the opportunity to recover other important substances such as oils, proteins, pigments, bioactive peptides, amino acids, collagen, chitin, gelatin, etc. [15–17].

More than two decades ago, research on the extraction of collagen from fish waste started to be conducted. Collagens are one of the most abundant proteins in animals, which are found in the extracellular matrix of connective tissues, including skin, bones, tendons, ligaments, cartilage, intervertebral discs, and blood vessels [18]. Collagens are not only implicated in tissue architecture maintenance and strength, but they also cover regulatory roles (i.e., through mechano-chemical transduction mechanisms) during tissue growth and repair [19,20]. Thanks to their nature, collagens are intrinsically bioactive, biocompatible, and biodegradable [21]. Hence, collagens are valued as the most commonly required and used biomaterials in many fields, including medical, cosmetic, nutraceutical, food and pharmaceutical industries in the forms of injectable solutions, thin substrates, porous sponges, nanofibrous matrices, and micro- and nano-spheres [22–25]. Recent studies revealed many similarities in the molecular structure and biochemical properties between collagen derived from fish and mammalian sources, despite the fact that fish collagen typically has a lower molecular weight and lower denaturation temperature than mammalian collagen [8,12,20,22,24,26–28]. Various extraction techniques for fish collagen have been developed depending on the selected tissue type and fish species. Hence, a considerable collection of literature has been developed on this subject [29–31]. Only in the past five years have researchers concentrated on innovative materials with improved characteristics in addition to developing extraction techniques for mass manufacture.

Collagen nanotechnology has a bright outlook because science in this area is always progressing and will continue to do so in the future. Nano collagen is ordinary collagen that has been sized down to a nanometer scale [32,33]. According to its nano-scale-based technology, which offers a high surface-area-to-volume ratio, an optimal penetration into wound sites and higher cell interaction is enabled. [34]. Moreover, nano collagen has the ability to deliver drugs and to supply a durable microenvironment at wounded sites to promote cellular regrowth and healing [35]. Collagen nanotechnology still presents many shortcomings, including the fact that only a small minority of therapeutic compounds have received commercial approval and that there are still numerous unsolved problems [32]. The complexity of pathophysiological symptoms and the lack of data on its real physiological effects is a further challenge for nanotechnology. Despite these downsides, nanotechnology is still a growing trend, with a huge amount of unrealized potential. This gives rise to the expectation that further research will assist in minimizing these downsides, leading to the creation of secure and efficient nano-based systems. In order to create approved therapeutic agents that take advantage of nanotechnology, additional research and studies must be performed [32]. Indeed, Figure 1 reveals the continuous increasing research interest on collagen, fish collagen, and nano collagen investigation in the last twenty years. In particular, it appears clear that there has been a significant increase in scientific works in the last five years. Nano collagen can be used for a variety of improvements and treatments, such as bone grafting, drug delivery, nerve tissue formation, vascular grafting, articular cartilage regeneration, cosmetics, and wound healing [21,22,36]. It is clear that nano collagen is a progressed type of nanotechnology; thus, further investigation must be attempted to advance this technology with the expectation that, in the future, nano collagen scaffolds will be more widely available [37].

This review aims to provide an overview of recent investigations into fish collagen, with a particular focus on its characteristics, types, and extraction methods, and, finally, on the valuation of fish industry waste for the preparation of biopolymers for various applications areas. Among others, fish-collagen application in the medical, pharmaceuticals, food, and cosmetic sectors are discussed.

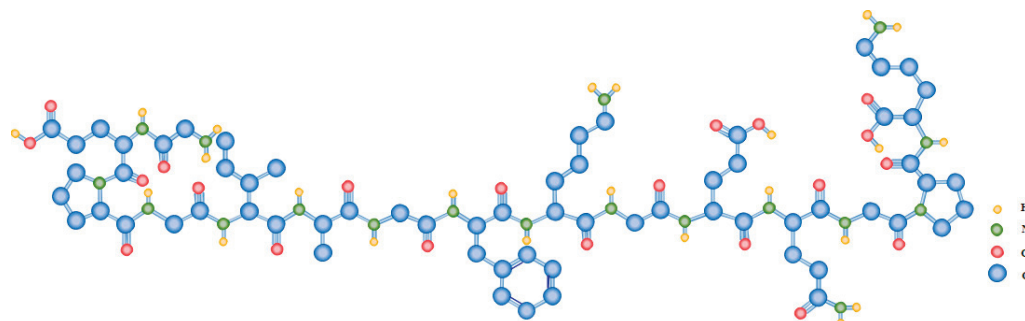


**Figure 1.** Increasing research interest in fish collagen (MC) and nano collagen (NC) compared with collagen (C), according to scientific papers analyzed by publication year in the last twenty years up to 2022 (from Scopus database: [www.scopus.com](http://www.scopus.com), accessed on 15 September 2022).

## 2. Collagen: Structure and Properties

Collagens represent about 30% of a mammal's weight [18,38]. Based on the historical order of their discovery, 28 types of collagens—type I through type XXVIII—have been identified and described up to the current day [39]. The oldest collagen identified to date was found in the soft tissue of a fossilized *Tyrannosaurus rex* bone that dates back 68 million years [40,41].

The molecular organization of collagens is highly variable, notwithstanding their general triple-helical structure and the triplet (Gly-X-Y)<sub>n</sub> repetition, where X and Y can be any amino acid, although proline and hydroxyproline are the most frequent occupants of these locations (Figure 2) [42,43]. Collagen's unit is composed of three  $\alpha$ -chains, the amino acid composition of which varies among collagen types. Furthermore, function and distribution in tissues play a role in the diversity of collagen, as well as molecular and supramolecular organization, such as occurrence and length of triple helical domains, packing of the triple helices, etc. [27,44].



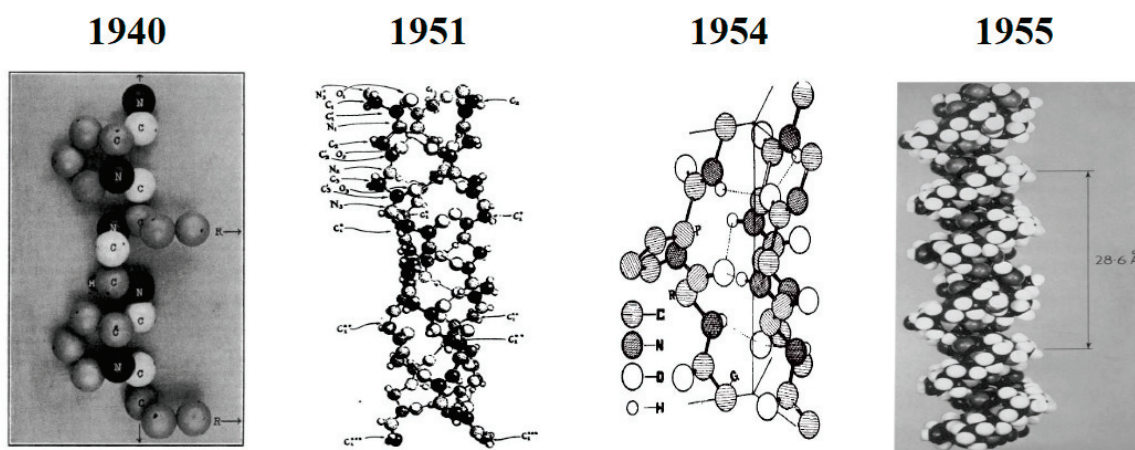
**Figure 2.** Exemplary amino acid repetition of the triplet (Gly-X-Y)<sub>n</sub> characteristic of type I collagen.

The most prevalent and thoroughly studied types of collagens are type I (almost present in all tissues and organs), type II (present in the cartilage, vitreous body, and nucleus pulposus), and type III (present in the skin, blood vessels, lungs, liver, and spleen) [45], which are used in tissue engineering and reconstructive medicine as well as in the pharmaceutical industry as compounds that extend the effects of drugs. Types I, II, and III

collagens, especially type I, are also used as plastics in medicine and cosmetology. Type I collagen represents over 70% of the entire collagen family and makes up more than 90% of the collagen in the human body. It is mainly found in connective tissues such as body joints, cartilages, bones, sclerae, ligaments, tendons, intervertebral discs, corneas, adventitia of blood vessels, skin, and most hollow organs including gastrointestinal and genitourinary tracts [24,39,46]. In contrast, types II, III, and IV collagen are frequently seen. Type II collagen, for instance, is a structurally important part of the hyaline cartilage that lines the adult's articular surfaces in addition to being present in other tissues including the intervertebral disc's nucleus pulposus and the retina, sclera, and lens of the eye. Skin, lungs, intestinal walls, and blood vessel walls all contain type III collagen.

Type I collagen is composed of three polypeptide chains, two identical  $\alpha 1(I)$  chains and one  $\alpha 2(I)$  chain, each of which has roughly 1000 amino acid residues [47]. Hydroxylation of proline residues is a typical post-translational modification of type I collagen that accounts for about 11–14% of amino acid residues and it is commonly used as a marker to detect and quantify collagen in tissues [48,49]. Whereas proline and hydroxyproline are essential for maintaining the triple helical structure under physiological conditions by forming hydrogen bonds that inhibit uncontrolled rotation, glycine is critical for packing the three helices [50,51].

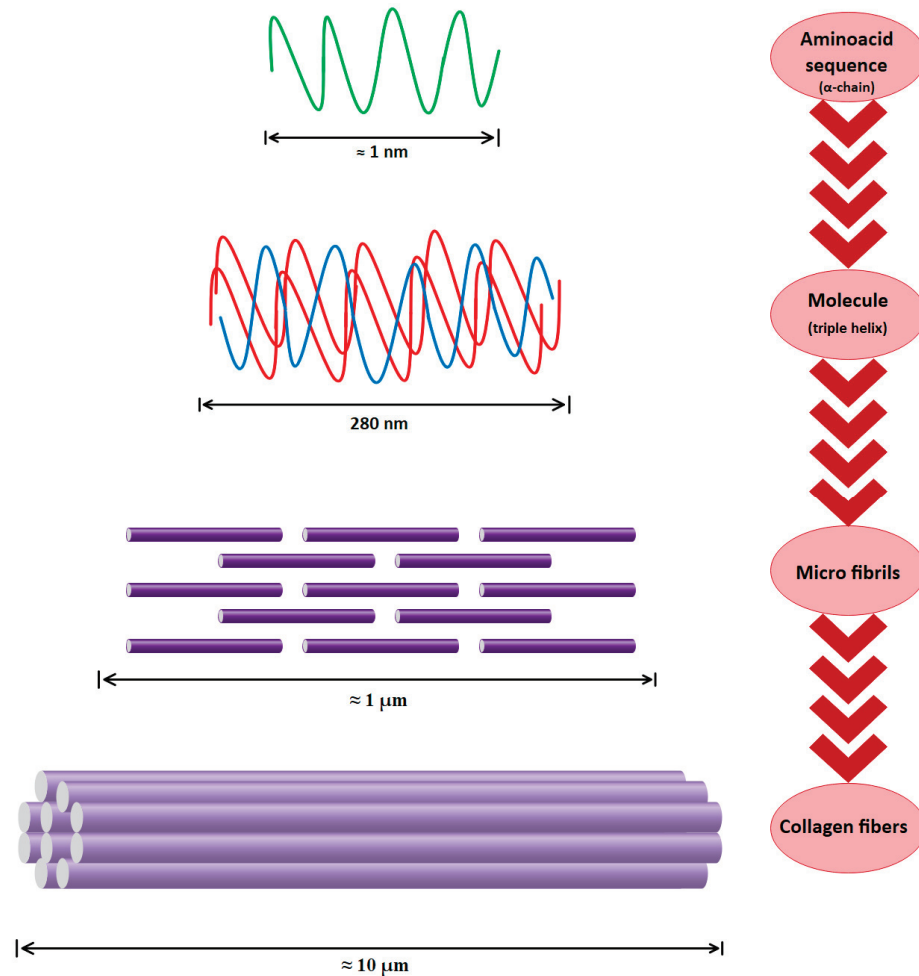
The idea that the type I collagen molecule is made up of a single extended polypeptide chain with all amide bonds was brought forward by Astbury and Bell in 1940 [51]. In 1951, Pauling and Corey provided the correct structures for the  $\alpha$ -helix and  $\beta$ -sheet [52]. In that proposal structure, three polypeptide chains were connected in a helical configuration by hydrogen bonds. These hydrogen bonds necessitated the production of two of the three peptide bonds and involved four of the six main chain heteroatoms inside each amino acid triplet [52]. The collagen triple helix structure was reconstructed in 1954 by Ramachandran and Kartha as a right-handed triple helix of three staggered, left-handed helices with one peptide bond and two hydrogen bonds within each triplet [53]. In 1955, this structure was improved by Rich and Crick, North, and Colleagues thanks to which the triple-helical structure that is still used today was unveiled. This structure has helical symmetry and just one crosslinking hydrogen bond per triplet [54]. Changes in the proposed structure of collagen from the beginning and its modification to the final structure accepted by the scientific community are shown in Figure 3.



**Figure 3.** Changes in the proposed structure of type I collagen from the beginning and its modification to the final accepted structure. Adapted from [52]. Reproduced from [51] with permission from Springer Nature, 1940. Reproduced from [53] with permission from Springer Nature, 1954. Reproduced from [54] with permission from Elsevier, 1955.

As is shown in Figure 4, three polypeptide  $\alpha$ -chains form the trimeric molecule that represents the type I collagen unit (length  $\approx$  300 nm, diameter  $\approx$  1.5 nm). Three parallel,

left-handed polyproline-II helices are arranged in a right-handed bundle [55,56]. Multiple collagen units are assembled into fibrils (length  $\approx \mu\text{m}$ , diameter  $\approx 100 \text{ nm}$ ) and then fibers (length  $\approx \text{mmm}$  diameter  $\approx 10 \mu\text{m}$ ) with dimensions and orientation that are strictly tissue-dependent [28,57].



**Figure 4.** Type I collagen hierarchical organization.

Thus, type I collagen is a hierarchically organized protein. The primary structure of type I collagen consists of three  $\alpha$  helices: two identical  $\alpha 1(\text{I})$  and one  $\alpha 2(\text{I})$  helices of approximately 1000 amino acids and a molecular weight of about 130–140 kDa and 110–120 kDa, respectively. The collagen molecule has a triple helical part and two non-helical parts at both ends (called telopeptides), with a molecular weight of 300–400 kDa, a length of 280 nm, and a width of 1.4 nm [58,59]. The secondary structure consists of each of these chains twisted in the form of a left-handed helix with three amino-acid repetitions in each turn. The tertiary structure, the inflexible structure, is created when the chains are then twisted three times around one another. Finally, in the quaternary structure, collagen molecules assemble into fibrils and then fibers. Because of the intermolecular and intramolecular interactions, this collagen organization is very stable [25,60]. Obviously, the collagen structure's stability is directly dependent on its chemical composition. For instance, the triple helix of collagen grows stronger as the percentage of amino acids is higher, such as proline and hydroxyproline. The pyrrolidine rings are directly responsible for the polypeptide chain's movement reduction [22,61]. Preservation of collagen's structural integrity results in an improvement in physical properties, an increase in thermal stability, and a decrease in the denaturation temperature [62–64].



Theoretical examination of the mechanical characteristics of collagen at several levels, including the main monomer, individual collagen fibrils, and collagen fibers, is possible by studying collagen's structured nature. Studying main monomers and fibrils made from type I collagen has likely provided the most direct measurements of the mechanical properties of collagen. Over the recent decades, researchers have used a variety of biophysical and theoretical methods, and recent developments in the Atomic Force Microscopy (AFM) approach have made it possible to perform more accurate evaluations [65]. According to estimates, the fracture strength of individual collagen triple helices is 11 GPa, which is much higher than that of collagen fibrils, which is 0.5 GPa [66]. This difference makes sense because, whereas the breaking of a fibril does not always entail the breakdown of covalent bonds, the breaking of individual collagen triple helices necessitates the unwinding of the triple helix and ultimately breaking of the covalent bonds [67]. In contrast to dehydrated type I collagen fibrils from mammalian sources, which have a Young's modulus of about 5 GPa according to AFM tests, individual collagen triple helices monomers have a Young's modulus between 6 and 7 GPa. Because collagen fibrils are anisotropic, another crucial measure of a collagen fibril's strength is its shear modulus, which determines stiffness [68].

Furthermore, AFM indicated that the shear modulus of dehydrated fibrils of type I collagen from mammalian sources is between 30 and 35 MPa. These fibrils' shear modulus was drastically decreased by hydration, but was increased by cross-linking. It is important to note that while some cross-linking is beneficial for the mechanical qualities of collagen fibrils, excessive cross-linking causes collagen fibrils to become highly brittle, which is a common sign of aging [69]. Investigation of the mechanical properties of collagen fibrils demonstrated that the length of the individual collagen triple helices monomer has been chosen by nature in a way to maximize the strength of the produced collagen fibril through effective energy dissipation. Simulations indicate that individual collagen triple helices monomers either longer or shorter than the length of a type I collagen triple helix, which is 300 nm, would form collagen fibrils with low mechanical properties [62]. The thermal and structural stability of the collagen triple helix is strongly influenced by the chemical composition of amino acid and its type, which is caused by the type of animal and the living conditions. Indeed, hydroxyproline stabilizes and strengthens the collagen structure [70]. In addition to preserving collagen's structure and enhancing its mechanical properties, hydroxyproline also plays an important role in its thermal stability. The denaturation temperature and denaturation enthalpy of collagen increases due to the presence of the hydroxyl group in hydroxyproline and the bonding with the pyrrolidine ring. The quantity of hydrogen bonds formed between hydroxyproline and pyrrolidine significantly influences the increment in enthalpy of denaturation. Therefore, the triple helix does have greater thermal stability the more water molecules that there are surrounding it [25,71].

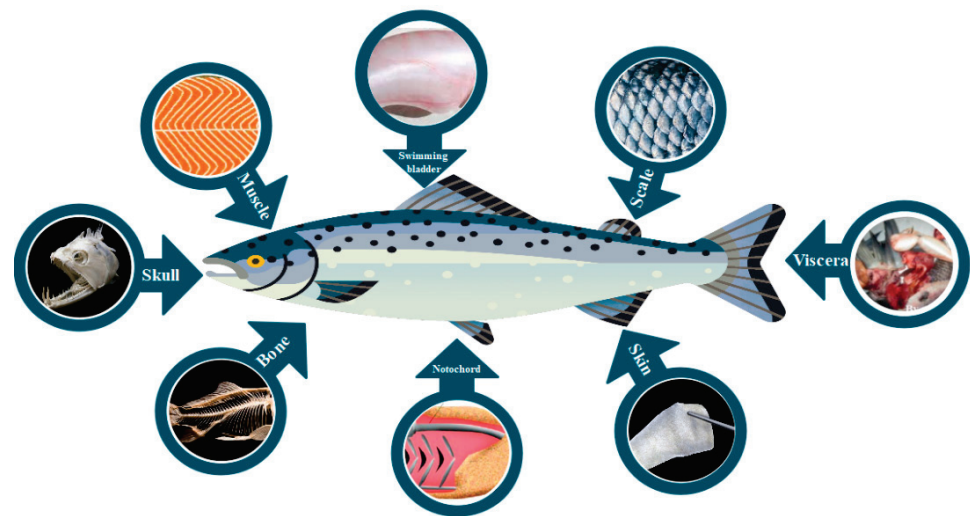
One of the most basic roles of collagen in the body is to provide connective tissues with stability, structure, and resistance to stresses [19,20]. Moreover, collagen has the ability to manage a wide range of nonstructural activities, including cell proliferation, migration, differentiation, and communication [60,72].

### 3. Fish Collagen

Collagen sources, types, pre-extraction conditions, and process methods are the main parameters that determine extracted product properties, including molecular weight of the peptide chain, amino acid composition, molecular structure, solubility, and functional activity. Although native type I collagen could be extracted from different mammalian sources, the main source of extraction is bovine due to availability and biocompatibility. [73]. There are other alternative sources for extracting type I collagen, among which pig, horse, sheep, and rat can be mentioned [74–77]. It is possible to obtain mammalian collagen from a wide range of tissues, notably skin, bones, tendons, lung tissue, and connective tissues. Due to some restrictions in terms of health, cultural, social, and religious issues that are implied by traditional sources, research has concentrated on the development of a new source of extraction. Various resources from the sea, including vertebrates as well as invertebrates,

have been studied and considered as collagen extraction sources. In particular, several fish species (e.g., *Rachycentron canadum*, *Esox lucius*, *Spotless smooth hound*, *Sciaenops ocellatus*, *Sardinella fimbriata*, *Coryphaena hippurus*, *Alaska pollock*, *Takifugu flavidus*, *Pacu*, *Labeo rohita*, *Labeo catla*, *Tuna*, *Thunnus obesus*, *Scomber japonicus*, *Gadus morhua*, *Prionace glauca*, *Cichla ocellaris*, *Cyprinus carpio*, *Oreochromis niloticus*, etc.) aquatic reptiles (such as the soft-shelled turtles), sponges, corals, octopuses, squids, starfish, jellyfish, cuttlefish and sea cucumbers, sea anemones, sea urchins, mussels, and shells were considered.

Skin, scales, bones, skull, swimming bladder, and remaining viscera, are by-products of fish that may be used as sources of collagen (Figure 5). Among all fish by-products, skin traditionally has been reported as the best source of fish collagen extraction [12,78–81].



**Figure 5.** By-products of fish as potential sources of collagen extraction.

Fish collagen physicochemical properties were found to be similar to mammalian collagen, but with some advantages such as (1) capability of purification and extraction; (2) aquaculture and accessibility to fishing by-product; (3) lower risk of disease transmission compared to mammalian collagen due to high ontogenetic difference between fish and humans; (4) lack of religious and cultural limitation; (5) slightly different chemical composition; (6) low viscosity; (7) non toxicity; (8) reasonable homeostatic properties; (9) bio-resorbability; (10) more simple extraction method; (11) more adaptable and metabolic compatibility; and (12) minimal inflammatory response (Figure 6) [82–85]. Although fish collagen has several advantages, it suffers from several disadvantages such as low denaturation temperature, low mechanical properties, and high degradation rate [78]. The major drawback of fish collagen compared to mammalian collagen is the lower denaturation temperature, which limits its medical applications [70]. During denaturation, collagen turns into gelatin, where the hydrogen bonds that support the helical structure are partially or completely destroyed, and it loses its structural role and its conformation-related biological activity [42,43]. The second main drawback of fish-derived collagen is its low mechanical resistance which limits its applications. Many efforts have been made to improve its mechanical properties and degradation profiles, including chemical or enzymatic cross-linking [86,87]. The different advantages and disadvantages of fish collagen are shown in Figure 6.

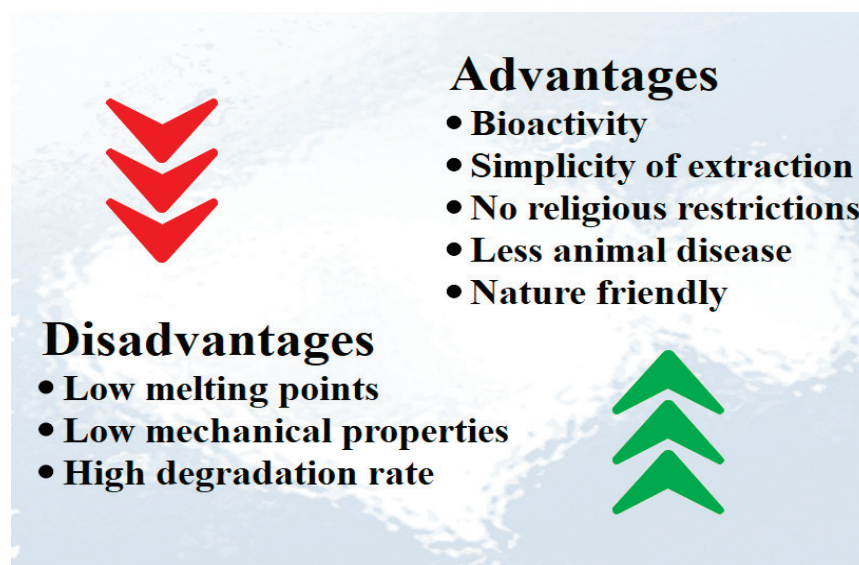


Figure 6. Advantages and disadvantages of fish collagen.

#### 4. Collagen Extraction Methods

Due to the enormous diversity of collagen types, it is challenging to design a standard extraction procedure for collagen from various tissues. However, the collagen extraction process usually consists of around five main steps (Table 1): (i) tissue separation and purification; (ii) tissue size reduction; (iii) non-collagenous components elimination; (vi) collagen extraction through acid and/or enzymatic treatment; (v) and, finally, recovery using salt precipitation. The extraction procedures start with the removal of unneeded portions. Fish by-products are then reduced in size to facilitate the following step which is the removal of non-collagen proteins, lipids, pigments, cell remnants, and minerals. Afterwards, collagen is extracted using an acidic treatment, followed by an optional enzymatic treatment, before being recovered using salt precipitation, dialyzation, and lyophilization. All these steps are performed at about 4° C to 10 °C, to prevent collagen denaturation [88–90].

Table 1. Five steps of collagen extraction process from fish sources [88–90].

No.	Step(s)	Time
1	Separation and purification	2 h
2	Size reduction	1 h
3	Non-collagenous components discarding	Up to 3 days
4	Collagen extraction through acid and/or enzyme treatment	Up to 6 days
5	Salt precipitation and recovery	2 days

The conventional process for collagen extraction, based on acid and/or enzymatic methods, has been improved in recent research. The fish ecosystem, the belonging tissue, and the method of extracting collagen from a fish source have a direct effect on the number of remaining impurities [83,91]. In the following, various sources, methods, advantages, and disadvantages of each method and effective parameters in the extraction of fish collagen have been investigated.

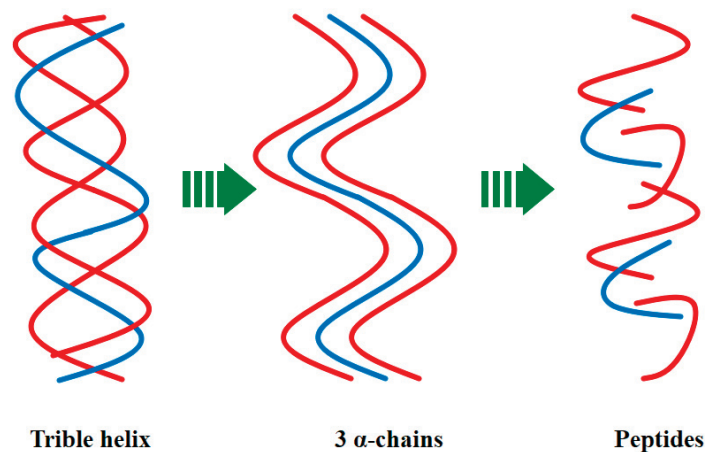
Fish tissues require special treatment before being recovered from fisheries and aquaculture byproducts, including washing with water and sodium chloride to remove impurities and lipids and milling the skin to increase its contact surface with the liquid phase [92]. Following the removal of contaminants and non-collagenous proteins using sodium hydroxide, hydrogen peroxide, calcium hydroxide, or a combination of these, the material is submerged in alkaline solutions, with butyl alcohol (10%) used to remove oily components [93,94].

The real extraction step is based on the solubility of the collagenous molecule taken after the pretreatment. The most common treatments are saline, acid, and/or enzymatic. The saline treatment employs neutral salt, such as sodium chloride and/or guanidine hydrochloride, for precipitation-based extraction, which, among its drawbacks, has a low extraction yield [95]. Once the sodium chloride concentration has been gradually raised through adding NaCl, the collagen is separated. It was shown that the basic salt extraction is ineffective after testing a number of collagen isolation techniques. Additionally, raising the salt content will enhance the ionic power of the resulting solution and boost the solubilization capacity. The ultimate yield is extremely low since, in normal tissues, the amount of neutral salt-soluble collagen is typically insignificant [96,97].

In the acid treatment, several acid types could be employed, such as acetic acid, lactic acid, citric acid, hydrochloric acid, formic acid, sulfuric acid, and tartaric acid [83]. Obviously, this method can solubilize collagen more effectively than basic salt extraction, but it is still only effective on young and uncross-linked collagen [97]. Collagen type I derived from fish skin is often extracted using an acidic treatment with acetic acid, hydrochloric acid, or phosphoric acid. However, this extraction method can be performed using either acids or alkali. These extraction techniques are extremely corrosive and, after neutralization, result in a high salt content. The pH value will influence the electrostatic interaction and structure depending on the acid's concentration. It establishes the ability of animal tissue to be extracted and dissolved [28,98,99].

Enzymatic treatment involves the use of enzymes, such as collagenase, papain, or pepsin [100,101]. Enzymatic hydrolysis has emerged as the best method for collagen extraction from fish because it tends to eliminate the non-helical extremities and increase the solubility of collagen molecules and, thus, increase the extracted material yield [102,103]. The potential for irreversible denaturation of the collagen structure by enzymatic digestion during this procedure could either be a drawback or not, since it could be used for the production of several collagen formulations with different hierarchical organization levels that will have different bioactivity profiles. A more effective collagen extraction method was obtained by integrating both the acidic and enzymatic treatments. The collagen molecule is affected by enzymes, which make it more soluble in an acidic media [61,104].

Figure 7 shows that the denaturation of native collagen results in the formation of randomly coiled  $\alpha$ -chains. Thermal treatments above collagen denaturation temperature can be used to obtain them. Proteolytic enzymes are able to hydrolyze the polypeptide chains in shorter polypeptide sequences. The final outcome is typically referred to as hydrolyzed collagen that is made up of short, low-molecular-weight peptides. The kind and level of hydrolysis, as well as the different type of enzyme used in the process, all affect collagen properties and functional activity [105–108].



**Figure 7.** Representative scheme of type I collagen denaturation into low-molecular-weight peptides (red and blue).



The molecule is not altered when collagen is extracted using ultrasonic as a substitute method; instead, this helps the enzymatic process [109,110]. This method can be used to produce higher collagen yields in shorter extraction durations. This approach is more effective than the traditional one because it increases mass transfer by opening the collagen fibrils, permitting acid and/or enzymatic hydrolysis, and subsequently improving the extraction yield [109–111].

Electro dialysis, a quick, effective, and affordable approach, was employed instead of traditional dialysis to boost extraction efficiency and process speed [112]. Isoelectric precipitation is a method frequently used to separate protein biomolecules, which can be used in collagen extraction from fish sources [113,114]. Thermal processing, or treating the protein to high pressure and temperature, constitute further extraction techniques. There is a subcritical water level (SCW) used in thermal processing, which can be found at pressures lower than 22 MPa and temperatures between 100 °C and 374 °C [97,115]. Figure 8 shows that the yield of collagen obtained varies from 0.05% to 94.4% [8].

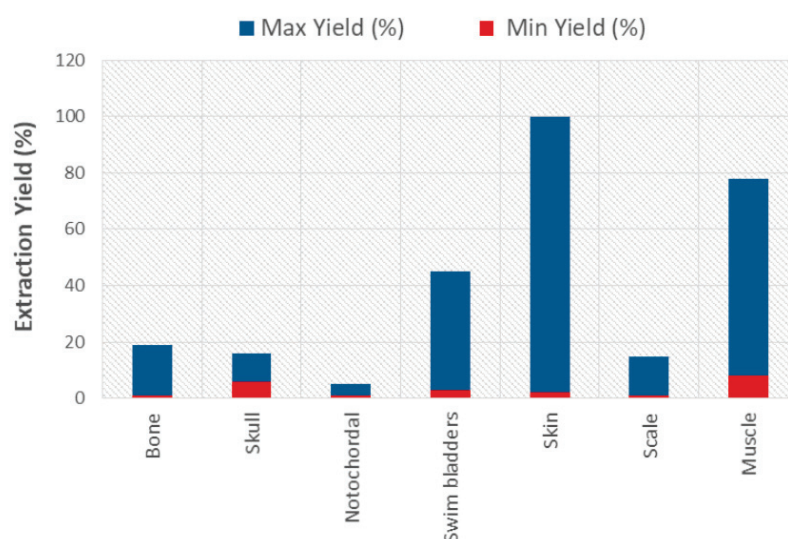


Figure 8. Yield of collagen obtained from fish sources [8].

Table 2 lists some recent studies on various techniques for collagen extraction from different fish sources. The primary objectives of introducing new methods during the collagen extraction phases are to shorten the extraction process time, energy, and chemicals compared to traditional methods. The efficiency of collagen extraction methods from animal by-products depends on the extraction source, age, and type of animal, as well as the condition of the processed by-products and the technology employed.

Table 2. Recent studies on various techniques for fish collagen extraction.

Source	Tissue	Extraction Method	Yield (%)	Reference
<i>Scomber japonicus</i>	Bone	Subcritical-water	1.75	[116]
	Skin		8.10	
<i>Thunnus obesus</i>	Skin	Acid (acetic acid)	13.5	[117]
	Skin	Enzymatic	16.7	
	Scale	(pepsin)	4.6	
	Bone		2.6	
<i>Nibe japonica</i>	Swim bladders	Acid (acetic acid)	11.33	[118]
		Enzymatic + Acid (pepsin + acetic acid)	15.35	



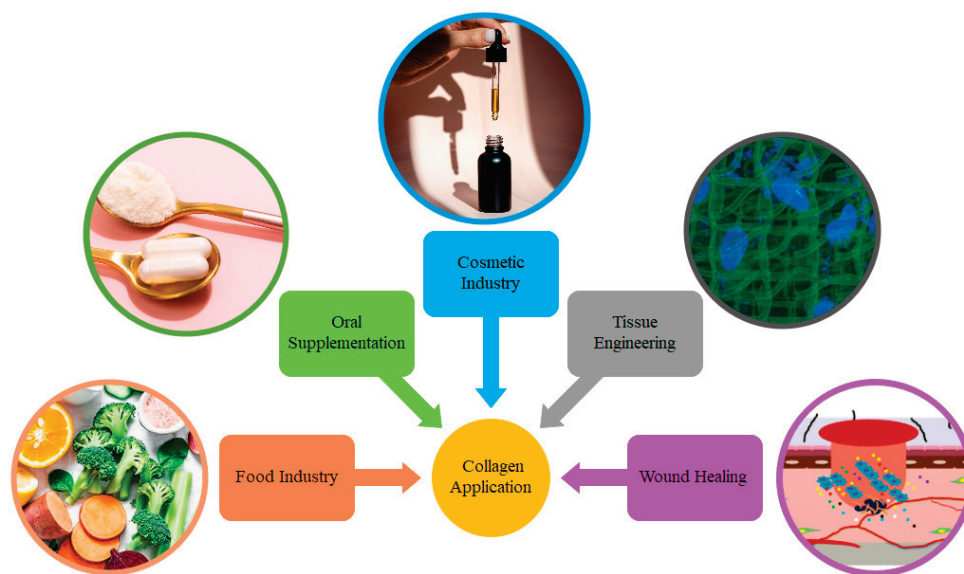
Table 2. Cont.

Source	Tissue	Extraction Method	Yield (%)	Reference
<i>Cyprinus carpio</i>	Scale	Acid (hydrochloric acid, phosphoric acid, and sulfuric acid)	13.6	[114]
<i>Sardinella fimbriata</i>	Fringescale	Acid (acetic acid)	7.48	[119]
		Enzymatic (pepsin)	0.94	
<i>Hybrid Sturgeon</i>	Skin	Acid (hydrochloric acid, acetic acid, citric acid, and lactic acid)	5.73	[120]
		Enzymatic (pepsin)	10.26	
<i>Oreochromis niloticus</i>	Skin	Acid (acetic acid)	19.07	[121]
		Enzymatic + Acid (pepsin + acetic acid)	19.61	
<i>Acipenser schrenckii</i>	Skin	Enzymatic + Acid (pepsin + hydrochloric acid)	13.4	[122]
	Swim bladders		16.5	
	Notochord		1.7	
<i>Misgurnus anguillicaudatus</i>	Skin	Acid (acetic acid)	22.4	[123]
		Enzymatic (pepsin)	27.32	
<i>Miichthys miuiuy</i>	Swim bladders	Acid	1.33	[124]
		Enzymatic (pepsin)	8.37	
<i>Saurida tumbil Bloch</i>	Skin	Acid (acetic acid)	11.73	[125]
		Acid (lactic acid)	11.63	
		Acid (citric acid)	11.39	
<i>Piaractus brachypomus</i>	Skin	Acid (acetic acid)	45.8	[126]
		Enzymatic (pepsin)	57.8	
<i>Nile Tilapia</i>	Skin	Acid (acetic acid)	4.76	[61]
		Enzymatic (pepsin)	8.14	
<i>Catla catla</i>	Skin	Acid (acetic acid)	63.40	[1,127]
		Enzymatic + Acid (pepsin + acetic acid)	69.53	
<i>Labeo rohita</i>	Skin	Acid (acetic acid)	46.13	[1,127]
		Enzymatic + Acid (pepsin + acetic acid)	64.94	
<i>Thunnus obesus</i>	Skin	Enzymatic (bromelain)	3.05	[128]
		Enzymatic (papain)	42.76	
		Enzymatic (pepsin)	52.02	
		Enzymatic (trypsin)	13.83	

## 5. Collagen Applications

Given its outstanding biocompatibility and biodegradability, low cytotoxicity, elevated versatility, significant therapeutic loading, affordability, lack of need for a multistep extrac-

tion procedure, high digestibility, and ease of absorption and distribution in the human body, fish collagen is even more frequently used in a many industrial areas [129,130]. Besides aforementioned advantages, it has a decreased viscosity in aqueous solution, low allergenicity, transparency, good solubility and dispersibility (i.e., uniform distribution in solution), emulsifying ability, and processability in different kinds of products such as powder, foam, and film [131,132]. Thus, throughout many different industrial sectors, including biomedical, pharmaceutical, food, cosmetic, and leather industries, type I collagen is widely employed, as presented in Figure 9. Some of these applications are mentioned below. For niche but promising applications in energy storage devices, the authors referred to a recent review [133].



**Figure 9.** Application of fish collagen in different industrial fields.

### 5.1. Food Industry

In the past, collagen has been used to prepare a variety of goods, including meat products, drinks, soups, and others [123,129]. It aids in enhancing and maintaining their physical, chemical, and sensory qualities. Compared to patties made without fish collagen, those prepared with fish collagen have a higher protein percentage, reduced fat content, comparable sensory acceptance, and better texture. Even in processed foodstuffs including sausages, sausage rolls, ham, hotdogs, and hamburgers, collagen has replaced half-content pork fat leading to enhanced hardness and chewiness, better stability after cooking, and a higher water-holding capacity. Additionally, fish collagen can be added to drinks such as natural fruit juice, to enhance their nutritional and functional qualities due to their greater protein content, bioavailability, moderate viscosity, and excellent water solubility [134–138]. More recently, studies are ongoing on the use of fish (minced fillet) waste in the manufacturing of foodstuffs [139].

### 5.2. Nutraceuticals

Collagen plays a crucial role in tissue and organ development, maintenance, and healing. The loss of collagen in the body begins at the end of the second decade of life and reaches 1% per year by the end of the fourth decade. This process continues until the eighth decade, when the body has lost about three quarters of its collagen compared to the youth. Additionally, other factors such as diseases, improper diet, alcoholism, and smoking accelerate this process [140–142].

The largest apparatus in the human body is the integumental system, which is primarily made of proteoglycans, hyaluronic acid and elastic fibers, and collagens (mainly types I, III, V; types IV, VI, VII to a minor extent). Natural aging involves changes in the human

body: the skin deteriorates morphologically, structurally, and functionally; collagen levels decline; and elastin fibers encourage the development of wrinkles. In the dermis, collagen has a double role: i) to serve as a building block for the formation of newly synthesized collagen and elastin fibers; ii) to interact with receptors on the fibroblasts' membrane to promote the synthesis of new collagen, elastin, and hyaluronic acid [143]. Considering that collagen peptides have antioxidant and antibacterial properties and vary in quality depending on the technique of extraction, they can be employed as a component in functional dietary supplements. In view of the fact that collagen oral supplementation reaches the deeper layers of the skin and improves skin physiology and appearance by enhancing hydration, elasticity, firmness, wrinkle reduction, and skin regeneration, oral collagen supplementation has gained popularity in recent years [123,144]. Many studies have concluded that hydrolyzed fish collagen applied as food supplement is able to provide positive effects on skin appearance with enhanced water-holding capacity, moisture absorption, retention, anti-aging, and anti-melanogenic effects [59,145].

Skin condition changes brought on by aging are a crucial concern for preserving the quality of life. As a result, the public is interested in dietary supplementation's ability to treat skin disorders. Naoki Ito postulated that, by elevating the plasma growth hormone, a supplement blend comprising ornithine and fish-derived collagen peptide could enhance skin conditions [146]. In this regard, two groups of volunteers used a supplement or identical placebo for two months. Skin condition, including elasticity and transepidermal water loss, as well as growth hormone levels, was significantly improved in the first group. The combination of amino acids in collagen hydrolysate, known as a safe nutraceutical, stimulated the production of collagen in the extracellular matrix of cartilage and other tissues. Porfírio performed research on the action of collagen hydrolysate in bone and cartilaginous tissue and its therapeutic use against osteoporosis and osteoarthritis, discovering a connection between the maintenance of bone strength and composition, as well as cartilage cell development and proliferation, and the administration of various doses of collagen hydrolysate [147]. This study concluded that hydrolyzed collagen has a protective effect on articular cartilage, and especially helps with symptomatic pain reduction considering the ability to raise bone mineral density [147]. Therefore, it has a good therapeutic effect on osteoporosis and osteoarthritis.

### 5.3. Cosmetics

As mentioned in the previous section, the role of collagen in the body is very important because it helps the skin, the largest organ of the human body. The skin protects the organism from external damage, regulates temperature, and performs other body functions. Over the years and in the process of aging, the amount of collagen in the skin decreases and this causes its morphological, structural, and functional deterioration. In fact, the presence of elastin fibers causes lines and wrinkles and shows aging. Controlling skin aging is a challenge in the cosmetic industry, but the use of collagen has been proven to be an alternative solution to reduce the effects of aging. In the studies that have been conducted, fish collagen has shown the capacity to retain water, absorb moisture, and retain it again, which can have anti-aging effects on the skin and can be used as a potential active ingredient in skin-care products [148–151].

### 5.4. Tissue Engineering and Regenerative Medicine

Historically, tissue engineering is based on the combination of scaffolds, cells, and signals. The term 'scaffold' is usually referred to as a temporal substitute that should structurally support tissue formation and provide the appropriate environment for cell migration, proliferation, and differentiation, and hence for repairing processes. The prevalence of collagen in human tissues and the important role it plays in the extracellular matrix make it a natural choice for its employment as raw material in the development of implantable devices for tissue engineering and regenerative medicine applications. Common

application areas include bone, vascular tissue, skin, cartilage, corneal tissue, oral mucosa, and dental regeneration [26,73,152].

Numerous studies demonstrated that collagens, especially fish collagens, have intriguing osteoconductive and biomechanical properties and are used more frequently in tissue engineering. Due to its exceptional biocompatibility, collagen has been reported to be employed as a biomaterial in a variety of vascular tissue applications. The bioactivity of collagen has caused this biopolymer to be widely used in skin tissue repair with its healing, antigenic, new-tissue-thickening, and adhesion properties.

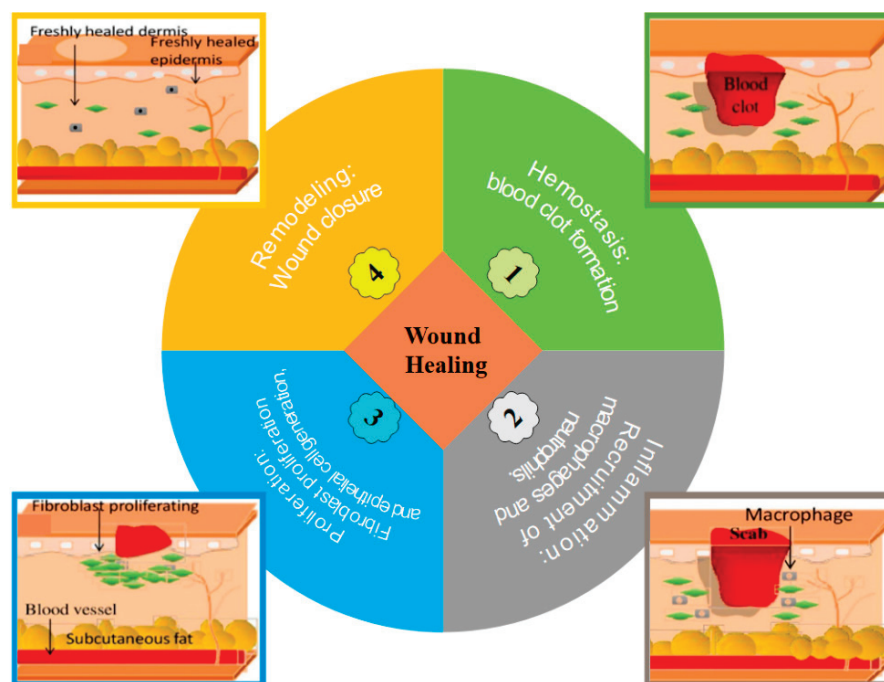
One such technique is tissue engineering, which relies on the utilization of autologous chondrocytes and resorbable matrices. Visual acuity depends on a healthy cornea, which is the eye's tough, transparent anterior surface. Damage to the cornea is a significant contributor to the lack of limbal stem cells that results in vision problems. To this goal, a number of treatment modalities are being created to address limbal stem cell insufficiency. The goal of this strategy was to create a biocompatible scaffold for growing limbal stem cells that completely replicate the human amniotic membrane. This was done by using a unique method based on fish collagen. It was discovered that the mechanical and physical forces of fish-scale-derived collagen were adequate for this purpose [153,154]. Collagen was also demonstrated to play a critical role in tooth tissue repair. Indeed, various collagen types retrieved using various procedures have demonstrated their ability to stimulate the regeneration of dental tissue; as a result, they can be employed in biomedical applications to regenerate tooth tissue [155,156].

Because of postoperative problems, including retears at the treated site, large and enormous rotator cuff tears pose a difficulty for surgeons. Since fish byproducts are regarded as a safer collagen source than other animal-derived scaffolds, collagen generated from fish scales has recently attracted more attention. Yamaura et al. [157] assessed the biological effectiveness of Tilapia-scales-derived collagen scaffolds for rotator cuff healing in rat models. In this research, by augmenting the repair site with a Tilapia-scale-derived collagen scaffold, after 6 weeks, an enhanced angiogenesis and fibrocartilage regeneration at the enthesis was observed. Due to osteogenic capacity and the connections between cells and the matrix, extracellular matrix and bioceramics are vital components in bone tissue regeneration. Since scaffolds are typically made up of synthetic polymers and bioceramics, surface modifications with hydrophilic materials, such as proteins, have great prospects for tissue engineering applications. In this study, which was provided by Kim et al. [158], marine atelocollagen was extracted from the bones and skins of *Paralichthys olivaceus*. Then, in vitro and in vivo calvarial implantation of the scaffolds with and without marine atelocollagen was performed to study bone tissue regeneration. The results of mineralization confirmed that scaffolds with marine atelocollagen showed an osteogenic increase from 300% to 1000% in different compositions, compared with pure scaffolds.

### 5.5. Wound Healing

The complex process of wound healing is essential for re-establishing the skin's barrier function. Numerous illnesses can halt this process, leaving behind chronic wounds that are extremely expensive to treat. Due to the complicated symptoms brought on by metabolic dysfunction of the wound microenvironment, such wounds fail to heal according to the stages of healing, and the comprehensive treatment of chronic wounds is still recognized as a huge unmet medical need. Consequently, there are three broad categories for wound classification: (i) superficial (involves only the epidermis), (ii) partial-thickness (involves epidermis and dermis), (iii) and full-thickness wound (involves also the underlying subcutaneous fat or deeper tissues) [159–163]. The process of wound healing is a physiological process that consists of four main steps: (i) hemostasis, (ii) inflammation, (iii) proliferation, and (iv) remodeling (Figure 10). Therefore, it is vital to choose the right polymers, bioactive chemicals, and wound dressings that can speed up the healing process. There is no one wound dressing that can be used to treat all types of wounds due to their varying etiology. Thus, the development of a smart wound dressing with antibacterial,

anti-inflammatory, and antioxidant capabilities that, most critically, can benefit nearly all types of wounds, is the future challenge [163–166].



**Figure 10.** Schematic of the wound healing steps: (1) hemostasis, (2) inflammation, (3) proliferation, and (4) remodeling.

The combination of polymers and bioactive compounds significantly speeds up wound healing. Although the use of natural remedies for wound healing has been extensively studied, only a small number have yet to be commercialized or employed in clinical settings. In order to fully understand the potential of naturally occurring bioactive compounds in skin tissue regeneration, more preclinical studies must be done. Collagen, as a biodegradable organic tissue matrix, is a common option when choosing safe and nontoxic materials because it is one of the most crucial elements in tissue regeneration and wound healing and gives the skin its tensile strength. Collagen also has antimicrobial qualities and can aid in the hemostasis process. Collagen is used in different forms of hydrogel, sponge, and film for wound treatment. The best example of wound dressing devices are hydrogels, three-dimensional networks which can maintain a moist environment at the wound site and promote quicker tissue regeneration [161,164,167].

Several attempts at wound healing using prototypal devices made of fish-derived type I collagen or decellularized fish skin have been made. Hu et al. demonstrated that marine collagen peptides promote wound closure at concentrations of  $50 \mu\text{g}\cdot\text{mL}^{-1}$  commencing at 12 h after treatment with collagen using an *in vitro* scratch assay [168]. It was demonstrated that the cell migration that was induced was comparable to migration seen when using  $10.0 \mu\text{g}/\text{mL}$  of epidermal growth factor, a factor known to be extremely important in wound healing. In addition, after 11 days, rabbits treated with marine collagen peptides extracted from the skin of *Tilapia* healed considerably quicker than the control group. Additionally, Yang et al. extracted collagen peptides from Alaska Pollock and showed that giving injured rats collagen peptides orally boosted recovery rates substantially more than those in the control groups [169]. Similarly, Chen et al. extracted collagen from bovine skin collagen nanofibers and marine *Tilapia* skin and demonstrated that collagen-treated rat groups recovered from wounds more quickly than control groups [170]. The study also discovered that collagen's hydroxyproline, which promotes re-epithelization, has a significant influence in the rate of wound healing. In comparison to the control groups,



the collagen-treated groups had more fibroblasts, higher vascularization, less inflammation, and more collagen fibers.

### 5.6. Food Packaging

Food packaging has the primary function of preserving and protecting food, primarily from oxidative and microbial degeneration, extending the shelf-life of the food by enhanced barrier and mechanical properties [171,172]. Fish collagen has attracted growing interest due to its potential for adding active and intelligent functions to conventional packaging [173,174]. In particular, active packaging can prevent the migration of H<sub>2</sub>O, O<sub>2</sub>, CO<sub>2</sub>, smells, and fats, and can include bioactive compounds such as antioxidants, antimicrobials, and taste to prolong the shelf life of the product [57,175,176]. Active packaging can appear in the form of edible films or coatings. Edible films are first produced by solution casting or compression molding and then applied to food surfaces by coating, wrapping, or spraying, while edible coatings are applied to food by spraying or dipping [177,178].

Films and coatings for food packaging must feature an elevated oxygen barrier and adequate thickness, mechanical properties, and transparency besides microbial stability, non-toxicity, and safety [179–182].

There are some necessary properties of biopolymers for food packaging, such as biodegradability, low water vapor permeability, oxygen barrier, thickness, transparency, edibility, and elasticity [183–186].

The application of fish collagen films is still constrained in the packaging industry due to drawbacks including poor mechanical qualities, low thermal stability, excessive water solubility and a large water vapor permeability. Several studies are in progress to overcome these limitations. For example, to reduce the brittleness, collagen films are usually prepared by using a plasticizer, mainly glycerol in the range 20–30 wt%, a small molecule of low volatility added to decrease attractive intermolecular forces along polymer chains and increase the free volume and chain mobility [187]. Moreover, suitable crosslinking treatments are being studied to improve the thermal stability of fish collagen [188,189]. Other possible solutions could be the blend of collagen with other biopolymers, mainly chitosan [77,190–193], and the addition of active compounds providing functional properties suitable for active packaging [187,194].

Gelatin, extracted from fish collagen by partial hydrolysis followed by thermal treatment, is attracting increasing interest for the development of edible films and coatings with probiotic properties, as recently reported in the literature [195–197]. In order to achieve the properties required for food packaging, several studies report on the physical or chemical modification of fish gelatin with chitosan, starch, soy protein isolate and carboxymethyl cellulose [198–202].

## 6. Collagen Market

Collagen and derivatives are widely used for various applications, including dietary supplements, anti-aging formulations, soft-tissue growth devices, wound dressings, and food packaging. The achievement of US Food and Drug Administration (FDA) GRAS status (Generally Recognized as Safe) in 1983 for collagen and in 1975 for gelatin [203] boosted collagen's use in several areas of application [204].

The increasing popularity of fish collagen for biomedical, food, cosmetic, nutraceutical, and nutricosmetic application has increased its demand. To this, the global marine collagen market was worth USD 685 million in 2020 [204] and USD 633 million in 2022 [205] and it was estimated to register over 5.3–7.5% of the compound annual growth rate (CAGR) between 2021 and 2029 [203,204] and is expected to reach a market size of USD 1123 million by 2032 [205]. In particular, the fish-collagen market was estimated to be worth USD 320.21 million in 2021 and is predicted to skyrocket to USD 624.12 million by 2029, with a CAGR of 8.7% during the forecast period 2022 to 2029 [206].

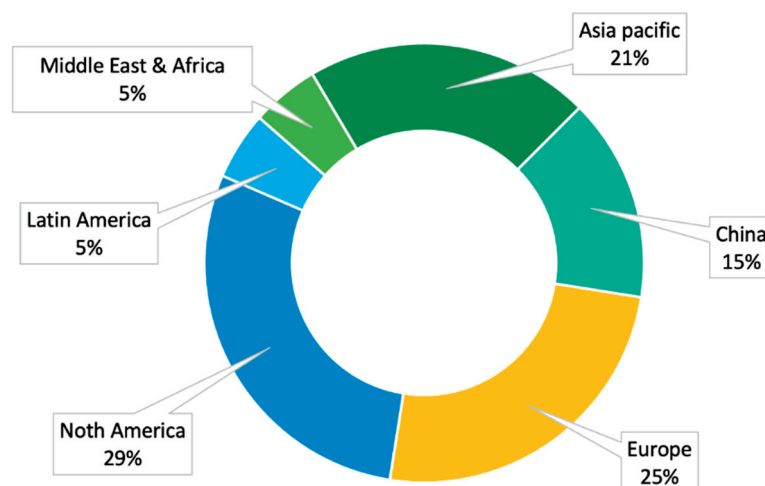
The increasing popularity of fish-collagen-based products is principally due to two main factors: (i) aging population, and (ii) environmental issues. The increase of the

mean population age is directly correlated with the increase of age-related diseases (i.e., joint disorders, wrinkles, and wounds) [206,207]. In these circumstances, collagen-based products have been revealed to be effective, quite low-cost, easily accessible, safe, non-invasive, and readily available, and, accordingly, fish-derived-collagen awareness has significantly increased thanks to its additional advantages compared to other collagen types [208]. Therefore, the fish-collagen market for nutraceutical application was valued at over USD 280 million in 2020. Moreover, the rising inclination of consumers towards fat-free and nutritious products has further increased the product demand [204]. Thus, the major factor that is expected to boost the growth of the marine collagen market in the forecast period is a rise in the demand for supplements to control healthcare costs [203]. On the other hand, the environmental problems linked to the disposal of the enormous quantity of by-products of the fishing industry and to the use of plastic have shifted focus toward the search for eco-friendly solutions. In particular, waste recovery technologies were developed to reduce the environmental impact on by-products and to develop new products with added value. Local enterprises profited from this arrangement because fish is more readily available for less money, and the collagen market is booming [207]. Therefore, fish collagen and derivatives started to be isolated, studied, and commercialized not only in health-related sectors but also in food packaging.

Fish collagen demand is related to its applications. In North America, it is mainly required for pharmaceutical applications [204]. In Europe and Australia, it is mainly used in the cosmetics industry [204,207]. The boost of fish collagen for cosmetic applications is principally due to the increasing preference for minimally or non-invasive surgical procedures compared to traditional surgical treatments. Additionally, the ease of treatment, the higher safety, and major accessibility have led the European population to prefer topical collagen formulations and food supplements for anti-aging and well-being treatments [209]. In Asia and Latin America, besides age-related issues, the major exploitation of fish collagen as a food supplement has arisen from the fact that, according to the European Nutraceutical Association (ENA), a lack of adequate nutrition accounted for 38.6% of deaths in China, India, and Brazil [204,207,209]. Indeed, the ENA's in-depth investigation highlighted that inadequate nutrition is not related to an economic gap, but to incorrect eating habits [209].

Regarding countries' contributions to the fish-collagen market, in 2012, the CARG of fish-collagen market by region was positive and was projected to reach +18% in North America, +31% in Latin America, +10% in Europe, and +28% in Asia by 2016 [209]. As shown in Figure 11, in 2019 North America (about 29%), Europe (about 30%), and Asia (Asia pacific: 21%, China: 15%) occupy the largest share of the market [209]. Among them, Asia is clearly expected to rule the market with about 36% of the total [207,209]. Actual fish-collagen market distribution by midlands is not available but it is known that North America's contribution remained almost unchanged (31%) and that, in Europe, Germany contributes 23.3% to the total fish-collagen market, while, in Asia, Japan contributes 6.6% and, in Oceania, Australia's contribution is about 2.6% [207].

The cost of fish-collagen is also application-related. The cost for the food industry (as binders, stabilizers, emulsifiers, film-formers, and fat replacers) was reported to be between EUR 8–12/kg, for the nutraceutical industry (for joint diseases) it was about EUR 10–12/kg, and for cosmetic applications it was reported to be about EUR 20–25/kg but could reach also EUR 40/kg [210]. However, the quality of the product obtained from marine life forms (USD 44539/metric ton) costs relatively higher than that from bovine sources (USD 33457/metric ton) [210] due to the complex and cost-intensive process of extracting collagen from marine organisms and by-products of the fishing industry. Moreover, fish waste has been somewhat decreased as a result of changes made to fishing regulations to combat overfishing, which limited the production of fish collagen and related goods. The high cost of fish collagen and the lack of awareness about its benefits among consumers are some of the major challenges faced by manufacturers [203]. These disadvantages allowed bovine collagen to have a leadership position as it holds a great cost advantage in lower-value products (e.g., food) [210].



**Figure 11.** Fish-collagen market segmentation by Continent in 2019 [207].

The major players operating in the marine collagen market are Ajinomoto (Tokyo, Japan), Amicogen Deyan Biotech (Jinseong-myeon, South Korea), Ashland (Wilmington, CA, USA), Athos collagen (Surat, India), BDF Biotech (Girona, Spain), BHN (Tokyo, Japan), Certified Nutraceuticals (Pauma Valley, CA, USA), Cobiosa (Madrid, Spain), ETChem (Suzhou, China), Gelita (Eberbach, Germany), Juncà Gelatines (Girona, Spain), Hangzhou Nutrition Biotechnology (Hangzhou, China), HealthyHey Nutrition (Mumbai, India), Hi-Media Laboratories (Maharashtra, India), Italgel (Cuneo, Italy), Lapi Gelatin (Empoly, Italy), Nippi Incorporated (Burnaby, Canada), Nitta Gelatin (Kokin, India), Norland Products (Jamesburg, NJ, USA), ProPlenish (Armadale, Australia), Rousselot (Gent, Belgium), Seagarden (Husøyvegen, Norway), Tessengerlo Group (Ixelles, Belgium), Weishardt Group (Graulhet, France), among others.

### 7. Challenges in the Industrial Implementation of Collagen Derived from Fish Waste

The collagen extraction process is a multistep, time-consuming procedure, which is a disadvantage in the industrial production of it. The issues and related challenges of fish collagen extraction are manifold and are principally linked to the extraction process and to the protein chemical-physical properties.

One of the main troubles is its low extraction yield, a parameter that is both species-related (i.e., taxonomy, age, tissue, and living conditions) and process-related (i.e., time, volumes, instrumentation, sample-volume ratio, types of acid and enzyme used and their concentrations, temperature, pH, ionic strength, and so on [211]). Several attempts were made in order to improve collagen extraction yield. The major steps forward have been made by optimizing solute and solvent concentrations and times in extraction steps 3–5. In particular, the implementation of a discarding phase of non-collagenous components (i.e., step 3 in Table 1) with NaOH 0.05–0.1 M, and an extraction phase (i.e., step 4 in Table 1) with an acetic acid concentration of 0.6 M for 36 h [212] brings a collagen yield increase. Regarding the enzymatic extraction, a pepsin concentration of 1200–1300 U/g is revered as the most effective in increasing collagen yield [98]. However, if, on one hand, the enzymatic extraction is able to significantly increase the yield of collagen, on the other hand, it significantly increases the time of the process and decreases the native conformation degree [213,214]. This consequence may not be industrially advantageous since it can lead to a higher cost of the process and therefore to a higher final cost of the product. For this reason, it is necessary to make a cost/benefit assessment before choosing whether or not to perform the enzymatic extraction. In addition to the ‘standard extraction process’ steps improvements, some innovative attempts have been made. Several authors demonstrated how the application of ultrasound increased yield and reduced processing time, as well as being greener compared to conventional extraction methods [79,109,213]. Huan et al.

developed a novel rapid extrusion-hydro-extraction process for collagen from fish scales at room temperature [215] as an alternative to traditional methods.

Regardless of the process, temperature affects all extraction steps, from the tissue separation to the final collagen precipitation and recovery. Because of fish collagen's low denaturation temperature ( $<37\text{ }^{\circ}\text{C}$ ), the need to carry out the entire extraction process at low temperatures ( $4\text{--}10\text{ }^{\circ}\text{C}$ ), to preserve its native structure and thus its structural properties and bioactivity, makes the procedure expensive. The low denaturation temperature of fish collagen is due to fish's evolutionary adaptation to the characteristics of the aquatic environment in which they live. For this reason, it is not possible to intervene in this aspect. The only thing that can be done is to carefully select the fish species. In particular, the selection of a fish species that lives in a tropical environment—and therefore will have collagen with a physiologically higher denaturation temperature (e.g.,  $32\text{--}36\text{ }^{\circ}\text{C}$  in catfish [215],  $36\text{--}38\text{ }^{\circ}\text{C}$  in carp [2,216],  $32\text{--}37\text{ }^{\circ}\text{C}$  in Tilapia [121], and  $43\text{ }^{\circ}\text{C}$  in lizardfish [217])—compared to a fish species living in cold waters, could be a solution. With this in mind, Pinedo et al. investigated the properties of collagen extracted from a hybrid fish line that, although similar to those of the original strains, was allowed to obtain a more controlled fish growth and, thus, a higher yield [81].

Despite the presence of various issues, it is clear how scientific and industrial research is moving towards the optimization of the extraction process and industrial implementation. In this regard, an advanced pilot plant automation was recently designed to maximize collagen extraction [218]. Therefore, since it is not possible to reduce the time and costs of the extraction process by optimizing it from the point of view of temperature control, a way to increase the denaturation temperature of marine collagen and make it more suitable for a wide range of applications is to induce post-synthesis crosslinking of the products. The increment of fish collagen denaturation temperature is another important issue since it is particularly relevant in some clinical applications. The application of crosslinking treatments also helps in the resolution of other two issues related to fish-collagen use which are the low mechanical properties and the low resistance to degradation, which make it unusable in some applications. Indeed, physical (e.g., UV [219,220], dehydrothermal treatment [219,221], chemical (e.g., methacrylation [222], pullulan [223], carbodiimide [221,224], N-hydroxysuccinimide-activated adipic acid [225]), and enzymatical (e.g., transglutaminase [225]) treatments were performed to enhance collagen properties. Maher et al. made a considerable step forward by successfully printing methacrylated fish collagen and realizing a 3D construct with desired properties, despite the fact that the applied treatment was not able to increase the resistance to degradation on par with collagen extracted from mammals [222]. Another strategy commonly adopted to improve collagen properties is to blend it with other biomaterials with higher mechanical properties, such as chitosan [77,226–228], poly(lactic acid) [228,229], alginate [230], polyvinyl alcohol [227,231], and cellulose [195,231].

## 8. Conclusions

Natural biopolymers have unique biophysical and biochemical properties, including biocompatibility, biodegradability, increased body fluid adsorption capacity, increased gel-forming ability, non-toxic and non-immunogenic capabilities, as well as antifungal, antibacterial, and anticancer activities. One of these biopolymers is collagen, which could be obtained from various sources such as fish, mammalian, and agro-food waste. By turning these wastes into new products with a high functional value, recycling these by-products can assist in decreasing the pollution caused by these sorts of wastes. A potential substitute for bovine collagen is thought to be fish collagen. Fish collagen is cited as an important biomaterial due to its wide range of biological characteristics, including remarkable biocompatibility, high levels of cell adhesion, exceptional biodegradability, and low antigenicity. This review provides a general overview of collagen and its properties, types of sources and extraction methods, and diverse applications in a variety of industries, with a spotlight on fisheries and aquaculture sources.



**Author Contributions:** Conceptualization, F.L. and Z.R.; methodology, Z.R. and F.L.; validation, Z.R., F.L., N.G. and L.S.; data curation, F.L.; writing—original draft preparation, Z.R. and F.L.; writing—review and editing, Z.R., F.L., N.G. and L.S.; supervision, F.L. All authors have read and agreed to the published version of the manuscript.

**Funding:** Z.R. acknowledges Regione Puglia for funding NANOCOLLAGEN-“Development of nanometric collagen from waste from the fish industry” (code 284e667a) in the framework of POC PUGLIA FESR-FSE 2014/2020 RIPARTI project.

**Institutional Review Board Statement:** Not applicable.

**Informed Consent Statement:** Not applicable.

**Data Availability Statement:** Data available on request.

**Conflicts of Interest:** The authors declare no conflict of interest.

## References

- Pal, G.K.; Nidheesh, T.; Suresh, P.V. Comparative study on characteristics and in vitro fibril formation ability of acid and pepsin soluble collagen from the skin of catla (*Catla catla*) and rohu (*Labeo rohita*). *Food Res. Int.* **2015**, *76*, 804–812. [CrossRef] [PubMed]
- Jia, Y.; Wang, H.H.; Wang, H.H.; Li, Y.; Wang, M.; Zhou, J. Biochemical properties of skin collagens isolated from black carp (*Mylopharyngodon piceus*). *Food Sci. Biotechnol.* **2012**, *21*, 1585–1592. [CrossRef]
- Wang, L.; An, X.; Yang, F.; Xin, Z.; Zhao, L.; Hu, Q. Isolation and characterisation of collagens from the skin, scale and bone of deep-sea redfish (*Sebastes mentella*). *Food Chem.* **2008**, *108*, 616–623. [CrossRef] [PubMed]
- Wang, S.; Zhang, Y. Study of writing problem in college general english course—Reflection on the reform of college english course. *J. Lang Teach. Res.* **2017**, *8*, 176–183. [CrossRef]
- Nagai, T.; Izumi, M.; Ishii, M. Fish scale collagen. Preparation and partial characterization. *Int. J. Food Sci. Technol.* **2004**, *39*, 239–244. [CrossRef]
- Silvipriya, K.S.; Krishna Kumar, K.; Bhat, A.R.; Dinesh Kumar, B.; John, A.; Lakshmanan, P. Collagen: Animal Sources and Biomedical Application. *J. Appl. Pharm. Sci.* **2015**, *5*, 123–127. [CrossRef]
- Shaw, C.; Knopf, K.; Kloas, W. Fish Feeds in Aquaponics and Beyond: A Novel Concept to Evaluate Protein Sources in Diets for Circular Multitrophic Food Production Systems. *Sustainability* **2022**, *14*, 4064. [CrossRef]
- de Melo Oliveira, V.; Assis, C.R.D.; de Aquino Marques Costa, B.; de Araújo Neri, R.C.; Monte, F.T.D.; da Costa Vasconcelos Freitas, H.M.S.; Franca, R.C.P.; Santos, J.F.; de Souza Bezerra, R.; Figueiredo Porto, A.L. Physical, biochemical, densitometric and spectroscopic techniques for characterization collagen from alternative sources: A review based on the sustainable valorization of aquatic by-products. *J. Mol. Struct.* **2021**, *1224*, 129023. [CrossRef]
- Sorushanova, A.; Delgado, L.M.; Wu, Z.; Shologu, N.; Kshirsagar, A.; Raghunath, R.; Mullen, A.M.; Bayon, Y.; Pandit, A.; Raghunath, M.; et al. The Collagen Suprafamily: From Biosynthesis to Advanced Biomaterial Development. *Adv. Mater.* **2019**, *31*, 1801651. [CrossRef]
- Shavandi, A.; Hou, Y.; Carne, A.; McConnell, M.; Bekhit, A.E.-D.A. Marine Waste Utilization as a Source of Functional and Health Compounds. *Adv. Food Nutr. Res.* **2019**, *87*, 187–254. [CrossRef]
- Furtado, M.; Chen, L.; Chen, Z.; Chen, A.; Cui, W. Development of fish collagen in tissue regeneration and drug delivery. *Eng. Regen.* **2022**, *3*, 217–231. [CrossRef]
- Maschmeyer, T.; Luque, R.; Selva, M. Upgrading of marine (fish and crustaceans) biowaste for high added-value molecules and bio(nano)-materials. *Chem. Soc. Rev.* **2020**, *49*, 4527–4563. [CrossRef] [PubMed]
- Hua, K.; Cobcroft, J.M.; Cole, A.; Condon, K.; Jerry, D.R.; Mangott, A.; Praeger, C.; Vucko, M.J.; Zeng, C.; Zenger, K.; et al. The Future of Aquatic Protein: Implications for Protein Sources in Aquaculture Diets. *One Earth* **2019**, *1*, 316–329. [CrossRef]
- Mishra, P.K.; Gautam, R.K.; Kumar, V.; Kakatkar, A.S.; Chatterjee, S. Synthesis of Biodegradable Films Using Gamma Irradiation from Fish Waste. *Waste Biomass Valorization* **2021**, *12*, 2247–2257. [CrossRef]
- Xu, C.; Nasrollahzadeh, M.; Selva, M.; Issaabadi, Z.; Luque, R. Waste-to-wealth: Biowaste valorization into valuable bio(nano)materials. *Chem. Soc. Rev.* **2019**, *48*, 4791–4822. [CrossRef]
- Al Khawli, F.; Pateiro, M.; Domínguez, R.; Lorenzo, J.M.; Gullón, P.; Kousoulaki, K.; Ferrer, E.; Berrada, H.; Barba, F.J. Innovative Green Technologies of Intensification for Valorization of Seafood and Their By-Products. *Mar. Drugs* **2019**, *17*, 689. [CrossRef]
- Caruso, G.; Floris, R.; Serangeli, C.; Di Paola, L. Fishery Wastes as a Yet Undiscovered Treasure from the Sea: Biomolecules Sources, Extraction Methods and Valorization. *Mar. Drugs* **2020**, *18*, 622. [CrossRef]
- Nimni, M.E.; Harkness, R.D. Molecular Structure and Functions of Collagen. In *Collagen*; CRC Press: Boca Raton, FL, USA, 2018; Volume 1, pp. 1–78. [CrossRef]
- Coppola, D.; Lauritano, C.; Esposito, F.P.; Riccio, G.; Rizzo, C.; De Pascale, D. Fish Waste: From Problem to Valuable Resource. *Mar. Drugs* **2021**, *19*, 116. [CrossRef]
- Mahmood, A.; Patel, D.; Hickson, B.; DesRochers, J.; Hu, X. Recent progress in biopolymer-based hydrogel materials for biomedical applications. *Int. J. Mol. Sci.* **2022**, *23*, 1415. [CrossRef]



21. Castile, J.D.; Taylor, K.M.G.; Buckton, G. The influence of incubation temperature and surfactant concentration on the interaction between dimyristoylphosphatidylcholine liposomes and poloxamer surfactants. *Int. J. Pharm.* **2001**, *221*, 197–209. [CrossRef]
22. El Blidi, O.; Omari, N.E.I.; Balahbib, A.; Ghchime, R.; El Menyiy, N.; Ibrahim, A.; Kaddour, K.B.; Bouyahya, A.B.; Chokairi, O.; Barkiyou, M. Extraction Methods, Characterization and Biomedical Applications of Collagen: A Review. *Biointerface Res. Appl. Chem.* **2021**, *11*, 13587–13613. [CrossRef]
23. Sbricoli, L.; Guazzo, R.; Annunziata, M.; Gobatto, L.; Bressan, E.; Natri, L. Selection of collagen membranes for bone regeneration: A literature review. *Materials* **2020**, *13*, 786. [CrossRef] [PubMed]
24. Xu, Q.; Torres, J.E.; Hakim, M.; Babiak, P.M.; Pal, P.; Battistoni, C.M.; Nguyen, M.; Panitch, A.; Solorio, L.; Liu, J.C. Collagen- and hyaluronic acid-based hydrogels and their biomedical applications. *Mater. Sci. Eng. R Rep.* **2021**, *146*, 100641. [CrossRef] [PubMed]
25. Naomi, R.; Ridzuan, P.M.; Bahari, H.; Vallejo-Giraldo, C. Current Insights into Collagen Type I. *Polymers* **2021**, *13*, 2642. [CrossRef]
26. Coppola, D.; Oliviero, M.; Vitale, G.A.; Lauritano, C.; D’Ambra, I.; Iannace, S.; de Pascale, D. Marine Collagen from Alternative and Sustainable Sources: Extraction, Processing and Applications. *Mar. Drugs* **2020**, *18*, 214. [CrossRef] [PubMed]
27. Gallo, N.; Natali, M.L.; Sannino, A.; Salvatore, L. An Overview of the Use of Equine Collagen as Emerging Material for Biomedical Applications. *J. Funct. Biomater.* **2020**, *11*, 79. [CrossRef] [PubMed]
28. Jafari, H.; Lista, A.; Siekapan, M.M.; Ghaffari-Bohlouli, P.; Nie, L.; Alimoradi, H.; Shavandi, A. Fish Collagen: Extraction, Characterization, and Applications for Biomaterials Engineering. *Polymers* **2020**, *12*, 2230. [CrossRef] [PubMed]
29. Ikoma, T.; Kobayashi, H.; Tanaka, J.; Walsh, D.; Mann, S. Physical properties of type I collagen extracted from fish scales of Pagrus major and Oreochromis niloticas. *Int. J. Biol. Macromol.* **2003**, *32*, 199–204. [CrossRef]
30. Nomura, Y.; Sakai, H.; Ishii, Y.; Shirai, K. Preparation and some properties of type I collagen from fish scales. *Biosci. Biotechnol. Biochem.* **1996**, *60*, 20922094. [CrossRef]
31. Nagai, T.; Suzuki, N. Isolation of collagen from fish waste material—skin, bone and fins. *Food Chem.* **2000**, *68*, 277–281. [CrossRef]
32. Rauta, P.R.; Mohanta, Y.K.; Nayak, D. *Nanotechnology in Biology and Medicine: Research Advancements & Future Perspectives*; CRC Press: Boca Raton, FL, USA, 2019.
33. Lo, S.; Fauzi, M.B. Current Update of Collagen Nanomaterials—Fabrication, Characterisation and Its Applications: A Review. *Pharmaceutics* **2021**, *13*, 316. [CrossRef] [PubMed]
34. Naskar, A.; Kim, K.S. Recent Advances in Nanomaterial-Based Wound-Healing Therapeutics. *Pharmaceutics* **2020**, *12*, 499. [CrossRef]
35. Ucar, B. Natural biomaterials in brain repair: A focus on collagen. *Neurochem. Int.* **2021**, *146*, 105033. [CrossRef] [PubMed]
36. Dong, C.; Lv, Y. Application of Collagen Scaffold in Tissue Engineering: Recent Advances and New Perspectives. *Polymers* **2016**, *8*, 42. [CrossRef]
37. Arun, A.; Malrautu, P.; Laha, A.; Luo, H.; Ramakrishna, S. Collagen Nanoparticles in Drug Delivery Systems and Tissue Engineering. *Appl. Sci.* **2021**, *11*, 11369. [CrossRef]
38. Neff, L.S.; Bradshaw, A.D. Cross your heart? Collagen cross-links in cardiac health and disease. *Cell Signal.* **2021**, *79*, 109889. [CrossRef] [PubMed]
39. Gelse, K.; Pöschl, E. Reviews TA-A drug delivery, 2003 U. Collagens—Structure, function, and biosynthesis. *Adv. Drug Deliv. Rev.* **2003**, *55*, 1531–1546. [CrossRef]
40. Schweitzer, M.H.; Suo, Z.; Avci, R.; Asara, J.M.; Allen, M.A.; Arce, F.T.; Horner, J.R. Analyses of Soft Tissue from Tyrannosaurus rex Suggest the Presence of Protein. *Science* **2007**, *316*, 277–280. [CrossRef]
41. Torres, J.M.; Borja, C.; Gibert, L.; Ribot, F.; Olivares, E.G. Twentieth-Century Paleoproteomics: Lessons from Venta Micena Fossils. *Biology* **2022**, *11*, 1184. [CrossRef]
42. Bächinger, H.P.; Mizuno, K.; Vranka, J.A.; Boudko, S.P. Collagen Formation and Structure. *Compr. Nat. Prod. II Chem. Biol.* **2010**, *5*, 469–530. [CrossRef]
43. Ricard-Blum, S. The Collagen Family. *Cold Spring Harb. Perspect. Biol.* **2011**, *3*, a004978. [CrossRef] [PubMed]
44. Kadler, K.E.; Baldock, C.; Bella, J.; Boot-Handford, R.P. Collagens at a glance. *J. Cell Sci.* **2007**, *120*, 1955–1958. [CrossRef] [PubMed]
45. Inoue, Y.; Itoh, H.; Aoki, M.; Ogawa, S.; Yamane, T.; Baba, T.; Tachibana, N.; Kohno, M.; Oishi, Y.; Kobayashi-Hattori, K. Accelerating effect of soy peptides containing collagen peptides on type I and III collagen levels in rat skin. *Biosci. Biotechnol. Biochem.* **2012**, *76*, 1549–1551. [CrossRef]
46. Minor, A.J.; Coulombe, K.L.K. Engineering a collagen matrix for cell-instructive regenerative angiogenesis. *J. Biomed. Mater. Res. Part B Appl. Biomater.* **2020**, *108*, 2407–2416. [CrossRef]
47. Bornstein, P.; Sage, H. Structurally distinct collagen types. *Annu. Rev. Biochem.* **1980**, *49*, 957–1003. [CrossRef] [PubMed]
48. Salvatore, L.; Gallo, N.; Aiello, D.; Lunetti, P.; Barca, A.; Blasi, L.; Madaghiele, M.; Bettini, S.; Giancane, G.; Hasna, M.; et al. An insight on type I collagen from horse tendon for the manufacture of implantable devices. *Int. J. Biol. Macromol.* **2020**, *154*, 291–306. [CrossRef] [PubMed]
49. Ignat’eva, N.Y.; Danilov, N.A.; Averkiev, S.V.; Obrezkova, M.V.; Lunin, V.V.; Sobol’, E.N. Determination of hydroxyproline in tissues and the evaluation of the collagen content of the tissues. *J. Anal. Chem.* **2007**, *62*, 51–57. [CrossRef]
50. Privalov, P.L.; Tiktopulo, E.I.; Tischenko, V.M. Stability and mobility of the collagen structure. *J. Mol. Biol.* **1979**, *127*, 203–216. [CrossRef]
51. Astbury, W.T.; Bell, F.O. Molecular Structure of the Collagen Fibres. *Nature.* **1940**, *145*, 421–422. [CrossRef]

52. Pauling, L.; Corey, R.B. The structure of fibrous proteins of the collagen-gelatin group. *Proc. Natl. Acad. Sci. USA* **1951**, *37*, 272–281. [CrossRef]
53. Ramachandran, G.N.; Kartha, G. Structure of Collagen. *Nature* **1954**, *174*, 269–270. [CrossRef] [PubMed]
54. Rich, A.; Crick, F.H.C. The molecular structure of collagen. *J. Mol. Biol.* **1961**, *3*, 483–506. [CrossRef] [PubMed]
55. Cowan, P.M.; McGavin, S.; North, A.C. The Polypeptide Chain Configuration of Collagen. *Nature* **1955**, *176*, 1062–1064. [CrossRef] [PubMed]
56. Bella, J. Collagen structure: New tricks from a very old dog. *Biochem. J.* **2016**, *473*, 1001–1025. [CrossRef]
57. Lim, Y.S.; Ok, Y.J.; Hwang, S.Y.; Kwak, J.Y.; Yoon, S. Marine collagen as a promising biomaterial for biomedical applications. *Mar. Drugs* **2019**, *17*, 467. [CrossRef]
58. Chen, L.; Cheng, G.; Meng, S.; Ding, Y. Collagen Membrane Derived from Fish Scales for Application in Bone Tissue Engineering. *Polymers* **2022**, *14*, 2532. [CrossRef]
59. León-López, A.; Morales-Peñaloza, A.; Manuel Martínez-Juárez, V.; Vargas-Torres, A.; Zeugolis, D.I.; Aguirre-Álvarez, G. Hydrolyzed Collagen—Sources and Applications. *Molecules* **2019**, *24*, 4031. [CrossRef]
60. Liu, X.; Gao, Y.; Long, X.; Hayashi, T.; Mizuno, K.; Hattori, S.; Fujisaki, H.; Ogura, T.; Wang, D.O.; Ikejima, T. Type I collagen promotes the migration and myogenic differentiation of C2C12 myoblasts: Via the release of interleukin-6 mediated by FAK/NF- $\kappa$ B p65 activation. *Food Funct.* **2020**, *11*, 328–338. [CrossRef]
61. Song, Z.; Liu, H.; Chen, L.L.; Chen, L.L.; Zhou, C.; Hong, P.; Deng, C. Characterization and comparison of collagen extracted from the skin of the Nile tilapia by fermentation and chemical pretreatment. *Food Chem.* **2021**, *340*, 128139. [CrossRef]
62. Peng, X.; Cui, Y.; Chen, J.; Gao, C.; Yang, Y.; Yu, W.; Rai, K.; Zhang, M.; Nian, R.; Bao, Z.; et al. High-Strength Collagen-Based Composite Films Regulated by Water-Soluble Recombinant Spider Silk Proteins and Water Annealing. *ACS Biomater. Sci. Eng.* **2022**, *8*, 3341–3353. [CrossRef]
63. Bao, Z.; Sun, Y.; Rai, K.; Peng, X.; Wang, S.; Nian, R.; Xian, M. The promising indicators of the thermal and mechanical properties of collagen from bass and tilapia: Synergistic effects of hydroxyproline and cysteine. *Biomater. Sci* **2018**, *6*, 3042–3052. [CrossRef] [PubMed]
64. Bao, Z.; Gao, M.; Fan, X.; Cui, Y.; Yang, J.; Peng, X.; Xian, M.; Sun, Y.; Nian, R. Development and characterization of a photo-cross-linked functionalized type-I collagen (*Oreochromis niloticus*) and polyethylene glycol diacrylate hydrogel. *Int. J. Biol. Macromol.* **2020**, *155*, 163–173. [CrossRef] [PubMed]
65. Shoulders, M.D.; Raines, R.T. Collagen Structure and Stability. *Annu. Rev. Biochem.* **2009**, *78*, 929–958. [CrossRef] [PubMed]
66. Buehler, M.J. Nature designs tough collagen: Explaining the nanostructure of collagen fibrils. *Proc. Natl. Acad. Sci. USA* **2006**, *103*, 12285–12290. [CrossRef] [PubMed]
67. Shen, Y.; Levin, A.; Kamada, A.; Toprakcioglu, Z.; Rodriguez-Garcia, M.; Xu, Y.; Knowles, T.P. From Protein Building Blocks to Functional Materials. *ACS Nano* **2021**, *15*, 5819–5837. [CrossRef]
68. Lin, J.; Shi, Y.; Men, Y.; Wang, X.; Ye, J.; Zhang, C. Mechanical roles in formation of oriented collagen fibers. *Tissue Eng.-Part B Rev.* **2020**, *26*, 116–128. [CrossRef]
69. Yang, L.; Van Der Werf, K.O.; Fitić, C.F.C.; Bennink, M.L.; Dijkstra, P.J.; Feijen, J. Mechanical properties of native and cross-linked type I collagen fibrils. *Biophys. J.* **2008**, *94*, 2204–2211. [CrossRef]
70. Tihăuan, B.-M.; Pircalabioru, G.G.; Axinie Bucos, M.; Marinaş, I.C.; Nicoară, A.-C.; Măruţescu, L.; Oprea, O.; Matei, E.; Maier, S.S. Crosslinked Collagenic Scaffold Behavior Evaluation by Physico-Chemical, Mechanical and Biological Assessments in an In Vitro Microenvironment. *Polymers* **2022**, *14*, 2430. [CrossRef]
71. Hossain, M.S.; Ebrahimi, H.; Ghosh, R. Fish scale inspired structures—A review of materials, manufacturing and models. *Bioinspir. Biomim.* **2022**, *17*, 061001. [CrossRef]
72. Sharma, S.; Dwivedi, S.; Chandra, S.; Srivastava, A.; Vijay, P. Collagen: A Brief Analysis. *Oral. Maxillofac. Pathol. J.* **2019**, *10*, 11–17. [CrossRef]
73. Salvatore, L.; Gallo, N.; Natali, M.L.; Campa, L.; Lunetti, P.; Madaghiele, M.; Blasi, F.S.; Corallo, A.; Capobianco, L.; Sannino, A. Marine collagen and its derivatives: Versatile and sustainable bio-resources for healthcare. *Mater. Sci. Eng. C* **2020**, *113*, 110963. [CrossRef] [PubMed]
74. Ferraro, V.; Gaillard-Martinie, B.; Sayd, T.; Chambon, C.; Anton, M.; Santé-Lhoutellier, V. Collagen type I from bovine bone. Effect of animal age, bone anatomy and drying methodology on extraction yield, self-assembly, thermal behaviour and. *Int. J. Biol. Macromol.* **2017**, *97*, 55–66. [CrossRef]
75. Davison-Kotler, E.; Marshall, W.S.; García-Gareta, E. Sources of Collagen for Biomaterials in Skin Wound Healing. *Bioengineering* **2019**, *6*, 56. [CrossRef] [PubMed]
76. Paschou, A.M.; Katsikini, M.; Christofilos, D.; Arvanitidis, J.; Ves, S.; Katsikini, C.M. High pressure Raman study of type-I collagen. *Wiley Online Libr.* **2018**, *285*, 2641–2653. [CrossRef] [PubMed]
77. Bhuiambar, M.V.; Bhagwat, P.K.; Dandge, P.B. Extraction and characterization of acid soluble collagen from fish waste: Development of collagen-chitosan blend as food packaging film. *J. Environ. Chem. Eng.* **2019**, *7*, 102983. [CrossRef]
78. Subhan, F.; Hussain, Z.; Tauseef, I.; Shehzad, A.; Wahid, F. A review on recent advances and applications of fish collagen. *Crit. Rev. Food Sci. Nutr.* **2021**, *61*, 1027–1037. [CrossRef]
79. Heidari, M.G.; Rezaei, M. Extracted pepsin of trout waste and ultrasound-promoted method for green recovery of fish collagen. *Sustain. Chem. Pharm.* **2022**, *30*, 100854. [CrossRef]

80. Morikawa, T.; Reátegui-Pinedo, N.; Salirrosas, D.; Sánchez-Tuesta, L.; Quiñones, C.; Jáuregui-Rosas, S.R.; Barraza, G.; Cabrera, A.; Ayala-Jara, C.; Miliari Martinez, R.; et al. Characterization of Collagen from Three Genetic Lines (Gray, Red and F1) of *Oreochromis niloticus* (Tilapia) Skin in Young and Old Adults. *Molecules* **2022**, *27*, 1123. [CrossRef]
81. Felician, F.; Xia, C.; Qi, W. Collagen from marine biological sources and medical applications. *Wiley Online Libr.* **2018**, *15*, e1700557. [CrossRef]
82. Nirmal, N.P.; Santivarangkna, C.; Rajput, M.S.; Benjakul, S.; Maqsood, S. Valorization of fish byproducts: Sources to end-product applications of bioactive protein hydrolysate. *Compr. Rev. Food Sci. Food Saf.* **2022**, *21*, 1803–1842. [CrossRef]
83. Fassini, D.; Wilkie, I.C.; Pozzolini, M.; Ferrario, C.; Sugni, M.; Rocha, M.S.; Giovine, M.; Bonasoro, F.; Silva, T.H.; Reis, R.L. Diverse and productive source of biopolymer inspiration: Marine collagens. *Biomacromolecules* **2021**, *22*, 1815–1834. [CrossRef] [PubMed]
84. Sanchez, A.; Blanco, M.; Correa, B.; Perez-Martin, R.I.; Sotelo, C.G. Effect of fish collagen hydrolysates on type I collagen mRNA levels of human dermal fibroblast culture. *Mar. Drugs* **2018**, *16*, 144. [CrossRef] [PubMed]
85. Lu, W.-C.; Chiu, C.-S.; Chan, Y.-J.; Guo, T.-P.; Lin, C.-C.; Wang, P.-C.; Po-Yu Lin, P.-Y.; Mulio, A.T.; Li, P.-H. An In Vivo Study to Evaluate the Efficacy of Blue Shark (*Prionace glauca*) Cartilage Collagen as a Cosmetic. *Mar. Drugs* **2022**, *20*, 633. [CrossRef] [PubMed]
86. Ahn, H.; Gong, D.J.; Lee, H.H.; Seo, J.Y.; Song, K.M.; Eom, S.J.; Yeo, S.Y. Mechanical Properties of Porcine and Fish Skin-Based Collagen and Conjugated Collagen Fibers. *Polymers* **2021**, *13*, 2151. [CrossRef]
87. Liu, S.; Lau, C.S.; Liang, K.; Wen, F.; Teoh, S.H. Marine collagen scaffolds in tissue engineering. *Curr. Opin. Biotechnol.* **2022**, *74*, 92–103. [CrossRef]
88. Luo, Q.; Hossen, M.A.; Zeng, Y.; Dai, J.; Li, S.; Qin, W.; Liu, Y. Gelatin-based composite films and their application in food packaging: A review. *J. Food Eng.* **2022**, *313*, 110762. [CrossRef]
89. Son, S.A.; Shin, E.S.; Park, Y.M.; Ma, A.; Yang, H.; Kim, S.H.; Shin, T.S. Composition of Collagen Extracted from the Skin of Three Different Varieties of Fish. *J. Korean Soc. Food Sci. Nutr.* **2022**, *51*, 71–81. [CrossRef]
90. Araujo, J.; Sica, P.; Costa, C.; Márquez, M.C. Enzymatic Hydrolysis of Fish Waste as an Alternative to Produce High Value-Added Products. *Waste Biomass Valorization* **2021**, *12*, 847–855. [CrossRef]
91. Zhang, J.; Jeevithan, E.; Bao, B.; Wang, S.; Gao, K.; Zhang, C.; Wu, W. Structural characterization, in-vivo acute systemic toxicity assessment and in-vitro intestinal absorption properties of tilapia (*Oreochromis niloticus*) skin acid and pepsin solubilized type I collagen. *Process Biochem.* **2016**, *51*, 2017–2025. [CrossRef]
92. Sierra, L.; Fan, H.; Zapata, J.; Wu, J. Antioxidant peptides derived from hydrolysates of red tilapia (*Oreochromis* sp.) scale. *LWT* **2021**, *146*, 111631. [CrossRef]
93. Chen, J.; Li, L.; Yi, R.; Gao, R.; He, J. Release kinetics of Tilapia scale collagen I peptides during tryptic hydrolysis. *Food Hydrocoll.* **2018**, *77*, 931–936. [CrossRef]
94. Das, J.; Dey, P.; Chakraborty, T.; Saleem, K.; Nagendra, R.; Banerjee, P. Utilization of marine industry waste derived collagen hydrolysate as peroxide inhibition agents in lipid-based food. *Wiley Online Libr.* **2018**, *42*, e13430. [CrossRef]
95. Schmidt, M.M.; Dornelles, R.C.P.; Mello, R.O.; Kubota, E.H.; Mazutti, M.A.; Kempka, A.P.; Demiate, I.M. Collagen extraction process. *Int. Food Res. J.* **2016**, *23*, 913–922.
96. Cao, C.; Xiao, Z.; Ge, C.; Wu, Y. Animal by-products collagen and derived peptide, as important components of innovative sustainable food systems—A comprehensive review. *Crit. Rev. Food Sci. Nutr.* **2021**, *62*, 8703–8727. [CrossRef]
97. Hong, H.; Fan, H.; Chalamaiah, M.; Wu, J. Preparation of low-molecular-weight, collagen hydrolysates (peptides): Current progress, challenges, and future perspectives. *Food Chem.* **2019**, *301*, 125222. [CrossRef]
98. Liu, D.; Wei, G.; Li, T.; Hu, J.; Lu, N.; Regenstein, J.M.; Zhou, P. Effects of alkaline pretreatments and acid extraction conditions on the acid-soluble collagen from grass carp (*Ctenopharyngodon idella*) skin. *Food Chem.* **2015**, *172*, 836–843. [CrossRef]
99. León-López, A.; Fuentes-Jiménez, L.; Delia Hernández-Fuentes, A.; Campos-Montiel, R.G.; Aguirre-Álvarez, G. Hydrolysed collagen from sheepskins as a source of functional peptides with antioxidant activity. *Int. J. Mol. Sci.* **2019**, *20*, 3931. [CrossRef]
100. Lee, H.J.; Roy, V.C.; Ho, T.C.; Park, J.S.; Jeong, Y.R.; Lee, S.C.; Kim, S.-Y.; Chun, B.-S. Amino Acid Profiles and Biopotentiality of Hydrolysates Obtained from Comb Panshell (*Atrina pectinata*) Viscera Using Subcritical Water Hydrolysis. *Mar. Drugs* **2021**, *19*, 137. [CrossRef]
101. Liu, C.; Ma, X.; Che, S.; Wang, C.; Li, B. The effect of hydrolysis with neutrase on molecular weight, functional properties, and antioxidant activities of Alaska pollock protein isolate. *J. Ocean Univ. China* **2018**, *17*, 1423–1431. [CrossRef]
102. Ahmed, R.; Chun, B.S. Subcritical water hydrolysis for the production of bioactive peptides from tuna skin collagen. *J. Supercrit. Fluids* **2018**, *141*, 88–96. [CrossRef]
103. Thirukumaran, R.; Anu Priya, V.K.; Krishnamoorthy, S.; Ramakrishnan, P.; Moses, J.A.; Anandharamakrishnan, C. Resource recovery from fish waste: Prospects and the usage of intensified extraction technologies. *Chemosphere* **2022**, *299*, 134361. [CrossRef] [PubMed]
104. Yu, D.; Chi, C.F.; Wang, B.; Ding, G.F.; Li, Z.R. Characterization of acid-and pepsin-soluble collagens from spines and skulls of skipjack tuna (*Katsuwonus pelamis*). *Chin. J. Nat. Med.* **2014**, *12*, 712–720. [CrossRef] [PubMed]
105. Wang, K.; Han, L.; Hong, H.; Pan, J.; Liu, H.; Luo, Y. Purification and identification of novel antioxidant peptides from silver carp muscle hydrolysate after simulated gastrointestinal digestion and transepithelial transport. *Food Chem.* **2021**, *342*, 128275. [CrossRef] [PubMed]



106. Kong, X.; Zhang, L.; Song, W.; Zhang, C.; Hua, Y.; Chen, Y.; Li, X. Separation, identification and molecular binding mechanism of dipeptidyl peptidase IV inhibitory peptides derived from walnut (*Juglans regia* L.) protein. *Food Chem.* **2021**, *347*, 129062. [CrossRef] [PubMed]
107. Oliveira Lima, K.; Alemán, A.; López-Caballero, M.E.; Gómez-Guillén, M.D.C.; Montero, M.P.; Prentice, C.; Huisa, A.J.T.; Monserrat, J.M. Characterization, stability, and in vivo effects in *Caenorhabditis elegans* of microencapsulated protein hydrolysates from stripped weakfish (*Cynoscion guatucupa*) industrial byproducts. *Food Chem.* **2021**, *364*, 130380. [CrossRef] [PubMed]
108. Ketnawa, S.; Benjakul, S.; Martínez-Alvarez, O.; Rawdkuen, S. Fish skin gelatin hydrolysates produced by visceral peptidase and bovine trypsin: Bioactivity and stability. *Food Chem.* **2017**, *215*, 383–390. [CrossRef] [PubMed]
109. Kim, H.K.; Kim, Y.H.Y.J.; Kim, Y.H.Y.J.; Park, H.J.; Lee, N.H. Effects of ultrasonic treatment on collagen extraction from skins of the sea bass *Lateolabrax japonicus*. *Fish Sci.* **2012**, *78*, 485–490. [CrossRef]
110. Li, D.; Mu, C.; Cai, S.; Lin, W. Ultrasonic irradiation in the enzymatic extraction of collagen. *Ultrason. Sonochem.* **2009**, *16*, 605–609. [CrossRef]
111. Melgosa, R.; Marques, M.; Paiva, A.; Bernardo, A.; Fernández, N.; Sá-Nogueira, I.; Simoes, P. Subcritical Water Extraction and Hydrolysis of Cod (*Gadus morhua*) Frames to Produce Bioactive Protein Extracts. *Foods* **2021**, *10*, 1222. [CrossRef] [PubMed]
112. Zhou, T.; Liu, X.; Sui, B.; Liu, C.; Mo, X.; Sun, J. Development of fish collagen/bioactive glass/chitosan composite nanofibers as a GTR/GBR membrane for inducing periodontal tissue regeneration. *Biomed. Mater.* **2017**, *12*, 55004. [CrossRef]
113. Li, P.H.; Lu, W.C.; Chan, Y.J.; Ko, W.C.; Jung, C.C.; Le Huynh, D.T.; Ji, Y.X. Extraction and characterization of collagen from sea cucumber (*Holothuria cinerascens*) and its potential application in moisturizing cosmetics. *Aquaculture* **2020**, *515*, 734590. [CrossRef]
114. Chinh, N.T.; Manh, V.Q.; Trung, V.Q.; Lam, T.D.; Huynh, M.D.; Tung, N.Q.; Trinh, N.D.; Hoang, T. Characterization of collagen derived from tropical freshwater carp fish scale wastes and its amino acid sequence. *Nat. Prod. Commun.* **2019**, *14*, 1934578X1986628. [CrossRef]
115. Powell, T.; Bowra, S.; Cooper, H.J. Subcritical Water Hydrolysis of Peptides: Amino Acid Side-Chain Modifications. *J. Am. Soc. Mass Spectrom.* **2017**, *28*, 1775–1786. [CrossRef] [PubMed]
116. Asaduzzaman, A.K.M.; Getachew, A.T.; Cho, Y.J.; Park, J.S.; Haq, M.; Chun, B.S. Characterization of pepsin-solubilised collagen recovered from mackerel (*Scomber japonicus*) bone and skin using subcritical water hydrolysis. *Int. J. Biol. Macromol.* **2020**, *148*, 1290–1297. [CrossRef] [PubMed]
117. Ahmed, R.; Haq, M.; Chun, B.S. Characterization of marine derived collagen extracted from the by-products of bigeye tuna (*Thunnus obesus*). *Int. J. Biol. Macromol.* **2019**, *135*, 668–676. [CrossRef]
118. Chen, Y.; Jin, H.; Yang, F.; Jin, S.; Liu, C.; Zhang, L.; Huang, J.; Wang, S.; Yan, Z.; Ca, X.; et al. Physicochemical, antioxidant properties of giant croaker (*Nibea japonica*) swim bladders collagen and wound healing evaluation. *Int. J. Biol. Macromol.* **2019**, *138*, 483–491. [CrossRef]
119. Hamdan, F.; Sarbon, N.M. Isolation and characterization of collagen from fringescale sardinella (*Sardinella fimbriata*) waste materials. *Int. Food. Res. J.* **2019**, *26*, 133–140.
120. Wei, P.; Zheng, H.; Shi, Z.; Li, D.; Xiang, Y. Isolation and Characterization of Acid-soluble Collagen and Pepsin-soluble Collagen from the Skin of Hybrid Sturgeon. *J. Wuhan Univ. Technol. Sci. Ed.* **2019**, *34*, 950–959. [CrossRef]
121. Song, W.K.; Liu, D.; Sun, L.L.; Li, B.F.; Hou, H. Physicochemical and Biocompatibility Properties of Type I Collagen from the Skin of Nile Tilapia (*Oreochromis niloticus*) for Biomedical Applications. *Mar. Drugs* **2019**, *17*, 137. [CrossRef]
122. Zhang, X.; Adachi, S.; Ura, K.; Takagi, Y. Properties of collagen extracted from Amur sturgeon *Acipenser schrenckii* and assessment of collagen fibrils in vitro. *Int. J. Biol. Macromol.* **2019**, *137*, 809–820. [CrossRef]
123. Wang, J.; Pei, X.; Liu, H.; Zhou, D. Extraction and characterization of acid-soluble and pepsin-soluble collagen from skin of loach (*Misgurnus anguillicaudatus*). *Int. J. Biol. Macromol.* **2018**, *106*, 544–550. [CrossRef] [PubMed]
124. Zhao, W.H.; Chi, C.F.; Zhao, Y.Q.; Wang, B. Preparation, Physicochemical and Antioxidant Properties of Acid- and Pepsin-Soluble Collagens from the Swim Bladders of Miiuy Croaker (*Miichthys miiuy*). *Mar. Drugs* **2018**, *16*, 161. [CrossRef] [PubMed]
125. Jaziri, A.A.; Shapawi, R.; Mokhtar, R.A.M.; Noordin, W.N.M.; Huda, N. Microstructural and Physicochemical Analysis of Collagens from the Skin of Lizardfish (*Saurida tumbil* Bloch, 1795) Extracted with Different Organic Acids. *Molecules* **2022**, *27*, 2452. [CrossRef] [PubMed]
126. Johny, L.C.; Kudre, T.G.; Suresh, P.V. Acid and Pepsin Soluble Collagens from Skin By-product of Red-bellied Pacu (*Piaractus brachypomus*): Extraction and Comparative Characterizations Towards Finding Substitute to Bovine and Porcine Collagen. *J. Aquat. Food Prod. Technol.* **2021**, *30*, 364–376. [CrossRef]
127. Mahboob, S. Isolation and characterization of collagen from fish waste material- skin, scales and fins of *Catla catla* and *Cirrhinus mrigala*. *J. Food Sci. Technol.* **2015**, *52*, 4296–4305. [CrossRef]
128. Devita, L.; Nurilmala, M.; Lioe, H.N.; Suhartono, M.T. Chemical and Antioxidant Characteristics of Skin-Derived Collagen Obtained by Acid-Enzymatic Hydrolysis of Bigeye Tuna (*Thunnus obesus*). *Mar. Drugs* **2021**, *19*, 222. [CrossRef]
129. Hashim, P.; Mohd Ridzwan, M.S.; Bakar, J.; Mat Hashim, D. Collagen in food and beverage industries. *Int. Food Res. J.* **2015**, *22*, 1–8.
130. Ahmad, M.; Benjakul, S. Extraction and characterisation of pepsin-solubilised collagen from the skin of unicorn leatherjacket (*Aluterus monoceros*). *Food Chem.* **2010**, *120*, 817–824. [CrossRef]

131. Tan, Y.; Chang, S.K.C. Isolation and characterization of collagen extracted from channel catfish (*Ictalurus punctatus*) skin. *Food Chem.* **2018**, *242*, 147–155. [CrossRef]
132. Bi, C.; Li, X.; Xin, Q.; Han, W.; Shi, C.; Guo, R.; Shi, W.; Qiao, R.; Wang, X.; Zhong, J. Effect of extraction methods on the preparation of electrospun/electrosprayed microstructures of tilapia skin collagen. *J. Biosci. Bioeng.* **2019**, *128*, 234–240. [CrossRef]
133. Lionetto, F.; Bagheri, S.; Mele, C. Sustainable Materials from Fish Industry Waste for Electrochemical Energy Systems. *Energies* **2021**, *14*, 7928. [CrossRef]
134. Bilek, S.E.; Bayram, S.K. Fruit juice drink production containing hydrolyzed collagen. *J. Funct. Foods* **2015**, *14*, 562–569. [CrossRef]
135. Nur Ibrahim, F.; Rashedi Ismail-Fitry, M.; Mat Yusoff, M.; Shukri, R. Effects of Fish Collagen Hydrolysate (FCH) as fat replacer in the production of buffalo patties. *J. Adv. Res. Appl. Sci. Eng. Technol.* **2018**, *11*, 108–117.
136. Sousa, S.C.; Fragoso, S.P.; Penna, C.R.A.; Arcanjo, N.M.O.; Silva, F.A.P.; Ferreira, V.C.S.; Barreto, M.D.S.; Araújo, I.B.S. Quality parameters of frankfurter-type sausages with partial replacement of fat by hydrolyzed collagen. *LWT-Food Sci. Technol.* **2017**, *76*, 320–325. [CrossRef]
137. Bhagwat, P.K.; Dandge, P.B. Isolation, characterization and valorizable applications of fish scale collagen in food and agriculture industries. *Biocatal. Agric. Biotechnol.* **2016**, *7*, 234–240. [CrossRef]
138. Pal, G.K.; Suresh, P.V. Sustainable valorisation of seafood by-products: Recovery of collagen and development of collagen-based novel functional food ingredients. *Innov. Food Sci. Emerg. Technol.* **2016**, *37*, 201–215. [CrossRef]
139. Zapata, J.I.H.; De La Pava, G.C.R. Physicochemical analysis of frankfurter type sausages made with red tilapia fillet waste (*Oreochromis* sp) and quinoa flour (*Chenopodium quinoa* W.). *Braz. J. Food Technol.* **2017**, *21*, 1–8. [CrossRef]
140. Guo, L.; Harnedy, P.A.; Zhang, L.; Li, B.; Zhang, Z.; Hou, H.; Zhao, X.; Fitzgerald, R.J. In vitro assessment of the multifunctional bioactive potential of Alaska pollock skin collagen following simulated gastrointestinal digestion. *J. Sci. Food Agric.* **2015**, *95*, 1514–1520. [CrossRef]
141. Pei, X.; Yang, R.; Zhang, Z.; Gao, L.; Wang, J.; Xu, Y.; Zhao, M.; Han, X.; Liu, Z.; Li, Y. Marine collagen peptide isolated from Chum Salmon (*Oncorhynchus keta*) skin facilitates learning and memory in aged C57BL/6J mice. *Food Chem.* **2010**, *118*, 333–340. [CrossRef]
142. Wang, L.; Jiang, Y.; Wang, X.; Zhou, J.; Cui, H.; Xu, W.; Xu, W.; He, Y.; Ma, H.; Gao, R. Effect of oral administration of collagen hydrolysates from Nile tilapia on the chronologically aged skin. *J. Funct. Foods* **2018**, *44*, 112–117. [CrossRef]
143. Venkatesan, J.; Anil, S.; Kim, S.K.; Shim, M.S. Marine Fish Proteins and Peptides for Cosmeceuticals: A Review. *Mar. Drugs* **2017**, *15*, 143. [CrossRef]
144. Hays, N.P.; Kim, H.; Wells, A.M.; Kajkenova, O.; Evans, W.J. Effects of Whey and Fortified Collagen Hydrolysate Protein Supplements on Nitrogen Balance and Body Composition in Older Women. *J. Am. Diet Assoc.* **2009**, *109*, 1082–1087. [CrossRef] [PubMed]
145. Chen, Y.P.; Wu, H.T.; Wang, G.H.; Liang, C.H. Improvement of skin condition on skin moisture and anti-melanogenesis by collagen peptides from milkfish (*Chanos chanos*) scales. *IOP Conf. Ser. Mater. Sci. Eng.* **2018**, *382*, 022067. [CrossRef]
146. Ito, N.; Seki, S.; Ueda, F. Effects of composite supplement containing collagen peptide and ornithine on skin conditions and plasma IGF-1 levels—A randomized, double-blind, placebo. *Mar. Drugs* **2018**, *16*, 482. [CrossRef] [PubMed]
147. Porfírio, E.; Fanaro, G.B. Collagen supplementation as a complementary therapy for the prevention and treatment of osteoporosis and osteoarthritis: A systematic review. *Rev. Bras. Geriatr. Gerontol.* **2016**, *19*, 153–164. [CrossRef]
148. Zouboulis, C.C.; Makrantonaki, E. Clinical aspects and molecular diagnostics of skin aging. *Clin. Dermatol.* **2011**, *29*, 3–14. [CrossRef]
149. Kim, D.U.; Chung, H.C.; Choi, J.; Sakai, Y.; Lee, B.Y. Oral Intake of Low-Molecular-Weight Collagen Peptide Improves Hydration, Elasticity, and Wrinkling in Human Skin: A Randomized, Double-Blind, Placebo-Controlled Study. *Nutrients* **2018**, *10*, 826. [CrossRef] [PubMed]
150. Haydont, V.; Bernard, B.A.; Fortunel, N.O. Age-related evolutions of the dermis: Clinical signs, fibroblast and extracellular matrix dynamics. *Mech. Ageing Dev.* **2019**, *177*, 150–156. [CrossRef]
151. Bolke, L.; Schlippe, G.; Gerß, J.; Voss, W. A Collagen Supplement Improves Skin Hydration, Elasticity, Roughness, and Density: Results of a Randomized, Placebo-Controlled, Blind Study. *Nutrients* **2019**, *11*, 2494. [CrossRef]
152. Tang, J.; Saito, T. Biocompatibility of Novel Type I Collagen Purified from Tilapia Fish Scale: An In Vitro Comparative Study. *Biomed. Res. Int.* **2015**, *2015*, 139476. [CrossRef]
153. Allan, B.; Ruan, R.; Landao-Bassonga, E.; Gillman, N.; Wang, T.; Gao, J.; Ruan, Y.; Xu, Y.; Lee, C.; Gonewardene, M.; et al. Collagen membrane for guided bone regeneration in dental and orthopedic applications. *Tissue Eng.-Part A* **2021**, *27*, 372–381. [CrossRef]
154. Binlath, T.; Thammanichanon, P.; Rittipakorn, P.; Thinsathid, N.; Jitprasertwong, P. Collagen-Based Biomaterials in Periodontal Regeneration: Current Applications and Future Perspectives of Plant-Based Collagen. *Biomimetics* **2022**, *7*, 34. [CrossRef] [PubMed]
155. Lin, K.; Zhang, D.; Macedo, M.H.; Cui, W.; Sarmiento, B.; Shen, G. Advanced Collagen-Based Biomaterials for Regenerative Biomedicine. *Adv. Funct. Mater.* **2019**, *29*, 1804943. [CrossRef]
156. Pankajakshan, D.; Voytik-Harbin, S.L.; Nör, J.E.; Bottino, M.C. Injectable highly tunable oligomeric collagen matrices for dental tissue regeneration. *ACS Appl. Bio. Mater.* **2020**, *3*, 859–868. [CrossRef] [PubMed]



157. Yamaura, K.; Mifune, Y.; Inui, A.; Nishimoto, H.; Mukohara, S.; Yoshikawa, T.; Shinohara, I.; Kato, T.; Furukawa, T.; Hoshino, Y.; et al. Novel therapy using a fish scale collagen scaffold for rotator cuff healing in rat models. *J. Shoulder Elb. Surg.* **2022**, *31*, 2629–2637. [CrossRef] [PubMed]
158. Kim, S.-C.; Heo, S.-Y.; Oh, G.-W.; Yi, M.; Jung, W.-K. A 3D-Printed Polycaprolactone/Marine Collagen Scaffold Reinforced with Carbonated Hydroxyapatite from Fish Bones for Bone Regeneration. *Mar. Drugs* **2022**, *20*, 344. [CrossRef]
159. Biranje, S.S.; Sun, J.; Cheng, L.; Cheng, Y.; Shi, Y.; Yu, S.; Jiao, H.; Zhang, M.; Lu, X.; Han, W.; et al. Development of Cellulose Nanofibril/Casein-Based 3D Composite Hemostasis Scaffold for Potential Wound-Healing Application. *ACS Appl. Mater. Interfaces* **2022**, *14*, 3792–3808. [CrossRef]
160. Mbese, Z.; Alven, S.; Aderibigbe, B.A. Collagen-based nanofibers for skin regeneration and wound dressing applications. *Polymers* **2021**, *13*, 4368. [CrossRef]
161. Nezhad-Mokhtari, P.; Javanbakht, S.; Asadi, N.; Ghorbani, M.; Milani, M.; Hanifehpour, Y.; Gholizadeh, P.; Akbarzadeh, A. Recent advances in honey-based hydrogels for wound healing applications: Towards natural therapeutics. *J. Drug Deliv. Sci. Technol.* **2021**, *66*, 102789. [CrossRef]
162. Sarrigiannidis, S.O.; Rey, J.M.; Dobre, O.; González-García, C.; Dalby, M.J.; Salmeron-Sanchez, M. A tough act to follow: Collagen hydrogel modifications to improve mechanical and growth factor loading capabilities. *Mater. Today Bio* **2021**, *10*, 100098. [CrossRef]
163. Kim, J.; Lee, K.M.; Han, S.H.; Ko, E.A.; Yoon, D.S.; Park, I.K.; Shin, H.; Park, K.-H.; Lee, J.-W. Development of stabilized dual growth factor-loaded hyaluronate collagen dressing matrix. *J. Tissue Eng.* **2021**, *12*, 2041731421999750. [CrossRef] [PubMed]
164. Ladhani, H.A.; Yowler, C.J.; Claridge, J.A. Burn Wound Colonization, Infection, and Sepsis. *Surg. Infect. (Larchmt)* **2021**, *22*, 44–48. [CrossRef] [PubMed]
165. Alven, S.; Nqoro, X.; Aderibigbe, B.A. Polymer-based materials loaded with curcumin for wound healing applications. *Polymers* **2020**, *12*, 2286. [CrossRef] [PubMed]
166. Hu, J.; Song, Y.; Zhang, C.; Huang, W.; Chen, A.; He, H.; Zhang, S.; Chen, Y.; Tu, C.; Liu, J.; et al. Highly Aligned Electrospun Collagen/Polycaprolactone Surgical Sutures with Sustained Release of Growth Factors for Wound Regeneration. *ACS Appl. Bio Mater.* **2020**, *3*, 965–976. [CrossRef]
167. Elibol, E.; Yilmaz, Y.F.; Ünal, A.; Ozcan, M.; Kum, N.Y.; Kum, R.O.; Kulaçoğlu, S. Effects of hyaluronic acid-collagen nanofibers on early wound healing in vocal cord trauma. *Eur. Arch. Otorhinolaryngol.* **2021**, *278*, 1537–1544. [CrossRef]
168. Hu, Z.; Yang, P.; Zhou, C.; Li, S. Marine Collagen Peptides from the Skin of Nile Tilapia (*Oreochromis niloticus*): Characterization and Wound Healing Evaluation. *Mar. Drugs* **2017**, *15*, 102. [CrossRef]
169. Yang, T.; Zhang, K.; Li, B.; Hou, H. Effects of oral administration of peptides with low molecular weight from Alaska Pollock (*Theragra chalcogramma*) on cutaneous wound healing. *J. Funct. Foods* **2018**, *48*, 682–691. [CrossRef]
170. Chen, J.; Gao, K.; Liu, S.; Wang, S.; Elango, J.; Bao, B.; Dong, J.; Liu, N.; Wu, W. Fish collagen surgical compress repairing characteristics on wound healing process in vivo. *Mar. Drugs* **2019**, *17*, 33. [CrossRef]
171. Kozłowicz, K.; Nazarewicz, S.; Góral, D.; Krawczuk, A.; Domin, M. Lyophilized protein structures as an alternative biodegradable material for food packaging. *Sustainability* **2019**, *11*, 7002. [CrossRef]
172. Wang, Z.; Hu, S.; Wang, H. Scale-up preparation and characterization of collagen/sodium alginate blend films. *J. Food Qual.* **2017**, *2017*, 4954259. [CrossRef]
173. Goyal, N.; Rastogi, D.; Jassal, M.; Agrawal, A.K. Chitosan as a potential stabilizing agent for titania nanoparticle dispersions for preparation of multifunctional cotton fabric. *Carbohydr. Polym.* **2016**, *154*, 167–175. [CrossRef] [PubMed]
174. Demitri, C.; Moscatello, A.; Giuri, A.; Raucci, M.G.; Esposito Corcione, C. Preparation and characterization of EG-Chitosan nanocomposites via direct exfoliation: A green methodology. *Polymers* **2015**, *7*, 2584–2594. [CrossRef]
175. Gokoglu, N. Innovations in seafood packaging technologies: A review. *Food Rev. Int.* **2019**, *36*, 340–366. [CrossRef]
176. Listrat, A.; Lebret, B.; Louveau, I.; Astruc, T.; Bonnet, M.; Lefaucheur, L.; Picard, B.; Bugeon, J. How muscle structure and composition influence meat and flesh quality. *Sci. World J.* **2016**, *2016*, 3182746. [CrossRef] [PubMed]
177. Antonio Vázquez, J.; Meduñña, A.; Durán, A.I.; Nogueira, M.; Fernández-Compás, A.; Pérez-Martín, R.I.; Rodríguez-Amado, I. Production of valuable compounds and bioactive metabolites from by-products of fish discards using chemical processing, enzymatic hydrolysis, and bacterial. *Mar. Drugs* **2019**, *17*, 139. [CrossRef] [PubMed]
178. Murrieta-Martínez, C.L.; Soto-Valdez, H.; Pacheco-Aguilar, R.; Torres-Arreola, W.; Rodríguez-Felix, F.; Márquez Ríos, E.; Encinas Rosales, L. Edible protein films: Sources and behavior. *Wiley Online Libr.* **2018**, *31*, 113–122. [CrossRef]
179. Medina, E.; Caro, N.; Abugoch, L.; Gamboa, A.; Díaz-Dosque, M.; Tapia, C. Chitosan thymol nanoparticles improve the antimicrobial effect and the water vapour barrier of chitosan-quinoa protein films. *J. Food Eng.* **2019**, *240*, 191–198. [CrossRef]
180. Gómez-Estaca, J.; Gómez-Guillén, M.C.; Fernández-Martín, F.; Montero, P. Effects of gelatin origin, bovine-hide and tuna-skin, on the properties of compound gelatin–chitosan films. *Food Hydrocoll.* **2011**, *25*, 1461–1469. [CrossRef]
181. de la Caba, K.; Guerrero, P.; Trung, T.S.; Cruz-Romero, M.; Kerry, J.P.; Fluhr, J.; Maurer, M.; Kruijssen, F.; Albalat, A.; Bunting, S.; et al. From seafood waste to active seafood packaging: An emerging opportunity of the circular economy. *J. Clean Prod.* **2019**, *208*, 86–98. [CrossRef]
182. Asgher, M.; Qamar, S.A.; Bilal, M.; Iqbal, H.M.N. Bio-based active food packaging materials: Sustainable alternative to conventional petrochemical-based packaging materials. *Food Res. Int.* **2020**, *137*, 109625. [CrossRef]
183. Paolucci, M.; Volpe, M.G. The Effect of Novel Packaging Technology on Food Safety and Quality. *Foods* **2021**, *10*, 269. [CrossRef] [PubMed]

184. Lionetto, F.; Esposito Corcione, C. Recent applications of biopolymers derived from fish industry waste in food packaging. *Polymers* **2021**, *13*, 2337. [CrossRef] [PubMed]
185. Ruiz-Salmón, I.; Margallo, M.; Laso, J.; Villanueva-Rey, P.; Mariño, D.; Quinteiro, P.; Dias, A.-C.; Nunes, M.-L.; Marques, A.; Feijoo, G.; et al. Addressing challenges and opportunities of the European seafood sector under a circular economy framework. *Curr. Opin. Environ. Sci. Health* **2020**, *13*, 101–106. [CrossRef]
186. Kang, Y.; Kim, H.J.; Moon, C.H. Eutrophication driven by aquaculture fish farms controls phytoplankton and dinoflagellate cyst abundance in the southern coastal waters of Korea. *J. Mar. Sci. Eng.* **2021**, *9*, 362. [CrossRef]
187. Ahmad, M.; Nirmal, N.P.; Chuprom, J. Molecular characteristics of collagen extracted from the starry triggerfish skin and its potential in the development of biodegradable packaging film. *RSC Adv.* **2016**, *6*, 33868–33879. [CrossRef]
188. Ahmed, M.; Verma, A.K.; Patel, R. Physiochemical, antioxidant, and food simulant release properties of collagen-carboxymethyl cellulose films enriched with *Berberis lyceum* root extract for. *J. Food Process. Preserv.* **2022**, *46*, e16485. [CrossRef]
189. Song, T.; Qian, S.; Lan, T.; Wu, Y.; Liu, J.; Zhang, H. Recent advances in bio-based smart active packaging materials. *Foods* **2022**, *11*, 2228. [CrossRef] [PubMed]
190. Kumar, S.; Mukherjee, A.; Dutta, J. Chitosan based nanocomposite films and coatings: Emerging antimicrobial food packaging alternatives. *Trends Food Sci. Technol.* **2020**, *97*, 196–209. [CrossRef]
191. Haghighi, H.; Licciardello, F.; Fava, P.; Siesler, H.W.; Pulvirenti, A. Recent advances on chitosan-based films for sustainable food packaging applications. *Food Packag. Shelf Life* **2020**, *26*, 100551. [CrossRef]
192. Zhuang, Y.; Ruan, S.; Yao, H.; Sun, Y. Physical Properties of Composite Films from Tilapia Skin Collagen with Pachyrhizus Starch and Rambutan Peel Phenolics. *Mar. Drugs* **2019**, *17*, 662. [CrossRef]
193. Freire Da Costa, G.; Grisi, C.V.B.; de Albuquerque Meireles, B.R.L.; de Sousa, S.; de Magalhães Cordeiro, A.M.T. Collagen films, cassava starch and their blends: Physical–chemical, thermal and microstructure properties. *Packag. Technol. Sci* **2022**, *35*, 229–240. [CrossRef]
194. Sommer, A.; Dederko-Kantowicz, P.; Staroszczyk, H.; Sommer, S.; Michalec, M. Enzymatic and chemical cross-linking of bacterial cellulose/fish collagen composites—A comparative study. *Int. J. Mol. Sci.* **2021**, *22*, 3346. [CrossRef] [PubMed]
195. Ahmed, M.W.; Haque, M.A.; Mohibullah, M.; Khan, M.S.I.; Islam, M.A.; Mondal, M.H.T.; Ahmmed, R. A review on active packaging for quality and safety of foods: Current trends, applications, prospects and challenges. *Food. Packag. Shelf Life* **2022**, *33*, 100913. [CrossRef]
196. Nur Hanani, Z.A.; Roos, Y.H.; Kerry, J.P. Use and application of gelatin as potential biodegradable packaging materials for food products. *Int. J. Biol. Macromol.* **2014**, *71*, 94–102. [CrossRef] [PubMed]
197. Lu, Y.; Luo, Q.; Chu, Y.; Tao, N.; Deng, S.; Wang, L.; Li, L. Application of Gelatin in Food Packaging: A Review. *Polymers* **2022**, *14*, 436. [CrossRef]
198. Sani, M.A.; Azizi-Lalabadi, M.; Tavassoli, M.; Mohammadi, K.; McClements, D.J. Recent Advances in the Development of Smart and Active Biodegradable Packaging Materials. *Nanomaterials* **2021**, *11*, 1331. [CrossRef]
199. Yao, X.; Qin, Y.; Zhang, M.; Zhang, J.; Qian, C.; Liu, J. Development of active and smart packaging films based on starch, polyvinyl alcohol and betacyanins from different plant sources. *Int. J. Biol. Macromol.* **2021**, *183*, 358–368. [CrossRef]
200. Irastorza, A.; Zarandona, I.; Andonegi, M.; Guerrero, P.; de la Caba, K. The versatility of collagen and chitosan: From food to biomedical applications. *Food Hydrocoll.* **2021**, *116*, 106633. [CrossRef]
201. Wang, H.; Ding, F.; Ma, L.; Zhang, Y. Edible films from chitosan-gelatin: Physical properties and food packaging application. *Food Biosci.* **2021**, *40*, 100871. [CrossRef]
202. Hu, H.; Yao, X.; Qin, Y.; Yong, H.; Liu, J. Development of multifunctional food packaging by incorporating betalains from vegetable amaranth (*Amaranthus tricolor* L.) into quaternary ammonium chitosan/fish gelatin blend films. *Int. J. Biol. Macromol.* **2020**, *159*, 675–684. [CrossRef]
203. Global Marine Collagen Market. Industry Trends Forecast to 2029. Available online: <https://www.databridgemarketresearch.com/reports/global-marine-collagen-market> (accessed on 3 November 2022).
204. Fish Collagen Peptides Market Size by Source n.d. Available online: <https://www.gminsights.com/industry-analysis/fish-collagen-peptides-market> (accessed on 15 October 2022).
205. Marine Collagen Market. Ind Trends Forecast to 2029 n.d. Available online: <https://www.futuremarketinsights.com/reports/sample/rep-gb-11528> (accessed on 5 November 2022).
206. Global Fish Collagen Peptides Market. Available online: <https://www.databridgemarketresearch.com/reports/global-fish-collagen-peptides-market> (accessed on 8 November 2022).
207. Fish Collagen Market n.d. Available online: <https://www.futuremarketinsights.com/reports/fish-collagen-market> (accessed on 2 November 2022).
208. Understanding Collagen Across Markets. n.d. Available online: [https://assets.ctfassets.net/pn8wbqitnzw9/59baJqNfCzOWFWBgYZ22s9/8b827e0e32946b3fc1ac567f1448bace/Understanding\\_Collagen\\_Across\\_Markets](https://assets.ctfassets.net/pn8wbqitnzw9/59baJqNfCzOWFWBgYZ22s9/8b827e0e32946b3fc1ac567f1448bace/Understanding_Collagen_Across_Markets) (accessed on 20 October 2022).
209. Fish Collagen Peptides Market Scenario. Available online: <https://www.databridgemarketresearch.com/news/global-fish-collagen-peptides-market> (accessed on 26 October 2022).
210. Collagen Business Case Report n.d. Available online: [https://www.mla.com.au/contentassets/ae2babccbb964211bad5556e86e9e627/v.rmh.0079\\_final\\_report.pdf/](https://www.mla.com.au/contentassets/ae2babccbb964211bad5556e86e9e627/v.rmh.0079_final_report.pdf/) (accessed on 5 November 2022).

211. Zhang, X.; Xu, S.; Shen, L.; Li, G. Factors affecting thermal stability of collagen from the aspects of extraction, processing and modification. *J. Leather Sci. Eng* **2020**, *2*, 19. [CrossRef]
212. Arumugam, G.K.S.; Sharma, D.; Balakrishnan, R.M.; Ettiyanappan, J.B.P. Extraction, optimization and characterization of collagen from sole fish skin. *Sustain. Chem. Pharm.* **2018**, *9*, 19–26. [CrossRef]
213. Huang, R.; Chen, S.; Ma, G.; Yang, B.; Guo, R.; Li, Q.; Zhong, J. Research on the extraction of collagen from scales of tilapia. *Adv. Mater. Res.* **2011**, *295–297*, 796–799. [CrossRef]
214. Yu, F.; Zong, C.; Jin, S.; Zheng, J.; Chen, N.; Huang, J.; Chen, Y.; Huang, F.; Yang, Z.; Tang, Y. Optimization of extraction conditions and characterization of pepsin-solubilised collagen from skin of giant croaker (*Nibea japonica*). *Mar. Drugs* **2018**, *16*, 29. [CrossRef]
215. Huang, C.Y.; Kuo, J.M.; Wu, S.J.; Tsai, H.T. Isolation and characterization of fish scale collagen from tilapia (*Oreochromis* sp.) by a novel extrusion-hydro-extraction process. *Food Chem.* **2016**, *190*, 997–1006. [CrossRef]
216. Dong, Y.; Dai, Z. Physicochemical, Structural and Antioxidant Properties of Collagens from the Swim Bladder of Four Fish Species. *Mar. Drugs* **2022**, *20*, 550. [CrossRef]
217. Zhang, B.; Chen, L.; Jaziri, A.A.; Shapawi, R.; Azli, R.; Mokhtar, M.; Norhana, W.; Noordin, M.; Huda, N. Physicochemical and Microstructural Analyses of Pepsin-Soluble Collagens Derived from Lizardfish (*Saurida tumbil* Bloch, 1795) Skin, Bone and Scales. *Gels* **2022**, *8*, 471. [CrossRef]
218. Gutierrez Cuba, C.; Cordova, A.; Loayza, J.; Carlo Cabrera, J.; Carrasco, L.; Sanchez, M. Advanced pilot plant automation for collagen production from hydrobiological waste in Callao, Perú. In Proceedings of the 20th LACCEI International Multi-Conference for Engineering, Education and Technology, Boca Raton, FL, USA, 18–22 July 2022. [CrossRef]
219. Yunoki, S.; Suzuki, T.; Takai, M. Stabilization of low denaturation temperature collagen from fish by physical cross-linking methods. *J. Biosci. Bioeng.* **2003**, *96*, 575–577. [CrossRef]
220. Sanz, B.; Albillos Sanchez, A.; Tangey, B.; Gilmore, K.; Yue, Z.; Liu, X.; Wallace, G. Light cross-linkable marine collagen for coaxial printing of a 3D model of neuromuscular junction formation. *Biomedicines* **2021**, *9*, 16. [CrossRef]
221. Safandowska, M.; Pietrucha, K. Effect of fish collagen modification on its thermal and rheological properties. *Int. J. Biol. Macromol.* **2013**, *53*, 32–37. [CrossRef]
222. Maher, M.; Glattauer, V.; Onofrillo, C.; Duchi, S.; Yue, Z.; Hughes, T.C.; Ramshaw, J.A.M.; Wallace, G.G. Suitability of Marine- and Porcine-Derived Collagen Type I Hydrogels for Bioprinting and Tissue Engineering Scaffolds. *Mar. Drugs* **2022**, *20*, 366. [CrossRef] [PubMed]
223. Roy, S.; Rhim, J.-W.; Li, S.; Fan, M.; Deng, S.; Tao, N. Characterization and Application in Packaging Grease of Gelatin–Sodium Alginate Edible Films Cross-Linked by Pullulan. *Polymers* **2022**, *14*, 3199. [CrossRef]
224. Suzuki, A.; Kodama, Y.; Miwa, K.; Kishimoto, K.; Hoshikawa, E.; Haga, K.; Sato, T.; Mizuno, J.; Izumi, K. Manufacturing micropatterned collagen scaffolds with chemical-crosslinking for development of biomimetic tissue-engineered oral mucosa. *Sci. Rep.* **2020**, *10*, 22192. [CrossRef]
225. Zhang, M.; Li, G. Partial Characterization of Fish Skin Collagen Cross-Linked by N-Hydroxysuccinimide Activated Adipic Acid. *J. Aquat. Food Prod. Technol.* **2014**, *23*, 44–58. [CrossRef]
226. Chen, J.; Luo, L.; Cen, C.; Liu, Y.; Li, H.; Wang, Y. The nano antibacterial composite film carboxymethyl chitosan/gelatin/nano ZnO improves the mechanical strength of food packaging. *Int. J. Biol. Macromol.* **2022**, *220*, 462–471. [CrossRef]
227. Guo, H.; Shao, C.; Ma, Y.; Zhang, Y.; Lu, P. Development of Active and Intelligent pH Film Based on Gelatin/Chitosan/Polyvinyl Alcohol with Litchi Shell Extract as an Indicator. *Int. J. Biol. Macromol.* **2023**, *226*, 77–89. [CrossRef] [PubMed]
228. Xia, Y.; Meng, F.; Wang, S.; Li, P.; Geng, C.; Zhang, X.; Zhou, Z.; Kong, F. Tough, antibacterial fish scale gelatin/chitosan film with excellent water vapor and UV-blocking performance comprising liquefied chitin and silica sol. *Int. J. Biol. Macromol.* **2022**, *222*, 3250–3260. [CrossRef] [PubMed]
229. Chen, J.; Li, Y.; Wang, Y.; Yakubu, S.; Tang, H.; Li, L. Active polylactic acid/tilapia fish gelatin-sodium alginate bilayer films: Application in preservation of Japanese sea bass (*Lateolabrax japonicus*). *Food Packag. Shelf Life* **2022**, *33*, 100915. [CrossRef]
230. Moya-Lopez, C.; Valcarcel, J.; Vázquez, J.A.; Bourson, P.; Chapron, D.; Solano, E.; Piñeiro, M.M.; Hermida-Merino, C.; Hermida-Merino, D. Biocompatibility enhancement of PLA by the generation of bionanocomposites with fish collagen derivatives. *Emergent Mater.* **2022**, *5*, 695–702. [CrossRef]
231. Kamer, D.D.A.; Kaynarca, G.B.; Yücel, E.; GÜMÜŞ, T. Development of gelatin/PVA based colorimetric films with a wide pH sensing range winery solid by-product (Vinasse) for monitor shrimp freshness. *Int. J. Biol. Macromol.* **2022**, *220*, 627–637. [CrossRef]

**Disclaimer/Publisher’s Note:** The statements, opinions and data contained in all publications are solely those of the individual author(s) and contributor(s) and not of MDPI and/or the editor(s). MDPI and/or the editor(s) disclaim responsibility for any injury to people or property resulting from any ideas, methods, instructions or products referred to in the content.

## Article

# Comparative Study of Flax and Pineapple Leaf Fiber Reinforced Poly(butylene succinate): Effect of Fiber Content on Mechanical Properties

Tawechai Amornsakchai <sup>1,2,3,\*</sup>, Sorn Duangsuwan <sup>1,2</sup>, Karine Mougín <sup>4</sup> and Kheng Lim Goh <sup>5,6</sup>

<sup>1</sup> Polymer Science and Technology Program, Department of Chemistry, Faculty of Science, Mahidol University, Phuttamonthon 4 Road, Salaya, Nakhon Pathom 73170, Thailand

<sup>2</sup> Center of Sustainable Energy and Green Materials, Faculty of Science, Mahidol University, Phuttamonthon 4 Road, Salaya, Nakhon Pathom 73170, Thailand

<sup>3</sup> TEAnity Team Co., Ltd., 40/494 Soi Navamintra 111, Khet Bueng Kum, Bangkok 10230, Thailand

<sup>4</sup> Institut de Science des Matériaux de Mulhouse, IS2M-CNRS-UHA, 15, Rue Jean Starcky, B.P.2488, 68057 Mulhouse, CEDEX, France; karine.mougin@uha.fr

<sup>5</sup> Mechanical Design and Manufacturing Engineering, Newcastle University in Singapore, 172A Ang Mo Kio Avenue 8 #05-01, SIT@NYP Building, Singapore 567739, Singapore; kheng-lim.goh@newcastle.ac.uk

<sup>6</sup> Faculty of Science, Agriculture & Engineering, Newcastle University, Newcastle upon Tyne NE1 7RU, UK

\* Correspondence: tawechai.amo@mahidol.ac.th

**Abstract:** In this study, we compare the reinforcing efficiency of pineapple leaf fiber (PALF) and cultivated flax fiber in unidirectional poly(butylene succinate) composites. Flax, known for robust mechanical properties, is contrasted with PALF, a less studied but potentially sustainable alternative. Short fibers (6 mm) were incorporated at 10 and 20% wt. levels. After two-roll mill mixing, uniaxially aligned prepreg sheets were compression molded into composites. At 10 wt.%, PALF and flax exhibited virtually the same stress–strain curve. Interestingly, PALF excelled at 20 wt.%, defying its inherently lower tensile properties compared to flax. PALF/PBS reached 70.7 MPa flexural strength, 2.0 GPa flexural modulus, and 107.3 °C heat distortion temperature. Comparable values for flax/PBS were 57.8 MPa, 1.7 GPa, and 103.7 °C. X-ray pole figures indicated similar matrix orientations in both composites. An analysis of extracted fibers revealed differences in breakage behavior. This study highlights the potential of PALF as a sustainable reinforcement option. Encouraging the use of PALF in high-performance bio-composites aligns with environmental goals.

**Keywords:** pineapple leaf fiber; flax; poly(butylene succinate); unidirectional composites; microstructure; mechanical properties

**Citation:** Amornsakchai, T.; Duangsuwan, S.; Mougín, K.; Goh, K.L. Comparative Study of Flax and Pineapple Leaf Fiber Reinforced Poly(butylene succinate): Effect of Fiber Content on Mechanical Properties. *Polymers* **2023**, *15*, 3691. <https://doi.org/10.3390/polym15183691>

Academic Editor: Raffaella Striani

Received: 11 August 2023

Revised: 3 September 2023

Accepted: 4 September 2023

Published: 7 September 2023



**Copyright:** © 2023 by the authors. Licensee MDPI, Basel, Switzerland. This article is an open access article distributed under the terms and conditions of the Creative Commons Attribution (CC BY) license (<https://creativecommons.org/licenses/by/4.0/>).

## 1. Introduction

In recent decades, escalating global concern over climate change has prompted a significant shift towards sustainable and environmentally friendly practices across various industries. One of the pressing issues we face today is the increasing level of carbon dioxide (CO<sub>2</sub>) in the Earth's atmosphere, contributing to the greenhouse effect and subsequent climate change. As scientists and researchers strive to combat this challenge, exploring alternative materials and manufacturing processes becomes crucial in reducing our reliance on petroleum-based products while simultaneously addressing CO<sub>2</sub> emissions using different concepts such as carbon capture utilization and storage (CCUS) using expensive modern technologies [1,2].

Plants, through the process of photosynthesis, have the remarkable ability to convert CO<sub>2</sub> into organic compounds, effectively sequestering this greenhouse gas and mitigating its impact on the environment. Leveraging the inherent qualities of natural fibers in composite materials offers a promising avenue to not only decrease dependence on fossil fuel-derived resources, but also actively sequester CO<sub>2</sub>. By incorporating these natural



fibers into polymer matrices, composites can be fabricated with improved mechanical properties [3–5] while simultaneously contributing to carbon capture and reduced environmental impact [6], similar to using wood, but much easier and with lower production cost. Although there are different types of natural fibers with a range of mechanical properties [4,7–10], perhaps it is fair to say that flax and hemp are the most successful commercial examples [11,12].

This study aims to conduct a comparative analysis between two types of natural fibers: flax and pineapple leaf fiber. Flax fiber, derived from the stem of the flax plant (*Linum usitatissimum*), has long been recognized for its mechanical strength and versatility [13,14]. On the other hand, pineapple leaf fiber, obtained from the waste of pineapple cultivation, has emerged as a potential alternative due to its abundance and renewability [15–19]. Although these two fibers have been studied for a long time, there is still some discrepancy in their reported mechanical properties (cf. Table 1 in [4], Table 2 in [15]). PALF has been used successfully in reinforcing different polymer matrices [20–22] despite the much lower than expected mechanical properties [23] compared to those of flax [24]. So far, there has been no direct comparison in the reinforcement efficiency of the two fibers, and thus this is the main objective of the present work. They are used to reinforce bio-based poly(butylene succinate) (PBS), which provokes an intensive interest among industry and researchers [25,26] and has been employed in automotive applications [27]. Here, we seek to investigate the influence of fiber content on the performance of the resulting composite materials.

Through this comparative study, we aim to contribute to the growing body of research dedicated to sustainable materials and their potential applications. By examining the mechanical properties of flax and pineapple leaf fiber composites, we can gain insights into their suitability for various engineering and manufacturing applications while also addressing the urgent need for carbon sequestration.

## 2. Materials and Methods

### 2.1. Materials

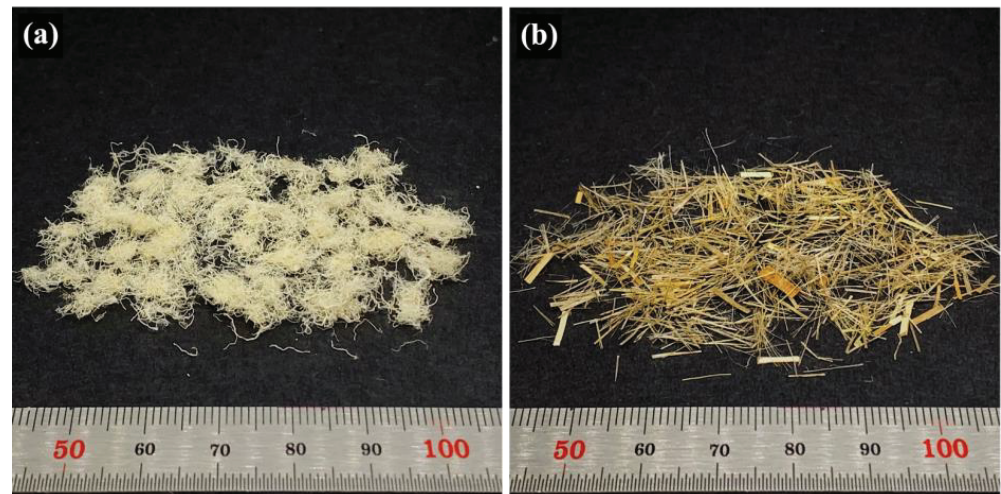
Poly (butylene succinate) (PBS, BioPBS FZ91PM/FZ91PB), produced from the polymerization of bio-based succinic acid and 1,4-butanediol, was used as the polymer matrix. The material was supplied by PTT MCC Biochem Company Limited (Bangkok, Thailand) and had a density of 1.26 g/cm<sup>3</sup> and a melt index of 5 g/10 min (190 °C, 2.16 kg). Its reported molecular weight ( $M_w$ ) was approximately 170 kDa [28].

Flax fiber (LINTEX, ~6 mm in length) was supplied by Dehondt Composites (Port-Jérôme-sur-Seine, France). According to the Alliance for European Flax-Linen and Hemp, the European flax is dew retted and mechanically scutched [29]. The fiber was supplied already cut to the specified calibrated length intended for composite reinforcement [30]. Pineapple leaf fibers (PALF, ~6 mm in length) were prepared from fresh pineapple leaves using the procedure presented in the literature [17]. Fresh pineapple leaves were collected from Bang Yang District, Phitsanulok Province, Thailand. The leaves were cut across their length into pieces 6 mm long, ground with a stone grinder, and dried to yield the whole ground leaf (WGL). The WGL was further processed by crushing it with a high-speed blender, followed by sieving to achieve the separation between the non-fibrous component and the PALF. The loose particulate non-fibrous component, with a particle size smaller than approximately 1 mm<sup>2</sup>, was able to pass through the sieve. In contrast, the curly and entangled PALF remained on the sieve, highlighting its distinctive physical properties. For visual reference, photographs of both PALF and flax fibers are presented in Figure 1.

### 2.2. Composite Prepreg Preparation

Prior to the melt-mixing process, all materials were dried overnight in a hot air oven at 80 °C. The PBS pellets were then heated and melted on a two-roll mill (W100T, Dr. Collin GmbH, Maitenbeth, Germany) for 2 min at a speed of 30 rpm. The front and back roll temperatures were 125 °C and 100 °C, respectively. Subsequently, a predetermined amount

of fiber (10 and 20 wt.% of total weight (PBS + fiber)) was gradually added over a period of 3 min. The mixing speed was then increased to 48 rpm, and the mixing continued for another 10 min to achieve a homogenous molten mixture.



**Figure 1.** Photographs of (a) PALF and (b) Flax fibers.

The resulting molten mixture was carefully pulled out with slight stretching to maintain the alignment of the fiber parallel to the machine direction. It was then allowed to cool and solidify, forming prepreg, as illustrated in Figure 2. The composites were designated as 10PALF, 20PALF, 10Flax and 20Flax, denoting the respective content of the fiber in the composites.



**Figure 2.** Fiber alignment on a two-roll mill during the uniaxial composite prepreg preparation.

### 2.3. Compressed Sheet Preparation

Composite sheets were prepared by stacking ten layers of prepreg between two flat metal sheets and a 3 mm spacer to prevent the excessive flow of the material and the disturbance of the fiber alignment. The stacked prepreps were preheated for 5 min under slight pressure. Then, they were pressed under a pressure of 1500 psi for 5 min, followed by cooling under the same pressure for 5 min. The compression molding was carried out at a temperature of 140 °C to destroy the matrix orientation and allow only fiber contribution to be observed [31].

## 2.4. Characterizations

### 2.4.1. Fibers' Chemical Composition

The chemical compositions of PALF and flax fibers were determined according to standard methods [32–35] through a certified local laboratory. Chemical composition is reported in terms of cellulose, holocellulose, acid-soluble lignin and acid-insoluble lignin.

The surface chemical compositions of PALF and flax fibers were observed using Fourier-transform infrared spectroscopy in an attenuated total reflectance mode (ATR-FTIR, Frontier, Perkin Elmer, Waltham, MA, USA). Spectra were recorded with 16 scans over the range of 4000 to 500  $\text{cm}^{-1}$  with a resolution of 4  $\text{cm}^{-1}$ .

### 2.4.2. X-ray Diffraction

X-ray diffraction patterns of the composites were recorded using an X-ray Diffractometer (XRD) (D8 DISCOVER, Bruker AXS GmbH, Karlsruhe, Germany) over the  $2\theta$  range between  $5^\circ$  and  $80^\circ$  with a step size of  $0.02^\circ$ . The X-ray wavelength was 1.54 Å (Ni-filtered  $\text{CuK}\alpha$ ). Pole figures for different samples were obtained with a cradle sample stage on the same machine. The data were analyzed with DEFFRAC.TEXTURE software (V4.1).

### 2.4.3. Scanning Electron Microscopy (SEM)

Fibers' shapes and sizes and the fractured surfaces of composites were observed using a scanning electron microscope (JSM-IT500, JEOL, Tokyo, Japan) with an accelerating voltage of 10 kV. Prior to observation, a thin layer of platinum was coated on the samples.

### 2.4.4. Thermal Properties

The melting and crystallization behavior of the composites were determined with a differential scanning calorimeter (DSC) (Q200-RCS90, TA Instruments, New Castle, DE, USA). The samples were first heated from 25 to 200  $^\circ\text{C}$ , held for 5 min to completely melt all the crystals, cooled to  $-70^\circ\text{C}$  and then heated again to 200  $^\circ\text{C}$ . The heating and cooling rate was 10  $^\circ\text{C}/\text{min}$  under a nitrogen atmosphere. The positions of the melting peak ( $T_m$ ), enthalpy of fusion ( $\Delta H_f$ ) and crystallization peak ( $T_c$ ) were determined for each sample using the instrument software. The degree of crystallinity ( $X_c$ ) was calculated using Equation (1).

$$X_c = \left( \frac{\Delta H_f}{\Delta H_f^0 (1 - W_f)} \right) \times 100\% \quad (1)$$

where  $\Delta H_f^0$  is the enthalpy of fusion for 100% crystalline PBS, which is taken as 110.3 J/g [36], and  $W_f$  is the weight fraction of fiber in the composites.

In addition, the heat deflection temperature (HDT) was determined with a Gotech testing machine (HV-3000-P3C, Gotech Testing Machines Inc., Taichung City, Taiwan). The specimen sizes were  $120 \times 13 \times 3 \text{ mm}^3$ . The test was performed following ASTM-D648 under the three-point bending mode with a span of 100 mm under a constant load of 0.455 MPa and a heating rate of 2  $^\circ\text{C}/\text{min}$ . HDT was determined as the temperature at which the specimen bends to 0.25 mm.

### 2.4.5. Mechanical Properties

**Flexural testing:** The test was carried out on a universal testing machine (Instron 5569, Instron, High Wycombe, UK) at a crosshead speed of 5 mm/min, 1 kN of load cell and a support span length of 48 mm. The specimens were cut from compressed sheets into strips 12.7 mm wide with a long axis parallel to the machine direction. The average values of flexural strength and secant modulus at 1% stain from 5 specimens were reported.

**Impact testing:** The test was carried out on a pendulum impact testing machine (HIT5.5P, Zwick/Roell, Ulm, Germany) in Izod configuration. The impact specimens were cut from compressed sheets into strips 60 mm long and 12.7 mm wide. The samples were

notched with a Zwick/Roell manual notch cutting machine. The notches were cut across the machine direction. Average values of 5 specimens were reported.

### 3. Results

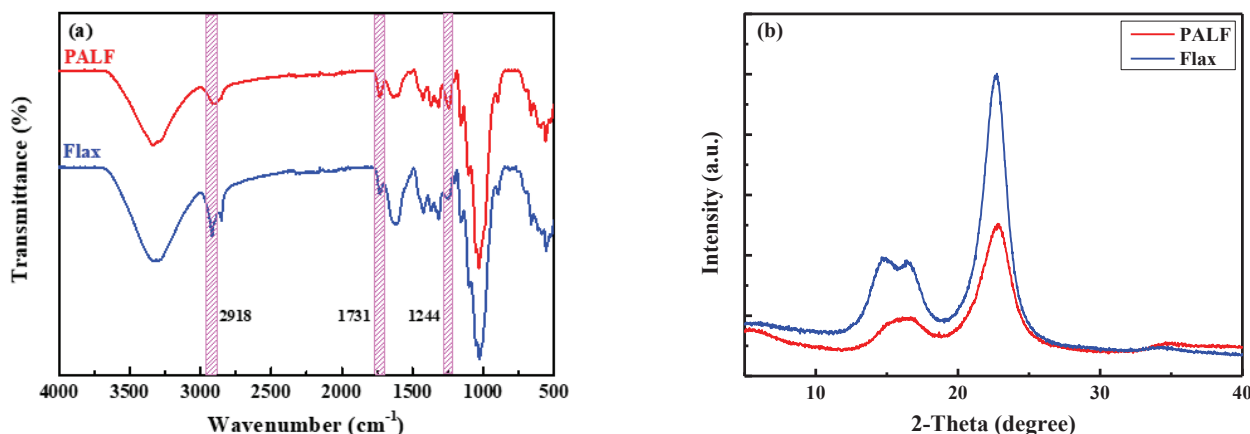
#### 3.1. PALF and Flax Characteristics

##### 3.1.1. Fiber Composition and Structure

Table 1 displays the chemical composition of PALF and flax fiber. In general, the chemical composition of the two fibers is very similar. PALF has a slightly higher holocellulose content than flax fiber, while flax has about 10% greater cellulose content than PALF. PALF also has about 1.5 times higher acid-soluble lignin content than flax. The greater content of hemicellulose (the difference between holocellulose and cellulose) is reflected in the FTIR spectra shown in Figure 3a, in which the peaks at  $1731\text{ cm}^{-1}$  and  $1244\text{ cm}^{-1}$  correspond to the C=O stretching of hemicellulose and lignin and the C–O stretching in lignin, respectively [37,38]. The peak at  $2918\text{ cm}^{-1}$  corresponds to the C–H stretching of methyl groups (–CH<sub>3</sub>) in both hemicellulose and cellulose [39].

**Table 1.** Chemical composition of PALF and flax fibers.

Chemical Constituent (%)	PALF	Flax
Cellulose (%)	57.2	67.2
Holocellulose (%)	85.5	82.6
Lignin (acid soluble)	2.6	0.9
Lignin (acid insoluble)	7.8	6.5



**Figure 3.** ATR-FTIR spectra (a) and XRD patterns (b) of PALF and flax fibers.

The lower hemicellulose content in flax is a result of the enzymatic degradation of the binding material during dew retting [14]. For PALF, only mechanical force was used in the preparation of the fiber. Therefore, not much material was removed.

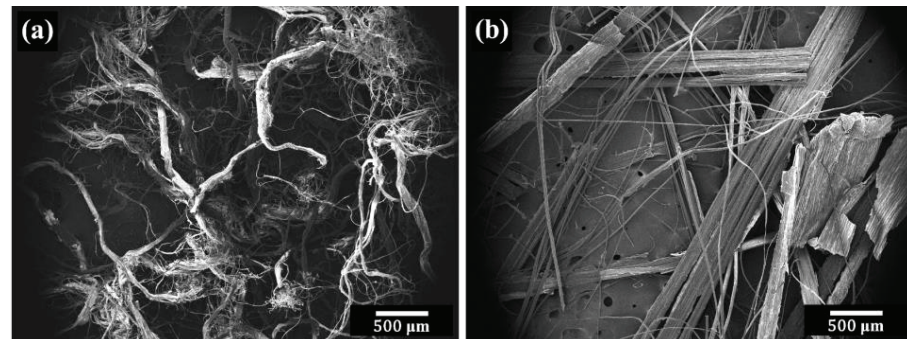
The crystalline structures of PALF and flax fibers were investigated using X-ray diffraction techniques. The diffraction patterns are shown in Figure 3b. Both fibers exhibited a similar characteristic pattern to cellulose Type I [40]. However, the patterns differed significantly in the resolution and sharpness of the peaks; flax fiber has much sharper peaks than PALF. This indicates that the crystalline structure in flax fiber is more perfect and possibly larger than in PALF. This difference could be the main reason for the higher mechanical performance of flax fiber.

##### 3.1.2. Scanning Electron Microscopy (SEM)

Figure 4 compares the size and shape of the two fibers. PALF had both large bundles and fine elementary fibers. The fibers were not straight, but contained a lot of kinks. On the other hand, flax fibers were rather straight and had both isolated small fibers and bundles



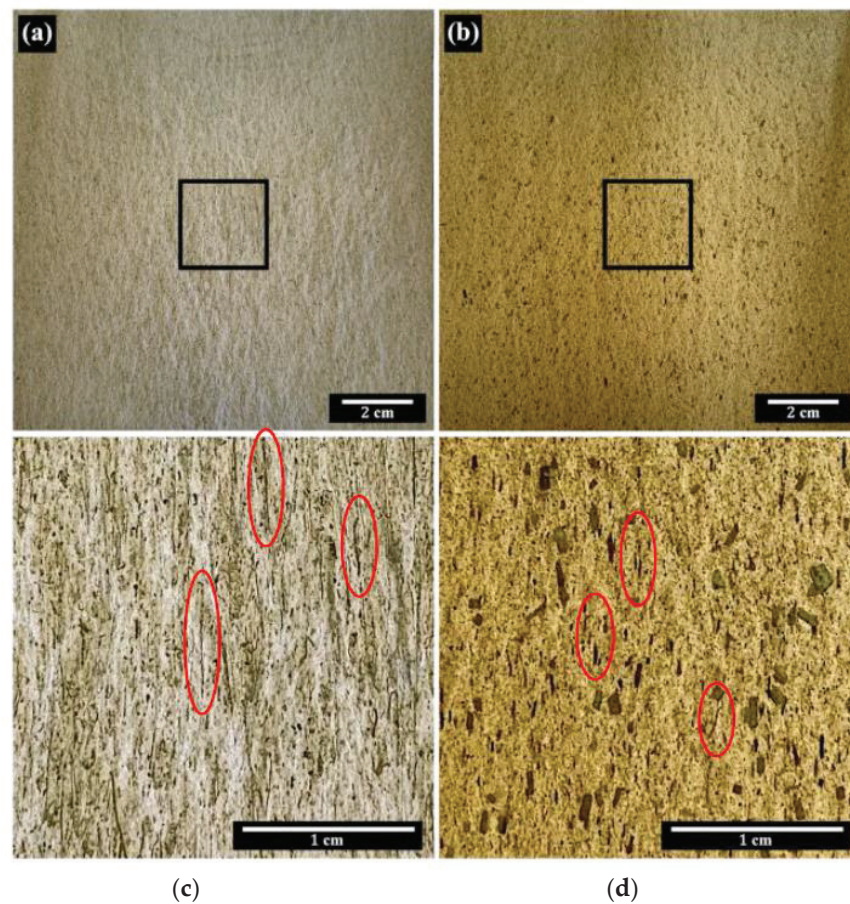
of fibers. Flax featured larger fiber bundles than PALF. Additionally, both PALF and flax fibers contained non-fibrous components. The variations in fiber size and shape can be attributed to the specific fiber preparation techniques employed.



**Figure 4.** SEM micrographs of (a) PALF and (b) flax fibers.

### 3.1.3. Prepreg Appearance

Figure 5 displays the photographs of PALF/PBS and flax/PBS prepregs. PALF/PBS has a pale color, while flax/PBS is brownish with a much greater number of dark spots of non-fibrous components. Both PALF and flax fibers appear evenly dispersed throughout the prepregs, indicating thorough mixing and alignment, as highlighted by the dark lines within elongated red circles.

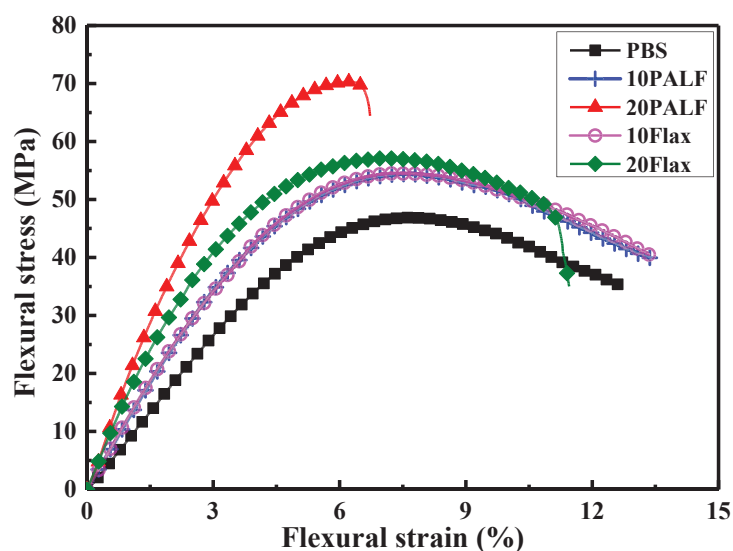


**Figure 5.** Optical images of composite prepregs: (a) PALF/PBS and (b) flax/PBS. Images (c) and (d) depict magnified views of the regions of interest indicated by squares in images (a) and (b), respectively. The red elongated circles highlight the alignment of fibers. Machine direction is vertical.

### 3.2. Mechanical Properties of Composites

#### 3.2.1. Flexural Properties

Figure 6 displays representative stress–strain curves of PALF/PBS and flax/PBS composites containing different fiber contents, and also that of PBS. With a fiber content of 10 wt.%, the stress at different strains increased over that of PBS throughout the whole range of strain. The composites had roughly similar failure strains to that of PBS. At 10 wt.% content, PALF/PBS and flax/PBS composites exhibited virtually the same behavior.



**Figure 6.** Representative flexural stress–strain curves of PALF/PBS and flax/PBS composites containing different fiber contents.

When the fiber content was increased to 20 wt.%, the stress for the flax/PBS composite increased slightly over that of 10 wt.%, and then the stress gradually decreased and the composite failed at a slightly lower strain than the composite with 10 wt.% fiber. The PALF/PBS composite with 20 wt.% fiber content exhibited a much-improved performance but failed at a much lower strain than the flax/PBS composite.

The average values for the flexural strength and flexural modulus of these composites are shown in Figure 7. The average flexural strength increased from 47 MPa to approximately 54 MPa for both PALF/PBS and flax/PBS composites containing 10 wt.% fiber, and to 70.7 and 57.8 MPa for PALF/PBS and flax/PBS with 20 wt.% fiber, respectively. A similar trend was observed for the flexural modulus. The average flexural modulus increased from 0.90 GPa to 1.25 GPa for both PALF/PBS and flax/PBS composites containing 10 wt.% fiber, and to 2.03 and 1.70 GPa for PALF/PBS and flax/PBS with 20 wt.% fiber, respectively.

The above results clearly indicate a better reinforcement efficiency of PALF over that of flax, despite its inferior mechanical properties. Doubling the flax content from 10 wt.% to 20 wt.% caused the flexural modulus to increase by approximately 10%, but it caused only a marginal change in flexural strength. PALF, on the other hand, caused both the flexural modulus and flexural strength to increase by approximately 62% and 31%, respectively, under a similar change. The reasons for this will be addressed later.

#### 3.2.2. Impact Properties

Figure 8 displays the notched Izod impact strengths of PALF/PBS and flax/PBS composites containing different fiber contents. The introduction of 10 wt.% of fiber to PBS resulted in an impact strength reduction to approximately 70% and 64% of that of PBS for PALF and flax, respectively. With a further increase in fiber content to 20 wt.%, the impact strength dropped even further, to approximately 62% and 54% of that of PBS for

PALF and flax, respectively. This indicates that PALF contributes to a smaller reduction in the impact strength of the composite compared to flax fibers. The decrease in impact strength in natural fiber-filled polymers is an anticipated outcome due to the increase in material stiffness and the presence of stress concentrators within [41–43]. A more detailed discussion on the reason for the comparatively smaller reduction in impact strength in the PALF system will follow.

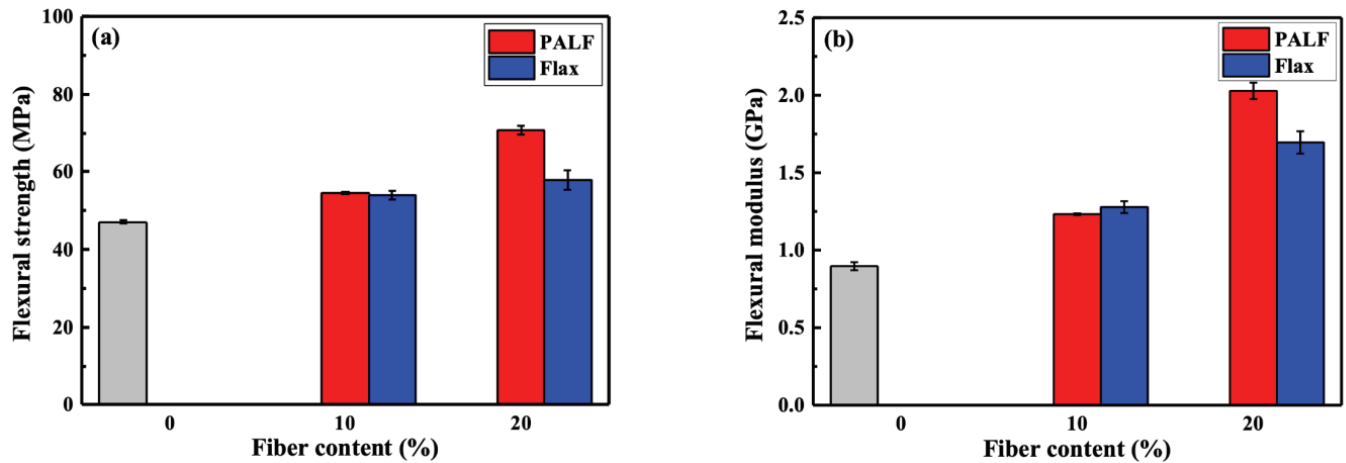


Figure 7. Flexural properties of PALF/PBS and flax/PBS composites containing different fiber contents, (a) flexural strength and (b) flexural modulus at 1% strain. Gray bar represents neat PBS.

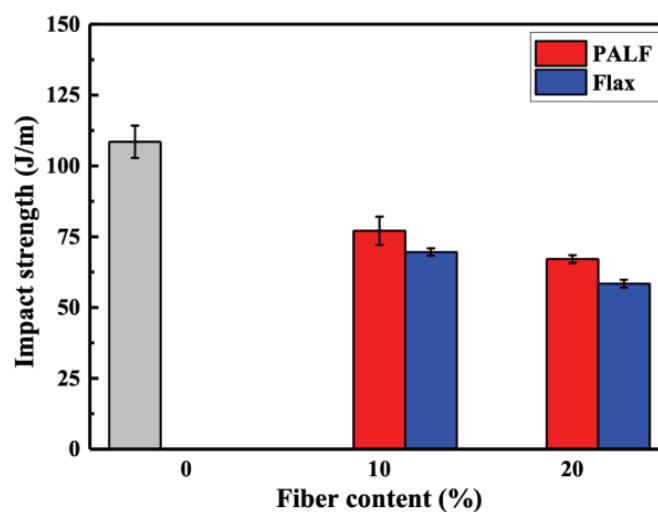


Figure 8. Impact properties of PALF/PBS and flax/PBS composites containing different fiber contents. Gray bar represents neat PBS.

### 3.3. Thermal Properties

#### 3.3.1. DSC

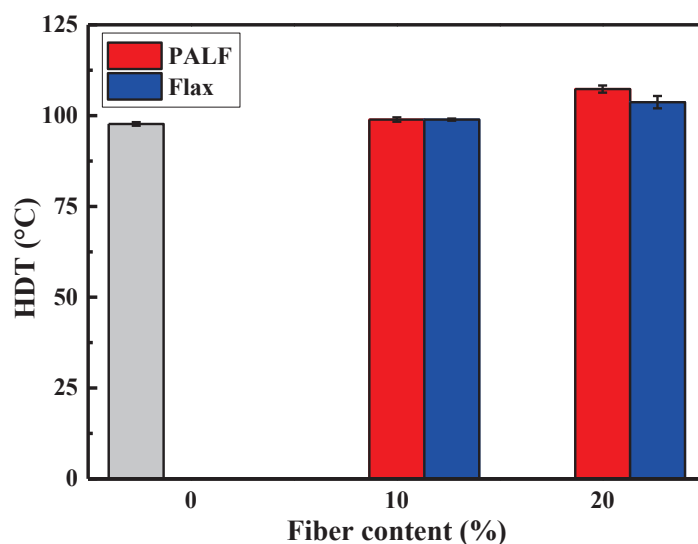
The melting and crystallization behavior of PBS in the composites is shown in Table 2. The presence of both PALF and flax fibers has a negligible effect on the melting temperature ( $T_m$ ), degree of crystallinity ( $X_c$ ), and crystallization temperature of PBS ( $T_c$ ). Thus, it may be stated that both PALF and flax fibers do not influence matrix crystallization, similar to the results observed in other systems [44,45].

**Table 2.** Thermal properties of PBS/PALF and PBS/flax composites.

Sample	First Heating		Cooling	Second Heating	
	$T_m$ (°C)	$X_c$ (%)	$T_c$ (°C)	$T_m$ (°C)	$X_c$ (%)
PBS	115.0	75.4	84.4	114.4	72.6
10PALF	114.2	78.9	81.4	114.2	75.7
20PALF	114.4	79.0	82.8	114.0	75.5
10Flax	114.8	76.2	81.0	114.8	72.9
20Flax	115.0	76.4	81.8	115.3	72.6

### 3.3.2. HDT

Figure 9 displays the heat distortion temperature (HDT) of the composites along with the base PBS. At 10 wt.%, both PALF and flax had a negligible effect on HDT. However, when the fiber content was increased to 20 wt.%, PALF caused a larger increase than flax fiber, being approximately 10 °C and 6 °C higher than that of the base matrix. This is the consequence of the increase in flexural modulus of the respective materials.

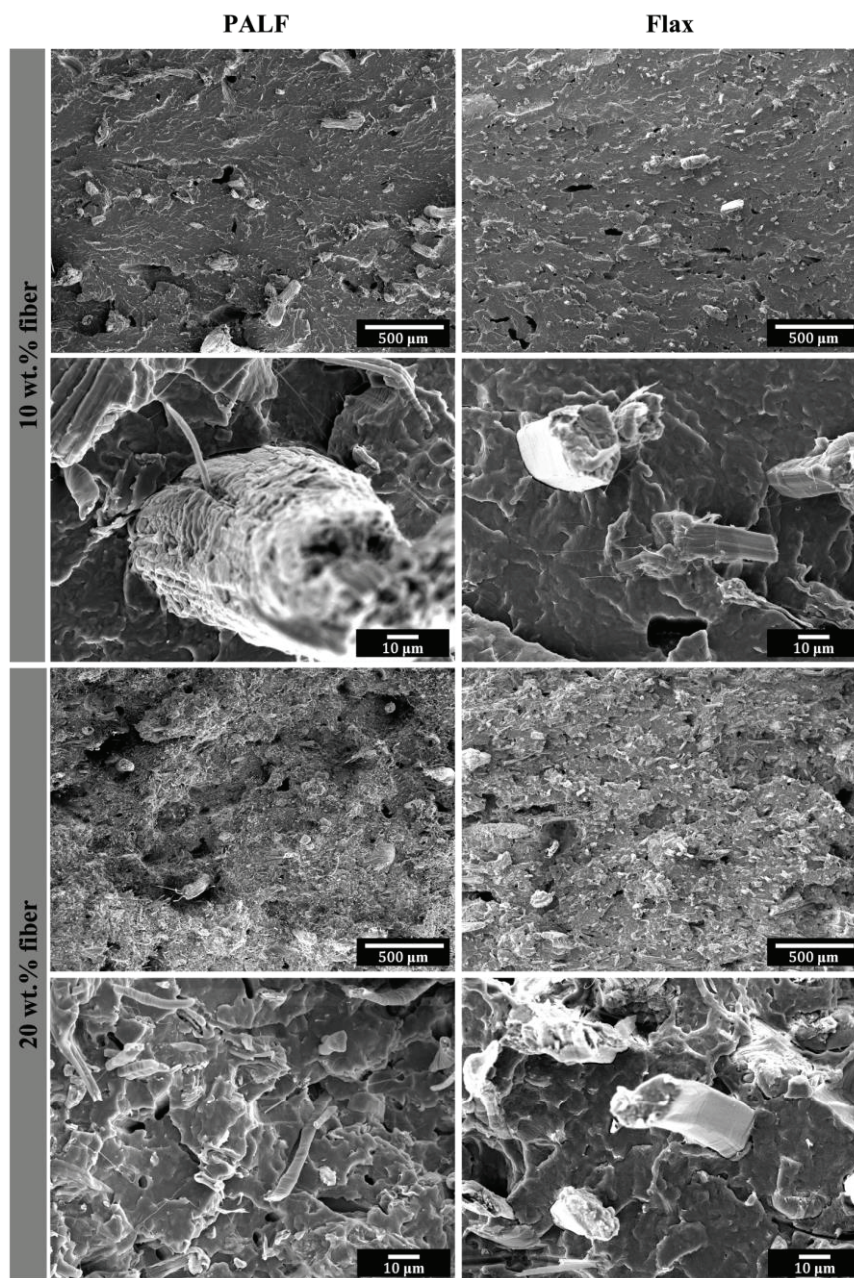


**Figure 9.** HDT of PALF and flax composites containing different fiber contents. Gray bar represents neat PBS.

### 3.4. Fracture Surfaces

Figure 10 shows the impact fracture surfaces of PALF/PBS and flax/PBS composites containing different fiber contents. Broken fibers are seen end-on, indicating a good alignment of the fibers along the machine direction (toward the observer). For 10 wt.% fiber, a larger number of fiber bundles can be seen in the PALF/PBS composite compared to the flax/PBS composite. When the fiber content was increased to 20 wt.%, a smaller number of large fiber bundles could be observed, indicating the breaking of large fiber bundles into finer elementary fibers. This phenomenon is likely due to the increase in the viscosity of the mixture (resulting from the higher fiber content), which facilitates higher stress transfer and thus breaks the bundles into finer elementary fibers.





**Figure 10.** Impact fracture surfaces of PALF/PBS and flax/PBS composites containing different fiber contents.

#### 4. Discussion

The nearly identical curves seen for 10 wt.% PALF/PBS and flax/PBS in Figure 6 signify a remarkable parity in reinforcing efficiency between the two types of fibers, even amidst their distinct mechanical properties. Intriguingly, at a higher fiber content of 20 wt.%, PALF exhibited significantly greater reinforcing efficiency than flax fiber. These findings merit a more in-depth examination.

It is known that for short fiber composites, the mechanical behavior of the composite is determined by several factors, including the mechanical properties of the reinforcing fiber, its orientation, the fiber aspect ratio, the fiber volume fraction, and the nature of the interface between the fiber and the matrix [46]. While we kept most starting parameters of the two types of fibers as close as possible, such as their length, amount, and mixing procedure, the only known parameter that was different was the mechanical properties of the fibers, with flax having much superior values. Surprisingly, this difference in mechanical properties

alone does not fully explain the stark difference in reinforcing efficiency. Therefore, a deeper analysis of the internal structure of the composites, including matrix structure, matrix orientation, and fiber dimension, is required.

4.1. Matrix Orientation via Pole Figures

The production method for uniaxial prepreg employed in this work could lead to matrix orientation [31]. This had been destroyed during the compression molding by using a high compression molding temperature, as previously described. XRD was used to confirm this. Figure 11a displays the XRD patterns of composite preregs and sheets. Preregs display very strong intensity, while the sheets show much less intensity, indicating much relaxation of the polymer matrix. Pole figures for all samples were then determined using the most intense peak, at around 22.7°, which was associated with the (110) plane of PBS crystalline [47].

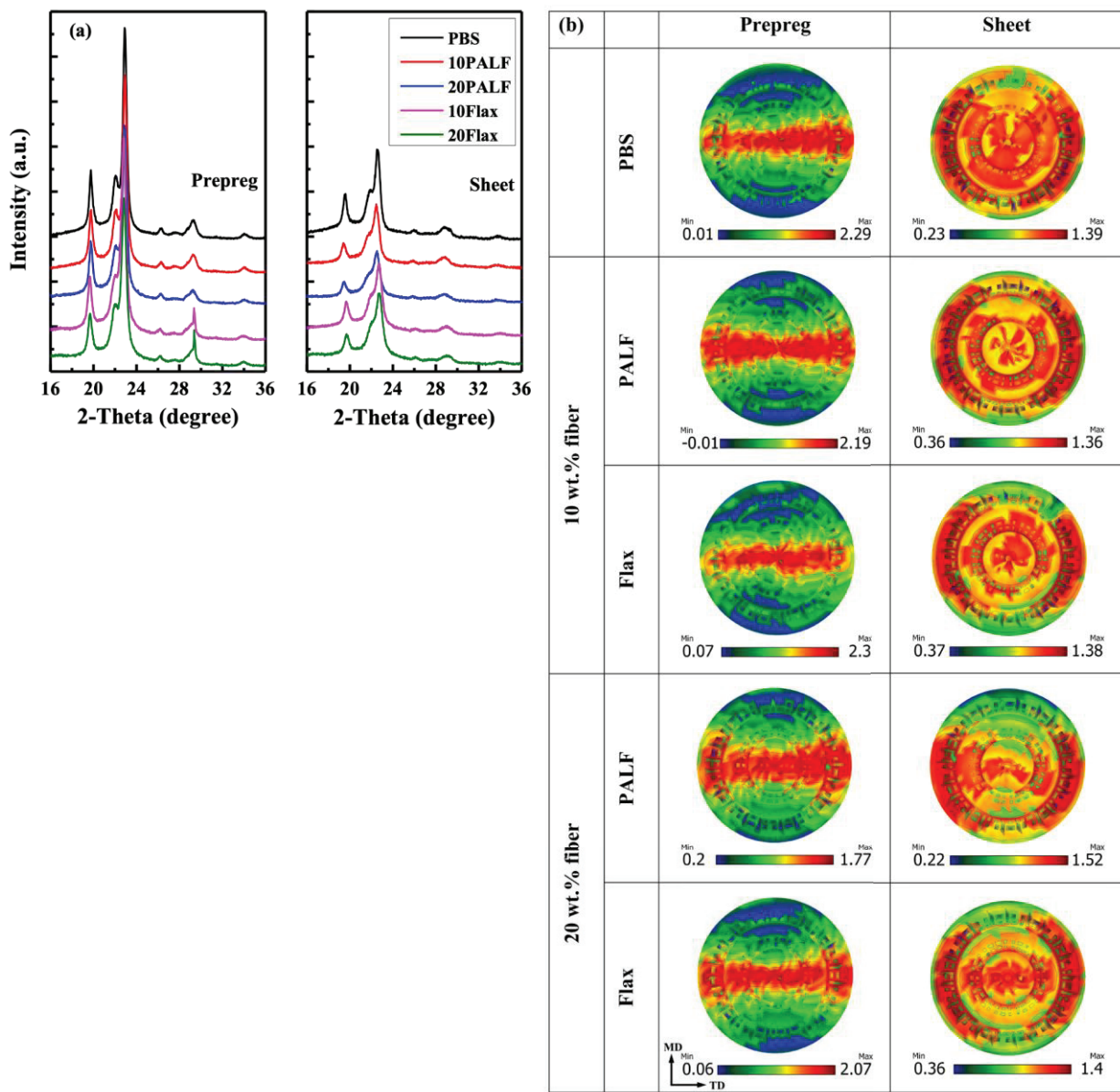


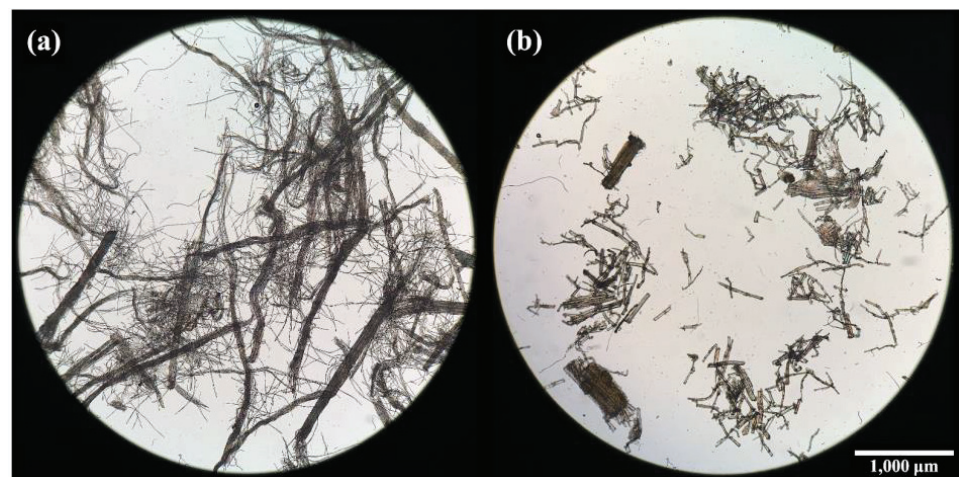
Figure 11. (a) XRD patterns of composite preregs and sheets; (b) X-ray pole figures for (110) plane of PALF/PBS and flax/PBS composite preregs and sheets compressed at 140 °C.



Pole figures for all samples for the (110) plane are shown in Figure 11b. It is clearly evident that the peak intensity of the prepregs is concentrated in the center, indicating a preferred matrix orientation in all prepregs. The presence of a high-intensity region supports the fact that the (110) reflection of the drawn PBS film lies on the equator [48]. However, when the sample was compressed at 140 °C, the previous orientation disappeared. These results are consistent with the previous XRD and DSC findings. Notably, with an increased fiber content in the sample compressed at 140 °C, a relatively weak molecular orientation can still be observed in the case of PALF/PBS. This suggests that the presence of fibers could slow down the relaxation of the matrix in the vicinity of the fiber, as suggested in the literature [31]. However, it could be assumed that such a marginal orientation of PBS in the PALF/PBS composite would play no role in enhancing the PALF/PBS composite over that of the flax/PBS composite (cf. Figure 7).

#### 4.2. Reinforcing Fiber in the Matrix

It has been reported that fibers such as jute, flax [49], PALF [50], kenaf [51], poplar wood, radiata pine, and rice husk [52] can break down during incorporation into a polymer matrix, resulting in a lower reinforcing efficiency. To determine whether such a situation had occurred, the fibers were extracted from the composites using hot chloroform. Figure 12 displays optical images (Olympus BX51TRF, Olympus Optical Co. Ltd., Tokyo, Japan) of PALF and flax fibers that were extracted from PALF/PBS and flax/PBS composites with 20 wt.% fiber. It is clear that PALF remained long, while flax broke into very short pieces. In both cases, fine elementary fibers and large bundles can be seen. Thus, it is unquestionable that such fragmented flax fibers would not be able to reinforce the composite effectively. PALF, which remains long, can still effectively reinforce the composite [53]. The longer PALF also gives composites with higher impact strength and HDT (cf. Figures 8 and 9). This observation supports our previous works, where PALF has been shown to outperform short Kevlar in reinforcing rubber matrices [22], and with an appropriate adhesion promoter the effectiveness can be further improved [54].



**Figure 12.** Low magnification optical micrographs of (a) PALF and (b) flax fibers after solvent extraction from their respective 20 wt.% composite prepregs.

As stated above, all kinds of fiber are prone to breakage during compounding with polymer matrices due to different breakage mechanisms [55] depending on the fiber characteristics, and this includes PALF. It can be easily envisaged that by reducing the stress involved during compounding, either by increasing the temperature or reducing mixing speed, the breakage could be reduced or minimized. Mixing with a two-roll mill involves a much lower shear stress than with an internal mixer or screw extruder. It is clear from the results above that flax fiber still breaks, while PALF does not. The fact that PALF can maintain its length during mixing with thermoplastics and provide a high reinforcement

efficiency certainly encourages its use in this form. Given that the starting length is long enough, and large fiber bundles break into finer elementary fibers during mixing, resulting in a significantly increased aspect ratio, composites with greatly improved properties can be obtained. Moreover, the utilization of PALF offers a promising ecological advantage. Compared to purposely cultivated fibers (such as flax, hemp, and kenaf), PALF exhibits lower carbon emissions and a reduced environmental footprint. Additionally, the use of PALF contributes to sustainable waste management practices by repurposing agricultural waste, making it a more environmentally friendly alternative for composite reinforcement. These ecological benefits further underscore the potential of PALF as a viable and eco-conscious solution in advancing sustainable materials across various industries, especially those that require higher performance or thinner parts.

## 5. Conclusions

In this study, we compared PALF with cultivated flax fiber as natural reinforcements in unidirectional PBS matrix composites. PALF showed remarkable potential as a sustainable alternative to flax fiber, well known for its high mechanical properties. PALF's ability to maintain length and integrity during mixing led to significant improvements in the flexural strength and modulus, particularly at 20 wt.% fiber content. Successful PALF dispersion in the matrix, along with fiber bundle disintegration, resulting in higher aspect ratio, further contributed to its superior performance. PALF offers valuable ecological benefits, with a lower carbon footprint and the utilization of agricultural waste. The study highlights PALF's underexplored potential as a sustainable and high-performance natural reinforcement, paving the way for eco-friendly materials in various industries. PALF's effective reinforcement and ecological advantages suggest that it is a promising candidate for developing sustainable and eco-friendly materials.

**Author Contributions:** Conceptualization, T.A. and K.M.; methodology, S.D., T.A. and K.L.G.; validation and data curation, S.D.; writing—original draft preparation, S.D. and T.A.; writing—review and editing, T.A., K.L.G. and K.M.; funding acquisition, T.A. All authors have read and agreed to the published version of the manuscript.

**Funding:** This research was funded by Mahidol University (Basic Research Fund: fiscal year 2022; Grant no. BRF1-046/2565).

**Institutional Review Board Statement:** Not applicable.

**Data Availability Statement:** Not applicable.

**Acknowledgments:** This research project is supported by Mahidol University (Basic Research Fund: fiscal year 2022; Grant no. BRF1-046/2565). We thank Mahidol University Frontier Research Facility (MU-FRF) for instrument support and the MU-FRF scientists, Nawapol Udpuay, Chawalit Takoon and Suwilai Chaveanghong, for their kind assistance in the operations of SEM and XRD.

**Conflicts of Interest:** T.A. declares a conflict of interest related to this research article: As a University Professor at Mahidol University, I have been engaged in developing an innovative method for extracting pineapple leaf fiber. This endeavor led to the establishment of TEAnity Team Co. Ltd., where I hold the position of Chief Technology Officer (CTO). While this research was conducted independently and supported solely by university funding, I acknowledge the potential for a conflict due to my dual roles. I affirm that the research and findings presented in the article remain unbiased and have not been influenced by any financial interests or affiliations with TEAnity Team Co. Ltd. The remaining authors declare no conflicts of interest.

## References

1. Hong, W.Y. A techno-economic review on carbon capture, utilisation and storage systems for achieving a net-zero CO<sub>2</sub> emissions future. *Carbon Capture Sci. Technol.* **2022**, *3*, 100044. [CrossRef]
2. Liu, E.; Lu, X.; Wang, D. A Systematic Review of Carbon Capture, Utilization and Storage: Status, Progress and Challenges. *Energies* **2023**, *16*, 2865. [CrossRef]
3. George, J.; Ivens, J.; Verpoest, I. Mechanical properties of flax fibre reinforced epoxy composites. *Angew. Makromol. Chem.* **1999**, *272*, 41–45. [CrossRef]



4. Kalia, S.; Kaith, B.S.; Kaur, I. Pretreatments of Natural Fibers and their Application as Reinforcing Material in Polymer Composites—A Review. *Polym. Eng. Sci.* **2009**, *49*, 1253–1272. [CrossRef]
5. Baley, C.; Gomina, M.; Breard, J.; Bourmaud, A.; Davies, P. Variability of mechanical properties of flax fibres for composite reinforcement. A review. *Ind. Crop Prod.* **2020**, *145*, 111984. [CrossRef]
6. Joshi, S.V.; Drzal, L.T.; Mohanty, A.K.; Arora, S. Are natural fiber composites environmentally superior to glass fiber reinforced composites? *Compos. Part A Appl. Sci. Manuf.* **2004**, *35*, 371–376. [CrossRef]
7. Nabi Saheb, D.; Jog, J.P. Natural fiber polymer composites: A review. *Adv. Polym. Technol.* **1999**, *18*, 351–363. [CrossRef]
8. Biagiotti, J.; Puglia, D.; Kenny, J.M. A review on natural fibre-based composites—Part I: Structure, processing and properties of vegetable fibres. *J. Nat. Fibers* **2004**, *1*, 37–68. [CrossRef]
9. Puglia, D.; Biagiotti, J.; Kenny, J.M. A review on natural fibre-based composites—Part II: Application of natural reinforcements in composite materials for automotive industry. *J. Nat. Fibers* **2004**, *1*, 23–65. [CrossRef]
10. Li, X.; Tabil, L.G.; Panigrahi, S. Chemical treatments of natural fiber for use in natural fiber-reinforced composites: A review. *J. Polym. Environ.* **2007**, *15*, 25–33. [CrossRef]
11. Pil, L.; Bensadoun, F.; Pariset, J.; Verpoest, I. Why are designers fascinated by flax and hemp fibre composites? *Compos. Part A Appl. Sci. Manuf.* **2016**, *83*, 193–205. [CrossRef]
12. Baley, C.; Bourmaud, A.; Davies, P. Eighty years of composites reinforced by flax fibres: A historical review. *Compos. Part A Appl. Sci. Manuf.* **2021**, *144*, 106333. [CrossRef]
13. Yan, L.; Chouw, N.; Jayaraman, K. Flax fibre and its composites—A review. *Compos. B Eng.* **2014**, *56*, 296–317. [CrossRef]
14. Baley, C.; Le Duigou, A.; Morvan, C.; Bourmaud, A. Tensile properties of flax fibers. In *Handbook of Properties of Textile and Technical Fibres*, 2nd ed.; Bunsell, A.R., Ed.; Elsevier: Kidlington, UK, 2018; pp. 275–300.
15. Mishra, S.; Mohanty, A.K.; Drzal, L.T.; Misra, M.; Hinrichsen, G. A review on pineapple leaf fibers, sisal fibers and their biocomposites. *Macromol. Mater. Eng.* **2004**, *289*, 955–974. [CrossRef]
16. Arib, R.M.N.; Sapuan, S.M.; Hamdan, M.A.M.M.; Paridah, M.T.; Zaman, H.M.D.K. A literature review of pineapple fibre reinforced polymer composites. *Polym. Polym. Compos.* **2004**, *12*, 341–348. [CrossRef]
17. Kengkhetkit, N.; Amornsakchai, T. Utilisation of pineapple leaf waste for plastic reinforcement: 1. A novel extraction method for short pineapple leaf fiber. *Ind. Crops. Prod.* **2012**, *40*, 55–61. [CrossRef]
18. Asim, M.; Abdan, K.; Jawaid, M.; Nasir, M.; Dashtizadeh, Z.; Ishak, M.R.; Hoque, M.E.; Deng, Y. A review on pineapple leaves fibre and its composites. *Inter. J. Polym. Sci.* **2015**, *2015*, 950567. [CrossRef]
19. Todkar, S.S.; Patil, S.A. Review on mechanical properties evaluation of pineapple leaf fibre (PALF) reinforced polymer composites. *Compos. B. Eng.* **2019**, *174*, 106927. [CrossRef]
20. Nopparut, A.; Amornsakchai, T. Influence of pineapple leaf fiber and its surface treatment on molecular orientation in, and mechanical properties of, injection molded nylon composites. *Polym. Test.* **2016**, *52*, 141–149. [CrossRef]
21. Kalapakdee, A.; Amornsakchai, T. Mechanical properties of preferentially aligned short pineapple leaf fiber reinforced thermoplastic elastomer: Effects of fiber content and matrix orientation. *Polym. Test.* **2014**, *37*, 36–44. [CrossRef]
22. Surajarusarn, B.; Hajjar-Garreau, S.; Schrodj, G.; Mougine, K.; Amornsakchai, T. Comparative study of pineapple leaf microfiber and aramid fiber reinforced natural rubbers using dynamic mechanical analysis. *Polym. Test.* **2020**, *82*, 106289. [CrossRef]
23. Surajarusarn, B.; Traiperm, P.; Amornsakchai, T. Revisiting the morphology, microstructure, and properties of cellulose fiber from pineapple leaf so as to expand its utilization. *Sains Malays.* **2019**, *48*, 145–154. [CrossRef]
24. Straumit, I.; Vandepitte, D.; Wevers, M.; Lomov, S.V. Identification of the flax fibre modulus based on an impregnated quasi-unidirectional fibre bundle test and X-ray computed tomography. *Compos. Sci. Technol.* **2017**, *151*, 124–130. [CrossRef]
25. Rafiqah, S.A.; Khalina, A.; Harmaen, A.S.; Tawakkal, I.A.; Zaman, K.; Asim, M.; Nurrazi, M.N.; Lee, C.H. A Review on Properties and Application of Bio-Based Poly(Butylene Succinate). *Polymers* **2021**, *13*, 1436. [CrossRef] [PubMed]
26. Mochane, M.J.; Magagula, S.I.; Sefadi, J.S.; Mokhena, T.C. A Review on Green Composites Based on Natural Fiber-Reinforced Polybutylene Succinate (PBS). *Polymers* **2021**, *13*, 1200. [CrossRef] [PubMed]
27. New High Biocontent Biopolymers. Available online: <https://plasticsengineering.wordpress.com/2015/09/03/new-high-biocontent-biopolymers> (accessed on 8 August 2023).
28. Bianchi, S.; Marchese, P.; Vannini, M.; Sisti, L.; Tassoni, A.; Ferri, M.; Mallegni, N.; Cinelli, P.; Celli, A. Evaluation of the activity of natural phenolic antioxidants, extracted from industrial coffee residues, on the stability of poly(1,4-butylene succinate) formulations. *J. Appl. Polym. Sci.* **2023**, *140*, e53878. [CrossRef]
29. European Flax: Environmentally Responsible. Available online: <https://allianceflaxlinenhemp.eu/en/european-flax-environmentally-responsible> (accessed on 24 August 2023).
30. Lintex. Available online: <http://www.dehondtcomposites.com/en/products/lintex/> (accessed on 24 August 2023).
31. Kengkhetkit, N.; Amornsakchai, T. Effect of matrix orientation and fiber content on the properties of uniaxial pineapple leaf fiber—Polypropylene composites. *KGK-Kaut. Gummi. Kunst.* **2020**, *73*, 44–50.
32. Updegraff, D.M. Semimicro determination of cellulose in biological materials. *Anal. Biochem.* **1969**, *32*, 420–424. [CrossRef]
33. Wise, L.E.; Murphy, M.; Adieco, A.A.D. A chlorite holocellulose, its fractionation and bearing on summative wood analysis and studies on the hemicelluloses. *Pap. Trade J.* **1946**, *122*, 35–43.
34. TAPPI UM 250. *Acid-Soluble Lignin in Wood and Pulp*; Technical Association of the Pulp and Paper Industry: Atlanta, GA, USA, 1991.

35. TAPPI T 222. *Acid-Insoluble Lignin in Wood and Pulp*; Technical Association of the Pulp and Paper Industry: Atlanta, GA, USA, 2002.
36. Deng, Y.; Thomas, N.L. Blending Poly(butylene succinate) with Poly(lactic acid): Ductility and Phase Inversion Effects. *Eur. Polym. J.* **2015**, *71*, 534–546. [CrossRef]
37. Huda, M.S.; Drzal, L.T.; Mohanty, A.K.; Misra, M. Effect of chemical modifications of the pineapple leaf fiber surfaces on the interfacial and mechanical properties of laminated biocomposites. *Compos. Interfaces* **2008**, *15*, 169–191. [CrossRef]
38. Gaba, E.W.; Asimeng, B.O.; Kaufmann, E.E.; Katu, S.K.; Foster, E.J.; Tiburu, E.K. Mechanical and Structural Characterization of Pineapple Leaf Fiber. *Fibers* **2021**, *9*, 51. [CrossRef]
39. Tanpichai, S.; Witayakran, S. All-cellulose composite laminates prepared from pineapple leaf fibers treated with steam explosion and alkaline treatment. *J. Reinf. Plast. Compos.* **2017**, *36*, 073168441770492. [CrossRef]
40. French, A.D. Idealized powder diffraction patterns for cellulose polymorphs. *Cellulose* **2014**, *21*, 885–896. [CrossRef]
41. Tantatherdtam, R.; Tran, T.; Chotineeranat, S.; Lee, B.H.; Sriroth, K.; Kim, H.J. Preparation and Characterization of Cassava Fiber-Based Polypropylene and Polybutylene Succinate Composites. *Agric. Nat. Resour.* **2009**, *43*, 245–251.
42. Then, Y.Y.; Ibrahim, N.; Zainuddin, N.; Ariffin, H.; Yunus, W. Oil Palm Mesocarp Fiber as New Lignocellulosic Material for Fabrication of Polymer/Fiber Biocomposites. *Int. J. Polym. Sci.* **2013**, *2013*, 797452. [CrossRef]
43. Frackowiak, S.; Ludwiczak, J.; Leluk, K. Man-Made and Natural Fibres as a Reinforcement in Fully Biodegradable Polymer Composites: A Concise Study. *J. Polym. Environ.* **2018**, *26*, 4360–4368. [CrossRef]
44. Muthuraj, R.; Misra, M.; Mohanty, A. Injection Molded Sustainable Biocomposites From Poly(butylene succinate) Bioplastic and Perennial Grass. *ACS Sustain. Chem. Eng.* **2015**, *3*, 2767–2776. [CrossRef]
45. Nanni, A.; Cancelli, U.; Montevecchi, G.; Masino, F.; Messori, M.; Antonelli, A. Functionalization and use of grape stalks as poly(butylene succinate) (PBS) reinforcing fillers. *Waste Manag.* **2021**, *126*, 538–548. [CrossRef]
46. Goh, K.L. Physical Properties of Fibres and Matrix. In *Discontinuous-Fibre Reinforced Composites: Fundamentals of Stress Transfer and Fracture Mechanics*; Springer: London, UK, 2017; pp. 21–74.
47. Cosquer, R.; Pruvost, S.; Gouanvé, F. Improvement of Barrier Properties of Biodegradable Polybutylene Succinate/Graphene Nanoplatelets Nanocomposites Prepared by Melt Process. *Membranes* **2021**, *11*, 151. [CrossRef]
48. Ihn, K.J.; Yoo, E.S.; Im, S.S. Structure and Morphology of Poly(tetramethylene succinate) Crystals. *Macromolecules* **1995**, *28*, 2460–2464. [CrossRef]
49. Tanguy, M.; Bourmaud, A.; Beaugrand, J.; Gaudry, T.; Baley, C. Polypropylene reinforcement with flax or jute fibre; Influence of microstructure and constituents properties on the performance of composite. *Compos. B Eng.* **2018**, *139*, 64–74. [CrossRef]
50. Berzin, F.; Amornsakchai, T.; Lemaitre, A.; Di Giuseppe, E.; Vergnes, B. Processing and properties of pineapple leaf fibers-polypropylene composites prepared by twin-screw extrusion. *Polym. Compos.* **2018**, *39*, 4115–4122. [CrossRef]
51. Lee, J.M.; Mohd Ishak, Z.A.; Mat Taib, R.; Law, T.T.; Ahmad Thirmizir, M.Z. Mechanical, Thermal and Water Absorption Properties of Kenaf-Fiber-Based Polypropylene and Poly(Butylene Succinate) Composites. *J. Polym. Environ.* **2013**, *21*, 293–302. [CrossRef]
52. Hao, X.; Zhou, H.; Mu, B.; Chen, L.; Guo, Q.; Yi, X.; Sun, L.; Wang, Q.; Ou, R. Effects of fiber geometry and orientation distribution on the anisotropy of mechanical properties, creep behavior, and thermal expansion of natural fiber/HDPE composites. *Compos. B Eng.* **2020**, *185*, 107778. [CrossRef]
53. Goh, K.L. Appendix A: Convergence to Continuous-Fibre Composites. In *Discontinuous-Fibre Reinforced Composites: Fundamentals of Stress Transfer and Fracture Mechanics*; Springer: London, UK, 2017; pp. 185–186.
54. Surajarusarn, B.; Thaiwattananon, S.; Thanawan, S.; Mougín, K.; Amornsakchai, T. Realising the Potential of Pineapple Leaf Fiber as Green and High-performance Reinforcement for Natural Rubber Composite with Liquid Functionalized Rubber. *Fibers Polym.* **2021**, *22*, 2543–2551. [CrossRef]
55. Albrecht, K.; Osswald, T.; Baur, E.; Meier, T.; Wartzack, S.; Müssig, J. Fibre Length Reduction in Natural Fibre-Reinforced Polymers during Compounding and Injection Moulding—Experiments Versus Numerical Prediction of Fibre Breakage. *J. Compos. Sci.* **2018**, *2*, 20. [CrossRef]

**Disclaimer/Publisher’s Note:** The statements, opinions and data contained in all publications are solely those of the individual author(s) and contributor(s) and not of MDPI and/or the editor(s). MDPI and/or the editor(s) disclaim responsibility for any injury to people or property resulting from any ideas, methods, instructions or products referred to in the content.



## Article

# Durability against Wetting-Drying Cycles of Sustainable Biopolymer-Treated Soil

Antonio Soldo <sup>1</sup> and Marta Miletic <sup>2,\*</sup><sup>1</sup> Department of Civil and Environmental Engineering, Auburn University, Auburn, AL 36849, USA<sup>2</sup> Department of Civil, Construction and Environmental Engineering, San Diego State University, San Diego, CA 92182, USA

\* Correspondence: mmiletic@sdsu.edu

**Abstract:** The world today is more oriented towards sustainable and environmental-friendly solutions in every field of science, technology, and engineering. Therefore, novel sustainable and eco-friendly approaches for soil improvement have also emerged. One of the effective, promising, and green solutions is the utilization of biopolymers. However, even though the biopolymers proved to be effective in enhancing the soil-mechanical properties, it is still unknown how they behave under real environmental conditions, such as fluctuating temperatures, moisture, plants, microorganisms, to name a few. The main research aim is to investigate the durability of biopolymer-improved soil on the cyclic processes of wetting and drying. Two types of biopolymers (Xanthan Gum and Guar Gum), and two types of soils (clean sand and silty sand) were investigated in this study. The results indicated that some biopolymer-amended specimens kept more than 70% of their original mass during wetting-drying cycles. During the compressive strength analysis, some biopolymer-treated specimens kept up to 45% of their initial strength during seven wetting-drying cycles. Furthermore, this study showed that certain damaged soil-biopolymer bonds could be restored with proper treatment. Repeating the process of wetting and drying can reactivate the bonding properties of biopolymers, which amends the broken bonds in soil. The regenerative property of biopolymers is an important feature that should not be neglected. It gives a clearer picture of the biopolymer utilization and makes it a good option for rapid temporary construction or long-standing construction in the areas with an arid climate.

**Citation:** Soldo, A.; Miletic, M. Durability against Wetting-Drying Cycles of Sustainable Biopolymer-Treated Soil. *Polymers* **2022**, *14*, 4247. <https://doi.org/10.3390/polym14194247>

Academic Editor: Magdalena Czemińska

Received: 14 September 2022

Accepted: 8 October 2022

Published: 10 October 2022



**Copyright:** © 2022 by the authors. Licensee MDPI, Basel, Switzerland. This article is an open access article distributed under the terms and conditions of the Creative Commons Attribution (CC BY) license (<https://creativecommons.org/licenses/by/4.0/>).

**Keywords:** biopolymer-treated soil; Xanthan Gum; Guar Gum; soil strength; durability; cyclic wetting-drying

## 1. Introduction

The expansion of cities often causes the need to construct in an unfavorable environment and on soils with undesirable mechanical characteristics. As a solution, soil's engineering properties can be improved by adding different chemical additives. Currently, cement is one of the most commonly used additives. However, the use of cement raises a series of environmental problems from which the contribution to CO<sub>2</sub> concentration on the planet is the most concerning. From the data in 2016, the production of cement contributes approximately 7.4% to the world's CO<sub>2</sub> emissions [1]. Furthermore, the use of cement can irreversibly affect the urban environment. Increased urban water runoff, vegetation growth prevention, and heat islands are some of the side effects of using cement as soil stabilizer [2]. Therefore, the need for a sustainable, green, and effective solution for enhancing soil characteristics is continuously increasing.

New bio-inspired solutions for the improvement of mechanical characteristics of soil, such as biopolymer-soil mixtures, are proved to be quite effective [2–6]. A biopolymer is a chain of smaller molecular units extracted from nature-made materials, such as wood, vegetable, algae, and animal shells. To the best of the authors' knowledge, no negative



effect of biopolymers on the environment has been reported. Throughout recent history, biopolymers were used in the food industry, the cosmetic industry, medicine, and agriculture [7–11]. In previous research, it was found that biopolymers, such as xanthan gum, guar gum, beta-glucan, and chitosan, can improve the strength of soil [5,6,12–15]. In addition, some biopolymers proved effective in reducing the collapsibility of soil [16] and erosion [17–19].

However, the main concern is the durability of biopolymer-amended soils while being exposed to environmental conditions such as wind, moisture, and temperature fluctuations. Kavazanjian et al. [18] investigated the effect of wind on erosion properties of the biopolymer-amended soil. Biopolymer emulsion was sprayed on the surface of the soil, and wind flow was blown over the soil surface. The major finding was that biopolymers could reduce wind-induced detachment of soil particles, but that ultraviolet radiation and heat can diminish their effect.

To date, the research on the durability of biopolymer-amended sand remains limited and insufficiently investigated. Chang et al. [20] explored the properties of biopolymer-amended sand against cyclic wetting-drying. They performed a series of unconfined compression tests on gellan gum-improved sand specimens after each wetting and drying cycle. Chen et al. [21] performed a series of direct shear tests on xanthan gum-improved sand. Both of the above-mentioned research studies have found that the strength of biopolymer-amended sand ultimately decreases due to cyclic wetting and drying. Some limitations of each of the mentioned studies are that one type of testing was conducted and the soil (sand) was amended with only one type of biopolymer. Some additional research in the field of cyclic wetting-drying of biopolymer-treated soil is presented in Table 1.

**Table 1.** Previous research related to wetting-drying of biopolymer-treated soil.

Authors	Soil	Biopolymer	Testing	Findings
Chen et al. 2015 [22]	Silty Sand	Xanthan Gum Guar Gum	Moisture retention	Moisture retention capacity was higher with the addition of biopolymers.
			Wind Tunnel	<ul style="list-style-type: none"> <li>- Biopolymer increased the erosion resistance of soil</li> <li>- At higher concentrations, the loss of mass was small during cyclic wetting-drying.</li> </ul>
			Penetration test	Increased surface strength with the increase of biopolymer concentration.
Chang et al. 2017 [20]	Poorly Graded Sand	Gellan Gum	Unconfined Compressive Strength Test	<ul style="list-style-type: none"> <li>- Reduction of the compressive strength was gradual.</li> <li>- The strength remained high after 10 wetting-drying cycles (i.e., &gt;70% of the initial strength).</li> </ul>
Chen et al. 2019 [21]	Well Graded Sand	Xanthan Gum	Direct Shear	Reduction of friction angle, cohesion, and peak shear stress was gradual.
Lemboye et al. 2021 [23]	Poorly Graded Sand	Acacia Gum Sodium Alginate Pectin	Wind Tunnel	<ul style="list-style-type: none"> <li>- Biopolymer increased the erosion resistance of the soil.</li> <li>- Wetting-drying increased the loss of mass.</li> </ul>
			Penetration Test	<ul style="list-style-type: none"> <li>- Biopolymer increased the surface strength of the soil.</li> <li>- Wetting-drying reduced surface strength.</li> </ul>
Adamczuk and Jozefaciuk, 2021 [24]	Sand Silt	Chitosan (two types)	Unconfined Compressive Strength Test	Strength changes after wetting-drying depended on soil type, biopolymer type, and biopolymer concentration.

The main research aim of our study is to investigate the durability of biopolymer-improved soil on the cyclic processes of wetting and drying. Two soil types were investi-

gated in this study, clean sand and silty sand. Additional testing variables were biopolymer type and concentration. In particular, the soil was treated with two types of biopolymer (Xanthan Gum and Guar Gum) at three different biopolymer concentrations (0.5%, 1%, 2%). Furthermore, plain and biopolymer-amended specimens were tested under two types of water-durability tests. Considering that Xanthan Gum and Guar Gum emerged as biopolymers with high potential for soil stabilization, the investigation of their durability will have a significant impact on their utilization in civil engineering practice.

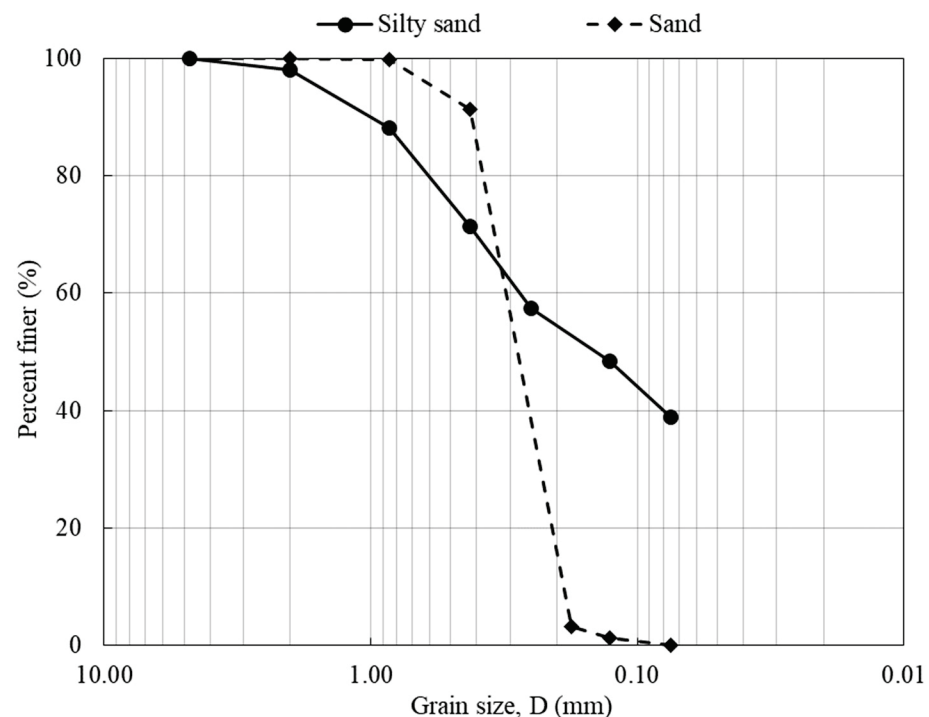
## 2. Materials and Methodology

### 2.1. Base Soil

To investigate the effect of the soil type on the biopolymer-amended soil durability, two types of soil were investigated in this study: silty sand (SM), and poorly graded sand (SP). The soils were classified according to the following standards: ASTM D6913-17—Standard Test Methods for Particle-Size Distribution of Soils Using Sieve Analysis [25], and ASTM D4318-17—Standard Test Methods for Liquid Limit, Plastic Limit, and Plasticity Index of Soils [26].

#### 2.1.1. Silty Sand

From the grain size distribution curve (Figure 1), the concentration of fine particles was 39% with a liquid limit of 49, a plastic limit of 29, and an index of plasticity of 20. According to the Unified Soil Classification System (USCS), the soil is classified as silty sand (SM).



**Figure 1.** Grain size distribution of the soils used in this study.

#### 2.1.2. Clean Sand

The sand was characterized by a high percentage of quartz and high uniformity. The coefficient of uniformity and coefficient of curvature were calculated as 1.46, and 0.93, respectively (Figure 1). The percentage of fine particles was below 5%. Therefore, the soil was classified as poorly graded sand (SP), according to USCS.

## 2.2. Biopolymers

To study the influence of the biopolymer type on the biopolymer-amended soil durability, two types of biopolymers were used in this study: Xanthan Gum and Guar Gum.

### 2.2.1. Xanthan Gum

*Xanthomonas campestris* bacterium creates the biopolymer polysaccharide Xanthan Gum (XG) by inducing the fermentation of a medium containing carbohydrate, such as glucose. In other words, XG is a long-chain polysaccharide having d-glucose, d-mannose, and d-glucuronic acid as building blocks in a molecular ratio of 3:3:2 with a high number of trisaccharide side chains [27]. Dissolving XG in hot or warm water creates non-Newtonian solutions with high pseudoplasticity. XG can be found in the cosmetic and food industry, agriculture, and oil drilling industry [9], and it has been researched for civil engineering purposes [5,6,28,29].

### 2.2.2. Guar Gum

Guar Gum (GG) is a galactomannan polysaccharide extracted from *Cyamopsis Tetragonolba*, known as guar beans or guar. Chemically, a GG biopolymer mainly consists of a high-molecular-weight polysaccharide galactomannan, which is based on a mannan backbone with galactose side groups. The ratio of the two building blocks in a molecular ratio seems to vary slightly depending on the origin of the seed, but the gum is generally considered to contain approximately one galactose building block for every two mannose building blocks [30]. In addition, GG shares certain similarities with XG. For instance, it can be dissolved in hot and cold water, and in the industry is used for similar purposes as XG. It can be found in cosmetic products, food products, oil, and gas drilling industries [30], and it has been researched in civil engineering [6,31–34].

## 2.3. Specimen Preparation

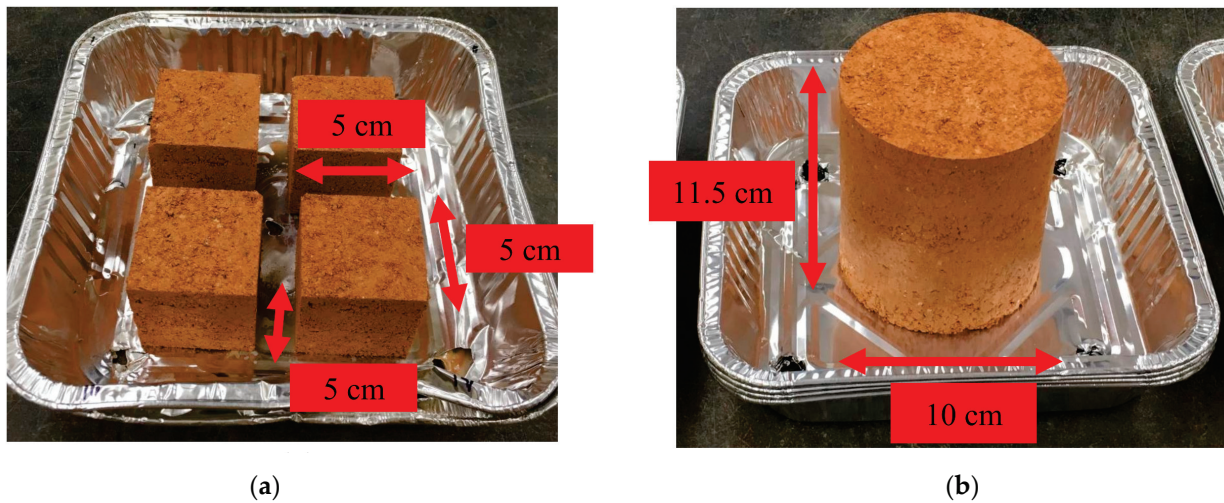
The dry base soils were placed in a metal dish and combined with biopolymer powders until uniformly mixed. The biopolymer concentrations used in this study were 0.5, 1, and 2% with respect to the mass of the plain soil. After carefully mixing the dry components (soil and biopolymers), water was added to the mix by spraying and constant stirring. The targeted water content was 16.5% for silty sand and 12% for the clean sand.

After achieving a uniform mixture, the soil-water-biopolymer mass was placed into molds. Two types of molds (Mold A and Mold B) were used for two different parts of this study.

Mold A was cylindrical with a diameter of 10.2 cm and a height of 11.6 cm. Silty sand was placed into the Mold A in three lifts and it was compacted with a hammer with a weight of 2.5 kg (Proctor hammer). The same type of mold is typically used for compaction efforts for ASTM D559 and ASTM D698. Each lift was compacted by releasing the hammer 25 times from the height of 30.5 cm. After each lift, the surface was scarified to achieve a better bond within the soil sample. Proctor hammer was omitted for the sand material due to its nature. Sand had a low concentration of fine particles that would have hindered the proper compaction if excessive compaction force was applied. Therefore, sand was carefully tapped into Mold A. Additionally, tapping the sand material into the mold kept the density of the biopolymer-treated sand close to its natural density. Specimens prepared in Mold A were used for durability testing during cyclic wetting and drying.

Mold B was cubical, with the inner dimensions of 5 cm. Cubical specimens were used for the testing of the compressive strength changes through the wetting-drying cycles. The specimens made out of silty sand were compacted with a metal rod in four lifts. Each lift was pressed 25 times. Sand specimens were gently tapped into the Mold B due to the aforementioned reasons relating to the nature of sand.

All specimens were air-dried in the laboratory at the temperature of 21 °C for five days (cubical specimens, Figure 2a) and seven days (cylindrical specimens, Figure 2b) to increase the biopolymer-soil strength and cure the specimens.



**Figure 2.** Photos of specimens for (a) unconfined compression, and (b) durability tests.

In addition, specimens made of plain silty sand were prepared in the same manner as the specimens with biopolymer additives. The plain specimens were used for comparison with the biopolymer-treated ones. The samples of the plain sand could not be made because the plain sand used in this research had no cohesion. Therefore, it could not be shaped to the desired dimensions.

#### 2.4. Testing

##### 2.4.1. Durability

The durability testing during cyclic wetting and drying was performed by the guidance of the ASTM D559—Standard Test Methods for Wetting and Drying Compacted Soil-Cement Mixtures [35]. Since ASTM D559 was originally designated for cemented soil, this study introduced certain modifications to the procedure described in ASTM D559. After compaction and air-drying, we measured the mass of specimens and submerged them in water for one hour. The specimens' mass was measured again after one hour, and specimens were placed in the oven at the temperature of 70 °C for 24 h. After 24 h, samples were taken out of the oven, gently stroked by a brush to remove all loose material, and weighed again before submerging them into the water. The same process was repeated ten times, where one hour in water and 24 h in the oven represents one wetting-drying cycle. This procedure was performed on XG-treated sand, XG-treated silty sand, and GG-treated silty sand. The cylindrical sand specimens with GG degraded after one hour in the water. Therefore, they could not be used for the continuation of the experiment. A similar degradation process happened with the cylindrical specimen of the plain silty sand. They degraded after one hour in the water. Thus, the durability testing of plain silty sand could not be continued.

##### 2.4.2. Unconfined Compression Test

The unconfined compression test is a widely used test to determine the compressive strength of cohesive materials. The test was performed on the plain and biopolymer-amended silty sand. Moreover, it was performed on the XG-improved sand, whereas untreated sand did not have any cohesion, which was required for this type of test. In addition, sand specimens with GG were not testable for this type of experiment due to their low resistance to water. The unconfined compression test was performed on cubical specimens five days after the preparation and air-drying. Three samples were compressed with an axial strain rate of 1.5%/min, which is in agreement with the ASTM D2166—Standard Test Method for Unconfined Compressive Strength of Cohesive Soil [36]. The remaining specimens were submerged in water at room temperature (21 °C) for 20 min. They were subsequently dried in the oven at 70 °C for 24 h. This process is referred to as



one wetting-drying cycle for unconfined compression specimens. Cubical samples of plain silty sand were not tested in the unconfined compression test after wetting and drying due to their degradation in water. After each wetting-drying period, three specimens were tested in the unconfined compression test, while the remaining samples were placed back in the water for 20 min. For the specimens with XG, seven cycles of wetting and drying were carried out through seven days. The unconfined compression test was performed after each cycle except for the fourth and sixth. Most of the cubical specimens with GG were heavily damaged after the first 20 min in water. Therefore, the remaining specimens with GG went through two or three cycles of wetting and drying.

Furthermore, the healing potential of the XG biopolymer was also investigated by wetting and re-testing previously loaded specimens after their first unconfined compression test. XG-sand cubes were placed in the water for 20 min after they were broken in the unconfined compression test for the first time. They were subsequently placed back in the oven and re-tested for the unconfined compression. The repeated cycle of wetting and drying was conducted to reactivate XG molecules and investigate their regenerative properties on the treated sand.

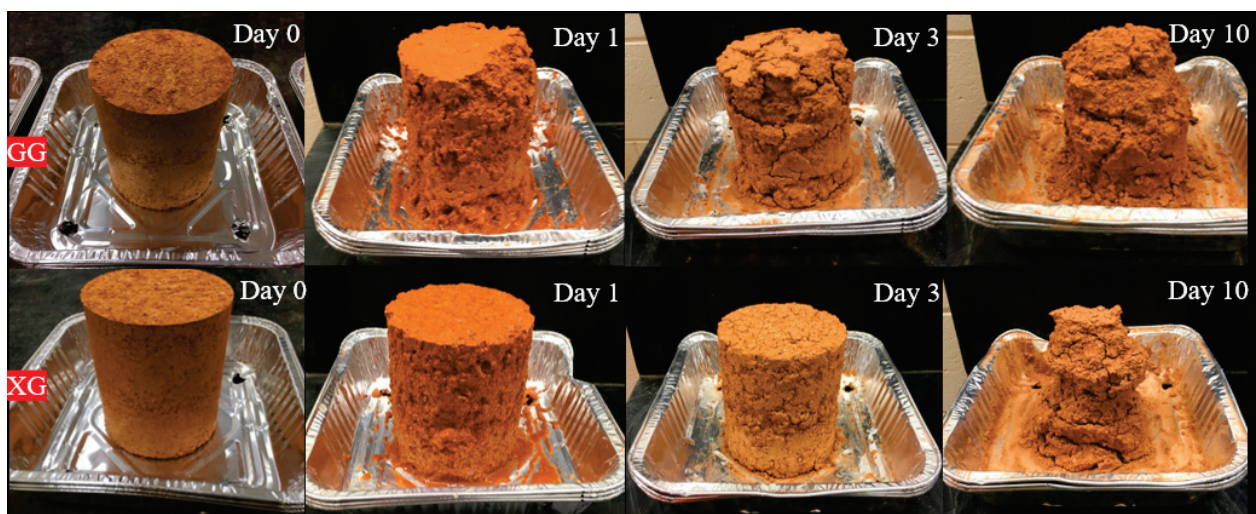
### 3. Results and Discussion

#### 3.1. Durability

The durability of the soil was observed through the change of mass through cyclic wetting and drying. The change of mass of the biopolymer-treated soil was calculated for each cycle by the following equation:

$$\% \text{ loss} = (A/B) \times 100 \quad (1)$$

where  $A$  is the mass of the soil after each cycle;  $B$  is the mass of the dry soil after seven days of curing in the air. Several samples were placed in the oven after the preparation and dried for 24 h at 70 °C. Those samples were not tested but they were used for comparison in mass with specimens that were air-dried for 7 days. The differences in mass for the same biopolymer-soil mix were between 2% and 7%. Therefore, we decided that the equation above would be appropriate for the analysis of the durability data. A visual representation of sample degradation through time is shown on biopolymer-treated silty sand in Figure 3.



**Figure 3.** Degradation of silty sand treated with 1% XG (upper row) and 1% GG (bottom row) due to cyclic wetting and drying.

Figure 4 shows the results of the mass percentages of biopolymer-soil remaining after each cycle. Plain soil samples degraded when submerged under the water for one hour and could not be tested in the designed experiment. The results from Figure 4 indicate that

the presence of biopolymers slowed the degradation process for both types of soil. Figure 4 also indicates that the resistance of the soil to cyclic wetting and drying depends on the type of the soil, type of biopolymer additive, and concentration of biopolymer additive. Different biopolymer types, like different soil types, show different reactions with water, which affects the behavior of the soil–biopolymer mixture when exposed to water.

Interestingly, the silty sand with XG showed the best resistance for cyclic wetting and drying at a concentration of 1% XG (Figure 4a). At that concentration, the specimens kept most of the mass up to the sixth wetting–drying cycle. After that, the loss of mass was more noticeable. The same soil type with 0.5% and 2% XG lost more soil mass which indicates that 1% XG could be the optimal water-resistance concentration for this type of soil. There are two reasons behind this: the binding properties of XG and the absorptive properties of the composite material (silty sand and XG). XG is a glue-like binding agent that bridges soil particles. In the mixture with 0.5% XG, soil particles have a weaker biopolymer bond when compared with mixtures with 1 and 2% XG. Therefore, samples with 0.5% XG lost approximately 65% of their initial mass after the first wetting cycle. The plain specimens of silty sand had the weakest particle bond which is the reason they degraded after the first cycle. On the other hand, a question emerges concerning why samples with the highest XG concentration (2%) did not show the best water resistance. The reason for that is the aforementioned absorptive properties of silty sand and XG. The XG attracts and binds water molecules, which further increases the absorbing potential of already swelling plain soil. In other words, the higher presence of XG caused more trapped water. Therefore, to achieve the same water content after each drying for the specimens with 1 and 2% XG, specimens with 2% XG would require a higher drying temperature or longer drying time. The constant higher presence of water can cause the reduction of negative pore pressures that can lower the apparent cohesion and cause the degradation of the soil mass. That resulted in the faster degradation of specimens with 2% XG. However, the loss of the mass under all biopolymer concentrations was significantly reduced when compared with the loss in mass of the plain soil.

In the case of silty sand amended with GG (Figure 4b), the specimens with higher concentrations have kept more of their soil mass during ten cycles of wetting and drying. When compared with higher concentrations, the samples treated with only 0.5% GG had significantly higher losses of mass between each cycle. Unlike the samples with 1% XG, the samples with 1% GG had a slight gradual loss of mass after each wetting–drying cycle. The samples with 2% GG showed a slight mass increase through the cyclic wetting–drying. That is because of the absorptive properties of silty sand and GG, similar as XG-treated silty sand. The samples with 2% GG lost some amount of soil during wetting–drying, but they also absorbed some water that did not completely evaporate during 24 h in the oven at 70 °C. Therefore, due to the higher absorptive properties of GG at 2% than at 0.5 and 1%, a longer period of drying or a higher drying temperature would be more appropriate for silty sand with 2% GG. Both GG and XG demonstrate a water-absorption nature. However, comparing results of silty sand with 2% GG and 2% XG indicates that GG chains release water molecules somewhat easier than XG chains. Even though XG and GG need to absorb water to activate their bonds with soils, releasing water molecules stiffens the soil–biopolymer bond, which gives GG-treated silty sand an edge over the XG-treated silty sand at a concentration of 2%.

For the clean sand specimens amended with XG (Figure 4c), the loss of mass is relatively low throughout the testing for higher concentrations when compared with silty sand. The reason for that is the fact that the sand has a higher porosity and lower water absorption capacity than silty sand. In other words, water absorption happens only due to the presence of XG. Higher porosity makes the water evaporation relatively faster in the sand than in silty sand. The cementitious effect of hardened XG gave the sand relatively good resistivity to water. However, sand with only 0.5% XG went successfully through only six cycles of wetting and drying before it became wholly degraded.

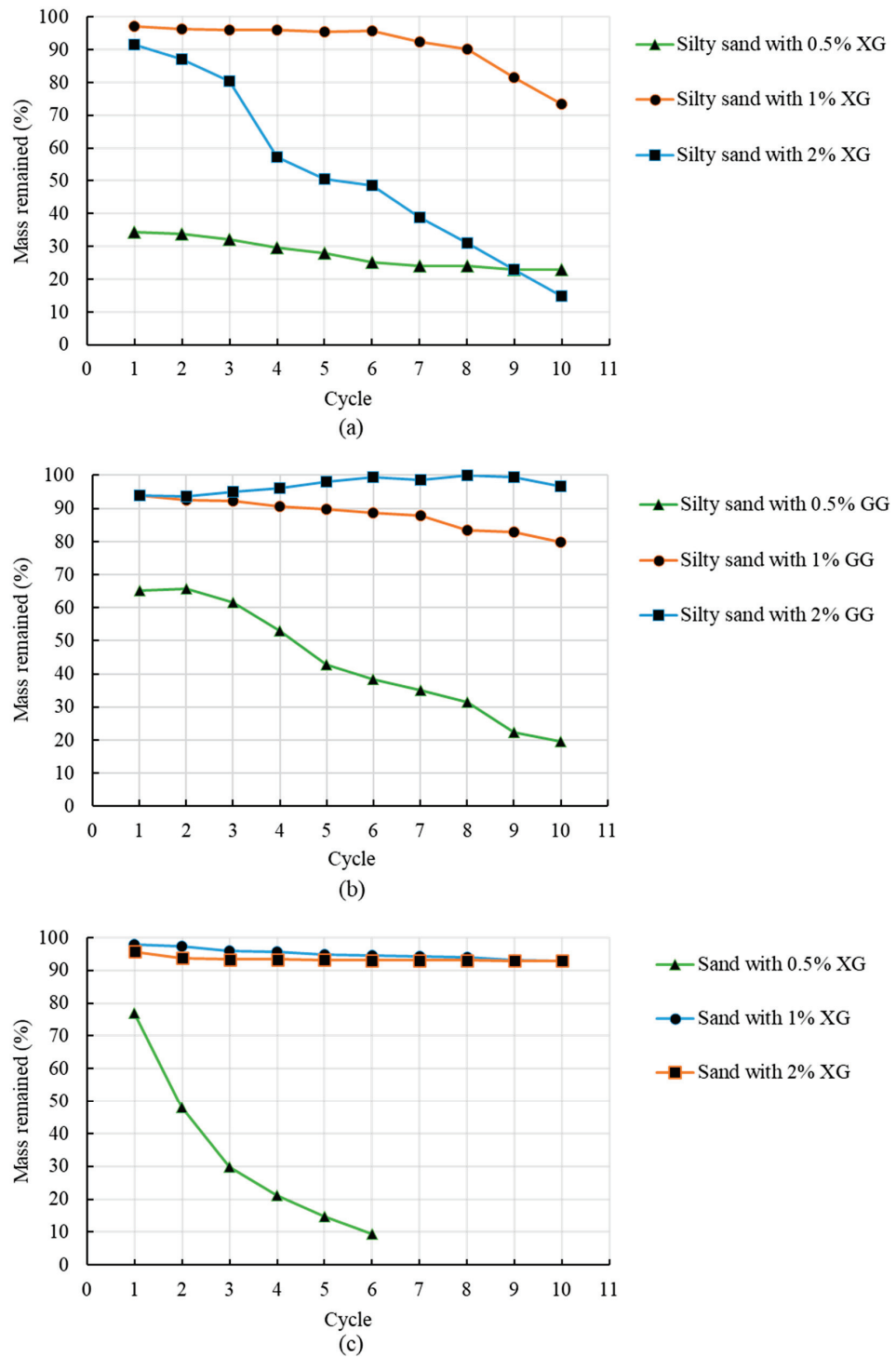


Figure 4. Change in mass for (a) Silty sand—XG, (b) Silty sand—GG, (c) Clean sand—XG.

3.2. Unconfined Compression Test

Figure 5 shows the relationship between the compressive strength and the number of wetting and drying cycles for silty sand (Figure 5a,b) and clean sand (Figure 5c). In all figures, the first point, at cycle zero, represents the compressive strength of specimens tested after five days of air-drying in the laboratory at room temperature. The plain silty sand samples degraded after 20 min in water and could not be tested through cyclic wetting and drying (Figure 5a,b). Plain clean sand samples were not testable because of non-existing cohesion that was needed to fabricate the specimens for this type of testing (Figure 5c). Both types of soil showed fast degradation in water for 0.5% of additives. Therefore, soils

amended with 0.5% of biopolymers could not be used for a detailed comparison with soil amended with higher biopolymer concentrations. The exception was the sand treated with 0.5% XG that showed a slightly higher level of water resistance (Figure 5c).

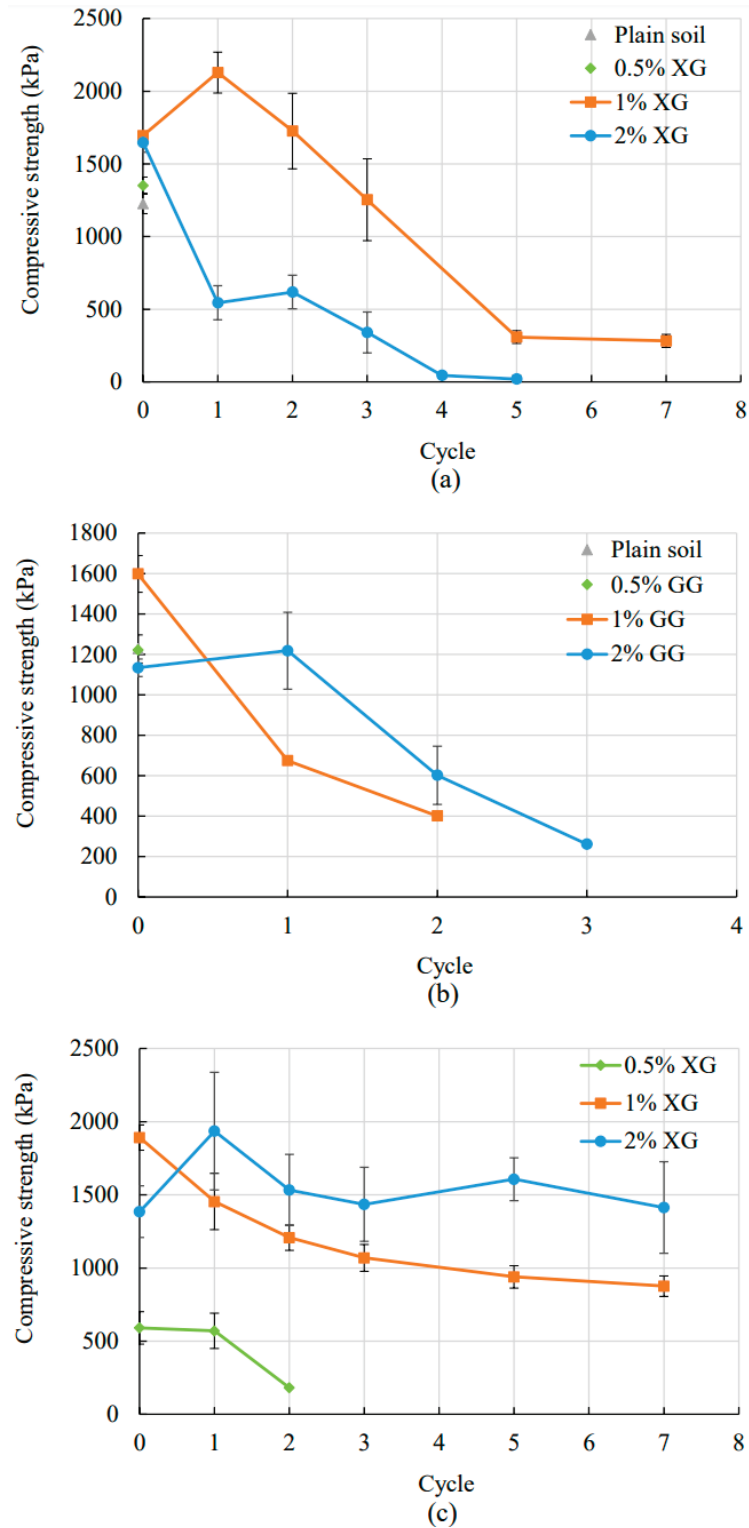
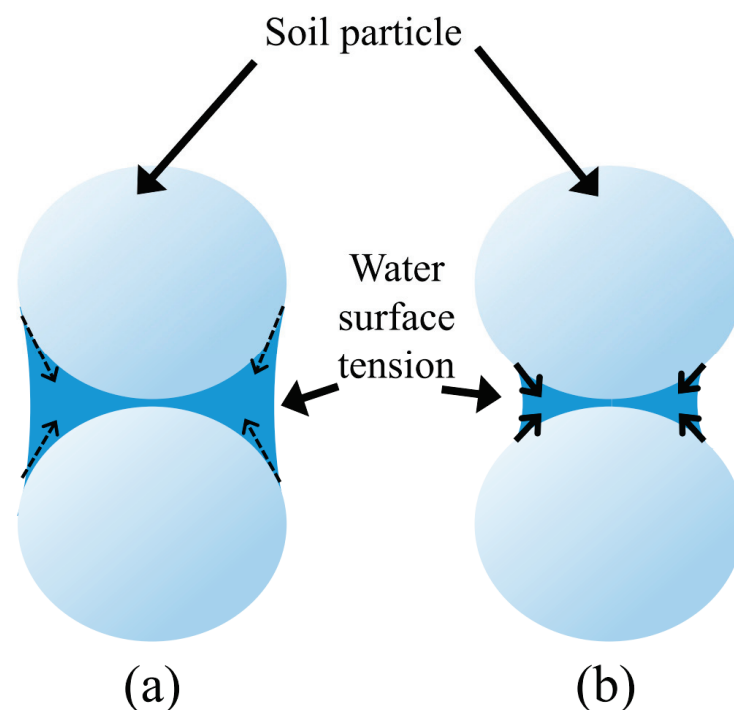


Figure 5. Change in compressive strength for (a) Silty sand—XG, (b) Silty sand—GG, (c) Clean sand—XG.



The change in the compressive strength of biopolymer-improved soil with wetting-drying cycles strongly depends on the biopolymer concentration, biopolymer type, and water content. Lower biopolymer concentration in soil results in a reduced number of biopolymer links and subsequent biopolymer–particle bonding. In other words, soils with a lower biopolymer concentration will have smaller compressive strength. On the other hand, a higher percentage of biopolymer causes greater water absorption. The decrease in the water content and degree of saturation increases the surface tension forces between soil particles, which subsequently increases the soil strength (Figure 6). It is noticeable that the biopolymer bond started to weaken after the first wetting and drying cycle because of constant water absorption and the thinning of the biopolymer links. For the specimens made out of the silty sand mixed with 2% XG, the increased biopolymer concentration resulted in higher water absorption than samples with 1% XG. The higher presence of the trapped water caused a more rapid decrease in the compressive strength because of reduced tension forces and loosened biopolymer links.



**Figure 6.** Interaction of water and soil particles: (a) a higher degree of saturation—lower surface tension forces, (b) lower degree of saturation—higher surface tension forces.

Figure 5b shows the decrease in the compressive strength for GG-treated silty sand with wetting-drying cycles. The vast majority of the 1% GG-treated cubicles were severely damaged and unusable for the unconfined compression test. Therefore, undischarged specimens went under two cycles of wetting and drying, where the change of their compressive strength was investigated. It is noticeable that after two cycles of wetting and drying, the compressive strength of 1% GG-treated cubicles decreased by 75%. In the case of 1% XG-treated silty sand, the decrease of the compressive strength by 75% would be estimated to happen after the fourth cycle of wetting and drying. The specimens with 2% GG showed better resistivity to water and higher strength through cyclic wetting and drying. The first points, at cycle zero, which represent the specimens after five days of air drying, indicate lower strength for the specimens with 2% GG. This trend was already observed with the samples treated with XG. The reason behind that is that higher concentrations of biopolymer need more air-drying time to completely harden and achieve the maximum strength. The same phenomena happened for the treated sand as well (Figure 5c).

Figure 5c represents the change of the compressive strength of XG-treated sand with wetting-drying cycles. During seven cycles of wetting and drying, sand with 1% XG kept 46% of the initial strength, while the sand with 2% XG kept 75% of the initial strength. However, the biopolymer-amended sand samples did not sustain their shape and strength at the lowest biopolymer concentration. At the concentration of 0.5% XG, they lost 70% of the initial strength after the second cycle and completely degraded during the third cycle.

### 3.3. Regenerative Properties of Biopolymers

Xanthan Gum is one of the partially reversible bond-based biopolymers. That means that it can be brought to the previous state by reapplying the processes that initially induced the change of that state. That reversible nature of XG was examined in biopolymer-treated sand samples that were tested under the unconfined compression test. After the third wetting-drying cycle, that was used to investigate the change in the compressive strength. The broken specimens were used to investigate the healing properties of XG. The broken specimens were submerged for 20 min and dried in the oven for 48 h, as described previously. After that, the same specimens were tested again under the unconfined compression test. The same process was repeated one more time. The results of two XG-treated sand specimens are summarized in Figure 7. The repeated process of wetting-drying stiffened the soil-biopolymer bond, and the XG-treated sand specimen regained some level of the initial strength, which is presented in Figure 7. Higher magnitudes of the compressive strength and the level of the regained strength were achieved for the higher concentration of XG. That is not surprising since a higher concentration of XG causes faster and broader linking of XG molecules with each other and with the surrounding sand particles.

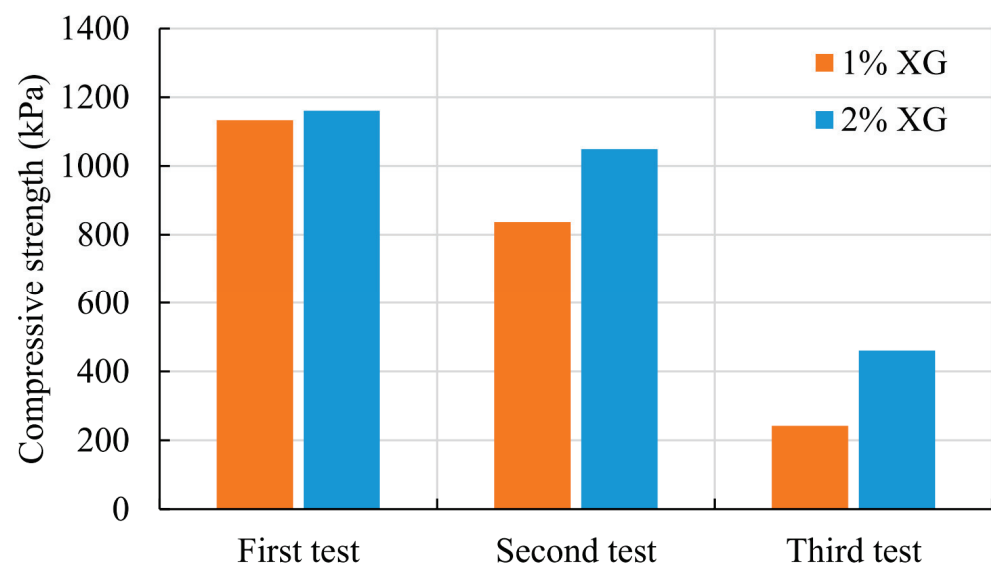
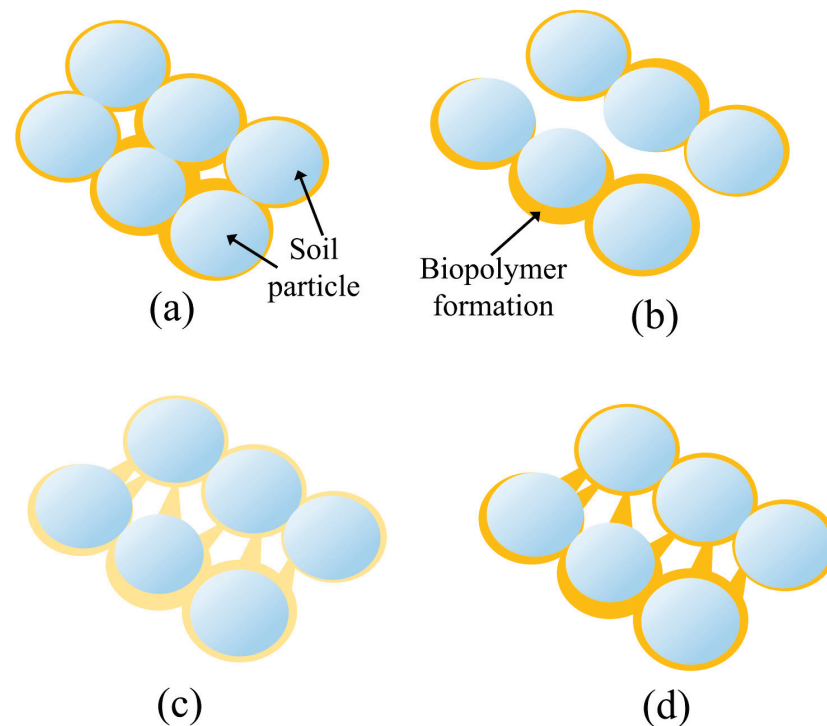


Figure 7. Compressive strength of regenerated sand XG-treated specimens.

That reversible nature of XG is schematically represented in Figure 8. The sand particles bonded by XG-links (Figure 8a) broke during the unconfined compression test (Figure 8b). After the broken specimens of XG-treated sand were put back together and submerged in water, the XG linkages loosened their structure, which allowed them to interact with the nearby sand particles again (Figure 8c) and mend the broken bonds (Figure 8d).



**Figure 8.** Healing cycle of biopolymer-treated sand: (a) sand particles bonded by XG-links, (b) breakage of the dry XG-links due to the applied mechanical loading, (c) XG-linkages loosen their structure in the contact with water which allows them to interact with the nearby sand particles; and (d) sand particles bonded again by new XG-links.

#### 4. Conclusions

Recently, biopolymers XG and GG have been shown to be promising environmentally friendly soil stabilization additives. However, they are prone to environmental influence, especially moisture changes. To best to the authors' knowledge, the previous research studies have not comprehensively investigated the effect of wetting-drying cycles on the strength and mass loss of the different biopolymer-treated soils. Therefore, the main aim of this study is to investigate the effect of wetting-drying cycles on the strength and mass loss of the biopolymer-stabilization. The types of soil used in this study were: silty sand and pure sand. In addition, two types of biopolymers (xanthan gum, and guar gum) and three biopolymer concentrations (0.5%, 1%, 2%) were used as testing variables in this research.

The first experimental study was focused on observing the change of the mass of the plain and biopolymer-treated soil during cyclic wetting and drying. It was shown that XG reduces the loss of mass for both tested soil types, while GG was only effective when mixed with silty sand. For the silty sand, the most effective concentration of XG to reduce the mass loss during the cyclic wetting and drying process was found to be 1%. The highest used concentration of XG (2%) caused higher entrapment of water, which ultimately led to faster loss of mass. On the other hand, the lowest concentration of XG (0.5%) resulted in too weak biopolymer-soil bonds, which degraded faster. That points to an optimum concentration of XG that works the best with a certain type of soil. For the GG-treated silty sand, the loss of mass was more prominent for lower concentrations. For the XG-treated sand, the loss of mass was relatively low for concentrations of 1% and 2%, which can be explained by higher porosity of sand, which makes water evaporation easier in comparison to the silty sand. A low concentration of 0.5% XG caused weak bonding between soil particles that rapidly degraded.

The second experiment investigated the change of the compressive strength of biopolymer-treated soil with wetting-drying cycles. XG proved able to reduce the loss of compressive strength in the silty sand and sand, while GG was only mildly effective in the silty sand.

However, the increase in the GG concentration reduced strength loss. The concentration of 1% XG was more effective than 2% in reducing the strength loss in the silty sand due to higher water absorption for higher concentrations of XG. The XG-treated sand showed extremely good resistivity to the loss of the compressive strength through cyclic wetting and drying. The higher concentrations of XG resulted in the higher compressive strength of sand. The concentration of 0.5% XG and GG was shown to be mildly or non-effective for the proposed type of testing.

The broken XG-treated sand specimens were re-submerged, dried, and subsequently tested in the unconfined compression test to study the healing properties of XG-treated sand. It was shown that re-wetting and drying could restore some level of the compressive strength of XG-treated sand. The reason behind it is the regenerative nature of XG, which loosens its structure in water and re-attaches to the nearby soil particles. The healed soil-biopolymer bond stiffens while the sample is subsequently dried and mends the cracks in sandy specimens. Sand samples with higher concentrations of XG were shown to regain more of their lost strength.

This research study showed that, even though biopolymers tend to be susceptible to water, certain biopolymer types and concentrations can significantly increase the durability of soil to water. It was also shown that the presence of water could activate the regenerative properties of XG, which accentuates its potential for soil stabilization. This research gives a clearer picture of XG and GG utilization, presenting a good option for rapid temporary construction (e.g., embankments) or long-standing construction in areas with an arid climate. The degradation of XG- and GG-treated soil due to longer exposure to water points to a practical way of disposing of the temporary construction elements that are made of the mentioned materials. Due to the non-hazardous nature of these biopolymers, watering and decomposing the XG- and GG-treated soil should not raise environmental concerns. XG and GG also showed favorable characteristics that can be utilized in dust control, erosion, and subgrade stabilization. However, since the water susceptibility of biopolymers is an important factor for their use in industry, this field of research still requires a significant amount of investigation.

**Author Contributions:** Conceptualization, M.M.; methodology, A.S.; validation, M.M.; formal analysis, M.M., A.S.; writing—original draft preparation, A.S.; writing—review and editing, M.M.; supervision, M.M. All authors have read and agreed to the published version of the manuscript.

**Funding:** This research received no external funding.

**Data Availability Statement:** The data presented in this study are available on request from the corresponding author.

**Conflicts of Interest:** The authors declare no conflict of interest.

## References

- Sanjuán, M.Á.; Andrade, C.; Mora, P.; Zaragoza, A. Carbon dioxide uptake by cement-based materials: A Spanish case study. *Appl. Sci.* **2020**, *10*, 339. [CrossRef]
- Chang, I.; Im, J.; Cho, G.-C. Introduction of Microbial Biopolymers in Soil Treatment for Future Environmentally-Friendly and Sustainable Geotechnical Engineering. *Sustainability* **2016**, *8*, 251. [CrossRef]
- Umar, M.; Kassim, K.A.; Ping Chiet, K.T. Biological process of soil improvement in civil engineering: A review. *J. Rock Mech. Geotech. Eng.* **2016**, *8*, 767–774. [CrossRef]
- Cho, G.-C.; Chang, I. Cementless Soil Stabilizer—Biopolymer. In Proceedings of the 2018 World Congress on Advances in Civil, Environmental & Materials Research (ACEM18), Incheon, Korea, 26–29 August 2012.
- Soldo, A.; Miletić, M. Study on Shear Strength of Xanthan Gum-Amended Soil. *Sustainability* **2019**, *11*, 6142. [CrossRef]
- Soldo, A.; Miletić, M.; Auad, M.L. Biopolymers as a sustainable solution for the enhancement of soil mechanical properties. *Sci. Rep.* **2020**, *10*, 1–13. [CrossRef]
- Hou, C.T.; Barnabe, N.; Greaney, K. Biodegradation of xanthan by salt-tolerant aerobic microorganisms. *J. Ind. Microbiol.* **1986**, *1*, 31–37. [CrossRef]
- Shahidi, F.; Synowiecki, J. Isolation and characterization of nutrients and value-added products from snow crab (*Chionoecetes opilio*) and shrimp (*Pandalus borealis*) processing discards. *J. Agric. Food Chem.* **1991**, *39*, 1527–1532. [CrossRef]
- Katzbauer, B. Properties and applications of xanthan gum. *Polym. Degrad. Stab.* **1998**, *59*, 81–84. [CrossRef]



10. Bourriot, S.; Garnier, C.; Doublier, J.-L. Phase separation, rheology and microstructure of micellar casein–guar gum mixtures. *Food Hydrocoll.* **1999**, *13*, 43–49. [CrossRef]
11. Volman, J.J.; Ramakers, J.D.; Plat, J. Dietary modulation of immune function by  $\beta$ glucans. *Physiol. Behav.* **2008**, *94*, 276–284. [CrossRef]
12. Chen, R.; Zhang, L.; Budhu, M. Biopolymer Stabilization of Mine Tailings. *J. Geotech. Geoenviron. Eng.* **2013**, *139*, 1802–1807. [CrossRef]
13. Latifi, N.; Horpibulsuk, S.; Meehan, C.L.; Abd Majid, M.Z.; Tahir, M.M.; Mohamad, E.T. Improvement of Problematic Soils with Biopolymer—An Environmentally Friendly Soil Stabilizer. *J. Mater. Civ. Eng.* **2017**, *29*, 04016204. [CrossRef]
14. Wiszniewski, M.; Skutnik, Z.; Biliniak, M.; Çabalar, A.F. Some geomechanical properties of a biopolymer treated medium sand. *Annals of Warsaw University of Life Sciences—SGGW. Land Reclam.* **2017**, *49*, 201–212.
15. Hataf, N.; Ghadir, P.; Ranjbar, N. Investigation of soil stabilization using chitosan biopolymer. *J. Clean. Prod.* **2018**, *170*, 1493–1500. [CrossRef]
16. Ayeldeen, M.; Negm, A.; El-Sawwaf, M.; Kitazume, M. Enhancing mechanical behaviors of collapsible soil using two biopolymers. *J. Rock Mech. Geotech. Eng.* **2017**, *9*, 329–339. [CrossRef]
17. Orts, W.J.; Sojka, R.E.; Glenn, G.M. Biopolymer additives to reduce erosion-induced soil losses during irrigation. *Ind. Crops Prod.* **2000**, *11*, 19–29. [CrossRef]
18. Kavazanjian, E.J.; Iglesias, E.; Karatas, I. Biopolymer soil stabilization for wind erosion control. In Proceedings of the 17th International Conference on Soil Mechanics and Geotechnical Engineering, Alexandria, Egypt, 5–9 October 2009; IOS Press: Amsterdam, The Netherlands, 2009; pp. 881–884.
19. Chang, I.; Prasadhi, A.K.; Im, J.; Cho, G.-C. Soil strengthening using thermo-gelation biopolymers. *Constr. Build. Mater.* **2015**, *77*, 430–438. [CrossRef]
20. Chang, I.; Im, J.; Lee, S.-W.; Cho, G.-C. Strength durability of gellan gum biopolymer treated Korean sand with cyclic wetting and drying. *Constr. Build. Mater.* **2017**, *143*, 210–221. [CrossRef]
21. Chen, C.; Wu, L.; Harbottle, M. Exploring the effect of biopolymers in near-surface soils using xanthan gum—Modified sand under shear. *Can. Geotech. J.* **2020**, *57*, 1109–1118. [CrossRef]
22. Chen, R.; Lee, I.; Zhang, L. Biopolymer stabilization of mine tailings for dust control. *J. Geotech. Geoenvironmental Eng.* **2015**, *141*, 04014100. [CrossRef]
23. Lemboye, K.; Almajed, A.; Alnuaim, A.; Arab, M.; Alshibli, K. Improving sand wind erosion resistance using renewable agriculturally derived biopolymers. *Aeolian Res.* **2021**, *49*, 100663. [CrossRef]
24. Adamczuk, A.; Jozefaciuk, G. Impact of Chitosan on the Mechanical Stability of Soils. *Molecules* **2022**, *27*, 2273. [CrossRef] [PubMed]
25. ASTM D6913-17; Standard Test Methods for Particle-Size Distribution (Gradation) of Soils Using Sieve Analysis. ASTM International Standards Organization: West Conshohocken, PA, USA, 2017; pp. 1–34.
26. ASTM D4318-17; Standard Test Methods for Liquid Limit, Plastic Limit, and Plasticity Index of Soils. ASTM International Standards Organization: West Conshohocken, PA, USA, 2017; pp. 1–20.
27. Jindal, N.; Singh Khattar, J. Chapter 4—Microbial Polysaccharides in Food Industry. In *Biopolymers for Food Design, Handbook of Food Bioengineering*; Grumezescu, A.M., Holban, A.M., Eds.; Academic Press: Cambridge, MA, USA, 2018; pp. 95–123.
28. Wiszniewski, M.; Skutnik, Z.; Cabalar, A.F. Laboratory assessment of permeability of sand and biopolymer mixtures. *Annals of Warsaw University of Life Sciences—SGGW. Land Reclam.* **2013**, *45*, 217–226.
29. Chang, I.; Im, J.; Prasadhi, A.K.; Cho, G.-C. Effects of Xanthan gum biopolymer on soil strengthening. *Constr. Build. Mater.* **2015**, *74*, 65–72. [CrossRef]
30. Rayment, P.; Ellis, P.R. GUMS | Nutritional Role of Guar Gum. In *Encyclopedia of Food Sciences and Nutrition*, 2nd ed.; Caballero, B., Ed.; Academic Press: Oxford, UK, 2003; pp. 3012–3021.
31. Thombare, N.; Jha, U.; Mishra, S.; Siddiqui, M.Z. Guar gum as a promising starting material for diverse applications: A review. *Int. J. Biol. Macromol.* **2016**, *88*, 361–372. [CrossRef] [PubMed]
32. Ayeldeen, M.K.; Negm, A.M.; El Sawwaf, M.A. Evaluating the physical characteristics of biopolymer/soil mixtures. *Arab. J. Geosci.* **2016**, *9*, 371. [CrossRef]
33. Dehghan, H.; Tabarsa, A.; Latifi, N.; Bagheri, Y. Use of xanthan and guar gums in soil strengthening. *Clean Technol. Environ. Policy* **2018**, *21*, 155–165. [CrossRef]
34. Toufigh, V.; Kianfar, E. The effects of stabilizers on the thermal and the mechanical properties of rammed earth at various humidities and their environmental impacts. *Constr. Build. Mater.* **2019**, *200*, 616–629. [CrossRef]
35. ASTM D559-15; Standard Test Methods for Wetting and Drying Compacted Soil-Cement Mixtures. ASTM: West Conshohocken, PA, USA, 2015; pp. 1–6.
36. ASTM D2166/D2166M-16; Standard Test Method for Unconfined Compressive Strength of Cohesive Soil. ASTM International: West Conshohocken, PA, USA, 2016.

## Article

# Durability, Strength, and Erosion Resistance Assessment of Lignin Biopolymer Treated Soil

Pouyan Bagheri <sup>1,\*</sup>, Ivan Gratchev <sup>1</sup>, Suwon Son <sup>2</sup> and Maksym Rybachuk <sup>3,4</sup>

<sup>1</sup> School of Engineering and Built Environment, Griffith University, Engineering Drive, Southport, QLD 4222, Australia

<sup>2</sup> Department of Architectural and Civil Engineering, Kyungil University, Gyeongsan 38428, Republic of Korea

<sup>3</sup> School of Engineering and Built Environment, Griffith University, 170 Kessels Rd., Nathan, QLD 4111, Australia

<sup>4</sup> Centre for Quantum Dynamics and Australian Attosecond Science Facility, Griffith University, Science Road, Nathan, QLD 4111, Australia

\* Correspondence: pouyan.bagheri@griffithuni.edu.au

**Abstract:** To mitigate the negative environmental effects of the overuse of conventional materials—such as cement—in soil improvement, sustainable engineering techniques need to be applied. The use of biopolymers as an alternative, environmentally friendly solution has received a great deal of attention recently. The application of lignin, a sustainable and ecofriendly biobased adhesive, to enhance soil mechanical properties has been investigated. The changes to engineering properties of lignin-infused soil relative to a lignin addition to soil at 0.5, 1, and 3.0 wt.% (including Atterberg limits, unconfined compression strength, consolidated undrained triaxial characteristics, and mechanical properties under wetting and drying cycles that mimic atmospheric conditions) have been studied. Our findings reveal that the soil's physical and strength characteristics, including unconfined compressive strength and soil cohesion, were improved by adding lignin through the aggregated soil particle process. While the internal friction angle of the soil was slightly decreased, the lignin additive significantly increased soil cohesion; the addition of 3% lignin to the soil doubled the soil's compressive strength and cohesion. Lignin-treated samples experienced less strength loss during wetting and drying cycles. After six repeated wetting and drying cycles, the strength of the 3% lignin-treated sample was twice that of the untreated sample. Soil treated with 3% lignin displayed the highest erosion resistance and minimal soil mass loss of ca. 10% under emulated atmospheric conditions. This study offers useful insights into the utilization of lignin biopolymer in practical engineering applications, such as road stabilization, slope reinforcement, and erosion prevention.

**Keywords:** lignin biopolymer; erosion; soil strength; triaxial test; wetting and drying cycles; silt

**Citation:** Bagheri, P.; Gratchev, I.; Son, S.; Rybachuk, M. Durability, Strength, and Erosion Resistance Assessment of Lignin Biopolymer Treated Soil. *Polymers* **2023**, *15*, 1556. <https://doi.org/10.3390/polym15061556>

Academic Editors: Raffaella Striani and Antonio Pizzi

Received: 2 January 2023

Revised: 11 March 2023

Accepted: 17 March 2023

Published: 21 March 2023



**Copyright:** © 2023 by the authors. Licensee MDPI, Basel, Switzerland. This article is an open access article distributed under the terms and conditions of the Creative Commons Attribution (CC BY) license (<https://creativecommons.org/licenses/by/4.0/>).

## 1. Introduction

Global climate change has dramatically influenced the environment, leading to irreversible changes in the limited resources we rely on. This has urged fundamental sustainable measures to be taken to reduce the consequences of these effects. A major impact of climate change that is significantly affecting the environment around us is extreme weather events, which results in intense localized rainfall in some geographic areas and drought in others. Intense rainfall events may cause instability in the ground properties, bringing a sudden increase in pore water pressure in soil which incurs a reduction in local soil strength, severe runoff, soil erosion, and eventually landslides and slope failures.

To improve the mechanical properties of soil and soil stability, a range of chemical treatments, including the addition of stabilizers to the soil, are often used. Portland cement has traditionally been the most commonly used additive to enhance soil properties. Although Portland cement has been widely used in different geotechnical engineering practices, its application for soil enhancement has been associated with a negative impact

on the environment, alongside the increase of carbon dioxide (CO<sub>2</sub>) emissions during cement production, as cement industries are believed to be responsible for up to 8% of global CO<sub>2</sub> emissions annually [1]. The application of cement for civil and geotechnical engineering purposes is believed to have contributed to several environmental concerns, including the increase in soil pH level [2], cement dust accumulation in soil resulting in soil infertility [3], urban runoff, heat islands, prevention of vegetation growth, and groundwater contamination [4].

Recently, research has been undertaken to use biopolymers, such as organic polymers that occur in abundance in nature and can be extracted from natural resources, as environmentally friendly additives in geotechnical engineering applications [5].

The improvement of soil strength by adding biopolymers, such as xanthan gum, guar gum, beta glucan, chitosan, and lignin, has been attempted before [4–13]. Bagheri et al. [5] examined the effect of xanthan gum on soil strength and confirmed substantial improvement in soil compressive strength within a certain curing time. Through lab studies, Soldo et al. [4] investigated the impact of xanthan gum, beta glucans, guar gum, chitosan, and alginate biopolymers on silty sand soil. They reported significant increases in biopolymer-treated soil strengths over a longer period. The effectiveness of gellan gum biopolymer against soil permeability [14] and dextran for surface erosion [13] were investigated. Ham et al. [13] added a microbial biopolymer, dextran, to the fine silica sand and showed that the biopolymer can increase erosion resistance. Zhang et al. [15] performed the shear-wave velocity test and unconfined compression test to assess the small-strain shear modulus and unconfined compressive strength of lignin-stabilised silty soil. They found that a small-strain shear modulus and the unconfined compressive strength of lignin-treated soil logarithmically increased with curing period.

To increase the effectiveness of biopolymer treatment, *in situ* influencing factors must be taken into consideration. Although lignin has been shown to boost soil strength [10,15], prior research largely focused on analyzing basic strengthening behavior and confirming viability. In particular, *in situ* three-dimensional stress conditions have not received significant consideration. In addition, studies that address changes in mechanical strength of lignin-treated soils under saturated conditions have been limited, including those concerned with the erosion resistance of biopolymer-treated soil. Furthermore, the earlier reports mostly evaluated the shear behaviour of biopolymer-treated soils by means of direct shear tests using dried soil samples that may not adequately represent the underground conditions.

Lignin was chosen for use in the current investigation because it has been demonstrated to be one of the most economically advantageous materials among all available biopolymers in geotechnical engineering [16].

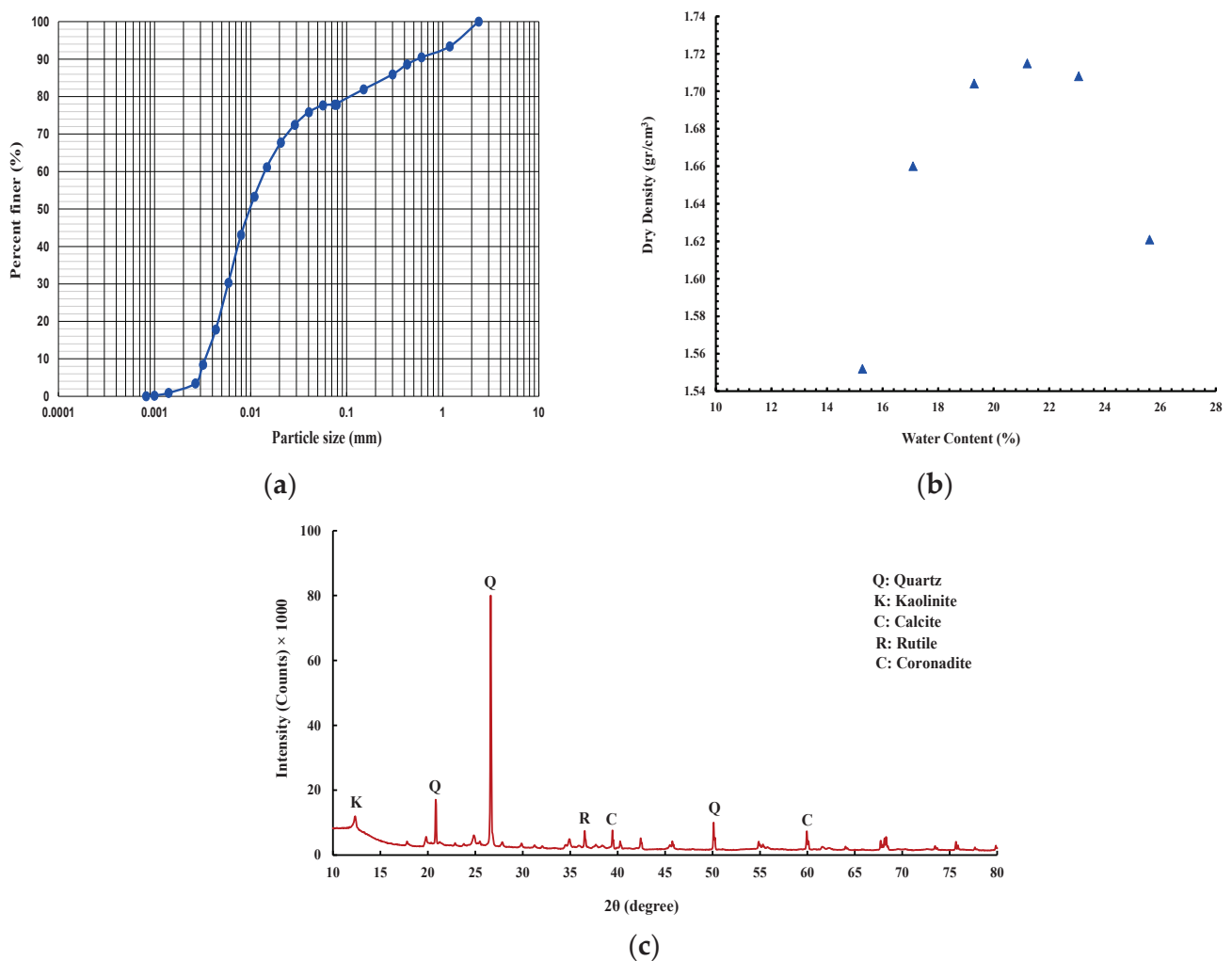
This study aims to address the mentioned gaps by performing a thorough study to examine the effect of lignin biopolymer agent on the soil mechanical properties subjected to various conditions. A range of laboratory experiments, including Atterberg limits tests and unconfined compressive strength (UCS) tests for the lignin-treated soil samples were conducted to obtain the engineering performance, soil strength, and plasticity behaviour. To investigate the effect of lignin additive on the soil shear strength and shear parameters and simulate *in situ* three-dimensional stress conditions, CU triaxial tests were performed. The durability and strength of lignin-treated soil under wetting and drying cycles were examined. The erosion resistance and soil loss of biopolymer-treated specimens exposed to natural atmospheric conditions were also examined. Finally, scanning electron microscopy (SEM) analyses were conducted to evaluate the microstructure mechanism of such treatment approaches.

The outcome of this study provides an enhanced understanding of the engineering behaviour of lignin-treated soil subjected to different conditions and facilitates the use of such sustainable techniques in civil and geotechnical practices.

## 2. Materials and Methods

### 2.1. Materials

Regarding soil, a low-plasticity silt soil (USCS classification: ML) according to ASTM D2487-17 [17] has been obtained from the Gold Coast area, Australia, with the grain size distribution as shown in Figure 1a obtained following the ASTM D422-63 [18]. The soil sample displayed plastic and liquid limits and a plasticity index of 26.9, 38, and 11.1, respectively, as measured in accordance with ASTM D4318-17 [19]. The specific gravity of the soil was 2.77, according to the ASTM D854-14 [20]. The standard proctor compaction test following ASTM D698-12 [21] was performed to obtain the maximum dry density of (1.72 g/cm<sup>3</sup>) and optimum moisture content of (21.7%) (Figure 1b).



**Figure 1.** (a) Grain size distribution. (b) Compaction test result. (c) X-ray diffraction (XRD) patterns of soil.

The mineral compositions of the soil were supplied by X-ray diffraction (XRD) analysis (Figure 1c). As seen from the soil XRD patterns, quartz is the main mineral with additional inclusions of kaolinite and calcite.

Regarding biopolymers, the lignin (LIG) was calcium lignosulphonate obtained from Dustex, Australia. The material was a brown viscose liquid with a pH (10% solution) of  $5.4 \pm 3.0$ , dry matter of  $55.0 \pm 1.0\%$ , and a density of  $1285 \text{ kg/m}^3$ . The LIG was a mixture of water (51%) and calcium lignosulfonate (49%).



## 2.2. Specimen Preparation

Initially, the soil was oven dried, and then the gravel was removed by crushing and sieving to 2.36 mm. Three concentrations of soil to LIG mixtures at 0.5 wt.%, 1.0 wt.%, and 3.0 wt.% were used in the study.

The wet mixture approach, as described by Ta'negonbadi et al. [10], was used to prepare LIG soil mixture. The LIG liquid was first added to the water to reach the desired moisture content, and then the diluted solution was sprayed and thoroughly mixed with the dry soil to prepare the homogenous blend.

The obtained mixtures were wrapped with double-layer plastic wrap and kept in a controlled temperature room for 24 h to prevent the formation of aggregations and ensure a uniform combination of biopolymer with soil particles. The soil mixtures were placed into a cylindrical metal mold (diameter 50 mm, length 150 mm) and evenly compacted in five layers to prepare the samples. The samples with the same diameter and length of around 110 mm were extruded from the mold following each compaction set. Each sample's dry density was guaranteed to be greater than 95% of the maximum dry soil density.

## 2.3. Experimental Measurements

Atterberg limits tests were conducted for the untreated and specified concentrations of LIG-treated soil to evaluate the impact of the biopolymer additive on the soil plasticity.

Regarding UCS tests, the samples were cured in a controlled temperature room for 0, 1, 4, 7, 10, 14, 28, and 35 days. The UCS tests in accordance with [22] were carried out for the cured samples. It is worth noting that three samples for each test were tested to minimize errors. From the outcome of UCS tests, the optimum curing time for treated and untreated samples was chosen for the following experiments.

Triaxial tests were used to examine how saturation conditions affected the strength of soil treated with LIG biopolymer. Consolidated undrained (CU) triaxial tests for the saturated samples were performed at confining pressures of 50, 100, and 200 kPa.

Regarding wetting and drying cycles tests, the durability of biopolymer-treated samples over six wetting/drying cycles was investigated. Polyvinyl chloride (PVC) molds were constructed with a diameter approximately equal to the sample (51 mm) and a higher length of 130 mm, allowing the sample to expand during the wetting cycle. Each wetting and drying cycle was initially started by placing the cured sample into a PVC mold, and then the mold was submerged in water for 24 h. The sample was then dried under room temperature conditions for the given optimum curing time. The UCS test was conducted following each cycle's completion to determine each sample's compressive strength.

Regarding the field experiment, five samples, including two untreated and three treated with the given concentrations of LIG, were exposed to the environment for 30 consecutive days, and soil mass loss of each specimen after exposure to the atmospheric conditions was measured and calculated. Daily temperature, relative humidity, and rainfall were recorded to evaluate the effect of environmental conditions on each sample's integrity.

Regarding SEM analysis, sample morphological examination was performed by using a scanning electron microscopy (SEM) analytical system (TESCAN Mira3, TESCAN Orsay Holdings, Czech Republic) under an acceleration voltage of 5 kV. Magnifications at 2500× and 15,000× were used and reported herein for the untreated, and 3% LIG-treated samples. The samples were platinum sputter coated (ca. 5 nm) immediately before collecting SEM image data.

## 3. Results and Discussion

The following provide the results and thorough examinations of the impact of LIG biopolymer on the soil.

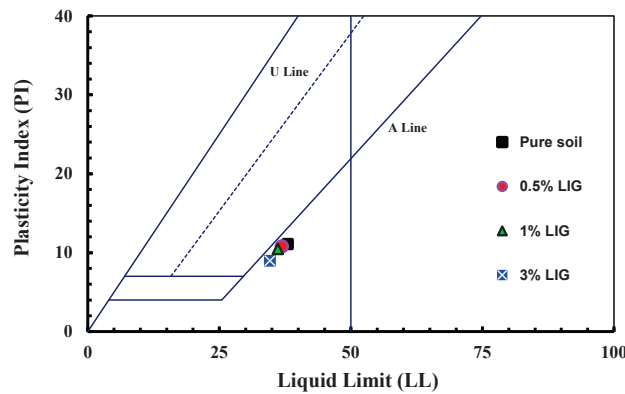
### 3.1. Atterberg Limits

The results of Atterberg limits tests considering different percentages of LIG are presented in Table 1.

**Table 1.** Results of Atterberg limits tests.

Soil Reference	Liquid Limit, LL (%)	Plastic Limit, PL (%)	Plasticity Index, PI (%)
Pure soil	38.0	26.9	11.1
0.5% LIG	36.9	26.1	10.8
1% LIG	36.1	25.6	10.5
3% LIG	34.6	25.6	9.0

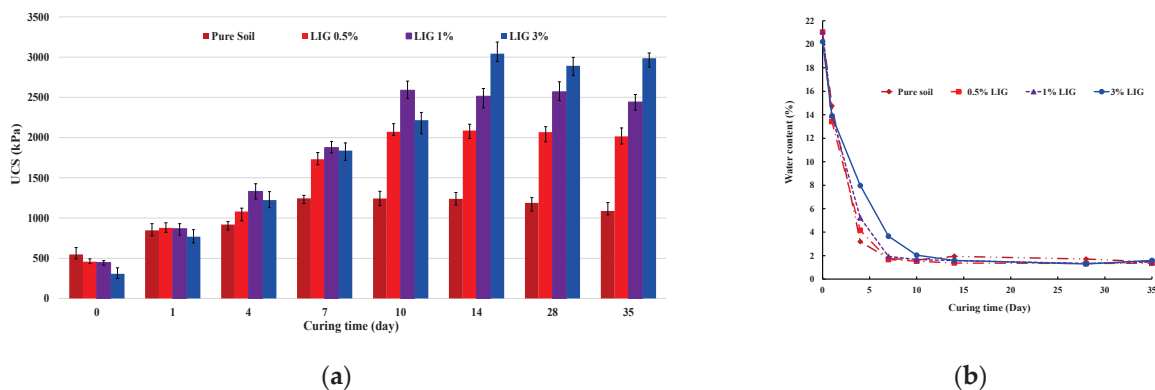
The presence of LIG did not significantly affect PL, while the LIG-treated soil experienced a slight reduction in LL (Table 1). This can be related to the clay particles flocculation [23]. By increasing the content of LIG, the LL slightly decreased while the PL remained almost unchanged. As the soil has some negative charges from clay minerals, LIG may neutralize the negative charges on the surface of soil particles. This brings less thickness to the double electric layer between the soil particles [24]. All LIG-treated samples were placed below the A-Line in the plasticity chart, indicating a slight change in soil plasticity (Figure 2).



**Figure 2.** Plasticity chart for the untreated and LIG-treated soil.

**3.2. Unconfined Compressive Strength (UCS)**

A series of UCS tests for the specified percentages of LIG-treated soils were conducted to ascertain the optimum curing time and analyze the compressive strength of the stabilized samples. Figure 3a displays the changes in UCS for the untreated and LIG-treated soils over various curing times.



**Figure 3.** (a) Changes in UCS for the LIG-treated soil with curing time. (b) Variation of water content with curing time.

Increased biopolymer concentration resulted in increased UCS. While the specimens treated with 0.5% and 1% LIG reached their peak strength after 10 days of curing, the 3% LIG-treated specimen reached its maximum strength after 14 days of curing. The

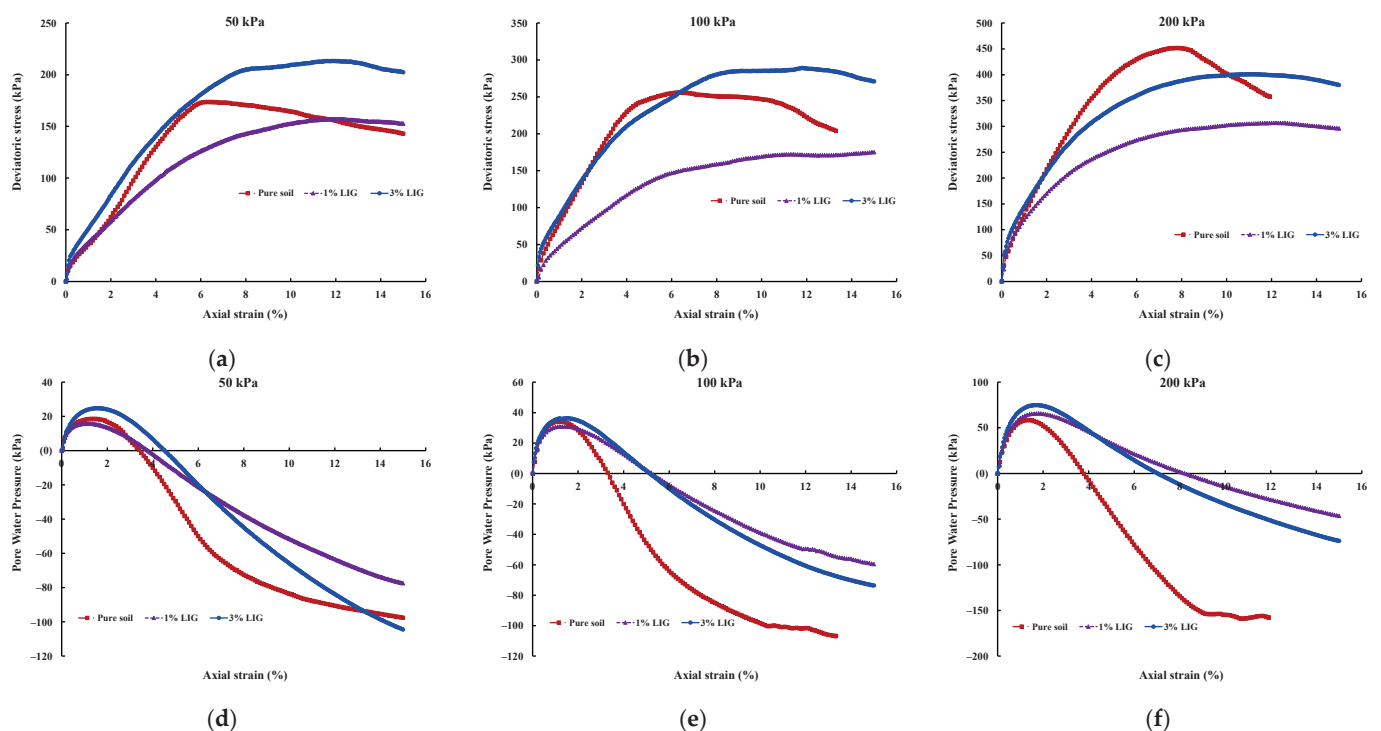
UCS considerably increased within a certain curing time for all LIG concentrations. It demonstrates that additional curing time slightly affects the soil strength. Since moisture content has a significant impact on soil behaviour, the moisture content of each specimen at the end of UCS tests was measured and represented in Figure 3b. A significant drop in water content corresponded to a substantial increase in the soil strength (Figure 3b). When the treated samples dried, the LIG biopolymer acted like a glue leading to a noticeable increase in soil strength.

The curing time corresponding to the highest UCS was considered the optimum and used for the following tests.

### 3.3. Shear Strength

#### CU Triaxial

The effect of LIG biopolymer on the stress-strain curves and shearing-induced pore water pressures for the pure soil, LIG treated specimens are shown in Figure 4.



**Figure 4.** Results of CU triaxial tests, deviatoric stress-axial strain curves for (a) 50 kPa confining pressure; (b) 100 kPa confining pressure; (c) 200 kPa confining pressure; and pore water pressures for (d) 50 kPa confining pressure; (e) 100 kPa confining pressure; (f) 200 kPa confining pressure.

As shown in Figure 4, LIG causes a reduction in the brittleness of soil. Pure soil exhibited brittle behaviour, and peak deviator stress is clearly defined; however, there is no well-outlined peak of shear stress for LIG-treated samples.

The soil treated with 3% LIG experienced slightly higher strength than pure soil, especially at lower confining pressures (Figure 4a). An approximate 10% increase in peak deviator stress was observed once the soil was treated with 3% LIG at 50 kPa confining pressure. This relatively small strength enhancement is attributed to the increase in soil cohesion. In addition, the absolute values of pore water pressures developed upon shearing for soil treated with 3% LIG were marginally higher than the shearing-induced pore water pressures in pure soil (Figure 4d). This implies higher suction upon the shearing stage, which resulted in higher deviatoric stress in 3% LIG treated soil. The higher negative pressure causes an increase in effective stress applied to the soil particles and leads to increased soil shear strength.

To combine the obtained results of shearing of pure soil and LIG-treated soil at various confining pressures, the maximum deviatoric stresses are shown in Figure 5.

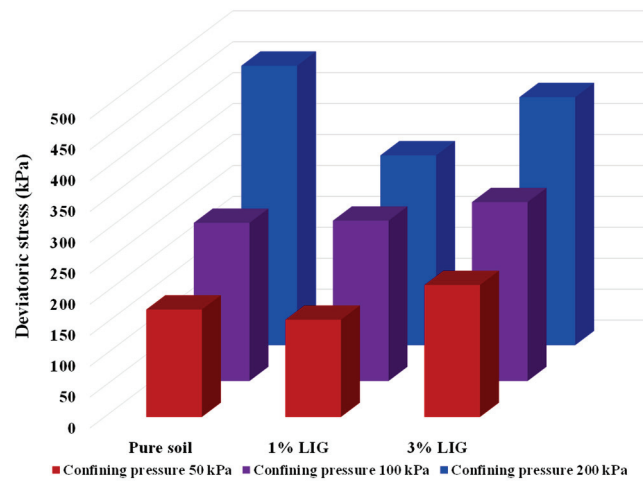


Figure 5. Results of CU triaxial tests, changes in maximum deviatoric stresses at various confining pressures.

Plotted failure envelope curves were used to derive the soil shear parameters for untreated and LIG-treated soil (Figure 6).

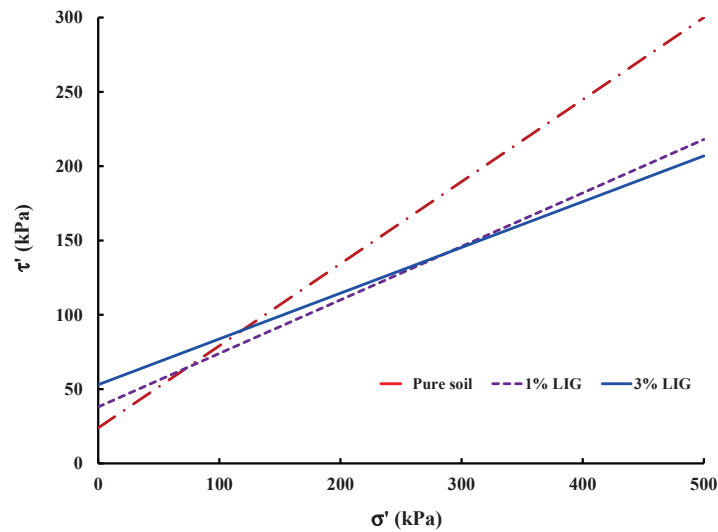


Figure 6. Effective shear stress vs. effective normal stress curves.

While soil friction angle reduced to some extent, a significant increase in soil cohesion occurred due to the LIG additive. Typically, the angularity of soil particles, soil gradation, and normal stress affect the soil friction angle. The LIG additive covers soil particles, smoothing the surface of particles, which causes a reduction in soil grain angularity. This results in a reduction in overall friction angle of soil. Table 2 provides the calculated shear parameters.

Table 2. Effective friction angle and cohesion of pure soil and LIG-treated soil.

Soil Reference	Effective Cohesion, $c'$ (kPa)	Effective Internal Friction Angle, $\phi'$ ( $^\circ$ )
Pure soil	24	28.9
1% LIG	38	24.0
3% LIG	53	22.5



### 3.4. Wetting and Drying Cycles

Figure 7 shows the changes in UCS values over six wetting and drying cycles. As the number of cycles increased, the UCS of the untreated soil gradually dropped. Following a dramatic reduction in the second cycle, the soil strength for the 1% LIG-treated soil was slightly decreased by increasing the wetting and drying cycles. For the highest dosage of LIG, as the number of cycles increased, there was a noticeable decline in soil strength. To clarify the effect of wetting/drying cycles and to better understand the rate of strength reduction over each cycle, the reduction factor ( $R_f$ ) defined as Equation (1) and changes in  $R_f$ , ( $\Delta R_f$ ), were computed and summarized in Table 3. We have

$$R_{f_i} = \left( \frac{|S_i - S_0|}{S_0} \right) \times 100; \Delta R_f = R_{f_{i+1}} - R_{f_i}, \tag{1}$$

where  $S_i$  is the UCS after each cycle, and  $S_0$  is the UCS at cycle 0 (before starting the experiment).

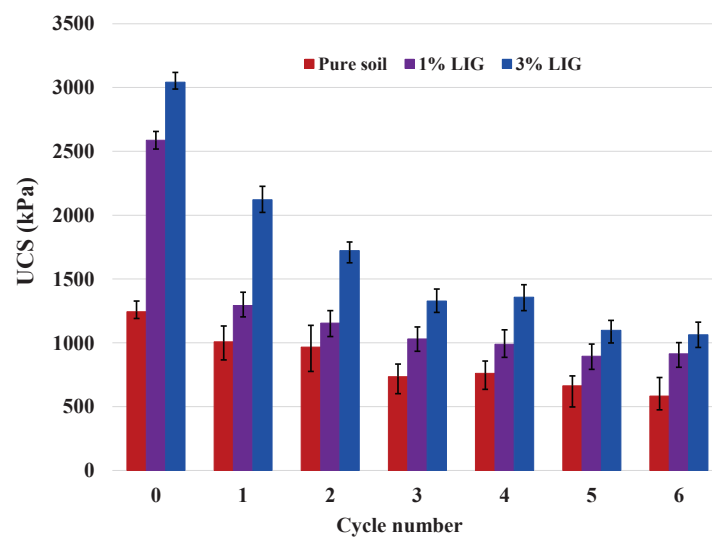


Figure 7. Changes of UCS with wetting and drying cycles.

Table 3. Values of reduction factor and difference in reduction factor during each wetting/drying cycle.

Cycle	$R_f$ (100%)			Cycles	$\Delta R_f$		
	Pure Soil	1% LIG	3% LIG		Pure Soil	1% LIG	3% LIG
0	0.0	0.0	0.0	0–1	19.0	50.1	30.3
1	19.0	50.1	30.3	1–2	3.2	5.3	13.1
2	22.2	55.4	43.4	2–3	16.3	4.8	13.0
3	38.5	60.2	56.4	3–4	0.3	1.6	–1.0
4	38.9	61.8	55.4	4–5	7.8	3.6	8.6
5	46.7	65.4	63.9	5–6	6.4	–0.7	1.1
6	53.1	64.7	65.0				

In all samples, the highest  $R_f$  occurred during the first cycle. As seen after the second cycle, the  $\Delta R_f$  were relatively low, confirming that further wetting/drying cycles did not significantly affect the soil strength. The LIG-treated samples showed higher soil strength than the pure soil sample despite UCS reduction in all specimens. The reason is that after each wetting cycle, once the sample was exposed to the drying cycle, the LIG reattached soil particles and mended the cracks in samples, leading to stronger grain-bonding. This proves the capability of LIG biopolymer in reduction of soil strength loss in comparison with the untreated soil.

### 3.5. Exposure to Atmosphere Conditions

Five samples, including two untreated and three treated with the given concentrations of LIG, were first prepared and placed under atmospheric influences. Daily temperature, relative humidity, and rainfall in the field were recorded (Figure 8). Figure 9 shows the samples exposed to natural atmospheric conditions within 30 days of testing. Even though all samples lost some soil mass during rainfall events, they kept their shapes after two weeks of exposure to the atmospheric conditions. While the untreated samples were damaged and lost almost 22% of their soil masses, the LIG-treated samples kept their shapes. The 3% LIG-treated sample remained nearly intact after 30 days of atmospheric condition exposure. The soil mass loss after 30 days of atmospheric exposure is given in Figure 10. The LIG-treated samples lost less soil mass compared to pure soil samples, confirming the applicability of such treatment technique in improving soil erosion resistance.

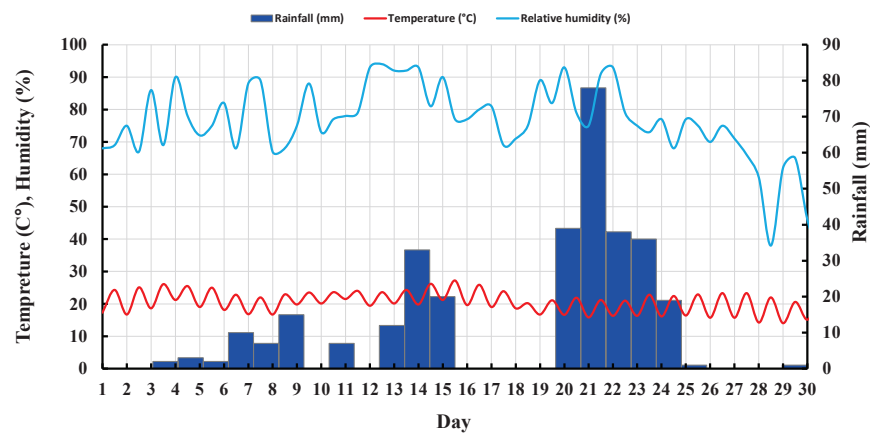


Figure 8. Recorded daily temperature, relative humidity, and rainfall in the field.

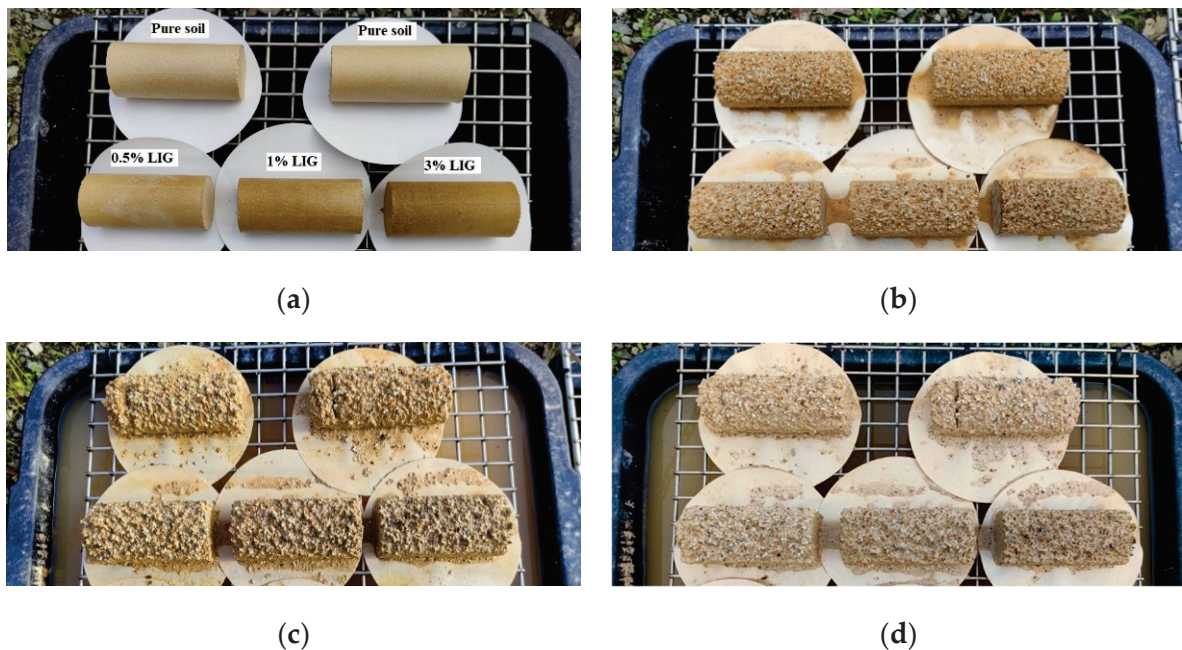


Figure 9. Samples exposed to the atmospheric conditions at (a) day 1, (b) day 14, (c) day 21, and (d) day 28.

### 3.6. SEM Analysis

SEM images of untreated and 3% LIG-treated soil are presented in Figure 11. The structure of soil changed due to lignin additive. The structure of pure soil has changed

from a clumpy and grained-based form (Figure 11a,b) to a combined and more conjunct configuration (Figure 11c,d).

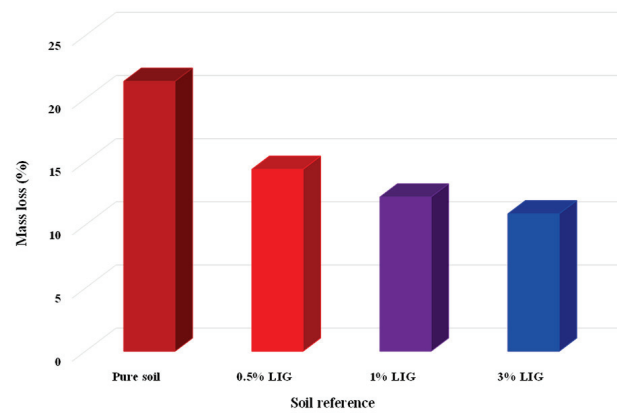


Figure 10. Soil mass loss after exposure to atmospheric conditions.

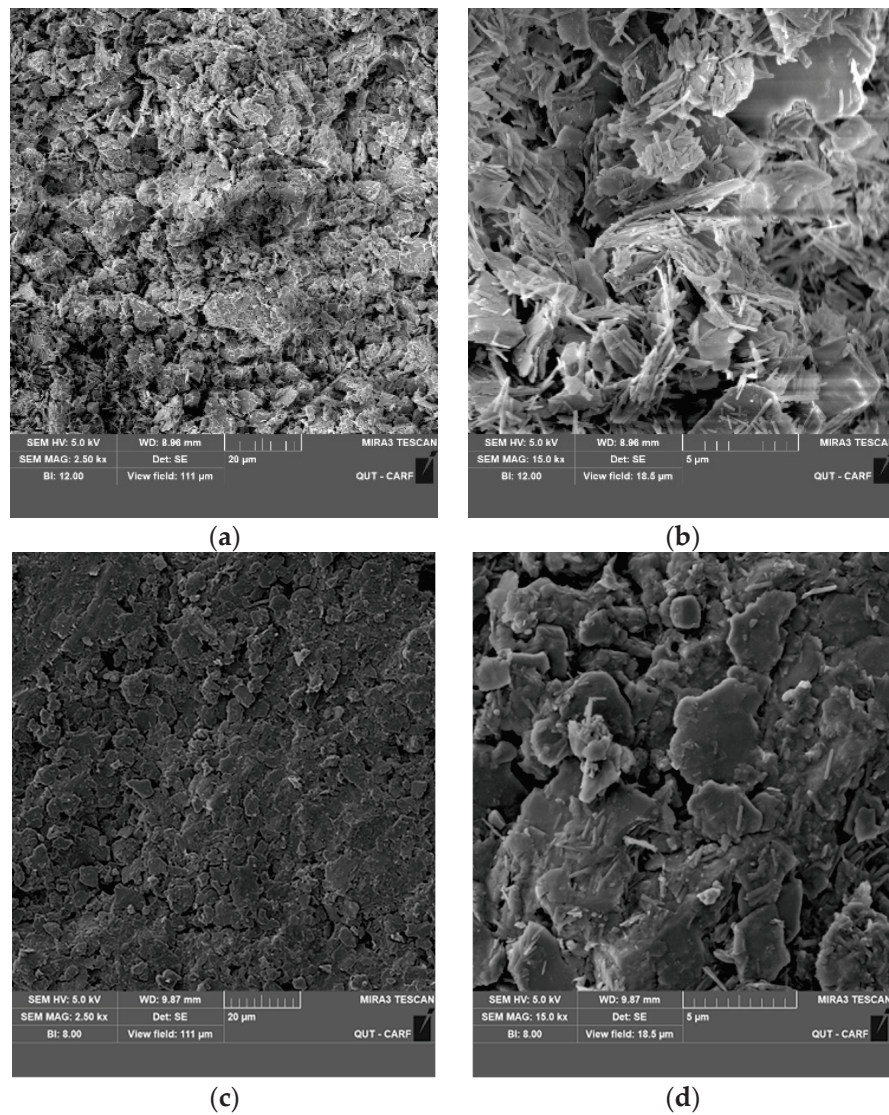


Figure 11. SEM images of the (a) pure soil with 2500× magnification; (b) untreated soil with 15,000× magnification; (c) LIG-treated soil with 2500× magnification; (d) LIG treated soil with 15,000× magnification.



The structure of pure soil is uneven, flaky, and disjointed. There are more obvious chunks of soil particles with larger spaces (Figure 11a,b). However, in treated soil, the pores among soil particles are partially filled with LIG, and a clear biopolymer coating of soil particles' surfaces and boundaries are seen. The soil particle aggregations by the LIG coating of the grains verify the soil strength improvement by adding biopolymer (Figure 11c,d).

#### 4. Conclusions

The major goals of this study were to create an environmentally friendly biopolymer-based soil improvement method and to conduct an experimental investigation into the impact of LIG biopolymer on the mechanical properties and erosion resistance of soil. To achieve these goals, various laboratory and field experiments on three different concentrations of LIG soil mixtures were performed. The following represents a summary of the most significant findings.

- The effect of LIG additive appeared to be insignificant on the soil PL, and a slight reduction in LL and plasticity index was seen.
- The soil compressive strength significantly increased with increasing curing time and LIG dosage. After 14 days of curing, the compressive strength of 3% LIG-treated samples did not go under major changes, and further curing did not affect their strengths. A similar trend was seen for 0.5% and 1% LIG-treated specimens after 10 days of curing.
- At lower confining pressures of CU triaxial tests, the 3% LIG-treated soil experienced slightly higher shear strength than the pure soil. The LIG additive caused significant improvement in soil cohesion and a slight reduction in soil friction angle.
- Despite biopolymers susceptibility to water, during wetting/drying cycles, the LIG biopolymer showed its capability to improve the strength and durability of soil to water. While all samples experienced compressive strength reduction during wetting and drying cycles, the LIG treated samples showed significantly higher strength than pure soil.
- The LIG-treated samples lost less soil mass compared to pure soil samples confirming the applicability of such treatment technique in improving soil erosion resistance.
- This study showed that the LIG biopolymer, a byproduct of paper and sugarcane factories, can effectively improve soil strength and erosion resistance under various conditions. The durability of LIG additive to water during wetting/drying cycles proves its potential application for quick temporary constructions in an arid climate area. Additionally, lower soil mass loss of LIG-treated samples verifies its application in erosion-prone areas.
- As the durability of biopolymers against soil erosion is an important factor and needs further investigation, large-scale field tests should be linked in future studies.

**Author Contributions:** Conceptualization, P.B.; methodology, P.B.; validation, P.B.; formal analysis, P.B.; writing—original draft preparation, P.B.; writing—review and editing, I.G., S.S. and M.R.; supervision, I.G. All authors have read and agreed to the published version of the manuscript.

**Funding:** This research was supported by Basic Science Research Program through the National Research Foundation of Republic of Korea (NRF) funded by the Ministry of Education (grant number: NRF-2022R1I1A1A01054495).

**Institutional Review Board Statement:** Not applicable.

**Data Availability Statement:** The data presented in this study are available on request from the corresponding author.

**Acknowledgments:** This study was performed with the financial support of the Griffith University Postgraduate Research Scholarship (GUPRS). Dustex Australia Pty Ltd is gratefully acknowledged for providing research samples (i.e., lignin) for this study.

**Conflicts of Interest:** The authors declare no conflict of interest.



## References

- Andrew, R.M. Global CO<sub>2</sub> emissions from cement production. *Earth Syst. Sci. Data* **2018**, *10*, 195.
- Bahmani, S.H.; Huat, B.B.K.; Asadi, A.; Farzadnia, N. Stabilization of residual soil using SiO<sub>2</sub> nanoparticles and cement. *Constr. Build. Mater.* **2014**, *64*, 350–359.
- Amani, J.; Babu, K.; Lakshmipathi, R.; Rao, G.R.; Chandrasekhar, K. Effect of Cement Dust Deposition on Soil Microbial Properties. *Int. J. Curr. Microbiol. Appl. Sci.* **2018**, *7*, 1230–1234.
- Soldo, A.; Miletic, M.; Auad, M.L. Biopolymers as a sustainable solution for the enhancement of soil mechanical properties. *Sci. Rep.* **2020**, *10*, 267. [PubMed]
- Bagheri, P.; Gratchev, I.; Rybachuk, M. Effects of Xanthan Gum Biopolymer on Soil Mechanical Properties. *Appl. Sci.* **2023**, *13*, 887. [CrossRef]
- Chang, I.; Cho, G.-C. Shear strength behavior and parameters of microbial gellan gum-treated soils: From sand to clay. *Acta Geotech.* **2019**, *14*, 361–375. [CrossRef]
- Latifi, N.; Horpibulsuk, S.; Meehan, C.L.; Majid, M.Z.A.; Tahir, M.M.; Mohamad, E.T. Improvement of problematic soils with biopolymer—An environmentally friendly soil stabilizer. *J. Mater. Civ. Eng.* **2017**, *29*, 04016204. [CrossRef]
- Chang, I.; Im, J.; Prasadhi, A.K.; Cho, G.-C. Effects of Xanthan gum biopolymer on soil strengthening. *Constr. Build. Mater.* **2015**, *74*, 65–72. [CrossRef]
- Chang, I.; Cho, G.-C. Strengthening of Korean residual soil with  $\beta$ -1, 3/1, 6-glucan biopolymer. *Constr. Build. Mater.* **2012**, *30*, 30–35. [CrossRef]
- Ta'negonbadi, B.; Noorzad, R. Physical and geotechnical long-term properties of lignosulfonate-stabilized clay: An experimental investigation. *Transp. Geotech.* **2018**, *17*, 41–50. [CrossRef]
- Chen, R.; Zhang, L.; Budhu, M. Biopolymer stabilization of mine tailings. *J. Geotech. Geoenviron. Eng.* **2013**, *139*, 1802–1807. [CrossRef]
- Hataf, N.; Ghadir, P.; Ranjbar, N. Investigation of soil stabilization using chitosan biopolymer. *J. Clean. Prod.* **2018**, *170*, 1493–1500. [CrossRef]
- Ham, S.-M.; Noh, D.-H.; Kwon, T.-H.; Muhunthan, B. Improvement of surface erosion resistance of sand by microbial biopolymer formation. *J. Geotech. Geoenviron. Eng.* **2018**, *144*, 06018004. [CrossRef]
- Chang, I.; Im, J.; Cho, G.-C. Geotechnical engineering behaviors of gellan gum biopolymer treated sand. *Can. Geotech. J.* **2016**, *53*, 1658–1670. [CrossRef]
- Zhang, T.; Cai, G.; Liu, S. Assessment of mechanical properties in recycled lignin-stabilized silty soil as base fill material. *J. Clean. Prod.* **2018**, *172*, 1788–1799. [CrossRef]
- Zhang, T.; Cai, G.; Liu, S. Application of lignin-stabilized silty soil in highway subgrade: A macroscale laboratory study. *J. Mater. Civ. Eng.* **2018**, *30*, 04018034. [CrossRef]
- ASTM D2487-17; Standard Practice for Classification of Soils for Engineering Purposes (Unified Soil Classification System). ASTM International: West Conshohocken, PA, USA, 2017.
- ASTM D422-63; Standard Test Method for Particle-Size Analysis of Soils. ASTM International: West Conshohocken, PA, USA, 2017.
- ASTM D4318-17; Standard Test Methods for Liquid Limit, Plastic Limit, and Plasticity Index of Soils. ASTM International: West Conshohocken, PA, USA, 2017.
- ASTM D854-14; Standard Test Methods for Specific Gravity of Soil Solids by Water Pycnometer. ASTM International: West Conshohocken, PA, USA, 2014.
- ASTM D698-12; Standard Test Methods for Laboratory Compaction Characteristics of Soil Using Standard Effort. ASTM International: West Conshohocken, PA, USA, 2014.
- ASTM D2166-06; Standard Test Method for Unconfined Compressive Strength of Cohesive Soil. ASTM International: West Conshohocken, PA, USA, 2010.
- Ta'negonbadi, B.; Noorzad, R. Stabilization of clayey soil using lignosulfonate. *Transp. Geotech.* **2017**, *12*, 45–55. [CrossRef]
- Xin, H.; Wei, M.; Li, G.-Y.; Mu, Y.-H.; Zhou, Z.-W.; Fei, W. Influence of lignosulfonate on mechanical properties of Lanzhou loess. *Rock Soil Mech.* **2017**, *38*, 18–26.

**Disclaimer/Publisher's Note:** The statements, opinions and data contained in all publications are solely those of the individual author(s) and contributor(s) and not of MDPI and/or the editor(s). MDPI and/or the editor(s) disclaim responsibility for any injury to people or property resulting from any ideas, methods, instructions or products referred to in the content.

## Article

# Effect of Spent Coffee Grounds on the Crystallinity and Viscoelastic Behavior of Polylactic Acid Composites

Anne Shayene Campos de Bomfim <sup>1,\*</sup>, Daniel Magalhães de Oliveira <sup>1</sup>, Kelly Cristina Coelho de Carvalho Benini <sup>1</sup>, Maria Odila Hilário Cioffi <sup>1</sup>, Herman Jacobus Cornelis Voorwald <sup>1</sup> and Denis Rodrigue <sup>2</sup>

<sup>1</sup> Fatigue and Aeronautical Materials Research Group, Department of Materials and Technology, UNESP-São Paulo State University, Guaratinguetá 12516-410, SP, Brazil; daniel.m.oliveira@unesp.br (D.M.d.O.); kccbini@gmail.com (K.C.C.d.C.B.); odila.cioffi@unesp.br (M.O.H.C.); h.voorwald@unesp.br (H.J.C.V.)

<sup>2</sup> Center for Research on Advanced Materials (CERMA), Department of Chemical Engineering, Université Laval, Quebec, QC G1V 0A6, Canada; denis.rodrigue@gch.ulaval.ca

\* Correspondence: anne.shayene@unesp.br

**Abstract:** This work investigated the addition of spent coffee grounds (SCG) as a valuable resource to produce biocomposites based on polylactic acid (PLA). PLA has a positive biodegradation effect but generates poor properties, depending on its molecular structure. The PLA and SCG (0, 10, 20 and 30 wt.%) were mixed via twin-screw extrusion and molded by compression to determine the effect of composition on several properties, including mechanical (impact strength), physical (density and porosity), thermal (crystallinity and transition temperature) and rheological (melt and solid state). The PLA crystallinity was found to increase after processing and filler addition (34–70% in the 1st heating) due to a heterogeneous nucleation effect, leading to composites with lower glass transition temperature (1–3 °C) and higher stiffness (~15%). Moreover, the composites had lower density (1.29, 1.24 and 1.16 g/cm<sup>3</sup>) and toughness (30.2, 26.8 and 19.2 J/m) as the filler content increased, which is associated with the presence of rigid particles and residual extractives from SCG. In the melt state, polymeric chain mobility was enhanced, and composites with a higher filler content became less viscous. Overall, the composite with 20 wt.% SCG provided the most balanced properties being similar to or better than neat PLA but at a lower cost. This composite could be applied not only to replace conventional PLA products, such as packaging and 3D printing, but also to other applications requiring lower density and higher stiffness.

**Keywords:** polylactic acid (PLA); spent coffee grounds (SCG); biocomposites; rheological properties; mechanical properties

**Citation:** de Bomfim, A.S.C.; de Oliveira, D.M.; Benini, K.C.C.d.C.; Cioffi, M.O.H.; Voorwald, H.J.C.; Rodrigue, D. Effect of Spent Coffee Grounds on the Crystallinity and Viscoelastic Behavior of Polylactic Acid Composites. *Polymers* **2023**, *15*, 2719. <https://doi.org/10.3390/polym15122719>

Academic Editors: Raffaella Striani and Swarup Roy

Received: 31 March 2023

Revised: 2 June 2023

Accepted: 8 June 2023

Published: 17 June 2023



**Copyright:** © 2023 by the authors. Licensee MDPI, Basel, Switzerland. This article is an open access article distributed under the terms and conditions of the Creative Commons Attribution (CC BY) license (<https://creativecommons.org/licenses/by/4.0/>).

## 1. Introduction

Polylactic acid (PLA) is a well-known biodegradable thermoplastic polymer and is vastly used for packaging and 3D printing applications. It is polymerized by polycondensation or ring-opening polymerization from the lactic acid monomer. Moreover, lactic acid can be fermented from natural sugars such as glucose or sucrose, including the sugars from spent coffee grounds fermentation [1]. The PLA molecular structure and molar mass directly affect the polymer's properties. In particular, thermal properties, such as melting temperature and glass transition temperature, are strongly related to the molecular structure, as well as the thermo-mechanical history of the polymer [2]. Despite its positive effect on the environment due to its biodegradability, PLA is reported to have low ductility, toughness, resistance to moisture, rate of crystallization, and glass transition temperature [3].

To improve the properties, several efforts have been made to fill PLA with different natural fillers as a disperse phase to modify the polymer chain mobility and consequently

enhance its properties [3–6]. Most of the PLA have low crystallinity (3–10%), and filler addition was reported to significantly improve PLA crystallinity by reorganizing the polymeric chains and influencing the crystallization rate via heterogeneous nucleation. For example, PLA filled with sisal (10 wt.%) was compared with polypropylene (PP) composites [7]. The results showed that the PLA composite had a 270% increase in crystallinity, while the PP composite was only improved by 12%. Moreover, a recent review concluded that PLA with improved properties could be developed by using different natural fillers, depending on the application requirements, since natural fibers are diversified and abundant [8].

Spent coffee grounds (SCG), as a residue of coffee beverages, is a valuable resource rich in polysaccharides, polyphenols, and proteins being widely studied for different applications, including composite filler [9]. A recent review discussed the valorization of SCG for biopolymers synthesis and as composites filler, highlighting the great versatility of SCG in improving different polymers properties [10]. Other works investigated PLA filled with different SCG concentrations and treatments to compare with other fillers and additives, showing promising results in improving PLA properties and biodegradability [11–14]. Although various techniques have been used to characterize the composites, none of the works focused on the effect of SCG addition on the material's crystallinity and viscoelastic properties. Combined dynamic mechanical analysis (DMA) and rheology, performed respectively in the solid and melt state of PLA filled with SCG, were not found in the current literature.

Moreover, PLA/SCG composites are a recent topic of research. According to the Scopus database, only 21 documents were published on this subject between 2013 and 2023 (May). The data show an increased tendency over the years. This subject is achieving scientific relevance, considering the number of citations peak in 2022 (177) [15].

Thus, the main objective of this work is to investigate the effect of spent coffee grounds content (0, 10, 20, and 30% wt.) on PLA crystallinity, as well as to determine the effect of crystallinity on the thermo-mechanical and viscoelastic properties of the composites produced via extrusion followed by compression molding. Although some previous works discussed the subject of PLA/SCG composites, the novelty of this work focuses on the characterizations being done in both the solid and melt state after SCG addition, as crystallinity and viscoelastic properties, which directly affect PLA processing and applications, are important for their applications.

## 2. Materials and Methods

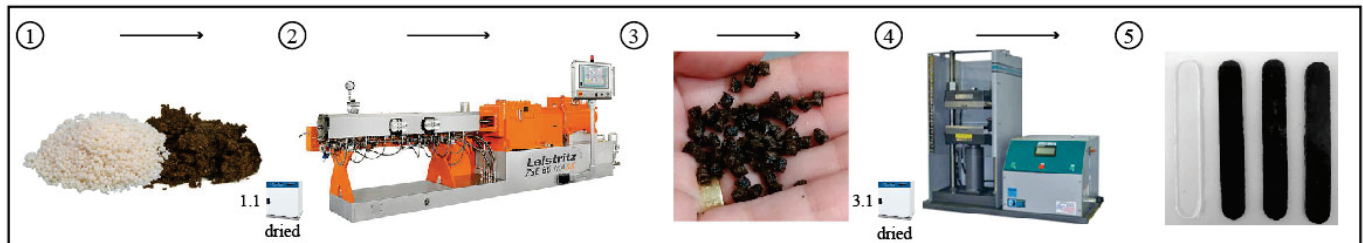
### 2.1. Materials

Pellets of PLA 2003D were supplied from NatureWorks (Minnetonka, MN, USA), while the spent coffee grounds (SCG) were collected as a post-consumer residue (mixture) from coffee shops on the campus of Laval University. Raw SCG was previously dried in an oven at 60 °C for a week to ensure that the moisture was completely removed.

### 2.2. Composite Preparation

The materials were first dried in an oven at 60 °C for 24 h and then mixed in a twin-screw extruder Leistritz ZSE-27 (Remscheid, Germany) having a screw diameter of 27 mm diameter, a L/D ratio (length/diameter) of 40 and 10 heating zone. The PLA pellets were fed in the first zone of the extruder, while the SCG was fed in the fourth zone via a side stuffer. The composition was determined by controlling the specific flow rate for each component (PLA and SCG) by calculating the weight/time ratio (SCG = 0, 10, 20, and 30 wt.%). The extruder was operated at the same constant mass flow rate of 100 g/min and a screw speed of 60 rpm for each composition. The temperature profile in the extruder was controlled at 175 °C (zone 1), 185 °C (zones 2–9), and 165 °C (last zone). A circular die (2.7 mm in diameter) was used to form the melt into a filament shape. The materials were cooled in a water bath close to the die exit (about 10 cm) and then pelletized using a model 304 pelletizer (Conair, Stamford, CT, USA). Then, the pellets were dried in an oven at 60 °C for 48 h before use. Finally, the pellets were molded in an SC7620 automatic

hydraulic press (Carver, Wabash, IN, USA) at 210 °C for 7 min with a constant force of 2 tons and compressing pressure in the mold of 0.5 MPa. The mold and plates were cooled with water circulation for about 3 min until getting to 70 °C. The plates were produced ( $210 \times 210 \times 2.4 \text{ mm}^3$ ) and cut into different specimens for characterization, as described next. The preparation of the composites is illustrated in Figure 1.



**Figure 1.** Preparation of the composites: (1) PLA pellets and raw SCG, (2) the extruder, (3) the composites' extruded pellets, (4) the hydraulic press, and (5) the obtained specimens.

### 2.3. Characterization

#### 2.3.1. Differential Scanning Calorimetry (DSC)

Dual scan analysis was carried out on a DSC Q20 (TA Instruments, New Castle, DE, USA) with a sample weight of around 5 mg in a temperature range from 0 to 200 °C under constant nitrogen flow (40 mL/min). The heating and cooling rate was 10 °C/min. Melting and cold crystallization temperatures ( $T_m$  and  $T_{cc}$ ), as well as melting and cold crystallization enthalpies ( $\Delta H_m$  and  $\Delta H_{cc}$ ) and crystallization degree ( $X_c$ ) were determined from the thermograms (heat flow as a function of temperature). The crystallinity degree was calculated as:

$$X_c = \left[ \frac{\Delta H_m - \Delta H_{cc}}{f \times \Delta H_{m100\%}} \right] 100 \quad (1)$$

where  $\Delta H_{m100\%}$  is the enthalpy of a fully crystalline PLA sample (93.7 J/g), while  $f$  is the weight fraction of PLA (matrix) in the samples [16–18].

#### 2.3.2. Thermo-Gravimetric Analysis (TGA)

TGA was carried out on SII Nanotechnology INC equipment model Exstar 6000—TG/DTA series (Tokyo, Japan) with a sample weight of around 10 mg. The analysis was performed in a platinum pan under a constant nitrogen flow (100 mL/min) in a temperature range from 30 to 600 °C and a heating rate of 10 °C/min. Thermal degradation temperature ( $T_{onset}$ ) was determined via DTG curves where an inflection point was observed in the baseline.

#### 2.3.3. Dynamic Mechanical Analysis (DMA)

DMA was carried out on a RSA3 (TA Instruments, New Castle, DE, USA) using rectangular specimens ( $82.3 \times 12.5 \times 2.4 \text{ mm}^3$ ) cut from the molded plates. A three-point bending geometry was selected with a span of 40 mm. Two types of characterization were performed after strain sweep verification to stay in the linear viscoelastic range of the materials. First, temperature sweeps were done from 25 to 80 °C with a heating rate of 0.5 °C/min and a frequency of 1 Hz. Then, frequency sweeps were performed at room temperature (23 °C) between 0.01 and 25 Hz with a strain of 0.01%.

#### 2.3.4. Rheology

The shear rheological properties in the melt state were studied using a rotational rheometer (ARES, Rheometric Scientific, TA Instruments, New Castle, DE, USA) with a parallel plate geometry (25 mm in diameter). All the analyses were performed under a nitrogen atmosphere. First, strain sweep tests (0.01 to 100%) were performed at a frequency of 1 Hz to determine the linear viscoelastic zone of the samples. Then, frequency sweeps



(0.01 to 40 Hz) were performed at a deformation of 5% using three temperatures: 180, 190, and 200 °C.

### 2.3.5. Impact Test

The Charpy impact strength was performed on a manual impact testing machine Wolfgang Ofist using a 4 J pendulum, type A. Seven rectangular “V” notched specimens ( $82.3 \times 12.5 \times 2.4 \text{ mm}^3$ ) of PLA and its composites were tested at room temperature according to ASTM D6110. The “V” notch was produced by a manual milling machine Vigorelli (type 1), using a bi-angular milling cutter.

### 2.3.6. Density and Porosity

The density of PLA and the composites ( $\rho_r$ ) was measured by a helium gas pycnometer Ultrapyc 1200e (Quantachrome Instruments, Boynton Beach, FL, USA) at room temperature. The samples were previously dried in an oven at 60 °C for 24 h and weighed. To calculate the porosity, the apparent density ( $\rho_a$ ) of the samples was measured via the Archimedes principle using water and calculated as:

$$\rho_a = \frac{w_0 \rho_f}{w_0 - w_1} \quad (2)$$

where  $\rho_f$  is the density of the fluid (water), while  $w_0$  and  $w_1$  are the samples' weight in air and immersed in water, respectively.

The porosity of the samples was calculated from the real ( $\rho_r$ ) and apparent density ( $\rho_a$ ) as:

$$\text{Porosity} = \left(1 - \frac{\rho_a}{\rho_r}\right) \times 100 \quad (3)$$

### 2.3.7. Scanning Electron Microscopy

Morphological analysis of the composites was carried out on the fractured surface of samples after impact testing. The specimens were previously dried and fixed on metal support using carbon adhesive tape before being coated (metalized) with gold. The images were taken with a Zeiss EVO LS-15 scanning electron microscopy (Cambridge, UK) combined with EDS/EBDS Oxford INCA Energy 250 system (Oxford Instruments, Oxfordshire, UK) operating at 5 kV.

### 2.3.8. Statistical Analysis

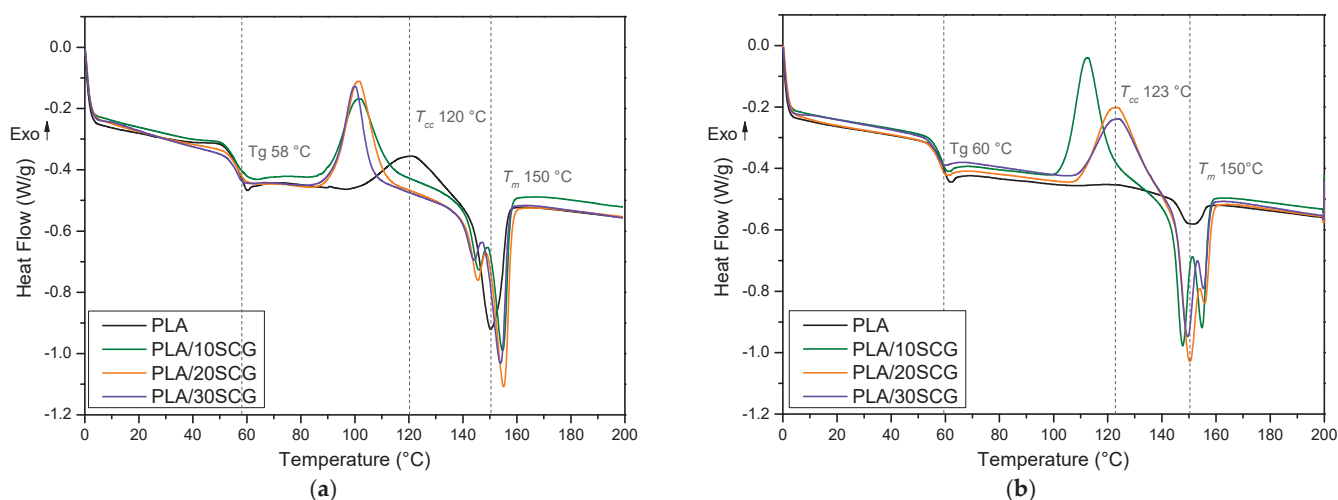
One-way ANOVA and grouping information using the Tukey method to calculate the statistical significance of impact test results were carried out using the statistical software Minitab 18.1 (Minitab Inc., State College, PA, USA). A significance index of 95% ( $p$ -value < 0.05) was used.

## 3. Results and Discussions

### 3.1. DSC and TGA

The DSC curves are presented in Figure 2, and the thermal parameters are summarized in Table 1. The first heating scan eliminates the thermal history from PLA and its composites, providing different values from the second heating scan. The thermal history is directly related to the compression molding conditions, mainly the cooling rate [19]. The cooling scan did not present thermal events, but a crystallization peak appeared in the heating scan, called cold crystallization. According to Table 1, PLA melting temperature ( $T_m$ ) was determined as the endothermic peak at around 150 °C, while cold crystallization temperature ( $T_{cc}$ ) occurred at around 122 °C. However,  $T_{cc}$  was not observed in the second heating scan (Figure 2b) due to a slow crystallization rate and low crystallinity degree (3.4%). For the composites, SCG addition generated the presence of two  $T_m$  in both heating scans. These peaks are related to the melting of the original crystals and the newly formed crystals due to the melt-recrystallization process or the presence of a dual lamellae structure formed

by the various heating scans [20]. Moreover,  $T_{cc}$  was well-defined around 112–123 °C for the composites in both heating scans. This shows that the polymeric chains were more organized after SCG addition due to a heterogeneous nucleation effect [21]. This observation can be confirmed by the significant improvement (34–70% in the 1st heating) of the composites' crystallinity compared to the neat PLA, especially in the second heating scan (about 1500%) (Table 1). The literature also reported PLA crystallinity increases after SCG addition, but the differences were not as high (93% at 15 wt.% and 66% at 20 wt.%) [11,22]. Although composites usually present higher crystallinity as the filler content increases, there is always a maximum related to chain mobility and spatial hindering. In our case, the maximum (70.3%) was observed for PLA/20SCG. This trend can also be related to particle agglomeration in PLA/30SCG acting as defects.



**Figure 2.** DSC curves for PLA and the composites: (a) first heating and (b) second heating.

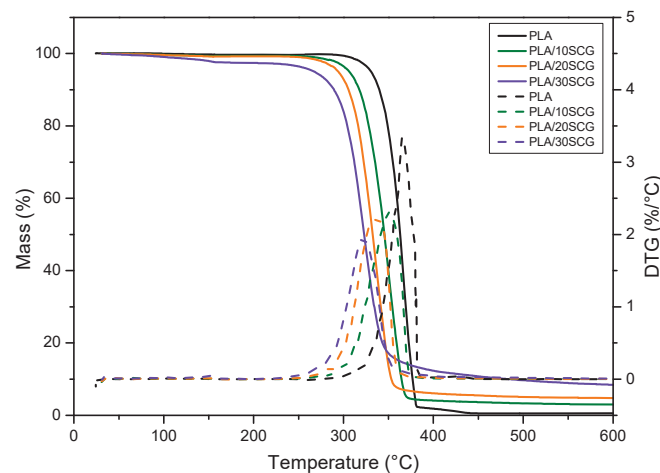
**Table 1.** Thermal parameters obtained via DSC and TGA curves.

Sample	1st Heating							2nd Heating					TGA			
	$T_{m1}$ (°C)	$T_{m2}$ (°C)	$T_{cc}$ (°C)	$\Delta H_m$ (J/g)	$\Delta H_{cc}$ (J/g)	$T_g$ (°C)	$X_c$ (%)	$T_{m1}$ (°C)	$T_{m2}$ (°C)	$T_{cc}$ (°C)	$\Delta H_m$ (J/g)	$\Delta H_{cc}$ (J/g)	$T_g$ (°C)	$X_c$ (%)	$T_{onset}$ (°C)	Residue <sub>600°C</sub> (%)
PLA	150.4	-	120.5	19.9	-18.5	58.3	41.0	150.0	-	-	3.2	-	59.9	3.4	291.3	0.6
PLA/10SCG	146.0	154.7	102.1	25.2	-21.1	55.5	54.9	147.7	154.9	112.5	25.6	-24.3	58.9	59.2	259.3	2.9
PLA/20SCG	145.5	155.1	101.4	28.7	-24.0	57.1	70.3	150.4	155.7	123.6	25.4	-22.5	58.1	63.9	252.7	4.8
PLA/30SCG	144.2	153.9	100.0	24.8	-17.7	56.7	64.8	149.5	155.4	123.9	20.5	-16.6	57.5	56.6	230.7	8.4

Finally, the glass transition temperature ( $T_g$ ) of neat PLA was found to be around 59 °C in the first and second heating scans. This result highlights that the thermal processing of the specimens did not significantly modify the PLA structure (degradation), leading to similar  $T_g$  of the matrix and the composites in the first and second heating scans. However, the composites presented slightly lower  $T_g$  values (2–3 °C difference) than the neat PLA in both scans due to higher polymer chain mobility associated with the presence of rigid particles releasing extractives from SCG. A similar trend of decreasing  $T_g$  was reported for PLA composites using treated SCG [22] and PLA with waste paper [23]. Another work used PLA with grapevine biochar (1 and 10 wt.%) and concluded that the filler acted as a nucleating agent by increasing the crystallinity and reducing the  $T_g$  values of the composites [24]. However, different behavior was identified for PLA/SCG (1–7 wt.%) 3D printed composites in which the  $T_g$  was the same for all samples, mostly influenced by the filler content and the processing conditions [25]. These results show the effect of SCG content, as well as the extrusion/compression steps, on the PLA's crystallinity and chain mobility. Although the presence of rigid fillers should limit polymer chain mobility, SCG

extractives can be released, leading to increased mobility as well as acting as nucleating agents/plasticizers, especially for a higher SCG concentration.

TGA curves are presented in Figure 3, and the thermal parameters are presented in Table 1. The thermal degradation temperature ( $T_{\text{onset}}$ ) was found to decrease as the filler content decreased (11% for PLA/10SCG and 21% for PLA/30SCG). This behavior is not in agreement with the results reported by previous works, such as PLA filled with SCG [26,27], PLA filled with rice straw hydrochar [28], and polypropylene (PP) filled with SCG [29,30]. Moreover, the  $T_{\text{onset}}$  values show that the composites were not degraded in the extrusion/compression processing ( $T < 210$  °C). Residual weight at 600 °C also increased with increasing filler content, which is related to extractives, mostly polysaccharides [31], and ashes from the natural filler. Some works reported that SCG residual weight was in the range of 5–25% [31,32].

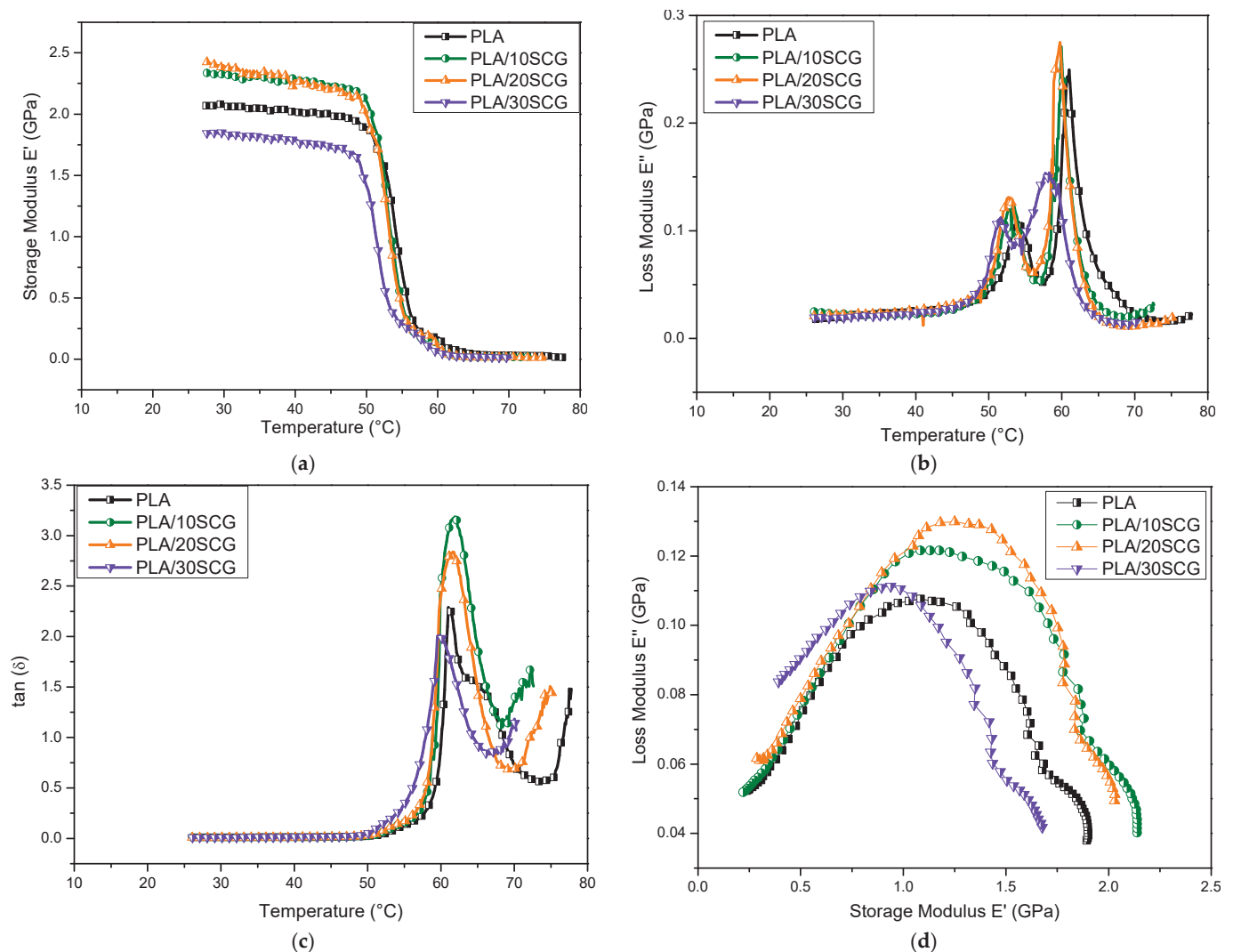


**Figure 3.** TGA curves for PLA and the composites.

### 3.2. Dynamic Mechanical Analysis (DMA)

In the solid state, DMA results are presented in terms of storage modulus ( $E'$ ), loss modulus ( $E''$ ), and  $\tan(\delta)$  ( $= E''/E'$ ) in Figure 4. Figure 4a shows that for  $E'$ , the values at 30 °C were selected for comparison. In this case, PLA/10SCG and PLA/20SCG presented higher values (2.32 and 2.39 GPa, respectively) than PLA/30SCG (1.84 GPa) and PLA (2.07 GPa), indicating that composites with intermediate SCG contents (10–20%) are slightly stiffer and store more energy than neat PLA and 30 wt.% SCG. This trend can be related to the DSC results (Table 1), showing that PLA/20SCG presented the highest crystallinity. Similar storage modulus increases were reported for injection-molded PLA composites filled with SCG and bamboo (30 wt.%) [32] and PLA composites filled with nanocellulose from sugarcane bagasse (1–5 wt.%) [33]. However, recent work reported that PLA/SCG (20 wt.%) with and without lactic acid oligomers had a lower storage modulus compared to neat PLA, which was associated with a plasticization effect caused by the SCG remaining oil [26]. Around 50–60 °C, the storage modulus significantly decreases for all samples, which corresponds to the glass transition range where the material significantly loses stiffness. For the loss modulus ( $E''$ ), Figure 4b shows that the maximum energy dissipation can be determined from the maximum on the  $E''$  curve. By increasing the SCG content, the peak temperature slightly decreased from 61.0 °C to 58.2 °C. Moreover, two transitions were identified in  $E''$  curves. The first one (51–55 °C) corresponds to a secondary transition related to the motion of localized links (bending and stretching) and the relaxation of lateral groups from the polymeric chain, while the second transition (58–61 °C) corresponds to the glass transition temperature ( $T_g$ ). Finally, the damping factor ( $\tan \delta$ ) followed the moduli trends: chain mobility restriction caused by SCG addition directly influenced the damping properties of the polymer [34]. Gonzalez-Lopez et al. (2019) observed a similar trend in PLA composites filled with agave fibers (10–30 wt.%)

and stated that lower  $\tan(\delta)$  with increasing filler concentration may be related to better polymer/filler interaction/adhesion [35]. Other studies supported this observation, such as PLA/polyester/kenaf laminated composite and PLA/silk composite [36,37]. As reported by Hassan et al. (2014), the  $\tan \delta$  peak shifts to higher temperatures, combined with a decreased peak intensity, indicating a restriction of molecular mobility due to improved interactions between the filler and matrix [38].



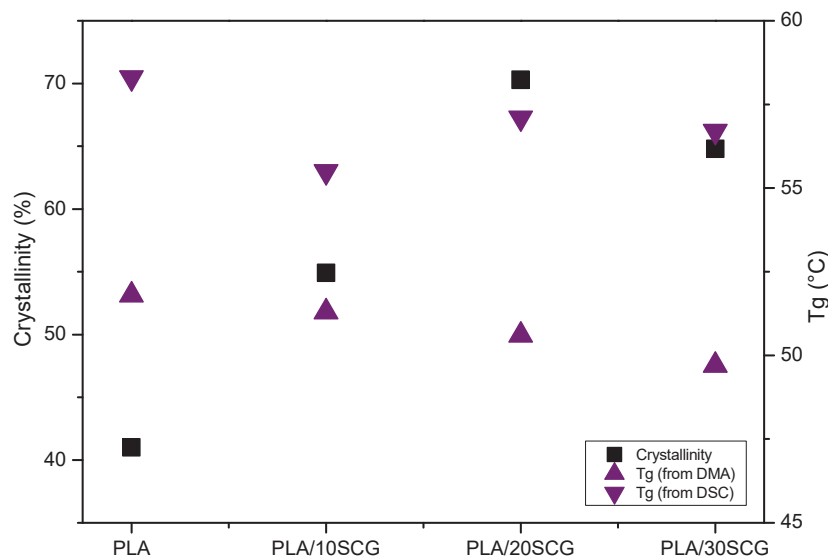
**Figure 4.** DMA curves for PLA and its composites: (a) storage modulus as a function of temperature, (b) loss modulus as a function of temperature, (c)  $\tan(\delta)$  as a function of temperature, and (d) Cole–Cole plots.

Cole–Cole plots ( $E''$  as a function of  $E'$ ) are presented in Figure 4d. It was noticed that semicircular curves are associated with homogenous systems and well-dispersed fillers in a polymeric matrix [33,39]. According to the curves, PLA/10SCG shows the most semicircular arc, similar to PLA, indicating a homogenous composite and good SCG dispersion. However, higher filler content has a more irregular curve, especially for PLA/30SCG. This indicates a more heterogeneous structure with poorly dispersed filler. This is also related to lower crystallinity (Table 1) and lower  $E'$  (Figure 4b) compared to the other composites.

To complete the analysis, Figure 5 compares the glass transition temperature ( $T_g$ ) from DSC (1st heating) and DMA. The  $T_g$  from DMA was determined from  $E'$  curves whose value decreased as the filler content increased: 51.8  $^{\circ}\text{C}$  for PLA, 51.3  $^{\circ}\text{C}$  for PLA/10SCG,



50.6 °C for PLA/20 SCG, and 49.7 °C for PLA/30SCG. This trend is also observed in the  $T_g$  obtained by DSC, emphasizing the effect of filler addition, especially with increasing filler content [40]. The relation between  $T_g$  and crystallinity as a function of filler content is also presented in Figure 5d. It was clearly identified that as the crystallinity increased, the  $T_g$  from DSC and DMA decreased, supporting the SCG effect observed on the polymeric chains.



**Figure 5.** PLA crystallinity (DSC) and  $T_g$  (DSC and DMA) as a function of SCG content.

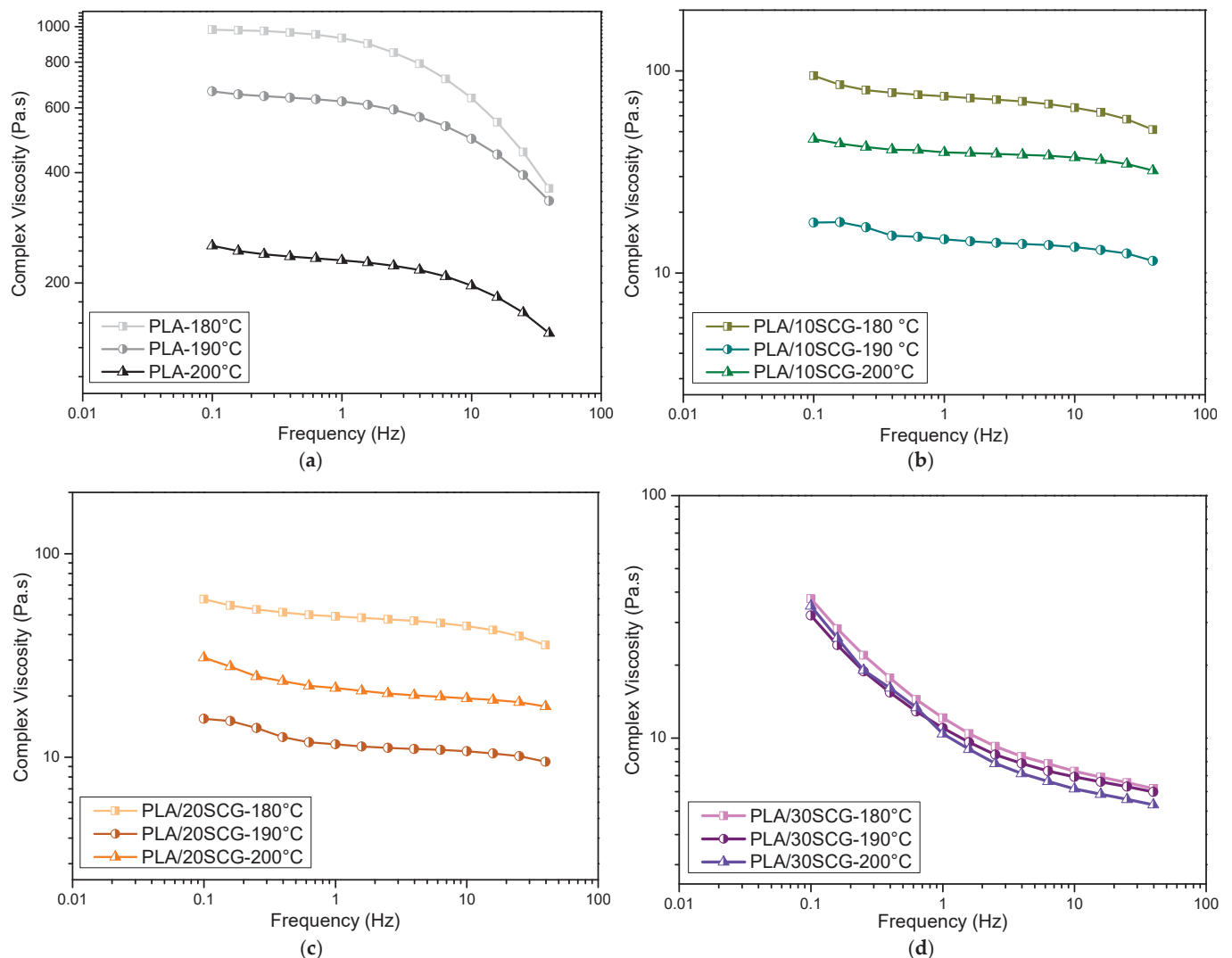
### 3.3. Rheology

The rheological properties in the melt state are reported in Figures 6 and 7 in terms of complex viscosity ( $\eta^*$ ), storage modulus ( $G'$ ), loss modulus ( $G''$ ), and damping factor ( $\tan \delta = G''/G'$ ). Figure 6 is used to determine the effect of temperature, while Figure 7 compares the effect of SCG content.

Figure 6 presents the complex viscosity as a function of frequency for different temperatures. As expected, the viscosity decreases with increasing temperature due to higher chain mobility and less interaction between them (more internal energy). However, the effect of frequency is different with increasing SCG content. For the neat PLA (Figure 6a), typical shear-thinning behavior for the neat polymer is observed with a Newtonian plateau at a low frequency and a power-law (decreasing trend) at a higher frequency. Then, PLA/10SCG and PLA/20SCG mainly have a Newtonian behavior (almost constant viscosity) and a slight shear-thinning behavior at a higher frequency (above 10 Hz). This behavior can be related to several factors, including complex interactions. First, the presence of rigid SCG particles modifies the chain mobility, especially as filler content increases.

The second factor is that higher filler content generates more shear in the extruder, possibly modifying the PLA molecular structure (more polymer degradation). However, this effect should be limited since negligible variations of the thermal properties were observed via DSC (Figure 2) and DMA (Figure 4). There is also a possibility that residual molecules (extractives such as mono/polysaccharides, carbohydrates, lipids, oils, proteins, etc.) are present from the SCG particles themselves (they were only dried and not washed before use) [41], i.e., low molecular weight materials that can act as plasticizers. Actually, this can be associated with the small bump around 155 °C that can be seen in TGA curves (Figure 4). As the SCG content increases, their concentration also increases, leading to different effects/trends on the PLA behavior. The effect is more important in the melt state (Figure 6) than in the solid state (Figure 4), and this is why both characterizations are needed to obtain complete information on these samples. Finally, PLA/30SCG presents a highly non-Newtonian behavior which is related to its higher filler content. The disappearance of

the Newtonian behavior (low frequency) has been associated with the presence of rigid particles having interactions between them, i.e., particle–particle contact [42].

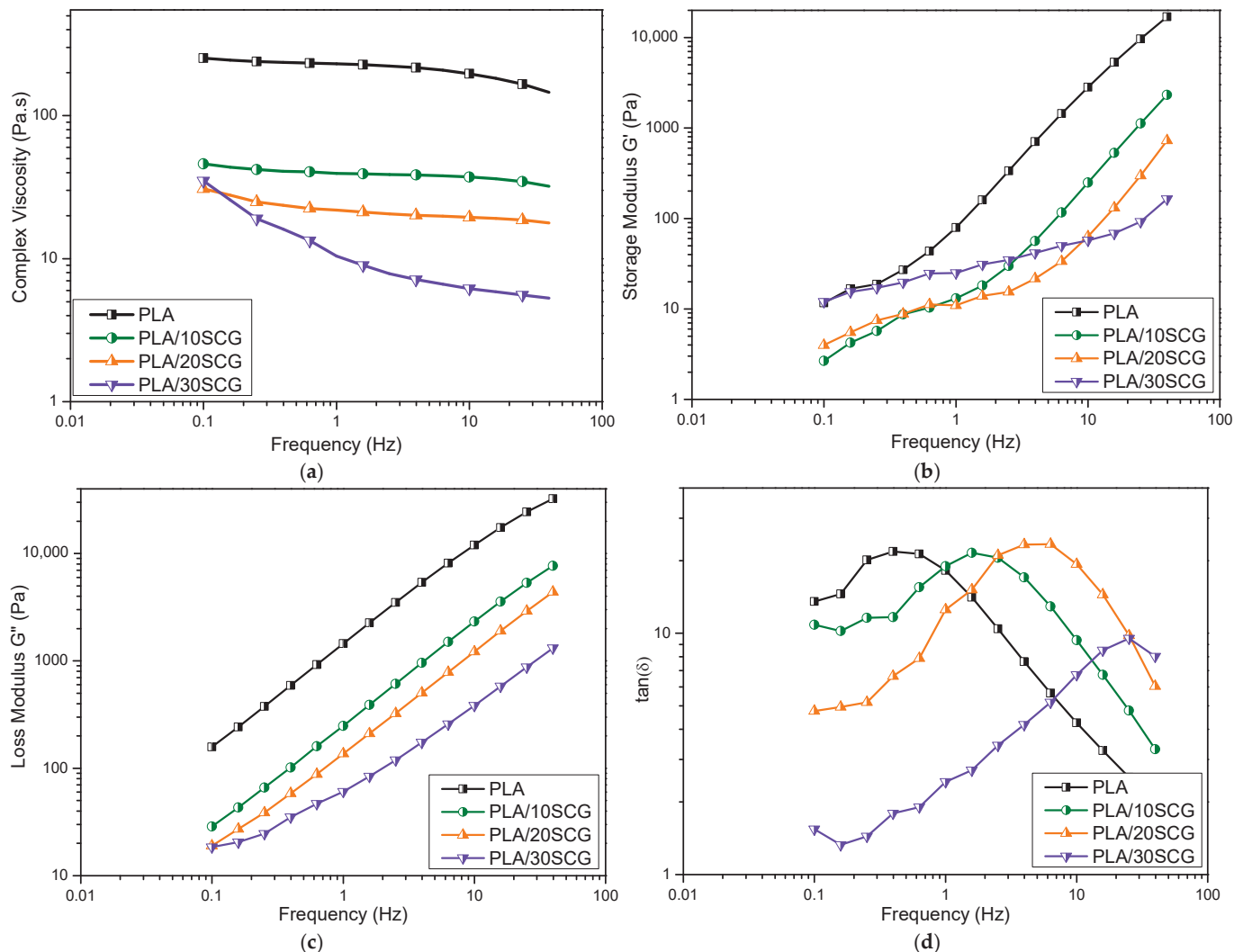


**Figure 6.** Complex viscosity as a function of frequency at different temperatures (180, 190, and 200 °C) for (a) PLA, (b) PLA/10SCG, (c) PLA/20SCG, and (d) PLA/30SCG.

According to Figure 7a, all the composites have a lower viscosity than the neat PLA at 200 °C. In fact, viscosity decreased as the filler content increased, which could be related to increased polymeric chain mobility in the melt state [43]. A similar trend was reported for PLA filaments filled with waste paper (5–15 wt.%) [23], PLA filled with biochar (1–7.5 wt.%) [42], and PLA filled with different waxes, such as beeswax, candelilla, carnauba, and cocoa (3–15 wt.%) [44]. A lower viscosity also suggests that the filler acted as a plasticizer from the presence of extractives, as described above [27]. This reduced viscosity would improve the processability of these materials [22].

The storage modulus ( $G'$ ), loss modulus ( $G''$ ) and loss tangent ( $\tan \delta$ ) are presented in Figure 7. All the samples show that  $G'$  and  $G''$  increase with frequency due to their viscoelastic nature, but the neat PLA again has higher values. At high frequencies (above 10 Hz),  $G'$  and  $G''$  decrease with increasing filler content. In the melt state, PLA is more rigid than the composites. However, as the filler content increases, the composites become less rigid [45]. Nizamuddin et al. (2021) reported on  $G'$  and  $G''$  behavior for PLA/rice straw hydrochar composites (5–20 wt.%), in which the values increased with filler content justified by the reduction of chain mobility leading to higher flow resistance [28]. Another

work investigated PLA filled with cocoa (3–15 wt.%) and observed that at lower frequencies,  $G'$  increased with increasing filler content, but at higher frequencies, a reversed trend was observed as  $G'$  decreased with filler content, which was justified by the plasticizing effect of the natural fillers extractives [44].



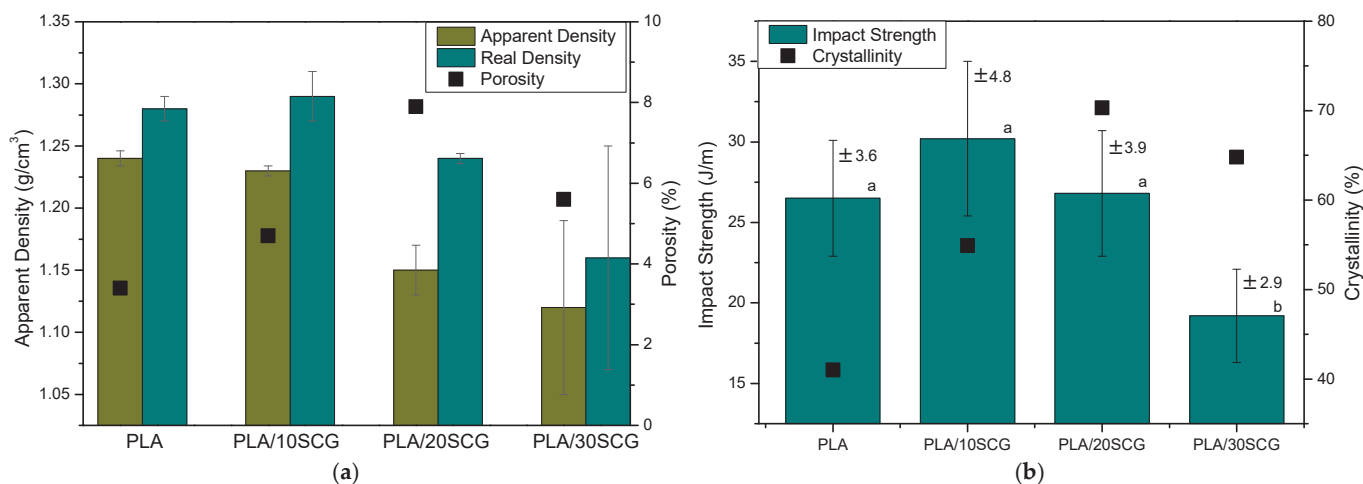
**Figure 7.** Viscoelastic properties as a function of frequency (200 °C) for PLA and the composites: (a) complex viscosity, (b) storage modulus, (c) loss modulus, and (d)  $\tan(\delta)$ .

The value of  $\tan(\delta)$  can be compared to unity to determine the viscous/elastic behavior of the materials [46]. According to Figure 7d, all the samples showed increased  $\tan(\delta)$  at a lower frequency, followed by a decrease at a higher frequency. PLA/10SCG and PLA/20SCG behave similarly to PLA at high frequency and then decreasing  $\tan(\delta)$ , while PLA/30SCG shows an increasing  $\tan(\delta)$  trend for most of the analysis performed. At lower frequency (0.1 Hz), PLA has the highest  $\tan(\delta)$ , indicating a more viscous behavior, while at higher frequency (40 Hz), PLA, PLA/10SCG, and PLA/20SCG present a stiffer behavior and PLA/30SCG a more elastic behavior. This decreasing  $\tan(\delta)$  trend with increasing frequency can be associated with chemical interaction between the polymer and the filler [28]. In this case, PLA/30SCG shows poor polymer-filler interactions, which is consistent with the density/porosity results as described next.

### 3.4. Impact Strength and Density

The real and apparent densities of the composites are presented in Figure 8a. It can be seen that the composites have a lower density than PLA, especially the apparent density.

The density decreased with increasing filler content as the polymer fraction was reduced, and natural fibers are known to be low-density materials. The density of SCG was reported to be  $0.45 \text{ g/cm}^3$  [47]. Such behavior (decreasing composites density) was also identified in PLA composites filled with nettle (10 and 25 wt.%) [48]. Furthermore, it was possible to calculate the porosity of the materials from density values. The results show that the composites have higher porosity than PLA. PLA/10SCG presented the lowest porous content (4.7%), while PLA/20SCG presented the highest value (7.9%), indicating poor dispersion and possible interfacial voids. In addition to the filler addition, the specimens' processing also influenced the porosity of the materials since neat PLA presented 3.4% of porosity. González-López et al. (2019) also reported a decreasing density trend with increasing porosity for PLA/agave composites as the filler content increased (10–30 wt.%), but porosity values were higher than in our work: about 35% for 20 wt.% composite and 60% for 30 wt.% composite [35]. Another work used SCG with high-density polyethylene (HDPE) and found that both density and porosity increased as the filler increased (10–30 wt.%), as 55% of porosity for the 30 wt.% composite [49].



**Figure 8.** Properties of PLA as a function of SCG content: (a) density and porosity, and (b) impact strength and crystallinity.

PLA has a well-known low toughness. From the PLA 2003D datasheet, a value of  $16 \text{ J/m}$  is reported [45]. Nevertheless, after extrusion/compression processing, PLA was found to have good impact strength ( $26.5 \text{ J/m}$ ). Although PLA/10SCG might have a slightly higher value, the composites present a slightly decreased impact strength with increasing filler content (Figure 8b) [11]. PLA filled with agave fibers (10–30 wt.%) was also reported to show lower impact strength with a reduction of 24% for 10 wt.% composite and 41% for the 30 wt.% composite [35]. In some cases, it was reported that filler addition could improve PLA toughness, but an optimum content of around 20 wt.% was observed [3]. Therefore, adding SCG could improve not only the crystallinity (DSC) and stiffness (DMA) of PLA but also its toughness (PLA/10SCG).

Statistical analysis (ANOVA) of the impact test has been carried out, and the results are shown in Table 2. As the  $F$  value (8.40) is greater than the  $F_{\text{critical}}$  value (3.01), the decision is to reject the null hypothesis ( $H_0$ ) (all means are equal) for a significance level of 0.05. In addition, considering that the  $p$ -value is less than the significance level ( $\alpha = 0.05$ ), the  $H_0$  was rejected since the  $p$ -value represents the probability against the null hypothesis. This result indicates that the impact strength of all the samples differs significantly. However, to determine whether the mean difference between any pair of groups is statistically significant, grouping information using the Tukey method and a significance level of 95% were carried out, which are presented with the letters a and b in Figure 8b. In these results, group a contains PLA, PLA/10SCG, and PLA/20SCG, while group b contains PLA/30SCG. The differences between the means of the PLA, PLA/10SCG, and PLA/20SCG, which share



the same letter, are not statistically significant. The PLA/30SCG does not share any letters, indicating a significantly lower mean value for impact strength than the other samples.

**Table 2.** ANOVA test for impact results of PLA and its composites.

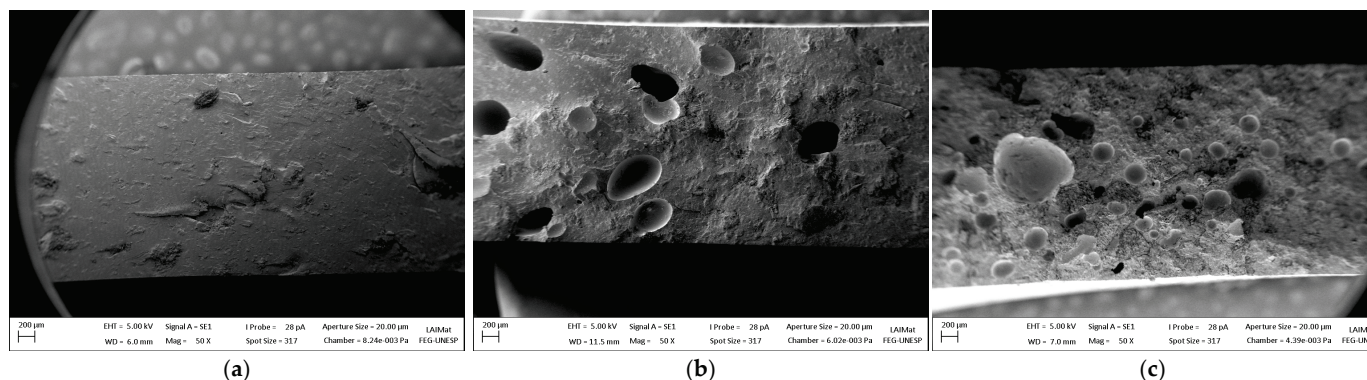
Source of Variation	SS	Df	MS	F	p-Value	F <sub>critical</sub>
AG	450.254	3	150.0847	<b>8.396984</b>	<b>0.000543</b>	<b>3.08787</b>
WG	428.9673	24	17.87364			
Total	879.2214	27				

Note: AG—among groups; WG—within groups; Df—degrees of freedom; SS—sum of squares; MS—mean square; F—F-test for one-way ANOVA; Number of observations = 7; Number of samples = 4.

Comparing toughness and crystallinity results, it is possible to identify that both properties increased for PLA/10SCG compared to PLA. Nevertheless, a different trend was observed for the other composites; PLA/20SCG presented the highest crystallinity leading to similar toughness compared to PLA despite presenting a higher porosity. Moreover, PLA/30SCG presented a high crystallinity but lower toughness compared to PLA, which is related to the filler content and the formation of agglomerates acting as stress concentration points, mainly for PLA/30SCG. Overall, it can be concluded that the final properties represent a balance between complex interactions.

### 3.5. Scanning Electron Microscopy

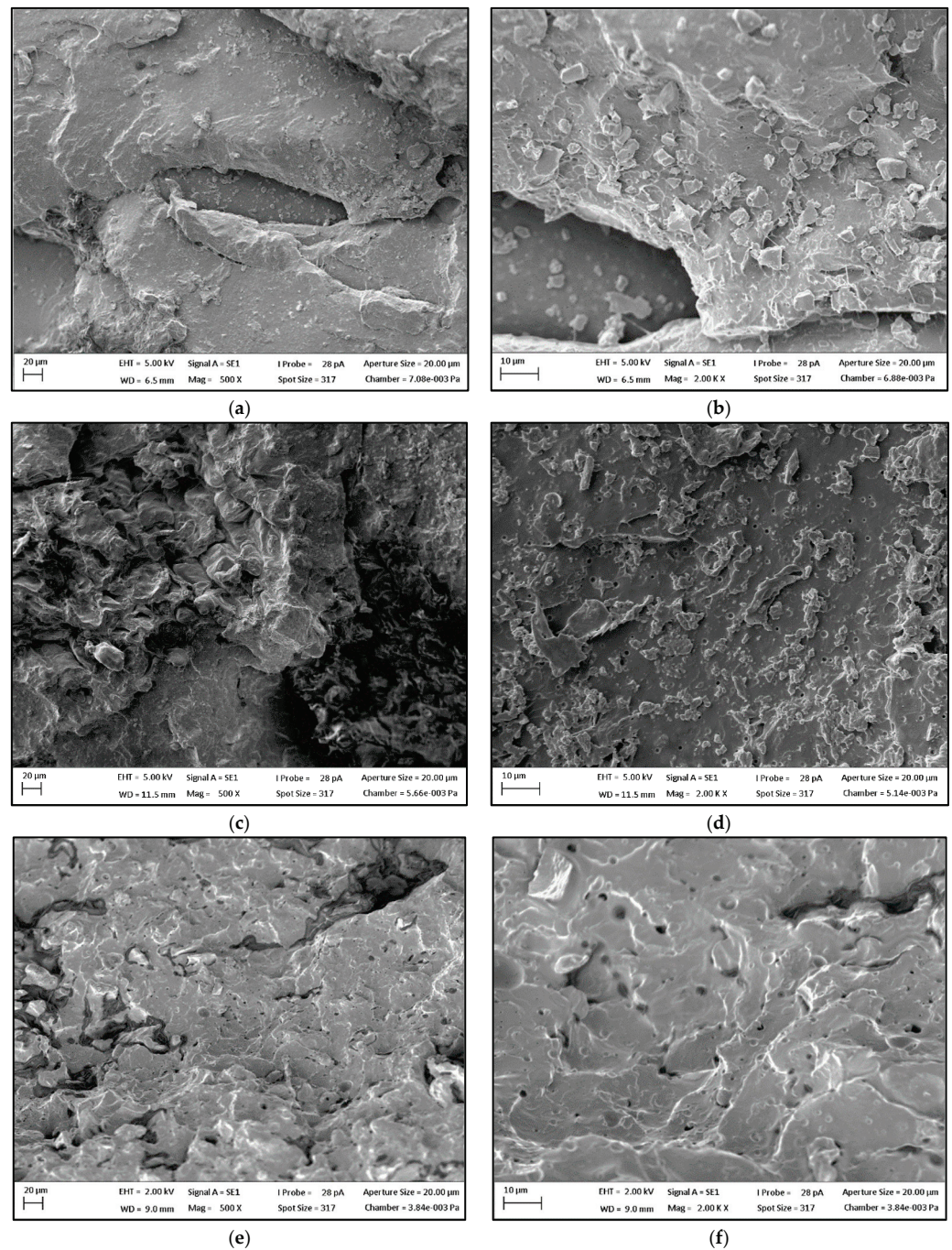
SEM images of the composites are presented in Figures 9 and 10. According to these images, it is possible to identify that PLA/20SCG and PLA/30SCG presented a higher volume and size of voids than PLA/10SCG, which can be seen at lower magnification (Figure 9). These images confirm the relatively high amount of porosity reported in Figure 8 for PLA/20SCG (7.9%) and PLA/30SCG (5.6%).



**Figure 9.** SEM images (magnification of 50×) for (a) PLA/10SCG, (b) PLA/20SCG, and (c) PLA/30SCG.

In addition, small voids were observed all over the matrix for all composites, but they are more evident for PLA/20SCG and PLA/30SCG (Figure 10). It can also be seen that SCG dispersion decreases with increasing filler content as less space is available between the particles leading to more particle–particle contact and agglomeration. Although PLA/30SCG has the highest filler concentration, the particles are very challenging to identify.

It can be concluded that the composites' morphology mostly influenced their thermo-mechanical and viscoelastic behavior, especially for PLA/20SCG and PLA/30SCG.



**Figure 10.** SEM images with different magnifications (500× and 2000×) for (a,b) PLA/10SCG, (c,d) PLA/20SCG, and (e,f) PLA/30SCG.

#### 4. Conclusions

PLA and its composites based on spent coffee grounds (SCG) were successfully prepared via twin-screw extrusion and compression molding. For the range of SCG content investigated (0–30 wt.%), a series of characterizations were performed with a focus on crystallinity, thermo-mechanical (solid state), and viscoelastic (melt state) properties.

The results showed that SCG can act as nucleating agents (solid particles) and plasticizers (extractive release). This led to several differences between the neat matrix (PLA) and the composites (effect of SCG content), as well as complex interactions.

For example, the thermal processing significantly increased the PLA crystallinity, which was further improved with filler addition. Although rigid particles limit polymeric



chain mobility, SCG extractives caused a higher crystallinity and lower  $T_g$ , which is related to higher polymeric chain mobility. Furthermore, as the crystallinity increased, the density and toughness decreased as the filler content increased, while the composite with the lower filler content (10 wt.%) provided a higher toughness than PLA. However, in the melt state, polymeric chain mobility was enhanced, and composites with a higher filler content became less viscous due to the increased chain mobility. This behavior might also be associated with possible residues/extractives acting as plasticizers in the composites.

Although PLA/20SCG showed a higher porosity (7.9%), it provided the best-balanced performances having similar or even better properties than neat PLA and all the other composites. For example, higher crystallinity (38.6%), higher storage modulus at 30 °C (2.38 GPa) and at high frequencies (4.3 GPa at 10 Hz), lower viscosity (19.3 Pa·s at 10 Hz), lower density (1.16 g/cm<sup>3</sup>) and comparable impact strength (26.8 J/m). Nevertheless, PLA/30SCG presented high crystallinity and low density that could influence, to a greater extent, the biodegradability of the material since it was reported that the presence of a biofiller could accelerate the biodegradation process [11].

This work represents a follow-up on previous studies in our groups and the literature. These materials are interesting because they are fully biobased. In the future, more work will focus on the effect of the SCG morphology (particle geometry and size) and composition (washing, extraction, surface modification, etc.) on the final biocomposites' properties. The effect of processing conditions (temperature, pressure, time, velocity, etc.) and method (injection molding, rotomolding, etc.) should also be compared for commercial and industrial applications. The presence of additives (coupling agents) can also be investigated to improve these results. Finally, it would be interesting to investigate the possibility of recycling and composting these materials.

**Author Contributions:** Conceptualization and methodology, A.S.C.d.B. and D.R.; validation, K.C.C.d.C.B., and H.J.C.V.; formal analysis, D.R.; investigation, A.S.C.d.B. and D.M.d.O.; resources, D.R.; data curation, A.S.C.d.B. and D.M.d.O.; writing—original draft preparation, A.S.C.d.B.; writing—review and editing, D.M.d.O., K.C.C.d.C.B., M.O.H.C., H.J.C.V. and D.R.; visualization, A.S.C.d.B. and D.R.; supervision, D.R. and H.J.C.V.; project administration, D.R.; funding acquisition, A.S.C.d.B. and D.M.d.O. All authors have read and agreed to the published version of the manuscript.

**Funding:** This research was funded by Coordenação de Aperfeiçoamento de Pessoal de Nível Superior—Brazil (CAPES), finance code 001, and grant number, 88887.495399/2020-00, and the Fundação de Amparo à Pesquisa do Estado de São Paulo (FAPESP), grants 2019/02607-6 and 2020/02361-4.

**Institutional Review Board Statement:** Not applicable.

**Data Availability Statement:** Not applicable.

**Acknowledgments:** The authors would like to acknowledge Université Laval and São Paulo State University for their administrative and technical support.

**Conflicts of Interest:** The authors declare no conflict of interest.

## References

1. Lee, K.H.; Jang, Y.W.; Lee, J.; Kim, S.; Park, C.; Yoo, H.Y. Statistical optimization of alkali pretreatment to improve sugars recovery from spent coffee grounds and utilization in lactic acid fermentation. *Processes* **2021**, *9*, 494. [CrossRef]
2. Inkinen, S.; Hakkarainen, M.; Albertsson, A.C.; Södergård, A. From lactic acid to poly(lactic acid) (PLA): Characterization and analysis of PLA and Its precursors. *Biomacromolecules* **2011**, *12*, 523–532. [CrossRef]
3. Murariu, M.; Dubois, P. PLA composites: From production to properties. *Adv. Drug Deliv. Rev.* **2016**, *107*, 17–46. [CrossRef] [PubMed]
4. Suaduang, N.; Ross, S.; Ross, G.M.; Pratumshat, S.; Mahasaranon, S. Effect of spent coffee grounds filler on the physical and mechanical properties of poly(lactic acid) bio-composite films. *Mater. Today Proc.* **2019**, *17*, 2104–2110. [CrossRef]
5. Su, J.; Jiang, Z.; Fang, C.; Zheng, Y.; Yang, M.; Pei, L.; Huang, Z. The Reinforcing Effect of Waste Corrugated Paper Fiber on Poly(lactic Acid). *Polymers* **2022**, *14*, 3562. [CrossRef] [PubMed]
6. Heidarian, P.; Behzad, T.; Karimi, K.; Sain, M. Properties investigation of recycled poly(lactic acid) reinforced by cellulose nanofibrils isolated from bagasse. *Polym. Compos.* **2018**, *39*, 3740–3749. [CrossRef]

7. Ngaowthong, C.; Borůvka, M.; Běhálek, L.; Lenfel, P.; Švec, M.; Dangtungee, R.; Siengchin, S.; Mavinkere, S.; Parameswaranpillai, J. Recycling of sisal fiber reinforced polypropylene and polylactic acid composites: Thermo-mechanical properties, morphology, and water absorption behavior. *Waste Manag.* **2019**, *97*, 71–81. [CrossRef]
8. Ilyas, R.A.; Zuhri, M.Y.M.; Aisyah, H.A.; Asyraf, M.R.M.; Hassan, S.A.; Zainudin, E.S.; Sapuan, S.M.; Sharma, S.; Bangar, S.P.; Jumaidin, R.; et al. Natural Fiber-Reinforced Polylactic Acid, Polylactic Acid Blends and Their Composites for Advanced Applications. *Polymers* **2022**, *14*, 202. [CrossRef]
9. McNutt, J.; He, Q. (Sophia) Spent coffee grounds: A review on current utilization. *J. Ind. Eng. Chem.* **2019**, *71*, 78–88. [CrossRef]
10. Bomfim, A.S.C.D.; de Oliveira, D.M.; Voorwald, H.J.C.; Benini, K.C.C.d.C.; Dumont, M.-J.; Rodrigue, D. Valorization of Spent Coffee Grounds as Precursors for Biopolymers and Composite Production. *Polymers* **2022**, *14*, 437. [CrossRef] [PubMed]
11. da Silva, A.P.; Pereira, M.d.P.; Passador, F.R.; Montagna, L.S. PLA/Coffee Grounds Composites: A Study of Photodegradation and Biodegradation in Soil. *Macromol. Symp.* **2020**, *394*, 1–9. [CrossRef]
12. Songtipya, L.; Limchu, T.; Phuttharak, S.; Songtipya, P.; Kalkornsurapranee, E. Poly(lactic acid)-based Composites Incorporated with Spent Coffee Ground and Tea Leave for Food Packaging Application: A Waste to Wealth. *IOP Conf. Ser. Mater. Sci. Eng.* **2019**, *553*, 1–9. [CrossRef]
13. Gama, N.; Ferreira, A.; Evtuguin, D.V. New poly(lactic acid) composites produced from coffee beverage wastes. *J. Appl. Polym. Sci.* **2021**, *139*, 51434. [CrossRef]
14. Yu, I.K.M.; Chan, O.Y.; Zhang, Q.; Wang, L.; Wong, K.-H.; Tsang, D.C.W. Upcycling of Spent Tea Leaves and Spent Coffee Grounds into Sustainable 3D-Printing Materials: Natural Plasticization and Low-Energy Fabrication. *ACS Sustain. Chem. Eng.* **2023**, *11*, 6230–6240. [CrossRef]
15. Scopus Database. Available online: <https://www.scopus.com/results/results.uri?sort=plf-f&src=s&st1=%28%28%22PLA%22+OR+%22polylactic+acid%22%29+AND+%22coffee+grounds%22%29&sid=2ee44e9e778e4ccad9588324a12431ae&sot=b&sdt=b&sl=66&st=TITLE-ABS-KEY%28%28%28%22PLA%22+OR+%22polylactic+acid%22%29+AND+%22coffee+grounds%22%29%29&origin=searchbasic&editSaveSearch=&yearFrom=Before+1960&yearTo=Present> (accessed on 31 May 2023).
16. Garlotta, D. A Literature Review of Poly (Lactic Acid) A Literature Review of Poly (Lactic Acid). *J. Polym. Environ.* **2001**, *9*, 63–84. [CrossRef]
17. Song, Y.; Tashiro, K.; Xu, D.; Liu, J.; Bin, Y. Crystallization behavior of poly(lactic acid)/microfibrillated cellulose composite. *Polymer* **2013**, *54*, 3417–3425. [CrossRef]
18. Perić, M.; Putz, R.; Paulik, C. 3D-printed pla filaments reinforced with nanofibrillated cellulose. *J. Renew. Mater.* **2020**, *8*, 759–772. [CrossRef]
19. Lim, L.T.; Auras, R.; Rubino, M. Processing technologies for poly(lactic acid). *Prog. Polym. Sci.* **2008**, *33*, 820–852. [CrossRef]
20. Yu, B.; Wang, M.; Sun, H.; Zhu, F.; Han, J.; Bhat, G. Preparation and properties of poly (lactic acid)/magnetic Fe<sub>3</sub>O<sub>4</sub> composites and nonwovens. *RSC Adv.* **2017**, *7*, 41929–41935. [CrossRef]
21. Cacciotti, I.; Mori, S.; Cherubini, V.; Nanni, F. Eco-sustainable systems based on poly(lactic acid), diatomite and coffee grounds extract for food packaging. *Int. J. Biol. Macromol.* **2018**, *112*, 567–575. [CrossRef]
22. Li, S.; Shi, C.; Sun, S.; Chan, H.; Lu, H.; Nilghaz, A.; Tian, J.; Cao, R. From brown to colored: Polylactic acid composite with micro/nano-structured white spent coffee grounds for three-dimensional printing. *Int. J. Biol. Macromol.* **2021**, *174*, 300–308. [CrossRef] [PubMed]
23. Tao, Y.; Liu, M.; Han, W.; Li, P. Waste office paper filled polylactic acid composite filaments for 3D printing. *Compos. Part B Eng.* **2021**, *221*, 108998. [CrossRef]
24. Huang, C.C.; Chang, C.W.; Jahan, K.; Wu, T.M.; Shih, Y.F. Effects of the Grapevine Biochar on the Properties of PLA Composites. *Materials* **2023**, *16*, 816. [CrossRef]
25. Yu, W.; Yuan, T.; Yao, Y.; Deng, Y.; Wang, X. PLA/Coffee Grounds Composite for 3D Printing and Its Properties. *Forests* **2023**, *14*, 367. [CrossRef]
26. Terroba-Delgado, E.; Fiori, S.; Gomez-Caturla, J.; Montanes, N.; Sanchez-Nacher, L.; Torres-Giner, S. Valorization of Liquor Waste Derived Spent Coffee Grains for the Development of Injection-Molded Poly lactide Pieces of Interest as Disposable Food Packaging and Serving Materials. *Foods* **2022**, *11*, 1162. [CrossRef] [PubMed]
27. Chang, Y.C.; Chen, Y.; Ning, J.; Hao, C.; Rock, M.; Amer, M.; Feng, S.; Falahati, M.; Wang, L.J.; Chen, R.K.; et al. No Such Thing as Trash: A 3D-Printable Polymer Composite Composed of Oil-Extracted Spent Coffee Grounds and Polylactic Acid with Enhanced Impact Toughness. *ACS Sustain. Chem. Eng.* **2019**, *7*, 15304–15310. [CrossRef]
28. Nizamuddin, S.; Hossain, N.; Qureshi, S.S.; Al-Mohaimed, A.M.; Tanjung, F.A.; Elshikh, M.S.; Siddiqui, M.T.H.; Baloch, H.A.; Mubarak, N.M.; Griffin, G.; et al. Experimental investigation of physicochemical, thermal, mechanical and rheological properties of polylactide/rice straw hydrochar composite. *J. Environ. Chem. Eng.* **2021**, *9*, 106011. [CrossRef]
29. García-García, D.; Carbonell, A.; Samper, M.D.; García-Sanoguera, D.; Balart, R. Green composites based on polypropylene matrix and hydrophobized spend coffee ground (SCG) powder. *Compos. Part B Eng.* **2015**, *78*, 256–265. [CrossRef]
30. Bomfim, A.S.C.d.; Voorwald, H.J.C.; Benini, K.C.C.d.C.; Oliveira, D.M.d.; Fernandes, M.F.; Cioffi, M.O.H. Sustainable application of recycled espresso coffee capsules: Natural composite development for a home composter product. *J. Clean. Prod.* **2021**, *297*, 1–13. [CrossRef]
31. Getachew, A.T.; Cho, Y.J.; Chun, B.S. Effect of pretreatments on isolation of bioactive polysaccharides from spent coffee grounds using subcritical water. *Int. J. Biol. Macromol.* **2018**, *109*, 711–719. [CrossRef]



32. Baek, B.S.; Park, J.W.; Lee, B.H.; Kim, H.J. Development and Application of Green Composites: Using Coffee Ground and Bamboo Flour. *J. Polym. Environ.* **2013**, *21*, 702–709. [CrossRef]
33. Gond, R.K.; Naik, T.P.; Gupta, M.K.; Singh, I. Development and characterisation of sugarcane bagasse nanocellulose/PLA composites. *Mater. Technol.* **2022**, *37*, 2942–2954. [CrossRef]
34. Lee, C.H.; Khalina, A.; Lee, S.H. Importance of interfacial adhesion condition on characterization of plant-fiber-reinforced polymer composites: A review. *Polymers* **2021**, *13*, 438. [CrossRef]
35. González-López, M.E.; Pérez-Fonseca, A.A.; Cisneros-López, E.O.; Manríquez-González, R.; Ramírez-Arreola, D.E.; Rodrigue, D.; Robledo-Ortiz, J.R. Effect of Maleated PLA on the Properties of Rotomolded PLA-Agave Fiber Biocomposites. *J. Polym. Environ.* **2019**, *27*, 61–73. [CrossRef]
36. Azlin, M.N.M.; Sapuan, S.M.; Zuhri, M.Y.M.; Zainudin, E.S.; Ilyas, R.A. Thermal Stability, Dynamic Mechanical Analysis and Flammability Properties of Woven Kenaf/Polyester-Reinforced Polylactic Acid Hybrid Laminated Composites. *Polymers* **2022**, *14*, 2690. [CrossRef] [PubMed]
37. Ho, M.P.; Wang, H.; Lau, K.T.; Leng, J. Effect of silk fiber to the mechanical and thermal properties of its biodegradable composites. *J. Appl. Polym. Sci.* **2013**, *127*, 2389–2396. [CrossRef]
38. Hassan, M.L.; Mathew, A.P.; Hassan, E.A.; Fadel, S.M.; Oksman, K. Improving cellulose/polypropylene nanocomposites properties with chemical modified bagasse nanofibers and maleated polypropylene. *J. Reinf. Plast. Compos.* **2014**, *33*, 26–36. [CrossRef]
39. Saba, N.; Safwan, A.; Sanyang, M.L.; Mohammad, F.; Pervaiz, M.; Jawaid, M.; Allothman, O.Y.; Sain, M. Thermal and dynamic mechanical properties of cellulose nanofibers reinforced epoxy composites. *Int. J. Biol. Macromol.* **2017**, *102*, 822–828. [CrossRef] [PubMed]
40. Cristea, M.; Ionita, D.; Iftime, M.M. Dynamic mechanical analysis investigations of pla-based renewable materials: How are they useful? *Materials* **2020**, *13*, 5302. [CrossRef] [PubMed]
41. Bomfim, A.S.C.D.; Oliveira, D.M.d.; Walling, E.; Babin, A.; Hersant, G.; Vaneeckhaute, C.; Dumont, M.-J.; Rodrigue, D. Spent Coffee Grounds Characterization and Reuse in Composting and Soil Amendment. *Waste* **2022**, *1*, 2–20. [CrossRef]
42. Arrigo, R.; Bartoli, M.; Malucelli, G. Poly(lactic Acid)–Biochar Biocomposites: Effect of Processing and Filler Content on Rheological, Thermal, and Mechanical Properties. *Polymers* **2020**, *12*, 892. [CrossRef] [PubMed]
43. Ares, A.; Bouza, R.; Pardo, S.G.; Abad, M.J.; Barral, L. Rheological, mechanical and thermal behaviour of wood polymer composites based on recycled polypropylene. *J. Polym. Environ.* **2010**, *18*, 318–325. [CrossRef]
44. Mendoza-Duarte, M.E.; Estrada-Moreno, I.A.; López-Martínez, E.I.; Vega-Rios, A. Effect of the Addition of Different Natural Waxes on the Mechanical and Rheological Behavior of PLA—A Comparative Study. *Polymers* **2023**, *15*, 305. [CrossRef]
45. Cipriano, T.F.; Silva, A.L.N.D.; Silva, A.H.M.D.F.T.D.; Sousa, A.M.F.D.; Silva, G.M.D.; Rocha, M.G. Thermal, rheological and morphological properties of poly (lactic acid) (PLA) and talc composites. *Polímeros Ciência E Tecnol.* **2014**, *24*, 276–282. [CrossRef]
46. Azizi, H.; Ghasemi, I. Investigation on the dynamic melt rheological properties of polypropylene/wood flour composites. *Polym. Compos.* **2009**, *30*, 429–435. [CrossRef]
47. Arulrajah, A.; Maghoolpilehrood, F.; Disfani, M.M.; Horpibulsuk, S. Spent coffee grounds as a non-structural embankment fill material: Engineering and environmental considerations. *J. Clean. Prod.* **2014**, *72*, 181–186. [CrossRef]
48. Kumar, N.; Das, D. Fibrous biocomposites from nettle (*Girardinia diversifolia*) and poly(lactic acid) fibers for automotive dashboard panel application. *Compos. Part B Eng.* **2017**, *130*, 54–63. [CrossRef]
49. Mendes, J.F.; Martins, J.T.; Manrich, A.; Luchesi, B.R.; Dantas, A.P.S.; Vanderlei, R.M.; Claro, P.C.; Neto, A.R.d.S.; Mattoso, L.H.C.; Martins, M.A. Thermo-physical and mechanical characteristics of composites based on high-density polyethylene (HDPE) e spent coffee grounds (SCG). *J. Polym. Environ.* **2021**, *29*, 2888–2900. [CrossRef]

**Disclaimer/Publisher’s Note:** The statements, opinions and data contained in all publications are solely those of the individual author(s) and contributor(s) and not of MDPI and/or the editor(s). MDPI and/or the editor(s) disclaim responsibility for any injury to people or property resulting from any ideas, methods, instructions or products referred to in the content.

Review

# Environmental Properties and Applications of Biodegradable Starch-Based Nanocomposites

Ashoka Gamage <sup>1,\*</sup>, Punniamoorthy Thiviya <sup>2</sup>, Sudhagar Mani <sup>3</sup>, Prabakaran Graceraj Ponnusamy <sup>3</sup>, Asanga Manamperi <sup>4</sup>, Philippe Evon <sup>5</sup>, Othmane Merah <sup>5,6,\*</sup> and Terrence Madhujith <sup>7</sup>

<sup>1</sup> Chemical and Process Engineering, Faculty of Engineering, University of Peradeniya, Peradeniya 20400, Sri Lanka

<sup>2</sup> Postgraduate Institute of Agriculture, University of Peradeniya, Peradeniya 20400, Sri Lanka

<sup>3</sup> School of Chemical, Materials and Biomedical Engineering, University of Georgia, Athens, GA 30602, USA

<sup>4</sup> Department of Chemical Engineering, College of Engineering, Kettering University, Flint, MI 48504-6214, USA

<sup>5</sup> Laboratoire de Chimie Agro-Industrielle (LCA), Institut National de la Recherche Agronomique, Université de Toulouse, CEDEX 4, 31030 Toulouse, France

<sup>6</sup> Département Génie Biologique, IUT A, Université Paul Sabatier, 32000 Auch, France

<sup>7</sup> Department of Food Science and Technology, Faculty of Agriculture, University of Peradeniya, Peradeniya 20400, Sri Lanka

\* Correspondence: ashogamage@gmail.com (A.G.); othmane.merah@ensiacet.fr (O.M.); Tel.: +94-714430714 (A.G.); +33-5-3432-3523 (O.M.)

**Abstract:** In recent years, the demand for environmental sustainability has caused a great interest in finding novel polymer materials from natural resources that are both biodegradable and eco-friendly. Natural biodegradable polymers can displace the usage of petroleum-based synthetic polymers due to their renewability, low toxicity, low costs, biocompatibility, and biodegradability. The development of novel starch-based bionanocomposites with improved properties has drawn specific attention recently in many applications, including food, agriculture, packaging, environmental remediation, textile, cosmetic, pharmaceutical, and biomedical fields. This paper discusses starch-based nanocomposites, mainly with nanocellulose, chitin nanoparticles, nanoclay, and carbon-based materials, and their applications in the agriculture, packaging, biomedical, and environment fields. This paper also focused on the lifecycle analysis and degradation of various starch-based nanocomposites.

**Keywords:** biodegradability; carbon nanotubes; graphene; life cycle analysis; nanocomposites; packaging; remediation; starch

**Citation:** Gamage, A.; Thiviya, P.; Mani, S.; Ponnusamy, P.G.; Manamperi, A.; Evon, P.; Merah, O.; Madhujith, T. Environmental Properties and Applications of Biodegradable Starch-Based Nanocomposites. *Polymers* **2022**, *14*, 4578. <https://doi.org/10.3390/polym14214578>

Academic Editor: Raffaella Striani

Received: 3 October 2022

Accepted: 25 October 2022

Published: 28 October 2022



**Copyright:** © 2022 by the authors. Licensee MDPI, Basel, Switzerland. This article is an open access article distributed under the terms and conditions of the Creative Commons Attribution (CC BY) license (<https://creativecommons.org/licenses/by/4.0/>).

## 1. Introduction

In recent days, nanocomposites have gained much attention over traditional composite materials and are widely used in food, packaging, biomedical applications, electronics, energy storage, optics, the automotive industry, bio-sorbants for environmental remediation, textiles, and many other applications [1,2]. Polymer nanocomposites consist of polymer matrices embedded with nanofillers [3]. Petroleum-based polymers are produced in huge amounts globally. Petroleum-based polymers are non-biodegradable, non-renewable, and produce hazardous substances which can threaten human health and the environment [4]. Furthermore, the depletion of these non-renewable petroleum-based fuels demands alternative resources [5].

Thus, biopolymer-based nanocomposites can be a sustainable alternative for petroleum-based nanocomposites in many applications due to their biodegradability, eco-friendliness, renewability, relatively inexpensive, low toxicity, abundance, and improved thermal, mechanical, physical, barrier, and functional properties [3,4]. Various natural biopolymers, including starch, cellulose, pectin, lignin, chitin/chitosan, alginates, hyaluronic acid, gelatin, terpenes, gluten, and polyhydroxyalkanoates (PHAs) from plants, animals, algae, microorganisms and synthetic biopolymers, including polycaprolactone (PCL),

poly(butylene succinate) (PBS), poly(lactic-co-glycolic acids) (PLGA), and polylactic acids (PLA), have been used in nanocomposite materials for various applications [1–3,6–8].

Starch is one of the most abundant natural polymers globally. Starch and its nanocomposites have been extensively studied for their abundance, low cost, ease of processibility, and chemical and physical properties [1,4]. Furthermore, starch can be used in natural or modified form. Native starch has drawbacks, such as poor mechanical properties, high hydrophilicity, and high biodegradability. Thus, researchers are exploring starch modification techniques to improve its properties and develop novel composites [1].

Starch can be modified into nanoparticles and can also undergo various physical (milling, blending with other polymers, extrusion, plasticizers, etc.) and chemical (substitution, graft co-polymerization, cross-linking, oxidation, etherification, esterification, dual modification, etc.) modifications to produce materials with novel properties [9–12].

Starch can be reinforced with starch nanoparticle/starch nanocrystals and nano polymers such as nanoclay (montmorillonites [MMTs], halloysites nanotubes [HNTs]), carbon nanotubes (CNTs), and nanofibers and nanowhiskers (cellulose, chitin) and metal and metal oxides (TiO<sub>2</sub> NPs, ZnO NPs, etc.) to achieve desirable properties and produce potential green sustainable nanocomposite materials [4,7,13]. The addition of nanofillers and additives with antioxidant and antimicrobial properties has been shown to improve or minimally affect biodegradation of starch-based nanocomposites [5,14,15]. Lifecycle assessments on starch and starch-based composites ensure their lower environmental impact and sustainable alternative for petrochemical-based polymers [16–18].

This review mainly discusses the starch-based nanocomposites in regard to starch and its nanostructures, various starch-based nanocomposites mainly reinforced with nano polymers, such as nanoclay, carbon-based materials, nanocellulose, and chitin NPs), and their applications, particularly in the fields of agriculture, packaging, biomedicine, and the environment. Moreover, this paper highlights the lifecycle analysis and degradation of various starch-based nanocomposites in order to analyze their environmental impact.

## 2. Starch

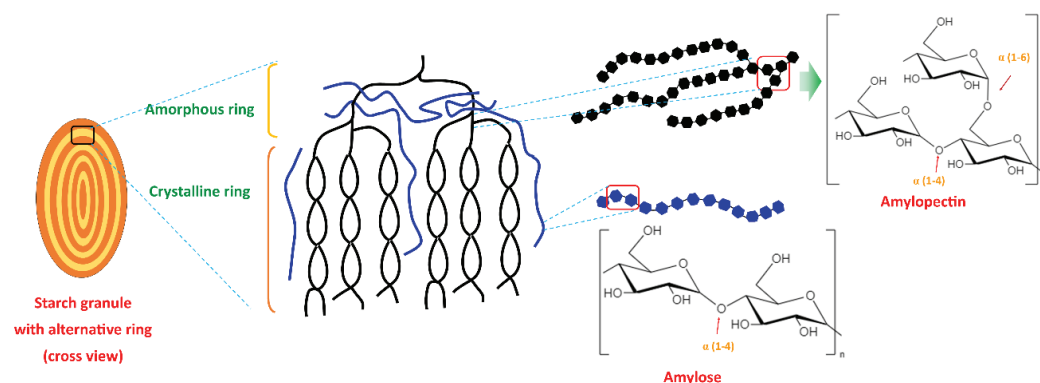
Starch is a polysaccharide and is renewable, inexpensive, biodegradable, and readily available. Starch contains two polymers (glucans) known as amylose (10–30%) and amylopectin (70–90%). Amylose is a linear chain of D-glucose units linked by the  $\alpha$ -(1,4) glycosylic bonds, while amylopectin is a highly branched and high molecular weight chain composed of D-glucose repeating units linked by  $\alpha$ -(1,4) glycosylic bonds and  $\alpha$ -(1,6) glycosidic bonds. The amylopectin chain contains 10–60 glucose units, and the side chains consist of 15–45 glucose units with about 5% of  $\alpha$ -(1,6) branching points [6,7]. Amylose and amylopectin are radially arranged in an alternating concentric (amorphous and semi-crystalline) ring in starch granules. Amylopectin is radially arranged in granules and contributes to its crystalline nature (double helices region), and single helices amylose is randomly distributed among amylopectin clusters. Amylose and the branching point of amylopectin form the amorphous region [19–21]. Figure 1 illustrates the structure of the starch granule and the chemical structure of amylopectin and amylose.

Starch is a primary energy source in plants, which is stored in various parts, including the roots, tubers, seeds, and stems [6]. Various plant sources, such as corn, potato, wheat, cassava, rice, corn, barley, rye, millet, peas, mung beans, lentils, arrowroot, sago, sorghum, banana, yam, and many others, are utilized to obtain starch [22–24].

Starches from different sources show variation in their chemical composition ( $\alpha$ -glucans, moisture, lipids, proteins, and phosphorylated residues), the structure of glucan components (amylose and amylopectin), and starch granule size and shape due to genetic and environmental factors [25,26].

Starch granules' size and shape can vary with the content, structure, and arrangement of amylose and amylopectin [25]. Starch granules are found in various sizes ranging from 2–150  $\mu$ m and packed with amylose and amylopectin content. Regular starch granules contain amylose in the range of 15–30% but can be varied in the range of 0–78%. Waxy

starch contains lower or no amylose, whereas high-amylose starch consists of more than 50% amylose [7,23]. Table 1 shows the amylose contents of various starch sources.



**Figure 1.** Starch granule structure and the chemical structure of amylopectin and amylose.

**Table 1.** Amylose and amylopectin contents of starch from various sources.

Starch Source	Amylose (%)	Reference
Arrowroot	35.52	[27]
Banana (pulp)	16.36–26.2	[28–30]
Banana (peel)	25.7	[29]
Barley (regular)	24.7	[31]
Cassava	2.5–32.12	[28,32,33]
Corn	0–79.05	[28,32]
Maize (normal)	22.7–28.9	[31,34]
Maize (waxy)	0.18	[34]
Maize (high amylose content)	35.5–64.8	[34]
Potato	18.6–31.9	[28,31–33]
Rice	0.1–28.7	[20,35]
Sweet potato (normal)	30.4	[36]
Wheat	6.2–22.8	[31,32]

Starch-based hydrogel is formed via gelatinization of starch during heating with excess water and followed by three-dimensional network formation by retrogradation [37]. Gelatinization of starch is an irreversible process that occurs through the absorption of water and disruption of the crystalline structure of starch granules by hydrogen bond breakage, swelling, the disintegration of starch granules, leaching of amylose that increases viscosity and solubilization of starch molecules [32,35,37].

Amylose and amylopectin content, amylopectin structure (molar mass or chain length), and starch granule size influence the chemical, physical, optical/transparency, and functional properties (water uptake, swelling, gelatinization, pasting [pasting viscosity and temperature], retrogradation, and susceptibility to enzymatic hydrolysis of starch [7,20,23,36,38].

Amylopectin contributes to water absorption, swelling, and pasting of starch granules, whereas amylose hinders the swelling property in the presence of lipids, thus preventing gelatinization power [32,38]. Furthermore, short-chain amylopectin showed better swelling power than that of long-chain amylopectin, indicating that starch with higher crystallinity reduces the swelling power [38]. Smaller granule size increases hydration, thus increasing the swelling, viscosity, and gelatinization properties [26].

Amylose content is negatively correlated with swelling power, gelatinization temperature, and the enthalpy of gelatinization required to disrupt the crystalline structure [35]. Waxy starch has a higher degree of crystallinity and higher gelatinization temperature than starch with high amylose content [31,35]. Amylose in starch has a high tendency for retrogradation due to its linear structure. However, the retrogradation properties of starch



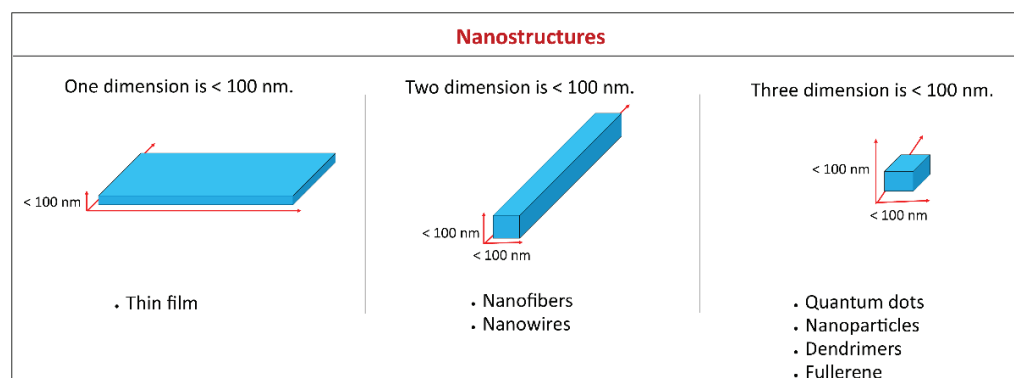
are mainly determined by the degree of crystallinity and gelatinization temperature than the amylose content [35].

Amylose–amylopectin ratio also influences thermal, mechanical, and barrier properties. Basiak et al. [23] reported that potato starch, containing lower amylose (20%) than that of wheat (25%) and corn (27%) starch, exhibited greater mechanical properties and lower water solubility, water vapor, and oxygen permeability. Other than that, optical properties were influenced by the amylose/amylopectin ratio: the potato (lower amylose) film was transparent, whereas corn and wheat films were opalescent.

However, applications of starch have been limited due to their poor performance, such as through their brittleness, high water sensitivity, poor gas and moisture barrier, susceptibility to retrogradation, high viscosity, and limited solubility [13,39]. Therefore, plasticizers, chemical modifiers, and incorporating nanofillers, such as starch nanoparticles, nanoparticles, nanoclay, nanofibers, and others, have been used to improve the properties of starch [39].

### 3. Nanomaterials and Nanocomposites

Nanomaterials are referred to as materials which have at least one of their dimensions less than 100 nm. Based on the definition, a thin film with <100 nm thickness is a nanomaterial as one of the dimensions is nanometric. Likewise, nanomaterials such as nanofibers, nanowires, and nanorods have two dimensions on the nanoscale, whereas quantum dots, nanoparticles, dendrimers, and fullerene have three dimensions in the nanometer range (Figure 2) [40].



**Figure 2.** Examples of various types of nanomaterials based on the number of dimensions in the nanometer range.

Nanomaterials can be classified based on dimensionality (number of dimensions with a length larger than 100 nm), as shown in Figure 3: 0D, 1D, 2D, and 3D. Zero dimension (0D), including spheres, hollow spheres, clusters, quantum dots, and metals, have no dimension of particles larger than 100 nm, i.e., all dimensions in the nanoscale. One-dimensional (1D) nanomaterials, such as nanorods, nanowires, nanofibers, and nanotubes, have one dimension, not in the nanoscale (>100 nm) and the other two are in the nanoscale, whereas two-dimensional (2D) nanomaterials, including thin film, nanocoatings, nanoplates, and nanolayers, have two dimensions, not in nanoscale and another one in nanoscale. Three-dimensional (3D) is the combination of nanocrystals in different directions which have various dimensions above 100 nm. Figure 3 depicts the classification of nanomaterials based on dimensionality [40–42].

Nanomaterials can be synthesized by two approaches: top-down and bottom-up approaches (Figure 4). In the top-down method, the bulk material is restructured into nanomaterials using mechanical grinding/milling, ball milling, polishing, lithography, and other means. While in the bottom-up method, nanomaterials are assembled from atomic range particles/molecules or nanoclusters through the sol–gel method, spinning,

molecular self-assembly, pyrolysis and condensation, vapor phase deposition, and other methods [40,41].

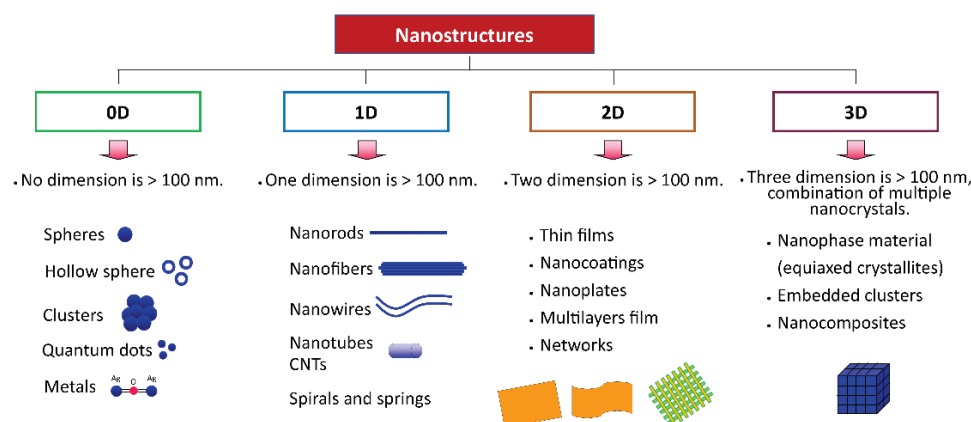


Figure 3. Classification of materials based on dimensionality.

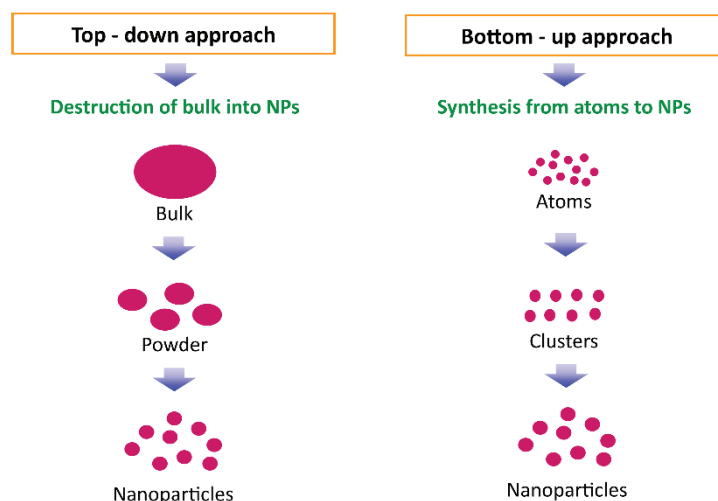
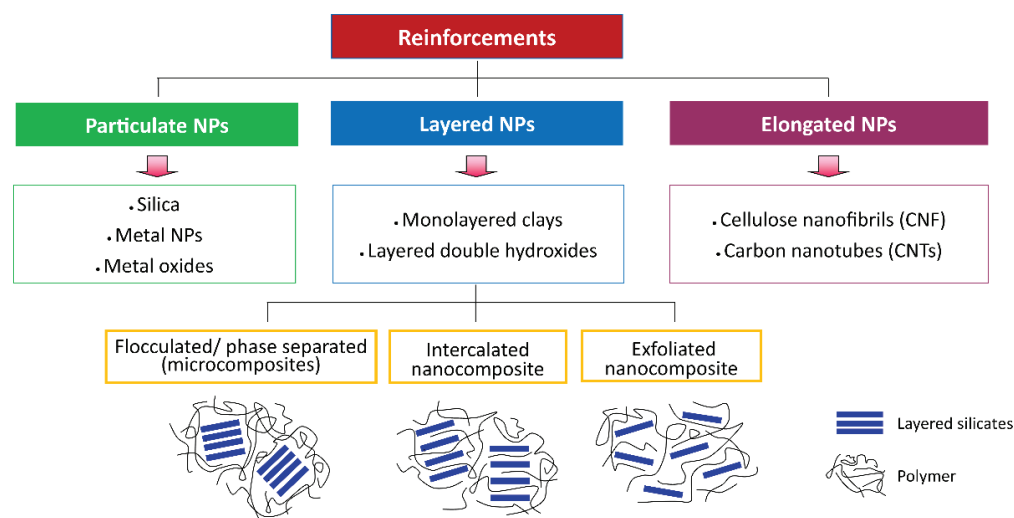


Figure 4. Nanoparticle synthesis methods: top-down and bottom-up approach.

Composite materials consist of two or more dissimilar materials, which are composed of two major constituents: (1) a matrix as a continuous phase (polymer, ceramic, or metal) and (2) reinforcement materials as an un-continuous phase. Bionanocomposites are composite materials that are composed of biopolymers and particles with at least one dimension in the nanometer range (1–100 nm). Bionanocomposites can also be referred to as green composites or biohybrids, or bioplastics [3,43].

Nanocomposites can be classified into three categories based on the morphology of reinforced nanoparticles: (1) particulate/iso-dimensional (silica, metal NPs, metal oxides), (2) layered (monolayered clays, layered double hydroxides), and (3) elongated (cellulose nanofibrils [CNF], carbon nanotubes [CNTs]) nanoparticles [3,44]. Particulate reinforcements are used to enhance resistance to flammability and reduce permeability and cost, whereas layered reinforcements are used for their superior mechanical behavior [43]. Furthermore, based on the degree of dispersion of particles in the matrix, layered nanocomposites have three subclasses, including intercalated, exfoliated, and flocculated/phase-separated nanocomposites (micro-composites) [3,6,43]. Flocculated/phase-separated nanocomposites are formed without a partition between individual layers due to the particle–particle interactions, polymer chains are intercalated between sheets of layered nanoparticles in intercalated nanocomposites, and exfoliated nanocomposites are formed by partition between individual layers (Figure 5) [43].



**Figure 5.** Classification of the nanocomposites.

#### 4. Starch Nanoparticles (SNPs)

Starch nanoparticles (SNPs) are mainly synthesized by the methods of hydrolysis (acid or enzymatic), regeneration, and physical treatments (milling, high-pressure homogenization, gamma radiation, and ultra-sonication) [45].

SNPs are mainly used as fillers in a polymer matrix to improve their reinforcing effect and mechanical and barrier properties [13]. Nanoparticles have a large surface area/volume ratio, allowing a great interaction capacity, which makes them potential reinforcement materials [46]. SNPs are non-toxic and can be used to prepare nanocomposite, absorbent, carrier (encapsulation), and emulsion stabilizers for food and non-food applications [45,47,48].

Santana et al. [46] reported the SNP obtained from ultrasound showed a significantly higher yield than SNP synthesized by acid hydrolysis. In addition, incorporating SNPs reduced the water vapor permeability of starch film [46]. Lin et al. [49] prepared debranched starch nanoparticles (DSNPs) by reverse emulsification using debranched waxy corn starch (98% of amylopectin), which showed a higher crystallinity and melting temperature than that of native waxy corn starch. Furthermore, the addition of debranched starch nanoparticles (5 wt.%) into corn starch films improved the tensile strength by 85.9% and decreased water vapor permeability and the oxygen transmission rate by 30.94% and 79.31%, respectively.

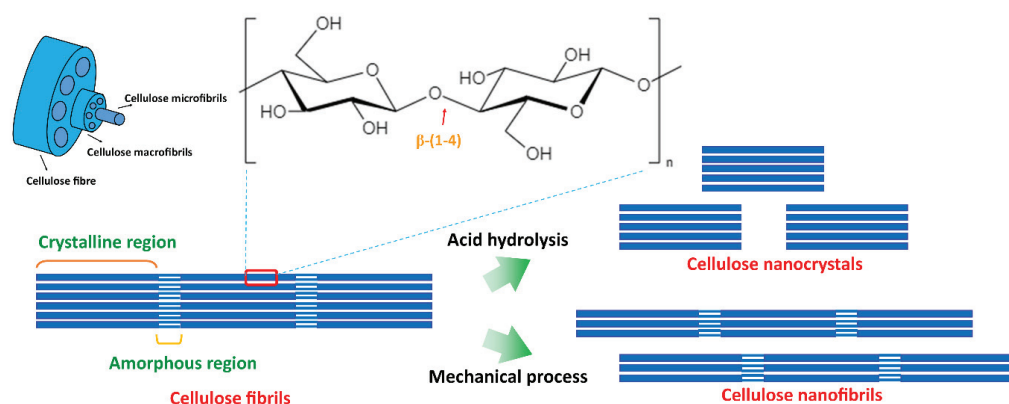
In another study, starch NPs prepared by acid hydrolysis containing Ag NPs showed good antibacterial activity against *Staphylococcus aureus*, *Salmonella typhi*, and *Escherichia coli* which has the potential to be used as a coating material for food packaging [50].

#### 5. Starch-Based Nanocomposites

Native starch or thermoplastic starch (TPS) has poor mechanical properties (fragility/brittleness), low thermal stability, hydrophilicity, high water vapor permeation, poor resistance to external factors (humidity, tearing, picking, etc.), and a lack of compatibility with hydrophobic polymers [7,12,51]. Therefore, starch is blended with other natural and synthetic polymers or incorporated with various nanomaterials to enhance the physical, mechanical, and barrier properties [7]. Compared with bulk materials, nanoparticles have a surface area/volume ratio and possess unique physical, mechanical, optical, magnetic, electrical, and other properties [42]. Hence, recently, bionanocomposites can be a promising material to enhance mechanical and barrier properties [52]. Starch reinforced with nanofillers, including nanocellulose, chitin nanoparticle, nanoclay, and carbon-based materials, are discussed below.

### 5.1. Starch/Nanocellulose Composite

Cellulose is the primary component of the plant cell wall and can be extracted from plants, invertebrates, marine animals, algae, fungi, and bacteria [53]. It is the most abundant natural polymer and is popular for its mechanical properties, reinforcement capabilities, low density, renewability, low toxicity, and biodegradability [54]. Cellulose is the polymer of D-glucose units linked by  $\beta$ -(1,4)-glycosidic bonds, and higher hydroxyl groups (-OH and -CH<sub>2</sub>-OH) at equatorial positions give higher stability (Figure 6) [55]. Cellulose fibres are formed with strong inter and intramolecular hydrogen bonds and aggregate with highly ordered (crystalline) and disordered regions (amorphous) [56]. Nanocellulose is a nanostructure of cellulose and has drawn much attention over the past years due to its excellent characteristics, including its high aspect ratio (length to diameter), improved mechanical and thermal properties, crystallinity, flexibility, renewability, abundance, biocompatibility, and biodegradability [55,57].



**Figure 6.** Cellulose chemical structure and schematic diagram of the formation of cellulose nanocrystals and cellulose nanofibrils.

Nanocellulose can be produced by top-down and bottom-down processes (Figure 6) [53,54] using various techniques, including enzymatic techniques, chemical hydrolysis, and mechanical treatments, including high-pressure homogenization, grinding, cryo-crushing, micro-fluidization, and high-intensity ultrasonication [46,53,54]. These synthetic techniques and conditions influence the dimensions, composition, and properties of nanocellulose. Nanocellulose can be generated in three forms: (1) cellulose nanofibrils (CNFs) and (2) cellulose nanocrystals (CNCs) from woods and other lignocellulosic materials using a top-down process, and (3) bacterial cellulose (BC) from the biosynthesis of bacteria using a bottom-to-top process. Figure 7 summarizes the three forms of cellulose and synthesis methods [53,55].

Cellulose nanofibrils or nanofibers (CNFs) nanofibrillated (NFC)/ microfibrillated (MFC) cellulose	Cellulose nanocrystals (CNCs)/ cellulose whiskers	Bacterial cellulose (BC) and electrospun cellulose nanofibers (ECNFs)
<ul style="list-style-type: none"> <li>• Top to bottom process: disintegration of cellulose fibers into nanocellulose.</li> <li>• Mechanical treatments (high pressure homogenization, grinding, milling, ultrasound, and steam explosion), chemical treatments, and the combination.</li> <li>• Diameter: 5 - 50 nm, length: few micrometers.</li> </ul>	<ul style="list-style-type: none"> <li>• Produced by top to bottom process: disintegration of cellulose fibers into nanocellulose.</li> <li>• Acid hydrolysis.</li> <li>• Diameter: 3 - 35nm, length: 200 - 500 nm.</li> </ul>	<ul style="list-style-type: none"> <li>• Bottom to top process: low molecular weight sugars or dissolved cellulose are generated by bacteria or electrospinning, respectively.</li> <li>• Biosynthesis by bacteria, such as <i>Acetobacterxylinum</i>.</li> <li>• Does not require pre-treatment to remove lignin and hemicellulose.</li> <li>• 20 - 100 nm long unique nanofiber system.</li> </ul>

**Figure 7.** Types of nanocelluloses.

Nanocellulose is widely used in various applications, such as biomedical engineering, the automotive industry, electronics, food packaging, cosmetics, construction, textiles, wood adhesives, and wastewater treatment applications [53,57].

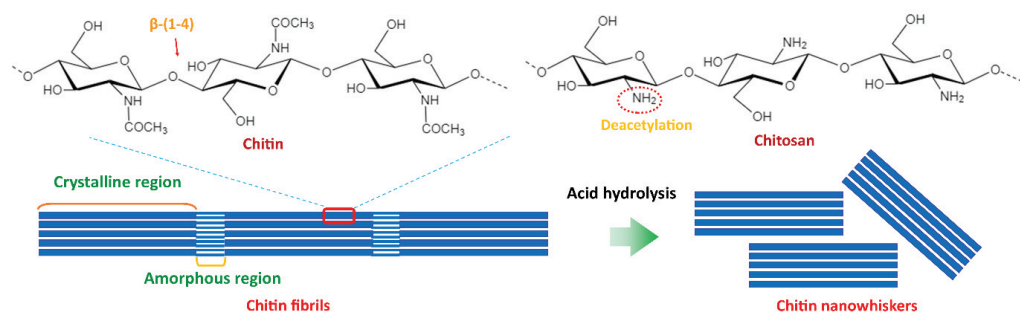
Othman et al. [58] prepared the corn starch (CS) film reinforced with nanocellulose fiber (NCF) and thymol, a compound extracted from the essential oil of thyme, which has



antioxidant and antimicrobial properties. They reported that adding 1.5% of NCF improved the thermal stability, mechanical, and barrier (water vapor and oxygen) properties of corn starch film. The CS/NCF/thymol composite reported improved thermal stability and flexibility. However, a significant reduction was observed with tensile strength, Young's modulus, and barrier properties [58]. In another study, starch from an unripe plantain bananas reinforced with cellulose nanofibers from banana peels improved the mechanical and water vapor barrier properties [59]. Starch/CNC nanocomposites were reported to improve the tensile strength (2.8 to 17.4 MPa), Young's modulus (112 to 520 MPa), and water barrier properties, as well as reduce the water solubility (26.6 to 18.5%) and contact angle 38.2 to 96.3° [60].

### 5.2. Starch/Chitin Nanoparticles Composites

Chitin is the second most abundant natural polysaccharide next to cellulose and is found in the shell of crustaceans (crab, lobster, and shrimp), the exoskeleton of arthropods, molluscan shells of squid, mushrooms, the cell wall of algae and fungi (yeast and mold). Chitin is composed of N-acetyl-2-amido-2-deoxy- $\beta$ -D-glucose (N-acetylglucosamine) units linked with a  $\beta$ -(1,4)-glycosidic bond, in which acetamide groups ( $-\text{NHCOCH}_3$ ) consists at the C2 of cellulose monomer. Chitosan is derived from the alkaline deacetylation of chitin (Figure 8). Chitin crystals are found in three forms:  $\alpha$ -chitins (which contain antiparallel cellulose chains),  $\beta$ -chitins (parallel cellulose chains), and  $\gamma$ -chitin (among three chains, two of them are in the same direction, and one is in the opposite direction) [61–63].



**Figure 8.** Chemical structure of chitin and schematic diagram of the formation of chitin nanowhiskers.

Chitin nanomaterial can be prepared through top-down and bottom-up approaches. Chitin fibrils consist of amorphous and crystalline regions and thus can be converted into three types of nano-chitins in a top-down approach: nanocrystals (via acid hydrolysis), nanofibers (via mechanical treatments), and nanowhiskers (consecutive acid hydrolysis at a high temperature and mechanical treatments) [39,62].

Nano-chitin has been widely studied for its high aspect ratio, high surface area, good mechanical properties, lightweight/low density, good chemical stability, renewability, non-toxicity, and antibacterial properties, and it is used in biomedicine, packaging, water treatment, green electronics, cosmetics, and many other applications [61,63].

A combination of chitin nanofibers and starch nanoparticles showed higher emulsion stability over a range of pHs and temperatures and can be used as an emulsion stabilizer in various products, such as food, paint, coating, cosmetics, and pharmaceuticals [48].

Chang et al. [64] reported chitin nanoparticles (CNPs) exhibited lower crystallinity than chitin whiskers. At a low level of CNPs, tensile strength, storage modulus, glass transition temperature, and water vapor barrier properties of plasticized potato starch/CNPs nanocomposite due to good interfacial interaction between CNPs' nanofiller and starch matrix.

By adding 5 wt.% chitin nanofibers (CNF) obtained from the fungus *Mucor indicus*, Young's modulus and the tensile strength of TPS were enhanced by 239% and 216%, respectively, and moisture absorption was reduced from 51% to 38%. However, the addition of CNF at a higher level increased moisture absorption and reduced the mechanical properties of TPS [39]. In another study, Heidari et al. [61] reported that CNF/TPS nanocomposite

films were more permeable to water vapor than pure CNF film. CNF at higher levels lowers the dispersion of nanofiller and tends to agglomerate, which leads to poor water vapor barrier and mechanical properties. In addition to that, the presence of excessive  $\text{NH}_2$  groups at the CNF surface may increase the affinity to water, thereby increasing water absorption [39,61].

### 5.3. Starch/Nanoclay Nanocomposites

Clay is a polymer composite of two-dimensional layered mineral silicates. The single layer is formed by the edge-linked octahedral sheet of aluminum or magnesium oxide sandwiched between two tetrahedral silicate sheets. As shown in Figure 6, three types of polymer-based nanocomposites can be obtained based on the polymer and silicate layers. Silicate clay is characterized by important physical properties, such as a cation exchange capacity and specific surface area [65,66]. Polymer/nanoclay composites are used in the automotive industry, aeronautical industry, packaging, flame-resistant materials, biomedical applications, and wastewater treatment [67,68]. Nanoclays can be categorized into several classes: smectite, chlorite, kaolinite, illite, and halloysite [68].

Plate-like montmorillonite (MMT) (smectite), a multilayer-aluminosilicates, has been widely studied as a reinforcing material in polymers due to its excellent cation exchange capacity, swelling behavior, and large surface area [68,69]. MMT also improved the thermal stability, mechanical, optical, and barrier properties, even at their lower concentration [70].

Mohan et al. [15] reported that the incorporation of MMT nanoclay into corn starch-based film resulted in a significant reduction in water absorption (by 22%), moisture uptake (40%), oxygen permeation (30%), and swelling thickness (31%) in comparison to corn starch film. Furthermore, the concentration of MMT nanoclay determines the structure of the nanocomposite. X-ray diffraction (XRD) analysis revealed that the intercalated nanoclay structure forms at a higher concentration (>2%), whereas the exfoliated structure forms at a lower concentration in the polymer matrix [15]. In another study, MMT addition was also shown to improve the tensile strength and biodegradability in cross-linked PLA/maleated TPS nanocomposite [71]. Biodegradable nanocomposites fabricated from cross-linked wheat starch (CLWS)/sodium montmorillonite (Na-MMT)/ $\text{TiO}_2$  NPs showed an exfoliated structure. Incorporating Na-MMT and  $\text{TiO}_2$  NPs reduced the water vapor permeability and water solubility of the CLWS film, whereas thermal stability, tensile strength, and Young's modulus were increased.  $\text{TiO}_2$  NPs showed better UV-blocking properties than Na-MMT [69]. Maize starch/glycerol (20%)/Na-MMT (10%) nanocomposite also showed intercalated structures and improved tensile properties [66].

Iamareerat et al. [72] prepared nanocomposite film with plasticized cassava starch incorporated with sodium-bentonite and cinnamon essential oil. The addition of sodium-bentonite nanoclay (0.5–0.75%) decreased the water vapor permeability in plasticized cassava starch with 2% glycerol film. Further addition of cinnamon essential oil into the CS/glycerol (2%)/sodium-bentonite (0.75%) showed better antibacterial activity and significantly inhibited microbial growth in pork meatballs, despite the increase in water vapor permeability.

Halloysites clay nanotubes (HNTs), aluminosilicate hollow cylinders, have a lower hydroxyl group on the surface than other silicates such as MMT, making them a promising reinforcement material for polymers [68,73]. Furthermore, HNTs exhibit exfoliated structures due to their high aspect ratio [73]. Dang et al. [73] revealed that the addition of modified or unmodified HNTs into the TPS/poly(butylene adipate-co-terephthalate) (PBAT) blend improved the thermal and mechanical properties without loss of ductility of the plasticized wheat starch matrix [74]. Another investigation on PVA/starch/glycerol/HNTs nanocomposites revealed that their hydrophobic nature and biodegradability decreased with the addition of HNTs [75].

#### 5.4. Starch/Carbonaceous Nanocomposites

Fullerenes, diamonds, carbon nanotubes (CNTs), graphene, and their derivatives are common carbon allotropes used in carbon-based nanocomposites [76].

CNTs found in two forms, single-walled (SWCNT) or multi-walled carbon nanotubes (MWCNT), have been widely studied as reinforcing fillers for TPS nanocomposite films [77]. CNTs have a larger surface area, excellent electrical conductivity, mechanical and thermal properties and they also have a higher volume-to-area ratio compared to that of other nanoparticles and they are widely used in various biomedical applications, environmental pollution control, sensing and detection, the automobile industry, and secondary food packaging. Direct contact food packaging materials are limited by their migration and potential toxicity [76,78,79].

Electrically conductive biocomposite films have gained popularity in various electronic, biomedical, and food packaging applications [22]. Potato starch-based film reinforced with MWCNT and ionic surfactants (sodium cholate, SC; cetyltrimethylammonium bromide, CTAB) decreased the contact angle and showed improved antioxidant properties (30.2 and 12% of scavenging activity, respectively) due to the presence of MWCNT. Surfactant SC showed better dispersibility of MWCNT in a potato starch matrix with improved mechanical properties and crystallinity [22].

Starch plasticized with ionic liquids reduces the retrogradation resulting in increased film stability and it has the potential use in ionically conducting solid polymers. The addition of nanofiller MWCNT at 0.5 wt.% in starch plasticized with ionic liquid, 1-ethyl-3-methylimidazolium acetate ([emim+][Ac−]) significantly increased the tensile strength by 327%, Young's modulus by 2484%, and elongation at break 82% (from 30 to 69%). Moreover, electrical conductivity was increased with MWCNT content (wt.%) and reached a maximum (56.3 S/m) at 5 wt.% MWCNT. MWCNT/starch plasticized with [emim+][Ac−] showed electroconductive properties because of its ionic nature of ionic liquids and the excellent electrical conductivity of MWCNT [77]. A starch-iodine complex matrix reinforced with a small amount of MWCNT (0.055%) reduced the water vapor permeability by 43% [78].

Graphene is a two-dimensional material arranged in a hexagonal lattice. Plasticized starch incorporated with reduced graphene oxide (rGO), a derivative of graphene, exhibited increased conductivity and dielectric properties, which could make it a potential candidate for producing sustainable bio-friendly electronic devices [80].

Investigation of poly(lactic acid) (PLA)/thermoplastic starch (TPS)/graphene nanoplatelets (GNP) blends revealed that the addition of GNP increased the crystallinity of the PLA/TPS blend, and the maximum crystallinity (68.39%) was observed with PLA (70%)/TPS (30%)/GNP (1%). Further increases in GNP resulted in the reduction of compatibility [81].

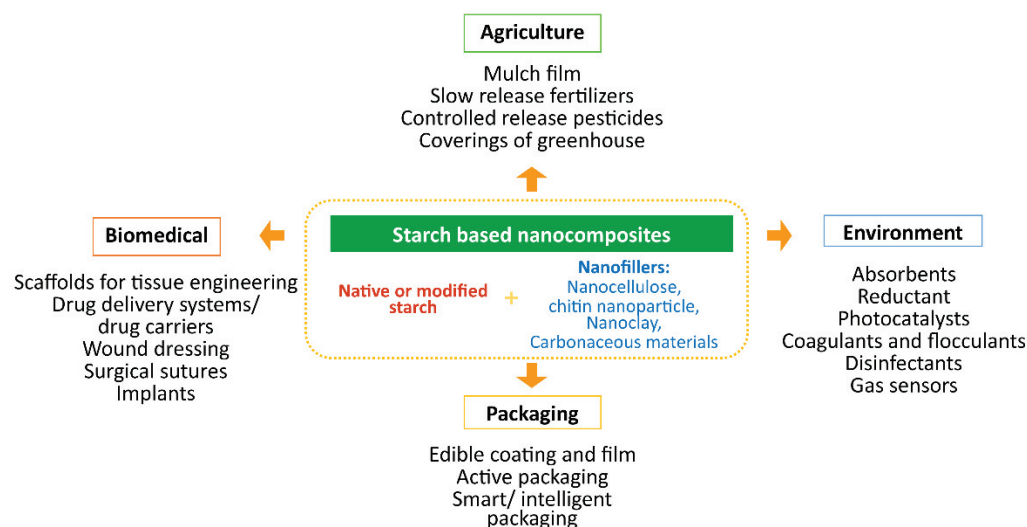
## 6. Applications of Biodegradable Starch-Based Nanocomposites

Biodegradable starch-based nanocomposites have been used in agriculture, packaging, biomedical, environment, and many other fields (Figure 9).

### 6.1. Agriculture

In recent years, biodegradable films have been developed for agricultural purposes, particularly for mulching applications, the coverings of a greenhouse, and the controlled/slow release of agrochemicals such as fertilizers and pesticides [82–84].

Agricultural mulches are used to prevent the hindrance caused by the weeds' growth, maintain soil wetness, and regulate soil temperature [85]. Interaction with water (water vapor permeability, contact angle, and water solubility/resistance) and environmental factors (thermal stability) are important parameters in mulch films. Mulch films must have a very low water vapor permeability to maintain the soil moisture by reducing the water loss by evaporation. Since mulch films are exposed to outdoor conditions, improving the thermal stability is therefore essential [83,86].



**Figure 9.** Applications of starch-based nanocomposites.

Pesticides protect the crop from pests, pathogens, weeds, and insects by destroying, attacking, mitigating, or repelling activity, whereas fertilizers are essential in agriculture to increase crop yield. However, in conventional applications, the efficiency of reaching their target sites is relatively low as they are hindered by immobilization, erosion, volatilization, leaching, surface runoff, or scavenging by soil. In addition, water is also an essential factor in crop growth and driving off fertilizers. Therefore, management of nutrient/pesticide active compounds and water loss is essential for crop production. To reduce the loss and improve their utilization efficiency, slow-release fertilizers or controlled-release pesticides with improved water retention and water holding capacity can be formulated by incorporating nanomaterial into biopolymers [82,84,87,88].

Merino et al. [83] investigated the water and light interaction with corn starch-based mulch film. The study revealed that the addition of chitosan/bentonite nanofiller into native and oxidized thermoplastic corn starch improved the water resistance, radiometric, and antibacterial properties without having a significant effect on the water vapor permeation and mechanical properties [83]. In another study, Merino et al. [86] reported that the addition of bentonite/chitosan into both matrixes, native and oxidized thermoplastic corn starch, increased the crystallinity (3.0 and 3.4%) and slightly increased thermal stability in comparison to the addition of natural bentonite.

Superabsorbent hydrogels are widely used in bi-functional (retain and supply water and nutrient over a long period) slow-release fertilizers due to their water retention properties. The addition of natural char nanoparticles (NCNPs) into corn starch-g-poly(AA-co-AAm) encapsulated urea provided high biodegradability and improved the soil water-retention capacity along with the slow release of urea [84]. Chitosan (CS)/sago starch (ST)/nano zeolite (NZ) nanocomposite released 64% of phosphorus and 41.93% of urea after 14 days and increased the water retention capacity. Furthermore, CS/ST/NZ nanocomposites showed better growth indexes in *Philodendron* spp. compared to the direct application of urea, suggesting the efficacy of nanocomposites in slow-release fertilizer formulation [88]. Urea encapsulated with starch (10%)/PVA (5%) with crosslinker acrylic acid (2%) and citric acid (2%) showed higher nitrogen-releasing efficiency, 70.10 and 50.74%, respectively, as well as improved growth factors in spinach plants [89]. Modified starch (esterified with dicarboxylic acid chloride)/organobentonite-based composites regulate the effective controlled release of encapsulated pesticide atrazine [90].

## 6.2. Packaging

Food packaging protects food from humidity, high/low temperatures, and other physiological factors and aids in food quality monitoring and control in the food supply chain and during storage (gas sensors, electronic nose) [91]. Starch has been used in food



packaging applications because of its strong mechanical properties, transparent/translucent appearance, and tasteless and flavorless characteristics [69]. Brittleness and poor water vapor barrier properties limit their applications. Nanoparticle reinforcement can improve the mechanical properties, hydrophobicity, water vapor and oxygen barrier, UV barrier, thermal properties, and other functional properties (antioxidant, antimicrobial, etc.) of starch which makes nanoparticles a potent material for edible film/coating, active and intelligent/smart packaging for protecting or maintaining and monitoring the quality of food materials [91–93].

Organic or inorganic nanofillers have been widely studied for food packaging applications, whereas organic nanofillers include nanoclay (MMTs, HNTs), natural biopolymers (chitosan, cellulose), and natural antimicrobial agents (nisin), and inorganic nanofillers includes metals (Ag, Au, Cu), and metal oxides (ZnO, TiO<sub>2</sub>, Ag<sub>2</sub>O, MgO, CuO, SnO<sub>2</sub>) [44,52,91].

The suitability of a film for packaging materials is mainly assessed by water vapor and oxygen barrier properties and good heat stability [94]. Furthermore, a film with improved mechanical strength and flexibility protects against shock and other physical damage. TiO<sub>2</sub> NPs reinforcement in potato starch-based composite films led to a reduction in water solubility, moisture uptake, and water vapor permeability, and an increment of UV barrier properties and tensile strength of the film, showing its potential for food packaging [92]. Na-MMT and TiO<sub>2</sub> NPs reduce the hydrophilicity and improve mechanical, water vapor, and UV barrier properties in cross-linked wheat starch, which makes them a suitable material for food packaging [69]. UV barrier packaging film from starch/kefiran/ZnO NPs showed improved tensile strength, Young's modulus, and thermal stability (increased melting temperature), which are beneficial to the packaging system [95]. Starch NPs/Ag NPs showed increased antibacterial activity against *Staphylococcus aureus*, *Salmonella typhi*, and *Escherichia coli* and can be used as an antibacterial food coating material [50]. Linseed polyol increased the contact angle, water absorption capacity, thermal stability, and biodegradation of polyvinyl alcohol/corn starch film. Further addition of Ag NPs showed antimicrobial behavior against *Proteus mirabilis*, *Candida albicans*, *Escherichia coli*, *Enterococcus faecalis*, *Staphylococcus aureus*, *Klebsiella pneumoniae*, among others, which shows the potential applications in antimicrobial packaging [96]. Poly(ethyl methacrylate)-co-starch (PEMA-co-starch)/graphene oxide/Ag NPs (2 wt.%) nanocomposite film showed improved thermal stability, chemical resistance, tensile strength, oxygen barrier properties, and antimicrobial properties against *Escherichia coli*, *Pseudomonas aeruginosa*, *Staphylococcus aureus*, and *Bacillus subtilis* [97].

Plasticised corn starch films reinforced with nanocellulose improved the mechanical strength, flexibility, and water vapor and oxygen barrier properties that have a beneficial effect on reducing the oxidation of oil during storage. This film showed good heat stability, which further prevents oxygen and water vapor transmission. Moreover, the storage study ensures that this plasticized corn starch-based nanocomposite can be used as an alternative packaging material for storing edible oils at ambient conditions (27 ± 3 °C temperature, 65 ± 5% RH) for more than three months without affecting the oil quality in terms of rancidity, viscosity, and color [94].

Starch from potato, wheat, and corn blended with carboxyl methylcellulose (CMC)/Na-MMT has potential applications in food packaging [98]. Cellulose nanocrystals (CNC) obtained from sugarcane bagasse blending with starch improved mechanical, water resistance, and water barrier properties and decreased surface hydrophilicity (contact angle > 90°), which makes this starch/CNC nanocomposite a potential food packaging material [60]. Heidari et al. [61] developed edible food packaging using chitin nanofibers (CNF)/TPS nanocomposite.

TPS/MMT/carvacrol essential oil showed biocidal effects against *Escherichia coli* due to the synergistic antibacterial effect of carvacrol essential oil and MMT suggesting the applications in antimicrobial packaging [99]. Packaging material fabricated with sweet potato starch (SPS)/MMT/thyme essential oil (TEO) was studied by Issa et al. [100]. They reported that the addition of MMT improved the mechanical and water barrier properties of SPS,

whereas biodegradability decreased. However, incorporating TEO decreased the tensile strength, elongation, Young's modulus, and water barrier with improved biodegradability in SPS/MMT. The nanocomposite made from cassava starch/glycerol (2%)/Na-bentonite (0.75%)/cinnamon essential oil (2.5%) exhibited antibacterial activity against *Escherichia coli*, *Salmonella typhimurium*, and *Staphylococcus aureus*, and significantly inhibited the microbial growth in pork meatballs stored under ambient and refrigeration conditions [72].

The addition of potassium sorbate, a commonly used preservative, into starch/nanoclay films controlled the migration of sorbate, resulting in the retention of antimicrobial activity for a long period [101]. Chen et al. [102] also developed a controlled-release active film from starch/polyvinyl alcohol (PVA) incorporated with cinnamaldehyde and microfibrillated cellulose (MFC). The addition of MFC was found to improve the tensile strength, crystallinity, hydrophobicity, and antimicrobial activity (against *S. putrefaciens*) with reduced flexibility. The oxygen and water vapor permeability reduced at 1.0 and 2.5% MFC but increased at higher concentrations. In addition, MFC, at 1 and 7.5%, controlled the release of cinnamaldehyde.

Smart packaging materials for monitoring the spoilage of milk packed in a bottle were developed by incorporating pH indicators, including bromocresol green (BG) and methyl orange (MO), into a starch/nanoclay nanocomposite [93]. Further nanometals (TiO<sub>2</sub>, SnO<sub>2</sub>, Ag<sub>2</sub>O, MgO, ZnO, CuO) can be used in gas sensors to monitor food quality [91].

### 6.3. Biomedical

Biodegradable polymers, including starch-based bionanocomposites, are widely used as scaffolds for tissue engineering, drug delivery systems/drug carriers, wound dressing, surgical sutures, and implants due to their mechanical properties, biocompatibility, biodegradability, and also the generation of non-toxic, biodegradable products [103–105].

Biopolymers in the repair of healing tissues accelerate treatment processes and eliminate implant removal surgery. Furthermore, implant materials and their biodegradable products must be non-cytotoxic and biocompatible [105]. Incorporating bioactive beta-tricalcium phosphate ( $\beta$ -TCP) nanoparticles (at 10%) into thermoplastic starch (TPS) drastically improved the mechanical properties and showed excellent biocompatibility with no cytotoxic effect for bone tissue engineering materials [105]. Waghmare et al. [106] fabricated starch-based nanofibrous scaffolds by electrospinning for wound healing applications.

Hydroxyapatite has been used widely in biomedical applications due to its biocompatibility and osteoconductive (cell regeneration process) properties. However, brittleness and lack of flexibility limit the applications. The combination of hydroxyapatite with starch materials can reduce brittleness, and the polar nature of starch encourages a good adhesion between starch and hydroxyapatite. Sadjadi et al. [107] synthesized a nanocomposite from starch/nano-hydroxyapatite, which possesses mechanical and biological properties identical to natural bone.

Abdel-Halim and Al-Deyab [108] reported that Ag NPs/starch/polyacrylamide nanocomposite hydrogel showed antimicrobial activity against fungi (*Aspergillus flavus* and *Candida albicans*) and bacteria (*Staphylococcus aureus* and *Escherichia coli*). PVA/starch incorporated with Ag NPs synthesized from green methods (*Diospyros lotus* fruit extract) has the potential to be used in wound dressing as it shows increased swelling and moisture retention capacity and reduced water vapor transmission that prevents the wound from dehydration and better antimicrobial activity against *Escherichia coli* and *Staphylococcus aureus* [109].

The ternary blend was developed by mixing polylactic acid (PLA)/starch (S)/poly- $\epsilon$ -caprolactone (PCL) with nano-hydroxyapatite (nHA) for controlled release of antibacterial triclosan. The incorporation of nHA (3%) improved the hydrolytic hydrophilicity, hydrolytic degradation, antibacterial activity (against *Escherichia coli* and *Staphylococcus aureus*), and drug release of PLA/S/PCL film. An increase in nHA content (1–7%) improved the biodegradation (13–10 months), and the antibacterial triclosan release rate of PLA/S/PCL/nHA film at 37 °C in buffer solution was increased (0.12–0.18  $\mu$ g/mL every day), which is in the range of MIC of triclosan (0.025–1  $\mu$ g/mL). Furthermore, the degra-

dation and release time of PLA/S/PCL/nHA (3 wt.%) nanocomposite showed similar profiles that ensure continuous drug release during the application [110]. Mallakpour and khodadadzadeh [111] also developed starch/MWCNT modified with glucose (MWCNT-G) nanocomposites for slow release of zolpidem drug delivery. Gao et al. [112] developed spherical core-shell Ag/starch NPs using green synthesis for slow-released nano silver as an antibacterial material which can be used in pharmaceutical and biomedical applications.

Nezami et al. [113] fabricated pH-sensitive magnetic nanocomposite hydrogel using graft copolymerization of itaconic acid (IA) and starch in the presence of magnetic Fe<sub>3</sub>O<sub>4</sub> NPs (St-IA/Fe<sub>3</sub>O<sub>4</sub>) for the controlled-release of guaifenesin (GFN) with low cytotoxicity. A nanocomposite with magnetic Fe<sub>3</sub>O<sub>4</sub> NPs at 0.83% significantly enhanced the drug release from 54.1 to 90.4% within 24 h in pH 7.4 [113].

Starch-based-fluorescent organic nanoparticles (FONs) reported high water dispersibility and excellent biocompatibility (cell viability was 99.69% at the concentration of FONs 100 µg/mL after 24 h). Thus, FONs are a promising candidate for biomedical applications that can be potentially used as fluorescence probes and carriers for delivering biologically active components [114].

#### 6.4. Environment

Extensive agricultural and industrial practices lead to the accumulation of various contaminants, including heavy metals and metalloids (Cr<sup>6+</sup>, Hg<sup>2+</sup>, Zn<sup>2+</sup>, Pb<sup>2+</sup>, Co<sup>2+</sup>, Cd<sup>2+</sup>, Cu<sup>2+</sup>, etc.), dyes, organic substances (pesticides, herbicides, fertilizers, aliphatic and aromatic hydrocarbons, volatile organic compounds [VOCs], oil spills), pathogenic microbes (virus, bacteria, fungi), and toxic gases (nitrogen oxides, SO<sub>2</sub>, CO) in water, soil, and air [115].

Starch-based nanocomposites with various nanofillers, including metal (Ag, Au, and Pd NPs), bimetal (Ag/Au), metal oxides (TiO<sub>2</sub>, ZnO, Fe<sub>2</sub>O<sub>3</sub>, MnO<sub>2</sub>), nanoscale zero-valent iron (nZVI) (Fe<sup>0</sup>), carbonaceous materials (CNTs [SWCNTs and MWCNTs], graphene, graphene oxide), nanoclays (MMTs, HNTs, bentonite), and polymers (chitin, cellulose nanowhiskers) are used in materials as recyclable and reusable filters, absorbents, reductants, photocatalysts, coagulants and flocculants, disinfectants, and gas sensors to detect or remediate contaminants, such as dyes, heavy metals ions (As, Pb<sup>2+</sup>, Cr<sup>6+</sup>, Cu<sup>2+</sup>, Cd<sup>2+</sup>, Hg<sup>2+</sup>, Ni<sup>2+</sup>, Co<sup>2+</sup>, etc.), various aromatic derivatives, fertilizers (urea), and other organic pollutants [116–124].

Green synthesis of Ag/Au bimetallic nanocomposite using graft copolymer hydroxyethyl starch-g-poly(acrylamide-co-acrylic acid) reported catalytic activities that involve the reduction of 4-nitrophenol to 4-aminophenol and degradation of azo dyes (congo red, Sudan-1, and methyl orange) by cleavage of –N = N-bond thus can be used in water treatment [122]. Gomes et al. [125] analyzed a starch/cellulose nanowhiskers hydrogel composite and highlighted the outstanding capacity for methylene blue dye removal.

Starch-graft-poly(acrylamide) (PAM)/graphene oxide (GO)/hydroxyapatite NPs (nHAp) nanocomposite was developed as a recyclable adsorbent for efficient removal of malachite green (MG) and other cationic dye from aqueous solution. The introduction of nHAp improved the biocompatibility of the PAM/GO composite, whereas the biodegradability, porosity, water content, and water uptake decreased with increasing nHAp content. Adsorption capacity increased with agitation time, pH, nHAp content, and initial dye concentration, and the optimum conditions were 60 min, pH 10, 5% nHAp, and 100 mg/L. PAM/GO and nHAp at 1–5 wt.% reported excellent porosity (31–11%), degradability (41–11% after 15 days), the maximum adsorption capacity of 297 mg/g, excellent regeneration capacity after five consecutive adsorption-desorption cycles of dye with high removal efficiency (77–86%) [126].

Adsorption is a basic principle of mechanism in targeted drug delivery, controlled release of pharmaceutically active compounds, and treatment of chemical water pollution [11]. The degree of the time dependency of kinetic coefficient ( $k_{obs}$ ) and the influencing factors (pH, temperature, initial concentration of tetracycline) are important to explore the suitability of materials in adsorption-based applications. Monodispersed starch stabilized magnetite nanoparticle (MSM) showed 70% absorption of antibiotic tetracycline within the

first 5 min and reached 90% after 1 h. The degree of the time dependency of the kinetic coefficient ( $k_{obs}$ ) had a negative correlation with the initial tetracycline concentration [11].

Chitin nanowhiskers (CNW) are better nano-adsorbents due to their high surface/volume ratio and abundant hydroxyl and acetamide functional groups on the surface [63]. MMT is hydrophilic and has a high specific area [127]. The bean starch/Na-MMT nanocomposite showed high absorption capacity for heavy metals  $Ni^{2+}$  (97.1% at pH 4.5, initial concentration of 100 ppm) and  $Co^{2+}$  (78.03% at pH 6, initial concentration of 140) in comparison to the starch matrix (72 and 74.2%, respectively) [116]. Yang et al. [123] studied the material nZVI loaded on biochar stabilized by starch to remediate  $Cr^{6+}$ .

Enzyme immobilization is an emerging technology for environmental remediation which gives many advantages over free enzymes, which include the efficiency and stability of catalytic enzymes and their enhanced recovery and reusability [128]. Further, the immobilized enzyme can be used as biosensors and biocatalysts to degrade dye from textile, leather, coloring, and printing industries [129]. Immobilized peroxidase on polymer/ $Fe_3O_4$  magnetic NPs has been successfully used to remediate wastewater containing different dyes in the textile industry [128]. Immobilized phenoloxidases other than peroxidase, including laccase and tyrosinase, are also used to degrade dyes and phenolic pollutants, and lipases are used to remediate oily wastewater [130]. Mehde [131] reported that magnetic NPs/tannic acid/starch/cross-linked enzyme aggregates-peroxidase are used to remove different types of dyes, such as methylene blue, Congo red, indigo carmine, and malachite green.

#### 6.5. Other Applications

Plasticized starch/reduced graphene oxide (rGO) nanocomposites with improved conductivity and dielectric properties can be used in bio-friendly flexible electronic devices [80]. The maize starch/glycerol (20%)/Na-MMT (10%) nanocomposite showed improved tensile properties, which can be used in lightweight architectural constructions [66]. Starch-based nanocomposites can also be used in lithium batteries, fuel cells, dye-sensitized solar cells, and electrically conductive biocomposite film for various other purposes [22,77].

Table 2 summarizes the studies reported on various biodegradable starch-based nanocomposites in regard to their applications and properties.

**Table 2.** Starch-based nanocomposites using various biodegradable polymers in regard to their applications and properties.

Starch-Based Nanocomposites	Application	Properties	References
Native (TPS) or oxidized (TPS-ox) corn starch/chitosan (CS)/bentonite (Bent)	Mulch film	The addition of 4% CS/Bent improved water resistance (decreased water solubility), radiometric, and antibacterial properties. Decreased mechanical property (tensile strength and elastic modulus: TPS-ox > TPS-ox/CS/Bent > TPS > TPS/CS/Bent).	[83]
Native (TPS) or oxidized (TPS-ox) corn starch/chitosan (CS)/bentonite (Bent)	Mulch film	The addition of 4% CS/Bent increased the crystallinity (3.30 and 3.00%) and led to a slight increase in thermal stability ( $T_{max}$ 139.2 and 126.9 °C) in TPS and TPS-ox, respectively.	[86]
Corn starch-g-poly(AA-co-AAm)/natural char nanoparticles (NCNPs)/urea	Bi-functional slow-release fertilizers	Provided improved biodegradability, soil water-retention capacity (35.6% and 33.2% at pH 4.5 and 5.5, respectively, after 6 days), water absorbency (215.1 g/g) along with the slow release of urea (73% in deionized water and 37% in NaCl).	[84]
Urea encapsulated with starch (10%)/PVA (5%) with crosslinker acrylic acid (2%) and citric acid (2%)	Slow release of fertilizer	Releasing efficiency of starch/PVA/acrylic acid and starch/PVA/citric acid were 70.10 and 50.74%, respectively. Improved the growth factors in spinach plants	[89]



Table 2. Cont.

Starch-Based Nanocomposites	Application	Properties	References
Corn starch/Debranched starch NPs (DSNPs)	Food packaging	Addition of 5% DSNPs increased the tensile strength (from 0.95 to 1.73 MPa) and decreased the water vapor permeability ( $7.11$ to $4.91 \times 10^{-10}$ gPa <sup>-1</sup> h <sup>-1</sup> m <sup>-1</sup> ) and oxygen transmission rate (394 to 81.61 cm <sup>3</sup> /m <sup>2</sup> ·day)	[49]
Starch NPs/Ag NPs	Coating material for food packaging	Antibacterial activity against <i>Staphylococcus aureus</i> , <i>Salmonella typhi</i> , and <i>Escherichia coli</i> .	[50]
Cross-linked wheat starch (CLWS)/sodium montmorillonite (Na-MMT)/TiO <sub>2</sub> NPs	Food packaging material	Shown exfoliated structure. Adding Na-MMT (5%) and TiO <sub>2</sub> NPs (1%) into CLWS showed reduced water vapor permeability (from 9.1 to $4.8 \times 10^{-5}$ g/m.d.Pa) and water solubility (100–50.35%), and increased thermal stability, tensile strength (2.49–5.56 MPa), and Young's modulus (0.71–1.09 MPa) in comparison to native wheat starch. CLWS/Na-MMT/TiO <sub>2</sub> NPs showed better UV-blocking properties than CLWS/Na-MMT.	[69]
Sweet potato starch (SPS)/montmorillonite (MMT)/thyme essential oil (TEO)	Food packaging	The addition of MMT improved the tensile (44.91%), Young's modulus (135.69 MPa), and water vapor barrier (0.022 gm/m <sup>2</sup> /day) and hindered the biodegradability of SPS. The addition of TEO decreased the mechanical and water vapor barrier properties of SPS/MMT nanocomposites. The addition of MMT and TEO improved water resistance by 50%.	[100]
Starch (potato, wheat, and corn, high amylose corn) carboxyl methylcellulose (CMC)/Na-MMT	Food packaging	Corn starch/CMC/Na-MMT nanocomposite showed higher tensile strength, glass transition temperature, thermal stability, crystallinity, lower solubility, and water vapor permeability.	[98]
Cassava starch/glycerol/Na-bentonite nanoclay/cinnamon essential oil	Antimicrobial food packaging pork meatballs	Antibacterial activity against <i>Escherichia coli</i> , <i>Salmonella typhimurium</i> , and <i>Staphylococcus aureus</i> . Improved the antimicrobial efficacy in pork meatballs stored under ambient and refrigeration conditions.	[72]
Starch/polyvinyl alcohol (PVA)/cinnamaldehyde (Cin)/micro fibrillated cellulose (MFC)	Controlled-release active packaging film	MFC improved the tensile strength, crystallinity, hydrophobicity, and antimicrobial activity (against <i>S. putrefaciens</i> ) with reduced flexibility. The oxygen and water vapor permeability reduced at 1 and 2.5% MFC and increased at higher concentrations. MFC at 1 and 7.5% controlled the release of Cin.	[102]
Corn starch (CS)/nanocellulose (NC)/glycerol (GL)/polyvinyl alcohol (PVOH)	Packaging material for edible oil	Optimum composition for CS-based nanocomposite: 0.89% NC, 2.53% GL, and 1.89% PVOH. Tensile strength 8.92 MPa, elongation at break 41.92%, bursting strength 556 kPa, and WVP $7.07 \times 10^{-10}$ g/m.s.Pa, oxygen transmission rate $3.56 \times 10^{-5}$ cm <sup>3</sup> /m <sup>2</sup> d.Pa. Good heat salability.	[94]
Starch from unripe plantain bananas/cellulose nanofibers from banana peels	Food packaging	Homogenized nanocomposite at five times higher pressure increased the tensile strength (from 7.3–9.9 MP), Young's modulus (478.6–663.1 MPa), decreased the elongation at break (32.2–20.7%), solubility (32.3–29.0%), WVP (10.7–6.0 $\times 10^{-11}$ g/m.s.Pa at low RH), sorption (2.73–2.20 $\times 10^{-7}$ mm <sup>2</sup> /s), and diffusion coefficient (0.42–0.27).	[59]
Corn starch (CS)/nanocellulose fiber (NCF)/thymol	Antioxidant and antimicrobial food packaging	Adding 1.5% of NCF improved the thermal stability, mechanical and water vapor, and oxygen barrier properties of corn starch film. CS/NCF/thymol composite reported improved thermal stability and flexibility with decreased tensile strength, Young's modulus, and barrier properties.	[58]
Starch/cellulose nanocrystals (CNC)	Food packaging	Improved the tensile strength (2.8 to 17.4 MPa), Young's modulus (112 to 520 MPa), water resistance (reduced solubility 26.6 to 18.5%), and water barrier properties and decreased surface hydrophilicity (contact angle 38.2 to 96.3°).	[60]

Table 2. Cont.

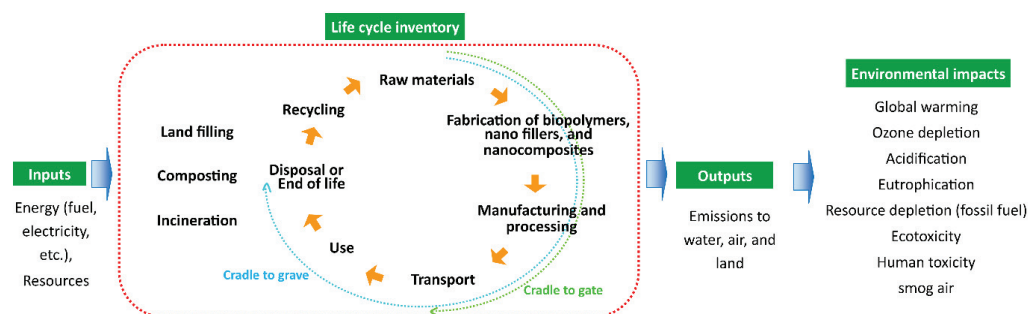
Starch-Based Nanocomposites	Application	Properties	References
TPS/chitin nanofibers (CNF) from fungus <i>Mucor indicus</i>	Nanocomposite for food packaging and other applications.	Addition of 5 wt.% CNF enhanced Young's modulus (239%) and tensile strength (by 180%) and reduced the elongation at break and moisture absorption compared to the TPS film.	[39]
PVA/starch/Ag NPs from <i>Diospyros lotus</i> fruit extract	Wound dressing applications	Increased swelling and moisture retention capacity, reduced water vapor transmission. Better antimicrobial activity against <i>Escherichia coli</i> and <i>Staphylococcus aureus</i>	[109]
Thermoplastic starch (TPS)/beta-tricalcium phosphate ( $\beta$ -TCP) NPs	Bone tissue engineering materials	Adding $\beta$ -TCP at 10% improved the tensile strength (from 1.67 to 4.8 MPa) and Young's modulus (from 66.54 to 390.5 MPa), and decreased elongation at break (78.56 to 18.03%) of TPS. Exhibited non-cytotoxicity effects and excellent biocompatibility.	[105]
Poly(lactic acid) (PLA)/starch (S)/poly- $\epsilon$ -caprolactone (PCL)/nano hydroxyapatite (nHAp)/	Controlled release of antibacterial triclosan	Incorporating nHA (3%) improved the hydrolytic hydrophilicity, hydrolytic degradation, antibacterial activity (against <i>Escherichia coli</i> and <i>Staphylococcus aureus</i> ), and continuous drug release of PLA/S/PCL film.	[110]
Starch-itaconic acid/ $\text{Fe}_3\text{O}_4$ NPs (St-IA/ $\text{Fe}_3\text{O}_4$ )	Controlled release of Guaifenesin (GFN)	The addition of magnetic $\text{Fe}_3\text{O}_4$ NPs at 0.83% enhanced the drug release percentage from 54.1 to 90.4% within 24 h in pH 7.4. Adding $\text{Fe}_3\text{O}_4$ NPs improved the wound healing ability in mice (healed after 10 days). Exhibited low cytotoxicity for human umbilical vein endothelial cells.	[113]
Graft copolymer hydroxyethyl starch-g-poly(acrylamide-co-acrylic acid)/Ag-Au bimetallic nanocomposite	Removal of toxic azo dyes from wastewater	Catalytic activities: reduction of 4-nitrophenol to 4-aminophenol and degradation by cleavage of $-\text{N}=\text{N}$ -the bond of azo dyes (Congo red, Sudan-1, and methyl orange).	[122]
Starch-graft-poly(acrylamide) (PAM)/graphene oxide (GO)/hydroxyapatite NPs (nHAp) nanocomposite	Recyclable adsorbent for efficient removal of malachite green (MG) dye from aqueous solution	PAM/GO and nHAp at 1–5 wt.% reported excellent porosity (31–11%), degradability (41–11% after 15 days), the maximum adsorption capacity of 297 mg/g, excellent regeneration capacity after five consecutive adsorption-desorption cycle of dye (27–14% of MG dye was liberated after 5th cycle, i.e., 77–86% removal efficiency)	[126].
Bean starch/sodium montmorillonite (Na-MMT)	Removal of $\text{Ni}^{2+}$ from water	Adding Na-MMT improved the absorption yield for $\text{Ni}^{2+}$ (from 72 to 97.1% at pH 4.5, initial concentration of 100 ppm) and $\text{Co}^{2+}$ (74.2 to 78.03% at pH 6, initial concentration of 140) in comparison to the bean starch matrix.	[116]
MWCNT/starch plasticized with ionic liquid, 1-ethyl-3-methylimidazolium acetate ([emim+][Ac-])	Packaging, lithium batteries, fuel cells, and dye-sensitized solar cells	MWCNT at 0.5 wt.% increased the tensile strength, Young's modulus, and elongation at the break by 327%, 2484%, and 82%, respectively. Electrical conductivity increased with MWCNT content with the maximum (56.3 S/m) at 5 wt.% MWCNT. Starch plasticizer [emim+][Ac-] slightly decreased the thermal stability in comparison to glycerol in the MWCNT/starch nanocomposite.	[77]
Starch/MWCNT/surfactants such as sodium dodecyl sulfate (SDS), cetyltrimethylammonium bromide (CTAB), and sodium cholate (SC)	Electrically conductive biocomposite film	CTAB reduced the mechanical properties of starch, while SC had no significant effect. SC (18.3–25.3°) and CTAB (20.8–32.3°) reduced the contact angle of starch (42.9–45.2°). CTAB (14.75 S/m) and SC (11.56 S/m) improved the electrical conductivity of starch ( $2.03 \times 10^{-6}$ S/m). CTAB (30.2%), SDS (24.4%), and SC (12%) increased the inhibition of free radicals more than starch.	[22].
Maize starch/glycerol (20%)/Na-MMT (10%) nanoclay	Lightweight architectural constructions	Showed intercalated structure and improved tensile properties.	[66]

## 7. Lifecycle Analysis of Nanocomposites

With increasing fossil depletion and environmental concerns, sustainable biobased materials have gained increasing interest. For biobased materials to be sustainable, preparation and processing should have limited environmental impacts [132].

The environmental credentials of bionanocomposites are evaluated by assessing their material production, product manufacturing, and product end-of-life. Many tools, including environmental impact analysis (EIA), life cycle analysis (LCA), material flow analysis (MFA), and ecological footprint (EF), are used for analyzing the environmental impacts of materials and manufacturing processes [133]. Life cycle assessment (LCA) is the most widely accepted method to assess environmental impact [134]. LCA is a science-based tool to comparatively analyze the environmental impacts of product systems concerning the extraction of raw materials, manufacturing, the use of final products, and their disposal [133,135,136].

The international organization for standardization (ISO) standardized the LCA via ISO 14040 series [134]. The two most commonly used methods are “*cradle to grave*” and “*cradle to gate*” [134,135]. The “*cradle to gate*” system covers all the steps from raw material extraction and energy to product conversion and delivery at the factory gate, whereas “*cradle to grave*” covers all phases of the lifecycle of a product, i.e., includes all steps of “*cradle to gate*” and usage and disposal phase [134]. LCA can be investigated through several environmental impact categories, such as global warming, ozone depletion, acidification, eutrophication, resource depletion (fossil fuel), ecotoxicity, human toxicity, photo oxidant formation, smog air, etc. [136–138]. Thus it is difficult to compare the results between studies [138]. Furthermore, there are only very few mentions in the literature about the environmental performance of nanomaterials based on LCA methods which also has some limitations, including a lack of life cycle inventory data and characterization factors for NMs’ emissions [139,140]. Figure 10 depicts the simplified framework for the LCA of nanocomposite materials.



**Figure 10.** A general framework for the LCA of nanocomposite materials.

This section covers the environmental profile of starch-based nanocomposites in comparison to nonconventional counterparts. The environmental impacts of starch-based composites production with PBS, PLA/PBAT, PHB, PLA, PBS/fiber, and recycled-PLA were greatly varied: non-renewable energy use (NREU) (33–72 MJ/kg, when using virgin starch), eutrophication (1.2–1.9 g P eq./kg), greenhouse gas (GHG) emissions (1.8–3.7 kg CO<sub>2</sub> eq./kg) and agricultural land use (0.3–1.3 m<sup>2</sup>yr/kg) (Table 3). Compared to petrochemical polymers, LDPE and PP, virgin starch-based polymers reduced GHG emissions (up to 80%, except starch/PBS, starch/PLA/PBAT) and NREU (up to 60%) but increased eutrophication potential (up to 400%) and agricultural land use. Furthermore, reclaimed starch from wastewater instead of virgin starch reduced environmental impacts [141].

The microwave-assisted technique can be an environmentally friendly alternative for glucose-reduced and starch-stabilized Ag NPs production [137].

LeCorre et al. [132] compared the sustainability of extraction of nanofillers’ starch nanocrystals (SNC) and organically modified nanoclay montmorillonite (OMMT). Though global warming and acidification potential indicators of SNC were higher than those of

OMMT, SNC has more positive impacts than OMMT, which contributes to non-renewable energy and mineral depletion.

The choice of starch sources and plasticizers influences the environmental impacts displayed by the production of composites. Corn starch/glycerol exhibited the lowest impact on the ecosystem, human health, and resources [142].

**Table 3.** Environmental impacts of starch polymer and nanofiller compared with LDPE polymer (Functional unit = 1 kg).

Impact Category	Ozone Depletion (kg CFC-11 eq.)	Global Warming Potential/Greenhouse Gas Emissions (kg CO <sub>2</sub> eq.)	Smog (kg O <sub>3</sub> eq.)	Acidification (kg SO <sub>2</sub> eq.)	Eutrophication (kg N eq.)	Human Toxicity, Carcinogen (CTUh)	Human Toxicity, Noncarcinogen (CTUh)	Respiratory Effects (kg PM <sub>2.5</sub> eq.)	Ecotoxicity (CTUe)	Water Consumption (Kg)	Agricultural Land Use (m <sup>2</sup> yr/kg)	Fossil Fuel Depletion/Non-Renewable Energy Use (MJ Surplus)	Reference
PE waste management	1.28 × 10 <sup>-5</sup>	3.82 × 10 <sup>3</sup>		5.77 × 10	1.39 × 10 <sup>c</sup>							1.05 × 10 <sup>-4</sup>	[143]
Starch-based polymers production with PBS, PLA/PBAT, PHB, PLA, PBS/fiber, and recycled-PLA		1.8–3.7			1.2–1.9 <sup>d</sup>						0.3–1.3	33–72	[141]
Starch-stabilized Ag NPs manufacturing via microwave-assisted heating	1.24 × 10 <sup>-7</sup>	8.44 × 10 <sup>-2</sup>	2.37 × 10 <sup>-1</sup>	2.51 × 10 <sup>-1</sup>	1.21 × 10 <sup>-1</sup>	4.44 × 10 <sup>-6</sup>	8.02 × 10 <sup>-4</sup>		6.41 × 10 <sup>2</sup>	5.85 × 10 <sup>5</sup>		7.08 × 10 <sup>2</sup>	[137]
Starch nanofiller preparation using various process	0.00	7.95–13.07	0.5–0.6 <sup>a</sup>	8.78–15.51 <sup>b</sup>	0.16–0.23	0.9–0.16 <sup>e</sup>	2216.99–3747.76 <sup>f</sup>	0.02	33.15–115.82 <sup>g</sup>			16–19	[132]
Nanofiller OMMT		1.52						1.139 <sup>g</sup>				40.079	[144]

<sup>a</sup>, kg/NO<sub>x</sub> eq.; <sup>b</sup>, H<sup>+</sup> moles eq.; <sup>c</sup>, kg PO<sub>4</sub><sup>3-</sup> eq.; <sup>d</sup>, g P eq./kg; <sup>e</sup>, kg benzene eq.; <sup>f</sup>, kg toluene eq.; <sup>g</sup>, g PM; <sup>h</sup>, kg 2,4-D eq. PM<sub>2.5</sub>, particulate matter of size under 2.5 μm; 2,4-D, 2,4-dichlorophenoxyacetic acid used as a herbicide and pesticide.

### 8. Biodegradation of Starch

Based on ASTM, biodegradable is defined as ‘capable of undergoing decomposition into carbon dioxide, methane, water, inorganic compounds, or biomass in which the predominant mechanism is the enzymatic action of microorganisms that can be measured by standard tests, in a specified period, reflecting available disposal condition’ [44]. Biodegradable polymers play a critical role in environmental sustainability as they take part in the natural cycle “from nature to nature” [145]. With regard to biopolymer, to be certified as a



biodegradable material, 90% of its mass should be decomposed in composting conditions within 90 days [146].

The type, nature, concentration, chemical modification, and antimicrobial properties of nanofiller, biodegradation test methods, and parameters, including temperature, moisture, humidity, pH, quantity and type of microorganisms, etc., can influence the biodegradability of nanocomposites [15,145,147].

Starch modification and incorporation of nanomaterials as nanofiller have been shown to alter biodegradability. For example, the biodegradability of starch increased with the addition of MMT at lower concentrations because of increased hydrophilicity that permits the microorganisms to enter into the polymer. In contrast, chemical modification of starch, nanofillers such as TiO<sub>2</sub>, graphene oxide, etc., reduce the biodegradability of starch-based nanocomposite because of their antioxidant potential [5,14,15,148].

Crosslinked nanocomposite film produced from thermoplastic corn starch crosslinked with oxidized sucrose and reinforced with cellulose nanofibrils from a pineapple leaf was reported to have a 30% weight loss rate after 30 days of burial, much lower than that of thermoplastic starch (80%) [5]. Crosslinking thermoplastic starch is hard to decompose due to the formation of acetal/hemiacetals and reduction of hydrophilicity and water permeability of nanocomposite, which decrease the attraction and permeability of microorganisms into the polymer matrix [5].

The addition of MMT into sweet potato starch (SPS) hindered biodegradability in soil burial tests due to the strong hydrogen bond between the hydroxyl groups of SPS and MMT and decreased water solubility that prevents water diffusion into the film [100]. However, the effect of MMT on biodegradability is concentration dependent. In corn starch-based film, adding MMT nanoclay at a lower concentration (1–3%) delayed the biodegradation rate (22–23 days for complete degradation), which may be attributed to the formation of the exfoliated structure at a lower concentration of MMT, which ensures good interaction between MMT and the polymer matrix. The biodegradability was increased at a higher level (>3%) of MMT due to agglomeration [15].

The cationic starch-based film incorporated with MMT and nanocrystalline cellulose degrade faster than the pure cationic starch film in composting at 58 °C, which may be attributed to hydrophilic nanocrystalline cellulose [127]. Thyme essential oil (TEO) and MMT incorporation have also been shown to increase biodegradation in SPS/MMT nanocomposites [100].

Incorporating fibrous TiO<sub>2</sub> (0.01 and 0.05 wt.%) in maize starch/PVA composite films improved the tensile strength, water vapor, and UV barrier properties with little effect on biodegradability in soil [146]. The addition of nanoclay fillers delays the biodegradation of corn starch when buried in a microbiological medium of pure *Micrococcus luteus* culture at room temperature for 30 days [15]. Incorporating antimicrobial Ag NPs into starch/PVA composite film reduced its biodegradability [14].

The addition of CaCO<sub>3</sub> in starch/polyethylhexylacrylate (PEHA)/PVA composite film improved the tensile strength, thermal stability, chemical resistance, and antimicrobial properties, which can be suitable for packaging. Starch/PEHA/PVA/CaCO<sub>3</sub> degraded by 65% after 15 days in activated sludge water [149]. Food packaging material prepared from poly(ethyl methacrylate)-co-starch/graphene oxide/AgNPs showed only a 4.5% biodegradation in active sludge water after 180 days [97].

Poly(lactic acid) (PLA)/thermoplastic cassava starch (TPCS)/graphene nanoplatelets (GRH) nanocomposite film showed a lower biodegradation rate than PLA film in vermiculite (0.11 to 0.06 d<sup>-1</sup>) and compost media (0.09 to 0.08 d<sup>-1</sup>) [148].

In slow-release fertilizer formulation, the incorporation of natural char nanoparticles (NCNPs) into corn starch-g-poly (acrylic acid-co-acrylamide)/urea composite increased the degradation rate (23.9% after 30 days in soil), which may be attributed to the increment in water absorbance that promotes the soil microorganisms to enter into the polymer matrix [84].

The biodegradability of nanocomposite film polylactic acid/starch/poly- $\epsilon$ -caprolactone/nano hydroxyapatite (nHAp) was increased with the nHAp content [110]. Hosseinzadeh and Ramin [126] reported that the degradability of starch-graft-poly(acrylamide) (PAM)/graphene oxide (GO) nanocomposite decreased with increasing nHAp addition in buffer solution due to the higher crystallinity, compressive strength, and elastic modulus of nanocomposite film.

In vitro degradation tests performed in a simulated body fluid (SBF) showed that thermoplastic starch (TPS)/beta-tricalcium phosphate ( $\beta$ -TCP) NPs degraded 51% after 28 days, higher than that of TPS (47%) [105]. Table 4 summarizes the recent findings about the biodegradability of different starch-based biopolymers.

**Table 4.** Biodegradability of different starch-based biopolymers.

Starch-Based Nanocomposite	Method	Biodegradation	Other Observation	Reference
Poly(ethyl methacrylate)-co-starch/graphene oxide/Ag NPs (PEMA-co-starch/GO/Ag NPs)	Active sludge water for 180 days.	4.5% after 180 days.	GO and Ag NPs (2 wt.%) increased thermal stability, chemical resistance, tensile strength, and oxygen barrier property. Antimicrobial activity against <i>Escherichia coli</i> , <i>Pseudomonas aeruginosa</i> , <i>Staphylococcus aureus</i> , and <i>Bacillus subtilis</i> .	[97]
Maize starch/PVA/TiO <sub>2</sub>	Soil burial test: buried at 2–3 cm depth in peaty soil with 60% moisture, 98% RH, at 30 °C for 3 months.	Around <20% remaining mass after 80 days.	The addition of fibrous TiO <sub>2</sub> (0.01 and 0.05 wt.%) decreased the elongation at break and improved the tensile strength, Young's modulus UV, and water vapor barrier properties.	[146]
Sweet potato starch (SPS)/montmorillonite (MMT)/thyme essential oil (TEO)	Soil burial degradation test.	The addition of MMT hindered the biodegradability (23.25%) of SPS (48.88%). Biodegradability of SPS/MMT increased with the addition of TEO (61–63%)	The addition of MMT and TEO improved water resistance by 50%. The addition of MMT at 3% and TEO at 2% improved the elongation, Young's modulus, and water vapor barrier properties of SPS.	[100]
Corn starch/glycerol/montmorillonite (MMT) nanoclay	Microbiological medium of pure <i>Micrococcus luteus</i> culture incubating at room temperature for 30 days.	Complete decay after 20 days in corn starch and 21–24 days in corn starch filled with nanoclay.	Addition of nanoclay (2–3 wt.%) in corn starch reduced water absorption (by 22%), moisture uptake (40%), oxygen permeation (30%), and swelling thickness (31%).	[15]
Cationic starch (CS)/montmorillonite (MMT)/nanocrystalline cellulose (NCC)	Composting conditions at 58 °C for 26 days.	CS/MMT/NCC nanocomposite films showed a higher decomposition rate than pure CS. 90% disintegration after 26 days.	Addition of MMT (5% wt) and NCC (5% wt) increased tensile strength (6.60 MPa) and modulus (2.17 GPa), and decreased elongation at break, water solubility (19.63%), moisture absorption (17.73%), water vapor permeability (4.61 gMm.m <sup>-2</sup> day.kPa), O <sub>2</sub> permeability (28.72 cm <sup>3</sup> m <sup>-1</sup> d <sup>-1</sup> Pa <sup>-1</sup> ).	[127]
Cross-linked poly(lactic acid) (PLA)/maleated thermoplastic starch (MTPS)/montmorillonite (MMT)	Samples (1.5 × 1.5 cm) in activated sludge for 3 months.	MTPS and nanoclay improved the biodegradation, while crosslinking of PLA reduced the biodegradation rate.	The addition of MMT improved tensile strength. Increasing MTPS (wt.%) content decreased the tensile strength and increased the elongation at break.	[71]
Corn starch-g-poly(AA-co-AAm)/natural char nanoparticles (NCNPs) nanocomposite encapsulated urea. Where: acrylic acid (AA), acrylamide (AAm).	Buried in the soil at pH 7.5 for 30 days.	The degradation rate after 30 days was 23.9%.	The addition of NCNPs decreased the leaching of nitrate and improved soil water-retention capacity.	[84]

Table 4. Cont.

Starch-Based Nanocomposite	Method	Biodegradation	Other Observation	Reference
Thermoplastic corn starch (TPS)/cellulose nanofibrils from pineapple leaf/oxidized sucrose	Sample (40 × 8 × 2 mm) buried at 10 cm depth of a sand and soil mixture (in equal ratio) at ambient temperature for 30 days.	About 30% weight loss in cross-linked films after 30 days, much lower than TPS (80%).	-	[5]
Starch/polyethylhexylacrylate (PEHA)/polyvinylalcohol (PVA)/nano CaCO <sub>3</sub> nanocomposite	Activated sludge water for 90 days.	Starch/PEHA/PVA/CaCO <sub>3</sub> (8 wt.%) degraded by 65% after 15 days	CaCO <sub>3</sub> increased the tensile strength, thermal conductivity, thermal stability, and chemical resistance. Antimicrobial activity against <i>Candida albicans</i> , <i>Escherichia coli</i> , <i>Pseudomonas aeruginosa</i> .	[149]
Poly(lactic acid) (PLA)/thermoplastic cassava starch (TPCS)/graphene nanoplatelets (GRH)	Samples (1 cm <sup>2</sup> ) buried in inoculated vermiculite and compost under aerobic controlled conditions: at 58 ± 2 °C, RH 50 ± 5%, and airflow rate 40 ± 2 cm <sup>3</sup> min <sup>-1</sup> .	The addition of GRH decreased the biodegradation rate from 0.11 to 0.06 d <sup>-1</sup> in vermiculite and 0.09 to 0.08 d <sup>-1</sup> in compost media.	In PLA, adding TPCS and GRH reduced the crystallinity (34.5 to 4.5%).	[148]
Poly(lactic acid) (PLA)/starch (S)/poly-ε-caprolactone (PCL)/nano hydroxyapatite (nHAp)/	In-vitro hydrolytic degradation test, 0.15 g samples (1 × 1 × 0.15 cm) was hot pressed and incubated in 50 mL phosphate buffer with pH 7.4 at 37 °C.	The increase in nHAp content (1–7%), faster the degradation (13–10 months).	Incorporating nHA (3%) improved the hydrophilicity and antibacterial activity (against <i>Escherichia coli</i> and <i>Staphylococcus aureus</i> ).	[110]
Starch-graft-poly(acrylamide) (PAM)/graphene oxide (GO)/hydroxyapatite NPs (nHAp) nanocomposite	Soaked in PBS buffer solutions (pH 7.4) containing lysozyme (5000 U/mL) at 37 °C for 15 days.	Biodegradation decreased with increasing nHAp content. Degradability was 41–11% lower than that of PAM/GO (55%) after 15 days.	With increasing nHAp content, porosity, water content, and water uptake were decreased.	[126]
Thermoplastic starch (TPS)/beta-tricalcium phosphate (β-TCP) NPs	In vitro degradation tests were performed in a simulated body fluid (SBF) for 28 days.	Degraded 51% after 28 days, higher than TPS (47%).	Adding β-TCP at 10% improved the mechanical properties of TPS.	[105]
Starch/PVA/Ag NPs	Under controlled aerobic composting conditions at 58 ± 2 °C for 45 days (based on EN ISO 14855-1: 2012 standard). Disintegration test under composting conditions: 5 g of film samples (25 × 25 mm) at 58 ± 2 °C for 73 days (ISO 20200: 2004).	Biodegradation is 58% after 45 days, which is higher than that of PVA (54%) and lower than starch (134%). Poor disintegration behavior in comparison to starch.	-	[14]
Polyvinyl alcohol (PVA)/corn starch (CS)/linseed polyol (LP)/Ag NPs	Soil burial of samples (2 × 2 cm) at a depth of 10 cm.	Biodegradability after 4 weeks PVA < PVA/CS < PVA/CS/LP < PVA/CS/LP/Ag NPs	Improved contact angle (53°), water absorption capacity (equilibrium swelling percentage 129%), thermal stability (10% weight loss at 308 °C), and biodegradation than PVA/CS film. Ag NPs improved antimicrobial behavior against <i>Proteus mirabilis</i> , <i>Candida albicans</i> , <i>Escherichia coli</i> , <i>Enterococcus faecalis</i> , <i>Staphylococcus aureus</i> , <i>Klebsiella pneumoniae</i> , among others.	[96]

## 9. Conclusions and Future Perspectives

In summary, starch is a natural polymer with outstanding biocompatible characteristics and can be used as both a matrix and reinforcement material for the development of new

bionanocomposites. Starch nanoparticles and other nanofillers, including nanocellulose, chitin NPs, nanoclay (MMT, HNTs, bentonites), carbon nanoparticles (MWCNTs, SWCNTs, graphene, graphene oxides), metal and metal oxides (Ag NPs, TiO<sub>2</sub>, ZnO, CaCO<sub>3</sub>, etc.), have been widely used for the creation of new starch-based bionanocomposites and are promising candidates for various industrial applications.

The excellent biocompatibility, complete degradability without toxic residues, low cost, wide availability, and renewability of starch-based nanocomposites would open up many applications in agriculture, packaging, environmental remediation, biomedicine, and many other fields. Some of the reported applications are edible food coating, active and intelligent food packaging, controlled/slow-released pesticides and fertilizers, mulch films, drug carriers (controlled/target specific), wound healing, scaffolds in tissue engineering, absorbents, filters, catalysts, or disinfectants for environmental remediation, electronic devices, lightweight architectural constructions, stabilizers in food and paints such as non-food applications, and many others.

Modification of starch or reinforcement with other materials to form a nanocomposite may alter biodegradability. Therefore, regarding the biodegradability of starch-based nanocomposites is important for them to be claimed as being biodegradable materials. Life cycle assessment of starch-based biocomposite materials for their respective applications provides critical information regarding the environmental and ecological benefits of the materials over fossil-based synthetic polymers for developing sustainable nanocomposites. However, only few studies have focused on life cycle assessment. Therefore, further studies on life cycle assessment of starch-based nanocomposites needs to be investigated. Nanomaterials can also enter the human body through inhalation, contact, and ingestion, which can lead to their accumulation in the human body. Therefore, further investigations on toxicity and risk factor analysis are necessary to find the most suitable starch-based nanocomposite materials.

**Author Contributions:** Writing—original draft, A.G., P.T., S.M., P.G.P., P.E. and T.M. Review and editing, A.G., P.T., S.M., P.G.P., A.M., O.M. and T.M. All authors have read and agreed to the published version of the manuscript.

**Funding:** This research received no external funding.

**Institutional Review Board Statement:** Not applicable.

**Data Availability Statement:** Not applicable.

**Conflicts of Interest:** The authors declare no conflict of interest.

## References

1. Ates, B.; Koytepe, S.; Ulu, A.; Gurses, C.; Thakur, V.K. Chemistry, Structures, and Advanced Applications of Nanocomposites from Biorenewable Resources. *Chem. Rev.* **2020**, *120*, 9304–9362. [CrossRef] [PubMed]
2. Saad, E.M.; Elshaarawy, R.F.; Mahmoud, S.A.; El-Moselhy, K.M. New Ulva Lactuca Algae Based Chitosan Bio-Composites for Bioremediation of Cd(II) Ions. *J. Biosour. Bioprod.* **2021**, *6*, 223–242. [CrossRef]
3. Puiggali, J.; Katsarava, R. Chapter 7—Bionanocomposites. In *Clay-Polymer Nanocomposites*; Jlassi, K., Chehimi, M.M., Thomas, S., Eds.; Elsevier: Amsterdam, The Netherlands, 2017; pp. 239–272, ISBN 978-0-323-46153-5.
4. Madhumitha, G.; Fowsiya, J.; Mohana Roopan, S.; Thakur, V.K. Recent Advances in Starch–Clay Nanocomposites. *Int. J. Polym. Anal. Charact.* **2018**, *23*, 331–345. [CrossRef]
5. Balakrishnan, P.; Geethamma, V.G.; Gopi, S.; Thomas, M.G.; Kunaver, M.; Huskić, M.; Kalarikkal, N.; Volova, T.; Rouxel, D.; Thomas, S. Thermal, Biodegradation and Theoretical Perspectives on Nanoscale Confinement in Starch/Cellulose Nanocomposite Modified via Green Crosslinker. *Int. J. Biol. Macromol.* **2019**, *134*, 781–790. [CrossRef]
6. Arora, B.; Bhatia, R.; Attri, P. 28—Bionanocomposites: Green Materials for a Sustainable Future. In *New Polymer Nanocomposites for Environmental Remediation*; Hussain, C.M., Mishra, A.K., Eds.; Elsevier: Wilmington, NC, USA, 2018; pp. 699–712, ISBN 978-0-12-811033-1.
7. García, N.L.; Famá, L.; D’Accorso, N.B.; Goyanes, S. Biodegradable Starch Nanocomposites. In *Eco-friendly Polymer Nanocomposites: Processing and Properties*; Thakur, V.K., Thakur, M.K., Eds.; Advanced Structured Materials; Springer: New Delhi, India, 2015; pp. 17–77, ISBN 978-81-322-2470-9.



8. Mohammad, F.; Arfin, T.; Bwatanglang, I.B.; Al-lohedan, H.A. Starch-Based Nanocomposites: Types and Industrial Applications. In *Bio-Based Polymers and Nanocomposites: Preparation, Processing, Properties & Performance*; Sanyang, M.L., Jawaid, M., Eds.; Springer International Publishing: Cham, Switzerland, 2019; pp. 157–181, ISBN 978-3-030-05825-8.
9. BeMiller, J.N. Chapter 5—Physical Modification of Starch. In *Starch in Food*, 2nd ed.; Sjöo, M., Nilsson, L., Eds.; Woodhead Publishing Series in Food Science, Technology and Nutrition; Woodhead Publishing: Cambridge, UK, 2018; pp. 223–253, ISBN 978-0-08-100868-3.
10. Gunawardene, O.H.P.; Gunathilake, C.A.; Amaraweera, A.P.S.M.; Fernando, N.M.L.; Manipura, A.; Manamperi, W.A.; Kulatunga, K.M.A.K.; Rajapaksha, S.M.; Gamage, A.; Dassanayake, R.S.; et al. Removal of Pb(II) Ions from Aqueous Solution Using Modified Starch. *J. Compos. Sci.* **2021**, *5*, 46. [CrossRef]
11. Okoli, C.P.; Ofomaja, A.E. Degree of Time Dependency of Kinetic Coefficient as a Function of Adsorbate Concentration; New Insights from Adsorption of Tetracycline onto Monodispersed Starch-Stabilized Magnetic Nanocomposite. *J. Environ. Manag.* **2018**, *218*, 139–147. [CrossRef]
12. Zarski, A.; Bajer, K.; Kapuśniak, J. Review of the Most Important Methods of Improving the Processing Properties of Starch toward Non-Food Applications. *Polymers* **2021**, *13*, 832. [CrossRef]
13. Le Corre, D.; Angellier-Coussy, H. Preparation and Application of Starch Nanoparticles for Nanocomposites: A Review. *React. Funct. Polym.* **2014**, *85*, 97–120. [CrossRef]
14. Cano, A.I.; Cháfer, M.; Chiralt, A.; González-Martínez, C. Biodegradation Behavior of Starch-PVA Films as Affected by the Incorporation of Different Antimicrobials. *Polym. Degrad. Stab.* **2016**, *132*, 11–20. [CrossRef]
15. Mohan, T.; Devchand, K.; Kanny, K. Barrier and Biodegradable Properties of Corn Starch-Derived Biopolymer Film Filled with Nanoclay Fillers. *J. Plast. Film Sheeting* **2017**, *33*, 309–336. [CrossRef]
16. Venkatesh, G.; Nyflött, Å.; Bonnerup, C.; Lestelius, M. An Economic-Environmental Analysis of Selected Barrier-Coating Materials Used in Packaging Food Products: A Swedish Case Study. *Env. Dev. Sustain.* **2018**, *20*, 1483–1497. [CrossRef]
17. Wani, A.A.; Singh, P. Application of Life Cycle Assessment for Starch and Starch Blends. In *Starch-Based Polymeric Materials and Nanocomposites*; Ahmed, J., Tiwari, B.K., Imam, S.H., Rao, M.A., Eds.; CRC Press: Boca Raton, FL, USA, 2012; ISBN 978-0-429-10818-1.
18. Kakadellis, S.; Harris, Z.M. Don't Scrap the Waste: The Need for Broader System Boundaries in Bioplastic Food Packaging Life-Cycle Assessment—A Critical Review. *J. Clean. Prod.* **2020**, *274*, 122831. [CrossRef]
19. Bertolini, A. (Ed.) *Starches: Characterization, Properties, and Applications*, 1st ed.; CRC Press: Boca Raton, FL, USA, 2009; ISBN 978-0-429-14172-0.
20. Govindaraju, I.; Zhuo, G.-Y.; Chakraborty, I.; Melanthota, S.K.; Mal, S.S.; Sarmah, B.; Baruah, V.J.; Mahato, K.K.; Mazumder, N. Investigation of Structural and Physico-Chemical Properties of Rice Starch with Varied Amylose Content: A Combined Microscopy, Spectroscopy, and Thermal Study. *Food Hydrocoll.* **2022**, *122*, 107093. [CrossRef]
21. Pérez, S.; Baldwin, P.M.; Gallant, D.J. Chapter 5—Structural Features of Starch Granules I. In *Starch*, 3rd ed.; BeMiller, J., Whistler, R., Eds.; Food Science and Technology; Academic Press: San Diego, CA, USA, 2009; pp. 149–192, ISBN 978-0-12-746275-2.
22. Alves, Z.; Abreu, B.; Ferreira, N.M.; Marques, E.F.; Nunes, C.; Ferreira, P. Enhancing the Dispersibility of Multiwalled Carbon Nanotubes within Starch-Based Films by the Use of Ionic Surfactants. *Carbohydr. Polym.* **2021**, *273*, 118531. [CrossRef]
23. Basiak, E.; Lenart, A.; Debeaufort, F. Effect of Starch Type on the Physico-Chemical Properties of Edible Films. *Int. J. Biol. Macromol.* **2017**, *98*, 348–356. [CrossRef]
24. Chaudhary, A.K.; Vijayakumar, R.P. Synthesis of Polystyrene/Starch/CNT Composite and Study on Its Biodegradability. *J. Polym. Res.* **2020**, *27*, 187. [CrossRef]
25. Copeland, L.; Blazek, J.; Salman, H.; Tang, M.C. Form and Functionality of Starch. *Food Hydrocoll.* **2009**, *23*, 1527–1534. [CrossRef]
26. Cornejo-Ramírez, Y.I.; Martínez-Cruz, O.; Del Toro-Sánchez, C.L.; Wong-Corral, F.J.; Borboa-Flores, J.; Cinco-Moroyoqui, F.J. The Structural Characteristics of Starches and Their Functional Properties. *CyTA—J. Food* **2018**, *16*, 1003–1017. [CrossRef]
27. Nogueira, G.F.; Fakhouri, F.M.; de Oliveira, R.A. Extraction and Characterization of Arrowroot (*Maranta Arundinaceae* L.) Starch and Its Application in Edible Films. *Carbohydr. Polym.* **2018**, *186*, 64–72. [CrossRef]
28. Lemos, P.V.F.; Barbosa, L.S.; Ramos, I.G.; Coelho, R.E.; Druzian, J.I. The Important Role of Crystallinity and Amylose Ratio in Thermal Stability of Starches. *J. Anal. Calorim.* **2018**, *131*, 2555–2567. [CrossRef]
29. Li, Z.; Guo, K.; Lin, L.; He, W.; Zhang, L.; Wei, C. Comparison of Physicochemical Properties of Starches from Flesh and Peel of Green Banana Fruit. *Molecules* **2018**, *23*, 2312. [CrossRef] [PubMed]
30. Thanyapanich, N.; Jimtaisong, A.; Rawdkuen, S. Functional Properties of Banana Starch (*Musa* Spp.) and Its Utilization in Cosmetics. *Molecules* **2021**, *26*, 3637. [CrossRef] [PubMed]
31. Schirmer, M.; Höchstätter, A.; Jekle, M.; Arendt, E.; Becker, T. Physicochemical and Morphological Characterization of Different Starches with Variable Amylose/Amylopectin Ratio. *Food Hydrocoll.* **2013**, *32*, 52–63. [CrossRef]
32. Chisenga, S.M.; Workneh, T.S.; Bultosa, G.; Alimi, B.A. Progress in Research and Applications of Cassava Flour and Starch: A Review. *J. Food Sci. Technol.* **2019**, *56*, 2799–2813. [CrossRef] [PubMed]
33. Han, H.; Hou, J.; Yang, N.; Zhang, Y.; Chen, H.; Zhang, Z.; Shen, Y.; Huang, S.; Guo, S. Insight on the Changes of Cassava and Potato Starch Granules during Gelatinization. *Int. J. Biol. Macromol.* **2019**, *126*, 37–43. [CrossRef] [PubMed]
34. Zhong, Y.; Liu, L.; Qu, J.; Blennow, A.; Hansen, A.R.; Wu, Y.; Guo, D.; Liu, X. Amylose Content and Specific Fine Structures Affect Lamellar Structure and Digestibility of Maize Starches. *Food Hydrocoll.* **2020**, *108*, 105994. [CrossRef]

35. Kong, X.; Zhu, P.; Sui, Z.; Bao, J. Physicochemical Properties of Starches from Diverse Rice Cultivars Varying in Apparent Amylose Content and Gelatinisation Temperature Combinations. *Food Chem.* **2015**, *172*, 433–440. [CrossRef] [PubMed]
36. Zhou, W.; Yang, J.; Hong, Y.; Liu, G.; Zheng, J.; Gu, Z.; Zhang, P. Impact of Amylose Content on Starch Physicochemical Properties in Transgenic Sweet Potato. *Carbohydr. Polym.* **2015**, *122*, 417–427. [CrossRef]
37. Biduski, B.; da Silva, W.M.F.; Colussi, R.; Halal, S.L.; De, M.E.; Lim, L.-T.; Dias, Á.R.G.; da Zavareze, E.R. Starch Hydrogels: The Influence of the Amylose Content and Gelatinization Method. *Int. J. Biol. Macromol.* **2018**, *113*, 443–449. [CrossRef]
38. Singh, S.; Singh, N.; Isono, N.; Noda, T. Relationship of Granule Size Distribution and Amylopectin Structure with Pasting, Thermal, and Retrogradation Properties in Wheat Starch. *J. Agric. Food Chem.* **2010**, *58*, 1180–1188. [CrossRef]
39. Bahrami, B.; Behzad, T.; Salehinik, F.; Zamani, A.; Heidarian, P. Incorporation of Extracted *Mucor Indicus* Fungus Chitin Nanofibers into Starch Biopolymer: Morphological, Physical, and Mechanical Evaluation. *Starch—Stärke* **2021**, *73*, 2000218. [CrossRef]
40. Ngô, C.; Van de Voorde, M.H. Nanomaterials: Doing More with Less. In *Nanotechnology in a Nutshell: From Simple to Complex Systems*; Ngô, C., Van de Voorde, M., Eds.; Atlantis Press: Paris, France, 2014; pp. 55–70, ISBN 978-94-6239-012-6.
41. Saleh, T.A. Nanomaterials: Classification, Properties, and Environmental Toxicities. *Environ. Technol. Innov.* **2020**, *20*, 101067. [CrossRef]
42. Singh, V.; Yadav, P.; Mishra, V. Recent Advances on Classification, Properties, Synthesis, and Characterization of Nanomaterials. In *Green Synthesis of Nanomaterials for Bioenergy Applications*; John Wiley & Sons, Ltd.: Hoboken, NJ, USA, 2020; pp. 83–97, ISBN 978-1-119-57678-5.
43. Zafar, R.; Zia, K.M.; Tabasum, S.; Jabeen, F.; Noreen, A.; Zuber, M. Polysaccharide Based Bionanocomposites, Properties and Applications: A Review. *Int. J. Biol. Macromol.* **2016**, *92*, 1012–1024. [CrossRef] [PubMed]
44. Turan, D.; Gunes, G.; Kilic, A. Perspectives of Bio-Nanocomposites for Food Packaging Applications. In *Bionanocomposites for Packaging Applications*; Jawaid, M., Swain, S.K., Eds.; Springer International Publishing: Cham, Switzerland, 2018; pp. 1–32, ISBN 978-3-319-67319-6.
45. Sandhu, K.S.; Nain, V. Starch Nanoparticles: Their Preparation and Applications. In *Plant Biotechnology: Recent Advancements and Developments*; Gahlawat, S.K., Salar, R.K., Siwach, P., Duhan, J.S., Kumar, S., Kaur, P., Eds.; Springer: Singapore, 2017; pp. 213–232, ISBN 978-981-10-4732-9.
46. Santana, J.S.; de Carvalho Costa, É.K.; Rodrigues, P.R.; Correia, P.R.C.; Cruz, R.S.; Druzian, J.I. Morphological, Barrier, and Mechanical Properties of Cassava Starch Films Reinforced with Cellulose and Starch Nanoparticles. *J. Appl. Polym. Sci.* **2019**, *136*, 47001. [CrossRef]
47. Campelo, P.H.; Sant’Ana, A.S.; Pedrosa Silva Clerici, M.T. Starch Nanoparticles: Production Methods, Structure, and Properties for Food Applications. *Curr. Opin. Food Sci.* **2020**, *33*, 136–140. [CrossRef]
48. Lee, Y.-S.; Tarté, R.; Acevedo, N.C. Synergistic Effects of Starch Nanoparticles and Chitin Nanofibers on the Stability of Oil-in-Water Pickering Emulsions. *Food Chem.* **2021**, *363*, 130301. [CrossRef]
49. Lin, Q.; Ji, N.; Li, M.; Dai, L.; Xu, X.; Xiong, L.; Sun, Q. Fabrication of Debranched Starch Nanoparticles via Reverse Emulsification for Improvement of Functional Properties of Corn Starch Films. *Food Hydrocoll.* **2020**, *104*, 105760. [CrossRef]
50. Amirsoleimani, M.; Khalilzadeh, M.A.; Sadeghifar, F.; Sadeghifar, H. Surface Modification of Nanostarch Using Nano Silver: A Potential Antibacterial for Food Package Coating. *J. Food Sci. Technol.* **2018**, *55*, 899–904. [CrossRef]
51. Krystyjan, M.; Khachatryan, G.; Khachatryan, K.; Konieczna-Molenda, A.; Grzesiakowska, A.; KuchtaGładysz, M.; Kawecka, A.; Grzebieniarski, W.; Nowak, N. The Functional and Application Possibilities of Starch/Chitosan Polymer Composites Modified by Graphene Oxide. *Int. J. Mol. Sci.* **2022**, *23*, 5956. [CrossRef]
52. Othman, S.H. Bio-Nanocomposite Materials for Food Packaging Applications: Types of Biopolymer and Nano-Sized Filler. *Agric. Agric. Sci. Procedia* **2014**, *2*, 296–303. [CrossRef]
53. Nasir, M.; Hashim, R.; Sulaiman, O.; Asim, M. 11—Nanocellulose: Preparation Methods and Applications. In *Cellulose-Reinforced Nanofibre Composites*; Jawaid, M., Boufi, S., Hps, A.K., Eds.; Woodhead Publishing Series in Composites Science and Engineering; Woodhead Publishing: Cambridge, UK, 2017; pp. 261–276, ISBN 978-0-08-100957-4.
54. Dufresne, A. Nanocellulose: A New Ageless Bionanomaterial. *Mater. Today* **2013**, *16*, 220–227. [CrossRef]
55. Reshmy, R.; Philip, E.; Paul, S.A.; Madhavan, A.; Sindhu, R.; Binod, P.; Pandey, A.; Sirohi, R. Nanocellulose-Based Products for Sustainable Applications—Recent Trends and Possibilities. *Rev. Env. Sci. Biotechnol.* **2020**, *19*, 779–806. [CrossRef]
56. Phanthong, P.; Reubroycharoen, P.; Hao, X.; Xu, G.; Abudula, A.; Guan, G. Nanocellulose: Extraction and Application. *Carbon Resour. Convers.* **2018**, *1*, 32–43. [CrossRef]
57. Trache, D.; Tarchoun, A.F.; Derradji, M.; Hamidon, T.S.; Masruchin, N.; Brosse, N.; Hussin, M.H. Nanocellulose: From Fundamentals to Advanced Applications. *Front. Chem.* **2020**, *8*, 392. [CrossRef] [PubMed]
58. Othman, S.H.; Nordin, N.; Azman, N.A.A.; Tawakkal, I.S.M.A.; Basha, R.K. Effects of Nanocellulose Fiber and Thymol on Mechanical, Thermal, and Barrier Properties of Corn Starch Films. *Int. J. Biol. Macromol.* **2021**, *183*, 1352–1361. [CrossRef]
59. Pelissari, F.M.; Andrade-Mahecha, M.M.; do Sobral, P.J.A.; Menegalli, F.C. Nanocomposites Based on Banana Starch Reinforced with Cellulose Nanofibers Isolated from Banana Peels. *J. Colloid Interface Sci.* **2017**, *505*, 154–167. [CrossRef]
60. Slavutsky, A.M.; Bertuzzi, M.A. Water Barrier Properties of Starch Films Reinforced with Cellulose Nanocrystals Obtained from Sugarcane Bagasse. *Carbohydr. Polym.* **2014**, *110*, 53–61. [CrossRef]

61. Heidari, M.; Khomeiri, M.; Yousefi, H.; Rafieian, M.; Kashiri, M. Chitin Nanofiber-Based Nanocomposites Containing Biodegradable Polymers for Food Packaging Applications. *J. Consum. Prot. Food Saf.* **2021**, *16*, 237–246. [CrossRef]
62. Thomas, M.S.; Koshy, R.R.; Mary, S.K.; Thomas, S.; Pothan, L.A. *Starch, Chitin and Chitosan Based Composites and Nanocomposites*; SpringerBriefs in Molecular Science; Springer International Publishing: Cham, Switzerland, 2019; ISBN 978-3-030-03157-2.
63. Yang, X.; Liu, J.; Pei, Y.; Zheng, X.; Tang, K. Recent Progress in Preparation and Application of Nano-Chitin Materials. *Energy Environ. Mater.* **2020**, *3*, 492–515. [CrossRef]
64. Chang, P.R.; Jian, R.; Yu, J.; Ma, X. Starch-Based Composites Reinforced with Novel Chitin Nanoparticles. *Carbohydr. Polym.* **2010**, *80*, 420–425. [CrossRef]
65. Alexandre, M.; Dubois, P. Polymer-Layered Silicate Nanocomposites: Preparation, Properties and Uses of a New Class of Materials. *Mater. Sci. Eng. R Rep.* **2000**, *28*, 1–63. [CrossRef]
66. Mansour, G.; Zoumaki, M.; Marinopoulou, A.; Raphaelides, S.N.; Tzetzis, D.; Zoumakis, N. Investigation on the Effects of Glycerol and Clay Contents on the Structure and Mechanical Properties of Maize Starch Nanocomposite Films. *Starch—Stärke* **2020**, *72*, 1900166. [CrossRef]
67. Abulyazied, D.E.; Ene, A. An Investigative Study on the Progress of Nanoclay-Reinforced Polymers: Preparation, Properties, and Applications: A Review. *Polymers* **2021**, *13*, 4401. [CrossRef] [PubMed]
68. Guo, F.; Aryana, S.; Han, Y.; Jiao, Y. A Review of the Synthesis and Applications of Polymer–Nanoclay Composites. *Appl. Sci.* **2018**, *8*, 1696. [CrossRef]
69. Yousefi, A.R.; Savadkoochi, B.; Zahedi, Y.; Hatami, M.; Ako, K. Fabrication and Characterization of Hybrid Sodium Montmorillonite/TiO<sub>2</sub> Reinforced Cross-Linked Wheat Starch-Based Nanocomposites. *Int. J. Biol. Macromol.* **2019**, *131*, 253–263. [CrossRef] [PubMed]
70. Campos-Requena, V.H.; Rivas, B.L.; Pérez, M.A.; Garrido-Miranda, K.A.; Pereira, E.D. Release of Essential Oil Constituent from Thermoplastic Starch/Layered Silicate Bionanocomposite Film as a Potential Active Packaging Material. *Eur. Polym. J.* **2018**, *109*, 64–71. [CrossRef]
71. Shayan, M.; Azizi, H.; Ghasemi, I.; Karrabi, M. Effect of Modified Starch and Nanoclay Particles on Biodegradability and Mechanical Properties of Cross-Linked Poly Lactic Acid. *Carbohydr. Polym.* **2015**, *124*, 237–244. [CrossRef]
72. Iamareerat, B.; Singh, M.; Sadiq, M.B.; Anal, A.K. Reinforced Cassava Starch Based Edible Film Incorporated with Essential Oil and Sodium Bentonite Nanoclay as Food Packaging Material. *J. Food Sci. Technol.* **2018**, *55*, 1953–1959. [CrossRef]
73. Dang, K.M.; Yoksan, R.; Pollet, E.; Avérous, L. Morphology and Properties of Thermoplastic Starch Blended with Biodegradable Polyester and Filled with Halloysite Nanoclay. *Carbohydr. Polym.* **2020**, *242*, 116392. [CrossRef]
74. Schmitt, H.; Prashantha, K.; Soulestin, J.; Lacrampe, M.F.; Krawczak, P. Preparation and Properties of Novel Melt-Blended Halloysite Nanotubes/Wheat Starch Nanocomposites. *Carbohydr. Polym.* **2012**, *89*, 920–927. [CrossRef]
75. Abdullah, Z.W.; Dong, Y. Biodegradable and Water Resistant Poly(Vinyl) Alcohol (PVA)/Starch (ST)/Glycerol (GL)/Halloysite Nanotube (HNT) Nanocomposite Films for Sustainable Food Packaging. *Front. Mater.* **2019**, *6*, 58. [CrossRef]
76. Ambika; Singh, P.P. Advances in Carbon Nanomaterial-Based Green Nanocomposites. In *Emerging Carbon-Based Nanocomposites for Environmental Applications*; Mishra, A.K., Hussain, C.M., Mishra, S.B., Eds.; John Wiley & Sons, Ltd.: Hoboken, NJ, USA, 2020; pp. 175–201, ISBN 978-1-119-55488-2.
77. Domene-López, D.; Delgado-Marín, J.J.; García-Quesada, J.C.; Martín-Gullón, I.; Montalbán, M.G. Electroconductive Starch/Multi-Walled Carbon Nanotube Films Plasticized by 1-Ethyl-3-Methylimidazolium Acetate. *Carbohydr. Polym.* **2020**, *229*, 115545. [CrossRef] [PubMed]
78. Famá, L.; Rojo, P.G.; Bernal, C.; Goyanes, S. Biodegradable Starch Based Nanocomposites with Low Water Vapor Permeability and High Storage Modulus. *Carbohydr. Polym.* **2012**, *87*, 1989–1993. [CrossRef]
79. Xu, D. Carbon Nanotubes (CNTs) Composite Materials and Food Packaging. In *Composites Materials for Food Packaging*; John Wiley & Sons, Ltd.: Hoboken, NJ, USA, 2018; pp. 235–249, ISBN 978-1-119-16024-3.
80. Mollik, S.I.; Alam, R.B.; Islam, M.R. Significantly Improved Dielectric Properties of Bio-Compatible Starch/Reduced Graphene Oxide Nanocomposites. *Synth. Met.* **2021**, *271*, 116624. [CrossRef]
81. Solati, M.; Saeidi, A.; Ghasemi, I. The Effect of Graphene Nanoplatelets on Dynamic Properties, Crystallization, and Morphology of a Biodegradable Blend of Poly(Lactic Acid)/Thermoplastic Starch. *Iran Polym. J.* **2019**, *28*, 649–658. [CrossRef]
82. Kalia, A.; Sharma, S.P.; Kaur, H.; Kaur, H. Chapter 5—Novel Nanocomposite-Based Controlled-Release Fertilizer and Pesticide Formulations: Prospects and Challenges. In *Multifunctional Hybrid Nanomaterials for Sustainable Agri-Food and Ecosystems*; Abd-Elsalam, K.A., Ed.; Micro and Nano Technologies; Elsevier: Amsterdam, The Netherlands, 2020; pp. 99–134, ISBN 978-0-12-821354-4.
83. Merino, D.; Gutiérrez, T.J.; Mansilla, A.Y.; Casalongué, C.A.; Alvarez, V.A. Critical Evaluation of Starch-Based Antibacterial Nanocomposites as Agricultural Mulch Films: Study on Their Interactions with Water and Light. *ACS Sustain. Chem. Eng.* **2018**, *6*, 15662–15672. [CrossRef]
84. Salimi, M.; Motamedi, E.; Motesharezedeh, B.; Hosseini, H.M.; Alikhani, H.A. Starch-g-Poly(Acrylic Acid-Co-Acrylamide) Composites Reinforced with Natural Char Nanoparticles toward Environmentally Benign Slow-Release Urea Fertilizers. *J. Environ. Chem. Eng.* **2020**, *8*, 103765. [CrossRef]
85. Gamage, A.; Liyanapathirana, A.; Manamperi, A.; Gunathilake, C.; Mani, S.; Merah, O.; Madhujith, T. Applications of Starch Biopolymers for a Sustainable Modern Agriculture. *Sustainability* **2022**, *14*, 6085. [CrossRef]



86. Merino, D.; Gutiérrez, T.J.; Alvarez, V.A. Structural and Thermal Properties of Agricultural Mulch Films Based on Native and Oxidized Corn Starch Nanocomposites. *Starch—Stärke* **2019**, *71*, 1800341. [CrossRef]
87. Pereira, E.I.; Giroto, A.S.; Bortolin, A.; Yamamoto, C.F.; Marconcini, J.M.; de Campos Bernardi, A.C.; Ribeiro, C. Perspectives in Nanocomposites for the Slow and Controlled Release of Agrochemicals: Fertilizers and Pesticides. In *Nanotechnologies in Food and Agriculture*; Rai, M., Ribeiro, C., Mattoso, L., Duran, N., Eds.; Springer International Publishing: Cham, Switzerland, 2015; pp. 241–265, ISBN 978-3-319-14024-7.
88. Pimsen, R.; Porrawatkul, P.; Nuengmatcha, P.; Ramasoot, S.; Chanthai, S. Efficiency Enhancement of Slow Release of Fertilizer Using Nanozeolite–Chitosan/Sago Starch-Based Biopolymer Composite. *J. Coat. Technol. Res.* **2021**, *18*, 1321–1332. [CrossRef]
89. Zafar, N.; Niazi, M.B.K.; Sher, F.; Khalid, U.; Jahan, Z.; Shah, G.A.; Zia, M. Starch and Polyvinyl Alcohol Encapsulated Biodegradable Nanocomposites for Environment Friendly Slow Release of Urea Fertilizer. *Chem. Eng. J. Adv.* **2021**, *7*, 100123. [CrossRef]
90. Jain, S.K.; Dutta, A.; Kumar, J.; Shakil, N.A. Preparation and Characterization of Dicarboxylic Acid Modified Starch-Clay Composites as Carriers for Pesticide Delivery. *Arab. J. Chem.* **2020**, *13*, 7990–8002. [CrossRef]
91. Galstyan, V.; Bhandari, M.P.; Sberveglieri, V.; Sberveglieri, G.; Comini, E. Metal Oxide Nanostructures in Food Applications: Quality Control and Packaging. *Chemosensors* **2018**, *6*, 16. [CrossRef]
92. Oleyaei, S.A.; Zahedi, Y.; Ghanbarzadeh, B.; Moayedi, A.A. Modification of Physicochemical and Thermal Properties of Starch Films by Incorporation of TiO<sub>2</sub> Nanoparticles. *Int. J. Biol. Macromol.* **2016**, *89*, 256–264. [CrossRef]
93. Pirsá, S.; Karimi Sani, I.; Khodayvandi, S. Design and Fabrication of Starch-Nano Clay Composite Films Loaded with Methyl Orange and Bromocresol Green for Determination of Spoilage in Milk Package. *Polym. Adv. Technol.* **2018**, *29*, 2750–2758. [CrossRef]
94. Patil, S.; Bharimalla, A.K.; Nadanathangam, V.; Dhakane-Lad, J.; Mahapatra, A.; Jagajanantha, P.; Saxena, S. Nanocellulose Reinforced Corn Starch-Based Biocomposite Films: Composite Optimization, Characterization and Storage Studies. *Food Packag. Shelf Life* **2022**, *33*, 100860. [CrossRef]
95. Babaei-Ghazvini, A.; Shahabi-Ghahfarrokhi, I.; Goudarzi, V. Preparation of UV-Protective Starch/Kefiran/ZnO Nanocomposite as a Packaging Film: Characterization. *Food Packag. Shelf Life* **2018**, *16*, 103–111. [CrossRef]
96. Sharmin, E.; Kafyah, M.T.; Alzaydi, A.A.; Fatani, A.A.; Hazazzi, F.A.; Babgi, S.K.; Alqarhi, N.M.; Sindi, A.A.H.; Akram, D.; Alam, M.; et al. Synthesis and Characterization of Polyvinyl Alcohol/Corn Starch/Linseed Polyol-Based Hydrogel Loaded with Biosynthesized Silver Nanoparticles. *Int. J. Biol. Macromol.* **2020**, *163*, 2236–2247. [CrossRef]
97. Mohanty, F.; Swain, S.K. Nano Silver Embedded Starch Hybrid Graphene Oxide Sandwiched Poly(Ethylmethacrylate) for Packaging Application. *Nano-Struct. Nano-Objects* **2019**, *18*, 100300. [CrossRef]
98. Jha, P.; Dharmalingam, K.; Nishizu, T.; Katsuno, N.; Anandalakshmi, R. Effect of Amylose–Amylopectin Ratios on Physical, Mechanical, and Thermal Properties of Starch-Based Bionanocomposite Films Incorporated with CMC and Nanoclay. *Starch—Stärke* **2020**, *72*, 1900121. [CrossRef]
99. de Souza, A.G.; dos Santos, N.M.A.; da Silva Torin, R.F.; dos Santos Rosa, D. Synergic Antimicrobial Properties of Carvacrol Essential Oil and Montmorillonite in Biodegradable Starch Films. *Int. J. Biol. Macromol.* **2020**, *164*, 1737–1747. [CrossRef] [PubMed]
100. Issa, A.T.; Schimmel, K.A.; Worku, M.; Shahbazi, A.; Ibrahim, S.A.; Tahergorabi, R. Sweet Potato Starch-Based Nanocomposites: Development, Characterization, and Biodegradability. *Starch—Stärke* **2018**, *70*, 1700273. [CrossRef]
101. Barzegar, H.; Azizi, M.H.; Barzegar, M.; Hamidi-Esfahani, Z. Effect of Potassium Sorbate on Antimicrobial and Physical Properties of Starch–Clay Nanocomposite Films. *Carbohydr. Polym.* **2014**, *110*, 26–31. [CrossRef] [PubMed]
102. Chen, Y.; Guo, Z.; Das, R.; Jiang, Q. Starch-Based Carbon Nanotubes and Graphene: Preparation, Properties and Applications. *ES Food Agrofor.* **2020**, *2*, 13–21. [CrossRef]
103. Gomes, M.E.; Godinho, J.S.; Tchalamov, D.; Cunha, A.M.; Reis, R.L. Alternative Tissue Engineering Scaffolds Based on Starch: Processing Methodologies, Morphology, Degradation and Mechanical Properties. *Mater. Sci. Eng. C* **2002**, *20*, 19–26. [CrossRef]
104. Lu, D.R.; Xiao, C.M.; Xu, S.J. Starch-Based Completely Biodegradable Polymer Materials. *Express Polym. Lett.* **2009**, *3*, 366–375. [CrossRef]
105. Taherimehr, M.; Bagheri, R.; Taherimehr, M. In-Vitro Evaluation of Thermoplastic Starch/ Beta-Tricalcium Phosphate Nano-Biocomposite in Bone Tissue Engineering. *Ceram. Int.* **2021**, *47*, 15458–15463. [CrossRef]
106. Waghmare, V.S.; Wadke, P.R.; Dyawanapelly, S.; Deshpande, A.; Jain, R.; Dandekar, P. Starch Based Nanofibrous Scaffolds for Wound Healing Applications. *Bioact. Mater.* **2018**, *3*, 255–266. [CrossRef]
107. Sadjadi, M.S.; Meskinfam, M.; Jazdarreh, H. Hydroxyapatite—Starch Nano Biocomposites Synthesis and Characterization. *Int. J. Nano Dimens.* **2010**, *1*, 57–63. [CrossRef]
108. Abdel-Halim, E.S.; Al-Deyab, S.S. Antimicrobial Activity of Silver/Starch/Polyacrylamide Nanocomposite. *Int. J. Biol. Macromol.* **2014**, *68*, 33–38. [CrossRef]
109. Batool, S.; Hussain, Z.; Niazi, M.B.K.; Liaqat, U.; Afzal, M. Biogenic Synthesis of Silver Nanoparticles and Evaluation of Physical and Antimicrobial Properties of Ag/PVA/Starch Nanocomposites Hydrogel Membranes for Wound Dressing Application. *J. Drug Deliv. Sci. Technol.* **2019**, *52*, 403–414. [CrossRef]
110. Davachi, S.M.; Shiroud Heidari, B.; Hejazi, I.; Seyfi, J.; Oliaei, E.; Farzaneh, A.; Rashedi, H. Interface Modified Polylactic Acid/Starch/Poly  $\epsilon$ -Caprolactone Antibacterial Nanocomposite Blends for Medical Applications. *Carbohydr. Polym.* **2017**, *155*, 336–344. [CrossRef] [PubMed]



111. Mallakpour, S.; Khodadadzadeh, L. Ultrasonic-Assisted Fabrication of Starch/MWCNT-Glucose Nanocomposites for Drug Delivery. *Ultrason. Sonochem.* **2018**, *40*, 402–409. [CrossRef] [PubMed]
112. Gao, X.; Wei, L.; Yan, H.; Xu, B. Green Synthesis and Characteristic of Core-Shell Structure Silver/Starch Nanoparticles. *Mater. Lett.* **2011**, *65*, 2963–2965. [CrossRef]
113. Nezami, S.; Sadeghi, M.; Mohajerani, H. A Novel PH-Sensitive and Magnetic Starch-Based Nanocomposite Hydrogel as a Controlled Drug Delivery System for Wound Healing. *Polym. Degrad. Stab.* **2020**, *179*, 109255. [CrossRef]
114. Shi, Y.; Xu, D.; Liu, M.; Fu, L.; Wan, Q.; Mao, L.; Dai, Y.; Wen, Y.; Zhang, X.; Wei, Y. Room Temperature Preparation of Fluorescent Starch Nanoparticles from Starch-Dopamine Conjugates and Their Biological Applications. *Mater. Sci. Eng. C* **2018**, *82*, 204–209. [CrossRef]
115. Guerra, F.D.; Attia, M.F.; Whitehead, D.C.; Alexis, F. Nanotechnology for Environmental Remediation: Materials and Applications. *Molecules* **2018**, *23*, 1760. [CrossRef]
116. García-Padilla, Á.; Moreno-Sader, K.A.; Realpe, Á.; Acevedo-Morantes, M.; Soares, J.B.P. Evaluation of Adsorption Capacities of Nanocomposites Prepared from Bean Starch and Montmorillonite. *Sustain. Chem. Pharm.* **2020**, *17*, 100292. [CrossRef]
117. Mallakpour, S.; Nouruzi, N. Application of Vitamin B1-Coated Carbon Nanotubes for the Production of Starch Nanocomposites with Enhanced Structural, Optical, Thermal and Cd(II) Adsorption Properties. *J. Polym. Environ.* **2018**, *26*, 2954–2963. [CrossRef]
118. Nasrollahzadeh, M.; Sajjadi, M.; Iravani, S.; Varma, R.S. Starch, Cellulose, Pectin, Gum, Alginate, Chitin and Chitosan Derived (Nano)Materials for Sustainable Water Treatment: A Review. *Carbohydr. Polym.* **2021**, *251*, 116986. [CrossRef]
119. Orooji, Y.; Nezafat, Z.; Nasrollahzadeh, M.; Kamali, T.A. Polysaccharide-Based (Nano)Materials for Cr(VI) Removal. *Int. J. Biol. Macromol.* **2021**, *188*, 950–973. [CrossRef] [PubMed]
120. del Orta, M.M.; Martín, J.; Santos, J.L.; Aparicio, I.; Medina-Carrasco, S.; Alonso, E. Biopolymer-Clay Nanocomposites as Novel and Ecofriendly Adsorbents for Environmental Remediation. *Appl. Clay Sci.* **2020**, *198*, 105838. [CrossRef]
121. Russo, T.; Fucile, P.; Giacometti, R.; Sannino, F. Sustainable Removal of Contaminants by Biopolymers: A Novel Approach for Wastewater Treatment. Current State and Future Perspectives. *Processes* **2021**, *9*, 719. [CrossRef]
122. Tripathy, T.; Kolya, H.; Jana, S.; Senapati, M. Green Synthesis of Ag-Au Bimetallic Nanocomposites Using a Biodegradable Synthetic Graft Copolymer; Hydroxyethyl Starch-g-Poly (Acrylamide-Co-Acrylic Acid) and Evaluation of Their Catalytic Activities. *Eur. Polym. J.* **2017**, *87*, 113–123. [CrossRef]
123. Yang, C.; Ge, C.; Li, X.; Li, L.; Wang, B.; Lin, A.; Yang, W. Does Soluble Starch Improve the Removal of Cr(VI) by NZVI Loaded on Biochar? *Ecotoxicol. Environ. Saf.* **2021**, *208*, 111552. [CrossRef]
124. Adeola, A.O.; Nomngongo, P.N. Advanced Polymeric Nanocomposites for Water Treatment Applications: A Holistic Perspective. *Polymers* **2022**, *14*, 2462. [CrossRef]
125. Gomes, R.F.; de Azevedo, A.C.N.; Pereira, A.G.B.; Muniz, E.C.; Fajardo, A.R.; Rodrigues, F.H.A. Fast Dye Removal from Water by Starch-Based Nanocomposites. *J. Colloid Interface Sci.* **2015**, *454*, 200–209. [CrossRef]
126. Hosseinzadeh, H.; Ramin, S. Fabrication of Starch-Graft-Poly(Acrylamide)/Graphene Oxide/Hydroxyapatite Nanocomposite Hydrogel Adsorbent for Removal of Malachite Green Dye from Aqueous Solution. *Int. J. Biol. Macromol.* **2018**, *106*, 101–115. [CrossRef]
127. Vaezi, K.; Asadpour, G.; Sharifi, S.H. Bio Nanocomposites Based on Cationic Starch Reinforced with Montmorillonite and Cellulose Nanocrystals: Fundamental Properties and Biodegradability Study. *Int. J. Biol. Macromol.* **2020**, *146*, 374–386. [CrossRef]
128. Darwesh, O.M.; Ali, S.S.; Matter, I.A.; Elsamahy, T.; Mahmoud, Y.A. Chapter Twenty—Enzymes Immobilization onto Magnetic Nanoparticles to Improve Industrial and Environmental Applications. In *Methods in Enzymology*; Kumar, C.V., Ed.; Nanoarmoring of Enzymes with Carbon Nanotubes and Magnetic Nanoparticles; Academic Press: Boca Raton, FL, USA, 2020; Volume 630, pp. 481–502.
129. Sharmeen, S.; Rahman, S.; Islam, M.; Islam, S.; Shahrzuzaman; Mallik, A.K.; Haque, P.; Rahman, M.M. 11—Application of Polysaccharides in Enzyme Immobilization. In *Functional Polysaccharides for Biomedical Applications*; Maiti, S., Jana, S., Eds.; Woodhead Publishing: Cambridge, UK, 2019; pp. 357–395, ISBN 978-0-08-102555-0.
130. Liu, D.-M.; Dong, C. Recent Advances in Nano-Carrier Immobilized Enzymes and Their Applications. *Process. Biochem.* **2020**, *92*, 464–475. [CrossRef]
131. Mehde, A.A. Development of Magnetic Cross-Linked Peroxidase Aggregates on Starch as Enhancement Template and Their Application for Decolorization. *Int. J. Biol. Macromol.* **2019**, *131*, 721–733. [CrossRef] [PubMed]
132. LeCorre, D.; Hohenthal, C.; Dufresne, A.; Bras, J. Comparative Sustainability Assessment of Starch Nanocrystals. *J. Polym. Environ.* **2013**, *21*, 71–80. [CrossRef]
133. Finnveden, G.; Moberg, Å. Environmental Systems Analysis Tools—An Overview. *J. Clean. Prod.* **2005**, *13*, 1165–1173. [CrossRef]
134. Shen, L.; Patel, M.K. Life Cycle Assessment of Polysaccharide Materials: A Review. *J. Polym. Environ.* **2008**, *16*, 154–167. [CrossRef]
135. Foroughi, F.; Rezvani Ghomi, E.; Morshedi Dehaghi, F.; Borayek, R.; Ramakrishna, S. A Review on the Life Cycle Assessment of Cellulose: From Properties to the Potential of Making It a Low Carbon Material. *Materials* **2021**, *14*, 714. [CrossRef] [PubMed]
136. Klöpffer, W.; Grahl, B. *Life Cycle Assessment (LCA): A Guide to Best Practice*; John Wiley & Sons: Hoboken, NJ, USA, 2014; ISBN 978-3-527-65564-9.
137. Bafana, A.; Kumar, S.V.; Temizel-Sekeryan, S.; Dahoumane, S.A.; Haselbach, L.; Jeffryes, C.S. Evaluating Microwave-Synthesized Silver Nanoparticles from Silver Nitrate with Life Cycle Assessment Techniques. *Sci. Total Environ.* **2018**, *636*, 936–943. [CrossRef]

138. Bishop, G.; Styles, D.; Lens, P.N.L. Environmental Performance Comparison of Bioplastics and Petrochemical Plastics: A Review of Life Cycle Assessment (LCA) Methodological Decisions. *Resour. Conserv. Recycl.* **2021**, *168*, 105451. [CrossRef]
139. Miseljic, M.; Olsen, S.I. LCA of Nanomaterials. In *Life Cycle Assessment: Theory and Practice*; Hauschild, M.Z., Rosenbaum, R.K., Olsen, S.I., Eds.; Springer International Publishing: Cham, Switzerland, 2018; pp. 817–833, ISBN 978-3-319-56475-3.
140. Nizam, N.U.M.; Hanafiah, M.M.; Woon, K.S. A Content Review of Life Cycle Assessment of Nanomaterials: Current Practices, Challenges, and Future Prospects. *Nanomaterials* **2021**, *11*, 3324. [CrossRef]
141. Broeren, M.L.M.; Kuling, L.; Worrell, E.; Shen, L. Environmental Impact Assessment of Six Starch Plastics Focusing on Wastewater-Derived Starch and Additives. *Resour. Conserv. Recycl.* **2017**, *127*, 246–255. [CrossRef]
142. Rojas-Bringas, P.M.; De-la-Torre, G.E.; Torres, F.G. Influence of the Source of Starch and Plasticizers on the Environmental Burden of Starch-Brazil Nut Fiber Biocomposite Production: A Life Cycle Assessment Approach. *Sci. Total Environ.* **2021**, *769*, 144869. [CrossRef]
143. Aryan, Y.; Yadav, P.; Samadder, S.R. Life Cycle Assessment of the Existing and Proposed Plastic Waste Management Options in India: A Case Study. *J. Clean. Prod.* **2019**, *211*, 1268–1283. [CrossRef]
144. Joshi, S. Can Nanotechnology Improve the Sustainability of Biobased Products? *J. Ind. Ecol.* **2008**, *12*, 474–489. [CrossRef]
145. Wróblewska-Krepsztul, J.; Rydzkowski, T.; Borowski, G.; Szczypiński, M.; Klepka, T.; Thakur, V.K. Recent Progress in Biodegradable Polymers and Nanocomposite-Based Packaging Materials for Sustainable Environment. *Int. J. Polym. Anal. Charact.* **2018**, *23*, 383–395. [CrossRef]
146. Kochkina, N.E.; Butikova, O.A. Effect of Fibrous TiO<sub>2</sub> Filler on the Structural, Mechanical, Barrier and Optical Characteristics of Biodegradable Maize Starch/PVA Composite Films. *Int. J. Biol. Macromol.* **2019**, *139*, 431–439. [CrossRef]
147. Glaskova-Kuzmina, T.; Starkova, O.; Gaidukovs, S.; Platnieks, O.; Gaidukova, G. Durability of Biodegradable Polymer Nanocomposites. *Polymers* **2021**, *13*, 3375. [CrossRef] [PubMed]
148. Bher, A.; Unalan, I.U.; Auras, R.; Rubino, M.; Schvezov, C.E. Graphene Modifies the Biodegradation of Poly(Lactic Acid)-Thermoplastic Cassava Starch Reactive Blend Films. *Polym. Degrad. Stab.* **2019**, *164*, 187–197. [CrossRef]
149. Prusty, K.; Swain, S.K. Nano CaCO<sub>3</sub> Imprinted Starch Hybrid Polyethylhexylacrylate/polyvinylalcohol Nanocomposite Thin Films. *Carbohydr. Polym.* **2016**, *139*, 90–98. [CrossRef]



## Article

# Fabrication, Characterization, and Microbial Biodegradation of Transparent Nanodehydrated Bioplastic (NDB) Membranes Using Novel Casting, Dehydration, and Peeling Techniques

Sherif S. Hindi <sup>1,\*</sup> and Mona Othman I. Albureikan <sup>2</sup>

<sup>1</sup> Department of Agriculture, Faculty of Environmental Sciences, King Abdulaziz University (KAU), P.O. Box 80208, Jeddah 21589, Saudi Arabia

<sup>2</sup> Department of Biological Sciences, Faculty of Science, King Abdulaziz University (KAU), P.O. Box 80208, Jeddah 21589, Saudi Arabia; malboraikan@kau.edu.sa

\* Correspondence: shindi@kau.edu.sa

**Abstract:** NDBs were fabricated from gum Arabic (GA) and polyvinyl alcohol (PVA) in different ratios using novel techniques (casting, dehydration, and peeling). The GA/PVA blends were cast with a novel vibration-free horizontal flow (VFHF) technique, producing membranes free of air bubble defects with a homogenous texture, smooth surface, and constant thickness. The casting process was achieved on a self-electrostatic template (SET) made of poly-(methyl methacrylate), which made peeling the final product membranes easy due to its non-stick behavior. After settling the casting of the membranous, while blind, the sheets were dried using nanometric dehydration under a mild vacuum stream using a novel stratified nano-dehydrator (SND) loaded with P<sub>2</sub>O<sub>5</sub>. After drying the NDB, the dry, smooth membranes were peeled easily without scratching defects. The physicochemical properties of the NDBs were investigated using FTIR, XRD, TGA, DTA, and AFM to ensure that the novel techniques did not distort the product quality. The NDBs retained their virgin characteristics, namely, their chemical functional groups (FTIR results), crystallinity index (XRD data), thermal stability (TGA and DTA), and ultrastructural features (surface roughness and permeability), as well as their microbial biodegradation ability. Adding PVA enhanced the membrane's properties except for mass loss, whereby increasing the GA allocation in the NDB blend reduces its mass loss at elevated temperatures. The produced bioplastic membranes showed suitable mechanical properties for food packaging applications and in the pharmaceutical industry for the controlled release of drugs. In comparison to control samples, the separated bacteria and fungi destroyed the bioplastic membranes. *Pseudomonas* spp. and *Bacillus* spp. were the two main strains of isolated bacteria, and *Rhizobus* spp. was the main fungus. The nano-dehydration method gave the best solution for the prompt drying of water-based biopolymers free of manufacturing defects, with simple and easily acquired machinery required for the casting and peeling tasks, in addition to its wonderful biodegradation behavior when buried in wet soil.

**Citation:** Hindi, S.S.; Albureikan, M.O.I. Fabrication, Characterization, and Microbial Biodegradation of Transparent Nanodehydrated Bioplastic (NDB) Membranes Using Novel Casting, Dehydration, and Peeling Techniques. *Polymers* **2023**, *15*, 3303. <https://doi.org/10.3390/polym15153303>

Academic Editor: Alberto Romero Garcia

Received: 21 May 2023

Revised: 15 July 2023

Accepted: 29 July 2023

Published: 4 August 2023

**Keywords:** hydrophilic bioplastics; gum Arabic; polyvinyl alcohol; casting of poly-(methyl methacrylate); dehydration; phosphorus pentoxide; peeling; microbial biodegradation



**Copyright:** © 2023 by the authors. Licensee MDPI, Basel, Switzerland. This article is an open access article distributed under the terms and conditions of the Creative Commons Attribution (CC BY) license (<https://creativecommons.org/licenses/by/4.0/>).

## 1. Introduction

Despite petroleum-based polymers' lower density and greater mechanical characteristics, biobased polymers have gained significant interest due to growing environmental concerns about their sustainability and biodegradability [1–6]. Many biopolymers, including poly-lactic acid/poly-lactide, poly-3-hydroxy-butyrate, starch, gelatin, alginate, agar agar, guar gum, and GA, have been used in various industrial applications.

GA is a type of edible and natural exudate gum arising from the mature trunks and branches of various acacia species, especially the *Acacia senegal*, *A. seyal*, *A. nilotica*, and *A. mellifera* (family: Fabaceae) [7]. The GA yield can be enhanced by drought conditions,



poor soil fertility, and injured or scratched plants to cover the huge demand for domestic and industrial applications due to its water-soluble and polysaccharide nature [8–10]. Chemically, GA has hydrophilic carbohydrates (arabinogalactans) as well as hydrophobic proteins (the arabinogalactan–protein complex and glycoproteins) that exhibit various functional properties in food additives [11–15]. It is well known that D-galactose, L-arabinose, L-rhamnose, D-glucuronic acid, and 4-O-methyl-d-glucuronic acid make up the highly branched complexes known as arabinogalactan proteins, along with a minor amount of proteins. While hydrophilic arabinogalactan provides steric and electrostatic stability, this hydrophobic polypeptide chain can tie gum to oil droplets in an emulsion [15]. The benefit of the amphiphilic nature of GA is that it prevents coalescence, which can promote film formation and display steric stabilization. Furthermore, GAs have significant effects on various emulsion factors, including opacity, specific gravity, zeta potential, and surface tension [15]. GA is used primarily in the food, medicinal pharmaceutical, and wood technology industries [15–33] and as a stabilizer, emulsifier, and thickening agent [15–18] because of its high hydrophilicity, low fluidic viscosity, good surficial activities, and ability to form a protective film around emulsion droplets [15]. Recently, the use of GA has been extended into the nanotechnology and nanomedicine fields due to its biocompatibility for both *in vivo* and *in vitro* applications and its stabilization of nanostructures. GA has been probed for its coating properties and increased biocompatibility of iron oxide magnetic nanoparticles [34,35], gold nanoparticles [36], carbon nanotubes [37], and quantum dot nanocolloids [38].

PVA is a synthetic polymer with a wide range of commercial applications due to its high crystallinity, good mechanical properties, water solubility, and adhesive properties [39–42]. These applications extend to the industrial, medical, pharmaceutical, and food sectors and include lacquers, resins, surgical threads, food packaging materials [26,29,40], paper coating, textile sizing [43], and coating purposes [44], where they are used in order to enhance the mechanical properties due to natural properties such as compatible structure and hydrophilic properties [45]. Furthermore, it is used as a thermoplastic polymer for living tissues because it is harmless and non-toxic, as well as functioning as a cross-linker and nanofiller [46–48]. Furthermore, since PVA has excellent chemical resistance, it is used as a good emulsifier [49]. Practically, PVA is widely blended with other hydrophilic polymers [45], such as GA, to enhance its mechanical properties as well as its biodegradability [42,50–56]. However, the drawbacks that are associated with the manufacturing of bioplastic materials are the drying process for the cast GA membrane due to the high water content of the parent material, thereby making the entire process time- and cost-intensive. Hence, there is a need to develop an apparatus or method that overcomes the above limitations [57]. The presence of a large number of hydroxyl, carboxylic, and carbonyl groups in the GA/PVA blends makes it a chemical reductant and environmentally benign medium [58]. PVA is easily degradable by biological organisms [39,58], and many microorganisms that are able to degrade PVA and GA have been identified [59–62].

Different GA composites were prepared and characterized by several researchers for fabricating films and membranes [63–65], as well as for the anodes of lithium-ion batteries [66]. In addition, Silvestri et al. [67] produced nanofibers from a blend containing GA (10 wt% solution), graphene oxide (GO), and PVA, while Lubambo et al. [68] obtained nanofibers from guar gum. The processing of GA includes impurity removal, kibbling, granulating, grinding, powdering, acid or enzymatic hydrolysis, clarification and discoloration, centrifugation (10,000–16,000 rpm/min), purification of the ceramic membrane, desalination, and spray drying [69–73].

Several researchers examined the mechanical characteristics of bioplastic materials [74–79]. These characteristics play a crucial role in determining the appropriateness of their use in particular applications. Electrospun scaffolds, for instance, should have adequate mechanical characteristics to withstand tension or compression pressures in bone tissue engineering. As assessed by Masti et al. [74], the mechanical properties of their fabricated bioplastic films were assessed by tensile strength (TS) and Young's modulus ( $Y_m$ ),

termed modulus of elasticity (MoE). The addition of gum acacia (GA) to the equal quantity of PVA/CS in the blend film shows improved  $T_s$  and  $Y_m$ . The increase in the  $T_s$  and  $Y_m$  of the blend due to the addition of the GA suggested that interfacial strength (adhesion) could be improved [74,76]. The further addition of GA decreased both  $T_s$  and  $Y_m$  [74,75].

Based on scientific investigations performed by Chougale et al. [76] and Ibrahim et al. [78], their FTIR studies confirmed that due to the crosslinking and intermolecular interactions caused by esterification during the heat treatment in the blend films, there is a significant interaction between each component of their bioplastic mix. Additionally, when compared to the transverse direction, the mechanical performance of the membranes demonstrated an increase in the elasticity modulus in the longitudinal direction from 85 MPa to 148 MPa [78].

A particular category of polymers known as biodegradable polymers [80–93] degrade naturally into byproducts such as gases ( $\text{CO}_2$  and  $\text{N}_2$ ), water, biomass, and inorganic salts [57] after serving their intended purpose. The abiotic and biotic components of the biodegradation mechanism coexist naturally in the soil [2,6]. Recently, a lot of biodegradable polymers have been created, and some known microbial enzymes can break them down [5]. Numerous microbial communities of bacteria, fungi, and yeasts, including but not limited to Gram-negative species, such as *Escherichia coli* and *Pseudomonas aeruginosa*, and Gram-positive species, such as *Staphylococcus aureus*, can use bioplastic as a nutrition source throughout the biodegradation process [1,3,4,55]. These include *Rhizobium meliloti* [5], *Bacillus* spp. [58], *Pseudomonas* spp., *Aspergillus* spp., *Rhizorpus* spp., *Fusarium* spp., *Penicillium* spp., *Saccharomyces* as yeast [59], and *Elite Aspergillus* [91]. Under aerobic (composting) or anaerobic (landfill) conditions, several petroleum-based polymers are biologically decomposable [47,94]. By combining synthetic and natural polymers, researchers have been able to improve the processing capacity, physicochemical characteristics, and biodegradability of synthetic polymers [1,4,6,50–53]. For various polymers, including PVA, the rates and environmental factors that influence breakdown might vary [47,60,95–97]. Composting can take place under different conditions, including anaerobic environments, underground soil layers, aqueous media, and even in the presence of oxygen.

The aims of the present work were: (a) to invent a more reliable bioplastic membrane that is suitable for different applications; (b) to overcome the casting, drying, and peeling problems of the hydrophilic bioplastic (GA/PVA) blends; (c) to compare the ordinary GA/PVA bioplastic membranes (ADB) with those synthesized using the novel methods in the present investigation (NDBs); and (d) to study the biodegradation behaviors of the NDBs when buried in wet soil.

## 2. Materials and Methods

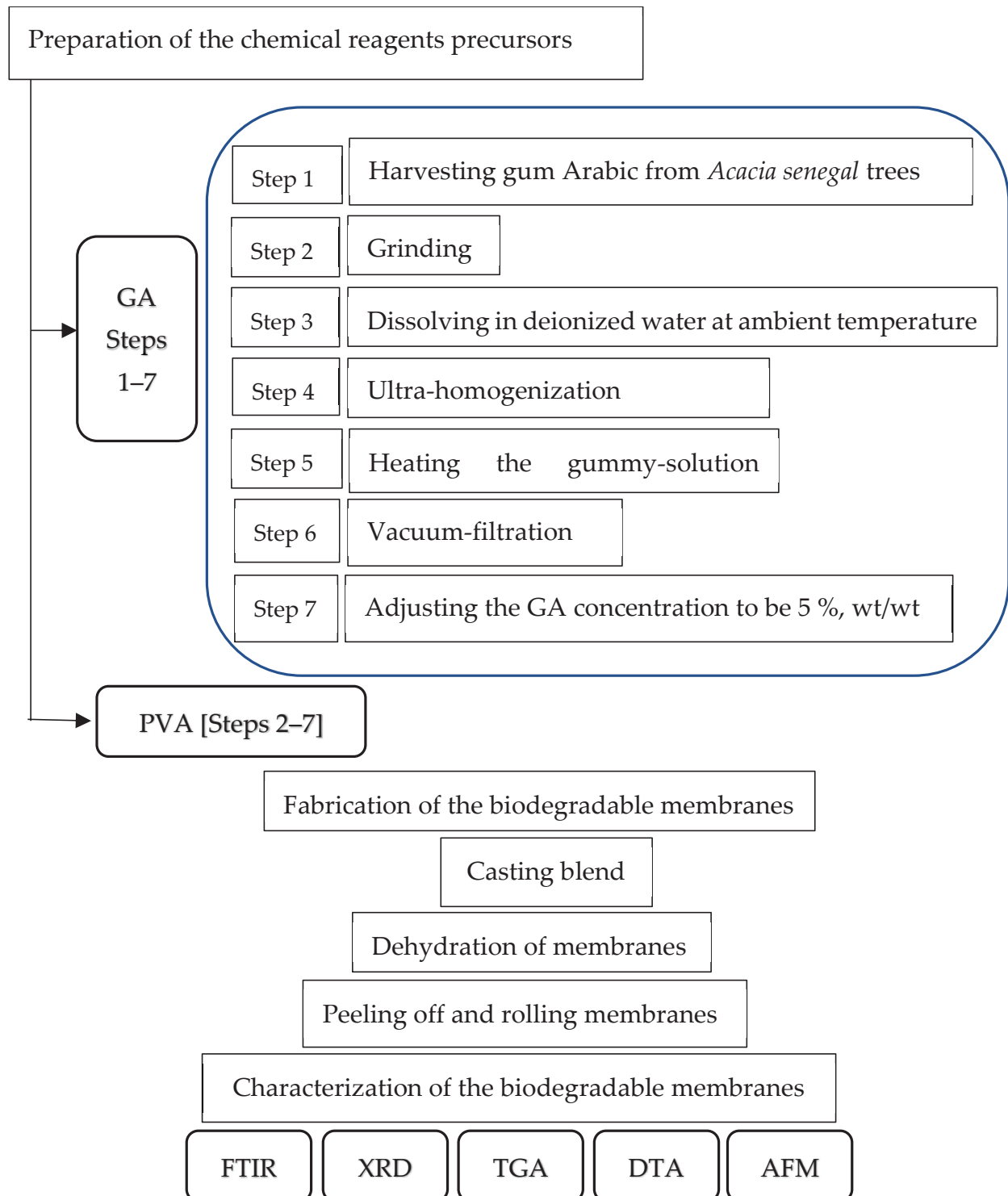
The management plan for the production of novel transparent NDBs is illustrated in Figure 1.

### 2.1. Raw Material

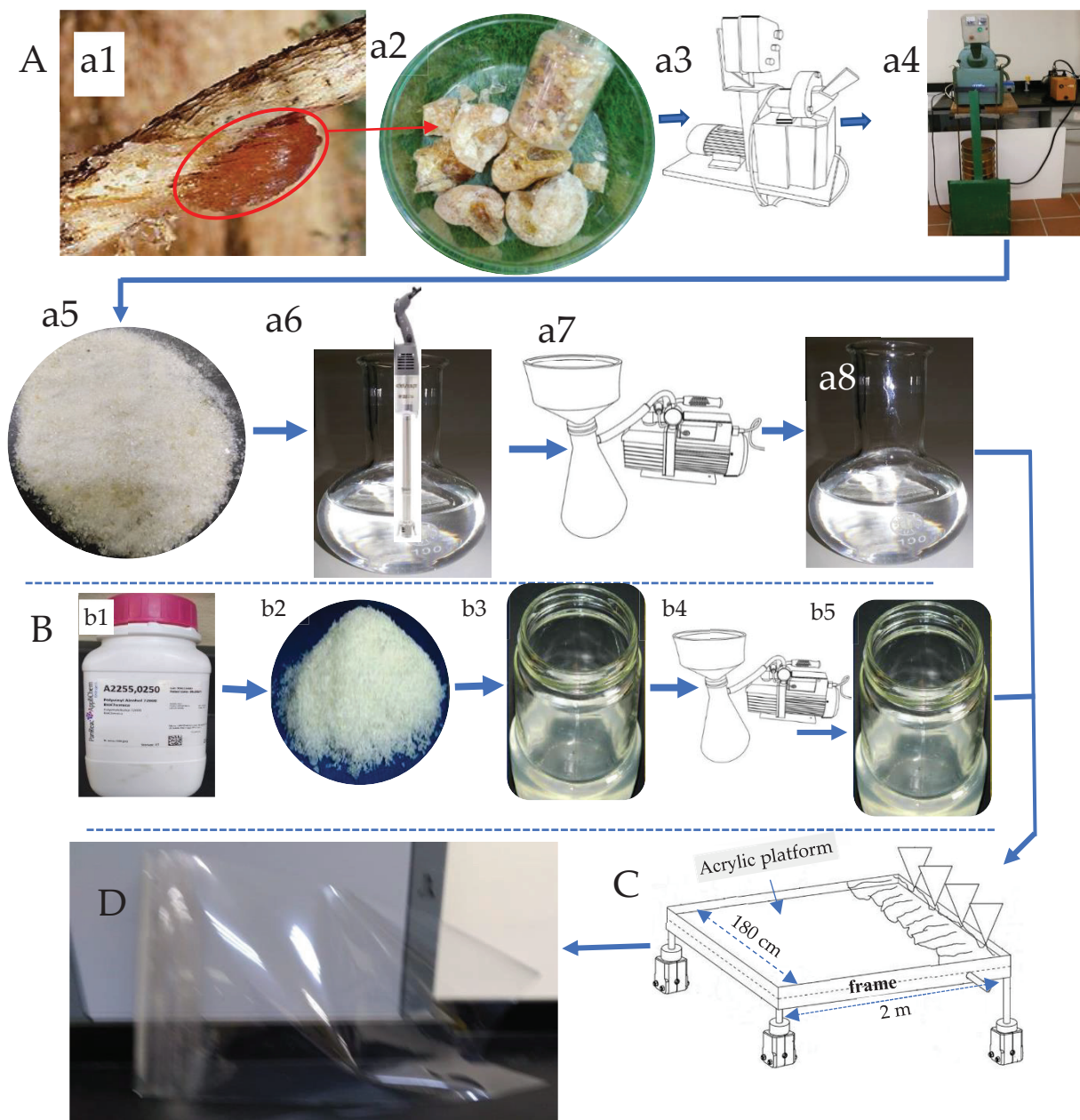
#### 2.1.1. GA

GA (~Mw:  $1.827 \times 10^6$  g/mol) was harvested from the trunks and branches of *Acacia seyal* trees (Figure 2(a1)) habituated at Hada Al-Sham (about 120 km apart from Jeddah), Saudi Arabia. As shown in Figure 2A, the naturally hardened sap excreted on a branch of an *Acacia seyal* tree was collected after tapping the woody tissues of the tree and making incisions (60 cm  $\times$  5 cm). (Figure 2(a1)) and cured into crude granules (Figure 2(a2)). The solid granules were ground using a mechanical grinding machine (Figure 2(a3)), passed through a standard 60 mesh sieve, and retained particles of 80 mesh size (60/80 mesh) using a vacuum-assisted sieving system (Figure 2(a4)). About 50 g of air-dried uniform GA powder (Figure 1(a5)) was dissolved in one liter of deionized water at ambient temperature (25 °C) and heated up to 80 °C with continuous stirring until all particles were completely dissolved (Figure 1(a6)). Removing the insoluble components of the resultant solution

was achieved via vacuum filtration (Figure 2(a7)) to obtain the clear GA precursor at a concentration of 5% wt/wt (Figure 2(a8)).



**Figure 1.** The management plan performed to study the efficiency of the novel manufacturing processes (vibrational casting, nano-dehydration, and self-electrostatic peeling) on the quality of the NDB membranes.



**Figure 2.** Manufacturing of NDBs: (A) Harvesting and processing of the GA principle precursor: (a1) hardened sap naturally excreted on a branch of an *Acacia seyal* tree; (a2) crude GA granules; (a3) mechanical grinder; (a4) vacuum-assisted sieving system; (a5) uniform powder of crude GA; (a6) crude solution of well-dissolved GA; (a7) vacuum-filtration device; and (a8) clear vacuum-filtered solution. (B) PVA-modifier precursor: (b1) analytical-grade bottle; (b2) powder form; (b3) crude solution of well-dissolved PVA; (b4) vacuum-filtration device; and (b5) clear vacuum-filtered solution; (C) VFHF device; (D) the NDB final product.

### 2.1.2. PVA

PVA was used as a modifier precursor to synthesize the NDB, along with GA. PVA used in this investigation (Figure 2B) was of ACS reagent quality (Figure 2(b1)), Mw 88,000 Da, and 88% deacetylated. About 50 g of PVA crystals (Figure 2(b2)) were dissolved in one liter of deionized water to obtain a crude solution (Figure 2(b3)) as a result of heating under continuous stirring at 80 °C until complete clearance and subsequently vacuum-filtered (Figure 2(b4)) to obtain the clear PVA precursor at a concentration of 5% *wt/wt* (Figure 2(b5)).



## 2.2. Preparation of the Bioplastic Blends

The practical procedure used for the novel casting of the bioplastic blends is presented in Figure S2. Six different bioplastic blends of GA and PVA in different ratios were prepared by mixing their aqueous solutions (5% *wt/wt* each) under continuous and calm stirring until the solution became completely homogenous (see Figure 2). It is crucial to stir slowly and carefully to prevent the addition of too many air bubbles to the solution, which can result in aeration defects in the final membranous product.

## 2.3. The Casting Platform

The practical procedure used for casting the bioplastic blends is presented at Figure S1 (see in Supplementary Materials). After mixing known concentrations of GA and PVA to obtain a homogenous clear solution, the blend was casted on a novel platform made up of poly-(methyl methacrylate) abbreviated as PMMA and known to be acrylic panel. We chose this material in the current experiment as an ideal casting platform for polymers, particularly water-based ones. This selection of PMMA was due to its non-stick surface, which can help the bioplastic blend be peeled easily after drying and curing [57]. The PMMA panel was irradiated using UV-waves to activate its electrostatic charges and rising its temperature up to 50 °C.

As shown in Table S1 and Figures 2C and S2, the PMMA panel (180 cm in width, 2 m longitudinally, 8 mm in thickness) was fixed on the upper panel of the casting table. Furthermore, adjacent strips of PMMA can be arranged to cover a movable belt that may be used as a casting surface [57]. Before pouring the bioplastic blend onto the PMMA's substrate, vibrational forces were generated by using suitable solenoids to ease spreading the blend in a definite velocity over the worm casting platform. After that, a mild air drying of the molten polymeric membrane was applied in order to thicken its viscosity.

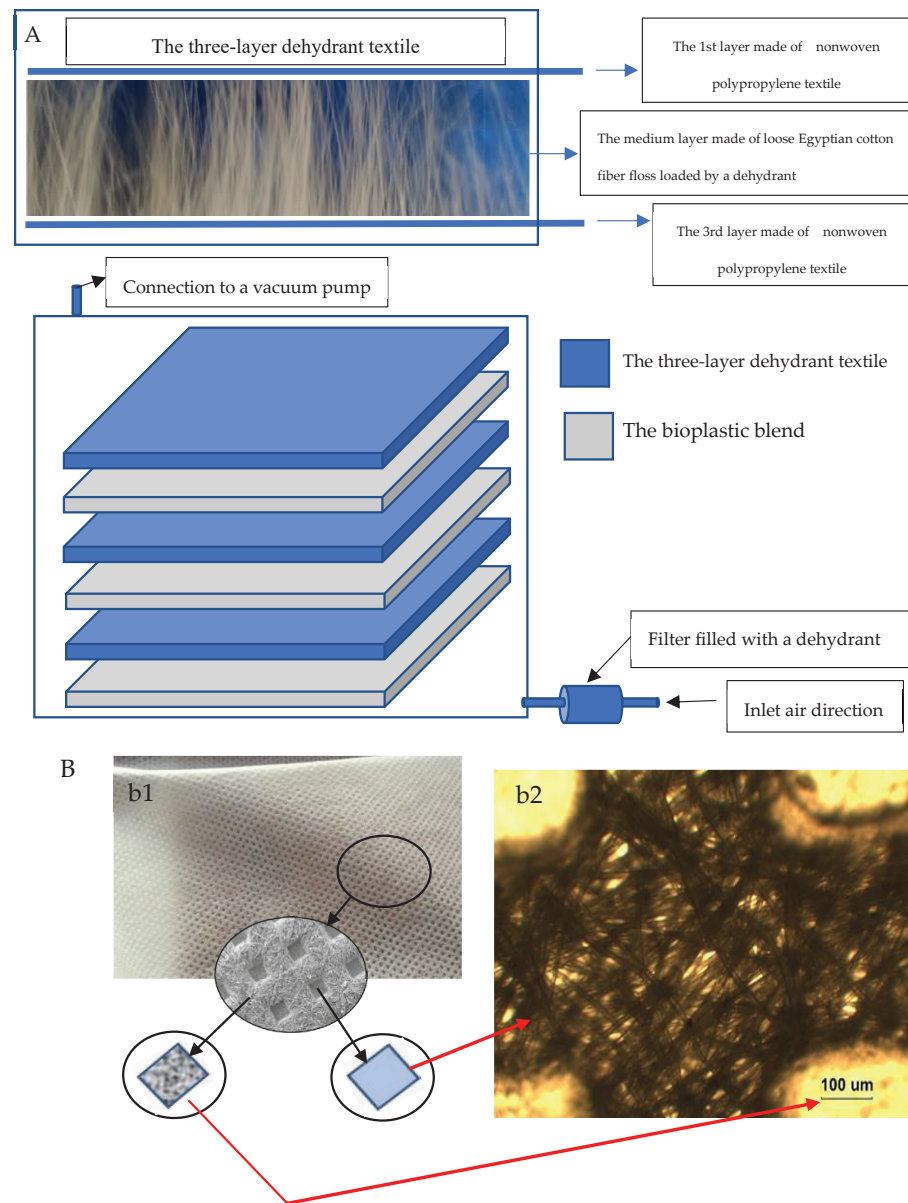
## 2.4. Casting the Bioplastic Blends

After obtaining complete homogeneity for the biopolymer blend, the bubble-free ternary blend solution was poured onto a clean acrylic panel. This panel is the surficial layer of the VFHF device (Figures 2C and S3), with a prominent frame where it is necessary to adjust the initial thickness of the bioplastic membrane to determine its final thickness. After that, the cast blend was allowed to dry at ambient temperature using the novel stratified nano-dehydrator (SND) apparatus [57,98,99], as shown in Figure 3.

The novel VFHF device (Figures 2C and S2, see in Supplementary Materials) features both the ease of casting the blend and peeling the membranes with a constant thickness free of air bubbles. For manufacturing a NDB, the blend was poured after adjusting the slope angle of the acrylic ground template (Figures 2C and S2) to a slight angle (about 15°) in order to accelerate the blended fluid movement. The slow motion of the blend protects its matrix from forcing more bubbles inside it. After the blend reached the opposite side of the template, the slope angle was re-adjusted to zero degrees to ensure exact horizontality in order to obtain identical thicknesses. It is worth mentioning that the thickness of the bioplastic sheets was controlled by two critical actions: (a) pouring a definite quantity of blend solution onto the same template area and (b) accurate adjustment for the viscosities of these blends [57].

In order to obtain a gentle, steady, and efficient flow for the viscous bioplastic blend, each of the four legs of the VFHF was fixed with a vibrating magnetic solenoid (a Kendrion OSR series shaker) that was designed with two excitation coils to generate a harmonious vibrating movement in the blend [57]. The magnetic vibrating system (Figure S3B) consists of a permanent magnet at the bottom, connecting the magnetic body's two halves and two excitation windings. The body to be vibrated, which serves as the armature, closes the magnetic circle through an air gap. A steady pulling force between the magnetic body and armature is produced by the permanent magnet that is integrated into the magnetic body, biasing the system. The alternating electromagnetic field's force effect superimposes itself onto the permanent magnet's force effect when an AC voltage is delivered to the

excitation coil. The fully encapsulated bobbin and coils achieve reliable long-life service and maintenance-free operation. In addition, OSR shaker solenoids are not susceptible to dust or moisture when operational under rough or adverse conditions [57]. It is worth mentioning that a permanent magnetic attachment serves to mount the OSR shaker solenoid freely and that it is detachable from the vibrating surface. Angle mounts permanently fix the OSR shaker solenoid to a vibrating surface. In addition, phase angle controllers were installed separately for the fine adjustment of vibration through alternating or direct current (via an integrated one-way rectifier), and they can be DIN-rail mounted within cabinets with minimal space.



**Figure 3.** The novel nano-dehydration technique: (A) the stratified air-dryer apparatus, and (B) the non-woven textile of polypropylene: (b1) an optical image, and (b2) microscope image (40×) according to Hindi and Albureikan [57].

### 2.5. Drying the NDBs

#### The Stratified Nano-Dehydrator (SND)

The most critical problem concerning the manufacturing of bioplastic sheets is their drying process, where it is crucial to obtain high-quality products. This problem arises from

the highly hydrophilic nature of bioplastic sheets blended with mixtures of hydrophilic GA and PVA in different ratios.

The SND was invented to accelerate the dehydration process of bioplastic sheets [57]. As shown in Figure 3, it consists of three stratified and perforated acrylic panels (poly-(methyl methacrylate)). These panels were arranged in a vertically alternating pattern, with three sub-layers consisting of dehydrant-loaded fibrous materials. Each sub-layer constitutes two non-woven polypropylene textiles, restricting an intermediate net of loosened Egyptian cotton floss (ECF). All fibrous materials constructing the sub-layer are saturated with a strong dehydrant, such as phosphorus pentoxide ( $P_4O_{10}$ ), the most highly preferred dehydrant reagent, rather than calcium chloride, magnesium sulfate, aluminum oxide, lithium aluminum hydride, metallic sodium, or silica gel. Removing water by  $P_2O_5$  was found to be more complete, quickly, effectively, and at a faster rate than many other dehydrants.

This cellulosic material was selected for this task due to its high content of alpha cellulose, well-known for its high hydrophilicity, which is essential to attaining good affinity to both moisture molecules as well as dehydrant crystals. The manner of loading dehydrant onto the cellulosic fibers can be summarized as follows: (1) air-drying of cellulosic fibers used as a core skeleton of the SND; (2) preparing dehydrant-saturated solution; (3) soaking cellulosic fibers in the salt-saturated solution via vacuum forces to ensure complete immersion and saturation of the fiber cells and penetration of the salt solution into the cell cavities, as well as the cell wall, through the internal border pits of the cellulosic fibers; (4) discarding excess salt solution and drying the cellulosic fibers by air-drying and finally oven-drying at  $80\text{ }^\circ\text{C} \pm 5\text{ }^\circ\text{C}$  for 2 h; and (5) this medium layer was inserted between the first and third layers, which were made of non-woven polypropylene textile. The edges of the outer layers were welded thermally due to the nature of polypropylene as a thermoplastic material. Furthermore, the three-layer textile was reinforced upon stitching using a sewing machine.

#### 2.6. Peeling off the Bioplastic Membranes

A self-electrostatic charged-template (SECT) made of poly-(methyl methacrylate) was used as a casting platform, which made peeling the final product membranes easy due to its non-stick behavior [57]. It can be used as a table cover termed an acrylic platform (Figure 2C) or as a covering layer (by coating or adhesion) for a movable belt to give production continuity.

The resulting transparent bioplastic sheet (Figure 2D) was peeled slowly and accurately away from the PMMA platform, rolled, and stored under dry circumstances until used.

#### 2.7. Characterization of the Bioplastic Membranes

The values of the different physical and chemical properties of the bioplastic sheets were calculated as presented in Table 1.

**Table 1.** Arithmetic formulas for calculating different chemical and physical properties of the bioplastic sheets.

Equation	Definitions
$^1 CI = (A_{pp}/A_t) \times 100$	$A_{pp}$ : Total planar area ( $\text{mm}^2$ ) of the XRD's diffractogram. $A_t$ : The planar area ( $\text{mm}^2$ ) of the principle peaks arises around $2\theta^\circ$ of $20^\circ$ .
$^2 M_L = [(W_2 - W_1)/W_1] \times 100$	$W_i$ : Initial weight of the bioplastic sample at a temperature zone, estimated from the TGA curves. $W_f$ : Final weight of the bioplastic sample at the same temperature zone, estimated from the TGA curves.

Table 1. Cont.

Equation	Definitions
${}^3 TR = T_i - T_f$	$T_i$ : Initial temperature of a certain thermogram. $T_f$ : Final temperature of the same thermogram.
${}^4 EC = E_f - E_i$	$E_f$ : Initial enthalpy of a certain thermogram. $E_i$ : Final enthalpy of the same thermogram.
${}^5 TS = F_f/A$	$F_f$ : Force at failure in Newton (N).
${}^6 MoE = \sigma/\epsilon$	A: Cross-section area (m <sup>2</sup> ) of the bioplastic sample.
${}^7 \epsilon = [\Delta L/L_0] = [(L_f - L_0)/L_0]$	$\sigma$ : Tensile stress (Pa).
${}^8 EaF = \Delta L_f = [(L_f - L_0)/L_0] \times 100$	$L_f$ : The length of the bioplastic sample at failure. $L_0$ : The initial length of the bioplastic sample at failure.
${}^9 \tan(\theta_n^\circ) = (y_2 - y_1)/(x_2 - x_1)$ $y = mx + C$ $m = \tan(\theta_n^\circ)$	$\theta^\circ$ : The incline angle ( $\theta$ ) in degrees of the hourly duplication (HD) curve for microbial populations. $x_1$ : The 1st incubation period (hr.) for the HD curve. $x_2$ : The 2nd incubation period (hr.) for the HD curve. $y_1$ : The initial HD of the colony-forming units (CFUs) in mega units (MCFU). $y_2$ : The final HD of the colony-forming units (CFUs) in mega units (MCFU). $m$ : The slope of the curve C: The intersecting section of the y-coordinate for the HD's curve.

<sup>1</sup> Crystallinity index (%), <sup>2</sup> Mass loss of the bioplastic membrane (g), <sup>3</sup> Temperature range (°C), <sup>4</sup> Enthalpy change ( $\mu\text{V}/\text{mg}$ ), <sup>5</sup> Tensile strength (MPa), <sup>6</sup> Modulus of elasticity (GPa), <sup>7</sup> Tensile strain, <sup>8</sup> Elongation at failure (%), <sup>9</sup> Slope of the HD-curve.

### 2.7.1. FTIR

Using a Bruker Tensor 37 FTIR spectrophotometer, the chemical constituents and functional groups of the six bioplastic membranous samples were investigated. The samples were combined with KBr at a ratio of 1:200 *wt/wt* and compressed under vacuum to form pellets after being oven-dried at 100 °C for 4–5 h. The materials' FTIR spectra were captured between 400 and 500  $\text{cm}^{-1}$  in transmittance mode.

### 2.7.2. X-ray Diffraction (XRD)

An XRD 7000 Shimadzu diffractometer (Kyoto, Japan) was used to determine the XRD spectra of the six bioplastic sheets. An anode generator, a copper target, and a wide-angle powder goniometer are all parts of the system. Measurements were performed with the aid of CuK radiation arising at 30 kV and 30 mA. The  $K\alpha_1$  (0.15406 nm) and  $K\alpha_2$  (0.15444 nm) components of the CuK radiation are present in the resulting XRD data.

A single-channel analyzer was used to extract the data resulting from the semiconductor detector. The reception slit was 0.15 mm at the same radius, and the divergence and scatter slits were each 10 m wide. Several droplets of diluted amorphous glue were used to mount dried bioplastic sheets (weighing around 0.5 g) onto a quartz platform. Each sample was scanned in the  $2\theta^\circ$  range between  $5^\circ$  and  $40^\circ$ . Every experiment was run in reflection mode, with increments of  $0.05^\circ$  and a scan speed of  $4^\circ/\text{min}$  [57,98].

The crystallinity index (CI) was computed by dividing the diffractogram area of crystalline cellulose by the entire area of the original diffractogram after smoothing the resulting crystalline peaks from the diffraction intensity profiles. Using Microsoft Excel (USA), the area under the curve was calculated by adding adjacent trapezoids [98–103].

### 2.7.3. Thermal Analysis

Since DTA typically complements TGA with information on phase transitions [93], the TGA and DTA of each blend were conducted simultaneously. These characterizations were carried out for TGA and DTA for all six bioplastic blends [57,98,99,101] using a Seiko and Star 6300 analyzer, Central Laboratory, Faculty of Science, Alexandria University, Egypt.



Using a heating rate of 20 °C/min under a nitrogen atmosphere, heating scans were carried out from 30 °C up to the final maximum temperature of 450 °C [57,98,101].

Determination of the NDB mass loss estimated from the TGA curves was achieved as illustrated in Table 1.

#### 2.7.4. Surface Topography (ST)

Atomic force microscopy (AFM) was used to examine the surfaces of the six NDBs in order to observe the full 3D membranous surface structures down to the nanometric scale. Four distinct characteristics of the NDB were revealed by AFM [57,98]: surface roughness (SR), nanometric particle size (NPS), pore diameter (PD), and void volume (VV).

#### 2.8. Mechanical Properties of the Bioplastic Membranes

The stress–strain behavior of the six bioplastic membranes, else ADB NDB, was measured using The Instron universal testing machine, model 1193, Instron Co., Ltd., London, UK, with a 200 N-load cell according to the ASTM D–882 standard test, 1989. The bioplastic membrane samples were rectangular-shaped (2.5 × 10 cm) for each of the ADBs and NDBs membranes. The device with two metallic grips was installed to hold the test sample at both ends. The starting grip separation for all samples was 50 mm, and the upper grip was extended at a constant rate of 50 mm per minute while the lower grip remained stationary. An automatic speed controller was fitted to the electrically powered machine to maintain the upper grip's speed. The ambient temperature was used for all measurements. From the plot of stress–strain curves, the UTS, MoE, and EaB for each film were estimated, as illustrated in Table 1.

The mechanical properties, namely, ultimate tensile strength (UTS) in MPa, modulus of elasticity (MoE) in MPa, and elongation at failure (EaF) as a percentage, were calculated.

##### 2.8.1. Ultimate Tensile Strength (UTS)

The UTS shows the film's maximum allowable tensile stress [74–76]. The UTS property of the bioplastic sample was calculated by dividing the maximum load causing the film failure by the cross-sectional area of the film, as explained in Table 1 [74–76].

##### 2.8.2. Modulus of Elasticity (MoE)

The membrane's MoE is a reliable indicator of its stiffness [74–76]. The MoE was computed by dividing the length of the membrane sample at yield by the stress at yield, as expressed in Table 1.

##### 2.8.3. Elongation at Failure (EaF)

The EaF was calculated by dividing the elongation at failure of the sample by the initial gauge length, as shown in Table 1 [74–76].

#### 2.9. Microbial Biodegradation

Microbial biodegradation was assessed to investigate the microbes' capacity to break down the buildup of bioplastic in soil. Upon calculating the percentage of biodegradation (weight loss), counting the microbe population isolated from the surfaces of bioplastic sheets, and evaluating the various morphological changes in these surfaces as a result of degradation, it was possible to determine the amount of biodegradation [98,99].

The soil was collected from the Agricultural Research Station (ARS) of King Abdullaziz University's Faculty of Environmental Sciences in Hada Al-Sham and was used to bury the bioplastic samples. The location is situated 240 m above sea level, around 120 km to the northwest of Jeddah (N = 21°48'3", E = 39°43'25"). The pH of the soil at the site ranged from 7.1 to 7.9, along with low levels of CaCO<sub>3</sub>, organic matter, and cation exchange capability [104,105].

### 2.9.1. Sample Preparation and Soil Burial Studies

The various bioplastic sheets were shredded into 2 cm × 2 cm pieces and buried 10 cm deep in 100-g wet soil boxes. Before being buried in the ground, each bioplastic piece was weighed (0.040–0.038 g). By adding sterile water to the soil samples to counteract water evaporation, the moisture content of the soil samples was kept constant [98].

Each sample box had a hole at the bottom for the excess water to drain through. After 30 and 60 days, soil samples were carefully removed, and the weight loss was calculated in order to separate, count, and compare the microbial community, as well as speculate on microbial morphology changes as a result of degradation [98,99,106].

### 2.9.2. Isolation and Counting of Microbial Communities

About 95 mL of sodium pyrophosphate solution at 0.1% *wt/v* was used to suspend one gram of soil collected from the surface of the bioplastic sheets from each sample. The samples were left to stand for 30 min. Then, using the serial dilution method, the supernatant was divided among six tubes, and one milliliter (mL) of each dilution was plated on nutrient agar medium, NA (Oxoid), for the isolation of bacteria, while potato dextrose agar medium, PDA (Oxoid), was used for isolation of fungi.

Finally, in order to determine the colony-forming units (CFUs), plates were incubated at 30 °C and pH 7 for 720 h (for bacteria) and at 25 °C and pH 5 for 1440 h (for fungi). Based on their cultural and physical characteristics, microorganisms were separated and identified using conventional assays [1,57,98,99].

### 2.10. Statistical Design and Analysis

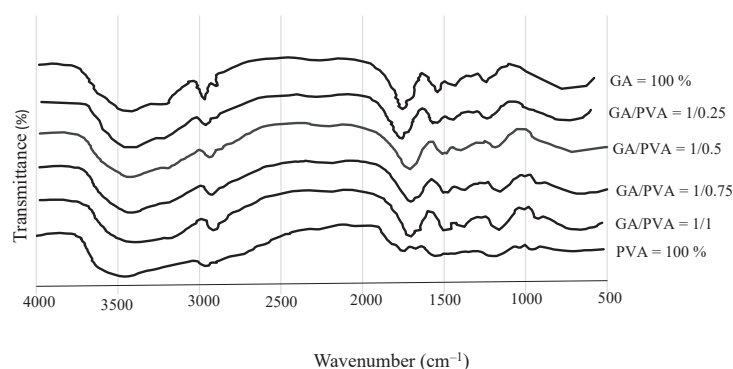
Various properties of the six bioplastic membranes synthesized from the aqueous solutions of GA and PVA were assessed using a randomized complete block design. According to El-Nakhlawy [107], a statistical analysis of the obtained data was carried out using the analysis of variance approach and the least significant difference test (LSD) at 0.05.

## 3. Results

### 3.1. Chemical and Physical Properties of the Bioplastic Membranes

#### 3.1.1. FTIR

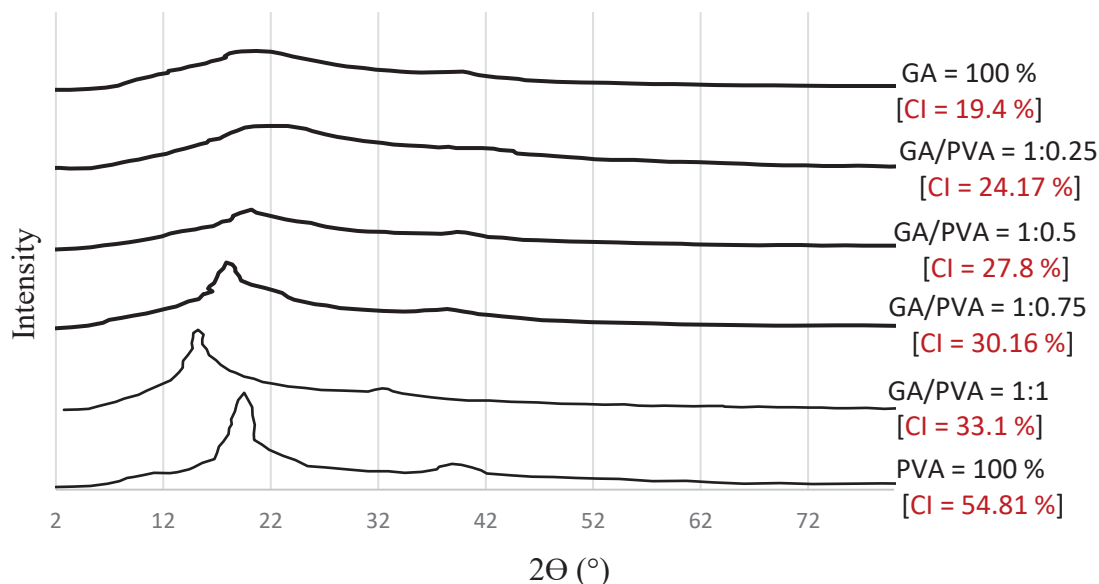
FTIR spectroscopy was used to determine the chemical functionality of the bioplastic sheets (the nanodehydrated membranes (NDBs)), as illustrated in Figure 4. The spectra of the resulting NDBs exhibited chemical group absorption bands that were typical of the gummy products made from both GA and PVA in different ratios. The absorption bands spanned an area between 500 and 4000  $\text{cm}^{-1}$ . Several chemical groups were precisely found at the following wavenumbers: 900–1250, 1426, 1402, 1625.4, 1627.4, 1430, 1436.91, 1437, 1641, 1047, 2800–3000, 2885, 2910.87, 2939, 3000, 3261, 3416, 3000, and 3600  $\text{cm}^{-1}$  [57,98,99,101,108–111].



**Figure 4.** FTIR spectra of the six transparent nanodehydrated bioplastic (NDB) membranes over the wavenumber range of 4000 to 500  $\text{cm}^{-1}$ , fabricated from various gum Arabic (GA)/polyvinyl alcohol (PVA) blends.

### 3.1.2. XRD

Figure 5 displays the XRD patterns of the six bioplastic membranes. The maximum intensity of the GA-broad diffractogram was obtained at  $2\theta = 20^\circ$ , which confirms the amorphous nature of the gum Arabic [13]. Moreover, a typical peak for pure PVA, a semi-crystalline polymer, was visible at  $2\theta = 19.9^\circ$ . With the increase in PVA allocation in the blend, the crystallinity index values increased (Figure 5).

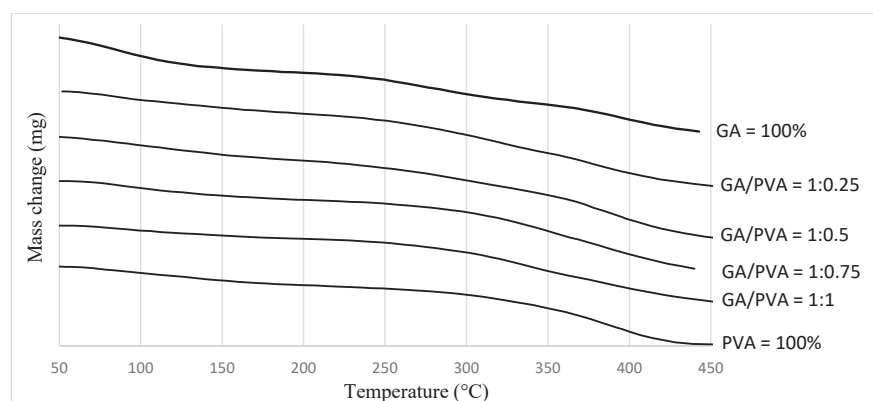


**Figure 5.** XRD diffractogram spectra of the six transparent nanodehydrated bioplastic (NDB) membranes over a wavenumber range of  $4000$  to  $500\text{ cm}^{-1}$ , fabricated from various gum Arabic (GA)/polyvinyl alcohol (PVA) blends, showing the crystallinity index (CI) values.

As demonstrated in Figure 5, the CI values of the NDBs were found to increase from 19.4% (for pure GA) to 54.81% (for pure PVA). Accordingly, it is clear that the increase in CI of the bioplastic blends can be attributed to an increase in the PVA allocation in the blend.

### 3.1.3. TGA

The TGA results are presented in Figure 6 and in Tables 2 and S2. The mass losses of the six NDBS samples were focused on eight temperature regions, namely,  $50$ – $100^\circ\text{C}$ ,  $100$ – $150^\circ\text{C}$ ,  $150$ – $200^\circ\text{C}$ ,  $200$ – $250^\circ\text{C}$ ,  $250$ – $300^\circ\text{C}$ ,  $300$ – $350^\circ\text{C}$ ,  $350$ – $400^\circ\text{C}$ , and  $400$ – $450^\circ\text{C}$  (Tables 2 and S2; Figure 6).



**Figure 6.** Thermogravimetric analysis (TGA) thermogram spectra of the six bioplastic membranes (NDBs) in the wavenumber range of  $4000$  to  $500\text{ cm}^{-1}$ , fabricated from various gum Arabic (GA)/polyvinyl alcohol (PVA) blends.

**Table 2.** Mean <sup>1–7</sup> values of mass loss (ML) of the six transparent nanodehydrated bioplastic (NDB) membranes over a wavenumber range of 4000 to 500 cm<sup>−1</sup>, fabricated from various gum Arabic (GA)/polyvinyl alcohol (PVA) blends over different ratios and temperature (T) zones.

T-Zones °C	GA/PVA Ratio					
	GA 100%	1:0.25	1:0.5	1:0.75	1:1	PVA 100%
50°–100°	13.68 <sup>A<sub>d</sub></sup>	4.57 <sup>B<sub>g</sub></sup>	4.85 <sup>B<sub>e</sub></sup>	5.02 <sup>B<sub>ef</sub></sup>	5.23 <sup>B<sub>ef</sub></sup>	5.69 <sup>B<sub>f</sub></sup>
100°–150°	11.11 <sup>A<sub>e</sub></sup>	6.32 <sup>AB<sub>f</sub></sup>	6.37 <sup>AB<sub>e</sub></sup>	6.93 <sup>AB<sub>e</sub></sup>	6.47 <sup>AB<sub>ef</sub></sup>	8.98 <sup>B<sub>ef</sub></sup>
150°–200°	4.18 <sup>BC<sub>g</sub></sup>	4.88 <sup>BC<sub>g</sub></sup>	6.46 <sup>B<sub>e</sub></sup>	4.26 <sup>BC<sub>ef</sub></sup>	3.23 <sup>C<sub>f</sub></sup>	8.07 <sup>A<sub>ef</sub></sup>
00°–250°	6.96 <sup>B<sub>f</sub></sup>	8.18 <sup>A<sub>e</sub></sup>	6.18 <sup>B<sub>e</sub></sup>	3.7 <sup>C<sub>f</sub></sup>	5.71 <sup>B<sub>ef</sub></sup>	3.9 <sup>C<sub>g</sub></sup>
250°–300°	7.48 <sup>C<sub>f</sub></sup>	14.9 <sup>A<sub>d</sub></sup>	7.36 <sup>C<sub>e</sub></sup>	10.77 <sup>AB<sub>d</sub></sup>	11.62 <sup>B<sub>d</sub></sup>	10.15 <sup>AB<sub>e</sub></sup>
300°–350°	22.2 <sup>B<sub>b</sub></sup>	12.62 <sup>E<sub>de</sub></sup>	15.93 <sup>D<sub>d</sub></sup>	22.41 <sup>B<sub>c</sub></sup>	28.57 <sup>A<sub>c</sub></sup>	18.08 <sup>C<sub>d</sub></sup>
350°–400°	18.2 <sup>E<sub>b</sub></sup>	21.13 <sup>D<sub>b</sub></sup>	26.32 <sup>C<sub>b</sub></sup>	33.3 <sup>B<sub>b</sub></sup>	34.4 <sup>B<sub>b</sub></sup>	44.14 <sup>A<sub>c</sub></sup>
400°–450°	28.6 <sup>D<sub>a</sub></sup>	27.68 <sup>D<sub>a</sub></sup>	41.43 <sup>C<sub>a</sub></sup>	39.17 <sup>BC<sub>a</sub></sup>	46.34 <sup>B<sub>a</sub></sup>	79.0 <sup>A<sub>a</sub></sup>
450°–500°	15.6 <sup>E<sub>c</sub></sup>	18.52 <sup>D<sub>c</sub></sup>	21.95 <sup>CD<sub>c</sub></sup>	24.66 <sup>C<sub>c</sub></sup>	45.5 <sup>B<sub>a</sub></sup>	58.8 <sup>A<sub>b</sub></sup>

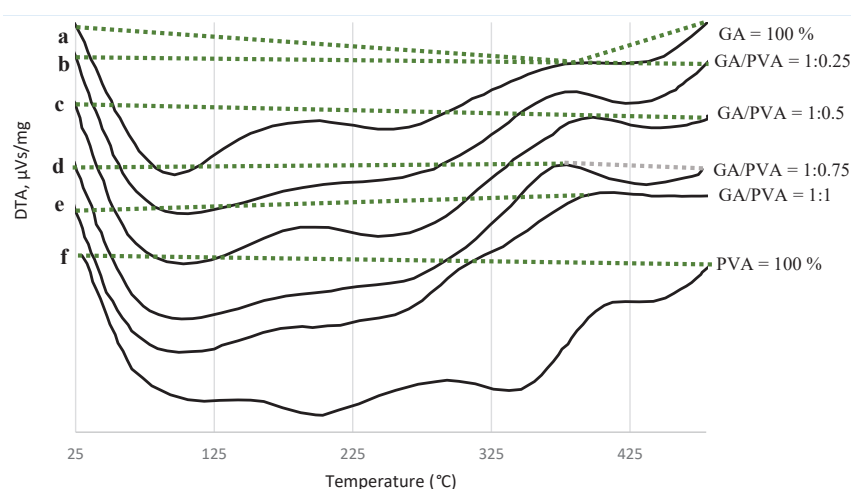
<sup>1</sup> Each value is an average of 3 samples. <sup>2</sup> Based on the original oven-dry weight. <sup>3</sup> Superscript capital letters for comparing blend ratios within the same temperature zone. <sup>4</sup> Subscript small letters for comparing temperature zones within the same blend ratio. <sup>5</sup> Means with the same letter are not significantly different at the 5% level. <sup>6</sup> Initial starting weight of the NDBs sample. <sup>7</sup> Final starting weight of the NDB sample.

The thermal degradation of the samples increased with rising temperatures for all six bioplastic blends, according to a comparison of mass losses between temperature zones (at the same bioplastic blend ratio).

Comparing the mass losses within the temperature zone meant studying the differences between bioplastic blend ratios in the same temperature zone. It is clear from Table 2 and Table S2 and from Figure 6 that at lower temperatures ( $\leq 150$  °C), PVA lost more weight (5.69% and 8.98% for 50–100 °C and 100–150 °C zones, respectively) than GA (13.68% and 11.11%) in the same temperature zones. On the other hand, at higher temperatures, this trend was reversed, whereby PVA lost more weight (79.01% and 58.8% for the 400–500 °C and 450–500 °C zones, respectively) than GA (28.6% and 15.6% for the same zones, respectively).

### 3.1.4. DTA

The DTA analysis findings of the six nanodehydrated NDBs are presented in Figure 7 and Table 3.



**Figure 7.** Thermograms of differential thermal analysis (DTA) of the six nanodehydrated bioplastic (NDB) membranes over a wavenumber range of 4000 to 500 cm<sup>−1</sup>, fabricated from various gum Arabic (GA)/polyvinyl alcohol (PVA) blends.



**Table 3.** DTA results of the six transparent nanodehydrated bioplastic (NDB) membranes in the wavenumber range of 4000 to 500  $\text{cm}^{-1}$ , fabricated from various gum Arabic (GA)/polyvinyl alcohol (PVA) blends: points of reaction, thermogram type, temperature range (TR), and enthalpy change (EC).

Points of Reaction	GA/PVA Ratio	Thermogram Type	TR $^{\circ}\text{C}$	EC $\mu\text{Vs}/\text{mg}$
a	GA = 100%	Endotherm Exotherm	25–265 265–435	−1017.25 +52.39
b	1:0.25	Endotherm	25–475	−2268.77
c	1:0.5	Endotherm Exotherm	25–397 397–480	−1127.7 −16.67
d	1:0.75	Endotherm Exotherm	25–375 375–475	−1276.04 −20.89
e	1:1	Endotherm	25–475	−1467.19
f	PVA = 100%	Endotherm	25–475	−2119.72

Examining Figure 7 and Table 3, the NDB thermograms were found to be divided into two sets representing the bioplastic blends, namely, the single-phase and double-phase thermograms. The single-phase thermogram is composed of one endothermic phase, namely, curve 'b' (GA/PVA of 1:0.25), curve 'e' (GA/PVA of 1:1), and curve 'f' (PVA = 100%). On the other hand, the double-phase thermogram is differentiated into two distinct regions (endothermic and exothermic), namely, curve 'a' (GA = 100%), curve 'c' (GA/PVA of 1:0.5), and curve 'd' (GA/PVA of 1:0.75).

For more information, see Table 3. It is evident that the temperature ranges of each thermogram and the absolute values of the heat change (HC) values for the endotherms (16 Vs/mg–52.4 Vs/mg) were larger than those for the exotherms. Additionally, among the other bioplastic blends, the pure PVA endotherm absorbed the most energy (2119.7 Vs/mg), but GA had the lowest value of heat change (−1017.3 Vs/mg).

### 3.2. Ultrastructure of the Bioplastic Membrane

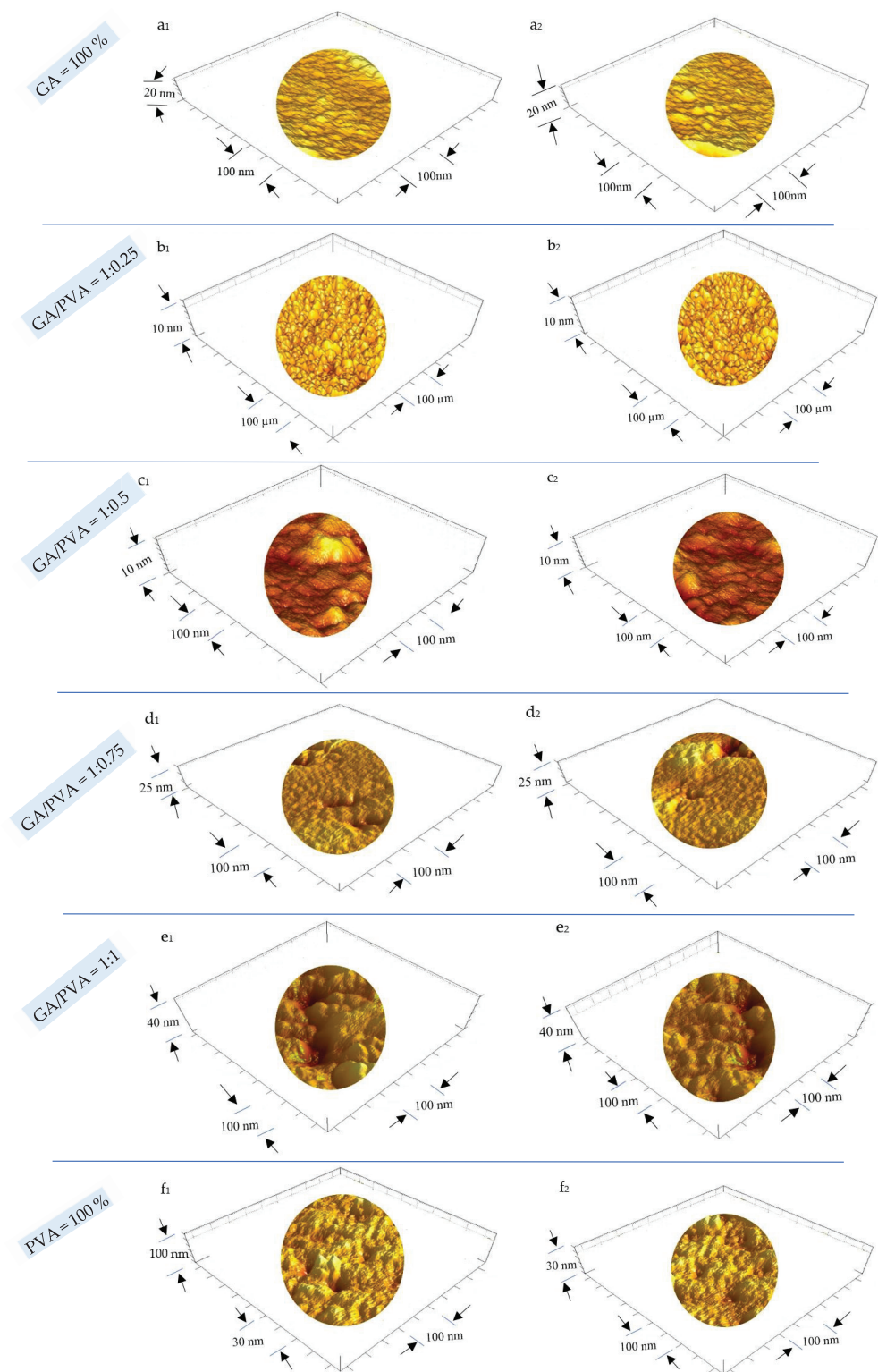
#### 3.2.1. Surface Roughness (SR) and Particle Size (PS)

In order to confirm the similarity between the ultrastructure features of ADBs and NDBs, the RS was investigated via atomic force microscopy (AFM) and is presented in Figure 8 for each of the six bioplastic blends. For clear, the GA/PVA blends' membranes dried by air are presented in Figure 8(a<sub>1</sub>–f<sub>1</sub>), while those for the NDBs are found in Figure 8(a<sub>2</sub>–f<sub>2</sub>). Since the nanometric PS is known to be intimately related to the SR, its data shown in Table 4 and Figure 9a are useful to shed an excess of light over the SR of the bioplastic membranes.

Paying attention to the AFM's images (Figure 8) revealed to that the RS was increased from the 1st blend ratio (GA = 100 %) until reaching the 6th blend ratio (PVA = 100 %). This finding can be attributed to the higher PS value of the PVA comparing to that for the pure GA as clear when speculating the gradual increasing of the PS values along with the six bioplastic blends. However, this trend was found to be similar for the ADBs and NDBs.

Regarding to the PS' results, see Table 4, statistical comparisons were performed between the membranes (ADEs and NDBs) as well as within the membranes (between the GA/PVA blends, namely, 1/0, 1/0.25, 1/0.5, 1/0.75, 1/1, and 0/1). Comparing membranes, there was no statistical difference between the ADBs and NDBs concerning their particle size (13.57 and 14.77 nm, respectively). On the other hand, comparing the blend ratios within the membrane (Table 4, Figures 8(a<sub>1</sub>,a<sub>2</sub>) and 9a) revealed that the GA membrane (GA = 100%) had the lowest PS for each of the means (13.57 nm), with a maximum value (55.44 nm). Furthermore, PVA sheets had the highest PS values (20.34 and 89.75 nm for the mean and maximum values, respectively). In between, increasing the PVA concentration

in the bioplastic blends increased the PS gradually (Table 4 and Figure 8( $f_1, f_2$ ) as well as Figure 9a).

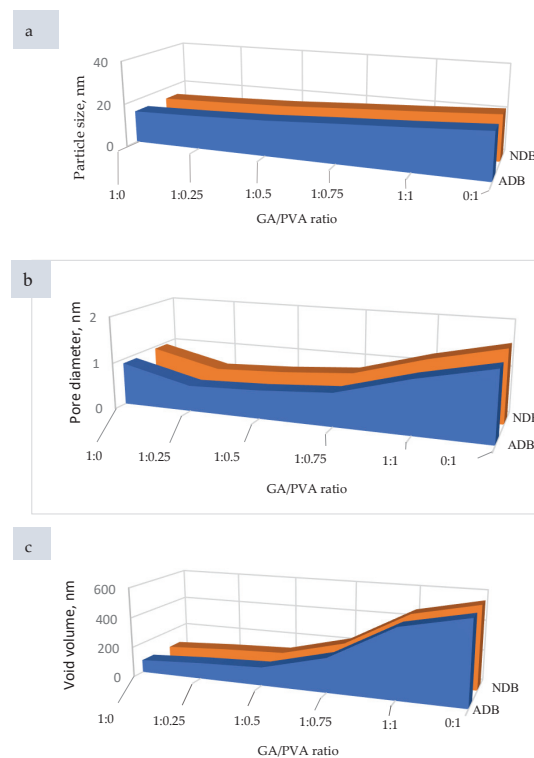


**Figure 8.** AFM images of surface roughness of the bioplastic membranes blended from gum Arabic (GA) and/or polyvinyl alcohol (PVA) precursors in different ratios: ( $a_1$ – $f_1$ ) air-dried membrane (ADB) and ( $a_2$ – $f_2$ ) nanodehydrated bioplastic membrane (NDB).

**Table 4.** Statistical parameters (SPs) of the ultrastructural features of the bioplastic membranes.

GA/PVA Ratio	GA Amount %	PVA Amount %	SPs	Particle Size nm		Permeability			
						Pore Diameter nm		Void Volume nm <sup>3</sup>	
				ADB	NDB	ADB	NDB	ADB	NDB
1/0	0	100	Mean <sup>1,2</sup>	13.57	14.77	0.91	0.953	83.24	84.29
			Max. <sup>3</sup>	55.44	56.68	3.905	3.948	1397.9	1398.91
			Min. <sup>4</sup>	4.24	5.49	0.002	0.045	0.007	1.057
			SD <sup>5</sup>	7.66	7.66	0.904	0.904	160.68	160.68
1:0.25	20	80	Mean <sup>1,2</sup>	14.17	15.42	0.553	0.606	105.74	106.74
			Max. <sup>2,3</sup>	76.94	78.19	3.54	3.593	1374.8	1375.47
			Min. <sup>2,4</sup>	4.24	5.49	0.001	0.055	0.005	1.008
			SD	8.93	8.93	0.457	0.457	156.17	156.17
1:0.5	66.7	33.3	Mean <sup>1,2</sup>	15.15	16.4	0.608	0.671	120.66	121.87
			Max. <sup>2,3</sup>	67.01	68.26	2.38	2.443	8009	8010.22
			Min. <sup>2,4</sup>	4.24	5.49	0.001	0.064	0.002	1.219
			SD <sup>5</sup>	8.51	8.51	0.469	0.469	309.6	309.6
1:0.75	57.1	42.9	Mean <sup>1,2</sup>	17.01	18.07	0.714	0.788	226.98	228.18
			Max. <sup>2,3</sup>	72.32	73.38	3.608	3.683	8411.8	8412.98
			Min. <sup>2,4</sup>	4.24	5.3	0.007	0.082	0.007	1.215
			SD <sup>5</sup>	9.26	9.26	0.615	0.615	631.41	631.41
1:1	50	50	Mean <sup>1,2</sup>	18.42	19.58	1.145	1.23	460.18	461.5
			Max. <sup>2,3</sup>	89.75	90.91	4.75	4.839	8411.8	8413.1
			Min. <sup>2,4</sup>	4.24	5.4	0.019	0.093	0.007	1.34
			SD <sup>5</sup>	12.69	12.69	2.342	1.002	1062.04	1062.04
0/1	100	0	Mean <sup>1,2</sup>	20.34	21.35	1.485	1.58	548.95	552.41
			Max. <sup>2,3</sup>	89.75	90.76	14.851	14.946	9315	9318.46
			Min. <sup>2,4</sup>	4.24	5.25	0.019	0.114	0.001	3.46
			SD <sup>5</sup>	14.58	14.58	2.342	2.342	1198.36	1198.36

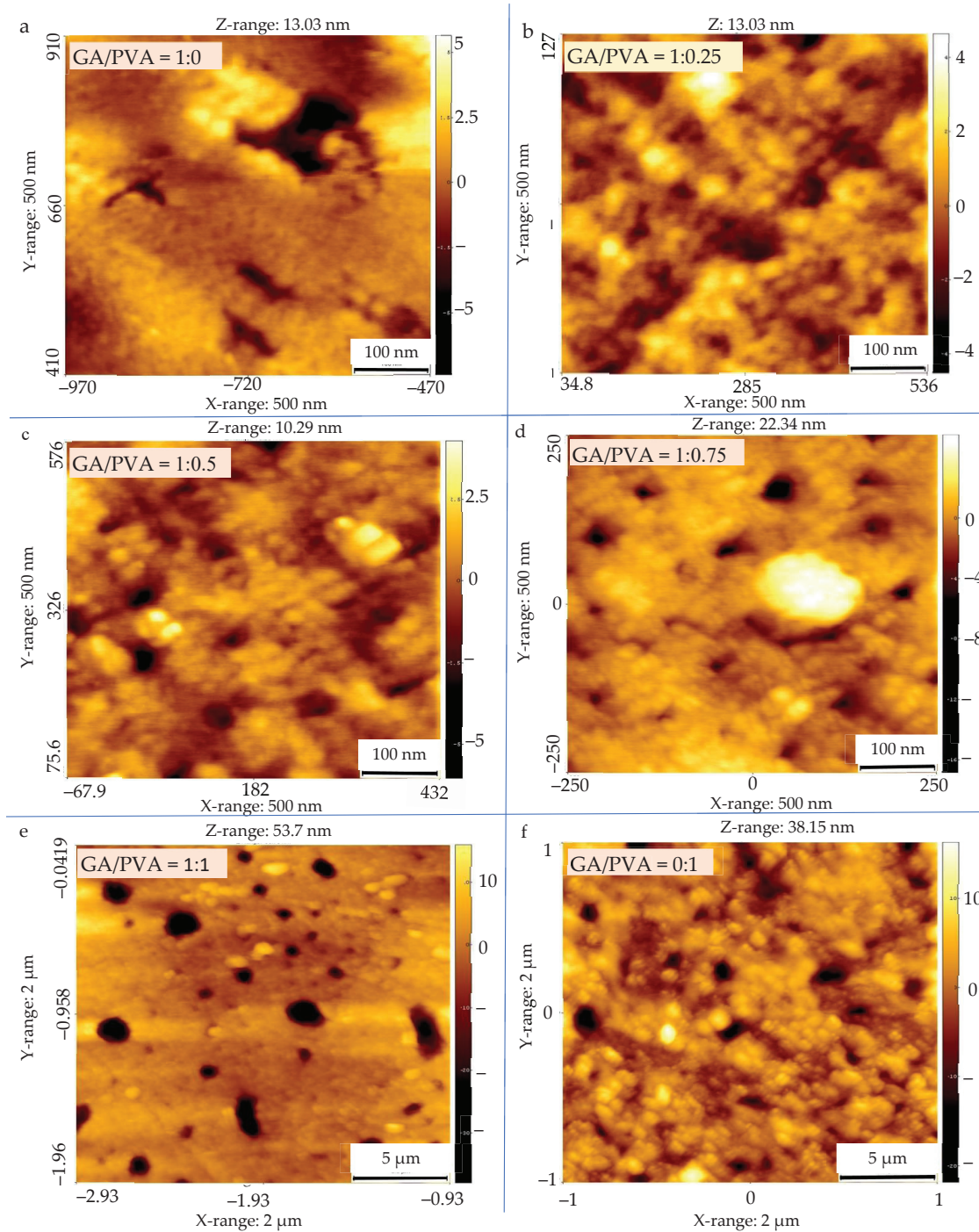
<sup>1</sup> Mean of the population members. <sup>2</sup> The number of observations is 1000 individuals. <sup>3</sup> Max. is the maximum value. <sup>4</sup> Min. is the minimum value. <sup>5</sup> SD are standard deviation values present within the parentheses.



**Figure 9.** Ultrastructure features of the air-dried membrane (ADB) and the nano-dehydrated-bioplastic membrane (NDB): (a) particle size, (b) pore diameter, and (c) void volume as affected by different allocations of GA and PVA (GA/PVA blends).

### 3.2.2. Pore Diameter (PD) and Void Volume (VV) of the NDB Membranes

Data produced for PD are presented in Table 4 and Figures 9b, 10 and S4, while Table 4 and Figure 9c represent the VV's results. The same ascending trend was noticed for both PD and VV regarding their influence, with an increase in the PVA allocation in the ADBs as well as the NDBs. The PD of the ADB increased from 0.91 nm to 1.485 nm for the GA/PVA ratios of 1/0 and 0/1, respectively. In addition, the VV of the ADB increased from 83.24 nm<sup>3</sup> to 548.95 nm<sup>3</sup> for the GA/PVA ratios of 1/0 and 0/1, respectively.



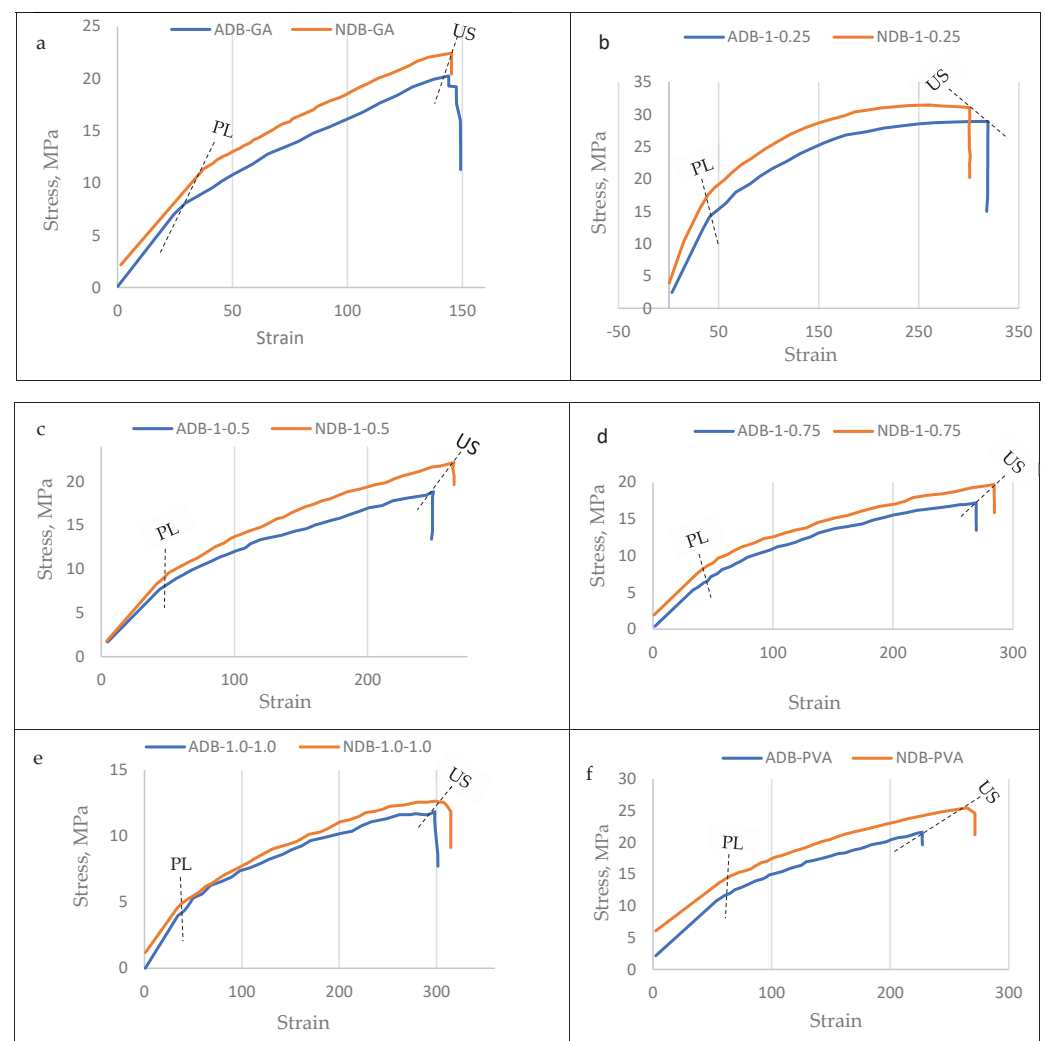
**Figure 10.** Permeability of the nanodehydrated bioplastic membranes blended from gum Arabic (GA) and polyvinyl alcohol (PVA) precursors in different ratios of GA/PVA: (a) 1/0, (b) 1:0.25, (c) 1:0.5, (d) 1:1.75, (e) 1:1, and (f) 0/1, respectively (AFM images).



In addition, there was no statistical difference between ADBs and NDBs in their PS, PD, and VV; consequently, there is no evidence that the novel procedures used in the bioplastic membrane preparation alter their parent ultrastructure.

### 3.3. Mechanical Properties of the Bioplastic Membranes

The results of the mechanical investigation of gum Arabic/poly (vinyl alcohol)/blend films were presented in Figures 11–14. Stress–strain curves of the six bioplastic membranes fabricated from GA and PVA are shown in Table 5 and Figure 11. For more specification, ultimate tensile strength (UTS), modulus of elasticity (MoE), and elongation at failure (EaF) are clear in Figures 12–14, respectively. Concerning Figure 11, it is worth mentioning that the disappearance of air bubbles in the bioplastic membranes as well as their clear transparency suggested the compatibility of the well-blended components [76] and consequently enhanced their mechanical properties. Simplifying illustration of the Figure 11, it presents the stress in mega Pascal units that affects the rheological endurance of each of the six bioplastic membranes expressed by the strain properties of the six blends. It is worth of mentioning that the mechanical relationship between stress and strain was determined for each of the ADB and NDB membranes.



**Figure 11.** Stress–strain graphs of the six bioplastic membranes fabricated from gum Arabic (GA) and polyvinyl alcohol (PVA) with different ratios for each of the air-dried (ADB) and nanodehydrated (NDB) membranes showing proportionality limit (PL) and ultimate stress (US).

**Table 5.** Proportionality limit (PL) and ultimate stress (US) of the six blends for each of the air-dried (ADB) and nanodehydrated (NDB) membranes.

GA/PVA Ratio	GA Amount %	PVA Amount %	Stress Type	ADB		NDB	
				Stress MPa	Strain	Stress MPa	Strain
1/0	0	100	PL	8.1	29.69	11.34	37.42
			US	20.42	145.24	21.42	145.25
1:0.25	20	80	PL	14.24	41.22	17.61	39.73
			US	28.91	319.13	31.05	300.9
1:0.5	66.7	33.3	PL	8.92	46.47	9.56	50.56
			US	18.84	249.5	20.64	264.98
1:0.75	57.1	42.9	PL	7.15	48.4	10.04	56.3
			US	15.92	269.39	19.7	284.39
1:1	50	50	PL	4.92	38.41	4.92	38.41
			US	11.86	297.99	12.33	310.55
0/1	100	0	PL	12.03	65.26	15.3	72.61
			US	21.64	227.09	25.47	264.91

As clear from Table 5 and Figure 11, the plotted stress-strain curves for the six blended membranes were differed concerning to their proportionality limit (PL) and ultimate strength (US). Regarding to sub-graphs of the bioplastic membranes in Figure 11a–f, both ADB (the red curve) and NDB (the blue curve) are similar in their ascending trend starting from the PL level up to the US. This behavior means that each membrane, else ADB or NDB was stressed through two stages: (1) in the 1st one, the stress was increased from zero up to the PL level, and (2) through the 2nd stage, each membrane transitioned from elastic to plastic nature as the load was increased from the PL up to the maximum load resulting the US stage.

Regarding to sub-graphs of the bioplastic membranes in Figure 11a–f, both ADB (the red curve) and NDB (the blue curve) are similar in their ascending trend starting from the PL level up to the US. This behavior means that each membrane, else ADB or NDB was stressed through two stages: (1) in the 1st one, the stress was increased from zero up to the PL level, (2) through the 2nd stage, each membrane transitioned from elastic to plastic nature as the load was increased from the PL up to the maximum load resulting the US stage.

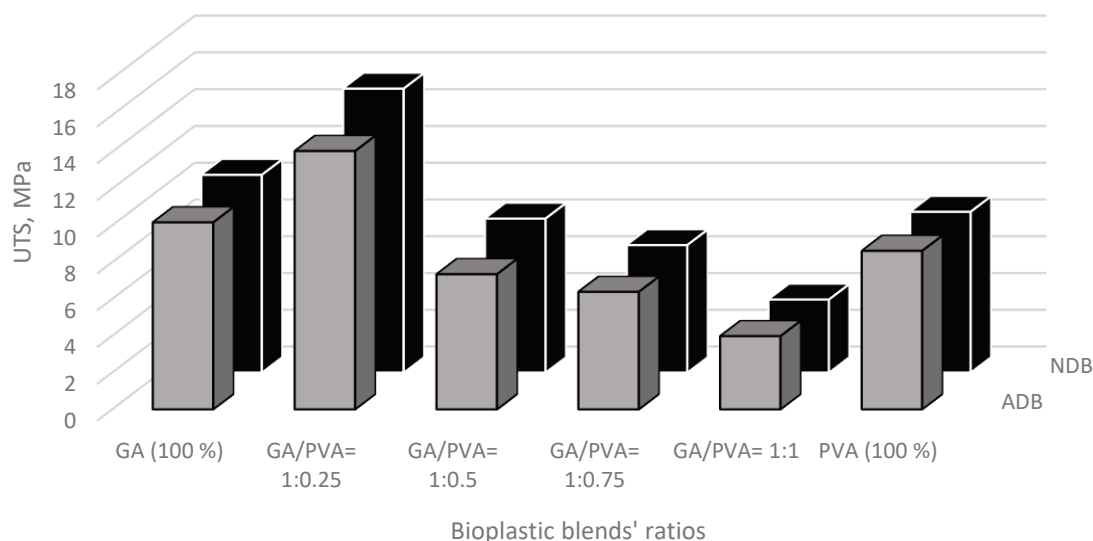
Regarding to proportionality limit (PL) of the bioplastic membranes, it is higher for the NDB than that for the ADB for all the six blend ratios. This indicates that the NDB membranes has higher elasticity endurance compared to their analogous membranes.

### 3.3.1. Ultimate Tensile Strength (UTS)

The observed curves of the UTS for the six polymeric blend membranes are presented in Figure 12.

The bioplastic membrane with the blend ratio of GA/PVA = 1:0.25 was found to have the highest UTS values (14.05 MPa and 15.44 MPa for ADB and NDB, respectively). It can also be seen from Figure 12 that the GA had a higher UTS' mean value than that for PVA (8.62 MPa and 8.74 MPa for ADB and NDB, respectively).

For more illustration, tensile stress increased as the GA content decreased from GA=100 % which has no PVA content (10.17 MPa, 10.75 MPa for ADB and NDB, respectively) up to the membrane with GA/PVA = 1:0.25 (14.05 MPa, 15.44 MPa for ADB and NDB, respectively). After that, the UTS decreased gradually with the consequent decrease in GA, thus increasing the PVA allocations in the bioplastic blend. Moreover, no significant difference was detected between the bioplastic membranes dehydrated by ordinary and nano-techniques (ADB and NDB) for all six bioplastic blends (Figure 12).

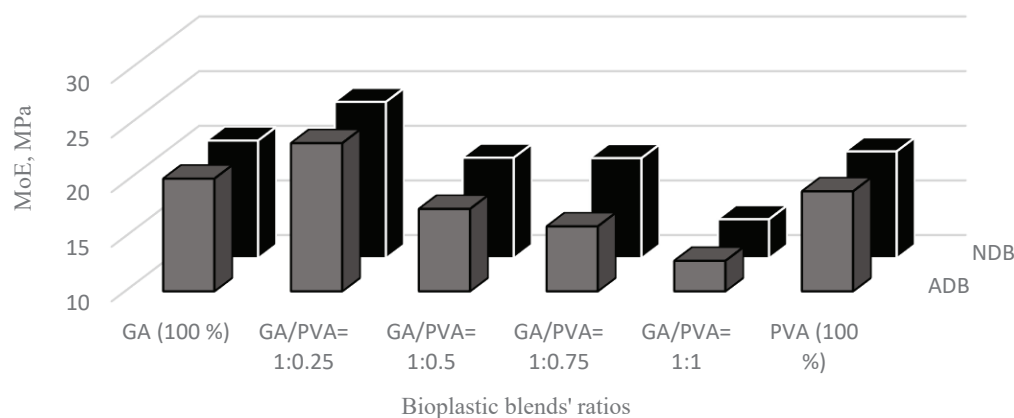


**Figure 12.** Ultimate tensile strength (UTS) of the six bioplastic membranes fabricated from gum Arabic (GA) and polyvinyl alcohol (PVA) with different ratios for each of the air-dried and nanodehydrated membranes.

### 3.3.2. Modulus of Elasticity (MoE)

Regarding the MoE graph presented in Figure 13 for the six bioplastic blends, the blend ratio of GA/PVA = 1:0.25 had the highest MoE values (14.05 MPa and 15.44 MPa for ADB and NDB, respectively). Moreover, GA was slightly higher in its MoE mean value than that for PVA (20.31 MPa and 20.77 MPa for ADB and NDB, respectively).

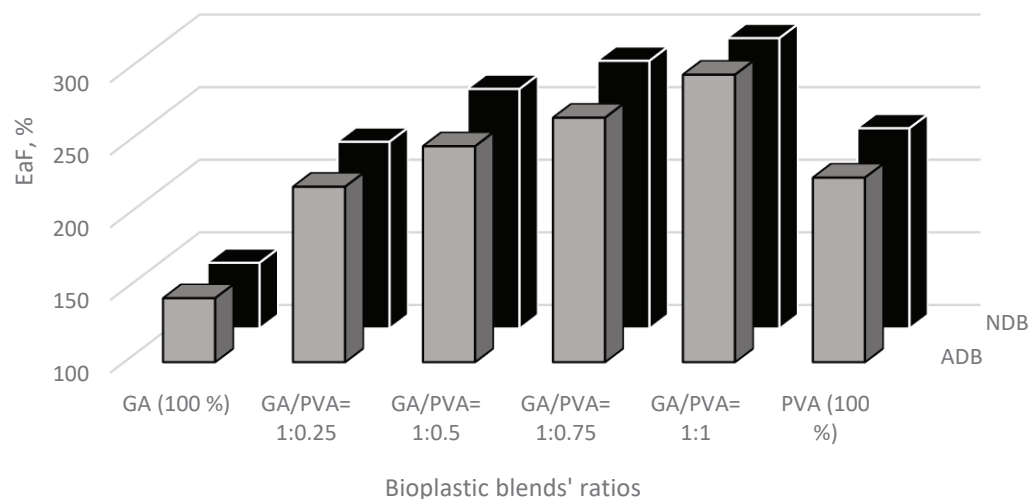
Also from Figure 13, it is worth mentioning that both graphs of ADB and NDB are similar in their trend concerning to the MoE curve, in which they increase with decreasing GA's and increasing PVA's allocation in the blend up to the blend ratio of 1:0.25. For more illustration, the mean value of the MoE was increased from the GA, 100%, and zero-allocation of PVA (20.31 MPa and 20.77 MPa for ADB and NDB, respectively) up to the membrane with GA/PVA = 1:0.25. After that, the UTS was decreased by decreasing the GA and increasing the PVA allocations in the bioplastic blend. Moreover, MoEs' mean values were found to be statistically similar concerning the bioplastic membranes dehydrated by ordinary and nano-techniques (ADB and NDB) for all six bioplastic blends (Figure 13).



**Figure 13.** Modulus of elasticity (MoE) of the six bioplastic membranes fabricated from gum Arabic (GA) and polyvinyl alcohol (PVA) with different ratios for air-dried (ADB) and nanodehydrated membranes (NDB).

### 3.3.3. Elongation at Failure (EaF)

The EaF data presented in Figure 14 indicates that adding PVA amounts to the bioplastic blends shows a significant increase in the EaF of the produced membranes for the GA/PVA's blending ratios of 1:0.25, 1:0.5, 1:0.75, and 1:1. In addition, it can also be seen from Figure 14 that the PVA had higher EaF's mean values (227.09% and 237.91%, for ADB and NDB, respectively) than those for GA (144.04% and 145.25%, for ADB and NDB, respectively). Moreover, there are no significant differences in the UTS belonging to the bioplastic membranes dried by means of ordinary and nano-dehydration methods (ADB and NDB) for all six bioplastic blends (Figure 14).



**Figure 14.** The percentage of elongation at failure (EaF) of the six bioplastic membranes fabricated from gum Arabic (GA) and polyvinyl alcohol (PVA) with different ratios for each of the air-dried (ADB) and nanodehydrated (NDB) membranes.

### 3.4. Bacterial and Fungal Biodegradation

The microbial communities for the initial soil samples as well as the buried bioplastic sheets were found to be different in number and species (Table 6). Depending on the type of buried membrane, different types of bacteria and fungi were found. *Pseudomonas* spp. [112,113], *Bacillus* spp. [58,112,113], *Aspergillus* spp. [114], and *Penicillium* spp. [112,115] were the predominant species for the buried PVA. *Bacillus* spp. [59], *Pseudomonas* spp., *Aspergillus* spp., *Rhizorpos* spp., *Fusarium* spp., *Penicillium* spp., and yeast *Saccharomyces* [59] were additional important species for the buried GA.

Moreover, the (GA/PVA = 1:1) bioplastic blend's microbial populations included *Bacillus* spp. [58,116], *Pseudomonas* spp., *Aspergillus* spp., *Rhizorpos* spp., *Fusarium* spp., and *Penicillium* spp. In addition, more fungal species than bacteria were found, which is consistent with the findings of Hindi et al. [98], who discovered that fungal isolates had a higher ability to use the sheets as growth substrates than bacteria.

Table 6 contains information about the colony-forming units (CFUs) of different microbial species. The total counts of bacteria, fungus, and yeast were determined to be  $2.28 \times 10^5$  and  $1.88 \times 10^3$  CFU/mL, respectively, in the first soil sample, and they were higher than those for GA and PVA (Table 5). After 30 and 60 days, pure GA (100%) had a higher CFU than pure PVA (100%). The CFU values measured after 30 and 60 days for each of the six bioplastic sheets showed no discernible differences.

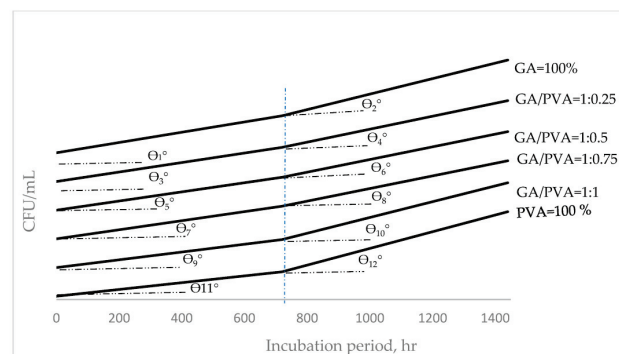
In addition, increasing colony-forming units (CFUs) over a defined period measured in hours was termed as hourly duplication (HD) of the CFU and was presented in Figures 15 and 16 for bacteria and fungi, respectively. For the prediction of the HD's values within the determined incubation periods, functional formulas were mathematically derived to reach this target, which is presented in Table 7.



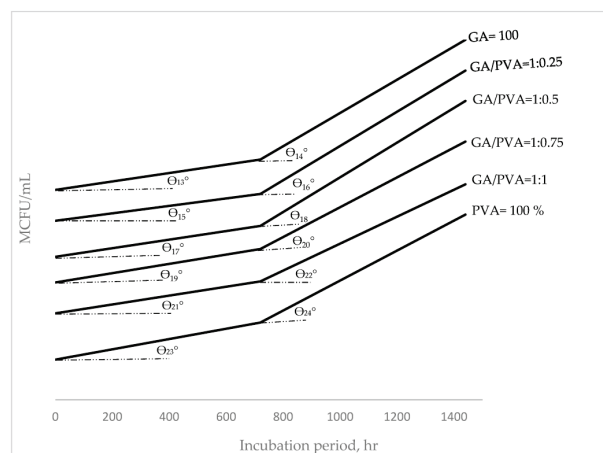
**Table 6.** Colony-forming units (CFUs) of microbial populations for bacterial and fungal species in the buried NDBs blended from gum Arabic (GA) and polyvinyl alcohol (PVA) in different ratios for soil burying.

AG/PVA Ratio	After 30 Days		After 60 Days	
	Bacteria CFU/mL	Fungi CFU/mL	Bacteria CFU/mL	Fungi CFU/mL
GA = 100%	$2.8 \times 10^6$ <sup>1</sup> [0.032]	$1.77 \times 10^3$ [0.008]	$6.69 \times 10^6$ [0.086]	$4.32 \times 10^3$ [0.077]
1:0.25	$2.6 \times 10^6$ [0.07]	$1.8 \times 10^3$ [0.042]	$5.86 \times 10^6$ [0.074]	$3.8 \times 10^3$ [0.093]
1:0.5	$2.52 \times 10^6$ [0.028]	$1.88 \times 10^3$ [0.094]	$5.7 \times 10^6$ [0.064]	$4.21 \times 10^3$ [0.086]
1:0.75	$2.5 \times 10^6$ [0.031]	$1.93 \times 10^3$ [0.095]	$5.67 \times 10^6$ [0.095]	$4.02 \times 10^3$ [0.086]
1:1	$2.17 \times 10^6$ [0.088]	$1.9 \times 10^3$ [0.012]	$6.14 \times 10^6$ [0.088]	$3.79 \times 10^3$ [0.044]
PVA = 100%	$1.93 \times 10^6$ [0.008]	$2.1 \times 10^3$ [0.083]	$6.12 \times 10^6$ [0.093]	$4.83 \times 10^3$ [0.046]
Soil control sample		Bacteria: $2.28 \times 10^5$ CFU/mL [0.058]		
		Fungi: $1.28 \times 10^3$ CFU/mL [0.022]		

<sup>1</sup> Values within parentheses are standard deviations.



**Figure 15.** Hourly duplication (HD) in colony-forming units (CFUs) of the bacterial population in the buried NDBs blended from gum Arabic (GA) and polyvinyl alcohol (PVA) in different ratios.



**Figure 16.** Hourly duplication (HD) in colony-forming units (CFUs) of fungi populations in the buried NDBs blended from gum Arabic (GA) and polyvinyl alcohol (PVA) in different ratios.

**Table 7.** Functional relationships between the incubation period (IP) as an independent variable (x) and hourly duplication (HD) as a dependent variable (y) of bacteria and fungi populations in the buried NDBs blended from gum Arabic (GA) and polyvinyl alcohol (PVA) in different ratios.

Microbial Type	AG/PVA Ratio	HD-Equation			
		<sup>1</sup> IA	The 1st Stage (0–720 h)	IAS	The 2nd Stage (720–1400 h)
Bacteria	GA = 100%	$\theta_1^\circ$	$y = 3572.2x + 228 \times 10^3$	$\theta_2^\circ$	$y = 8975x + 228 \times 10^3$
	1:0.25	$\theta_3^\circ$	$y = 3294.4x + 228 \times 10^3$	$\theta_4^\circ$	$y = 7822.2x + 228 \times 10^3$
	1:0.5	$\theta_5^\circ$	$y = 3183.3x + 228 \times 10^3$	$\theta_6^\circ$	$y = 7600x + 228 \times 10^3$
	1:0.75	$\theta_7^\circ$	$y = 3155.56x + 228 \times 10^3$	$\theta_8^\circ$	$y = 7558.3x + 228 \times 10^3$
	1:1	$\theta_9^\circ$	$y = 2697.2x + 228 \times 10^3$	$\theta_{10}^\circ$	$y = 7100x + 228 \times 10^3$
	PVA = 100%	$\theta_{11}^\circ$	$y = 2363.89x + 228 \times 10^3$	$\theta_{12}^\circ$	$y = 6794.4x + 228 \times 10^3$
Fungi	GA = 100%	$\theta_{13}^\circ$	$y = 0.8194x + 1.28 \times 10^3$	$\theta_{14}^\circ$	$y = 3.2361x + 1.87 \times 10^3$
	1:0.25	$\theta_{15}^\circ$	$y = 0.7222x + 1.28 \times 10^3$	$\theta_{16}^\circ$	$y = 3.3333x + 1.8 \times 10^3$
	1:0.5	$\theta_{17}^\circ$	$y = 0.8333x + 1.28 \times 10^3$	$\theta_{18}^\circ$	$y = 3.375x + 1.88 \times 10^3$
	1:0.75	$\theta_{19}^\circ$	$y = 0.9028x + 1.28 \times 10^3$	$\theta_{20}^\circ$	$y = 2.90278x + 1.93 \times 10^3$
	1:1	$\theta_{21}^\circ$	$y = 0.8611x + 1.48 \times 10^3$	$\theta_{22}^\circ$	$y = 2.625x + 2.1 \times 10^3$
	PVA = 100%	$\theta_{23}^\circ$	$y = x + 1.78 \times 10^3$	$\theta_{24}^\circ$	$y = 2.9167x + 2.5 \times 10^3$

<sup>1</sup> Incline angle in degrees.

Belonging to both bacterial (Figure 15) and fungi (Figure 16) communities, the HD values determined during and just after 800 h and up to 1400 h for each of the six bioplastic sheets showed the same ascending trend. For both trends, the HD's mean values for all the blends' ratios through the 1st duration (0–800 h) showed a slower duplication rate than those within the 2nd region (800–1400 h). These duplication rates can be noticed from the slope angle of the HD curves, as shown in Figures 15 and 16 [117,118].

In addition, it can also be seen when comparing the HDs of bacteria (Figure 15) with those for fungi (Figure 16) that the HDs' rate for fungi communities grown on the six bioplastic membranes was higher than those recorded for their analogous curves belonging to the bacteria. Moreover, the higher level of HD for the fungi community was more obvious at the 2nd stage of the incubation period. This finding can be observed by speculating the curves' slopes ( $\tan \theta_n$ , where  $n = 1-24$ ).

#### 4. Discussion

##### 4.1. Scientific Illustration of the Ease of Peeling the Bioplastic Membranes Away from the Acrylic Platform

In addition to the issue of drying the bioplastic sheets facing all hydrophilic natural polymer-based membranes, peeling these sheets to be rolled up is a major problem in the hydrophilic bioplastic blend field. Studying the ease of peeling the bioplastic membrane away from the casting panel template was achieved by investigating the chemical and physical properties of each of three parameters, namely, the bioplastic blend (fluid phase), the PMMA's platform (solid phase), and the liquid/solid interface, as shown in Figure S4 [57,98,119–125].

Regarding the triboelectric series that classifies materials based on their propensity to take electrons (tribo-positive) or not (tribo-negative), it is important to note that PMMA is a biocompatible polymer, which due to its propensity for either donating or absorbing electrons, occupies the middle position on the triboelectric series [119].

The following examples show how simple it is to separate the bioplastic membrane from the acrylic platform:

- a. Materials with relatively low surface energies are regarded as non-stick surfaces [125] and vice versa. As shown in Table S1, the acrylic platform exhibits modest surface energy (41 dynes/cm) and contact angle ( $82^\circ$ ), both of which are indicative of a non-stick surface [126].

- b. Acrylic is a powerful static generator in terms of electrostatic charge. When its surface is wiped back and forth, positive and negative surficial charges arise that draw and hold microscopic particles. Surficial charge variations have the potential to cause agglomerated particles to discharge in an unanticipated manner, endangering contamination-sensitive materials [127]. PMMA is positioned close to the middle of this empirical series for the surface potential and is regarded as a tribo-positive electron-donating material [119,127].

GA is composed of three distinct fractions, as shown in Figure S3, including the arabinogalactan–protein complex (MW 1500 kDa; approximately 10% of the total gum solids), arabinogalactan (MW 280 kDa; approximately 88% of the total gum solids), and glycoprotein (MW 250 kDa; approximately 2% of the total gum solids [128–130]. Due to their low molecular weight and branching pattern, arabinogalactan films are challenging to produce [131,132].

According to Winiewska et al. [133], PVA chains have a particular percentage of acetate groups (14%), which are the source of the polymer molecules negative charges. The structure of the PVA adsorption layer is impacted by even the comparatively modest portion of these groups. The presence of more acetate groups in the polymeric chains resulted in increased PVA adsorption levels, indicating that these groups are crucial to PVA adsorption [134]. As the pH of the solution rises, so does the contribution of charged acetate groups.

Due to the electrostatic attraction of negative charges present along the polymeric chains, the polymer chains extend further. The amount of PVA is directly influenced by the degree of development in the polymer macromolecules.

In general, plastics are categorized into four categories by Nuraje et al. [135]: super hydrophilic, hydrophilic, hydrophobic, and super hydrophobic, with contact angles ( $\theta^\circ$ ) of below  $5^\circ$ , below  $90^\circ$ ,  $90^\circ$ – $150^\circ$ , and  $150^\circ$ – $180^\circ$ , respectively.

The liquid–fluid–solid system exhibits three different interfaces in its configuration when a liquid drop is placed on a solid surface (Figure S4), namely, liquid–fluid, solid–fluid, and liquid–solid. It is noticed that adhesive and cohesive forces are present at each interface as a result of the intermolecular forces at work there. Cohesive forces cause the drop to return to its spherical shape, whereas adhesion forces encourage it to spread out. The conflict between these two forces determines the contact angle [57,73,133–137]. It is feasible to establish a connection between the static contact angle and the interfacial stresses under equilibrium conditions. The Young–Dupre equation is the name of this relationship. By applying the Hild [126] formula, it was discovered that the spreading of a droplet of a bioplastic blend is equal to  $A - (B + C)$ , where  $A$  is the surface tension of the bioplastic blend,  $B$  is the surface tension of the acrylic panel, and  $C$  is the surface energy of the interface between the bioplastic blend and the acrylic panel. While liquid will spread when the spreading is zero to positive, it will not if the spreading is negative.

#### 4.2. Scientific Illustration of the Nanodehydration of the Bioplastic Membranes

It is well known that drying bioplastic membranes is a critical issue when manufacturing these products. This crucial problem arises from the highly hydrophilic nature of their natural-based precursors, such as the hydrophilic GA and PVA used in this study. Accordingly, a novel technique and device were invented to accelerate the dehydration process of such products [57]. The invention, termed the stratified nano-dehydrator (SND), is constructed from accurately selected materials, including perforated acrylic panels (poly(methyl methacrylate)), polypropylene’s non-woven textile, cellulosic cotton floss, and an effective dehydrant agent such as P2O5, which is the most effective dehydrant reagent, rather than calcium chloride, magnesium sulfate, aluminum oxide, lithium aluminum hydride, metallic sodium, or silica gel.

The reasons for choosing PMMA material as barrier panels within the dehydrator apparatus were due to its self-electrostatic charging property as well as its ability to force the evaporated water molecules to have higher surface tension, which facilitates their

escape outside the SND atmosphere and, subsequently, accelerates drying the bioplastic membranes. Furthermore, the cellulosic material (loosened Egyptian cotton floss) was selected for this task due to its high content of alpha cellulose, well-known for its high hydrophilicity, which is essential to attaining good affinity to both moisture molecules as well as dehydrant crystals.

The scientific concepts of ion dehydration reported by Pavluchkov et al. [138] can be used to explain the water molecules' diffusion, especially in the transition state, by converting the water liquid into gaseous or steam matter.

Polar covalent bonds between the O- and H-atoms were extensively reported to generate an asymmetric distribution of electrons in a water molecule, with two excess electrons on the O-atom's side of the molecule and two deficient electrons on the H-atom's side. This asymmetry accepts water molecules with both molecular cohesion that attracts water molecules to each other and/or adhesion that attracts water molecules to their neighboring asymmetrically charged materials like ions, polarized molecules, and charged surfaces, including but not limited to glass [139] and the PMMA's casting platform used in the present investigation [57].

Since water molecules have high polarity, their transportation (evaporation) from the bioplastic membranes upon the drying process can be viewed like the ion dehydration phenomenon that regulates ionic transport through sub-nanopores, which can permit selectivity between similar sized and charged ions, as referred to by Pavluchkov et al. [138]. Transition-state theory gives an idea about molecular activation parameters (enthalpy and entropy) that determine the interaction level between the transported species and the wet bioplastic blend, as well as the freedom of molecular motion within it. Since hydration and dehydration effects are characterized by substantial enthalpic (due to changes in the chemical bonds between the ion and its surroundings) and entropic (due to changes in the spatial structure of the ion) changes at the molecular level, this theory has been successfully suggested to explore dehydration-related transport phenomena in membranes [138].

The enclosed system within the SND was partially vacuumed to give mildly driven forces that accelerate the water vapor molecules' escape outside the dehydrator [57] and subsequently enhance the drying process itself.

### 4.3. Chemical and Physical Properties of the Bioplastic Membranes

#### 4.3.1. FTIR

Different organic functional groups found in naturally occurring substances can be recognized using Fourier transform infrared (FTIR) spectroscopy. The complicated vibrational modes were seen in the FTIR spectra for the various bioplastic samples over a wide range of wavenumbers (Figure 4).

Figure 4 shows the strong and broad O-H stretching vibrations at  $3416\text{ cm}^{-1}$  dominating the primary FTIR spectra of the six bioplastic sheets. At  $2939\text{ cm}^{-1}$ , the C-H stretching modes are riding above the board peak. Along with the bulk ring mode at  $1426\text{ cm}^{-1}$ , the carbonyl stretching modes are seen at  $1641\text{ cm}^{-1}$ . At  $1047\text{ cm}^{-1}$ , the typical C-O-C anti-symmetric stretching mode was found. These findings are modified from those attained by other researchers [108–111] for the study of biopolymeric materials.

For an additional illustration, the overall banding of the FTIR analysis showed a carbohydrate fingerprint at  $900\text{--}1250\text{ cm}^{-1}$  [138]; C-O-C anti-symmetric stretching at  $1426$  and  $1047\text{ cm}^{-1}$  [57,98,99];  $\text{COO}^-$  asymmetric stretching at  $1402\text{ cm}^{-1}$  [139]; an O-H in-plane bending band in carboxylic acids at  $1625.4$ ,  $1627.4$ ,  $1430$ ,  $1436.91$ , and  $1437\text{ cm}^{-1}$  [132,133];  $\text{COO}^-$  symmetric stretching and carbonyl stretching modes at  $1641\text{ cm}^{-1}$  [57,98,99,101]; C-H stretching at  $2800\text{--}3000$ ,  $2885$ , and  $2939\text{ cm}^{-1}$  [57,98,99,101,137,140–142]; vibrational modes of the C-H group at  $2910.87\text{ cm}^{-1}$  [141,142]; O-H stretching vibrations at  $3261$ ,  $3416$ , and  $3000\text{--}3600\text{ cm}^{-1}$  [57,98,137,141,143], and the unique presence of O-H groups at  $3526.35\text{ cm}^{-1}$  [142,143].

The FTIR for the NDB used in the current work and the ADB created by Hindi et al. [98] have main functional groups that share chemical characteristics, accord-



ing to the comparison. As a result, the chemical components of the bioplastic products have been preserved by the use of innovative casting blends, nano-dehydration, and membrane peeling.

#### 4.3.2. XRD

The GA-broad diffractogram's greatest intensity was recorded at  $2\theta^\circ = 20^\circ$  (Figure 5), which supports the amorphous nature of gum Arabic [13]. Moreover, a typical peak for pure PVA, a semi-crystalline polymer detected at  $2\theta^\circ = 19.9^\circ$  (Figure 4f), confirmed its semi-crystallinity feature [57,92,111].

With the increase in PVA allocation in the blend, the crystallinity index values increased. The growing CI of the bioplastic blends can be correlated to the increasing PVA allocation in the blend because the CI value of PVA (54.81%) was found to be greater than that of GA (19.4%).

#### 4.3.3. TGA

TGA analyzes the mass change behavior in bioplastic membranes that occurs as a function of temperature and time in a controlled environment. The best uses for it are to evaluate reaction kinetics, volatile contents, thermal stability, degradation traits, aging/lifetime breakdown, and degradation features.

The thermal deterioration of the samples (Figure 6) increased at higher temperatures (up to 500 °C) than at lower temperatures, according to a comparison of the mass losses between the temperature zones. Furthermore, a comparison of the mass losses across the temperature ranges revealed that PVA shed more weight in the higher temperature zones than GA. A mass loss of up to 100 °C can be attributed to the water molecule's large solvation capacity, which results in the evaporation of loosely bound moisture on the surface, or "free water". Furthermore, mass loss at temperatures up to 150 °C can be due to hygroscopic water evaporation [57,92].

#### 4.3.4. DTA

Similar information is provided by DTA, which measures the temperature difference between a sample and a reference due to thermal treatments in a material. The DTA typically provides phase transition information in addition to the TGA.

It is commonly known that two types of thermograms can be distinguished for a given material during thermal reactions: endothermic, which uses energy, and exothermic, which excludes energy. The depolymerization of the bioplastic materials themselves as a result of heat treatment causes exograms to occur (Figure 7). Moreover, the endotherm can be attributed to the fusing or melting of crystallites as well as the evaporation of free moisture (up to 100 °C) and hygroscopic moisture (up to 120 °C) [57].

As shown in Figure 7 and Table 3, GA had the lowest value of heat change (−1017.3 Vs/mg), but the endotherm of pure PVA absorbed the maximum amount of energy (2119.7 Vs/mg) among the other bioplastic blends. As a result, PVA is more thermally stable than GA because it absorbs heat more effectively, shielding the bioplastic sample from potential thermal degradation brought on by rising temperatures. Moreover, the enhanced PVA allocation in the blends boosted the thermal stability of the bioplastic sheets.

GA exhibits greater thermal stability than PVA at higher temperatures (about 350 °C). As a result, altering a bioplastic blend to increase PVA or decrease GA enhances the thermal stability of the resulting bioplastic membrane [57,92].

### 4.4. Anatomical Ultrastructure of the Bioplastic Membranes

#### 4.4.1. Surface Roughness and Nanometric Particle Size

While the pure PVA sheets (0/1 blend ratio) had the greatest PS values for both the ADB and NDM, the pure GA membrane (1/0) had the lowest PS values. Gradually raising the PVA concentration in the bioplastic blend increased the PS. The surface roughness (SR) features examined via atomic force microscopy (AFM), as shown in Table 4 and Figure 8,

provide confirmation of this. The results obtained for PVA-based membranes and the median value for those cast from GA/PVA (1:1) are compared.

As a result, the presence of PVA causes the SR of the water-based polymeric blends to increase, generating a surface that is rougher. This is supported by the surface roughness features examined using atomic force microscopy (AFM), as shown in Table 4 and Figure 8.

Increases in PVA allocation make the blend's texture coarser since PVA membranes have a rougher structure than GA membranes. According to the comparison of the membranes, there is no statistically significant difference between the ADB and NDB in their PS, along with the six bioplastic blends. Additionally, analyses of the effects of different bioplastic blend ratios on a membrane showed that, in both cases, blends with higher PVA concentrations produced membranes with higher porosities (PD and VV).

It is important to note that smoother sheets are preferred for packaging over coarser ones because the latter tend to gather more dust on their surfaces. Although PVA is a crucial part of the bioplastic mixture that improves the quality of the final membrane and makes it easier for it to peel off the casting surface after drying, a careful balance must be taken into account to have the best quality and smoothest surfaces.

Moreover, there is no statistical distinction in the PS between the ADB and the NDB. Because of this, the unique techniques created to make it easier to cast their mixes, dry them faster, and peel membranes off easily using a self-electrostatic template did not alter the parent roughness properties. Because of this, the unique approaches employed in the current study did not alter the permeability of the membranes (PD and VV).

#### 4.4.2. Membrane Permeability

For the membrane ultrastructure presented in Figure 9, the GA membranes had the lowest PD and VV compared to those for PVA, which had the highest ones for both air-dried bioplastic (ADB) membrane and nanodehydrated transparent bioplastic (NDB) membrane. Accordingly, increasing the PVA allocation increased the membrane permeability, which facilitated the water evaporation from the blend during the nano-dehydration procedures.

When compared to PVA membranes, which had the highest PD and VV for both the air-dried bioplastic (ADB) and nanodehydrated (NDB) membranes, the GA membranes had the lowest ultrastructures. As a result, increasing the PVA allocation also increased the membrane permeability, which made it easier for the blend's water to evaporate throughout the nano-dehydration processes.

Moreover, there is no statistical difference between the ADB and NDB for each case of the PS, PD, or VV. Because of this, the unique approaches employed in the current study did not alter the permeability of the membranes (PD and VV), as shown in Figure 9 and Table 4.

#### 4.5. Mechanical Properties of the Bioplastic Membranes

The evaluation of a film's capability and mechanical integrity heavily relies on its mechanical properties. The interactions between the blend's components had a significant impact on the matrices of blended films. The mechanical properties were reported to be solely dependent on the chemical structure, which could be best described by using UTS, MoE, and EaF [74]. In addition, it was reported by Gomaa et al. [77] that the internal molecular force, the crystallinity shape, and the content of the polymer all have a significant impact on the mechanical characteristics [77].

The findings understood from Table 5 and Figure 11 revealed that both ADB (the red curve) and NDB (the blue curve) are similar in their ascending trend starting from the PL level up to the US. This behavior means that each membrane, else ADB or NDB was stressed through two stages: (1) in the 1st one, the stress was increased from zero up to the PL level, (2) through the 2nd stage, each membrane transitioned from elastic to plastic nature as the load was increased from the PL up to the maximum load resulting the US stage.

In addition, regarding to proportionality limit (PL) of the bioplastic membranes, it is higher for the NDB than that for the ADB for all the six blend ratios. This indicates that the NDB membranes has higher elasticity endurance compared to their analogous membranes.

As clear from Table 5 and Figure 11, the plotted stress-strain curves for the six blended membranes were differed concerning to their proportionality limit (PL) and ultimate strength (US).

Regarding to sub-graphs of the bioplastic membranes in Figure 11a–f, the similarity between the ADB and NDB in their ascending trend starting from the PL level up to the US can be explained that these membranes was stressed through two stages: (1) in the 1st one, the stress was increased from zero up to the PL level, and (2) through the 2nd stage, each membrane transitioned from elastic to plastic nature as the load was increased from the PL up to the maximum load resulting the US stage.

Since the proportionality limit (PL) of the bioplastic membranes was found to be higher for the NDB than that for the ADB for all the six blend ratios. This indicates that the NDB membranes has higher elasticity endurance compared to their analogous membranes.

The highest values of the UTS (Figure 12) and the MoE (Figure 13) for the membranous sample at the blend ratio of 1:0.25 can be attributed to the strong interaction between the GA and PVA at this optimum blend ratio, which permitted complete miscible blending [76].

The EaF of the bioplastic film samples is explained by the maximum change in its length before failure or breaking as clear from Figure 14 [74].

As shown in Figure 14, adding the GA to the blends enhanced the EaF's membranes up to the blend ratio of GA/PVA of 0.5/0.5. This could be attributed to the good interfacial adhesion among the polymer components (GA and PVA). These findings of the mechanical study confirm the addition of gum acacia can improve mechanical properties, which decrease with an increase in the allocation of gum Arabic [74].

Adding polyvinyl alcohol to the gum Arabic for preparing the bioplastic blend films improved the mechanical properties of these membranes, especially in the blend ratio of GA/PVA of 1:0.25, which enhanced both UTS and MoE, while EaF was enhanced for the blend ratio's membrane GA/PVA of 1:1. Therefore, the results of this work may show that the functional properties of GA/PVA blend films are adequate for food packaging applications and in the pharmaceutical industry for controlled release of drugs [74].

#### 4.6. Microbial Biodegradation

Biodegradation of the NDB material was confirmed significantly by its reduction in weight for all six NDB samples, and it was found that degradation commenced within 30 and 60 days [144–147].

The microbial communities in all the buried bioplastic sheets, including the control one, were different in number and species. The species of bacteria and fungi differed according to the type of buried sheet.

The microbiological study revealed that all six bioplastic sheets are able to be degraded, contrary to petroleum-based sheets.

Biodegradation is the process by which microorganisms can degrade bioplastic membrane materials, leading to a loss of weight after a period of time. Our results show that all blended bioplastic membranes have reduced weight, especially GA. Our results agree with those of Sasaki et al. [92], who prepared films of phenolic extracts incorporated into GA and found that the highest weight loss of films was 45.81%, compared with GA (26.87%) after 30 days.

Microorganisms can degrade bioplastic membranes through a process called biodegradation, which eventually causes the membranes to lose their weight. Our findings indicate that the weights of all blended bioplastic membranes, particularly GA, decreased. Our findings are consistent with those of Sasaki et al. [92], who created films using phenolic extracts mixed with GA and discovered that after 30 days, the weight loss of the films was higher than that of the GA (45.81%).

These findings were contrary to Ibrahim et al. [78], who discovered that for nanofiber membranes based on homogenous polymeric blends of gum Arabic, polyvinyl alcohol, and silver nanoparticles, the biodegradation tests of the generated nanofibers revealed that 99.09% of the material was broken down after 28 days (Table 7). These variations in the results can be explained by the fact that a variety of factors, including microbes, humidity, sunshine, and oxygen, can affect the bioplastic's capacity to degrade [80].

In addition, because it affects the microbial population and shapes it, the depth of the soil that bioplastic membranes are buried in is a crucial component for biodegradation [78]. In addition, as a result of using gum as a source of nutrients, the number of bacteria increased over time [82,98].

Our results proved that *Pseudomonas* spp., *Bacillus* spp., and *Micrococcus* spp. were the most commonly isolated bacterial strains appearing in different samples, while *Rhizobus* spp., *Penicillium* spp., and *Fusarium* spp. were the most commonly isolated fungus strains that appeared in our different samples. These findings agree with those found by Santos-Beneit et al. [93] and Sasaki et al. [92], which were isolates of *Bacillus cereus*, *Bacillus polymyxa*, *Bacillus licheniformis*, *Corynebacterium xerosis*, *Staphylococcus epidermis*, *Streptococcus bovis*, and the fungi *Penicillium notatum*, *Rhizopus nigricans*, *Aspergillus niger*, and *Fusarium moniliforme* from gum Arabic [68,87,89,90,92,144,145].

Belonging to comparisons within communities, it was found that the HD values determined during and just after 800 h and 1400 h for each of the six bioplastic sheets buried in the soil were similar in their trend concerning each of the bacteria (Figure 15) and fungi (Figure 16) as well as Table 7. This similarity in trends can be attributed to the constancy of the burying depth of the bioplastic membranes [78] and/or various factors, including microbes, humidity, sunshine, and oxygen, which can affect the bioplastic's capacity to degrade [80].

Moreover, a common trend was registered between the NDB products fabricated in the current investigation and the ADB synthesized by Hindi et al. [98] and Hindi and Albureikan [57]. Accordingly, the nano-dehydration invention did not affect the parent's ability to biodegrade the bioplastic membranous product.

## 5. Conclusions and Future Perspectives

Great success was achieved for the fabrication of bioplastic membranes from gum Arabic mixed with polyvinyl alcohol by applying a novel casting method, termed static vibrated-free horizontal flow, which produces free air bubble sheets. The novel nano-dehydration technique gave the best solution for drying the bioplastic sheets and can be used for any water-based biopolymeric-based product. It is the first time that an acrylic (poly-(methyl methacrylate)) panel used as an ideal template surface features an electrostatically charged hydrophobic surface. As a result, peeling off its template surface is made simpler.

The most important properties of the nanodehydrated bioplastic membranes were studied using Fourier transform infrared spectroscopy, X-ray powder diffraction, thermogravimetric analysis, differential thermal analysis, and atomic force microscopy to ensure that the novel techniques did not distort the product quality. The nanodehydrated bioplastic membranes retained their parent properties, including chemical functional groups, crystallinity index, mass loss, thermal stability, ultrastructure features (surface roughness and permeability), and their ability for microbial biodegradation. PVA had a higher crystallinity index (CI), a greater mass loss at higher temperatures, higher thermal stability due to its higher heat content, and greater clearance of surface roughness due to its high particle size (PS), as well as higher permeability parameters, namely, pore diameter (PD) and void volume (VV), than those for GA. Accordingly, increasing the PVA allocation in the bioplastic blends could enhance their properties except for mass loss, whereas increasing the GA allocation in the NDB blend reduced its mass loss at elevated temperatures.

There is no statistical difference between the bioplastic membranes synthesized elsewhere with ordinary air drying or nano-dehydration in terms of their particle size and



permeability, indicating that the novel procedures used did not distort the parent properties examined as well as their ability for biodegradation. Adding polyvinyl alcohol to the gum Arabic for preparing the bioplastic blend films improved the mechanical properties of these membranes, especially in the blend ratio of GA/PVA of 1:0.25, which enhanced both UTS and MoE, while EaF was enhanced for the blend ratio's membrane GA/PVA of 1:1. Therefore, the results of this work may show that the functional properties of GA/PVA blend films are adequate for food packaging applications and in the pharmaceutical industry for controlled release of drugs [74]. The biodegradation of the nanodehydrated bioplastic membranes was confirmed significantly by the reduction in weight for all six blended samples, and degradation was found to start within 30 and 60 days. Pure GA was the most commonly biodegraded sample among the other bioplastic samples. The microbial communities in all of the buried bioplastic sheets, including the control sample, were different in number, species, and duplication rates. The microbiological survey revealed that all six bioplastic sheets are able to be degraded, contrary to petroleum-based sheets.

## 6. Patent

System, apparatus, and methods for manufacturing biodegradable biopolymeric materials (US Patent No. 11548192).

**Supplementary Materials:** The following supporting information can be downloaded at: <https://www.mdpi.com/article/10.3390/polym15153303/s1>, Figure S1. The practical procedure used for the novel casting of the (NDB) membranes; Figure S2. The vibrational casting process of the polymeric blends into sheets; Figure S3. Chemical constituents of the polymers used to synthesize the nanodehydrated-bioplastic (NDB) membranes: (a) gum Arabic (GA) precursor, (b) polyvinyl alcohol (PVA) precursor, (c) (poly-(methyl methacrylate), PMMA); Figure S4. Visualization analysis of void volumes (VV, nm<sup>3</sup>) of the six nanodehydrated-bioplastic membranes (NBMs): (a) GA (100%); (b) GA/PVA = 1:0.25; (c) GA/PVA = 1:0.5; (d), GA/PVA = 1:0.75; and (e) GA/PVA = 1:1, and (f) PVA = 100% based on AFM-image analysis; Table S1. Surface energy and contact angle of the most important industrial polymers; Table S2. Calculating means of mass loss (ML) of the NDB membranes blended from gum Arabic (GA) and polyvinyl alcohol (PVA) in the six ratios and different temperature zones (T-zones).

**Author Contributions:** Conceptualization, S.S.H. and M.O.I.A.; methodology, S.S.H.; validation, S.S.H. and M.O.I.A.; formal analysis, S.S.H.; investigation, S.S.H. and M.O.I.A.; writing—original draft preparation, S.S.H. and M.O.I.A.; writing—review and editing, S.S.H. and M.O.I.A. All authors have read and agreed to the published version of the manuscript.

**Funding:** This work was funded by the Deanship of Scientific Research (DSR), KAU, Jeddah, under grant No. G: 85/155/1434.

**Institutional Review Board Statement:** Not applicable.

**Data Availability Statement:** The supporting data for the reported results, including a link to the publicly archived datasets analyzed or generated during this study, can be found under the following patent: US Patent for System, apparatus, and methods for manufacturing biodegradable biopolymeric materials (Patent #11548192, issued 10 January 2023)—Justia Patents Search, <https://patents.justia.com/patent/11060208> (accessed on 17 November 2022).

**Acknowledgments:** The P.I. author is deeply thankful to DSR, KAU, Jeddah for funding this research work. The project that revealed this invention was funded by the Deanship of Scientific Research (DSR), King Abdulaziz University, Jeddah, under grants no. G: 85/155/1434 and, respectively. The P.I. author therefore acknowledges with thanks the DSR for technical and financial support. Appreciation is given to the Center of Nanotechnology (CN) for its technical assistance. Deep thanks to Rakan A. Alanazi for his scientific assistance throughout this investigation.

**Conflicts of Interest:** The authors declare no conflict of interest.

## Nomenclature

ADB	Air-dried bioplastic
ACS	The American Chemical Society
AFM	Atomic force microscopy
CI	Crystallinity index
CFU	Colony-forming unit of microbial populations
DSC	Differential scanning calorimetry
DTA	Differential thermal analysis
EaF	Elongation at failure
EC	Enthalpy change
FTIR	Fourier transform infrared spectroscopy
GA	Gum Arabic
HC	Heat change in $\mu\text{Vs}/\text{mg}$
HD	Hourly duplication
MoE	Modulus of elasticity
$\mu\text{Vs}/\text{mg}$	Microvolts per milligram
NDB	Nanodehydrated bioplastic
NPS	Nanometric particle size
PubChem	Open chemistry database managed by the National Institutes of Health (NHI)
PVA	Polyvinyl alcohol
SD	Standard deviation
SECT	Self-electrostatic charged-template
SP	Statistical parameters
SR	Surface roughness
PD	Pore diameter
PS	Particle size
TGA	Thermogravimetric analysis
TR	Temperature range ( $^{\circ}\text{C}$ )
UTS	Ultimate tensile strength
XRD	X-ray diffraction
VFHF	Vibrated-free horizontal flow
VV	Void volume

## References

- Mergaert, J.; Anderson, C.; Wouters, A.; Swings, J.; Kersters, K. Biodegradation of polyhydroxyalkanoates. *FEMS Microbiol. Lett.* **1992**, *9*, 317–321. [CrossRef] [PubMed]
- Nampoothiri, K.M.; Nair, N.R.; John, R.P. An overview of the recent developments in polylactide (PLA) research. *Bioresour. Technol.* **2010**, *101*, 8493–8501. [CrossRef]
- Boyandin, A.N.; Prudnikova, S.V.; Filipenko, M.L.; Khrapov, E.A.; Vasil'ev, A.D.; Volova, T.G. Biodegradation of polyhydroxyalkanoates by soil microbial communities of different structures and detection of PHA degrading microorganisms. *Appl. Biochem. Microbiol.* **2012**, *48*, 28–36. [CrossRef]
- Merugu, R. Studies on PHB (Polyhydroxy butyrate) degradation by some species of *Aspergillus*. *Studies* **2012**, *4*, 1111–1113.
- Gautam, N.; Kaur, I. Soil burial biodegradation studies of starch grafted polyethylene and identification of *Rhizobium meliloti* therefrom. *J. Environ. Chem. Ecotoxicol.* **2013**, *5*, 147–158.
- Karamanlioglu, M. Environmental Degradation of the Compostable Plastic Packaging Material Poly (lactic) acid and Its Impact on Fungal Communities in Compost. Ph.D. Thesis, Manchester University, Manchester, UK, 2013; p. 198.
- Badreldin, H.A.; Al-Husseni, I.; Beegam, S.; Al-Shukaili, A.; Nemmar, A.; Schierling, S.; Queisser, N.; Schupp, N. Effect of gum Arabic on oxidative stress and inflammation in adenine-induced chronic renal failure in rats. *PLoS ONE* **2013**, *8*, e55242.
- Feddersen, R.L.; Thorp, S.N. Sodium carboxymethyl cellulose. In *Industrial Gums, Polysaccharides and Their Derivatives*; Whistler, R.L., Bemiller, J.N., Eds.; Academic Press: New York, NY, USA, 1993; pp. 537–578.
- Verbeke, D.; Dierckx, S.; Dewettinck, K. Exudate gums: Occurrence, production, and applications. *Appl. Microbiol. Biotechnol.* **2003**, *63*, 10–21. [CrossRef]
- Williams, P.A.; Phillips, G.O. *Handbook of Hydrocolloids*; Williams, P.A., Phillips, G.O., Eds.; CRC Press: Cambridge, UK; Elsevier: Amsterdam, The Netherlands, 2000; pp. 155–168.
- Anonymous; FAO. *Food and Nutrition*; Food and Agriculture Organization: Rome, Italy, 1990; p. 49.
- Buffo, R.A.; Reineccius, G.A.; Oehlert, G.W. Factors affecting the emulsifying and rheological properties of gum acacia in beverage emulsions. *Food Hydrocoll.* **2001**, *15*, 53–66. [CrossRef]

13. Almuslet, N.A.; Hassan, E.A.; Al-Sherbini, A.A.M.; Muhgoub, M.G.A. Diode laser (532 nm) induced grafting of polyacrylamide onto gum Arabic. *J. Phys. Sci.* **2012**, *23*, 43–53.
14. Anonymous. *Production and Marketing of Gum Arabic*; Network for Natural Gums and Resins in Africa (NGARA): Nairobi, Kenya, 2016.
15. Krempel, M.; Griffin, K.; Khouryieh, H. Hydrocolloids as emulsifiers and stabilizers in beverage preservation. In *Preservatives and Preservation Approaches in Beverages; The Science of Beverages*; Grumezescu, A.M., Holban, A.M., Eds.; Academic Press: Cambridge, MA, USA, 2019; Volume 15, pp. 427–465.
16. Rinsky, L.H.; Rinsky, G. *The Pastry Chef's Companion: A Comprehensive Resource Guide for the Baking and Pastry Professional*; John Wiley & Sons: Chichester, UK, 2009; Volume 1, p. 134.
17. Maqbool, M.; Ali, A.; Alderson, P.G.; Zahid, N. Exploring the new applications of gum Arabic obtained from acacia species to preserve fresh fruits and vegetables. In Proceedings of the II International Symposium on Underutilized Plant Species: Crops for the Future—Beyond Food Security, Kuala Lumpur, Malaysia, 27 June–1 July 2013; Volume 2, pp. 2406–6168.
18. McEachran, R. Gum Arabic: The Invisible Ingredient in Soft Drink Supply Chains. *Guardian* **2013**. Available online: [www.theguardian.com](http://www.theguardian.com) (accessed on 16 February 2023).
19. Anderson, D.M.W.; Farquhar, J.G.K. Gum exudates from the genus *Prosopis*. *Int. Tree Crops J.* **1982**, *2*, 15–24. [CrossRef]
20. Anderson, D.M.W.; McNab, C.G.A.; Anderson, C.G.; Brown, P.M.; Pringuer, M.A. Studies of uronic acid materials, Part 58: Gum exudates from the genus *Sterculia* (gum karaya). *Int. Tree Crops J.* **1983**, *2*, 147–154. [CrossRef]
21. Suliman, S.M.; Hamdouk, M.I.; Elfaki, M.B. Gum Arabic fibre as a supplement to low protein diet in chronic renal failure patients. Sudan Association of Physicians. In Proceedings of the 17th Conference, Friendship Hall, Khartoum, Sudan, 21–23 March 2000.
22. Gamal el-din, A.M.; Mostafa, A.M.; Al-Shabanah, O.A.; Al-Bekairi, A.M.; Nagi, M.N. Protective effect of Arabic gum against acetaminophen-induced hepatotoxicity in mice. *Pharmacol. Res.* **2003**, *48*, 631–635. [CrossRef]
23. Eltayeb, I.B.; Awad, A.I.; Elderbi, M.A.; Shadad, S.A. Effect of gum Arabic on the absorption of a single oral dose of amoxicillin in healthy Sudanese volunteers. *J. Antimicrob. Chemother.* **2004**, *54*, 577–578. [CrossRef]
24. Ali, A.A.; Ali, K.E.; Fadlalla, A.; Khalid, K.E. The effects of gum Arabic oral treatment on the metabolic profile of chronic renal failure patients under regular haemodialysis in central Sudan. *Nat. Prod. Res.* **2008**, *22*, 12–21. [CrossRef]
25. Hills, S. Gum Arabic Caloric Value Lowered. 2008. Available online: [www.foodnavigator-usa.com](http://www.foodnavigator-usa.com) (accessed on 24 January 2023).
26. Ali, B.H.; Ziada, A.; Blunden, G. Biological effects of gum Arabic: A review of some recent research. *Food Chem. Toxicol.* **2009**, *47*, 1–8. [CrossRef]
27. Omer, A.E.; Ayed, I.A.M.; El Badwi, S.M.A. Effect of gum Arabic on nephrotoxicity induced by *Aristolochia bracteolata* in rats. *Sch. Acad. J. Biosci.* **2013**, *1*, 377–380.
28. Luo, Y.; Zhang, Y.; Pan, K.; Critzer, F.; Davidson, P.M.; Zhong, Q. Self-emulsification of alkaline-dissolved clove bud oil by whey protein, gum Arabic, lecithin, and their combinations. *J. Agric. Food. Chem.* **2014**, *62*, 4417–4424. [CrossRef]
29. Wang, H.; Williams, P.A.; Senan, C. Synthesis, characterization and emulsification properties of dodecanyl succinic anhydride derivatives of gum Arabic. *Food Hydrocoll.* **2014**, *37*, 143–148. [CrossRef]
30. Lawrence, R.; Jeyakumar, E.; Gupta, A. Antibacterial activity of *Acacia Arabica* (Bark) extract against selected multi drug resistant pathogenic bacteria. *Int. J. Curr. Microbiol. Appl. Sci.* **2015**, *1*, 213–222.
31. Hadavi, M.; Hasannia, S.; Faghihi, S.; Mashayekhi, F.; Zadeh, H.; Mostofi, S. Novel calcified gum Arabic porous nano-composite scaffold for bone tissue regeneration. *Biochem. Biophys. Res. Commun.* **2017**, *488*, 671–678. [CrossRef]
32. Salih, N.K. Applications of gum Arabic in medical and health benefits. In *Gum Arabic*; Academic Press: Cambridge, MA, USA, 2018; pp. 269–281.
33. Kraaijpoel, D.; Herenius, C. *Het Kunstschilderboek—Handboek voor Materialen en Technieken, Cantecler*; Tirion Art: Utrecht, The Netherlands, 2007; p. 183.
34. Banerjee, S.S.; Chen, D.-H. Magnetic nanoparticles grafted with cyclodextrin for hydrophobic drug delivery. *Chem. Mater.* **2007**, *19*, 6345–6349. [CrossRef]
35. Wilson, O.C., Jr.; Blair, E.; Kennedy, S.; Rivera, G.; Mehl, P. Surface modification of magnetic nanoparticles with oleylamine and gum Arabic. *Mater. Sci. Eng. C* **2008**, *28*, 438–442. [CrossRef]
36. Kattumuri, V.; Katti, K.; Bhaskaran, S.; Boote, E.J.; Casteel, S.W.; Fent, G.M.; Robert-son, D.J.; Chandrasekhar, M.; Kannan, R.; Katti, K.V. Gum Arabic as a photochemical construct for the stabilization of gold nanoparticles: In vivo pharmacokinetics and X-ray-contrast-imaging studies. *Small* **2007**, *3*, 333–341. [CrossRef]
37. Kumar, M.K.; Reddy, A.L.M.; Ramaprabhu, S. Exfoliated single-walled carbonnanotube-based hydrogen sensor. *Sens. Actuators B* **2008**, *130*, 653–660. [CrossRef]
38. Park, C.; Lim, K.H.; Kwon, D.; Yoon, T.H. Biocompatible quantum dot nanocolloids stabilized by gum Arabic. *Bull. Kor. Chem. Soc.* **2008**, *29*, 1277–1279.
39. Razzak, M.T.; Darwis, D. Irradiation of polyvinyl alcohol and polyvinyl pyrrolidone blended hydrogel for wound dressing. *Radiat. Phys. Chem.* **2001**, *62*, 107–113. [CrossRef]
40. DeMerlis, C.C.; Schoneker, D.R. Review of the oral toxicity of polyvinyl alcohol (PVA). *Food Chem. Toxicol.* **2003**, *41*, 319–326. [CrossRef]

41. Dos Reis, E.F.; Campos, F.S.; Lage, A.P.; Leite, R.C.; Heneine, L.G.; Vasconcelos, W.L.; Portela Lobato, Z.I.; Mansur, H.S. Synthesis and characterization of Poly (Vinyl Alcohol) Hydrogels and Hybrids for rMPB70 Protein Adsorption. *Mat. Res.* **2006**, *9*, 185–191. [CrossRef]
42. Nair, N.R.; Nampoothiri, K.M.; Pandey, A. Preparation of poly (L-lactide) blends and biodegradation by *Lentzea waywayandensis*. *Biotechnol. Lett.* **2012**, *34*, 2031–2035. [CrossRef]
43. Liu, M.; Guo, B.; Du, M.; Jia, D. Drying induced aggregation of halloysite nanotubes in polyvinyl alcohol/halloysite nanotubes solution and its effect on properties of composite film. *Appl. Phys. A* **2007**, *88*, 391–395. [CrossRef]
44. Masti, S.P.; Chougale, R.B. Influence of Poly (Vinylpyrrolidone) on Binary Blend Films Made from Poly(Vinyl Alcohol)/Chitosan. *Inter. Res. J. Env. Sci.* **2014**, *3*, 11–13.
45. Limpan, N.; Prodpran, T.; Benjakul, S.; Prasarnpran, S. Influences of degree of hydrolysis and molecular weight of poly (vinyl alcohol), PVA on properties of fish myofibrillar protein/PVA blend films. *Food Hydrocoll.* **2012**, *29*, 226–233. [CrossRef]
46. Qiu, K.; Netravali, A.N. Fabrication and characterization of biodegradable composites based on microfibrillated cellulose and polyvinyl alcohol. *Compos. Sci. Technol.* **2012**, *72*, 1588–1594. [CrossRef]
47. Qiu, K.; Netravali, A.N. A Composting study of membrane-like polyvinyl alcohol based resins and nanocomposites. *J. Polym. Environ.* **2013**, *21*, 658–674. [CrossRef]
48. Qiu, K.; Netravali, A.N. Halloysite nanotube reinforced biodegradable nanocomposites using noncrosslinked and malonic acid crosslinked polyvinyl alcohol. *Polym. Compos.* **2013**, *34*, 799–809. [CrossRef]
49. Mudigoudra, B.S.; Masti, S.P.; Chougale, R.B. Thermal behavior of poly (vinyl alcohol). Poly(vinyl pyrrolidone)/chitosan ternary polymer blend films. *Res. J. Recent Sci.* **2012**, *1*, 83–86.
50. Onyari, J.M.; Mulaa, F.; Muia, J.; Shiundu, P. Biodegradability of poly (lactic acid), preparation and characterization of PLA/gum Arabic blends. *J. Polym. Environ.* **2008**, *16*, 205–212. [CrossRef]
51. Cozic, C.; Picton, L.; Garda, M.R.; Marlhoux, F.; Le Cerf, D. Analysis of Arabic gum: Study of degradation and water desorption processes. *Food Hydrocoll.* **2009**, *23*, 1930–1934. [CrossRef]
52. Tiwari, A.; Terada, D.; Kobayash, H. Polyvinyl modified guar–gum bioplastics for packaging applications. *Handb. Bioplastics Biocomposites Eng. Appl.* **2011**, *24*, 177.
53. Nakashima, T.; Xu, C.; Bin, Y.; Matsuo, M. Morphology and mechanical properties of poly (vinyl alcohol) and starch blends prepared by gelation/crystallization from solutions. *Colloid. Polym. Sci.* **2001**, *279*, 646–654. [CrossRef]
54. Huang, X.; Netravali, A. Biodegradable green composites made using bamboo micro/nano-fibrils and chemically modified soy protein resin. *Compos. Sci. Technol.* **2009**, *69*, 1009–1015. [CrossRef]
55. Padil, V.V.T.; Nguyen, N.H.; Ševcū, A.; Černík, M. Fabrication, characterization, and antibacterial properties of electrospun membrane composed of gum karaya, polyvinyl alcohol, and silver nanoparticles. *J. Nanomater.* **2015**, *271*, 32–38.
56. Padil, V.V.T.; Cernik, M.; Vellora, V. Tree gum based electrospun nanofibre sheets: Process optimization, characterization and environmental application. In Proceedings of the Nanocon 2014, 6th International Conference, Brno, Czech Republic, 4–7 November 2014.
57. Hindi, S.S.; Albureikan, M.O.I. System, Apparatus, and Methods for Manufacturing Biodegradable Biopolymeric Materials. U.S. Patent No. 11548192, 1 October 2023.
58. Volova, T.G.; Boyandin, A.N.; Vasil'ev, A.D.; Karpov, V.A.; Kozhevnikov, I.V.; Prudnikova, S.V.; Gitel'Zon, I.I. Biodegradation of polyhydroxyalkanoates (PHAs) in the South China Sea and identification of PHA-degrading bacteria. *Microbiology* **2011**, *80*, 252. [CrossRef]
59. Chen, J.; Zhang, Y.; Du, G.C.; Hua, Z.Z.; Zhu, Y. Biodegradation of polyvinyl alcohol by a mixed microbial culture. *Enzym. Microb. Technol.* **2007**, *40*, 1686–1691. [CrossRef]
60. Corti, A.; Solaro, R.; Chiellini, E. Biodegradation of poly (vinyl alcohol) in selected mixed microbial culture and relevant culture filtrate. *Polym. Degrad. Stab.* **2002**, *75*, 447–458. [CrossRef]
61. Rong, D.; Usui, K.; Morohoshi, T.; Kato, N.; Zhou, M.; Ikeda, T. Symbiotic degradation of polyvinyl alcohol by *Novosphingobium* sp. and *Xanthobacter flavus*. *J. Environ. Biotechnol.* **2009**, *9*, 131–134.
62. Abd Alla, F.A.A. The Effects of Microbiological Biodegradation on Gum Arabic Structure and Molecular Mass. Ph.D. Thesis, Sudan University of Science and Technology, Khartoum, Sudan, 2012.
63. Wail, F.; Sabir, A.; Jacob, K.I. Novel reverse osmosis membranes composed of modified PVA/gum Arabic conjugates: Biofouling mitigation and chlorine resistance enhancement. *Carbohydr. Polym.* **2017**, *155*, 28–39.
64. Solomon, M.M.; Gerengi, H.; Umoren, S.A.; Essien, N.B.; Essien, U.B.; Kaya, E. Gum Arabic-silver nanoparticles composite as a green anticorrosive formulation for steel corrosion in strong acid media. *Carbohydr. Polym.* **2018**, *181*, 43–55. [CrossRef]
65. Tahsiri, Z.; Mirzaei, H.; Hosseini, S.M.H.; Khalesi, M. Gum Arabic improves the mechanical properties of wild almond protein film. *Carbohydr. Polym.* **2019**, *222*, 114994. [CrossRef]
66. Ling, M.; Xu, Y.; Zhao, H.; Gu, X.; Qiu, J.; Li, S.; Wu, M.; Song, X.; Yan, C.; Liu, G.; et al. Dual-functional gum Arabic binder for silicon anodes in lithium ion batteries. *Nano Energy* **2015**, *12*, 178–185. [CrossRef]
67. Silvestri, D.; Mikšiček, J.; Waclawek, S.; Torres-Mendieta, R.; Padil, V.V.; Černík, M. Production of electrospun nanofibers based on graphene oxide/gum Arabic. *Int. J. Biol. Macromol.* **2019**, *124*, 396–402. [CrossRef] [PubMed]
68. Lubambo, A.F.; de Freitas, R.A.; Sierakowski, M.R.; Lucyszyn, N.; Sasaki, G.L.; Serafim, B.M.; Saul, C.K. Electrospinning of commercial guar–gum: Effects of purification and filtration. *Carbohydr. Polym.* **2013**, *93*, 484–491. [CrossRef] [PubMed]



69. Tieguhong, J.C.; Ndoye, O. Development of trade and marketing of non-wood forest products for poverty alleviation Africa. In Proceedings of the Lessons Learnt on SFM in Africa, Uppsala, Sweden, 18–22 October 2004.
70. Anonymous. Policy Note: Export Marketing of Gum Arabic from Sudan. Washington, D.C. World Bank Group. Available online: <http://documents.worldbank.org/curated/en/736741468334873447/Policy-note-export-marketing-of-gum-arabic-from-sudan> (accessed on 2 March 2023).
71. ElKhawad, H.; ElBagher, M.A. Gum Arabic Processing and Marketing in the Sudan. Master's Thesis, Chemical Engineering, Khartoum, Sudan, 2008.
72. Naili, D.; Wenzhi, D. Technology for Producing Gum Arabic Powder. Chinese Patent Application No. CN 101143995A, 19 March 2008.
73. Chikamai, B.N.; Banks, W.B.; Anderson, D.M.W.; Weiping, W. Processing of gum Arabic and some new opportunities. *Food Hydrocoll.* **1996**, *10*, 309–316. [CrossRef]
74. Masti, S.; Kasai, D.; Mudigoudra, B.; Chougale, R. Effect of gum acacia (GA) on tensile properties of biodegradable chitosan (CS)/poly (vinyl alcohol) (PVA) polymer blend films. *J. Mater. Sci.* **2016**, *4*, 5–8.
75. Chougale, S.I.; Mamza, P.A.P.; Ja'o, A.M. Effect of pure and modified gum Arabic on the mechanical properties of poly (vinyl chloride). *Int. J. Sci. Res. Publ.* **2015**, *5*, 7.
76. Chougale, R.B.; P Masti, S.P.; Kasai, D.R.; Mudigoudra, B.S. Influence of gum ghatti on morphological and mechanical properties of poly(vinyl alcohol)/poly(vinyl pyrrolidone) blend films. *Pharma Chem.* **2018**, *10*, 1–6.
77. Gomaa, M.M.; El Fadly, E.; Salama, M.A.; Abdin, M. Production of bio composite films from gum Arabic and galangal extract to prolong the shelf life of *Agaricus bisporus*. *J. Polym. Environ.* **2022**, *30*, 4787–4799. [CrossRef]
78. Ibrahim, M.; Krejčík, M.; Havlíček, K.; Petřík, S.; Eldessouki, M. Evaluation of chemical and physical properties of biodegradable gum Arabic/PVA/Ag nanofibrous membranes as a potential wrapping material. *J. Eng. Fibers Fabr.* **2020**, *15*, 1–9. [CrossRef]
79. Jain, N.; Singh, V.K.; Chauhan, S. A review on mechanical and water absorption properties of polyvinyl alcohol based composites/films. *J. Mech. Behav. Mater.* **2017**, *26*, 213–222. [CrossRef]
80. Schmidt, M.W.; Torn, M.S.; Abiven, S.; Dittmar, T.; Guggenberger, G.; Janssens, I.A.; Trumbore, S.E. Persistence of soil organic matter as an ecosystem property. *Nature* **2011**, *478*, 49–56. [CrossRef] [PubMed]
81. Abdalla, I.G.E. Enzymatic Degradation and Analysis of Gum Arabic. Ph.D. Thesis, UOFK, Lexington, KY, USA, 2015.
82. Freedman, Z.; Zak, D.R. Soil bacterial communities are shaped by temporal and environmental filtering: Evidence from a long-term chronosequence. *Environ. Microbiol.* **2015**, *17*, 3208–3218. [CrossRef]
83. Turner, S.; Mikutta, R.; Meyer-Stüve, S.; Guggenberger, G.; Schaarschmidt, F.; Lazar, C.S.; Schippers, A. Microbial community dynamics in soil depth profiles over 120,000 years of ecosystem development. *Front. Microbiol.* **2017**, *8*, 874. [CrossRef]
84. Adam, F.A.; Abdallah, A.M.; Abdel-Magid, H.M.; Osman, M.E.; Al-Aassaf, S.; Phillips, G.O. Effect of some isolated bacterial species on the physicochemical aspects and main components of gum arabic (*Acacia senegal* var. *senegal*). *Int. J. Dev. Res.* **2018**, *8*, 18436–18442.
85. Wu, H.F.; Yue, L.Z.; Jiang, S.L.; Lu, Y.Q.; Wu, Y.X.; Wan, Z.Y. Biodegradation of polyvinyl alcohol by different dominant degrading bacterial strains in a baffled anaerobic bioreactor. *Int. J. Dev. Res.* **2019**, *79*, 2005–2012. [CrossRef] [PubMed]
86. Hao, J.; Chai, Y.N.; Lopes, L.D.; Ordóñez, R.A.; Wright, E.E.; Archontoulis, S.; Schachtman, D.P. The effects of soil depth on the structure of microbial communities in agricultural soils in Iowa, USA. *Appl. Environ. Microbiol.* **2021**, *87*, e02673-20. [CrossRef] [PubMed]
87. Sichert, A.; Cordero, O.X. Polysaccharide–bacteria interactions from the lens of evolutionary ecology. *Front. Microbiol.* **2021**, *12*, 705082. [CrossRef]
88. Polman, E.M.; Gruter, G.J.M.; Parsons, J.R.; Tietema, A. Comparison of the aerobic biodegradation of biopolymers and the corresponding bioplastics: A review. *Sci. Total Environ.* **2021**, *753*, 141953. [CrossRef]
89. Villa-Rivera, M.G.; Cano-Camacho, H.; López-Romero, E.; Zavala-Páramo, M.G. The role of arabinogalactan type II degradation in plant–microbe interactions. *Front. Microbiol.* **2021**, *12*, 730543. [CrossRef]
90. Sasaki, Y.; Uchimura, Y.; Kitahara, K.; Fujita, K. Characterization of a GH36  $\alpha$ -D-galactosidase associated with assimilation of gum Arabic in *Bifidobacterium longum* subsp. *longum* JCM7052. *J. Appl. Glycosci.* **2021**, *68*, 47–52. [CrossRef]
91. Chien, H.-L.; Tsai, Y.-T.; Tseng, W.-S.; Wu, J.-A.; Kuo, S.-L.; Chang, S.-L.; Huang, S.-J.; Liu, C.-T. Biodegradation of PBSA films by *Elite Aspergillus* isolates and farmland soil. *Polymer* **2022**, *14*, 1320. [CrossRef]
92. Sasaki, Y.; Komeno, M.; Ishiwata, A.; Horigome, A.; Odamaki, T.; Xiao, J.Z.; Fujita, K. Mechanism of cooperative degradation of gum arabic arabinogalactan protein by *bifidobacterium longum* surface enzymes. *Appl. Environ. Microbiol.* **2022**, *88*, e02187-21. [CrossRef]
93. Santos-Beneit, F.; Chen, L.M.; Bordel, S.; Frutos de la Flor, R.; García-Depraect, O.; Lebrero, R.; Rodríguez-Vega, S.; Muñoz, R.; Börner, R.A.; Börner, T. Screening enzymes that can depolymerize commercial biodegradable polymers: Heterologous expression of *Fusarium solani* cutinase in *Escherichia coli*. *Microorganisms* **2023**, *11*, 328. [CrossRef]
94. Tang, Y.; Zhou, D.; Zhang, J. Novel polyvinyl alcohol/styrene butadiene rubber latex/carboxymethyl cellulose nanocomposites reinforced with modified halloysite nanotubes. *J. Nanomater.* **2013**, *2013*, 1–8. [CrossRef]
95. Chiellini, E.; Corti, A.; Solaro, R. Biodegradation of poly (vinyl alcohol) based blown films under different environmental conditions. *Polym. Degrad. Stab.* **1999**, *64*, 305–312. [CrossRef]

96. Jayasekara, R.; Harding, I.; Bowater, I.; Christie, G.B.; Lonergan, G.T. Biodegradation by composting of surface modified starch and PVA blended films. *J. Polym. Environ.* **2003**, *11*, 49–56. [CrossRef]
97. Matsumura, S.; Tanaka, T. Novel malonate-type copolymers containing vinyl alcohol blocks as biodegradable segments and their builder performance in detergent formulations. *J. Appl. Polym. Sci.* **1994**, *2*, 89–97. [CrossRef]
98. Hindi, S.S.; Albureikan, M.; Othman, I.; Al-ghamdy, A.A.; Alhummiyany, H.; Ansari, M.S. Synthesis and characterization of gum Arabic based bioplastic membranes. *J. Nanosci. Nanotechnol. Res.* **2017**, *4*, 32–42.
99. Hindi, S.S.; Albureikan, M.O.I.; Attieh, A.; Al-ghamdy, A.A.; Alhummiyany, H.; Al-Sharabi, S.M. Effect of potassium dichromate on properties and biodegradation of gum Arabic based bioplastic membranes. *Nanosci. Nanotechnol. Res.* **2017**, *4*, 49–58. [CrossRef]
100. Hindi, S.S. Some crystallographic properties of cellulose I as affected by cellulosic resource, smoothing, and computation methods. *Int. J. Innov. Res. Sci.* **2017**, *6*, 732–752.
101. Hindi, S.S. Suitability of date palm leaflets for sulphated cellulose nanocrystals synthesis. *J. Nanosci. Nanotechnol. Res.* **2017**, *4*, 7–16. [CrossRef]
102. Hindi, S.S. Nanocrystalline cellulose: Synthesis from pruning waste of *Zizyphus spina christi* and characterization. *J. Nanosci. Nanotechnol.* **2017**, *4*, 106–114.
103. Fortunati, E.; Puglia, D.; Monti, M.; Peponi, L.; Santulli, C.; Kenny, J.M.; Torre, L. Extraction of cellulose nanocrystals from *Phormium tenax* fibres. *J. Polym. Environ.* **2013**, *21*, 319–328. [CrossRef]
104. Al-Solaimani, S.G. Chemical properties of soils and underground water of Hada Al-Sham Research Station, Kingdom of Saudi Arabia. *J. Environ. Sci. Ain Shams Univ.* **2003**, *6*, 257–284.
105. Al-Solaimani, S.G.; Al-Toukhy, A.; Al-Zahrani, S. Mineral characteristics, classification and evaluation of soils of Hada Al-Sham Res. Station, Kingdom of Saudi Arabia. *J. Environ. Sci. Ain Shams Univ.* **2003**, *6*, 285–322.
106. Mostafa, H.M.; Sourell, H.; Bockisch, F.J. Mechanical properties of some bioplastics under different soil types used as biodegradable drip tubes. *Agric. Eng. Int. CIGR J.* **2010**, *12*, 12–21.
107. El-Nakhlawy, F.S. *Principles of Statistics, Biostatistical Experimental Design and Analysis*; KAU Pub. Center KSA: Jeddah, Saudi Arabia, 2008.
108. Şişmanoğlu, T.; Karakuş, S.; Birer, Ö.; Soyly, G.S.P.; Kolan, A.; Tan, E.; Ürk, Ö.; Akdüt, G.; Kilislioglu, A. Preparation and characterization of antibacterial Senegalia (acacia) Senegal/iron—Silica bio-nanocomposites. *Appl. Surf. Sci.* **2015**, *354*, 250–255. [CrossRef]
109. Bouaziz, F.; Koubaa, M.; Barba, F.J.; Roothinejad, S.; Chaabouni, S.E. Antioxidant properties of water-soluble gum from flaxseed hulls. *Antioxidants* **2016**, *5*, 26. [CrossRef]
110. Anicuta, S.-G.; Dobre, L.; Stroescu, M.; Jipa, I. Fourier transform infrared (FTIR) spectroscopy for characterization of antimicrobial films containing chitosan. *Analele Univ. Din Oradea Fasc. Ecotoxicologie Zooteh. Si Tehnol. Ind. Aliment.* **2010**, 1234–1240.
111. Rathna, G.V.N.; Jog, J.P.; Gaikwad, A.B. Development of non-woven nanofibers of egg albumen-poly (vinyl alcohol) blends: Influence of solution properties on morphology of nanofibers. *Polym. J.* **2011**, *43*, 654–661. [CrossRef]
112. Mori, T.; Sakimoto, M.; Kagi, T.; Sakai, T. Isolation and characterization of a strain of *Bacillus megaterium* that degrades poly (vinyl alcohol). *Biosci. Biotechnol. Biochem.* **1996**, *60*, 330–332. [CrossRef] [PubMed]
113. Patil, R.; Bagde, U.S. Enrichment and isolation of microbial strains degrading bioplastic polyvinyl alcohol and time course study of their degradation potential. *Afr. J. Biotechnol.* **2015**, *14*, 2216–2226.
114. Jecu, L.; Gheorghe, A.; Rosu, A.; Raut, I.; Grosu, E.; Ghiurea, M. Ability of fungal strains to degrade PVA based materials. *J. Polym. Environ.* **2010**, *18*, 284–290. [CrossRef]
115. Kawai, F.; Hu, X. Biochemistry of microbial polyvinyl alcohol degradation. *Appl. Microbiol. Biotechnol.* **2009**, *84*, 227–237. [CrossRef] [PubMed]
116. Cadmus, M.C.; Jackson, L.K.; Burton, K.A.; Plattner, R.D.; Slodki, M.E. Biodegradation of xanthan gum by *Bacillus* sp. *Appl. Environ. Microbiol.* **1982**, *44*, 5–11. [CrossRef]
117. Hossain, I.; Sarafat, A. Fungi grow faster than Gram-negative bacteria in Emb media and also deterring the growth of these bacteria by reducing the pH of that media. *J. Pharmacogenomics* **2020**, *12*, 1–10.
118. Johannes, R.; Bååth, E. Growth of saprotrophic fungi and bacteria in soil. *FEMS Microbiol. Ecol.* **2011**, *78*, 17–30.
119. Busoloa, T.; Urab, D.P.; Kima, S.K.; Marzecc, M.M.; Bernasik, A.; Stachewicz, U.; Kar-Narayan, S. Surface potential tailoring of PMMA fibers by electrospinning for enhanced triboelectric performance. *Nano Energy* **2019**, *57*, 500–506. [CrossRef]
120. Anonymous. National Center for Biotechnology Information. PubChem Compound Summary for CID 11199, Polyvinyl Alcohol. 2023. Available online: <https://pubchem.ncbi.nlm.nih.gov/compound/Vinyl-alcohol> (accessed on 11 March 2023).
121. Anonymous. National Center for Biotechnology Information. PubChem Substance Record for SID 50019090, 2-Methyl-2-Propenoic Acid Methyl Ester Homopolymer, Source: LeadScope. 2023. Available online: <https://pubchem.ncbi.nlm.nih.gov/substance/50019090> (accessed on 12 March 2023).
122. Anonymous. PubChem, Compound Summary for CID 24847856, Galactoarabinan. 2023. Available online: <https://pubchem.ncbi.nlm.nih.gov/compound/Galactoarabinan> (accessed on 8 March 2023).
123. Anonymous. National Center for Biotechnology Information. PubChem, compound Summary for CID 439212, Glycoprotein. 2023. Available online: <https://pubchem.ncbi.nlm.nih.gov/compound/Glycoprotein> (accessed on 13 March 2023).

124. Anonymous. National Center for Biotechnology Information. PubChem, Substance Record for SID 405234199, a Plant Arabinogalactan-[Protein], Source: BioCyc. 2023. Available online: <https://pubchem.ncbi.nlm.nih.gov/substance/405234199> (accessed on 22 March 2023).
125. Schmidt, D.L.; Coburn, C.E.; DeKoven, B.M.; Potter, G.E.; Meyers, G.F.; Fischer, D.A. Water-based non-stick hydrophobic coatings. *Nature* **1994**, *368*, 39–41. [CrossRef]
126. Hild, F. Surface Energy of Plastics. 2009. Available online: <https://www.tstar.com/blog/bid/33845/surface-energy-of-plastics> (accessed on 22 March 2023).
127. Zi, Y.; Wang, Z.L. Nanogenerators: An emerging technology towards nanoenergy. *APL Mater.* **2017**, *5*, 074103. [CrossRef]
128. Randall, R.C.; Phillips, G.O.; Williams, P.A. The role of the proteinaceous component on the emulsifying properties of gum arabic. *Food Hydrocoll.* **1988**, *2*, 131–140. [CrossRef]
129. Randall, R.C.; Phillips, G.O.; Williams, P.A. Fractionation and characterization of gum from *Acacia senegal*. *Food Hydrocoll.* **1989**, *3*, 65–75. [CrossRef]
130. Azzaoui, K.; Hammouti, B.; Lamhamdi, A.; Mejdoubi, E.; Berrabah, M. The gum Arabic in the southern region of Morocco. *Mor. J. Chem.* **2014**, *3*, 99–107.
131. Elsabee, M.Z.; Naguib, H.F.; Morsi, R.E. Chitosan based nanofibers, review. *Mater. Sci. Eng. C* **2012**, *32*, 1711–1726. [CrossRef] [PubMed]
132. Pakravan, M.; Heuzey, M.C.; Aji, A. A fundamental study of chitosan/PEO electrospinning. *Polym. J.* **2011**, *52*, 4813–4824. [CrossRef]
133. Wiśniewska, M.; Bogatyrov, V.; Ostolska, I.; Szewczuk-Karpisz, K.; Terpiłowski, K.; Nosal-Wiercińska, A. Impact of poly(vinyl alcohol) adsorption on the surface characteristics of mixed oxide  $Mn_xO_y-SiO_2$ . *Adsorption* **2016**, *22*, 417–423. [CrossRef]
134. Chibowski, S.; Paszkiewicz, M.; Krupa, M. Investigation of the influence of the polyvinyl alcohol adsorption on the electrical properties of  $Al_2O_3$ -solution interface, thickness of the adsorption layers of PVA. *Powder Technol.* **2000**, *107*, 251–255. [CrossRef]
135. Nuraje, N.; Khan, W.S.; Lei, Y.; Ceylan, M.; Asmatulu, R. Superhydrophobic electrospun nanofibers. *J. Mater. Chem. A.1* **2013**, *1*, 1929–1946. [CrossRef]
136. Osti, G.B.F.; Wolf, F.G.; Philippi, P.C. Spreading of liquid drops on acrylic surfaces. In Proceedings of the 20th International Congress of Mechanical Engineering, Gramado, Brazil, 15–20 November 2009.
137. Johnson, R.E.; Dettre, R.H. *Wetting of Low-Energy Surfaces*; Marcel Dekker: New York, NY, USA, 1993.
138. Pavluchkov, V.; Shefer, I.; Peer-Haim, O.; Blotvogel, J.; Epsztein, R. Indications of ion dehydration in diffusion-only and pressure-driven nanofiltration. *J. Membr. Sci.* **2022**, *648*, 120358. [CrossRef]
139. Walker, J.A. Physics for Introductory Biology. 2020. Available online: [https://www.middleprofessor.com/files/physics\\_for\\_biologicals/\\_book/index.html](https://www.middleprofessor.com/files/physics_for_biologists/_book/index.html) (accessed on 11 July 2023).
140. Ibekwe, C.A.; Oyatogun, G.M.; Esan, T.A.; Oluwasegun, K.M. Synthesis and characterization of chitosan/gum Arabic nanoparticles for bone regeneration. *Am. J. Mater. Sci. Eng.* **2017**, *5*, 28–36.
141. Mir, M.B.; Haripriya, S. Assessment of physical and structural characteristics of almond gum. *Int. J. Biol. Macromol.* **2016**, *93*, 476–482.
142. Stuart, B.H. *Infrared Spectroscopy: Fundamentals and Applications*, 1st ed.; John Wiley & Sons Ltd.: West Sussex, UK, 2004.
143. Kumar, A.; Negi, Y.S.; Choudhary, V.; Bhardwaj, N.K. Characterization of cellulose nanocrystals produced by acid-hydrolysis from sugarcane bagasse as agro-waste. *Mater. Chem. Phys.* **2014**, *2*, 1–8. [CrossRef]
144. Yoshimi, Y.; Yaguchi, K.; Kaneko, S.; Tsumuraya, Y.; Kotake, T. Properties of two fungal endo-beta-1,3-galactanases and their synergistic action with an exo-beta-1,3-galactanase in degrading arabinogalactan-proteins. *Carbohydr. Res.* **2017**, *45*, 26–35. [CrossRef]
145. Yoshimi, Y.; Hara, K.; Yoshimura, M.; Tanaka, N.; Higaki, T.; Tsumuraya, Y.; Kotake, T. Expression of a fungal exo-beta-1,3-galactanase in *Arabidopsis* reveals a role of type II arabinogalactans in the regulation of cell shape. *J. Exp. Bot.* **2020**, *71*, 5414–5424. [CrossRef]
146. Gao, X.; Fu, C.; Li, M.; Qi, X.; Jia, X. Effects of biodegradation of corn-starch-sodium alginate-biobased liquid mulch film on soil microbial functions. *Int. J. Environ. Res. Public Health* **2022**, *19*, 8631. [CrossRef]
147. Augustine, R.; Kalarikkal, N.; Thomas, S. Effect of zinc oxide nanoparticles on the invitro degradation of electrospun polycaprolactone membranes in simulated body fluid. *Int. J. Polym. Mater. Polym. Biomater.* **2016**, *65*, 28–37. [CrossRef]

**Disclaimer/Publisher’s Note:** The statements, opinions and data contained in all publications are solely those of the individual author(s) and contributor(s) and not of MDPI and/or the editor(s). MDPI and/or the editor(s) disclaim responsibility for any injury to people or property resulting from any ideas, methods, instructions or products referred to in the content.

## Article

# Improving the Recyclability of an Epoxy Resin through the Addition of New Biobased Vitrimer

Antonio Veloso-Fernández <sup>1,\*</sup>, Leire Ruiz-Rubio <sup>1,2</sup>, Imanol Yugueros <sup>1</sup>, M. Isabel Moreno-Benítez <sup>3</sup>, José Manuel Laza <sup>1</sup> and José Luis Vilas-Vilela <sup>1,2</sup>

<sup>1</sup> Grupo de Química Macromolecular (LABQUIMAC), Departamento de Química Física, Facultad de Ciencia y Tecnología, Universidad del País Vasco UPV/EHU, 48940 Leioa, Spain; leire.ruiz@ehu.eus (L.R.-R.); iyugueros004@ikasle.ehu.eus (I.Y.); and josemanuel.laza@ehu.eus (J.M.L.); joseluis.vilas@ehu.eus (J.L.V.-V.)

<sup>2</sup> BCMaterials, Basque Center for Materials, Applications and Nanostructures, UPV/EHU Science Park, 48940 Leioa, Spain

<sup>3</sup> Grupo de Química Macromolecular (LABQUIMAC), Departamento de Química Orgánica e Inorgánica, Facultad de Ciencia y Tecnología, Universidad del País Vasco UPV/EHU, 48940 Leioa, Spain; mariaisabel.moreno@ehu.eus

\* Correspondence: antonio.veloso@ehu.eus; Tel.: +34-946-01-5965

**Abstract:** In recent decades, the use of thermoset epoxy resins (ER) has spread to countless applications due to their mechanical properties, heat resistance and stability. However, these ERs are neither biodegradable nor recyclable due to their permanent crosslinked networks and usually, they are synthesized from fossil and toxic precursors. Therefore, reducing its consumption is of vital importance to the environment. On the one hand, the solution to the recyclability problems of epoxy resins can be achieved through the use of vitrimers, which have thermoset properties and can be recycled as thermoplastic materials. On the other hand, vitrimers can be made from natural sources, reducing their toxicity. In this work, a sustainable epoxy vitrimer has been efficiently synthesized, VESOV, by curing epoxidized soybean oil (ESO) with a new vanillin-derived Schiff base (VSB) dynamic hardener, aliphatic diamine (1,4-butanediamine, BDA) and using 1,2-dimethylimidazole (DMI) as an accelerator. Likewise, using the same synthesized VSB agent, a commercial epoxy resin has also been cured and characterized as ESO. Finally, different percentages (30, 50 and 70 wt%) of the same ER have been included in the formulation of VESOV, demonstrating that only including 30 wt% of ER in the formulation is able to improve the thermo-mechanical properties, maintaining the VESOV's inherent reprocessability or recyclability. In short, this is the first approach to achieve a new material that can be postulated in the future as a replacement for current commercial epoxy resins, although it still requires a minimum percentage of RE in the formulation, it makes it possible to recycle the material while maintaining good mechanical properties.

**Keywords:** sustainable materials; epoxy resin; Schiff base; epoxidized soybean oil; epoxy vitrimer; reprocessability; recyclability

**Citation:** Veloso-Fernández, A.; Ruiz-Rubio, L.; Yugueros, I.; Moreno-Benítez, M.I.; Laza, J.M.; Vilas-Vilela, J.L. Improving the Recyclability of an Epoxy Resin through the Addition of New Biobased Vitrimer. *Polymers* **2023**, *15*, 3737. <https://doi.org/10.3390/polym15183737>

Academic Editor: Raffaella Striani

Received: 26 July 2023

Revised: 4 September 2023

Accepted: 5 September 2023

Published: 12 September 2023



**Copyright:** © 2023 by the authors. Licensee MDPI, Basel, Switzerland. This article is an open access article distributed under the terms and conditions of the Creative Commons Attribution (CC BY) license (<https://creativecommons.org/licenses/by/4.0/>).

## 1. Introduction

In recent years, special attention has been paid to the use of epoxy resins (ER). This type of thermoset polymer has distinguished properties, such as thermal stability, mechanical strength, creep resistance, electrical insulation, and chemical resistance [1–7]. These polymers are industrially synthesized to use as coatings, adhesives, electronic packaging materials or composites for automobile, aerospace or transportation industries [1,2,8,9]. In fact, the global annual production in 2020 reached almost 10 million tons [10].

Nevertheless, most of the current epoxy thermosets (~90%) are prepared from non-renewable diglycidyl ether of bisphenol A (DGEBA) and cannot be reprocessed or recycled due to their permanent crosslinking, which causes significant waste and environmental problems after their service lifetime [11–13]. In addition to the non-renewability, bisphenol



A and epichlorohydrin, which are the raw materials of DGEBA, are toxic, fossil derivatives and both are categorized as hazardous to living organisms [14].

Therefore, recently, more attention has been paid to designing sustainable epoxy thermoset resins from diverse renewable resources, such as epoxidized vegetable oils [15], cardanol [16], isosorbide [17], vanillin [18,19], etc. Specifically, vegetable oils are prime candidates to replace fossil-based derivatives in polymer materials due to: (i) their universal availability, (ii) low toxicity and (iii) low price [20]. Moreover, the presence of carbon-carbon double bonds enables them to be easily transformed into epoxidized vegetable oils (EVOs) through a curing process with hardening agents. Nevertheless, their highly crosslinked structure combined with slightly flexible backbones provides EVOs with poor mechanical strength fusing with poor ductility and low glass transition temperature ( $T_g$ ) [21,22].

To address these issues, new studies to develop new epoxy resins that contain the remarkable properties of thermosets, as well as the intrinsic capacity of thermoplastics to be recycled after their useful life, are needed. One of the possible solutions is the development of covalent adaptable networks (CANs).

The so-called CANs are polymeric materials with permanent crosslinks, which can reversibly transform into dynamic crosslinks, allowing their chains to flow (analogous to thermoplastics) when they are induced by an external stimulus, such as temperature [23,24], exposure to ultraviolet light [25] or pH [26,27]. In the absence of this stimulus, their reticulated structure offers them stiffness and durability as thermosetting materials. Thus, these polymeric materials, which have thermosetting polymer properties due to their crosslinking networks, are recyclable and reusable due to the dynamic nature of these crosslinks.

In 2011, Leibler et al. reported [28] a new class of CANs called vitrimers, which resemble vitreous silica due to their change in viscosity and the fact that they also follow an Arrhenius relationship that increases with temperature. Vitrimers belong to a sub-class of CANs in which the crosslinking bonds have an associative nature, resulting in the ability of the material to change its topology via exchange reactions [29–33]. Certainly, vitrimer crosslink density can be recognized as almost constant regardless of external stimuli, resulting in two principal effects [34–38]. First, unlike dissociative CANs, which transform from a solid state more suddenly [39], an extended gummy/rubbery phase can be observed in vitrimers when heated. Second, some researchers have also remarked a greater creep/solvent resistance for vitrimers [37,40,41]. Moreover, vitrimers are distinguished according to their temperature-dependent viscoelastic behavior, as the covalent exchange rate is related to the transition temperature. At high temperatures, when the exchange reactions become fast enough, the viscosity of vitrimers is basically controlled by the exchange reactions, leading to a decrease in viscosity with the temperature that follows the Arrhenius law.

The viscoelastic behavior of vitrimers changes with the topology freezing temperature ( $T_v$ ) [28]. The  $T_v$  is chosen by agreement as the temperature at which the viscosity reaches  $10^{12}$  Pa·s [42]. Below  $T_v$ , vitrimers behave as conventional thermosets, and above  $T_v$ , they can undergo creeping and relaxing stresses. The control of this temperature is essential since the exchange of covalent bonds and permanent crosslinking allows or does not allow thermal recycling [43–45]. Thus, epoxy vitrimers are a substantial advance for the replacement of current thermosets.

The developed vitrimers so far have been overviewed according to the nature of the dynamic exchange reaction. The most common dynamic interactions used in the design of vitrimers have been carboxylate transesterification [28], transamination of vinyllogous urethanes [46], transalkylation of triazolium salts [47], disulfide exchange [48] or Schiff base (imine) exchange [49]. Among them, Schiff bases show great potential in the fabrication of epoxy vitrimers due to the presence of a reversible covalent bond since it can be hydrolyzed to aldehyde or ketone and to amine under acid conditions [50]. Furthermore, compounds obtained from natural resources can be used as reagents, which are more attractive and interesting compared with the existing materials. Among them, recent studies show the design of sustainable epoxy vitrimers with natural phenolic compounds such as vanillin

(VAN) as the starting material due to the stiffness structure provided by the benzene ring leading to high- $T_g$  epoxy vitrimers combined with superior mechanical strength and modulus [51–53]. It should be noted that VAN is one of the few compounds with a phenolic group manufactured on an industrial scale from biomass, especially from tannin and lignin [54]. Therefore, this reagent has the potential to become a key precursor for the synthesis of bio-based polymers as it presents an aromatic structure that can achieve good thermo-mechanical properties.

Taking into account all the premises described, in this work, a biovitrimer is developed from components obtained from natural resources, such as epoxidized soybean oil (ESO) and VAN. ESO is used as a bio-based monomer and a vanillin derivative as a new Schiff base to act as a biobased hardener. First, the Schiff base is prepared using VAN and aliphatic diamine (1,4-butanediamine, BDA). Second, ESO and the new Schiff base are combined to form the vitrimer. However, numerous studies have shown the susceptibility of vitrimers to creep substantially under use conditions [55–57]. For that reason, in order to improve the properties of this new material, a critical fraction of permanent crosslinks (30, 50 and 70 wt%) is added to the new biovitrimer, which has little or no detrimental effect on reprocessability [48,52,58,59]. During this work, the poly(bisphenol A-co-epichlorohydrin) glycidyl end-capped is used as a commercial epoxy resin (ER). Finally, in all the samples, thermal and mechanical properties, as well as their reprocessability or recyclability, have been investigated.

## 2. Experimental Section

### 2.1. Reagents

Vanillin (VAN, 99%), 1,4-butanediamine (BDA, 99%), 1,2-dimethylimidazole (DMI, 97%) and commercial epoxy resin (ER) poly(bisphenol A-co-epichlorohydrin) glycidyl end-capped ( $M_n \sim 355 \text{ g mol}^{-1}$ ) were purchased from Sigma Aldrich (Saint Louis, MO, USA). Methanol (MeOH,  $\geq 99.5\%$ ) was obtained from PANREAC (Barcelona, Spain). Epoxidized soybean oil (ESO) EPOVINSTAB H-800-D was kindly supplied by Hebron S.A. (Barcelona, Spain). All the chemicals were used as received.

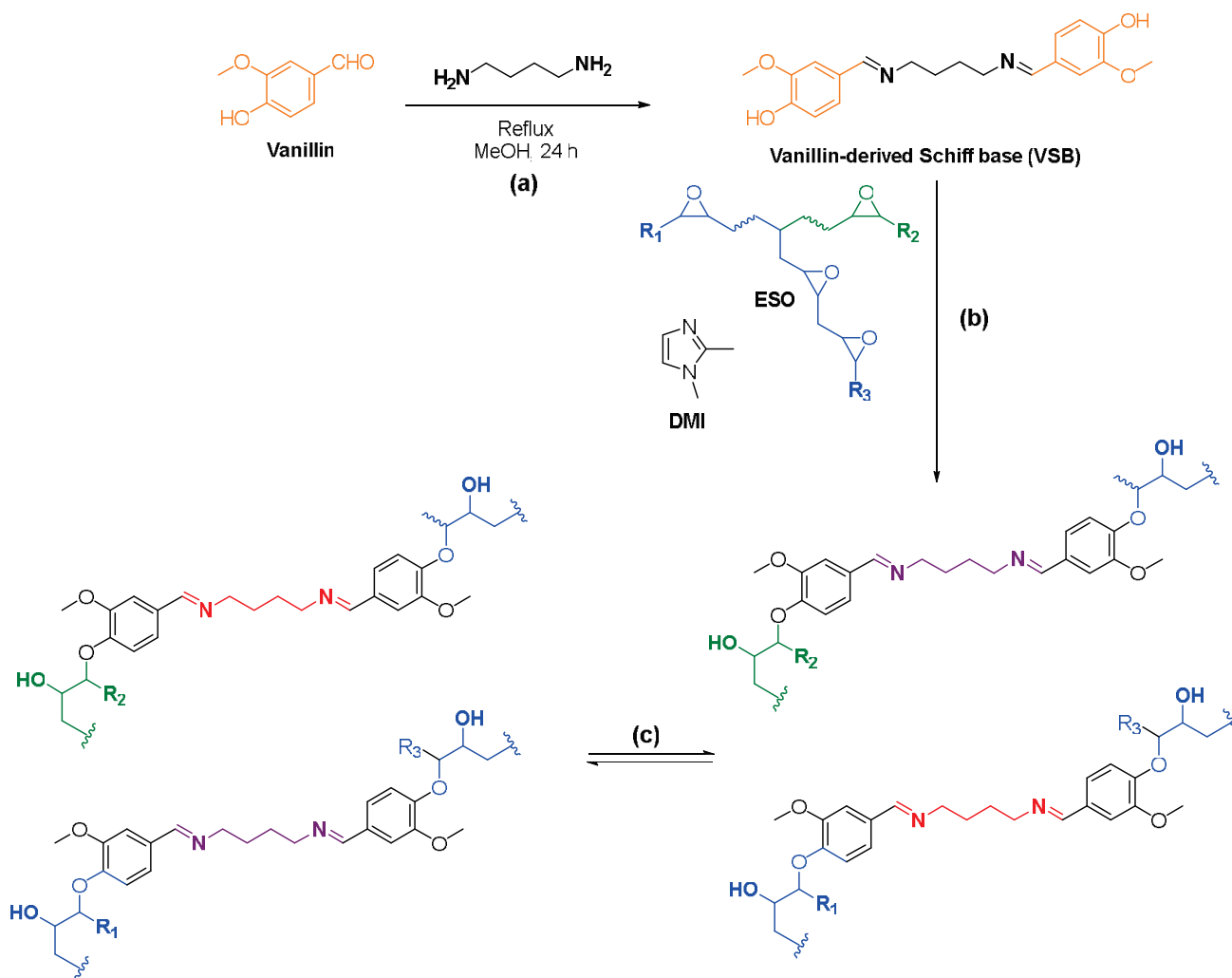
### 2.2. Synthesis of Vanillin-Derived Schiff Base Curing Agent

The vanillin-derived Schiff base (VSB) curing agent was synthesized by dissolving 10.0 g (66 mmol) of vanillin in 100 mL of methanol and mixed in a 500 mL single-necked round-bottomed flask with 3.3 mL (33 mmol) of 1,4-butanediamine. A yellow powdered product (VSB) was obtained (Scheme 1a) after solvent evaporation, which was washed with methanol and vacuum dried at 50 °C for 24 h.

### 2.3. Synthesis of Vitrimers

The VSB-cured ESO biovitrimer (VESOV) was synthesized by a two-stage procedure pre- and post-curing. To achieve the pre-curing stage, predetermined amounts of VSB and ESO were added to the reaction using an equivalent phenolic/epoxy hydroxyl ratio (simplified as X). Previous works performed by Zhao et al. [60] and Zeng et al. [61] demonstrated that the optimal ratio to obtain a vitrimer with a highly crosslinked network is  $X = 0.7$ . First, the VSB was heated until reaching its melting point in a 100 mL single-necked round-bottomed flask placed into an oil bath and stirred with a magnetic stirring bar under a nitrogen atmosphere. When the VSB was completely melted, the corresponding amount of ESO was added. After ESO and VSB were fully mixed, the catalyst 1,2-dimethylimidazole (DMI) (0.5 wt%) was added, allowing the resulting mixture to react until the magnetic stirrer could not turn due to the increase in the viscosity of the medium (Scheme 1b). Then, the post-curing stage started with the transfer of the resultant mixture to a 10 cm  $\times$  10 cm  $\times$  1.0 mm stainless steel mold, which was placed in a compression molding machine at 150 °C under 10 bar for 2 h. After allowing the sample to reach room temperature, a film was obtained. Scheme 1c shows in purple and red how the network

structure is reorganized by the thermal-induced exchange reaction of Schiff base in the crosslinking structure of VESOV, leading to the stress relaxation behavior.



**Scheme 1.** (a) Preparation of the dynamic curing agent (VSB), (b) curing reaction of ESO with VSB to form VESOV, and (c) exchange reaction of the Schiff base in the vitrimer, indicating in color the outcome exchange.

For the synthesis of VESOV+ER, the same procedure was used, adding the epoxy resin at the same time as the ESO. Thus, it was decided to add progressive amounts by weight of epoxy resin (30, 50 and 70 wt%) to determine the influence of the addition of epoxy resin to the VESOV. Additionally, to investigate the reaction between VSB+ER, the same procedure as ESO was followed, adding ER to the VSB. Therefore, the mechanical and thermal properties of five samples were studied: VESOV, VESOV+ER (30 wt% of ER), VESOV+ER (50 wt%), VESOV+ER (70 wt%) and VSB+ER.

### 3. Characterization

Fourier transform infrared (FTIR) spectra with wavelengths from 4000 to 400  $\text{cm}^{-1}$  were recorded by a Nicolet Nexus spectrophotometer (Thermo Fisher Scientific Inc., Madison, WI, USA), where the samples were measured within KBr pellets. The resolution and scanning number were 4  $\text{cm}^{-1}$  and 32 times, respectively. The data were analyzed using OMNIC 8.2 software.

Proton nuclear magnetic resonance ( $^1\text{H-NMR}$ ) spectra were recorded on a Bruker AV-600 (600 MHz) spectrometer (Billerica, MA, USA) using deuterated chloroform ( $\text{CDCl}_3$ ) as the solvent.

The melting temperature of VSB and the glass transition temperature of the vitrimers were measured by differential scanning calorimeter (DSC) with a DSC METTLER TOLEDO 822<sup>e</sup> instrument (Greifensee, Switzerland) equipped with STAR<sup>®</sup> v14.0 software. The samples (~10 mg) were placed in 100  $\mu\text{L}$  aluminum crucibles. Samples were heated from  $-10\text{ }^\circ\text{C}$  to  $250\text{ }^\circ\text{C}$ , in the case of the VSB, and from  $-10\text{ }^\circ\text{C}$  to  $150\text{ }^\circ\text{C}$  for the vitrimers. A scanning rate of  $10\text{ }^\circ\text{C}\cdot\text{min}^{-1}$  under a nitrogen atmosphere with a flow rate of  $20\text{ mL}\cdot\text{min}^{-1}$ .

The thermal stability of the samples (~10 mg) was measured by thermal gravimetric analysis (TGA) under a nitrogen atmosphere ( $20\text{ mL}\cdot\text{min}^{-1}$ ) with a temperature range of  $25\text{--}800\text{ }^\circ\text{C}$  and a heating rate of  $10\text{ }^\circ\text{C}\cdot\text{min}^{-1}$  by a SHIMADZU DTG-60 thermal gravimetric analyzer (Kyoto, Japan). The statistic heat-resistant index temperature ( $T_s$ ) is a characteristic of the thermal stability of the cured resin [62] and was calculated according to Equation (1):

$$T_s = 0.49 \times [T_{5\%} + 0.6 \times (T_{30\%} - T_{5\%})] \quad (1)$$

where  $T_{5\%}$  and  $T_{30\%}$  are the temperatures at, respectively, 5% and 30% weight loss.  $T_{5\%}$  was considered the onset decomposition temperature ( $T_o$ ) of the sample.

Dynamic mechanical analysis (DMA) was carried out in the tensile mode by a DMA1-METTLER TOLEDO instrument (Greifensee, Switzerland) equipped with STAR<sup>®</sup> v14.0 software for curve analysis. Storage modulus ( $E'$ ), loss modulus ( $E''$ ) and loss factors ( $\tan \delta$ ) values were collected at  $3\text{ }^\circ\text{C}\cdot\text{min}^{-1}$  heating rate from  $-10$  to  $150\text{ }^\circ\text{C}$ , displacement of  $20\text{ }\mu\text{m}$ , and 1, 3 and 10 Hz frequencies. Rectangular-shaped testing bars with a width of 5.0 mm, length of 10.0 mm and thickness of 0.5 mm were prepared. The glass transition was assigned at the maximum of the loss factor ( $\tan \delta = E''/E'$ ).

Reprocessing tests were performed on the compression molding machine (20 TM Hot Plates Press, Hidrotecno S.L., Oiartzun, Spain). The films were cut into small pieces with scissors, placed into the  $10\text{ cm} \times 10\text{ cm} \times 1.0\text{ mm}$  stainless steel mold, and reprocessed at  $150\text{ }^\circ\text{C}$  for 60 min at 10 bar. After cooling to room temperature, the reprocessed films were obtained, and their thermo-mechanical properties were measured.

#### 4. Results and Discussion

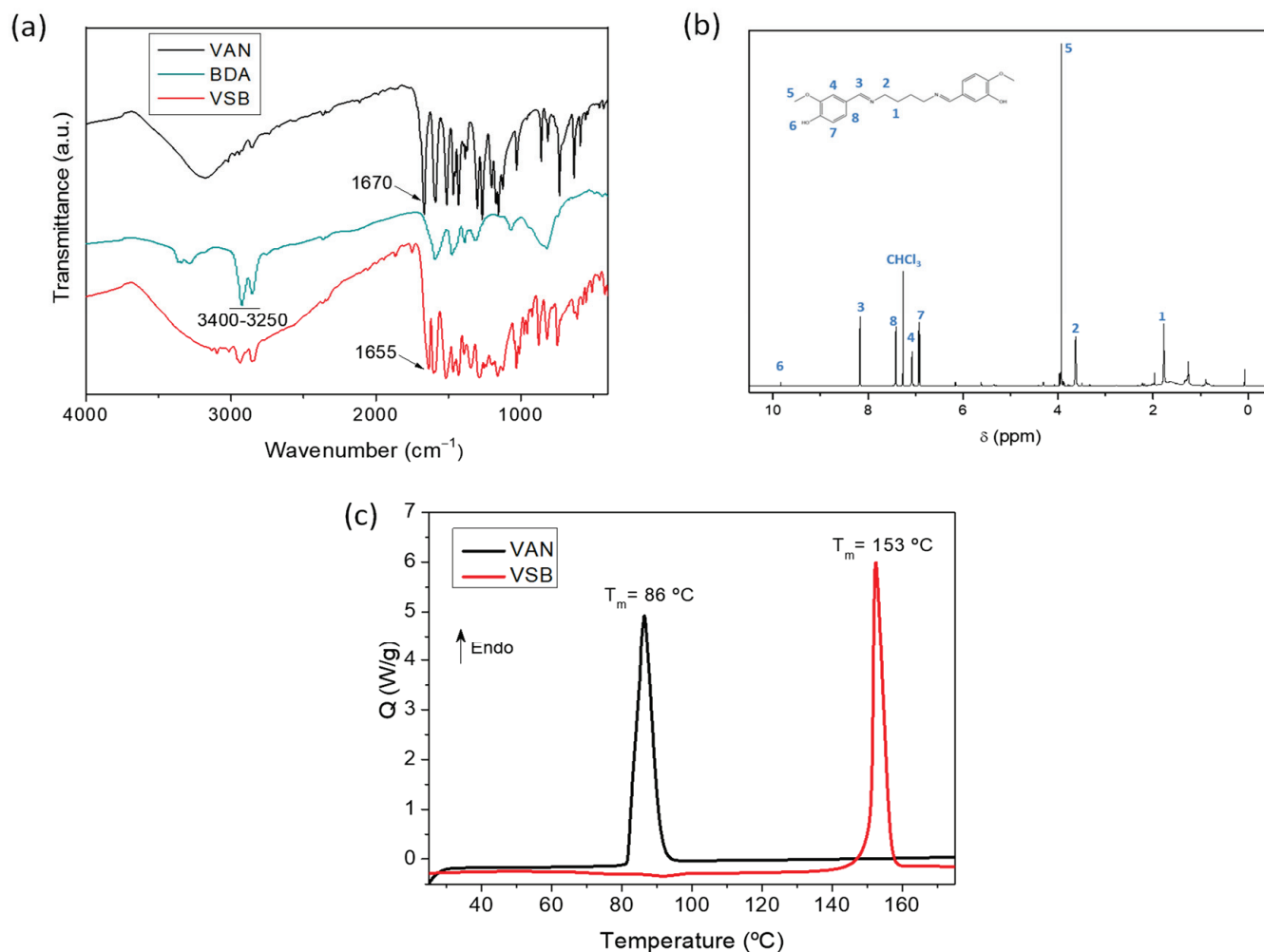
Epoxy thermosets exhibit tremendous thermo-mechanical properties; however, they lack the capacity to be reprocessed after their use. The main objective of this work is to obtain a substitute for epoxy resins that can be considered biobased. In this regard, it must be taken into account that to consider a material as biobased, a minimum of 50% of the compounds incorporated into its formulation must be obtained from natural resources. For this, first, the Schiff base is synthesized using VAN and aliphatic diamine (1,4-butandiamine, BDA). Then, a sustainable epoxy vitrimer derived from vegetable oil ESO is prepared, and finally, to improve the thermo-mechanical properties of the reprocessable vitrimer, a small amount of commercial epoxy resin (ER) is added.

##### 4.1. Synthesis and Characterization of Vanillin-Derived Schiff Base (VSB) Hardener

VSB hardener was synthesized by refluxing VAN and BDA in methanol for 24 h. The chemical structure of VSB was confirmed by FTIR and  $^1\text{H-NMR}$ . Figure 1a shows how the characteristic stretching peak of  $\text{C}=\text{O}$  on the aldehyde group ( $1670\text{ cm}^{-1}$ ) of the VAN and the broad stretching of  $\text{N-H}$  (between  $3400$  and  $3250\text{ cm}^{-1}$ ) of BDA is not observed in the VSB FTIR spectrum. Instead, a new characteristic peak appears at  $1655\text{ cm}^{-1}$  for VSB, attributing to the formed Schiff base unit (the most significant FTIR signals were compiled in the Supporting Information). Moreover,  $^1\text{H-NMR}$  easily (Figures S1 and S2) allows the Schiff base identification via the disappearance of the signal from the aldehyde group of the VAN and the presence of a new signal in the VSB typical of an imine (Figure 1b). Precisely, the signals for the H proton of alcohol, imine, benzene ring, methoxy and butane were observed at shifts of 9.8, 8.2, 7.4–6.9, 3.9 and 1.8 ppm, respectively. These facts indicate



that the Schiff base bond has been successfully formed by the reaction between the amino and aldehyde groups. In addition, the DSC curve of VSB shows only one sharp melting peak at 153 °C (Figure 1c), observing that the VSB was successfully synthesized, as the correspondent melting peak of VAN (~86 °C) was not observed in the DSC curve of VSB. In short, it is corroborated that the vanillin-derived Schiff base was prepared successfully.

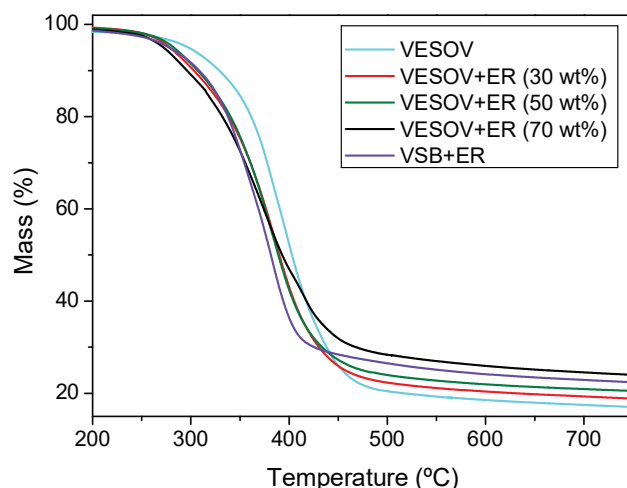


**Figure 1.** (a) FTIR spectra of VAN, BDA and VSB, (b) <sup>1</sup>H-NMR spectrum of VSB and (c) DSC heating curve for VAN and VSB.

#### 4.2. Synthesis and Characterization of VESOV, VESOV+ER (Different Percentages) and VSB+ER

Once the VSB was formed (Scheme 1a), using DMI as a catalyst, five different formulations of ESO and/or ER vitrimers were developed: VESOV, VESOV+ER (30 wt%), VESOV+ER (50 wt%), VESOV+ER (70 wt%) and VSB+ER. In all cases, the synthetic procedure was the same as described above; after a pre-curing stage where the VSB is reacted with the ESO, the ER or a mixture of both, the post-curing is accomplished (Scheme 1b). Subsequently, the thermo-mechanical properties of the samples were studied.

First, the thermal stability of the samples was studied to confirm that the material remains stable and does not suffer any degradation during the reprocessing procedure. The thermal stability profiles of the obtained vitrimers are displayed in Figure 2 and Tables 1 and S1. Clearly, all samples are thermally stable up to a temperature of at least 272–297 °C (onset decomposition temperature, T<sub>o</sub>, in Table 1), demonstrating that they possess acceptable thermal stability under all conventional modeling approaches and that they are also thermally resistant during reprocessing, which is important for the recycling of the vitrimer through thermal processing [63].



**Figure 2.** Thermogravimetric curves for VESOV, VESOV+ER (with different weight ratio) and VSB+ER.

**Table 1.**  $T_o$  and  $T_s$  values determined by TGA Analysis.

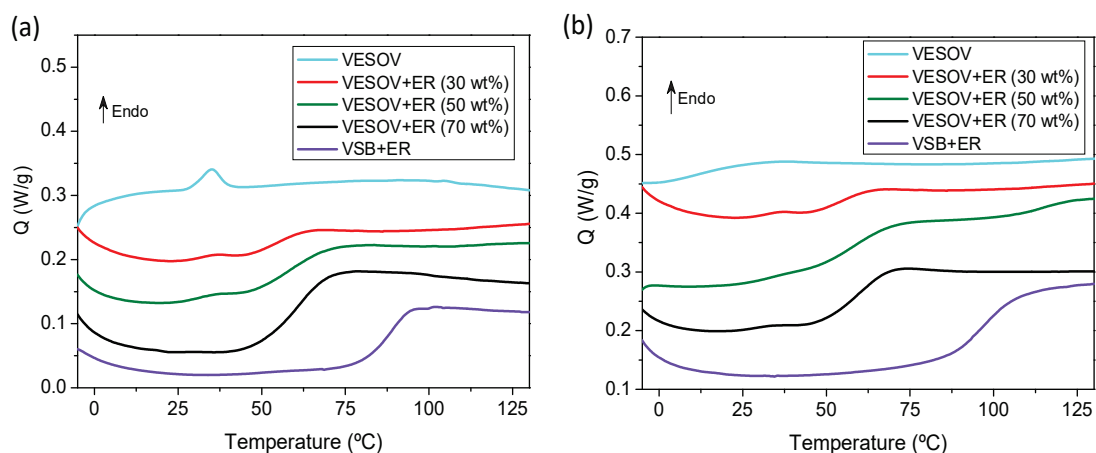
Sample	$T_o$ (°C)	$T_s$ (°C)
VESOV	297.3	169.3
VESOV+ER (30 wt%)	278.3	160.5
VESOV+ER (50 wt%)	282.4	161.4
VESOV+ER (70 wt%)	272.2	157.8
VSB+ER	277.6	158.5

From Table 1, it can be observed that the statistic heat-resistant index temperature values ( $T_s$ ) show the same trend as  $T_o$  (or  $T_{5\%}$ ) values. The results demonstrate that samples with low epoxy resin (ER) content exhibit higher thermal stability (VESOV has the highest), whereas increasing the ER content (VESOV+ER) decreases the thermal stability. The reason for this behavior could be associated with the higher amount of VSB in the network, involving a higher content of imine bonds. Moreover, the higher the oxirane ring content, the more ester and hydroxyl groups are created through the curing. These functions can also promote the thermal scissions of the networks [64].

The glass transition temperature ( $T_g$ ), which usually acts as the upper limit use temperature for thermosetting materials, is a major parameter [65]. Figure 3a,b shows the DSC curves of epoxy vitrimers to make a comparison of the  $T_{g-onset}$  (simplified as  $T_g$ ) between VESOV, VESOV+ER (different percentages) and VSB+ER.

In Figure 3a, it was observed that in the VESOV+ER samples (30 and 50 wt%), two glass transition temperatures coexist. The first one appears at the same range as the  $T_g$  peak of VESOV, whilst the other  $T_g$  appears a little more displaced at higher temperatures. This may be due to the formation of two polymeric networks that do not mix with each other; that is, a heterogeneous mixture was obtained. However, as noted below, it is most likely that the post-curing process (2 h at 150 °C) was not enough to obtain a fully cured vitrimer. In Table 2, the  $T_g$  of the different samples is summarized ( $T_{g-onset}$ ).

As can be noticed in Table 2, when the fraction of epoxy resin increases, the  $T_g$  values rise significantly; that is, higher stiffness is achieved by making the fluidity of the chains more difficult. Therefore, the addition of a small amount of epoxy resin helps VESOV to improve its thermal properties. Indeed, VESOV has a  $T_g$  equal to 28.7 °C, while the addition of only 30 wt% of ER increases the  $T_g$  to 48.2 °C. However, by continuing to add more percentage in weight in ER (50 and 70 wt%), the increase that occurs in  $T_g$  is not as significant ( $T_g = 48.7$  and 50.3 °C for 50 and 70 wt% in ER, respectively). That is, a larger increase in the added proportion of ER did not provide significantly higher  $T_g$ .

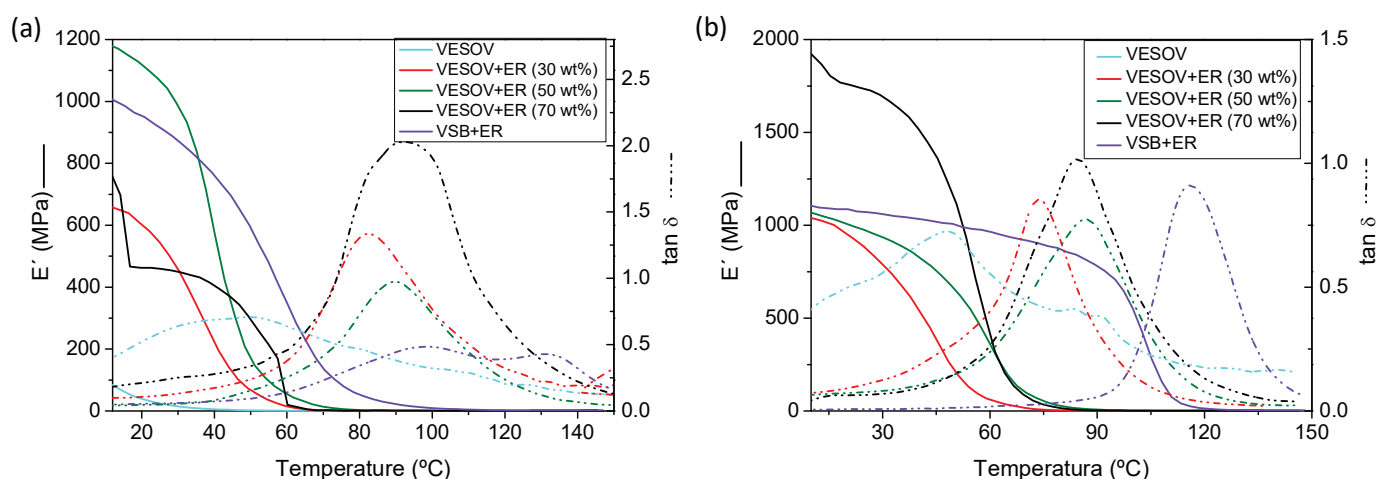


**Figure 3.** (a) Calorimetric curves of the original and (b) reprocessed vitrimers: VESOV, VESOV+ER (with different proportion by weight) and VSB+ER.

**Table 2.**  $T_g$  values obtained in the calorimetric curves (DSC) and the maximum peak of the  $\tan \delta$  (DMA) in the original and reprocessed samples.

Sample	DSC $T_g$ (°C)		DMA $T_g$ (°C)	
	Original	Reprocessed	Original	Reprocessed
VESOV	28.7	6.8	44.0	50.7
VESOV+ER (30 wt%)	48.2	45.1	70.2	75.1
VESOV+ER (50 wt%)	48.7	55.0	78.0	88.4
VESOV+ER (70 wt%)	50.3	50.6	78.7	85.3
VSB+ER	78.6	91.5	111.5	116.1

Further, the  $T_g$  of the samples was determined via DMA. Figure 4 shows both the storage modulus ( $E'$ ) and the loss factor ( $\tan \delta$ ) (its maximum peak is the  $T_g$  of each sample) versus temperature. In addition, Table 2 shows the glass transition temperatures of all the samples obtained by DMA. All the curves with their corresponding numerical data are presented at a frequency of 3 Hz.



**Figure 4.** DMA curves obtained for (a) original and (b) reprocessed vitrimers at 3 Hz frequency: VESOV, VESOV+ER (with different weight proportion) and VSB+ER.

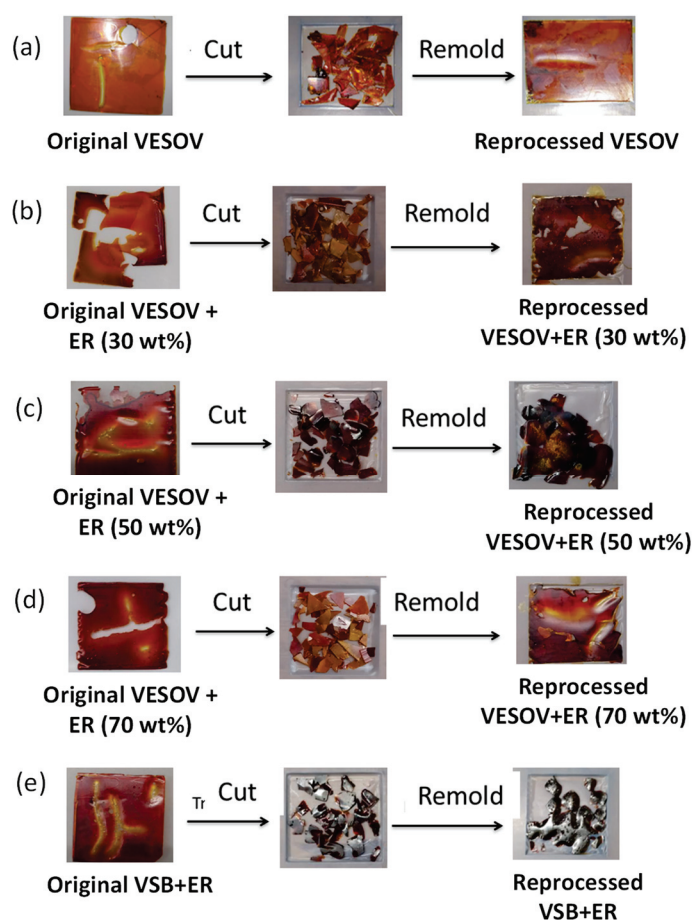
As in the DSC, it is observed that while increasing the amount of epoxy resin, the glass transition temperature of the sample increases progressively. On the other hand, in Figure 4a, the  $\tan \delta$  curve of VSB+ER exhibits two peaks, implying it is not completely

cured, as not all the chains of the system have reacted effectively. That is, as said before, the post-curing process is not enough to reach a total curing, and samples need a greater post-curing. Furthermore, the difference in the storage modulus is notable amongst samples. Thus, while VESOV has a very low storage modulus, it is remarkably increased by adding a small amount of epoxy resin.

In conclusion, analyzing the results obtained so far, it can be said that adding a small amount of epoxy resin (30 wt%) considerably improves the thermo-mechanical properties of the VESOV vitrimer. Finally, the reprocessability of these vitrimers was studied.

#### 4.3. Reprocessability of VESOV, VESOV+ER (Different Percentages) and VSB+ER

The dynamic character of the Schiff base exchanges improves the ability of the samples to be reprocessed. The reprocessing is performed as explained before: The samples were cut into small pieces with scissors, placed into a steel mold and reprocessed at 150 °C for 60 min at 10 bar. These reprocessed samples are shown in Figure 5, observing that VESOV has a considerable ability to be reprocessed (Figure 5a) since it contains dynamic covalent bonds. On the contrary, after carrying out this test with the VSB+ER (Figure 5e), incomplete recovery of the original shape is achieved, as it includes permanent crosslinks due to epoxy resin's nature as a thermoset. Figure 5b–d also shows the reprocessability of those vitrimers synthesized using different proportions of ESO and epoxy resin (VESOV+ER). In Figure 5b, it can be seen that only with the inclusion of 30 wt% of epoxy resin is it observed that the reprocessability of the sample substantially improves. In order to compare and verify if any degradation occurs after reprocessability, FTIR analysis was performed. In the supporting information, FTIR spectra of all the samples are included. No differences were observed between pre- and post-reprocessed spectra (Figure S3).



**Figure 5.** Digital photos demonstrating the reprocessability of (a) VESOV, (b) VESOV+ER (30 wt%), (c) VESOV+ER (50 wt%), (d) VESOV+ER (70 wt%) and (e) VSB+ER.



Yet, it is necessary to verify that this reprocessing does not diminish the good thermo-mechanical properties obtained for the original samples. For this, the characterizations via DSC and DMA of the different reprocessed samples were accomplished. Moreover, a comparison between the original and remolded samples is performed to evaluate how many times samples can be reprocessed without losing their thermo-mechanical properties.

In DSC, the reprocessed samples only present a  $T_g$ , showing that they are totally cured (Figure 3b). In addition, as seen in Table 2, all the glass transition temperatures obtained for the reprocessed samples are similar or even higher than those corresponding to the samples without reprocessing. The only exception is precisely the vitrimer synthesized only with ESO (VESOV), which showed a clear decrease in its  $T_g$ .

However, DMA measurements (Figure 4b) demonstrate that all the reprocessed samples slightly increase their glass transition temperatures (Table 2) because they undergo a post-curing process in which the crosslinking of their bonds increases. This fact is confirmed by the width of the  $\tan \delta$  peaks, as in the original samples, the width of the peak is greater, denoting that the samples are more heterogeneous. In the reprocessed samples, peak width decreases considerably, denoting that the crosslinking of the bonds has been superior and obtained a larger homogeneity of the system.

## 5. Conclusions

In conclusion, it has been possible to verify that 1,4-butanediamine is a suitable reagent to synthesize a vanillin-derived Schiff base (VSB) that can be used as a curing agent in the development of a new vitrimer from epoxidized soybean oil (VESOV). Furthermore, the inclusion of a commercial epoxy resin to the VESOV helped to improve its mechanical and thermal properties, observing by DSC and DMA techniques that when the percentage of epoxy resin increases, the  $T_g$  increases remarkably. However, these new epoxy materials must have a balance between their thermo-mechanical properties and their reprocessability to be considered vitrimers. In this way, a circular economy can be established, such as thermoplastics. Standing on this, it can be concluded that the VESOV+ER 30 wt% sample seems to be the most suitable to achieve this objective since it has the qualities of a thermoset (high storage modulus and  $T_g$ ) and contains elements of a thermoplastic (good reprocessability), with this last property not attributable to conventional epoxy resins.

In short, this new dynamic hardener based on vanillin and 1,4-butanediamine obtained good properties as expected; a sustainable vitrimer was synthesized based only on epoxidized vegetable oil. The first approach to this objective has been made by developing a new material with remarkable features by adding a small amount of commercial epoxy resin (30 wt%), so the material can be considered biobased with good mechanical properties and the possibility of recycling. Therefore, this material can be postulated in the future, with slight improvements, to be a replacement for current commercial epoxy resins.

**Supplementary Materials:** The following supporting information can be downloaded at: <https://www.mdpi.com/article/10.3390/polym15183737/s1>, Figure S1:  $^1\text{H-NMR}$  spectrum of 1,4-butanediamine. Figure S2:  $^1\text{H-NMR}$  spectrum of vanillin; Figure S3: FTIR spectra of pre- (black) and post-reprocessed (red) sample; Table S1: TGA results obtained for samples:  $T_{30\%}$  and final residual mass %.

**Author Contributions:** Conceptualization, A.V.-F. and J.M.L.; methodology, J.M.L.; validation, L.R.-R., M.I.M.-B. and J.L.V.-V.; formal analysis, A.V.-F.; investigation, I.Y.; resources, L.R.-R.; data curation, I.Y.; writing—original draft preparation, A.V.-F.; writing—review and editing, J.M.L.; visualization, M.I.M.-B.; supervision, J.L.V.-V.; project administration, J.L.V.-V.; funding acquisition, J.L.V.-V. All authors have read and agreed to the published version of the manuscript.

**Funding:** This research was funded by Basque Government ELKARTEK (KK-2023/00056; KK-2023/00016; KK-2022/0082; KK-2022/0040) and Grupos Consolidados (IT1756-22).

**Institutional Review Board Statement:** Not applicable.

**Informed Consent Statement:** Not applicable.

**Data Availability Statement:** Not applicable.

**Acknowledgments:** The authors are thankful for the funding from the Government of the Basque Country under the Grupos de Investigación del Sistema Universitario Vasco, (IT1756-22) program and the ELKARTEK program. The authors also thank the technical support of SGIker (UPV/EHU).

**Conflicts of Interest:** The authors declare no conflict of interest.

### Abbreviations

BDA	1,4-butandiamine
CAN	Covalent Adaptable Network
CDCl <sub>3</sub>	deuterated chloroform
DGEBA	diglycidyl ether of bisphenol A
DMA	Dynamic Mechanic Analysis
DMI	1,2-dimethylimidazole
DSC	Differential Scanning Calorimetry
E′	Storage modulus
E″	Loss modulus
ESO	Epoxidized Soybean Oil
ER	Epoxy resin
EVO	Epoxidized Vegetable Oil
FTIR	Fourier Transform Infrared
MeOH	Methanol
NMR	Nuclear Magnetic Resonance
tan δ	loss factor
T <sub>5%</sub>	temperature at 5% weight loss
T <sub>30%</sub>	temperature at 30% weight loss
T <sub>g</sub>	Glass transition temperature
TGA	Thermogravimetric Analysis
T <sub>o</sub>	onset decomposition temperature
T <sub>s</sub>	statistic heat-resistant index temperature
T <sub>v</sub>	Topology freezing point temperature
VAN	Vanillin
VESOV	VSB cured ESO vitrimer
VSB	Vanillin-derived Schiff Base

### References

- Jin, F.L.; Park, S.J.; Li, X.J. Synthesis and application of epoxy resins: A review. *Ind. Eng. Chem.* **2015**, *29*, 1–11. [CrossRef]
- Auvergne, R.; Caillol, S.; David, G.; Boutevin, B.; Pascault, J. Biobased thermosetting epoxy: Present and future. *Chem. Rev.* **2014**, *114*, 1082–1115. [CrossRef] [PubMed]
- Mullins, M.J.; Liu, D.; Sue, H.J. Mechanical properties of thermosets. In *Thermosets: Structure, Properties and Applications*, 2nd ed.; Guo, Q., Ed.; Fudan University: Shanghai, China; Elsevier: Amsterdam, The Netherlands, 2018; pp. 35–68.
- Shiota, A.; Ober, C.K. Rigid rod and liquid crystalline thermosets. *Prog. Polym. Sci.* **1997**, *22*, 975–1000. [CrossRef]
- Raquez, J.; Deléglise, M.; Lacrampe, M.; Krawczak, P. Thermosetting (bio) materials derived from renewable resources: A critical review. *Prog. Polym. Sci.* **2010**, *35*, 487–509. [CrossRef]
- Rutz, B.H.; Berg, J.C. Thermosetting (bio) materials derived from renewable resources: A critical review. *Adv. Colloid Interface Sci.* **2010**, *160*, 56–75. [CrossRef]
- Wang, S.; Ma, S.; Xu, C.; Liu, Y.; Dai, J.; Wang, Z.; Liu, X.; Chen, J.; Shen, X.; Wei, J. Vanillin-derived high-performance flame retardant epoxy resins: Facile synthesis and properties. *Macromolecules* **2017**, *50*, 1892–1901. [CrossRef]
- Senthilkumar, K.; Saba, N.; Rajini, N.; Chandrasekar, M.; Jawaid, M.; Siengchin, S.; Alotman, O.Y. Mechanical properties evaluation of sisal fibre reinforced polymer composites: A review. *Constr. Build. Mater.* **2018**, *174*, 713–729. [CrossRef]
- Jensen, J.P.; Skelton, K. Wind turbine blade recycling: Experiences, challenges and possibilities in a circular economy. *Renew. Sust. Energ. Rev.* **2018**, *97*, 165–176. [CrossRef]
- O’Dea, R.M.; Willie, J.A.; Epps, T.H. 100th anniversary of macromolecular science viewpoint: Polymers from lignocellulosic biomass. Current challenges and future opportunities. *ACS Macro Lett.* **2020**, *9*, 476–493. [CrossRef] [PubMed]
- Jian, X.; An, X.; Li, Y.; Chen, J.; Wang, M.; Zeng, J. All plant oil derived epoxy thermosets with excellent comprehensive properties. *Macromolecules* **2017**, *50*, 5729–5738. [CrossRef]
- Vollmer, I.; Jenks, M.J.; Roelands, M.C.; White, R.J.; van Harmelen, T.; de Wild, P.; van Der Laan, G.P.; Meirer, F.; Keurentjes, J.T.; Weckhuysen, B.M. Beyond mechanical recycling: Giving new life to plastic waste. *Angew. Chem. Int. Ed.* **2020**, *59*, 15402–15423. [CrossRef] [PubMed]

13. Hahladakis, J.N.; Iacovidou, E. An overview of the challenges and trade-offs in closing the loop of post-consumer plastic waste (PCPW): Focus on recycling. *J. Hazard. Mater.* **2019**, *380*, 120887–120897. [CrossRef] [PubMed]
14. Maiorana, A.; Spinella, S.; Gross, R.A. Bio-based alternative to the diglycidyl ether of bisphenol A with controlled materials properties. *Biomacromolecules* **2015**, *16*, 1021–1031. [CrossRef]
15. Stemmelen, M.; Pessel, F.; Lapinte, V.; Caillol, S.; Habas, J.; Robin, J. A fully biobased epoxy resin from vegetable oils: From the synthesis of the precursors by thiol-ene reaction to the study of the final material. *J. Polym. Sci. A Polym. Chem.* **2011**, *49*, 2434–2444. [CrossRef]
16. Dworakowska, S.; Cornille, A.; Bogdał, D.; Boutevin, B.; Caillol, S. Formulation of bio-based epoxy foams from epoxidized cardanol and vegetable oil amine. *Eur. J. Lipid Sci. Technol.* **2015**, *117*, 1893–1902. [CrossRef]
17. Feng, X.; East, A.J.; Hammond, W.B.; Zhang, Y.; Jaffe, M. Overview of advances in sugar-based polymers. *Polym. Adv. Technol.* **2011**, *22*, 139–150. [CrossRef]
18. Fache, M.; Viola, A.; Auvergne, R.; Boutevin, B.; Caillol, S. Biobased epoxy thermosets from vanillin-derived oligomers. *Eur. Polym. J.* **2015**, *68*, 526–535. [CrossRef]
19. Fache, M.; Auvergne, R.; Boutevin, B.; Caillol, S. New vanillin-derived diepoxy monomers for the synthesis of biobased thermosets. *Eur. Polym. J.* **2015**, *67*, 527–538. [CrossRef]
20. Tremblay-Parrado, K.; García-Astrain, C.; Avérous, L. Click chemistry for the synthesis of biobased polymers and networks derived from vegetable oils. *Green Chem.* **2021**, *23*, 4296–4327. [CrossRef]
21. Wang, X.; Chen, L.; Wu, J.; Fu, T.; Wang, Y. Flame-retardant pressure-sensitive adhesives derived from epoxidized soybean oil and phosphorus-containing dicarboxylic acids. *ACS Sustain. Chem. Eng.* **2017**, *5*, 3353–3361. [CrossRef]
22. Jian, X.; He, Y.; Li, Y.; Wang, M.; Zeng, J. Curing of epoxidized soybean oil with crystalline oligomeric poly (butylene succinate) towards high performance and sustainable epoxy resins. *Chem. Eng. J.* **2017**, *326*, 875–885. [CrossRef]
23. Sun, X.; Wu, H.; Long, R. Thermomechanics of a temperature sensitive covalent adaptable polymer with bond exchange reactions. *Soft Matter* **2016**, *12*, 8847–8860. [CrossRef] [PubMed]
24. Murphy, E.B.; Bolanos, E.; Schaffner-Hamann, C.; Wudl, F.; Nutt, S.R.; Auad, M.L. Synthesis and characterization of a single-component thermally remendable polymer network: Staudinger and Stille revisited. *Macromolecules* **2008**, *41*, 5203–5209. [CrossRef]
25. Lendlein, A.; Jiang, H.; Juenger, O.; Langer, R. Light-induced shape-memory polymers. *Nature* **2005**, *434*, 879–882. [CrossRef]
26. Zheng, J.; Png, Z.M.; Ng, S.H.; Tham, G.X.; Ye, E.; Goh, S.S.; Loh, X.J.; Li, Z. Vitrimers: Current research trends and their emerging applications. *Mater. Today Commun.* **2021**, *51*, 586–625. [CrossRef]
27. Pepels, M.; Pilot, I.; Klumperman, B.; Goossens, H. Self-healing systems based on disulfide–thiol exchange reactions. *Polym. Chem.* **2013**, *4*, 4955–4965. [CrossRef]
28. Leibler, L.; Tournilhac, F.; Capelot, M.; Montarnal, D. Silica-like malleable materials from permanent organic networks. *Science* **2011**, *334*, 965–968.
29. Huang, Z.; Wang, Y.; Zhu, J.; Yu, J.; Hu, Z. Surface engineering of nanosilica for vitrimer composites. *Compos. Sci. Technol.* **2018**, *154*, 18–27. [CrossRef]
30. Li, H.; Zhang, B.; Yu, K.; Yuan, C.; Zhou, C.; Dunn, M.L.; Qi, H.J.; Shi, Q.; Wei, Q.; Liu, J. Influence of treating parameters on thermomechanical properties of recycled epoxy-acid vitrimers. *Soft Matter* **2020**, *16*, 1668–1677. [CrossRef]
31. Snyder, R.L.; Fortman, D.J.; De Hoe, G.X.; Hillmyer, M.A.; Dichtel, W.R. Reprocessable acid-degradable polycarbonate vitrimers. *Macromolecules* **2018**, *51*, 389–397. [CrossRef]
32. Zhou, Y.; Goossens, J.G.; Sijbesma, R.P.; Heuts, J.P. Poly (butylene terephthalate)/glycerol-based vitrimers via solid-state polymerization. *Macromolecules* **2017**, *50*, 6742–6751. [CrossRef]
33. Stukenbroeker, T.; Wang, W.; Winne, J.M.; Du Prez, F.E.; Nicolaÿ, R.; Leibler, L. Polydimethylsiloxane quenchable vitrimers. *Polym. Chem.* **2017**, *8*, 6590–6593. [CrossRef]
34. Porath, L.E.; Evans, C.M. Importance of broad temperature windows and multiple rheological approaches for probing viscoelasticity and entropic elasticity in vitrimers. *Macromolecules* **2021**, *54*, 4782–4791. [CrossRef]
35. Meng, F.; Saed, M.O.; Terentjev, E.M. Elasticity and relaxation in full and partial vitrimer networks. *Macromolecules* **2019**, *52*, 7423–7429. [CrossRef]
36. Li, L.; Chen, X.; Jin, K.; Rusayyis, M.B.; Torkelson, J.M. Arresting Elevated-Temperature Creep and Achieving Full Cross-Link Density Recovery in Reprocessable Polymer Networks and Network Composites via Nitroxide-Mediated Dynamic Chemistry. *Macromolecules* **2021**, *54*, 1452–1464. [CrossRef]
37. Lessard, J.J.; Scheutz, G.M.; Sung, S.H.; Lantz, K.A.; Epps, T.H., III; Sumerlin, B.S. Block copolymer vitrimers. *J. Am. Chem. Soc.* **2020**, *142*, 283–289. [CrossRef]
38. Ling, F.; Liu, Z.; Chen, M.; Wang, H.; Zhu, Y.; Ma, C.; Wu, J.; Huang, G. Compatibility driven self-strengthening during the radical-responsive remolding process of poly-isoprene vitrimers. *J. Mater. Chem. A* **2019**, *7*, 25324–25332. [CrossRef]
39. Jourdain, A.; Asbai, R.; Anaya, O.; Chehimi, M.M.; Drockenmuller, E.; Montarnal, D. Rheological properties of covalent adaptable networks with 1, 2, 3-triazolium cross-links: The missing link between vitrimers and dissociative networks. *Macromolecules* **2020**, *53*, 1884–1900. [CrossRef]
40. Elling, B.R.; Dichtel, W.R. Reprocessable cross-linked polymer networks: Are associative exchange mechanisms desirable? *ACS Cent. Sci.* **2020**, *6*, 1488–1496. [CrossRef]

41. Guerre, M.; Taplan, C.; Winne, J.M.; Du Prez, F.E. Vitrimers: Directing chemical reactivity to control material properties. *Chem. Sci.* **2020**, *11*, 4855–4870. [CrossRef]
42. Dyre, J.C. Colloquium: The glass transition and elastic models of glass-forming liquids. *Rev. Mod. Phys.* **2006**, *78*, 953–972. [CrossRef]
43. Fortman, D.J.; Brutman, J.P.; De Hoe, G.X.; Snyder, R.L.; Dichtel, W.R.; Hillmyer, M.A. Approaches to sustainable and continually recyclable cross-linked polymers. *ACS Sustain. Chem. Eng.* **2018**, *6*, 11145–11159. [CrossRef]
44. Hayashi, M. Implantation of Recyclability and Healability into Cross-Linked Commercial Polymers by Applying the Vitriimer Concept. *Polymers* **2020**, *12*, 1322. [CrossRef]
45. Alabiso, W.; Schlögl, S. The Impact of Vitrimers on the Industry of the Future: Chemistry, Properties and Sustainable Forward-Looking Applications. *Polymers* **2020**, *12*, 1660. [CrossRef] [PubMed]
46. Denissen, W.; Rivero, G.; Nicolaj, R.; Leibler, L.; Winne, J.M.; Du Prez, F.E. Vinylogous urethane vitrimers. *Adv. Funct. Mater.* **2015**, *25*, 2451–2457. [CrossRef]
47. Obadia, M.M.; Mudraboyina, B.P.; Serghei, A.; Montarnal, D.; Drockenmuller, E. Reprocessing and recycling of highly cross-linked ion-conducting networks through transalkylation exchanges of C–N bonds. *J. Am. Chem. Soc.* **2015**, *137*, 6078–6083. [CrossRef]
48. de Luzuriaga, A.R.; Martin, R.; Markaide, N.; Rekondo, A.; Cabañero, G.; Rodríguez, J.; Odriozola, I. Epoxy resin with exchangeable disulfide crosslinks to obtain reprocessable, repairable and recyclable fiber-reinforced thermoset composites. *Mater. Horiz.* **2016**, *3*, 241–247. [CrossRef]
49. Liu, H.; Zhang, H.; Wang, H.; Huang, X.; Huang, G.; Wu, J. Weldable, malleable and programmable epoxy vitrimers with high mechanical properties and water insensitivity. *Chem. Eng. J.* **2019**, *368*, 61–70. [CrossRef]
50. Wang, H.; Zhang, Y.; Possanza, C.M.; Zimmerman, S.C.; Cheng, J.; Moore, J.S.; Harris, K.; Katz, J.S. Trigger chemistries for better industrial formulations. *ACS Appl. Mater. Interfaces* **2015**, *7*, 6369–6382. [CrossRef]
51. Zhao, S.; Abu-Omar, M.M. Recyclable and malleable epoxy thermoset bearing aromatic imine bonds. *Macromolecules* **2018**, *51*, 9816–9824. [CrossRef]
52. Yu, Q.; Peng, X.; Wang, Y.; Geng, H.; Xu, A.; Zhang, X.; Xu, W.; Ye, D. Vanillin-based degradable epoxy vitrimers: Reprocessability and mechanical properties study. *Eur. Polym. J.* **2019**, *117*, 55–63. [CrossRef]
53. Memon, H.; Liu, H.; Rashid, M.A.; Chen, L.; Jiang, Q.; Zhang, L.; Wei, Y.; Liu, W.; Qiu, Y. Vanillin-based epoxy vitriimer with high performance and closed-loop recyclability. *Macromolecules* **2020**, *53*, 621–630. [CrossRef]
54. Fache, M.; Boutevin, B.; Caillol, S. Vanillin production from lignin and its use as a renewable chemical. *ACS Sustain. Chem. Eng.* **2016**, *4*, 35–46. [CrossRef]
55. Liu, W.; Schmidt, D.F.; Reynaud, E. Catalyst selection, creep, and stress relaxation in high-performance epoxy vitrimers. *Ind. Eng. Chem. Res.* **2017**, *56*, 2667–2672. [CrossRef]
56. Snijkers, F.; Pasquino, R.; Maffezzoli, A. Curing and viscoelasticity of vitrimers. *Soft Matter* **2017**, *13*, 258–268. [CrossRef]
57. Winne, J.M.; Leibler, L.; Du Prez, F.E. Dynamic covalent chemistry in polymer networks: A mechanistic perspective. *Polym. Chem.* **2019**, *10*, 6091–6108. [CrossRef]
58. Li, L.; Chen, X.; Jin, K.; Torkelson, J.M. Vitrimers designed both to strongly suppress creep and to recover original cross-link density after reprocessing: Quantitative theory and experiments. *Macromolecules* **2018**, *51*, 5537–5546. [CrossRef]
59. Sun, Y.; Sheng, D.; Wu, H.; Tian, X.; Xie, H.; Shi, B.; Yang, Y. Bio-based vitriimer-like polyurethane based on dynamic imine bond with high-strength, reprocessability, rapid-degradability and antibacterial ability. *Polymer* **2021**, *233*, 124208. [CrossRef]
60. Zhao, X.; Liu, Y.; Weng, Y.; Li, Y.; Zeng, J. Sustainable epoxy vitrimers from epoxidized soybean oil and vanillin. *ACS Sustain. Chem. Eng.* **2020**, *8*, 15020–15029. [CrossRef]
61. Zeng, R.; Wu, Y.; Li, Y.; Wang, M.; Zeng, J. Curing behavior of epoxidized soybean oil with biobased dicarboxylic acids. *Polym. Test.* **2017**, *57*, 281–287. [CrossRef]
62. Di Mauro, C.; Malburet, S.; Genua, A.; Graillot, A.; Mija, A. Sustainable series of new epoxidized vegetable oil-based thermosets with chemical recycling properties. *Biomacromolecules* **2020**, *21*, 3923–3935. [CrossRef] [PubMed]
63. Liu, Y.Y.; He, J.; Li, Y.D.; Zhao, X.L.; Zeng, J.B. Biobased, reprocessable and weldable epoxy vitrimers from epoxidized soybean oil. *Ind. Crops Prod.* **2020**, *153*, 112576–112584. [CrossRef]
64. Ma, Z.; Wang, Y.; Zhu, J.; Yu, J.; Hu, Z.J. Bio-based epoxy vitrimers: Reprocessability, controllable shape memory, and degradability. *Polym. Sci. A Polym. Chem.* **2017**, *55*, 1790–1799. [CrossRef]
65. Pascault, J.P.; Williams, R.J.J. Glass transition temperature versus conversion relationships for thermosetting polymers. *J. Polym. Sci. B Polym. Phys.* **1990**, *28*, 85–95. [CrossRef]

**Disclaimer/Publisher’s Note:** The statements, opinions and data contained in all publications are solely those of the individual author(s) and contributor(s) and not of MDPI and/or the editor(s). MDPI and/or the editor(s) disclaim responsibility for any injury to people or property resulting from any ideas, methods, instructions or products referred to in the content.





## Article

# Investigating the Mechanical, Thermal, and Crystalline Properties of Raw and Potassium Hydroxide Treated *Butea Parviflora* Fibers for Green Polymer Composites

Abisha Mohan <sup>1</sup>, Retnam Krishna Priya <sup>1,\*</sup>, Krishna Prakash Arunachalam <sup>2,\*</sup>, Siva Avudaiappan <sup>3,4,5</sup>, Nelson Maureira-Carsalade <sup>6</sup> and Angel Roco-Videla <sup>7,\*</sup>

<sup>1</sup> PG & Research Department of Physics, Holy Cross College, Nagercoil, Affiliated to Manonmaniam Sundaranar University, Tirunelveli 627012, India; mabisha@proton.me

<sup>2</sup> Department of Civil Engineering, University College of Engineering Nagercoil, Anna University, Nagercoil 629004, India

<sup>3</sup> Departamento de Ingeniería Civil, Universidad de Concepción, Concepción 4070386, Chile; savudaiappan@udec.cl

<sup>4</sup> Centro Nacional de Excelencia para la Industria de la Madera (CENAMAD), Pontificia Universidad Católica de Chile, Av. Vicuña Mackenna 4860, Santiago 8330024, Chile

<sup>5</sup> Department of Physiology, Saveetha Dental College and Hospitals, SIMATS, Chennai 600077, India

<sup>6</sup> Departamento de Ingeniería Civil, Universidad Católica de la Santísima Concepción, Concepción 4090541, Chile

<sup>7</sup> Facultad de Salud y Ciencias Sociales, Universidad de las Américas, Providencia, Santiago 7500975, Chile

\* Correspondence: rkrishnapriya@protonmail.com (R.K.P.); krishnaprakash3191@gmail.com (K.P.A.); aroco@udla.cl (A.R.-V.)

**Citation:** Mohan, A.; Priya, R.K.; Arunachalam, K.P.; Avudaiappan, S.; Maureira-Carsalade, N.; Roco-Videla, A. Investigating the Mechanical, Thermal, and Crystalline Properties of Raw and Potassium Hydroxide Treated *Butea Parviflora* Fibers for Green Polymer Composites. *Polymers* **2023**, *15*, 3522. <https://doi.org/10.3390/polym15173522>

Academic Editor: Raffaella Striani

Received: 24 June 2023

Revised: 13 August 2023

Accepted: 17 August 2023

Published: 24 August 2023



**Copyright:** © 2023 by the authors. Licensee MDPI, Basel, Switzerland. This article is an open access article distributed under the terms and conditions of the Creative Commons Attribution (CC BY) license (<https://creativecommons.org/licenses/by/4.0/>).

**Abstract:** The only biotic factor that can satisfy the needs of human species are plants. In order to minimize plastic usage and spread an immediate require of environmental awareness, the globe urges for the development of green composite materials. Natural fibers show good renewability and sustainability and are hence utilized as reinforcements in polymer matrix composites. The present work concerns on the usage of *Butea parviflora* fiber (BP), a green material, for high end applications. The study throws light upon the characterization of raw and potassium hydroxide (KOH)-treated *Butea Parviflora* plant, where its physical, structural, morphological, mechanical, and thermal properties are analyzed using the powder XRD, FTIR spectroscopy, FESEM micrographs, tensile testing, Tg-DTA, Thermal conductivity, Chemical composition, and CHNS analysis. The density values of untreated and KOH-treated fibers are 1.238 g/cc and 1.340 g/cc, respectively. The crystallinity index of the treated fiber has significantly increased from 83.63% to 86.03%. The cellulose content of the treated fiber also experienced a substantial increase from 58.50% to 60.72%. Treated fibers exhibited a reduction in both hemicelluloses and wax content. Spectroscopic studies registered varying vibrations of functional groups residing on the fibers. SEM images distinguished specific changes on the raw and treated fiber surfaces. The Availability of elements Carbon, Nitrogen, and Hydrogen were analyzed using the CHNS studies. The tensile strength and modulus of treated fibers has risen to 192.97 MPa and 3.46 Gpa, respectively. Thermal conductivity (K) using Lee's disc showed a decrement in the K values of alkalinized BP. The activation energy  $E_a$  lies between 55.95 and 73.15 kJ/mol. The fibers can withstand a good temperature of up to 240 °C, presenting that it can be tuned in for making sustainable composites.

**Keywords:** green composites; stem fiber; crystallinity; thermal behavior; reinforcement material

## 1. Introduction

For centuries, the distinctive characteristics of natural fibers have made them valuable for diverse purposes. The properties of natural fibers, including their mechanical, physical, and chemical attributes, are contingent on factors such as the specific fiber type, the plant

species from which they are derived, and the environmental conditions in which they are cultivated. Natural fibers are categorized based on their chemical composition, which can be either cellulose-based or lignin-based. Cellulose-based fibers such as cotton, jute, flax, hemp, and sisal have high tensile strength, suitable flexibility, and low density, making them suitable for applications such as textiles, paper, and composites. Lignin-based fibers, such as wood fibers, have high stiffness and strength, making them suitable for applications such as building materials and composites. Due to their environmentally friendly and sustainable behavior, natural fibers are progressively being utilized as substitutes for synthetic fibers in a wide range of applications. The lowered density of natural fiber composites (NFCs), along with their advantageous tribological and insulating qualities, could increase the cargo capacity of aircraft. Boeing and Airbus, two aviation industry titans, applied considerable effort to learn more about the usage of natural fibers in airplane interiors [1].

Natural fiber composites (NFCs) are composite materials that are made from a combination of natural fibers and a matrix material. NFCs are becoming increasingly popular as a sustainable and environmentally friendly substitute for conventional composite materials, which predominantly rely on synthetic fibers. The natural fibers used in NFCs can come from plant, animal, or mineral sources. The matrix material can be made from a variety of materials such as bio-based polymers, thermosetting resins, or thermoplastics. The characterization of natural fibers are instrumental in developing and optimizing new applications. NFCs have numerous advantages over traditional composite materials. The efficient properties possessed by natural fibers are light weight, high aspect ratio, low density, soundproof, thermal, mechanical properties, and biodegradability [2–4]. The combined effect of cellulose, hemicellulose, lignin, and wax dictates the overall properties of fibers. However, the hydrophilicity of the fibers turn in as a threat while intriguing fibers in making composites [5,6]. Microwave drying systems using halogen lamps were employed to bring down the moisture absorption in bast fibers [7]. The inadequate interfacial bonding contributes to diminished mechanical properties, which can be influenced by factors such as contact angle, orientation of microfibrils relative to the cell axis, and the Young's modulus of the fiber [8]. By subjecting fibers to different treatments, it is possible to transit their hydrophilic nature to hydrophobic, resulting in improved performance and easier disposal [9–11]. Studies in the literature demonstrate that alkali treatment has caused notable changes in the mechanical properties of reinforcements [12–15]. Specifically, alkali-treated *Borassus* fruit fibers exhibited significant increase of 41% in tensile strength, 69% in modulus and 40% in elongation [16]. 5% NaOH action on *Acacia Caesia* bark fibers had removed amorphous constituents and improved its tensile nature [17]. KOH-treated *Ijuk* fibers displayed enhanced tensile and stiffness in the fabricated composites [18]. Furthermore, natural fibers typically require lower processing temperatures compared to synthetic alternatives, which could be overthrown by employing flame retardants like phosphates, phosphoric acids, N-methynol functional phosphorus esters, antimony-halogen combinations, boron and nitrogen compounds [1]. Generally practiced chemical treatment process are bleaching, benzoylation, acetylation, silane, permanganate, etc.

The present work focuses on the *Butea Parviflora* (BP) plant, which is native to most South East Asian countries, including India. It is one among the many plants of the Fabaceae family with the genus name 'Butea'. It has a trifoliate alternate spiral leaf arrangement and bears flowers and seeds. Seeds are imbibed with many pharmaceutical benefits and are crushed for oil [19]. Being a deciduous climbing shrub, it could extend up to 20 m in height. Long fiber strands are torn out for domestic utilities by localities.

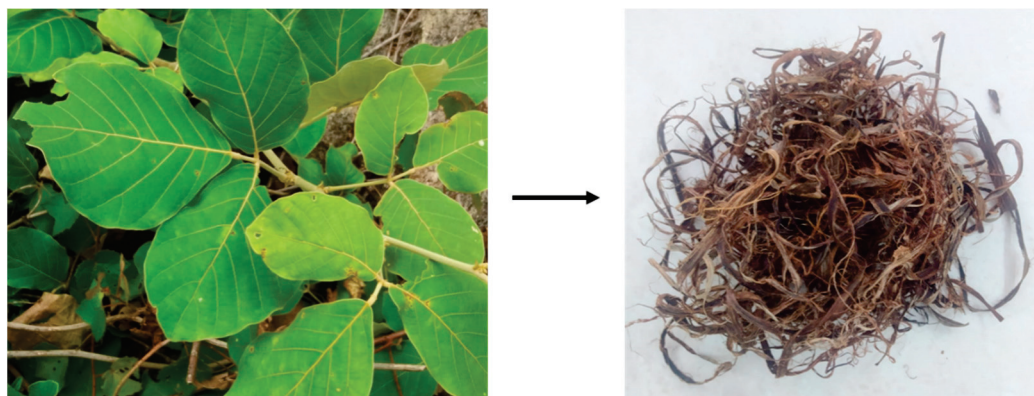
The *Butea parviflora* (BP) fiber is believed to possess most characters, as found in other stem fibers discovered to date, and there has been limited research conducted on it. The BP plant has climbing branches twined strongly around each other. The roots are strongly fixed to the ground, thus rendering a mechanical support from retrieving its path of growth. They are scattered all over India mostly in the Western and Eastern ghats and are widely flourished from moist to arid region. Fibers for the present study are collected from the village of Thirunandikarai, Kanniyakumari District, Tamil Nadu. Characterization

of BP fibers is necessary to understand their properties and potential applications. Raw and 0.1 M of KOH-treated Butea fibers are prepared for the characterization procedures including physical, mechanical, spectroscopic, thermal, crystalline, morphological, and chemical testing methods. Physical testing methods involve measurements of fiber diameter, length, density and aspect ratios. Mechanical testing techniques are employed to assess the strength and rigidity of fibers, while the spectroscopic, thermal, crystalline, and morphologies are studied using the FTIR, Thermogravimetric analysis (TG-DTA), X-ray diffraction (XRD), and Scanning Electron Microscopic studies (SEM) [20]. Chemical testing methods are used to identify the chemical composition of fibers, including the detection of impurities and extractives. The experimental data indicate that BP has the potential to serve as a superior reinforcing material in the formulation of sustainable composites.

## 2. Materials and Methods

### 2.1. Material Extraction

The collected BP fibers are mechanically removed from the branchy stems using a metal teeth. The peeled fibers are then dried in the absence of sunlight for about 7 days in a clean environment. Fibers are drenched in water and surface modification is attained by soaking it in 0.1 M of KOH environment for 30 min. Alkali pre-treatment is performed to eliminate impurities such as wax, oil, etc., from the fibers, while also inducing modifications to enhance their properties [21,22]. Fibers are kept at room temperature for over 10–15 days. Potassium hydroxide was chosen over NaOH in the current study, because it is less alkaline. In Ijuk fibers, KOH-treated fibers generated the highest tensile and stiffness than NaOH [18]. Given that KOH treatment was not performed prior on Butea fibers, KOH with 0.1 molarity was carried on Butea fibers. Fibers mercerized with 0.1 M KOH solution on other fibers demonstrated an enhancement in the mechanical properties [23]. Sisal fibers from the literature showed an improved hydrophobic behavior while treated with same molarity of alkali solution [24]. Alkali-treated fibers are proceeded with vacuum desiccating for 2 days [25]. Figure 1 shows the fibers extracted from Butea parviflora (BP).



**Figure 1.** Collected fibers from Butea parviflora plant.

### 2.2. Physical Properties of Butea Parviflora (BP) Fiber

The physical factors of unprocessed and alkali-treated Butea parviflora (BP) fibers are crucial in making composites. Randomly selected BP fibers 30 in number are taken to establish the physical aspects.

Diameter of BP is calculated using an optical microscope. KOH-treated fibers show a decrease in the diameter of the raw fibers. It can be believed that the interfacial strength decreases with an increase in diameter regardless of surface modifications [26].

Aspect ratios of natural fibers are found by calculating the ratio between the length and diameter. The aspect ratios of alkali-treated BP (203.91) are greater than raw BP (174.59). Higher the aspect ratios, more will be the compressive strength of composites. The addition of coconut and oil palm fibers to soil building blocks resulted in an augmentation



of both compressive and tensile strength, which is correlated with higher aspect ratios of the fibers [27].

The linear density (LD) is a measure to determine the fineness of a fiber, and excellency in tensile strength is observed with higher LD values. An average length of 10 cm was chosen to calculate the fiber's LD using the equation [28].

$$\text{Linear density (LD)} = \frac{\text{mass of fibers (grams)}}{\text{length of fibers (meter)}} \quad (1)$$

Density plays a crucial role in determining the suitability of natural fiber composites for various applications. It is a prime factor that distinguishes and discriminates natural fiber composites from their synthetic counterparts. Density is analyzed using the liquid pycnometer method, with the immersion liquid toluene, using the equation [9,29],

$$\rho = \frac{(mb - ma)}{[(mc - ma) - (md - mb)]} \rho_t \quad (2)$$

In the given context,  $ma$  represents the mass of the empty pycnometer (in kilograms),  $mb$  denotes the mass of the pycnometer filled with fibers (in kilograms),  $mc$  represents the mass of the pycnometer filled with toluene (in kilograms), and  $md$  indicates the mass of the pycnometer filled with both fibers and toluene (in kilograms).

The density of KOH-treated BP (1.340 g/cc) is higher than raw BP (1.238 g/cc). Less-dense extractives of fibers like lignin and hemicellulose, along with airspaces, might get removed by the alkalization. Hence, the density of treated BP has been incremented [28]. Density values of BP are comparable with other fibers like *Thespesia populnea* (1.412 g/cc) [30], carbon (1.40 g/cc), and aramid fibers (1.40 g/cc) and are much smaller than E-glass fibers (2050 g/cc) [31]. Physical aspects of *Butea* fibers are displayed in Table 1.

**Table 1.** Comparison made between the physical and chemical attributes of untreated and alkaliized BP fibers, alongside other types of fibers.

Fibers	Diameter	Aspect Ratio (L/D)	Linear Density	Density (g/cc)	Reference
Raw BP	0.048 mm	174.59	312 tex	1.238	Present work
Treated BP	0.027 mm	203.91	346 tex	1.340	Present work
<i>Acacia leucophlea</i>	168.5 $\mu\text{m}$	-	-	1.385	[32]
<i>Coccinia grandis</i>	543–621 $\mu\text{m}$	-	130.9 tex	1.517	[33]

### 3. Characterization Studies

#### 3.1. X-ray Diffraction (XRD) Analysis

The crystalline nature of *Butea* fibers was measured using powder X-ray diffraction. The analysis was conducted using a D8 Advance Model diffractometer from the manufacturer, Bruker AXS, Karlsruhe, Germany. Recording the spectrum for  $2\theta$  values was taken between  $3^\circ$  and  $80^\circ$  under 40 kV and a current supply of 35 mA. The Segal empirical formula was utilized to calculate the crystallinity index of BP fibers [34,35].

$$\text{CI} = \frac{I_{200} - I_{\text{am}}}{I_{200}} * 100\% \quad (3)$$

where  $I_{200}$ —maximum intensity of the crystalline diffraction peak at  $2\theta$  angle range of  $22^\circ$  to  $23^\circ$ , and  $I_{\text{am}}$ —minimum intensity of an amorphous peak at  $2\theta$  angle of  $18^\circ$ . Additionally, the crystallite size was calculated utilizing Scherrer's equation [36].

$$\text{CS} = \frac{K\lambda}{\beta_{200}\cos\theta} \quad (4)$$

where  $K$ —Scherrer's constant,  $\lambda$ —wavelength of X-rays (0.154 nm),  $\beta_{200}$ —the peak's full width at half maximum, and  $\theta$ —Bragg angle.

### 3.2. Scanning Electron Microscopy (SEM)

Scanning electron microscopy gives outstanding results in identifying the morphological features; thereby, the fundamental characters of the fibers are lit up with detailed clarity. The surface images of fibers were scanned with the working voltage from 0.5 to 30 kV, using an instrument, Jeol 6390LA/OXFORD XMXN, from JEOL India PVT LTD; South Delhi, India, a subsidiary company of JEOL Limited, Tokyo, Japan.

### 3.3. Thermogravimetric Analysis

Heat resistance is very much needed for making composites [37]. By indulging fibers in thermal analysis, the nature of samples under various environments of heating and cooling, along with inert oxidation-reduction atmospheres, can be cited. The change in mass is adjoined with a variety of reactions such as decomposition, degradation, adsorption, vaporization, oxidation, reduction, etc. Tg-dta and DSC analyses were carried out using the Perkin Elmer STA 6000 Model, from the manufacturer Perkin Elmer Inc., Mumbai, India. The heating process was monitored at a rate of 20 °C per minute under a dynamic nitrogen atmosphere within the temperature range of 40–800 °C.

### 3.4. Thermal Conductivity Using Lee's Disc Method

Thermal conductivity was assessed using Lee's disc method, wherein the mass, diameter, and thickness of Lee's disc were measured using a digital weighing machine, Vernier caliper, and screw gauge. At the onset of steady temperature, the disc is let to cool down, and dropping temperatures are noted. The thermal conductivity was determined by employing a specific equation for the calculation process [38].

$$k = \frac{mxd(r + 2h)}{\pi r^2(T_1 - T_2)(2r + 2h)} dT/dt \text{ W/m/K} \quad (5)$$

The various parameters involved are:  $m$  represents the mass of the Lee's disc,  $d$  refers to the sample thickness,  $x$  denotes the specific heat,  $r$  represents the radius of the Lee's disc,  $h$  signifies the thickness of the Lee's disc, and  $dT/dt$  represents the tangential slope. Additionally,  $T_1$  represents the steady temperature of the vapor chamber, and  $T_2$  represents the steady temperature of the Lee's disc.

### 3.5. CHNS Analyzer

CHNS elemental analysis offers a quick method to determine the levels of carbon, hydrogen, nitrogen, and sulfur in organic samples and various other materials, including volatile or viscous samples. The analysis was performed using the model Elementar Vario EL III, Micro Cube manufactured by Elementar, Langenselbold, Germany with a precision > 0.1% absorbance.

### 3.6. Single Fiber Tensile Testing

The tensile strength of BP fibers were measured using single fiber strength and elongation (Zwick/Roell) from the Physical Testing Laboratory, SITRA, Coimbatore. All analyses were conducted at a controlled temperature of approximately 21 °C with a tolerance of  $\pm 1$  °C, along with a relative humidity of 65%. The gauge length was set at 50 mm, and the transverse rate was maintained at 30 mm/min. The tensile strength of BP fibers was determined using [39]

$$\text{Tensile strength}(\sigma) = \frac{\text{Tensile force (F)}}{\text{cross sectional area of fibers (A)}} \quad (6)$$

The microfibril angles of BP fibers are calculated using the global deformation equation [40].

$$\varepsilon = \ln \left( 1 + \frac{\Delta L}{L} \right) = -\ln (\cos \alpha) \quad (7)$$

where  $\varepsilon$ —strain developed,  $\alpha$ —microfibril angle (MFA),  $L$ —fiber length, and  $\Delta L$ —elongation at the time of breaking.

### 3.7. FTIR Analysis

The FTIR spectrometer (Model FTIR-8400S spectrum, SHIMADZU, Kyoto, Japan) was employed to identify the functional groups present in both untreated and alkali-treated fibers. The analysis was conducted using a KBr matrix with a scan rate of 45 scans per minute and a resolution of  $4 \text{ cm}^{-1}$ , within a wavenumber range of  $400 \text{ cm}^{-1}$  to  $4000 \text{ cm}^{-1}$ .

## 4. Results and Discussion

### 4.1. Determination of Chemical Composition

The presence of cellulose, lignin, hemicellulose, and wax content in the fiber sample was determined through chemical analysis. Extraction methods, maturity of plant parts, and the habitat of plants would have a direct outcome on the cellular compositions [41]. Standardized methods were followed to find the cellular composition. Percentage of cellulose and hemicellulose was found from the acid and neutral detergent method. Lignin content was found using the Klason method, and moisture quantity was measured by drying the sample. The wax percentage was determined using the Soxhlet extraction method, where the chosen solvent's vapor dissolves wax from the fiber samples. The variance between the extracted mass and the dried mass calculates the wax% present in the samples.

The cellulose content of 0.1 M KOH-treated BP was 60.72%, which is higher than the raw fiber (58.5%) and is thought to withstand hydrostatic pressure gradients of the fibers. After alkali treatment, fibers showed a visible improvement to serve as reinforcement material [42]. The cellulose values are in agreement with Kenaf (53.14%) [43] and Okra fibers (60–70%) [44]. Hemicellulose in alkalinized BP deeply declined to 19.2% from 40.13%. There are almost no comprehensive treatment methods to extract hemicellulose completely without dissolving the cell components [45]. Complete removal of hemicelluloses could potentially lead to a reduction in composite strength while enhancing its stiffness [46]. Molecular weights of hemicellulose are lower than cellulose, and also, the alkali treatment on BP has eliminated a high degree of hemicelluloses, and because of that, physical properties such as density, aspect ratio, and linear density show an increase [47].

Furthermore, the complete removal of hemicellulose or lignin through alkalization may not be foolproof due to the presence of hydrogen bonding between residual hemicellulose and cellulose fibrils [48,49]. Lignin contributes to the structural integrity of fibers. A higher lignin percentage (18.09%) of BP can possibly favor excellent rigidity compared to other fibers. The physical properties of BP fibers were not negatively influenced by lignin. However, the presence of lignin impacted the thermal stability of BP fibers by stretching its degradation temperature [50]. The cellulose/lignin ratio in BP fibers was almost around 3:1. It is necessary to obtain a high cellulose/lignin ratio in samples to receive better crystalline, structural, and physical properties while introducing these fibers for composite making [51]. Modifying the cellulose/lignin ratio through diverse oxidative treatments is essential for these fibers, as this approach could yield improved fiber properties, namely (higher thermal stability, high mechanical strength), beyond those observed in the current study.

The amount of wax housed in the BP fibers (0.31%) was minimized to 0.25% using KOH action, and hence, initial flushing of samples prior to alkali treatment was considered optional. Dewaxing occurred during the alkali action had introduced a rough surface, which is shown in the SEM images. Moreover, the elimination of wax and other contaminants contributed to the enhancement of the tensile properties of the BP fibers [52]. A comparison

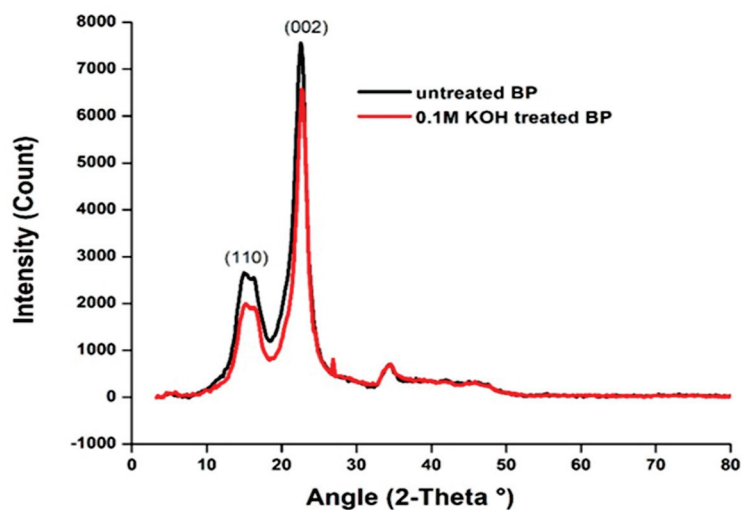
of the chemical composition between BP fibers and other natural fibers is presented in Table 2 [40].

**Table 2.** Comparison of chemical characteristics of raw and alkali-treated BP with other fibers.

Fibers	Cellulose (wt%)	Hemicellulose (wt%)	Lignin (wt%)	Moisture (wt%)	Wax (wt%)	Pectin (wt%)
Raw BP	58.5	40.13	18.09	11.63	0.31	6.77
Treated BP	60.72	19.2	20.5	12.4	0.25	3.4
Acacia leucophlea	68.09	13.6	17.73	8.83	-	-
Coccinia grandis	63.22	-	24.42	9.14	0.32	-
Prosopis juliflora bark	61.65	16.14	17.11	9.48	0.61	-

4.2. X-ray Diffraction (XRD) Analysis

The XRD analysis revealed the crystalline nature of the BP fibers in Figure 2. The lattice planes at (110) and (002) belong to the crystallographic plane group of celluloses [44]. It turns out that the crystallinity index (CI) of 0.1 M KOH-treated BP (86%) was more than the untreated BP (83%). SEM images also display an ordered arrangement of cellular components in the alkali-treated fiber. High CI indicates a better orientation of cellulose around the fiber axis, which attributes to the higher strength of fibers [53]. Additionally, the thermal degradation of fibers is also toggled to higher temperatures with the rise in CI. The CI for BP fiber is greater than other fibers and is tabulated in Table 3. Under certain conditions, it is possible for the crystalline regions to undergo rearrangement, leading to an increased level of crystallinity in the fiber [54]. Meanwhile, the crystallite size of the alkali-treated BP has risen from 7.5 nm to 8.04 nm. The CS of Butea fibers is smaller than the Sida cordifolia stem (18 nm). The increment of CS in the treated BP is suspected owing to the varying strain caused by the intrusion of K<sup>+</sup> ions on the cellular arrangement during treatment [39].



**Figure 2.** X-ray diffractogram of raw and 0.1 M KOH-treated Butea parviflora (BP).

**Table 3.** Comparison of crystallinity index of raw and alkali-treated BP with other fibers.

Sample	Crystallinity Index (%)	Crystallite Size (nm)	Reference
Untreated BP	83.63	7.50	Present work
Alkali-treated BP	86.03	8.04	Present work
Thespesia populnea	48.17	3.57	[55]
Sida cordifolia stem	56.92	18	[56]



#### 4.3. CHNS Analysis

The presence of elements like carbon, nitrogen, hydrogen, and sulfur in Butea fibers can be detected using the CHNS analyzer. The analysis employs finely chopped raw and alkali-treated fibers. Samples with a high carbon content are regarded advantageous when used as fillers in strengthening composites [12]. The low heat conductivity values obtained from Lee's disc setup of alkaliized BP can be accredited due to its high carbon content. Table 4 shows the weight percent of carbon, hydrogen, and nitrogen.

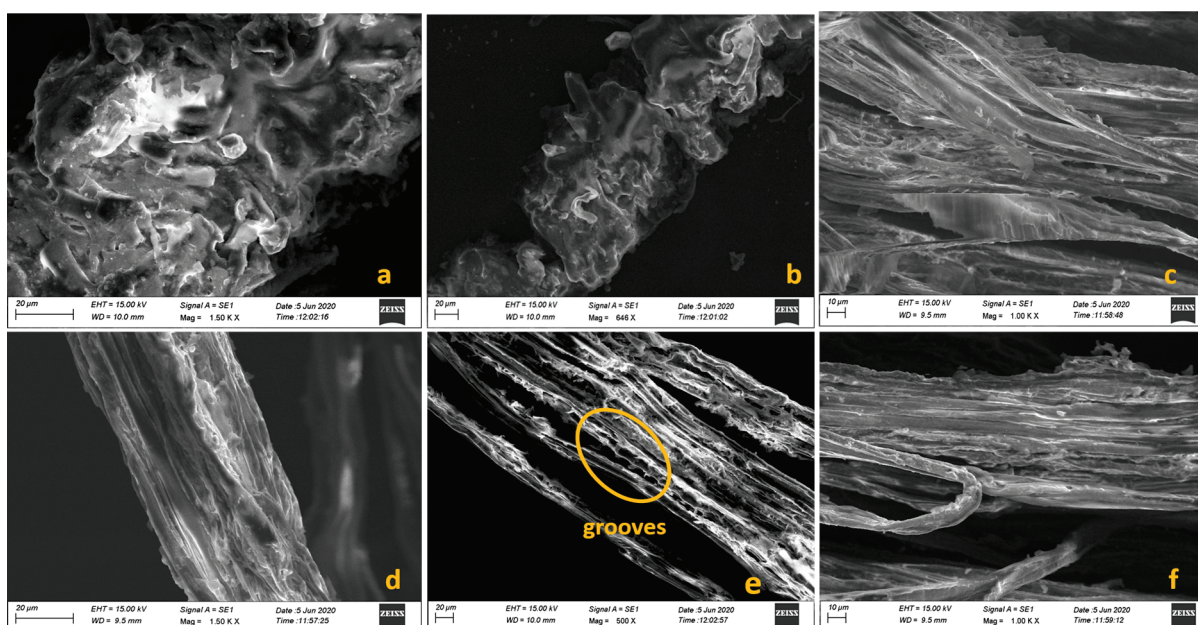
**Table 4.** CHNS analysis of BP fiber.

Sample	N%	C%	H%	S%	Weight (mg)
0.1 M KOH-treated	0.93	41.66	6.60	ND	7.60
Untreated	0.84	39.75	6.30	ND	7.12

ND—not detected.

#### 4.4. FESEM Analysis

The surface characteristics of both untreated and 0.1 M alkali-treated BP fibers are depicted in Figure 3a–f. SEM analysis is highly used to question the failure approach at the micro level [57]. The presence of small peaks against the long stripes is seen in the raw fiber. Epidermal projections appear on the longitudinal surface. The clouded irregularities in Figure 3a could be part of non-cellulosic debris [58]. This imperfection is removed in the alkaliized fibers. It is assumed that the KOH treatment has washed away most of the oil and waxy impurities tied up with the microfibrils, generating a rough interface on the top of the fibers. The elimination of non-cellulosic structures, mainly wax and hemicellulose, could have created fine grooves along the axis. This might greatly improve the expansive adhesion with the matrix interface [41]. The axial arrangement of treated fibrils is more coordinated than the raw fiber.

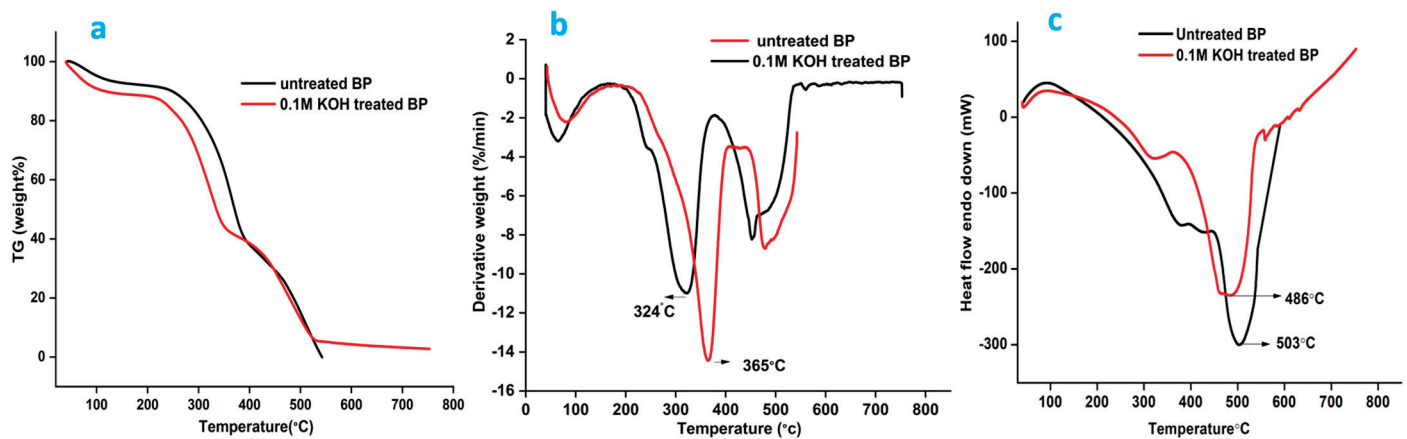


**Figure 3.** (a–c) SEM photographs of raw BP, (d–f) SEM photographs of 0.1 M KOH treated BP.

#### 4.5. Thermogravimetric Analysis

The thermal nature of BP was monitored between 40 and 800 °C at a heating rate of 20 °C/min. The Tg-dta and DSC curves are provided in Figure 4a,b. Three-step thermal degradation was observed in both fibers. The initial stage of mass loss is anticipated due to the evaporation of moisture present in the fiber [59,60]. The degradation pattern observed

in the dtg graph of both fibers between 200 and 260 °C is because of the elimination of hemicellulose. The quick dismissal of cellulose occurs around 240–350 °C leaving anhydro cellulose and levoglucosan [61]. A mass loss of 50 and 45.06% was registered for the raw and treated BP in the second stage, which concerns the exclusion of hemicellulose, lignin, and a tiny fraction of celluloses. The swift reaction is cascaded to the next step with the huge dismissal of hemicellulose. Lignin degradation is registered between the range 280 and 500 °C [62]. Patterns of mass loss noted around specific temperatures are shown in Table 5.



**Figure 4.** (a). Thermogravimetry plot of untreated and alkalinized Butea fiber; (b). differential thermogravimetry plot of untreated and alkalinized BP; (c). differential scanning calorimetry curve of raw and alkalinized BP.

**Table 5.** Mass loss with temperature from TG.

Fibers	Temperature (°C)	Mass Loss (%)	Residual Char (%)
Raw BP	54–251	17.72	0.4
	251–394	50.78	
	394–540	39.1	
KOH-treated BP	42–209	11.68	2.59
	209–356	45.06	
	356–544	40.67	

DTG shows that the maximum degradation peak for the alkali-treated fibers has been backtracked to 324 °C compared to that of the raw fiber, which was marked at 365 °C. Alkali action might have dismissed lignin, and hence, the treated fibers have noticed an early decomposition. Minor peaks were noted for the raw and alkalinized BP between 400 and 500 °C. Removal of lignin could have occurred within this limit. Weight loss of fibers was stabilized around 500 °C leaving the residues [63]. Other cellulosic fibers like *Eucalyptus grandis* and *Pinus taeda* spotted their maximum decomposition temperatures at 353 °C and 360 °C [61].

#### 4.6. Differential Scanning Calorimetry

The DSC curves are plotted in Figure 4c. As the temperature increases, notable peaks appear, signaling various thermal events or transitions taking place within the fiber. A prominent endothermic peak was obtained for the KOH-treated fibers at 486 °C. It indicates the pyrolysis and exclusion of lignified compounds, leaving behind char. For the untreated profile, a peak was spotted at 503 °C, owing to the loss of diversified functional groups of lignin. This peak value clearly correlates with the elevated decomposition temperature indicated in the DTG curve. A minor peak was spotted at 360 and 330 °C in the raw and treated BP, marking the removal of cellulose and hemicelluloses. A small hump seen

initially around 100 °C in both fibers is because of moisture removal [64]. All the outcomes show that BP fiber can be signed in for making fiber reinforcement composites as long as its thermal stand-by temperature does not exceed 240 °C.

#### 4.7. Activation Energy of Fibers

The kinetic activation energy (Ea) of BP was determined using the Coast–Redfern method [65].

$$\log \left[ \frac{-\log(1 - \alpha)}{T^2} \right] = \log \frac{AR}{\beta Ea} \left[ 1 - \frac{2RT}{Ea} \right] = \frac{Ea}{2.303RT} \tag{8}$$

Ea was estimated through linear interpolation of data points between  $\log[-\log(1 - \alpha)/T^2]$  and  $1000/T$ . The plot is shown in Figure 5. It speaks more about the aptness of the fibers to be used in composite making. Ea of cellulose fibers show different patterns due to variations in the fiber contents and structure [66].

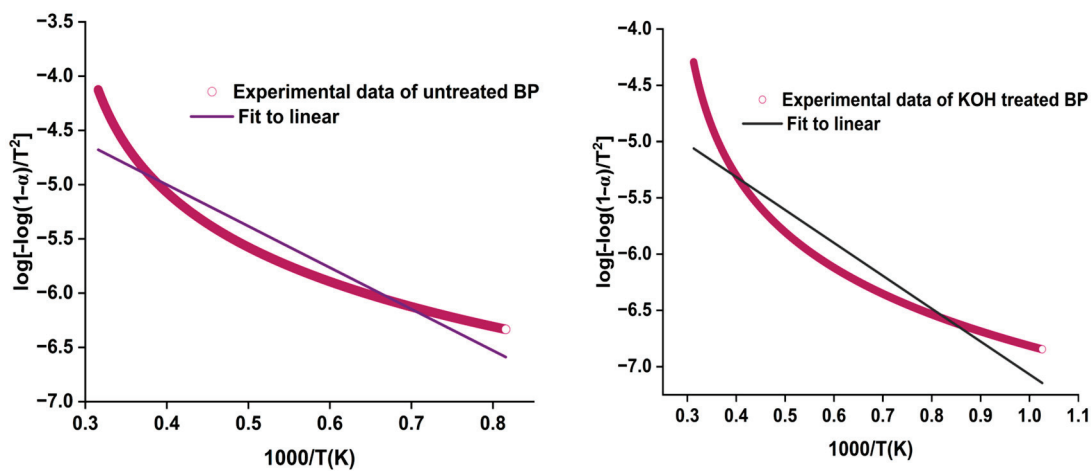


Figure 5. Ea curve of raw and KOH-treated BP.

The activation energy calculated for the raw BP ( $Ea = 73.15$  kJ/mol) was higher than for alkalinized fiber ( $Ea = 55.95$  kJ/mol). The activation energy has its impact more on the untreated fiber rather than the alkalinized BP. The thermal stability of green fibers is primarily determined by their decomposition temperature. The kinetic activation energy (Ea) values of other fibers are: Prosopis juliflora (76.72 kJ/mol), C. quadrangularis (74.18 kJ/mol), and Coccinia grandis (82.3 kJ/mol) [33,67]. The thermal outcomes of Butea fibers are shown in Table 6.

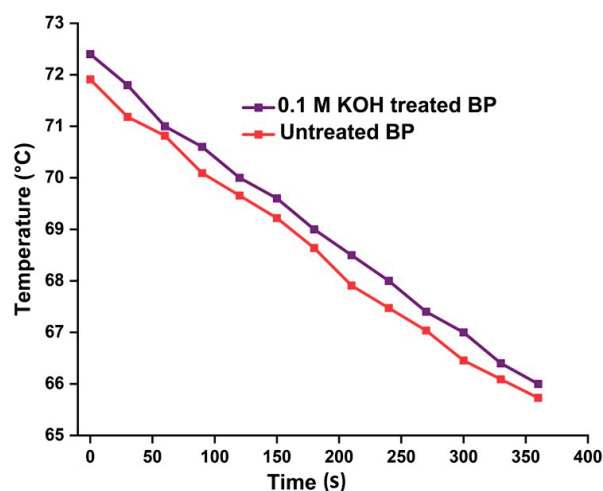
Table 6. Thermal outcomes of Butea parviflora fibers.

Fibers	Activation Energy (Ea)	Max Degradation Temperature (°C)	Thermal Conductivity (K)
Raw BP	73.15 kJ/mol	365	0.029 W/mk
Alkalinized BP	55.95 kJ/mol	324	0.020 W/mk

#### 4.8. Thermal Conductivity

Natural fiber-based materials are highly influential because of their potential insulation behavior. The thermal conductivity (K) of untreated and alkalinized BP fiber, found using Lee’s disc method, was  $K = 0.029 \text{ Wm}^{-1}\text{k}^{-1}$  and  $K = 0.020 \text{ Wm}^{-1}\text{k}^{-1}$ . Thermal conductivity plots of BP fibers are shown in Figure 6. K values of BP fibers are much lower than wood-based thermal insulation foam ( $k = 0.038 \text{ Wm}^{-1}\text{k}^{-1}$ ) [68]. The activity was performed at two Lee’s disc setups at room temperature, with the fibers woven tightly without void spaces. The steady temperature of the untreated and 0.1 M KOH-treated fibers are at 73.5 °C and 67.4 °C. Based on the observations, it can be deduced that as the material

thickness decreases, its conductivity also reduces, resulting in improved thermal insulation properties [69].



**Figure 6.** A linear plot of heat transport of raw and KOH-treated BP fibers.

The K value of the treated BP fibers is comparatively lower than other plant fibers, like corn stalks ( $K = 0.121 \text{ Wm}^{-1}\text{k}^{-1}$ ) and Areca husk fiber ( $K = 0.021 \text{ Wm}^{-1}\text{k}^{-1}$ ) [70]. The reduced K value of the alkalinized BP accounts for the amorphous content dwelling in the fiber. Lowered heat conducting behavior of BP fibers may lay a path to act as a better thermal insulator, or it can appease the synthetic thermal insulators the least.

#### 4.9. Single Fiber Tensile Test

Tensile properties of fiber predominantly gear on a number of things, like the maturity of plant parts, habitat, fibers chosen for testing, and so on. The presence of cellulose is a crucial factor influencing the mechanical behavior of fiber composites, as it exhibits a diverse range of polymeric actions [71,72]. The tensile strength of the alkalinized fiber increased by 192.97 MPa compared to the raw fiber's value of 92.64 MPa. Additionally, the treated fiber exhibits a high tensile modulus of 3.462 GPa, whereas the raw fiber had 2.164 GPa. The removal of amorphous components resulted in a more organized alignment of microfibrils along the fiber axis, thereby significantly enhancing the strength of the fibers.

Higher MFA ( $\alpha$ ) might result in poor fiber orientation. The tensile values are on the rise when the MFA is low and vice versa [40]. The elongation at break and strain experienced by the fibers play a crucial role in enhancing the MFA (microfibril angle). Higher MFA introduces higher ductility of fibers, which is also dependent on the orientation of microfibrils. Meanwhile, the MFA ( $\alpha$ ) of treated fiber ( $19.67 \pm 10.49^\circ$ ) is lower than the raw fiber ( $21.11 \pm 14.08^\circ$ ). The range of MFA values of BP appease with the other fibers and can be introduced for composite reinforcements. A semiempirical relation shown in Equation 9 was formulated by Satyanarayanan et al. It relates to MFA and fiber elongation, and the relation agrees with the BP fibers as well [73].

$$\varepsilon = 2.78 + 7.28 \times 10^{-2}\theta + 7.7 \times 10^{-3}\theta^2 \quad (9)$$

where  $\varepsilon$  is the % elongation, and  $\theta$  is the MFA with the cellulose content. These tensile values of Butea fibers were compared with various fibers in Table 7.

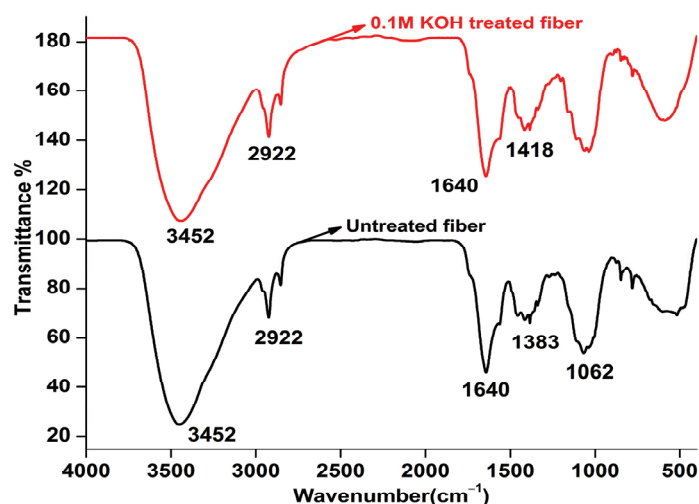


**Table 7.** Tensile properties of BP and other natural fibers.

Fibers	Tensile Strength (MPa)	Young's Modulus (GPa)	Elongation at Break (%)	Microfibril Angle (°)	References
Raw BP	92.64	2.164	7.2 ± 3.1	21.11 ± 14.08	Present work
Alkalized BP	192.97	3.462	6.2 ± 1.7	19.67 ± 10.49	Present work
Napier grass	75	6.8	2.8	-	[74]
Cordia dichotoma	36.2	3.6	2.0	-	[75]
Sansevieria ehrenbergii	50–585	1.5–7.67	2.8–21.7	-	[76]
Aerial roots of Banyan	19.37 ± 7.72	1.8 ± 0.40	1.8 ± 0.40	10.88 ± 1.198	[40]
Pennisetum purpureum	73 ± 6	5.68 ± 0.14	1.40 ± 0.23	-	[77]

#### 4.10. FTIR Analysis

Spectroscopic investigation on fibers gives a detailed account of the structure and presence of constituents binding with the fiber arrangements like cellulose, hemicellulose, pectin, lignin, and others [78]. The FTIR absorption peak of the raw and treated fibers are provided in Figure 7, and the spectroscopic assignments are listed in Table 8. The presence of a prominent band in the range of 3600–3000  $\text{cm}^{-1}$  can be attributed to the stretching of hydrogen-bonded O–H groups in cellulose and/or hemicellulose [79]. A strong peak at 2922 and 2916  $\text{cm}^{-1}$  of fibers is the outcome of the C–H stretching vibration of cellulose [80,81]. Due to the free vibration of the carboxyl group, a peak is visible in both fibers at 1640  $\text{cm}^{-1}$  [44].

**Figure 7.** FTIR image of raw and 0.1 M KOH-treated BP.**Table 8.** Spectroscopic vibrations in BP fibers.

Wavenumber ( $\text{cm}^{-1}$ )		Vibrational Band Assignments
Raw BP	KOH-Treated BP	
3451	3452	O–H stretching with hydrogen bonding in cellulose/hemicellulose
2922	2916	C–H stretching of cellulose
2850	2850	C–H stretching of hemicelluloses
1644	1644	Stretching of C=O in the acetyl group of hemicellulose
-	1418	C–H <sub>2</sub> symmetric bending in cellulose
1383	-	Asymmetric stretching of C–O–C in lignin
1064	-	C–O and C–C stretching of cellulose
847	-	$\beta$ -glycosidic linkage in monosaccharides
781	781	CO stretching
517	-	Off-plane OH bending

Asymmetric stretching of C–O–C in lignin caused a vibration in the raw fiber at  $1383\text{ cm}^{-1}$ , whereas the vibration was removed in the treated fibers. Alkaline reagents facilitate the breakdown of lignin into smaller, low-molecular-weight compounds [61,82]. An observable peak split was noticed around  $1064\text{ cm}^{-1}$  in the raw BP due to O–H vibrations [83,84]. A glitch noted at  $847\text{ cm}^{-1}$  in the raw BP has been unseen in the treated BP. Slight differences in the vibrations of functional groups were observed between the raw and alkalinized BP. These variances can be attributed to the removal of specific chemical groups during the alkalization process.

## 5. Conclusions

The aptness of raw and 0.1 M KOH-treated *Butea parviflora* (BP) fiber to be consumed for green composites was examined, and the following observations were drawn. The density and fineness of the alkalinized fiber have risen to (1.34 g/cc) and 346 tex, then the raw fiber, which is (1.23 g/cc) and 312 tex. The chemical composition of fibers clearly witnessed the changes in the levels of cellulose and hemicellulose between the raw and alkalinized fibers cellulose hiked to 60.72% while hemicellulose dropped from 40 to 19% in the alkalinized BP. The elimination of wax and pectin has a significant impact on the semicrystalline fiber, resulting in enhanced crystallinity. XRD analysis revealed a substantial increase in cellulose content (up to 86.03%) and an enlargement in crystallite size (8.04 nm) after the treatment. FTIR assignments marked slender vibrational changes in the raw and KOH-treated fiber.

The SEM images neatly distinguish the presence and absence of components on the fiber surface, aiding in the analysis of their effective bonding with the matrix phase. Due to their low thermal conductivity ( $K = 0.020\text{ W/mK}$ ), BP fibers are suitable to act as thermal insulators in structural applications. Choosing natural fibers for thermal insulation would significantly reduce carbon footprints compared to synthetic insulators.

Complete analysis of the Tg-dta and DSC studies provided insights into the mass loss of cellulosic and amorphous components at specific temperatures. From the DTG curves, degradation peaks for *Butea* fibers were observed. The maximum temperature up to which the fibers can stay active was noted to be around  $240\text{ }^{\circ}\text{C}$ . The activation energy of the raw fiber ( $E_a = 73.15\text{ kJ/mol}$ ) was higher than that of the treated fiber, indicating that the thermal potentials of the raw fibers are better than the treated BP fibers.

Increments in the crystallinity values and cellulose content directly influence the tensile behavior, showing an abrupt rise in the tensile values of raw BP from 92.64 to 192.97 MPa for the alkalinized BP. Only the thermal behavior of raw fibers showed a trifling swiftness than the KOH-treated BP. However, all the properties of treated fibers, except the thermal outcome, surpass those of the untreated fiber.

Summing up the text, the present work highlights the enormity of *Butea parviflora* fiber through various studies and analyses. The low density, high crystallinity, and thermal stability of BP fibers differentiate its novelty from other green fibers available in the market. It can stand as a suitable contender in the global market of composites in minimizing carbon emissions and safeguarding green territory. The findings provide a positive way to introduce fiber as a reinforcement material in composite making. The impeccable assets of the plant fiber can be further harvested by subjecting them to various treatments along with assessing their properties.

**Author Contributions:** A.M.—Conceptualization, Data curation, Formal analysis, Methodology, Validation, Visualization, Writing—original draft, Writing—review and editing. R.K.P.—Conceptualization, Data curation, Formal analysis, Methodology, Supervision, Validation, Visualization, Writing—original draft, Writing—review and editing. K.P.A.—Conceptualization, Data curation, Formal analysis, Methodology, Supervision, Validation, Visualization, Writing—review and editing. S.A.—Data curation, Formal analysis, Methodology, Supervision, Validation, Visualization, Writing—review and editing. N.M.-C.—Data curation, Funding acquisition, Project administration, Validation, Writing—review and editing. A.R.-V.—Data curation, Project administration, Validation, Project administration, Visualization. All authors have read and agreed to the published version of the manuscript.

**Funding:** The author thanks Vicerrectoria de Investigacion y Desarrollo (VRID) y Direccion de Investigacion y Creacion Artistica DICA, Proyecto presentado al Concurso VRID-Iniciación 2022, VRID N°2022000449-INI, Universidad de Concepción, Concepción, Chile. Centro Nacional de Excelencia para la Industria de la Madera (ANID BASAL FB210015 CENAMAD), Pontificia Universidad Católica de Chile, Vicuña Mackenna 7860, Santiago, Chile, and Dirección de Investigación de la Universidad Católica de la Santísima Concepción, Concepción, Chile.

**Institutional Review Board Statement:** Not Applicable.

**Data Availability Statement:** Will be provided on request.

**Acknowledgments:** The authors gratefully appreciate the support provided by the Research scholar, M. Abisha (Reg. No. 20213042132004) PG & Research Department of Physics, Holy Cross College (Autonomous) Nagercoil, Affiliated to Manonmaniam Sundaranar University, Tirunelveli, 627012, Tamil Nadu, India.

**Conflicts of Interest:** The authors declare no conflict of interest.

## References

1. Arockiam, N.J.; Jawaid, M.; Saba, N. Sustainable Bio Composites for Aircraft Components. In *Sustainable Composites for Aerospace Applications*; Elsevier: Amsterdam, The Netherlands, 2018; pp. 109–123.
2. Jawaid, M.; Abdul Khalil, H.P.S. Cellulosic/Synthetic Fibre Reinforced Polymer Hybrid Composites: A Review. *Carbohydr. Polym.* **2011**, *86*, 1–18. [CrossRef]
3. Sanjay, M.; Yogesha, B. Studies on Natural/Glass Fiber Reinforced Polymer Hybrid Composites: An Evolution. *Mater. Today Proc.* **2017**, *4*, 2739–2747. [CrossRef]
4. Yusriah, L.; Sapuan, S.M.; Zainudin, E.S.; Mariatti, M. Characterization of Physical, Mechanical, Thermal and Morphological Properties of Agro-Waste Betel Nut (*Areca catechu*) Husk Fibre. *J. Clean. Prod.* **2014**, *72*, 174–180. [CrossRef]
5. Ali, A.; Shaker, K.; Nawab, Y.; Jabbar, M.; Hussain, T.; Militky, J.; Baheti, V. Hydrophobic Treatment of Natural Fibers and Their Composites—A Review. *J. Ind. Text.* **2018**, *47*, 2153–2183. [CrossRef]
6. Sepe, R.; Bollino, F.; Boccarusso, L.; Caputo, F. Influence of Chemical Treatments on Mechanical Properties of Hemp Fiber Reinforced Composites. *Compos. Part B Eng.* **2018**, *133*, 210–217. [CrossRef]
7. Huda, M.S.; Drzal, L.T.; Ray, D.; Mohanty, A.K.; Mishra, M. Natural-Fiber Composites in the Automotive Sector. In *Properties and Performance of Natural-Fibre Composites*; Elsevier: Amsterdam, The Netherlands, 2008; pp. 221–268.
8. Biswas, S.; Kindo, S.; Patnaik, A. Effect of Fiber Length on Mechanical Behavior of Coir Fiber Reinforced Epoxy Composites. *Fibers Polym.* **2011**, *12*, 73–78. [CrossRef]
9. Mohanty, A.K.; Misra, M.; Hinrichsen, G. Biofibres, Biodegradable Polymers and Biocomposites: An Overview. *Macromol. Mater. Eng.* **2000**, *276–277*, 1–24. [CrossRef]
10. Fiore, V.; Scalici, T.; Valenza, A. Effect of Sodium Bicarbonate Treatment on Mechanical Properties of Flax-Reinforced Epoxy Composite Materials. *J. Compos. Mater.* **2018**, *52*, 1061–1072. [CrossRef]
11. Rajeshkumar, G. An Experimental Study on the Interdependence of Mercerization, Moisture Absorption and Mechanical Properties of Sustainable Phoenix Sp. Fibre-Reinforced Epoxy Composites. *J. Ind. Text.* **2020**, *49*, 1233–1251. [CrossRef]
12. Popescu, C.-M.; Kavitha, S.A.; Krishna Priya, R.; Arunachalam, K.P.; Avudaiappan, S.; Maureira-Carsalade, N.; Roco-Videla, Á. Investigation on Properties of Raw and Alkali Treated Novel Cellulosic Root Fibres of Zea Mays for Polymeric Composites. *Polymers* **2023**, *15*, 1802. [CrossRef]
13. Arunachalam, K.P.; Avudaiappan, S.; Flores, E.I.S.; Parra, P.F. Experimental Study on the Mechanical Properties and Microstructures of Cenosphere Concrete. *Materials* **2023**, *16*, 3518. [CrossRef]
14. Avudaiappan, S.; Cendoya, P.; Arunachalam, K.P.; Maureira-Carsalade, N.; Canales, C.; Amran, M.; Parra, P.F. Innovative Use of Single-Use Face Mask Fibers for the Production of a Sustainable Cement Mortar. *J. Compos. Sci.* **2023**, *7*, 214. [CrossRef]
15. Arunachalam, K.P.; Avudaiappan, S.; Maureira, N.; Da Costa Garcia Filho, F.; Monteiro, S.N.; Batista, I.D.; de Azevedo, A.R.G. Innovative Use of Copper Mine Tailing as an Additive in Cement Mortar. *J. Mater. Res. Technol.* **2023**, *25*, 2261–2274. [CrossRef]
16. Sathish, S.; Karthi, N.; Prabhu, L.; Gokulkumar, S.; Balaji, D.; Vigneshkumar, N.; Ajeem Farhan, T.S.; AkilKumar, A.; Dinesh, V.P. A Review of Natural Fiber Composites: Extraction Methods, Chemical Treatments and Applications. *Mater. Today Proc.* **2021**, *45*, 8017–8023. [CrossRef]
17. Sivasubramanian, P.; Kalimuthu, M.; Palaniappan, M.; Alavudeen, A.; Rajini, N.; Santulli, C. Effect of Alkali Treatment on the Properties of Acacia Caesia Bark Fibres. *Fibers* **2021**, *9*, 49. [CrossRef]
18. Santhiarsa, I.G.N.N. Effects of Alkaline Treatment and Fiber Length towards the Static and Dynamic Properties of Ijuk Fiber Strengthened-Epoxy Composite. In Proceedings of the International Mechanical Engineering and Engineering Education Conferences, East Java, Indonesia, 7–8 October 2016; p. 030022.
19. Kaki, S.S.; Jabeen, T.; Reddy, J.R.C.; Ram Mohan, M.; Anjaneyulu, E.; Prasad, R.B.N.; Rao, B.V.S.K. Isolation and Physico-Chemical Characterization of Butea Parviflora Seed Oil. *Grasas Aceites* **2016**, *67*, e151. [CrossRef]

20. RajeshKumar, K.; Awoyera, P.O.; Shyamala, G.; Kumar, V.; Gurumoorthy, N.; Kayikci, S.; Romero, L.M.B.; Prakash, A.K. Structural Performance of Biaxial Geogrid Reinforced Concrete Slab. *Int. J. Civ. Eng.* **2022**, *20*, 349–359. [CrossRef]
21. Mayandi, K.; Rajini, N.; Pitchipoo, P.; Sreenivasan, V.; Jappes, J.W.; Alavudeen, A. A Comparative Study on Characterisations of *Cissus Quadrangularis* and *Phoenix Reclinata* Natural Fibres. *J. Reinf. Plast. Compos.* **2015**, *34*, 269–280. [CrossRef]
22. Li, X.; Tabil, L.G.; Panigrahi, S. Chemical Treatments of Natural Fiber for Use in Natural Fiber-Reinforced Composites: A Review. *J. Polym. Environ.* **2007**, *15*, 25–33. [CrossRef]
23. Prakash, S.O.; Sahu, P.; Madhan, M.; Johnson Santhosh, A. A Review on Natural Fibre-Reinforced Biopolymer Composites: Properties and Applications. *Int. J. Polym. Sci.* **2022**, *2022*, 7820731. [CrossRef]
24. Dorneles de Castro, B.; Machado Neves Silva, K.M.; Maziero, R.; de Faria, P.E.; Pereira Silva-Caldeira, P.; Campos Rubio, J.C. Influence of Gamma Radiation Treatment on the Mechanical Properties of Sisal Fibers to Use into Composite Materials. *Fibers Polym.* **2020**, *21*, 1816–1823. [CrossRef]
25. Mukhopadhyay, S.; Fangueiro, R. Physical Modification of Natural Fibers and Thermoplastic Films for Composites—A Review. *J. Thermoplast. Compos. Mater.* **2009**, *22*, 135–162. [CrossRef]
26. Moon, C.K.; Lee, J.-O.; Cho, H.H.; Kim, K.S. Effect of Diameter and Surface Treatment of Fiber on Interfacial Shear Strength in Glass Fiber/Epoxy and HDPE. *J. Appl. Polym. Sci.* **1992**, *45*, 443–450. [CrossRef]
27. Danso, H.; Martinson, D.B.; Ali, M.; Williams, J. Effect of Fibre Aspect Ratio on Mechanical Properties of Soil Building Blocks. *Constr. Build. Mater.* **2015**, *83*, 314–319. [CrossRef]
28. Abisha, M.; Priya, R.K.; Arunachalam, K.P.; Avudaiappan, S.; Saavedra Flores, E.I.; Parra, P.F. Biodegradable Green Composites: Effects of Potassium Permanganate (KMnO<sub>4</sub>) Treatment on Thermal, Mechanical, and Morphological Behavior of *Butea Parviflora* (BP) Fibers. *Polymers* **2023**, *15*, 2197. [CrossRef] [PubMed]
29. Truong, M.; Zhong, W.; Boyko, S.; Alcock, M. A Comparative Study on Natural Fibre Density Measurement. *J. Text. Inst.* **2009**, *100*, 525–529. [CrossRef]
30. Kathirselvam, M.; Kumaravel, A.; Arthanarieswaran, V.P.; Saravanakumar, S.S. Isolation and Characterization of Cellulose Fibers from *Thespesia Populnea* Barks: A Study on Physicochemical and Structural Properties. *Int. J. Biol. Macromol.* **2019**, *129*, 396–406. [CrossRef]
31. Fan, M.; Weclawski, B. Long Natural Fibre Composites. In *Advanced High Strength Natural Fibre Composites in Construction*; Elsevier: Amsterdam, The Netherlands, 2017; pp. 141–177.
32. Arthanarieswaran, V.P.; Kumaravel, A.; Saravanakumar, S.S. Characterization of New Natural Cellulosic Fiber from *Acacia Leucophloea* Bark. *Int. J. Polym. Anal. Charact.* **2015**, *20*, 367–376. [CrossRef]
33. Jebadurai, S.G.; Raj, R.E.; Sreenivasan, V.S.; Binoj, J.S. Comprehensive Characterization of Natural Cellulosic Fiber from *Coccinia Grandis* Stem. *Carbohydr. Polym.* **2019**, *207*, 675–683. [CrossRef]
34. Segal, L.; Creely, J.J.; Martin, A.E.; Conrad, C.M. An Empirical Method for Estimating the Degree of Crystallinity of Native Cellulose Using the X-ray Diffractometer. *Text. Res. J.* **1959**, *29*, 786–794. [CrossRef]
35. Sheeba, K.R.J.; Priya, R.K.; Arunachalam, K.P.; Avudaiappan, S.; Maureira-Carsalade, N.; Roco-Videla, Á. Characterisation of Sodium Acetate Treatment on *Acacia Pennata* Natural Fibres. *Polymers* **2023**, *15*, 1996. [CrossRef] [PubMed]
36. Belouadah, Z.; Ati, A.; Rokbi, M. Characterization of New Natural Cellulosic Fiber from *Lygeum spartum* L. *Carbohydr. Polym.* **2015**, *134*, 429–437. [CrossRef] [PubMed]
37. Van De Velde, K.; Kiekens, P. Thermal Degradation of Flax: The Determination of Kinetic Parameters with Thermogravimetric Analysis. *J. Appl. Polym. Sci.* **2002**, *83*, 2634–2643. [CrossRef]
38. Alam, M. Lee's and Charlton's Method for Investigation of Thermal Conductivity of Insulating Materials. *IOSR J. Mech. Civ. Eng.* **2012**, *3*, 53–60. [CrossRef]
39. Gaba, E.W.; Asimeng, B.O.; Kaufmann, E.E.; Katu, S.K.; Foster, E.J.; Tiburu, E.K. Mechanical and Structural Characterization of Pineapple Leaf Fiber. *Fibers* **2021**, *9*, 51. [CrossRef]
40. Ganapathy, T.; Sathiskumar, R.; Senthamaraiannan, P.; Saravanakumar, S.S.; Khan, A. Characterization of Raw and Alkali Treated New Natural Cellulosic Fibres Extracted from the Aerial Roots of Banyan Tree. *Int. J. Biol. Macromol.* **2019**, *138*, 573–581. [CrossRef]
41. Maepa, C.E.; Jayaramudu, J.; Okonkwo, J.O.; Ray, S.S.; Sadiku, E.R.; Ramontja, J. Extraction and Characterization of Natural Cellulose Fibers from Maize Tassel. *Int. J. Polym. Anal. Charact.* **2015**, *20*, 99–109. [CrossRef]
42. Binoj, J.S.; Edwin Raj, R.; Sreenivasan, V.S.; Rexin Thusnavis, G. Morphological, Physical, Mechanical, Chemical and Thermal Characterization of Sustainable Indian Areca Fruit Husk Fibers (*Areca catechu* L.) as Potential Alternate for Hazardous Synthetic Fibers. *J. Bionic Eng.* **2016**, *13*, 156–165. [CrossRef]
43. Yu, H.; Yu, C. Study on Microbe Retting of Kenaf Fiber. *Enzyme Microb. Technol.* **2007**, *40*, 1806–1809. [CrossRef]
44. Saravanakumar, S.S.; Kumaravel, A.; Nagarajan, T.; Sudhakar, P.; Baskaran, R. Characterization of a Novel Natural Cellulosic Fiber from *Prosopis Juliflora* Bark. *Carbohydr. Polym.* **2013**, *92*, 1928–1933. [CrossRef]
45. Svärd, A.; Brännvall, E.; Edlund, U. Rapeseed Straw as a Renewable Source of Hemicelluloses: Extraction, Characterization and Film Formation. *Carbohydr. Polym.* **2015**, *133*, 179–186. [CrossRef] [PubMed]
46. Liu, M.; Meyer, A.S.; Fernando, D.; Silva, D.A.S.; Daniel, G.; Thygesen, A. Effect of Pectin and Hemicellulose Removal from Hemp Fibres on the Mechanical Properties of Unidirectional Hemp/Epoxy Composites. *Compos. Part A Appl. Sci. Manuf.* **2016**, *90*, 724–735. [CrossRef]



47. Komuraiah, A.; Kumar, N.S.; Prasad, B.D. Chemical Composition of Natural Fibers and Its Influence on Their Mechanical Properties. *Mech. Compos. Mater.* **2014**, *50*, 359–376. [CrossRef]
48. Pejic, B.M.; Kostic, M.M.; Skundric, P.D.; Praskalo, J.Z. The Effects of Hemicelluloses and Lignin Removal on Water Uptake Behavior of Hemp Fibers. *Bioresour. Technol.* **2008**, *99*, 7152–7159. [CrossRef] [PubMed]
49. Saha, P.; Manna, S.; Chowdhury, S.R.; Sen, R.; Roy, D.; Adhikari, B. Enhancement of Tensile Strength of Lignocellulosic Jute Fibers by Alkali-Steam Treatment. *Bioresour. Technol.* **2010**, *101*, 3182–3187. [CrossRef]
50. Manral, A.; Bajpai, P.K. Analysis of Natural Fiber Constituents: A Review. *IOP Conf. Ser. Mater. Sci. Eng.* **2018**, *455*, 012115. [CrossRef]
51. Zhu, Z.H.; Mo, B.H.; Hao, M.Y. Study of Contents Ratio of Cellulose, Hemicellulose and Lignin on the Mechanical Properties of Sisal Fibers Reinforced Polylactic Acid (PLA) Composites. *IOP Conf. Ser. Mater. Sci. Eng.* **2019**, *544*, 012012. [CrossRef]
52. Das, R.; Dash, C.; Behera, P.; Bisoyi, D.K. Influence Of Dewaxing on Mechanical Properties of Kapok Fiber-Reinforced Polymer Composite. *IOP Conf. Ser. Earth Environ. Sci.* **2022**, *1086*, 012054. [CrossRef]
53. Reddy, N.; Yang, Y. Characterizing Natural Cellulose Fibers from Velvet Leaf (*Abutilon theophrasti*) Stems. *Bioresour. Technol.* **2008**, *99*, 2449–2454. [CrossRef]
54. Pan, M.-Z.; Zhou, D.-G.; Deng, J.; Zhang, S.Y. Preparation and Properties of Wheat Straw Fiber-Polypropylene Composites. I. Investigation of Surface Treatments on the Wheat Straw Fiber. *J. Appl. Polym. Sci.* **2009**, *114*, 3049–3056. [CrossRef]
55. Kathirselvam, M.; Kumaravel, A.; Arthanarieswaran, V.P.; Saravanakumar, S.S. Assessment of Cellulose in Bark Fibers of *Thespesia Populnea*: Influence of Stem Maturity on Fiber Characterization. *Carbohydr. Polym.* **2019**, *212*, 439–449. [CrossRef] [PubMed]
56. Manimaran, P.; Senthamarai Kannan, P.; Murugananthan, K.; Sanjay, M.R. Physicochemical Properties of New Cellulosic Fibers from *Azadirachta Indica* Plant. *J. Nat. Fibers* **2018**, *15*, 29–38. [CrossRef]
57. Kamal, M. Scanning Electron Microscopy Study of Fiber Reinforced Polymeric Nanocomposites. In *Scanning Electron Microscopy*; InTech: London, UK, 2012.
58. Gonçalves, A.P.B.; De Miranda, C.S.; Guimarães, D.H.; De Oliveira, J.C.; Cruz, A.M.F.; Da Silva, F.L.B.M.; Luporini, S.; José, N.M. Physicochemical, Mechanical and Morphologic Characterization of Purple Banana Fibers. *Mater. Res.* **2015**, *18*, 205–209. [CrossRef]
59. Surya Rajan, B.; Balaji, M.A.S.; Saravanakumar, S.S. Effect of Chemical Treatment and Fiber Loading on Physico-Mechanical Properties of *Prosopis Juliflora* Fiber Reinforced Hybrid Friction Composite. *Mater. Res. Express* **2018**, *6*, 035302. [CrossRef]
60. Vijay, R.; Lenin Singaravelu, D.; Vinod, A.; Sanjay, M.R.; Siengchin, S.; Jawaid, M.; Khan, A.; Parameswaranpillai, J. Characterization of Raw and Alkali Treated New Natural Cellulosic Fibers from *Tridax Procumbens*. *Int. J. Biol. Macromol.* **2019**, *125*, 99–108. [CrossRef]
61. Seki, Y.; Sarikanat, M.; Sever, K.; Durmuşkahya, C. Extraction and Properties of *Ferula communis* (Chakshir) Fibers as Novel Reinforcement for Composites Materials. *Compos. Part B Eng.* **2013**, *44*, 517–523. [CrossRef]
62. Maache, M.; Bezazi, A.; Amroune, S.; Scarpa, F.; Dufresne, A. Characterization of a Novel Natural Cellulosic Fiber from *Juncus effusus* L. *Carbohydr. Polym.* **2017**, *171*, 163–172. [CrossRef]
63. Prithivirajan, R.; Narayanasamy, P.; Al-Dhabi, N.A.; Balasundar, P.; Shyam Kumar, R.; Ponmurugan, K.; Ramkumar, T.; Senthil, S. Characterization of *Musa Paradisiaca* L. Cellulosic Natural Fibers from Agro-Discarded Blossom Petal Waste. *J. Nat. Fibers* **2020**, *17*, 1640–1653. [CrossRef]
64. Sinha, E.; Rout, S.K. Influence of Fibre-Surface Treatment on Structural, Thermal and Mechanical Properties of Jute Fibre and Its Composite. *Bull. Mater. Sci.* **2009**, *32*, 65–76. [CrossRef]
65. Paswan, S.K.; Kumari, S.; Kar, M.; Singh, A.; Pathak, H.; Borah, J.P.; Kumar, L. Optimization of Structure-Property Relationships in Nickel Ferrite Nanoparticles Annealed at Different Temperature. *J. Phys. Chem. Solids* **2021**, *151*, 109928. [CrossRef]
66. Yao, F.; Wu, Q.; Lei, Y.; Guo, W.; Xu, Y. Thermal Decomposition Kinetics of Natural Fibers: Activation Energy with Dynamic Thermogravimetric Analysis. *Polym. Degrad. Stab.* **2008**, *93*, 90–98. [CrossRef]
67. Senthamarai kannan, P.; Kathiresan, M. Characterization of Raw and Alkali Treated New Natural Cellulosic Fiber from *Coccinia Grandis*.L. *Carbohydr. Polym.* **2018**, *186*, 332–343. [CrossRef] [PubMed]
68. Siciliano, A.P.; Zhao, X.; Fedderwitz, R.; Ramakrishnan, K.; Dai, J.; Gong, A.; Zhu, J.Y.; Kośny, J.; Hu, L. Sustainable Wood-Waste-Based Thermal Insulation Foam for Building Energy Efficiency. *Buildings* **2023**, *13*, 840. [CrossRef]
69. Zhou, X.; Zheng, F.; Li, H.; Lu, C. An Environment-Friendly Thermal Insulation Material from Cotton Stalk Fibers. *Energy Build.* **2010**, *42*, 1070–1074. [CrossRef]
70. Chethan, G.; Sunil, K.C.; Sandesh, A.; Narayana, Y. Determination of Thermal Conductivity of Areca Husk Fiber by Lee's Disc Method. *Res. J. Chem. Env.* **2020**, *24*, 17–20.
71. Divyah, N.; Prakash, R.; Srividhya, S.; Avudaiappan, S.; Guindos, P.; Carsalade, N.M.; Arunachalam, K.P.; Noroozinejad Farsangi, E.; Roco-Videla, Á. Experimental and Numerical Investigations of Laced Built-Up Lightweight Concrete Encased Columns Subjected to Cyclic Axial Load. *Buildings* **2023**, *13*, 1444. [CrossRef]
72. Jayanthi, V.; Avudaiappan, S.; Amran, M.; Arunachalam, K.P.; Qader, D.N.; Delgado, M.C.; Saavedra Flores, E.I.; Rashid, R.S.M. Innovative Use of Micronized Biomass Silica-GGBS as Agro-Industrial by-Products for the Production of a Sustainable High-Strength Geopolymer Concrete. *Case Stud. Constr. Mater.* **2023**, *18*, e01782. [CrossRef]

73. Djafari Petroudy, S.R. Physical and Mechanical Properties of Natural Fibers. In *Advanced High Strength Natural Fibre Composites in Construction*; Elsevier: Amsterdam, The Netherlands, 2017; pp. 59–83.
74. Kommula, V.P.; Reddy, K.O.; Shukla, M.; Marwala, T.; Rajulu, A.V. Physico-Chemical, Tensile, and Thermal Characterization of Napier Grass (Native African) Fiber Strands. *Int. J. Polym. Anal. Charact.* **2013**, *18*, 303–314. [CrossRef]
75. Jayaramudu, J.; Maity, A.; Sadiku, E.R.; Guduri, B.R.; Varada Rajulu, A.; Ramana, C.V.V.; Li, R. Structure and Properties of New Natural Cellulose Fabrics from *Cordia Dichotoma*. *Carbohydr. Polym.* **2011**, *86*, 1623–1629. [CrossRef]
76. Sathishkumar, T.P.; Navaneethakrishnan, P.; Shankar, S.; Rajasekar, R. Characterization of New Cellulose *Sansevieria Ehrenbergii* Fibers for Polymer Composites. *Compos. Interfaces* **2013**, *20*, 575–593. [CrossRef]
77. Ridzuan, M.J.M.; Abdul Majid, M.S.; Afendi, M.; Aqmariah Kanafiah, S.N.; Zahri, J.M.; Gibson, A.G. Characterisation of Natural Cellulosic Fibre from *Pennisetum Purpureum* Stem as Potential Reinforcement of Polymer Composites. *Mater. Des.* **2016**, *89*, 839–847. [CrossRef]
78. Fan, M.; Dai, D.; Huang, B.; Fan, M.; Dai, D.; Huang, B. Fourier Transform Infrared Spectroscopy for Natural Fibres. In *Fourier Transform: Materials Analysis*; BoD—Books on Demand: Norderstedt, Germany, 2012. [CrossRef]
79. Amroune, S.; Bezazi, A.; Belaadi, A.; Zhu, C.; Scarpa, F.; Rahatekar, S.; Imad, A. Tensile Mechanical Properties and Surface Chemical Sensitivity of Technical Fibres from Date Palm Fruit Branches (*Phoenix dactylifera* L.). *Compos. Part A Appl. Sci. Manuf.* **2015**, *71*, 95–106. [CrossRef]
80. Manimaran, P.; Saravanakumar, S.S.; Mithun, N.K.; Sentharamaikannan, P. Physicochemical Properties of New Cellulosic Fibers from the Bark of *Acacia arabica*. *Int. J. Polym. Anal. Charact.* **2016**, *21*, 548–553. [CrossRef]
81. Reddy, K.O.; Uma Maheswari, C.; Muzenda, E.; Shukla, M.; Rajulu, A.V. Extraction and Characterization of Cellulose from Pretreated *Ficus* (Peepal Tree) Leaf Fibers. *J. Nat. Fibers* **2016**, *13*, 54–64. [CrossRef]
82. Elalami, D.; Barakat, A. *Clean Energy and Resources Recovery*; Elsevier: Amsterdam, The Netherlands, 2021; ISBN 9780323852234.
83. Hossain, S.; Jalil, M.A.; Islam, T.; Rahman, M.M. A Low-Density Cellulose Rich New Natural Fiber Extracted from the Bark of Jack Tree Branches and Its Characterizations. *Heliyon* **2022**, *8*, e11667. [CrossRef] [PubMed]
84. Sandak, J.; Niemz, P.; Hänsel, A.; Mai, J.; Sandak, A. Feasibility of Portable NIR Spectrometer for Quality Assurance in Glue-Laminated Timber Production. *Constr. Build. Mater.* **2021**, *308*, 125026. [CrossRef]

**Disclaimer/Publisher’s Note:** The statements, opinions and data contained in all publications are solely those of the individual author(s) and contributor(s) and not of MDPI and/or the editor(s). MDPI and/or the editor(s) disclaim responsibility for any injury to people or property resulting from any ideas, methods, instructions or products referred to in the content.



## Article

# Marginal Micro-Seal and Tensile Bond Strength of a Biopolymer Hybrid Layer Coupled with Dental Prosthesis Using a Primerless-Wet System

Morakot Piemjai <sup>1,\*</sup>, Onusa Waleepitackdej <sup>1</sup> and Franklin Garcia-Godoy <sup>2,3</sup><sup>1</sup> Department of Prosthodontics, Faculty of Dentistry, Chulalongkorn University, Bangkok 10330, Thailand<sup>2</sup> Department of Bioscience Research, College of Dentistry, University of Tennessee Health Science Center, Memphis, TN 38163, USA<sup>3</sup> Adjunct Faculty, The Forsyth Institute, Cambridge, MA 02142, USA

\* Correspondence: tmorakot@chula.ac.th

**Abstract:** The aim of this study is to compare the marginal seal and tensile bond strength (TBS) of prostheses fixed to enamel-dentin using different adhesive systems. Resin-composite inlays directly fabricated from Class V cavities of extracted human molars/premolars and mini-dumbbell-shaped specimens of bonded enamel-dentin were prepared for microleakage and tensile tests, respectively. Four adhesive systems were used: primerless-wet (1-1 etching for 10-, 30-, or 60-s, and 4-META/MMA-TBB), primer-moist (All-Bond2 + Duolink or Single-Bond2 + RelyX ARC), self-etch (AQ-Bond + Metafil FLO), and dry (Super-Bond C&B) bonding. Dye penetration distance and TBS data were recorded. Failure modes and characteristics of the tooth-resin interface were examined on the fractured specimens. All specimens in 10-, 30-, and 60-s etching primerless-wet, Super-Bond, and AQ-Bond had a microleakage-free tooth-resin interface. Primer-moist groups showed microleakage at the cementum/dentin-resin margin/interface. Significantly higher TBSs ( $p < 0.05$ ) were recorded in primer-less-wet and Super-Bond groups with the consistent hybridized biopolymer layer after the chemical challenge and mixed failure in tooth structure, luting-resin, and at the PMMA-rod interface. There was no correlation between microleakage and TBS data ( $p = -0.148$ ). A 1–3  $\mu\text{m}$  hybrid layer created in the 10–60 s primerless-wet technique, producing complete micro-seal and higher tensile strength than enamel and cured 4-META/MMA-TBB, may enhance clinical performances like Super-Bond C&B, the sustainable luting resin.

**Citation:** Piemjai, M.; Waleepitackdej, O.; Garcia-Godoy, F. Marginal Micro-Seal and Tensile Bond Strength of a Biopolymer Hybrid Layer Coupled with Dental Prosthesis Using a Primerless-Wet System. *Polymers* **2023**, *15*, 283. <https://doi.org/10.3390/polym15020283>

Academic Editor: Raffaella Striani

Received: 18 November 2022

Revised: 23 December 2022

Accepted: 25 December 2022

Published: 5 January 2023



**Copyright:** © 2023 by the authors. Licensee MDPI, Basel, Switzerland. This article is an open access article distributed under the terms and conditions of the Creative Commons Attribution (CC BY) license (<https://creativecommons.org/licenses/by/4.0/>).

**Keywords:** primerless-wet bonding; resin adhesive system; hybrid layer; tensile bond strength; micro-seal; luting resin; dental prosthesis; fixed prosthodontics

## 1. Introduction

Dental enamel naturally protects the dentin and pulp from invasion by external stimuli. Therefore, non- or minimally invasive restorations or prostheses that protect the enamel from tooth reduction, recurrent caries, or tooth fracture are crucial in maintaining healthy dentin and pulp. High tensile bond strength adhesives are required when restorations or prostheses are not sufficiently resistant to displacement under functional loading [1]. Severe tooth reduction to gain more retention, resistance form, or strength for restorations/prostheses removes dentin, especially when restoring with non-hybrid layer formation materials, such as amalgam restorations and dental prostheses fixed with acid-base cement.

The total-etch concept was developed to simplify bonding to both enamel and dentin by etching the entire cavity with 40% phosphoric acid gel [2]. Strong phosphoric acid demineralizes enamel deeper than mild acid [3]. Thus, demineralized enamel might remain after resin polymerization allowing oral acid penetration. However, monomer diffusion



into etched enamel is more accessible than demineralized dentin, as phosphoric acid-conditioned dentin collapses when air-dried [4]. Therefore, phosphoric acid demineralized dentin cannot provide adequate permeability for complete monomer impregnation in either dry or moist systems [4,5]. In addition, it leads to a leakage pathway [6,7], post-operative hypersensitivity, and secondary caries [8,9].

Ferric ions in an acid conditioner can aggregate glycosaminoglycan (GAG) in demineralized dentin and provide permeability for potential monomers to diffuse through completely in dry or wet conditions [6–11]. Therefore, a hybridized dentin with a leakage-free interface was formed [6–9]. Self-etch bonding systems and self-adhesive cement were introduced to simplify the bonding steps and minimize aggressive phosphoric acid etching on dentin. However, bonded restorations using these self-etching or self-adhesive systems could not reliably provide a leakage-free dentin-resin interface [12–15] because of the limitation of monomer diffusion through any smear layer into the intact dentin [14,16]. Ferric chloride (1%) in 1% citric acid aqueous conditioner (1-1), a mild acid for smear layer removal, and 4-methacryloyloxyethyl trimellitate anhydride in methyl methacrylate initiated by tri-*n*-butyl borane resin (4-META/MMA-TBB) can provide reliable hybridized dentin when wet bonding with primer in the long-range periods (10–60 s) of conditioning [10]. A 1–3  $\mu\text{m}$  hybridized dentin layer suggested that 1-1 conditioned dentin was sufficiently permeable for water to evaporate and for monomers to impregnate. Thus, only blot-drying with or without primer (primerless-wet bonding) can produce a complete hybrid layer that reinforces the dentin [10,17] and prevents dye penetration of direct restorations [7,17].

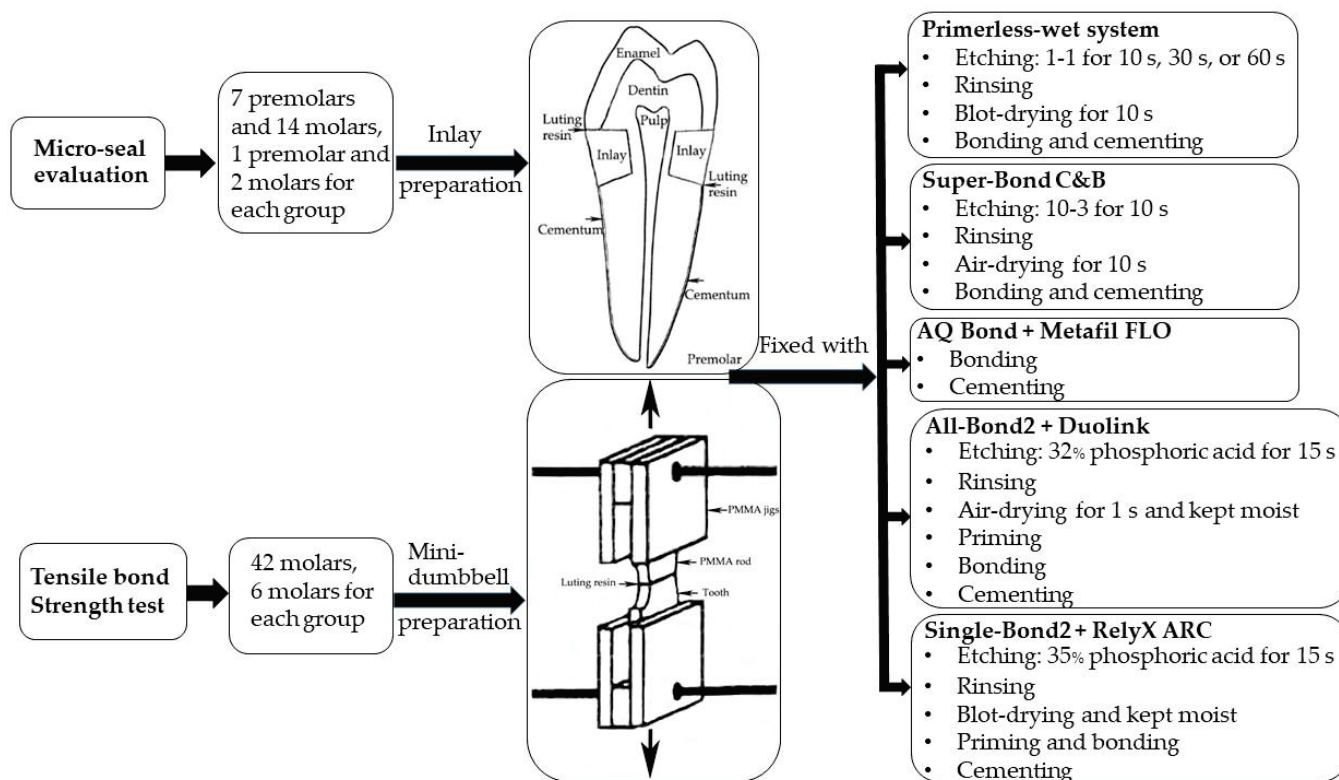
Dental clinical failures are often found in direct or indirect restorations and fixed partial prostheses due to secondary caries, especially at the cementum/dentin margin [18–21]. Detachment of restorations or prostheses is a minor complication that leads to failure [21–24]. The demineralized dentin, the defect, remains in restored-dentin, which may lead to a leakage pathway and recurrent caries [6,8,9], strongly influencing the failure of restorations or prostheses [18–21]. The hybrid layer formed by dry bonding using 10% citric acid and 3% ferric chloride aqueous solution (10-3) conditioned for 10 s and 4-META/MMA-TBB resin (Super-Bond C&B, Sun Medical, Shiga, Japan; a sustainable luting resin since 1983), provides a significantly higher 15-year survival with less secondary caries and prosthesis detachment complication rates of full coverage retainers than those of acid-base cement [21]. However more extended 10-3 etching period of 30–60 s creates demineralized dentin too deep ( $>4 \mu\text{m}$ ) to be fully impregnated by the monomers before starting polymerization. Thus, exposed demineralized dentin remains to allow leakage, caries, or pulp infection [8,21]. A tensile test using a mini-dumbbell-shaped bonded specimen [2,25] and a microleakage test [6,8] can detect this remaining demineralized dentin, the weakening part of the restored dentin.

We hypothesized that primerless-wet bonding could create a reliable hybrid layer on enamel-dentin and provide a complete micro-seal and tensile bond strength comparable with Super-Bond C&B. Moreover, a complete seal might not relate to the tensile bond strength of tooth-resin interface luting with various resin adhesives.

The objective of this study was to compare the dye penetration distance and the tensile bond strength at the tooth-resin interface of a prosthesis fixed to enamel-dentin using different adhesive systems: dry (Super-Bond C&B), moist with primer (All-Bond2 + Duoink or Single-Bond2 + RelyX ARC), self-etch (AQ-Bond + Metafil FLO), and primerless-wet (1-1 conditioner and 4-META/MMA-TBB resin) bonding.

## 2. Materials and Methods

Previously frozen extracted human molars and premolars without caries, restorations, or cracked lines were collected and stored in water at  $-20 \text{ }^{\circ}\text{C}$  for 2–3 months. Then, all teeth were randomly divided into two experimental groups of 7 premolars and 14 molars for micro-seal evaluation and 42 molars to prepare the mini-dumbbell-shaped specimens for tensile testing. The primary experimental steps are illustrated in Figure 1.



**Figure 1.** An illustrated diagram for the steps carried out in this experiment.

### 2.1. Micro-Seal Evaluation Using Dye Penetration

Class V cavities at the cementoenamel junction (CEJ) on the buccal and lingual surfaces of seven premolars and all axial surfaces for fourteen molars were outlined. A box cavity of  $2 \times 3$  mm and 1.5 mm depth with approximately  $5^\circ$  divergent axial walls was prepared with occlusal and gingival margins on enamel and cementum, respectively, using a diamond bur with an air-water sprayed high-speed handpiece. Resin composite inlays of  $2 \times 3 \times 1.5$  mm were directly fabricated from the cavities with light-cured resin composite (Metafil CX, Sun Medical, Shiga, Japan). Each inlay was light-cured for 60 s on both outer and inner surfaces. All cavities were randomly divided into 7 groups of 10 specimens (1 premolar and 2 molars) for different tooth conditionings and/or resin cement. Primerless-wet bonding using 1-1 conditioning for 10 s, 30 s, 60 s (Groups 1-1-10s, 1-1-30s, 1-1-60s respectively) and 4-META/MMA-TBB resin; and commercially available adhesive resin cement: Super-Bond C&B (Sun Medical, Shiga, Japan), All-Bond2 + Duolink (Bisco, Schaumburg, IL, USA), Single-Bond2 + RelyX ARC (3M ESPE, Saint Paul, MN, USA), or AQ-Bond Plus + Metafil FLO (Sun Medical, Shiga, Japan) was used to fix an inlay prosthesis into the cavity. The manipulation of commercial systems followed manufacturers' recommendations, as shown in Table 1, and the main chemical composition of luting adhesives and resin composite inlay, as shown in Table 2. Fine diamond burs in a high-speed handpiece were used to finish the restored margins after the polymerization of adhesives. After storing in water at  $37^\circ\text{C}$  for 24 h, all tooth surfaces except an area of the inlay and 1 mm away from the occlusal (enamel) and gingival (cementum) margins were coated with two layers of nail varnish (Pias, Bangkok, Thailand). Specimens were then immersed in 0.5% basic fuchsin dye for 24 h. After soaking, all specimens were cleaned with tap water before being vertically sectioned at the center of each restoration using a diamond disc with a slow-speed handpiece. The distance of dye penetration was measured under a stereomicroscope (ECLIPSE E400 POL, Nikon, Japan) at  $\times 50$ – $\times 200$  magnifications.

**Table 1.** Manipulation of tooth-conditioning, luting adhesive, and prosthesis cementation.

Systems	Primerless-Wet			Dry	Self-Etched	Moist with Primer	
Groups	1-1-10s	1-1-30s	1-1-60s	Super-Bond C&B	AQ-Bond	All-Bond2	Single-Bond2
Acid conditioner	1-1	1-1	1-1	10-3	-	32% phosphoric acid	35% phosphoric acid
Conditioning time	10 s	30 s	60 s	10 s	-	15 s	15 s
Rinse off	10 s	10 s	10 s	10 s	-	15 s	10 s
Surface treatment	Blot-dried 10 s			Air-dried 10 s	-	Air-dried 1 s, kept moist	Blot-dried and kept moist
Manipulations of luting adhesives	Mixed 4 drops of 4-META/MMA and 1 drop of TBB in a cool porcelain container applied using brush-dip technique with PMMA powder for auto-curing on the conditioned tooth-surface and resin-composite inlay or PMMA block prior fixation			Same as primerless-wet groups	Scrubbed sponge impregnated with monomers on tooth surface for 20 s, air-dried for 5 s, light-cured for 10 s. Applied metafil FLO on resin-composite inlay or PMMA block prior to fixation, light-cured for 60 s.	Mixed 1 drop of primer A: B, coated on conditioned tooth-surface 5 times, gently air-dried for 5 s, applied D&E resin, light-cured for 20 s. Mixed Duolink cement and applied on resin-composite inlay or PMMA block prior to fixation, light-cured for 60 s.	Applied Single-Bond 2 on conditioned tooth surface for 15 s, gently air-dried for 5 s, light cured for 10 s. Mixed RelyX ARC cement and applied on resin-composite inlay or PMMA block before fixation, light-cured 60 s.

**Table 2.** The main chemical composition of luting adhesives and resin composite inlay.

Materials	Chemical Composition
Primerless-wet	Etchant: 1% citric acid and 1% ferric chloride (1-1); water Monomers: 4-methacryloyloxyethyl trimellitate anhydride in methyl methacrylate initiated by tri- <i>n</i> -butyl borane (4-META/MMA-TBB) Powder: poly(methyl methacrylate) (PMMA)
Super-Bond C&B	Etchant: 10% citric acid and 3% ferric chloride (10-3); water Monomers: 4-META/MMA-TBB Powder: PMMA
AQ-Bond Plus Metafil FLO	Monomers: methyl methacrylate (MMA); 4-META; urethane dimethacrylate (UDMA); 2-hydroxyethyl methacrylate (HEMA); acetone; water Sponge: polyurethane foam; amine- <i>p</i> -toluenesulfonic acid sodium salt ( <i>p</i> -TSNa) Luting: UDMA; triethylene glycol dimethacrylate (TEGDMA); trimethylolpropane trimethacrylate (TMPT); barium glass
All-Bond2 Duolink	Etchant: 32% phosphoric acid; water Primer: 2% NTG-GMA (N-tolyglycine-glycidyl methacrylate); 16% BPDm (biphenyl dimethacrylate); acetone Bonding: bisphenol A-glycidyl methacrylate (bis-GMA); UDMA, HEMA Luting: bis-GMA; TEGDMA; UDMA; glass filler
Single-Bond2 RelyX ARC	Etchant: 35% phosphoric acid; water Bonding: bis-GMA; HEMA; dimethacrylates, ethanol, water; methacrylate functional copolymer of polyacrylic and polyitaconic acids Luting: bis-GMA; TEGDMA; zirconia/silica filler
Metafil CX	Inlay: UDMA; TEGDMA; TMPT; colloidal silica

## 2.2. Tensile Bond Strength Test

Forty-two extracted sound human molars without cracks were root-embedded in acrylic blocks (Formatray, Kerr, Orange, CA, USA). A 2 mm occlusal portion was horizontally removed using a sectioning machine (Isomet 1000 series 15, Buehler, Lake Bluff, IL, USA) to expose a surface which was then ground with a wheel diamond bur (111 Intensiv, Grancia, Switzerland). A prepared surface of 2 mm in width (0.5 mm of enamel/DEJ and 1.5 mm of dentin) and 4 mm in length was outlined with double-sided tape. One of the tooth conditionings and adhesive systems, as previously mentioned in the micro-leakage test (Table 1), was randomly selected to bond that area with a square PMMA rod (7 × 7 × 4 mm) to form a handle for tensile testing. A 2.0-mm thick vertical section

was prepared using the sectioning machine. A mini-dumbbell bonded specimen with a cross-section of  $3.0 \times 2.0$  mm was shaped using a diamond fissure bur (B11, GC Dental Industrial Co., Tokyo, Japan) operated in a high-speed handpiece under the air-water spray. All specimens were stored in  $37^\circ\text{C}$  water for 24 h prior to tensile testing ( $n = 6$ ) [2,10,16]. Each mini-dumbbell specimen was securely bonded to disposable PMMA jigs using 1-1-10s bonding on the tooth surface and self-cured acrylic (Unifast, Trad, GC Int. Co., Tokyo, Japan) on the PMMA surface to facilitate tensile testing [16]. An assembled specimen was aligned in a universal testing machine (Instron 8872, Norwood, MA, USA) and vertically loaded in tension at a crosshead speed of 1.0 mm/min. The force at failure was recorded in Newtons. The mode of failure, the cross-sectional area of the fractured surface, and the enamel and dentin area were examined under a stereomicroscope and SEM. Tensile bond strengths were calculated in MPa.

### 2.3. Characteristics Evaluation of Tooth-Resin Interfacial Biopolymer Layer

Fracture specimens from each bonding system were randomly selected and vertically sectioned (without epoxy embedding) into 1 mm thick pieces. The tooth-resin interface surface to be examined was finished with #600 and #1200 grit abrasive papers and finally polished with  $0.05\ \mu\text{m}$  alumina paste and then ultrasonically cleaned for 15 min. The chemical challenge, either soaking in 6 mol/L HCl for 30 s or soaking in 6 mol/L HCl for 30 s followed by 1% NaOCl for 60 min, was carried out to test the resistance of acidic and proteolytic degradation, akin to caries formation. For SEM examination, all polished and chemically soaked specimens were desiccated and gold-sputtered. The characteristics of the newly formed interfacial biopolymer layer between the tooth and cured resin were examined at  $\times 35$  to  $\times 5000$  magnifications.

### 2.4. Statistical Analysis

Normal distribution and homoscedasticity of dye penetration distance and tensile bond strength data were analyzed using one-sample Kolmogorov-Smirnov and Levene tests, respectively. In addition, Pearson correlation between leakage distance and tensile bond strength data was performed using SPSS for Windows version 22 (IBM Corporation, Somers, NY, USA). The significant difference was set at  $\alpha = 0.05$ .

## 3. Results

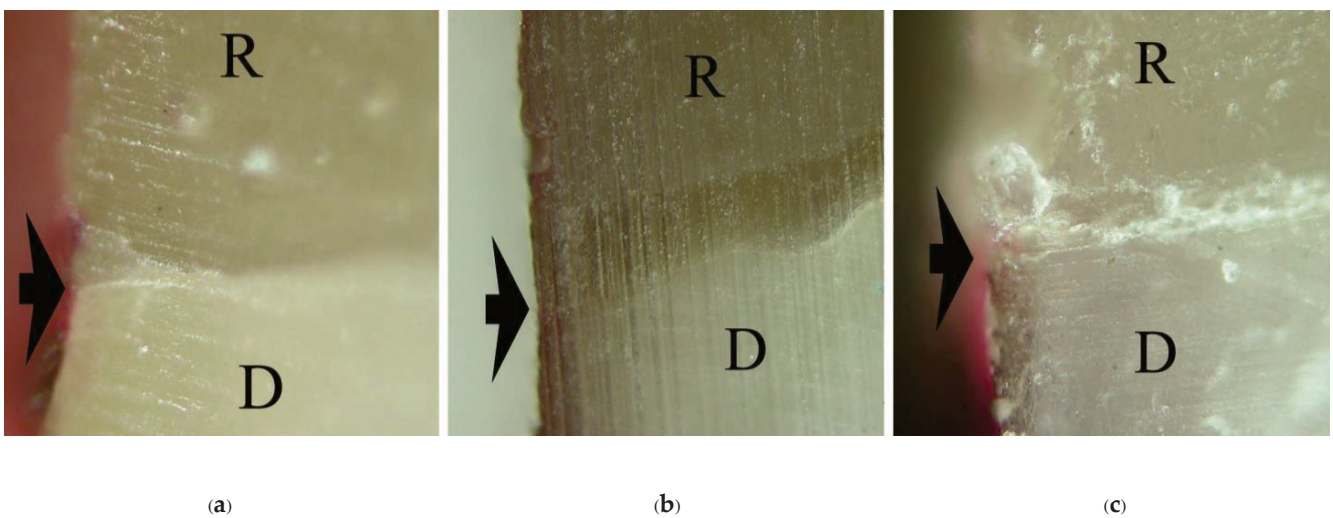
Means and standard deviations (SD) of dye penetration distance, tensile bond strength, and mode of failure for all groups are summarized in Table 3. No dye penetration at the cementum/dentin-resin interface was found in the primerless-wet groups (1-1-10s, 1-1-30s, 1-1-60 s) (Figure 2), Super-Bond C&B (Figure 3a), and AQ-Bond (Figure 3b) specimens and at the enamel-resin interface in all groups. No statistically significantly different dye penetration distance at the dentin-resin interfaces was found between All-Bond2 and Single-Bond2 when analyzed using a t-test. All specimens in these moist bonding with primer groups leaked at the dentin-resin interface (Figure 4).



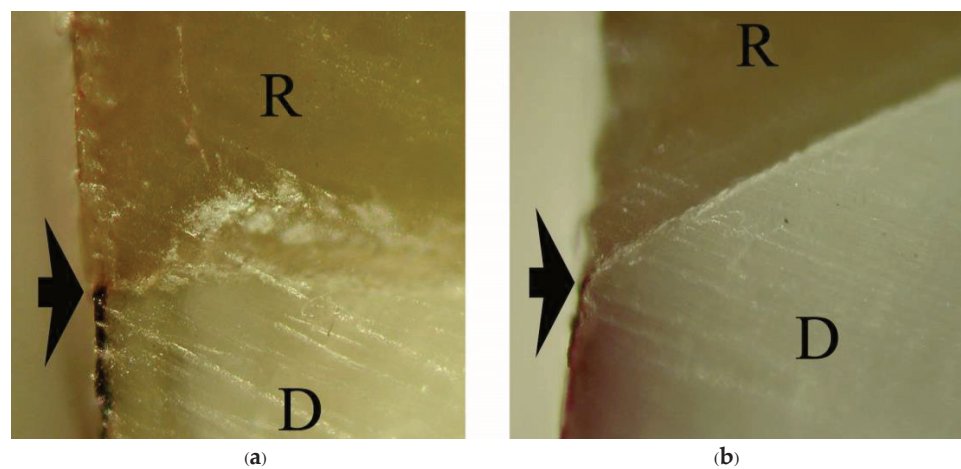
**Table 3.** Mean  $\pm$  SD of dye penetration distance at tooth-resin interface (n = 10), tensile bond strength, and failure modes of enamel/DEJ/dentin-resin dumbbell-shaped specimens (n = 6) for all groups.

Groups	Dye Penetration Distance (mm)		TBS (MPa)	Mode of Failure
	Enamel-Resin	Dentin-Resin		
1-1-10s	0	0	20.57 $\pm$ 3.83	E/DEJ/D, R, R/PMMA
1-1-30s	0	0	20.33 $\pm$ 1.81	E/DEJ/D, R, R/PMMA
1-1-60s	0	0	20.61 $\pm$ 1.81	E/DEJ/D, R, R/PMMA
Super-Bond	0	0	20.03 $\pm$ 2.38	E/DEJ/D, R, R/PMMA
Single-Bond2	0	0.228 $\pm$ 0.190	13.73 $\pm$ 8.82	E/DEJ/D, DD, R
All-Bond2	0	0.145 $\pm$ 0.878	10.85 $\pm$ 4.23	E/DEJ/D, DD, R
AQ-Bond	0	0	6.57 $\pm$ 3.50	HsE, R

0 = No dye penetration. E/DEJ/D = cohesive failure in enamel, DEJ or dentin, R = cohesive failure in luting resin, R/PMMA = failure at the resin-PMMA-rod interface, DD = failure at demineralized dentin-resin interface, HsE = failure in hybridized suspended enamel smears. There was no significant difference between groups connected with a vertical line ( $p > 0.05$ ).

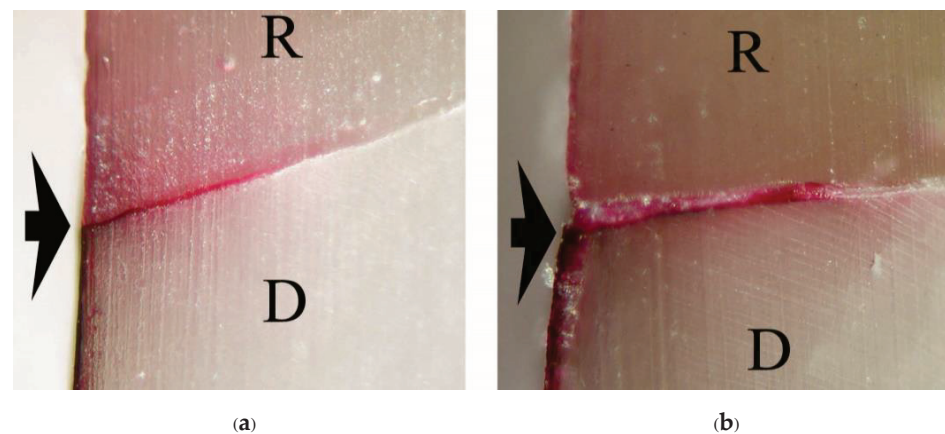


**Figure 2.** No dye penetration at the cementum/dentin-resin interface (arrowed) of primerless-wet bonding groups: (a) 1-1-10s, (b) 1-1-30s, (c) 1-1-60s (original  $\times 200$ , D = dentin, R = resin-composite in-lay).



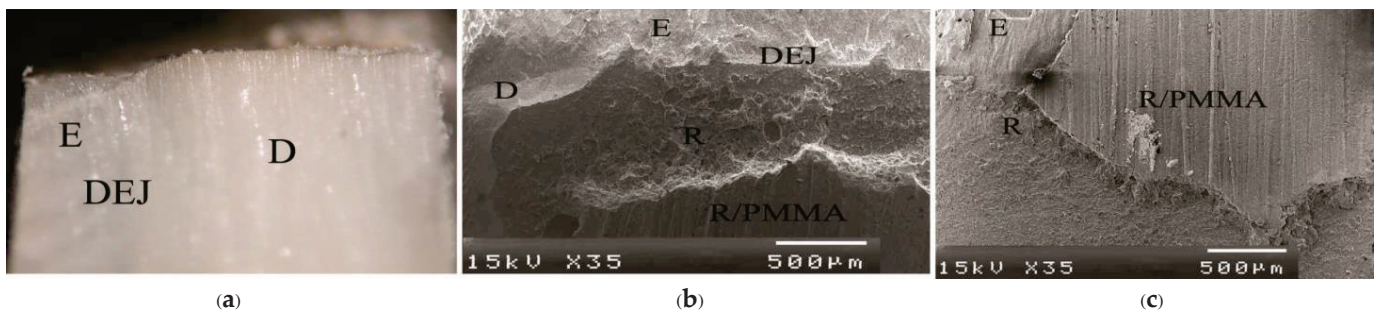
**Figure 3.** No dye penetration at the cementum/dentin-resin interface (arrowed) of Super-Bond (a) and AQ-Bond (b) specimens (original  $\times 200$ , D = dentin, R = resin-composite inlay).





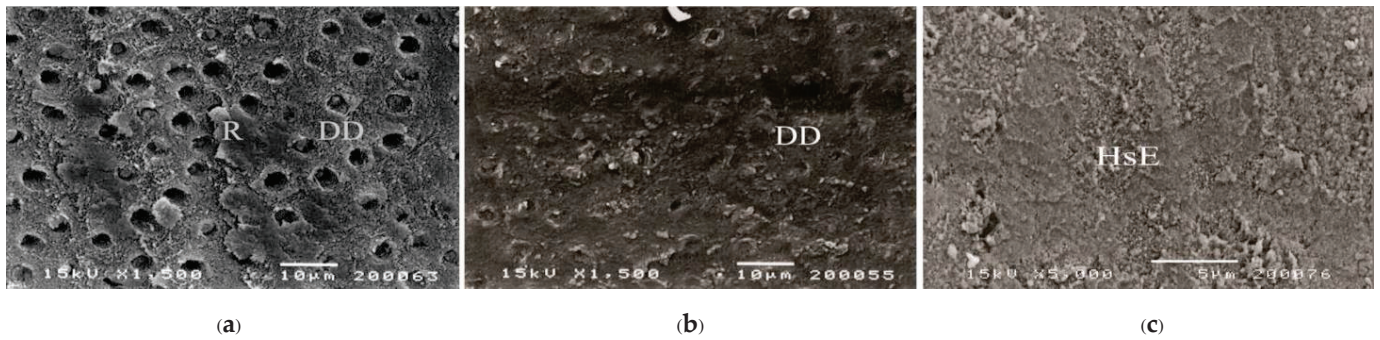
**Figure 4.** Dye penetration at the cementum/dentin-resin interface (arrowed) of moist bonding with primer groups: (a) All-Bond2, (b) Single-Bond2 (original  $\times 200$ , D = dentin, R = resin-composite inlay).

As a significant difference was found in the test of homogeneity of variances, Brown-Forsythe and Tamhane multiple comparisons were used to reveal a significant difference in tensile bond strength between groups. No significant difference in tensile bond strength was found among 1-1-10s, 1-1-30s, 1-1-60s, Super-Bond, and Single-Bond2; Single-Bond2, All-Bond2, and AQ-Bond groups. Cohesive failure originated in enamel followed by either dentino-enamel junction (DEJ), dentin, cured luting resin or adhesive failure at resin-PMMA rod interfaces mainly occurred in fractured specimens of primerless-wet and Super-Bond groups (Figure 5). In contrast, failure occurring in demineralized dentin or at the resin-demineralized dentin interface was found in Single-Bond2 (Figure 6a), and All-Bond2 fractured specimens (Figure 6b). The lowest tensile bond strength was measured in AQ-Bond specimens, where the original failure was found at the suspended resin-smear layer of the enamel-resin interface (Figure 6c).

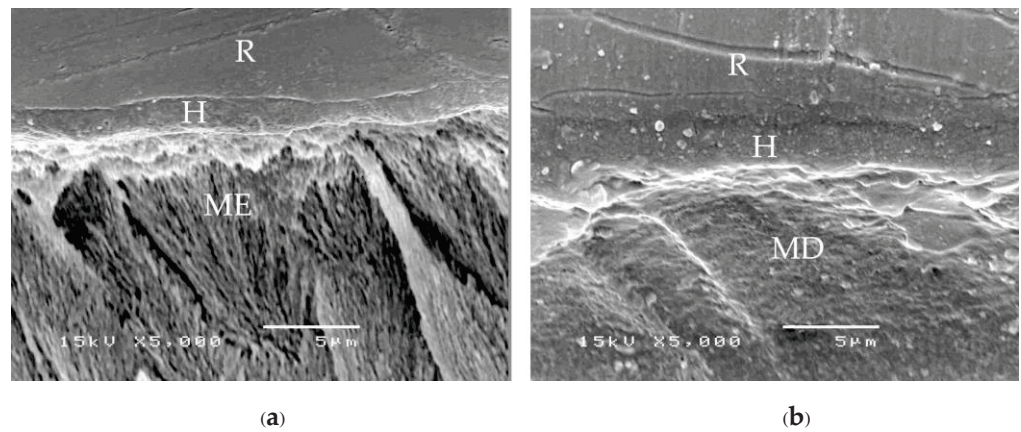


**Figure 5.** Stereo and SEM micrograph of the fractured surface showing cohesive failure originating in enamel followed by either DEJ, dentin, cured resin, or adhesive failure at resin-PMMA rod interfaces (R/PMMA) primarily found in primerless-wet and Super-Bond groups: sagittal view at  $\times 50$  magnification (a) and cross-sectional view of 1-1-60s (b) and Super-Bond (c) specimens (D = dentin, E = enamel, R = luting resin).

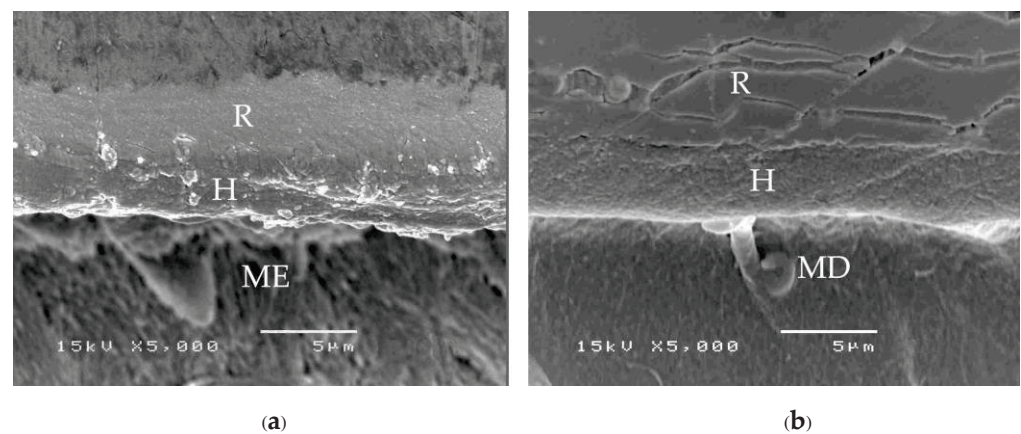
A consistent thickness of hybridized enamel or hybridized dentin after loading and the chemical challenge was found in primerless-wet (Figure 7) and dry bonding (Super-Bond C&B) (Figure 8) systems. A detached or degraded enamel- or dentin-resin interfacial layer was found in moist with primer (All-Bond2 and Single-Bond2) (Figure 9) and self-etch (AQ-Bond) (Figure 10) systems. The correlation between the dye penetration distance and the tensile bond strength data for the enamel and dentin-bonded interface was very weak (Pearson correlation =  $-0.148$ )



**Figure 6.** SEM micrograph of the fractured surface showing failure: in the remaining demineralized dentin of Single-Bond2 (a) and at the demineralized dentin-resin interface of All-Bond2 (b) moist bonding with primer specimens, and in the hybridized suspended smears at the enamel-resin interface of AQ-Bond (c) specimen (DD = demineralized dentin, HsE = hybridized suspended enamel smears, R = luting resin).

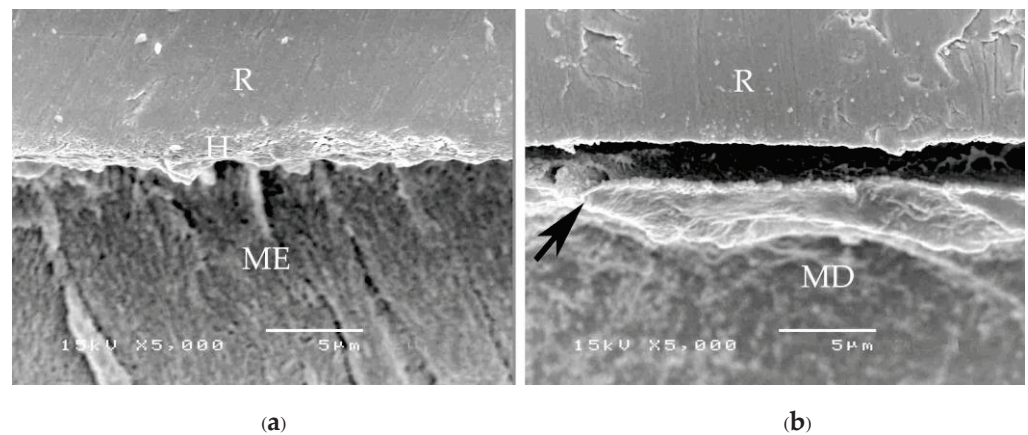


**Figure 7.** SEM micrographs of fractured specimens after chemical challenge demonstrating: the stable hybridized enamel (a) and hybridized dentin (b) of 1-1-30s primerless-wet specimens (H = hybrid layer, R = resin, ME = modified enamel, MD = modified dentin).

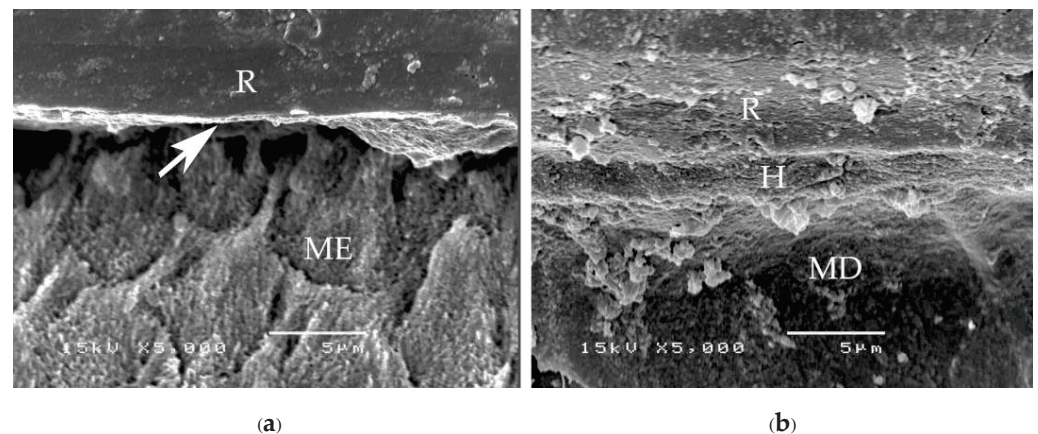


**Figure 8.** SEM micrographs of fractured specimens after chemical challenge demonstrating: the stable hybridized enamel (a) and hybridized dentin (b) of Super-Bond C&B specimens (H = hybrid layer, R = resin, ME = modified enamel, MD = modified dentin).





**Figure 9.** SEM micrographs of fractured specimens after chemical challenge demonstrating: the degraded hybridized enamel (a) and the detached and degraded dentin-resin interface (black arrow) of All-Bond2 specimens (b) (H = hybrid layer, R = resin, ME = modified enamel, MD = modified dentin).



**Figure 10.** SEM micrograph of fractured specimens after chemical challenge demonstrating: the degraded hybridized enamel (white arrow) (a) and the hybridized dentin (b) of AQ-Bond specimens (H = hybrid layer, R = resin, ME = modified enamel, MD = modified dentin).

#### 4. Discussion

The complete marginal seal, no significant differences in TBSs, and the same failure mode among primerless-wet and Super-Bond groups suggest that the milder acid of 1-1 conditioner using primerless-wet bonding could adequately prepare the etched enamel-dentin for 4-META/MMA-TBB resin to entirely impregnate as well as that of the 10-3 conditioner in dry bonding (Figures 2, 3a and 5, Table 3). Furthermore, long etching periods of 10–60 s of 1-1 dissolved less content of calcium ions, therefore even blot-drying without primer could provide the permeability of acid-etched enamel-DEJ-dentin for 4-META/MMA-TBB to penetrate completely before being polymerized to form a 1–3  $\mu\text{m}$  hybrid layer. Therefore, no adhesive failure at the tooth-resin interface was noticed with the average strength like dry bonding using 10-3 solution for 10 s etching of Super-Bond C&B.

The mode of failure originating on the enamel surface suggests that resin infiltration into acid-etched enamel-DEJ-dentin using primerless-wet bonding and dry bonding using Super-Bond C&B could provide a tensile bond strength higher than that of the tensile strength of enamel itself (Figure 5). The complete hybridization of resin into the total etched enamel-DEJ-dentin depends on the demineralized tooth substrate's permeability and the monomers' diffusion potential. Non-detachment with consistent thickness hybridized layers against loading force for failure and chemical challenge found in the primerless-wet and Super-Bond groups (Figures 7 and 8) suggest the high resin content encapsulates the tooth component in the hybrid layer. Therefore, the enamel- and dentin-resin hybrid layer,

created using a primerless-wet bonding with 10 s to 60 s 1-1 conditioning, 4-META/MMA-TBB, and PMMA powder could be a sustainable biopolymer to provide a complete micro-seal and high tensile bond strength comparable with that of Super-Bond C&B. The long-range conditioning period of 1-1 for 10 s to 60 s ensures more safety manipulation in the clinical situation.

The adhesive failure at the demineralized dentin-resin interface or cohesive failure in the remaining demineralized dentin found in Single-Bond2 and All-Bond2 fractured specimens minimized the tensile bond strength and was probably the cause of the leakage (Figures 4 and 6a,b). This demineralized dentin is the leakage pathway for dye or lactic acid to penetrate [6,8,9]. After tensile loading and chemical challenge, the inconsistent enamel-resin interface and the detached and degraded dentin-resin interface confirmed monomers' incomplete impregnation into the demineralized tooth substrate (Figure 8). These results suggest that moist bonding using 32% or 35% phosphoric acid for a 15 s etching period, kept moist and either primed and bonded using one or separate steps cannot provide a complete marginal seal of cementum/dentin and a stable hybrid layer.

Although achieving a complete seal for the enamel and cementum/dentin margin/interface (Figure 3b), AQ-Bond specimens had a significantly lower tensile strength than the primerless-wet and Super-Bond groups. The fracture mode originated in the hybridized suspended smear layer of the enamel-resin interface (Figure 6c); the thin hybridized enamel with degradation and the detached hybridized dentin after chemical immersion (Figure 10) suggest the remaining smear and the low resin content of the hybrid layer. These results imply that scrubbing this self-etch monomer for 20 s could not sufficiently remove all the smear layer to provide high adhesion to enamel and dentin. Therefore, careful removal of more smear layers by aggressively air-blowing off or an additional scrubbing application [9] is recommended for cavities with no retentive form and require higher retention, such as a large wedge shape abrasion lesion.

As the primer and bonding agents of all groups contain the methacrylate monomers with hydrophobic and hydrophilic groups, the significantly different factor is the conditioned tooth surface of each system. This study's results suggest that the permeability of conditioned tissue of the adhesive system that provides the durable biopolymer hybridized dentin influences the complete micro-seal and higher tensile bond strength. Moreover, the complete micro-seal or dye penetration distance was unrelated to the TBS data. Therefore, luting resin or resin adhesives that provide a complete marginal seal should be primarily considered to protect dentin and pulp for long-term function. In other words, a complete seal margin with an impermeable hybrid layer is more reliable than a high tensile bond strength adhesive with the leaked margin in preventing recurrent or secondary caries [8,9,21], the most common dental restoration failure, ensuring the lifelong survival of restored vital teeth. In clinical cases where high retention and completely sealed dentin is required, i.e., a short clinical crown or severe tooth wear and partial coverage retainers, a complete hybrid layer with high tensile strength and micro-seal margins can extend the long-term survival of vital teeth with less invasive treatment or without intentional pulp removal [21,26,27]. The results of this study support the hypothesis.

The novelty of this study is that a primerless-wet system using mild acid (1-1) conditioning for 10–60 s and blot-drying to remove all smears and water is less aggressive and safer than a dry bonding system using a 10-3 conditioner. Furthermore, its total etching creates durable hybridized enamel and dentin, providing the micro-seal and tensile bond strength (TBS) better than a primer-moist system. In addition, its TBS is higher than the self-etch system. However, an in-vivo study should be carried out to evaluate the effect of dentinal fluid in a vital tooth before introducing this system into the market. In the future, dentists can use this adhesive system as long-term dentin protection to treat patients at home.



## 5. Conclusions

Primerless-wet bonding using 1-1 conditioning for 10 s to 60 s and 4-META/MMA-TBB luting resin provided a reliable hybrid layer, a biopolymer, with a marginal micro-seal and tensile strength of the bonded enamel/DEJ/dentin similar to that of a dry system using Super-Bond C&B and higher than that of enamel itself. It can be a sustainable luting resin or adhesive agent with a sustainable hybrid layer. A basic fuchsin dye penetration was found when demineralized cementum/dentin was left underneath to provide a leakage pathway. To successfully prevent biological failure, a luting resin providing a complete marginal seal is preferable to the one with a leaked margin, even with high bond strength, as there is no correlation between complete marginal micro-seal and TBS data.

**Author Contributions:** Conceptualization, M.P.; data curation, M.P. and O.W.; formal analysis, M.P. and O.W.; investigation, M.P. and O.W.; methodology, M.P. and O.W.; project administration, M.P.; resources, M.P. and O.W.; supervision, M.P.; validation, M.P. and O.W.; visualization, M.P. and O.W.; writing—original draft, M.P.; writing—review and editing, M.P. and F.G.-G. All authors have read and agreed to the published version of the manuscript.

**Funding:** This research received no funding.

**Institutional Review Board Statement:** The study was conducted in accordance with the Declaration of Helsinki, and approved by the Institutional Review Board of Faculty of Dentistry, Chulalongkorn University. The study did not require ethical approval.

**Informed Consent Statement:** Not applicable.

**Data Availability Statement:** Not applicable.

**Acknowledgments:** The authors would like to express their appreciation to Nobuo Nakabayashi for his support and comments; John Harcourt, The University of Melbourne, for assistance with English clarity.

**Conflicts of Interest:** The authors declare no conflict of interest.

## References

1. Anusavice, K.J.; Shen, C.; Rawls, H.R. *Phillips's Science of Dental Materials*, 12th ed.; Saunders: Philadelphia, PA, USA, 2013; pp. 309–313.
2. Nakabayashi, N.; Pashley, D.H. *Hybridization of Dental Hard Tissue*; Quintessence: Tokyo, Japan, 1998; pp. 13–14, 76–77.
3. Shinchii, M.J.; Soma, K.; Nakabayashi, N. The effect of phosphoric acid concentration on resin tag length and bond strength of a photo-cured resin to acid-etched enamel. *Dent. Mater.* **2000**, *16*, 324–329. [CrossRef] [PubMed]
4. Inokoshi, S.; Hosoda, H.; Harniratissai, C.; Shimida, Y.; Tatsumi, T. A study on the resin-impregnated layer of dentin. Part A. Comparative study on the decalcified and undecalcified sections and the application of argon ion beam etching to disclose the resin-impregnated layer of dentin. *Jpn. J. Conser Dent.* **1990**, *33*, 427–442.
5. Tay, F.R.; Gwinnett, A.J.; Wei, S.H. The overwet phenomenon: A scanning electron microscopic study of surface moisture in the acid-conditioned, resin-dentin interface. *Am. J. Dent.* **1996**, *9*, 109–114. [PubMed]
6. Piemjai, M.; Watanabe, A.; Iwasaki, Y.; Nakabayashi, N. Effect of remaining demineralised dentin on dental microleakage accessed by a dye penetration: How to inhibit microleakage? *J. Dent.* **2004**, *32*, 495–501. [CrossRef]
7. Piemjai, M.; Waleepitackdej, O.; Garcia-Godoy, F.; Nakabayashi, N. Dentin protection by a primer-less adhesive technique. *Am. J. Dent.* **2011**, *24*, 284–288.
8. Piemjai, M.; Chantarawej, P.; Nakabayashi, N.; Garcia-Godoy, F. Prognosis test by visualization of demineralized dentin under restorations to prevent initial wall-lesions initiated by lactic acid. *Am. J. Dent.* **2017**, *30*, 119–124.
9. Piemjai, M.; Chantarawej, P.; Nakabayashi, N. Evaluation of caries-free restorations bonded with various adhesive systems: In-vitro study. *Int. J. Dent.* **2020**, *2020*, 5859835. [CrossRef]
10. Piemjai, M.; Nakabayashi, N. Effect of dentin conditioners on wet bonding of 4- META/MMA-TBB resin. *J. Adhesive Dent.* **2001**, *3*, 325–331.
11. Iwasaki, Y.; Toida, T.; Nakabayashi, N. Improved wet bonding of methyl methacrylate-tri-n-butylborane resin to dentin etched with ten percent phosphoric acid in the presence of ferric ions. *J. Biomed. Mater. Res.* **2004**, *68A*, 566–572. [CrossRef]
12. Watanabe, I.; Nakabayashi, N. Bonding durability of Photocured phenyl-P in TEGDMA to smear layer—Retained bovine dentin. *Quintessence Int.* **1993**, *24*, 335–342.
13. Piemjai, M.; Thaveeratana, A.; Nakabayashi, N. Marginal integrity between a prefabricated composite block and enamel, DEJ and dentin bonded by three adhesive resins. *Am. J. Dent.* **2010**, *23*, 285–291. [PubMed]

14. Monticelli, F.; Osorio, R.; Mazzitelli, C.; Ferrari, M.; Toledado, M. Limited decalcification/diffusion of self-adhesive cements into dentin. *J. Dent. Res.* **2008**, *87*, 974–979. [CrossRef] [PubMed]
15. Sengar, E.V.; Mulay, S.; Beri, L.; Gupta, A.; Almohareb, T.; Binalrimal, S.; Robaian, A.; Bahammam, M.A.; Bahammam, H.A.; Bahammam, S.A.; et al. Comparative evaluation of microleakage of flowable composite resin using etch and rinse, self-etch adhesive systems, and self-adhesive flowable composite resin in Class V cavities: Confocal laser microscopic study. *Materials* **2022**, *15*, 4963. [CrossRef] [PubMed]
16. Koibuchi, H.; Yasuda, N.; Nakabayashi, N. Bonding to dentin with a self-etching primer: The effect of smear layers. *Dent. Mater.* **2001**, *17*, 122–126. [CrossRef] [PubMed]
17. Piemjai, M.; Waleepitackdej, O.; Nakabayashi, N. Influence of dentin substrates to simplify wet-bonding: A leakage-free and reliable tensile strength interface for long-lasting restorations. *J. Biomed. Mater. Res.* **2011**, *99B*, 321–327. [CrossRef]
18. Manhart, J.; Chen, H.Y.; Hamm, G.; Hickel, R. Buonocore memorial lecture: Review of the clinical survival of direct and indirect restorations in posterior teeth of the permanent dentition. *Oper Dent.* **2004**, *29*, 481–508.
19. De Backer, H.; Van Maele, G.; De Moor, N.; Van den Berghe, L.; De Boever, J. An 18-year retrospective survival study of full crowns with or without posts. *Int. J. Prosthodont.* **2006**, *19*, 136–142.
20. Walton, T.R. The up to 25-year survival and clinical performance of 2,340 high gold-based metal-ceramic single crowns. *Int. J. Prosthodont.* **2013**, *26*, 151–160. [CrossRef]
21. Piemjai, M.; Adunphichet, N. Impact of hybrid layer formation on the 15-year survival, complications and failures of full-coverage retainers. *J. Prosthodont. Res.* **2022**, *66*, 131–140. [CrossRef]
22. Bart, I.; Dobler, B.; Schmidlin, K.; Zwahlen, M.; Salvi, G.E.; Lang, N.P.; Bragger, U. Complication and failure rates of tooth-supported fixed dental prostheses after 7 to 19 years in function. *Int. J. Prosthodont.* **2012**, *25*, 360–367.
23. Beier, U.S.; Kapferer, I.; Dumfahrt, H. Clinical long-term evaluation and failure characteristics of 1,335 all-ceramic restorations. *Int. J. Prosthodont.* **2012**, *25*, 70–78. [PubMed]
24. Kenyon, B.J.; Frederickson, D.; Hagge, M.S. Gingival seal of deep Class II direct and indirect composite restorations. *Am. J. Dent.* **2007**, *21*, 3–6.
25. Piemjai, M.; Nakabayashi, N. Direct tensile strength and characteristics of dentin restored with all-ceramic, resin-composite and cast metal prostheses cemented with resin adhesives. *BioMed Res. Int.* **2015**, *2015*, 656948. [CrossRef] [PubMed]
26. Piemjai, M. *Advanced Fixed Prosthodontics: Dentin Protection for Life-long Function*; Samcharoen Panich: Bangkok, Thailand, 2015; pp. 160–197.
27. Masaka, N.; Yoneda, S.; Masaka, K. An up to 43-year longitudinal study of fixed prosthetic restorations retained with 4-META/MMA-TBB resin cement or zinc phosphate cement. *J. Prosthet. Dent.* **2021**. *Online ahead of print*. [CrossRef] [PubMed]

**Disclaimer/Publisher’s Note:** The statements, opinions and data contained in all publications are solely those of the individual author(s) and contributor(s) and not of MDPI and/or the editor(s). MDPI and/or the editor(s) disclaim responsibility for any injury to people or property resulting from any ideas, methods, instructions or products referred to in the content.

Review

# Modification of Starches and Flours by Acetylation and Its Dual Modifications: A Review of Impact on Physicochemical Properties and Their Applications

Edy Subroto \*, Yana Cahyana , Rossi Indiaranto and Tiara Aray Rahmah

Department of Food Industrial Technology, Faculty of Agro-Industrial Technology, Universitas Padjadjaran, Bandung 45363, Indonesia; y.cahyana@unpad.ac.id (Y.C.); rossi.indiaranto@unpad.ac.id (R.I.); tiara16005@mail.unpad.ac.id (T.A.R.)

\* Correspondence: edy.subroto@unpad.ac.id

**Abstract:** Various modification treatments have been carried out to improve the physicochemical and functional properties of various types of starch and flour. Modification by acetylation has been widely used to improve the quality and stability of starch. This review describes the effects of acetylation modification and its dual modifications on the physicochemical properties of starch/flour and their applications. Acetylation can increase swelling power, swelling volume, water/oil absorption capacity, and retrogradation stability. The dual modification of acetylation with cross-linking or hydrothermal treatment can improve the thermal stability of starch/flour. However, the results of the modifications may vary depending on the type of starch, reagents, and processing methods. Acetylated starch can be used as an encapsulant for nanoparticles, biofilms, adhesives, fat replacers, and other products with better paste stability and clarity. A comparison of various characteristics of acetylated starches and their dual modifications is expected to be a reference for developing and applying acetylated starches/flours in various fields and products.

**Keywords:** acetylation; starch; flour; physicochemical properties; modification

**Citation:** Subroto, E.; Cahyana, Y.; Indiaranto, R.; Rahmah, T.A. Modification of Starches and Flours by Acetylation and Its Dual Modifications: A Review of Impact on Physicochemical Properties and Their Applications. *Polymers* **2023**, *15*, 2990. <https://doi.org/10.3390/polym15142990>

Academic Editor: Raffaella Striani

Received: 13 June 2023

Revised: 6 July 2023

Accepted: 7 July 2023

Published: 9 July 2023



**Copyright:** © 2023 by the authors. Licensee MDPI, Basel, Switzerland. This article is an open access article distributed under the terms and conditions of the Creative Commons Attribution (CC BY) license (<https://creativecommons.org/licenses/by/4.0/>).

## 1. Introduction

Native starches/flours generally have several drawbacks related to functional, pasting, and physicochemical properties, which can limit their use in various applications. These limitations include low swelling ability, absorption capacity, solubility, starch clarity, and freeze stability [1–4]. Most of the starches tend to retrograde easily when the starch paste is stored at low temperatures. This is caused by the amylose chains that had previously come out of the granules binding to each other again to form a crystalline structure [5,6]. Retrogradation causes an increase in starch viscosity, crystallinity, gel structure, and gel texture [7,8]. Various treatments and modifications have been used to improve these properties, one of which is by modifying acetylation. Acetylation is a modification involving the substitution of hydroxyl groups with acetyl groups; the number of substituted acetyl groups affects the characteristics of starch/flour [9–11].

The modification of acetylation in starch/flour has been reported to increase swelling ability, clarity of starch paste, and stability of starch against retrogradation [12–14]. Acetylated starch is often applied to improve the texture and appearance of products whose quality may decrease due to damage during processing or retrogradation. Acetylated starch can also provide a good thickening effect in various foods. However, acetylated starch is unstable to thermal processes characterized by increased breakdown viscosity [15–17]. This can be overcome by combining acetylation with other modifications that can improve thermal stability, such as cross-linking modifications and hydrothermal treatments, such as heat moisture treatment (HMT) and annealing (ANN). Hydrothermal modification can

improve the formation of amylose-lipid complexes and the regularity of the crystalline matrix to control the swelling capacity and increase stability to heating and friction [18–20].

Modifying acetylation combined with cross-linking or hydrothermal treatment can improve the clarity of the paste, texture, and thermal stability [21,22]. Several studies have stated that hydrothermal treatment is able to increase the effectiveness of acetylation reactions with starch molecules so that more acetyl groups are substituted and can minimize the use of chemicals for the acetylation process [10,23]. However, several dual-modified treatments have contradictory effects, so the resulting characteristics depend on the dominant treatment [10,22].

Changes in the characteristics of starch/flour due to the modification of acetylation are highly dependent on the degree of substitution (DS) and treatment conditions such as the source of starch, type of reagent, pH, temperature, and time [12,15,24]. The starch source determines the amylose-amylopectin content, which determines the amorphous and crystalline structures of the starch granules. This type of acetylation reagent generally uses acetic acid, vinyl acetate, or acetic anhydride, which can be catalyzed using bases such as NaOH and KOH. At the same time, temperature and time reaction determine the level of DS obtained, which greatly affects the characteristics of the starch/flour produced. This review describes studies on modifications of various types of starch and flour by acetylation or dual modification of their physicochemical characteristics, as well as their applications in various fields/products, so that they can become a reference for the development of starches/flours.

## 2. Applications of Acetylated Modified Starch/Flour

Modifying a starch affects its characteristics, and the changes that occur depend on the type of modification applied. Chemical modifications such as acetylation weaken the starch's structure, thereby increasing its hydration capacity and reducing its tendency to retrograde [25,26]. Meanwhile, the combination of acetylation with cross-linking and hydrothermal modification (HMT and ANN) can increase the orderliness of the crystalline matrix so that the gelatinization process becomes slower and granule swelling is limited [1,27,28]. Therefore, acetylated modified starch or its dual modification is often used to improve the hydration quality and thermal stability of the product [24,29]. However, the application of acetylated starch and its dual modifications has been developed in various fields and various products. Some applications of acetylated modified starches/flours for various products and fields can be seen in Table 1.

**Table 1.** Some applications of acetylated modified starches/flours for various products and fields.

Starch/Flour and Treatment	Products/Applications	Characteristics	References
Acetylated cassava starch	Starch-based nanoparticles for encapsulation of antioxidants	Acetylated starch interacts well with antioxidant compounds, especially BHT, and protects antioxidants from degradation. Acetylated starch can increase the thermal stability of nanoparticles.	[30]
Acetylated rice starch nanocrystals	Nanocrystal for protein delivery	BSA protein release is significantly slowed. Acetylated rice starch nanocrystals can be good for protein delivery.	[31]
Acetylated debranched waxy corn starch	Nanocarrier for curcumin	Acetylated starch to be amphiphilic, having polar and non-polar groups. Curcumin micelles were spherical with a particle size of about 50–100 nm. Micelles of acetylated starch can accommodate curcumin until the concentration of 0.45 mg/mL	[32]



Table 1. Cont.

Starch/Flour and Treatment	Products/Applications	Characteristics	References
Retrograded acetylated corn starch	Drug (budesonide) delivery	Acetylation increased the hydrophobicity and reduced the swelling power and granule porosity. Tablets from retrograded acetylated corn starch released the drug in ileocolonic by 81.38%. Tablets were potentially suitable for the treatment of ileocolonic diseases.	[33]
Acetylated cassava starch and Maltol Incorporated	Active biodegradable film/packaging	The film based on acetylated cassava starch, which was incorporated with 10% maltol reduced molecular mobility and hydrophilicity; elongation was reduced by 34%, while the tensile strength was reduced by 37%. The active film inhibited the fungal growth for up to 6 times longer and maintained the flavor of bakery products.	[34]
Acetylated corn starch	Starch-based bioplastics	Acetylated corn starch improved the homogeneity and mechanical properties of biocomposites. The solubility of starch-based bioplastics decreased to 24.9–28.2%	[35]
Acetylated corn starch	Biodegradable polymers poly(lactic acid) for packaging materials	Acetylated corn starch increased the thermal stability of biodegradable polymers. Acetylated corn starch improved mechanical properties such as toughness and tensile strength.	[36]
Acetylated cassava starch	Starch nanoparticles for emulsion stabilizer	Acetylated starch nanoparticles with DS of 0.53 improved the hydrophobicity by a contact angle of more than 89.56°. Acetylated starch nanoparticles of 1.5% improved storage stability for up to 35 days and emulsion capacity by improving the droplet size and homogeneity.	[37]
Cross-linked acetylated cassava starch	Set yogurt	Cross-linked acetylated cassava starch improved the stability, viscous modulus ( $G''$ ), and elastic modulus ( $G'$ ) of the set yogurt.	[38]
Acetylated corn starch	Fat replacer of beef patties	The use of 15% acetylated corn starch improved the acceptance of organoleptic, microstructure, and physicochemical properties in beef patties, Acetylated corn starch is a suitable fat replacer for meat products.	[16]
Acetylated arenga starch	Bread	The addition of acetylated arenga starch up to 50% improved the quality of the bread produced, including sensorial properties, oven spring, oil absorption, and oil holding capacity.	[39]
Acetylated corn starch	Noodles	Acetylated corn starch increased the brightness of noodles. Acetylated starch reduced the tensile properties, chewiness, adhesion, and hardness of noodles. Acetylated starch increased the resistant starch and slowly digestible starch of noodles.	[40]

Table 1. Cont.

Starch/Flour and Treatment	Products/Applications	Characteristics	References
Acetylated rice starch and potato starch	Gut microbiota fermentation	Acetylated starch produced more SCFA than native starch. Acetylated starches were easier to use and more quickly fermentable by the gut microbiota.	[41]
Acetylated-crosslinked corn starch	Wood-based panel adhesive	The adhesive had better water resistance up to 1 MPa, The adhesive was also heat resistant, so it can be used in high-temperature pressing.	[42]
Acetylated waxy corn starch	Wood adhesive	The adhesive resistance to water increased up to 61.1% The shear strength increased up to 321% in the wet state and 59.4% in the dry state.	[43]
Acetylated corn starch and potato starch	Coagulants for wastewater treatment	Acetylated starch from corn and potato starch was effective as a coagulant for wastewater treatment by significantly reducing pH, color, turbidity, and electrical conductivity.	[44]

Acetylation modification can increase the functionality of starch and its applications, especially in foods. The high hydration ability of acetylated starch has the potential to be used as a thickening agent. Several studies also reported that acetylation modification has good stability and resistance to retrogradation and syneresis, so it has the potential to be applied as a stabilizer in products that require low-temperature storage [13,45]. In addition, acetylation modification can increase OAC so that it can be applied as a filming agent. Acetylated starch has many applications in the food industry, some of which are in products such as retorted soups, sauces, canned pie fillings, frozen food, baby food, and salad dressings [15,24,46].

Acetylated modified starch, especially in nanocrystal form, has been effectively applied for encapsulation and as a delivery system for various drugs and other active compounds [47]. de Oliveira et al. [30] applied acetylated cassava starch as starch-based nanoparticles for the encapsulation of antioxidants; it was reported that acetylated cassava starch interacted well with antioxidant compounds, especially BHT and protected antioxidants from the degradation process, and increased the thermal stability of nanoparticles. Liu et al. [32] applied acetylated debranched waxy corn starch as a nanocarrier for curcumin, and it was reported that curcumin micelles of acetylated starch had a spherical shape with a particle size of about 50–100 nm and could accommodate curcumin until the concentration of 0.45 mg/mL. Gangopadhyay et al. [33] applied retrograded acetylated corn starch to drug (budesonide) delivery, and it was reported that tablets from retrograded acetylated corn starch were able to release the drug in ileocolonic by 81.38% and were potentially suitable for the treatment of ileocolonic diseases. Meanwhile, Xiao et al. [31] reported that acetylated rice starch nanocrystals could be used for protein (BSA) delivery by significantly slowing BSA protein release.

Acetylated modified starch, especially in nanocrystal form, has been applied to improve the quality of bioactive films. Promhuad et al. [34] applied acetylated cassava starch and Maltol Incorporated in active biodegradable film/packaging fabrication; it was reported that film based on acetylated cassava starch, which was incorporated with 10% maltol, reduced molecular mobility, hydrophilicity, elongation, and tensile strength. The active film based on acetylated cassava starch inhibited the fungal growth by up to six times longer and maintained the flavor of bakery products. Fitch-Vargas et al. [35] applied acetylated corn starch in the manufacture of starch-based bioplastics; it was reported that acetylated corn starch improved homogeneity and mechanical properties, while the solubility of starch-based bioplastics decreased to 24.9–28.2%. Meanwhile, Nasser et al. [36]

reported that acetylated corn starch could be applied to biodegradable polymers poly(lactic acid) for packaging materials, where acetylated corn starch can increase the thermal stability of biodegradable polymers and improve mechanical properties such as toughness and tensile strength.

Acetylated modified starch and its dual modification can also be used as a stabilizer in various emulsion products and can act as a fat replacer. Yao et al. [37] applied acetylated cassava starch nanoparticles as an emulsion stabilizer; it was reported that acetylated starch nanoparticles improved hydrophobicity and improved emulsion capacity by improving the droplet size and homogeneity so that the storage stability increased up to 35 days. Cui et al. [38] applied cross-linked acetylated cassava starch to the manufacture of set yogurt, and it was reported that cross-linked acetylated cassava starch improved the stability, viscous modulus, and elastic modulus of the set yogurt. Meanwhile, Osman et al. [16] utilized acetylated corn starch as a fat replacer in beef patties, and it was found that it was suitable as a fat replacer for meat products. At the same time, the use of 15% acetylated corn starch improved the acceptance of organoleptic, microstructural, and physicochemical properties in beef patties.

Acetylated starch can also be applied directly in the manufacture of various food products such as bread and noodles. For some food products, such as bread, retrogradation causes bread staling, where the quality of the bread decreases in the form of a harder texture [48]. Acetylated starch could slow down and improve retrogradation, thereby improving the texture and quality of bread. Rahim et al. [39] applied acetylated arenga starches to bread making; it was reported that adding acetylated starch up to 50% was able to improve the quality of the bread produced, which included sensorial properties, oven spring, oil absorption, and oil holding capacity. Meanwhile, Lin et al. [40] applied acetylated corn starch to the manufacture of noodles, and it was reported that acetylated corn starch increased the brightness and reduced the tensile properties, chewiness, adhesion, and hardness of noodles. Acetylated starch was also reported to increase resistant starch and slowly digestible starch in noodles. Wang et al. [41] also reported that acetylated rice starch and potato starch improved the gut microbiota fermentation by producing more SCFA and were easier to use and more quickly fermentable by the gut microbiota.

Acetylated modified starch and its dual modification can also be used in the chemical field, namely as a waste treatment coagulant and as an adhesive, especially to increase its water resistance and shear strength [49]. Gu et al. [42] applied acetylated-crosslinked corn starch as a wood-based panel adhesive, where the adhesive had better water resistance up to 1 MPa, and the adhesive was also heat-resistant so that it could be used in high-temperature pressing. Wang et al. [43] applied acetylated waxy corn starch as a wood adhesive, and it was found that the adhesive's resistance to water increased up to 61.1%, and the shear strength increased up to 321% in the wet state and 59.4% in the dry state. Meanwhile, Posada-Velez et al. [44] applied acetylated potato starch and corn starch as coagulants for wastewater treatment, and it was found that acetylated starch from both corn and potato starch had good effectiveness as a coagulant for wastewater treatment by significantly reducing pH, color, turbidity, and electrical conductivity.

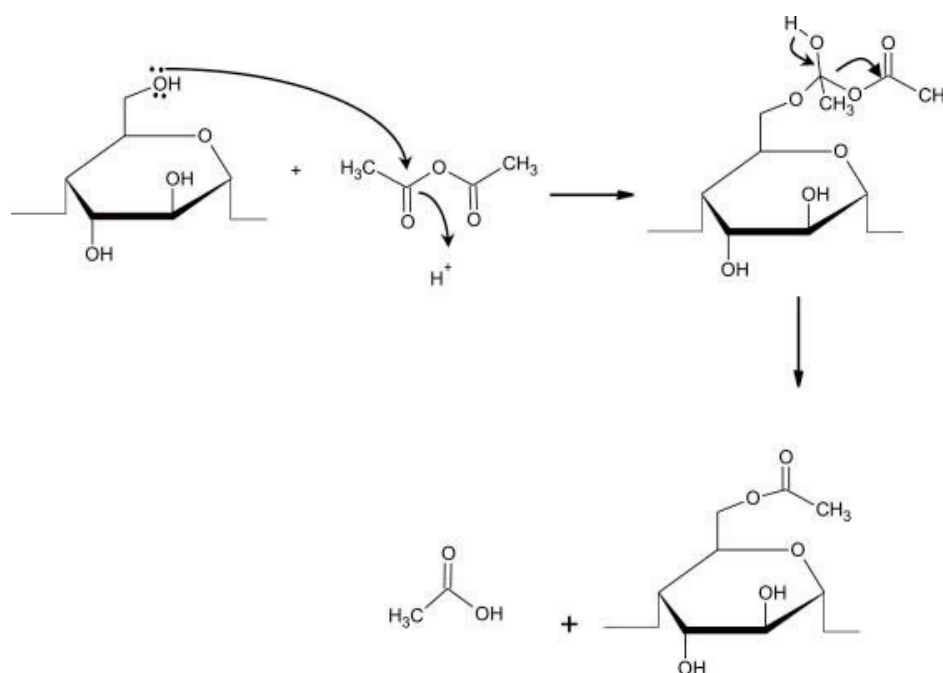
### 3. Acetylation Modification Process in Starch/Flour

#### 3.1. Mechanism of Acetylation

The characteristics of starches and flours could be improved by chemical, physical, and combination or dual modifications. These modifications aim to change some of the properties of starch by altering its original structure through physical treatment or changing the hydroxyl groups in starch through chemical reactions such as oxidation and esterification [50–53]. The modification of starch includes the use of heat, oxidizing agents, alkalis, acids, and other chemicals that will generate new chemical groups, resulting in changes in size, morphology, molecular structure, and other physicochemical characteristics [54,55].

Chemical modification can change the significant characteristics of starch and flour. Chemical modifications can be carried out through acid hydrolysis, oxidation, cross-linking, and the addition of functional groups such as acetylation. In general, chemical modification adds new functional groups to the starch, which then affect the physicochemical properties of the modified starch [52,56–58]. The chemical modification of acetylation has been widely applied to various food industries. Several studies have been developed by combining acetylation modification with physical or other chemical modifications, such as acetylation + hydrothermal and acetylation + crosslinking, in order to increase starch's functional value and expand its application [26,59,60].

Acetylation is a chemical modification technique conducted through the esterification of starch using acetic anhydride, acetic acid, and vinyl acetate reagents and alkali (NaOH, KOH,  $\text{Ca}(\text{OH})_2$ , and  $\text{Na}_2\text{CO}_3$  as catalysts [61,62]. The basic principle of the acetylation reaction is the substitution of starch-free hydroxyl groups with acetyl groups (Figure 1) by weakening the bonds between starch molecules to produce starch that is amphiphilic (hydrophilic and hydrophobic) [63,64]. Acetylation is an indirect esterification process, so it is necessary to add a catalyst so that the reaction can take place. Before the reaction, the starch is first conditioned in an alkaline state to form the starch base. An acetate reagent is then added to form starch acetate [30,65–67]. The basic principle of the acetylation reaction by the substitution of starch-free hydroxyl groups with acetyl groups can be seen in Figure 1.



**Figure 1.** The basic principle of the acetylation reaction by the substitution of starch-free hydroxyl groups with acetyl groups [67], with permission from Elsevier, 2015.

Figure 1 shows that the acetylation reaction occurs via the substitution of the acyl group with the free hydroxyl group portion of the glucose monomers as a constituent of starch molecules. There are many hydroxyl groups, so more free hydroxyl groups being substituted with acetyl groups will result in a greater degree of substitution. Acetylation can reach equilibrium, and if the reverse reaction occurs, it indicates the hydrolysis reaction of the ester bond. The rate of the acetylation reaction is affected by several factors as well as other esterification reactions, especially the structures of the acids and alcohols that react and the catalyst used [68]. The catalyst usually uses strong bases such as KOH and NaOH using anhydride reagents such as acetic anhydride. However, using organic acids or carboxylic acids as organocatalytics is also competitive to produce safer and more environmentally friendly processes. Organocatalytics that can be used include L-aspartic, citric, L-tartaric, L-malic, L-lactic, glycolic, fumaric acids, and L-proline. These



organic catalysts can also produce high esterification reaction rates and high degrees of substitution [69,70].

The degrees of substitution (DS) affect the physicochemical and functional characteristics of acetylated modified starch/flour [71,72]. The DS values ranged from 0.01 to 3, describing the number of substituted acetyl groups in one glucose unit. Starch acetate with DS 0.01 indicates that there is one substituted acetyl group in 100 units of glucose. In contrast, starch acetate with DS 3 indicates that there are 300 substituted acetyl groups in 100 units of glucose. This is based on the theory that acetylation reactions can substitute three free hydroxyl groups of glucose units on C2, C3, and C6 atoms with acetyl groups [16,73]. Acetic starch with low DS has been widely applied in the food industry for many years. The Food and Drug Administration (FDA) stipulates that the maximum permissible limit for the percentage of acetyl groups in foodstuffs is 2.5% or the equivalent of a DS value of 0.1, but generally, for commercial food products, starch acetate is used with a low DS (<0.1) or medium DS (0.1–1.0) [15,74].

### 3.2. Effect of Acetylation Methods on Properties of Starch/Flour

The acetylation method involving reactant types and concentrations can affect the acetylation reaction's efficiency. The DS of starch acetate is greater when the reactant concentration is high [75]. Generally, the ability and efficiency of acetic anhydride in substituting acetyl groups were greater than that of vinyl acetate at the same conditions and concentrations. In addition, the type of catalyst and reaction medium (solvent) also affect the efficiency of the reaction. Solvents that can be used in acetylation reactions include water, pyridine, and DMSO. Pyridine and DMSO have greater efficiency than water but can have adverse environmental and health impacts [24]. Thus, the number of substituted acetyl groups is affected by several factors, including the source or type of starch, the concentration of the reactants, pH, reaction time, and the catalyst used [65,76]. The starch type with many amorphous parts, such as starch from tubers, is more easily penetrated or substituted by acetyl groups. An example is the acetylation of potato starch, which produced a higher DS (DS: 0.180–0.238) than corn starch (DS: 0.133–0.184) [77]. The use of reactants with higher concentrations can produce higher DS; for example, the use of an acetylation of sweet potato starch using acetic anhydride at concentrations of 2, 4, 6, and 8% produced DS of 0.032, 0.059, 0.091, and 0.123 respectively [78]. pH can also affect DS, where the use of a higher pH could increase DS; for example, the acetylation of yellow pea starch at pH 9–10 produced a higher DS (DS: 0.071) than pH 7.5–9.0 (DS: 0.066) [62]. Longer reaction times can increase DS; for example, a chestnut starch acetylation at 30, 60, and 90 min reaction times resulted in the DS being 0.010, 0.020, and 0.024, respectively [14]. The type of catalyst used can also affect the DS; for example, the use of catalysts of  $\text{Ca}(\text{OH})_2$ , NaOH, and KOH 1 N in the acetylation of waxy cornstarch produced DS of 0.077, 0.081, and 0.085, respectively [61]. The DS value can be determined by several techniques, including headspace gas chromatography (HS-GC), infrared spectroscopy or FT-IR, nuclear magnetic resonance (NMR), and titration [53]. Several methods of modifying acetylation on various types of starch/flour and their effect on DS values can be seen in Table 2.

**Table 2.** Several methods of modifying acetylation on various types of starch/flour and their effect on DS values.

Starches or Flours	Reagents/Acetylation Condition	Degree of Substitution (DS)	References
<b>One Step Acetylation</b>			
Corn starch Waxy corn starch	Acetic anhydride, pH 8–9 using NaOH 2%.	Corn (0.05–0.07) Waxy corn (0.08–0.09)	[79]
Maize starch	Choline carboxylate, imidazolium carboxylate, and imidazolium chloride	0.26–2.63	[80]

Table 2. Cont.

	Starches or Flours	Reagents/Acetylation Condition	Degree of Substitution (DS)	References
	Corn starch	Acetic anhydride using toluene sulfuric acid as the catalyst.	1.5 and 3.0	[81]
	Sweet potato starch Potato starch	Acetic anhydride	0.041–0.076	[82]
	Sweet potato starch	Acetic anhydride 0–8%, pH 8.1–8.3, NaOH 3%	0.032–0.123	[78]
	Potato starch Cassava starch	pH 8, NaOH 3%, 10–20 min	Potato starch (0.10–0.26) Cassava starch (0.10–0.18)	[83]
	Potato starch Corn starch	pH 8.0–8.4, NaOH 3%, 10 min	Potato (0.180–0.238) Corn (0.133–0.184)	[77]
	Purple yam (PY) starch White yam (WY) starch	pH 8.0–8.4, NaOH 3%, 10 min and 240 min	Purple yam (0.034–0.051) White yam (0.036–0.043)	[84]
	Cocoyam starch	pH 8.0–8.5, 1 M NaOH, 5 min	0.30	[85]
	Waxy maize starch	NaOH 20% for 40 min, and NaOH 2% for 120 min	0.12	[86]
	Waxy maize starch	pH 8.0–8.5, NaOH 1 N, KOH 1 N, and Ca(OH) <sub>2</sub> 1 N for 60 min	0.077–0.085	[61]
	Maize starch	pH 8, 1 M NaOH, 60 min	0.080–0.210	[87]
	High amylose maize starch	pH 8, NaOH 50%, 15–240 min	0.57–2.23	[73]
	Rice starch	pH 8, NaOH 3%	0.03	[88]
	Oat starch	pH 8–8.5, NaOH 1 M for 5 min	0.02–0.05	[89]
	Sword bean starch	pH 8.0–8.4, 1 M NaOH, 30 min	0.14	[90]
	Yellow pea starch Chickpea starch Cowpea starch	Acetic anhydride, pH 7.5–9.0, 1–2 h, 20–25 °C, vinyl acetate, pH 9–10, 1–2 h, 20–25 °C	Acetic anhydride (0.059–0.066) Vinyl acetate (0.064–0.071)	[62]
	Japonica rice starch Indica rice starch	NaOH 4%, pH 7.8–8.2, 5 min	Japonica rice (0.066) Indica rice (0.060)	[91]
	Small granule wheat starch Large granule wheat starch	Acetic anhydride 8%, 30 °C, pH 8, NaOH 1 M, 15–20 min	0.039–0.043	[92]
	Sago starch	Acetylation (acetic anhydride, pH 7–10, NaOH 3%, T = room temperature, t = 50 min)	0.21–0.58	[93]
	Oat starch	Acetic anhydride (6% and 8%), pH 8.0–8.4, NaOH 3%, T = 25 °C, t = 10 min.	0.05–0.11	[21]
<b>Two steps acetylation</b>				
<b>Second step</b>	<b>Starches or flours</b>	<b>Reagents/Acetylation Condition</b>	<b>Degree of Substitution (DS)</b>	<b>References</b>
HMT	Buckwheat starch	Acetic anhydride, HMT= Moisture content 25%, temperature 110 °C, 4 h.	0.0289	[59]
Retrogradation	Purple sweet potato flour and starch	pH 8.5, NaOH 0.5 M, 15 min.	Purple sweet potato flour (0.08) Purple sweet potato starch (0.165)	[94]

Table 2. Cont.

Two steps acetylation				
Second step	Starches or flours	Reagents/Acetylation Condition	Degree of Substitution (DS)	References
Retrogradation	Potato starch	Acetic acid anhydride, pH 8–9, NaOH 3%, 15 min. Retrogradation using extruder, T = 60–65–70 °C, 100–110–120 °C or 150–160–170 °C.	3.1–4.4	[95]
Extrusion	Corn starch	Acetic anhydride 7.88%. Extrusion at Screw Speed (SS, 100 rpm) and Barrel Temperature (BT, 80 °C).	0.2	[96]
ANN	Mung bean starch	Acetic acid anhydride 20%, 15 min, pH 8 by NaOH 3%, 25 °C 25 min, ANN = 60 °C, 6 h.	0.02–0.26	[97]
ANN	Potato starch	Acetic acid anhydride, pH 8–9 by NaOH 0.5 M, 15 min, ANN = 51–61 °C, 48 h.	0.07–0.1	[26]
ANN	Waxy potato (WP) starch Waxy rice (WR) starch Waxy barley (WB) starch Waxy corn (WC) starch	Acetic anhydride 20 g/100 g, at pH 8, using NaOH 3%, 15 min, ANN = Moisture 75%, 10 °C below gelatinization temperature, 2–72 h.	WC (0.03–0.13) WB (0.06–0.24) WR (0.03–0.25) WP (0.01–0.12)	[10]

Infrared spectroscopy or FT-IR is also frequently used to determine the DS value of acetylated modified starch/flour. An example of the effect of acetylation modification on the FTIR spectra of starch can be seen in Figure 2. The FTIR spectrum of acetylated starch is shown by the appearance of several peaks or new absorption bands at wave numbers 1240, 1375, 1435, and 1754 or 1742  $\text{cm}^{-1}$ , which interprets C–O carbonyl stretching vibrations,  $\text{CH}_3$  symmetry deformation vibrations,  $\text{CH}_3$  antisymmetric deformation vibrations, and carbonyl C=O, respectively [98–100]. The appearance of these new absorption peaks indicates the occurrence of an esterification reaction, namely the substitution of hydroxyl groups by acetyl groups. The greater intensity of the absorption peaks indicates that the DS value is also greater and is followed by a weakening of the peaks at wave numbers 3421, 1082, and 1014  $\text{cm}^{-1}$ , which interprets the reduction of hydroxyl groups. Additionally, the spectrum of acetylated starch also shows that the anhydroglucose units tend to shift towards high wave numbers [100].

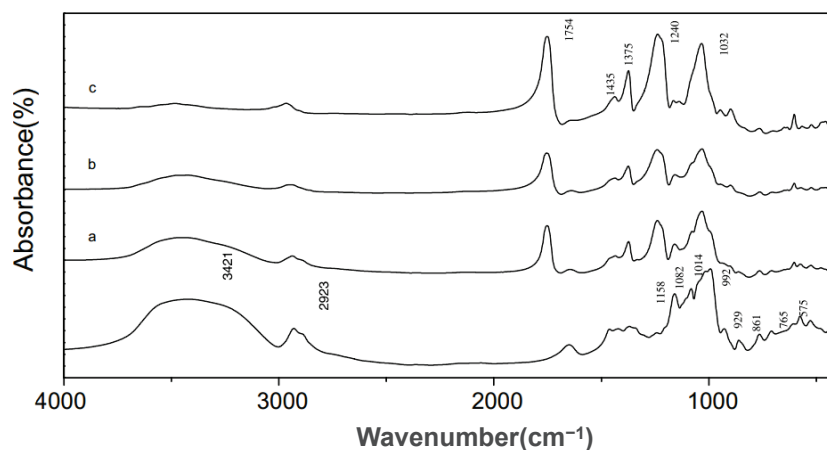
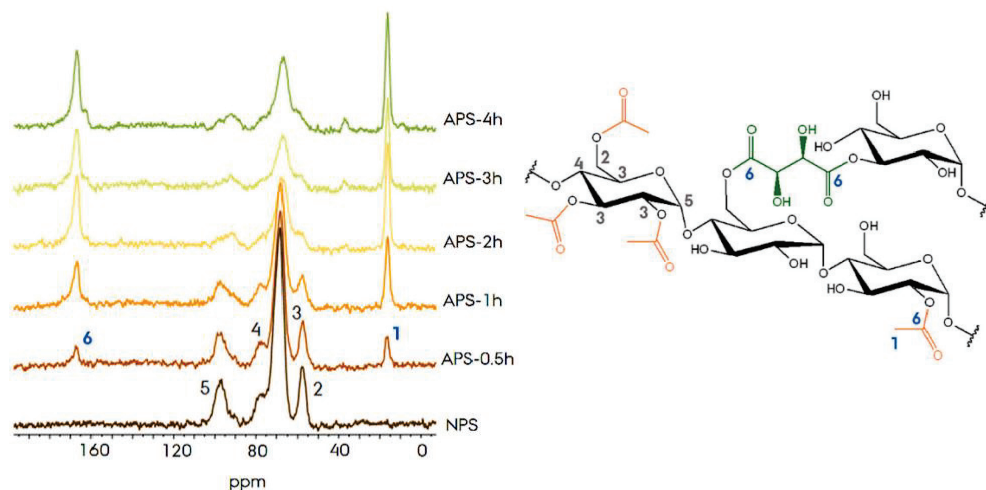


Figure 2. FTIR spectra of native corn starch and acetylated corn starches at different DS (a) 0.85, (b) 1.78, (c) 2.89 [100], with permission from Elsevier, 2008.

The DS value of acetylated starch can also be determined based on nuclear magnetic resonance (NMR) spectra, which generally use  $^1\text{H}$  NMR,  $^{13}\text{C}$  NMR, or  $^{13}\text{C}$ - $^1\text{H}$  COSY. NMR spectra can show changes in anhydroglucose units due to the substitution of hydroxyl groups by acetyl groups. An example of the effect of acetylation modification on the NMR spectra of starch can be seen in Figure 3.



**Figure 3.** Single Pulse- $^{13}\text{C}$  NMR spectra of native pea starch (NPS) and acetylated pea starch (APS) by organocatalytic acetylation at different reaction times. Signal 1 corresponds to the carbon of the alkyl group, and signal 6 corresponds to the carbon of the ester groups of starch [101].

The hydroxyl (-OH) groups of  $\text{C}_2$ ,  $\text{C}_3$ , and  $\text{C}_6$  show a proton signal from the anhydroglucose unit between 4.4 and 5.6 ppm; the signal at 5.10 ppm corresponds to the anomeric proton of the link ( $\alpha$ -1, 4), whereas the anomeric proton of the junction ( $\alpha$ -1,6) exhibits a small signal at 4.86 ppm [101,102]. Figure 3 shows that in acetylated starch, an additional signal between 1.8 and 2.2 ppm indicates a methyl proton from the acyl group, thus indicating that the acetylation process was successful. The level of acetylation increases with the length of the reaction time. The spectrum of native starch shows four main signals (Signals 2, 3, 4, and 5). In comparison, in acetylated pea starch, there are two additional signals, namely signal 1 at 16.4 ppm and signal 6 at 166.6 ppm, which interpret the carbon of the methyl proton from the acyl group ( $-\text{CH}_3$ ) and the ester group ( $\text{C}=\text{O}$ ). The longer the reaction time, the greater the area of the two signals, which means that the DS value of the acetylation increases [101].

Some of the advantages of acetylation modification include increasing starch clarity, lowering the gelatinization temperature, increasing the stability of frozen storage, and being more resistant to retrogradation [24,103]. Therefore, acetylated starch is commonly used in the food industry for the production of salad dressings, retorted soups, frozen foods, baby food, and snacks [86,104]. Chang and Lv [105] reported that acetylation reactions could also produce resistant starch in the form of RS type 4, which has a low glycemic index. In addition to its application in food ingredients, several studies have stated that acetylated starch with high DS is commonly used as a packaging material or in cigarette filters and has several applications in the pharmaceutical field [96,106]. Although it can improve the characteristics of starch, this modification tends to produce starch that is less resistant to high-temperature heating. Therefore, several researchers carried out a combination of physical modification + acetylation to improve the thermal stability of starch. Several modification combinations have been carried out, including annealing-acetylation [10,97] and sonication + acetylation [63].



#### 4. Characteristics of Acetylated Modified Starch/Flour

##### 4.1. Functional Properties of Acetylated Modified Starch/Flour

Functional characteristics are the properties of starch/flour that affect the usability of starch when applied. The functional characteristics of starch/flour can be viewed through several parameters, including amylose leaching/solubility, oil absorption capacity (OAC), water absorption capacity (WAC), freeze-thaw stability (FTS), and swelling power (SP). Swelling power is related to the amount of water absorbed, where the greater the swelling power value, the more water is absorbed. Starch granules will swell when heated in water, which is caused by the breaking of hydrogen bonds between starch molecules so that starch molecules will bind with water [54,107].

The swelling of granules is closely related to the release of starch molecules from granules or what is known as amylose leaching. As gelatinization proceeds, the water present in the starch suspension enters the outer amorphous and crystalline regions (located near the amorphous lamellae) [108,109]. The process of entry of water into the amorphous region causes granule swelling and weakens the hydrogen bonds between amylose and amylopectin chains. The continuous heating process takes place, causing starch molecules dissolved in water to easily move in and out of the solution system. Starch molecules that dissolve in hot water (amylose) will come out with the water, causing amylose leaching [110,111]. Solubility and swelling power are affected by several factors, including the amylose-lipid complex, molecular weight, granule size, amylose/amylopectin ratio, distribution of amylopectin chain lengths, amylose-amylopectin chain interactions, the molecular structure of starch granules, and crystal arrangement [28,112–115]. The solubility is more affected by the amylose content, while the swelling power is affected by the amylopectin component [116].

Water absorption capacity (WAC) is defined as the ability of granules to absorb water. WAC determines the amount of water available for starch gelatinization during cooking [117]. The gel formation cannot reach optimum conditions if the amount of water is lower. The greater the WAC, the more starch constituent material is lost, while the lower the WAC, the more compact the structure. Solubility, swelling power, and WAC are related to other parameters, namely viscosity, and crystallinity. Increases in solubility, SP, and WAC are associated with decreased crystallinity of starch and cause an increase in viscosity [118,119].

Starch paste stored at freezing temperatures will cause the water contained in the paste to form ice crystals, and these ice crystals will melt during thawing and release of water from the granules, which is called syneresis [120]. Freeze-thaw stability (FTS) describes the ability of pasta to withstand repeated freezing and thawing cycles without any physical changes. FTS is correlated with retrograde tendencies. The increased aggregation of starch molecules causes an increase in the release of water molecules from starch granules, so the syneresis increases, and FTS decreases [6,89]. Modification treatments, both acetylation and hydrothermal, can affect the interactions between starch molecules, which can affect the stability of the paste in frozen storage [74,121].

Retrogradation occurs when starch components that have been gelatinized re-associate. This association causes the starch structure to become more compact, making the paste more turbid. The modification of acetylation in corn starch was reported to increase starch's stability against retrogradation and increase the clarity of starch paste [15,87]. Based on the level of clarity, the paste is classified into three types, namely transparent, moderately transparent, and cloudy. The clarity of the starch paste can be observed through a spectrophotometer by measuring the % transmittance, where the higher the %transmittance, the more transparent the paste. The level of clarity of the paste varies depending on the type of paste, solubility, swelling power (SP), and the aggregation of starch molecules [122,123]. Starch with high clarity and viscosity is suitable for application as a thickening agent, while some food products, such as salad dressings, require opaque starch [9,15,124].

Starch with high solubility and hydration ability is needed in several processed food industries, such as in the manufacture of noodles, bakery products, jelly, and many more [56,125]. Acetylation modification can increase SP and WAC, while hydrothermal modification generally causes a decrease in SP and WAC. Information regarding the effect of acetylation modification and its dual modification on the functional properties of starch/flour is available in Table 3.

**Table 3.** The effect of acetylation and its dual modification on the functional properties of starch/flour.

Treatments	Materials	Functional Properties	References
Acetylation by vinyl acetate	Amaranth starch	Swelling power (SP) increased while solubility, WAC, and OAC decreased.	[126]
Acetylation	Sweet potato starch and flour Potato starch and flour	Starch: swelling volume (SV) increased; whiteness decreased. Flour: SV increased; whiteness increased. The whiteness degree of starch was higher than flour	[127]
Acetylation (pH 8.0–8.5, NaOH 1 M, 5 min)	Sweet potato starch	An increase in WAC, OAC, swelling power (SP), solubility, starch clarity, and gel strength. More stable to low-temperature storage.	[128]
Acetylation (Acetic anhydride 0–8%, pH 8.1–8.3, NaOH 3%)	Sweet potato starch	Swelling (SV) and solubility increased with increasing DS	[78]
Acetylation (pH 8, NaOH 3%, 10–20 min)	Potato starch Cassava starch	Water binding capacity (WBC), paste clarity, and solubility increased Whiteness was decreased Acetylated potato starch, which was reacted for 20 min, caused a decrease in WBC.	[83]
Acetylation (pH 8.0–8.4, NaOH 3%, 10 and 240 min)	Purple yam (PY) starch White yam (WY) starch	In PY, there is an increase in WAC, SV, and solubility, but in 240 min of acetylated PY, the changes were not significant. At 240 min of acetylated WY, the increase in WAC and SV was greater, but the solubility value was lower than at 10 min of acetylated WY.	[84]
Acetylation (pH 8.0–8.5, 1 M NaOH, 5 min)	Cocoyam starch	SV increased with increasing temperature and pH Solubility was decreased Improved WAC, OAC, and paste clarity	[85]
Acetylation (pH 8.0–8.4, NaOH 3%, 10 min)	Potato starch Maize starch	SV and paste clarity increased Paste clarity potato starch > corn starch Solubility increased until the concentration of 8%, then decreased at 10–12%. WAC decreased	[77]
Acetylation (pH 8–8.5, 1 M NaOH, 5 min)	Oat starch	WAC and OAC increased Frozen storage stability increased	[89]
Acetylation (pH 8, NaOH 3%)	Rice starch	Aggregation and deformation of starch granules occurred Size of starch granules reduced Granules become perforated	[88]
Acetylation (pH 8.0–8.4, 1 M NaOH, 30 min)	Sword bean starch	WAC and SV increased Solubility decreased	[90]

Table 3. Cont.

Treatments	Materials	Functional Properties	References
Acetylation (acetic anhydride, pH 7.5–9.0, 20–25 °C, 1–2 h,) and (vinyl acetate, pH 9–10, 20–25 °C, 1–2 h)	Yellow pea starch Chickpea starch Cowpea starch	Acetylation by vinyl acetate had a greater swelling ability Acetylation by acetic anhydride in cowpea reduced the swelling ability	[62]
Acetylation (acetic anhydride, pH 7–10, NaOH 3%, T = room temperature, t = 50 min)	Sago starch	There was an increase in solubility, SP, oil absorption capacity, water absorption capacity, and clarity.	[93]
Acetylation and ANN	Black bean starch Pinto bean starch	Acetylation: SV increased ANN: SV decreased	[129]
Acetylation and HMT	Buckwheat seed starch	Acetylation: OAC, WAC, solubility, SV, paste clarity, and whiteness increased. HMT: WAC, OAC, and paste clarity increased, while solubility, SV, and whiteness decreased	[59]
Acetylation (8% Acetic anhydride, 30 °C, pH 8, 1 M NaOH, 15–20 min)	Small-sized granule wheat starch Large-sized granule wheat starch	SV and paste clarity increased, while FTS decreased SV in large granules was greater than in small granules	[92]
Acetylation (4% NaOH, pH 7.8–8.2, 5 min)	Japonica rice starch Indica rice starch	SV and solubility decreased	[91]
Acetylation (Acetic anhydride 6% and 8%, pH 8.0–8.4, NaOH 3%, T = 25 °C, t = 10 min.)	Oat starch	Swelling factor increased Swelling temperature decreased Synaeresis decreased	[21]
Sonication-Acetylation (25, 40, and 25 + 40 Hz, 5 min, 45–75 °C)	Wheat starch	WAC and solubility increased frozen storage stability increased	[130]
Acetylation-ANN	Potato starch	Swelling power (SP) was higher than native starch and annealed starch	[26]
Acetylation-ANN	Mung beans starch	SV and solubility decreased	[97]
Acetylation and Acetylation-ANN	Waxy potato (WP) starch Waxy rice (WR) starch Waxy barley (WB) starch Waxy corn (WC) starch	Acetylation caused an increase in SV. Dual modification caused an increase in the SV of cereal starch, but there was no significant change in WP starch. Acetylation and Dual modified stable to low-temperature storage and paste clarity increased.	[10]
Acetylation-retrogradation (pH 8.5; NaOH 0.5 M, 15 min)	Purple sweet potato flour and starch	Solubility increased WAC and SP decreased	[94]
Acetylation-retrogradation (pH 8–9; NaOH 3%, 15 min)	Potato starch	Solubility increased water absorbability increased	[95]
Acetylation-Extrusion (Acetic anhydride 7.88%, Extrusion at BT = 80 °C, SS = 100 rpm)	Corn starch	Water absorption index decreased Water solubility index decreased	[96]

Modification by acetylation could increase the swelling power, solubility, and WAC as the DS increases. The modification of acetylation causes an increase in SP in sweet potato starch [128], potato starch [10,77,83], purple yam, white yam, and cocoyam starches [84,85], sword bean starch [90], chickpea and yellow pea starches [62], corn and waxy corn starches [10,77,87], rice and waxy rice starches [10,88], sago starch [93], wheat starch [92], and waxy barley starch [10]. This increase is due to the substitution of the hydrophilic (acetyl) group, which facilitates water penetration into the starch granules [87,89].

Improvements in starch hydration and water absorption capacity after modification by acetylation were found in sweet potato starch [128], potato starch [83], purple yam, white yam, and cocoyam starches [84,85], sword bean starches [90], oat starch [89], rice starch [88], and sago starch [93]. The increased hydration power of the granules due to the substitution of acetyl groups causes increased flexibility of the structure, making it easier to bind water [46]. Increased starch solubility due to modification of acetylation was found in sweet potato starch [128], potato starch [77,83], sword bean starch [90], corn and waxy corn starch [77,87], rice starch [88], and sago starch [93].

The modification of acetylation can also affect the solubility of starch and flour. Acetylation will generally increase solubility, mainly due to the addition of acetyl groups that disrupt the interactions between starch molecules, which in turn increases the affinity of starch molecules to dissolve in water [88]. The increase in starch solubility due to the substitution of acetyl groups will weaken the hydrogen bonds that connect starch on an intermolecular level as well as inhibit intermolecular associations so that the starch molecules will bind with water and dissolve along with the water coming out of the starch granules [84]. Nevertheless, several studies have found a decrease in WAC in acetylated potato and corn starch [77], a decrease in solubility in acetylated cocoyam starch [85], and a decrease in SP in acetylated japonica and indica rice starch [91]. The effect of acetylation modification on the hydration and solubility of granules is influenced by the number of substituted acetyl groups (DS); the higher the DS, the greater the changes that occur [88,93].

Several studies reported that the combination of modification by esterification (acetylation) + hydrothermal treatment was able to increase SP, WAC, and starch solubility [10,23,97]. This is because the esterification modification is related to the substitution of ester groups (acetyl/hydroxypropyl), which weakens the granule structure, thereby facilitating the penetration of water into the granules and increasing the interaction of starch molecules with water [10,23].

The acetylation modification can also reduce retrogradation tendencies and increase the clarity level of starch paste [46,59,77,85,128,129,131]. Increasing the clarity of the paste is related to the hydration ability of the granules. The greater the hydration ability of the granules, the higher the level of clarity. The substitution of acetyl groups will limit the intermolecular interactions of starch, thereby reducing the tendency for starch syneresis [87,89,129]. The decrease in syneresis tendencies in acetylated starch is related to the substitution of acetyl groups, which limits intermolecular interactions when the paste is stored at low temperatures [46]. In addition, the modification of acetylation and its combination can also affect the whiteness of starch, where most of the modification treatments cause a decrease in whiteness [10,26].

Modification by acetylation can lead to an increase in the hydration ability of starch granules. This is due to the disorganization of the intragranular structure followed by the following events: (1) disruption of the intermolecular hydrogen bonds of the starch and increased penetration of water into the amorphous regions [75,88], (2) the presence of repulsive forces rejecting intermolecular starch due to the substitution of acetyl groups, (3) the partial depolymerization of the amylopectin structure, which causes a decrease in molecular weight (MW) [88,132], (4) a decrease in starch crystallinity [92,132,133] and the limitation of starch intermolecular interactions [84].

The acetyl group can have two properties, namely hydrophilic and hydrophobic. Acetylation at low DS makes starch tend to be hydrophilic, while acetylation at high DS makes starch tend to be hydrophobic [93,134]. Therefore, several studies reported that acetylation causes an increase in OAC [85,89,90,93]. The high OAC value has the potential to improve the flavor and mouthfeel of food products, such as whipped cream, sausages, chiffon cakes, and various processed desserts [135].

Several studies have reported that acetylation can reduce the tendency of starch to experience retrogradation and syneresis and shows a better level of clarity and transparency of starch than natural starch [77,85,89]. This is due to the substitution of acetyl groups which will hinder the association between starch molecules [88]. The clarity of starch is



related to the ability of starch hydration (WAC and SP). The increased hydration ability of the granules causes more water molecules to be trapped in the granules so that when observed using a spectrophotometer, more light can be transmitted by the paste [136].

Acetylation can reduce the occurrence of syneresis in starch. A decrease in the percentage of syneresis indicates an increase in the stability of the paste against frozen storage [13,15]. Syneresis is related to retrogradation events in which reassociation occurs between starch molecules when stored at low temperatures. Syneresis causes a decrease in the water content of amylose/amylopectin, which can affect product characteristics. The substitution of acetyl groups can prevent the reassociation of the starch molecules so that the retrogradation tendency decreases. In addition, the substitution of acetyl groups also increases the water storage capacity so that the retention power of granules to water is also greater [10,46,83,88,130]. Mendoza et al. [84] reported that limiting the intermolecular associations of starch due to acetylation was necessary to produce starch with high hydration, good storage stability, and high clarity.

Acetylation modifications can also be combined with other modifications. The combination of acetylation with hydrothermal treatments (ANN and HMT) can increase the hydration and solubility of starch [26,97]. A single hydrothermal modification generally reduces the hydration power and solubility of starch. The addition of esterification modifications (acetylation or hydroxypropylation) can increase the hydration ability of granules and starch solubility. This statement is supported by several studies, which reported that the combination of acetylation + ANN modification in waxy cereal and potato starches had a higher swelling power (SP) than native starch and ANN starch, while the combination with HMT could increase SP, but this combination decreased the solubility of starch [10].

The substitution of ester groups (acetyl/hydroxypropyl) can weaken the crystalline structure of granules so that water penetration into the granules becomes easier and SP increases [10,23]. Nonetheless, Sitanggang et al. [97] reported that the combination of acetylation + ANN modification in black bean and pinto bean starches reduced SP and starch solubility. This decrease was due to an increase in starch crystallinity due to ANN modification, so the hydration power of the granules decreased [28]. In addition, the substitution of the acetyl group in this dual-modified starch causes the starch to become more hydrophobic [86,93].

Egodage [10] reported that the combination of acetylation + ANN modification in waxy rice and waxy potato starches increased the percentage of transmittance, which indicated an increase in the clarity of the paste. Low-temperature storage conditions caused a decrease in the clarity of the paste caused by the retrogradation process. The decrease in clarity of acetylated and acetylated + ANN-modified starch paste was not as big as that of natural starch and ANN-modified starch. The substitution of the acetyl group prevented amylopectin molecules from aggregating in the paste so that the retrogradation tendency decreased [10,77]. Reducing the retrogradation tendency could reduce the level of paste syneresis. Abedi et al. [130] reported that the combination of acetylation + sonication modifications reduced the percentage of syneresis due to the substitution of acetyl groups, which prevented the retrogradation process. Thus, the combination of acetylation + hydrothermal modification can improve the functional characteristics of starch. Changes in the functional properties of starch depend on the dominant modification treatment. Acetylation modification tends to weaken the crystalline structure of starch, so if this modification is combined with hydrothermal-modified starch, it can weaken the perfect structure. The substitution of ester groups with low DS tends to cause hydrophilic starch, thereby increasing the hydration ability of the modified starch, but if the DS is too low, the esterification reaction does not change the characteristics of the starch [93,137].

#### *4.2. Pasting Properties of Acetylated Modified Starch/Flour*

Pasting properties are indicators that determine starch properties during processing, which affect the cooking quality and functionality. Pasting properties described as an amylographic curve can be used to determine the application of starch in food

ingredients [138,139]. Starch with low viscosity is suitable for liquid-based foodstuffs, while starch with high viscosity is suitable for use as a thickening agent [140–142].

Based on the amylographic curve, starch is classified into four types, namely types A, B, C, and V [143,144]. Starch type A shows high swelling of starch granules followed by a rapid decrease in viscosity during cooking, commonly found in potato starch, cassava starch, and several types of cereals. Type B starch, which has almost the same curved shape as type A but has a lower viscosity, is usually found in cereals. Type C starch, which exhibits limited swelling of the granules, has no peak viscosity, and tends to be heat-stable, is commonly found in modified starches and legumes. Type V starch, showing limited swelling of the granules, is usually found in starch that interacts with alcohol or fatty acid [144,145]. The effect of acetylation modification and its dual modification on the pasting properties of starch/flour is presented in Table 4.

**Table 4.** The effect of acetylation and its dual modification on the pasting properties of starch/flour.

Treatments	Starch/Flour	Pasting Properties	References
Acetylation (pH 8.0–8.5, NaOH 1 M, 5 min)	Sweet potato starch	Peak viscosity (PV), setback viscosity (SB), breakdown viscosity (BD), and pasting temperature (PT) decreased.	[128]
Acetylation by vinyl acetate	Amaranth starch	PV and BD increased, while PT and final viscosity (FV) decreased.	[126]
Acetylation-Enzymatic	Sweet potato flour Potato flour	PV, BD, and SB decreased.	[104]
Acetylation	Sweet potato starch Potato starch	PT and SB of potato starch did not change significantly, but PV and BD decreased. Whereas in sweet potato starch, there was a decrease in PT, PV, BD, and SB. There was a decreased PT, PV, BD, and SB in acetylated flour.	[127]
Acetylation	Commercial potato starch	PT, PV, BD, SB, and final viscosity (FV) decreased.	[146]
Acetylation	Potato starch	PT, PV, and SB decreased, while BD increased.	[147]
Acetylation (pH 8.0–8.4, NaOH 3%, 10 and 240 min)	Purple yam (PY) starch White yam (WY) starch	The initial gelatinization temperature decreased, but heating to 95 °C increased the viscosity. PV and SB in purple yam increased, while PV and BD in white yam decreased.	[84]
Acetylation (pH 8.0–8.5, NaOH 1 M, 5 min)	Cocoyam starch	PT, PV, hot paste viscosity (HPv), cold paste viscosity (CPv), and SB decreased. BD increased.	[85]
Acetylation, NaOH (pH 8.0–8.5, NaOH 1 N, KOH 1 N, Ca(OH) <sub>2</sub> 1 N, 60 min)	Waxy maize starch	PV increased, while PT decreased	[61]
Acetylation and HMT	Buckwheat seed starch	PV, FV, trough viscosity (TV), and PT for acetylated starch increased, while BD and SB decreased. PT in HMT-starch increased, while PV, FV, TV, BD, and SB decreased.	[59]
Acetylation (pH 8, NaOH 3%)	Rice starch	PV and TV increased, while PT and SB decreased.	[88]

Table 4. Cont.

Treatments	Starch/Flour	Pasting Properties	References
Acetylation and ANN	Black bean starch Pinto bean starch	Acetylation-ANN reduces PV, HPV, CPV, BD, and SB Acetylation lowers PT and faster gelatinization time ANN increases PT and longer gelatinization time	[129]
Acetylation (pH 8.0–8.4, NaOH 1 M, 30 min)	Sword bean starch	PV, BD, and PT increased, while SB decreased	[90]
Cross-linked Acetylation starch (Acetic anhydride, pH 8, and sodium trimetaphosphate 0.7–0.9%)	Maize starch	PV and SB increased, while PT and BD decreased	[60]
Acetylation (acetic anhydride, pH 7.5–9.0, 1–2 h, 20–25 °C) and (vinyl acetate, pH 9–10, 1–2 h, 20–25 °C)	Yellow pea starch Chickpea starch Cowpea starch	The smaller the particle size of the chickpea and yellow pea, the greater the viscosity of the paste, while the particle size of the cowpea does not affect the viscosity. Acetylation using vinyl acetate produces a paste with a greater viscosity.	[62]
Acetylation (8% Acetic anhydride, 30 °C, pH 8, NaOH 1 M, 15–20 min)	Small granule wheat starch Large granule wheat starch	Acetylation increased paste viscosity, but PT decreased	[92]
Acetylation (4% NaOH, pH 7.8–8.2, 5 min)	Japonica rice starch Indica rice starch	PV and PT decreased; the reduction was greater with the single acetylation modification. BD and SB increased.	[91]
Acetylation-sonication (25, 40, and 25 + 40 Hz, 5 min, 45–75 °C)	Wheat starch	PV and BD increased, while PT and SB decreased	[130]
Acetylation-ANN	Mung bean starch	PV, BD, HPv, and CPv decreased, while PT and SB increased	[97]
Acetylation-retrogradation (pH 8.5, NaOH 0.5 M, 15 min)	Purple sweet potato flour and starch	Gelatinization occurs more quickly PV, BD, TV, FV, and SB decreased drastically	[94]

In general, acetylation modification causes a decrease in starch gelatinization temperature so that it facilitates product application in terms of energy saving and its utilization in products that are susceptible to heat [128]. Several studies reported that the modification of acetylation causes a decrease in gelatinization temperature in sweet potato starch [128]; potato starch [147]; yam starches [84,85]; cowpea, yellow pea, and chickpea starches [62]; pinto bean and black bean starches [129]; rice starch [88,91]; waxy cornstarch [61]; and wheat starch [92], as well as decreased setback viscosity in sweet potato starch [104,128]; potato starch [127]; sword bean starch [90]; yellow pea, and chickpea starches [62]; black bean and pinto bean starches [129]; and rice starch [88]. A decrease in SB indicates a decreased retrogradation tendency, making the starch more stable at low-temperature storage. Meanwhile, most studies report that acetylation causes an increase in viscosity followed by an increase in starch hydration ability [59,62,88,90,92].

Table 4 also shows that acetylation modification combined with hydrothermal treatment can improve the pasting properties of starch to cover the weaknesses in hydrothermal modification. Sitanggang et al. [97] reported that the combination of acetylation + ANN modification could increase PT and SB and reduce PV and BD. The addition of the esterification treatment (acetylation/hydroxypropylation) was able to weaken the crystalline matrix so that it had a higher viscosity and a lower gelatinization temperature when compared to the single hydrothermal treatment [23,148,149].

The substitution of acetyl groups causes weak intermolecular forces, which decreases the gelatinization temperature of starch acetate. This statement is supported by several researchers who reported a decrease in gelatinization temperature after the modification of acetylation, including sweet potato starch [128], potato starch [147], yam starches [84,85], cowpea, yellow pea, and chickpea starches [62], pinto bean and black bean starches [129], rice starch [88,91], waxy maize starches [61], and wheat starch [92]. A decrease in the pasting temperature of the acetylated starch indicates that a large amount of energy is not required for the starch to gelatinize. This can be used to save energy in cooking or processing using acetylated starch [128].

The substitution of the acetyl group weakens the intermolecular bonds between amylose and amylopectin, thereby facilitating the penetration of water into the amorphous region, which is followed by an increase in the ability to absorb water during gelatinization [59,85,88,90]. Increasing the hydration ability of starch granules during gelatinization can increase the viscosity of the paste. Several studies reported an increase in paste viscosity after the modification of acetylation in sweet potato starch [127], purple yam starch [84], sword bean starch [90], yellow pea cowpea, and chickpea starches [62], buckwheat starch [59], waxy maize starch [61], rice starch [88], and wheat starch [92]. However, the effect of acetylation modification on starch viscosity is not always the same. Several studies reported that acetylation can have a different effect on each type of starch. The difference in results obtained is influenced by several factors, including the distribution of amylopectin chains, amylose content, molecular arrangement of granules, and the degree of substitution of acetyl groups [62,84].

Acetylation modification can reduce the setback viscosity (SB), which indicates an increase in starch storage stability, especially at cold temperatures. This statement is reinforced by several studies which reported a decrease in SB after modification of acetylation [62,88,90,104,127,129]. Acetyl group substitution inhibits intermolecular interactions of starch, thereby minimizing the tendency of starch retrogradation [88,94,104].

The modification of acetylation with different materials and types of starch can produce different pasting properties as well. Acetylation with vinyl acetate and acetic anhydride in starch can cause a decrease in the gelatinization temperature due to the weakening of the intermolecular interactions of starch [25,150]. However, acetylation with vinyl acetate in yellow pea and chickpea starches changed the type of starch gelatinization from type C to type B. In contrast, acetylation with acetic anhydride did not change the gelatinization pattern. The peak viscosity of all types of starch increased after acetylation modification with vinyl acetate. In contrast, acetylation with acetic anhydride caused a decrease in the peak viscosity of cowpea and chickpea starches. Both types of reagents caused a decrease in the SB of cowpea starch but an increase in SB in yellow pea starch. Meanwhile, acetylation with either acetate anhydride or vinyl acetate did not change the SB chickpea starch. Thus, the modification of acetylation with different reagents and starch sources has a different effect on its pasting properties [62,84,127].

Hydrothermal modification can increase the starch gelatinization temperature followed by a decrease in peak, BD, and SB viscosity, while acetylation causes a decrease in PT and SB followed by an increase in PV and BD [59,151,152]. Changes in the pasting properties of hydrothermally modified starch are contradictory to acetylation modifications. Sitanggang et al. [97] reported that the combination of acetylation + ANN modification led to an increase in PT and SB, followed by a decrease in peak viscosity and BD. This indicates that ANN modification is dominant because the resulting characteristics resemble ANN starch. In other studies, the dual modification of retrogradation + acetylation [94] and sonication + acetylation [130] produced starch with characteristics like acetylated starch. Yu et al. [94] reported that acetylation of retrograded starch caused a greater decrease in viscosity. This may be due to the substitution of acetyl groups causing starch to be hydrophobic. Referring to Rahim et al. [93], the greater the substituted acetyl group, the more hydrophobic the starch. In addition, acetylation treatment can increase the PV and BD and decrease the pasting temperature (PT). This is due to the substitution of acetyl



groups weakening the crystalline structure so that water penetration into the granules is easier [11,41]. Thus, the pasting properties of the dual-modified starch will lead to the dominant treatment.

#### 4.3. Starch Granule Morphology of Acetylated Modified Starch/Flour

The shape and size of starch granules vary depending on the starch source. Most of the tuber starches have oval-shaped granules, but some have round, polygonal, and spherical ones, and some are irregular; the size varies from 1 to 110  $\mu\text{m}$  depending on the type of starch [153]. For example, sweet potato starch has polygonal granules [154,155], round, hexagonal, and spherical with a size of 4–26  $\mu\text{m}$  and a smooth surface without cracks [104].

Changes in the morphology of starch granules are commonly found in modified starches. Several studies have stated that acetylation modification causes granule damage (deformation, fusion, cracking, resulting in holes) [84,88,94]. However, some modifications, such as annealing, generally do not cause significant changes in granule morphology. The morphological characteristics of modified starch may vary in each sample and are influenced by several factors, including the source of starch, the type of modification, and the modification conditions (time, temperature, and reagents used). The morphological characteristics of starch granules can be analyzed in several ways, including light microscopy, scanning electron microscope (SEM), transmission electron microscope (TEM), atomic force microscope (AFM), and confocal laser scanning microscope (CLSM) [27,156,157]. Information on the morphological characteristics of acetylated and its dual modification of starch/flour can be seen in Table 5.

**Table 5.** The effect of acetylation and its dual modification on the morphological characteristics of starch/flour.

Treatments	Starch/Flour	Granule Morphology	References
Acetylated-Enzymatic	Sweet potato flour Potato flour	Aggregation of starch granules was formed, and the surface became irregular/rough.	[104]
Acetylation by vinyl acetate	Amaranth starch	The surface of the granules was smooth, showing, and no significant changes occurred.	[126]
Acetylated (pH 8, NaOH 3%, 10–20 min)	Potato starch Cassava starch	No significant changes occurred Slight granule fusion occurred	[83]
Acetylation (acetic acid, pH 8.0–8.5 by NaOH 0.5 N)	Corn starch Potato starch	The surface of starch granules in corn and potato starch becomes rough due to breakdown and erosion.	[44]
Acetylation	Potato starch	Fragmentation of starch granules	[147]
Acetylated (pH 8.0–8.4, NaOH 3%, 10 min)	Potato starch Corn starch	Fusion of starch granules occurred where potato starch granules were more susceptible than corn starch. The greater the concentration of reactants and DS, the greater the damage that occurred.	[77]
Acetylated (acetic anhydride) and acetylated distarch adipate (acetic anhydride and adipic acid)	Potato starch	Hole formation occurred in the middle of the granules (doughnut-like forms) in acetylated starch. There was no significant change, but the modified acetylated distarch adipate starch had a more compact surface.	[158]
Acetylated (pH 8.0–8.4, NaOH 3%, 10 and 240 min)	Purple yam (PY) starch White yam (WY) starch	Holes appeared, but starch granules tended to retain their shape	[84]
Acetylated (pH 8, NaOH 1 M, 60 min)	Corn starch	Granule aggregation occurred; the aggregation between granules was getting bigger along with the greater concentration of acetic anhydride.	[87]

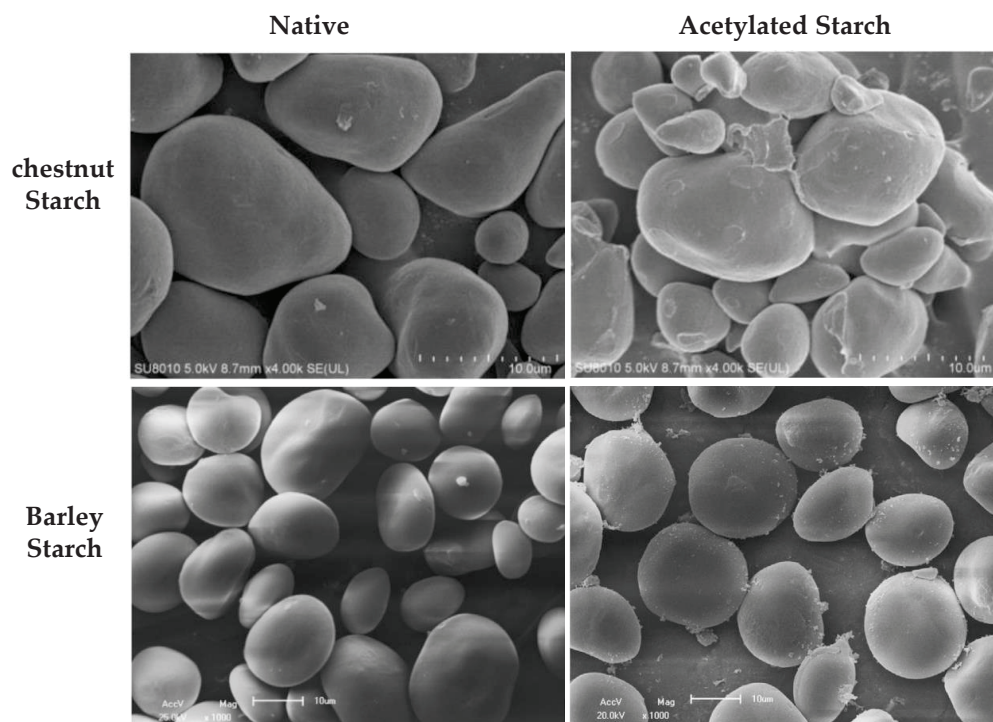
Table 5. Cont.

Treatments	Starch/Flour	Granule Morphology	References
Acetylated (pH 8, NaOH 50%, 15–240 min)	High-amylose maize starch	In the largest DS (2.23), granule fusion occurred, which caused the surface to become rougher and shaped like fibers. Granular damage was getting bigger along with the bigger the DS value.	[73]
Acetylated (pH 8, NaOH 3%)	Rice starch	Aggregation and deformation of starch granules occurred The size of the starch granules became smaller Starch granules became hollow	[88]
Acetylated (pH 8–8.5, NaOH 1 M, 5 min)	Oat starch	The texture of the starch granules becomes coarser, and small pores appear on the surface.	[89]
Acetylated (pH 8.0–8.4, NaOH 1 M, 30 min)	Sword bean starch	Some of the starch granules were broken (<10%) and caused the surface texture to become rough.	[90]
Acetylated (8% Acetic anhydride, 30 °C, pH 8, NaOH 1 M, 15–20 min)	Small granule wheat starch Large granule wheat starch	Starch granule damaged Starch with a larger granule size was easily damaged	[92]
Acetylation (Acetic anhydride 6% and 8%, pH 8.0–8.4, NaOH 3%, T = 25 °C, t = 10 min.)	Oat starch	The whole surface of starch granules was slightly damaged.	[21]
Acetylated and HMT	Buckwheat seed starch	The granules decreased slightly in size and became more separated from each other. Combination with HMT caused some starch granules to perforate.	[59]
Cross-linked Acetylation starch (Acetic anhydride, pH 8, and sodium trimetaphosphate 0.7–0.9%)	Maize starch	No significant changes occurred Starch granules have smooth surfaces and clear edges.	[60]
Acetylated and retrogradation (pH 8.5, NaOH 0.5 M, 15 min)	Purple sweet potato starch and flour	Acetylation caused granule aggregation and an increase in size Modification of acetylation + retrogradation resulted in a more compact structure, where the granule structure of starch is more compact than that of flour	[94]
Acetylated -sonication (25, 40, 65 Hz, 5 min, 45–75 °C)	Wheat starch	Starch granule fusion occurred There were holes and cracks on the surface of the starch granules	[130]
Acetylated and ANN	Mung bean starch	The granules became weaker and had a rougher surface The distance between granules became more tenuous, especially in dual-modified starch	[97]
Acetylated and ANN	Waxy potato (WP) starch Waxy rice (WR) starch Waxy barley (WB) starch Waxy corn (WC) starch	Acetylated starch had a rougher surface than native starch; the greater the damage, the greater the DS. The combination of acetylation + ANN caused a slight change in the granule surface in the form of a rougher surface.	[10]

In general, acetylation can cause the fusion and aggregation of starch granules [73,77, 88,147]. This is related to the substitution of acetyl groups, which causes the disintegration of the structure and the more porous nature of the granules [104,159]. Xu et al. [73] reported

that the substitution of acetyl groups in high numbers caused granule fragmentation, where the starch granules melted to form a fiber-like structure.

In addition, several studies have stated that acetylation reactions can also cause the formation of holes or pores so that the surface of the granules becomes rough [89,90,158]. These changes may occur due to partial hydrolysis by acids and reactions with alkalis. Fornal et al. [158] reported that the formation of holes or pores could be associated with the gelatinization of the granule surface due to the neutralization reaction with alkali (NaOH) in the acetylation modification process. However, several studies stated that acetylation modification at low DS did not cause changes in granule morphology [10,59,83,84]. Examples of morphological changes in acetylated starch can be seen in Figure 4.



**Figure 4.** Morphological changes in acetylated modified chestnut starch [14] and barley starch [160], with permission from Elsevier, 2015.

Figure 4 shows that the modification of acetylation can cause starch granules to deform to form small fragments. The substitution of acetyl groups into starch molecules weakens the inter-/intramolecular bonds of starch and causes starch granules to lose their integrity [88,159]. The integrity of the starch is weakened, and its structure becomes increasingly porous during the acetylation reaction; then, the starch granules experience fragmentation and aggregate with each other [15,159].

Changes in the morphology of starch granules due to acetylation modifications can have different results. Several factors affect the morphological diversity of acetylated starch, namely internal factors such as the content of amylose-amylopectin and external factors such as type of reactant, concentration of reactant, reaction time, temperature, type of alkali, and concentration of alkali. Morphological changes will increase with the greater substitution of acetyl groups [126,160]. This may be due to the low DS acetylation reaction only taking place in the amorphous area of the granule surface so that it does not cause changes in the granule structure, whereas, at high DS, acetylation reactions can take place in the internal structure of the granules which causes greater damage [84,159].

The combination of acetylation with other modifications (dual modifications), such as hydrothermal treatment, also produces a variety of granule morphology. Acetylation modifications generally cause granule aggregation and fusion, whereas hydrothermal modifications (HMT and ANN) are more likely to maintain their integrity [10,161,162].

Therefore, in the dual treatment, the resulting modification of the morphological characteristics depends on the dominant modified treatment. However, there are dual-modified treatments that give a synergistic effect, while others depend on the most dominant treatment. The dual modification treatment that is synergistic includes sonication-acetylation modification. The sonication modification facilitates the acetylation reaction so that the effectiveness of the acetylation reaction in starch granules increases [130].

The dual modification of ANN-acetylation can produce starch with morphological characteristics resembling acetylated starch. This indicates that the modification of esterification/acetylation has a dominant effect [97]. Egodage [10] reported that the use of 5% ANN-Acetylation treatment did not cause granule changes, but 10% ANN-Acetylation treatment caused morphological changes resembling acetylated modified starch. This was due to the 5% acetylation of substituted acetyl groups that are too low to change the morphology of the granules. Although there was a slight change in the acetylated and dual-modified starch granules, the sizes and shapes of the granules did not change significantly; this indicates that the integrity of the granules was maintained during modification [10]. Different results were reported by Yu et al. [94], who stated that the dual modification of acetylation-retrogradation in starch and sweet potato flour caused granule deformation where the granules undergo fusion and aggregation. This could lead to granule damage when the ANN modification is smaller than during the retrogradation modification, so the ANN-acetylated starch is more stable in maintaining its structure than the retrogradation-acetylated starch. The differences in the characteristics produced are influenced by several factors, including the type of modification, the type of starch and its structure, as well as the conditions and treatment of the modification [56,163].

#### 4.4. Starch Crystallinity of Acetylated Modified Starch/Flour

The crystallinity of starch can be determined by observing the X-ray diffraction pattern. The X-ray diffraction pattern is related to the formation of semicrystalline regions during modification so that the amorphous and crystalline areas can be identified [164,165]. The basic principle of this test is the exposure of X-rays to the sample by scanning the diffraction area at an angle of  $2\theta$  from  $4^\circ$ . The diffractogram pattern will produce a series of diffraction peaks with varying relative intensities along a certain value ( $2\theta$ ). Amorphous and crystalline regions can be distinguished by making curves and linear lines. The curve is made by connecting each point of minimum intensity; the area above the curve is known as the crystalline region ( $\alpha_c$ ). The linear line is made by connecting two intensity points at  $4^\circ$  and  $37^\circ$  ( $2\theta$ ); the area that lies between the curve and the linear line is known as the amorphous region ( $\alpha_a$ ). The ratio of the upper area ( $\alpha_c$ ) to the total diffracted area ( $\alpha_c + \alpha_a$ ) is known as the degree of crystallinity or relative crystallinity [165–168].

Based on the intensity peaks formed, the starch crystallinity is divided into three types, namely types A, B, and C. The type A diffraction pattern has a distinctive pattern with peaks of  $23^\circ$ ,  $18^\circ$ ,  $17^\circ$ , and  $15^\circ$  ( $2\theta$ ), commonly found in cereal starch (rice) [169,170], and sweet potatoes [153–155,171]. The type B starch diffraction pattern is characterized by a small peak at  $5.6^\circ$  ( $2\theta$ ) and double peaks at  $24^\circ$  and  $22^\circ$  ( $2\theta$ ), commonly found in fruits, tubers, and high amylose starch [172,173]. Type C starch is a combination of different type A and type B crystal structures and is further classified into type  $C_A$  (close to type A) and  $C_B$  (close to type B). Type C starch showed strong diffraction peaks at  $17^\circ$  and  $23^\circ$  ( $2\theta$ ) and some small peaks around  $5.6^\circ$  and  $15^\circ$  ( $2\theta$ ).  $C_A$ -type starch showed a shoulder peak at  $18^\circ$  ( $2\theta$ ), while  $C_B$  type showed two shoulder peaks at  $22^\circ$  and  $24^\circ$  ( $2\theta$ ) [167]. Type C starch is commonly found in beans and sweet potatoes. Besides types A, B, and C, there is type V, which is formed due to the presence of amylose-fat complexes. Lopez-Rubio et al. [174] V-type crystals show diffraction peaks at points  $7^\circ$ ,  $13^\circ$ , and  $20^\circ$  ( $2\theta$ ). Guo et al. [141], in their research, stated that sweet potato has a type C diffraction pattern. The acetylation modification process and its combination can affect starch crystallinity. Information regarding the effect of acetylation modification and its combination on various types of starch on crystallinity can be seen in Table 6.



**Table 6.** The effect of acetylation and its dual modification on the crystallinity of starch/flour.

Treatments	Starch/Flour	Crystallinity	References
Acetylation by acetic anhydride and toluene sulfuric acid	Corn starch	Acetylation reduced the degree of crystallinity of corn starch by increasing the amorphous regions. Acetylated starch with a DS of 3 had a slightly higher Tg than acetylated starch with a DS of 1.5.	[81]
Acetylation	Sweet potato Potato	There was no significant change in the crystalline region	[82]
Acetylation by vinyl acetate	Amaranth starch	There was no change in the crystalline diffraction pattern, but the relative crystallinity (RC) decreased.	[126]
Acetylation (pH 8, NaOH 3%, 10–20 min)	Potato starch Cassava starch	There was no change in the crystalline diffraction pattern, but the crystallinity index increased.	[83]
Acetylation	Potato starch	The degree of crystallinity increased	[147]
Acetylation (pH 8, NaOH 3%, 30–55 min)	Banggai yam starch	The crystalline diffraction pattern remained the same, but the degree of crystallinity increased. Acetylation for 50 min had the highest degree of crystallinity	[175]
Acetylation (pH 8.0–8.4, NaOH 3%, 10 and 240 min)	Purple yam (PY) starch White yam (WY) starch	The type of crystallinity remained the same, but the degree of crystallinity decreased with increasing DS.	[84]
Acetylation (pH 8.0–8.5, NaOH 1 M, 5 min)	Cocoyam	The crystalline diffraction pattern and degree of crystallinity did not change significantly.	[85]
Acetylation (NaOH 20%, 40 min, and NaOH 2%, 120 min)	Waxy maize starch	The crystalline diffraction pattern remained the same, but there was a decrease in the degree of crystallinity.	[86]
Acetylation (pH 8.0–8.5, NaOH 1 N, KOH 1 N, and Ca(OH) <sub>2</sub> 1 N, 60 min)	Waxy maize starch	The crystalline diffraction pattern remained the same.	[61]
Acetylation (pH 8, NaOH 50%, 15–240 min)	High amylose maize starch	The crystalline diffraction pattern remained the same, but an increase in the degree of crystallinity.	[73]
Acetylation (pH 8–8.5, NaOH 1 M, 5 min)	Oat starch	The crystalline diffraction pattern remained the same, but there was a decrease in the degree of crystallinity.	[89]
Acetylation (pH 8.0–8.4, NaOH 1 M, 30 min)	Sword bean starch	There was a change in the type of starch crystallinity from type B to type C	[90]
Acetylation (acetic anhydride, pH 7.5–9.0, 1–2 h, 20–25 °C) and (vinyl acetate, pH 9–10, 1–2 h, 20–25 °C)	Yellow pea starch Chickpea starch Cowpea starch	The crystalline diffraction pattern and the degree of crystallinity of the starch did not change significantly.	[62]
Acetylation (acetic acid, pH 8.0–8.5 by NaOH 0.5 N)	Corn starch Potato starch	There was a similar diffraction pattern of starch crystallinity but a slight loss in the degree of starch crystallinity.	[44]
Acetylation	Corn starch Waxy corn starch	The crystalline diffraction pattern remained the same, but there was a decrease in the degree of starch crystallinity.	[79]

Table 6. Cont.

Treatments	Starch/Flour	Crystallinity	References
ANN-Acetylation	Mung bean starch	The crystalline diffraction pattern remained the same, The crystalline index increased, where the crystallinity of ANN was greater than the crystallinity of the dual modification.	[97]
ANN-Acetylation	Waxy corn (WC) starch Waxy barley (WB) starch Waxy rice (WR) starch Waxy potato (WP) starch	The degree of crystallinity decreased in acetylated starch, where the greater the DS, the greater the decrease. The greatest decrease in crystallinity occurred in the dual modification (ANN- Acetylation)	[10]
Sonication- Acetylation (25, 40, and 25 + 40 Hz, 5 min, 45–75 °C)	Wheat starch	There was a change in the type of starch crystallinity and a decrease in the degree of starch crystallinity as the sonication frequency increased in the dual modification (sonication-acetylation).	[130]

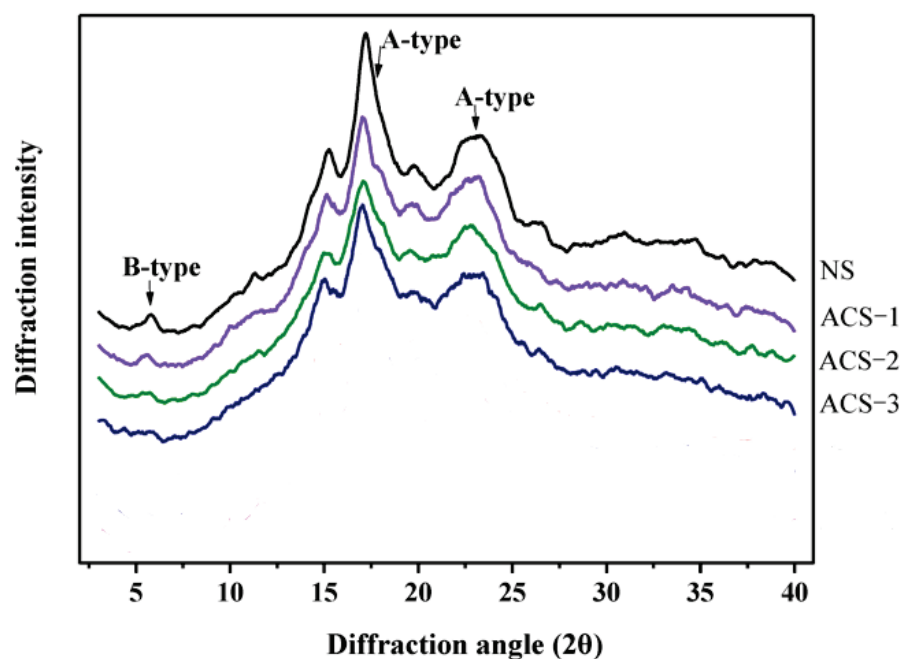
The type of starch crystallinity due to modification treatment can change, as indicated by the change in diffraction intensity. The acetylation treatment conditions and the dual modifications applied can change the polymorphic properties of starch. In general, acetylation at low DS can weaken the diffraction intensity, but no change in the crystalline diffraction pattern was found. This is supported by several studies, which stated that starch acetate weakened diffraction intensity but still retained its type of crystallinity [10,61,62,73,77,83–86,175]. However, the results obtained in each study were not always the same. Shah et al. [89] reported that acetylation did not change the type of starch crystallinity but caused a decrease in the diffraction intensity peak and found an increase in the peak  $2\theta$  of  $20^\circ$ . This peak may reflect the formation of amylose complexes with other compounds, such as amylose-lipids. In comparison, Adebowale et al. [90] reported that acetylation modification changed the crystallinity type of sword bean starch from type B to type C, indicating that polymorph A began to form during the modification.

The modification treatment of both acetylation and dual modification can increase, decrease, or not change the relative crystallinity (RC) of starch. The rearrangement of the double helix structure in starch granules can increase starch crystallinity, while the decrease occurs due to the partial gelatinization of starch granules [28,176]. The modification of starch caused an increase in RC, as seen in studies of acetylation modification of potato and cassava starch [83,147] and on the dual ANN-acetylation modification in mung bean starch [97]. Meanwhile, a decrease in RC occurred in the modified acetylation of white and purple yam starch [84], oat starch [89], high amylose maize starch [73], Banggai yam starch [175], waxy maize starch [86], waxy barley, waxy corn, waxy potato, waxy rice starch [10], and corn starch [79]. RC reduction also occurred in dual modifications acetylation-ANN of waxy potato starch, waxy barley starch, waxy rice starch, and waxy corn starch [10]. However, no RC changes were found in the modified acetylation of peas starch [62], cocoyam starch [85], and waxy maize starch [61].

The effect of acetylation on crystallinity depends on the type of starch and the treatment conditions. Differences in starch crystallinity are affected by several internal components of starch, including the interaction of double helices in crystals, the arrangement of double helices in the crystalline area, and the number of crystalline areas, which is affected by amylopectin content and chain length, and crystal size [164,165]. The polymorphic type and crystallinity of starch are also strongly affected by the internal components of starch and external factors such as environmental conditions and the presence of fat, which can form amylo-lipid complexes [28,177,178].

The substitution of hydroxyl groups with acetyl groups can weaken the hydrogen bonds that connect between starch molecules, which then causes a decrease in starch crys-

tallinity [159]. This statement is supported by several studies, which stated that acetylation modification caused a decrease in RC [10,73,79,84,89,175]. Nonetheless, the crystallinity index of cassava and potato starch increased after acetylation modification [83,147]. This was due to the weakening of the amorphous area of the granules followed by an increase in the crystalline area. Meanwhile, in several studies, acetylation with low DS only took place in the amorphous area of the granules, so it did not cause any changes in the crystalline area [61,62,85]. The effect of acetylation modification on the X-ray diffractogram profile can be seen in Figure 5.



**Figure 5.** XRD profiles of acetylated modified chestnut starch at different reaction times (NS = native starch, ACS-1 = acetylated starch 30 min, ACS-2 = acetylated starch 60 min, ACS-3 = acetylated starch 90 min) [14].

Figure 5 shows that the acetylation process does not cause changes in the diffraction peaks. Acetylation reactions with a low degree of substitution tend to attack amorphous areas so that no significant changes are found in the crystalline structure and do not change the diffraction pattern [14,85,175]. In Figure 5, two types of peaks are observed, namely the B-type peaks at  $5.6^\circ$  ( $2\theta$ ) and A-type peaks at  $17.0^\circ$  and  $23.0^\circ$  ( $2\theta$ ). The acetylation modification did not significantly change the A-type polymorphs at  $17.0^\circ$  and  $23.0^\circ$  ( $2\theta$ ) because these A-type polymorphs have a strong crystalline structure that is difficult to penetrate by acetylating reagents. However, the longer acetylation was able to reduce the number of B-type polymorphs at  $5.6^\circ$  ( $2\theta$ ), which had a weak crystalline structure. This could be due to the longer acetylation increasing the substitution of acetyl groups and reducing the hydroxyl groups in the amylose and amylopectin molecular chains, thereby damaging the long-range order of double helices so that the intra- and intermolecular bonds of starch weakened and caused a decrease in crystallinity [14]. However, an increase in crystallinity was found after 50 min of acetylation. This may have been due to the acid residue left after modification. This residue can cause the degradation of starch amorphous areas [175]. Wang et al. [179] reported an increase in crystallinity after the modification of acid hydrolysis because acid tends to attack amorphous areas. Acetylation with high DS can leave more acid residues and cause damage to amorphous areas. Thus, DS on acetylation modification in starch and flour greatly affects the crystallinity of the resulting starch.

Acetylation modification can be combined with several other modifications, especially hydrothermal modification, to obtain the desired crystallinity characteristics. In general, the combination of acetylation and hydrothermal modification (HMT, ANN) did not cause

a change in the crystalline diffraction pattern, but a change in the RC did occur. The combination of ANN + acetylation modification caused a decrease in crystallinity in waxy (rice, barley, corn, and potato) starches [10]. Nonetheless, the dual ANN + AS modification of mung bean starch caused an increase in crystallinity, but the crystallinity was lower when compared to the single ANN treatment. This indicated that acetylation modification could disrupt the crystal structure of ANN starch, which was already perfect. The dual modification treatment could also weaken the effect of changing one of the treatments, such as the ANN + acetylation modification in mung bean starch [97].

The modification of acetylation and the combination of ANN + acetylation did not cause any changes in the starch crystalline diffraction pattern. However, the modification of acetylation could cause a decrease in RC and increases in DS. This was due to the substitution of acetyl groups weakening the formation of intermolecular hydrogen bonds, causing a weakening of the crystalline structure [86]. The dual combination of ANN + acetylation modification could cause a greater decrease in RC than ANN modification. This decrease indicated that the effects of these two modifications are opposite to each other. Structural changes that occurred during ANN led to an increase in the mobility of the amylopectin chains in the amorphous lamellae and the movement of molecules in the crystalline region, facilitating the entry of acetyl groups into the granules. This increase in acetyl group substitution then caused greater damage [10,15].

#### 4.5. Comparison of Acetylated Modified Starch/Flour with Other Modifications

The modification of acetylation in starch/flour has several advantages, including a relatively easy modification process that can produce starch/flour, which has a high swelling ability, clear starch paste, and good stability against retrogradation [14,98,100,102]. However, acetylation modification has several drawbacks because it requires a process to clean up chemical residues, which is quite expensive; the potential for waste is not environmentally friendly; and acetylated starch is unstable to thermal processes [15–17]. In addition, different characteristics may occur depending on the type of starch/flour and the processing conditions. The general comparison of acetylated modified starch/flour with other modifications can be seen in Table 7.

**Table 7.** The general comparison of acetylated modified starch/flour with other modifications.

Parameters	Acetylated Starch	Oxidized Starch	Crosslinked Starch	Hydrothermal Starch (HMT and Others)
Energy consumption for process modification	Low	Low	Low	High
Environmental friendliness	Less environmentally friendly	Less environmentally friendly	Less environmentally friendly	Environmentally friendly
Starch paste clarity	Paste clarity increases	Paste clarity increases	Paste clarity increases	Paste clarity decreases
Starch solubility	Solubility increases	Solubility increases	Solubility decreases	Solubility decreases
Swelling power (SP)	SP increases	SP increases	SP decreases	SP increases
Water absorption capacity (WAC)	WAC increases	WAC increases	WAC increases	WAC increases
Stability at high temperatures	The stability decreases	The stability increases	The stability increases	The stability increases
Stability against retrogradation	The stability increases	The stability increases	The stability decreases	The stability decreases
Degree of crystallinity	The degree of crystallinity decreases	The degree of crystallinity decreases	The degree of crystallinity increases	The degree of crystallinity increases
Starch granule morphology	The starch granules are rougher	The starch granules are rougher and more porous	The starch granules are rougher	The starch granules are rougher



## 5. Conclusions and Future Research

The modification of acetylation in starch/flour generally causes the fusion of starch granules, increasing the granule hydration ability, solubility, paste viscosity, storage stability and decreasing the gelatinization temperature and retrogradation stability. Acetylation generally does not change the crystalline structure of starch because it takes place in the amorphous areas of the granules, and some of them reduce the degree of crystallinity. Changes in starch/flour characteristics due to acetylation are strongly affected by the degree of acetyl group substitution. Dual acetylation modification with hydrothermal treatments such as HMT/ANN or cross-linking can produce starch/flour with better cooking and storage stability than native starch or single-modified starch and broaden its application to various products.

The modification of acetylation in starch/flour is continuing to develop, especially to increase the efficiency of the modification process and the application of acetylated starch in various fields and products. The efficiency of the modification process is being improved, including via pre-treatment through the formation of porous starch, such as by ultrasonication, partial hydrolysis, or oxidation. Acetylated starch/flour was also developed through dual modifications, including cross-linking and hydrothermal treatments, to increase thermal stability. The application of acetylated starch has also been developed more broadly to produce starch nanoparticles, which can then be used for encapsulation, starch-based composite, biofilms, drug delivery systems, and other applications.

**Author Contributions:** Conceptualization, E.S. and Y.C.; methodology, E.S., R.I. and T.A.R.; software, R.I.; validation, Y.C., R.I. and T.A.R.; formal analysis, E.S. and T.A.R.; investigation, E.S. and T.A.R.; resources, Y.C. and R.I.; data curation, R.I. and T.A.R.; writing—original draft preparation, E.S. and T.A.R.; writing—review and editing, Y.C. and R.I.; visualization, E.S. and R.I.; supervision, Y.C.; project administration, E.S. and R.I.; funding acquisition, E.S. All authors have read and agreed to the published version of the manuscript.

**Funding:** This article was supported by Universitas Padjadjaran, Indonesia.

**Institutional Review Board Statement:** Not applicable.

**Data Availability Statement:** Not applicable.

**Acknowledgments:** The authors would like to thank the Rector of Universitas Padjadjaran and The Ministry of Education, Culture, Research, and Technology of the Republic of Indonesia.

**Conflicts of Interest:** The authors declare no conflict of interest.

## References

1. Fonseca, L.M.; El Halal, S.L.M.; Dias, A.R.G.; da Rosa Zavareze, E. Physical Modification of Starch by Heat-Moisture Treatment and Annealing and Their Applications: A Review. *Carbohydr. Polym.* **2021**, *274*, 118665. [CrossRef] [PubMed]
2. Majzoobi, M.; Pesaran, Y.; Mesbahi, G.; Farahnaky, A. Evaluation of the Effects of Hydrothermal Treatment on Rice Flour and Its Related Starch. *Int. J. Food Prop.* **2016**, *19*, 2135–2145. [CrossRef]
3. Majzoobi, M.; Farahnaky, A. Granular Cold-Water Swelling Starch; Properties, Preparation and Applications, a Review. *Food Hydrocoll.* **2021**, *111*, 106393. [CrossRef]
4. Subroto, E.; Sitha, N.; Filianty, F.; Indiarso, R.; Sukri, N. Freeze Moisture Treatment and Ozonation of Adlay Starch (Coix Lacryma-Jobi): Effect on Functional, Pasting, and Physicochemical Properties. *Polymers* **2022**, *14*, 3854. [CrossRef]
5. Chang, Q.; Zheng, B.; Zhang, Y.; Zeng, H. A Comprehensive Review of the Factors Influencing the Formation of Retrograded Starch. *Int. J. Biol. Macromol.* **2021**, *186*, 163–173. [CrossRef]
6. Wang, S.; Li, C.; Copeland, L.; Niu, Q.; Wang, S. Starch Retrogradation: A Comprehensive Review. *Compr. Rev. Food Sci. Food Saf.* **2015**, *14*, 568–585. [CrossRef]
7. Liu, X.; Chao, C.; Yu, J.; Copeland, L.; Wang, S. Mechanistic Studies of Starch Retrogradation and Its Effects on Starch Gel Properties. *Food Hydrocoll.* **2021**, *120*, 106914. [CrossRef]
8. Chung, H.J.; Liu, Q.; Hoover, R. Effect of Single and Dual Hydrothermal Treatments on the Crystalline Structure, Thermal Properties, and Nutritional Fractions of Pea, Lentil, and Navy Bean Starches. *Food Res. Int.* **2010**, *43*, 501–508. [CrossRef]
9. Colussi, R.; Pinto, V.Z.; El Halal, S.L.M.; Vanier, N.L.; Villanova, F.A.; Marques e Silva, R.; da Rosa Zavareze, E.; Dias, A.R.G. Structural, Morphological, and Physicochemical Properties of Acetylated High-, Medium-, and Low-Amylose Rice Starches. *Carbohydr. Polym.* **2014**, *103*, 405–413. [CrossRef]

10. Egodage, R. *The Impact of Annealing, Acetylation, and Dual Modification on the Structure and Physicochemical Properties of Waxy Starches*; Memorial University of Newfoundland: Corner Brook, NL, Canada, 2019.
11. Shaari, S.; Samsudin, H.; Uthumporn, U. Effect of Acetylation Treatment on Surface Modified Tapioca Starches. *Food Res.* **2021**, *5*, 340–347. [CrossRef]
12. Gagnetten, M.; Cáceres, S.G.; Rodríguez Osuna, I.A.; Olaiz, N.M.; Schebor, C.; Leiva, G.E. Modification of Cassava Starch by Acetylation and Pulsed Electric Field Technology: Analysis of Physical and Functional Properties. *Innov. Food Sci. Emerg. Technol.* **2023**, *85*, 103344. [CrossRef]
13. Abba, H.; Ibrahim, A.; Shallangwa, G.A.; Uba, S.; Dallatu, Y.A. Effect of Acetylation on Stability to Retrogradation of Starch Extracted from Wild Polynesian Arrowroot (*Tacca Leontopetaloides* (L.) Kuntze) for Utilization as Adhesive on Paper. *J. Polym.* **2014**, *2014*, 732174. [CrossRef]
14. Liu, C.; Yan, H.; Liu, S.; Chang, X. Influence of Phosphorylation and Acetylation on Structural, Physicochemical and Functional Properties of Chestnut Starch. *Polymers* **2022**, *14*, 172. [CrossRef] [PubMed]
15. Colussi, R.; El Halal, S.L.M.; Pinto, V.Z.; Bartz, J.; Gutkoski, L.C.; da Rosa Zavareze, E.; Dias, A.R.G. Acetylation of Rice Starch in an Aqueous Medium for Use in Food. *LWT Food Sci. Technol.* **2015**, *62*, 1076–1082. [CrossRef]
16. Eshag Osman, M.F.; Mohamed, A.A.; Mohamed Ahmed, I.A.; Alamri, M.S.; Al Juhaimi, F.Y.; Hussain, S.; Ibraheem, M.A.; Qasem, A.A. Acetylated Corn Starch as a Fat Replacer: Effect on Physicochemical, Textural, and Sensory Attributes of Beef Patties during Frozen Storage. *Food Chem.* **2022**, *388*, 132988. [CrossRef]
17. Miyazaki, M.; Maeda, T.; Morita, N. Gelatinization Properties and Bread Quality of Flours Substituted with Hydroxypropylated, Acetylated and Phosphorylated Cross-Linked Tapioca Starches. *J. Appl. Glycosci.* **2005**, *52*, 345–350. [CrossRef]
18. Lu, X.; Shi, C.; Zhu, J.; Li, Y.; Huang, Q. Structure of Starch-Fatty Acid Complexes Produced via Hydrothermal Treatment. *Food Hydrocoll.* **2019**, *88*, 58–67. [CrossRef]
19. Pukkahuta, C.; Suwannawat, B.; Shobsngob, S.; Varavinit, S. Comparative Study of Pasting and Thermal Transition Characteristics of Osmotic Pressure and Heat-Moisture Treated Corn Starch. *Carbohydr. Polym.* **2008**, *72*, 527–536. [CrossRef]
20. Subroto, E.; Indiaro, R.; Marta, H.; Shalihah, S. Effect of Heat Moisture Treatment on Functional and Pasting Properties of Potato. *Food Res.* **2019**, *3*, 469–476. [CrossRef]
21. Mirmoghtadaie, L.; Kadivar, M.; Shahedi, M. Effects of Cross-Linking and Acetylation on Oat Starch Properties. *Food Chem.* **2009**, *116*, 709–713. [CrossRef]
22. Ashogbon, A.O. Dual Modification of Various Starches: Synthesis, Properties and Applications. *Food Chem.* **2021**, *342*, 128325. [CrossRef] [PubMed]
23. Gunaratne, A.; Corke, H. Effect of Hydroxypropylation and Alkaline Treatment in Hydroxypropylation on Some Structural and Physicochemical Properties of Heat-Moisture Treated Wheat, Potato and Waxy Maize Starches. *Carbohydr. Polym.* **2007**, *68*, 305–313. [CrossRef]
24. Ačkar, Đ.; Babić, J.; Jozinović, A.; Miličević, B.; Jokić, S.; Miličević, R.; Rajič, M.; Šubarić, D. Starch Modification by Organic Acids and Their Derivatives: A Review. *Molecules* **2015**, *20*, 19554–19570. [CrossRef] [PubMed]
25. Nawaz, M.A.; Singh, T.K.; Tan, M.; Prakash, S.; Fukai, S.; Bhandari, B. Acetylation of Intact White Rice Grains to Alter the Physicochemical Properties. *J. Cereal Sci.* **2020**, *92*, 102928. [CrossRef]
26. Zdybel, E.; Wilczak, A.; Kapelko-Żeberska, M.; Tomaszewska-Ciosk, E.; Gryszkin, A.; Gawrońska, A.; Zięba, T. Physicochemical Properties and Digestion Resistance of Acetylated Starch Obtained from Annealed Starch. *Polymers* **2021**, *13*, 4141. [CrossRef]
27. Subroto, E.; Mahani; Indiaro, R.; Yarlina, V.P.; Izzati, A.N. A Mini Review of Physicochemical Properties of Starch and Flour by Using Hydrothermal Treatment. *Polymers* **2022**, *14*, 5447. [CrossRef]
28. Zavareze, E.D.R.; Dias, A.R.G. Impact of Heat-Moisture Treatment and Annealing in Starches: A Review. *Carbohydr. Polym.* **2011**, *83*, 317–328. [CrossRef]
29. Raina, C.S.; Singh, S.; Bawa, A.S.; Saxena, D.C. Some Characteristics of Acetylated, Cross-Linked and Dual Modified Indian Rice Starches. *Eur. Food Res. Technol.* **2006**, *223*, 561–570. [CrossRef]
30. de Oliveira, N.R.; Fornaciari, B.; Mali, S.; Carvalho, G.M. Acetylated Starch-Based Nanoparticles: Synthesis, Characterization, and Studies of Interaction With Antioxidants. *Starch-Stärke* **2018**, *70*, 1700170. [CrossRef]
31. Xiao, H.; Yang, F.; Lin, Q.; Zhang, Q.; Tang, W.; Zhang, L.; Xu, D.; Liu, G.-Q. Preparation and Properties of Hydrophobic Films Based on Acetylated Broken-Rice Starch Nanocrystals for Slow Protein Delivery. *Int. J. Biol. Macromol.* **2019**, *138*, 556–564. [CrossRef]
32. Liu, Q.; Li, F.; Ji, N.; Dai, L.; Xiong, L.; Sun, Q. Acetylated Debranched Starch Micelles as a Promising Nanocarrier for Curcumin. *Food Hydrocoll.* **2021**, *111*, 106253. [CrossRef]
33. Gangopadhyay, A.; Bose, A.; Rout, S.S.; Mohapatra, R. Application of Dual Modified Corn Starch as a Polymer for the Colon Targeted Direct Compressible Budesonide Tablet. *J. Drug Deliv. Sci. Technol.* **2022**, *74*, 103556. [CrossRef]
34. Promhuad, K.; Bumbudsanpharoke, N.; Wadaugsorn, K.; Sonchaeng, U.; Harnkarnsujarit, N. Maltol-Incorporated Acetylated Cassava Starch Films for Shelf-Life-Extension Packaging of Bakery Products. *Polymers* **2022**, *14*, 5342. [CrossRef] [PubMed]
35. Fitch-Vargas, P.R.; Camacho-Hernández, I.L.; Rodríguez-González, F.J.; Martínez-Bustos, F.; Calderón-Castro, A.; Zazueta-Morales, J.d.J.; Aguilar-Palazuelos, E. Effect of Compounding and Plastic Processing Methods on the Development of Bioplastics Based on Acetylated Starch Reinforced with Sugarcane Bagasse Cellulose Fibers. *Ind. Crops Prod.* **2023**, *192*, 116084. [CrossRef]

36. Nasser, R.; Ngunjiri, R.; Moresoli, C.; Yu, A.; Yuan, Z.; Xu, C. (Charles) Poly(Lactic Acid)/Acetylated Starch Blends: Effect of Starch Acetylation on the Material Properties. *Carbohydr. Polym.* **2020**, *229*, 115453. [CrossRef]
37. Yao, X.; Lin, R.; Liang, Y.; Jiao, S.; Zhong, L. Characterization of Acetylated Starch Nanoparticles for Potential Use as an Emulsion Stabilizer. *Food Chem.* **2023**, *400*, 133873. [CrossRef]
38. Cui, B.; Lu, Y.; Tan, C.; Wang, G.; Li, G.-H. Effect of Cross-Linked Acetylated Starch Content on the Structure and Stability of Set Yoghurt. *Food Hydrocoll.* **2014**, *35*, 576–582. [CrossRef]
39. Rahim, A.; Kadir, S.; Jusman, J.; Zulkippli, Z.; Hambali, T.N.A. Physical, Chemical and Sensory Characteristics of Bread with Different Concentrations of Acetylated Arenga Starches. *Int. Food Res. J.* **2019**, *26*, 841–848.
40. Lin, D.; Zhou, W.; Yang, Z.; Zhong, Y.; Xing, B.; Wu, Z.; Chen, H.; Wu, D.; Zhang, Q.; Qin, W.; et al. Study on Physicochemical Properties, Digestive Properties and Application of Acetylated Starch in Noodles. *Int. J. Biol. Macromol.* **2019**, *128*, 948–956. [CrossRef]
41. Wang, R.; Wang, J.; Liu, M.; Strappe, P.; Li, M.; Wang, A.; Zhuang, M.; Liu, J.; Blanchard, C.; Zhou, Z. Association of Starch Crystalline Pattern with Acetylation Property and Its Influence on Gut Microbota Fermentation Characteristics. *Food Hydrocoll.* **2022**, *128*, 107556. [CrossRef]
42. Gu, Y.; Cheng, L.; Gu, Z.; Hong, Y.; Li, Z.; Li, C. Preparation, Characterization and Properties of Starch-Based Adhesive for Wood-Based Panels. *Int. J. Biol. Macromol.* **2019**, *134*, 247–254. [CrossRef] [PubMed]
43. Wang, Z.; Li, Z.; Gu, Z.; Hong, Y.; Cheng, L. Preparation, Characterization and Properties of Starch-Based Wood Adhesive. *Carbohydr. Polym.* **2012**, *88*, 699–706. [CrossRef]
44. Posada-Velez, M.C.; Pineda-Gomez, P.; Martinez-Hernandez, H.D. Acetylated Corn and Potato Starches as an Alternative to the Toxic Inorganic Coagulants/Flocculants for Wastewater Treatment. *Environ. Nanotechnol. Monit. Manag.* **2023**, *20*, 100786. [CrossRef]
45. Pang, Z.; Xu, R.; Luo, T.; Che, X.; Bansal, N.; Liu, X. Physicochemical Properties of Modified Starch under Yogurt Manufacturing Conditions and Its Relation to the Properties of Yogurt. *J. Food Eng.* **2019**, *245*, 11–17. [CrossRef]
46. Singh, H.; Sodhi, N.S.; Singh, N. Structure and Functional Properties of Acetylated Sorghum Starch. *Int. J. Food Prop.* **2012**, *15*, 312–325. [CrossRef]
47. Li, H.; Wang, Y.; Zhao, P.; Guo, L.; Huang, L.; Li, X.; Gao, W. Naturally and Chemically Acetylated Polysaccharides: Structural Characteristics, Synthesis, Activities, and Applications in the Delivery System: A Review. *Carbohydr. Polym.* **2023**, *313*, 120746. [CrossRef] [PubMed]
48. Collar, C.; Rosell, C.M. Bakery and Confectioneries. In *Valorization of by Products from Plant Based Food Processing Industries*; Chandrasekaran, M., Ed.; CRC Press: Boca Raton, FL, USA, 2013; pp. 554–582.
49. Watcharakitti, J.; Win, E.E.; Nimnuan, J.; Smith, S.M. Modified Starch-Based Adhesives: A Review. *Polymers* **2022**, *14*, 2023. [CrossRef]
50. Zia-ud-Din; Xiong, H.; Fei, P. Physical and Chemical Modification of Starches: A Review. *Crit. Rev. Food Sci. Nutr.* **2017**, *57*, 2691–2705. [CrossRef]
51. Adiyanti, T.; Subroto, E. Modifications Of Banana Starch And Its Characteristics: A Review. *Int. J. Sci. Technol. Res.* **2020**, *9*, 3–6.
52. Masina, N.; Choonara, Y.E.; Kumar, P.; du Toit, L.C.; Govender, M.; Indermun, S.; Pillay, V. A Review of the Chemical Modification Techniques of Starch. *Carbohydr. Polym.* **2017**, *157*, 1226–1236. [CrossRef]
53. Hong, J.; Zeng, X.-A.; Brennan, C.S.; Brennan, M.; Han, Z. Recent Advances in Techniques for Starch Esters and the Applications: A Review. *Foods* **2016**, *5*, 50. [CrossRef] [PubMed]
54. Ojogbo, E.; Ogunsona, E.O.; Mekonnen, T.H. Chemical and Physical Modifications of Starch for Renewable Polymeric Materials. *Mater. Today Sustain.* **2020**, *7–8*, 100028. [CrossRef]
55. Tharanathan, R.N. Starch-Value Addition by Modification. *Crit. Rev. Food Sci. Nutr.* **2005**, *45*, 371–384. [CrossRef] [PubMed]
56. Wang, Z.; Mhaske, P.; Farahnaky, A.; Kasapis, S.; Majzoobi, M. Cassava Starch: Chemical Modification and Its Impact on Functional Properties and Digestibility, a Review. *Food Hydrocoll.* **2022**, *129*, 107542. [CrossRef]
57. Hermansson, A.M.; Svegmarm, K. Developments in the Understanding of Starch Functionality. *Trends Food Sci. Technol.* **1996**, *7*, 345–353. [CrossRef]
58. Nurmilah, S.; Subroto, E. Chemical Modification of Starch for the Production of Resistant Starch Type-4 (Rs4): A Review. *Int. J. Eng. Trends Technol.* **2021**, *69*, 45–50. [CrossRef]
59. Sarkar, S. Influence of Acetylation and Heat-Moisture Treatment on Physio-Chemical, Pasting and Morphological Properties of Buckwheat (*Fagopyrum esculentum*) Starch. *Asian J. Dairy Food Res.* **2016**, *35*, 298–303. [CrossRef]
60. Xue, X.; Liang, Q.; Gao, Q.; Luo, Z. One-Step Synthesis of Cross-Linked Esterified Starch and Its Properties. *Appl. Sci.* **2022**, *12*, 4075. [CrossRef]
61. Wang, Y.J.; Wang, L. Characterization of Acetylated Waxy Maize Starches Prepared under Catalysis by Different Alkali and Alkaline-Earth Hydroxides. *Starch/Staerke* **2002**, *54*, 25–30. [CrossRef]
62. Huang, J.; Schols, H.A.; Jin, Z.; Sulmann, E.; Voragen, A.G.J. Characterization of Differently Sized Granule Fractions of Yellow Pea, Cowpea and Chickpea Starches after Modification with Acetic Anhydride and Vinyl Acetate. *Carbohydr. Polym.* **2007**, *67*, 11–20. [CrossRef]
63. Aadil, R.M.; Zeng, X.A.; Sun, D.W.; Wang, M.S.; Liu, Z.W.; Zhang, Z.H. Combined Effects of Sonication and Pulsed Electric Field on Selected Quality Parameters of Grapefruit Juice. *LWT Food Sci. Technol.* **2015**, *62*, 890–893. [CrossRef]



64. Lidstrom, P.; Tierney, J.; Wathey, B.; Westman, J. Microwave Assisted Organic Synthesis-A Review. *Tetrahedron* **2001**, *57*, 9225–9283. [CrossRef]
65. Kumoro, A.C.; Amalia, R.; Budiyati, C.S.; Retnowati, D.S.; Ratnawati, R. Preparation and Characterization of Physicochemical Properties of Glacial Acetic Acid Modified Gadung (*Diocorea Hispida* Dennst) Flours. *J. Food Sci. Technol.* **2015**, *52*, 6615–6622. [CrossRef] [PubMed]
66. Tian, S.; Chen, Y.; Chen, Z.; Yang, Y.; Wang, Y. Preparation and Characteristics of Starch Esters and Its Effects on Dough Physicochemical Properties. *J. Food Qual.* **2018**, *2018*, 1395978. [CrossRef]
67. Teodoro, A.P.; Mali, S.; Romero, N.; de Carvalho, G.M. Cassava Starch Films Containing Acetylated Starch Nanoparticles as Reinforcement: Physical and Mechanical Characterization. *Carbohydr. Polym.* **2015**, *126*, 9–16. [CrossRef]
68. Otache, M.A.; Duru, R.U.; Achugasim, O.; Abayeh, O.J. Advances in the Modification of Starch via Esterification for Enhanced Properties. *J. Polym. Environ.* **2021**, *29*, 1365–1379. [CrossRef]
69. Casas, J.; Persson, P.V.; Iversen, T.; Córdova, A. Direct Organocatalytic Ring-Opening Polymerizations of Lactones. *Adv. Synth. Catal.* **2004**, *346*, 1087–1089. [CrossRef]
70. Imre, B.; Vilaplana, F. Organocatalytic Esterification of Corn Starches towards Enhanced Thermal Stability and Moisture Resistance. *Green Chem.* **2020**, *22*, 5017–5031. [CrossRef]
71. Trela, V.D.; Ramallo, A.L.; Albani, O.A. Synthesis and Characterization of Acetylated Cassava Starch with Different Degrees of Substitution. *Brazilian Arch. Biol. Technol.* **2020**, *63*, e20180292. [CrossRef]
72. Sodhi, N.S.; Singh, N. Characteristics of Acetylated Starches Prepared Using Starches Separated from Different Rice Cultivars. *J. Food Eng.* **2005**, *70*, 117–127. [CrossRef]
73. Xu, Y.; Miladinov, V.; Hanna, M.A. Synthesis and Characterization of Starch Acetates with High Substitution. *Cereal Chem.* **2004**, *81*, 735–740. [CrossRef]
74. Zhang, K.; Zhao, D.; Ma, X.; Guo, D.; Tong, X.; Zhang, Y.; Qu, L. Effect of Different Starch Acetates on the Quality Characteristics of Frozen Cooked Noodles. *Food Sci. Nutr.* **2022**, *10*, 678–688. [CrossRef] [PubMed]
75. Babic, J.; Subaric, D.; Ackar, D.; Kovacevic, D.; Pilizota, V.; Kopjar, M. Preparation and Characterization of Acetylated Tapioca Starches. *Dtsch. Leb.* **2007**, *103*, 580–585.
76. Huang, J.; Schols, H.A.; Klaver, R.; Jin, Z.; Voragen, A.G.J. Acetyl Substitution Patterns of Amylose and Amylopectin Populations in Cowpea Starch Modified with Acetic Anhydride and Vinyl Acetate. *Carbohydr. Polym.* **2007**, *67*, 542–550. [CrossRef]
77. Singh, N.; Chawla, D.; Singh, J. Influence of Acetic Anhydride on Physicochemical, Morphological and Thermal Properties of Corn and Potato Starch. *Food Chem.* **2004**, *86*, 601–608. [CrossRef]
78. Lee, H.L.; Yoo, B. Dynamic Rheological and Thermal Properties of Acetylated Sweet Potato Starch. *Starch/Stärke* **2009**, *61*, 407–413. [CrossRef]
79. Pietrzyk, S.; Fortuna, T.; Łabanowska, M.; Juszczak, L.; Gałkowska, D.; Bączkiewicz, M.; Kurdziel, M. The Effect of Amylose Content and Level of Oxidation on the Structural Changes of Acetylated Corn Starch and Generation of Free Radicals. *Food Chem.* **2018**, *240*, 259–267. [CrossRef]
80. Ren, F.; Wang, J.; Yu, J.; Zhong, C.; Xie, F.; Wang, S. Green Synthesis of Acetylated Maize Starch in Different Imidazolium Carboxylate and Choline Carboxylate Ionic Liquids. *Carbohydr. Polym.* **2022**, *288*, 119353. [CrossRef]
81. Nasser, R.; Moresoli, C.; Yu, A.; Yuan, Z.; Xu, C. (Charles) Structural Dependence of the Molecular Mobility in Acetylated Starch. *Polymer* **2021**, *215*, 123371. [CrossRef]
82. Chen, Z.; Schols, H.A.; Voragen, A.G.J. Differently Sized Granules from Acetylated Potato and Sweet Potato Starches Differ in the Acetyl Substitution Pattern of Their Amylose Populations. *Carbohydr. Polym.* **2004**, *56*, 219–226. [CrossRef]
83. Mbougoung, P.D.; Tenin, D.; Scher, J.; Tchiégang, C. Influence of Acetylation on Physicochemical, Functional and Thermal Properties of Potato and Cassava Starches. *J. Food Eng.* **2012**, *108*, 320–326. [CrossRef]
84. Mendoza, J.S.; RuyDíaz, J.H.; Quintero, A.F. Effect of the Acetylation Process on Native Starches of Yam (*Dioscorea* spp.). *Rev. Fac. Nac. Agron. Medellín* **2016**, *69*, 7997–8006. [CrossRef]
85. Lawal, O.S. Composition, Physicochemical Properties and Retrogradation Characteristics of Native, Oxidised, Acetylated and Acid-Thinned New Cocoyam (*Xanthosoma sagittifolium*) Starch. *Food Chem.* **2004**, *87*, 205–218. [CrossRef]
86. Luo, Z.G.; Shi, Y.C. Distribution of Acetyl Groups in Acetylated Waxy Maize Starches Prepared in Aqueous Solution with Two Different Alkaline Concentrations. *Food Hydrocoll.* **2018**, *79*, 491–497. [CrossRef]
87. Ayucitra, A. Preparation and Characterisation of Acetylated Corn Starches. *Int. J. Chem. Eng. Appl.* **2012**, *3*, 156–159. [CrossRef]
88. González, Z.; Pérez, E. Effect of Acetylation on Some Properties of Rice Starch. *Starch-Stärke* **2002**, *54*, 148–154. [CrossRef]
89. Shah, A.; Masoodi, F.A.; Gani, A.; Ashwar, B.A. Physicochemical, Rheological and Structural Characterization of Acetylated Oat Starches. *LWT Food Sci. Technol.* **2017**, *80*, 19–26. [CrossRef]
90. Adebowale, K.O.; Afolabi, T.A.; Olu-Owolabi, B.I. Functional, Physicochemical and Retrogradation Properties of Sword Bean (*Canavalia gladiata*) Acetylated and Oxidized Starches. *Carbohydr. Polym.* **2006**, *65*, 93–101. [CrossRef]
91. Lee, S.J.; Hong, J.Y.; Lee, E.J.; Chung, H.J.; Lim, S.T. Impact of Single and Dual Modifications on Physicochemical Properties of Japonica and Indica Rice Starches. *Carbohydr. Polym.* **2015**, *122*, 77–83. [CrossRef]
92. Van Hung, P.; Morita, N. Effects of Granule Sizes on Physicochemical Properties of Cross-Linked and Acetylated Wheat Starches. *Starch/Stärke* **2005**, *57*, 413–420. [CrossRef]



93. Rahim, A.; Mahfudz; Muhandi; Kadir, S.; Rostiati; Alam, N.; Hutomo, G.S.; Priyantono, E.; Salingkat, C.A.; Abdullah, R. Effect of PH and Acetic Anhydride Concentration on Physicochemical Characteristics of Acetylated Sago Starch. *IOP Conf. Ser. Earth Environ. Sci.* **2022**, *1107*, 12124. [CrossRef]
94. Yu, S.X.; Mu, T.H.; Zhang, M.; Ma, M.M.; Zhao, Z.K. Effects of Retrogradation and Further Acetylation on the Digestibility and Physicochemical Properties of Purple Sweet Potato Flour and Starch. *Starch/Staerke* **2015**, *67*, 892–902. [CrossRef]
95. Kapelko, M.; Zięba, T.; Gryszkin, A.; Styczyńska, M.; Wilczak, A. Properties of Retrograded and Acetylated Starch Produced via Starch Extrusion or Starch Hydrolysis with Pullulanase. *Carbohydr. Polym.* **2013**, *97*, 551–557. [CrossRef] [PubMed]
96. Calderón-Castro, A.; Jacobo-Valenzuela, N.; Félix-Salazar, L.A.; Zazueta-Morales, J.d.J.; Martínez-Bustos, F.; Fitch-Vargas, P.R.; Carrillo-López, A.; Aguilar-Palazuelos, E. Optimization of Corn Starch Acetylation and Succinylation Using the Extrusion Process. *J. Food Sci. Technol.* **2019**, *56*, 3940–3950. [CrossRef] [PubMed]
97. Sitanggang, A.; Sani, P.; Mastuti, T. Modification of Mung Bean Starch by Annealing Treatment and Acetylation. In Proceedings of the 2nd SEAFST International Seminar—2nd SIS, Bogor, Indonesia, 4–5 September 2019; SciTePress: Setubal, Portugal, 2020; pp. 10–19, ISBN 978-989-758-466-4. [CrossRef]
98. Rahim, A.; Siswo Huto, G.; Rahman, N.; Bohari, H.S.A. Structure and Functional Properties of Arenga Starch by Acetylation with Different Concentrations of Acetic Anhydride. *Asian J. Sci. Res.* **2019**, *12*, 220–228. [CrossRef]
99. Otemuyiwa, I.O.; Aina, A.F. Physicochemical Properties and In-Vitro Digestibility Studies of Microwave Assisted Chemically Modified Breadfruit (*Artocarpus altilis*) Starch. *Int. J. Food Prop.* **2021**, *24*, 140–151. [CrossRef]
100. Chi, H.; Xu, K.; Wu, X.; Chen, Q.; Xue, D.; Song, C.; Zhang, W.; Wang, P. Effect of Acetylation on the Properties of Corn Starch. *Food Chem.* **2008**, *106*, 923–928. [CrossRef]
101. Vidal, N.P.; Bai, W.; Geng, M.; Martinez, M.M. Organocatalytic Acetylation of Pea Starch: Effect of Alkanoyl and Tartaryl Groups on Starch Acetate Performance. *Carbohydr. Polym.* **2022**, *294*, 119780. [CrossRef]
102. Kemas, C.U.; Ngwuluka, N.C.; Ocheke, N.A.; Nep, E.I. Starch-Based Xerogels: Effect of Acetylation on Physicochemical and Rheological Properties. *Int. J. Biol. Macromol.* **2017**, *98*, 94–102. [CrossRef]
103. Chakraborty, I.; N, P.; Mal, S.S.; Paul, U.C.; Rahman, M.H.; Mazumder, N. An Insight into the Gelatinization Properties Influencing the Modified Starches Used in Food Industry: A Review. *Food Bioprocess Technol.* **2022**, *15*, 1195–1223. [CrossRef]
104. Yadav, A.R.; Guha, M.; Reddy, S.Y.; Tharanathan, R.N.; Ramteke, R.S. Physical Properties of Acetylated and Enzyme-Modified Potato and Sweet Potato Flours. *J. Food Sci.* **2007**, *72*, E249–E253. [CrossRef] [PubMed]
105. Chang, Y.; Lv, Y. Structure, Functionality, and Digestibility of Acetylated Hullless Barley Starch. *Int. J. Food Prop.* **2017**, *20*, 1818–1828. [CrossRef]
106. Wu, X.; Liu, P.; Ren, L.; Tong, J.; Zhou, J. Optimization of Corn Starch Succinylation Using Response Surface Methodology. *Starch-Stärke* **2014**, *66*, 508–514. [CrossRef]
107. Debet, M.R.; Gidley, M.J. Three Classes of Starch Granule Swelling: Influence of Surface Proteins and Lipids. *Carbohydr. Polym.* **2006**, *64*, 452–465. [CrossRef]
108. Vermeylen, R.; Derycke, V.; Delcour, J.A.; Goderis, B.; Reynaers, H.; Koch, M.H.J. Gelatinization of Starch in Excess Water: Beyond the Melting of Lamellar Crystallites. A Combined Wide- and Small-Angle X-Ray Scattering Study. *Biomacromolecules* **2006**, *7*, 2624–2630. [CrossRef]
109. Song, M.-R.; Choi, S.-H.; Oh, S.-M.; Kim, H.; Bae, J.-E.; Park, C.-S.; Kim, B.-Y.; Baik, M.-Y. Characterization of Amorphous Granular Starches Prepared by High Hydrostatic Pressure (HHP). *Food Sci. Biotechnol.* **2017**, *26*, 671–678. [CrossRef]
110. Tao, K.; Li, C.; Yu, W.; Gilbert, R.G.; Li, E. How Amylose Molecular Fine Structure of Rice Starch Affects Functional Properties. *Carbohydr. Polym.* **2019**, *204*, 24–31. [CrossRef]
111. Nikolenko, M.V.; Myrhorodska-Terentieva, V.D.; Sakhno, Y.; Jaisi, D.P.; Likozar, B.; Kostyniuk, A. Hydrothermal Leaching of Amylose from Native, Oxidized and Heat-Treated Starches. *Processes* **2023**, *11*, 1464. [CrossRef]
112. Sondari, D.; Amanda, P.; Suryaningrum, R.; Burhani, D.; Pramasari, D.A.; Septevani, A.A.; Restu, W.K.; Agustian, E.; Irawan, Y.; Oktaviani, M. Effect of Different Amount of Cross-Linker and Catalyst on Modified Cassava towards Its Chemical Characteristic. *IOP Conf. Ser. Earth Environ. Sci.* **2021**, *759*, 12007. [CrossRef]
113. Li, W.; Shan, Y.; Xiao, X.; Luo, Q.; Zheng, J.; Ouyang, S. Physicochemical Properties of A- and B- Starch Granules Isolated from Hard Red and Soft Red Winter Wheat. *Agric. Food Chem.* **2013**, *61*, 6477–6484. [CrossRef]
114. Waduge, R.N.; Hoover, R.; Vasanthan, T.; Gao, J.; Li, J. Effect of Annealing on the Structure and Physicochemical Properties of Barley Starches of Varying Amylose Content. *Food Res. Int.* **2006**, *39*, 59–77. [CrossRef]
115. Wani, A.A.; Singh, P.; Shah, M.A.; Schweiggert-Weisz, U.; Gul, K.; Wani, I.A. Rice Starch Diversity: Effects on Structural, Morphological, Thermal, and Physicochemical Properties—A Review. *Compr. Rev. Food Sci. Food Saf.* **2012**, *11*, 417–436. [CrossRef]
116. Ratnayake, W.S.; Hoover, R.; Warkentin, T. Pea Starch: Composition, Structure and Properties—A Review. *Starch/Staerke* **2002**, *54*, 217–234. [CrossRef]
117. Bello, M.O.; Tolaba, M.P.; Suarez, C. Water Absorption and Starch Gelatinization in Whole Rice Grain during Soaking. *LWT Food Sci. Technol.* **2007**, *40*, 313–318. [CrossRef]
118. Ulfa, G.M.; Putri, W.D.R.; Fibrianto, K.; Prihatiningtyas, R.; Widjanarko, S.B. The Influence of Temperature in Swelling Power, Solubility, and Water Binding Capacity of Pregelatinised Sweet Potato Starch. *IOP Conf. Ser. Earth Environ. Sci.* **2020**, *475*, 12036. [CrossRef]
119. Wang, S.; Jin, F.; Yu, J. Pea Starch Annealing: New Insights. *Food Bioprocess Technol.* **2013**, *6*, 3564–3575. [CrossRef]

120. Hoover, R.; Ratnayake, W.S. Starch Characteristics of Black Bean, Chick Pea, Lentil, Navy Bean and Pinto Bean Cultivars Grown in Canada. *Food Chem.* **2002**, *78*, 489–498. [CrossRef]
121. Iuga, M.; Mironeasa, S. A Review of the Hydrothermal Treatments Impact on Starch Based Systems Properties. *Crit. Rev. Food Sci. Nutr.* **2020**, *60*, 3890–3915. [CrossRef]
122. Shen, Y.; Zhang, N.; Xu, Y.; Huang, J.; Yuan, M.; Wu, D.; Shu, X. Physicochemical Properties of Hydroxypropylated and Cross-Linked Rice Starches Differential in Amylose Content. *Int. J. Biol. Macromol.* **2019**, *128*, 775–781. [CrossRef]
123. Lan, H.; Hoover, R.; Jayakody, L.; Liu, Q.; Donner, E.; Baga, M.; Asare, E.K.; Hucl, P.; Chibbar, R.N. Impact of Annealing on the Molecular Structure and Physicochemical Properties of Normal, Waxy and High Amylose Bread Wheat Starches. *Food Chem.* **2008**, *111*, 663–675. [CrossRef]
124. Sobini, N.; Darsiga, S.; Kananke, T.C.; Srivijeindran, S. Characterization of Modified Palmyrah Tuber Starch by Pre-Gelatinization, Acid and Dextrinization Processes and Its Applicability. *Food Chem. Adv.* **2022**, *1*, 100143. [CrossRef]
125. Marta, H.; Cahyana, Y.; Djali, M.; Pramafisi, G. The Properties, Modification, and Application of Banana Starch. *Polymers* **2022**, *14*, 3092. [CrossRef] [PubMed]
126. Sindhu, R.; Devi, A.; Khatkar, B.S. Morphology, Structure and Functionality of Acetylated, Oxidized and Heat Moisture Treated Amaranth Starches. *Food Hydrocoll.* **2021**, *118*, 106800. [CrossRef]
127. Chen, Z.; Schols, H.A.; Voragen, A.G.J. The Use of Potato and Sweet Potato Starches Affects White Salted Noodle Quality. *J. Food Sci.* **2003**, *68*, 2630–2637. [CrossRef]
128. Chibuzo, I.M. Physicochemical and Retrogradation Characteristics of Modified Sweet Potato (*Ipomoea Batatas* L. (Lam)) Sarch. *J. Agric. Food. Tech* **2012**, *2*, 49–55.
129. Simsek, S.; Ovando-Martínez, M.; Whitney, K.; Bello-Pérez, L.A. Effect of Acetylation, Oxidation and Annealing on Physicochemical Properties of Bean Starch. *Food Chem.* **2012**, *134*, 1796–1803. [CrossRef]
130. Abedi, E.; Pourmohammadi, K.; Abbasi, S. Dual-Frequency Ultrasound for Ultrasonic-Assisted Esterification. *Food Sci. Nutr.* **2019**, *7*, 2613–2624. [CrossRef]
131. Van Hung, P.; Morita, N. Dough Properties and Bread Quality of Flours Supplemented with Cross-Linked Cornstarches. *Food Res. Int.* **2004**, *37*, 461–467. [CrossRef]
132. Liu, H.; Corke, H.; Ramsden, L. Functional Properties and Enzymatic Digestibility of Cationic and Cross-Linked Cationic Ae, Wx, and Normal Maize Starch. *J. Agric. Food Chem.* **1999**, *47*, 2523–2528. [CrossRef]
133. Bello-Pérez, L.A.; Agama-Acevedo, E.; Zamudio-Flores, P.B.; Mendez-Montealvo, G.; Rodriguez-Ambriz, S.L. Effect of Low and High Acetylation Degree in the Morphological, Physicochemical and Structural Characteristics of Barley Starch. *LWT Food Sci. Technol.* **2010**, *43*, 1434–1440. [CrossRef]
134. Singh, J.; Kaur, L.; Singh, N. Effect of Acetylation on Some Properties of Corn and Potato Starches. *Starch-Stärke* **2004**, *56*, 586–601. [CrossRef]
135. Kaushal, P.; Kumar, V.; Sharma, H.K. Comparative Study of Physicochemical, Functional, Antinutritional and Pasting Properties of Taro (*Colocasia esculenta*), Rice (*Oryza sativa*) Flour, Pigeonpea (*Cajanus cajan*) Flour and Their Blends. *LWT Food Sci. Technol.* **2012**, *48*, 59–68. [CrossRef]
136. Han, F.; Liu, M.; Gong, H.; Lü, S.; Ni, B.; Zhang, B. Synthesis, Characterization and Functional Properties of Low Substituted Acetylated Corn Starch. *Int. J. Biol. Macromol.* **2012**, *50*, 1026–1034. [CrossRef]
137. Ren, L.; Dong, Z.; Jiang, M.; Tong, J.; Zhou, J. Hydrophobization of Starch Nanocrystals through Esterification in Green Media. *Ind. Crops Prod.* **2014**, *59*, 115–118. [CrossRef]
138. Suh, D.S.; Jane, J. Comparison of Starch Pasting Properties at Various Cooking Conditions Using the Micro Visco-Amylo-Graph and the Rapid Visco Analyser. *Cereal Chem.* **2003**, *80*, 745–749. [CrossRef]
139. BeMiller, J.N. Pasting, Paste, and Gel Properties of Starch–Hydrocolloid Combinations. *Carbohydr. Polym.* **2011**, *86*, 386–423. [CrossRef]
140. Collado, L.S.; Mabesa, L.B.; Oates, C.G.; Corke, H. Bihon-Type Noodles from Heat-Moisture-Treated Sweet Potato Starch. *J. Food Sci.* **2001**, *66*, 604–609. [CrossRef]
141. Guo, K.; Liu, T.; Xu, A.; Zhang, L.; Bian, X.; Wei, C. Structural and Functional Properties of Starches from Root Tubers of White, Yellow, and Purple Sweet Potatoes. *Food Hydrocoll.* **2019**, *89*, 829–836. [CrossRef]
142. Pranoto, Y.; Rahmayuni; Haryadi; Rakshit, S.K. Physicochemical Properties of Heat Moisture Treated Sweet Potato Starches of Selected Indonesian Varieties. *Int. Food Res. J.* **2014**, *21*, 2031–2038.
143. Hutabarat, D.J.C.; Stevensen, J. Physicochemical Properties of Enzymatically Modified Starch: A Review. *IOP Conf. Ser. Earth Environ. Sci.* **2023**, *1169*, 12093. [CrossRef]
144. Sun, Y.; Wang, M.; Ma, S.; Wang, H. Physicochemical Characterization of Rice, Potato, and Pea Starches, Each with Different Crystalline Pattern, When Incorporated with Konjac Glucomannan. *Food Hydrocoll.* **2020**, *101*, 105499. [CrossRef]
145. He, W.; Wei, C. Progress in C-Type Starches from Different Plant Sources. *Food Hydrocoll.* **2017**, *73*, 162–175. [CrossRef]
146. Lewandowicz, J.; Le Thanh-Blicharz, J.; Szwengiel, A. The Effect of Chemical Modification on the Rheological Properties and Structure of Food Grade Modified Starches. *Processes* **2022**, *10*, 938. [CrossRef]
147. Lewandowicz, G.; Blaszcak, W.; Fornal, J. Effect of Acetylation on Microstructure of Potato Starch. *Polish J. Food Nutr. Sci.* **1998**, *7*, 78–84.

148. Iftikhar, S.A.; Chakraborty, S.; Dutta, H. Effect of Acetylation, Hydroxypropylation and Dual Acetylation-Hydroxypropylation on Physicochemical and Digestive Properties of Rice Starches with Different Amylose Content. *Biointerface Res. Appl. Chem.* **2022**, *12*, 6788–6803. [CrossRef]
149. Perera, C.; Hoover, R.; Martin, A.M. The Effect of Hydroxypropylation on the Structure and Physicochemical Properties of Native, Defatted and Heat-Moisture Treated Potato Starches. *Food Res. Int.* **1997**, *30*, 235–247. [CrossRef]
150. Wickramasinghe, M.; Yamamoto, K.; Yamauchi, H.; Noda, T. Effect of Low Level of Starch Acetylation on Physicochemical Properties of Potato Starch. *Food Sci. Biotechnol.* **2009**, *18*, 118–123.
151. Subroto, E.; Filianty, F.; Indiarso, R.; Andita Shafira, A. Physicochemical and Functional Properties of Modified Adlay Starch (Coix Lacryma-Jobi) by Microwave and Ozonation. *Int. J. Food Prop.* **2022**, *25*, 1622–1634. [CrossRef]
152. Marta, H.; Cahyana, Y.; Bintang, S.; Soeherman, G.P.; Djali, M. Physicochemical and Pasting Properties of Corn Starch as Affected by Hydrothermal Modification by Various Methods. *Int. J. Food Prop.* **2022**, *25*, 792–812. [CrossRef]
153. Hoover, R. Composition, Molecular Structure, and Physicochemical Properties of Tuber and Root Starches: A Review. *Carbohydr. Polym.* **2001**, *45*, 253–267. [CrossRef]
154. Trung, P.T.B.; Ngoc, L.B.B.; Hoa, P.N.; Tien, N.N.T.; Hung, P. Van Impact of Heat-Moisture and Annealing Treatments on Physicochemical Properties and Digestibility of Starches from Different Colored Sweet Potato Varieties. *Int. J. Biol. Macromol.* **2017**, *105*, 1071–1078. [CrossRef] [PubMed]
155. Vieira, F.C.; Sarmiento, S.B.S. Heat-Moisture Treatment and Enzymatic Digestibility of Peruvian Carrot, Sweet Potato and Ginger Starches. *Starch/Staerke* **2008**, *60*, 223–232. [CrossRef]
156. Chen, P.; Yu, L.; Simon, G.; Petinakis, E.; Dean, K.; Chen, L. Morphologies and Microstructures of Cornstarches with Different Amylose-Amylopectin Ratios Studied by Confocal Laser Scanning Microscope. *J. Cereal Sci.* **2009**, *50*, 241–247. [CrossRef]
157. Glaring, M.A.; Koch, C.B.; Blennow, A. Genotype-Specific Spatial Distribution of Starch Molecules in the Starch Granule: A Combined CLSM and SEM Approach. *Biomacromolecules* **2006**, *7*, 2310–2320. [CrossRef] [PubMed]
158. Fornal, J.; Sadowska, J.; Błaszczak, W.; Jeliński, T.; Stasiak, M.; Molenda, M.; Hajnos, M. Influence of Some Chemical Modifications on the Characteristics of Potato Starch Powders. *J. Food Eng.* **2012**, *108*, 515–522. [CrossRef]
159. Zhang, L.; Xie, W.; Zhao, X.; Liu, Y.; Gao, W. Study on the Morphology, Crystalline Structure and Thermal Properties of Yellow Ginger Starch Acetates with Different Degrees of Substitution. *Thermochim. Acta* **2009**, *495*, 57–62. [CrossRef]
160. El Halal, S.L.M.; Colussi, R.; Pinto, V.Z.; Bartz, J.; Radunz, M.; Carreño, N.L.V.; Dias, A.R.G.; Zavareze, E.D.R. Structure, Morphology and Functionality of Acetylated and Oxidised Barley Starches. *Food Chem.* **2015**, *168*, 247–256. [CrossRef]
161. Ariyantoro, A.R.; Fitriyani, A.; Affandi, D.R.; Muhammad, D.R.A.; Yulviatun, A.; Nishizu, T. The Effect of Dual Modification with Annealing and Heat Moisture Treatment (HMT) on Physicochemical Properties of Jack Bean Starch (*Canavalia ensiformis*). *Food Res.* **2022**, *6*, 189–198. [CrossRef]
162. Marboh, V.; Gayary, M.A.; Gautam, G.; Mahanta, C.L. Comparative Study of Heat-Moisture Treatment and Annealing on Morphology, Crystallinity, Pasting, and Thermal Properties of Sohphlang (*Flemingia vestita*) Starch. *Starch-Stärke* **2022**, *74*, 2100294. [CrossRef]
163. Alcázar-Alay, S.C.; Meireles, M.A.A. Physicochemical Properties, Modifications and Applications of Starches from Different Botanical Sources. *Food Sci. Technol.* **2015**, *35*, 215–236. [CrossRef]
164. Rodríguez-García, M.E.; Hernández-Landaverde, M.A.; Delgado, J.M.; Ramírez-Gutiérrez, C.F.; Ramírez-Cardona, M.; Millán-Malo, B.M.; Londoño-Restrepo, S.M. Crystalline Structures of the Main Components of Starch. *Curr. Opin. Food Sci.* **2021**, *37*, 107–111. [CrossRef]
165. Dome, K.; Podgorbunskikh, E.; Bychkov, A.; Lomovsky, O. Changes in the Crystallinity Degree of Starch Having Different Types of Crystal Structure after Mechanical Pretreatment. *Polymers* **2020**, *12*, 641. [CrossRef] [PubMed]
166. Chukhchin, D.G.; Malkov, A.V.; Tyshkunova, I.V.; Mayer, L.V.; Novozhilov, E. V Diffractometric Method for Determining the Degree of Crystallinity of Materials. *Crystallogr. Rep.* **2016**, *61*, 371–375. [CrossRef]
167. Cheetham, N.W.H.; Tao, L. Variation in Crystalline Type with Amylose Content in Maize Starch Granules: An X-Ray Powder Diffraction Study. *Carbohydr. Polym.* **1998**, *36*, 277–284. [CrossRef]
168. Buléon, A.; Colonna, P.; Planchot, V.; Ball, S. Starch Granules: Structure and Biosynthesis. *Int. J. Biol. Macromol.* **1998**, *23*, 85–112. [CrossRef]
169. Buléon, A.; Gallant, D.J.; Bouchet, B.; Mouille, G.; D’Hulst, C.; Kossmann, J.; Ball, S. Starches from A to C: Chlamydomonas Reinhardtii as a Model Microbial System to Investigate the Biosynthesis of the Plant Amylopectin Crystal. *Plant Physiol.* **1997**, *115*, 949–957. [CrossRef] [PubMed]
170. Zeng, S.; Wu, X.; Lin, S.; Zeng, H.; Lu, X.; Zhang, Y.; Zheng, B. Structural Characteristics and Physicochemical Properties of Lotus Seed Resistant Starch Prepared by Different Methods. *Food Chem.* **2015**, *186*, 213–222. [CrossRef]
171. Ahn, J.H.; Baek, H.R.; Kim, K.M.; Han, G.J.; Choi, J.B.; Kim, Y.; Moon, T.W. Slowly Digestible Sweetpotato Flour: Preparation by Heat-Moisture Treatment and Characterization of Physicochemical Properties. *Food Sci. Biotechnol.* **2013**, *22*, 383–391. [CrossRef]
172. Buléon, A.; Gérard, C.; Riekkel, C.; Vuong, R.; Chanzy, H. Details of the Crystalline Ultrastructure of C-Starch Granules, Revealed by Synchrotron Microfocus Mapping. *Macromolecules* **1998**, *31*, 6605–6610. [CrossRef]
173. Pan, T.; Lin, L.; Wang, J.; Liu, Q.; Wei, C. Long Branch-Chains of Amylopectin with B-Type Crystallinity in Rice Seed with Inhibition of Starch Branching Enzyme I and IIb Resist in Situ Degradation and Inhibit Plant Growth during Seedling Development. *BMC Plant Biol.* **2018**, *18*, 9. [CrossRef]

174. Lopez-Rubio, A.; Flanagan, B.M.; Gilbert, E.P.; Gidley, M.J. A Novel Approach for Calculating Starch Crystallinity and Its Correlation with Double Helix Content: A Combined XRD and NMR Study. *Biopolymers* **2008**, *89*, 761–768. [CrossRef] [PubMed]
175. If'all, I.; Hasanuddin, A.; Rahim, A.; Kadir, S. Modification of Starch by Acetylation of the Acetyl Function Group and the Kristanility of Banggai Yam Starch Acetate. *Rekayasa* **2019**, *12*, 135–140. [CrossRef]
176. Xu, M.; Saleh, A.S.M.; Gong, B.; Li, B.; Jing, L.; Gou, M.; Jiang, H.; Li, W. The Effect of Repeated versus Continuous Annealing on Structural, Physicochemical, and Digestive Properties of Potato Starch. *Food Res. Int.* **2018**, *111*, 324–333. [CrossRef] [PubMed]
177. Gunaratne, A.; Hoover, R. Effect of Heat-Moisture Treatment on the Structure and Physicochemical Properties of Tuber and Root Starches. *Carbohydr. Polym.* **2002**, *49*, 425–437. [CrossRef]
178. Miao, M.; Zhang, T.; Jiang, B. Characterisations of Kabuli and Desi Chickpea Starches Cultivated in China. *Food Chem.* **2009**, *113*, 1025–1032. [CrossRef]
179. Wang, Y.J.; Den Truong, V.; Wang, L. Structures and Rheological Properties of Corn Starch as Affected by Acid Hydrolysis. *Carbohydr. Polym.* **2003**, *52*, 327–333. [CrossRef]

**Disclaimer/Publisher's Note:** The statements, opinions and data contained in all publications are solely those of the individual author(s) and contributor(s) and not of MDPI and/or the editor(s). MDPI and/or the editor(s) disclaim responsibility for any injury to people or property resulting from any ideas, methods, instructions or products referred to in the content.



## Article

# Optimization of Cellulose Nanofiber Loading and Processing Conditions during Melt Extrusion of Poly(3-hydroxybutyrate-co-3-hydroxyhexanoate) Bionanocomposites

Siti Shazra Shazleen <sup>1</sup>, Fatimah Athiyah Sabaruddin <sup>1</sup>, Yoshito Ando <sup>2</sup> and Hidayah Ariffin <sup>1,3,\*</sup>

<sup>1</sup> Department of Bioprocess Technology, Faculty of Biotechnology and Biomolecular Sciences, Universiti Putra Malaysia UPM, Serdang 43400, Selangor, Malaysia

<sup>2</sup> Graduate School of Life Science and Systems Engineering, Kyushu Institute of Technology, 2-4 Hibikino, Wakamatsu-ku, Kitakyushu-shi, Fukuoka 808-0196, Japan

<sup>3</sup> Laboratory of Biopolymer and Derivatives, Institute of Tropical Forestry and Forest Products, Universiti Putra Malaysia UPM, Serdang 43400, Selangor, Malaysia

\* Correspondence: hidayah@upm.edu.my

**Abstract:** This present study optimized the cellulose nanofiber (CNF) loading and melt processing conditions of poly(3-hydroxybutyrate-co-3-hydroxyhexanoate) P(HB-co-11% HHx) bionanocomposite fabrication in twin screw extruder by using the response surface methodology (RSM). A face-centered central composite design (CCD) was applied to statistically specify the important parameters, namely CNF loading (1–9 wt.%), rotational speed (20–60 rpm), and temperature (135–175 °C), on the mechanical properties of the P(HB-co-11% HHx) bionanocomposites. The developed model reveals that CNF loading and temperature were the dominating parameters that enhanced the mechanical properties of the P(HB-co-11% HHx)/CNF bionanocomposites. The optimal CNF loading, rotational speed, and temperature for P(HB-co-11% HHx) bionanocomposite fabrication were 1.5 wt.%, 20 rpm, and 160 °C, respectively. The predicted tensile strength, flexural strength, and flexural modulus for these optimum conditions were 22.96 MPa, 33.91 MPa, and 1.02 GPa, respectively, with maximum desirability of 0.929. P(HB-co-11% HHx)/CNF bionanocomposites exhibited improved tensile strength, flexural strength, and modulus by 17, 6, and 20%, respectively, as compared to the neat P(HB-co-11% HHx). While the crystallinity of P(HB-co-11% HHx)/CNF bionanocomposites increased by 17% under the optimal fabrication conditions, the thermal stability of the P(HB-co-11% HHx)/CNF bionanocomposites was not significantly different from neat P(HB-co-11% HHx).

**Keywords:** poly(3-hydroxybutyrate-co-3-hydroxyhexanoate); cellulose nanofiber; bionanocomposite; melt-extrusion processing; optimization; response surface methodology

**Citation:** Shazleen, S.S.; Sabaruddin, F.A.; Ando, Y.; Ariffin, H. Optimization of Cellulose Nanofiber Loading and Processing Conditions during Melt Extrusion of Poly(3-hydroxybutyrate-co-3-hydroxyhexanoate) Bionanocomposites. *Polymers* **2023**, *15*, 671. <https://doi.org/10.3390/polym15030671>

Academic Editor: Raffaella Striani

Received: 10 November 2022

Revised: 2 December 2022

Accepted: 30 December 2022

Published: 28 January 2023



**Copyright:** © 2023 by the authors. Licensee MDPI, Basel, Switzerland. This article is an open access article distributed under the terms and conditions of the Creative Commons Attribution (CC BY) license (<https://creativecommons.org/licenses/by/4.0/>).

## 1. Introduction

The growing use of plastics around the world has led to an increase in plastic waste. In Malaysia, plastic waste constituted 19% of the total waste generated where most of the commodity plastics are derived from petroleum, and they are single use, i.e., they are discarded after being used only once [1]. This leads to the accumulation of disposal plastic waste that mostly ends up in landfills or dumps in the open environment. According to Jambeck et al. [2], Malaysia was placed eighth among the world's top 10 countries for having poorly managed plastic waste. In light of the environmental damage caused by plastic waste pollution, and also the difficulties of managing that waste on land and in water, there is indeed an urgent need to establish sustainable and cost-effective solutions. Therefore, recent advancements in biodegradable and recyclable polymers are essential, considering the uncertainty of petroleum usage worldwide. Manufacturing industries are transitioning to more eco-friendly, sustainable economic production as a consequence of the

intense pace of scientific and technological advancement. Today, the most well-known and widely used polymers in a multitude of areas are polylactic acid (PLA), polycaprolactone (PCL), polyglycolide (PGA), and polyhydroxyalkanoates (PHAs). Among all, PHA has drawn significant attention as one of the most viable substitutes for synthetic polymers. This is because PHAs are more compostable and biodegradable in marine conditions than PLA. Although PLA is compostable, it may remain in the ocean for up to 1000 years before it can be composted [3]. PCL and PGA are considered to be non-toxic, yet because of their higher crystallinity they degrade more slowly than PLA [4]. Moreover, PHA properties are comparable to most non-degradable materials [5], making PHA suitable for industrial uses, particularly in packaging.

PHA is recognized as a sustainable alternative among the most prominent synthesized and commercialized biodegradable polymers as it can be converted into water and carbon dioxide in the presence of oxygen, or into methane under anaerobic conditions without forming toxic products, by microorganisms found in water and soil [6]. PHAs are a type of linear biopolyester made up of hydroxyalkanoate (HA) units organized in a basic structure produced via bacterial fermentation and are currently being marketed as a means of creating a more sustainable future [7]. Their properties differ significantly depending on the structure and composition of their monomers [8]. PHAs offer several benefits over petroleum-based polymers, including the ability to be synthesized from renewable carbon sources, processability, and biodegradability. The most widespread and extensively studied member of this family is the homopolymer poly(3-hydroxybutyrate) (PHB) and the copolymers poly(3-hydroxybutyrate-co-3-hydroxyvalerate) (PHBV) and poly(3-hydroxybutyrate-co-3-hydroxyhexanoate) (PHBHHx).

PHBHHx is one of the most promising biodegradable aliphatic polyesters of the PHA family due to the fact that it has unique combination properties including full anaerobic degradability, moisture resistance, and good barrier properties [9]. PHBHHx has higher elastic characteristics and a wider processing window than PHB and PHBV due to the relatively long alkyl side chain, making it a suitable biopolymeric source for developing biocomposites with increased flexibility [10,11]. However, despite their potential, the effective utilization of PHBHHx-based materials is exacerbated by their low mechanical properties and difficulties in processing as compared to synthetic polymers [12]. In addition, PHBHHx-based materials are still hindered by their high production costs and are dependent on the performance of bacterial fermentation [13]. Their high manufacturing cost has surpassed the cost of manufacturing conventional plastics. These limitations have restrained the applicability of these materials in a wide range of applications. The incorporation of nanofillers, particularly bio-based nanofillers in PHBHHx, is seen as an ideal strategy for developing bio-based nanocomposites with superior mechanical properties.

Nanofillers have a higher aspect ratio than micro-sized fillers, giving them better reinforcement effects. Recent studies have focused on the use of nanocellulose, particularly cellulose nanofiber (CNF) as reinforcing bio-based nanomaterials. CNF has been known for its outstanding properties such as high mechanical properties and thermal stability, large specific surface area, renewability, biodegradability, and biocompatibility properties that can be produced by mechanical or chemical treatments which are advantageous for reinforced polymers [14]. CNF has a low coefficient of thermal expansion of 0.1 ppm/K; an estimated strength of 2–3 GPa, which is five times stronger than mild steel; and a high Young's modulus of 130–150 GPa [15]. Recently, the effect of CNF as a reinforcement material for PHBHHx has been widely reported [14–17]. Most studies agreed that the addition of CNF can enhance the mechanical properties of PHBHHx bionanocomposites significantly.

Nonetheless, CNF loading beyond a certain percentage can be detrimental as it may lead to significant nanofiller agglomerations. Several studies have documented that the improvement of polymer nanocomposite may endure immense difficulty attributable to the dispersion of nanofibers [18–22]. The hypothesis is that if the nanofibers are evenly distributed throughout the polymer matrix, the optimal nanocomposite properties can be attained. It should be highlighted at this stage that proper alignment and control of

nanofiber dispersion have remained a key problem for many years [23]. The effectiveness of load transfer between the nanofibers and the polymer matrix and subsequently the mechanical properties of nanocomposite are both governed by the strength of adhesion in the interface region [23]. Consequently, the characteristics of the nanocomposite deteriorate if there is inadequate adhesion at the interphase.

In complement to the CNF reinforcing effect, in practice, the applied melt-processing process and conditions can have a profound effect on the mechanical properties [12]. Nonetheless, studies on the mechanical properties of PHBHHx/CNF bionanocomposites under the influence of processing temperature and shear stress have been scarcely reported. To our knowledge, there are no studies that explicitly correlate variations in mechanical properties to the practical processing parameters and CNF loading used in melt extrusion of PHBHHx. Identifying the optimal values for these parameters to enhance the mechanical properties of the bionanocomposite is a challenging and complicated task as there are so many design parameters to consider. In light of this, the prediction and assessment of design parameters is vital for the optimum design of bionanocomposites for a particular application. However, few studies to date have quantitatively optimized the mechanical characteristics of PHBHHx/CNF bionanocomposites depending on the design parameters. Hence, the present in-depth research was performed with the purpose of improving the mechanical characteristics of P(HB-co-11% HHx) through the optimization of CNF loading and processing conditions. Through the use of Design-Expert software, mathematical models were generated between the aforementioned parameters and responses. The validation experiment was conducted to verify whether the obtained optimal conditions result in the intended mechanical properties for P(HB-co-11% HHx)/CNF bionanocomposites.

## 2. Materials and Methods

### 2.1. Materials

Poly(3-hydroxybutyrate-co-3-hydroxyhexanoate) with 11 mol% of HHx unit, P(HB-co-11% HHx) as determined by  $^1\text{H-NMR}$  was supplied by ©KANEKA Biodegradable Polymer <sup>TM</sup> (Kaneka Co., Osaka, Japan). Spray-dried CNF was purchased from ZoepNano Sdn. Bhd., (Serdang, Malaysia) and used in this experiment as nanofiller. The CNF powder had an average particle size of less than 100 nm.

### 2.2. P(HB-co-11% HHx) Bionanocomposite Fabrication and Molding

P(HB-co-11% HHx)/CNF bionanocomposite was fabricated by using twin-screw extruder (Labtech Engineering Co., Ltd., Bangkok, Thailand) with the screw diameter of 16 mm. Prior to mixing, P(HB-co-11% HHx) powder was dried in an oven at 60 °C for 24 h to remove moisture because it is very essential to minimize the hydrolytic degradation during the processing at high temperature [24]. The P(HB-co-11% HHx) and CNF powder were mechanically mixed before being fed into the extruder. After the extrusion, the obtained filament was granulated by a pelletizer (SHEER SGS 25-E4, MAAG Group manufactures, Zurich, Switzerland) and then molded into 11 × 11 cm film with thickness of 1 mm by direct compression molding using a hydraulic hot press at temperature of 160 °C and 110 kg.cm<sup>-2</sup> pressure for 10 min. Cooling was then performed for 30 min under the same pressure.

### 2.3. Characterization of P(HB-co-11% HHx) Bionanocomposite

#### 2.3.1. Mechanical Analysis

Mechanical properties of bionanocomposites were analyzed using an Instron Universal Testing Machine—Instron 5566 (Instron, Norwood, MA, USA) with load cell of 10 kN at room temperature. Five dog-bone-shaped specimens for tensile strength were tested according to the standard method of ASTM D 638-05 with crosshead speed of 1 mm/min. Meanwhile, flexural strength and modulus tests were performed at 1.21 mm/min speed according to the standard method of ASTM D790. One-way ANOVA and Duncan's multiple range test were

used to statistically evaluate the mechanical properties of the fabricated bionanocomposites following the validation experiment.

### 2.3.2. Experimental Design and Optimization

A face-centered central composite design (CCD), comprising three different factors, was used to run the experiment: CNF content ( $X_1$ ) (1 to 9 wt.%), rotational speed ( $X_2$ ) (20 to 60 rpm), and temperature ( $X_3$ ) (135 to 175 °C). In this study, CCD was used to determine the optimum melt-extrusion conditions in fabrication of P(HB-co-11% HHx)/CNF bionanocomposites with maximum mechanical properties. The temperature was set between 135 and 175 °C in consideration of the onset melting point of P(HB-co-11% HHx) from differential scanning calorimetry (DSC), which is approximately 155 °C, and onset degradation of CNF and P(HB-co-11% HHx) from thermogravimetric (TG) analysis around 280–290 °C. These variables were studied at five different levels coded as  $-\alpha$ ,  $-1$ ,  $0$ ,  $+1$ , and  $+\alpha$ , where  $\alpha = 2$ . Actual and coded values of the variables are summarized in Table 1. The CCD consists of 19 runs including five replications of center points to determine pure error and reduce the variability in the data collection. The mechanical properties of the tensile strength ( $Y_1$ ), flexural strength ( $Y_2$ ), and flexural modulus ( $Y_3$ ) were recorded as responses. The experimental design arrangement was randomized to prevent systematic error and minimize the effects of uncontrolled factors.

**Table 1.** Central composite design matrix of coded and actual factor level.

Run	CNF Loading (wt.%), $X_1$		Rotational Speed (rpm), $X_2$		Temperature (°C), $X_3$	
	Coded	Actual	Coded	Actual	Coded	Actual
1	0	5	2	60	0	155
2	0	5	0	40	0	155
3	0	5	0	40	0	155
4	-2	1	0	40	0	155
5	-1	3	-1	30	1	165
6	0	5	0	40	0	155
7	0	5	0	40	0	155
8	1	7	-1	30	1	165
9	0	5	0	40	2	175
10	0	5	-2	20	0	155
11	0	5	0	40	0	155
12	-1	3	1	50	1	165
13	-1	3	-1	30	-1	145
14	2	9	0	40	0	155
15	1	7	1	50	1	165
16	1	7	1	50	-1	145
17	-1	3	1	50	-1	145
18	1	7	-1	30	-1	145
19	0	5	0	40	-2	135

The experimental data were analyzed, and response surface plots were generated using Design-Expert statistical software (Version 7.0, Stat-Ease Inc., Minneapolis, MN, USA). Analysis of variance (ANOVA) was used to determine the significance of each factor and the regression coefficient of the linear, quadratic, and interaction terms with a confidence level over 95% or a  $p$ -value lower than 0.05. The influence of the factors on the responses was illustrated using a contour plot, and the optimal levels were identified. Actual experimentation was performed to verify and validate the predicted optimal conditions obtained from software for CNF content, rotational speed, and temperature. Data were fitted to a second-order polynomial equation as shown in Equation (1), where  $Y_1$ ,  $Y_2$ , and  $Y_3$  are the responses;  $X_1$ ,  $X_2$ , and  $X_3$  are the varied factors ranging from  $-2$  to  $2$ , which influence the response  $Y$ ;  $\beta_0$  is the constant coefficient;  $\beta_1$ ,  $\beta_2$ , and  $\beta_3$  are linear coefficients;  $\beta_{11}$ ,  $\beta_{22}$ , and  $\beta_{33}$  are quadratic coefficients; and  $\beta_{12}$ ,  $\beta_{13}$ , and  $\beta_{23}$  are interaction coefficients. The validity



and adequacy of the regression models were verified by comparing the experimentally obtained data with the fitted value predicted by the models.

$$Y = \beta_0 + \beta_1 X_1 + \beta_2 X_2 + \beta_3 X_3 + \beta_{11} X_1^2 + \beta_{22} X_2^2 + \beta_{33} X_3^2 + \beta_{12} X_1 X_2 + \beta_{13} X_1 X_3 + \beta_{23} X_2 X_3 \quad (1)$$

### 2.3.3. Thermal Stability Analysis

Thermal stability of neat P(HB-co-11% HHx) and P(HB-co-11% HHx)/1.5% CNF bionanocomposites were analyzed using a thermogravimetric analyzer (TGA 4000, Perkin Elmer, Waltham, MA, USA). The samples weighing around 8–12 mg were placed on a ceramic pan and heated from 50 to 500 °C at a heating rate of 10 °C/min under nitrogen flow of 100 mL/min.

### 2.3.4. X-ray Diffraction Analysis

X-ray diffraction (XRD) spectroscopy was used to quantify the crystallinity of bionanocomposites. An automated Shimadzu 6000 X-ray diffractometer (Tokyo, Japan) operating at 40 kV with a current of 20 mA and Cu radiation of  $\lambda = 1.5406$  between  $2\theta = 10$  and  $50^\circ$  was used for the experiment.

## 3. Results and Discussion

### 3.1. Response Surface Model Analysis

The design matrix generated by Design-Expert software included data on tensile strength, flexural strength, and flexural modulus allowed regression analysis to be performed to identify the best-fit model for the experimental data, with the derived regression equation being used to predict a particular response at points that are not included in regression [25]. The tensile strength, flexural strength, and flexural modulus were indicated to be correlated with CNF loading, rotating speed, and temperature by regression analysis of the experimental data. Different parameters including the model F value, the lack of fit F value, the coefficient of determination  $R^2$ , adjusted  $R^2$ , press value, and coefficient of variation (CV) were used to assess the model's adequacy. The experimental and predicted values of responses are summarized in Table 2.

**Table 2.** The experimental and predicted values of responses.

Run	CNF Loading (wt. %), $X_1$		Rotational Speed (rpm), $X_2$		Temperature (°C), $X_3$	
	* Exp.	** Pred.	* Exp.	** Pred.	* Exp.	** Pred.
1	21.27	20.58	31.36	31.34	1.05	1.05
2	21.63	21.35	31.74	31.49	1.09	1.06
3	21.73	21.35	31.61	31.49	1.05	1.06
4	22.96	22.49	33.91	33.87	1.00	1.00
5	21.21	21.35	30.64	30.93	1.03	1.03
6	21.93	21.35	31.96	31.49	1.05	1.06
7	21.61	21.35	31.00	31.49	1.04	1.06
8	18.78	19.43	30.25	30.45	1.06	1.07
9	16.50	15.86	25.26	24.96	0.99	0.99
10	21.41	21.26	32.46	32.26	1.04	1.03
11	20.67	21.35	31.37	31.49	1.08	1.06
12	18.61	19.58	29.68	29.72	1.00	1.01
13	20.12	20.60	31.55	31.49	0.96	0.97
14	20.41	20.04	31.58	31.40	1.06	1.05
15	17.80	18.16	29.15	29.43	1.07	1.08
16	19.95	20.65	29.67	29.60	0.98	0.98
17	21.01	21.19	31.58	31.59	0.97	0.97
18	19.70	19.56	29.14	29.31	0.95	0.95
19	17.79	17.60	25.61	25.69	0.84	0.83

\* Exp.: experimental; \*\* Pred.: predicted.

Full quadratic models were adopted as the best-fitting model for all responses as detailed in Table 3. The models were chosen using an ANOVA with a sufficient coefficient of determination ( $R^2$ ) (above 80%), insignificant lack-of-fit probability ( $p > 0.005$ ), and significant model probability ( $p < 0.05$ ). A significant  $p$ -value and an insignificant lack of fit, respectively, indicate a good model and a good fit of the model to the data [2,3]. The linear ( $X_1, X_2, X_3$ ), interactive ( $X_1X_2, X_1X_3, X_2X_3$ ), and quadratic ( $X_1^2, X_2^2, X_3^2$ )  $p$ -values are presented in the same table. A lower  $p$ -value ( $p < 0.05$ ) suggests that the corresponding coefficient is more significant.

**Table 3.** Analysis of variance (ANOVA) for response surface quadratic model.

	Tensile Strength (MPa), $Y_1$	Flexural Strength (MPa), $Y_2$	Flexural Modulus (GPa), $Y_3$
Model	0.0010 *	<0.0001 *	<0.0001 *
Linear	–	–	–
$X_1$ –CNF content	0.0078 *	<0.0001 *	0.0085 *
$X_2$ –Rotational speed	0.3705	0.0197 *	0.4362
$X_3$ –Temperature	0.0391 *	0.0523	<0.0001 *
Interaction	–	–	–
$X_1X_2$	0.6425	0.7058	0.1807
$X_1X_3$	0.4108	0.0051 *	0.0812
$X_2X_3$	0.0460 *	0.0195 *	0.2325
Quadratic	–	–	–
$X_1^2$	0.8958	0.0021 *	0.0441 *
$X_2^2$	0.4919	0.2788	0.1997
$X_3^2$	<0.0001 *	<0.0001 *	<0.0001 *
Lack of fit	0.1462 **	0.6977 **	0.8991 **
$R^2$	0.9092	0.9883	0.9619
Standard deviation	0.72	0.33	0.017

\* Statistically significant at  $p < 0.05$  for model; \*\* statistically insignificant at  $p > 0.05$  for the lack of fit.

The  $p$ -values for the lack-of-fit of tensile strength, flexural strength, and modulus were 0.1462, 0.6977, and 0.8991, respectively, which were higher than 0.05, signifying that the model had insignificant lack-of-fit. This is a good indicator that the proposed model fits the experimental data, and the factors have a significant effect on the responses. If the model exhibits significant lack-of-fit, it should not be applied to predict a particular response as it fails to represent data at points that were not included in the regression [25,26]. Ghelich et al. [27] mentioned that the significant lack-of-fit may be related to (i) replicate measurements with repetitive center point data that are consistent with each other, (ii) missing significant higher order non-standard terms or engagement in the model, (iii) larger residual errors compared to the pure error, or (iv) inadequate equal error at any points, i.e., heteroscedasticity (significant disparity between sizes of the observations), implying a more appropriate model fitting.

The coefficient of determination  $R^2$  measures the quality of experimental data fitting to the model where the value was approximately near 1, highlighting that the dependent variable was predicted with less error than the independent variables of CNF loading, rotational speed, and temperature. The  $R^2$  values for tensile strength, flexural strength, and modulus were 0.9092, 0.9883, and 0.9619, respectively, signaling a high proportion of variability predicted by the models of 91%, 99%, and 96%, respectively, from CNF loading, rotational speed, and temperature of P(HB-co-11% HHx)/CNF bionanocomposite fabrication, as seen in Table 3. Moreover, a high  $R^2$  value close to 1 displays good agreement between predicted and reported results within the experimental range [28]. Figure 1 shows the plot of experimental by predicted values, where the proximity of the points scattered along the fitted line demonstrates agreement between experimental and predicted values, evidencing the adequacy of models to estimate the mechanical properties of P(HB-co-11%

HHx)/CNF bionanocomposites prepared at varying CNF loadings, rotational speeds, and temperatures. Hence, these findings affirm that all the responses are affected by experimental factors.

The mathematical relationship between the response and variable process parameters can be established using response surface modeling. The final regression equations (in terms of coded factors) to predict the effect of factors on the responses are shown in Equations (2)–(4), where  $Y_1$ ,  $Y_2$ , and  $Y_3$  represent tensile strength, flexural strength, and flexural modulus, respectively;  $X_1$ ,  $X_2$ , and  $X_3$  are CNF loading, rotational speed, and temperature, respectively.

$$Y_1 = 21.35 - 0.61 X_1 - 0.17 X_2 - 0.44 X_3 - 0.020 X_1^2 - 0.11 X_2^2 - 1.15 X_3^2 + 0.12 X_1 X_2 - 0.22 X_1 X_3 - 1.15 X_2 X_3 \quad (2)$$

$$Y_2 = 31.49 - 0.62 X_1 - 0.23 X_2 - 0.18 X_3 + 0.29 X_1^2 + 0.077 X_2^2 - 1.54 X_3^2 + 0.045 X_1 X_2 + 0.43 X_1 X_3 - 0.33 X_2 X_3 \quad (3)$$

$$Y_3 = 1.06 + 0.014 X_1 + 0.003375 X_2 + 0.038 X_3 - 0.007963 X_1^2 - 0.004713 X_2^2 - 0.037 X_3^2 + 0.0085 X_1 X_2 + 0.012 X_1 X_3 - 0.007963 X_2 X_3 \quad (4)$$

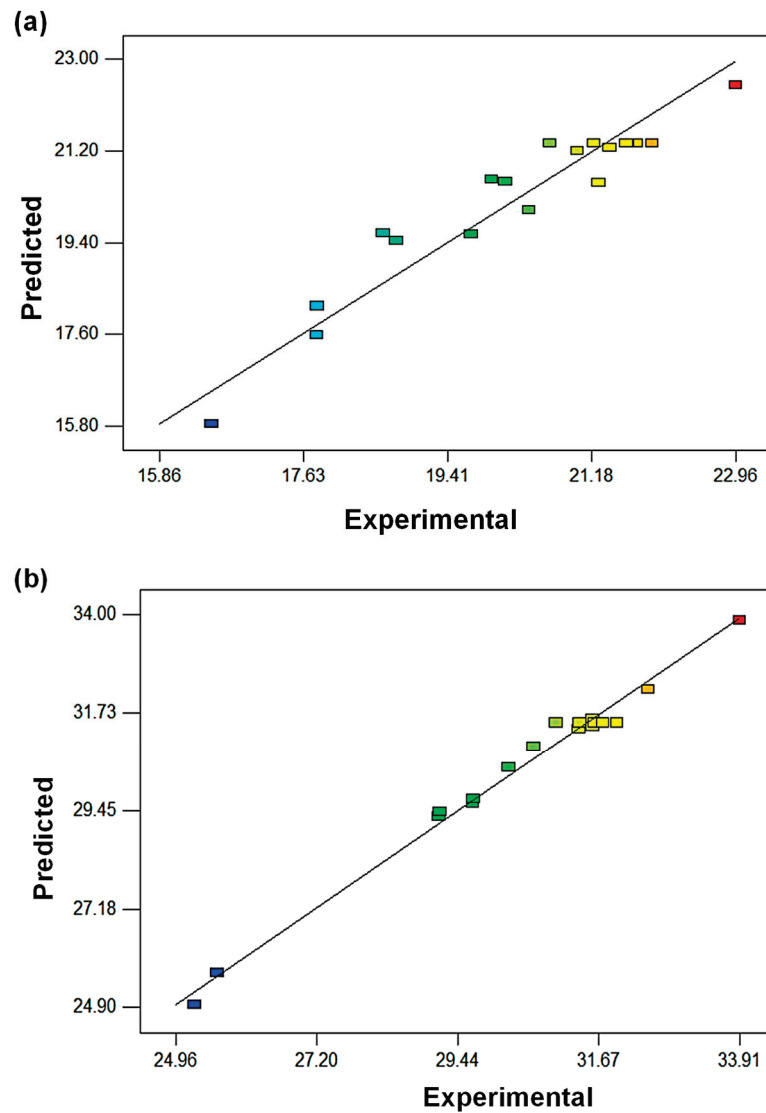
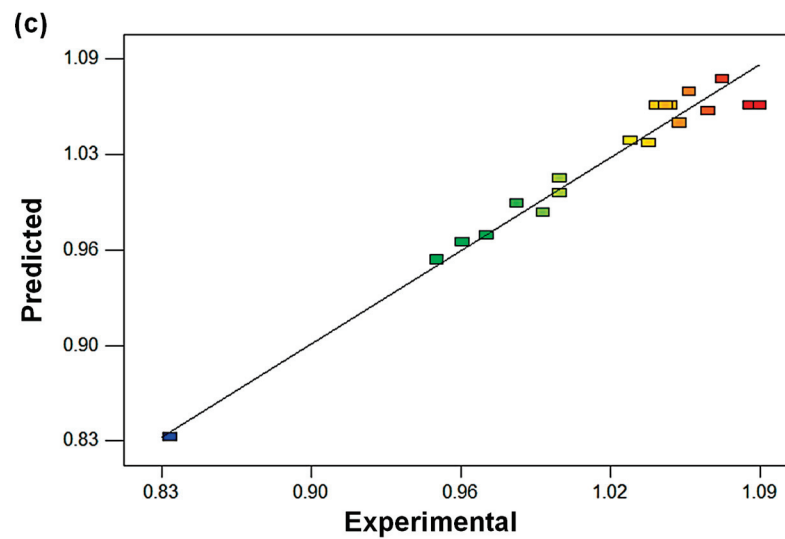


Figure 1. Cont.



**Figure 1.** Experimental and predicted values for (a) tensile strength, (b) flexural strength, and (c) flexural modulus of P(HB-co-11% HHx)/CNF bionanocomposites.

The polynomial equation in terms of uncoded variables of factors was obtained by exchange of coded variables with actual values as shown in Equations (5)–(7).

$$Y_1 = -292.88125 + 1.20304 (\text{CNF content}) + 0.95185 (\text{Rotational speed}) + 3.82790 (\text{Temperature}) - 0.00499155 (\text{CNF content})^2 - 0.00106216 (\text{Rotational speed})^2 - 0.011550 (\text{Temperature})^2 + 0.006125 (\text{CNF content})(\text{Rotational speed}) - 0.011 (\text{CNF content})(\text{Temperature}) - 0.0059 (\text{Rotational speed})(\text{Temperature}) \quad (5)$$

$$Y_2 = -333.88437 - 4.40841 (\text{CNF content}) + 0.41136 (\text{Rotational speed}) + 4.78479 (\text{Temperature}) + 0.071529 (\text{CNF content})^2 + 0.000773649 (\text{Rotational speed})^2 - 0.015414 (\text{Temperature})^2 + 0.00225 (\text{CNF content})(\text{Rotational speed}) + 0.021250 (\text{CNF content})(\text{Temperature}) - 0.00327 (\text{Rotational speed})(\text{Temperature}) \quad (6)$$

$$Y_3 = -8.61259 - 0.079280 (\text{CNF content}) + 0.013608 (\text{Rotational speed}) + 0.11970 (\text{Temperature}) - 0.0019907 (\text{CNF content})^2 - 0.0000471284 (\text{Rotational speed})^2 - 0.000373378 (\text{Temperature})^2 + 0.000425 (\text{CNF content})(\text{Rotational speed}) + 0.000575 (\text{CNF content})(\text{Temperature}) - 0.000075 (\text{Rotational speed})(\text{Temperature}) \quad (7)$$

### 3.2. Effect of Melt-Extrusion Processing Conditions on Mechanical Properties of P(Hb-Co-11% HHx)/CNF Bionanocomposites

The effect of each processing factor, namely CNF loading, rotating speed, and temperature, on the mechanical characteristics of P(HB-co-11% HHx)/CNF bionanocomposite was assessed using a quadratic regression model. The contour and response surface plots generated from the empirical predicted model in Equations (2)–(4) can be used to better assess the whole relationship between the independent variable  $X$  and the response variable  $Y$ , as depicted in Figures 2–4. The response surface plots, which are shown from the pairwise combination of targeted variables by keeping other variables at their center point level, demonstrate the mutual interaction of the independent factors. The response surface plots were converted into a three-dimensional (3D) diagram to determine the optimal conditions for each variable towards maximum mechanical properties. Thus, in all response surface and 3D contour plots, the fixed variable is held at a rotational speed of 30 rpm.



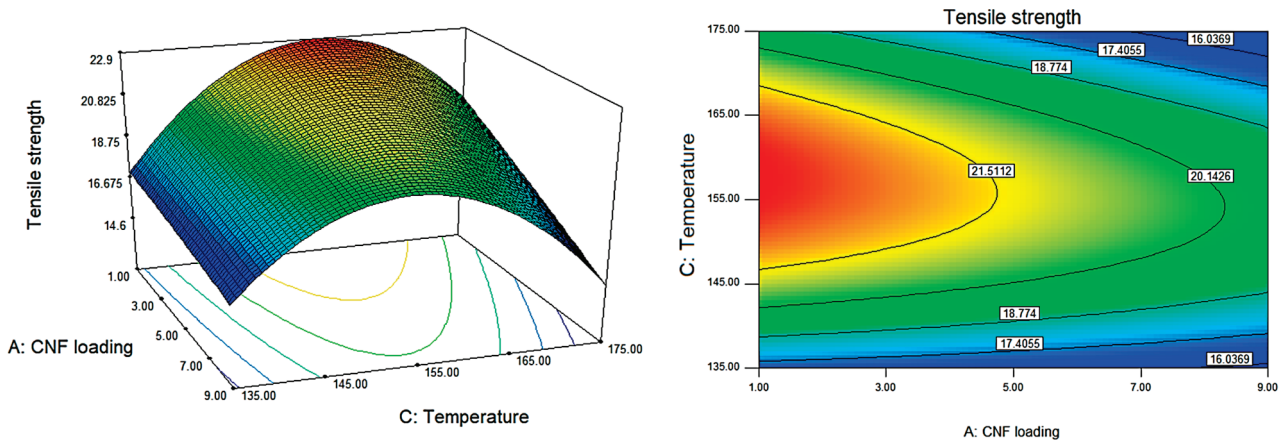


Figure 2. The 3D and response surface contour plots for the dependence of P(HB-co-11% HHX)/CNF bionanocomposite’s tensile strength on CNF loading and temperature as significant factors.

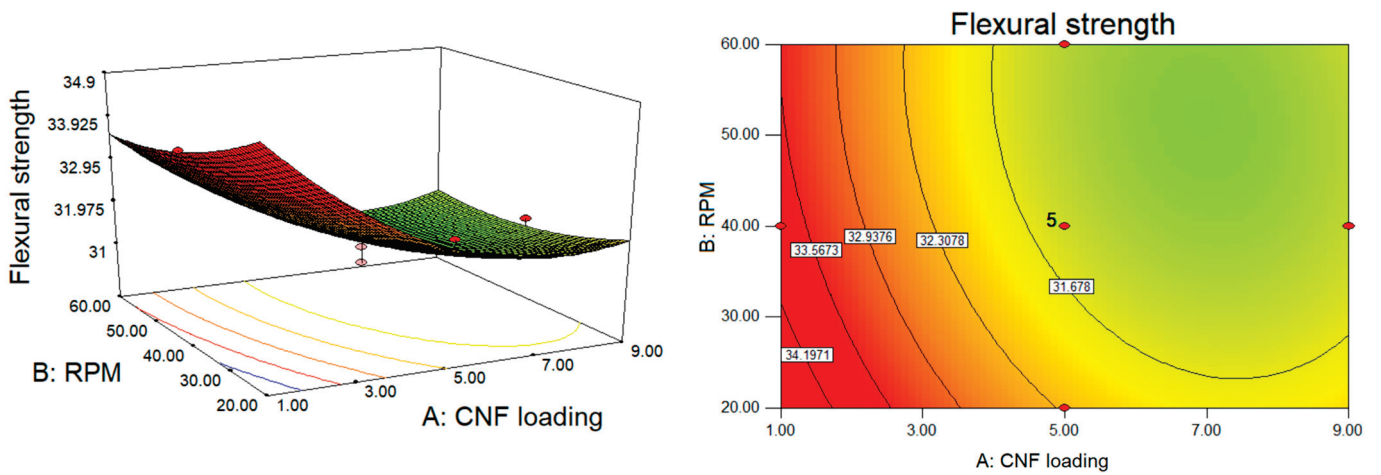


Figure 3. The 3D and response surface contour plots for the dependence of P(HB-co-11% HHX)/CNF bionanocomposite’s flexural strength on CNF loading and rotational speed as significant factors.

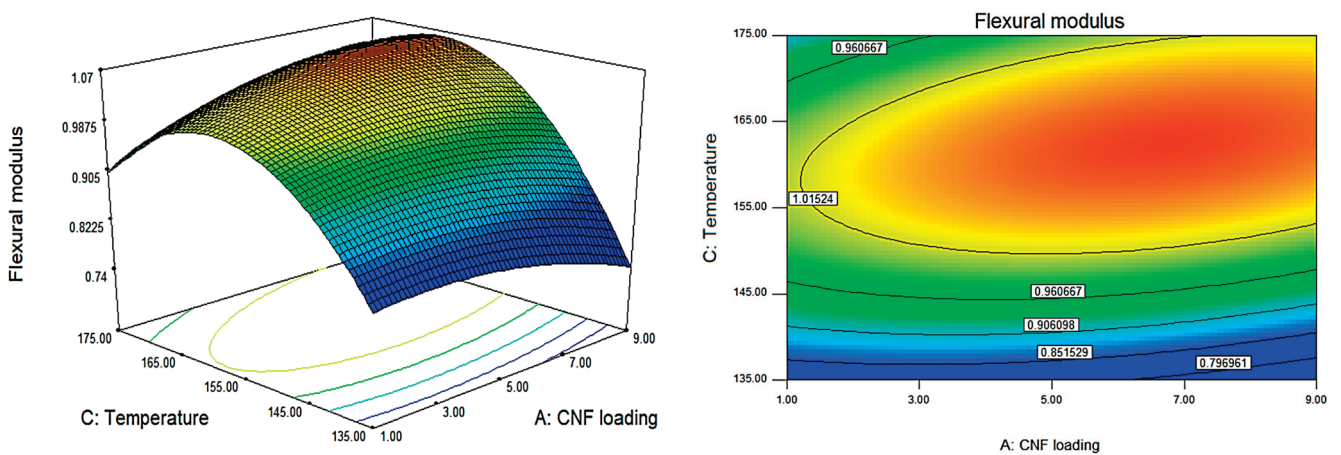


Figure 4. The 3D and response surface contour plots for the dependence of P(HB-co-11% HHX)/CNF bionanocomposite’s flexural modulus on CNF loading and temperature as significant factors.

Figure 2 depicts the 3D and response surface contour plots for the effects of CNF loading and temperature on tensile strength based on Equation (1). Results indicate that these variables are the most important factors influencing tensile strength (Table 3). It was

observed that further increment in CNF loading of more than 3 wt.% reduced the tensile strength of the bionanocomposites. This might be due to the agglomeration of the CNF within P(HB-co-11% HHx) matrix which disrupted the compactness and the spherulite structure of the bionanocomposites [29,30]. Meanwhile, the tensile strength of P(HB-co-11% HHx)/CNF bionanocomposites increased as temperature rose from 135 to 155 °C before declining from 155 to 175 °C. This result may be explained by the fact that P(HB-co-11% HHx) twin-screw extrusion at high temperature can result in a reduction in molecular weight owing to thermal degradation [10,24]. It has been discovered that random chain scission is the process of degradation causing PHAs to rapidly lose molecular weight when exposed to heat [31].

Figure 3 depicts 3D and response surface contour plots for the effects of CNF loading and rotational speed on flexural strength based on Equation (3). CNF loading (linear and quadratic) had a significant effect ( $p < 0.05$ ) on flexural strength, as well as the linear effect of rotational speed, interaction effect of CNF loading-rotational speed, and CNF loading-temperature and also the quadratic effect of temperature (Table 3). In comparison to the quadratic effect of temperature, the quadratic effect of CNF loading was less pronounced, with the coefficient of each factor of 1.54 and 0.29, respectively (Equation (3)). It was discovered that CNF dispersion in P(HB-co-11% HHx) was unaffected by rotational speed, as demonstrated by insignificant changes in tensile strength and flexural modulus. Conversely, a significant linear effect was noticed for flexural strength (Table 3), where a minor improvement could be noticed while processing P(HB-co-11% HHx) bionanocomposite at a slower rotational speed (Figure 3). Flexural strength decreases with the increase in CNF loading and rotational speed from 1 to 9 wt.% and 20 to 60 rpm, respectively.

Similar to flexural strength, significant quadratic effects of both CNF loading and temperature were observed against flexural modulus with no significant interactions between all factors (Table 3). Flexural modulus decreased with the increase in processing temperature from 155 to 175 °C, which is similar to the results of tensile and flexural strength. As aforementioned, fabricating bionanocomposites at high processing temperature leads to polymer degradation due to random chain scission, resulting in brittleness of the bionanocomposites [32,33]. Since the polymer molecular weight substantially decreases at temperatures above 155 °C, processing at those temperatures seems unsuitable. However, different from tensile and flexural strength, the addition of CNF up to 9 wt.% did not negatively affect the flexural modulus (Figure 4). In this study, CNF distribution in P(HB-co-11% HHx) was found to be unaffected by rotational speed, as proved by in Table 3, where no significant interaction can be seen between CNF loading and screw speed.

### 3.3. Response Surface Optimization of P(HB-co-11% HHx)/CNF Bionanocomposites

Numerical optimization was performed in accordance with the design and analysis, taking each criterion into consideration (Table 4). Due to the severity of the effect on tensile and flexural strength as well as flexural modulus, these responses were set at a maximum value. As shown in Table 4, the optimal CNF loading, rotational speed, and temperature for P(HB-co-11% HHx)/CNF bionanocomposite fabrication were 1.5 wt.% CNF, 20 rpm, and 160 °C, respectively. For these ideal conditions, it was predicted that the tensile strength, flexural strength, and modulus would be 22.96 MPa, 33.91 MPa, and 1.022 GPa, respectively, with a maximum desirability of 0.929.

### 3.4. Validation Experiment

The mechanical properties of the P(HB-co-11% HHx)/CNF bionanocomposite fabricated at the proposed parameter were consistent with the predicted value throughout the validation experiment as tabulated in Table 5, with the exception of the tensile strength, which was 9% higher. This finding was very good and favorable in light of the objective of this study, which was to attain high mechanical properties.

**Table 4.** The settings and solutions of the numerical optimization criterion.

Factor Constraints							
Name	Goal	Lower Limit		Upper Limit			
X <sub>1</sub>	Is in range	1.00		9.00			
X <sub>2</sub>	Is in range	20.00		60.00			
X <sub>3</sub>	Is in range	135.00		175.00			
Response Constraints							
Y <sub>1</sub>	Maximize	16.50		22.96			
Y <sub>2</sub>	Maximize	25.26		33.91			
Y <sub>3</sub>	Maximize	0.836		1.086			
Optimum Solutions							
Number	X <sub>1</sub>	X <sub>2</sub>	X <sub>3</sub>	Y <sub>1</sub>	Y <sub>2</sub>	Y <sub>3</sub>	Desirability
1	1.54	20.00	159.53	22.96	33.91	1.022	0.929
2	1.54	20.00	159.33	22.96	33.94	1.022	0.928
3	1.50	20.67	159.40	22.96	33.91	1.022	0.928
4	1.46	21.28	158.84	22.96	33.99	1.021	0.927

**Table 5.** Comparison between predicted and experimental values of P(HB-co-11% HHx)/CNF bionanocomposites fabricated at optimal conditions.

	Predicted	Experimental
Tensile strength (MPa), Y <sub>1</sub>	22.16	25.11 ± 0.4
Flexural strength (MPa), Y <sub>2</sub>	33.91	32.46 ± 0.4
Flexural modulus (GPa), Y <sub>3</sub>	1.02	1.00 ± 0.1

The mechanical properties of the neat P(HB-co-11% HHx) and P(HB-co-11% HHx)/CNF bionanocomposites prepared under these ideal conditions are shown in Table 6. This result demonstrated the ability of CNF to increase tensile strength, flexural strength, and flexural modulus by 17, 6, and 20%, respectively.

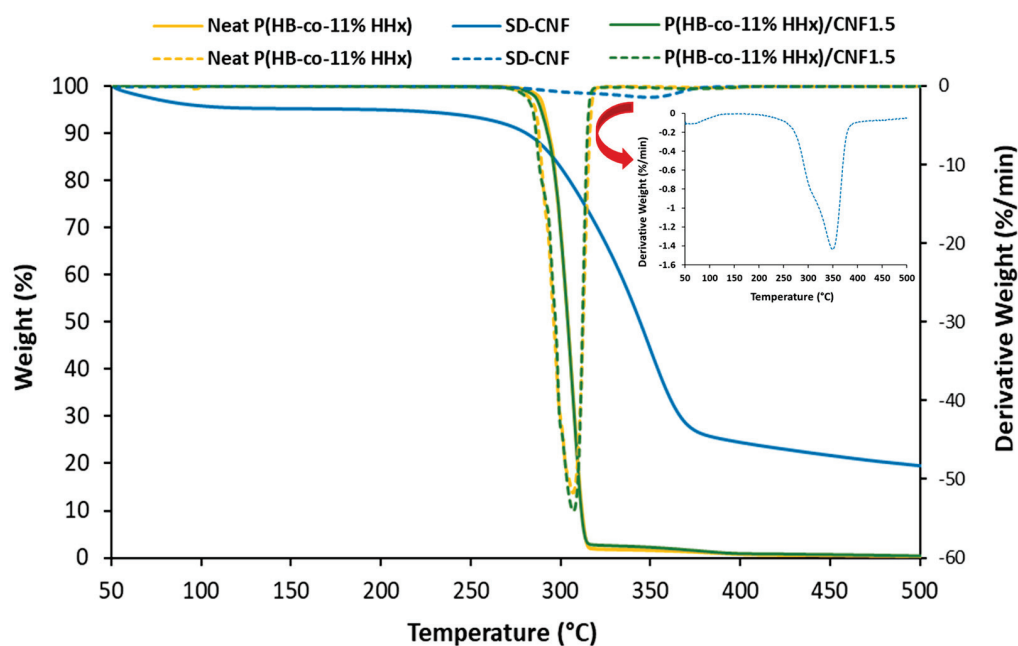
**Table 6.** Mechanical properties of neat P(HB-co-11% HHx) and P(HB-co-11% HHx)/CNF1.5 bionanocomposites.

	Neat P(HB-co-11% HHx)	P(HB-co-11% HHx)/CNF1.5
Tensile strength (MPa)	21.48 ± 0.4 <sup>b</sup>	25.11 ± 0.4 <sup>a</sup>
Flexural strength (MPa)	30.54 ± 0.7 <sup>b</sup>	32.46 ± 0.4 <sup>a</sup>
Flexural modulus (GPa)	0.83 ± 0.1 <sup>b</sup>	1.00 ± 0.1 <sup>a</sup>

All data are means of five replicates ± S.D. The superscript letters indicate significant difference ( $p < 0.05$ ) according to Duncan's multiple range test.

### 3.5. Effect of CNF on Thermal Stability and Crystallinity Properties of P(HB-co-11% HHx)/CNF Bionanocomposites

The thermal stability of spray dried-CNF, neat P(HB-co-11% HHx) and P(HB-co-11% HHx)/CNF1.5 bionanocomposites was investigated by thermogravimetric analysis. The TG and DTG curves are presented in Figure 5, and the thermal degradation data are summarized in Table 7. T<sub>10</sub> represents the temperature at which 10% of mass reduction was recorded, while T<sub>max</sub> represents the temperature at maximum mass loss, which was taken from the DTG thermogram.



**Figure 5.** TG and DTG curves for neat P(HB-co-11% HHx) and P(HB-co-11% HHx)/CNF1.5 bionanocomposites (Red arrow shows the zoom in peak for SD-CNF for DTG).

**Table 7.** Thermal degradation temperatures of neat P(HB-co-11% HHx) and P(HB-co-11% HHx)/CNF at 10 wt.% of weight loss ( $T_{10}$ ) and maximum degradation temperature ( $T_{max}$ ).

Sample	$T_{10}$ (°C)	$T_{max}$ (°C)
Neat P(HB-co-11% HHx)	294	307
SD-CNF	281	350
Optimized P(HB-co-11% HHx)/CNF1.5	293	307

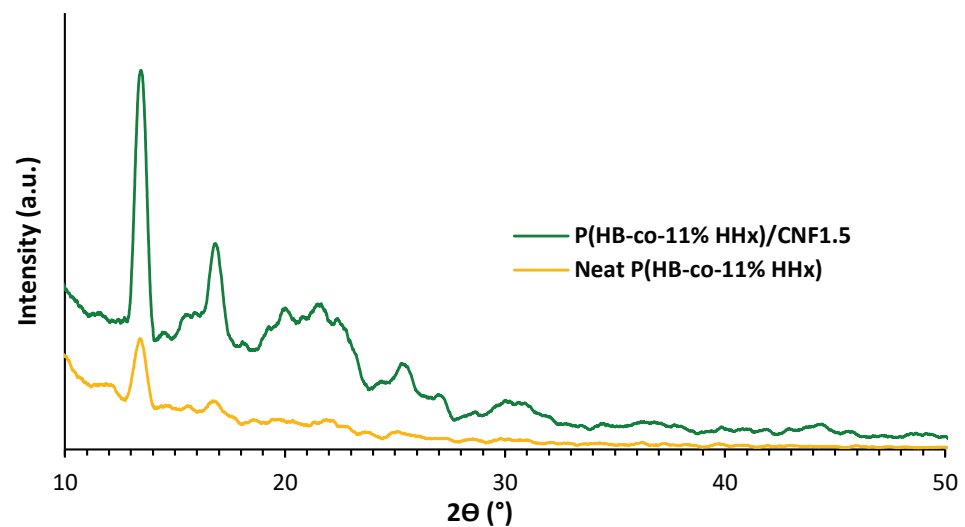
P(HB-co-11% HHx) thermal decomposition commenced at 280 °C and was completed at 320°C with single step degradation profile. As seen from Table 7, the  $T_{10}$  and  $T_{max}$  of neat P(HB-co-11% HHx) were 294 and 307 °C, respectively. Spray dried-CNF was less thermally stable at the beginning, where some weight loss started to occur at temperature around 100 °C, indicating the removal of moisture. Nevertheless, the  $T_{max}$  value was higher compared to P(HB-co-11% HHx). The addition of 1.5 wt.% CNF did not change the thermal stability of neat P(HB-co-11% HHx).

X-ray diffraction (XRD) analysis was performed to determine the crystallinity properties of neat P(HB-co-11% HHx) and optimized P(HB-co-11% HHx)/CNF1.5 bionanocomposites. Figure 6 displays the XRD patterns for both bionanocomposite samples, and the crystallinity index calculated is tabulated in Table 8.

**Table 8.** Crystallinity index (CI) of neat P(HB-co-11% HHx) and P(HB-co-11% HHx)/CNF bionanocomposites.

Sample	Crystallinity Index (%)
Neat P(HB-co-11% HHx)	25.1
P(HB-co-11% HHx)/CNF1.5	30.1





**Figure 6.** XRD patterns of neat P(HB-co-11% HHx) and optimized P(HB-co-11% HHx)/CNF1.5 bionanocomposites.

Sharp crystal peaks are visible in this sample, and their intensity was noticeably higher than that seen in the neat P(HB-co-11% HHx) sample, in accordance with the pattern of a bionanocomposite film containing 1.5 wt.% of CNF. This can be linked to the effective CNF distribution in the film matrix. This finding demonstrated that the addition of CNF promotes the growth of crystalline areas in the P(HB-co-11% HHx) matrix as evidenced by the increase in crystallinity index from 25.1 to 30.1%. As proved in Table 6, it has been suggested that an increase in crystallinity leads to an increase in the strength and modulus of bionanocomposites. Additionally, there is no peak shift in the XRD pattern of P(HB-co-11% HHx)/CNF bionanocomposites, indicating that the melt compounding by the twin screw extrusion process did not alter their crystal structures [24].

#### 4. Conclusions

P(HB-co-11% HHx)/CNF bionanocomposites fabricated using twin screw extruders were evaluated and predicted, and their melt-extrusion processing parameters were optimized using response surface modeling analysis based on the CCD method. The individual and interaction effects of three important melt-extrusion processing conditions, namely CNF loading, rotation speed, and temperature, on mechanical properties of P(HB-co-11% HHx)/CNF bionanocomposites (tensile strength, flexural strength, and modulus) were adequately modeled and optimized. It was discovered that CNF loading and temperature have a substantial effect on the mechanical properties of the P(HB-co-11% HHx)/CNF bionanocomposites; however, rotational speed has a less influential effect on mechanical properties except flexural modulus. At optimum CNF loading, rotational speed, and temperature of 1.5 wt.%, 20 rpm, and 160 °C, tensile strength, flexural strength, and flexural modulus are reported to be 22.96 MPa, 33.91 MPa, and 1.022 GPa, respectively. The response values obtained from the validation experiment were in good agreement with the predicted values. Validation tests proved that the response surface equations were adequate for predicting responses. The results of the TG and DTG study indicated that the thermal stability of the P(HB-co-11% HHx) matrix did not differ significantly from neat P(HB-co-11% HHx) when the optimum amount of CNF was introduced. The XRD analysis revealed that the addition of CNF increased crystallinity, which promotes the formation of crystalline regions in the P(HB-co-11% HHx) matrix. This research highlights the importance of optimal melt-extrusion processing conditions and their influence on the mechanical properties of P(HB-co-11% HHx)/CNF bionanocomposites. The findings of this research are anticipated to aid in the invention of novel P(HB-co-11% HHx) materials for packaging and other applications, taking into consideration the relevance of the correlation between melt-extrusion process parameters and the potential for process optimization to

enhance the mechanical properties of P(HB-co-11% HHx). This process optimization can be further used as one of the technical developments for bio-based nanocomposites derived from green materials with excellent prospects in novel high performance food packaging materials. With the optimum process conditions, the properties such as high mechanical performance with additional desired function such good thermal and barrier properties can be achieved. In addition, the application of bio-based materials to replace the synthetic fossil-based materials provides a range of benefits for various economic entities. Positive feedback has also been reported concerning ecological, economic, and social aspects associated with the transition from traditional plastic to bio-based plastics that can be widely used as packaging materials and act as a significant driver of the industry's growth.

**Author Contributions:** The manuscript was completed through the contributions of all authors. Conceptualization, H.A. and S.S.S.; methodology, H.A. and S.S.S.; software, H.A.; formal analysis, S.S.S. and F.A.S.; investigation, S.S.S. and F.A.S.; data curation, H.A.; writing—original draft, S.S.S.; writing—review and editing, H.A. and F.A.S.; visualization: S.S.S. and F.A.S.; supervision, H.A. and Y.A.; project administration, H.A.; funding acquisition, H.A. and Y.A. All authors have read and agreed to the published version of the manuscript.

**Funding:** This research was funded by the UPM-Kyutech Matching Grant (UPM-Kyutech/2020/9300471).

**Institutional Review Board Statement:** Not applicable.

**Informed Consent Statement:** Not applicable.

**Data Availability Statement:** Not applicable.

**Conflicts of Interest:** The authors declare no conflict of interest.

## References

- Chen, H.L.; Nath, T.K.; Chong, S.; Foo, V.; Gibbins, C.; Lechner, A.M. The Plastic Waste Problem in Malaysia: Management, Recycling and Disposal of Local and Global Plastic Waste. *SN Appl. Sci.* **2021**, *3*, 437. [CrossRef]
- Jambeck, J.R.; Geyer, R.; Wilcox, C.; Siegler, T.R.; Perryman, M.; Andrady, A.; Narayan, R.; Law, K.L. The Ocean. *Mar. Pollut.* **2015**, *347*, 768–771. [CrossRef]
- Naser, A.Z.; Deiab, I.; Darras, B.M. Poly(Lactic Acid) (PLA) and Polyhydroxyalkanoates (PHAs), Green Alternatives to Petroleum-Based Plastics: A Review. *RSC Adv.* **2021**, *11*, 17151–17196. [CrossRef]
- Kaniuk, Ł.; Stachewicz, U. Development and Advantages of Biodegradable PHA Polymers Based on Electrospun PHBV Fibers for Tissue Engineering and Other Biomedical Applications. *ACS Biomater. Sci. Eng.* **2021**, *7*, 5339–5362. [CrossRef]
- Ojumu, T.V.; Yu, J.; Solomon, B.O. Production of Polyhydroxyalkanoates, a Bacterial Biodegradable Polymer. *Afr. J. Biotechnol.* **2004**, *3*, 18–24. [CrossRef]
- Rivera-Briso, A.L.; Serrano-Aroca, Á. Poly(3-Hydroxybutyrate-Co-3-Hydroxyvalerate): Enhancement Strategies for Advanced Applications. *Polymers.* **2018**, *10*, 732. [CrossRef]
- Gumel, A.M.; Annuar, M.S.M. Nanocomposites of Polyhydroxylalkanoates (PHAs). In *RSC Green Chemistry*; Roy, I., Visakh, P., Eds.; Royal Society of Chemistry: Cambridge, UK, 2015; pp. 98–118. ISBN 1757-7039.
- Li, Z.; Yang, J.; Loh, X.J. Polyhydroxyalkanoates: Opening Doors for a Sustainable Future. *NPG Asia Mater.* **2016**, *8*, e265. [CrossRef]
- Zhang, Q.; Liu, Q.; Mark, J.E.; Noda, I. A Novel Biodegradable Nanocomposite Based on Poly (3-Hydroxybutyrate-Co-3-Hydroxyhexanoate) and Silylated Kaolinite/Silica Core-Shell Nanoparticles. *Appl. Clay Sci.* **2009**, *46*, 51–56. [CrossRef]
- Corrado, I.; Abdalrazeq, M.; Pezzella, C.; Di Girolamo, R.; Porta, R.; Sannia, G.; Giosafatto, C.V.L. Design and Characterization of Poly (3-Hydroxybutyrate-Co-Hydroxyhexanoate) Nanoparticles and Their Grafting in Whey Protein-Based Nanocomposites. *Food Hydrocoll.* **2021**, *110*, 106167. [CrossRef]
- Puppi, D.; Morelli, A.; Chiellini, F. Additive Manufacturing of Poly(3-Hydroxybutyrate-Co-3-Hydroxyhexanoate)/ Poly( $\epsilon$ -Caprolactone) Blend Scaffolds for Tissue Engineering. *Bioengineering* **2017**, *4*, 49. [CrossRef]
- Vanheusden, C.; Samyn, P.; Goderis, B.; Hamid, M.; Reddy, N.; Ethirajan, A.; Peeters, R.; Buntinx, M. Extrusion and Injection Molding of Poly(3-Hydroxybutyrate-Co-3-Hydroxyhexanoate) (Phbhx): Influence of Processing Conditions on Mechanical Properties and Microstructure. *Polymers* **2021**, *13*, 4012. [CrossRef] [PubMed]
- Rebia, R.A.; Rozet, S.; Tamada, Y.; Tanaka, T. Biodegradable PHBH/PVA Blend Nanofibers: Fabrication, Characterization, in Vitro Degradation, and in Vitro Biocompatibility. *Polym. Degrad. Stab.* **2018**, *154*, 124–136. [CrossRef]
- Nogi, M.; Kim, C.; Sugahara, T.; Inui, T.; Takahashi, T. High Thermal Stability of Optical Transparency in Cellulose Nanofiber Paper. *Appl. Phys. Lett.* **2013**, *102*, 181911. [CrossRef]

15. Nogi, M.; Iwamoto, S.; Nakagaito, A.N.; Yano, H. Optically Transparent Nanofiber Paper. *Adv. Mater.* **2009**, *21*, 1595–1598. [CrossRef]
16. Giubilini, A.; Sciancalepore, C.; Messori, M.; Bondioli, F. New Biocomposite Obtained Using Poly (3-Hydroxybutyrate-Co-3-Hydroxyhexanoate) (PHBH) and Micro Fibrillated Cellulose. *J. Appl. Polym. Sci.* **2020**, *137*, 48953. [CrossRef]
17. Valentini, F.; Dorigato, A.; Rigotti, D.; Pegoretti, A. Polyhydroxyalkanoates/Fibrillated Nanocellulose Composites for Additive Manufacturing. *J. Polym. Environ.* **2019**, *27*, 1333–1341. [CrossRef]
18. Yasim-Anuar, T.A.T.; Sharip, N.S.; Megashah, L.N.; Ariffin, H.; Nor, N.A.M. Cellulose Nanofibers from Waste Paper and Their Utilization as Reinforcement Materials in Poly((R)-3-Hydroxybutyrate-Co-(R)3-Hydroxyhexanoate Bionanocomposite. *Pertanika J. Sci. Technol.* **2020**, *28*, 259–271. [CrossRef]
19. Lee, J.; Hikima, Y.; Sekiguchi, T.; Ohshima, M. Thermal, Rheological, and Mechanical Properties of Cellulose Nanofiber (CNF) and Poly(3-Hydroxybutyrate-Co-3-Hydroxyhexanoate) (PHBH) Biopolymer Nanocomposites. *Cellulose* **2022**, *29*, 3901–3913. [CrossRef]
20. Andrade Pizarro, R.D.; Skurtys, O.; Osorio-Lira, F. Effect of Cellulose Nanofibers Concentration on Mechanical, Optical, and Barrier Properties of Gelatin-Based Edible Films. *Dyna* **2015**, *82*, 219–226. [CrossRef]
21. Shazleen, S.S.; Yasim-Anuar, T.A.T.; Ibrahim, N.A.; Hassan, M.A.; Ariffin, H. Functionality of Cellulose Nanofiber as Bio-Based Nucleating Agent and Nano-Reinforcement Material to Enhance Crystallization and Mechanical Properties of Polylactic Acid Nanocomposite. *Polymers* **2021**, *13*, 389. [CrossRef]
22. Yasim-Anuar, T.A.T.; Ariffin, H.; Norrahim, M.N.F.; Hassan, M.A.; Andou, Y.; Tsukegi, T.; Nishida, H. Well-Dispersed Cellulose Nanofiber in Low Density Polyethylene Nanocomposite by Liquid-Assisted Extrusion. *Polymers* **2020**, *12*, 927. [CrossRef] [PubMed]
23. Rabothata, M.; Muthu, J.; Wegner, L. Optimum Design Parameters and Mechanical Properties of Polymeric Nanocomposites Using NSGA-II Optimization Method. *J. Compos. Mater.* **2020**, *55*, 949–972. [CrossRef]
24. Berrabah, I.; Dehouche, N.; Kaci, M.; Bruzard, S.; Deguines, C.H.; Delaite, C. Morphological, Crystallinity and Thermal Stability Characterization of Poly(3-Hydroxybutyrate-Co-3-Hydroxyhexanoate)/Zinc Oxide Nanoparticles Bionanocomposites: Effect of Filler Content. *Mater. Today Proc.* **2022**, *53*, 223–227. [CrossRef]
25. Sharip, N.S.; Ariff, H.; Andou, Y.; Shirosaki, Y.; Bahrin, E.K.; Jawaid, M.; Tahir, P.M.; Ibrahim, N.A. Process Optimization of Ultra-High Molecular Weight Polyethylene / Cellulose Nanofiber Bionanocomposites in Triple Screw Kneading Extruder by Response. *Molecules* **2020**, *25*, 4498. [CrossRef]
26. Azeredo, H.M.C.; Mattoso, L.H.C.; Avena-Bustillos, R.J.; Filho, G.C.; Munford, M.L.; Wood, D.; McHugh, T.H. Nanocellulose Reinforced Chitosan Composite Films as Affected by Nanofiller Loading and Plasticizer Content. *J. Food Sci.* **2010**, *75*, N1–N7. [CrossRef] [PubMed]
27. Ghelich, R.; Jahannama, M.R.; Abdizadeh, H.; Torknik, F.S.; Vaezi, M.R. Central Composite Design (CCD)-Response Surface Methodology (RSM) of Effective Electrospinning Parameters on PVP-B-Hf Hybrid Nanofibrous Composites for Synthesis of HfB<sub>2</sub>-Based Composite Nanofibers. *Compos. Part B Eng.* **2019**, *166*, 527–541. [CrossRef]
28. Bagheri, V.; Ghanbarzadeh, B.; Ayaseh, A.; Ostadrahimi, A.; Ehsani, A.; Alizadeh-Sani, M.; Adun, P.A. The Optimization of Physico-Mechanical Properties of Bionanocomposite Films Based on Gluten/Carboxymethyl Cellulose/Cellulose Nanofiber Using Response Surface Methodology. *Polym. Test.* **2019**, *78*, 105989. [CrossRef]
29. Zhou, J.; Ma, X.; Li, J.; Zhu, L. Preparation and Characterization of a Bionanocomposite from Poly (3-Hydroxybutyrate-Co-3-Hydroxyhexanoate) and Cellulose Nanocrystals. *Cellulose* **2019**, *26*, 979–990. [CrossRef]
30. Post, W.; Kuijpers, L.J.; Zijlstra, M.; van der Zee, M.; Molenveld, K. Effect of Mineral Fillers on the Mechanical Properties of Commercially Available Biodegradable Polymers. *Polymers* **2021**, *13*, 394. [CrossRef]
31. Montano-Herrera, L.; Pratt, S.; Arcos-Hernandez, M.V.; Halley, P.J.; Lant, P.A.; Werker, A.; Laycock, B. In-Line Monitoring of Thermal Degradation of PHA during Melt-Processing by Near-Infrared Spectroscopy. *New Biotechnol.* **2014**, *31*, 357–363. [CrossRef]
32. Lin, P.; Xu, Q.; Cheng, S.; Li, X.; Zhao, Z.; Sun, S.; Peng, C.; Joy, A.; Wang, S.Q. Effects of Molecular Weight Reduction on Brittle-Ductile Transition and Elastic Yielding Due to Noninvasive Irradiation on Polymer Glasses. *Macromolecules* **2017**, *50*, 2447–2455. [CrossRef]
33. Song, Y.; Deng, J.; Xu, Z.; Nie, Y.; Lan, Z. Effect of Thermal Aging on Mechanical Properties and Color Difference of Glass Fiber/Polyetherimide (GF/PEI) Composites. *Polymers* **2022**, *14*, 67. [CrossRef] [PubMed]

**Disclaimer/Publisher’s Note:** The statements, opinions and data contained in all publications are solely those of the individual author(s) and contributor(s) and not of MDPI and/or the editor(s). MDPI and/or the editor(s) disclaim responsibility for any injury to people or property resulting from any ideas, methods, instructions or products referred to in the content.





Article

# Part B: Improvement of the Optical Properties of Cellulose Nanocrystals Reinforced Thermoplastic Starch Bio-Composite Films by Ex Situ Incorporation of Green Silver Nanoparticles from *Chaetomorpha linum*

Nour Houda M'sakni <sup>1,2,\*</sup> and Taghreed Alsufyani <sup>1,\*</sup><sup>1</sup> Department of Chemistry, College of Science, Taif University, P.O. Box 11099, Taif 21944, Saudi Arabia<sup>2</sup> Laboratory of Interfaces and Advanced Materials (LIMA), Faculty of Science, Monastir University, Monastir 5019, Tunisia\* Correspondence: [nour.h@tu.edu.sa](mailto:nour.h@tu.edu.sa) (N.H.M.); [taghreed.alsufyani@tu.edu.sa](mailto:taghreed.alsufyani@tu.edu.sa) (T.A.)

† These authors contributed equally to this work.

**Abstract:** The study was used in the context of realigning novel low-cost materials for their better and improved optical properties. Emphasis was placed on the bio-nanocomposite approach for producing cellulose/starch/silver nanoparticle films. These polymeric films were produced using the solution casting technique followed by the thermal evaporation process. The structural model of the bio-composite films (CS:CL-CNC7:3–50%) was developed from our previous study. Subsequently, in order to improve the optical properties of bio-composite films, bio-nanocomposites were prepared by incorporating silver nanoparticles (AgNPs) ex situ at various concentrations (5–50% w/w). Characterization was conducted using UV-Visible (UV-Vis), Fourier Transform Infrared (FTIR), Scanning Electron Microscope (SEM) and Transmission Electron Microscope (TEM) to understand the structure–property relationships. The FTIR analysis indicated a reduction in the number of waves associated with the OH functional groups by adding AgNPs due to the formation of new hydrogen bonds between the bio-composite matrix and the CL-WE-AgNPs. Based on mathematical equations, the optical bandgap energy, the energy of Urbach, the edge of absorption (Ed), and the carbon clusters (N) were estimated for CS:CL-CNC and CS:CL-CNC-AgNPs (5–50%) nanocomposite films. Furthermore, the optical bandgap values were shifted to the lower photon energy from 3.12 to 2.58 eV by increasing the AgNPs content, which indicates the semi-conductor effect on the composite system. The decrease in Urbach's energy is the result of a decrease in the disorder of the biopolymer matrix and/or attributed to an increase in crystalline size. In addition, the cluster carbon number increased from 121.56 to 177.75, respectively, from bio-composite to bio-nanocomposite with 50% AgNPs. This is due to the presence of a strong H-binding interaction between the bio-composite matrix and the AgNPs molecules. The results revealed that the incorporation of 20% AgNPs into the CS:CL-CNC7:3–50% bio-composite film could be the best candidate composition for all optical properties. It can be used for potential applications in the area of food packaging as well as successfully on opto-electronic devices.

**Keywords:** green macroalga; red sea; *Chaetomorpha linum*; cellulose nanocrystals; starch; green silver nanoparticles; bio-nanocomposite films; optical properties

**Citation:** M'sakni, N.H.; Alsufyani, T. Part B: Improvement of the Optical Properties of Cellulose Nanocrystals Reinforced Thermoplastic Starch Bio-Composite Films by Ex Situ Incorporation of Green Silver Nanoparticles from *Chaetomorpha linum*. *Polymers* **2023**, *15*, 2148. <https://doi.org/10.3390/polym15092148>

Academic Editor: Marcelo Antunes

Received: 25 March 2023

Revised: 26 April 2023

Accepted: 28 April 2023

Published: 30 April 2023



**Copyright:** © 2023 by the authors. Licensee MDPI, Basel, Switzerland. This article is an open access article distributed under the terms and conditions of the Creative Commons Attribution (CC BY) license (<https://creativecommons.org/licenses/by/4.0/>).

## 1. Introduction

The development of the bio-composites was based on the environmental knowledge that was generated over time. The remaining natural starch is a vital biomaterial for making environmentally friendly materials. In order to improve the properties of these biomaterials, a new area was created, including the development of bio-nanocomposites [1]. This is a continuous polymer phase in which loads of at least one size on a nanoscale are dispersed.

At this scale, the surface effects become predominant with volume effects in order to obtain original properties different from massive objects. The synthesized nanocomposites have demonstrated their versatility as a catalyst in the esterification response for the production of bio-diesel, a very good potential substitute for Gram-positive antimicrobial activity, as well as Gram-negative micro-organisms and an effective material for energy storage applications [2]. In this regard, nanostructures and nanocomposites, due to their small size, good catalytic activity, high surface area and outstanding selectivity, can play an important role in the near future [3]. Nanofillers, by their specific properties and the multitude of forms they can take, produce functional materials of interest in a number of areas such as electronics, medicine, cosmetics, optical physics and packaging [1].

Polymer matrices used for the production of CNC-reinforced composites could be divided into two parts: biodegradable and non-biodegradable polymers [4]. For example, natural polymers including by-products of cellulose, starch, natural rubber, and biopolymers such as polyhydroxyalkanoate (PHA), polylactic acid (PLA), polycaprolactone (PCL), etc., were widely used as biodegradable polymers to prepare bio-nanocomposites reinforced with cellulose nanocrystals [4,5]. Therefore, in our recent studies [6], we sought to reinforce the bio-composite film, with the introduction of a green *C. linum* silver nanoparticle in order to improve the optical properties of the biofilm. The study provided not only the optical property but also the characterization that led to the development of an optoelectronic bio-nanocomposite.

Due to remarkable physical and chemical properties, noble metallic nanoparticles play their role in various domains such as biological markers [7], treatment of cancer tumors [8], fluorescence [9], improving the efficiency of solar panels [10] or the signal in Raman spectroscopy [11]. Moreover, through enhanced optical response, these nanoparticles are indirectly used to characterize the physical properties of other particles such as catalysis [12]. However, integrating metallic nanoparticles in the polymer matrix is a fundamental and critical industrial challenge. In fact, their load properties, their nature and their presence in the matrix considerably alter the mechanical, thermal, electrical or optical properties, as well as contributing to simplifying and reducing the cost of the transformed material. In recent years, silicon nanowires decorated with silver nanoparticles have also been identified as semi-conductor and antibacterial unidimensional synthetic nanomaterials [13]. AgNPs with diverse properties such as catalytic activity [14], Raman diffusion [15], good conductivity [16], anti-microbial [17] and optical activity [18] have generated considerable interest in the area of nanotechnology [19]. AgNPs can be synthesized using physical, biological and chemical approaches [20]. However, physical-chemical techniques are highly productive in designing well-defined nanoparticles, but they have certain limitations, such as the use of hazardous chemicals, high costs, time-consuming processes, and the generation of impurities [21]. Green synthesis has gained more interest and actively increased progress in the fields of science and industry due to its ecological, cost-effective and non-hazardous nature [22]. To synthesize AgNPs, a metal precursor, reducing agents, and a non-toxic stabilizing/capping agent were required [23,24]. However, the presence of biomolecules of natural active agents in plants plays a significant role in reducing and stabilizing nanoparticles [24,25]. The phytochemical substances involved in reducing and capping nanoparticles are terpenoids, flavonoids, phenols, alkaloids, polysaccharides, proteins, enzymes, amino acids, etc. [26]. In addition, other active agents were reported such as linalool, quinol, methyl chavicol, eugenol, chlorophyll, caffeine, theophylline, ascorbic acids, and so on [27,28]. Several methods have been developed for incorporating nanoparticles into a polymer matrix in two ways, which are known as *ex situ* and *in situ* [29].

Each organic semiconductor has its own energy levels that basically depend on the molecular structure. Thus, the electronic bandgap is the energy difference between the lowest unoccupied molecular orbital (LUMO) and highest occupied molecular orbital (HOMO) level [30]. This difference in energy reveals the bandgap that electrons can only penetrate by external excitation. In general, it is 1 to 3 eV for organic semiconductors and

zero for conductors with overlapping valence and a conductive band. When it is high (>6 eV), the material is insulating, since it does not transfer electrons [31].

The objective of this study was to Integrate ex situ AgNPs as an electron donor reinforcement at the bandwidth of the bio-composite developed in our recent study [6] in order to develop new low-bandgap bio-nanocomposites for an optoelectronic application. The main requirement was to reduce the HOMO energy level as well as the bandgap of the polymers in order to increase the open circuit voltage of organic photovoltaic solar cells.

## 2. Experimental Work

### 2.1. Materials

Macroalgae thalli belonging to the order Cladophorales, *Chaetomorpha linum* were used as raw material to prepare AgNPs. Green algae were collected on the southwest coast of the Red Sea in Jeddah KSA (coordinates 21°37'41" N and 39°6'11" E). A CS:CL-CNC7:3–50% bio-composite (Table 1) was developed by reinforcing the thermoplastic starch matrix with cellulose nanocrystals (CL-CNCs) derived from *C. linum* algae biomass, according to the treatment detailed in our previous studies [6]. Silver nitrate-AgNO<sub>3</sub> (99.8%) was purchased from VWR, PROLABO.

**Table 1.** Composition of the cellulose nanocrystals, starch, glycerol, and CL-WE-AgNPs used in the investigation for the development of bio-composite and, bio-nanocomposites films.

Sample Code	CL-CNC (g)	% NaOH (mL)	CS (g)	Distilled Water (mL)	Glycerol (mL)	CL-WE-AgNPs (mL)
CS:CL-CNC7: 3–50% [6]	3.00	40	7.00	140	90.0	-
CS:CL-CNC7:3-AgNPs 5%	2.85	38	6.65	133	85.5	9
CS:CL-CNC7:3-AgNPs 10%,	2.70	36	6.30	126	81.0	18
CS:CL-CNC7:3-AgNPs 15%	2.55	34	5.95	119	76.5	27
CS:CL-CNC7:3-AgNPs 20%	2.40	32	5.60	112	72.0	36
CS:CL-CNC7:3-AgNPs 40%	1.80	24	4.20	84	54	72
CS:CL-CNC7:3-AgNPs 50%	1.50	20	3.50	70	45	90

#### 2.1.1. Colloidal Silver Nanoparticle (AgNP) Synthesis

The hydrosoluble polymers were obtained from 2 g of dry *C. linum* powder (CL-R) by extraction for 2 h in hot deionized water (1:40 w:w, 80 °C) with mechanical stirring. The mixture was filtered through a cloth and then centrifuged (5000 rpm) for 20 min to produce the CL-W fraction, as illustrated in Figure 1a. The filtrate was precipitated with the addition of 95% ethanol (40:60 v:v) to remove the remaining salts as well as low-molecular-mass polymers (proteins and polysaccharides) [32]. After decanting for 12 h (4 °C), the insoluble material was centrifuged out (5000 rpm) for 30 min to obtain the CL-WE fraction and recovered in deionized water. This fraction was used as a reducing and stabilizing agent for AgNPs synthesis [32]. To synthesize the colloidal AgNPs, 10 mL of seaweed extract was added to 90 mL of a 1 mM aqueous solution of silver nitrate (AgNO<sub>3</sub>) with constant stirring. The pH was adjusted to 9 by using 1 M NaOH solution to promote the reduction of Ag<sup>+</sup> ions at ambient temperature. Within hours, the color changed from yellow to dark brown, which confirmed the formation of AgNPs [33]. The synthesized material was labeled CL-WE-AgNPs.

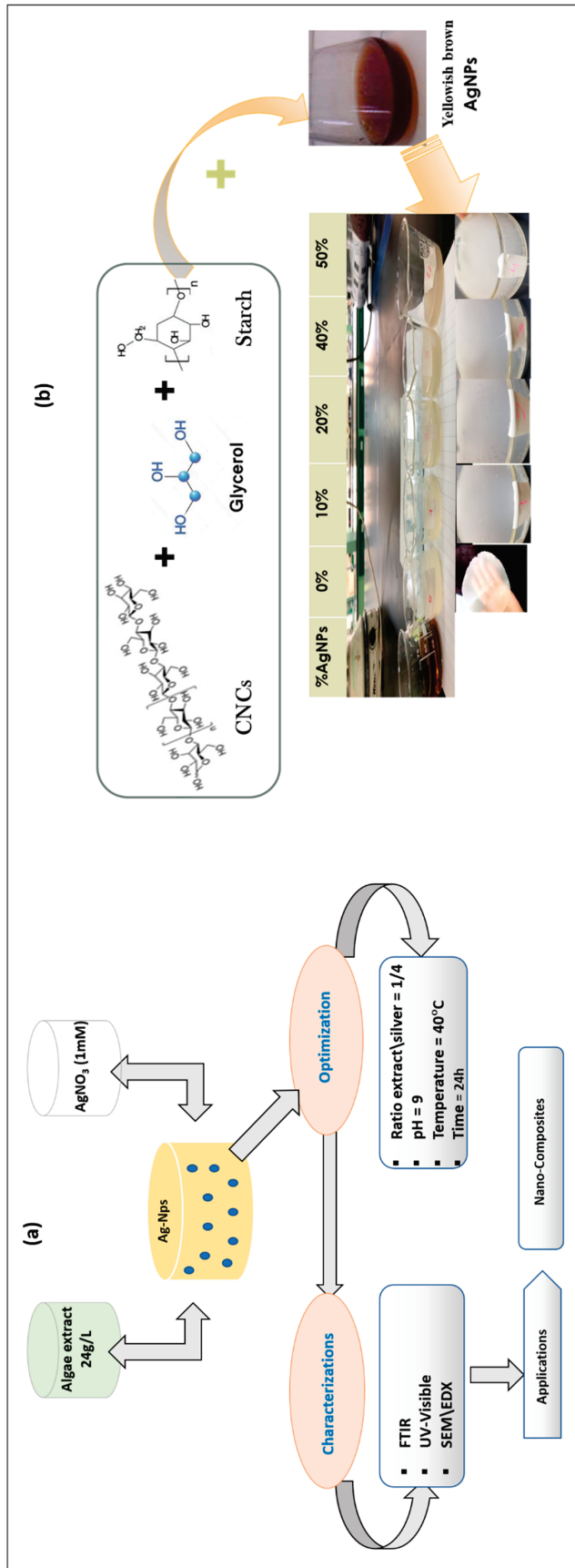


Figure 1. Schematic diagram of (a) elaboration of CL-WE-AgNPs from *C. linum*, and (b) elaboration of bio-nanocomposites.

### 2.1.2. Development of Optical Bio-Nanocomposite Films

To improve the performance of the bio-composite packaging, which was produced with the best formulation made for the biodegradable film (containing cellulose nanocrystals and thermoplastic starch), CL-WE-AgNPs were added in order to enhance the optical properties of bio-composite films.

Firstly, five solutions were prepared using the CS:CL-CNC7:3–50% bio-composite, and they were mixed successively with different compositions of CL-WE-AgNPs by weight with 190 mL of distilled water, stirred for five minutes and sonicated for 15 min. Then, the solutions were heated in a water bath at 85 °C for 30 min. The solution was moved into a Petri dish and stored in the oven for 24 h at 45 °C for drying. The films were peeled and retained in a desiccator (48 h) to control moisture (Figure 1b). The composition of the materials was fixed in cellulose nanocrystals, starch, and glycerol, which vary only with the percentage by weight of AgNPs, as shown in Table 1. Consequently, the percentage by weight of CL-WE-AgNPs was derived from the total quantity of mixture added. The resulting biofilms are named: CS:CL-CNC7:3-AgNPs (5%), CS:CL-CNC7:3-AgNPs (10%), CS:CL-CNC7:3-AgNPs (20%), CS:CL-CNC7:3-AgNPs (40%), and CS:CL-CNC7:3-AgNPs (50%) for the bio-nanocomposite films and CS: CL-CNC7:3–50% for the control bio-composite film.

## 2.2. Characterization Methods

### 2.2.1. UV-Visible Analysis

For optical properties, the UV-Vis-NIR (JASCO; V670) (JASCO; V670, Easton, Portland, OR, USA) spectrophotometer was used to study the optical transmittance (T) and absorbance (A) of films prepared over the wavelength range of 190 to 900 nm (Figure 8a,b).

Determining the bandgap value of both amorphous materials and polymers is crucial for their applications. The most popular technique to stimulate the bandgap is a measurement of the optical absorption coefficient. This coefficient was determined by mean absorbance (A), and Equation (1) was followed [34]:

$$\alpha = \frac{2.303 A}{d(\text{cm})} \quad (1)$$

where  $d = 0.02$  cm, and the film thickness was determined by a Vernier caliper. The functions of the absorption coefficient with incident photon energy for bio-composite films CS:CL-CNC7:3–50% and for bio-nanocomposite films CS:CL-CNC7:3-AgNP (5–50%) are shown, respectively, in Figure 9a,b.

The energy bandgap ( $E_g$ ) deviation of all the prepared films was determined by intercepting the plotted linear portion  $(\alpha hv)^2$  versus  $hv$ , as shown in Figure 10a, pursuing Tauc's method (Equation (2)) [35,36]:

$$\alpha hv = B(hv - E_g)^n \quad (2)$$

where  $B$  is the width parameter of the absorption edge,  $hv$  is the incident photon energy calculated from  $hv$  (eV) =  $1240/\lambda$  (nm), and  $n$  is the factor that takes 3/2 or 1/2 for direct transitions and 2 or 3 for indirect transitions relying on the forbidden or allowed transition, respectively.

For determining the band tail that refers to the width of localized states, the absorption coefficient  $\alpha(v)$  near the band edge as exponential dependence of photon energy ( $hv$ ) was determined from the Urbach relationship (Equation (3)) [37,38]:

$$\alpha(hv) = \alpha_0 e^{\left(\frac{hv}{E_e}\right)} \quad (3)$$

where  $\alpha_0$  is known as the constant and  $E_e$  denotes the band tail (Urbach tail), referring to the localized state's width (Figure 10b).



The number of carbon atoms (N) in a cluster is calculated from the optical energy bandgap (Eg) using the following relation (Equation (4)) [39,40]:

$$E_g = 34.4/\sqrt{N} \quad (4)$$

### 2.2.2. FTIR Analysis

Several stages involved in the development of bio-nanocomposite films were studied by FTIR (Thermo spectrophotometer, Nicolet IR 200, Madison, WI, USA). FTIR spectra were recorded between 4000 and 400  $\text{cm}^{-1}$  and compared with data already reported to distinguish the signal in a specific manner.

### 2.2.3. SEM and TEM Analyses

The JEOL model JEM-2000FX (Tokyo, Japan) instrument operated at an accelerating voltage of 200 Kilo voltage used to determine SEM (scanning electron microscope), EDX (energy-dispersive X-ray spectroscopy), and TEM (transmissions electron microscopy) measurement.

SEM and EDX images were taken for the characterization of the morphology, and the microstructures of all the materials were obtained at different stages of the bio-nanocomposite film development process.

In order to better clarify the morphology and size of the particles, TEM analysis was applied. A few drops of sonicated powdered sample were prepared and placed on a carbon-coated copper grid and air-dried for 1 h. The CL-WE-AgNP sample was selected for TEM analysis.

## 3. Results and Discussion

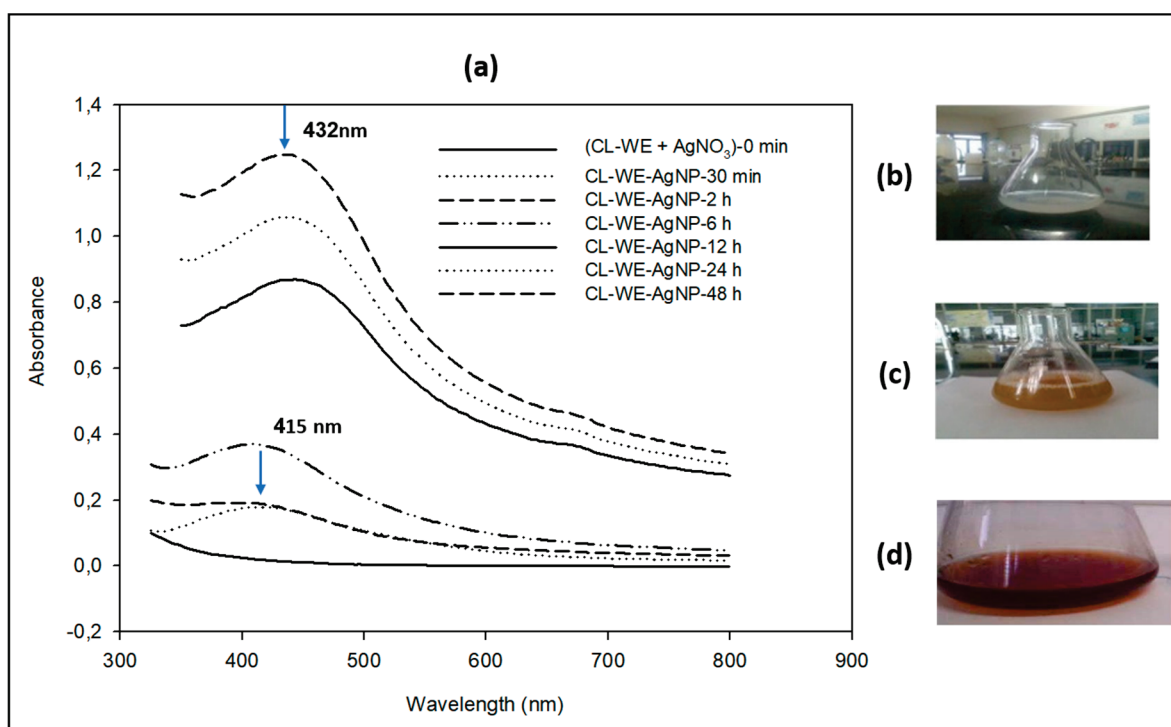
### 3.1. Impact of AgNPs Density on Optical Responses of Bio-Nanocomposite Films

#### 3.1.1. Synthesis of Colloid Silver Nanoparticles (AgNPs)

AgNPs (5, 10, 20, 40 and, 50%) were ex situ incorporated in (CS:CL-CNC7:3–50%) biofilm employing the matrix containing CL-CNC from *C. linum* (3 g), CS (7 g) and 50% glycerol as plasticizer agent to improve the optical properties of our previous biofilm [6]. The reduction of AgNPs was carried out by UV-Visible, SEM-EDX, TEM, and FTIR.

The reduction of the  $\text{Ag}^+$  ion into AgNPs was analyzed by color change (Figure 2a–d). Before adding the solution ( $\text{AgNO}_3$ , 1 mM), the supernatant of the *C. linum* extract precipitated in ethanol (CL-WE) was pale white–yellow (Figure 2b); it turned to a yellow–brown color after 30 min of contact (Figure 2c) and then brownish at the end of the reaction with the ions (after 48 h of contact) (Figure 2d).

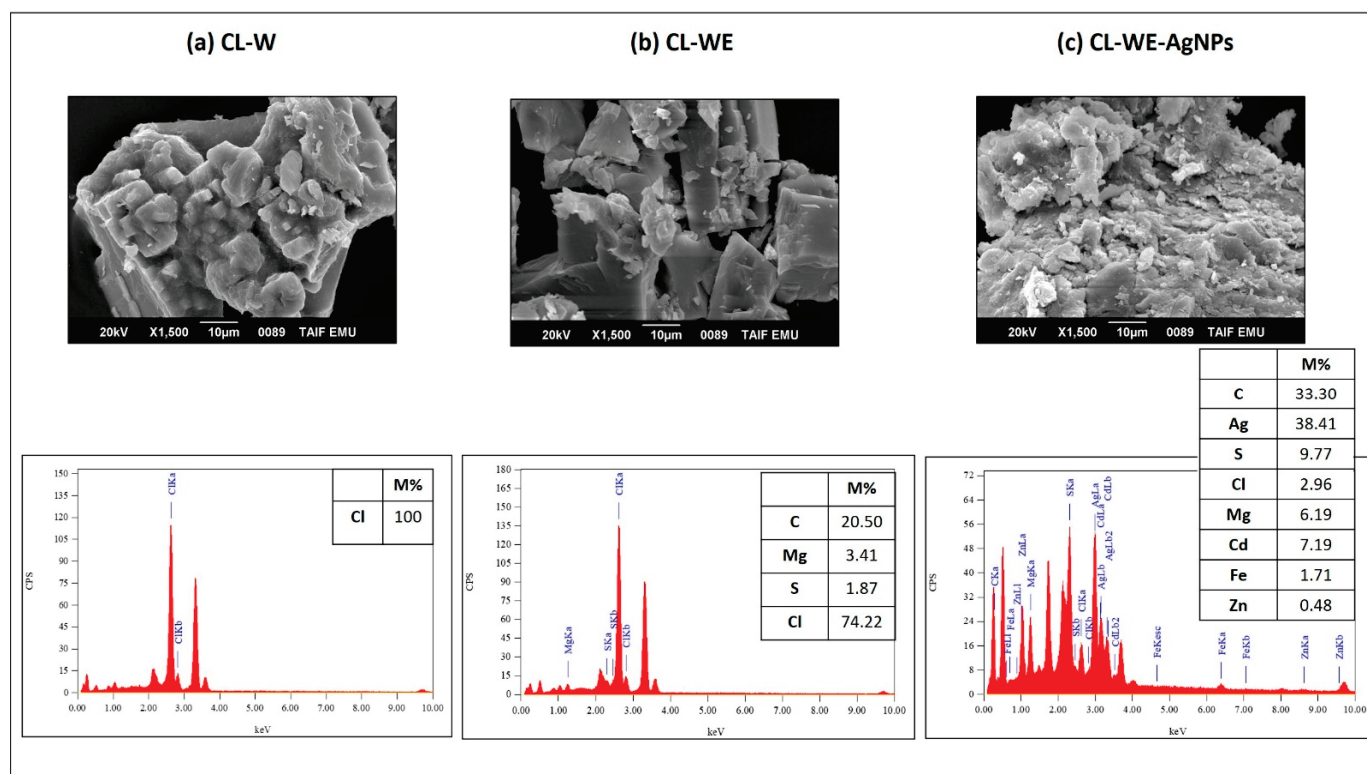
These results were confirmed by UV-Visible characterization spectrophotometry, which is a technique that proved to be very useful for the rapid analysis of colloidal solutions of AgNPs. This helps to determine whether the synthesis process was terminated by the formation of nanoparticles. The formation and stability of the reduced silver nanoparticles in the colloidal solution were monitored by UV-Vis spectrophotometric analysis [41]. The UV-Vis spectra showed a maximum absorbance at 415 nm that increased with the incubation time of silver nitrate with *C. linum* extract (Figure 2a) [42]. The presence of an absorbance peak at approximately 415 nm makes clear the formation of AgNPs in the solution, which is due to surface plasmon resonance (SPR) electrons present on the nanoparticle surface. The intensity of the SPR band increased with reaction time (30 min, 2 h, 6 h, 12 h, 24 and 48 h) and showed a maximum absorbance at 432 nm after 48 h (Figure 2a), indicating the synthesis of the AgNPs [42]. It is reported earlier that the absorbance at about 430 nm for silver is a feature of these noble metallic particles [43,44]. These results confirmed that 48 h time is the longest synthesis time at the present temperature and pH. It was observed that with an increase in the contact time between CL-WE and  $\text{AgNO}_3$ , the absorption peak shifted to a higher wavelength (from 415 to 432 nm), indicating an increase in the size of the AgNPs synthesized extract. These results are similar to those reported in the literature [41,42,45].



**Figure 2.** (a) UV-Vis absorption spectrum of silver nanoparticles CL-WE-AgNPs synthesized using aqueous dialyzed extract of fresh *C. linum* (CL-WE) as a function of reaction time, (b) beginning of the reaction (pale white–yellow), (c) after 30 min (yellow–brown color) and (d) after 48 h (brownish color) at 40 °C, and pH = 9.

### 3.1.2. Morphological Analysis of Synthesized AgNP and Its By-Products

A scanning electron microscope with an energy-dispersive X-ray spectrometer (SEM-EDX) was used to determine the silver concentration of the nanoparticles (Figure 3a–c). However, the EDX analysis of the aqueous extract of *C. linum* (CL-W) (Figure 3a) showed a high percentage of chlorine and salt, while after precipitation with ethanol (Figure 3b), the percentage of chlorine was decreased, so we note the presence of sulfur specific for glucosamines, which confirms the role of ethanol purification. After the reduction of the silver ions with the aqueous extract (CL-WE) (Figure 3c) which performs both reducing and stabilizing effects, a new distinct peak was detected at 2.983 keV in the CL-WE-AgNPs. Prasad, Kambala [46] have shown that AgNPs generally exhibit an absorption peak in the region of 3 keV due to the phenomenon of surface plasma resonance. The appearance of this peak (Figure 3c) confirmed the presence of elemental silver in the nanoparticles thus produced (CL-WE-AgNPs) with a silver concentration of around  $38.41 \pm 1.06\%$ , which was detected after an incubation of 48 h. The morphology of the CL-WE-AgNPs shows that several co-components appear alongside silver: in particular, iron, magnesium, zinc, cadmium, chlorine, sulfate . . . This is due to the reduction of silver by the aqueous *C. linum* extract, which was accompanied by the reduction of those trace metals and led to the formation of co-nanoparticles as a trace. Despite the low metal content (zinc and cadmium  $\leq 1$  ppm, iron  $\leq 2$  ppm, and magnesium  $\leq 5$  ppm per mass) that coexist with silver (originally VWR Chemicals commercial silver nitrate), ethanol precipitates of aqueous extract have been able to reduce these metals and obtain co-nanocomposites alongside nanocomposite silver synthesis. This explains the effect of ethanol precipitation of the plant extract that characterizes our method of green synthesis of AgNPs, which promotes the increase in the reducing properties of the plant extract following the purification of ethanol.



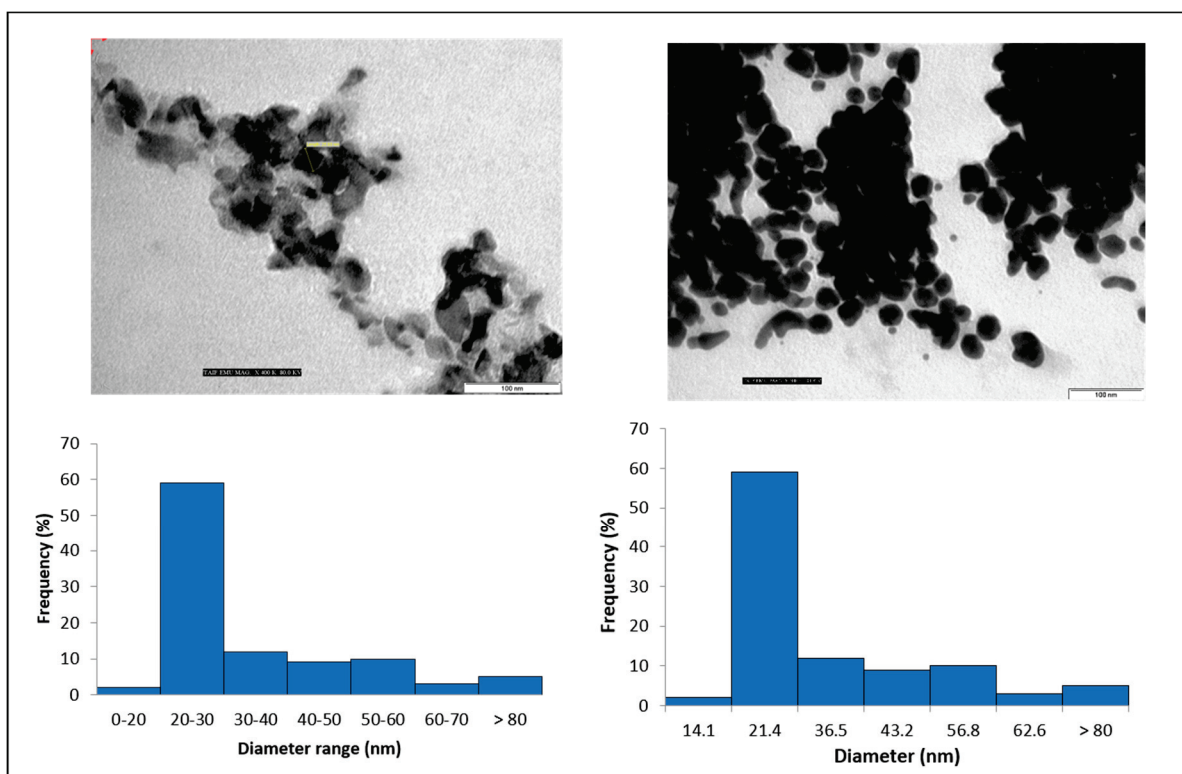
**Figure 3.** SEM and EDX image of silver nanoparticles synthesized steps: (a) CL-W, (b) CL-WE, (c) CL-WE-AgNPs.

Figure 4 represents the TEM image of CL-WE-AgNPs (48 h) determining that the AgNPs are well defined and are spherical with slight agglomeration. The presence of agglomeration could be due to the drying effects produced during sample preparation [47,48]. The aggregation behavior of AgNPs is mostly affected by pH and electrolyte concentration [49], while the presence of biomolecules can improve particle stability due to the biomolecular coronary effect [49]. In our work, we show that a degree of detected aggregation can be attributed to the ethanol precipitation effect of water extract (CL-W) that removes the salt that coexists with biomolecules. As shown, the size of nanoparticles increases with increasing concentration of  $\text{AgNO}_3$ . The Ag size range thus detected varied from 20 to 30 nm with an average of 21.4 nm. In comparison to the previous research, it was concluded that AgNPs with 20 nm size have a plasmon resonance band around 430 nm (violet absorption) and are brown [50].

### 3.1.3. FTIR Analysis of Synthesized AgNPs and Its By-Products

The biomolecules present in the root extract of *C. linum* played an active role in reducing  $\text{Ag}^+$  to AgNPs, as confirmed by the FTIR analysis. Figure 5a,b represent the FTIR spectrum of *C. linum* extract before and after ethanol precipitation. The FTIR spectra of dried *C. linum* extract before purification by ethanol (CL-W) (Figure 5a) have shown many peaks at  $614\text{ cm}^{-1}$ ,  $645\text{ cm}^{-1}$ ,  $706\text{ cm}^{-1}$ ,  $839\text{ cm}^{-1}$ ,  $863\text{ cm}^{-1}$ ,  $924\text{ cm}^{-1}$ ,  $1004\text{ cm}^{-1}$ ,  $1047\text{ cm}^{-1}$ ,  $1095\text{ cm}^{-1}$ ,  $1224\text{ cm}^{-1}$ ,  $1412\text{ cm}^{-1}$ ,  $1538\text{ cm}^{-1}$ ,  $1645\text{ cm}^{-1}$ ,  $2297\text{ cm}^{-1}$ ,  $2842\text{ cm}^{-1}$ ,  $2910\text{ cm}^{-1}$ ,  $2938\text{ cm}^{-1}$ ,  $3279\text{ cm}^{-1}$  and  $3338\text{ cm}^{-1}$ . However, the FTIR spectra of dried *C. linum* extract after purification with ethanol precipitation (CL-WE) have shown disparate peaks at  $614\text{ cm}^{-1}$ ,  $645\text{ cm}^{-1}$ ,  $924\text{ cm}^{-1}$ , and  $2297\text{ cm}^{-1}$  specifying aliphatic bromo compound, aliphatic-chloro compound, nucleic acid (other phosphate-containing compounds) [51,52] and nitrile compounds [53], respectively. Meanwhile, the decrease in the peak at  $1539\text{ cm}^{-1}$  is of amide II [54], explaining the effect of precipitation in ethanol which eliminates the salt compounds and minimizes the presence of free protein and increases the level of polysaccharides in the solution [32]. The appearance of the strong peak at  $1220\text{ cm}^{-1}$  is

specific to the asymmetric stretching vibration of sulfate groups commonly available in *C. linum* in the form of sulfated polysaccharides [55], which are used for the stabilization of AgNPs [56]. However, the corresponding bands observed at  $1545\text{ cm}^{-1}$  and  $1643\text{ cm}^{-1}$  are assigned successively to the amide II from proteins and the stretching vibration of the (NH) C=O group. After the reduction of  $\text{AgNO}_3$ , the shift of the bands from  $1538\text{ cm}^{-1}$  and  $1524\text{ cm}^{-1}$  is attributed to the involvement of the secondary amines in the reduction process and the binding of the (NH) C=O group with nanoparticles. Since a member of the (NH) C=O group within the cage of cyclic peptides is involved in stabilizing the nanoparticles, the shift of the (NH) C=O band is quite small. Thus, the peptides play a major role for the reduction of  $\text{Ag}^+$  to AgNPs. New bands in CL-WE-AgNPs at  $1133\text{ cm}^{-1}$  and  $1467\text{ cm}^{-1}$  (Figure 5b) may be attributed as vibrations of the glycosidic C-O bond (C-O-C) stretches from carbohydrates as well as to C=C-C, aromatic ring stretch, and the aromatic compound.



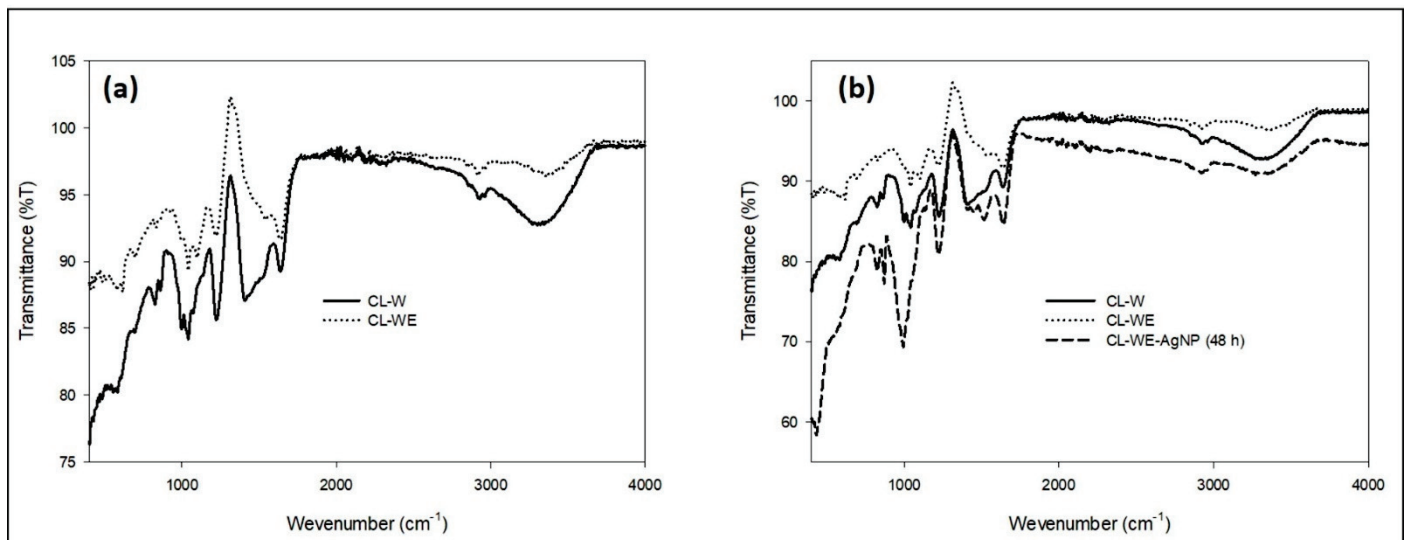
**Figure 4.** TEM image of CL-WE-AgNPs (48 h).

### 3.2. Characterization of Bio-Nanocomposite Films

#### 3.2.1. Morphological Analysis

To analyze the surface morphology of the films produced, and to show the distribution of AgNPs in the bio-nanocomposites (Starch/Cellulose/AgNPs) thus formed, a scanning electron microscope with an energy-dispersive X-ray spectrometer (SEM-EDX) was used. Figure 6a–e provides specific information about the structure and changes in the optical properties of films resulting from the addition of AgNPs. The SEM image of the film without AgNPs (CS:CL-CNC7:3–50%) in one of our recent studies [6] shows a porous surface with rough tufts. In contrast, the SEM images of the films with AgNPs (CS:CL-CNC7:3-AgNP5–50%) (Figure 6a–e) show more or less smooth surfaces with the emergence of some small aggregates corresponding to CL-WE-AgNPs in the form of white markings merged into nanoclusters [57,58]. The SEM images (Figure 6c) show a better distribution of CL-WE-AgNPs in CS/CL-CNC7:3–50% films with a percentage of 20% of AgNPs, indicating sufficient interfacial interaction with the matrix of the CS/CL-CNC mixture and the CL-WE-AgNPs [59].





**Figure 5.** FTIR analysis of (a) *C. linum* water extract before and after purification with ethanol precipitation and (b) colloidal silver nanoparticle CL-WE-AgNPs synthesis.

### 3.2.2. FTIR Analysis

After the preparation of the bio-nanocomposites by the modification of CS:CL-CNC7:3–50% films, by the incorporation of different levels of CL-WE-AgNPs (5–50%), FTIR measurements (Figure 7, Table S1) were performed to verify the formation of chemical bonds between the functionalized CL-WE-AgNPs and the matrix of CS:CL-CNC7:3–50%, which was carried on from our previous article for the current study [6]. The shape of the curves showed that the interactions of the matrix chains increase with the velocity of the nanoparticles (Figure 7). For all the matrices (CS:CL-CNC7:3–50%-AgNPs), new bands have appeared ( $1642\text{ cm}^{-1}$  and  $1787\text{ cm}^{-1}$ ) showing a better interaction in the order of CL-WE-AgNPs rate: 5%, 10%, 40%, 50%, to 20%. Although the bio-nanocomposite containing 20% CL-WE-AgNPs seems best in terms of composition, it suggests a good intermolecular interaction between the different compositions of the matrix.



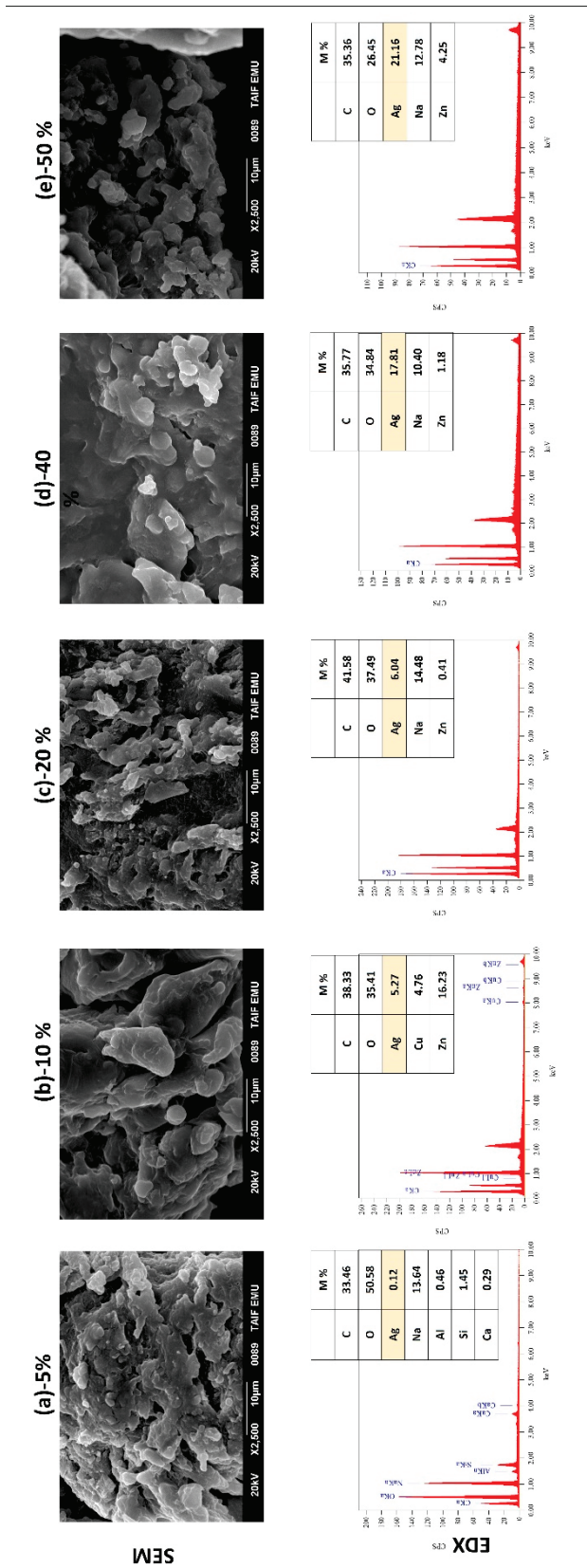


Figure 6. SEM and EDX analysis of bio-nanocomposite films CS:CL-CNC7:3-AgNPs (5–50%).

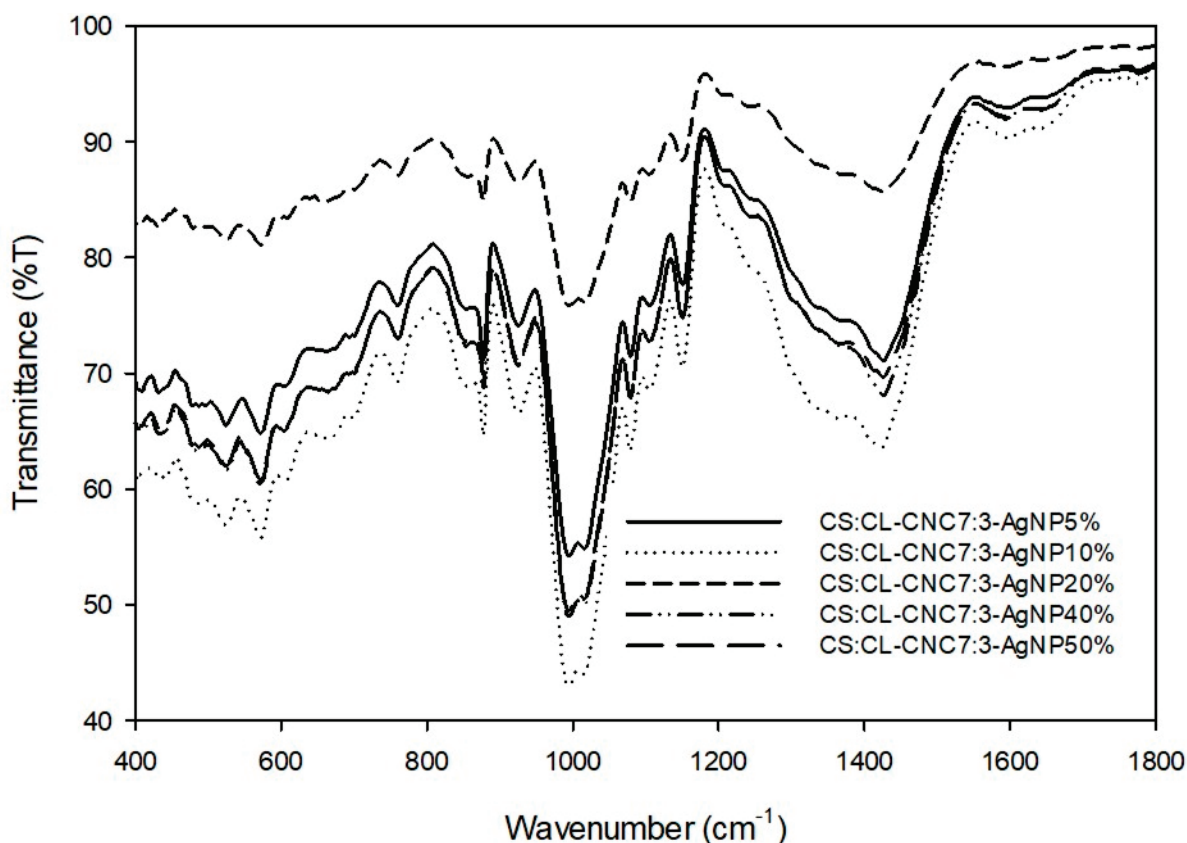


Figure 7. FTIR analysis of development bio-nanocomposite films (400–1800  $\text{cm}^{-1}$ ).

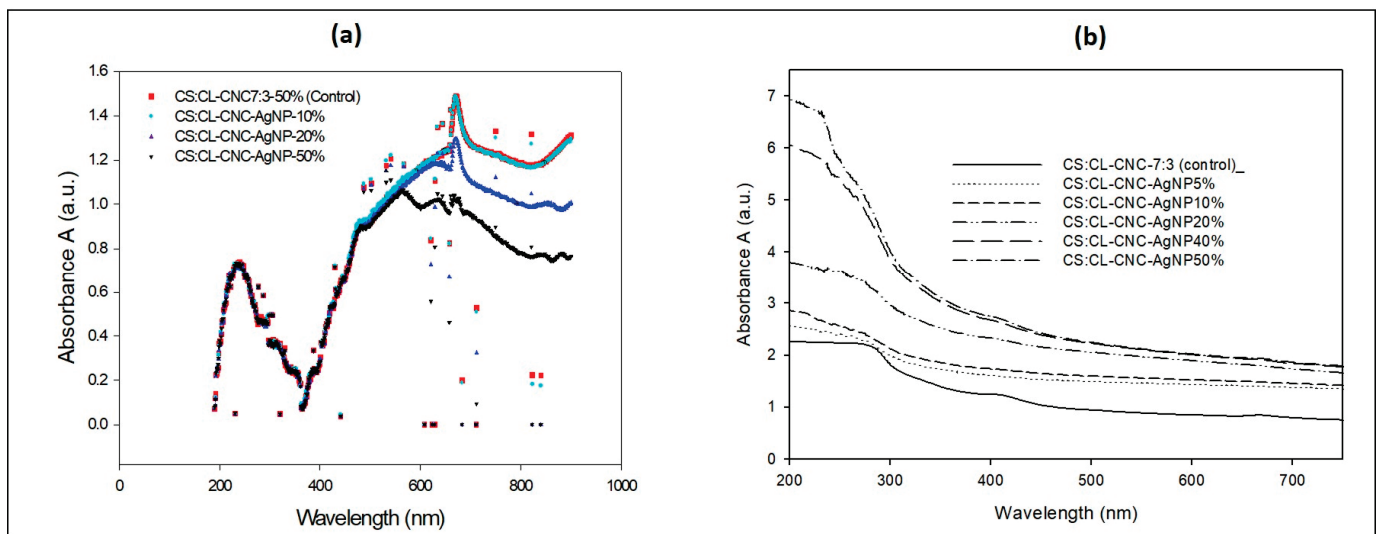
The band appeared at  $1643\text{ cm}^{-1}$  specifying the groups of water released from CL-CNC, as we stated in one of our recent studies [6]. The absorbance increases as CL-WE-AgNPs are added, indicating that water absorption is inversely proportional to the proportion of hydrophilic CL-WE-AgNPs [60–62]. However, the band around  $1787\text{ cm}^{-1}$  is attributed to the elongational vibrations of the C=O bond which occur due to the presence of hemicellulose residues from the CL-WE-AgNPs matrix on cellulose chains [60,63].

The number of waves associated with OH functional groups at  $3321\text{ cm}^{-1}$  was reduced due to the formation of new hydrogen bonds between the bio-composite matrix and the CL-WE-AgNPs [64]. A similar result was reported by previous research, which is explained in terms of weakened hydrogen bonding due to electron delocalization [65,66].

### 3.3. Optical Properties of the Synthesized Bio-Nanocomposites Films: The Ability to Protect Films against UV

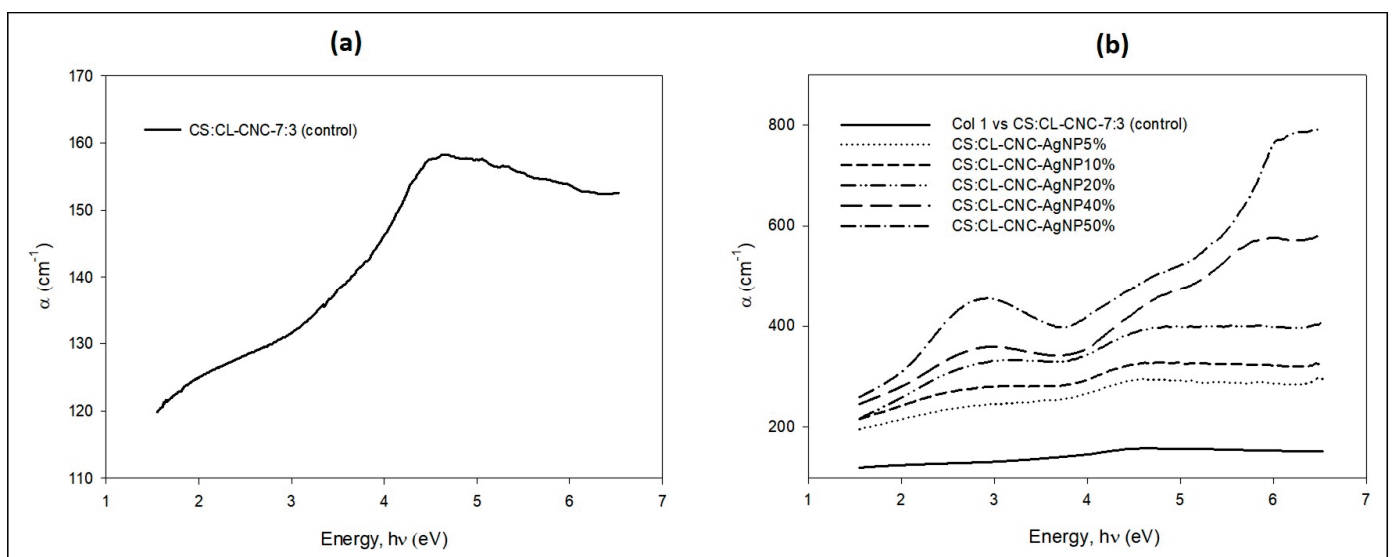
The absorbance of the bio-composite films of CS:CL-CNC:7:3–50% (control) [6] and with 5 to 50% of CL-WE-AgNPs was incorporated over the wavelength range of 190 to 900 nm, as shown in Figure 8a. As we stated in one of our recent studies [6], the starch/cellulose/glycerol-based bio-composite film exhibited UV absorbance at 273 nm but was not present in visible regions. In contrast, CS-CL-CNC-AgNPs (5–50%) films showed strong absorbance bands in the UV range around 212–300 nm (Figure 8a), which was due to the presence of AgNPs in the matrix. This explains that these bio-nanocomposites could be used in different fields of application. This is due to efficient UV absorbers, mainly for UV-C rays (100–280 nm), but also for UV-B rays (280–315 nm). He also noted that the intensity of the absorption peaks increases with the increase in the AgNPs content in CS-CL-CNC-AgNPs films (5–50% by weight), explaining a higher UV absorption ability for CS-CL-CNC-AgNPs 50% film compared to other matrices. Figure 8b revealed a strong absorption peak between 336 and 600 nm with a maximum absorbance of about 420–434 nm,

which is the typical plasmon resonance band of AgNPs [33,67]. The peak indicates that the  $\text{Ag}^+$  ions in the solution ( $\text{AgNO}_3$ , 1 mM) were successfully reduced to AgNPs.



**Figure 8.** (a) UV-visible absorption spectra of bio-composite formulation with the integration of CL-WE-AgNPs (10%, 20%, and 50%), and (b) Optical absorbance spectra of development bio-nanocomposite films.

The absorption coefficient ( $\alpha$ ) of the bioplastic film (CS-CL-CNC7:3–50%) is calculated according to Equation (1) and illustrated in (Figure 9a,b). The  $\alpha$ -values of the film (Figure 9a) are high and draw a broad spectrum in the spectral region  $> 1.55$  eV, which recommends the film for specific applications in the field of solar cells. Two absorption peaks also appeared at  $h\nu \approx 2.1$  eV and 4.6 eV in the visible and UV spectra range, respectively. These peaks are attributed to the  $\pi$ - $\pi^*$  transition between bonding and molecular orbital antibonding [68,69].



**Figure 9.** Optical absorption coefficient as a function of photon energy of (a) CS-CL-CNC7:3–50% bio-composite film [6] and (b) CS-CL-CNC-AgNPs (5–50%) development bio-nanocomposite films at ambient temperature.

The band structure of solid materials can be identified by studying the optical absorption spectrum [70,71]. Optical absorption studies on polymer blend films without and

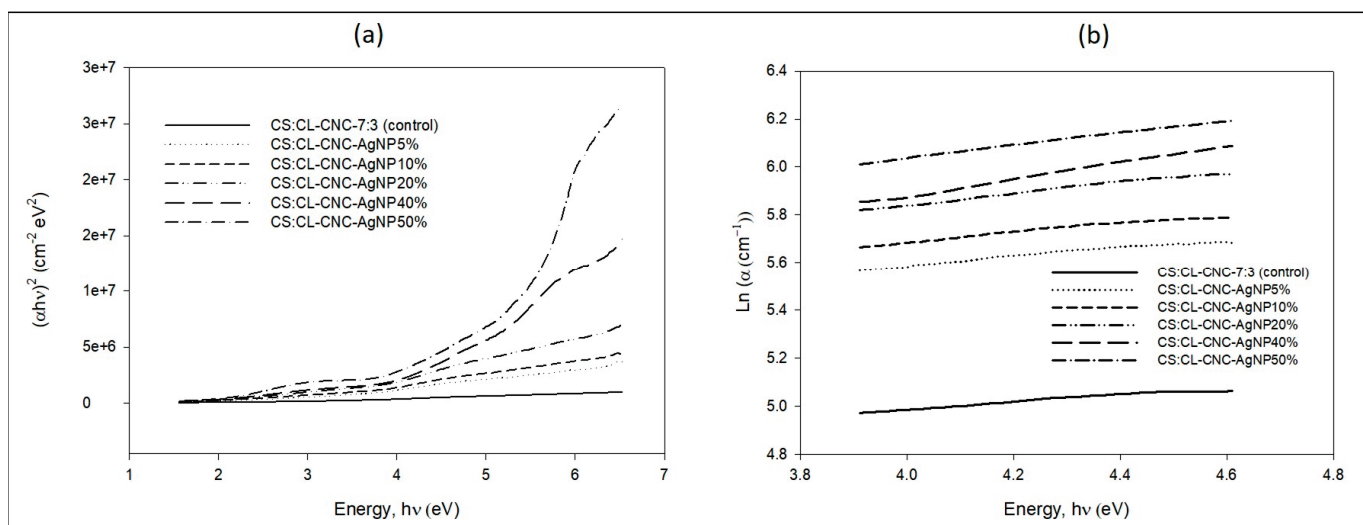
containing various concentrations of CL-WE-AgNPs (5–50%) are presented in Figure 9b. It was carried out to determine the optical constants: namely the position of the edge of the fundamental band and the optical bandgap (Table 2).

**Table 2.** Values of absorption edge (Ed), bandgap (Eg), band tail (Ee), and carbon cluster number N of CS-CL-CNC7:3–50% bio-composite film [6], and CS-CL-CNC-AgNPs (5–50%) development bio-nanocomposite films, at ambient temperature.

	Absorption Edge (Ed) (eV)	Optical Bandgap (Eg) (eV)	Urbach Energy (Ee) (eV)	Carbon Cluster Number (N)
CS:CL-CNC7:3–50% [6]	2.47	3.12	6.89	121.56
CS:CL-CNC-AgNPs 5%	1.51	2.91	5.41	139.74
CS:CL-CNC-AgNPs 10%	1.44	2.88	5.21	142.67
CS:CL-CNC-AgNPs 20%	1.32	2.82	4.25	148.80
CS:CL-CNC-AgNPs 40%	1.20	2.76	3.65	155.35
CS:CL-CNC-AgNPs 50%	1.08	2.58	3.62	177.78

Figure 9b demonstrated the optical absorption coefficients versus the photon energy of the biofilm mixture of CL-NCN and starch (CS-CL-CNC7:3–50%) and the bio-nanocomposites films (CS-CL-CNC-AgNPs (5–50%)). In particular, the optical absorption coefficients of the CS-CL-CNC7:3–50% film decrease as the AgNP content increases (Table 2). This reduction in Ed is attributed to the increase in the number of charge carriers by the structural modifications of the polymer matrix, which is due to molecular interactions between polymeric chains and CL-WE-AgNP [72]. They are also related to the changes in the number of electrons and the holes in the conductive and valence bands [73]. Specifically, the optical absorption edge shift explains the electronic coupling between CL-WE-AgNPs and CS-CL-CNC7:3–50% [72,73].

The optical bandgap energy (Eg) is the most interesting parameter for integrated optical optoelectronic and photovoltaic devices [74]. Therefore, by extrapolating the linear region to the abscissa, we obtain the energy of the optical bandgap of the amorphous material (Figure 10a). Table 2 shows that the energy value of the bandgap of the CS-CL-CNC7:3–50% film without CL-WE-AgNPs is 3.12 eV and decreases with increasing AgNPs content to 2.58 eV for the CS:CL-CNC-AgNPs 50% nanocomposite film. In this case, the bandgap energy is lower (<3 eV), indicating that it is a semi-conductor [75]. In particular, the reduction of Eg of the polymer matrix of the different films is attributed to the fact that the content of CL-WE-AgNPs is responsible for modifying the degree of disorder of the polymer as well as its structure. As a result, these changes reflect the localized states in the bandgap, which are responsible for decreasing the bandgap energy of the polymer [39,76]. Thus, the reduction in the bandgap is due to the addition of CL-WE-AgNPs in the CS:CL-CNC-7:3–50% matrix, which was carried on from our previous article for the current study [6]. This is due to the increased carrier–carrier interaction in the valence and conduction bands and subsequently the displacement of the valence and conduction band. However, the decrease in Eg reflects the formation of charge transfer complexes (CTCs) as trap levels between the bands of the HOMO, which is mainly carried by the silver metal and is an MO type Ag-d( $\pi$ ), and the LUMO, which is carried by the polymer matrix and it is an MO type ( $\pi^*$ ) [77]. This highlights the good miscibility between the CL-WE-AgNPs and the polymer matrix [39].



**Figure 10.** (a) Relationship between  $(\alpha hv)^2$  versus photon energy ( $h\nu$ ), (b) Absorption coefficient  $\ln \alpha$  versus photon energy for CS-CL-CNC7:3–50% bio-composite film [6], and CS-CL-CNC-AgNPs (5–50%) development bio-nanocomposite films at ambient temperature.

The Urbach curve is shown in Figure 10b, and the logarithm of the absorption coefficient ( $\alpha$ ) is plotted as a function of the photon energy ( $h\nu$ ). Table 2 groups the estimated values of the tail of the samples ( $E_e$ ) which were obtained by the inverse of the slope of the linear part of these curves (Equation (3)). The absorption edge called the Urbach energy, and it depends on induced disorder, static disorder, temperature, thermal vibrations in the lattice, strong ionic bonds and on average photon energies [78]. In our study, the temperature and the thickness of films were fixed, respectively, at ambient temperature and 0.02 cm. It is apparent in Figure 10b that the incorporation of CL-WE-AgNPs significantly reduces the absorption edge and decreases the  $E_e$  values in the films (Table 2) [79]. Indeed, the values of  $E_e$  decrease from 6.89 to 3.62 eV with the increase in the concentration of CL-WE-AgNPs from 0 to 50% by weight. This decrease in the Urbach energy is the result of the decreased disorder of the biopolymers matrix, and/or this was attributed to an increase in crystalline size [78]. Results were explained by several studies, showing that AgNPs [39] and other nanoparticles such as carbon nanotubes [79] lead to a redistribution of states from the band to the tail and thus promote a large number of tail-to-tail transitions [39,79]. Other studies showed that the width of the Urbach tail decreased by moving from thicker film to finer film, which meant from order to disorder [80]. However, the addition of CL-WE-AgNPs costs a charge transfer complex and reduces both  $E_g$  and  $E_e$ . At the same time, nanocomposite films achieve a good transparency of about 20%, and these values are suitable for certain applications. The correlation between Urbach energy and film thickness should be investigated.

The carbon atom number in clusters of CS-CL-CNC7:3–50% films and different bio-nanocomposite films were calculated (Equation (4)) and are regrouped in Table 2. The value of  $N$  for a bio-composite film without CL-WE-AgNPs is around 121.56, which increases to 177.78 in CS:CL-CNC-AgNPs 50% bio-nanocomposites. The increase in  $N$  value is due to the conjugation in monomer units of CS:CL-CNC7:3–50% matrix post embedding of AgNPs. Meanwhile, the band tail and the number of carbon clusters in the samples increased with increasing AgNPs contents [39].

The increase might be due to the breaking of electrons in the C–H bonds due to the liberation of hydrogen [81]. During irradiations, there is the release of gases from the polymeric material. These released gases such as  $\text{H}_2$ ,  $\text{H}$ ,  $\text{CO}$ , and  $\text{CO}_2$  can be led to the carbonaceous clusters (being rich charge carriers) in the polymer matrix. This carbonaceous cluster impacts the various physical properties of the polymeric material. Hence, the increase may be due to the carbon network and bonding of polymer–metal, and it ensures



the conductivity of polymers [40]. Another study also shows that the value of the optical bandgap  $E_g$  shows a decreasing trend with the fluence of the irradiated ions and with two kinds of ions ( $\text{Si}^{8+}$  and  $\text{Ne}^{6+}$ ) [82]. In addition, the number of carbon atoms per conjugation length increases with the increase in the ion dose built into the bio-composite matrix [82]. The formation of these clusters in polymer films with ion irradiation has been investigated extensively [82,83], and it is explained by the carbon clusters, which are supposed to be carriers in electrical conductivity, being formed along the latent pathways of energy ions in polymers.

#### 4. Conclusions

The improvement of the optical properties of the bio-composite film was obtained by integrating ex situ variable percentages of CL-WE-AgNPs (5–50%) synthesized from *C. linum* by green means. SEM/EDX confirmed a uniform dispersion of CL-WE-AgNPs in the bio-composite matrix with small agglomerations. A fundamental study of the optical properties of films was carried out to determine the absorption of UV with the presence of AgNPs in composites. However, a decrease in optical bandgap, edge absorption, and Urbach energy was observed compared to the CS:CL-CNC7:3–50% film developed in our recent study. The bandgap of the bio-composites decreases from 3.12 to 2.58 eV with the increase in the AgNPs content to 50%. In this case, the bandgap energy is lower (<3 eV), indicating that it is an improved semi-conductor. The decrease in Urbach energy results from a decrease in the matrix of biopolymers and/or an increase in crystalline size. Furthermore, the cluster carbon number increased, respectively, from 121.56 to 177.75 from bio-composite to bio-nanocomposite with 50% AgNPs. This is due to the presence of a strong H-binding interaction between the bio-composite matrix and the AgNP molecules. Consequently, the incorporation of AgNPs into the bio-composite film CS/CNC costs a load transfer complex and reduces  $E_g$  and  $E_e$ . At the same time, nanocomposite films attain a good transparency of about 20%. It could be applied to potential applications in the field of food packaging and can be used successfully on opto-electronic devices. Due to the promising properties of bio-composites, several new ones are emerging, and the assessment of their risks requires an individual approach of each nanomaterial. As a result of concerns about the safe use of bio-nanocomposites, further research into their mechanical properties and biological activity is required to provide a clear response regarding how and what nanomaterials can be a viable alternative to applications in many different areas.

**Supplementary Materials:** The following supporting information can be downloaded at: <https://www.mdpi.com/article/10.3390/polym15092148/s1>, Table S1: Assignment of bands found in FTIR spectra of different isolated water extract, silver nanoparticles and bio-nanocomposite.

**Author Contributions:** Both authors contributed equally to this study, including experiment performance, data analyses, discussion, writing, and reviewing. All authors have read and agreed to the published version of the manuscript.

**Funding:** The publication was funded by the Deanship of Scientific Research, Taif University for funding this work.

**Institutional Review Board Statement:** Not applicable.

**Informed Consent Statement:** Not applicable.

**Data Availability Statement:** The data presented in this study are available on request from the corresponding author.

**Acknowledgments:** The researchers would like to acknowledge Deanship of Scientific Research, Taif University for funding this work.

**Conflicts of Interest:** The authors declare that they have no conflict of interest.

## References

- Karimah, A.; Ridho, M.R.; Munawar, S.S.; Adi, D.S.; Ismadi; Damayanti, R.; Subiyanto, B.; Fatriasari, W.; Fudholi, A. A review on natural fibers for development of eco-friendly bio-composite: Characteristics, and utilizations. *J. Mater. Res. Technol.* **2021**, *13*, 2442–2458. [CrossRef]
- Philip, C.S.; Nivetha, A.; Sakthivel, C.; Veena, C.G.; Prabha, I. Novel fabrication of cellulose sprinkled crystalline nanocomposites using economical fibrous sources: High performance, compatible catalytic and electrochemical properties. *Microporous Mesoporous Mater.* **2021**, *318*, 111021. [CrossRef]
- Irfan, M.; Qurashi, A.; Alam, M.W. Metal oxide nanostructures and nanocomposites for selective catalytic reduction of NOx: A review. *Arab. J. Sci. Eng.* **2010**, *35*, 79–92.
- Hassan, I.; Ai-Jawhari, H. *Polymer Nanocomposite Matrices*; Springer: Cham, Switzerland, 2019. [CrossRef]
- Ilyas, R.A.; Sapuan, S.; Ishak, M.; Zainudin, E.S.; Mahamud, A. Nanocellulose Reinforced Starch Polymer Composites: A Review of Preparation, Properties and Application. In Proceedings of the 5th International Conference on Applied Sciences and Engineering Application (ICASEA 2018), Cameron Highlands, Malaysia, 7–8 April 2018.
- Alsufyani, T.; M'sakni, N.H. Part A: Biodegradable Bio-Composite Film Reinforced with Cellulose Nanocrystals from *Chaetomorpha linum* into Thermoplastic Starch Matrices. *Polymers* **2023**, *15*, 1542. [CrossRef] [PubMed]
- Anker, J.; Hall, W.P.; Lyandres, O.; Shah, N.; Zhao, J.; Duynne, R. Biosensing with Plasmonic Nanosensors. *Nat. Mater.* **2008**, *7*, 442–453. [CrossRef] [PubMed]
- Sotiriou, G.; Starsich, F.; Dasargyri, A.; Wurnig, M.; Krumeich, F.; Boss, A.; Leroux, J.-C.; Pratsinis, S. Photothermal Killing of Cancer Cells by the Controlled Plasmonic Coupling of Silica-Coated Au/Fe<sub>2</sub>O<sub>3</sub> Nanoaggregates. *Adv. Funct. Mater.* **2014**, *24*, 2818–2827. [CrossRef]
- Capadona, L.; Vinson, A.; Bartko, A.; Dickson, R. Photoactivated Fluorescence from Individual Silver Nanoclusters. *Science* **2001**, *291*, 103–106. [CrossRef]
- Marco, N.; Kristy, V.; Alison, C.; Muhsen, A.; Jinzhang, L.; Nunzio, M. Plasmonic effect of gold nanoparticles in organic solar cells. *Sol. Energy* **2014**, *106*, 23–37. [CrossRef]
- Sebastian, S. Surface-enhanced Raman spectroscopy: Concepts and chemical applications. *Angew. Chem.* **2014**, *53*, 4756–4795.
- Heiz, U.; Landman, U. *Nanocatalysis*; Springer: Berlin/Heidelberg, Germany, 2006. [CrossRef]
- Alam, M.W.; Al Qahtani, H.S.; Souayeh, B.; Ahmed, W.; Albalawi, H.; Farhan, M.; Abuzir, A.; Naeem, S. Novel Copper-Zinc-Manganese Ternary Metal Oxide Nanocomposite as Heterogeneous Catalyst for Glucose Sensor and Antibacterial Activity. *Antioxidants* **2022**, *11*, 1064. [CrossRef]
- Wang, J.; Liu, J.; Guo, X.; Yan, L.; Lincoln, S.F. The formation and catalytic activity of silver nanoparticles in aqueous polyacrylate solutions. *Front. Chem. Sci. Eng.* **2016**, *10*, 432–439. [CrossRef]
- Kochylas, I.; Gardelis, S.; Likodimos, V.; Giannakopoulos, K.P.; Falaras, P.; Nassiopoulou, A.G. Improved Surface-Enhanced-Raman Scattering Sensitivity Using Si Nanowires/Silver Nanostructures by a Single Step Metal-Assisted Chemical Etching. *Nanomaterials* **2021**, *11*, 1760. [CrossRef] [PubMed]
- Li, Y.; Wu, Y.; Ong, B.S. Facile synthesis of silver nanoparticles useful for fabrication of high-conductivity elements for printed electronics. *J. Am. Chem. Soc.* **2005**, *127*, 3266–3267. [CrossRef] [PubMed]
- Martínez-Castañón, G.-A.; Nino, N.; Martínez-Gutiérrez, F.; Martínez, J.R.; Ruiz, F. Synthesis and antibacterial activity of silver nanoparticles with different sizes. *J. Nanoparticle Res.* **2008**, *10*, 1343–1348. [CrossRef]
- Kumar, A.; Madhu, G.; John, E.; Kuttinarayanan, S.; Nair, S.K. Optical and antimicrobial properties of silver nanoparticles synthesized via green route using honey. *Green Process. Synth.* **2020**, *9*, 268–274. [CrossRef]
- Almatroudi, A. Silver nanoparticles: Synthesis, characterisation and biomedical applications. *Open Life Sci.* **2020**, *15*, 819–839. [CrossRef] [PubMed]
- Vidyasagar; Patel, R.R.; Singh, S.K.; Singh, M. Green synthesis of silver nanoparticles: Methods, biological applications, delivery and toxicity. *Mater. Adv.* **2023**, *4*, 1831–1849. [CrossRef]
- Iravani, S.; Korbekandi, H.; Mirmohammadi, S.; Zolfaghari, B. Synthesis of silver nanoparticles: Chemical, physical and biological methods. *Res. Pharm. Sci.* **2014**, *9*, 385–406.
- Ying, S.; Guan, Z.; Ofoegbu, P.C.; Clubb, P.; Rico, C.; He, F.; Hong, J. Green synthesis of nanoparticles: Current developments and limitations. *Environ. Technol. Innov.* **2022**, *26*, 102336. [CrossRef]
- Goel, M.; Sharma, A.; Sharma, B. Recent Advances in Biogenic Silver Nanoparticles for Their Biomedical Applications. *Sustain. Chem.* **2023**, *4*, 61–94. [CrossRef]
- Hasan, K.M.F.; Xiaoyi, L.; Shaoqin, Z.; Horváth, P.G.; Bak, M.; Bejő, L.; Sipos, G.; Alpár, T. Functional silver nanoparticles synthesis from sustainable point of view: 2000 to 2023—A review on game changing materials. *Heliyon* **2022**, *8*, e12322. [CrossRef] [PubMed]
- Monowar, T.; Rahman, M.; Bhore, S.; Raju, G.; Sathasivam, K. Silver Nanoparticles Synthesized by Using the Endophytic Bacterium *Pantoea ananatis* are Promising Antimicrobial Agents against Multidrug Resistant Bacteria. *Molecules* **2018**, *23*, 3220. [CrossRef] [PubMed]
- Shaikh, W.A.; Chakraborty, S.; Owens, G.; Islam, R.U. A review of the phytochemical mediated synthesis of AgNP (silver nanoparticle): The wonder particle of the past decade. *Appl. Nanosci.* **2021**, *11*, 2625–2660. [CrossRef] [PubMed]

27. Rauwel, P.; Küünal, S.; Ferdov, S.; Rauwel, E. A Review on the Green Synthesis of Silver Nanoparticles and Their Morphologies Studied via TEM. *Adv. Mater. Sci. Eng.* **2015**, *2015*, 682749. [CrossRef]
28. Siddiqi, K.S.; Husen, A.; Rao, R.A.K. A review on biosynthesis of silver nanoparticles and their biocidal properties. *J. Nanobiotechnol.* **2018**, *16*, 14. [CrossRef]
29. Pandey, P.P. Preparation and Characterization of Polymer Nanocomposites. *Soft Nanosci. Lett.* **2020**, *10*, 1–15. [CrossRef]
30. Bertrandie, J.; Han, J.; De Castro, C.; Yengel, E.; Gorenflot, J.; Anthopoulos, T.; Laquai, F.; Sharma, A.; Baran, D. The Energy Level Conundrum of Organic Semiconductors in Solar Cells. *Adv. Mater.* **2022**, *34*, e2202575. [CrossRef]
31. Geoghegan, M.A.; Hadziioannou, G. *Polymer Electronics*; Oxford University Press: Oxford, UK, 2013; p. 256. [CrossRef]
32. M'sakni, N.H.; Zayane, H.; Majdoub, H.; Morvan, C.; Roudesli, S.; Deratani, A. Extraction and characterization of polysaccharides from *Mesembryanthemum crystallinum*. *e-Polymers* **2005**, *5*, 63. [CrossRef]
33. Virender, K.S.; Ria, A.Y.; Yekaterina, L. Silver nanoparticles: Green synthesis and their antimicrobial activities. *Adv. Colloid Interface Sci.* **2009**, *145*, 83–96. [CrossRef]
34. ElMetwally, M.A.; Amr, M.A.; Shalabya, I.B.; Mohamed, A.M. Structural, optical, morphological and thermal properties of PEO/PVP blend containing different concentrations of biosynthesized Au nanoparticles. *J. Mater. Res. Technol.* **2018**, *7*, 419–431. [CrossRef]
35. Soliman, T.; Abouhaswa, A. Synthesis and structural of Cd<sub>0.5</sub>Zn<sub>0.5</sub>F<sub>2</sub>O<sub>4</sub> nanoparticles and its influence on the structure and optical properties of polyvinyl alcohol films. *J. Mater. Sci. Mater. Electron.* **2020**, *31*, 9666–9674. [CrossRef]
36. Zeyada, H.; Elshabaan, M. Gamma-ray irradiation induced structural and optical constants changes of thermally evaporated neutral red thin films. *J. Mater. Sci.* **2012**, *47*, 493–502. [CrossRef]
37. Ledinský, M.; Schönfeldová, T.; Holovský, J.; Aydin, E.; Hájková, Z.; Landová, L.; Neykova, N.; Fejfar, A.; De Wolf, S. Temperature Dependence of the Urbach Energy in Lead Iodide Perovskites. *J. Phys. Chem. Lett.* **2019**, *10*, 1368–1373. [CrossRef]
38. Urbach, F. The Long-Wavelength Edge of Photographic Sensitivity and of the Electronic Absorption of Solids. *Phys. Rev.* **1953**, *92*, 1324. [CrossRef]
39. Abdelhamied, M.M.; Atta, A.K.; Abdelreheem, A.; Farag, A.T.M.; El Okr, M. Synthesis and Optical Properties of PVA/PANI/Ag Nanocomposite films. *J. Mater. Sci. Mater. Electron.* **2020**, *31*, 22629–22641. [CrossRef]
40. Abdel Reheem, A.; Atta, A.; Afify, T. Optical and electrical properties of argon ion beam irradiated PVA/Ag nanocomposites. *Surf. Rev. Lett.* **2016**, *24*, 1750038. [CrossRef]
41. Abdussalam-Mohammed, W.; Mohamed, L.; Abraheem, M.S.; Mansour, M.M.A.; Sherif, A.M. Biofabrication of Silver Nanoparticles Using Teucrium Apollinis Extract: Characterization, Stability, and Their Antibacterial Activities. *Chemistry* **2023**, *5*, 54–64. [CrossRef]
42. Kocadağ Kocazorbaz, E. Green Synthesis, Optimization, and Characterization of Silver Nanoparticles from *Euphorbia rigida* Leaf Extract and Investigation of Their Antimicrobial Activities. *Bilecik Şeyh Edebali Üniv. Fen Bilim. Derg.* **2021**, *8*, 512–522. [CrossRef]
43. Hemlata; Meena, P.R.; Singh, A.P.; Tejavath, K.K. Biosynthesis of Silver Nanoparticles Using *Cucumis prophetarum* Aqueous Leaf Extract and Their Antibacterial and Antiproliferative Activity Against Cancer Cell Lines. *ACS Omega* **2020**, *5*, 5520–5528. [CrossRef]
44. Logeswari, P.; Silambarasan, S.; Abraham, J. Synthesis of silver nanoparticles using plants extract and analysis of their antimicrobial property. *J. Saudi Chem. Soc.* **2015**, *19*, 311–317. [CrossRef]
45. Shakeel, A.; Saifullah; Mudasir, A.; Babu Lal, S.; Saiqa, I. Green synthesis of silver nanoparticles using *Azadirachta indica* aqueous leaf extract. *J. Radiat. Res. Appl. Sci.* **2016**, *9*, 1–7. [CrossRef]
46. Prasad, T.N.V.K.V.; Kambala, V.; Naidu, R. Phyconanotechnology: Synthesis of silver nanoparticles using brown marine algae *Cystophora moniliformis* and their characterisation. *J. Appl. Phycol.* **2013**, *25*, 177–182. [CrossRef]
47. Mulenós, M.R.; Lujan, H.; Pitts, L.K.R.; Sayes, C.M. Silver Nanoparticles Agglomerate Intracellularly Depending on the Stabilizing Agent: Implications for Nanomedicine Efficacy. *Nanomaterials* **2020**, *10*, 1953. [CrossRef]
48. Michen, B.; Geers, C.; Vanhecke, D.; Voss, C.; Rothen-Rutishauser, B.; Balog, S.; Fink, A. Avoiding drying-artifacts in transmission electron microscopy: Characterizing the size and colloidal state of nanoparticles. *Sci. Rep.* **2015**, *5*, 9793. [CrossRef] [PubMed]
49. Bélteky, P.; Rónavári, A.; Igaz, N.; Szerencsés, B.; Tóth, I.Y.; Pfeiffer, I.; Kiricsi, M.; Kónya, Z. Silver nanoparticles: Aggregation behavior in biorelevant conditions and its impact on biological activity. *Int. J. Nanomed.* **2019**, *14*, 667–687. [CrossRef] [PubMed]
50. Zimmer, S.; Chupin, G.; Bon, C.; Yannis, C.; Jonathan, P. Synthèse et détermination de la taille de nanoprismes d'argent. *Bull. De L'union Des Phys.* **2016**, *110*, 1339–1368.
51. Tang, Z.; Zhou, C.; Cai, Y.; Tang, Y.; Sun, W.; Huipeng, Y.; Zheng, T.; Chen, H.; Xiao, Y.; Shan, Z.; et al. Purification, characterization and antioxidant activities in vitro of polysaccharides from *Amaranthus hybridus* L. *PeerJ* **2020**, *8*, e9077. [CrossRef]
52. Pawar, H.A.; Lalitha, K.G. Isolation, purification and characterization of galactomannans as an excipient from *Senna tora* seeds. *Int. J. Biol. Macromol.* **2014**, *65*, 167–175. [CrossRef]
53. Subrhamanian, H.; Suriyamoorthy, P.; Rajasekar, D. Fourier transform infra-red spectroscopy analysis of *Erythrina variegata* L. *J. Pharm. Sci. Res.* **2017**, *9*, 2062–2067.
54. Charles, E.; Lakshmi, P.K.; Selvaraj, M.; Vaidyanathan, S.; Srisudha, S.; Mary, M.B. Biomolecular transitions and lipid accumulation in green microalgae monitored by FTIR and Raman analysis. *Spectrochim. Acta Part A Mol. Biomol. Spectrosc.* **2019**, *224*, 117382. [CrossRef]

55. Trabelsi, L.; M'Sakni, N.H.; Ouada, H.B.; Bacha, H.; Roudesli, S. Partial characterization of extracellular polysaccharides produced by cyanobacterium *Arthrospira platensis*. *Biotechnol. Bioprocess Eng.* **2009**, *14*, 27–31. [CrossRef]
56. Kannan, R.; Arumugam, R.; Ramya, D.; Manivannan, D.K.; Anantharaman, P. Green synthesis of silver nanoparticles using marine macroalga *Chaetomorpha linum*. *Appl. Nanosci.* **2012**, *3*, 229–233. [CrossRef]
57. Butoi, B.; Groza, A.; Dinca, P.; Balan, A.; Barna, V. Morphological and Structural Analysis of Polyaniline and Poly(o-anisidine) Layers Generated in a DC Glow Discharge Plasma by Using an Oblique Angle Electrode Deposition Configuration. *Polymers* **2017**, *9*, 732. [CrossRef]
58. Zafar, S.; Zafar, A. Biosynthesis and Characterization of Silver Nanoparticles Using Phoenix dactylifera Fruits Extract and their In Vitro Antimicrobial and Cytotoxic Effects. *Open Biotechnol. J.* **2019**, *13*, 37–46. [CrossRef]
59. Yu, Y.; Zhou, Z.; Huang, G.; Cheng, H.; Han, L.; Zhao, S.; Chen, Y.; Meng, F. Purifying water with silver nanoparticles (AgNPs)-incorporated membranes: Recent advancements and critical challenges. *Water Res.* **2022**, *222*, 118901. [CrossRef] [PubMed]
60. Asrofi, M.; Abrial, H.; Kasim, A.; Pratoto, A.; Mahardika, M.; Hafizulhaq, F. Characterization of the sonicated yam bean starch bionanocomposites reinforced by nanocellulose water hyacinth fiber (WHF): The effect of various fiber loading. *J. Eng. Sci. Technol.* **2018**, *13*, 2700–2715.
61. Abrial, H.; Hartono, J. Moisture absorption of starch based biocomposites reinforced with water hyacinth fibers. *IOP Conf. Ser. Mater. Sci. Eng.* **2017**, *213*, 012035. [CrossRef]
62. Balakrishnan, P.; Sreekala, M.S.; Kunaver, M.; Huskić, M.; Thomas, S. Morphology, transport characteristics and viscoelastic polymer chain confinement in nanocomposites based on thermoplastic potato starch and cellulose nanofibers from pineapple leaf. *Carbohydr. Polym.* **2017**, *169*, 176–188. [CrossRef]
63. Maréchal, Y.; Chanzy, H. The hydrogen bond network in I $\beta$  cellulose as observed by infrared spectrometry. *J. Mol. Struct.* **2000**, *523*, 183–196. [CrossRef]
64. Lubis, M.; Harahap, M.; Ginting, M.H.S.; Sartika, M.; Azmi, H. Production of bioplastic from avocado seed starch reinforced with microcrystalline cellulose from sugar palm fibers. *J. Eng. Sci. Technol.* **2018**, *13*, 381–393.
65. Jutarat, P.; Sudarat, C.; Suwat, M.; Areeya, H. Effect of jute and kapok fibers on properties of thermoplastic cassava starch composites. *Mater. Des.* **2013**, *47*, 309–315. [CrossRef]
66. Kaewta, K.; Jariya, T. Studies on the structure and properties of thermoplastic starch/luffa fiber composites. *Mater. Des.* **2012**, *40*, 314–318. [CrossRef]
67. Fan, L.; Zhang, H.; Gao, M.; Zhang, M.; Liu, P.; Liu, X. Cellulose nanocrystals/silver nanoparticles: In-situ preparation and application in PVA films. *Holzforchung* **2020**, *74*, 523–528. [CrossRef]
68. Nasher, M.A.; Youssif, M.I.; El-Ghamaz, N.A.; Zeyada, H.M. Structural, optical and electrical studies of Toluidine Blue thin films prepared by thermal evaporation technique. *J. Lumin.* **2018**, *204*, 428–435. [CrossRef]
69. Davydov, A.S.; Dresner, S.B.; Knox, R.S. Theory of Molecular Excitons. *Phys. Today* **1972**, *25*, 55–57. [CrossRef]
70. Buruiana, L.; Avram, E.; Popa, A.; Musteata, V.; Ioan, S. Electrical conductivity and optical properties of a new quaternized polysulfone. *Polym. Bull.* **2012**, *68*, 1641–1661. [CrossRef]
71. Aziz, S.B.; Abdullah, O.; Saber, D.; Rasheed, M.; Ahmed, H. Investigation of Metallic Silver Nanoparticles through UV-Vis and Optical Micrograph Techniques. *Int. J. Electrochem. Sci.* **2017**, *12*, 363–373. [CrossRef]
72. Atta, A.; Abdel Reheem, A.; Abdeltwab, E. Ion Beam Irradiation Effects on Surface Morphology and Optical Properties of ZnO/PVA Composites. *Surf. Rev. Lett.* **2020**, *27*, 1950214. [CrossRef]
73. Atta, A.; Abdelhamied, M.; Abdel Reheem, A.; Berber, M. Flexible Methyl Cellulose/Polyaniline/Silver Composite Films with Enhanced Linear and Nonlinear Optical Properties. *Polymers* **2021**, *13*, 1225. [CrossRef]
74. Abdulwahid, R.; Abdullah, O.; Aziz, S.B.; Hussien, S.; Muhammadsharif, F.; Yahya, M.Y. The study of structural and optical properties of PVA:PbO<sub>2</sub> based solid polymer nanocomposites. *J. Mater. Sci. Mater. Electron.* **2016**, *27*, 12112–12118. [CrossRef]
75. Isac, D.J. Urbach and Bandgap Energy along with Optical Constants Analysis of nanocrystalline LZBCCO Ceramics. *IJournals Int. J. Soc. Relev. Concern (IJSRC)* **2015**, *3*, 1–11.
76. Khairy, Y.; Yahia, I.S.; Elhosiny Ali, H. Facile synthesis, structure analysis and optical performance of manganese oxide-doped PVA nanocomposite for optoelectronic and optical cut-off laser devices. *J. Mater. Sci. Mater. Electron.* **2020**, *31*, 8072–8085. [CrossRef]
77. Omed Gh, A.; Shujahadeen, B.A.; Mariwan, A.R. Structural and optical characterization of PVA:KMnO<sub>4</sub> based solid polymer electrolyte. *Results Phys.* **2016**, *6*, 1103–1108. [CrossRef]
78. Dejam, L.; Sabbaghzadeh, J.; Ghaderi, A.; Solaymani, S.; Matos, R.S.; Țălu, Ș.; da Fonseca Filho, H.D.; Sari, A.H.; Kiani, H.; Shayegan, A.H.S.; et al. Advanced nano-texture, optical bandgap, and Urbach energy analysis of NiO/Si heterojunctions. *Sci. Rep.* **2023**, *13*, 6518. [CrossRef]
79. Awad, S.; El-Gamal, S.; El Sayed, A.M.; Abdel-Hady, E.E. Characterization, optical, and nanoscale free volume properties of Na-CMC/PAM/CNT nanocomposites. *Polym. Adv. Technol.* **2020**, *31*, 114–125. [CrossRef]
80. Katerina Chryssou, M.S.a.E.L. A Study of the Optical Bandgap Energy and Urbach Energy Tail of Two White A4 Copy Paper Samples. *Ann. Chem. Sci. Res.* **2021**, *3*, 1–6. [CrossRef]
81. Abdul-Kader, A.M.; Turos, A.; Jagielski, J.; Nowicki, L.; Ratajczak, R.; Stonert, A.; AlMa'adeed, M. Hydrogen release in UHMWPE upon He-ion bombardment. *Vacuum* **2005**, *78*, 281–284. [CrossRef]



82. Kumar, R.; Ali, S.; Naqvi, A.; Virk, H.; De, U.; Avasthi, D.; Prasad, R. Study of optical band gap and carbon cluster sizes formed in 100 MeV Si<sup>8+</sup> and 145 MeV Ne<sup>6+</sup> ions irradiated polypropylene polymer. *Indian J. Phys.* **2009**, *83*, 969–976. [CrossRef]
83. Fink, D.; Müller, M.; Chadderton, L.T.; Cannington, P.H.; Elliman, R.G.; McDonald, D.C. Optically absorbing layers on ion beam modified polymers: A study of their evolution and properties. *Nucl. Instrum. Methods Phys. Res. Sect. B Beam Interact. Mater. At.* **1988**, *32*, 125–130. [CrossRef]

**Disclaimer/Publisher’s Note:** The statements, opinions and data contained in all publications are solely those of the individual author(s) and contributor(s) and not of MDPI and/or the editor(s). MDPI and/or the editor(s) disclaim responsibility for any injury to people or property resulting from any ideas, methods, instructions or products referred to in the content.



## Article

# Physico-Mechanical, Thermal, Morphological, and Aging Characteristics of Green Hybrid Composites Prepared from Wool-Sisal and Wool-Palf with Natural Rubber

Seiko Jose <sup>1,2</sup>, Puthenpurackal Shajimon Shanumon <sup>3</sup>, Annmi Paul <sup>3</sup>, Jessen Mathew <sup>3</sup> and Sabu Thomas <sup>1,3,\*</sup><sup>1</sup> School of Chemical Sciences, Mahatma Gandhi University, Kottayam 686560, Kerala, India<sup>2</sup> Textile Manufacturing and Textile Chemistry Division, ICAR-Central Sheep and Wool Research Institute, Avikanagar 304501, Rajasthan, India<sup>3</sup> School of Energy Materials, Mahatma Gandhi University, Kottayam 686560, Kerala, India

\* Correspondence: sabuthomas@mgu.ac.in

**Abstract:** In the reported study, two composites, namely sisal-wool hybrid composite (SWHC) and pineapple leaf fibre(PALF)-wool hybrid composite (PWHC) were prepared by mixing natural rubber with equal quantities of wool with sisal/PALF in a two-roll mixing mill. The mixture was subjected to curing at 150 °C inside a 2 mm thick mold, according to the curing time provided by the MDR. The physico-mechanical properties of the composite *viz.*, the tensile strength, elongation, modulus, areal density, relative density, and hardness were determined and compared in addition to the solvent diffusion and thermal degradation properties. The hybrid composite samples were subjected to accelerated aging, owing to temperature, UV radiation, and soil burial tests. The cross-sectional images of the composites were compared with a scanning electron microscopic analysis at different magnifications. A Fourier transform infrared spectroscopic analysis was conducted on the hybrid composite to determine the possible chemical interaction of the fibres with the natural rubber matrix.

**Keywords:** aging; coarse wool fibre; hybrid composites; natural rubber; PALF; sisal fibre

**Citation:** Jose, S.; Shanumon, P.S.; Paul, A.; Mathew, J.; Thomas, S. Physico-Mechanical, Thermal, Morphological, and Aging Characteristics of Green Hybrid Composites Prepared from Wool-Sisal and Wool-Palf with Natural Rubber. *Polymers* **2022**, *14*, 4882. <https://doi.org/10.3390/polym14224882>

Academic Editor: Raffaella Striani

Received: 20 October 2022

Accepted: 10 November 2022

Published: 12 November 2022



**Copyright:** © 2022 by the authors. Licensee MDPI, Basel, Switzerland. This article is an open access article distributed under the terms and conditions of the Creative Commons Attribution (CC BY) license (<https://creativecommons.org/licenses/by/4.0/>).

## 1. Introduction

Green composites are expected to be the next generation of sustainable composite materials, and both academia and industry are interested in them [1]. These materials are made from natural resources that are renewable, recyclable, and biodegradable. Green composites are typically made by combining natural resins with plant and animal fibres. Natural fibres are demonstrating that they are a more ecologically friendly, cost-effective, and a lighter alternative to synthetic fibres [2]. Bio-resins, which are derived from protein, starch, and vegetable oils, have been created as an alternative to petroleum-based polymers. Compared to synthetic fibres, natural plant-based fibres have a number of clear advantages, such as a reasonable price, good mechanical properties, thermal and acoustic insulation, and can degrade naturally. The short natural fibre reinforced rubber composites have been found to possess a good dimensional stability and high green strength [3].

Sisal is a commercially valuable fibre, extracted from *Agave sisalana* leaves. It is primarily utilized in the production of carpets, insulating panels, and maritime ropes and is commercially grown in Brazil, Tanzania, Kenya, and Madagascar. It has tremendous tensile strength and is quite robust. Many research attempts have been reported for the use of sisal fibre in composites [4]. Pineapple is one of the most popular fruits extensively grown in Costa Rica, the Philippines, Brazil, Thailand, China, and India. The pineapple leaf fibre (PALF) is extracted from the leftover leaves of the pineapple plant. Of all of the natural fibres derived from plant leaves, PALF has the largest proportion of cellulose content and the lowest microfibrillar angle, which results in an exceptionally good tensile strength. PALF is used for a variety of purposes, such as the creation of textiles [5], paper [6], and

composites [7]. Both PALF and sisal fibres are extracted by a mechanical extraction process known as decortication.

Wool is a protein fibre obtained from sheep. Based on the fibre fineness, it is categorized as fine, medium coarse and very coarse (kempy). The fine and medium coarse wool is employed in the apparel and carpet industries, respectively. The very coarse wool fibre has medullation, as result it is highly brittle and does not find applications in the above said industries. Currently, they are used in decentralized sectors, *viz.*, quilt industries, handmade felt, and so forth [8]. Few studies have been reported about the use of coarse wool in composites [9–11]. Natural rubber (NR) is one of the unavoidable polymers in the world. It is extracted as a resin from the *Hevea brasiliensis* tree and further dried into sheets or blocks. The plastic qualities of the natural rubber are transformed into elastic through vulcanization, ultimately resulting in the hardness and resilience of NR. The NR is a highly preferred matrix for the composite researchers.

Several recent studies have been reported, regarding the fabrication of PALF and sisal fibre reinforced natural rubber composite [12,13]. Sisal fibre is considered as an important reinforcement, due to the presence of excess cellulose components which make them less susceptible to moisture [14]. The physical and mechanical characteristics of the hybrid composites are determined by factors, such as type of fibre, aspect ratio, orientation, length, and interfacial adherence to the matrix [15].

The objective of our work is to give a value addition to the highly coarse wool, which has no other purpose at the moment. In our previous work, we employed coarse wool fibre as reinforcement in the rubber matrix and subsequently made few prototypes. However, we realized the need of improving the mechanical properties of the wool- NR composite, without compromising the “natural touch”. Thus, it is decided to mix coarse wool with appropriate plant fibre and to prepare the hybrid composites with better mechanical properties. As per the author’s knowledge, the hybrid composite of wool with other plant fibres in the natural rubber matrix, has never been reported. Hybrid composites are often prepared to conceal the flaws of one or more component fibres. Many research attempts have been reported on the hybrid composites of natural fibres [16,17]. In this study, two hybrid composites (wool + sisal + rubber) and (wool + PALF + rubber) were prepared by mixing equal quantities of wool with sisal/PALF in a rubber matrix. The morphological, thermal, physico-mechanical properties, and accelerated aging of these hybrid composites were analyzed and compared.

## 2. Materials and Methods

The natural rubber of grade ISNR-5 (Indian Standard Natural Rubber) was sourced from M/S Malankara Plantations, Thodupuzha, Kerala, India. The coarse wool fibre (Patawadi sheep breed) (bundle strength—13.67 g/tex, fibre diameter—44 microns), sisal fibre (bundle strength—30.9 g/tex, fineness—30 tex, density—1.45 g/cm<sup>3</sup>) was supplied by ICAR- Central Sheep and Wool Research Institute, Avikanagar, Rajasthan, India, and ICAR- Sisal Research Station, Odisha, India, respectively. The PALF was extracted from remnant pineapple leaves after cultivation, using a decorticator at Mahatma Gandhi University, Kottayam, Kerala, India. (bundle strength—38.5 g/tex, fineness—3.5 tex, density—1.43 g/cm<sup>3</sup>). The chemicals used in the rubber vulcanization *viz.*, sulphur (sp. gravity 2.05), zinc oxide (sp. gravity 5.55), stearic acid (sp. gravity 0.85), Wingstay L (antioxidant), and CBS (N-cyclohexylbenzothiazylsulphenamide), were purchased from Sameera Chemicals, Kottayam, Kerala, India.

### 2.1. Preparation of the SWHC and PWHC

The wool, sisal, and PALF fibre were chopped in to 1.5 cm length. The NR was adequately masticated in a two-roll mixing mill (300 × 500 cm) for two minutes. The masticated rubber, the vulcanizing agents, and the fibres were combined, as mentioned in Table 1. Just before adding sulphur, the wool fibre was added to the NR polymer matrix, along with the sisal fibre for the SWHC and with the PALF for the PWHC. Care was taken

to preserve the compound flow direction so that the majority of the fibres followed the same flow path. In order to ensure an equal distribution of the fibres in the polymer matrix, samples were milled for 10 min [18].

**Table 1.** List of rubber compounding ingredients [19,20].

Ingredients	SWHC (phr)	PWHC (phr)
Natural Rubber	100	100
Zinc Oxide	5.0	5.0
Stearic Acid	2.5	2.5
Wingstay L	1.0	1.0
CBS	1.5	1.5
Wool Fibre	50	50
Sisal Fibre	50	-
PALF	-	50
Sulphur	2.5	2.5

phr indicates parts per hundred of rubber.

Using a Moving Die Rheometer (Rheometer MDR 2000, Alpha Technology), the curing properties of the SWHC and the PWHC were studied, in accordance with the ASTM D5289 method at 150 °C. The composites were vulcanized at 150 °C inside a 2 mm thick mold, according to the curing time provided by the MDR at 100 bar pressure (5 min for curing for both composites (see  $t_{90}$  values in Table 2). Following the vulcanization, the hybrid composite samples were removed from the mold and cooled. The samples were pre-conditioned at 25 °C and 65% RH before further analysis. For each set of composites, five replicas were prepared. The cure rate index, which is a measurement of difference between  $t_{90}$  (optimum cure time) and  $ts_2$  (insipient scorch time), was calculated using the formula [21]

$$\text{Cure rate index} = 100 / (t_{90} - ts_2) \quad (1)$$

**Table 2.** Torque and cure time values of the SWHC and PWHC samples.

Sample Name	Maximum Torque (dNm)	Minimum Torque (dNm)	$t_{90}$ (min)	$ts_2$ (min)	Cure Rate Index ( $\text{min}^{-1}$ )
SWHC	38.36	0.76	5.12	2.29	35.34
PWHC	48.68	1.72	5.14	2.29	35.09

## 2.2. Analysis of the Physico-Mechanical Properties of the Composites

A universal testing machine (Tinius Olsen H50KT) was employed for the determination of the tensile and tear strength of the SWHC and PWHC. The samples were analyzed, in accordance with the ASTM D412 and ASTM D624 standards, respectively. Three samples were tested for each composite and the average result was calculated. The moisture content of the hybrid composites was determined, in accordance with ASTM D2495-07. The hardness of the SWHC and PWHC was assessed with the aid of a Shore-A hardness tester (Presto), following the ASTM D-2240 guidelines. The areal density of the composites was calculated, using the following formula.

$$\text{Areal density} = \frac{\text{Weight of the composite (g)}}{\text{Area of the composite (cm}^2\text{)}} \times 10000 \quad (2)$$

The relative density of the SWHC and PWHC in water was calculated according to ASTM D792, using the equation below.

$$\text{Relative density} = \left( \frac{\text{Weight in air}}{\text{Weight in air} - \text{Weight in water}} \right) \times \text{Density of water} \quad (3)$$

The SWHC and PWHC were analyzed for their solvent diffusion properties using water and toluene. Three replicas from each composite were cut in a round disc shape (2 cm diameter). Prior to dipping in the solvent, both specimens underwent preconditioning (25 °C and 65% RH) and were weighed. The hybrid composite samples were dipped in their respective solvents and removed from the solvents in predefined intervals. The specimens were gently hand pressed in between a blotting paper, to remove the surplus solvent and weighed. The procedure was repeated until a swelling equilibrium was reached [18]. The mole% solvent uptake of the composite samples was calculated using the Equation (4).  $Q_t$  represents the solvent's mole% uptake at a certain time  $t$ . Further, to investigate the diffusion properties of the SWHC and PWHC with water and toluene, a graph of  $Q_t$  vs.  $\sqrt{t}$  was generated.

$$Q_t = \left( \frac{(\text{Mass of solvent absorbed by the composite} / \text{Molar mass of the solvent})}{\text{Initial mass of the composite}} \right) \times 100 \quad (4)$$

The crosslink density, associated with the composites immersed in toluene is calculated using the following sets of equations below [18]

$$\mathbf{U} = 1/2Mc \quad (5)$$

$$Mc = - \frac{\rho_p V_s \phi^{1/3}}{\left( \ln [1 - \phi] + \phi + \chi \phi^2 \right)} \quad (6)$$

$$\phi = \frac{\frac{W_1}{\rho_p}}{\left( \frac{W_1}{\rho_p} \right) + \left( \frac{W_2}{\rho_s} \right)} \quad (7)$$

$$\chi = \beta + \frac{V_s}{RT} (\delta_p - \delta_s)^2 \quad (8)$$

The crosslinking density of the material is given by Equation (5). Equation (6) is used to compute the molar masses between the crosslinks, or " $Mc$ ". Equation (7) is used to compute " $\phi$ ", which is the volume fraction of rubber at the swelling equilibrium. " $\rho_p$ " stands for the polymer density, " $\rho_s$ " for the solvent density, and " $V_s$ " for the molar volume of each solvent. Equation (8) can be used to calculate " $\chi$ " which is the interaction parameter between the polymer and the solvent. Equation (6) would be used to derive " $Mc$ ", using the values of " $\phi$ " and " $\chi$ ", as determined by Equations (7) and (8), respectively. In Equation (4), " $\beta$ " " $\delta_s$ ", and " $\delta_p$ " stand in for the lattice constant (zero for polymers), the solubility parameter of the solvent, and the solubility parameter of the polymer, respectively. " $R$ " is the universal gas constant and " $T$ " is the temperature. For all testing, five replicas were made and the average value was taken.

### 2.3. FTIR, SEM, TGA, and the Aging Analysis of the Composites

With a Perkin Elmer Spectrum-2 spectrometer, the FT-IR spectra of the SWHC and PWHC were recorded across a range of 4000  $\text{cm}^{-1}$  to 400  $\text{cm}^{-1}$ , using the attenuated total reflection (ATR). The spectrum was obtained after 24 consecutive scans. The JEOL-JSM-6390 scanning electron microscope was used to examine the surface morphological properties of the hybrid composites. The samples were sputter coated with gold-palladium to prevent electron beams from having any charge effects during the examination. The images were captured at various magnifications at a 20 kV accelerating voltage. The

thermogravimetric analysis was carried out, using TA instruments (SDT Q600) in an inert atmosphere at temperatures ranging from 25 °C to 700 °C. The heating rate, 10 °C/min and a DTA sensitivity of 0.001 °C were maintained throughout the analysis. The composite samples were subjected to accelerated aging to temperature (ASTMD 573-04), UV, and biodegradation as per the standard methods reported in our previous studies [22].

### 3. Results and Discussion

#### 3.1. Cure Characteristics

Figure 1 shows the cure characteristics of the SWHC and PWHC. It is apparent from the figure that both composite mixtures followed almost the same pattern in the MDR curve. It can be clearly understood from the graph that the time required for the initiation of the crosslinking is nearly the same for the SWHC and PWHC. There is an initial decrease in torque that was noted in both the SWHC and PWHC, because of the softening of the rubber polymer matrix, when subjected to heat. When the crosslinking was initiated, with respect to time, the torque increased to a maximum, where the crosslinking was the highest and then showed a slight reduction, and then became almost constant. The corresponding torque and cure time values are shown in Table 2.

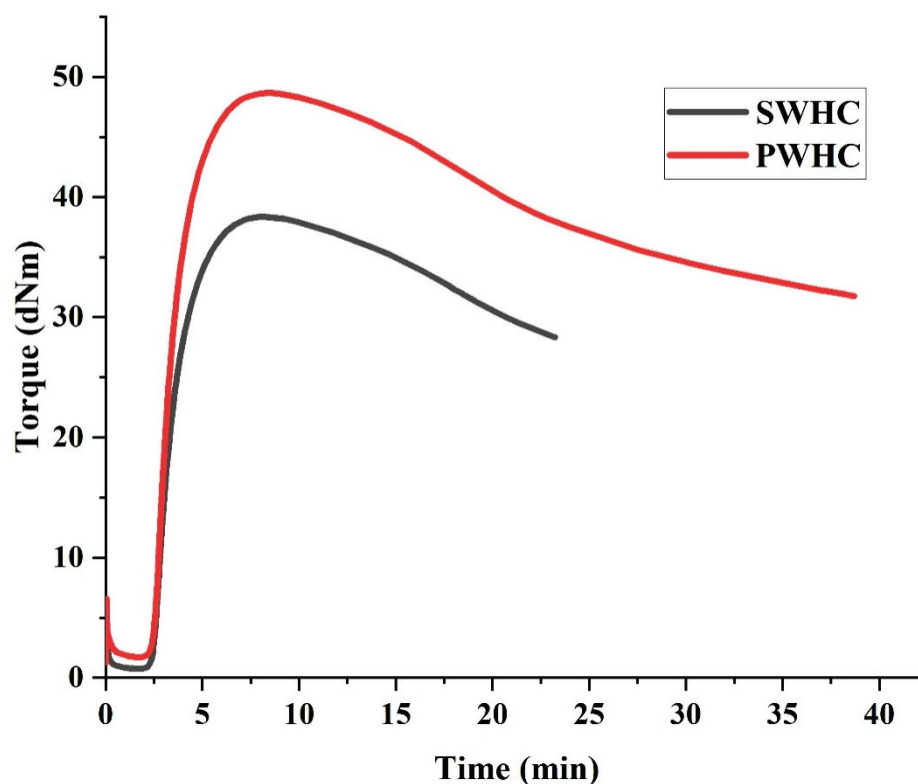


Figure 1. Cure characteristics of the SWHC and PWHC.

In fibre reinforced rubber composites, the maximum torque is an indication of the extent of the crosslinking and the stiffness, while the minimum torque indicates the fibre content present in it [23]. The maximum torque for the PWHC (48.68) is marginally higher than that for the SWHC (38.36). The value of  $t_{s2}$  (insipient scorch time) is same for both composites, which indicate that the vulcanization in both composites begins at the same time and the similar value of  $t_{90}$  shows that the vulcanization proceeds to a completion at the similar time, for the composites.

Regardless of the same values for  $t_{90}$  and  $t_{s2}$  in both the SWHC and PWHC, the maximum torque for the PWHC was found to be high. This indicates that the crosslinking associated with the vulcanization was increased by the addition of PALF in the wool-NR matrix, in comparison to the addition of the sisal fibre. The cure rate index is almost same



for both composites, which indicates that the rate of curing is almost the same for the SWHC and PWHC [24]. Since the rubber content is lower in the NR hybrid composite, the cure curve declined after reaching  $t_{90}$ . This might be due to the over curing of the composites. Similar observations have been reported elsewhere [25].

### 3.2. Tensile and Tear Properties

The stress–strain curve of the composite samples is depicted in Figure 2. The curves indicate that the PWHCs could withstand more stress in comparison with SWHC, meanwhile the latter possess a higher elongation. The corresponding tensile strength data is shown in the Table 3.

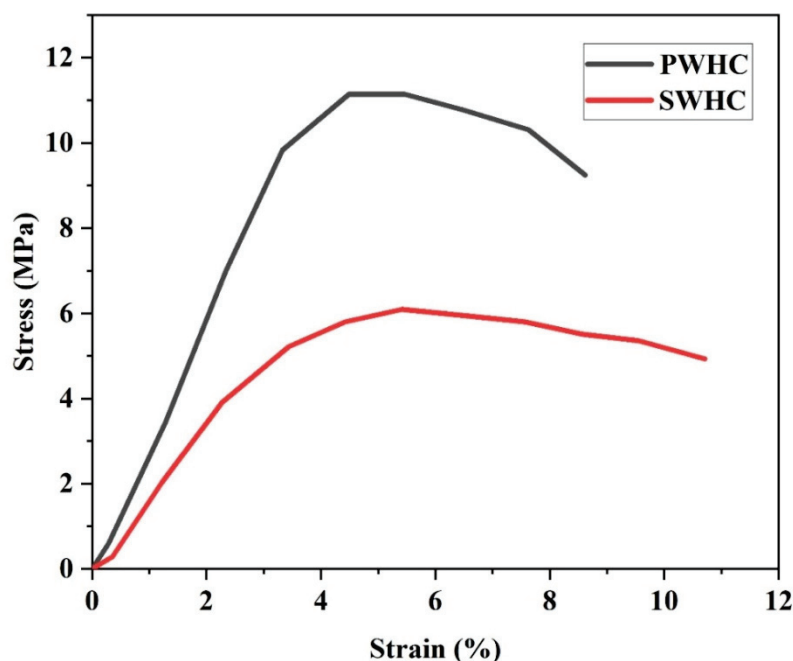


Figure 2. Stress–strain curve of the SWHC and PWHC.

Table 3. Tensile and tear properties of the SWHC and PWHC.

Sample	Tensile Strength at Break (MPa)	Elongation at Break (%)	Young’s Modulus (MPa)	Tear Strength (N/mm)
SWHC	6.09 (3.30)	5.42 (8.85)	169.3 (1.36)	45.9 (6.48)
PWHC	11.14 (7.08)	4.49 (3.1)	334 (3.00)	85.0 (6.18)

It is evident from Table 3 that the tensile strength for the PWHC (11.14 MPa) is almost double than that for the SWHC (6.09 MPa). The higher tensile strength of the PWHC, in comparison with the SWHC may be due to the following reasons. (i) The higher tensile strength of the PALF (38.5 g/tex) than sisal fibre (30.9 g/tex), (ii) the dense packing of the fibre, the lack of voids and a better interfacial adhesion of the PALF in the rubber matrix, as observed from the SEM images, (iii) the better transfer of stress between the NR and PALF, compared to that between the NR and sisal fibre, as indicated by the tear analysis (Table 3). Thus, Young’s modulus associated with the PWHC is higher than that of the SWHC. The lower value of Young’s modulus and the elongation (%) indicates that the PWHC has a much better resistance to elastic deformation, compared to the SWHC.

The tear strength of a polymer indicates the ability of the polymer to withstand tearing or cracking, when they are subjected to an external force. The tear strength of the PWHC (85.0 N/mm) is significantly higher than that for the SWHC (45.9 N/mm). This is because the transfer of stress in the PALF incorporated composite, is better than that in the sisal fibre incorporated composite. The lower tear strength is also an indication of a poor interaction between the fibre and the polymer matrix [26]. The SWHC possessed a higher elongation at break (5.42%) than the PWHC (4.49%).

### 3.3. Moisture Absorption and the Hardness Properties

In comparison with the synthetic fibre composites, the moisture content of the SWHC and the PWHC was found to be in a higher range (Table 4). The higher moisture content of the developed hybrid composites may be due to the high inclusion (100 phr) of hydrophilic natural fibres. In comparison with the SWHC, the PWHC has a marginally lower moisture content (5.90%), perhaps due to the fact that sisal fibres absorb more moisture than the PALF [27]. In the context of composites, the high moisture content of the natural fibre is a major concern to researchers. Sisal and PALF are lignocellulosic, and the presence of hemicelluloses causes a high moisture uptake. The presence of moisture in the natural fibre reinforced composites causes a weaker interaction between the fibres and the matrix [28].

**Table 4.** Moisture content and hardness of the PWHC and SWHC.

Sample	Moisture Content (%)	Hardness (Shore A)	Areal Density (g/m <sup>2</sup> )	Relative Density (g/cm <sup>3</sup> )
PWHC	5.90	91.56	2719.36	1.11
SWHC	6.57	91.30	2707.84	1.09

Rubber is a soft polymer. The inclusion of natural fibres, such as wool, sisal, and PALF, in large quantity significantly increase the hardness of the composites. A good network formation of a natural fibre inside of the soft rubber polymer matrix may be the reason behind it, as a result, the Shore A hardness increased. The hardness of the PWHC was 91.56 and that of the SWHC was 91.3. Though there exists a considerable difference in the mechanical properties, hardness (91), areal density (2700 g/m<sup>2</sup>), and relative densities (1.11 g/cm<sup>3</sup>) of both, the PWHC and SWHC were found to be almost the same. It can be seen from Table 4 that the relative density of both hybrid composites is almost same.

### 3.4. FTIR Analysis

Figure 3a displays the FTIR spectra of sisal, PALF, and wool fibre. The sharp peak for wool fibre, seen at 1640 cm<sup>-1</sup>, is due to the amide I group present in the wool protein, while the peak at 3272 cm<sup>-1</sup> denotes the amide N-H stretching vibration. The bending vibration of the C-N-H bond corresponds to the peaks at 1520 cm<sup>-1</sup> [29–31]. The FTIR spectra shows similar peaks for both the PALF and sisal, as they are lignocellulosic fibres. In case of the sisal fibre and PALF, the broad peak at 3332 cm<sup>-1</sup> corresponds to the -OH stretching vibrations from cellulose while the symmetric and asymmetric stretching of the CH<sub>2</sub> groups is indicated by the peak at 2886 cm<sup>-1</sup> [32]. The peaks at 1732 cm<sup>-1</sup> can be attributed to the stretching vibration of C=O groups in hemicellulose and the peaks in between 1627–1606 cm<sup>-1</sup>, indicate the aromatic C=C stretching vibrations in lignin [33,34]. It can also be observed that the intensity of the peak at 1606 cm<sup>-1</sup> is higher for the sisal fibre, compared to PALF, indicating that the lignin content is higher for the sisal. The C-O/C-C group stretching is indicated by the peaks at 1017 cm<sup>-1</sup> [35].

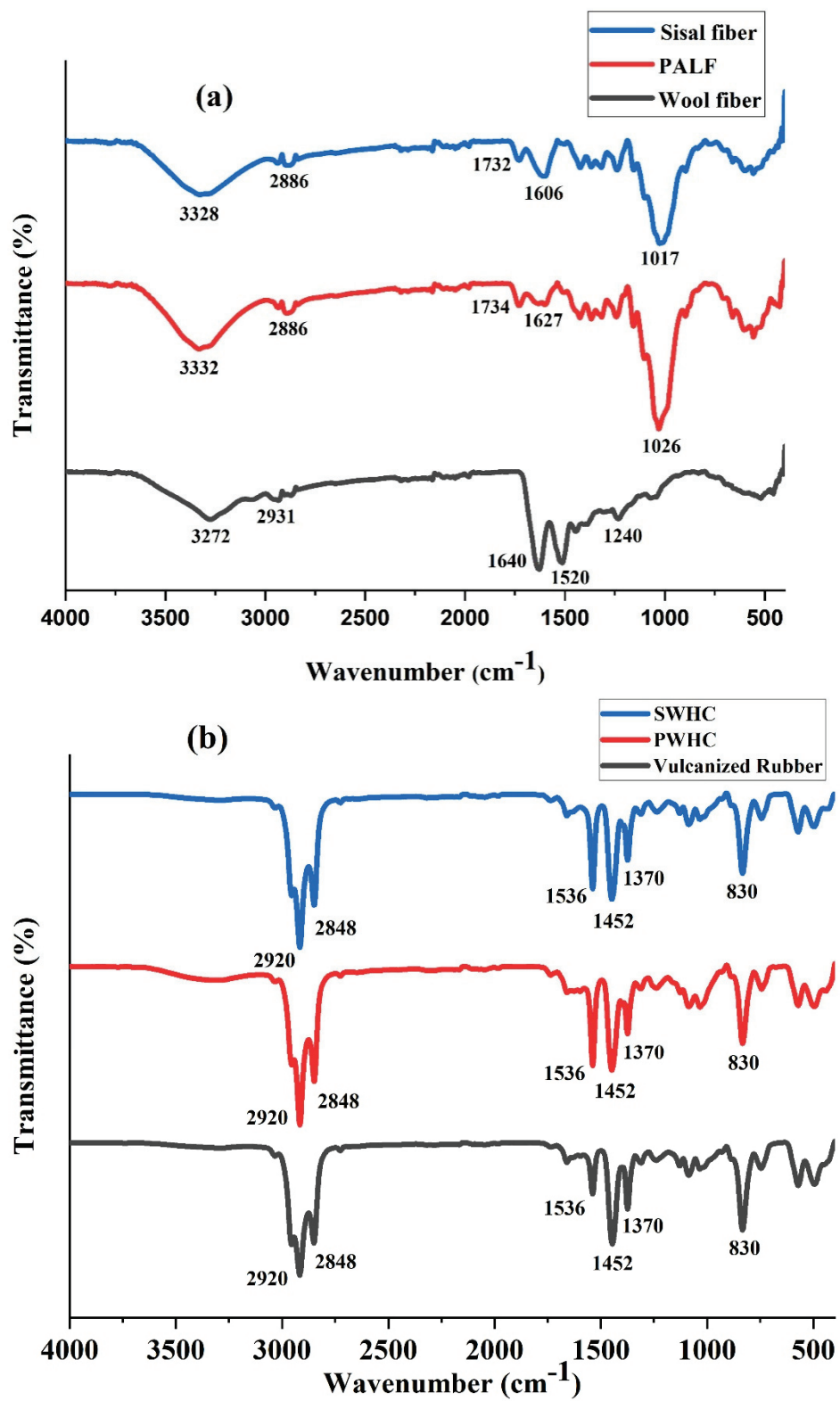


Figure 3. FTIR spectrum of (a) sisal fibre, PALF and wool fibre (b) vulcanized rubber, PWHC and SWHC.

It can be clearly observed, from the Figure 3b, that the SWHC, PWHC, and the vulcanized rubber shows almost the same peaks. The peaks observed at  $2920\text{ cm}^{-1}$  and  $2848\text{ cm}^{-1}$  indicate the symmetrical stretching of the  $-\text{CH}_3$  bonds and  $-\text{CH}_2-$  bonds, respectively. The characteristic in-plane bending of the amide II group in the wool protein is denoted by the peak at  $1536\text{ cm}^{-1}$ . The sharp peaks observed at  $1452\text{ cm}^{-1}$  and  $1370\text{ cm}^{-1}$  indicate the deformation of the  $-\text{CH}_3$  bonds, while the out of plane bending for the  $\text{C}=\text{C}-\text{H}$  group is shown by the peak at  $830\text{ cm}^{-1}$  [36]. All of these peaks are characteristic of the vulcanized rubber sample. It is observed from the spectra that the peaks corresponding to the wool, PALF, and sisal are not prominent and are masked by the natural rubber. No shifts in the peaks, even after the addition of the fibres, indicates that there is no chemical interaction between the fibres and the polymer matrix, leading to the conclusion that the interaction may be physical, involving van der Waals forces or hydrogen bonds.

### 3.5. SEM Analysis

Figure 4a–d shows the cross-sectional scanning electron microscopic images of the SWHC and Figure 4e–h shows that of the PWHC. It is visible from the images that in both the composites, a good network of fibres is present throughout the polymer matrix. It can also be seen from the images that the wool fibre (with scales) is distributed evenly with the sisal fibre (without scales) in the SWHC and with PALF (without scales) in the PWHC. Most of the fibres are in a uniform direction inside the rubber matrix. The absence of large voids in the composites indicates that the hybrid composites are properly prepared without the entrapment of air inside them. However; while comparing the SEM images (Figure 4d,h), which is of the cross sectional images of the SWHC and PWHC, respectively, it is found that the number of voids are comparatively higher in the SWHC than in the PWHC. This indicates a good adhesion between the PALF and NR matrix. The fibre pull-out is visible from the matrix in Figure 4b,f, and the images suggest that in the PWHC (Figure 4h), the voids formed at the root of the pulled-out fibres, are relatively small when compared to that in the SWHC. The higher interfacial adhesion between the natural fibres and the polymer matrix keeps the fibres intact with the matrix, which can also be the reason for the higher tensile strength, shown by the PWHC (11.14 MPa), compared to the SWHC (6.09 MPa) [37]. It has been reported that the formation of large voids is an indication of the poor interfacial adhesion between the fibres and the matrix [13]. It is inferred from the SEM analysis that the failure mechanism in these composites was the fibre pull-out, the fibre fracture, and the interfacial debonding.

Figure 5a shows the TG curve of the SWHC and PWHC. Due to the similarity in the chemical nature and composition, both composites followed almost the same pattern. As discussed regarding the physical properties of the composites, the composites have a moisture content of 6–7%. The minor weight loss at  $110\text{ }^\circ\text{C}$ , may be due to the removal of moisture from the composites. The TGA shows a major weight reduction between  $250\text{ }^\circ\text{C}$  and  $400\text{ }^\circ\text{C}$  and both composites showed a weight loss of 84.14%, until a constant weight was reached at a temperature of  $442.5\text{ }^\circ\text{C}$ .

The thermal degradation of the composites may be explained, based on the degradation of the individual components. In the case of the wool fibre, the thermal degradation takes place in three steps [38]. The first stage of the degradation takes place between  $100\text{ }^\circ\text{C}$  and  $135\text{ }^\circ\text{C}$  and is attributed to the loss of moisture content [39]. During the second step, a maximum weight loss occurred between  $218\text{ }^\circ\text{C}$  and  $390\text{ }^\circ\text{C}$ , due to the breakdown of the microfibril-matrix structure and the disulfide linkages [38]. In the third step, various peptide bonds present in the wool were broken at around  $390\text{--}500\text{ }^\circ\text{C}$ . Above  $500\text{ }^\circ\text{C}$ , the char oxidation reactions dominated [31,40].



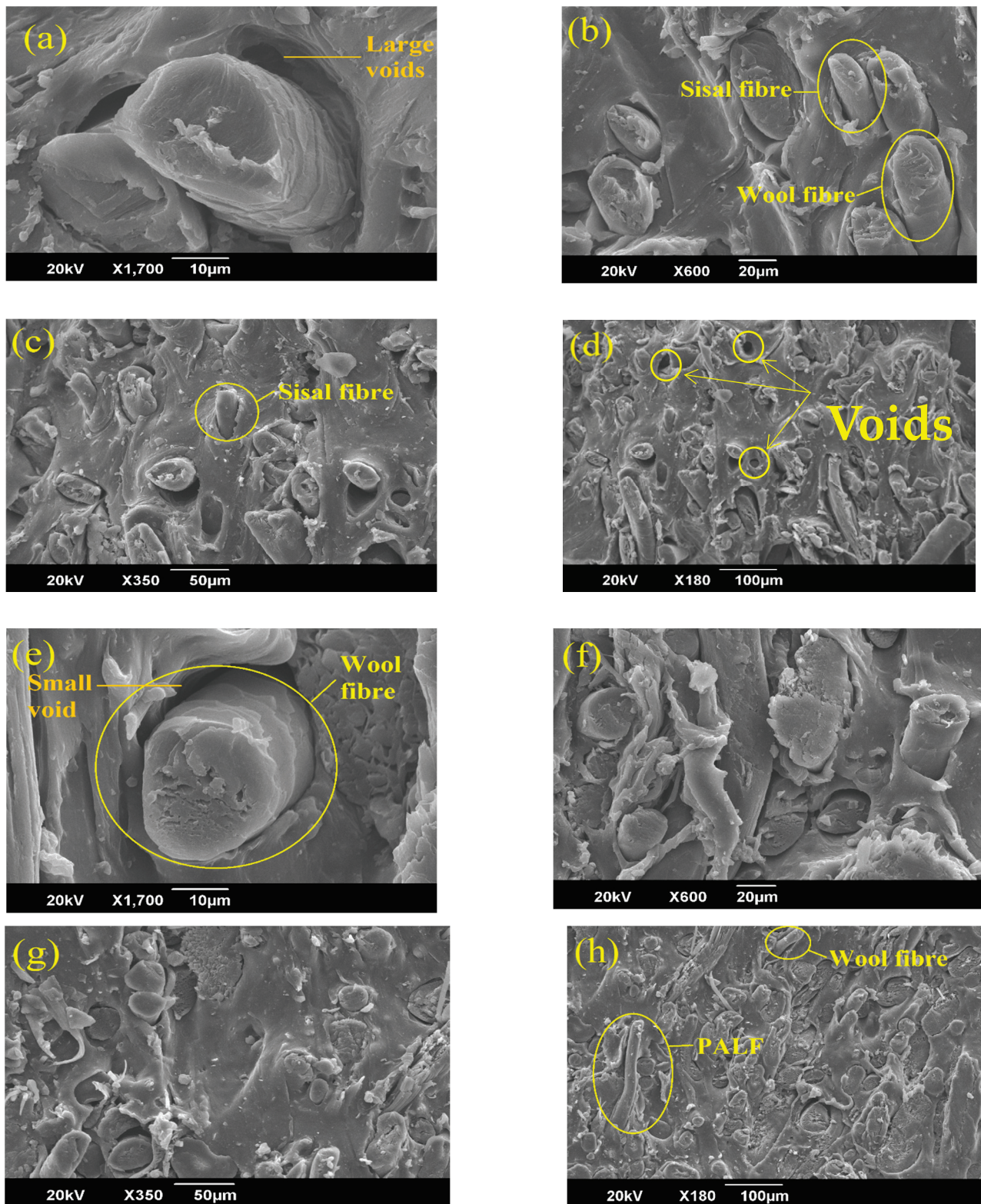


Figure 4. SEM images of the SWHC (a–d) and the PWHC (e–h) at various magnifications.

### 3.6. Thermogravimetric Analysis

Being lignocellulosic in nature, in both the sisal and PALF, after the removal of moisture at 110 °C, the second weight loss corresponds to hemicellulose’s degradation that starts at about 190 °C. Further, cellulose starts degrading from 290 °C up to 360 °C. The lignin degradation starts at about 280 °C and continues even above 500 °C [32]. For the vulcanized



rubber, the degradation begins at about 200 °C and is completed at about 475 °C, where the maximum weight loss is obtained at 358 °C, which may be attributed to the oxidation of the rubber [41]. It is also inferred from the data that the incorporation of wool, sisal, and PALF, slightly increases the thermal stability of the vulcanized rubber.

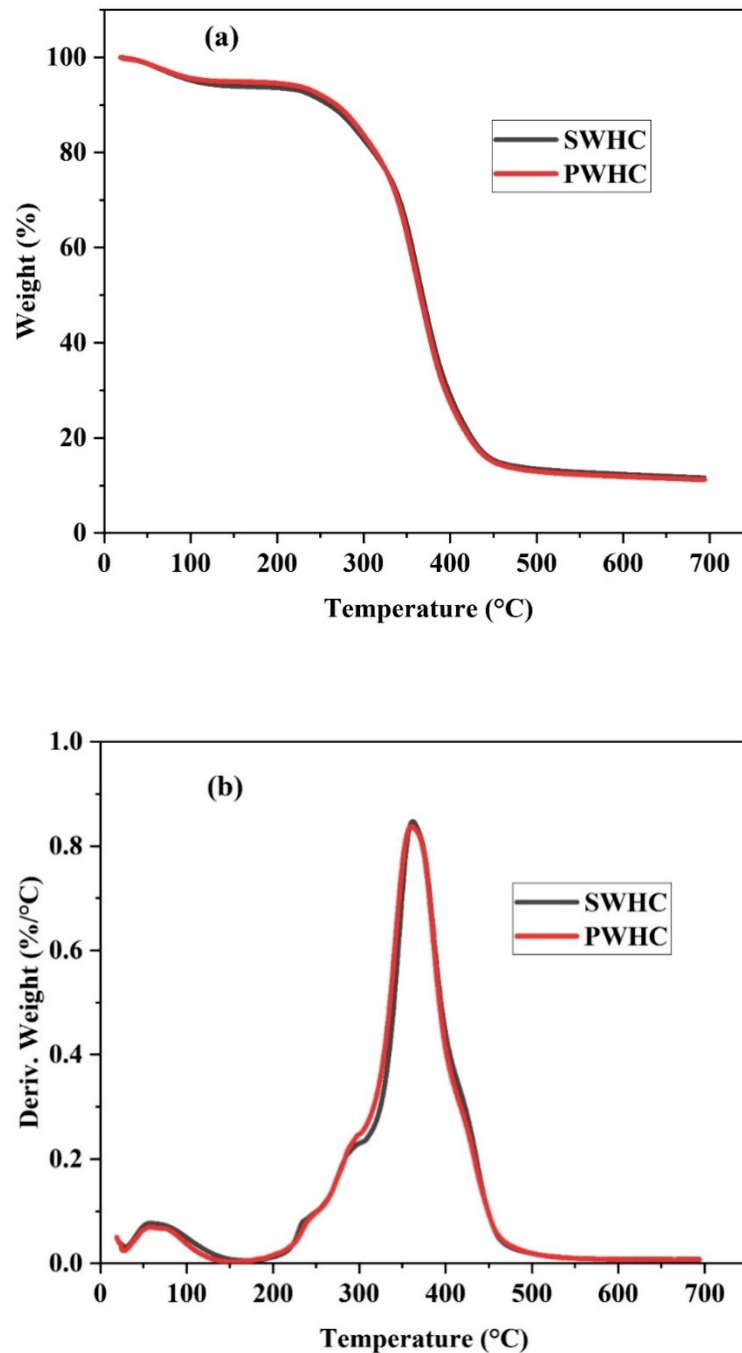


Figure 5. (a) TGA and (b) DTG curve of the SWHC and PWHC.

The degradation process has demonstrated one corresponding weight-loss peak in the DTG curves, as shown in Figure 5b, which corresponds to a single turn in the TG curves and was caused by thermal scissions of the C-C chain bonds in the natural rubber matrix [42]. The DTG curves show that at 361.67 °C, both composites show an equal rate of weight loss (0.8373%/°C), with respect to the temperature. The results indicate that the SWHC and PWHC possess a similar range of magnitude when considering their thermal

stability, which may be due to the fact that both sisal fibre and PALF are plant fibres that have almost similar chemical structure and properties.

### 3.7. Solvent Diffusion

The uptake of toluene and water by the SWHC and PWHC, via the diffusion, was analyzed and plotted between  $Q_t$  (mole% uptake of solvent) and  $\sqrt{t}$  (min). The process of diffusion is a parameter for the kinetics and is related to the nature of the polymer, the nature of the fillers added, its free volume, the extent of crosslinking, etc. [18]. It is apparent from Figure 6a that the rate of diffusion and the quantity of the toluene absorption is higher in the SWHC, in comparison with the PWHC. The low absorption and diffusion of toluene in the PWHC may be due to the dense packing of PALF inside the rubber matrix, which restrict the diffusion of the aromatic solvent [43]. This is also supported by the SEM images, which showed a higher packing density, a better adhesion, and less void contents in the PWHC than the SWHC. At the time of saturation, the SWHC showed a weight gain of 184.65%, while it was 95.85% for the PWHC.

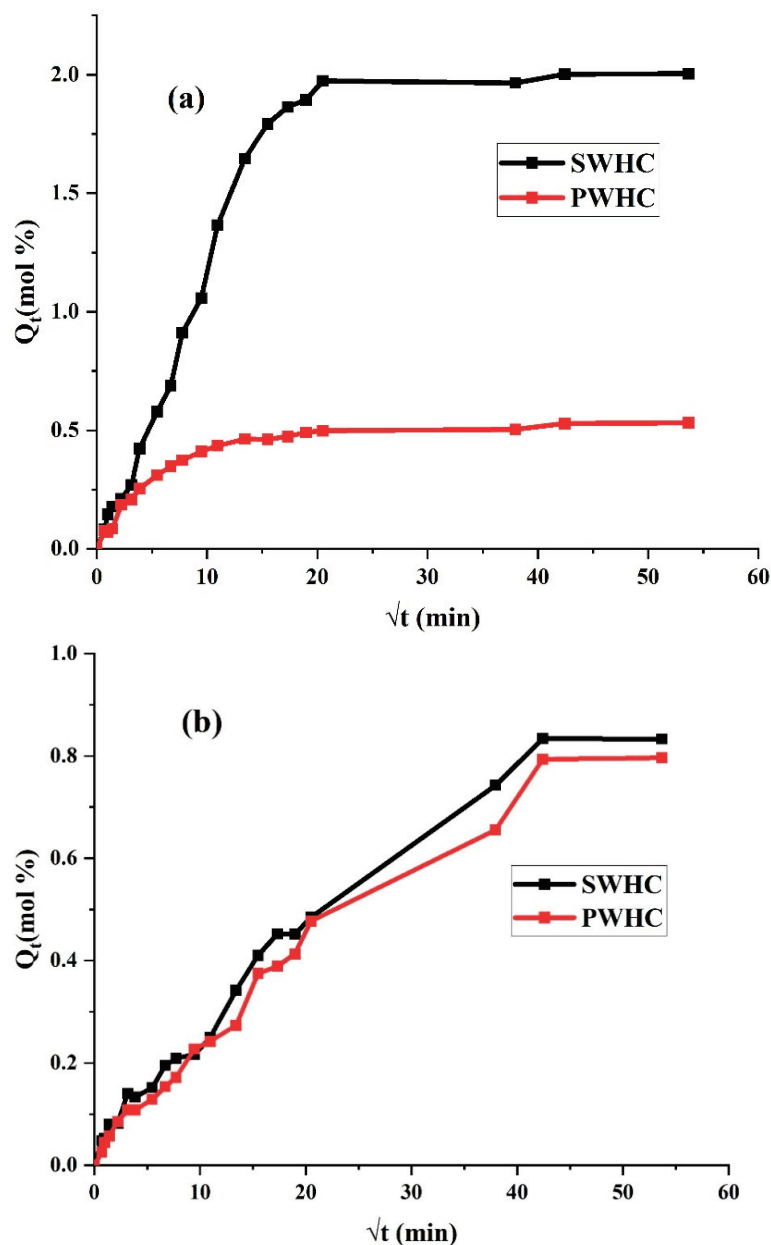


Figure 6. Diffusion curve of the SWHC and PWHC in (a) toluene (b) water.

Interestingly, it can be also seen from Figure 6b, that the mole% uptake of water does not show much difference for both the SWHC and PWHC, although the SWHC graph shows a marginally higher uptake of water. Both composites showed similar rates of diffusion up to the saturation. The water may enter the composite through the small cracks and pores and generates diffusion pathways. Both the sisal fibre and PALF are hygroscopic and allow the diffusion of water through them whilst, the matrix is hydrophobic. At the time of saturation, the SWHC gained 14.99% and the PWHC gained 14.39% weight, respectively. These high water absorption properties, though common in natural fibre-reinforced composites, are not in an appreciable quality for the composites.

It can also be observed from Table 5 that both composites possess a similar crosslink density. The crosslink density was defined as the density of chains or segments that connect two infinite sections of the polymer network [44]. The value of “ $M_c$ ”, which is the molar masses between the crosslinks, is so high that it can be considered as an indication of the greater crosslinking of the networks present in the composites [44].

**Table 5.** Crosslink density and  $M_c$  of the SWHC and PWHC.

Composite	$M_c$ (g/mol)	Crosslink Density (g·mol/cc)
SWHC	62,840.43	$7.96 \times 10^{-6}$
PWHC	65,247.92	$7.66 \times 10^{-6}$

### 3.8. Accelerated Thermal and UV Aging

The composites of the NR are susceptible to degradation by heat, UV radiation, ozone, humidity, etc. [45]. The PWHC and SWHC (Figure 7) were subjected to the accelerated thermal and UV degradation and the change in their mechanical properties were analyzed. In large chain macromolecules with complicated crosslinked structures, the application of heat, as well as radiation, can cause scissions, not only to the main chain, but also to the side chains which may lead to a loss of weight and the emission of gases with low molecular weights. As a result, the exposure to heat/radiation can cause changes to the chemical structure of the composites, such as the chain scission, crosslink formation, and breakage [46]. It can be observed from Figure 8 that there is a slight increase in the tensile strength and Young’s modulus after the thermal aging for both the SWHC and PWHC. This increase might be due to the formation of new crosslinks when the vulcanized NR is subjected to heating [47]. When exposed to prolonged UV radiation, the tensile strength increased for both the SWHC and PWHC, although there was a significant reduction in Young’s modulus of the material. The trend shown by the un-aged, thermal aged, and UV aged samples for both the PWHC and SWHC, was similar, such that there is an increase in their tensile strengths. In the case of their stress % (elongation at break %), the two composites showed a different trend, such as in the SWHC, the stress % demonstrates an increase after the UV aging, with respect to the un-aged samples, where the stress % for the PWHC remains stagnant. Similarly, Young’s modulus for both the PWHC and SWHC showed a similar trend, such as an increase in the modulus after thermal aging and a decrease in the modulus after UV aging.

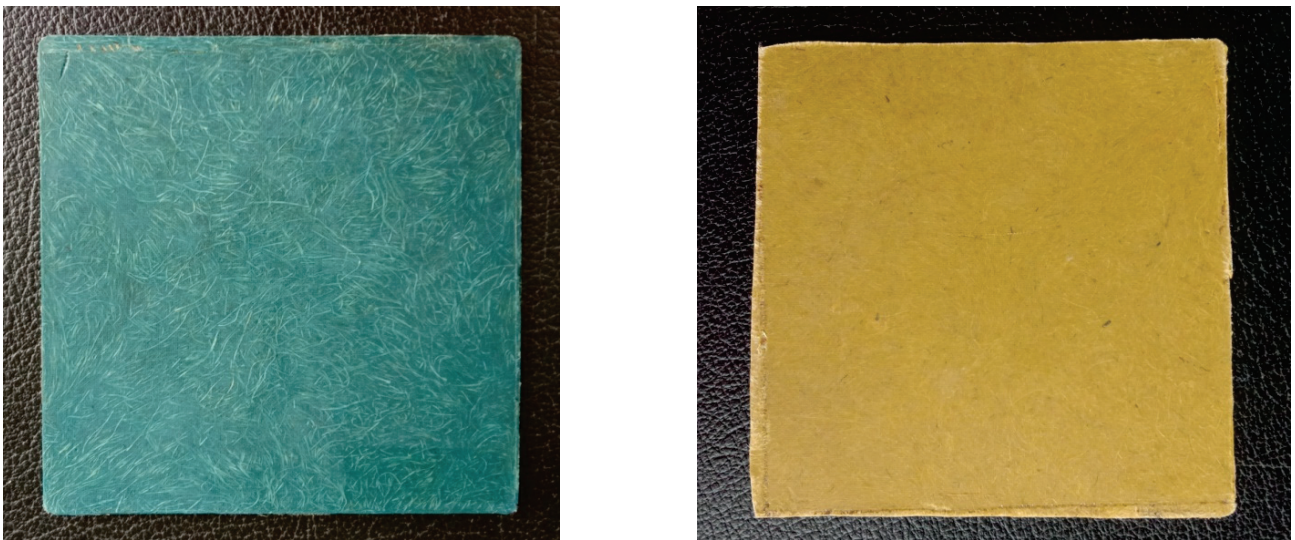


Figure 7. Images of the SWHC (green) and the PWHC (yellow). Note: Pigments were added during the composite preparation for identification.

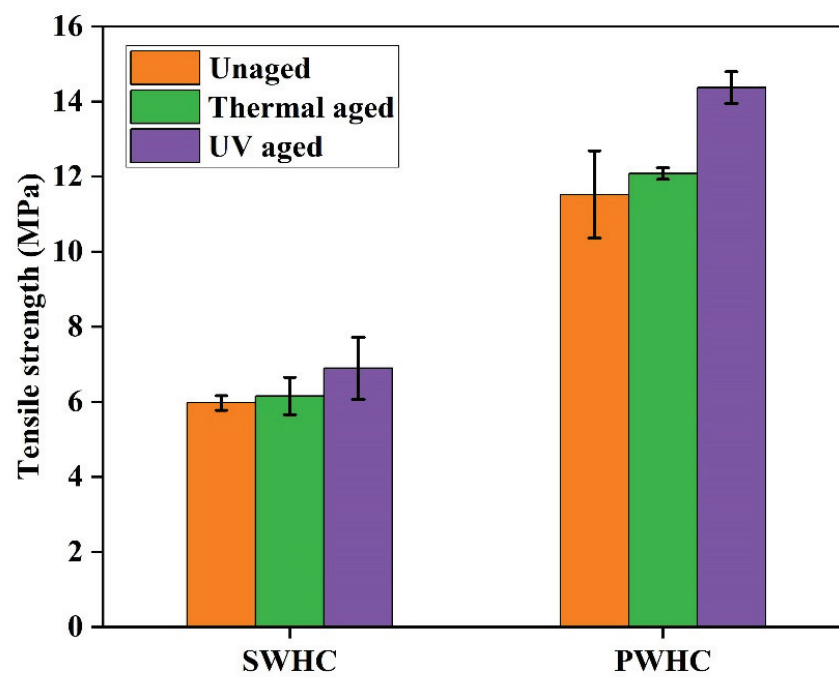


Figure 8. Cont.

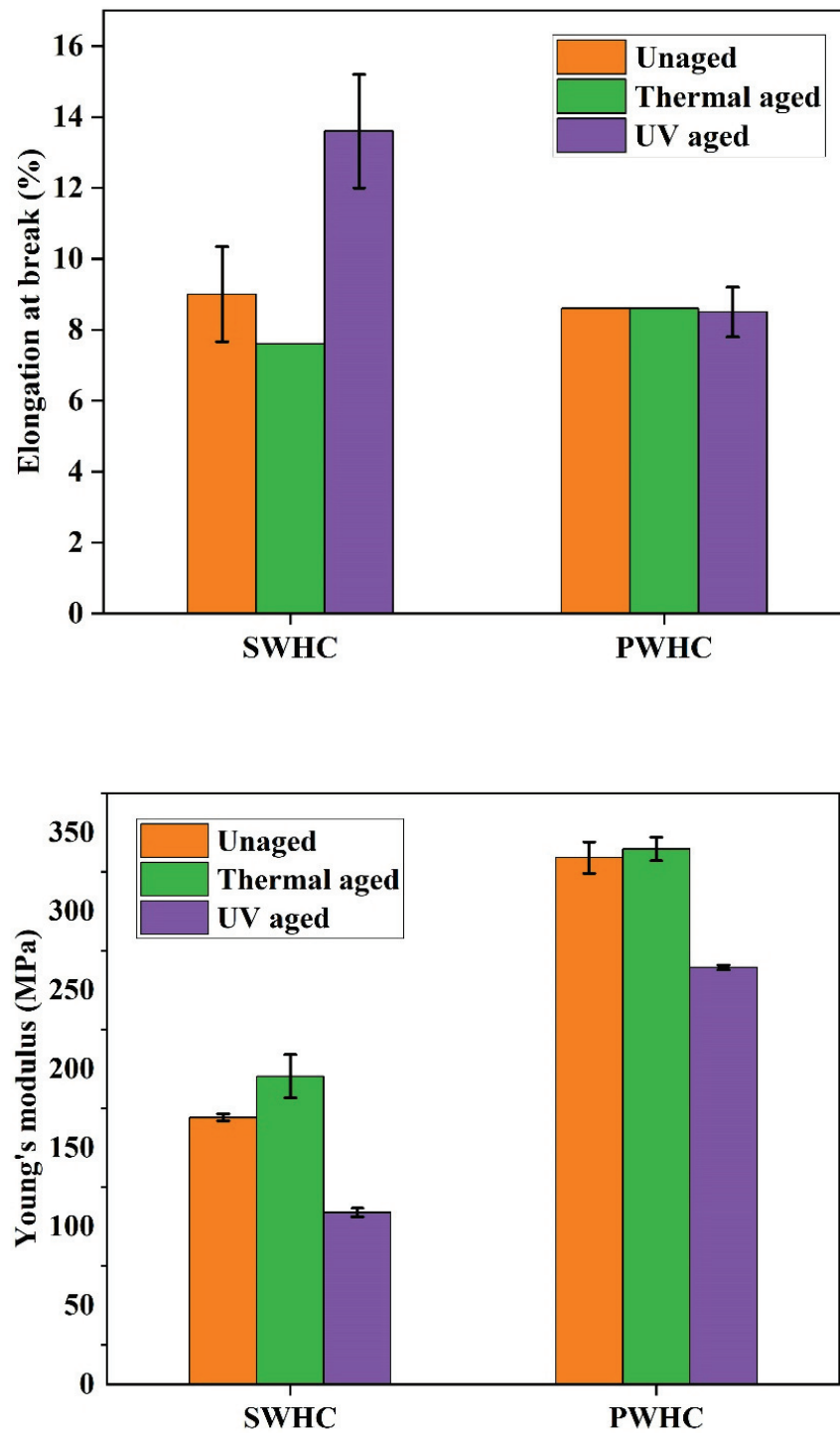


Figure 8. Mechanical properties of the SWHC and PWHC after the thermal and UV aging.

### 3.9. Biodegradation

Biodegradation is a process in which a compound decomposes due to the enzymes or chemicals secreted by bacteria or fungi present in soil. Both the SWHC and PWHC were subjected to accelerated biodegradation for 60 days through a soil burial test, as mentioned earlier. Once the stated period was over, the reduction in weight for the SWHC was found to be 2.43%, while it was 2.34% for the PWHC. It can be seen from Table 6 that both composites showed an almost equal loss of weight. It appears that the biological decomposition occurred at a very slow rate. This may be due to the following reason. (1) The vulcanized rubber, as it is poorly biodegradable, due to the presence of



high crosslinking. (2) Though wool, sisal, and PALF are natural fibres that degrade over time, the presence of lignin in the PALF and the sisal mask and protects the cellulose and hemicellulose from a rapid degradation by the microorganisms, due to the presence of the aromatic and crosslinked structure of the lignin [13]. (3) The extensive packing of fibres in the matrix can slow down the degradation process, since the tight network prevents the excessive growth of microorganisms [48]. Above all, these facts and the presence of high amounts of natural fibres in the developed composites resulted in an increase in the absorption of moisture which eventually led to the growth of microorganisms that caused the mass degradation of the composite.

**Table 6.** Weight reduction of the SWHC and PWHC after 60 days of soil burial test.

Sample	Weight Reduction (%)
SWHC	2.43 (0.38)
PWHC	2.34 (0.49)

Note: The values in the parenthesis indicate the standard deviation.

#### 4. Conclusions

Hybrid green composites, SWHC (sisal fibre + coarse wool fibre + NR) and PWHC (PALF + coarse wool fibre + NR) were fabricated and compared for their morphological, physical, mechanical, and aging properties. In comparison with the SWHC, the PWHC showed a higher tensile strength and modulus, a higher tear strength, a low moisture absorption and low mole% uptake (diffusion) of toluene and water. The PHWC showed a higher torque during the cure analysis. The results obtained from the FTIR spectra provided no valid evidence for any chemical interaction between the polymer matrix and the natural fibres in both the SWHC and PWHC. An analysis of the SEM images showed that the PWHC had a better packing of fibres, thereby an increased interfacial adhesion between the fibres and the polymer matrix. The thermal degradation characteristics remained as constant. Both the hybrid composites showed a slow pace of degradation while subjected to the soil burial test. It is concluded that the newly developed hybrid composites can be regarded as good substitutes for non-biodegradable composites and can be considered as potential material for packing and household applications.

**Author Contributions:** Conceptualization, S.J.; Methodology, J.M.; Validation, S.T.; Formal analysis, J.M., P.S.S., A.P. and S.J.; Investigation, S.J., J.M. and S.T.; writing, P.S.S., A.P. and S.J.; Original draft preparation, P.S.S. All authors have read and agreed to the published version of the manuscript.

**Funding:** This research received no external funding.

**Institutional Review Board Statement:** Not applicable.

**Informed Consent Statement:** Not applicable.

**Data Availability Statement:** Not applicable.

**Conflicts of Interest:** The authors declare no conflict of interest.

#### References

1. Shekar, H.S.S.; Ramachandra, M. Green Composites: A Review. *Mater. Today Proc.* **2018**, *5*, 2518–2526. [CrossRef]
2. Mitra, B.C. Environment Friendly Composite Materials: Biocomposites and Green Composites. *Def. Sci. J.* **2014**, *64*, 244–261. [CrossRef]
3. Nair, A.B.; Joseph, R. Eco-Friendly Bio-Composites Using Natural Rubber (NR) Matrices and Natural Fibre Reinforcements. *Chem. Manuf. Appl. Nat. Rubber* **2014**, 249–283. [CrossRef]
4. Li, Y.; Mai, Y.; Ye, L. Sisal Fibre and Its Composites: A Review of Recent Developments In Pa Us As Do Me Us Ex On As. *Compos. Sci. Technol.* **2000**, *60*, 2037–2055.
5. Jose, S.; Das, R.; Mustafa, I.; Karmakar, S.; Basu, G. Potentiality of Indian Pineapple Leaf Fibre for Apparels. *J. Nat. Fibres* **2019**, *16*, 536–544. [CrossRef]

6. Salleh, S.; Majid, R.A.; Yahya, W.J.; Abd Kadir, H.; Chan AF, E.; Munthoub, D.I.; Rusman, R. Composite Paper from an Agricultural Waste of Bagasse Sugarcane and Pineapple Leaf Fibre: A Novel Random and Multilayer Hybrid Fibre Reinforced Composite Paper. *Nord. Pulp Pap. Res. J.* **2021**, *36*, 475–490. [CrossRef]
7. Arib, R.M.N.; Sapuan, S.M.; Hamdan, M.A.M.M.; Paridah, M.T.; Zaman, H.M.D.K. A Literature Review of Pineapple Fibre Reinforced Polymer Composites. *Polym. Polym. Compos.* **2004**, *12*, 341–348. [CrossRef]
8. Kumar, A.; Prince, L.L.; Jose, S. *Sustainable Wool Production in India*; Elsevier Ltd.: Amsterdam, The Netherlands, 2017; ISBN 9780081020425.
9. Conzatti, L.; Giunco, F.; Stagnaro, P.; Patrucco, A.; Tonin, C.; Marano, C.; Rink, M.; Marsano, E. Wool Fibres Functionalised with a Silane-Based Coupling Agent for Reinforced Polypropylene Composites. *Compos. Part A Appl. Sci. Manuf.* **2014**, *61*, 51–59. [CrossRef]
10. Bharath, K.N.; Pasha, M.; Nizamuddin, B.A. Characterization of Natural Fibre (Sheep Wool)-Reinforced Polymer-Matrix Composites at Different Operating Conditions. *J. Ind. Text.* **2016**, *45*, 730–751. [CrossRef]
11. Kim, N.K.; Lin, R.J.T.; Bhattacharyya, D. Effects of Wool Fibres, Ammonium Polyphosphate and Polymer Viscosity on the Flammability and Mechanical Performance of PP/Wool Composites. *Polym. Degrad. Stab.* **2015**, *119*, 167–177. [CrossRef]
12. Sivasubramanian, P.; Mayandi, K.; Santulli, C.; Alavudeen, A.; Rajini, N. Effect of Fibre Length on Curing and Mechanical Behavior of Pineapple Leaf Fibre (PALF) Reinforced Natural Rubber Composites. *J. Nat. Fibres* **2020**, *19*, 4326–4337. [CrossRef]
13. Abdel-Hakim, A.; El-Wakil, A.E.A.A.; El-Mogy, S.; Halim, S. Effect of Fibre Coating on the Mechanical Performance, Water Absorption and Biodegradability of Sisal Fibre/Natural Rubber Composite. *Polym. Int.* **2021**, *70*, 1356–1366. [CrossRef]
14. Senthilkumar, K.; Saba, N.; Rajini, N.; Chandrasekar, M.; Jawaid, M.; Siengchin, S.; Alotman, O.Y. Mechanical Properties Evaluation of Sisal Fibre Reinforced Polymer Composites: A Review. *Constr. Build. Mater.* **2018**, *174*, 713–729. [CrossRef]
15. Jawaid, M.; Abdul Khalil, H.P.S. Cellulosic/Synthetic Fibre Reinforced Polymer Hybrid Composites: A Review. *Carbohydr. Polym.* **2011**, *86*, 1–18. [CrossRef]
16. Siakeng, R.; Jawaid, M.; Asim, M.; Saba, N.; Sanjay, M.R.; Siengchin, S.; Fouad, H. Alkali Treated Coir/Pineapple Leaf Fibres Reinforced Pla Hybrid Composites: Evaluation of Mechanical, Morphological, Thermal and Physical Properties. *Express Polym. Lett.* **2020**, *14*, 717–730. [CrossRef]
17. Veerasimman, A.; Shanmugam, V.; Rajendran, S.; Johnson, D.J.; Subbiah, A.; Koilpichai, J.; Marimuthu, U. Thermal Properties of Natural Fibre Sisal Based Hybrid Composites—A Brief Review. *J. Nat. Fibres* **2021**, *19*, 4696–4706. [CrossRef]
18. Kaliyathan, A.V.; Rane, A.V.; Jackson, S.; Thomas, S. Analysis of Diffusion Characteristics for Aromatic Solvents through Carbon Black Filled Natural Rubber/ Butadiene Rubber Blends. *Polym. Compos.* **2021**, *42*, 375–396. [CrossRef]
19. Yakubu, M.K.; Gumel, M.S.; Umar, A.; Metelerkamp, R. Physico-Mechanical Effects of Surface-Modified Sorgum Stalk Powder on Reinforced Rubber. *J. Reinf. Plast. Compos.* **2010**, *29*, 2855–2868. [CrossRef]
20. Palanisamy, S.; Mayandi, K.; Palaniappan, M.; Alavudeen, A. Mechanical Properties of Phormium Tenax Reinforced Natural. *Fibers* **2021**, *9*, 11.
21. Surya, I.; Khosman, H. The Compounds of Montmorillonite-Filled Natural Rubber: Cure Rate Index, Swelling and Hardness Properties. *AIP Conf. Proc.* **2020**, *2237*, 020076. [CrossRef]
22. Jose, S.; Thomas, S.; Jibin, K.P.; Sisanth, K.S.; Kadam, V.; Shakyawar, D.B. Surface Modification of Wool Fabric Using Sodium Lignosulfonate and Subsequent Improvement in the Interfacial Adhesion of Natural Rubber Latex in the Wool/Rubber Composites. *Ind. Crops Prod.* **2022**, *177*, 114489. [CrossRef]
23. John, M.J.; Varughese, K.T.; Thomas, S. Green Composites from Natural Fibres and Natural Rubber: Effect of Fibre Ratio on Mechanical and Swelling Characteristics. *J. Nat. Fibres* **2008**, *5*, 47–60. [CrossRef]
24. Surya, I.; Sukeksi, L.; Hayeemasae, N. Studies on Cure Index, Swelling Behaviour, Tensile and Thermooxidative Properties of Natural Rubber Compounds in the Presence of Alkanolamide. *IOP Conf. Ser. Mater. Sci. Eng.* **2018**, *309*, 012060. [CrossRef]
25. Setyadewi, N.M.; Indrajati, I.N.; Darmawan, N. Mechanical Properties and Curing Characteristics of Shape Memory Natural Rubber. *IOP Conf. Ser. Mater. Sci. Eng.* **2019**, *541*, 012012.
26. Ismail, H.; Edyham, M.R.; Wirjosentono, B. Bamboo Fibre Filled Natural Rubber Composites: The Effects of Filler Loading and Bonding Agent. *Polym. Test.* **2002**, *21*, 139–144. [CrossRef]
27. Aguele, F.O.; Madufor, C.I.; Adekunle, K.F. Comparative Study of Physical Properties of Polymer Composites Reinforced with Uncarbonised and Carbonised Coir. *Open J. Polym. Chem.* **2014**, *4*, 73–82. [CrossRef]
28. Ouarhim, W.; Essabir, H.; Bensalah, M.O.; Rodrigue, D.; Bouhfid, R.; Qaiss, A. el kacem Hybrid Composites and Intra-Ply Hybrid Composites Based on Jute and Glass Fibres: A Comparative Study on Moisture Absorption and Mechanical Properties. *Mater. Today Commun.* **2020**, *22*, 100861. [CrossRef]
29. Rani, S.; Kadam, V.; Rose, N.M.; Jose, S.; Yadav, S.; Shakyawar, D.B. Wheat Starch, Gum Arabic and Chitosan Biopolymer Treatment of Wool Fabric for Improved Shrink Resistance Finishing. *Int. J. Biol. Macromol.* **2020**, *163*, 1044–1052. [CrossRef]
30. Rani, S.; Kadam, V.; Rose, N.M.; Jose, S.; Shakyawar, D.B.; Yadav, S. Effect of Enzyme Treatment on Wool Fabric Properties and Dimensional Stability. *Indian J. Fibre Text. Res.* **2021**, *46*, 83–90. [CrossRef]
31. Jose, S.; Shanmugam, N.; Das, S.; Kumar, A.; Pandit, P. Coating of Lightweight Wool Fabric with Nano Clay for Fire Retardancy. *J. Text. Inst.* **2019**, *110*, 764–770. [CrossRef]
32. Basu, G.; Mishra, L.; Jose, S.; Samanta, A.K. Accelerated Retting Cum Softening of Coconut Fibre. *Ind. Crops Prod.* **2015**, *77*, 66–73. [CrossRef]

33. Hazarika, D.; Gogoi, N.; Jose, S.; Das, R.; Basu, G. Exploration of Future Prospects of Indian Pineapple Leaf, an Agro Waste for Textile Application. *J. Clean. Prod.* **2017**, *141*, 580–586. [CrossRef]
34. Singh, G.; Jose, S.; Kaur, D.; Soun, B. Extraction and Characterization of Corn Leaf Fibre. *J. Nat. Fibres* **2022**, *19*, 1581–1591. [CrossRef]
35. Zhou, F.; Cheng, G.; Jiang, B. Effect of Silane Treatment on Microstructure of Sisal Fibres. *Appl. Surf. Sci.* **2014**, *292*, 806–812. [CrossRef]
36. Mohan, S. Vibrational Spectra of Cis-1, 4-Polyisoprene. *Arab. J. Sci. Eng.* **2015**, *29*, 17–26.
37. Hu, C.; Zhou, Y.; Zhang, T.; Jiang, T.; Zeng, G. Effect of Fibre Modified by Alkali/Polyvinyl Alcohol Coating Treatment on Properties of Sisal Fibre Plastic Composites. *J. Reinf. Plast. Compos.* **2020**, *39*, 880–889. [CrossRef]
38. Ahmed, A.; Qayoum, A. Investigation on the Thermal Degradation, Moisture Absorption Characteristics and Antibacterial Behavior of Natural Insulation Materials. *Mater. Renew. Sustain. Energy* **2021**, *10*, 4. [CrossRef]
39. Forouharshad, M.; Montazer, M.; Moghadam, M.B.; Saligheh, O. Flame Retardant Wool Using Zirconium Oxychloride in Various Acidic Media Optimized by RSM. *Thermochim. Acta* **2011**, *516*, 29–34. [CrossRef]
40. Davies, P.J.; Horrocks, A.R.; Mirafab, M. Scanning Electron Microscopic Studies of Wool/Intumescent Char Formation. *Polym. Int.* **2000**, *49*, 1125–1132. [CrossRef]
41. Sircar, A.K.; Lamond, T.G. Identification of Elastomer Blends by Thermal Analysis. *Thermochim. Acta* **1973**, *7*, 287–292.
42. Li, S.D.; Peng, Z.; Kong, L.X.; Zhong, J.P. Thermal Degradation Kinetics and Morphology of Natural Rubber/Silica Nanocomposites. *J. Nanosci. Nanotechnol.* **2006**, *6*, 541–546. [CrossRef]
43. Obasi, H.C.; Arukalam, I.O.; Nwanonenyi, S.C.; Eze, I.O.; Chiemenem, L.I.; Nwosu-Obieogu, K.; Opara, H. Mechanical and Transport Properties of Natural Rubber Reinforced with Piassava (*Raphia Hookeri*) Fibre Composites. *J. Mater. Environ. Sci.* **2019**, *10*, 119–131.
44. Wool, R.P. Properties of Triglyceride-Based Thermosets. *Bio-Based Polym. Compos.* **2005**, 202–255. [CrossRef]
45. Vinod, V.S.; Varghese, S.; Kuriakose, B. Degradation Behaviour of Natural Rubber-Aluminium Powder Composites: Effect of Heat, Ozone and High Energy Radiation. *Polym. Degrad. Stab.* **2002**, *75*, 405–412. [CrossRef]
46. Gull, N.; Khan, S.M.; Islam, A.; Butt, M.T.Z.; Jamil, T. *Modification of Polyaniline*; Elsevier: Amsterdam, The Netherlands, 2018; ISBN 9780128095515.
47. Choi, S.S. Influence of Rubber Composition on Change of Crosslink Density of Rubber Vulcanizates with EV Cure System by Thermal Aging. *J. Appl. Polym. Sci.* **2000**, *75*, 1378–1384. [CrossRef]
48. Ji, M.; Li, F.; Li, J.; Li, J.; Zhang, C.; Sun, K.; Guo, Z. Enhanced Mechanical Properties, Water Resistance, Thermal Stability, and Biodegradation of the Starch-Sisal Fibre Composites with Various Fillers. *Mater. Des.* **2021**, *198*, 109373. [CrossRef]

## Article

# PLA-Based Hybrid Biocomposites: Effects of Fiber Type, Fiber Content, and Annealing on Thermal and Mechanical Properties

Supitcha Yaisun <sup>1,2</sup> and Tatiya Trongsatitkul <sup>1,2,3,\*</sup>

<sup>1</sup> School of Polymer Engineering, Institute of Engineering, Suranaree University of Technology, Nakhon Ratchasima 30000, Thailand; supitcha\_yaisun@hotmail.com

<sup>2</sup> Center for Excellence on Petrochemical and Materials Technology, Chulalongkorn University, Bangkok 10330, Thailand

<sup>3</sup> Research Center for Biocomposite Materials for Medical Industry and Agricultural and Food Industry, Suranaree University of Technology, Nakhon Ratchasima 30000, Thailand

\* Correspondence: tatiya@sut.ac.th

**Abstract:** In this study, we utilized a hybridization approach for two different fibers to overcome the drawbacks of single-fiber-reinforced PLA composites. Coir fiber and bamboo leaf fiber were used as reinforcing natural fibers as their properties complement one another. Additionally, we combined thermal annealing with hybridization techniques to further improve the overall properties of the composites. The results showed that the hybridization of BF: CF with a ratio of 1:2 gave PLA-based hybrid composites optimal mechanical and thermal properties. Furthermore, the improvement in the thermal stability of hybrid composites, attributable to an increase in crystallinity, was a result of thermal annealing. The improvement in HDT in annealed 1BF:2CF hybrid composite was about 13.76% higher than that of the neat PLA. Annealing of the composites led to increased crystallinity, which was confirmed using differential scanning calorimetry (DSC). The synergistic effect of hybridization and annealing, leading to the improvement in the thermal properties, opened up the possibilities for the use of PLA-based composites. In this study, we demonstrated that a combined technique can be utilized as a strategy for improving the properties of 100% biocomposites and help overcome some limitations of the use of PLA in many applications.

**Keywords:** polylactic acid; coir fiber; bamboo leaf fiber; hybrid composites; annealing; biocomposite

**Citation:** Yaisun, S.; Trongsatitkul, T. PLA-Based Hybrid Biocomposites: Effects of Fiber Type, Fiber Content, and Annealing on Thermal and Mechanical Properties. *Polymers* **2023**, *15*, 4106. <https://doi.org/10.3390/polym15204106>

Academic Editor: Raffaella Striani

Received: 30 June 2023

Revised: 7 October 2023

Accepted: 9 October 2023

Published: 16 October 2023



**Copyright:** © 2023 by the authors. Licensee MDPI, Basel, Switzerland. This article is an open access article distributed under the terms and conditions of the Creative Commons Attribution (CC BY) license (<https://creativecommons.org/licenses/by/4.0/>).

## 1. Introduction

Biopolymers are presently viewed as promising substitutes for traditional petroleum-based polymers, as the latter have contributed to environmental issues related to pollution, greenhouse gas emissions, and the depletion of fossil fuel reserves. Growing environmental awareness and sustainability concerns among consumers have driven industries to search for alternative, more environmentally friendly materials [1]. Polylactic acid or PLA stands out as one of the extensively studied and commonly used biopolymers, garnering significant interest for traditional uses like packaging materials, fiber production, and more recently, in composite materials for diverse practical and mechanical applications. PLA occupies a central role in the eco-friendly polymer market and emerges as a highly promising choice for future advancements [2–4]. However, the use of PLA has been limited by its thermal properties. It has a low heat-softening temperature and low thermal stability as compared with petroleum-based polymers polyethylene (HDPE), polypropylene (PP), and polystyrene (PS).

To overcome these limitations while maintaining a status of being 100% biodegradable, natural fibers used as reinforcement in PLA-based biocomposites have been investigated to improve PLA performance [5]. An increasing tendency has been observed in favor of incorporating natural fibers as a reinforcement in polymer composites. This inclination is driven by their adaptability during processing, well-defined strength characteristics,



ready availability, biodegradable nature, cost-effectiveness (in terms of volume), and environmentally friendly attributes. Polymer composites incorporating natural fibers present numerous notable benefits compared with traditional synthetic alternatives, including their biodegradability, environmentally friendly characteristics, affordability, ready availability, low weight, and more. These natural fiber-reinforced polymer composites are receiving increasing recognition and wider acceptance across various applications, such as food packaging, interiors of automobiles, railway coaches, and airplanes, as well as storage solutions and construction.

Recently, coir fibers (CFs) have stood out as excellent choices due to the fruit's remarkable versatility, serving a purpose as a food and contributing to the production of a diverse array of industrial products. The extensive cultivation of coir crops results in substantial biomass accumulation, often leading to its disposal in landfills or inappropriate sites, giving rise to significant social and environmental challenges. On the other hand, coir fiber-reinforced polylactic acid (PLA) biocomposites have gained substantial research attention for their use in various applications [6–10]. Coir fibers possess low cellulose (36–43%) and hemicellulose (0.2%), a high lignin content (41–45%), and a high microfibrillar angle (30–45°, which results in their relatively low tensile strength and modulus as well as the highest elongation at the break among other typical natural fibers [11–13], as shown in Table 1. Because coir fibers possess a significant amount of lignin, they exhibit durability, resistance to weather, a degree of waterproofing, and the potential for chemical modification. Additionally, these fibers can be stretched beyond their elastic limit without breaking, showcasing a high elongation at the break [14]. Many studies in the literature contain comprehensive analyses of the structural, morphological, mechanical, and thermal characteristics of coir fibers [15–20]. Bamboo leaf fiber (BF) is one of the most abundantly available waste materials. BF has a shorter growing time than its culm. Studies on the use of BF as a reinforcement material have not yet been widespread. Up to now, studies have indicated that adding fibers into PLA matrices can improve the performance of PLA composites. The selection of plant fibers determines the end properties of composites [21].

Incorporating natural fibers into polymer composites can be challenging due to certain inherent characteristics that have potential downsides. These characteristics include limited protection against microbial attacks, inadequate resistance to moisture, poor adhesion in the fiber–matrix surface, and a tendency to form aggregates during processing. These limitations can be addressed by alterations to the surface of fibers; this is achievable using chemical techniques like mercerization [22], dewaxing, acetylation, chemical grafting, bleaching, delignification, and salinization [23].

Because each fiber possesses unique advantages and drawbacks, reinforcing a given polymer with a combination of two or more fiber types may help to overcome the drawbacks of each fiber and, subsequently, improve the properties of the composite overall. This technique is known as “hybrid composite” and has recently attracted significant attention from researchers [9,24,25].

To further improve the mechanical properties and service temperatures of PLA-based composites, we used thermal annealing together with hybridization in this study. Thermal annealing can be carried out by subjecting specimens to a high temperature, above its cold-crystallization temperature, and then using a slow cooling rate to induce the formation of a crystallized structure that enhances the thermal properties of the material, as well as the mechanical properties [26–28]. Thus, the service temperature and mechanical performance of the PLA-based composite are expected to improve.

Many researchers try to improve natural fiber composite properties by carrying out chemical treatment of the natural fiber [29]. However, because most of the chemical treatment techniques use strong acidic or basic chemicals, they are inherently harmful to the environment. Therefore, we focused on developing a 100% eco-friendly material in this work. We strategically combined fiber hybridization and annealing to overcome the drawbacks of PLA composites. In this study, first, we investigated the effect of fiber types (coir and bamboo leaf fibers), fiber loading (5, 10, and 15 wt%), and thermal annealing



on morphology, tensile properties, thermal properties, crystallinity, and heat distortion temperature (HDT) of a PLA-based single-fiber composite. Then, we combined the fiber in various ratios to create PLA-based hybrid composites. The fiber loading of 10 wt% was kept constant. The ratio of coir fiber and bamboo leaf fiber was varied. The BF: CF ratios were 1:1, 1:2, and 2:1. The fibers were incorporated into the PLA matrix using twin screw extrusion, and the test specimens were prepared with compression molding. To enhance the crystallization of PLA, annealing of PLA-based hybrid composites was performed at 120 °C for 30 min [30]. With these combined techniques, an improvement in the overall properties of composites could be expected.

**Table 1.** The chemical, mechanical, and physical properties of natural fibers [31].

Sample	Coir	Bamboo	Bamboo Leaf	Sisal
Density (g/m <sup>3</sup> )	1.25–1.5	0.9	-	1.26–1.33
Diameter (μm)	100–450	-	-	100–300
Cellulose (%)	36–43	26–43	19.5–26.3	74–75.2
Hemicellulose (%)	0.2	30	11.3–13.5	10–13.9
Lignin (%)	41–45	21–30	8.7–11.6	8–12
Microfibrillar angle (°)	30–45	-	-	10–20
Tensile strength (MPa)	105–175	-	-	600–700
Young's modulus (GPa)	4–6	-	-	38
Elongation at break (%)	17–47	-	-	3.64–5.12
Moisture absorption (%)	10	-	-	11

## 2. Materials and Methods

### 2.1. Materials

Poly(lactic acid (PLA) (grade LX175, Purac Ltd., Ban Chang, Thailand) used was at an extrusion grade with a density of 1.24 g/cm<sup>3</sup> and a melt flow index of 3 g/10 min. Coir (*Cocos nucifera* L., Thailand) and bamboo leaf (*Bambusa ventricosa* McClure, Thailand) were purchased from local farmers in Nakhon Ratchasima, Thailand.

#### 2.1.1. Fiber Preparation

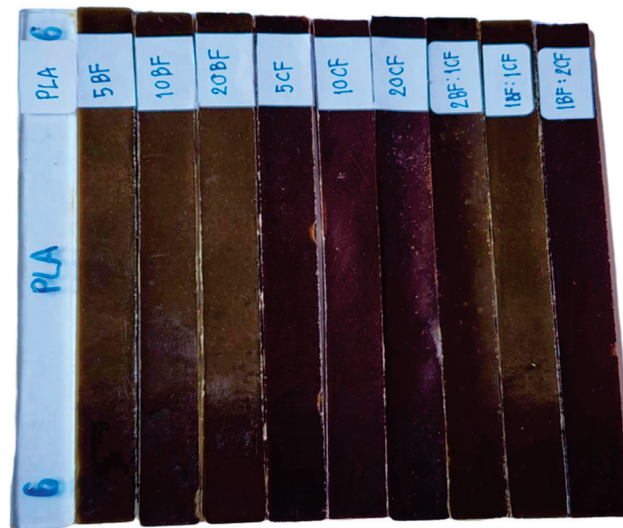
The dried bamboo leaf and coir were crushed into fine fibers with shorter lengths using a wood crusher machine (CT, CGR-20, Chareon Tut Co., Ltd., Samutprakarn, Thailand) for 1 h. The fibers with a diameter in the range of 45–106 μm were obtained. The obtained fibers were given code names as bamboo leaf fiber (BF) and coir fiber (CF).

#### 2.1.2. Preparation of PLA-Based Composites

A list of samples used in this study is shown in Table 2. The composites were prepared with the melt mixing technique using a co-rotating twin screw extruder (Brabender, DSE 35/17D, Brabender GmbH & Co. KG, Duisburg, Germany). The fibers and PLA were dried in a hot air oven at 80 °C for 4 h before use. Immediately after drying, the PLA and fiber underwent melt mixing in the twin screw extruder at the screw speed of 20 rpm and melting temperature of 170 °C. The compound pellets were then compression molded at 170 °C for 10 min to form test specimens (See Figure 1). To investigate the effect of annealing on the composite's properties, samples were annealed at 120 °C for 30 min in a hot air oven (Despatch, LAC series, Despatch Industries, Inc., Lakeville, MN, USA) before being left cool at room temperature.

**Table 2.** Composition of PLA-based composites.

Sample	PLA (wt%)	BF (wt%)	CF (wt%)
Neat PLA	100	-	-
5BF/PLA	95	5	-
10BF/PLA	90	10	-
20BF/PLA	80	20	-
5CF/PLA	95	-	5
10CF/PLA	90	-	10
20CF/PLA	80	-	20
1BF:2CF	90	3.33	6.67
1BF:1BF	90	5	5
2BF:1CF	90	6.67	3.33

**Figure 1.** Photograph of PLA, PLA composite, and PLA-based hybrid composite specimens.

## 2.2. Characterization and Test

### 2.2.1. Tensile Test

The tensile test of PLA and its composite was carried out according to ASTM D638 [32]. Five dog bone-shape specimens with a gauge length of 50 mm were tested at room temperature ( $\sim 25$  °C) using a universal testing machine (UTM, INSTRON/5565, Instron Co., Ltd., Norwood, MA, USA). The test was performed using a 5 kN load cell at 5 mm/min crosshead speed. The reported value is an average value from five replications. The error bars shown in the graph represent the standard deviation value.

### 2.2.2. Morphological Study

The tensile fractured surfaces of PLA and its composites were used in the investigation of the composites' morphological structure. The fractured surface was used as it can reveal information on the distribution and dispersion of the reinforcing agents and the adhesion between the fibers and matrix as well as the failure mode (brittle or ductile fracture). The fractured surfaces were then sputtered coated with gold for 3 min before being examined using a scanning electron microscope, SEM (JEOL, model JSM6400, JEOL Ltd., Tokyo, Japan), at 5–10 kV.

### 2.2.3. Differential Scanning Calorimetry (DSC)

The crystallization and melting behaviors of PLA and PLA-based hybrid composites were determined using differential scanning calorimetry (DSC: Mettler Toledo STAre SW 8.1, Mettler-Toledo International Inc., Greifensee, Switzerland). A sample was heated from 25 to 200 °C with a heating rate of 10 °C/min (first heating scan). After keeping the sample

at 200 °C for 1 min, it was cooled to 25 °C. Finally, it was heated again to 200 °C (second heating scan). The degree of crystallinity ( $X_c$ ) of the neat PLA, PLA composites, and PLA hybrid composites was calculated using Equation (1) [33].

$$X_c = \frac{\Delta H_m - \Delta H_{cc}}{\omega \Delta H_m^0} \times 100\% \quad (1)$$

where  $\Delta H_m$  is the heat of melting and  $\Delta H_{cc}$  is determined by integrating the areas (J/g) under the peaks.  $\Delta H_m^0$  is a reference value and represents the heat of melting if the polymer were 100% crystallinity (93.7 J/g for PLA) [34] and  $\omega$  is the weight fraction of the PLA in the composites.

### 2.3. Heat Deflection Temperature (HDT)

An HDT/VICAT manual heat deflection tester (model HDV1, Atlas Electric Devices Co., Chicago, IL, USA) was used to measure the heat deflection temperature (HDT) of PLA and its composites. The test was carried out using a load of 0.455 MPa, as specified by ASTM D648 [35].

## 3. Results and Discussion

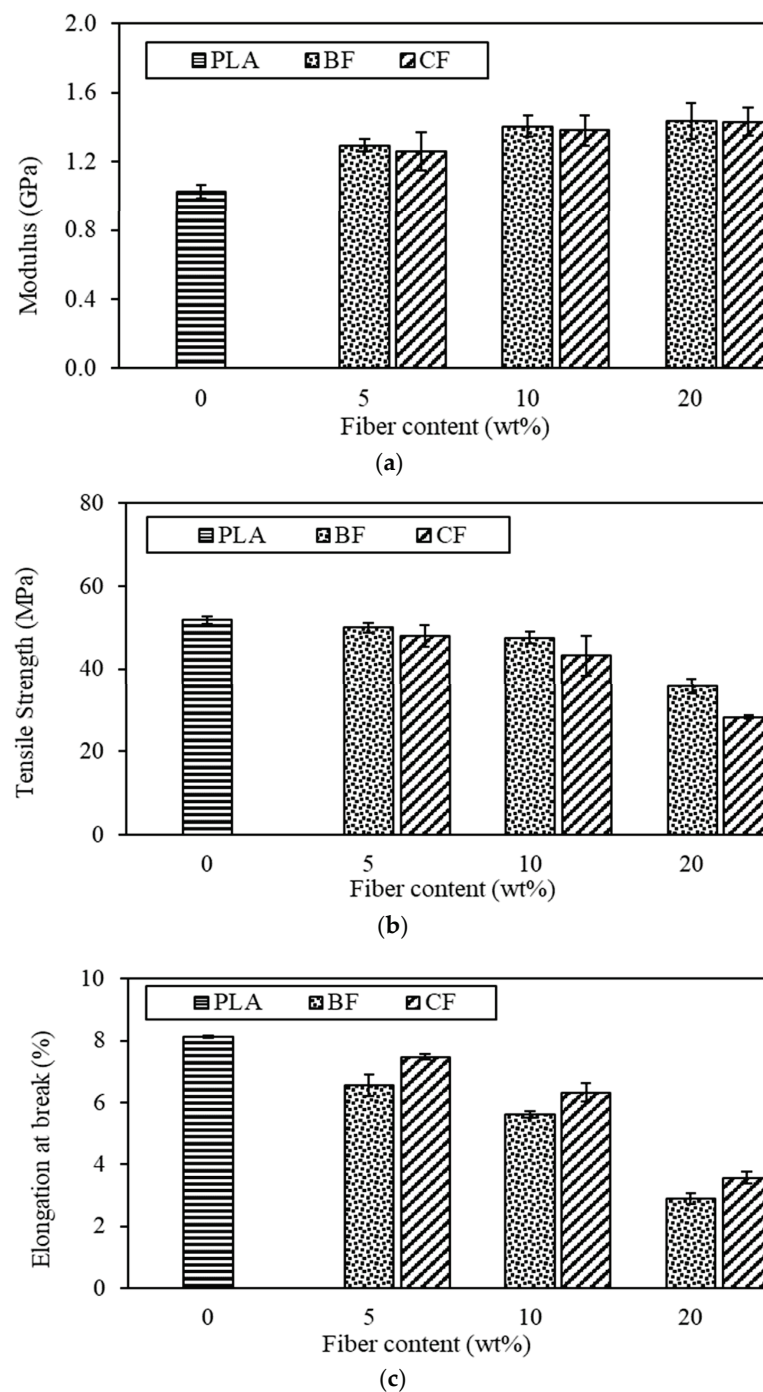
### 3.1. Effect of Fiber Type and Content on Tensile Properties of PLA-Based Composites

The tensile properties including modulus tensile strength, and elongation at break of PLA and PLA single-fiber composites at various fiber loading are depicted in Figure 2. Generally, neat PLA showed better tensile strength and elongation at break than those of the PLA composites. This finding is in agreement with those reported by others [36,37]. The neat PLA possessed the highest tensile strength and elongation at break of 51.85 MPa and 8.13%, respectively. The presence of natural fiber in PLA composite increased the tensile modulus. The maximum tensile moduli were obtained from the composites containing 20 wt% fiber loading. Improvements in tensile moduli in the PLA composites over the neat PLA were 41.18% and 40.20% for 20BF/PLA and 20CF/PLA, respectively.

Increasing the fiber loading resulted in an increase in the tensile moduli of PLA composites, whereas the tensile strength and elongation at break of PLA composites were decreased. The results suggested that with the presence of the natural fiber, the PLA-based composite became more brittle. These results were expected, and they indicated a poor adhesion between the natural fiber and the PLA matrix. Similar results were reported by other researchers who suggested that these findings were associated with a low strength of adhesion among the fibers within composite materials. The decrease in tensile strength with the increasing fiber content may also be due to an agglomeration of fibers in the PLA matrix [36–38]. The poor adhesion among the composite components stemmed from the low hydrophilicity and polarity of PLA as compared with those of the plant fibers, which possess polar hydroxyl groups on their surfaces. The PLA composites reinforced with plant fibers tend to display inadequate interfacial adhesion, consequently leading to ineffective stress transfer from the matrix to the fibers [39–41]. A poor adhesion between the fibers and the PLA matrix could be seen in the results of the morphological study reported in the next section. In addition, it was known that adding rigid particles into a polymer matrix generally resulted in an increased stiffness of the polymer.

As compared with the same fiber content, the presence of BF and CF in the PLA matrix gave the same moduli value, which increased with the fiber loading. Therefore, the type of fiber was an insignificant parameter in increasing the composite stiffness. In other words, the fiber content played a dominant role in controlling the composite moduli. On the other hand, the type of fiber seemed to have a significant effect on the tensile strength and elongation at break. The BF/PLA composites showed slightly higher tensile strength, while the CF/PLA composites presented higher elongation at break. These findings could plausibly be explained by the nature of the fiber (see Table 1). The coir fiber possessed a low tensile strength and high stretching ability as compared with the other fibers. Therefore, a composite of such fiber would sustain the same characteristics as its

component [11–14]. Additionally, one could speculate that combining the two fibers would yield the best characteristic of both fibers. To investigate the effect of fiber hybridization, we considered using 10 wt% fiber for further study. Although the PLA composite containing 20 wt% of fiber possessed the highest modulus, because of the diminishing tensile strength and elongation at break, it may not be optimal for further improvement in the composite properties. PLA composites with 10 wt% fiber content possessed overall optimal properties and offered the possibility for greater improvement as well as the opportunity to understand the different effects of different fibers in hybridization on the composite performance. Therefore, hybrid composites with different ratios of BF: CF were prepared with a constant fiber loading of 10 wt%.



**Figure 2.** Tensile properties of PLA and PLA composites with varied fiber content 5–20 wt% (a) tensile modulus, (b) tensile strength, and (c) elongation at break.

### 3.2. Effect of Fiber Ratio and Annealing on Tensile Properties of PLA-Based Composites

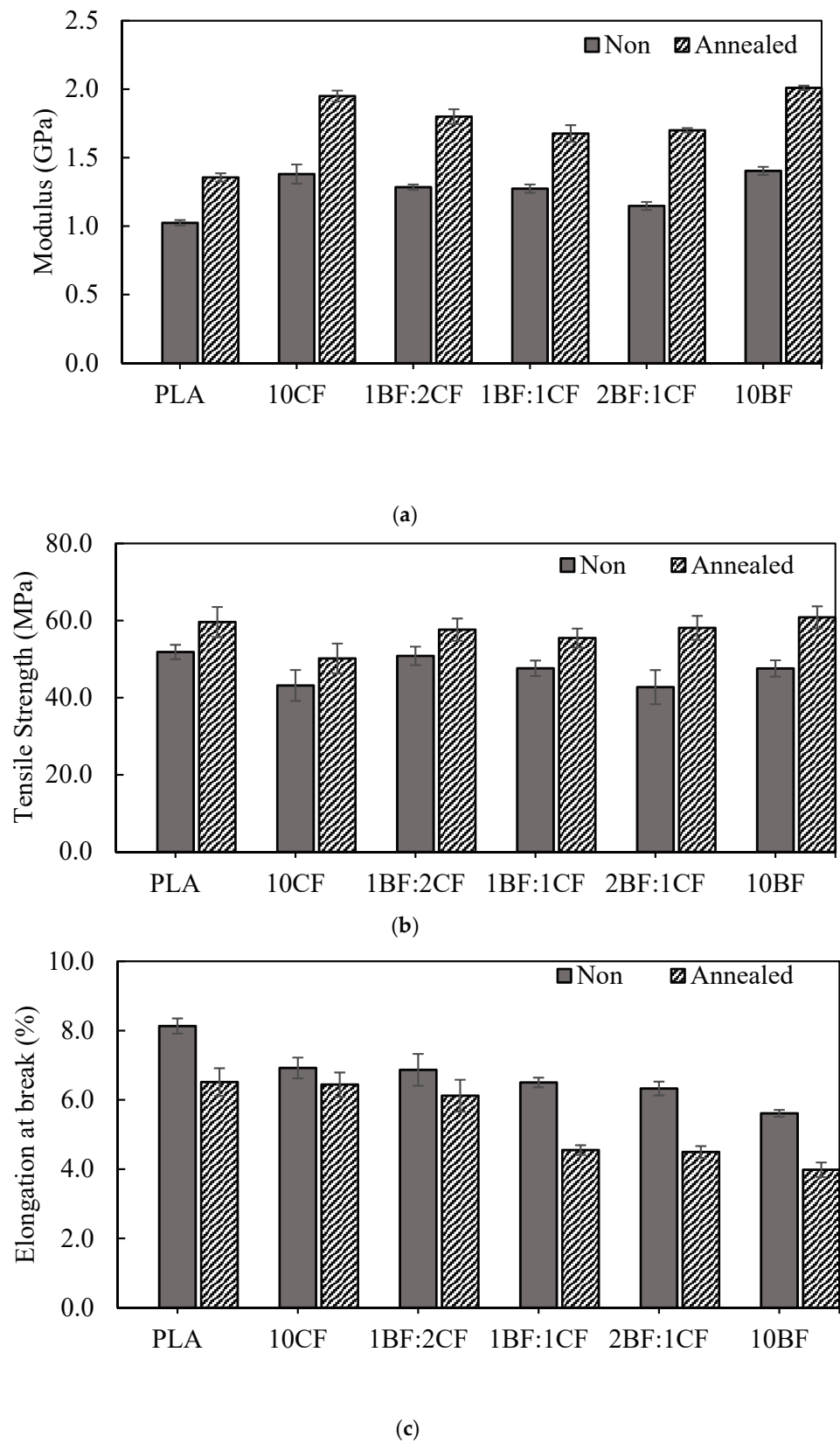
Hybrid composites with a constant fiber loading of 10 wt% were prepared with different BF: CF ratios (1:1, 1:2, and 2:1). As can be seen in Figure 3, similar to the results found for single-fiber composites, the modulus of the hybrid composites was dependent only on the fiber loading. Different BF: CF fiber ratios gave insignificantly different modulus as well as tensile strength. Among the hybrid composites, 1BF: 2CF showed the highest tensile properties including tensile modulus, tensile strength, and elongation at break. It was interesting to note that elongation at break of the composites seemed to improve with the CF fiber content. As the ratio of the reinforced fiber changed, the decrease in CF content in the composite resulted in a decrease in elongation at break. This finding that CF was beneficial in improving elongation at break of single-fiber-reinforced PLA remained true even in the hybrid composite, where two different fibers were combined.

Annealing was the strategy we used in combination with fiber hybridization. The increases in modulus and tensile strength were expected as annealing generally increased and improved crystallinity and crystal growth. The crystalline phase in a semicrystalline polymer is known to be the main contributor to the hardening and strengthening of the polymer. As expected, further increases in modulus and tensile strength were obtained after thermal treatment/annealing of the PLA hybrid composites. However, elongation at break of all annealed samples suffered, as shown in Figure 3. These could also be explained by the increase in crystallinity in post-annealing samples. Higher crystalline materials resulted in harder material, whereas the portion of amorphous regions providing the elasticity of the sample was reduced. The presence of an increased crystal portion restricted the chain movement in the samples, resulting in lower extensibility. The DSC results reported in the next section confirm this speculation. It should be noted that the hybrid composite containing a high content of coir fiber showed a lower degree of elongation at break dimension after annealing. The decrease in elongation at break was about 7% and 10% in 10CF and 1:2 BF: CF composites, respectively, and about 30% for the other composites. This result indicated the strong dependency of elongation at break on fiber type even after annealing, where crystallinity should be dominant. To our knowledge, this particular point has not been reported elsewhere and may be worth investigating in depth in future studies.

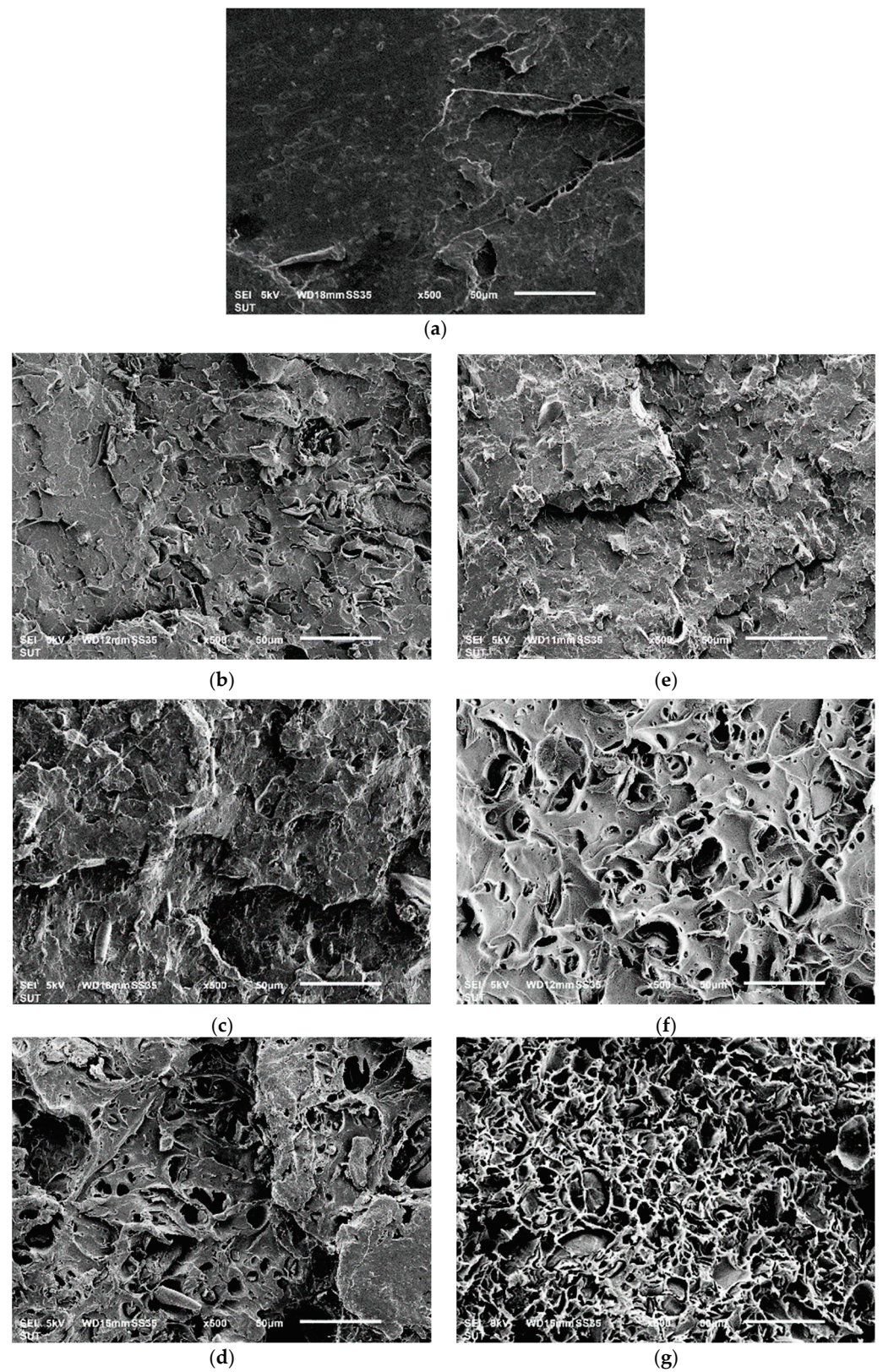
### 3.3. Morphology of PLA-Based Composites

SEM micrographs of the tensile fractured surface of PLA and its composites are shown in Figure 4. The surface of neat PLA was smooth, all the composites were present with voids. Figure 4b–g shows the void due to fiber pull-out and poor adhesion between the fibers and matrix [42]. The void size tends to increase with increasing fiber content. Composites with CF showed more voids with greater sizes than those with BF. These voids generate weak zones where the load-bearing capacity tends to drop, leading to a reduction in tensile strength and elongation at break of PLA composites. When comparing BF composites and CF composites, the fractured surface investigation revealed that CF composites were more ductile as compared with the BF composites. The yielding feature of the PLA matrix on the fractured surface of CF composites was plausibly due to the ability of CF to elongate to a greater extent than BF [14]. Thus, when the extensional force was applied, the CF held the composites together, impeding a brittle failure and allowing a greater extension length before breaking. This finding agreed well with the tensile results shown in Figure 2. The results also suggested that CF may have a better adhesion between fibers and the PLA matrix; otherwise, fracture surface yield could not occur.





**Figure 3.** Tensile properties of PLA, PLA composites, and PLA hybrid composites with and without thermal treatment (annealing at 120 °C for 30 min): (a) tensile modulus, (b) tensile strength, and (c) elongation at break.



**Figure 4.** SEM micrographs of the tension-fractured surfaces of (a) neat PLA, (b) 5BF/PLA, (c) 10BF/PLA, (d) 20BF/PLA, (e) 5CF/PLA, (f) 10CF/PLA, and (g) 20 CF/PLA.

### 3.4. Thermal and Crystallinity of PLA-Based Composites

Differential scanning calorimetry (DSC) was used to investigate the effect of fiber type, fiber content, and thermal treatment in promoting the crystallinity of the PLA matrix. The

DSC data including crystallinity ( $X_c$ ) calculated using Equation (1), melting temperature ( $T_m$ ), and cold crystallization temperature ( $T_{cc}$ ) from the first heating scan are presented in Figure 5 and Table 3. It can be seen that the  $T_g$  of PLA was 61.18 °C. The  $T_g$  slightly decreased with the addition of fiber into the PLA matrix. The  $T_{cc}$  was observed in all non-annealed samples, indicating that PLA molecules were unable to crystallize during the cooling phase. It is well-known that PLA’s crystal formation is naturally low and requires significant encouragement to induce crystallization [43]. An increase in crystallinity in PLA results in an improvement in several properties such as tensile and thermal properties [44].  $T_{cc}$  of PLA composites increased with the presence of fiber. This indicated a greater amount of the non-crystalline phase in the composite as compared with that of the neat PLA. The result agreed well with the crystallinity ( $X_c$ ). This was plausibly due to the incorporated fiber restricting the mobility of PLA chains together with the fast-cooling conditions during compression molding [45]. However, the  $T_g$  and  $T_{cc}$  peaks disappeared from the curve after thermal annealing. The disappearance of the peaks signified the growth of crystals in PLA (crystal perfection). This phenomenon was attributed to the rearrangement of PLA molecules upon high temperature and slow cooling. The molecules had sufficient time to slowly crystallize.

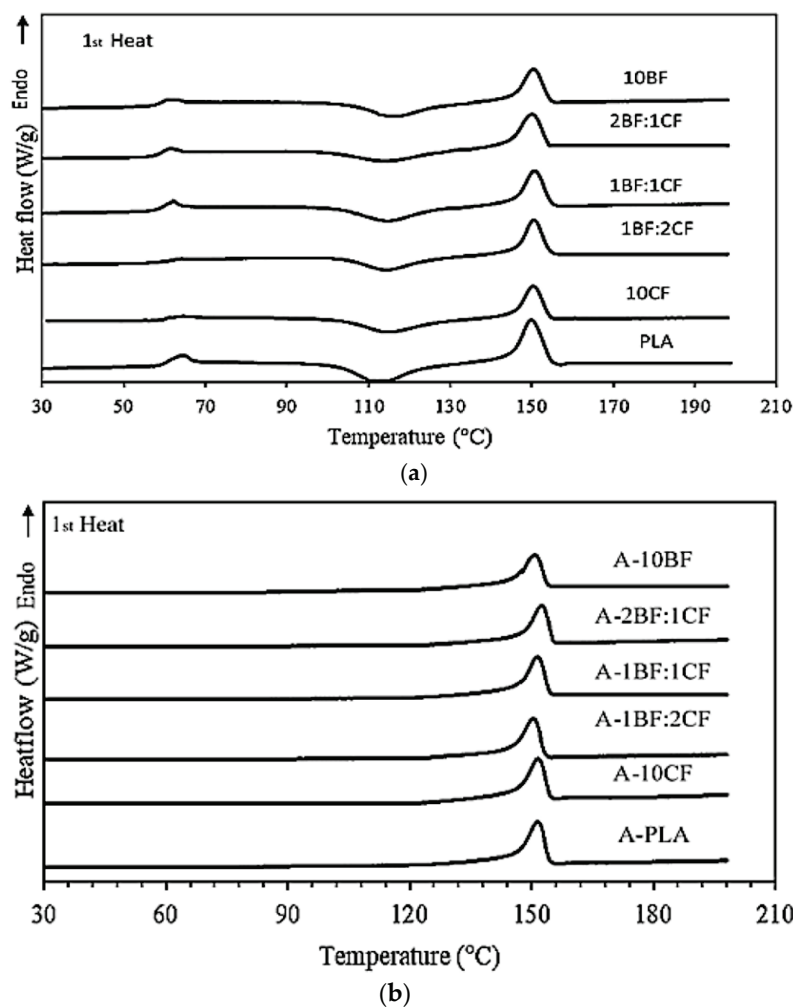


Figure 5. DSC thermograms of PLA, PLA composites, PLA hybrid composites (a) before and (b) after heat treatment.



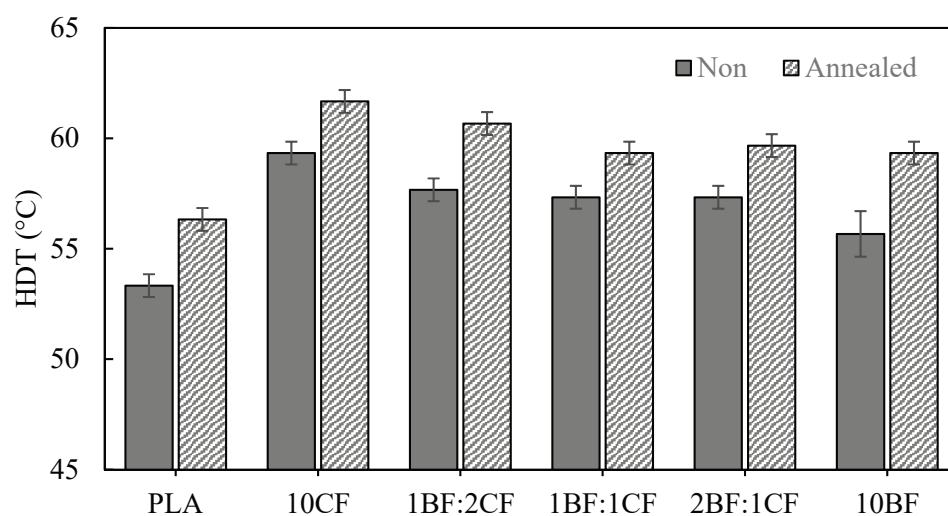
**Table 3.** Transition temperatures obtained from the DSC first heating scan of PLA and its composites, with and without thermal treatment.

Sample	Non-Annealed				Annealed			
	T <sub>g</sub> (°C)	T <sub>cc</sub> (°C)	T <sub>m</sub> (°C)	X <sub>C</sub> (%)	T <sub>g</sub> (°C)	T <sub>cc</sub> (°C)	T <sub>m</sub> (°C)	X <sub>C</sub> (%)
PLA	61.18	112.43	149.84	6.10	-	-	151.82	38.90
10CF	61.28	115.22	150.30	2.85	-	-	151.32	36.73
1BF:2CF	59.99	114.20	150.45	4.68	-	-	151.62	37.38
1BF:1CF	59.63	114.53	150.62	3.63	-	-	150.29	36.36
2BF:1CF	59.59	114.04	150.12	2.08	-	-	150.76	36.23
10BF	59.75	116.25	150.47	2.44	-	-	150.47	35.72

The X<sub>C</sub> of the neat, non-annealed PLA was 6.1%, which showed the tendency to decrease with increasing fiber content. The nucleating ability of both fillers was insufficient to obtain the dominant crystallinity of the PLA-based composites. The existence of both fibers hindered the mobility of PLA chains, leading to the poor rearrangement of PLA molecules and thus, lower crystallinity. The higher results for X<sub>C</sub> of post-annealed samples were due to sufficient time and energy for the PLA molecules to rearrange and overcome the hindrance of the fiber to crystallization during the annealing process.

### 3.5. Heat Deflection Temperature (HDT)

The heat deflection temperature (HDT) is commonly used to determine the maximum service temperature of a material. PLA possesses a low service temperature, which limits its use in various applications. For semicrystalline polymers such as PLA, HDT is strongly dependent on crystallinity. The poor HDT of PLA is partly due to its naturally low crystallinity. Figure 6 shows the HDT results of PLA and its composites. The HDT of neat PLA was about 53.33 °C, which was rather low for various applications such as automotive parts and packaging. With the presence of natural fiber in the PLA matrix, the HDT increased to 55.67 and 59.33 °C for the 10BF/PLA and 10CF/PLA composites, respectively. The increase in HDT in this case was due to the higher stiffness (moduli) of the single-fiber composites. As discussed previously, the presence of fiber in the composites reduced the crystallinity slightly; therefore, the increase in HDT in the composite was not from the crystallinity.

**Figure 6.** HDT data for PLA, PLA composites, and PLA hybrid composites before and after heat treatment.

In the case of hybrid composites created by adding BF: CF in different ratios (1BF:2CF, 1BF:1CF, and 2BF:1CF) into the PLA matrix, the HDT value of 1BF:2CF was the highest among those hybrid composites. The HDT value of 2BF:1CF was 57.33 °C, which was a

7.5% improvement as compared with the neat PLA. The increases in HDT for PLA hybrid composites were also due to the increase in stiffness with the presence of fiber and not because of crystallinity. Stiffness is defined as the ability of a material to resist deformation under load. On the other hand, HDT is a measurement of the material while temperature is increased. Therefore, the modulus of PLA composites and PLA hybrid composites were also examined for an analysis of HDT. Referring to Figures 2a and 3a, it was shown that the modulus of PLA composites and PLA hybrid composites were higher than that of the neat PLA.

Annealing of the PLA composites gave rise to HDT in all samples. This was because annealing increased both the crystallinity and modulus. The increase in HDT value of the post-annealing samples might be due to the increase in crystallinity and consequently, the modulus/stiffness. The high-temperature exposure and slow cooling process of PLA composites induce the formation of a crystallized structure that enhances thermal properties. The maximum HDT obtained in this work was 61.7 °C in an annealed 10CF sample, which was an 8.3 °C increase over the non-annealed neat PLA. Other researchers also reported an increase in HDT over the same temperature range. A further increase in HDT up to 120 °C could be achieved using nucleating agents together with thermal treatment manipulation [46].

#### 4. Conclusions

In summary, we illustrated the possibility of improving PLA properties using combined techniques of hybridization and thermal treatment. The hybrid composites created using two different fibers can offer beneficial properties of the individual fibers used. Selecting a proper pair of fibers is critical to obtaining properties that complement one another. In this work, the PLA composite reinforced with coir fiber offers better elongation at break and HDT than BF composites, while bamboo leaf fiber offers better tensile strength than CF composites. The fiber content played an important role in dominating the mechanical properties of the final composite, specifically the stiffness (moduli). The PLA composites consisting of 10 wt% of fiber possessed the most balanced properties in terms of tensile modulus, tensile strength, and elongation at break. Hybridization of the BF: CF with the ratio of 1:2 gave the most desirable properties. Thermal treatment or annealing further improved the mechanical and thermal properties of hybrid composites. These improvements are attributed to the increased degree of crystallinity brought about by the exposure to high temperatures and slow cooling. However, the result of tensile properties showed lower tensile strength, as compared with the neat PLA, due to poor adhesion between fiber and matrix. Further studies can be performed to investigate several strategies to improve the adhesion between fibers and the PLA matrix. It can be expected that when the adhesion between fibers and the matrix is improved, the properties of PLA-based hybrid composites will be greatly improved, which will consequently open more possibilities for the utilization of PLA in various applications.

**Author Contributions:** Conceptualization, T.T. and S.Y.; methodology, T.T. and S.Y.; validation, T.T. and S.Y.; formal analysis, S.Y.; investigation, S.Y.; writing—original draft preparation, S.Y.; writing—review and editing, T.T. and S.Y.; visualization T.T. and S.Y.; supervision, T.T.; project administration, T.T.; funding acquisition, T.T. All authors have read and agreed to the published version of the manuscript.

**Funding:** This work was funded by Suranaree University of Technology (SUT) and the Center of Excellence on Petrochemical and Materials Technology (PETROMAT) High Performance and Smart Materials (HPSMs) program, 2016.

**Institutional Review Board Statement:** Not applicable.

**Data Availability Statement:** The data presented in this study are available upon request from the corresponding author.



**Acknowledgments:** The authors thank the Suranaree University of Technology for providing equipment and facilities.

**Conflicts of Interest:** The authors declare no conflict of interest.

## References

- Mohanty, A.K.; Misra, M.; Drzal, L.T. Sustainable Bio-Composites from Renewable Resources: Opportunities and Challenges in the Green Materials World. *J. Polym. Environ.* **2002**, *10*, 19–26. [CrossRef]
- Siracusa, V.; Rocculi, P.; Romani, S.; Rosa, M.D. Biodegradable polymers for food packaging: A review. *Trends Food Sci. Technol.* **2008**, *19*, 634–643. [CrossRef]
- Pongtanayut, K.; Thongpin, C.; Santawitee, O. The Effect of Rubber on Morphology, Thermal Properties and Mechanical Properties of PLA/NR and PLA/ENR Blends. *Energy Procedia* **2013**, *34*, 888–897. [CrossRef]
- Yang, Y.; Zhang, L.; Xiong, Z.; Tang, Z.; Zhang, R.; Zhu, J. Research progress in the heat resistance, toughening and filling modification of PLA. *Sci. China Chem.* **2016**, *59*, 1355–1368. [CrossRef]
- Trifol, J.; Plackett, D.; Sillard, C.; Szabo, P.; Bras, J.; Daugaard, A.E. Hybrid poly(lactic acid)/nanocellulose/nanoclay composites with synergistically enhanced barrier properties and improved thermomechanical resistance. *Polym. Int.* **2016**, *65*, 988–995. [CrossRef]
- Coskun, K.; Mutlu, A.; Dogan, M.; Bozacı, E. Effect of various enzymatic treatments on the mechanical properties of coir fiber/poly(lactic acid) biocomposites. *J. Thermoplast. Compos. Mater.* **2019**, *34*, 1066–1079. [CrossRef]
- Dong, Y.; Ghataura, A.; Takagi, H.; Haroosh, H.J.; Nakagaito, A.N.; Lau, K.-T. Polylactic acid (PLA) biocomposites reinforced with coir fibres: Evaluation of mechanical performance and multifunctional properties. *Compos. Part A Appl. Sci. Manuf.* **2014**, *63*, 76–84. [CrossRef]
- Sun, Z.; Zhang, L.; Liang, D.; Xiao, W.; Lin, J. Mechanical and Thermal Properties of PLA Biocomposites Reinforced by Coir Fibers. *Int. J. Polym. Sci.* **2017**, *2017*, 2178329. [CrossRef]
- Yusoff, R.B.; Takagi, H.; Nakagaito, A.N. Tensile and flexural properties of polylactic acid-based hybrid green composites reinforced by kenaf, bamboo and coir fibers. *Ind. Crops Prod.* **2016**, *94*, 562–573. [CrossRef]
- Zhang, L.; Sun, Z.; Liang, D.; Lin, J.; Xiao, W. Preparation and performance evaluation of PLA/coir fibre biocomposites. *BioResources* **2017**, *12*, 7349–7362. [CrossRef]
- Adeniyi, A.G.; Onifade, D.V.; Ighalo, J.O.; Adeoye, A.S. A review of coir fiber reinforced polymer composites. *Compos. Part B Eng.* **2019**, *176*, 107305. [CrossRef]
- Mathura, N.; Cree, D. Characterization and mechanical property of Trinidad coir fibers. *J. Appl. Polym. Sci.* **2016**, *133*, 43692. [CrossRef]
- Nam, T.H.; Ogihara, S.; Tung, N.H.; Kobayashi, S. Effect of alkali treatment on interfacial and mechanical properties of coir fiber reinforced poly(butylene succinate) biodegradable composites. *Compos. Part B Eng.* **2011**, *42*, 1648–1656. [CrossRef]
- Geethamma, V.G.; Kalaprasad, G.; Groeninckx, G.; Thomas, S. Dynamic mechanical behavior of short coir fiber reinforced natural rubber composites. *Compos. Part A Appl. Sci. Manuf.* **2005**, *36*, 1499–1506. [CrossRef]
- Zainudin, E.S.; Yan, L.H.; Haniffah, W.H.; Jawaid, M.; Alothman, O.Y. Effect of coir fiber loading on mechanical and morphological properties of oil palm fibers reinforced polypropylene composites. *Polym. Compos.* **2014**, *35*, 1418–1425. [CrossRef]
- Arrakhiz, F.Z.; El Achaby, M.; Malha, M.; Bensalah, M.; Fassi-Fehri, O.; Bouhfid, R.; Benmoussa, K.; Qaiss, A. Mechanical and thermal properties of natural fibers reinforced polymer composites: Doum/low density polyethylene. *Mater. Des.* **2013**, *43*, 200–205. [CrossRef]
- Essabir, H.; Bensalah, M.O.; Rodrigue, D.; Bouhfid, R.; Qaiss, A. Structural, mechanical and thermal properties of bio-based hybrid composites from waste coir residues: Fibers and shell particles. *Mech. Mater.* **2016**, *93*, 134–144. [CrossRef]
- Morandim-Giannetti, A.A.; Agnelli, J.A.M.; Lanças, B.Z.; Magnabosco, R.; Casarin, S.A.; Bettini, S.H.P. Lignin as additive in polypropylene/coir composites: Thermal, mechanical and morphological properties. *Carbohydr. Polym.* **2012**, *87*, 2563–2568. [CrossRef]
- Rosa, M.F.; Chiou, B.-S.; Medeiros, E.S.; Wood, D.F.; Williams, T.G.; Mattoso, L.H.C.; Orts, W.J.; Imam, S.H. Effect of fiber treatments on tensile and thermal properties of starch/ethylene vinyl alcohol copolymers/coir biocomposites. *Bioresour. Technol.* **2009**, *100*, 5196–5202. [CrossRef]
- Islam, M.N.; Haque, M.M.; Huque, M.M. Mechanical and Morphological Properties of Chemically Treated Coir-Filled Polypropylene Composites. *Ind. Eng. Chem. Res.* **2009**, *48*, 10491–10497. [CrossRef]
- Peltola, H.; Pääkkönen, E.; Jetsu, P.; Heinemann, S. Wood based PLA and PP composites: Effect of fibre type and matrix polymer on fibre morphology, dispersion and composite properties. *Compos. Part A Appl. Sci. Manuf.* **2014**, *61*, 13–22. [CrossRef]
- Suardana, N.; Lokantara, I.P.; Lim, J.K. Influence of water absorption on mechanical properties of coconut coir Fiber/Poly-Lactic acid biocomposites. *Mater. Phys. Mech.* **2011**, *12*, 113–125.
- Saw, S.K.; Sarkhel, G.; Choudhury, A. Surface modification of coir fibre involving oxidation of lignins followed by reaction with furfuryl alcohol: Characterization and stability. *Appl. Surf. Sci.* **2011**, *257*, 3763–3769. [CrossRef]
- Irina, M.M.W.; Azmi, A.I.; Tan, C.L.; Lee, C.C.; Khalil, A.N.M. Evaluation of Mechanical Properties of Hybrid Fiber Reinforced Polymer Composites and their Architecture. *Procedia Manuf.* **2015**, *2*, 236–240. [CrossRef]

25. Sanjay, M.R.; Yogesha, B. Studies on Natural/Glass Fiber Reinforced Polymer Hybrid Composites: An Evolution. *Mater. Today Proc.* **2017**, *4*, 2739–2747. [CrossRef]
26. Kong, W.; Zhu, B.; Su, F.; Wang, Z.; Shao, C.; Wang, Y.; Liu, C.; Shen, C. Melting temperature, concentration and cooling rate-dependent nucleating ability of a self-assembly aryl amide nucleator on poly(lactic acid) crystallization. *Polymer* **2019**, *168*, 77–85. [CrossRef]
27. Tábi, T.; Sajó, I.E.; Szabó, F.; Luyt, A.S.; Kovacs, J.G. Crystalline structure of annealed polylactic acid and its relation to processing. *Express Polym. Lett.* **2010**, *4*, 659–668. [CrossRef]
28. Wang, J.; Kazemi, Y.; Wang, S.; Hamidinejad, M.; Mahmud, M.B.; Pötschke, P.; Park, C.B. Enhancing the electrical conductivity of PP/CNT nanocomposites through crystal-induced volume exclusion effect with a slow cooling rate. *Compos. Part B Eng.* **2020**, *183*, 107663. [CrossRef]
29. Bouzouita, A.; Notta-Cuvier, D.; Raquez, J.-M.; Lauro, F.; Dubois, P. Poly(lactic acid)-Based Materials for Automotive Applications. In *Industrial Applications of Poly(Lactic Acid)*; Di Lorenzo, M., Androsch, R., Eds.; Advances in Polymer Science; Springer: Cham, Switzerland, 2017; pp. 1–43.
30. Shi, Q.F.; Mou, H.Y.; Li, Q.Y.; Wang, J.K.; Guo, W.H. Influence of heat treatment on the heat distortion temperature of poly(lactic acid)/bamboo fiber/talc hybrid biocomposites. *J. Appl. Polym. Sci.* **2012**, *123*, 2828–2836. [CrossRef]
31. Nam, T.H.; Ogihara, S.; Kobayashi, S. Interfacial, Mechanical and Thermal Properties of Coir Fiber-Reinforced Poly(Lactic Acid) Biodegradable Composites. *Adv. Compos. Mater.* **2012**, *21*, 103–122. [CrossRef]
32. ASTM D638-22; Standard Test Method for Tensile Properties of Plastics. ASTM International: West Conshohocken, PA, USA, 2022. [CrossRef]
33. Choi, H.-J.; Kim, M.S.; Ahn, D.; Yeo, S.Y.; Lee, S. Electrical percolation threshold of carbon black in a polymer matrix and its application to antistatic fibre. *Sci. Rep.* **2019**, *9*, 6338. [CrossRef]
34. Davachi, S.M.; Kaffashi, B. Preparation and Characterization of Poly L-Lactide/Triclosan Nanoparticles for Specific Antibacterial and Medical Applications. *Int. J. Polym. Mater. Polym. Biomater.* **2015**, *64*, 497–508. [CrossRef]
35. ASTM D648-18; Standard Test Method for Deflection Temperature of Plastics Under Flexural Load in the Edgewise Position. ASTM International: West Conshohocken, PA, USA, 2018. [CrossRef]
36. Oksman, K.; Skrifvars, M.; Selin, J.-F. Natural fibres as reinforcement in polylactic acid (PLA) composites. *Compos. Sci. Technol.* **2003**, *63*, 1317–1324. [CrossRef]
37. Sitticharoen, W.; Uthiyoung, C.; Passadee, N.; Wongprom, C. Surface treated bagasse fiber ash on rheological, mechanical properties of PLA/BFA biocomposites. *Polimeros* **2018**, *28*, 187–195. [CrossRef]
38. Agunsoye, J.O.; Aigbodion, V.S. Bagasse filled recycled polyethylene bio-composites: Morphological and mechanical properties study. *Results Phys.* **2013**, *3*, 187–194. [CrossRef]
39. Chun, K.S.; Husseinsyah, S.; Osman, H. Mechanical and thermal properties of coconut shell powder filled polylactic acid biocomposites: Effects of the filler content and silane coupling agent. *J. Polym. Res.* **2012**, *19*, 9859. [CrossRef]
40. Duan, J.; Wu, H.; Fu, W.; Hao, M. Mechanical properties of hybrid sisal/coir fibers reinforced poly(lactide) biocomposites. *Polym. Compos.* **2018**, *39*, E188–E199. [CrossRef]
41. Liang, Z.; Wu, H.; Liu, R.; Wu, C. Preparation of Long Sisal Fiber-Reinforced Polylactic Acid Biocomposites with Highly Improved Mechanical Performance. *Polymers* **2021**, *13*, 1124. [CrossRef]
42. Petinakis, E.; Liu, X.; Yu, L.; Way, C.; Sangwan, P.; Dean, K.; Bateman, S.; Edward, G. Biodegradation and thermal decomposition of poly(lactic acid)-based materials reinforced by hydrophilic fillers. *Polym. Degrad. Stab.* **2010**, *95*, 1704–1707. [CrossRef]
43. Jiang, L.; Shen, T.; Xu, P.; Zhao, X.; Li, X.; Dong, W.; Ma, P.; Chen, M. Crystallization modification of poly(lactide) by using nucleating agents and stereocomplexation. *e-Polymers* **2016**, *16*, 1–13. [CrossRef]
44. Suryanegara, L.; Nakagaito, A.N.; Yano, H. Thermo-mechanical properties of microfibrillated cellulose-reinforced partially crystallized PLA composites. *Cellulose* **2010**, *17*, 771–778. [CrossRef]
45. Shih, Y.-F.; Huang, C.-C. Polylactic acid (PLA)/banana fiber (BF) biodegradable green composites. *J. Polym. Res.* **2011**, *18*, 2335–2340. [CrossRef]
46. Aliotta, L.; Sciarra, L.M.; Cinelli, P.; Canesi, I.; Lazzeri, A. Improvement of the PLA Crystallinity and Heat Distortion Temperature Optimizing the Content of Nucleating Agents and the Injection Molding Cycle Time. *Polymers* **2022**, *14*, 977. [CrossRef] [PubMed]

**Disclaimer/Publisher’s Note:** The statements, opinions and data contained in all publications are solely those of the individual author(s) and contributor(s) and not of MDPI and/or the editor(s). MDPI and/or the editor(s) disclaim responsibility for any injury to people or property resulting from any ideas, methods, instructions or products referred to in the content.

Review

# Polymer-Based Hydrogel Loaded with Honey in Drug Delivery System for Wound Healing Applications

Siti Nor Najihah Yasin, Zulfahmi Said \*, Nadia Halib, Zulaiha A Rahman and Noor Izzati Mokhzani

Department of Basic Sciences and Oral Biology, Faculty of Dentistry, Universiti Sains Islam Malaysia, Tower B, Persiaran MPAJ, Jalan Pandan Utama, Pandan Indah, Kuala Lumpur 55100, Malaysia; sitinajihah.yasin@gmail.com (S.N.N.Y.); nadia.halib@usim.edu.my (N.H.); zulaiha@usim.edu.my (Z.A.R.); n.izzati9802@raudah.usim.edu.my (N.I.M.)

\* Correspondence: zulfahmi@usim.edu.my

**Abstract:** Excellent wound dressings should have crucial components, including high porosity, non-toxicity, high water absorption, and the ability to retain a humid environment in the wound area and facilitate wound healing. Unfortunately, current wound dressings hamper the healing process, with poor antibacterial, anti-inflammatory, and antioxidant activity, frequent dressing changes, low biodegradability, and poor mechanical properties. Hydrogels are crosslinked polymer chains with three-dimensional (3D) networks that have been applicable as wound dressings. They could retain a humid environment on the wound site, provide a protective barrier against pathogenic infections, and provide pain relief. Hydrogel can be obtained from natural, synthetic, or hybrid polymers. Honey is a natural substance that has demonstrated several therapeutic efficacies, including anti-inflammatory, antibacterial, and antioxidant activity, which makes it beneficial for wound treatment. Honey-based hydrogel wound dressings demonstrated excellent characteristics, including good biodegradability and biocompatibility, stimulated cell proliferation and reepithelization, inhibited bacterial growth, and accelerated wound healing. This review aimed to demonstrate the potential of honey-based hydrogel in wound healing applications and complement the studies accessible regarding implementing honey-based hydrogel dressing for wound healing.

**Citation:** Yasin, S.N.N.; Said, Z.; Halib, N.; Rahman, Z.A.; Mokhzani, N.I. Polymer-Based Hydrogel Loaded with Honey in Drug Delivery System for Wound Healing Applications. *Polymers* **2023**, *15*, 3085. <https://doi.org/10.3390/polym15143085>

Academic Editors: Raffaella Striani and Marcel Popa

Received: 29 March 2023

Revised: 1 May 2023

Accepted: 18 May 2023

Published: 18 July 2023



**Copyright:** © 2023 by the authors. Licensee MDPI, Basel, Switzerland. This article is an open access article distributed under the terms and conditions of the Creative Commons Attribution (CC BY) license (<https://creativecommons.org/licenses/by/4.0/>).

**Keywords:** wound healing; wound dressings; hydrogel; honey; natural polymer; synthetic polymer

## 1. Introduction

Wounds are typically defined as damage to the skin as well as to epidermal- or dermal-layer structures. They can be categorized as acute or chronic wounds depending on their duration and the nature of the healing process [1]. Wound healing is a dynamic and sophisticated tissue regeneration process that repairs the damaged skin and other soft tissues locally or systematically. It involves four temporal stages: hemostasis, inflammation, proliferation, and remodeling [2].

Wound dressings play a significant role in offering the optimum conditions for wound healing and protecting the wounds from further damage and infection. Conventional dressings, including gauzes, plasters, and bandages, are used as primary and secondary dressings for protection against microbial infections [3]. However, these dressings absorb a high amount of moisture on the wound, and can dry and adhere to the wound surface and cause pain when removed [4]. Additionally, some of these dressings might not have antimicrobial, antioxidant, and other bioactive components [5]. Therefore, it is essential to design appropriate dressings that can be easily detached and do not cause any harm to the surface of wounds during dressing replacement [6]. Additionally, it should offer excellent antimicrobial activity, excellent mechanical properties, be able to deliver bioactive agents [7], provide a physical protective barrier, promote the deposition of the extracellular matrix (ECM), and maintain an optimal environment on the wound site, as well as promote the process of wound healing [8].

Hydrogels are three-dimensional (3D) networks made up of hydrophilic polymers formed through hydrogen or covalent crosslinking using the process of a physical or chemical reaction [9]. Hydrogels are commonly employed as wound dressings and have been proven effective, mainly for treating wounds and skin ulcers [10]. These 3D polymer networks can absorb a tremendous amount of liquid, offer a humid environment, excellent biocompatibility [11], biodegradability, and adhesion that can efficiently stimulate cell proliferation and facilitate the process of wound healing as well as improve the stage of wound repair [5]. In addition, the hydrophilic groups in the polymeric chains cause the hydrogel dressings to retain water, with a higher water content ensuring a good porosity, softness, and elasticity [12] and a cooling effect, thus minimizing pains upon removal [13].

Hydrogels can be prepared through natural polymers, including alginate, chitosan, hyaluronic acid, cellulose, starch, gelatin, etc., or synthetic polymers such as polyvinyl alcohol (PVA), polyacrylamide, polyethylene glycol (PEG), etc., or a combination of both polymers [14]. These combinations, which are known as hybrid polymers, could enhance their individual physicochemical, mechanical, and biological properties and promote healing [13]. Some examples of this combination include PVA/chitosan [15], PVA/starch [16], polyacrylamide/chitosan [17], etc. Hydrogel-based wound dressings are well recommended for their healing-promoting properties, which speed up the proliferation and epithelialization processes [8]. Therefore, they are acceptable as first aid for wound care [18]. Excellent wound dressings that are prepared from the polymers as mentioned earlier can be further enhanced by incorporating nature-based bioactive agents [19].

Honey has been applied for centuries as a treatment for infected wounds to accelerate the process of wound healing. Honey is gaining considerable attention as a regenerative agent to treat ulcers, bed sores, skin infections, wounds, and burns. It offers antimicrobial, anti-inflammatory, and antioxidant activity and maintains a moist wound environment that acts as a protective barrier to prevent infection [20]. It also demonstrates the ability to recover the development of new tissue to heal the wound through epithelization. Honey rapidly clears wounds when applied topically to promote the deep healing of wounds with infection [21]. The lower pH of honey (pH 3.5–4.0) could inhibit protease activity, which increases oxygen release from hemoglobin, and promotes macrophage and fibroblast activity on a wound site. In contrast, hydrogen peroxide sterilizes the wound and stimulates vascular endothelial growth factor (VEGF) production [22].

The application of honey-based hydrogel wound dressings has been practiced in the biomedical field. Some studies have demonstrated that honey-based hydrogel dressings can increase water absorption and swellability, support epithelization, stimulate cell proliferation, inhibit bacteria growth, and accelerate wound healing [23–25]. This review aimed to focus on the potential of using honey incorporated into hydrogel patch formulation as a promising approach for wound healing applications and highlight the honey-based hydrogel's properties in treating wound infection.

## 2. The Phase of Wound Healing

The process of wound healing is dynamic and sophisticated, consisting of four overlapping phases: hemostasis, inflammation, proliferation, and remodeling [26,27] (Figure 1). Hemostasis begins with blood coagulation, including the formation of fibrin clots, degranulation, platelet accumulation, and release of growth factors. As a result, fibroblasts, macrophages, and endothelial cells become involved in wound healing [28].

In the inflammatory stage, neutrophils protect the wound against pathogenic infections and cleanse the wound from cellular debris to create a favorable condition for rapid healing [29]. Exudates are responsible for inflammation symptoms, such as redness, warmth, erythema, and swelling of the damaged skin. New epithelial cells infiltrate the wound environment to replace the dead cells due to damaged skin [19]. The severity of the damage determines the duration of the hemostasis and inflammatory stages [30].

In the proliferative stage, cell proliferation and connective tissue formation occur. Next, ECM components, such as hyaluronic acid and glycosaminoglycan, contribute to the



production of granulation tissue to replace the primary clot development. This stage can last several days to a few weeks following injury [31]. The final stage is a remodeling or maturation phase that starts around weeks and lasts up to months. Finally, the surface of the damaged tissue is fully recovered with fibroblast cells with a scar formation [32,33].

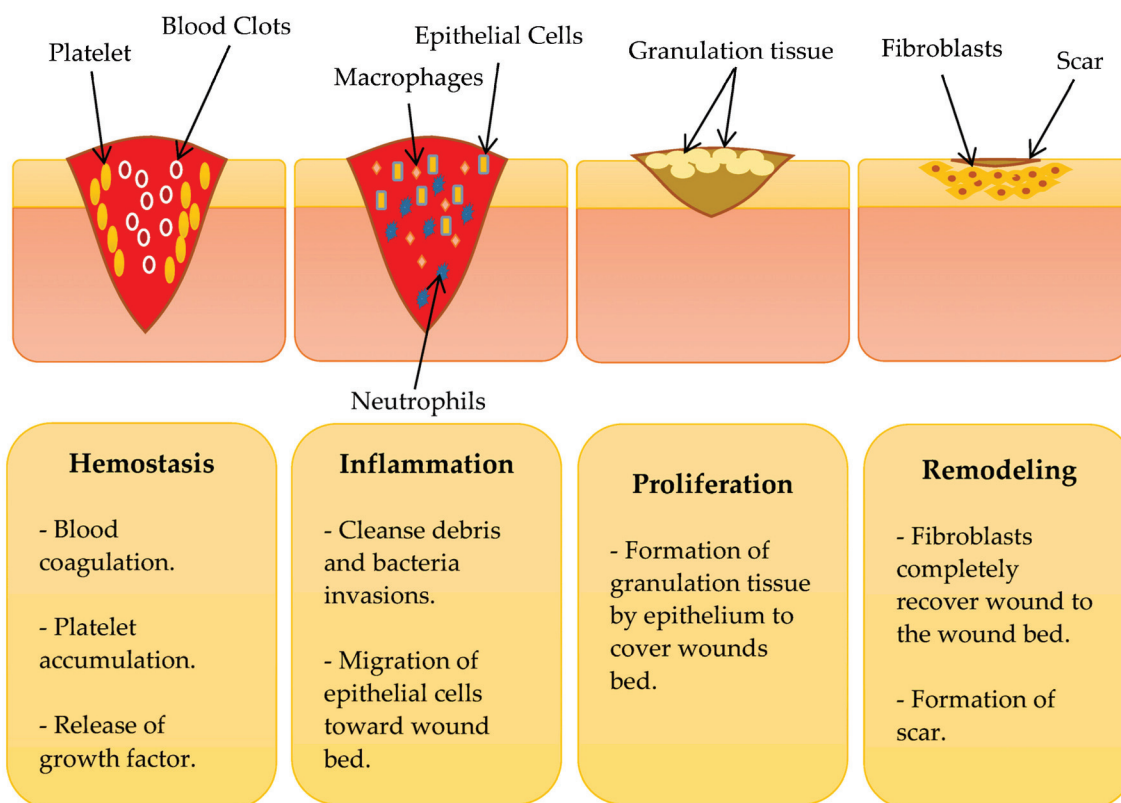


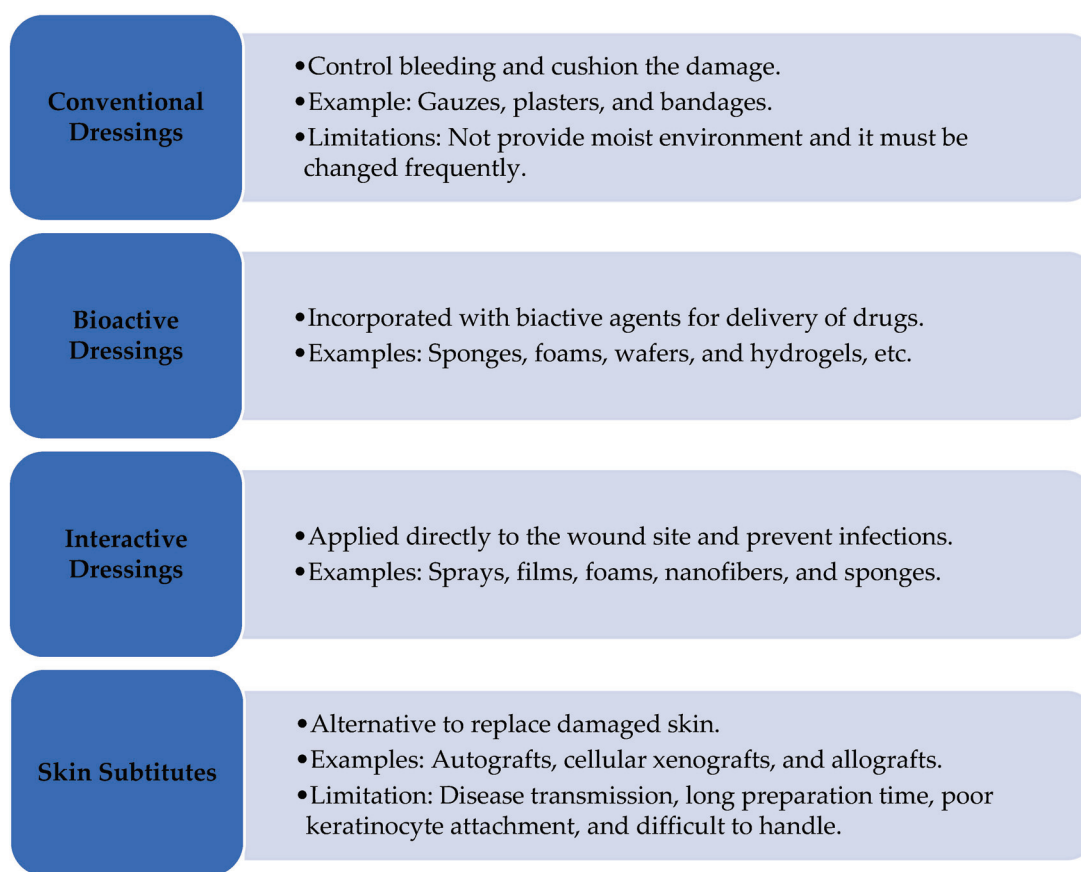
Figure 1. The phases of wound healing. Adapted from Ref. [33].

### 3. Classification of Wound Dressings

Acute or chronic wounds need proper treatment to evade any shortcomings that may arise throughout the healing process. Conventional, bioactive, and interactive dressings and skin substitutes are applied to treat wounds [19] (Figure 2). Conventional wound dressings, or passive dressings, protect wounds against external substances, infection, and damage. Additionally, these dressings function to control blood, cover and absorb wounds, and cushion the damage. Examples of conventional dressings are gauze, plasters, and bandages. However, some limitations of these dressings are that they do not provide a moist environment to the wound bed [34] and must be changed frequently during the healing process, which may cause more skin damage [35].

Bioactive wound dressings are designed to provide bioactive compounds. To improve the therapeutic efficiency of these dressings, they might be incorporated with antimicrobial agents, growth factors, nutrients, nanoparticles, vitamins, plant extracts, and other natural biomaterials to the wound site to promote the healing process [36]. Some formulation-based bioactive wound dressing examples include sponges, foams, wafers, hydrogels, films, membranes, and nanofibers [37]. In addition, bioactive wound dressings have properties that include non-toxicity, excellent biocompatibility, and biodegradability [19].





**Figure 2.** Classification of wound dressings. Adapted from Ref. [19].

Interactive dressings are applied directly to the wound site, removing debris, providing a moist environment, and preventing infections [38]. Examples of these dressings include sprays, films, foams, nanofibers, and sponges. In addition, they are favorable for re-epithelization due to excellent oxygen concentration and pH control [39].

Skin substitutes are wound dressings that are developed to restore damaged skin. They are made up of epidermal and dermal layers that are formed by fibroblasts and keratinocytes on collagen matrices. The primary mechanism of these dressings is to secrete and stimulate growth factors through which epithelization is achieved [3]. Autografts, acellular xenografts, and allografts are some forms of skin substitute wound dressings. The advantages of these wound dressings include minimizing scar formation, providing pain relief, and accelerating healing. However, some limitations of these dressings are possible disease transmission, long preparation time, poor keratinocyte attachment, difficulty handling, etc. [40].

#### 4. Polymer-Based Hydrogels for Wound Healing

The polymer-based hydrogel can be employed in biomedical applications for wound healing, drug delivery, and tissue engineering [41]. They can be classified as natural, synthetic, and hybrid (combination of natural and synthetic) polymers (Figure 3). Excellent polymer-based hydrogel wound dressings should have appropriate features, including good biocompatibility and biodegradability, meaning the hydrogels could fully degrade after a duration [5,11,42]. Additionally, it should have adequate adhesion and excellent mechanical properties to ensure it can adhere to and cover the wounds entirely to prevent microbial infection [43]. In addition, the hydrogels should provide and maintain a humid environment at the wound site for cell migration and proliferation [11,44]. Therefore, dressing selection needs careful consideration before promoting the healing process [45].

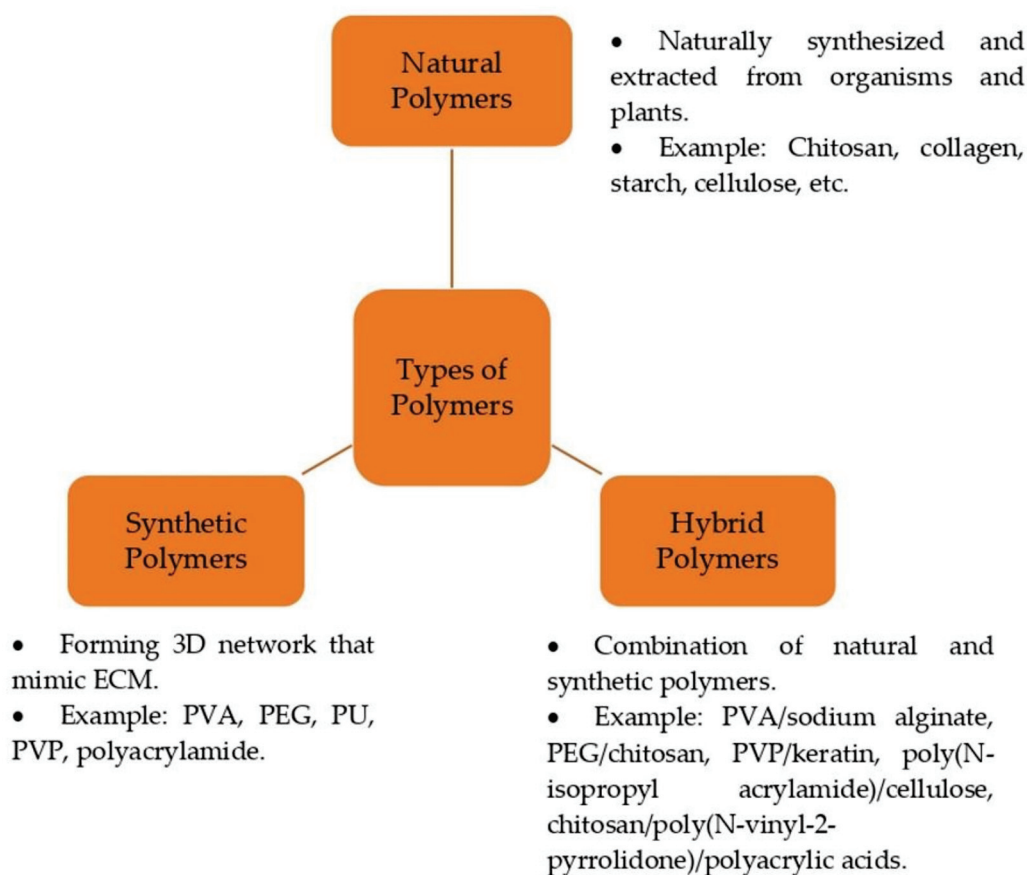


Figure 3. Types of polymers.

#### 4.1. Natural Polymer

Natural polymers have been applied over the centuries as the primary bioactive substance in biomedical fields [45]. These polymers are naturally synthesized and extracted from organisms and plants. Natural polymers including chitosan, collagen, starch, cellulose, sodium alginate, agarose, gelatin, and hyaluronic acid are some examples that are broadly utilized in synthesizing hydrogel wound dressings [14,46].

The interest in utilizing natural polymers as a hydrogel includes for their biodegradability, biocompatibility, non-toxicity, and low immunogenicity, and the structures are similar to that of ECM [47]. They may also produce by-products that are well tolerated by living organisms without triggering toxic reactions when subjected to enzymatic degradation [48]. However, they have some limitations, such as pathogenic contamination, uncontrollable degradation rate, complex modification, and low mechanical properties, which may restrain tissue regeneration application [49].

#### 4.2. Synthetic Polymer

Synthetic polymers are beneficial in a few properties over natural polymers, such as endless forms, tunable properties, non-toxicity, and established structures [45]. Synthetic polymers are typically designed to mimic the structures of natural polymers, with minor modifications to enhance desired properties. These polymers contribute to forming a controlled 3D network with a high molecular weight, new functional groups, and charged groups. Some examples of synthetic polymers include PVA, PEG, polyurethane (PU), polyvinyl pyrrolidone (PVP), and polyacrylamide [5]. In addition, the derivations of cellulose, acrylic acid polymers, and vinyl polymers are some of the most commonly used synthetic polymers [46]. The limitations of these polymers are that they have insufficient cell adhesion sites, require chemical modifications to improve cell adhesion [50], are impermeable to drugs and proteins, and have poor mechanical stability [51].

#### 4.3. Hybrid-Based Polymers

Hybrid-based polymers are developed through the combination of at least two or more polymer-based natural and synthetic polymers. Each polymer holds specific physicochemical and biological properties in a blending [52]. Several researchers have investigated if hybrid hydrogels can be widely used to overcome the limitations of both polymer types [13], as they possess the advantages of both natural and synthetic polymers in terms of their physicochemical, mechanical, and biological activities [53]. Additionally, these hybrid hydrogels could offer excellent flexibility, biocompatibility, biodegradability, and high absorption capacity and promote wound healing [54]. Some examples of hybrid polymers include PVA/sodium alginate [55], PEG/chitosan [56], PVP/keratin [57], poly(N-isopropyl acrylamide)/cellulose [58], chitosan/poly(N-vinyl-2-pyrrolidone)/polyacrylic acids [59], etc.

### 5. Physicochemical Properties and Composition of Honey

Honey is a raw substance with a sophisticated chemical composition and wound-healing properties. In addition, it has a broad range of physicochemical properties and compositions dependent upon its botanical and geographical areas [60].

The physicochemical composition of honey includes acidity, pH, moisture, ash content, hydroxymethylfurfural (HMF), sugar content, and enzyme activity. The chemical composition of honey encompasses various constituents that contribute to its biological activities. These constituents include proteins, organic acids, enzymes, phenols, flavonoids, vitamins, etc. These components play a role in honey's beneficial effects and potential wound-healing properties [61].

A previous study has investigated the nutritional index of honey from diverse botanical areas. They found that honey's moisture content ranges from 27–31% of honey. The ash levels were 0.15–0.9%, while the protein content was 0.2–0.8%. Additionally, the sugar content for glucose, fructose, and sucrose was 29–31%, 45–48%, and 2–4%, respectively. The HMF value also should not be more than 60 mg/kg. Its pH levels are between 3.24 to 6.1. Honey contains several active compounds, including flavonoids, organic acids, phenolic acid, vitamins, and enzymes, that may improve wound healing [62].

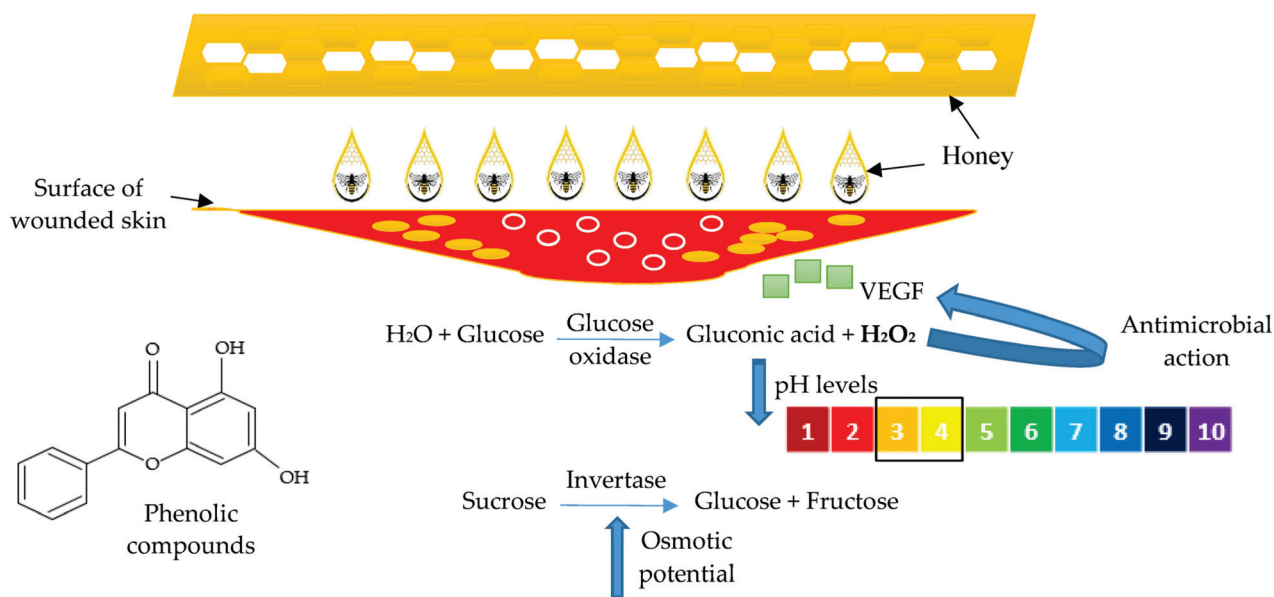
### 6. Biological Activity of Honey in Wound Healing

Honey has been well-known for wound treatment since ancient times. The healing properties of honey are related to its antioxidant, anti-inflammatory, and antimicrobial activities, and its capabilities of maintaining a moist wound environment, protecting the wound, and preventing pathogenic infection [20]. The immunological activity of honey is also crucial in wound healing as it has pro- and anti-inflammatory properties [63]. In addition, honey has antimicrobial properties and has the potential to counter wound infections and function as a physical barrier to the wound area, as well as promote wound healing [21]. The antimicrobial properties found in honey play a significant role in the body's response to tissue damage [64].

Honey may aid in regenerating damaged tissues and wound healing as it contains a high sugar content, reactive oxygen species generation, and anti-inflammatory properties [65]. Additionally, honey can sterilize wound infection, stimulate the growth of tissues and re-epithelization, and reduce scar formation. These factors contribute to the four phases of wound healing, as stated above [66]. Honey demonstrates diverse effects in each stage of the wound-healing process [67]. During the inflammatory stage, honey inhibits bacterial placement, lowers pH, increases antioxidant action, increases peroxide generation, and releases pro-inflammatory cytokines [68]. It then promotes epithelization and proliferation while decreasing edema and exudate in the wound during the proliferative stage. Next, during the remodeling stage, honey helps to recover the wound and prevent scar formation [32].

Additionally, hydrogen peroxide ( $H_2O_2$ ) production on glucose is another characteristic of honey that causes antimicrobial action. This compound catalyze by glucose oxidation of glucose which lead to the production of gluconic acid and hydrogen peroxide [68]. The

formation of gluconic acid contributes to a decrease in pH levels, while hydrogen peroxide enhances the antimicrobial properties of honey. This cascade of events, which includes pH reduction to levels between 3.5–4.0, is crucial for initiating the tissue repair process [68,69]. Furthermore,  $H_2O_2$ -dependent honey may stimulate the synthesis of vascular endothelial growth factor (VEGF) and sterilize the wound site [22]. In addition to glucose oxidase, bees create invertase, which enhances the osmotic potential of honey by breaking down sucrose into fructose and glucose (Figure 4) [69]. The production of  $H_2O_2$  also tends to be toxic to the cellular tissue when it is too saturated. However, it can be countered with an antioxidant compound inside the honey [70].



**Figure 4.** The fundamental principle of honey in wound healing. Adapted from Ref. [69].

The antioxidant properties are also other medicinal properties of honey that have been studied. The antioxidant action in honey is enhanced by the presence of phenolic compounds [66]. Plants create various secondary metabolites in response to environmental stresses and oxidative damage. These compounds are transferred to honey through nectar. The phenolic compounds are divided into two categories, which are phenolic acids and flavonoids. Free radicals are scavenged by phenolic acids and flavonoids, which reduce tissue damage and inflammation. In biomedical fields, honey has been employed to treat wounds, burns, and inflammation, and has a synergistic effect when combined with antimicrobial agents [22,71]. Previous research discovered that the relative positions of OH groups in the aromatic ring affect the antioxidant effect of phenolic acids and are also found to be the most potent antioxidant among all phenolic acid compounds [72].

The current therapeutic applications used in wound management are beneficial for inhibiting bacterial infection and promoting healing [73]. Using natural products with antimicrobial properties in biomedical research has garnered considerable attention in modern medicine [71]. The excellent properties of natural products, including honey, curcumin, and aloe vera, are the most prominent arguments for applying natural products in treating wounds [74]. Honey has been a topical treatment since ancient times and has been officially recognized as a medical device in conventional medicine, and can be combined with silver dressings or other formulations [56,63]. Table 1 shows the comparison between honey and some bioactive substances that are commonly utilized in wound healing applications.

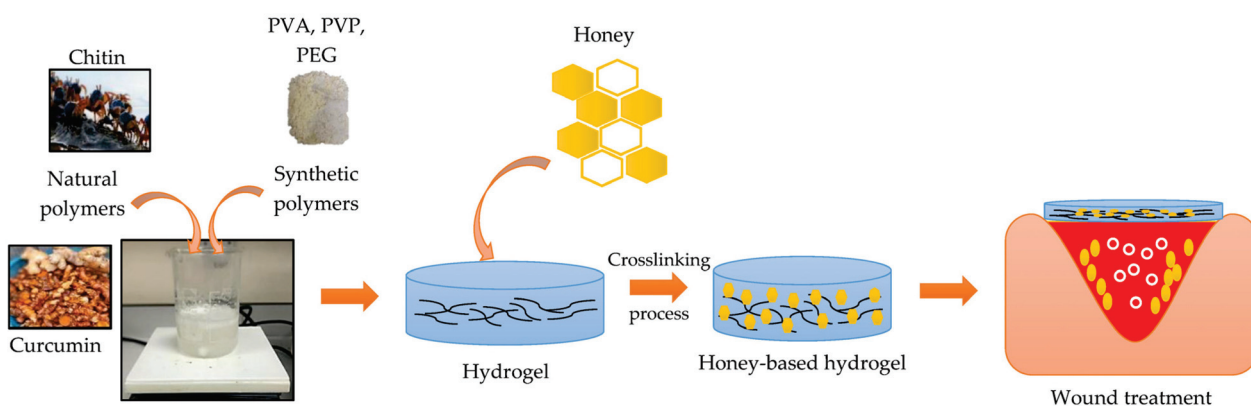
**Table 1.** Comparison between honey and other bioactive substances for wound healing applications.

Bioactive Substances	Advantages	Disadvantages	References
Honey	<ul style="list-style-type: none"> <li>- Rapid epithelization and wound contraction.</li> <li>- Reduced pain and inflammation.</li> <li>- Cost-effective.</li> </ul>	<ul style="list-style-type: none"> <li>- Give a stinging sensation in some patients that can cause some discomfort.</li> </ul>	[20]
Epidermal Growth Factor	<ul style="list-style-type: none"> <li>- Maintains tissue hemostasis by regulating cell survival, proliferation, migration, and differentiation.</li> </ul>	<ul style="list-style-type: none"> <li>- Short in vivo half-life due to low stability.</li> <li>- Restricted absorption to the wound site.</li> <li>- Elimination by exudation before reaching the wound site.</li> <li>- High-cost dressings.</li> </ul>	[75]
ECM Protein	<ul style="list-style-type: none"> <li>- Regulates cell differentiation, migration, and proliferation.</li> </ul>	<ul style="list-style-type: none"> <li>- Uncontrolled cell growth and invasion.</li> <li>- Impaired apoptosis and cell differentiation.</li> <li>- Dysfunction of all the normal functions of the skin.</li> </ul>	[76]
Silver sulfadiazine	<ul style="list-style-type: none"> <li>- Prevent and treat wound infection (second and third-degree burns).</li> </ul>	<ul style="list-style-type: none"> <li>- Toxic to fibroblasts when applied in high concentrations.</li> </ul>	[77]

## 7. Application of Honey-Based Hydrogel for Wound Healing

Hydrogels combined with honey have multiple benefits and are considered ideal wound dressings to promote healing [20,78,79] (Figure 5). Hydrogels are 3D structures crosslinked with hydrophilic characteristics that can hold abundant volumes of water and other liquids [11,80]. Thus, it is applicable for wound healing due to its high porosity, excessive water content, ability to release therapeutic agents, excellent biocompatibility, biodegradability, and it can accelerate the wound healing process [5,19,81]. Furthermore, honey has been traditionally utilized as a wound dressing to accelerate and enhance the process of wound healing. Therefore, incorporating honey into the hydrogel could be effective for wound healing [20,82].





**Figure 5.** Schematic of honey-based hydrogel for wound healing. Adapted from Ref. [82].

Chopra et al. prepared a natural chitosan and PVA to formulate a hydrogel film incorporating honey for wound healing treatment and evaluated their physicochemical and mechanical properties. The findings showed that the thickness and weight of the films were between  $0.041 \pm 0.006$  to  $0.055 \pm 0.004$  mm, and  $0.425 \pm 0.02$  to  $0.480 \pm 0.04$  g, respectively. The folding endurance ranged from  $350 \pm 15$  to  $445 \pm 7$ . The folding endurance values increase as the chitosan concentration increases from F1–F5 (0.25–2%). The formulation of batch F5 (2% of chitosan) gives a smooth surface and homogenous form with little porosity, exhibiting excellent structural integrity. Additionally, the hydrogel's moisture content increases as the chitosan concentration increases. Swelling analysis indicates that increasing the chitosan concentration may increase the water's swelling ratio. The F5 showed the highest swelling ratio, with 300% after 24 h. For mechanical characteristics, the results showed a value from  $4.74 \pm 0.83$  to  $38.36 \pm 5.39$  N for tensile strength, and  $30.58 \pm 3.64$  to  $33.51 \pm 2.47$  mm for elongation at the break, respectively. A strong interaction and network between the polymers could enhance the mechanical characteristics of the hydrogel film. In addition, an antimicrobial study against *Staphylococcus aureus* (*S. aureus*) demonstrated that a honey-based hydrogel film exhibited antimicrobial activity with excellent bacteriostatic ability. The F4 showed an excellent antimicrobial effect, with the diameter of the inhibition zone being  $5.01 \pm 0.32$  mm [83].

Additionally, a study by Gopal et al. incorporated Kelulut honey and Tualang honey into cellulose/PEG hydrogels to treat wound infections. The finding showed that the honey hydrogels showed excellent antimicrobial activity compared to the control hydrogels. Tualang honey hydrogels exhibited the highest zone of inhibition for negative *Escherichia coli* (*E. coli*), and *S. aureus*, which could be influenced by the highly acidic component with pH 3.55–4.0 which may inhibit both bacteria. For *E. coli*, the Kelulut honey hydrogels showed slightly higher inhibition zones than the Tualang honey hydrogels. Meanwhile, for *S. aureus*, the Tualang honey hydrogels exhibited higher inhibition zones than the Kelulut honey hydrogels. In vitro cell viability testing indicated that both honey-based hydrogels recorded the maximum cell viability (90%) compared to control hydrogels without the incorporation of honey, which recorded the minimum viability [23].

Lo et al. conducted a study that formulated cellulose/poly(lactic-co-glycolic acid) (PLGA) patches incorporated with Kelulut honey for aphthous stomatitis treatment. The ATR–FTIR study was utilized to analyze the morphology of the patches. In vitro cell viability analysis indicated that the Kelulut honey patch stimulated an increase in cell viability percentage by more than 90% compared to the control, which can promote angiogenesis by supporting tissue regeneration and skin re-epithelization. Additionally, the PLGA polymer released the honey into the extracellular matrix and rapidly closed the wound gap. In vivo analysis also demonstrated that the honey patches could inhibit the growth of *E. coli* in the first 2 h, followed by the inhibition of *S. aureus* in the next 2 h [84].

Zekry et al. investigated the PVA/honey hydrogel for wound healing. They prepared Manuka honey (MH)/pomegranate peel powder (PPP)/PVA (10%/1%/12%), MH/PPP/PVA (20%, 2%,

10.5%), MH/PPP/PVA (25%/2.5%/9.7%), MH/PPP/BV/PVA (25%/2.5%/0.01%/9.7%), and LH/PPP/BV/PVA (25%/2.5%/0.01%/9.7%). Scanning electron microscopy (SEM) was used to analyze the morphological structures of all formulations. The *in vitro* release study displayed that the honey was released over 24 h with a low adhesion to the wound site, stimulating cell proliferation and re-epithelization. Additionally, *in vivo* analysis of the wound healing activity indicated that all treated groups achieved complete healing on day 10, compared to the PVA control group (day 13) and no treatment groups (day 14) which demonstrated slowed healing processes. Moreover, at day 3 and 5, the commercial Medihoney<sup>®</sup> group showed a higher percentage of wound closure compared to the PVA control and no treatment groups. Additionally, the honey hydrogel inhibited 90–98% of the *S. aureus* and *E. coli* growth, which showed good antimicrobial activity compared to controls [85].

Samraj et al. studied a combination of Kelulut honey with curcumin in the nanofibrous composite hydrogel membrane to treat wound healing. The findings showed that the impregnation of curcumin and honey promotes healing by stimulating cell migration and promoting recovery through anti-inflammatory properties. In addition, impregnating honey with curcumin promotes new cell regeneration and prevents scar formation. *In vitro* and *in vivo* rat models showed improved recovery and no cytotoxicity compared to control groups without treatment. Furthermore, antioxidant and antimicrobial studies demonstrated that the activity of wound healing with the hydrogel membrane was significantly higher than curcumin and honey alone. Therefore, incorporating honey into composite hydrogel membranes may assist in wound healing [86].

A previous study by Noori et al. developed a nanocomposite hydrogel using PVA/chitosan/honey/montmorillonite (PCMH). SEM and XRD were employed to perform the morphological analysis of the hydrogel film. Additionally, swelling tests were performed at 37 °C, and the results demonstrated that the swelling increased as the temperature increased. Furthermore, the 3-(4,5-dimethylthiazol-2)-2,5-diphenyltetrazolium bromide (MTT) analysis revealed that the PCMH hydrogel had a higher cell viability above 75% after 24 h, indicating no cytotoxicity. For pure chitosan, it was shown that the cell viability was more than the control group. This indicated that the pure chitosan itself could stimulate cell proliferation. An *in vitro* study against *S. aureus* has shown that PCMH hydrogel showed a more significant antibacterial value of higher than 99%, which demonstrated that it can restrict the growth of bacteria. Additionally, wound healing activity was evaluated in rats through *in vivo* analysis, and the results showed that PCMH hydrogel reduced the wound area more significantly than the control group and showed better wound healing ability, a rapid rate of honey release, restricted bacterial growth, and reduced the length of the wound healing process through cell reepithelization and proliferation. These results indicate that honey-based hydrogels could be applied as a wound-healing treatment [24].

The studies *in vitro* and *in vivo* performed by El-Kased have incorporated Egyptian honey (25, 50, and 75%) into chitosan/polyacrylic acid hydrogels for treating burn-wound healing. The findings showed that all hydrogel formulations exhibited a rapid swelling behavior due to their porous structure, providing a large surface area for rapid solvent uptake. Additionally, the swelling index was found to be inversely proportional to the honey concentration, indicating that an increase in honey concentration results in a decrease in the hydrogel's swelling percentage. This factor may be affected by the polymer's viscosity, which can impact the swelling process. *In vitro* release studies revealed that the release of honey from the hydrogel depended upon the honey concentration. Among all formulations, hydrogels with the lowest concentration of honey (25%) showed superior sustained release with 70% of release over 3 h. *In vitro* antimicrobial analysis showed that 75% of honey incorporated into hydrogels showed the highest healing rate as it stimulated cell re-epithelization and excellent antimicrobial activity compared to pure honey and commercial products [87].

Yang et al. developed nanofibrous silk fibroin and polyethylene oxide (PEO) with various concentrations of Manuka honey (10%, 30%, 50%, and 70% *w/v*) using an electrospinning technique. The FTIR was used to study the structural behavior of the fibrous matrices. The findings showed that the honey-based hydrogel dressings exhibited an-

antimicrobial activity against *E. coli*, *S. aureus*, *P. aeruginosa*, and MRSA, in which the results revealed that the non-honey dressing was approximately zero, but antimicrobial activity improved to around a 50%, 28%, 57% and 40% inhibition of *E. coli*, *S. aureus*, *P. aeruginosa*, and MRSA, respectively, for the 70% *w/v* honey hydrogel over 24 h. Furthermore, *in vitro* biocompatibility analysis showed that hydrogel containing honey had a higher viability than the control. However, the increasing concentration of honey did not change the cell viability, demonstrating that the incorporation of honey does not negatively affect the excellent biocompatibility of the hydrogel. Additionally, *in vivo* analysis in a rat dorsal wound model showed that the wounds treated with 70% honey hydrogel wholly recovered, whereas both the control group and commercial Aquacel<sup>®</sup> Ag wound dressing group had only slight reductions in wound size [88].

Another study by Tavakoli and Tang fabricated a polyvinyl alcohol/Manuka honey hybrid hydrogel wound dressing with borax as a crosslinking agent. Hydrogels prepared with 1% borax demonstrated adequate biocompatibility, a sustained release of honey in the ulcer bed, and no burst release of antibiotics. The addition of borax also increased the mechanical durability of the honey/PVA hybrid and prevented hydrogel degradation during the swelling process. This thin layer of hydrophilic gel may improve the wound-healing process and reduce the risk of contamination. The results demonstrated that the honey showed good antibacterial activity against *S. aureus* in all samples, especially in the samples with a 1% crosslinking agent. The results showed that the PVA/borax/honey hybrid hydrogel demonstrated the greatest swellability and stability and had excellent antimicrobial activity, and indicated that PVA/honey hydrogel produced the best characteristics for applying to wound dressing [25].

Durai and Sizing fabricated chitosan hydrogel films impregnated with 8% Manuka honey to treat wounds. The results revealed that honey increased the folding endurance, with the honey hydrogel films surviving a mean of 289 folds compared to 143 folds for the non-honey films. This result demonstrates a greater flexibility of the honey hydrogel film due to the hygroscopic effect of honey. Additionally, honey reduced the swelling ratios of the hydrogel films and inhibited the growth of *S. aureus* and *E. coli*. In an *in vivo* analysis of a rat dorsal wound model, the honey hydrogel showed an increased wound gap compared with control groups of non-honey and ointment. The honey hydrogel and non-honey hydrogel showed closures of 94% and 78% after 12 days of treatment, compared with the ointment-treated group and the non-treated control whose wounds showed closures of 86% and 64%, respectively [89].

Zohdi et al. developed a hydrogel dressing incorporating Gelam honey into the polyvinyl pyrrolidone (PVP)/protein-free agar/polyethylene glycol (PEG) hydrogel with a 6%, 8%, 10%, and 15% concentration of honey. The finding showed that the honey hydrogel and the control group had good uniformity and transparency with a 3–4 mm thickness. Additionally, the pH of the honey hydrogel was slightly acidic, with a value of pH 4.3, while the control group had a pH of 5.3. This slight acidity in the hydrogel may be due to the natural acidic properties of honey, which typically has a pH ranging from 3.2 to 4.5. For swelling analysis, the honey hydrogel demonstrated a high capability in absorbing fluid compared to the control group. The *in vivo* analysis in rats revealed that the honey hydrogel dressing stimulated wound closure and promoted the process of reepithelization better than the control group. Furthermore, the histopathological analysis showed that the honey hydrogel attenuated the inflammatory response on day 7, earlier than the control group. Moreover, honey hydrogel facilitates the growth of granulation tissue and blood capillary and collagen synthesis, which is effected by the generation of hydrogen peroxide by honey [90].

Khoo et al. compared a Tualang honey wound dressing and hydrofiber silver-treated wound dressing. The results demonstrated that the Tualang honey dressing had more flexibility, less adherence, easily peeled, and caused less fluid accumulation in the wound site. Furthermore, according to an *in vivo* study, using Tualang honey for dressing burn wounds resulted in significantly greater wound contraction than applying hydrofiber silver dress-

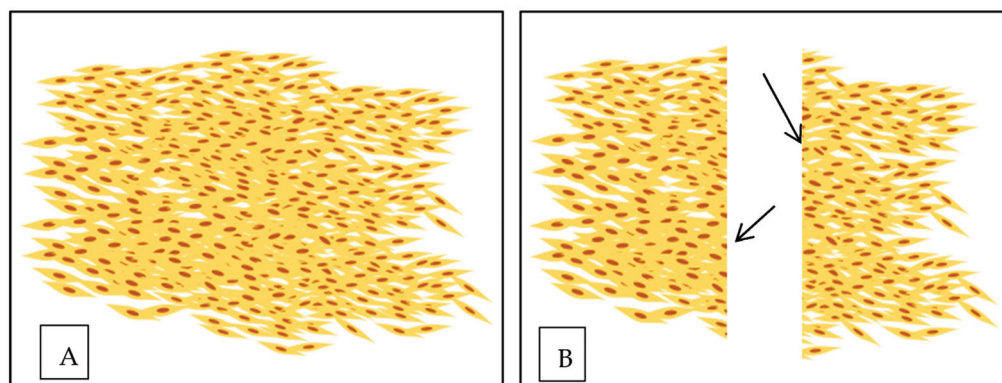
ing. Furthermore, on day 6, the wound area became smaller and showed increasing cell epithelization. Additionally, the Tualang honey -treated wound dressing showed a lower bacterial growth of *Pseudomonas aeruginosa*-inoculated wounds and excellent antibacterial activity [91].

### 8. Cell Migration and Proliferation on Honey-Based Wound Dressings

The scratch- or wound-healing assay is a cost-effective and straightforward experimental method for investigating cell migration [92]. The assay involves growing a cell monolayer in a multiwell assay plate, creating a “wound” or scratch, and then capturing images at regular intervals to measure and quantify cell migration [93] as shown in Figure 6. Scratch assays are commonly employed to study the molecular mechanisms that influence cell migration and to identify therapeutic compounds that can modulate cell migration for potential treatments. Therefore, it is crucial to develop reliable methods for quantifying and comparing migration rates of different scratch assays to advance biomedical research [94]. The wound closure percentage was calculated using the following formula:

$$\% \text{ Wound Closure} = \frac{A_0 - A_T}{A_0} \times 100\%$$

where  $A_0$  is the wound area measured after scratching, and  $A_T$  is the area of the wound measured at a predetermined time.



**Figure 6.** Illustration of in vitro wound healing assay. (A) Fibroblast cells form a confluent monolayer. (B) In vitro “wound” was created by a straight line scratch across the fibroblast monolayer [94].

There are limited studies on utilizing cell-culture applications to perform cellular migration upon honey-based dermal wound dressings, as there are broad studies that have carried out the application of honey dressing in animals to study the effectiveness of honey in wound healing. However, several studies utilize pure honey (with a dilution factor) for wound healing analysis.

For instance, Chaudhary et al. studied the cell migration assay under 0.1% of Manuka honey and 0.1% Jamun honey on primary fibroblast cells from a neuron differentiation medium (NDM) and a decalcified bone matrix (DBM) skin. The results showed that both kinds of honey could stimulate cell proliferation against fibroblast cells over 24 h. However, DBM cells with Manuka honey and Jamun honey migrated faster than NDM cells at 24 h [95].

Ranzato et al. performed a scratch-wound assay on the fibroblast cells using 0.1% *v/v* Manuka, buckwheat, acacia honey, and platelet lysate (PL). The finding showed that the cells exposed to buckwheat and acacia honey showed a higher rate of wound closure at 24 h compared to controls, while Manuka honey showed a lower effect against fibroblast cells [96].

The study by Ebadi and Fazeli performed a wound healing analysis on human dermal fibroblasts using honey and an ethanol extract of propolis (EEP). The finding showed that 100  $\mu\text{g/mL}$  and 200  $\mu\text{g/mL}$  concentrations of EEP demonstrated the highest percentages



of wound closure compared to the control and DMSO control. After 48 h, the wound healed entirely at the 100 µg/mL and 200 µg/mL concentrations. For the honey analysis, the 25 µg/mL to 200 µg/mL concentrations showed a slight increase in the percentage of wound closure, while for the 100 µg/mL and 200 µg/mL concentrations, the wound healed after 48 h, faster than both control groups. The EEP and honey concentrations of 100 µg/mL and 200 µg/mL showed remarkable wound closure after 24 and 48 h compared to both control groups [97].

An MTT assay also can be performed to assess cell proliferation. A study by Lau et al. performed a cell proliferation assay under different concentrations of Tualang honey on human periodontal ligament fibroblast cells (HPDLF). The finding showed that 0.02% Tualang honey concentration stimulated a higher proliferation rate than the control. However, at a higher concentration of Tualang honey (5%), the cells became rounded and floating, indicating that a higher honey concentration could inhibit cell proliferation [98].

Additionally, Shamloo et al. studied the cell proliferation and biocompatibility of human fibroblast cells using various concentrations (0, 5, 10, and 20%) of a chitosan/honey hydrogel. The finding demonstrated that a 10% concentration of chitosan/honey hydrogel stimulated the highest cell proliferation compared to other hydrogels. It also demonstrated that the addition of honey into hydrogel could offer maximum nutrients for cells, which may increase cell proliferation, as well as cell viability [99].

A study by Sarhan et al. analyzed the cell proliferation of human fibroblast cells when using various types of honey hydrogel (0, 25, 50, 75, and 100% extraction). The findings showed that 100% honey extraction stimulated the highest cell proliferation (>90%) compared to other hydrogels and the positive control, commercial Aquacel<sup>®</sup> Ag. In this study, the Aquacel<sup>®</sup> Ag showed cytotoxic signs with a cell viability of 9% [100].

## 9. Toxicological Information of Honey-Based Wound Dressings

It is essential to consider the toxicological aspects associated with honey-based wound dressings [101]. Among many types of toxicological analyses, the MTT assay is a widely utilized method to evaluate cell viability and cytotoxicity in vitro, which makes it suitable for toxicological analysis in wound-healing applications [102]. Table 2 shows in vitro MTT assays related to applying honey-based wound dressings.

**Table 2.** In vitro MTT assay of honey-based hydrogel wound dressings.

Type of Formulation	Formulation Matrices	Percentage of Honey in the Formulation	Site of Application	Findings	References
Cellulose hydrogel	Sodium carbomethyl cellulose (SCMC)/hydroxypropyl methyl cellulose (HPMC)/polyethylene glycol (PEG)/honey	Kelulut honey (22%) Tualang honey (22%) Asian honey (33%)	Human skin fibroblast cells	All samples showed higher cell viability (<90–100%) compared to control group. Kelulut honey > Asian honey > Tualang honey.	[23]
Hybrid hydrogel film	6% w/w PVA/3, 6, 10% w/w borax/honey	5 g honey	Human fibroblast cells	All samples with different borax concentrations showed <90% cell viability compared to control group.	[25]
Hybrid hydrogel	Cellulose/poly(lactic-co-glycolic acid)(PLGA)/Kelulut honey	Not stated	Human skin fibroblast cell	Honey hydrogel showed maximum cell viability with 218.35 ± 7.80% compared to control.	[84]
Nanofibrous hydrogel	Pomegranate/PVA/honey	Manuka honey: 25% Bee venom honey: 0.01% Lyophilized multiflora honey: 25%	L929 mouse fibroblast cells	All hydrogel scaffolds with different concentrations (and different types of honey) showed <100% cell viability compared to control group, which indicates that all hydrogels have no cytotoxicity against skin cells. Promotes cell migration and proliferation.	[85]
Hybrid hydrogel	3% v/v chitosan/5% w/v gelatin/10% w/v PVA/Iran honey	0, 5, 10, and 20% v/v honey	Human fibroblast cells	Chitosan-based hydrogel showed non-toxicity impacts on the cells, and showed highest biocompatibility. It demonstrated that the addition of honey-based hydrogel could offer the cells with nutrients and increase cell proliferation.	[99]



**Table 2.** *Cont.*

Type of Formulation	Formulation Matrices	Percentage of Honey in the Formulation	Site of Application	Findings	References
Electrospun nanofibrous hydrogel	<ul style="list-style-type: none"> <li>- 3.5% w/v chitosan/7% w/v PVA/30% honey</li> <li>- honey/PVA/chitosan (HPCS)</li> <li>- Honey/PVA/chitosan/<i>Cleome droserifolia</i> (HPCS-CE)</li> <li>- honey/PVA/chitosan/<i>Allium sativum</i> (HPCS-AE)</li> <li>- HPCS/AE/CE</li> </ul>	30% w/v(25, 50, 75, 100% extraction)	HFD4 human fibroblast cells	<ul style="list-style-type: none"> <li>- HPCS and HPCS-CE showed 90% and 87% of cell viability in the 100% extract solution compared to control and commercial Aquacel<sup>®</sup> Ag.</li> <li>- HPCS-AE and HPCS-AE/CE showed decreased cell viability (68% and 75%) in the 100% extract solution.</li> </ul>	[100]
Electrospun nanofibrous hydrogel	<ul style="list-style-type: none"> <li>- 0.8% w/v sodium alginate/7.2% w/v PVA/acacia honey</li> </ul>	0, 5, 10, 15, and 20% v/v honey	NIH3T3 fibroblast cells	<ul style="list-style-type: none"> <li>- The nanofibrous hydrogel loaded with 10% honey showed the highest cell viability with 102.71 ± 1.31%. However, at 20% honey, cell viability decreased to 96.42 ± 0.93%.</li> </ul>	[103]
Electrospun nanofibrous hydrogel sheet	Poly( $\epsilon$ -caprolactone)(PCL)/Manuka honey	1%, 5%, 10%, and 20% v/v	Fibroblast cells	Sample with 20% honey showed the highest cell viability compared to other group and control group.	[104]

### 10. Regulatory Information of Honey-Based Wound Dressing

Honey-based wound dressings are classified as medical devices. They are regulated by various regulatory agencies worldwide [66], including the US Food and Drug Administration (FDA) [105], European Medicines Agency (EMA) [106], National Medical Products Administration (NMPA) [107], Therapeutic Goods Administration (TGA) [108], Health Sciences Authority (HSA) [109], and Medical Device Authority (MDA) [110]. It should be noted that the regulatory requirements for honey-based wound dressings may vary depending on the country and region in which they are commercialized [66].

The importance of providing the regulation information before they can be sold in a country is to assure the quality, efficacy, and safety of products that are used for wound care [111]. Regulatory bodies set standards and guidelines for manufacturing, labeling, and marketing wound-care products, including honey-based wound dressings, to ensure that they meet specific criteria and do not harm patients [112]. By adhering to these regulations, manufacturers can ensure that their products are effective and safe for use, and healthcare providers and patients can have confidence in their products [113]. Additionally, regulatory information can help healthcare providers. Patients make informed decisions about wound care products based on their specific needs and circumstances [111,114]. Table 3 describes the regulatory requirements for honey-based wound dressings based on the country.

**Table 3.** Description of the regulatory body in different countries.

Country Name	Regulatory Body	Regulatory Guidelines	Classification of Wound Dressings	Regulatory Requirements	References
United States	USFDA	21 CFR Part 820	Class I: low to moderate risk Class II: moderate to high risk Class III: high risk	Premarket approval or 510(k) application is required.	[105]
Europe	EMA	Council Directive 93/42/EEC	Class I: low risk Class IIa & IIb: medium risk Class III: high risk	Quality Management Systems (QMS) approval is required.	[106]
China	NMPA	Medical Devices Act	Class I: low to moderate risk Class II: moderate to high risk Class III: high risk	Application form is required, and need an approval before marketing.	[107]

Table 3. Cont.

Country Name	Regulatory Body	Regulatory Guidelines	Classification of Wound Dressings	Regulatory Requirements	References
Australia	TGA	Australian Therapeutic Goods Regulations	Class I: low risk Class II: medium risk	EU approval and CE markage is required.	[108]
Singapore	HSA	Health Product Act	Class A: Low-risk Class B: Moderate-risk Class C: High-risk Class D: In vitro diagnostic (IVD) medical devices	Approval is required.	[109]
Malaysia	MDA	Medical Devices Act 2012 (Act 737)	Class A: Low-risk Class B: Low to moderate-risk Class C: Moderate to high-risk Class D: High-risk	Conformity Assessment Body (CAB) approval is required.	[110]

### 11. Patent Information on Honey-Based Wound Dressings

Patent information in wound dressing refers to the documentation of a novel invention or discovery related to wound dressings, registered with the appropriate government agency for exclusive rights of use and distribution by the inventor or assignee for a certain period [115]. This information can include detailed descriptions of the wound dressing composition, manufacturing methods, potential applications, and any relevant testing or clinical trial results [116].

The importance of patent information in wound dressing lies in the potential value it can offer to researchers, manufacturers, and clinicians involved in wound care. By studying patented wound dressings, researchers can gain insights into new materials and technologies that may improve the efficacy and safety of wound healing [117]. In addition, manufacturers can use this information to develop and market innovative wound dressings that offer unique benefits to patients. Moreover, clinicians can stay informed about new wound dressing options that may help their patients heal faster and with fewer complications [118]. Overall, patent information in wound dressing is an essential resource for anyone involved in wound-care research, development, and clinical practice, providing insights into new technologies and innovations that may help improve patient outcomes and advance the field of wound healing [117–119]. Table 4 describes patent information for honey-based wound dressings.

Table 4. Patent information of honey-based wound dressings.

Type of Patents	Inventor(s)	Issued	Assignee	Descriptions	References
US7714183B2 Use of honey in dressings	Phillip Roy Caskey	11 May 2010	Derma Science Inc	- The patent application describes a flexible dressing designed for direct application to wounds to absorb exudates. - The dressing consists of an alginate fiber sheet that is fully impregnated with honey, and transforms into a gel-like state as it absorbs exudate. - The combination of the alginate fiber sheet and honey provides benefits such as moisture retention, antimicrobial properties, and wound-healing promotion.	[120]

Table 4. Cont.

Type of Patents	Inventor(s)	Issued	Assignee	Descriptions	References
WO2002087644A1 Wound dressings comprising a carboxymethyl cellulose fabric impregnated with honey	James William Edmonds	7 November 2002	Not listed	The patent describes the wound dressings comprising honey as also containing carboxymethyl cellulose filaments in amounts up to 50% of the weight of the honey, preferably in the form of a fabric.	[121]
US5980875A Honey preparations	Mahmoud A. Mousa	11 November 1999	Not listed	- The patent describes the methods and preparations designed to address challenges related to the local application of honey for therapeutic, cosmetic, and nutritional purposes. These preparations consist of active ingredients derived from honey and a base containing components such as oils, gelling agents, emulsifiers, or combinations thereof. - The active ingredients found in honey, such as vitamins, sugars, enzymes, hormones, amino acids, and minerals, can be extracted from honey or other natural sources or be synthesized.	[122]
US9107974B2 Honey impregnated composite dressing having super-absorbency and an intelligent management of wound exudate, and methods of making the same	Howard Kenneth Payne, Gregory Frank Devenish	18 August 2015	Links Medical Products Inc	- The patent relates to a specialized wound dressing called a super-absorbent, honey-dosed foam/fiber composite with a gap pattern. - This dressing consists of a structured composite material made of foam and fiber, which is patterned with gaps on one side while the other side lacks such gaps.	[123]
AU2006272366B2 Therapeutic honey and method of producing same	Peter Taylor	22 September 2011	Honey Research & Development Pty Ltd.	- The patent relates to a specific type of honey characterized by the following attributes: (i) It exhibits antimicrobial activity that is not derived from peroxide; and (ii) It is derived from <i>Leptospermum</i> sub-tenu. - The honey undergoes a storage process for a certain duration and under specific conditions necessary to enhance its non-peroxide-based antimicrobial activity.	[124]
US10500235B2 Wound healing compositions comprising buckwheat honey and methylglyoxal and methods of use	Mark R. Wardell	10 December 2019	San Melix Laboratories Inc, Sannelix Laboratories Inc	- The patent application presents compositions based on medicinal honey that possess broad-spectrum antibacterial properties attributed to the presence of peroxide, polyphenols, and methylglyoxal. - The application describes methods of treating wounds by directly applying the aforementioned composition or utilizing wound dressings that incorporate the composition.	[125]
WO2007045931A2 Compositions and dressings for the treatment of wounds	Stephen Cotton	26 April 2007	Not listed	- The patent describes the composition of honey ranging from 30% to 99.5% w/w, and a naturally occurring plant extract with antibacterial properties ranging from 0.5% to 15% w/w as having proven effectiveness in wound treatment. - These compositions can be directly applied to wounds or can be applied to a flexible material, either as a coating or impregnation.	[126]
US6956144B2 Honey-based wound dressing	Peter Molan	18 October 2005	ApiMed Medical Honey Ltd.	- The patent application describes the utilization of honey in medical dressings. It involves the modification of honey by incorporating a viscosity increasing agent, which enables the creation of various compositions such as ointments, salves, and self-adhesive gels for mouth ulcers and pustules, as well as pliable or flexible sheets suitable for wound coverings. - The invention emphasizes the use of selected honeys that possess antibacterial properties beyond those attributed solely to osmolarity and sugar concentration effects.	[127]
AU2007100007A4 Improvements in and Relating to the use of Honey in Dressings	Phillip Roy, Caskey, Mardi Lewis	1 February 2007	ApiMed Medical Honey Ltd.	- This invention proposes utilizing honey with desirable qualities and viscosity in combination with various therapeutic or suitable medical dressings. - Example: Honey-impregnated dressings are expected to have significant potential in the treatment of chronic wounds, whether infected or non-infected, especially in cases where moist wound care is required.	[128]

## 12. Commercialized Product of Honey-Based Wound Dressings

Commercializing a honey-based wound dressing involves bringing the product to market and selling it to healthcare providers, medical facilities, and end-users [129]. Table 5 shows some recent honey-based wound dressings commercialized in the market. These commercialized honey-based wound dressings effectively manage and treat various wounds, including burns, diabetic ulcers, surgical wounds, pressure ulcers, etc. [25,130]. They are also known for reducing inflammation and promoting faster healing compared to traditional wound dressings. However, they should be used under the guidance of a healthcare professional before independent application of these dressings [1,131].

**Table 5.** Product commercialization of honey-based wound dressings.

Type of Dressing	Examples/Products	Intended Usage	References
Hydrocolloid Dressing	MediHoney®	<ul style="list-style-type: none"> <li>- Chronic (diabetic ulcers, venous ulcers, pressure ulcers) and acute wounds (surgical wounds) and burns.</li> <li>- Promotes wound healing by reducing healing time and promoting tissue growth.</li> </ul>	[132]
Film Dressing	TheraHoney®	<ul style="list-style-type: none"> <li>- Diabetic ulcers, venous ulcers, pressure ulcers, surgical wounds, traumatic wounds, and burns.</li> <li>- Stimulates wound healing by providing a moist environment, reducing pain and inflammation, and providing antimicrobial activity.</li> </ul>	[133]
Foam Dressing	Actilite®	<ul style="list-style-type: none"> <li>- Pressure ulcers, leg ulcers, diabetic ulcers, surgical wounds, traumatic wounds, and burns.</li> <li>- Protects wounds from antimicrobial activity, and provides a moist wound environment.</li> </ul>	[134]
Alginate Dressing	Algivon®	<ul style="list-style-type: none"> <li>- Leg ulcers, pressure ulcers, diabetic foot ulcers, and surgical wounds.</li> <li>- Provides antimicrobial properties, helps to absorb exudate, and promotes healing.</li> </ul>	[135]
Mesh Dressing	Activon®	<ul style="list-style-type: none"> <li>- Diabetic foot ulcers, pressure ulcers, venous leg ulcers, surgical wounds, traumatic wounds, and burns.</li> <li>- Promotes healing by providing a moist wound environment, managing exudate, reducing inflammation, and preventing infection.</li> </ul>	[136]

### 13. Conclusions and Future Perspectives

Wound healing is a sophisticated process that involves the replacement of damaged tissue layers and cellular structures. Numerous approaches have focused on wound-care management, including developing new therapeutic approaches and technologies for

wound management. Hydrogel wound dressings have gained attention among researchers due to their rapid wound healing properties and their ability to offer a moist environment, good biodegradability, and protection against bacterial infections. Improving the physicochemical, mechanical, and biological properties, and the wound-healing ability of hydrogel materials, is the primary goal when developing hydrogels, mainly achieved through blending natural and synthetic polymers with the addition of other bioactive substances, such as honey, which is beneficial for wound healing. The addition of honey during in vivo and in vitro studies into formulated hydrogel wound dressings has been found to prevent bacterial infections, enhance their absorption capacity, and accelerate wound healing, due to its anti-inflammatory, antimicrobial, and antioxidant activities. Moreover, the blending of polymers could be enhanced by incorporating other additives, such as cross-linkers, to enhance their mechanical properties, flexibility, biocompatibility, biodegradability, high absorption, etc. Although there are extensive in vivo and in vitro analyses that have shown efficacy in wound healing, its implementation in clinical fields still needs to be managed to ensure the safety and effectiveness of polymer-based hydrogel formulations in human applications.

**Author Contributions:** Conceptualization, S.N.N.Y., Z.S., N.H., Z.A.R. and N.I.M.; writing—original draft preparation, S.N.N.Y., Z.S. and N.I.M.; writing—review and editing, S.N.N.Y., Z.S., N.H., Z.A.R. and N.I.M.; supervision, Z.S. All authors have read and agreed to the published version of the manuscript.

**Funding:** This research was funded by the Ministry of Higher Education (MoHE) of Malaysia under the Fundamental Research Grant Scheme (FRGS) (FRGS/1/2020/STG05/USIM/03/1).

**Institutional Review Board Statement:** Not applicable.

**Data Availability Statement:** Not applicable.

**Acknowledgments:** The authors thank the Universiti Sains Islam Malaysia (USIM) and the Ministry of Higher Education (MoHE) of Malaysia.

**Conflicts of Interest:** The authors declare no conflict of interest.

## References

1. Shi, C.; Wang, C.; Liu, H.; Li, Q.; Li, R.; Zhang, Y.; Liu, Y.; Shao, Y.; Wang, J. Selection of Appropriate Wound Dressing for Various Wounds. *Front. Bioeng. Biotechnol.* **2020**, *8*, 182. [CrossRef] [PubMed]
2. Wilkinson, H.N.; Hardman, M.J. Wound healing: Cellular mechanisms and pathological outcomes. *Open Biol.* **2020**, *10*, 200223. [CrossRef] [PubMed]
3. Dhivya, S.; Padma, V.V.; Santhini, E. Wound dressings—A review. *Biomedicine* **2015**, *5*, 22. [CrossRef] [PubMed]
4. Ghomi, E.R.; Khalili, S.; Khorasani, S.N.; Neisiany, R.E.; Ramakrishna, S. Wound dressings: Current advances and future directions. *J. Appl. Polym. Sci.* **2019**, *136*, 47738. [CrossRef]
5. Su, J.; Li, J.; Liang, J.; Zhang, K.; Li, J. Hydrogel Preparation Methods and Biomaterials for Wound Dressing. *Life* **2021**, *11*, 1016. [CrossRef]
6. Bosworth, L.A.; Downes, S. *Electrospinning for Tissue Regeneration*; Woodhead Publishing Limited eBooks: Amsterdam, The Netherlands, 2011. [CrossRef]
7. Kalaycıoğlu, Z.; Kahya, N.; Adımcılar, V.; Kaygusuz, H.; Torlak, E.; Akın-Evingür, G.; Erım, F.B. Antibacterial nano cerium oxide/chitosan/cellulose acetate composite films as potential wound dressing. *Eur. Polym. J.* **2020**, *133*, 109777. [CrossRef]
8. Chin, C.-Y.; Jalil, J.; Ng, P.Y.; Ng, S.-F. Development and formulation of Moringa oleifera standardised leaf extract film dressing for wound healing application. *J. Ethnopharmacol.* **2018**, *212*, 188–199. [CrossRef]
9. Bustamante-Torres, M.; Romero-Fierro, D.; Arcentales-Vera, B.; Palomino, K.; Magaña, H.; Bucio, E. Hydrogels Classification According to the Physical or Chemical Interactions and as Stimuli-Sensitive Materials. *Gels* **2021**, *7*, 182. [CrossRef]
10. Brumberg, V.; Astrelina, T.; Malivanova, T.; Samoilov, A. Modern Wound Dressings: Hydrogel Dressings. *Biomedicines* **2021**, *9*, 1235. [CrossRef]
11. Gavan, A.; Colobatiu, L.; Hanganu, D.; Bogdan, C.; Olah, N.K.; Achim, M.; Mirel, S. Development and Evaluation of Hydrogel Wound Dressings Loaded with Herbal Extracts. *Processes* **2022**, *10*, 242. [CrossRef]
12. Chai, Q.; Jiao, Y.; Yu, X. Hydrogels for Biomedical Applications: Their Characteristics and the Mechanisms behind Them. *Gels* **2017**, *3*, 6. [CrossRef] [PubMed]
13. Aderibigbe, B.A. Hybrid-Based Wound Dressings: Combination of Synthetic and Biopolymers. *Polymers* **2022**, *14*, 3806. [CrossRef] [PubMed]



14. Hamed, H.; Moradi, S.; Hudson, S.M.; Tonelli, A.E. Chitosan based hydrogels and their applications for drug delivery in wound dressings: A review. *Carbohydr. Polym.* **2018**, *199*, 445–460. [CrossRef] [PubMed]
15. Khorasani, M.T.; Joorabloo, A.; Adeli, H.; Mansoori-Moghadam, Z.; Moghaddam, A. Design and optimization of process parameters of poly(vinyl alcohol)/chitosan/nano zinc oxide hydrogels as wound healing materials. *Carbohydr. Polym.* **2018**, *207*, 542–554. [CrossRef] [PubMed]
16. Ahmed, A.; Niazi, M.B.K.; Jahan, Z.; Ahmad, T.; Hussain, A.; Pervaiz, E.; Janjua, H.A.; Hussain, Z. In-vitro and in-vivo study of superabsorbent PVA/Starch/g-C<sub>3</sub>N<sub>4</sub>/Ag@TiO<sub>2</sub> NPs hydrogel membranes for wound dressing. *Eur. Polym. J.* **2020**, *130*, 109650. [CrossRef]
17. Xue, H.; Hu, L.; Xiong, Y.; Zhu, X.; Wei, C.; Cao, F.; Zhou, W.; Sun, Y.; Endo, Y.; Liu, M.; et al. Quaternized chitosan-Matrigel-polyacrylamide hydrogels as wound dressing for wound repair and regeneration. *Carbohydr. Polym.* **2019**, *226*, 115302. [CrossRef]
18. Koehler, J.; Brandl, F.; Goepferich, A. Hydrogel wound dressings for bioactive treatment of acute and chronic wounds. *Eur. Polym. J.* **2018**, *100*, 1–11. [CrossRef]
19. Alven, S.; Nqoro, X.; Aderibigbe, B.A. Polymer-Based Materials Loaded with Curcumin for Wound Healing Applications. *Polymers* **2020**, *12*, 2286. [CrossRef]
20. Yaghoobi, R.; Kazerouni, A.; Kazerouni, O. Evidence for Clinical Use of Honey in Wound Healing as an Anti-bacterial, Anti-inflammatory Anti-oxidant and Anti-viral Agent: A Review. *Jundishapur J. Nat. Pharm. Prod.* **2013**, *8*, 100–104. [CrossRef]
21. Mandal, M.D.; Mandal, S. Honey: Its medicinal property and antibacterial activity. *Asian Pac. J. Trop. Biomed.* **2011**, *1*, 154–160. [CrossRef]
22. Minden-Birkenmaier, B.A.; Bowlin, G.L. Honey-Based Templates in Wound Healing and Tissue Engineering. *Bioengineering* **2018**, *5*, 46. [CrossRef] [PubMed]
23. Gopal, R.; Lo, A.Z.K.; Masrol, M.; Lai, C.-H.; Zain, N.M.; Saidin, S. Susceptibility of Stingless Bee, Giant Bee and Asian Bee Honeys Incorporated Cellulose Hydrogels in Treating Wound Infection. *Malays. J. Fundam. Appl. Sci.* **2021**, *17*, 242–252. [CrossRef]
24. Noori, S.; Kokabi, M.; Hassan, Z.M. Poly(vinyl alcohol)/chitosan/honey/clay responsive nanocomposite hydrogel wound dressing. *J. Appl. Polym. Sci.* **2018**, *135*, 46311. [CrossRef]
25. Tavakoli, J.; Tang, Y. Honey/PVA hybrid wound dressings with controlled release of antibiotics: Structural, physico-mechanical and in-vitro biomedical studies. *Mater. Sci. Eng. C* **2017**, *77*, 318–325. [CrossRef] [PubMed]
26. Ibrahim, N.; Ima-Nirwana, S.; Mohamed, I.N.; Mohamed, N.; Chin, K.; Shuid, A.N. Wound Healing Properties of Selected Natural Products. *Int. J. Environ. Res. Public Health* **2018**, *15*, 2360. [CrossRef]
27. Benito-Martínez, S.; Pérez-Köhler, B.; Rodríguez, M.; Izco, J.M.; Recalde, J.I.; Pascual, G. Wound Healing Modulation through the Local Application of Powder Collagen-Derived Treatments in an Excisional Cutaneous Murine Model. *Biomedicines* **2022**, *10*, 960. [CrossRef]
28. Zuliani-Alvarez, L.; Midwood, K.S. Fibrinogen-Related Proteins in Tissue Repair: How a Unique Domain with a Common Structure Controls Diverse Aspects of Wound Healing. *Adv. Wound Care* **2014**, *4*, 273–285. [CrossRef]
29. Fredric, S.; Gowda, D.V.; Yashashwini, M. Wafers for Wound Healing. *J. Chem. Pharm. Res.* **2015**, *7*, 450–468. Available online: <https://www.jocpr.com/articles/wafers-for-wound-healing.pdf> (accessed on 14 May 2023).
30. Frykberg, R.G.; Banks, J. Challenges in the Treatment of Chronic Wounds. *Adv. Wound Care* **2015**, *4*, 560–582. [CrossRef]
31. Gainza, G.; Villullas, S.; Pedraz, J.L.; Hernandez, R.M.; Igartua, M. Advances in drug delivery systems (DDSs) to release growth factors for wound healing and skin regeneration. *Nanomed. Nanotechnol. Biol. Med.* **2015**, *11*, 1551–1573. [CrossRef]
32. Gonzalez, A.C.D.O.; Costa, T.F.; de Araújo Andrade, Z.; Medrado, A.R.A.P. Wound healing—A literature review. *An. Bras. Dermatol.* **2016**, *91*, 614–620. [CrossRef] [PubMed]
33. Alven, S.; Peter, S.; Mbese, Z.; Aderibigbe, B.A. Polymer-Based Wound Dressing Materials Loaded with Bioactive Agents: Potential Materials for the Treatment of Diabetic Wounds. *Polymers* **2022**, *14*, 724. [CrossRef] [PubMed]
34. Stoica, A.E.; Chircov, C.; Grumezescu, A.M. Nanomaterials for Wound Dressings: An Up-to-Date Overview. *Molecules* **2020**, *25*, 2699. [CrossRef] [PubMed]
35. Ndlovu, S.P.; Ngece, K.; Alven, S.; Aderibigbe, B.A. Gelatin-Based Hybrid Scaffolds: Promising Wound Dressings. *Polymers* **2021**, *13*, 2959. [CrossRef]
36. Vivcharenko, V.; Przekora, A. Modifications of Wound Dressings with Bioactive Agents to Achieve Improved Pro-Healing Properties. *Appl. Sci.* **2021**, *11*, 4114. [CrossRef]
37. Mandla, S.; Huyer, L.D.; Radisic, M. Review: Multimodal bioactive material approaches for wound healing. *APL Bioeng.* **2018**, *2*, 021503. [CrossRef]
38. Weller, C.D.; Team, V.; Sussman, G. First-Line Interactive Wound Dressing Update: A Comprehensive Review of the Evidence. *Front. Pharmacol.* **2020**, *11*, 155. [CrossRef]
39. Schoukens, G. 5—Bioactive dressings to promote wound healing. In *Advanced Textiles for Wound Care*; Elsevier: Amsterdam, The Netherlands, 2019; pp. 135–167. [CrossRef]
40. Savoji, H.; Godau, B.; Hassani, M.S.; Akbari, M. Skin Tissue Substitutes and Biomaterial Risk Assessment and Testing. *Front. Bioeng. Biotechnol.* **2018**, *6*, 86. [CrossRef]
41. Ho, T.-C.; Chang, C.-C.; Chan, H.-P.; Chung, T.-W.; Shu, C.-W.; Chuang, K.-P.; Duh, T.-H.; Yang, M.-H.; Tyan, Y.-C. Hydrogels: Properties and applications in Biomedicine. *Molecules* **2022**, *27*, 2902. [CrossRef]

42. Pourshahrestani, S.; Zeimaran, E.; Kadri, N.A.; Mutlu, N.; Boccaccini, A.R. Polymeric Hydrogel Systems as Emerging Biomaterial Platforms to Enable Hemostasis and Wound Healing. *Adv. Health Mater.* **2020**, *9*, 2000905. [CrossRef]
43. Chen, T.; Chen, Y.; Rehman, H.U.; Chen, Z.; Yang, Z.; Wang, M.; Li, H.; Liu, H. Ultratough, Self-Healing, and Tissue-Adhesive Hydrogel for Wound Dressing. *ACS Appl. Mater. Interfaces* **2018**, *10*, 33523–33531. [CrossRef]
44. Wang, H.; Xu, Z.; Zhao, M.; Liu, G.; Wu, J. Advances of hydrogel dressings in diabetic wounds. *Biomater. Sci.* **2020**, *9*, 1530–1546. [CrossRef] [PubMed]
45. Reddy, M.S.B.; Ponnamma, D.; Choudhary, R.; Sadasivuni, K.K. A Comparative Review of Natural and Synthetic Biopolymer Composite Scaffolds. *Polymers* **2021**, *13*, 1105. [CrossRef] [PubMed]
46. Ramineni, S.K. Mucoadhesive Films for Treatment of Local Oral Disorders: Development, Characterization and *In Vivo* Testing. Ph.D. Thesis, University of Kentucky, Lexington, KY, USA, 2013. Available online: [https://uknowledge.uky.edu/cbme\\_etds/19](https://uknowledge.uky.edu/cbme_etds/19) (accessed on 14 May 2023).
47. Suamte, L.; Turkey, A.; Babu, P.J. Design of 3D smart scaffolds using natural, synthetic and hybrid derived polymers for skin regenerative applications. *Smart Mater. Med.* **2023**, *4*, 243–256. [CrossRef]
48. Negut, I.; Dorcioman, G.; Grumezescu, V. Scaffolds for Wound Healing Applications. *Polymers* **2020**, *12*, 2010. [CrossRef] [PubMed]
49. Donnalaja, F.; Jacchetti, E.; Soncini, M.; Raimondi, M.T. Natural and Synthetic Polymers for Bone Scaffolds Optimization. *Polymers* **2020**, *12*, 905. [CrossRef] [PubMed]
50. Nune, S.K.; Rama, K.S.; Dirisala, V.R.; Chavali, M. *Electrospinning of Collagen Nanofiber Scaffolds for Tissue Repair and Regeneration*; Elsevier eBooks: Amsterdam, The Netherlands, 2017; pp. 281–311. [CrossRef]
51. Kamoun, E.A.; Kenawy, E.-R.S.; Chen, X. A review on polymeric hydrogel membranes for wound dressing applications: PVA-based hydrogel dressings. *J. Adv. Res.* **2017**, *8*, 217–233. [CrossRef]
52. Jayakumar, A.; Radoor, S.; Radhakrishnan, E.K.; Nair, I.; Siengchin, S.; Siengchin, S. *Soy Protein-Based Polymer Blends and Composites*; Elsevier eBooks: Amsterdam, The Netherlands, 2022; pp. 39–57. [CrossRef]
53. Aswathy, S.; Narendrakumar, U.; Manjubala, I. Commercial hydrogels for biomedical applications. *Heliyon* **2020**, *6*, e03719. [CrossRef]
54. Follmann, H.D.; Messias, I.; Queiroz, M.V.O.; Araujo, R.A.; Rubira, A.F.; Muniz, E.C. Designing hybrid materials with multi-functional interfaces for wound dressing, electrocatalysis, and chemical separation. *J. Colloid Interface Sci.* **2019**, *533*, 106–125. [CrossRef]
55. Kong, F.; Fan, C.; Yang, Y.; Lee, B.H.; Wei, K. 5-hydroxymethylfurfural-embedded poly (vinyl alcohol)/sodium alginate hybrid hydrogels accelerate wound healing. *Int. J. Biol. Macromol.* **2019**, *138*, 933–949. [CrossRef] [PubMed]
56. Masood, N.; Ahmed, R.; Tariq, M.; Ahmed, Z.; Masoud, M.S.; Ali, I.; Asghar, R.; Andleeb, A.; Hasan, A. Silver nanoparticle impregnated chitosan-PEG hydrogel enhances wound healing in diabetes induced rabbits. *Int. J. Pharm.* **2019**, *559*, 23–36. [CrossRef] [PubMed]
57. Tajik, F.; Eslahi, N.; Rashidi, A.; Rad, M.M. Hybrid antibacterial hydrogels based on PVP and keratin incorporated with lavender extract. *J. Polym. Res.* **2021**, *28*, 1–10. [CrossRef]
58. Zubik, K.; Singhsa, P.; Wang, Y.; Manuspiya, H.; Narain, R. Thermo-Responsive Poly(*N*-Isopropylacrylamide)-Cellulose Nanocrystals Hybrid Hydrogels for Wound Dressing. *Polymers* **2017**, *9*, 119. [CrossRef]
59. Rasool, A.; Ata, S.; Islam, A. Stimuli responsive biopolymer (chitosan) based blend hydrogels for wound healing application. *Carbohydr. Polym.* **2019**, *203*, 423–429. [CrossRef]
60. Eteraf-Oskouei, T.; Najafi, M. Traditional and Modern Uses of Natural Honey in Human Diseases: A Review. *Iran. J. Basic Med. Sci.* **2013**, *16*, 731–742.
61. Al-Kafawene, M.A.; Alwahsh, M.; Hilmi, A.B.M.; Abulebdah, D.H. Physicochemical Characteristics and Bioactive Compounds of Different Types of Honey and Their Biological and Therapeutic Properties: A Comprehensive Review. *Antibiotics* **2023**, *12*, 337. [CrossRef]
62. Lim, D.C.C.; Abu Bakar, M.F.; Majid, M. Nutritional composition of stingless bee honey from different botanical origins. *IOP Conf. Ser. Earth Environ. Sci.* **2019**, *269*, 012025. [CrossRef]
63. Alvarez-Suarez, J.M.; Gasparrini, M.; Simal-Gandara, J.; Mazzoni, L.; Giampieri, F. The Composition and Biological Activity of Honey: A Focus on Manuka Honey. *Foods* **2014**, *3*, 420–432. [CrossRef]
64. Samarghandian, S.; Farkhondeh, T.; Samini, F. Honey and health: A review of recent clinical research. *Pharmacogn. Res.* **2017**, *9*, 121–127.
65. Mieles, J.Y.; Vyas, C.; Aslan, E.; Humphreys, G.; Diver, C.; Bartolo, P. Honey: An Advanced Antimicrobial and Wound Healing Biomaterial for Tissue Engineering Applications. *Pharmaceutics* **2022**, *14*, 1663. [CrossRef]
66. Bahari, N.; Hashim, N.; Akim, A.M.; Maringgal, B. Recent Advances in Honey-Based Nanoparticles for Wound Dressing: A Review. *Nanomaterials* **2022**, *12*, 2560. [CrossRef] [PubMed]
67. Anis, A.; Sharshar, A.; El Hanbally, S.; Sadek, Y. A Novel Organic Composite Accelerates Wound Healing: Experimental and Clinical Study in Equine. *J. Equine Vet.-Sci.* **2021**, *99*, 103406. [CrossRef]
68. Yilmaz, A.C.; Aygin, D. Honey Dressing In Wound Treatment: A Systematic Review. *Complement. Ther. Med.* **2020**, *51*, 102388. [CrossRef] [PubMed]
69. Tashkandi, H. Honey in wound healing: An updated review. *Open Life Sci.* **2021**, *16*, 1091–1100. [CrossRef]

70. Al-Jadi, A.-M.; Enchang, F.K.; Yusoff, K.M. The effect of Malaysian honey and its major components on the proliferation of cultured fibroblasts. *Turk. J. Med. Sci.* **2014**, *44*, 733–740. [CrossRef]
71. Thirupathi, K.; Raorane, C.J.; Ramkumar, V.; Ulagesan, S.; Santhamoorthy, M.; Raj, V.; Krishnakumar, G.S.; Phan, T.T.V.; Kim, S.-C. Update on Chitosan-Based Hydrogels: Preparation, Characterization, and Its Antimicrobial and Antibiofilm Applications. *Gels* **2022**, *9*, 35. [CrossRef]
72. Oryan, A.; Alemzadeh, E.; Moshiri, A. Biological properties and therapeutic activities of honey in wound healing: A narrative review and meta-analysis. *J. Tissue Viability* **2016**, *25*, 98–118. [CrossRef]
73. Vaou, N.; Stavropoulou, E.; Voidarou, C.; Tsigalou, C.; Bezirtzoglou, E. Towards Advances in Medicinal Plant Antimicrobial Activity: A Review Study on Challenges and Future Perspectives. *Microorganisms* **2021**, *9*, 2041. [CrossRef]
74. Liu, E.; Gao, H.; Zhao, Y.; Pang, Y.; Yao, Y.; Yang, Z.; Zhang, X.; Wang, Y.; Yang, S.; Ma, X.; et al. The potential application of natural products in cutaneous wound healing: A review of preclinical evidence. *Front. Pharmacol.* **2022**, *13*, 900439. [CrossRef]
75. Bodnar, R.J. Epidermal Growth Factor and Epidermal Growth Factor Receptor: The Yin and Yang in the Treatment of Cutaneous Wounds and Cancer. *Adv. Wound Care* **2013**, *2*, 24–29. [CrossRef] [PubMed]
76. Huang, Y.; Kyriakides, T.R. The role of extracellular matrix in the pathophysiology of diabetic wounds. *Matrix Biol. Plus* **2020**, *6–7*, 100037. [CrossRef] [PubMed]
77. Gupta, S.S.; Singh, O.; Bhagel, P.S.; Moses, S.; Shukla, S.; Mathur, R.K. Honey dressing versus silver sulfadiazene dressing for wound healing in burn patients: A retrospective study. *J. Cutan. Aesthetic Surg.* **2011**, *4*, 183. [CrossRef] [PubMed]
78. Pasupuleti, V.R.; Sammugam, L.; Ramesh, N.; Gan, S.H. Honey, Propolis, and Royal Jelly: A comprehensive review of their biological actions and health benefits. *Oxidative Med. Cell. Longev.* **2017**, *2017*, 1–21. [CrossRef]
79. Molan, P.C. Re-introducing honey in the management of wounds and ulcers—Theory and practice. *J. Wound Ostomy Cont. Nurs.* **2002**, *48*, 28–40.
80. Ousey, K.; Cutting, K.; Rogers, A.; Rippon, M. The importance of hydration in wound healing: Reinvigorating the clinical perspective. *J. Wound Care* **2016**, *25*, 122–130. [CrossRef]
81. Sood, A.; Granick, M.S.; Tomaselli, N.L. Wound Dressings and Comparative Effectiveness Data. *Adv. Wound Care* **2014**, *3*, 511–529. [CrossRef]
82. Esa, N.E.F.; Ansari, M.N.M.; Razak, S.I.A.; Ismail, N.I.; Jusoh, N.; Zawawi, N.A.; Jamaludin, M.I.; Sagadevan, S.; Nayan, N.H.M. A Review on Recent Progress of Stingless Bee Honey and Its Hydrogel-Based Compound for Wound Care Management. *Molecules* **2022**, *27*, 3080. [CrossRef]
83. Chopra, H.; Bibi, S.; Kumar, S.; Khan, M.S.; Kumar, P.; Singh, I. Preparation and Evaluation of Chitosan/PVA Based Hydrogel Films Loaded with Honey for Wound Healing Application. *Gels* **2022**, *8*, 111. [CrossRef]
84. Lo, A.Z.K.; Lukman, S.K.; Lai, C.-H.; Zain, N.M.; Saidin, S. Stingless Bee Honey Incorporated Cellulose Hydrogel/Poly(Lactic-Co-Glycolic Acid) Patch as an Alternative Treatment for Aphthous Stomatitis. *Cell. Chem. Technol.* **2021**, *55*, 539–603. [CrossRef]
85. Zekry, S.S.A.; Abdellatif, A.; Azzazy, H.M. Fabrication of pomegranate/honey nanofibers for use as antibacterial wound dressings. *Wound Med.* **2020**, *28*, 100181. [CrossRef]
86. Samraj, S.M.D.; Kirupha, S.D.; Elango, S.; Vadodaria, K. Fabrication of nanofibrous membrane using stingless bee honey and curcumin for wound healing applications. *J. Drug Deliv. Sci. Technol.* **2021**, *63*, 102271. [CrossRef]
87. El-Kased, R.F.; Amer, R.I.; Attia, D.; Elmazar, M.M. Honey-based hydrogel: In vitro and comparative In vivo evaluation for burn wound healing. *Sci. Rep.* **2017**, *7*, 9692. [CrossRef] [PubMed]
88. Yang, X.; Fan, L.; Ma, L.; Wang, Y.; Lin, S.; Yu, F.; Pan, X.; Luo, G.; Zhang, D.; Wang, H. Green electrospun Manuka honey/silk fibroin fibrous matrices as potential wound dressing. *Mater. Des.* **2017**, *119*, 76–84. [CrossRef]
89. Durai, B.; Sizing, S. Development and Evaluation of Chitosan Honey Hydrogel Sheets as Wound Dressing. *Int. J. Pharm. Bio. Sci.* **2015**, *6*, 26–37. Available online: [http://www.ijpbs.net/cms/php/upload/3829\\_pdf.pdf](http://www.ijpbs.net/cms/php/upload/3829_pdf.pdf) (accessed on 14 May 2023).
90. Zohdi, R.M.; Zakaria, Z.A.B.; Yusof, N.; Mustapha, N.M.; Abdullah, M.N.H. Gelam (*Melaleuca* spp.) Honey-Based Hydrogel as Burn Wound Dressing. *Evid.-Based Complement. Altern. Med.* **2011**, *2012*, 1–7. [CrossRef]
91. Khoo, Y.-T.; Halim, A.S.; Singh, K.-K.B.; Mohamad, N.-A. Wound contraction effects and antibacterial properties of Tualang honey on full-thickness burn wounds in rats in comparison to hydrofibre. *BMC Complement. Altern. Med.* **2010**, *10*, 48. [CrossRef]
92. Liang, C.-C.; Park, A.Y.; Guan, J.-L. In vitro scratch assay: A convenient and inexpensive method for analysis of cell migration in vitro. *Nat. Protoc.* **2007**, *2*, 329–333. [CrossRef]
93. Jonkman, J.E.N.; Cathcart, J.A.; Xu, F.; Bartolini, M.E.; Amon, J.E.; Stevens, K.M.; Colarusso, P. An introduction to the wound healing assay using live-cell microscopy. *Cell Adhes. Migr.* **2014**, *8*, 440–451. [CrossRef]
94. Grada, A.; Otero-Viñas, M.; Prieto-Castrillo, F.P.; Obagi, Z.; Falanga, V. Research Techniques Made Simple: Analysis of Collective Cell Migration Using the Wound Healing Assay. *J. Investig. Dermatol.* **2017**, *137*, e11–e16. [CrossRef]
95. Chaudhary, A.; Bag, S.; Banerjee, P.; Chatterjee, J. Wound healing efficacy of Jamun honey in diabetic mice model through reepithelialization, collagen deposition and angiogenesis. *J. Tradit. Complement. Med.* **2019**, *10*, 529–543. [CrossRef] [PubMed]
96. Ranzato, E.; Martinotti, S.; Burlando, B. Honey exposure stimulates wound repair of human dermal fibroblasts. *Burn. Trauma* **2013**, *1*, 32. [CrossRef] [PubMed]
97. Ebadi, P.; Fazeli, M. Evaluation of the potential in vitro effects of propolis and honey on wound healing in human dermal fibroblast cells. *S. Afr. J. Bot.* **2020**, *137*, 414–422. [CrossRef]



98. Lau, X.Y.; Taib, H.; Berahim, Z.; Ahmad, A.; Zainuddin, S.L.A. The Effect of Tualang Honey on Human Periodontal Ligament Fibroblast Proliferation and Alkaline Phosphatase Level. *Sains Malays.* **2015**, *44*, 1021–1025. [CrossRef]
99. Shamloo, A.; Aghababaie, Z.; Afjoul, H.; Jami, M.; Bidgoli, M.R.; Vossoughi, M.; Ramazani, A.; Kamyabhesari, K. Fabrication and evaluation of chitosan/gelatin/PVA hydrogel incorporating honey for wound healing applications: An in vitro, in vivo study. *Int. J. Pharm.* **2020**, *592*, 120068. [CrossRef] [PubMed]
100. Sarhan, W.A.; Azzazy, H.M.E.; El-Sherbiny, I.M. Honey/Chitosan Nanofiber Wound Dressing Enriched with *Allium sativum* and *Cleome droserifolia*: Enhanced Antimicrobial and Wound Healing Activity. *ACS Appl. Mater. Interfaces* **2016**, *8*, 6379–6390. [CrossRef] [PubMed]
101. Scephankova, H.; Combarros-Fuertes, P.; Fresno, J.M.; Tornadijo, M.E.; Dias, M.S.; Pinto, C.A.; Saraiva, J.A.; Estevinho, L.M. Role of Honey in Advanced Wound Care. *Molecules* **2021**, *26*, 4784. [CrossRef] [PubMed]
102. Li, W.; Zhou, J.; Xu, Y. Study of the in vitro cytotoxicity testing of medical devices. *Biomed. Rep.* **2015**, *3*, 617–620. [CrossRef]
103. Tang, Y.; Lan, X.; Liang, C.; Zhong, Z.; Xie, R.; Zhou, Y.; Miao, X.; Wang, H.; Wang, W. Honey loaded alginate/PVA nanofibrous membrane as potential bioactive wound dressing. *Carbohydr. Polym.* **2019**, *219*, 113–120. [CrossRef]
104. A Minden-Birkenmaier, B.; Neuhalfen, R.M.; Janowiak, B.E.; Sell, S.A. Preliminary Investigation and Characterization of Electrospun Polycaprolactone and Manuka Honey Scaffolds for Dermal Repair. *J. Eng. Fibers Fabr.* **2015**, *10*, 155892501501000. [CrossRef]
105. Center for Devices and Radiological Health—U.S. Food and Drug Administration. Medical Devices. Available online: <https://www.fda.gov/medical-devices> (accessed on 14 May 2023).
106. EMA. Scientific Guidelines. European Medicines Agency. Available online: <https://www.ema.europa.eu/en/human-regulatory/research-development/scientific-guidelines> (accessed on 14 May 2023).
107. China's National Medical Products Administration (NMPA). Global Regulatory Partners, Inc. Available online: <https://globalregulatorypartners.com/countries/china-national-national-medical-products-administration-nmpa/> (accessed on 14 May 2023).
108. TGA. Therapeutic Goods Administration (TGA). Available online: <https://www.tga.gov.au/> (accessed on 14 May 2023).
109. HSA. Guidance Documents for Medical Devices. HSA. Available online: <https://www.hsa.gov.sg/medical-devices/guidance-documents> (accessed on 14 May 2023).
110. Guideline—Medical Device Authority (MDA). Portal.mda.gov.my. Available online: <https://portal.mda.gov.my/doc-list/guideline.html> (accessed on 14 May 2023).
111. Assakina, L. FAQ: Product Registration. National Pharmaceutical Regulatory Agency (NPRA). Available online: <https://www.npra.gov.my/index.php/en/component/content/article/37-english/faq/623-product-registration.html?Itemid=1391> (accessed on 14 May 2023).
112. Ministry of Health. Drug Registration Guidance Document (DRGD). Available online: <https://www.npra.gov.my/easyarticles/images/users/1153/DRGD%20January%202023/Complete-Drug-Registration-Guidance-Documents-DRGD-3rd-Edition-3rd-Revision-July-2022.pdf> (accessed on 14 May 2023).
113. Young, M.; Smith, M.A. *Standard and Evaluation of Healthcare Quality, Safety, and Person Centered Care*; PubMed; StatPearls Publishing: Philadelphia, PA, USA, 2022. Available online: <https://www.ncbi.nlm.nih.gov/books/NBK576432/> (accessed on 14 May 2023).
114. Heerschap, C.; Nicholas, A.; Whitehead, M. Wound management: Investigating the interprofessional decision-making process. *Int. Wound J.* **2018**, *16*, 233–242. [CrossRef]
115. Mayfield, D.L. Medical Patents and How New Instruments or Medications Might Be Patented. *Mo. Med.* **2016**, *113*, 456–462. [PubMed]
116. Bhattacharya, S.; Saha, C. Intellectual property rights: An overview and implications in pharmaceutical industry. *J. Adv. Pharm. Technol. Res.* **2011**, *2*, 88–93. [CrossRef]
117. Gwak, J.H.; Sohn, S.Y. Identifying the trends in wound-healing patents for successful investment strategies. *PLoS ONE* **2017**, *12*, e0174203. [CrossRef] [PubMed]
118. Laurano, R.; Boffito, M.; Ciardelli, G.; Chiono, V. Wound dressing products: A translational investigation from the bench to the market. *Eng. Regen.* **2022**, *3*, 182–200. [CrossRef]
119. Sen, C.K.; Gordillo, G.M.; Roy, S.; Kirsner, R.; Lambert, L.; Hunt, T.K.; Gottrup, F.; Gurtner, G.C.; Longaker, M.T. Human skin wounds: A major and snowballing threat to public health and the economy. *Wound Repair Regen.* **2009**, *17*, 763–771. [CrossRef] [PubMed]
120. Caskey, P.R. Use of Honey in Dressings. U.S. Patent US7714183B2, 11 May 2010. Available online: <https://patents.google.com/patent/US7714183B2/en> (accessed on 14 May 2023).
121. Edmonds, J.W. Wound Dressings Comprising a Carboxymethyl Cellulose Fabric Impregnated with Honey. WIPO (PCT) WO2002087644A1, 7 November 2002. Available online: <https://patents.google.com/patent/WO2002087644A1/en> (accessed on 14 May 2023).
122. Mousa, M.A. Honey Preparations. U.S. Patent US5980875A, 11 November 1999. Available online: <https://patents.google.com/patent/US5980875A/en?q=US5980875A+> (accessed on 14 May 2023).

123. Payne, H.K.; Devenish, G.F. Honey Impregnated Composite Dressing Having Super Absorbency and Intelligent Management of Wound Exudate and Method of Making Same. U.S. Patent US9107974B2, 18 August 2015. Available online: <https://patents.google.com/patent/US9107974B2/en> (accessed on 14 May 2023).
124. Peter, T. Therapeutic Honey and Method of Producing Same. AU Patent AU2006272366B2, 22 September 2011. Available online: <https://patents.google.com/patent/AU2006272366B2/en> (accessed on 14 May 2023).
125. Wardell, M.R. Wound Healing Compositions Comprising Buckwheat Honey and Methylglyoxal and Methods of Use. U.S. Patent 10500235, 10 December 2019. Available online: <https://patents.google.com/patent/US10500235B2/en> (accessed on 14 May 2023).
126. Cotton, S. Compositions and Dressings for the Treatment of Wounds. WIPO (PCT) WO2007045931A2, 26 April 2007. Available online: <https://patents.google.com/patent/WO2007045931A2/en> (accessed on 14 May 2023).
127. Molan, P. Honey Based Wound Dressing. U.S. Patent US6956144B2, 18 October 2005. Available online: <https://patents.google.com/patent/US6956144B2/en> (accessed on 14 May 2023).
128. Roy, P.; Lewis, M. Improvements in and Relating to the Use of Honey in Dressing. AU Patent AU2007100007A4, 1 February 2007. Available online: <https://patents.google.com/patent/AU2007100007A4/en> (accessed on 14 May 2023).
129. Pieper, B. Honey-Based Dressings and Wound Care. *J. Wound Ostomy Cont. Nurs.* **2009**, *36*, 60–66. [CrossRef] [PubMed]
130. Clark, M.; Adcock, L. Honey for Wound Management: A Review of Clinical Effectiveness and Guidelines. Canadian Agency for Drugs and Technologies in Health. Ottawa, Canada. 2018. Available online: [https://www.ncbi.nlm.nih.gov/books/NBK538361/#\\_ncbi\\_dlg\\_cpyrght\\_NBK538361](https://www.ncbi.nlm.nih.gov/books/NBK538361/#_ncbi_dlg_cpyrght_NBK538361) (accessed on 14 May 2023).
131. Nguyen, H.M.; Le, T.T.N.; Nguyen, A.T.; Le, H.N.T.; Pham, T.T. Biomedical materials for wound dressing: Recent advances and applications. *RSC Adv.* **2023**, *13*, 5509–5528. [CrossRef]
132. U.S. Food & Drug Administration. 510(k) Summary for Derma Sciences Medihoney Gel Dressings with Active Manuka Honey. Available online: [https://www.accessdata.fda.gov/cdrh\\_docs/pdf8/K080315.pdf](https://www.accessdata.fda.gov/cdrh_docs/pdf8/K080315.pdf) (accessed on 14 May 2023).
133. Medline. TheraHoney: Honey Wound Dressings. Available online: [https://www.medline.com/media/catalog/Docs/MKT/LIT241\\_BRO\\_TheraHoney\\_1673178.pdf](https://www.medline.com/media/catalog/Docs/MKT/LIT241_BRO_TheraHoney_1673178.pdf) (accessed on 14 May 2023).
134. Actilite Manuka Honey Impregnated Tulle Dressing. Available online: <https://medicaldressings.co.uk/actilite-manuka-honey-impregnated-tulle-dressing/> (accessed on 14 May 2023).
135. Algivon—100% Manuka Honey. Advancis Medical. Available online: <https://uk.advancismedical.com/products/algivon> (accessed on 14 May 2023).
136. Medline. 100% Medical Grade Manuka Honey. Available online: <https://www.medline.com/media/catalog/Docs/MKT/manuka%20honey%20v4.pdf> (accessed on 14 May 2023).

**Disclaimer/Publisher’s Note:** The statements, opinions and data contained in all publications are solely those of the individual author(s) and contributor(s) and not of MDPI and/or the editor(s). MDPI and/or the editor(s) disclaim responsibility for any injury to people or property resulting from any ideas, methods, instructions or products referred to in the content.





Review

# Polymeric Materials Obtained by Extrusion and Injection Molding from Lignocellulosic Agroindustrial Biomass

Ada Pacheco <sup>1</sup>, Arian Evangelista-Osorio <sup>1</sup>, Katherine Gabriela Muchaypiña-Flores <sup>1</sup>, Luis Alejandro Marzano-Barreda <sup>1</sup>, Perla Paredes-Concepción <sup>2</sup>, Heidy Palacin-Baldeón <sup>1</sup>, Maicon Sérgio Nascimento Dos Santos <sup>3</sup>, Marcus Vinícius Tres <sup>3</sup>, Giovani Leone Zabet <sup>3</sup> and Luis Olivera-Montenegro <sup>1,2,\*</sup>

- <sup>1</sup> Bioprocesses and Biomass Conversion Research Group, Universidad San Ignacio de Loyola, La Molina 15024, Peru; ada.pacheco.gil@gmail.com (A.P.); arian.evangelista@usil.pe (A.E.-O.); katherine.muchaypina@usil.pe (K.G.M.-F.); lmarzano@usil.edu.pe (L.A.M.-B.); heidy.palacin@usil.pe (H.P.-B.)
- <sup>2</sup> Grupo de Ciencia, Tecnología e Innovación en Alimentos, Universidad San Ignacio de Loyola, La Molina 15024, Peru; pparedes@usil.edu.pe
- <sup>3</sup> Laboratory of Agroindustrial Processes Engineering (LAPE), Federal University of Santa Maria, 1040 Sete de Setembro St., Center DC, Cachoeira do Sul, Santa Maria 96508-010, RS, Brazil; maiconsergions@gmail.com (M.S.N.D.S.); marcus.tres@ufsm.br (M.V.T.); giovani.zabet@ufsm.br (G.L.Z.)
- \* Correspondence: lolivera@usil.edu.pe

**Abstract:** This review presents the advances in polymeric materials achieved by extrusion and injection molding from lignocellulosic agroindustrial biomass. Biomass, which is derived from agricultural and industrial waste, is a renewable and abundant feedstock that contains mainly cellulose, hemicellulose, and lignin. To improve the properties and functions of polymeric materials, cellulose is subjected to a variety of modifications. The most common modifications are surface modification, grafting, chemical procedures, and molecule chemical grafting. Injection molding and extrusion technologies are crucial in shaping and manufacturing polymer composites, with precise control over the process and material selection. Furthermore, injection molding involves four phases: plasticization, injection, cooling, and ejection, with a focus on energy efficiency. Fundamental aspects of an injection molding machine, such as the motor, hopper, heating units, nozzle, and clamping unit, are discussed. Extrusion technology, commonly used as a preliminary step to injection molding, presents challenges regarding fiber reinforcement and stress accumulation, while lignin-based polymeric materials are challenging due to their hydrophobicity. The diverse applications of these biodegradable materials include automotive industries, construction, food packaging, and various consumer goods. Polymeric materials are positioned to offer even bigger contributions to sustainable and eco-friendly solutions in the future, as research and development continues.

**Keywords:** agroindustrial wastes; biomaterials; cellulose; lignocellulosic biomass

**Citation:** Pacheco, A.; Evangelista-Osorio, A.; Muchaypiña-Flores, K.G.; Marzano-Barreda, L.A.; Paredes-Concepción, P.; Palacin-Baldeón, H.; Dos Santos, M.S.N.; Tres, M.V.; Zabet, G.L.; Olivera-Montenegro, L. Polymeric Materials Obtained by Extrusion and Injection Molding from Lignocellulosic Agroindustrial Biomass. *Polymers* **2023**, *15*, 4046. <https://doi.org/10.3390/polym15204046>

Academic Editor: Raffaella Striani

Received: 21 August 2023

Revised: 3 October 2023

Accepted: 3 October 2023

Published: 10 October 2023



**Copyright:** © 2023 by the authors. Licensee MDPI, Basel, Switzerland. This article is an open access article distributed under the terms and conditions of the Creative Commons Attribution (CC BY) license (<https://creativecommons.org/licenses/by/4.0/>).

## 1. Introduction

The growing awareness of environmental challenges and the search for sustainable solutions have led to a critical evaluation of the way natural resources and waste are managed [1,2]. The continuous growth of the global population and the increasing demand for food and energy have made the effective management of agricultural and food waste a fundamental area of concern [3,4]. On an annual basis, a considerable quantity of agroindustrial wastes, arising from the production of food and crops, amasses on a global scale. This accumulation has adverse repercussions not only for the environment, but also for the global economy [5]. These residues not only represent a loss of valuable resources, but also cause increasing emissions of greenhouse gases, thus contributing to climate change [6]. Furthermore, at various stages across the food supply chain, from production to consumption, there is a disconcerting level of food loss and waste [7,8]. The food industry

has embarked on a concerted endeavor to curtail food loss and waste, embracing strategies that champion the reevaluation of food waste. In this process, the concept of the circular economy has assumed a central role, advocating for the conversion of waste into valuable resources [9,10].

These waste materials, primarily composed of lignocellulosic biomass, can be efficiently converted into biopolymers [11,12]. Biomass, mainly comprising cellulose, hemicellulose, and lignin, necessitates pretreatment to reduce its refractory nature and enhance accessibility within its structure [13]. There are four types of pretreatment methods: physical (milling, extrusion, sonication, microwave, ultrasound, ozonolysis, and pyrolysis), chemical (alkali, dilute acid, ionic liquid, organic solvent, and oxidative delignification), physicochemical (CO<sub>2</sub> explosion, steam explosion, hydrothermal, liquid hot water, and ammonia fiber explosion), and biological [14–16]. The characteristics of the feedstock, energy requirements, cost, and product recovery should be considered when choosing the pretreatment method [17].

Extrusion and injection molding are widely used manufacturing technologies in the plastics industry [18]. By leveraging this technology, biomass can be transformed into high-quality polymeric materials with desirable properties. Extrusion involves the continuous melting, mixing, and shaping of the biopolymers, while injection molding enables the precise and efficient formation of complex shapes through the injection of molten materials into molds [19].

The use of lignocellulosic agroindustrial biomass for polymeric materials offers numerous advantages, such as reduced dependence on polymers based on non-renewable fossil fuels, thereby promoting sustainability, and reducing the environmental impact [20]. In addition, this approach contributes to efficient waste management, reducing the burden on landfills [21].

Reinforced polymers, also called composites, are the union of two materials, a matrix, and a reinforcement, characterized by one being lightweight and the other strong [22]. The matrix can be polymeric, ceramic, or metallic, while the reinforcement can be fibers, particles, or laminates [23]. A challenge in the formation of composites is the coupling of the hydrophilic interfaces in the reinforcement and the hydrophobic interfaces in the polymeric matrix [24]. Fiber reinforcement is mainly composed of lignocellulosic mass. Agroindustrial wastes are increasingly used due to their low cost, biodegradability, improved properties, and composite quality [24].

This review delves into the latest innovations and research trends in the use of lignocellulosic biomass from agroindustrial wastes, with the purpose of developing polymeric materials using extrusion and injection molding technologies. Additionally, it provides an overview of agroindustrial biomass, its properties, pretreatment methods, and extrusion and injection molding processes. The review also underscores the wide-ranging industrial applications of these materials and outlines potential future developments.

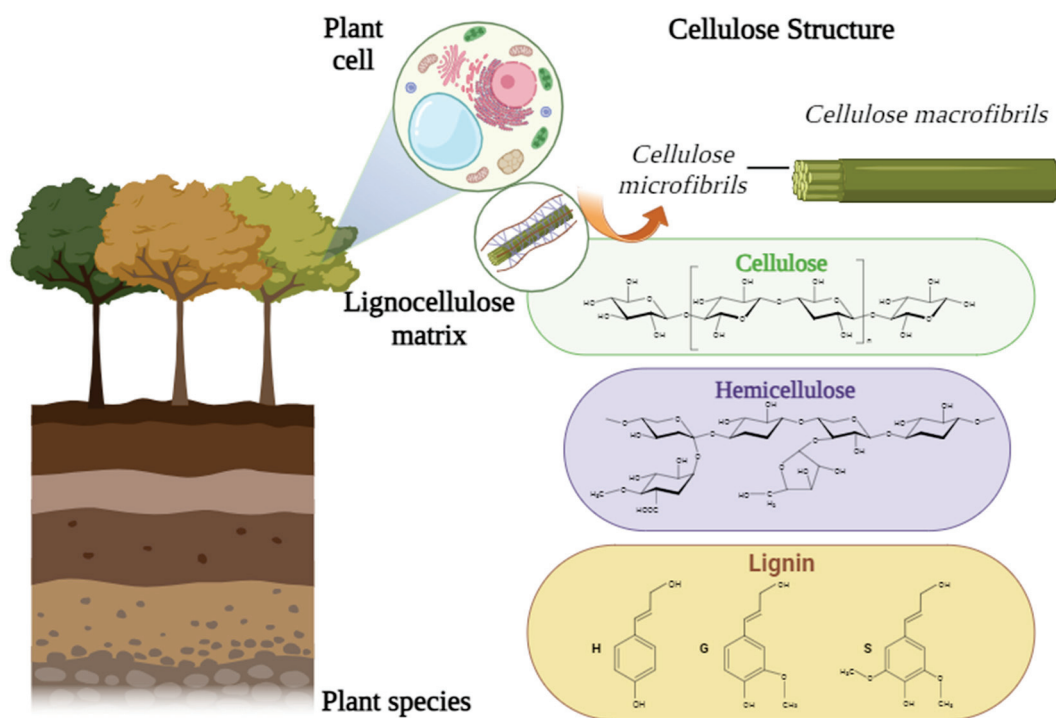
## 2. Sources and Components of Lignocellulosic Agroindustrial Biomass

Lignocellulosic agroindustrial biomass, a highly renewable and cost-effective natural resource, is derived from agricultural residues (husks, bagasse, seeds, roots, leaves, stems, seed pods, and straw), food processing waste (peels, skin, shells, oil cakes, and egg waste), and forestry by-products [9,25]. The primary components of biomass are cellulose, hemicellulose, and lignin. The components can vary based on factors such as the type of biomass, location, climate, and harvesting season [12].

### 2.1. Cellulose

Cellulose (C<sub>6</sub>H<sub>10</sub>O<sub>5</sub>)<sub>n</sub> is the most abundant renewable natural polymer in nature. In general, lignocellulose-based biomaterials have a large proportion of total cellulose content, highly interlaced by a significant amount of covalent bonds with high rigidity to form extremely strong and resilient components [26]. Generally, cellulose from algae is approximately 70 wt% and cellulose from plant-based materials ranges from 40 to

60 wt% [27]. Nonetheless, some studies indicate that the cellulose content in some plants, such as hop stems, can reach 70 wt%, which allows the substance to be widely used for biopolymer production and applications [28]. Spontaneously, cellulose molecules form large agglomerates that aggregate into microfibrils, which are constituents commonly called crystalline and amorphous zones [29]. The structure of the multiple components that comprise the complex are presented in Figure 1. The structure of cellulolytic chains is made up of cellulose microfibrils, intimately intertwined in complexes based on lignin and hemicellulose.



**Figure 1.** Matrix with cellulose macrofibrils and microfibrils intimately intertwined by the matrix of lignin and hemicellulose.

One of the main assertions about cellulose, and its stocked reserve of highly renewable and widely investigated organic constituents, is directed at the ease of obtaining the biopolymer. Expressive amounts of cellulose are easily verified in a series of plant species, marine algae, marine animals, bacteria, and vegetable residual biomass, which represent up to 50 wt% of the total weight of the biowaste [30]. Additionally, cellulose promotes high resistance in the plant cell wall, mainly due to the large number of glucose monomeric units covalently linked through  $\beta$ -1,4 glycosidic bonds [31].

Furthermore, other characteristics of the cellulose complex give rise to the recalcitrant characteristic of lignocellulose-based materials, such as the high crystalline performance of the matrix, a significant degree of polymerization (up to 10,000 units), and the presence of an intricate network of hydroxyl groups associated with intramolecular hydrogen bonds in cellulose [32]. The glucose-rich aggregate of hydroxyl compounds forms intertwined hydrogen bonds that provide resilience to the molecular structure and connect with neighboring particles to form a network of microfibrils. The hundreds of bonds that involve intermolecular and intramolecular hydrogen molecules and the intertwining of crystalline and non-crystalline zones are intimately responsible for the two-phase structure of cellulose, in which the regions of high crystallinity or cellulose nanocrystals (CNC) stand out [33]. Conversely, more susceptible molecular chains are called amorphous zones, which are easily degraded to obtain a highly soluble and reactive amorphous material. This performance promotes a drastic decline in solubility in liquid contents and an increase in resistance to molecular chain disfigurement by the action of water [34]. Additionally, cellulolytic chains

include  $\beta$ -D-glucopyranose elements interconnected via  $\beta$ -(1,4)-glycosidic bonds. Cellulose holds up to 1400 D-glucose units directly disposed to structure microfibrils units, which are broadly grouped to configure cellulose fibrils, which are structured under a highly rigid and vigorous matrix, rich in cellulose and hemicellulose [35].

The diversity of applications of cellulose complexes is closely associated with a range of matrix dominances, such as low density, biodegradability, significant porosity, and improved physical and mechanical mechanisms [36]. Cellulose is easily obtained from natural sources, which corroborates its high accessibility, cost effectiveness, applicability, reduced or minimal toxicity, and biocompatibility [37]. The total cellulose content and the arrangement of the crystalline zones are dependent on the plant species and the lignocellulose content, which is directly associated with the resistance potential of the biomaterial and the difficulty of breaking the complex by the action of hydrolysis [38]. Furthermore, there is a diversity in the secondary structures derived from cellulose, or crystal arrangements, such as cellulose I, cellulose II, cellulose III, and cellulose IV [39]. Cellulose I is associated with natural cellulose, easily found in nature. Cellulose II and cellulose III are by-products of the original cellulose, generally obtained through the regeneration of cellulose I. Finally, cellulose IV is obtained from cellulose III using procedures involving high temperatures and glycerol. The different crystal arrangements vary in terms of the characteristic attributes, such as hydrophilicity, mechanical potential, and stability performance [40].

Recently, cellulose-based exploration has been promoted due to a series of benefits, such as cost effectiveness, efficiency, physical and mechanical properties, the low degree of the environmental impact, exuberance, and capacity for nanoscale structure, among others [41]. A variety of technological innovations have been widely explored for the isolation of cellulose from lignocellulosic waste. The high interest has broken sustainability boundaries under the concept of biorefineries, because there is a wide spectrum of applications for cellulose-rich biomaterials or secondary bioproducts. Among the main industrial complexes that instigate research associated with cellulose are the food industry [42], textile industry [43], energy production [44], building and engineering industry [45], biomedicine [46], pharmaceuticals industry [47], adsorption [48], and wastewater treatment [49], among others.

### Nanocellulose

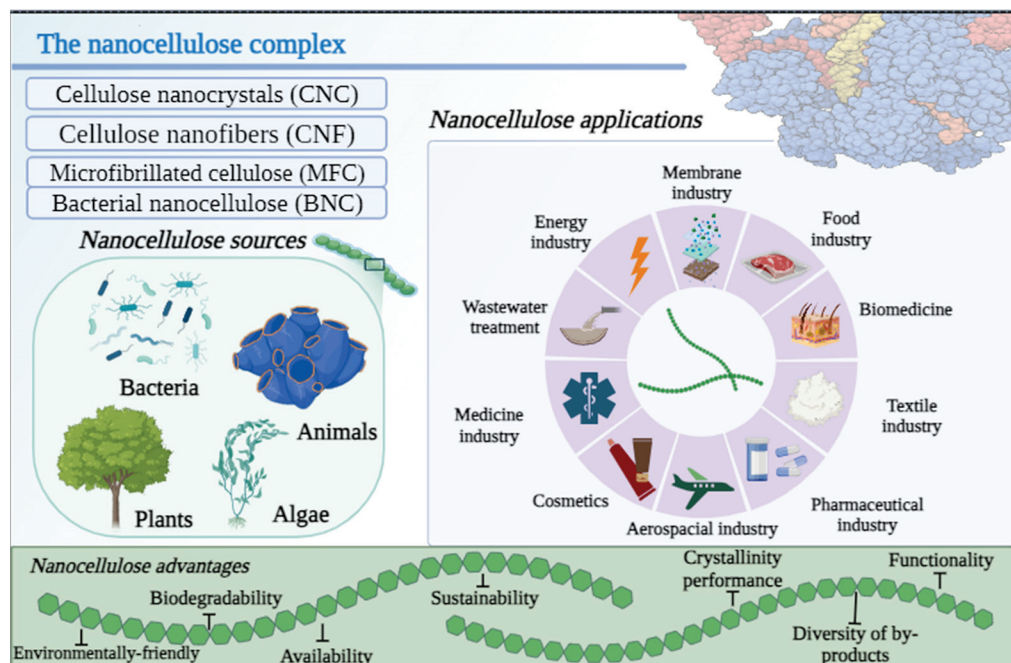
Nanocellulose is a biopolymer originating from cellulose and occurring at the nanoscale, obtained mainly from marine and land plants, animals, and bacteria in four primary forms: CNC, cellulose nanofibers or nanofibrillated cellulose (NFC), microfibrillated cellulose (MFC), and microbial or bacterial nanocellulose (BNC) [50]. Nanocellulose is characterized as highly resistant fibers, with a diameter of less than 100 nm and a density of up to  $1.6 \text{ g/cm}^3$ . A high abundance of hydroxyl functional groups can be easily adapted to express high performance [51]. Nanocellulose provides a highly modifiable surface, significant mechanical strength, high hydrophilicity, and biocompatibility [52]. During the hydrolytic process, the amorphous zone of the cellulose fibers is cleaved to form an extremely strong and crystalline nanoscale structure with a rod-like arrangement [53]. Most commonly seen, CNC features lengths of up to 100–300 nm and up to 5–50 nm in diameter, with a rich hydrogen bonding matrix, allowing for high voltage transfer. An NFC is commonly synthesized using chemical pretreatments and homogenization is carried out in high-pressure conditions [54]. NFCs constitute nanoscale fibrils, with a width between 2 and 60 nm, and are established from the agglomeration of cellulose chains, generated by hydrogen bonds, and comprise crystalline and amorphous zones, easily synthesized from the discharge of fibrils from microfiber bundles under strategies of mechanical fibrillation [55]. Furthermore, BNC consists of the application of microorganisms as primary sources of biopolymers, mainly due to the rapid microbial growth and high availability of the product. The literature indicates two dominant procedures to produce BNC based on microbial agents: static culture and agitated culture. Static culture refers to the accumulation of BNC forming a thick and whitish layer or cuticle. Agitated culture spontaneously



produces cellulose in the culture medium, forming irregular agglomerates or suspended fibers [54].

CNCs are nanoparticles abundantly rich in fragments of the cellulose chain, rigorously ordered in a crystalline structure of up to 100 nm. CNCs indicate high thermal stability, in addition to a higher surface area and crystallinity compared to primitive cellulose [41]. NFCs are frequently produced by many mechanical procedures, such as milling/refining, high-pressure homogenization, ultrasound-assisted treatment, microwave, steam explosion, and microfluidization, and by a series of chemical processes, such as TEMPO oxidation, persulfate oxidation ammonium, carboxymethylation, and cationization [40].

The direct alteration of the surface of the cellulose nanoparticles allows access to the biopolymer for a variety of purposes (Figure 2). Modifications based on hydroxyl groups allow the improvement of the biomaterial and intensify its potential use. Chemical reactions involving oxidation and acetylation processes or the addition of functional materials, polymers, and functional groups on the surface of the nanogranules allow the surface properties of the nanocellulose to be improved and associate with different non-polar matrices or change its affinity with certain polar and non-polar molecules [56]. The use of nanocellulose has aroused extensive industrial interest and has shed light on a variety of operations, such as the paper industry [57], packaging [58], cosmetics [59], the pharmaceuticals industry [60], medicine [61], biomedicine [62], paints and coating [63], hydrogel synthesis [64], and filtrations [65]. Nanocellulose has two basic disadvantages, namely a high number of hydroxyl compounds, which causes strong and resistant interactions by hydrogen molecules between two bundles of nanofibrils, and high hydrophilicity, which does not allow its application for a variety of industrial purposes, such as coating paper or composites, for example, without inducing a prominent surface modification to degrade the number of hydroxyl interactions and to stimulate compatibility with several other matrices [66].



**Figure 2.** Main advantages and current applications of cellulose-based biomaterials and cellulose primary configurations.

## 2.2. Lignin

Lignin is one of the most exuberant organic materials in nature and its content range is 15–30% in plants. However, these concentrations are variable depending on the type of biomass, plant characteristics, plant growth environment, and constitution of the cellulose wall [67]. Moreover, lignin is the only renewable aromatic polymer in nature [68].

Approximately 50 to 70 million tons of lignin are produced worldwide [69]. This panorama is directly associated with the widespread use of lignin as a source for the production of biofuels, since about 60 billion gallons of biofuels should be produced annually. Approximately 0.75 billion tons of biomass rich in lignin is required, indicating that the conversion of plant biomass will result in at least 0.225 billion tons of lignin as a by-product [70]. In the plant spectrum, lignin encompasses the free space between the cellulose and hemicellulose bands, establishing a highly resistant and rigid structure, whose purpose is to act in the performance of water and nutrient transport in the stems of plants [68]. The lignin matter is closely associated with the mechanical properties of the plant cell wall and the mechanical resistance provided by the biopolymer is significantly superior to the resistance provided by the cellulose content [71].

The inflexibility of lignin is highly influenced by the aromatic chains in the compounds in signapyl alcohol, *p*-coumaryl alcohol, and coniferyl alcohol. Furthermore, plant species with high lignin production have large amounts of lignin-synthesizing enzymes, such as phenylalanine ammonia lyase (PAL), caffeic acid *O*-methyltransferase (COMT), 4-coumarate coenzyme A ligase 3 (4CL<sub>3</sub>), cinnamyl alcohol dehydrogenase 2/7 (CAD2/7), cinnamoyl-CoA reductase 20 (CCR20), and cinnamate 4-hydroxylase (C<sub>4</sub>H) [72]. Lignin is also composed of three hydroxycinnamic alcohols, ceteryl alcohol, and mustard alcohol via ether associations, C-C chains, among others [33]. There is a significant diversity in distinct, highly polar chemical groups allocated in the structural complex of lignin, such as methoxyl, hydroxyl, carbonyl, and carboxyl, granting lignin high resistance to the action of enzymes, chemical solvents, or water hydrolysis [20].

Lignin acts as a carrier of fundamental materials, such as water and nutritional substances, and as a component of structural support for plant organs, arranging the matrix that also composes cellulose and hemicellulose in the complex [73]. The lignin content in the plant may vary with the species and the morphological organ, since there is a diversity in the scientific investigations that have indicated different concentrations of lignin in different organs of the same plant [74–76]. The high accessibility and ease of obtaining lignin from natural sources is key to a wide range of industrial applications, from adsorbent materials to biofuels and power generation [77]. The sustainable footprint of lignin provides the basis for the synthesis of biomaterials that convert the uncontrolled use of chemical resources to the production of electricity [78]. The spectrum of direct applications of lignin includes the engineering industry [79], biomedicine and biotechnology [80], medicine [81], biopesticides and biofertilizers [82], wastewater treatment [83], biofuels [84], adsorbents [85], carbon fibers [86], adhesives [87], dispersants [88], anti-UV filters [89], and the pharmaceuticals industry [90].

### 3. Modification and Characterization of Cellulose

Cellulose is widely obtained from lignocellulose-rich materials, bacteria, marine animals, and algae [91]. With the intensification of sustainable assertions in recent years, the exploration of polymers of natural origin has gained attention, which directly reflects the exploration of technological strategies and processes that involve the modification of these materials to enhance performance. The structural modification of the cellulose surface aims to reduce the high hydrophilicity of biomaterials, as well as to intensify the rupture of the long chain of hydroxyl groups that sustain the material. To improve treatment performance, it offers appropriate cost effectiveness and generates bioproducts in an environmentally friendly context. Pretreatments involving cellulose materials can be of enzymatic origin or TEMPO (2,2,6,6-tetramethylpiperidine-1-oxyl). These procedures aim to increase the reactivity of cellulose, especially in the transfiguration of hydroxyl groups into carboxylate groups [54]. The subtopics described below provide a better understanding of the processes involved in configuration changes in cellulose-based biomaterials.

### 3.1. Surface Modification

The surface arrangement of nanocellulose can be easily configured through the continuous action of surfactants rich in highly hydrophobic and hydrophilic groups, or the adsorptive process based on polyelectrolytes [66]. There is a diversity of surfactants, such as fluorosurfactants adherent to the cellulose structure, cationic surfactants, and polyelectrolyte compounds, adapting the hydrophobic potential and improving specific properties [54]. Alterations in the hydroxyl groups that form the surface structure of nanocellulose are appropriate to enhance the spectrum of action of these biopolymers, especially in association with other materials to configure the structural properties of nanocellulose and improve the field of affinity with highly polar and/or non-polar matrices [56]. The modification of the surface structure using the adsorption method is segmented into two main classifications: the polyelectrolyte method and specific groups aimed at the adsorption of some points. The polyelectrolyte method has high potential as it involves different polyelectrolytes with opposite charges and specific nanoparticles to adapt the desired properties to the nanoparticles, with ease of modification through the adsorption of the nanoparticles and CNFs [92].

### 3.2. Grafting

Graft polymerization is a cellulose modification strategy whose purpose is to stimulate highly resistant covalent bonds to generate a branched copolymer, without affecting the primary characteristics of the biomaterial [37]. The grafting procedure drastically reduces the interaction between solutes and unattractive aggregates with the cellulolytic surface, providing groups suitable for designing electrostatic repulsion from the membrane surface or enhancing hydrophilicity to enhance water-surface interactivity [93]. The grade of the grafted polymer directly affects the properties of the natural fiber, mainly the mechanical characteristics, elasticity, potential absorption, ion exchange competence, propensity for rupture of the resistant structure with extreme conditions of temperature and abrasion, and resistance [94].

Generally, the grafting procedure involves different mechanisms of action: (i) “grafting into” a step directly related to reactions between the functional groups of different polymers; (ii) “grafting from” refers to a polymer with functional groups that enhance the polymerization of vinylic monomers, in which the highly reactive sites belonging to the main chain are stimulated by chemical treatments or irradiation; and (iii) “grafting through” which implies the (co)polymerization of macromonomers [95]. Modification of the surface of cellulose by polymerization provides for the alteration of specific physical and chemical properties that may suit the desired purpose [96].

The effect of the grafting of cellulose in polylactide was evaluated after the synthesis of a series of cellulose ester-graft-poly(lactide) (CeEs-g-PLA) copolymers. A series of CeEs-g-PLA copolymers was synthesized using one-pot reactions involving acylation and ring-opening polymerization. With the increasing degree of acyl group substitution, the copolymers presented enhanced thermal stability and thermoplasticity due to the intermolecular interactions between the acyl groups and poly(lactide) sidechains. Therefore, the feed content of the acyl agent has a significant influence on the structural characteristics of the graft copolymer, because the acylation proceeds predominantly at the hydroxy groups in the cellulose backbone and, then, the PLA chains are grafted onto the remaining unreacted hydroxy groups [97].

Green biofilms with antimicrobial activity were developed from PLA and cyclic N-halamine 1-chloro-2,2,5,5-tetramethyl-4-imidazolidinone (MC) grafted microcrystalline cellulose (g-MCC) fibers. The grafting percentage was 10.24%. The grafting improved the compatibility between g-MCC and PLA, leading to an excellent dispersion of g-MCC in the film matrix, and a superior transparency of the g-MCC/PLA compared to that of the MCC/PLA films. The enhanced compatibility of the g-MCC/PLA films produced better mechanical properties, including the mechanical strength, elongation at break and initial modulus than those of both the MCC/PLA and MC/PLA composites. The oxidative

chlorine of g-MCC/PLA was highly stable compared to that of MC/PLA films, providing long-term antimicrobial activity [98].

Incorporating the surface-grafted cellulose nanocrystals (CNCs) with enantiomeric polylactide (PLLA or PDLA) was presented as an effective and sustainable way to modify PLLA. The CNCs with identical content and length of PLLA and PDLA were prepared and blended with PLLA. The rheological properties of PLLA/CNC-g-D are improved, indicating that the stereocomplexation can improve the interfacial strength as compared with the conventional van der Waals force in PLLA/CNC-g-L. The matrix crystallizes at a higher rate in PLLA/CNC-g-L than PLLA/CNC-g-D. PLLA/CNC-g-L15 reached its half crystallinity in 8.26 min, while a longer period of 13.41 min was required for PLLA/CNC-g-D15. The formation of low content sc-PLA at the interface may restrict the diffusion of PLLA, but contribute less to generate crystalline nuclei, which synergistically leads to the retarded crystallization kinetics in PLLA/CNC-g-D [99].

### 3.3. Chemical Procedures

Chemical-based modification procedures involve changes in the basic properties of cellulose, such as the hydrophilic or hydrophobic potential, elasticity, water absorption, adsorptive or ion exchange performance, and resistance to adversity. The dominant basic chemical modification strategies for cellulose are esterification, etherification, halogenations, oxidation, and treatment with alkaline compounds [54]. Changes in the nanocellulose complex significantly increase the degradability and biocompatibility of the biopolymer with other biomaterials [53]. Furthermore, considering the low cost–benefit and process efficiency, Table 1 indicates the main segments and pretreatments for modifying the pulp structure, from specific chemical methods to mechanical base changes. The procedures increase the cellulolytic reactivity and enhance the conversion of compounds into desired functional groups to adapt to promising characteristics and properties.

### 3.4. Other Treatments

Furthermore, the diversity of viable alternatives has been applied to biowaste treatment. These strategies concentrate techniques of mechanical and/or thermal and chemical activities to alter the physicochemical properties of the feedstocks. Among the mechanical and physical methods, the drying method and the milling strategy are valid alternatives that have been widely explored. The drying method is extremely necessary for preparing the raw material before applying other pretreatment strategies, especially for eliminating moisture from the material, which improves process efficiency and requires lower temperature and calorific value [100]. Cellulose drying conditions directly influence its dissolution and some studies have led to a parameterization of conditions to optimize the cellulose dissolution process [95]. The drying process can be conducted by oven drying and/or freeze drying, hot pressing, and supercritical drying with CO<sub>2</sub>. Furthermore, the drying procedure or wetting/drying cycles, called hornification, provide higher dimensional stability and less material degradation through increases in molecular packing. This procedure can be controlled, for example, by the time and/or number of cycles and drying requirements [101].

Among the mechanical methods, strategies aimed at reducing the particle size and increasing the contact area between the solid matrix and the solvent are widely applied. The milling strategy involves the effectiveness of the mechanical and thermal effects to redesign the fiber matrix and provide a wide spectrum of applications for the biomaterials, based on the adjustment of high pressure, collision, and absorption, in addition to a significant increase in temperature [102]. Additionally, the milling procedure is an extremely efficient strategy for modifying the crystalline structure of cellulose, as it enables the optimization of cellulose hydrolysis, interrupting the crystallinity (cellulose I) of native cellulose through increased contact with acid by cellulose [103].

According to physiochemical methods, they are the most common alternatives, mainly due to the modifications in the properties of the material, as well as the increase in inter-



molecular interactions. These methods involve steam explosion, wet oxidation, liquid hot water (LHW), and microwave-assisted and ultrasound-assisted extractions, and have been widely explored due to the high rupturing of the lignocellulose complex and minimization of the crystallinity of the cellulose. Accordingly, the steam explosion process is an environmentally viable strategy to modify cellulose fibers through the intensification of fibrillation, providing the synthesis of nanofibers [104]. Furthermore, the steam explosion procedure promotes the rupture of lignocellulosic biomass components by steam heating, shear forces, and hydrolysis of glycosidic bonds by the organic acid formed during the process. The steam explosion procedure facilitates the rupture of lignocellulosic structures, promoting the modification of the physical properties of the material (specific surface area, water retention capacity, color, etc.) and increasing the rate of enzymatic hydrolysis of the cellulose components [105].

Wet oxidation is an interesting alternative applied to the functionalization of cellulose because the process results in products with different structures and properties depending on the substrate, reagents, reaction parameters, and medium. The strategy provides new, high-performance materials based on cellulose, with the possibility of a variety of applications [106]. The oxidation process involves changing the performance of nanofibrils, facilitating their dissolution in water. This scenario results in a high degree of cellulose processing, without requiring the use of chemical products [107]. Furthermore, pretreatment with liquid hot water (LHW) is an interesting strategy, since it does not involve the addition of chemicals and has moderate process operating conditions. The procedure involves the application of water associated with an increase in temperature, drastically reducing the pH of the medium releasing carboxylic acids and intensifying the rupture of the structural matrix of the lignocellulosic biomass. Consequently, there is a significant increase in the accessible surface area, intensifying the action of the enzymes and the fermentation process [108].

Furthermore, microwave-assisted technology is a promising technique applied to lignocellulose-rich structure modification processes and extraction procedures. The alternative applies microwaves to significantly increase the temperature of the medium, reducing the reaction time, improving the process efficiency, and establishing uniform operating conditions, such as fast heating speed, uniform heating, and no temperature gradient occurrence [109]. In the hydrolysis processes, the microwave-assisted treatment significantly promotes the transformation of cellulose into C6 molecules with high selectivity. High-temperature conditions act positively on hydrolysis performance, since the microwave-assisted process allows superior operating conditions compared to conventional hydrothermal systems. It was pointed out that high temperatures promoted an intensification of the association at the molecular level between the microwaves and cellulose (through the primary alcohol groups,  $-\text{CH}_2\text{OH}$  groups), redirecting the energy to the surrounding molecular structure to initiate the cleavage of polysaccharide chains [110].

Ultrasound-assisted technology has been indicated as an efficient strategy in the extraction and rupture processes of the lignocellulosic complex. The energy intensity of the process increases the mass transfer of the biomass components to the extraction solution and, under established conditions, causes the acoustic cavitation process, in which the waves produced by the equipment propagate in expansion and compression cycles. Large amounts of microbubbles are formed and collide with strong motion. The friction between the microbubbles releases a significant amount of energy in the configuration of shock waves, which come into contact with the material rich in lignocellulose and promote its disintegration, facilitating the extraction and modification processes [111]. The hydrodynamic forces produced lead to the defibrillation of the biomass, which may be pure cellulose, microcrystalline cellulose, or other components of interest. The direct rupture of the biomass promotes the formation of filament aggregates with different sizes. The performance of the process depends directly on the characteristics of the material, since the ultrasonic bath acts on the crystalline structure of cellulose in different ways, based on



the type of biomass, operating conditions, concentration of lignocellulose, and degree of crystallinity [112].

On the other hand, the use of organic solvents is still one of the main alternatives adopted as a pretreatment. The replacement of the primary hydroxyl groups in cellulose by other molecules results in the intensification of the diversity of chemical reactions, in addition to contributing to an increase in grafting efficiency and the performance of functional groups for structural modifications. The main chemical reaction alternatives applied for the structural modification of cellulose are esterification, oxidation/amidation, and silanization. Esterification is generally carried out by an acylation process with carboxylic acid anhydride and 4-dimethylaminopyridine or strong acid as a catalyst. The oxidation process involves distinct C6 hydroxyl groups under moderate aqueous conditions; in addition to modifying the biopolymers and causing strong bonds at one end and adapting them with specific functional groups at the other to adapt to the matrix [113]. The application of silane is widely carried out, since the process intensifies the interfacial interaction between the hydroxyl groups of cellulose. The silanol agent is produced and can react with the hydroxyl groups of cellulose or condense on cellulose surfaces since they have the same reactive groups (-OH). Furthermore, thermal treatments can allow condensation between the OH groups of hydrolyzed silanes and cellulose, assuming chemical modification [114]. Nevertheless, these materials are highly harmful and their recovery after the extraction procedure requires additional steps, which results in higher process complexity and increased cost-benefit [115]. The continued use of solvents in pretreatment procedures is still inevitable, mainly due to the high proportion of solid dissolution, mass and heat transfer, viscosity reduction, and effectiveness in the separation and purification operation [116].

**Table 1.** Current advantages and limitations to the main cellulose-based modification processes.

Modification Methods	Process Methods	Advantages	Drawbacks	References
Surface adsorption	<ul style="list-style-type: none"> <li>- Plasma</li> <li>- Photochemistry</li> <li>- Radiation</li> <li>- Enzymes</li> </ul>	<ul style="list-style-type: none"> <li>- Hydrophilicity</li> <li>- High efficiency</li> <li>- Environmentally friendly</li> <li>- Biocompatibility</li> <li>- Properties adjustment</li> <li>- Cellulose profile preservation</li> <li>- Biodegradability</li> </ul>	<ul style="list-style-type: none"> <li>- High moisture absorption</li> <li>- Uncontrolled di-isocyanate and cellulose reaction</li> </ul>	[37,96,117]
Chemicals	<ul style="list-style-type: none"> <li>- Carboxylic acid groups</li> <li>- Specific functional groups</li> <li>- Alkyne-acid associations</li> <li>- Carbonylation</li> <li>- Esterification</li> <li>- Acylation</li> <li>- Ionic liquids</li> <li>- Etherification</li> </ul>	<ul style="list-style-type: none"> <li>- Functionality</li> <li>- Viability for a variety of functional groups</li> <li>- Process agility</li> <li>- Efficiency</li> <li>- By-products generation</li> <li>- Structural durability</li> <li>- High adsorption potential</li> </ul>	<ul style="list-style-type: none"> <li>- Pollution rate</li> <li>- High costs</li> <li>- Recycling resistance</li> <li>- Low dispersibility</li> <li>- Purification necessity</li> </ul>	[37,54,118]
Grafting	<ul style="list-style-type: none"> <li>- Grafting to</li> <li>- Grafting from</li> <li>- Grafting through</li> </ul>	<ul style="list-style-type: none"> <li>- Versatility</li> <li>- Biocompatibility</li> <li>- Properties adaptability</li> <li>- Weight adjustment</li> <li>- Dispersity adjustment</li> </ul>	<ul style="list-style-type: none"> <li>- Homopolymer synthesis</li> <li>- High graft density</li> <li>- Degradation of cellulose complex</li> <li>- No generation of block copolymer grafts</li> </ul>	[95,96,119,120]
Molecule chemical grafting	<ul style="list-style-type: none"> <li>- Ionic transference</li> <li>- Esterification</li> <li>- Acetylation</li> <li>- Gaseous methods</li> </ul>	<ul style="list-style-type: none"> <li>- Cellulose structure improvement</li> <li>- High cellulose derivates production</li> <li>- Process conditions adjustment</li> <li>- Accessibility of the cellulose surface</li> </ul>	<ul style="list-style-type: none"> <li>- High complexity in ester bond production</li> <li>- No total cellulose dissolution</li> <li>- Toxicity</li> <li>- Harsh reactant conditions</li> </ul>	[37,54,66,120]

#### 4. Modification and Characterization of Lignin

Lignin is the second most abundant biopolymer in nature, with a highly resilient structure and strong antioxidant activity. The molecular design of lignin indicates a significant concentration of functional groups, with easy alteration of properties based on chemical modification procedures [121]. The concentration and design of the lignin matrix varies depending on the type of biomass and lignocellulose content [122]. The golden age of exploring highly sustainable energy sources based on the use of materials rich in lignocellulose comes from strategies for a diversity of applications, such as the mass production of biofuels and other biochemical products to satisfy energy demand. Some essential plant materials from widely cultivated crops, such as sugar cane, corn, and sorghum, are promising for processes involving the synthesis of first-generation biofuels and chemical products of interest [33]. Under biorefinery concepts, the type of biomass is also strongly influenced by local characteristics, such as agricultural management, climate performance, and raw material availability. Since the bioeconomy approach has emerged as a strategy faithfully associated with the valorization of residues of plant origin, the requirement for natural biopolymers has fueled interest in technological alternatives and methods associated with the modification of lignin [123].

Considering that the structure of lignin is rich in a diversity of active groups, lignin can react chemically from different aspects, such as halogenation, nitration, phenylation, graft copolymerization, alkylation, dealkylation, sulfomethylation, acylation, ammonization, esterification, and hydrogenolysis. Furthermore, lignin has satisfactory compatibility with other biopolymers or natural fibers due to its hydrophilic nature, which establishes the application of lignin polar groups as agents to increase compatibility with essentially hydrophobic polymers. Furthermore, cross-linking with other polymers is desirable from the application of their hydroxyl groups to give rise to new materials, such as aromatic chemicals and bio-based polymeric materials [124].

One of the main methods of modifying lignin consists of the esterification of the biopolymer in reactions involving carboxylic acids, anhydrides, and acid chlorides. In this case, the modification of lignin by esterification reaction causes significant changes in its properties, such as better UV absorption, altered thermal stability, higher compatibility with the matrix, improved mechanical properties, better dimensional stability, improved hydrophobicity, and higher resistance to microbial decomposition [125]. Other surface modification strategies, such as conductive polymer coating, gold spray coating, and metal oxide coating, have received attention, due to the tunable physicochemical properties that have a wide range of uses, such as energy storage, sensors, and adsorption propensity [126]. Other methods involve physical modification techniques, which do not involve reactions between the functional groups present in lignin, but explore physical strategies that promote new and distinct properties of the modified material. Among these techniques, the application of gamma irradiation, sorption of metal ions, and plasma treatment are excellent exemplifications. These alternatives cause strong variations in the morphology of lignin, ease the rupture of the rigid matrix, and cause alterations in the surface characteristics of the material.

#### 5. Manufacturing Technology

##### 5.1. Extrusion Technology

An extrusion machine can be a single or twin-screw machine. A twin-screw extruder offers better efficiency results by reducing the melting and mixing time. Three important aspects related to extrusion technology are polymer melting, solids transport, and melt flow, which are controlled by computer models. These extrusion models are limited to pure polymers, so when making a composite there are difficulties in the fluidity of the reinforcing material [122]. However, a model called global GSEM has recently been developed for the extrusion of reinforced polymers in single-screw extruders with flood and starvation feeding, where starvation feeding has advantages to melting, less agglomeration, and better compound mixing [127].

Extrusion is a technology that is generally used as a preliminary step to injection molding. In extrusion, the matrix and the reinforcement are mixed to form granules, which are then laminated with injection technology [23,128].

There is research using extrusion as a pre-injection stage using vegetable-based materials. Mainly when producing pellets, this is the case in the study of thermoplastic starch and polylactic acid with tannins to delay biodegradation [129], to evaluate compatibilizers between polylactic acid and thermoplastic starch [130], with residues of soy, polyvinyl alcohol, and starch [131], or the use of bagasse cassava with polylactic acid for the production of tubes for seedlings [132].

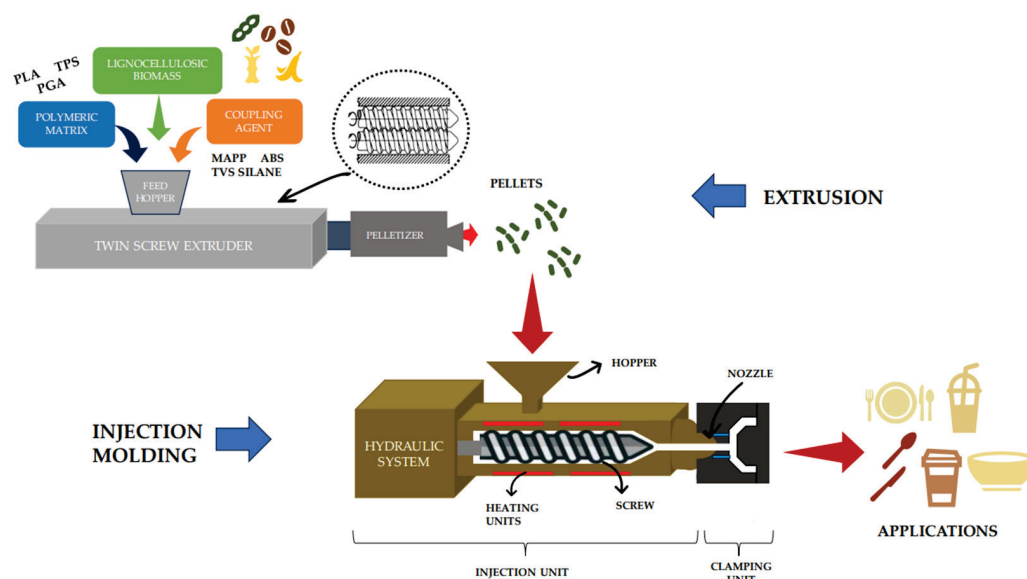
### 5.2. Injection Molding (IM)

The injection molding process has four relevant phases: plasticization, injection, cooling, and ejection [133]. During the first phase, the material is inserted into the barrel through a hopper and is melted using a rotating screw and internal heating units. Once the material is melted, it continues to the next phase, where the material is injected into the mold at a set speed and pressure parameters. For this, the screw is shifted to the front to avoid pressure variation and backward movement of the material in the barrel or deformation of the material. After this, the molded part goes to the cooling phase where the pressure and temperature decrease. This phase ends when the material solidifies. Finally, in the ejection, the part is removed by opening the mold [134–136]. IM technology demands high-energy consumption during processing [137]. The cooling phase is the most time-consuming stage in the cycle, taking between 50% to 80% of the cycle, so it is the stage that consumes the most energy [138]. As a result, there are more and more studies on improving energy efficiency at different stages of the process [139–142].

#### Parts of an Injection Molding Machine

The fundamental aspects to consider for IM are the machine specifications and the material to be used. Optimizing these aspects can ensure the reduction of defects and the quality of the final products [143]. An injection molding machine has a motor. It can be an AC motor or a hydraulic motor, with the hydraulic motor being the most used due to its excellent characteristics, such as less force required to start the movement and less overload on the rotating screw [134]. Then, it has a hopper to receive and store the material until it passes into the barrel to be melted, with the help of the heating units and the rotary screw. As the pellets are moved forward by the screw, they gradually melt, and are entirely molten by the time they reach the front of the barrel. In this part, there are temperature control sensors for the resistors. To complete the injection unit parts, we have the non-return check valve and the nozzle that contacts the mold and through which the material is injected. In the clamping unit, there are the fixed platen and the mobile platen that hold the mold [22,144].

Additionally, water is involved in the injection process. The plastic, which has the consistency of warm honey, is too viscous to flow through the narrow vents. To speed up the plastic's solidification, coolant, typically water, flows through channels inside the mold just beneath the surface of the interior. After the injected part solidifies, the mold opens. As the mold opens, the volume increases without introducing air, which creates tremendous suction that holds the mold together [145]. The extrusion and injection molding process described is illustrated in the following Figure 3.



**Figure 3.** Extrusion and injection molding to produce composite-based parts.

### 5.3. Materials

The materials used for IM can be thermoplastic or thermosetting. Some of the polymers used are PA 6, PC, PE-HD, PE-LD, PP, and PS, although there is an extensive variety [146]. Currently, due to the growing interest in biodegradable compounds, petroleum-derived polymers are being replaced by biopolymers obtained naturally or synthetically, such as PLA, TPS, PGA, PHB, PLLA, etc. To select the most suitable polymer for IM, it is important to consider some of the relevant inherent properties, such as strength, flexibility, toughness, thermoresistance, and cost [147].

### 5.4. Polymer Composites: Issues, Challenges, and Progress

#### 5.4.1. Cellulose and Hemicellulose Used in Injection Molding

Cellulose and hemicellulose in injection molding are generally used as reinforcing materials in bonding to a matrix polymer. The mechanical, thermal, and morphological properties of injection molded reinforced composites are the focus of research and discussion, since these properties are parameters to evaluate the improvements that the addition of lignocellulose to the polymer matrix can provide. The parameters of reinforced polymers are mainly linked to the pretreatment of the fiber, the percentage of the filler to be used, the dispersion of the fibers in the matrix, the technology used, the fiber length, and the properties of the matrices [148].

The compatibility between the matrix and the reinforcement represents a challenge due to the hydrophilic behavior of the filler and the hydrophobic behavior of the matrix, resulting in fiber agglomeration [149]. For this reason, coupling agents that act both in the matrix and the filler are currently used to improve the adhesion, heat resistance, and mechanical properties of the composite. The most used coupling agents are epoxy and maleic groups and glycidyl methacrylate because of their favorable compatibility [150–152]. One of the agents most widely used as a compatibilizer is maleic anhydride grafted polypropylene (MAPP), as it provides good adhesion when a polypropylene matrix is used [153,154]. The correct adhesion between the fiber and the matrix will integrate the fiber-dependent strength and modulus and the matrix-dependent thermal stability.

For the formation of parts by extrusion and IM using biomass as reinforcement, it is important to consider the processing temperature. Lignocellulose has two zones where its main components are lost, between 200–250 °C where amorphous cellulose and hemicellulose are degraded, and between 360–540 °C where lignin is degraded [150,155–157]. This parameter can affect the tensile strength and stiffness of the obtained product [158]. Organoleptic characteristics, such as odor and color, are also affected by high temperatures,

even though cellulose has a high thermal resistance. Hemicellulose, on the other hand, decomposes producing an inappropriate odor, however, this can be minimized with odor attenuators [159]. The color of the molded part can undergo variations depending on the reinforcement material used, such as turning a dark brown color due to the Maillard reaction [160].

In injection molding and extrusion, the reinforcement material and the matrix material influence the rheological, mechanical, and thermal characteristics. Overfilling can reduce the contact between the reinforcement surfaces and the matrix due to the lack of available contact surfaces in the matrix, which will affect the mechanical properties by preventing energy absorption and enhancement of the matrix polymer [161]. Regarding the rheological properties, the increase in filler material does not significantly affect the viscosity or melt temperature [153], but it can generate an increase in pressure, which can cause clogging of the nozzle during injection and generate defective parts [162]. In some cases, the coupling agent has been shown to reduce viscosity by providing lubrication, which may reduce the pressure required during injection [163]. In the study on a composite reinforced with coffee husk flour, they evidenced fractures in the rough surface due to the increase in filler [160]. Increased filler and poor adhesion can affect the toughness of the composite and promote brittleness, as evidenced in tests conducted between linseed meal and PLA. However, this can be significantly reduced with the use of linseed derivatives, such as oil, which serve as a plasticizer during extrusion [164].

Extrusion is commonly used as a previous step to IM, used to make the blend of the reinforced composite. Hence, it is very important to try to optimize the parameters during this process. A failure related to the extrusion of fiber-reinforced polymers is breakage due to stress accumulation in the fibers. This is mainly due to the control of parameters through the extruder flow [165]. The size of the fibers and the shearing can also affect the mechanical properties since the adhesion between the compounds is reduced [151,166]. It reduces the surface interaction between the filler and the matrix, as well as overfilling, promoting agglomeration and a reduction of Young's modulus [167]. The tensile modulus will increase as the fiber length increases [158]. One technique that has shown promising results in the processing of polymer composites before injection is solid-state extrusion (SSE), as it favors fiber distribution and dispersion [149].

#### 5.4.2. Lignin-Based Polymeric Materials

Due to its hydrophobicity and rigidity, lignin is of direct use, however, it requires hard work for its integration with a polymer matrix [168]; in addition to being incompatible with various aliphatic polyesters, such as PLA and PLC, impairing its mechanical properties [169]. In the evaluation of the addition of unmodified lignin extracted from tobacco in HDPE, it was found that the injection molding parameters are not affected and the dispersion using a single-screw extruder is adequate; however, the increase in lignin decreases the resistance to traction [170]. A coupling agent in lignin-reinforced composites, such as maleic anhydride grafting, can improve the tensile strength and ethylenebutylacrylate glycidylmethacrylate terpolymer (EBGMA) impact resistance. The combination of both can offer better results in terms of both characteristics [171]. More recent studies have seen advances in composites by extrusion and injection with hybrid components (pp/lignin/linen) using MAPP to ensure adhesion, obtaining improvements in stiffness and strength [172].

Regarding advances in extrusion and injection technologies, biobased polyethylene and kraft lignin processed using reactive extrusion with dicumyl peroxide (DCP) offer suitable results in terms of the mechanical properties and dispersion in lignin, thus being an effective and sustainable alternative [173]. Kraft lignin can also be used as a bio-coupling agent when modified by phenolation or glyoxalation, giving similar results to those obtained with maleic anhydride grafting concerning the mechanical properties [174].



## 6. Applications

In recent years, the number of biodegradable materials from different agroindustrial wastes and by-products has increased because of the need to replace the use of conventional petroleum-based plastics. In this context, developing biodegradable plastic (natural polymers or biopolymers) is necessary to avoid recycling and environmental pollution issues. It also has several advantages, such as renewability and biodegradability, and can be part of sustainable consumption that minimally affects the environment [175]. This agroindustrial biomass may be directly incorporated into polymer matrices, reinforcing filler composites [175], or used as the source of particular compounds to modify the polymer materials [176].

Corn, wheat, rice, soybean straw, sugarcane bagasse, orange waste, coffee industry by-products (coffee husk, spent coffee grounds) [177], avocado seed flour [175], banana and pineapple wastes, cornhusk, malt bagasse, and a diversity of residues are used in polymer matrices (polyolefins, low-density polyethylene, polyhydroxybutyrate, high-density polyethylene, and polypropylene). They are used for the manufacturing of natural fiber composites (NFCs), mainly to promote mechanical reinforcement and thermal or acoustic insulation [178], since they have thermal conductivity similar to these materials. They have already been implemented in the automotive, aerospace, and defense industries, where innovations are being made [179]. It uses trays prepared by thermopressing in a compression molding machine to fabricate biodegradable trays for semi-rigid packaging [180].

In agricultural, agroindustrial wastes, such as corn and wheat-waste flour, sunflower seed husks, rice husks, yerba mate waste, and cellulose paper, are used in the development of biodegradable and compostable pots for seedling growth containers molded from the obtained thermocompressed sheets using a mold with the specified dimensions [181]. In civil construction, studies have been developed on the application of vegetable fibers as reinforcement in cement-based composites and particleboards for building construction and infrastructure, for applications as ceilings and as structural components [182].

Applications of polymeric materials from agroindustrial biomass include household goods, sports equipment, musical instruments, toys, office supplies, flexible cards, and within the automotive industry in the form of pellets by injection molding and extrusion [67,158]. Regarding the food industry, it has been used extensively for the formulation of food packaging and containers, such as trays, plates, bags, cups, and lids. In the food services sector, it has been used to produce spoons, forks, knives, and drinking straws, as shown in Table 2.

**Table 2.** Applications of compounds.

Application	Matrix	Reinforcing Material	Processing Method	Coupling Agent	Improved Properties	Ref.
Seedling tubes	PLA	Cassava bagasse	Extrusion and IM	-	Increased biodegradability	[132]
Food-serving utensils and tableware	PLA	Spent coffee grounds	Extrusion and IM	Oligomers of lactic acid (OLAs)	Tensile strength ductility and thermal stability	[183]
Masking panels, fiberboards, and plywood	PP	Walnut shells	Twin-screw extrusion and IM	MAPP	Thermal stability	[184]
Floors, doors, and furniture	BioPP	Mango peel flour	Reactive extrusion and IM	PP-g-IA and DCP	Elongation at break and thermal stability	[185]
Bio packaging materials, and food films	PBSA/PHBV	Faba bean stems and pods	Twin-screw extrusion and IM	-	Mechanical and barrier	[166]
Pellets (for packaging and disposable utensils)	PBS	Raw wheat bran	Extrusion	-	Increased biodegradability	[186]

Table 2. Cont.

Application	Matrix	Reinforcing Material	Processing Method	Coupling Agent	Improved Properties	Ref.
Rigid food packaging	PLA	Mango seeds	Extrusion and IM	-	Mechanical and barrier	[187]
Thermoplastic composite products	HDPE	Yerba mate	Extrusion and IM	MAPE	Tensile strength and modulus	[188]
Protective bags for banana fruits	Mater-Bi	Banana fiber	Twin-screw extrusion and film blowing/IM	-	Flexibility and mechanical properties	[189]
Bio composites	PP	Bagasse cane	Twin-screw extrusion and IM	SEBS-g-MA	Yung's modulus, tensile strength, and hardness	[190]
Rigid food packaging	Bio PET	Recycled cotton fibers	Twin-screw extrusion and IM	-	Elasticity, hardness, and thermal stability	[191]
Coffee capsules	PHBV/ATBC/CaCO <sub>3</sub>	Coffee silverskin	Melt extrusion and IM	-	Elastic modulus, crystallinity, and biodegradability	[192]
Industrial materials	PLA/MLO	Sheep wool fibers	Extrusion and IM	TVS silane	Matrix/reinforcement interaction	[193]
Packaging products	LLDPE	Carbocal	Extrusion and IM	-	Mechanical and rheological	[194]
Food packaging and industrial applications	HDPE	Coffee husk	Extrusion and IM	Acrylonitrilo butadieno estireno (ABS)	Tensile modulus, tensile strength, and melting temperature	[195]
Food stretch film, food shrink film, and bags of fruit	PE	Sour cherry shell powder	Single-screw extrusion with blowing die film	Maleic anhydride polyethylene	Mechanical and moisture absorption	[196]
Flexible bioactive packaging	Starch/glycerol/water	Acerola residue	Extrusion and IM	-	Antioxidant characteristics	[197]
Rigid bioactive packaging	Starch/glycerol/water	Grape skin	Extrusion and IM	-	Antioxidant characteristic	[197]
Biodegradable food packaging	PLA	Durian skin fiber	Extrusion and IM	-	Biodegradability	[198]
Agricultural film products	PLA	Spent coffee grounds	Twin-screw extruder and blow film extrusion	-	Flow rate increasing and viscosity decreasing	[199]
Fruit and vegetable packaging	PLA	Wheat straw	Twin-screw extrusion and IM	-	Flexural modulus and mechanical and thermal performance	[200]

The use of PLA in combination with cassava bagasse accelerates biodegradation faster, its use as seedling tubes increases the phosphorus content of the soil [132], cassava bagasse also increases the tensile strength, the modulus of elasticity, and lowers the water absorption capacity [201]. Besides, their use as lignocellulosic nanofibers, in combination with cassava starch, they obtain good intermolecular interaction and barrier properties, which can be applied in food packaging [202]. Moreover, cassava could also be used as a matrix. One study used cassava starch with glycerol and water, this mixture in combination with acerola improves the elongation at break, but reduces the mechanical properties and elasticity due to its high sugar content, while the mixture with added grape residues, improves the mechanical properties and elasticity [197]. Furthermore, grape pomace extract as an antimicrobial additive in bactericidal isotactic polypropylene shows low water vapor permeability [203]. PLA composites in combination with wheat straw were also developed, demonstrating rapid crystallization for a shorter molding time, and increased flexural modulus, and water permeability for packaging [200]. In addition, the use of ultrafine wheat fiber, blended with PHBV, improves the water vapor transfer rate, favoring

its use in fresh produce packaging [204]. On the other hand, lignocellulosic nanofibers developed from wheat straw, blended with PLA and Ecoflex<sup>®</sup>, resulted in high water vapor permeability and antioxidant capacity for lettuce packaging [205]. Other research, using raw wheat bran composites and PBS, showed a noticeable impact on the rate of decomposition in an accelerated ageing environment [206]. PLA with mango by-products (20% tegument) achieves good mechanical properties, such as an elastic modulus up to 38% by IM, fiber provides higher stiffness, applicable for rigid packaging [187]. Mango seed and its use as a flour, mixed with glycerol, increases the mechanical and barrier properties, and has good antioxidant capacity [207,208]. In addition, the development of bioPP/mango peel flour for wood product applications and compatibilized with an itaconic acid copolymer, results in increased Shore D hardness, tensile strength, and an increased fracture toughness of 29.69% [185]. PLA with coffee grounds (SCG) by IM and compatible with oligomers, possesses high thermal stability, tensile strength, and elongation at a break of 39.6%, due to its lipid content. These were applicable for utensils and tableware [183]. Another study also incorporated the use of PLA and SCG through the blown extrusion process to produce biocomposite films, showing that the elongation at break increases with increasing SCG, while the tensile strength and hardness decrease [199]. This is because oil extraction from SCG increases the flexibility in films [208], and its incorporation also increases the content of antioxidants and microbial activity [209]. The use of coffee waste continues to increase, such as the production of coffee capsules based on coffee silverskin (tegument covering the endosperm) with PHBV copolymers by IM, resulting in a low breaking strength but an increase in the elastic modulus and crystallinity [192]. Food packaging was also made from coffee husks, HDPE, and ABS, as a result of the increased tensile modulus and tensile strength [195].

Yerba mate waste at 20% by weight, blended with PP and HDPE, showed good modulus and tensile strength, viable for wood composites [188]. Likewise, the use of yerba mate residue with PLA increases the flexibility and preserves the antioxidant properties, applicable in films [210]. Bean waste can also be applied in film making, its use at 30% by weight, in combination with PBSA/PHBV, increases the modulus of elasticity and decreases the tensile strength, applicable in the production of films [166]. Banana fiber and Mater-Bi<sup>®</sup> were used in the creation of biodegradable bags, presenting greater strength and flexibility due to the fibers. In addition, the ripening of bananas is delayed by 1 to 2 weeks [189]. On the other hand, banana fibers with PVA increase the tensile strength and minimum water absorption for film making [211]. Similarly, banana fiber (especially canary fiber) has a higher tensile strength and modulus of elasticity compared to other fibers, such as sisal, jute, flax, cotton, and coconut [212].

Walnut shells were combined with PP by means of IM for panel, board, and plywood production, demonstrating that using PP and MAPP as a bonding precursor provides stiffness and thermal stability [184]. In the production of wood-based panels, walnut shells could be added up to 20% in order to fulfil their mechanical properties [213]. In addition, it has been shown that nut shells are very fragile in combination with PLA, so alkaline treatments are used [214] or plasticizers, for example, epoxidized oils are used [215]. Another study used PLA with durian skin fiber and additionally epoxidized palm oil, which resulted in improved processability and energy reduction, applied in biodegradable packaging [198]. Moreover, sheep wool fibers were used as reinforcement for PLA plasticized with maleinized linseed oil, resulting in poor tensile properties, but an increase in the modulus of elasticity and the elongation at break [193]. The increased use of wool fibers does not generate good adhesion in the polymer matrix, which decreases the tensile forces [216]. As a solution, silane treatment generates good compatibility and adhesion to wool fibers, increasing the mechanical properties [217]. Recycled cotton fiber waste has been used with bio-PET by IM and showed poor mechanical properties, such as tensile strength, due to different polarities; however, they have a high modulus of elasticity and hardness, applicable for rigid packaging [191]. On the other hand, films with cotton and elastane residues through dissolution and regeneration, obtain high transparency

and good tensile strength, applicable for packaging materials [218]. Another study used Carbocal<sup>®</sup> (sugar-beet residue) with LLDPE, resulting in stiffer composites; the thermal resistance and modulus of elasticity increased by 150% with the use of 50% Carbocal<sup>®</sup> [194]. The use of sugar beet with PVA increases the mechanical properties and water resistance for the formation of biodegradable films [219].

## 7. Concluding Remarks and Future Trends

Advances in polymeric materials derived from agroindustrial biomass using extrusion and injection molding techniques present a promising avenue for sustainable material development. Biomass offers renewable, eco-friendly feedstock for biomaterial production, reducing the environmental impact and providing cost savings. The modification of cellulose, achieved through surface modification, grafting, chemical procedures, and molecule chemical grafting, improves the properties and versatility of these materials. However, more studies are needed to optimize the modification and processing techniques, improve material compatibility, and explore new applications. Extrusion technology melts, mixes, and homogenizes the composites to form granules. Twin-screw extrusion is suggested as it provides greater efficiency in the process, followed by the use of injection molding technology to obtain the desired shape. The parameters in extrusion and injection molding should be optimized, as they will depend on its shear and composition. The fiber size is of vital importance because it can reduce the mechanical properties, such as Young's modulus of elasticity, which is why solid-state extrusion is recommended, as it favors a better distribution of the fibers. In addition, to overcome the differences in polarity between the matrix and the reinforcements, coupling agents are used to improve the adhesion, mechanical properties, and thermal stability of the reinforcements. Continued advancements in this field will contribute to the transition towards more eco-friendly and resource-efficient material solutions. Extrusion and injection molding techniques offer remarkable advantages as a result of their application in multiple industrial sectors, such as the automotive industry, textiles, pharmaceuticals, the biomedical industry, various packaging applications, and many others.

According to this review, it is evident that the trend is for biodegradable materials applied to the area of agriculture and food. The most common biodegradable polymer used is polylactic acid. Depending on the application and rigidity of the material, extrusion or injection is preferable. For example, more flexible materials, such as bags, are better for extrusion and more rigid materials, such as utensils or tableware, are preferable.

**Author Contributions:** Conceptualization, L.O.-M. and L.A.M.-B.; methodology, G.L.Z.; Project administration, L.O.-M.; investigation, A.P., A.E.-O., K.G.M.-F., L.A.M.-B., H.P.-B., P.P.-C., M.S.N.D.S., M.V.T., G.L.Z. and L.O.-M.; resources, G.L.Z., H.P.-B. and K.G.M.-F.; writing—original draft preparation, K.G.M.-F., L.A.M.-B., H.P.-B., P.P.-C., M.S.N.D.S., M.V.T., G.L.Z. and L.O.-M.; writing—review and editing, L.O.-M. and G.L.Z.; visualization, L.O.-M. and H.P.-B.; supervision, L.O.-M., P.P.-C., L.A.M.-B. and G.L.Z.; Data curation, A.P. and A.E.-O. All authors have read and agreed to the published version of the manuscript.

**Funding:** This research received no external funding.

**Institutional Review Board Statement:** Not applicable.

**Data Availability Statement:** Not applicable.

**Acknowledgments:** The authors acknowledge the scientific and technical support from the Pilot Plant of Agroindustrial Engineering at the University San Ignacio de Loyola and the Integrated Laboratory of Agroindustrial Processes Engineering (LAPE) at the Federal University of Santa Maria.

**Conflicts of Interest:** The authors declare no conflict of interest.

## References

- Blasi, A.; Verardi, A.; Lopresto, C.G.; Siciliano, S.; Sangiorgio, P. Lignocellulosic Agricultural Waste Valorization to Obtain Valuable Products: An Overview. *Recycling* **2023**, *8*, 61. [CrossRef]
- Varghese, S.A.; Pulikkalparambil, H.; Promhuad, K.; Srisa, A.; Laorenza, Y.; Jarupan, L.; Nampitch, T.; Chonhenchob, V.; Harnkarnsujarit, N. Renovation of Agro-Waste for Sustainable Food Packaging: A Review. *Polymers* **2023**, *15*, 648. [CrossRef] [PubMed]
- Daszkiewicz, T. Food Production in the Context of Global Developmental Challenges. *Agriculture* **2022**, *12*, 832. [CrossRef]
- Sala, S.; Anton, A.; McLaren, S.J.; Notarnicola, B.; Saouter, E.; Sonesson, U. In Quest of Reducing the Environmental Impacts of Food Production and Consumption. *J. Clean. Prod.* **2017**, *140*, 387–398. [CrossRef]
- Campoy-Muñoz, P.; Cardenete, M.A.; Delgado, M.C. Economic Impact Assessment of Food Waste Reduction on European Countries through Social Accounting Matrices. *Resour. Conserv. Recycl.* **2017**, *122*, 202–209. [CrossRef]
- Oluseun Adejumo, I.; Adebukola Adebisi, O. Agricultural Solid Wastes: Causes, Effects, and Effective Management. In *Strategies of Sustainable Solid Waste Management*; Saleh, H.M., Ed.; IntechOpen: London, UK, 2021; ISBN 978-1-83962-559-6.
- Bedoya-Perales, N.S.; Dal' Magro, G.P. Quantification of Food Losses and Waste in Peru: A Mass Flow Analysis along the Food Supply Chain. *Sustainability* **2021**, *13*, 2807. [CrossRef]
- Ishangulyev, R.; Kim, S.; Lee, S. Understanding Food Loss and Waste—Why Are We Losing and Wasting Food? *Foods* **2019**, *8*, 297. [CrossRef]
- Sharma, V.; Tsai, M.-L.; Nargotra, P.; Chen, C.-W.; Kuo, C.-H.; Sun, P.-P.; Dong, C.-D. Agro-Industrial Food Waste as a Low-Cost Substrate for Sustainable Production of Industrial Enzymes: A Critical Review. *Catalysts* **2022**, *12*, 1373. [CrossRef]
- Wang, Y.; Yuan, Z.; Tang, Y. Enhancing Food Security and Environmental Sustainability: A Critical Review of Food Loss and Waste Management. *Resour. Environ. Sustain.* **2021**, *4*, 100023. [CrossRef]
- Mujtaba, M.; Fernandes Fraceto, L.; Fazeli, M.; Mukherjee, S.; Savassa, S.M.; Araujo De Medeiros, G.; Do Espírito Santo Pereira, A.; Mancini, S.D.; Lipponen, J.; Vilaplana, F. Lignocellulosic Biomass from Agricultural Waste to the Circular Economy: A Review with Focus on Biofuels, Biocomposites and Bioplastics. *J. Clean. Prod.* **2023**, *402*, 136815. [CrossRef]
- Nargotra, P.; Sharma, V.; Tsai, M.-L.; Hsieh, S.-L.; Dong, C.-D.; Wang, H.-M.D.; Kuo, C.-H. Recent Advancements in the Valorization of Agro-Industrial Food Waste for the Production of Nanocellulose. *Appl. Sci.* **2023**, *13*, 6159. [CrossRef]
- Saravanan, A.; Yaashikaa, P.R.; Kumar, P.S.; Thamarai, P.; Deivayanai, V.C.; Rangasamy, G. A Comprehensive Review on Techno-Economic Analysis of Biomass Valorization and Conversional Technologies of Lignocellulosic Residues. *Ind. Crops Prod.* **2023**, *200*, 116822. [CrossRef]
- Bhatia, S.K.; Jagtap, S.S.; Bedekar, A.A.; Bhatia, R.K.; Patel, A.K.; Pant, D.; Rajesh Banu, J.; Rao, C.V.; Kim, Y.-G.; Yang, Y.-H. Recent Developments in Pretreatment Technologies on Lignocellulosic Biomass: Effect of Key Parameters, Technological Improvements, and Challenges. *Bioresour. Technol.* **2020**, *300*, 122724. [CrossRef]
- Singh, N.; Singhania, R.R.; Nigam, P.S.; Dong, C.-D.; Patel, A.K.; Puri, M. Global Status of Lignocellulosic Biorefinery: Challenges and Perspectives. *Bioresour. Technol.* **2022**, *344*, 126415. [CrossRef]
- Zhang, Y.; Ding, Z.; Shahadat Hossain, M.; Maurya, R.; Yang, Y.; Singh, V.; Kumar, D.; Salama, E.-S.; Sun, X.; Sindhu, R.; et al. Recent Advances in Lignocellulosic and Algal Biomass Pretreatment and Its Biorefinery Approaches for Biochemicals and Bioenergy Conversion. *Bioresour. Technol.* **2023**, *367*, 128281. [CrossRef]
- Raj, T.; Chandrasekhar, K.; Naresh Kumar, A.; Kim, S.-H. Lignocellulosic Biomass as Renewable Feedstock for Biodegradable and Recyclable Plastics Production: A Sustainable Approach. *Renew. Sustain. Energy Rev.* **2022**, *158*, 112130. [CrossRef]
- Synyuk, O.; Musiał, J.; Zlotenko, B.; Kulik, T. Development of Equipment for Injection Molding of Polymer Products Filled with Recycled Polymer Waste. *Polymers* **2020**, *12*, 2725. [CrossRef]
- Wilczyński, K.; Wilczyński, K.J.; Buziak, K. Modeling and Experimental Studies on Polymer Melting and Flow in Injection Molding. *Polymers* **2022**, *14*, 2106. [CrossRef]
- Yang, J.; Ching, Y.C.; Chuah, C.H. Applications of Lignocellulosic Fibers and Lignin in Bioplastics: A Review. *Polymers* **2019**, *11*, 751. [CrossRef]
- Ortega, F.; Versino, F.; López, O.V.; García, M.A. Biobased Composites from Agro-Industrial Wastes and by-Products. *Emergent Mater.* **2022**, *5*, 873–921. [CrossRef]
- Rabbi, M.S.; Islam, T.; Islam, G.M.S. Injection-Molded Natural Fiber-Reinforced Polymer Composites—A Review. *Int. J. Mech. Mater. Eng.* **2021**, *16*, 15. [CrossRef]
- Pannu, A.S.; Singh, S.; Dhawan, V. Composite manufacturing techniques—A review on injection, compression, pultrusion and extrusion process. *J. Adv. Sci. Res.* **2019**, *10*, 146–151.
- Root, K.P.; Pal, A.K.; Pesaranhajiabbas, E.; Mohanty, A.K.; Misra, M. Injection Moulded Composites from High Biomass Filled Biodegradable Plastic: Properties and Performance Evaluation for Single-Use Applications. *Compos. Part C Open Access* **2023**, *11*, 100358. [CrossRef]
- Ashokkumar, V.; Venkatkarthick, R.; Jayashree, S.; Chuetor, S.; Dharmaraj, S.; Kumar, G.; Chen, W.-H.; Ngamcharussrivichai, C. Recent Advances in Lignocellulosic Biomass for Biofuels and Value-Added Bioproducts—A Critical Review. *Bioresour. Technol.* **2022**, *344*, 126195. [CrossRef] [PubMed]



26. Wang, Y.; Gui, C.; Wu, J.; Gao, X.; Huang, T.; Cui, F.; Liu, H.; Sethupathy, S. Spatio-Temporal Modification of Lignin Biosynthesis in Plants: A Promising Strategy for Lignocellulose Improvement and Lignin Valorization. *Front. Bioeng. Biotechnol.* **2022**, *10*, 917459.
27. Stepanova, M.; Korzhikova-Vlakh, E. Modification of cellulose micro- and nanomaterials to improve properties of aliphatic polyesters/cellulose composites: A review. *Polymers* **2022**, *14*, 1477. [CrossRef] [PubMed]
28. Szymanska-Chargot, M.; Ciesla, J.; Pekala, P.; Pieczywek, P.M.; Oleszek, W.; Zyla, M.; Szkopek, Z.; Zdunek, A. The Influence of High-Intensity Ultrasonication on Properties of Cellulose Produced from the Hop Stems, the Byproduct of the Hop Cones Production. *Molecules* **2022**, *27*, 2624. [CrossRef]
29. Anwar, Z.; Gulfranz, M.; Irshad, M. Agro-Industrial Lignocellulosic Biomass a Key to Unlock the Future Bio-Energy: A Brief Review. *J. Radiat. Res. Appl. Sci.* **2014**, *7*, 163–173. [CrossRef]
30. Haq, I.U.; Qaisar, K.; Nawaz, A.; Akram, F.; Mukhtar, H.; Zohu, X.; Xu, Y.; Mumtaz, M.W.; Rashid, U.; Ghani, W.A.W.A.K.; et al. Advances in Valorization of Lignocellulosic Biomass towards Energy Generation. *Catalysts* **2021**, *11*, 309. [CrossRef]
31. Xie, Y.; Zhang, K.; Cui, S.; Liu, Y. A Review on the Structure and Biodegradation of Cellulose-Lignin Complexes. *Pap. Biomater.* **2020**, *5*, 44–50. [CrossRef]
32. Mankar, A.R.; Pandey, A.; Modak, A.; Pant, K.K. Pretreatment of Lignocellulosic Biomass: A Review on Recent Advances. *Bioresour. Technol.* **2021**, *334*, 125235. [CrossRef] [PubMed]
33. Wu, W.; Li, P.; Huang, L.; Wei, Y.; Li, J.; Zhang, L.; Jin, Y. The Role of Lignin Structure on Cellulase Adsorption and Enzymatic Hydrolysis. *Biomass* **2023**, *3*, 96–107. [CrossRef]
34. Adewuyi, A. Underutilized Lignocellulosic Waste as Sources of Feedstock for Biofuel Production in Developing Countries. *Front. Energy Res.* **2022**, *10*, 741570. [CrossRef]
35. Zoghlami, A.; Paës, G. Lignocellulosic Biomass: Understanding Recalcitrance and Predicting Hydrolysis. *Front. Chem.* **2019**, *7*, 874. [CrossRef]
36. Seddiqi, H.; Oliyai, E.; Honarkar, H.; Jin, J.; Geonzon, L.C.; Bacabac, R.G.; Klein-Nulend, J. Cellulose and Its Derivatives: Towards Biomedical Applications. *Cellulose* **2021**, *28*, 1893–1931. [CrossRef]
37. Aziz, T.; Farid, A.; Haq, F.; Kiran, M.; Ullah, A.; Zhang, K.; Li, C.; Ghazanfar, S.; Sun, H.; Ullah, R.; et al. A Review on the Modification of Cellulose and Its Applications. *Polymers* **2022**, *14*, 3206. [CrossRef]
38. Przypis, M.; Wawoczny, A.; Gillner, D. Biomass and Cellulose Dissolution—The Important Issue in Renewable Materials Treatment. *Appl. Sci.* **2023**, *13*, 1055. [CrossRef]
39. Potenza, M.; Bergamonti, L.; Lottici, P.P.; Righi, L.; Lazzarini, L.; Graiff, C. Green Extraction of Cellulose Nanocrystals of Polymorph II from *Cynara scolymus* L.: Challenge for a “Zero Waste” Economy. *Crystals* **2022**, *12*, 672. [CrossRef]
40. Uusi-Tarkka, E.-K.; Skrifvars, M.; Haapala, A. Fabricating Sustainable All-Cellulose Composites. *Appl. Sci.* **2021**, *11*, 10069. [CrossRef]
41. Magagula, L.P.; Masemola, C.M.; Ballim, M.A.; Tetana, Z.N.; Moloto, N.; Linganiso, E.C. Lignocellulosic Biomass Waste-Derived Cellulose Nanocrystals and Carbon Nanomaterials: A Review. *Int. J. Mol. Sci.* **2022**, *23*, 4310. [CrossRef]
42. Heydorn, R.L.; Lammers, D.; Gottschling, M.; Dohnt, K. Effect of Food Industry By-Products on Bacterial Cellulose Production and Its Structural Properties. *Cellulose* **2023**, *30*, 4159–4179. [CrossRef]
43. Lawson, L.; Degenstein, L.M.; Bates, B.; Chute, W.; King, D.; Dolez, P.I. Cellulose Textiles from Hemp Biomass: Opportunities and Challenges. *Sustainability* **2022**, *14*, 15337. [CrossRef]
44. Zhou, J.; Wang, H.; Du, C.; Zhang, D.; Lin, H.; Chen, Y.; Xiong, J. Cellulose for Sustainable Triboelectric Nanogenerators. *Adv. Energy Sustain. Res.* **2022**, *3*, 2100161. [CrossRef]
45. Rocha Ferreira, S.; Ukrainczyk, N.; Defáveri do Carmo e Silva, K.; Eduardo Silva, L.; Koenders, E. Effect of Microcrystalline Cellulose on Geopolymer and Portland Cement Pastes Mechanical Performance. *Constr. Build. Mater.* **2021**, *288*, 123053. [CrossRef]
46. Fatema, N.; Ceballos, R.M.; Fan, C. Modifications of Cellulose-Based Biomaterials for Biomedical Applications. *Front. Bioeng. Biotechnol.* **2022**, *10*, 993711. [CrossRef]
47. Ciolacu, D.E.; Nicu, R.; Ciolacu, F. Cellulose-Based Hydrogels as Sustained Drug-Delivery Systems. *Materials* **2020**, *13*, 5270. [CrossRef]
48. Rahman, U.U.; Humayun, M.; Khan, A.; Farooq, S.; Sadiq, M.; Bououdina, M.; Shah, N. Thermo-Chemical Modification of Cellulose for the Adsorptive Removal of Titan Yellow from Wastewater. *Molecules* **2023**, *28*, 3955. [CrossRef]
49. Zhang, R.; Tian, Y. Characteristics of Natural Biopolymers and Their Derivative as Sorbents for Chromium Adsorption: A Review. *J. Leather Sci. Eng.* **2020**, *2*, 24. [CrossRef]
50. Das, S.; Ghosh, B.; Sarkar, K. Nanocellulose as Sustainable Biomaterials for Drug Delivery. *Sens. Int.* **2022**, *3*, 100135. [CrossRef]
51. Tahir, D.; Karim, M.R.A.; Hu, H.; Naseem, S.; Rehan, M.; Ahmad, M.; Zhang, M. Sources, Chemical Functionalization, and Commercial Applications of Nanocellulose and Nanocellulose-Based Composites: A Review. *Polymers* **2022**, *14*, 4468. [CrossRef]
52. Ghasemlou, M.; Daver, F.; Ivanova, E.P.; Habibi, Y.; Adhikari, B. Surface Modifications of Nanocellulose: From Synthesis to High-Performance Nanocomposites. *Prog. Polym. Sci.* **2021**, *119*, 101418. [CrossRef]
53. Randhawa, A.; Dutta, S.D.; Ganguly, K.; Patil, T.V.; Patel, D.K.; Lim, K.-T. A Review of Properties of Nanocellulose, Its Synthesis, and Potential in Biomedical Applications. *Appl. Sci.* **2022**, *12*, 7090. [CrossRef]
54. Omran, A.A.B.; Mohammed, A.A.B.A.; Sapuan, S.M.; Ilyas, R.A.; Asyraf, M.R.M.; Rahimian Kolor, S.S.; Petrú, M. Micro- and Nanocellulose in Polymer Composite Materials: A Review. *Polymers* **2021**, *13*, 231. [CrossRef] [PubMed]

55. Tayeb, A.H.; Amini, E.; Ghasemi, S.; Tajvidi, M. Cellulose Nanomaterials—Binding Properties and Applications: A Review. *Molecules* **2018**, *23*, 2684. [CrossRef]
56. Abushammala, H.; Mao, J. A Review of the Surface Modification of Cellulose and Nanocellulose Using Aliphatic and Aromatic Mono- and Di-Isocyanates. *Molecules* **2019**, *24*, 2782. [CrossRef]
57. Li, A.; Xu, D.; Luo, L.; Zhou, Y.; Yan, W.; Leng, X.; Dai, D.; Zhou, Y.; Ahmad, H.; Rao, J.; et al. Overview of Nanocellulose as Additives in Paper Processing and Paper Products. *Nanotechnol. Rev.* **2021**, *10*, 264–281. [CrossRef]
58. Silva, F.A.G.S.; Dourado, F.; Gama, M.; Poças, F. Nanocellulose Bio-Based Composites for Food Packaging. *Nanomaterials* **2020**, *10*, 2041. [CrossRef]
59. Almeida, T.; Silvestre, A.J.D.; Vilela, C.; Freire, C.S.R. Bacterial Nanocellulose toward Green Cosmetics: Recent Progresses and Challenges. *Int. J. Mol. Sci.* **2021**, *22*, 2836. [CrossRef]
60. Huo, Y.; Liu, Y.; Xia, M.; Du, H.; Lin, Z.; Li, B.; Liu, H. Nanocellulose-Based Composite Materials Used in Drug Delivery Systems. *Polymers* **2022**, *14*, 2648. [CrossRef]
61. Ghilan, A.; Nicu, R.; Ciolacu, D.E.; Ciolacu, F. Insight into the Latest Medical Applications of Nanocellulose. *Materials* **2023**, *16*, 4447. [CrossRef]
62. Bacakova, L.; Pajorova, J.; Bacakova, M.; Skogberg, A.; Kallio, P.; Kolarova, K.; Svorcik, V. Versatile Application of Nanocellulose: From Industry to Skin Tissue Engineering and Wound Healing. *Nanomaterials* **2019**, *9*, 164. [CrossRef] [PubMed]
63. Fornari, A.; Rossi, M.; Rocco, D.; Mattiello, L. A Review of Applications of Nanocellulose to Preserve and Protect Cultural Heritage Wood, Paintings, and Historical Papers. *Appl. Sci.* **2022**, *12*, 12846. [CrossRef]
64. Yang, J.; Luo, Z.; Wang, M. Novel Fluorescent Nanocellulose Hydrogel Based on Nanocellulose and Carbon Dots for Detection and Removal of Heavy Metal Ions in Water. *Foods* **2022**, *11*, 1619. [CrossRef]
65. Mautner, A. Nanocellulose Water Treatment Membranes and Filters: A Review. *Polym. Int.* **2020**, *69*, 741–751. [CrossRef]
66. Missoum, K.; Belgacem, M.N.; Bras, J. Nanofibrillated Cellulose Surface Modification: A Review. *Materials* **2013**, *6*, 1745–1766. [CrossRef]
67. Borrero-López, A.M.; Valencia, C.; Franco, J.M. Lignocellulosic Materials for the Production of Biofuels, Biochemicals and Biomaterials and Applications of Lignocellulose-Based Polyurethanes: A Review. *Polymers* **2022**, *14*, 881. [CrossRef]
68. Roy, R.; Rahman, M.S.; Amit, T.A.; Jadhav, B. Recent Advances in Lignin Depolymerization Techniques: A Comparative Overview of Traditional and Greener Approaches. *Biomass* **2022**, *2*, 130–154. [CrossRef]
69. Bajwa, D.S.; Pourhashem, G.; Ullah, A.H.; Bajwa, S.G. A Concise Review of Current Lignin Production, Applications, Products and Their Environmental Impact. *Ind. Crops Prod.* **2019**, *139*, 111526. [CrossRef]
70. Iram, A.; Berenjian, A.; Demirci, A. A Review on the Utilization of Lignin as a Fermentation Substrate to Produce Lignin-Modifying Enzymes and Other Value-Added Products. *Molecules* **2021**, *26*, 2960. [CrossRef]
71. Hussain, S.; Iqbal, N.; Rahman, T.; Liu, T.; Brestic, M.; Safdar, M.E.; Asghar, M.A.; Farooq, M.U.; Shafiq, I.; Ali, A.; et al. Shade Effect on Carbohydrates Dynamics and Stem Strength of Soybean Genotypes. *Environ. Exp. Bot.* **2019**, *162*, 374–382. [CrossRef]
72. Li, Q.; Fu, C.; Liang, C.; Ni, X.; Zhao, X.; Chen, M.; Ou, L. Crop Lodging and The Roles of Lignin, Cellulose, and Hemicellulose in Lodging Resistance. *Agronomy* **2022**, *12*, 1795. [CrossRef]
73. Gbenezor, O.P.; Olanrewaju, O.A.; Usman, M.A.; Adeosun, S.O. Lignin from Brewers' Spent Grain: Structural and Thermal Evaluations. *Polymers* **2023**, *15*, 2346. [CrossRef] [PubMed]
74. Abaide, E.R.; Ugalde, G.; Di Luccio, M.; Moreira, R.d.F.P.M.; Tres, M.V.; Zabet, G.L.; Mazutti, M.A. Obtaining Fermentable Sugars and Bioproducts from Rice Husks by Subcritical Water Hydrolysis in a Semi-Continuous Mode. *Bioresour. Technol.* **2019**, *272*, 510–520. [CrossRef] [PubMed]
75. Garcia-Maraver, A.; Salvachúa, D.; Martínez, M.J.; Diaz, L.F.; Zamorano, M. Analysis of the Relation between the Cellulose, Hemicellulose and Lignin Content and the Thermal Behavior of Residual Biomass from Olive Trees. *Waste Manag.* **2013**, *33*, 2245–2249. [CrossRef]
76. Dos Santos, M.S.N.; Zabet, G.L.; Mazutti, M.A.; Ugalde, G.A.; Rezzadori, K.; Tres, M.V. Optimization of Subcritical Water Hydrolysis of Pecan Wastes Biomasses in a Semi-Continuous Mode. *Bioresour. Technol.* **2020**, *306*, 123129. [CrossRef]
77. Sharma, S.; Tsai, M.-L.; Sharma, V.; Sun, P.-P.; Nargotra, P.; Bajaj, B.K.; Chen, C.-W.; Dong, C.-D. Environment Friendly Pretreatment Approaches for the Bioconversion of Lignocellulosic Biomass into Biofuels and Value-Added Products. *Environments* **2023**, *10*, 6. [CrossRef]
78. Fabbri, F.; Bischof, S.; Mayr, S.; Gritsch, S.; Jimenez Bartolome, M.; Schwaiger, N.; Guebitz, G.M.; Weiss, R. The Biomodified Lignin Platform: A Review. *Polymers* **2023**, *15*, 1694. [CrossRef]
79. Gaudenzi, E.; Cardone, F.; Lu, X.; Canestrari, F. The Use of Lignin for Sustainable Asphalt Pavements: A Literature Review. *Constr. Build. Mater.* **2023**, *362*, 129773. [CrossRef]
80. Stanisz, M.; Klapiszewski, L.; Collins, M.N.; Jesionowski, T. Recent Progress in Biomedical and Biotechnological Applications of Lignin-Based Spherical Nano- and Microstructures: A Comprehensive Review. *Mater. Today Chem.* **2022**, *26*, 101198. [CrossRef]
81. Verdini, F.; Gaudino, E.C.; Canova, E.; Tabasso, S.; Behbahani, P.J.; Cravotto, G. Lignin as a Natural Carrier for the Efficient Delivery of Bioactive Compounds: From Waste to Health. *Molecules* **2022**, *27*, 3598. [CrossRef]
82. Chen, M.; Li, Y.; Liu, H.; Zhang, D.; Shi, Q.-S.; Zhong, X.-Q.; Guo, Y.; Xie, X.-B. High Value Valorization of Lignin as Environmental Benign Antimicrobial. *Mater. Today Bio* **2023**, *18*, 100520. [CrossRef]

83. Wang, B.; Sun, Y.-C.; Sun, R.-C. Fractional and Structural Characterization of Lignin and Its Modification as Biosorbents for Efficient Removal of Chromium from Wastewater: A Review. *J. Leather Sci. Eng.* **2019**, *1*, 5. [CrossRef]
84. Kocaturk, E.; Salan, T.; Ozcelik, O.; Alma, M.H.; Candan, Z. Recent Advances in Lignin-Based Biofuel Production. *Energies* **2023**, *16*, 3382. [CrossRef]
85. Nikolic, M.; Cáceres Najarro, M.; Johannsen, I.; Iruthayaraj, J.; Ceccato, M.; Feilberg, A. Copper Adsorption on Lignin for the Removal of Hydrogen Sulfide. *Molecules* **2020**, *25*, 5577. [CrossRef] [PubMed]
86. Zhou, L.; You, X.; Wang, L.; Qi, S.; Wang, R.; Uraki, Y.; Zhang, H. Fabrication of Graphitized Carbon Fibers from Fusible Lignin and Their Application in Supercapacitors. *Polymers* **2023**, *15*, 1947. [CrossRef]
87. Vieira, F.R.; Gama, N.; Magina, S.; Barros-Timmons, A.; Evtuguin, D.V.; Pinto, P.C.O.R. Polyurethane Adhesives Based on Oxyalkylated Kraft Lignin. *Polymers* **2022**, *14*, 5305. [CrossRef]
88. Hopa, D.Y.; Fatehi, P. Using Sulfobutylated and Sulfomethylated Lignin as Dispersant for Kaolin Suspension. *Polymers* **2020**, *12*, 2046. [CrossRef]
89. Piccinino, D.; Capecchi, E.; Tomaino, E.; Gabellone, S.; Gigli, V.; Avitabile, D.; Saladino, R. Nano-Structured Lignin as Green Antioxidant and UV Shielding Ingredient for Sunscreen Applications. *Antioxidants* **2021**, *10*, 274. [CrossRef]
90. Kumar, R.; Butreddy, A.; Kommineni, N.; Reddy, P.G.; Bunekar, N.; Sarkar, C.; Dutt, S.; Mishra, V.K.; Aadil, K.R.; Mishra, Y.K.; et al. Lignin: Drug/Gene Delivery and Tissue Engineering Applications. *Int. J. Nanomed.* **2021**, *16*, 2419–2441. [CrossRef]
91. Vasić, K.; Knez, Ž.; Leitgeb, M. Bioethanol Production by Enzymatic Hydrolysis from Different Lignocellulosic Sources. *Molecules* **2021**, *26*, 753. [CrossRef]
92. Yi, T.; Zhao, H.; Mo, Q.; Pan, D.; Liu, Y.; Huang, L.; Xu, H.; Hu, B.; Song, H. From Cellulose to Cellulose Nanofibrils—A Comprehensive Review of the Preparation and Modification of Cellulose Nanofibrils. *Materials* **2020**, *13*, 5062. [CrossRef] [PubMed]
93. Tyrka, M.; Nowak, M.; Misic, D.; Póľbrat, T.; Koter, S.; Trusek, A.; Zizovic, I. Cellulose Acetate Membranes Modification by Aminosilane Grafting in Supercritical Carbon Dioxide towards Antibiofilm Properties. *Membranes* **2022**, *12*, 33. [CrossRef] [PubMed]
94. Cichosz, S.; Masek, A.; Rylski, A. Cellulose Modification for Improved Compatibility with the Polymer Matrix: Mechanical Characterization of the Composite Material. *Materials* **2020**, *13*, 5519. [CrossRef] [PubMed]
95. Liyanage, S.; Acharya, S.; Parajuli, P.; Shamshina, J.L.; Abidi, N. Production and Surface Modification of Cellulose Bioproducts. *Polymers* **2021**, *13*, 3433. [CrossRef]
96. Wohlhauser, S.; Delepierre, G.; Labet, M.; Morandi, G.; Thielemans, W.; Weder, C.; Zoppe, J.O. Grafting Polymers from Cellulose Nanocrystals: Synthesis, Properties, and Applications. *Macromolecules* **2018**, *51*, 6157–6189. [CrossRef]
97. Lee, H.Y.; Seok, J.H.; Lee, J.-C.; Lee, W.; Iwata, T. One-pot synthesis of cellulose ester-graft-poly lactide copolymers in an ionic liquid and the effect of graft-chain composition on their thermoplasticities and enzymatic degradabilities. *Polym. Degrad. Stab.* **2023**, *214*, 110401. [CrossRef]
98. An, L.; Perkins, P.; Yi, R.; Ren, T. Development of polylactic acid based antimicrobial food packaging films with N-halamine modified microcrystalline cellulose. *Int. J. Biol. Macromol.* **2023**, *242*, 124685. [CrossRef]
99. Fang, H.-G.; Yang, K.-J.; Xie, Q.-Z.; Chen, X.; Wu, S.-L.; Ding, Y.-S. Influence of Interfacial Enantiomeric Grafting on Melt Rheology and Crystallization of Polylactide/Cellulose Nanocrystals Composites. *Chin. J. Polym. Sci.* **2022**, *40*, 93–106. [CrossRef]
100. Taylor, M.; Alabdrabalameer, H.; Skoulou, V. Choosing Physical, Physicochemical and Chemical Methods of Pre-Treating Lignocellulosic Wastes to Repurpose into Solid Fuels. *Sustainability* **2019**, *11*, 3604. [CrossRef]
101. Cichosz, S.; Masek, A. Drying of the Natural Fibers as A Solvent-Free Way to Improve the Cellulose-Filled Polymer Composite Performance. *Polymers* **2020**, *12*, 484. [CrossRef]
102. Zheng, H.; Sun, Y.; Zheng, T.; Zeng, Y.; Fu, L.; Zhou, T.; Jia, F.; Xu, Y.; He, K.; Yang, Y. Effects of Shear Emulsifying/Ball Milling/Autoclave Modification on Structure, Physicochemical Properties, Phenolic Compounds, and Antioxidant Capacity of Lotus (Nelumbo) Leaves Dietary Fiber. *Front. Nutr.* **2023**, *10*, 1064662. [CrossRef] [PubMed]
103. Liu, X.; Yan, P.; Xu, Z.; Zhang, Z.C. The effect of mix-milling with P2O5 on cellulose physicochemical properties responsible for increased glucose yield. *Carbohydr. Polym.* **2021**, *258*, 117652. [CrossRef] [PubMed]
104. Jacquet, N.; Vanderghem, C.; Danthine, S.; Quiévy, N.; Blecker, C.; Devaux, J.; Paquot, M. Influence of steam explosion on physicochemical properties and hydrolysis rate of pure cellulose fibers. *Bioresour. Technol.* **2012**, *121*, 221–227. [CrossRef]
105. Tienne, L.G.P.; Cordeiro, S.B.; Brito, E.B.; Marques, M.F.V. Microcrystalline cellulose treated by steam explosion and used for thermo-mechanical improvement of polypropylene. *J. Compos. Mater.* **2020**, *54*, 3611–3624. [CrossRef]
106. Muthamma, K.; Sunil, D. cellulose as an eco-friendly and sustainable material for optical anticounterfeiting applications: An up-to-date appraisal. *ACS Omega* **2022**, *7*, 42681–42699. [CrossRef]
107. Duceac, I.A.; Tanasa, F.; Coseri, S. Selective oxidation of cellulose—A multitask platform with significant environmental impact. *Materials* **2022**, *15*, 5076. [CrossRef]
108. Jimenez-Gutierrez, J.M.; Verlinden, R.A.J.; Van Der Meer, P.C.; Van Der Wielen, L.A.M.; Straathof, A.J.J. Liquid Hot Water Pretreatment of Lignocellulosic Biomass at Lab and Pilot Scale. *Processes* **2021**, *9*, 1518. [CrossRef]
109. Cui, J.-Y.; Zhang, N.; Jiang, J.-C. Effects of Microwave-Assisted Liquid Hot Water Pretreatment on Chemical Composition and Structure of Moso Bamboo. *Front. Bioeng. Biotechnol.* **2021**, *9*, 821982. [CrossRef]



110. Jiang, S.; Daly, H.; Xiang, H.; Yan, Y.; Zhang, H.; Hardacre, C.; Fan, X. Microwave-assisted catalyst-free hydrolysis of fibrous cellulose for deriving sugars and biochemicals. *Front. Chem. Sci. Eng.* **2018**, *13*, 718–726. [CrossRef]
111. Santos, D.; Giacobe, K.; Silva, C.M.; Saldanha, L.F.; Martins, A.F.; Flores, E.M.M.; Bizzi, C.A. Ultrasound-Assisted Demineralization Process of Sugarcane Straw and Its Influence on the Further Biomass Conversion. *Sustainability* **2022**, *14*, 557. [CrossRef]
112. Mazela, B.; Perdoch, W.; Peplińska, B.; Zieliński, M. Influence of Chemical Pre-Treatments and Ultrasonication on the Dimensions and Appearance of Cellulose Fibers. *Materials* **2020**, *13*, 5274. [CrossRef] [PubMed]
113. Nadányi, R.; Ház, A.; Lisý, A.; Jablonský, M.; Šurina, I.; Majová, V.; Baco, A. Lignin Modifications, Applications, and Possible Market Prices. *Energies* **2022**, *15*, 6520. [CrossRef]
114. Courtenay, J.C.; Sharma, R.I.; Scott, J.L. Recent Advances in Modified Cellulose for Tissue Culture Applications. *Molecules* **2018**, *23*, 654. [CrossRef] [PubMed]
115. Montesantos, N.; Maschietti, M. Supercritical Carbon Dioxide Extraction of Lignocellulosic Bio-Oils: The Potential of Fuel Upgrading and Chemical Recovery. *Energies* **2020**, *13*, 1600. [CrossRef]
116. Viñas-Ospino, A.; López-Malo, D.; Esteve, M.J.; Frígola, A.; Blesa, J. Green Solvents: Emerging Alternatives for Carotenoid Extraction from Fruit and Vegetable By-Products. *Foods* **2023**, *12*, 863. [CrossRef]
117. Leszczyńska, A.; Radzik, P.; Szefer, E.; Mičušík, M.; Omastová, M.; Pielichowski, K. Surface Modification of Cellulose Nanocrystals with Succinic Anhydride. *Polymers* **2019**, *11*, 866. [CrossRef]
118. Zhu, H.; Han, Z.; Cheng, J.-H.; Sun, D.-W. Modification of Cellulose from Sugarcane (*Saccharum Officinarum*) Bagasse Pulp by Cold Plasma: Dissolution, Structure and Surface Chemistry Analysis. *Food Chem.* **2022**, *374*, 131675. [CrossRef]
119. Kang, H.; Liu, R.; Huang, Y. Graft Modification of Cellulose: Methods, Properties and Applications. *Polymer* **2015**, *70*, A1–A16. [CrossRef]
120. Zhang, Z.; Sèbe, G.; Hou, Y.; Wang, J.; Huang, J.; Zhou, G. Grafting Polymers from Cellulose Nanocrystals via Surface-Initiated Atom Transfer Radical Polymerization. *J. Appl. Polym. Sci.* **2021**, *138*, 51458. [CrossRef]
121. Sugiarto, S.; Leow, Y.; Tan, C.L.; Wang, G.; Kai, D. How far is Lignin from being a biomedical material? *Bioact. Mater.* **2022**, *8*, 71–94. [CrossRef]
122. Wilczyński, K.; Nastaj, A.; Lewandowski, A.; Wilczyński, K.J.; Buziak, K. Fundamentals of Global Modeling for Polymer Extrusion. *Polymers* **2019**, *11*, 2106. [CrossRef]
123. Dutta, N.; Usman, M.; Luo, G.; Zhang, S. An Insight into Valorization of Lignocellulosic Biomass by Optimization with the Combination of Hydrothermal (HT) and Biological Techniques: A Review. *Sustain. Chem.* **2022**, *3*, 35–55. [CrossRef]
124. Komisarz, K.; Majka, T.M.; Pielichowski, K. Chemical and Physical Modification of Lignin for Green Polymeric Composite Materials. *Materials* **2023**, *16*, 16. [CrossRef]
125. Shi, K.; Liu, G.; Sun, H.; Weng, Y. Polylactic Acid/Lignin Composites: A Review. *Polymers* **2023**, *15*, 2807. [CrossRef]
126. Attia, A.A.M.; Abas, K.M.; Nada, A.A.A.; Shouman, M.A.H.; Šišková, A.O.; Mosnáček, J. Fabrication, modification, and characterization of lignin-based electrospun fibers derived from distinctive biomass sources. *Polymers* **2021**, *13*, 2277. [CrossRef] [PubMed]
127. Nastaj, A.; Wilczyński, K. Optimization and Scale-Up for Polymer Extrusion. *Polymers* **2021**, *13*, 1547. [CrossRef] [PubMed]
128. Forsgren, L.; Venkatesh, A.; Rigoulet, F.; Sahlin-Sjövold, K.; Westman, G.; Rigdahl, M.; Boldizar, A. Water-Assisted Extrusion and Injection Moulding of Composites with Surface-Grafted Cellulose Nanocrystals—An Upscaling Study. *Compos. Part B Eng.* **2021**, *208*, 108590. [CrossRef]
129. Moreira, A.A.; De Carvalho, F.A.; Bilck, A.P.; De Paula, M.T.; Mali, S.; Yamashita, F.; De Oliveira, A.L.M. Tannin Improves the Processability and Delays the Biodegradability of Poly (Lactic Acid)-starch-based Thermoset Materials Produced by Injection Molding Made with Renewable Compounds. *J. Appl. Polym. Sci.* **2023**, *140*, e53815. [CrossRef]
130. Da Silva, S.C.; Simões, B.M.; Yamashita, F.; de Carvalho, F.A. Compatibilizers for Biodegradable Starch and Poly (Lactic Acid) Materials Produced by Thermoplastic Injection. *Res. Soc. Dev.* **2022**, *11*, e476111436521. [CrossRef]
131. Bortolatto, R.; Bittencourt, P.R.S.; Yamashita, F. Biodegradable Starch / Polyvinyl Alcohol Composites Produced by Thermoplastic Injection Containing Cellulose Extracted from Soybean Hulls (*Glycine max* L.). *Ind. Crops Prod.* **2022**, *176*, 114383. [CrossRef]
132. De Carvalho, F.A.; Moreira, A.A.; De Oliveira, A.L.M.; Yamashita, F. Biodegradation of Poly(Lactic Acid)—Cassava Bagasse Composites Produced by Injection Molding. *J. Appl. Polym. Sci.* **2021**, *138*, 50667. [CrossRef]
133. Finkeldey, F.; Volke, J.; Zarges, J.-C.; Heim, H.-P.; Wiederkehr, P. Learning Quality Characteristics for Plastic Injection Molding Processes Using a Combination of Simulated and Measured Data. *J. Manuf. Process.* **2020**, *60*, 134–143. [CrossRef]
134. Fu, H.; Xu, H.; Liu, Y.; Yang, Z.; Kormakov, S.; Wu, D.; Sun, J. Overview of Injection Molding Technology for Processing Polymers and Their Composites. *ES Mater. Manuf.* **2020**, *8*, 3–23. [CrossRef]
135. Khosravani, M.R.; Nasiri, S. Injection Molding Manufacturing Process: Review of Case-Based Reasoning Applications. *J. Intell. Manuf.* **2020**, *31*, 847–864. [CrossRef]
136. Tosello, G.; Charalambis, A.; Kerbache, L.; Mischkot, M.; Pedersen, D.B.; Calaon, M.; Hansen, H.N. Value Chain and Production Cost Optimization by Integrating Additive Manufacturing in Injection Molding Process Chain. *Int. J. Adv. Manuf. Technol.* **2019**, *100*, 783–795. [CrossRef]
137. Spiering, T.; Kohlitz, S.; Sundmaeker, H.; Herrmann, C. Energy Efficiency Benchmarking for Injection Moulding Processes. *Robot. Comput. Integr. Manuf.* **2015**, *36*, 45–59. [CrossRef]

138. Park, H.S.; Phuong, D.X.; Kumar, S. AI Based Injection Molding Process for Consistent Product Quality. *Procedia Manuf.* **2019**, *28*, 102–106. [CrossRef]
139. He, H.; Xing, Y.; Wang, R.; Lu, Y.; Zhang, L.; Li, F. Optimization Design of Cooling System for Injection Molding Mold of Non-Pneumatic Tire. *Therm. Sci. Eng. Prog.* **2023**, *42*, 101866. [CrossRef]
140. Kuo, C.-C.; Nguyen, T.-D.; Zhu, Y.-J.; Lin, S.-X. Rapid Development of an Injection Mold with High Cooling Performance Using Molding Simulation and Rapid Tooling Technology. *Micromachines* **2021**, *12*, 311. [CrossRef] [PubMed]
141. Park, H.-S.; Dang, X.-P.; Nguyen, D.-S.; Kumar, S. Design of Advanced Injection Mold to Increase Cooling Efficiency. *Int. J. Precis. Eng. Manuf. Green Technol.* **2020**, *7*, 319–328. [CrossRef]
142. Torres-Alba, A.; Mercado-Colmenero, J.M.; Diaz-Perete, D.; Martin-Doñate, C. A New Conformal Cooling Design Procedure for Injection Molding Based on Temperature Clusters and Multidimensional Discrete Models. *Polymers* **2020**, *12*, 154. [CrossRef] [PubMed]
143. Cheng, C.-C.; Wu, Y.-L. Diagnosis of Multi-Stage Injection Molding Process by Ultrasonic Technology at a T-Shape Extension Nozzle. *J. Mater. Process. Technol.* **2020**, *282*, 116650. [CrossRef]
144. Zhao, N.; Lian, J.; Wang, P.; Xu, Z. Recent Progress in Minimizing the Warpage and Shrinkage Deformations by the Optimization of Process Parameters in Plastic Injection Molding: A Review. *Int. J. Adv. Manuf. Technol.* **2022**, *120*, 85–101. [CrossRef] [PubMed]
145. Selvaraj, S.K.; Raj, A.; Rishikesh Mahadevan, R.; Chadha, U.; Paramasivam, V. A Review on Machine Learning Models in Injection Molding Machines. *Adv. Mater. Sci. Eng.* **2022**, *2022*, e1949061. [CrossRef]
146. Dizon, J.R.C.; Valino, A.D.; Souza, L.R.; Espera, A.H.; Chen, Q.; Advincula, R.C. Three-dimensional-printed molds and materials for injection molding and rapid tooling applications. *MRS Commun.* **2019**, *9*, 1267–1283. [CrossRef]
147. Ramkumar, P.L.; Gupta, N.; Shukla, A.; Kumar, A. Bio-Polymer Selection for Injection Molding Process Using Multi Objective Optimization by Ratio Analysis Method. *Mater. Today Proc.* **2021**, *45*, 4447–4450. [CrossRef]
148. Singh, G.; Missiaen, J.-M.; Bouvard, D.; Chaix, J.-M. Copper Extrusion 3D Printing Using Metal Injection Moulding Feedstock: Analysis of Process Parameters for Green Density and Surface Roughness Optimization. *Addit. Manuf.* **2021**, *38*, 101778. [CrossRef]
149. Oliveira, G.H.M.; Maia, T.H.S.; Talabi, S.I.; Canto, L.B.; Lucas, A.A. Characterization of Cellulose Nano/Microfibril Reinforced Polypropylene Composites Processed via Solid-State Shear Pulverization. *Polym. Compos.* **2021**, *42*, 1371–1382. [CrossRef]
150. Agüero, Á.; Garcia-Sanoguera, D.; Lascano, D.; Rojas-Lema, S.; Ivorra-Martinez, J.; Fenollar, O.; Torres-Giner, S. Evaluation of Different Compatibilization Strategies to Improve the Performance of Injection-Molded Green Composite Pieces Made of Polylactide Reinforced with Short Flaxseed Fibers. *Polymers* **2020**, *12*, 821. [CrossRef]
151. Berzin, F.; Lemkhanter, L.; Marcuello, C.; Chabbert, B.; Aguié-Béghin, V.; Molinari, M.; Castellani, R.; Vergnes, B. Influence of the Polarity of the Matrix on the Breakage Mechanisms of Lignocellulosic Fibers during Twin-Screw Extrusion. *Polym. Compos.* **2020**, *41*, 1106–1117. [CrossRef]
152. Robledo-Ortiz, J.R.; González-López, M.E.; Martín del Campo, A.S.; Pérez-Fonseca, A.A. Lignocellulosic Materials as Reinforcement of Polyhydroxybutyrate and Its Copolymer with Hydroxyvalerate: A Review. *J. Polym. Environ.* **2021**, *29*, 1350–1364. [CrossRef]
153. Dolça, C.; Fages, E.; Gongá, E.; Garcia-Sanoguera, D.; Balart, R.; Quiles-Carrillo, L. The Effect of Varying the Amount of Short Hemp Fibers on Mechanical and Thermal Properties of Wood–Plastic Composites from Biobased Polyethylene Processed by Injection Molding. *Polymers* **2022**, *14*, 138. [CrossRef] [PubMed]
154. Merijs-Meri, R.; Zicans, J.; Ivanova, T.; Bochkov, I.; Varkale, M.; Franciszczak, P.; Bledzki, A.K.; Danilovas, P.P.; Gravitis, J.; Rubenis, K.; et al. Development and Characterization of Grain Husks Derived Lignocellulose Filler Containing Polypropylene Composites. *Polym. Eng. Sci.* **2019**, *59*, 2467–2473. [CrossRef]
155. Hidalgo-Salazar, M.A.; Salinas, E. Mechanical, Thermal, Viscoelastic Performance and Product Application of PP- Rice Husk Colombian Biocomposites. *Compos. Part B Eng.* **2019**, *176*, 107135. [CrossRef]
156. Soto-Salcido, L.A.; Anugwom, I.; Ballinas-Casarrubias, L.; Mänttari, M.; Kallioinen, M. NADES-Based Fractionation of Biomass to Produce Raw Material for the Preparation of Cellulose Acetates. *Cellulose* **2020**, *27*, 6831–6848. [CrossRef]
157. Tsegaye, B.; Ström, A.; Hedenqvist, M.S. Thermoplastic Lignocellulose Materials: A Review on Recent Advancement and Utilities. *Carbohydr. Polym. Technol. Appl.* **2023**, *5*, 100319. [CrossRef]
158. Zarna, C.; Opedal, M.T.; Echtermeyer, A.T.; Chinga-Carrasco, G. Reinforcement Ability of Lignocellulosic Components in Biocomposites and Their 3D Printed Applications—A Review. *Compos. Part C Open Access* **2021**, *6*, 100171. [CrossRef]
159. Domenek, S.; Berzin, F.; Ducruet, V.; Plessis, C.; Dhakal, H.; Richaud, E.; Beaugrand, J. Extrusion and Injection Moulding Induced Degradation of Date Palm Fibre—Polypropylene Composites. *Polym. Degrad. Stab.* **2021**, *190*, 109641. [CrossRef]
160. Ortiz-Barajas, D.L.; Arévalo-Prada, J.A.; Fenollar, O.; Rueda-Ordóñez, Y.J.; Torres-Giner, S. Torrefaction of Coffee Husk Flour for the Development of Injection-Molded Green Composite Pieces of Polylactide with High Sustainability. *Appl. Sci.* **2020**, *10*, 6468. [CrossRef]
161. Koffi, A.; Koffi, D.; Toubal, L. Mechanical Properties and Drop-Weight Impact Performance of Injection-Molded HDPE/Birch Fiber Composites. *Polym. Test.* **2021**, *93*, 106956. [CrossRef]
162. Parres, F.; Peydro, M.A.; Juarez, D.; Arrieta, M.P.; Aldas, M. Study of the Properties of a Biodegradable Polymer Filled with Different Wood Flour Particles. *Polymers* **2020**, *12*, 2974. [CrossRef] [PubMed]



163. Montanes, N.; Quiles-Carrillo, L.; Ferrandiz, S.; Fenollar, O.; Boronat, T. Effects of Lignocellulosic Fillers from Waste Thyme on Melt Flow Behavior and Processability of Wood Plastic Composites (WPC) with Biobased Poly(Ethylene) by Injection Molding. *J. Polym. Environ.* **2019**, *27*, 747–756. [CrossRef]
164. Agüero, Á.; Lascano, D.; Garcia-Sanoguera, D.; Fenollar, O.; Torres-Giner, S. Valorization of Linen Processing By-Products for the Development of Injection-Molded Green Composite Pieces of Polylactide with Improved Performance. *Sustainability* **2020**, *12*, 652. [CrossRef]
165. Berzin, F.; David, C.; Vergnes, B. Use of Flow Modeling to Optimize the Twin-Screw Extrusion Process for the Preparation of Lignocellulosic Fiber-Based Composites. *Front. Mater.* **2020**, *7*, 218. [CrossRef]
166. Masanabo, M.A.; Tribot, A.; Luoma, E.; Sharmin, N.; Sivertsvik, M.; Emmambux, M.N.; Keränen, J. Faba Bean Lignocellulosic Sidestream as a Filler for the Development of Biodegradable Packaging. *Polym. Test.* **2023**, *123*, 108047. [CrossRef]
167. Andrzejewski, J.; Barczewski, M.; Szostak, M. Injection Molding of Highly Filled Polypropylene-Based Biocomposites: Buckwheat Husk and Wood Flour Filler: A Comparison of Agricultural and Wood Industry Waste Utilization. *Polymers* **2019**, *11*, 1881. [CrossRef]
168. Lamm, M.E.; Wang, L.; Kishore, V.; Tekinalp, H.; Kunc, V.; Wang, J.; Gardner, D.J.; Ozcan, S. Material Extrusion Additive Manufacturing of Wood and Lignocellulosic Filled Composites. *Polymers* **2020**, *12*, 2115. [CrossRef]
169. Fal, J.; Bulanda, K.; Traciak, J.; Sobczak, J.; Kuzioła, R.; Grąz, K.M.; Budzik, G.; Oleksy, M.; Żyła, G. Electrical and Optical Properties of Silicon Oxide Lignin Polylactide (SiO<sub>2</sub>-L-PLA). *Molecules* **2020**, *25*, 1354. [CrossRef]
170. Menta, V.G.K.; Tahir, I.; Abutunis, A. Effects of Blending Tobacco Lignin with HDPE on Thermal and Mechanical Properties. *Materials* **2022**, *15*, 4437. [CrossRef]
171. Abdelwahab, M.A.; Misra, M.; Mohanty, A.K. Injection Molded Biocomposites from Polypropylene and Lignin: Effect of Compatibilizers on Interfacial Adhesion and Performance. *Ind. Crops Prod.* **2019**, *132*, 497–510. [CrossRef]
172. Pregi, E.; Faludi, G.; Kun, D.; Móczó, J.; Pukánszky, B. Three-Component Polypropylene/Lignin/Flax Composites with High Natural Additive Content for Structural Applications. *Ind. Crops Prod.* **2022**, *182*, 114890. [CrossRef]
173. Rojas-Lema, S.; Ivorra-Martinez, J.; Lascano, D.; Garcia-Garcia, D.; Balart, R. Improved Performance of Environmentally Friendly Blends of Biobased Polyethylene and Kraft Lignin Compatibilized by Reactive Extrusion with Dicumyl Peroxide. *Macromol. Mater. Eng.* **2021**, *306*, 2100196. [CrossRef]
174. Younesi-Kordkheili, H.; Pizzi, A. Ionic Liquid- Modified Lignin as a Bio- Coupling Agent for Natural Fiber- Recycled Polypropylene Composites. *Compos. Part B Eng.* **2020**, *181*, 107587. [CrossRef]
175. Aguilar, G.J.; Tapia-Blácido, D.R. Evaluating How Avocado Residue Addition Affects the Properties of Cassava Starch-Based Foam Trays. *Int. J. Biol. Macromol.* **2023**, *240*, 124348. [CrossRef] [PubMed]
176. Rao, J.; Lv, Z.; Chen, G.; Peng, F. Hemicellulose: Structure, Chemical Modification, and Application. *Prog. Polym. Sci.* **2023**, *140*, 101675. [CrossRef]
177. Martelli-Tosi, M.; Esposto, B.S.; Cristina da Silva, N.; Tapia-Blácido, D.R.; Jafari, S.M. 14—Reinforced Nanocomposites for Food Packaging. In *Handbook of Food Nanotechnology*; Jafari, S.M., Ed.; Academic Press: Cambridge, MA, USA, 2020; pp. 533–574. ISBN 978-0-12-815866-1.
178. Ochi, D.; Barbieri, D.; Reis, A.F.; Severino, P.; Venturini, A.C.; Pedroso Yoshida, C.M.; Souto, E.B.; da Silva, C.F. Chapter 1—Agro-Industrial Waste as Fillers for Green Composites. In *Green Sustainable Process for Chemical and Environmental Engineering and Science*; Inamuddin Altalhi, T., Alrooqi, A., Eds.; Elsevier: Amsterdam, The Netherlands, 2023; pp. 1–26. ISBN 978-0-323-95183-8.
179. Bruton, K.; Hazael, R.; Critchley, R.; Bloodworth-Race, S. Lignocellulosic Natural Fibers in Polymer Composite Materials: Benefits, Challenges and Applications. In *Encyclopedia of Materials: Plastics and Polymers*; Hashmi, M.S.J., Ed.; Elsevier: Oxford, UK, 2022; pp. 353–369. ISBN 978-0-12-823291-0.
180. Ferreira, D.C.M.; Molina, G.; Pelissari, F.M. Biodegradable Trays Based on Cassava Starch Blended with Agroindustrial Residues. *Compos. Part B Eng.* **2020**, *183*, 107682. [CrossRef]
181. Fuentes, R.A.; Berthe, J.A.; Barbosa, S.E.; Castillo, L.A. Development of Biodegradable Pots from Different Agroindustrial Wastes and Byproducts. *Sustain. Mater. Technol.* **2021**, *30*, e00338. [CrossRef]
182. Cravo, J.C.M.; Sartori, D.L.; Fiorelli, J. 2—Agro-Industrial Waste Composites as Components for Rural Buildings. In *Lignocellulosic Fibre and Biomass-Based Composite Materials*; Jawaid, M., Paridah, M.T., Saba, N., Eds.; Woodhead Publishing Series in Composites Science and Engineering; Woodhead Publishing: Sawston, UK, 2017; pp. 13–25. ISBN 978-0-08-100959-8.
183. Terroba-Delicado, E.; Fiori, S.; Gomez-Caturla, J.; Montanes, N.; Sanchez-Nacher, L.; Torres-Giner, S. Valorization of Liquor Waste Derived Spent Coffee Grains for the Development of Injection-Molded Polylactide Pieces of Interest as Disposable Food Packaging and Serving Materials. *Foods* **2022**, *11*, 1162. [CrossRef]
184. Dobrzyńska-Mizera, M.; Knitter, M.; Barczewski, M. Walnut Shells as a Filler for Polymeric Materials. *Drew. Pr. Nauk. Doniesienia Komun.* **2019**, *62*, 153–168. [CrossRef]
185. Gomez-Caturla, J.; Balart, R.; Ivorra-Martinez, J.; Garcia-Garcia, D.; Dominici, F.; Puglia, D.; Torre, L. Biopolypropylene-Based Wood Plastic Composites Reinforced with Mango Peel Flour and Compatibilized with an Environmentally Friendly Copolymer from Itaconic Acid. *ACS Appl. Polym. Mater.* **2022**, *4*, 4398–4410. [CrossRef]
186. Sasimowski, E.; Majewski, Ł.; Grochowicz, M. Artificial Ageing, Chemical Resistance, and Biodegradation of Biocomposites from Poly(Butylene Succinate) and Wheat Bran. *Materials* **2021**, *14*, 7580. [CrossRef]

187. Lima, E.M.B.; Middea, A.; Neumann, R.; da Silva Moreira Thiré, R.M.; Pereira, J.F.; de Freitas, S.C.; Penteadó, M.S.; Lima, A.M.; da Silva Minguita, A.P.; da Costa Mattos, M.; et al. Biocomposites of PLA and Mango Seed Waste: Potential Material for Food Packaging and a Technological Alternative to Reduce Environmental Impact. *Starch Stärke* **2021**, *73*, 2000118. [CrossRef]
188. Bavasso, I.; Bracciale, M.P.; Sbardella, F.; Tirillò, J.; Sarasini, F.; Di Palma, L. Effect of Yerba Mate (*Ilex paraguariensis*) Residue and Coupling Agent on the Mechanical and Thermal Properties of Polyolefin-Based Composites. *Polym. Compos.* **2020**, *41*, 161–173. [CrossRef]
189. Bordón, P.; Paz, R.; Peñalva, C.; Vega, G.; Monzón, M.; García, L. Biodegradable Polymer Compounds Reinforced with Banana Fiber for the Production of Protective Bags for Banana Fruits in the Context of Circular Economy. *Agronomy* **2021**, *11*, 242. [CrossRef]
190. Boussetta, A.; Benhamou, A.A.; Barba, F.J.; Grimi, N.; Simirgiotis, M.J.; Moubarik, A. Effect of Cellulose Microfibers from Sugar Beet Pulp By-Product on the Reinforcement of HDPE Composites Prepared by Twin-screw Extrusion and Injection Molding. *J. Bionic Eng.* **2023**, *20*, 349–365. [CrossRef]
191. Montava-Jordà, S.; Torres-Giner, S.; Ferrandiz-Bou, S.; Quiles-Carrillo, L.; Montanes, N. Development of Sustainable and Cost-Competitive Injection-Molded Pieces of Partially Bio-Based Polyethylene Terephthalate through the Valorization of Cotton Textile Waste. *Int. J. Mol. Sci.* **2019**, *20*, 1378. [CrossRef] [PubMed]
192. Gigante, V.; Seggiani, M.; Cinelli, P.; Signori, F.; Vania, A.; Navarini, L.; Amato, G.; Lazzeri, A. Utilization of Coffee Silverskin in the Production of Poly(3-Hydroxybutyrate-Co-3-Hydroxyvalerate) Biopolymer-Based Thermoplastic Biocomposites for Food Contact Applications. *Compos. Part A Appl. Sci. Manuf.* **2021**, *140*, 106172. [CrossRef]
193. Pawlak, F.; Aldas, M.; Parres, F.; López-Martínez, J.; Arrieta, M.P. Silane-Functionalized Sheep Wool Fibers from Dairy Industry Waste for the Development of Plasticized PLA Composites with Maleinized Linseed Oil for Injection-Molded Parts. *Polymers* **2020**, *12*, 2523. [CrossRef]
194. Suffo, M.; de la Mata, M.; Molina, S.I. A Sugar-Beet Waste Based Thermoplastic Agro-Composite as Substitute for Raw Materials. *J. Clean. Prod.* **2020**, *257*, 120382. [CrossRef]
195. Amena, B.T.; Altenbach, H.; Tibba, G.S.; Hossain, N. Investigation of Mechanical Properties of Coffee Husk-HDPE-ABS Polymer Composite Using Injection-Molding Method. *J. Compos. Sci.* **2022**, *6*, 354. [CrossRef]
196. Farhadi, S.; Javanmard, M. Mechanical and Physical Properties of Polyethylene/Sour Cherry Shell Powder Bio-Composite as Potential Food Packaging. *Food Sci. Nutr.* **2021**, *9*, 3071–3077. [CrossRef]
197. Reinaldo, J.S.; Milfont, C.H.R.; Gomes, F.P.C.; Mattos, A.L.A.; Medeiros, F.G.M.; Lopes, P.F.N.; Filho, M.d.s.M.S.; Matsui, K.N.; Ito, E.N. Influence of Grape and Acerola Residues on the Antioxidant, Physicochemical and Mechanical Properties of Cassava Starch Biocomposites. *Polym. Test.* **2021**, *93*, 107015. [CrossRef]
198. Anuar, H.; Rashid, S.M.S.A.; Nordin, N.M.; Ali, F.; Buys, Y.F.; Thomas, S.; Nasir, N.A.M.; Asri, S.E.A.M. Potential of fabrication of durian skin fiber biocomposites for food packaging application through the electricity impact analysis. *IIUM Eng. J.* **2021**, *22*, 294–305. [CrossRef]
199. Suaduang, N.; Ross, S.; Ross, G.M.; Wangsoub, S.; Mahasaranon, S. The Physical and Mechanical Properties of Biocomposite Films Composed of Poly(Lactic Acid) with Spent Coffee Grounds. *Key Eng. Mater.* **2019**, *824*, 87–93. [CrossRef]
200. Yang, S.; Bai, S.; Wang, Q. Sustainable Packaging Biocomposites from Polylactic Acid and Wheat Straw: Enhanced Physical Performance by Solid State Shear Milling Process. *Compos. Sci. Technol.* **2018**, *158*, 34–42. [CrossRef]
201. Abotbina, W.; Sapuan, S.M.; Ilyas, R.A.; Sultan, M.T.H.; Alkbir, M.F.M. Preparation and Characterization of Black Seed/Cassava Bagasse Fiber-Reinforced Cornstarch-Based Hybrid Composites. *Sustainability* **2022**, *14*, 12042. [CrossRef]
202. Travalini, A.P.; Lamsal, B.; Magalhães, W.L.E.; Demiate, I.M. Cassava Starch Films Reinforced with Lignocellulose Nanofibers from Cassava Bagasse. *Int. J. Biol. Macromol.* **2019**, *139*, 1151–1161. [CrossRef]
203. da Silva, D.J.; de Oliveira, M.M.; Wang, S.H.; Carastan, D.J.; Rosa, D.S. Designing Antimicrobial Polypropylene Films with Grape Pomace Extract for Food Packaging. *Food Packag. Shelf Life* **2022**, *34*, 100929. [CrossRef]
204. Berthet, M.-A.; Angellier-Coussy, H.; Chea, V.; Guillard, V.; Gastaldi, E.; Gontard, N. Sustainable Food Packaging: Valorising Wheat Straw Fibres for Tuning PHBV-Based Composites Properties. *Compos. Part A Appl. Sci. Manuf.* **2015**, *72*, 139–147. [CrossRef]
205. Bascón-Villegas, I.; Pereira, M.; Espinosa, E.; Sánchez-Gutiérrez, M.; Rodríguez, A.; Pérez-Rodríguez, F. A New Eco-Friendly Packaging System Incorporating Lignocellulose Nanofibres from Agri-Food Residues Applied to Fresh-Cut Lettuce. *J. Clean. Prod.* **2022**, *372*, 133597. [CrossRef]
206. Gomez-Caturla, J.; Ivorra-Martinez, J.; Quiles-Carrillo, L.; Balart, R.; Garcia-Garcia, D.; Dominici, F.; Puglia, D.; Torre, L. Improvement of the Barrier and Mechanical Properties of Environmentally Friendly Mango Kernel Flour/Glycerol Films by Varying the Particle Size of Mango Kernel Flour. *Ind. Crops Prod.* **2022**, *188*, 115668. [CrossRef]
207. Torres-León, C.; Vicente, A.A.; Flores-López, M.L.; Rojas, R.; Serna-Cock, L.; Alvarez-Pérez, O.B.; Aguilar, C.N. Edible Films and Coatings Based on Mango (Var. Ataulfo) by-Products to Improve Gas Transfer Rate of Peach. *LWT* **2018**, *97*, 624–631. [CrossRef]
208. Da Silva, A.P.; de Paula Pereira, M.; Passador, F.R.; Montagna, L.S. PLA/Coffee Grounds Composites: A Study of Photodegradation and Biodegradation in Soil. *Macromol. Symp.* **2020**, *394*, 2000091. [CrossRef]
209. Ounkaew, A.; Kasemsiri, P.; Kamwilaisak, K.; Saengprachatanarug, K.; Mongkolthananruk, W.; Souvanh, M.; Pongsa, U.; Chindaprasirt, P. Polyvinyl Alcohol (PVA)/Starch Bioactive Packaging Film Enriched with Antioxidants from Spent Coffee Ground and Citric Acid. *J. Polym. Environ.* **2018**, *26*, 3762–3772. [CrossRef]

210. Arrieta, M.P.; Peponi, L.; López, D.; Fernández-García, M. Recovery of Yerba Mate (*Ilex paraguariensis*) Residue for the Development of PLA-Based Bionanocomposite Films. *Ind. Crops Prod.* **2018**, *111*, 317–328. [CrossRef]
211. Srivastava, K.R.; Singh, M.K.; Mishra, P.K.; Srivastava, P. Pretreatment of Banana Pseudostem Fibre for Green Composite Packaging Film Preparation with Polyvinyl Alcohol. *J. Polym. Res.* **2019**, *26*, 95. [CrossRef]
212. Benítez, A.N.; Monzón, M.D.; Angulo, I.; Ortega, Z.; Hernández, P.M.; Marrero, M.D. Treatment of Banana Fiber for Use in the Reinforcement of Polymeric Matrices. *Measurement* **2013**, *46*, 1065–1073. [CrossRef]
213. Pirayesh, H.; Khazaeian, A.; Tabarsa, T. The Potential for Using Walnut (*Juglans regia* L.) Shell as a Raw Material for Wood-Based Particleboard Manufacturing. *Compos. Part B Eng.* **2012**, *43*, 3276–3280. [CrossRef]
214. Orue, A.; Eceiza, A.; Arbelaiz, A. The Use of Alkali Treated Walnut Shells as Filler in Plasticized Poly(Lactic Acid) Matrix Composites. *Ind. Crops Prod.* **2020**, *145*, 111993. [CrossRef]
215. Orue, A.; Eceiza, A.; Arbelaiz, A. Preparation and Characterization of Poly(Lactic Acid) Plasticized with Vegetable Oils and Reinforced with Sisal Fibers. *Ind. Crops Prod.* **2018**, *112*, 170–180. [CrossRef]
216. Aldas Carrasco, M.F.; Rouault, N.J.; Ferri Azor, J.M.; López-Martínez, J.; Samper Madrigal, M.D. A New Bio-Based Fibre-Reinforced Polymer Obtained from Sheep Wool Short Fibres and PLA. *Green Mater.* **2020**, *8*, 79–91. [CrossRef]
217. Conzatti, L.; Giunco, F.; Stagnaro, P.; Patrucco, A.; Tonin, C.; Marano, C.; Rink, M.; Marsano, E. Wool Fibres Functionalised with a Silane-Based Coupling Agent for Reinforced Polypropylene Composites. *Compos. Part A Appl. Sci. Manuf.* **2014**, *61*, 51–59. [CrossRef]
218. Wang, L.; Huang, S.; Wang, Y. Recycling of Waste Cotton Textile Containing Elastane Fibers through Dissolution and Regeneration. *Membranes* **2022**, *12*, 355. [CrossRef]
219. Shen, Z.; Ghasemlou, M.; Kamdem, D.P. Development and Compatibility Assessment of New Composite Film Based on Sugar Beet Pulp and Polyvinyl Alcohol Intended for Packaging Applications. *J. Appl. Polym. Sci.* **2015**, *132*. [CrossRef]

**Disclaimer/Publisher’s Note:** The statements, opinions and data contained in all publications are solely those of the individual author(s) and contributor(s) and not of MDPI and/or the editor(s). MDPI and/or the editor(s) disclaim responsibility for any injury to people or property resulting from any ideas, methods, instructions or products referred to in the content.



Review

# Polymeric Scaffolds Used in Dental Pulp Regeneration by Tissue Engineering Approach

Vinna K. Sugiaman <sup>1,\*</sup>, Jeffrey <sup>2</sup>, Silvia Naliani <sup>3</sup>, Natallia Pranata <sup>1</sup>, Rudy Djuanda <sup>4</sup> and Rosalina Intan Saputri <sup>5,6</sup>

<sup>1</sup> Department of Oral Biology, Faculty of Dentistry, Maranatha Christian University, Bandung 40164, West Java, Indonesia

<sup>2</sup> Department of Pediatric Dentistry, Faculty of Dentistry, Jenderal Achmad Yani University, Cimahi 40531, West Java, Indonesia

<sup>3</sup> Department of Prosthodontics, Faculty of Dentistry, Maranatha Christian University, Bandung 40164, West Java, Indonesia

<sup>4</sup> Department of Conservative Dentistry and Endodontic, Faculty of Dentistry, Maranatha Christian University, Bandung 40164, West Java, Indonesia

<sup>5</sup> College of Medicine, Veterinary, and Life Sciences, University of Glasgow, Glasgow G12 8QQ, UK

<sup>6</sup> Faculty of Dentistry, Maranatha Christian University, Bandung 40164, West Java, Indonesia

\* Correspondence: vinnakurniawati@yahoo.co.id

**Abstract:** Currently, the challenge in dentistry is to revitalize dental pulp by utilizing tissue engineering technology; thus, a biomaterial is needed to facilitate the process. One of the three essential elements in tissue engineering technology is a scaffold. A scaffold acts as a three-dimensional (3D) framework that provides structural and biological support and creates a good environment for cell activation, communication between cells, and inducing cell organization. Therefore, the selection of a scaffold represents a challenge in regenerative endodontics. A scaffold must be safe, biodegradable, and biocompatible, with low immunogenicity, and must be able to support cell growth. Moreover, it must be supported by adequate scaffold characteristics, which include the level of porosity, pore size, and interconnectivity; these factors ultimately play an essential role in cell behavior and tissue formation. The use of natural or synthetic polymer scaffolds with excellent mechanical properties, such as small pore size and a high surface-to-volume ratio, as a matrix in dental tissue engineering has recently received a lot of attention because it shows great potential with good biological characteristics for cell regeneration. This review describes the latest developments regarding the usage of natural or synthetic scaffold polymers that have the ideal biomaterial properties to facilitate tissue regeneration when combined with stem cells and growth factors in revitalizing dental pulp tissue. The utilization of polymer scaffolds in tissue engineering can help the pulp tissue regeneration process.

**Keywords:** biocompatible; biodegradable; polymers; scaffolds; tissue engineering

**Citation:** Sugiaman, V.K.; Jeffrey; Naliani, S.; Pranata, N.; Djuanda, R.; Saputri, R.I. Polymeric Scaffolds Used in Dental Pulp Regeneration by Tissue Engineering Approach.

*Polymers* **2023**, *15*, 1082. <https://doi.org/10.3390/polym15051082>

Academic Editor: Raffaella Striani

Received: 8 January 2023

Revised: 16 February 2023

Accepted: 18 February 2023

Published: 21 February 2023



**Copyright:** © 2023 by the authors. Licensee MDPI, Basel, Switzerland. This article is an open access article distributed under the terms and conditions of the Creative Commons Attribution (CC BY) license (<https://creativecommons.org/licenses/by/4.0/>).

## 1. Introduction

Pulpal pathosis is one of the most common oral diseases due to persistent stimulation from trauma, dental caries, or iatrogenic causes. Dental caries occur because of bacterial infection on the tooth surface, which consists of enamel and dentin. Untreated dental caries trigger an inflammation response in the dental pulp, and chronic inflammation in the pulp tissue leads to permanent healthy tissue loss [1,2].

The current pulp pathosis treatments are root canal treatment and pulp revascularization [2]. Root canal treatment is the treatment of choice in dentistry, which is effective for severe pulp pathosis conditions. This treatment has a high success rate, but the tooth loses pulp tissue as a result. Thus, despite the treatment's benefits, the treated tooth becomes nonvital, which increases the risk of fracture and a decrease in the pulp defense mechanism and sensory function [2,3].



Therefore, regenerative endodontic treatment to restore normal pulp functioning via complex dentin–pulp regeneration has recently been developed. The treatment aims to replace the pathological or nonvital pulp tissue with new healthy tissue [2,4].

Regenerative tissue engineering technology is improving rapidly. In pulp tissue regeneration, three important aspects have been developed for their utilization in the technique: stem cells, growth factors, and biomaterials/scaffolds [2,5]. Stem cells represent one of the key elements in tissue engineering technology. Stem cells are unspecialized cells that have the ability to regenerate, proliferate, and differentiate into specific cells [6,7]. After an injury, these cells play a role in healing via tissue regeneration [2,8].

A growth factor or morphogen is a protein or signaling molecule that bonds to specific membrane cell receptors which control and coordinate all cellular functions, such as cell signaling, cell proliferation, and matrix synthesis [6,9]. Growth factors play an important role in increasing the regenerative effect and control function of stem cells. Examples of growth factors that play a role in the signaling process of dentin and pulp regeneration are bone morphogenic proteins (BMP) such as BMP-2, BMP-4, BMP-7, and transforming growth factor  $\beta$ -1(TGF- $\beta$ 1) [4,10,11].

A scaffold or biomaterial is a framework or structure that provides a three-dimensional (3D) growth space for cells and regulates cell function and metabolism. The scaffold creates a microenvironment that promotes cells' regenerative capacities and multipotentialities. These conditions promote tissue regeneration. Recently, many natural or synthetic scaffold materials have been used for pulp regeneration [2,12]. Bioactive scaffolds stimulate the proliferation and differentiation of stem cells into odontoblast-like cells to regenerate pulp tissue [13,14]. Therefore, the role of scaffolds in tissue regeneration is important, becoming the mediator that facilitates the transfer of stem cells and/or growth factors at the location of the local receptor [15].

Each component in tissue engineering has a different effect in supporting the pulp regenerative process, but a combination of these three components gives the best results [2,4]. Dental tissue engineering is expected to provide tooth vitality, with pulp tissue similar to that of a normal tooth. Therefore, it is important to guide cell interactions with extracellular matrices, which is accomplished by using scaffolds and cell culture techniques [15].

This review will describe the latest developments regarding the usage of natural or synthetic scaffold polymers that have the ideal biomaterial properties to facilitate tissue regeneration when combined with stem cells and growth factors to revitalize dental pulp tissue. The utilization of polymer scaffolds in tissue engineering can help the pulp tissue regeneration process. This article is the first to discuss the various types of scaffolds with their various advantages and disadvantages that can be utilized in regenerating dental pulp tissue.

## 2. The Dental Pulp

Dental pulp is a loose connective tissue that occupies the root canal and is surrounded by dentin. Dental pulp consists of blood vessels, nerves, and odontoblasts, which line the predentine layer in the pulp tissue. Thus, pulp plays a role in providing nutrition, vitality, and pathogen detection through its sensory function as an infection response. Pulp tissue has sensitivity and immunoprotective attributes that maintain pulp homeostasis, facilitate its regenerative ability, and form reactionary dentin [2,16–18].

Histologically, dental pulp consists of several zones: the dentinoblastic zone, the cell-free zone, the cell-rich zone, and the pulp core. The primary cells of the pulp layer are odontoblasts, fibroblasts, macrophages, undifferentiated ecto-mesenchymal cells, and other immunocompetent cells [19,20]. The dentinoblastic zone functionally forms the pulp–dentin complex. This zone is the first line of reparative dentine formation and provides protective responses toward external stimulation, whereas the pulp core is rich in nerves and blood vessels which provide the pulp with nutrition and sensory functioning [2,19].

Therefore, the loss of pulp tissue causes a loss of vitality and sensitivity in the tooth and leads to uncontrolled infections in the surrounding tissues. This condition needs

complex treatment, such as root canal treatment, which renders the tooth nonvital and brittle, which influences the patient's quality of life [17,18].

### 3. Dental Pulp Regeneration

Pulp regeneration is a healing process regarding the injured or lost parts of the dental pulp and results in the re-establishment of its complete biological function [2,21]. Ideal pulp regeneration should generate pulp structure and function as similar as possible to healthy tissue. This regeneration involves the regeneration of the dentin–pulp complex, blood vessels, and nerves, which reach a favorable level of reconstruction through the angiogenesis and neurogenesis processes. Other than that, it also involves the rehabilitation of pulp physiological functioning, represented by sensation, nutrition, and immunological defense [2,6].

Illustrated by the formation of connective tissue, with cell density and an architecture similar to that of healthy pulp, successful pulp regeneration consists of nerves and blood vessels able to secrete new dentin as healthy pulp at a controlled rate. Vascular tissue plays a role in providing nutrition, oxygen, cell immunity, and the recruitment and circulation of cells, which maintains the tissue's vitality and viability, while the nerves are fundamental to cell regulation, which manages the regeneration process and provides defense mechanisms and tissue repair [6,22].

Regenerated blood vessels should be connected to the periapical bone tissue, which surrounds the tooth; therefore, it can receive regular blood flow and transport nutrition for regenerating the tissue or dentin. Other than that, the regenerating tissue should be innervated, with the tooth maintaining heat/cold and pain sensations [17,23]. Therefore, vascular and nerve supply should be maintained through the apical foramen, which is one of the aims of the pulp regenerative process.

In the regeneration process, stem cells proliferate and differentiate into endothelial cells for angiogenesis/vasculogenesis and move into odontoblasts to carry out the dentin reparative process. At the beginning of the process, angiogenic signals, such as fibroblast growth factor (bFGF), vascular endothelial growth factor (VEGF), and transforming growth factor  $\beta$  (TGF- $\beta$ ), are released by endothelial cells, injured pulp cells, and the extracellular matrix (ECM), which causes stem cell migration and stimulates neo-angiogenesis [24,25].

### 4. Endodontic Regeneration

Infected dental pulp needs root canal treatment (RCT), which is a conservative but effective treatment. Traditionally, in this treatment, the pulp tissue is removed and replaced by synthetic obturation materials, such as paste or gutta-percha [13,17]. RCT aims to remove the space for potential microbiome reinfection and create a healing environment by mechanical or chemical disinfection, which is continued by inert material closure [2,26]. The treatment has a high success rate in dentistry, with 97% of one million teeth able to retain functionality for around 8 years [13,17].

Teeth that receive RCT experience severe defects regarding hard tissue, devitalized pulp from denervation, and avascularity. This leads to an increased risk of fracture, the disruption of the pulpal defense mechanisms, and a loss of physiological functions, such as nutrition and sensation [2,17,27]. In order to prevent these side effects, an effective treatment strategy is needed for the revitalization of the pulp. The emergence of tissue engineering technology and regenerative treatments provides the possibility of developing regenerative endodontic treatments [17].

RCT causes the tooth to be nonvital and susceptible to structural changes [28]; the challenge in modern dentistry is to maintain pulp vitality. Thus, an interdisciplinary approach to regenerative treatments has developed, which utilizes living cells to heal, replace, and restore damaged human tissues and organs to reach their normal level of functioning. One of these treatments is stem cell engineering, which has the potential to be the future of regenerative treatment [29,30].

Dental tissue regeneration can be obtained by the regeneration of each part of a tooth's structure, which consists of enamel, dentin, pulp, alveolar bone, cementum, and periodontal ligament or by regenerating the whole tooth structurally and functionally [15,31]. Regenerative endodontics is one of the endodontic treatments that focus on replacing the damaged pulp tissue through tissue regeneration to restore tooth vitality, leading to an increase in patient quality of life. Regenerative tissue should have healthy pulp properties, such as the ability of the dentin-deposition process, reinnervation, and vascularization [17,26].

## 5. Tissue Engineering

Tissue engineering technology is an interdisciplinary science that implements the biological principles of regenerative treatment techniques, with a focus on repairing and restoring the biological function of cells, tissues, and organs that have been injured by internal or external factors [6,32]. Tissue engineering technology aims to contribute to the restoration of damaged tissue function and structure by utilizing stem cell interactions, scaffolds/biomaterials, and growth factors. The proper combination of these three elements enables the manipulation of the biomimetic microenvironment containing the vascular system, which normally maintains nutrition supply, waste disposal, inflammatory response, and pulp regeneration [2,6,33]. In tissue engineering, angiogenesis has an important role in nutrition supply and the potential recruitment of stem cells [4,34].

In tissue engineering technology, pulp regeneration might be achieved via the utilization of three key elements: (i) stem cells, (ii) scaffolds, and (iii) signaling molecules such as growth factors. Firstly, the pulp regeneration process might be achieved through stem cell isolation and *in vitro* manipulation. After this, the cells are cultured in the scaffold and combined with the growth factor, which is then all transplanted into the root canal [35–37].

Every individual element has a different impact on pulp regeneration, but with all elements supporting each other, this might provide a favorable result. The proper combination of these three elements provides a micro-biomimetic environment, influencing the overall accomplishment of pulp regeneration. This result might be achieved by the formation of a fully functional vascular system, thus providing adequate nutrition supply, waste disposal, and inflammation response, leading to satisfactory pulp regeneration [2].

### 5.1. Dental Stem Cells

Mesenchymal stem cells (MSCs) are a type of stem cell that is suitable for regenerative treatment because of its high proliferation and multipotential ability [29,38]. According to the minimal criteria of the International Society for Cellular Therapy, MSCs are marked with positive (CD29, CD44, CD73, CD90, CD105, and Stro-1) and with negative hematopoietic markers (CD14, CD34, and CD45) [13,39].

MSCs can be isolated from different locations in the oral and maxillofacial regions, such as from dental pulp stem cells (DPSCs) and the stem cells exfoliated from human deciduous teeth (SHED) and can be isolated from healthy pulp tissue. These cells could be differentiated *in vitro* into adipocytes, odontoblasts, osteoblasts, and chondroblasts, which form dentin or pulp tissue after *in vivo* transplantation [13,29]. Other cells, such as dental follicle progenitor stem cells (DFPCs), periodontal ligament stem cells (PDLSCs), and stem cells from apical papilla (SCAPs), can be differentiated *in vitro* into adipocytes, odontoblasts, cementoblast-like cells, and connective tissue [5,13,29,40].

Each type of stem cell has different properties: SHED and SCAP have higher proliferation activity compared to DPSC, although all stem cells possess the potential to regenerate dentin and pulp [5,13].

### 5.2. Growth Factors

Signaling molecules, such as stem cell factor (SCF), stromal-cell-derived factor (SDF-1 $\alpha$ ), platelet-derived growth factor (PDGF), basic fibroblast growth factor (bFGF), and granulocyte colony-stimulating factor (G-CSF), can be used for pulp tissue regeneration [17]. Several growth factors, such as SDF-1 $\alpha$ , bFGF, and PDGF, are chemotaxis molecules and

correlate to blood vessels, nerves, and dentin in the pulp regeneration process. PDGF and VEGF contribute to vasculogenesis/angiogenesis, while NGF contributes to the growth and survival of the nerves; BMP-7 contributes to the differentiation and mineralization of odontoblasts [36,37]. Growth factors play a role in the restoration of stimulation of a structure and the physiology of tissue function in damaged tissue [2].

### 5.3. Scaffolds

A scaffold is a three-dimensional frame microenvironment that facilitates attachment, cellular infiltration, differentiation, proliferation, and stem cell metabolism with the aid of growth factors. The frame has to provide support for nutrition and oxygen diffusion in the regeneration process and should have biodegradable properties because it will be replaced by the new tissue [4,6,41].

Different types of developed scaffold materials or models have certain levels of flexibility and degradability [6]. Currently, natural or synthetic scaffolds have started to be commonly used in pulp tissue regeneration [2]. The scaffolds that have been used are tissue extracts, such as blood clots, platelet-rich fibrin (PRF), platelet-rich plasma (PRP), tricalcium phosphate ceramic, hydroxyapatite calcium, and mineral trioxide aggregate and synthetic polymers such as polylactic-co-glycolic acid, polylactic acid, and biopolymers such as collagen, hydrogel, hyaluronan, and chitosan [4].

Blood clots represent one type of scaffold that has natural properties from which natural substances such as collagen, chitosan, fibrin, hyaluronic acid, gelatin, alginate, and peptide-based scaffolds can be derived. These scaffolds have been studied as scaffolds for pulp regeneration because of their biocompatibility, biomimetic properties, availability, cost-effectiveness, and ease of conversion (into hydrogel) [13,42].

Other than natural scaffolds, there have been several synthetic polymers developed, such as polyglycolic acid (PGA), poly(d,l-lactide-coglycolide) (PLGA), polylactic acid (PLA), poly(l-lactic) acid (PLLA), and polycaprolactone (PCL), and inorganic calcium phosphates, such as hydroxyapatite (HA) or beta-tricalcium phosphate ( $\beta$  TCP), as well as a combination of silica glass and phosphate. Synthetic scaffolds have been studied considerably as scaffolds that have the potential for tooth regeneration because of their nontoxicity, biodegradability, and ease with which to manipulate properties, including mechanical rigidity and degradation rate [2,15,42].

In contrast to natural scaffolds, synthetic scaffolds can be prepared in unlimited numbers because they are produced in a controlled environment according to a desirable shape. This condition allows for the obtainment of the scaffold in accordance with cell differentiation properties, certain pore characteristics, and certain mechanical, chemical, and degradation rate properties according to the desired application [15,43,44].

This polymer is a biomaterial that is commonly used to form scaffolds with characteristics that are related to differentiation in their composition, structure, and macromolecule arrangement [15]. In recent studies, scaffolds have shown the potential to be bioactive carriers and have recapitulated the interaction between stem cells, progenitor cells, microphysiological environments, and extracellular matrices [13]. In regenerative endodontic treatment, polymer scaffold usage could provide physiological environments to increase the biological performance in the pulp regeneration process. This process consists of revascularization and revitalization processes. This scaffold influences cell migration, viability, discharge, proliferation, recruitment, and degradability [45].

Although scaffolds have huge potential, there are challenges that need to be overcome, such as integrating the scaffold with complicated morphologies without damaging the surrounding tissues. For tooth regeneration, scaffolds require several general characteristics, such as being easy to manipulate, having bioactive and biodegradable properties, having adequate porosity and physical and mechanical strength, having low immunogenicity, and being able to support vascularization [15,43].

Other criteria, such as having an adequate shape, size, and pore volume, are important for the penetration and diffusion of growth factors, nutrition, and waste discharge between

the cells [13,15]. Therefore, a scaffold's criteria and design create favorable microenvironments that are important as a foundation to then perform tissue engineering technology processes. This microenvironment supports the organization of cell functioning regarding self-renewal and differentiation, supporting cell and growth factor transportation, creating an environment for cell activities, and promoting communication between cells, which leads to tissue regeneration [2,13,46]. These scaffold characteristics represent important keys to the process of tissue regeneration because they play vital roles in defining cell behavior and tissue formation [13].

To confirm the success of the cell growth and differentiation processes in tissue engineering, scaffold materials must be able to interact with host tissues and provide an ideal environment for tissue growth [29,46]. The ideal scaffold for pulp regeneration should fulfill three criteria: biocompatibility, adequate rigidity to withstand mastication force, and tight sealing with dentin to prevent micro-organism infiltration [29,44]. Other than that, the degradation process of a scaffold is usually one of the factors that plays a role in treatment failure [47]. The rate of scaffold degradation should be complementary to the rate of new tissue formation and should not produce harmful waste side products [15,48,49]. Utilization of the use of scaffolds in tissue engineering technology must fulfill several characteristics which can be seen in Figure 1.



**Figure 1.** Scaffold for Tissue Engineering.

### 5.3.1. Scaffolds Made of Natural Polymers

One of the tissue engineering triad elements in regenerative endodontics is scaffolds, which work as biological and structural support for cell growth and differentiation. Proper scaffold selection is a challenge in the dentin–pulp regeneration process [50]. Cells' migration, proliferation, and differentiation correlate with the choice of a scaffold's physical properties, such as appropriate viscoelasticity to mimic the real pulp tissue [51]. The application of scaffolds for dental pulp regeneration should be able to mimic the microenvironment in the root canal and provide mechanical support [52,53].

The application of 3D bioprinting technology to scaffold-making can precisely mimic external and internal morphologies. The 3D scaffold has moderate porosity, which allows nutrition and oxygen infiltration, leading to the occurrence of metabolic activities [53]. The application of scaffolds via the injection process is recommended because it can adapt well to the shape of the pulp chamber and root canal so that cell and matrix interaction can occur efficiently [50].

To date, scaffolds are classified as natural and synthetic scaffolds based on the material source and biomaterial properties used [54]. Scaffolds for tissue regeneration using natural or synthetic materials are continually being developed [55]. Natural scaffolds come from the host or natural materials. Examples of host scaffolds are blood clots, autologous platelet concentrates, and decellularized extracellular matrices [54]. Examples of natural material scaffolds are collagen, alginate, chitosan, hyaluronic acid, and fibrin [50,51,53,54]. Natural



material scaffolds have the advantage of cell recognition and adhesion from molecular signaling, although the application of this type of scaffold has the limitation of product variation, risk of pathogen transmission, poor mechanical properties, and immunological responses to foreign objects [52]. The shape of the scaffold can be a porous sponge, a solid block, a sheet, or a hydrogel [56].

Collagen is a scaffold material that has the closest viscoelasticity to real pulp tissue [51]. The combination of natural materials, such as collagen and the host's blood clot, show predictable patterns for tissue formation and mineralization in human dental structures when compared to collagen or blood clots individually. The application of one type of scaffold, such as a blood clot, does not provide stable results for the tissue regeneration process [57]. Instability and unpredictable clinical results from the blood clot are the consequences of unregulated stem cells in the pulp chambers, including the difficulties of bleed formation and hemostasis [52].

When compared to blood clots, platelet-rich plasma (PRP) and platelet-rich fibrin (PRF) provided lower increases in dental root length and less effectivity in root development [58]. PRP from the host's blood contains high platelet, growth factor, and cytokine concentrations, which increase the ability of wound healing and stem cell recruitment from the pulp and increase SCAP proliferation. While PRF contains plentiful growth factors, which can stimulate cell differentiation as well as cell adhesion and migration [59]. The advantages of materials with rich platelet concentrations, such as PRF or PRP, are the increases in the level of angiogenesis and revascularization, which is fundamental to accomplishing endodontic regeneration therapy [56]. Hydrogel-based collagen could mimic the interaction between cells and extracellular matrices in vivo and organize cell growth, which is used for tissue engineering [60].

Polymer materials, such as gelatin and fibrin, are commonly used as natural scaffolds. Gelatin is a biopolymer protein that comes from collagen hydrolysis, which facilitates the proliferation and differentiation of odontoblasts in dental pulp stem cells (DPSCs) [50]. Gelatin is a partial hydrolysate from animals. When compared to gelatin, hydrogel gelatin has better biocompatibility because of its low immunogenicity properties [50,53]. A gelatin-based matrix showed better endodontic therapy results when compared to fibrin-based matrix groups after 12 weeks follow-up in mini-pig immature dental models [50].

Other studies into fibrin-based scaffolds in hydrogel showed that this material was compatible with dental pulp regeneration by supporting pulp-like tissue formation [61]. Fibrin is a natural protein polymer that forms part of blood clot formation. Hydrogel-based fibrin can stimulate pulp-like tissue formation with an odontoblast layer in the root canal system [50]. The advantages of these materials are good cytocompatibility, physical kinetic degradation, and nontoxic degradation products, and they are also easy to inject into the pulp canal. Other natural materials, such as alginate, chitosan, collagen, and hyaluronic acid, or synthetic materials, such as polyethylene glycol, poly (D,L) lactic acid, and fibrin-based bio-ink for 3D printing, were added to increase the structural and functional properties of fibrin scaffolds [61].

Alginate is a natural polymer from algae, which has good biocompatibility properties, is cost-effective, has low cytotoxicity, and has an optimal structure for nutrition exchange [45,52,53]. Alginate hydrogels were formed by crosslinking polysaccharide and divalent cations to form an ion bridge in water-insoluble tissue [52]. Alginate hydrogels are able to arrange themselves in accordance with mechanical properties, such as rigidity and stress relaxation, to regulate stem cell activity [45]. Alginate has proper mechanical properties but can be applied in the form of hydrogel injection or bone porosity, which enables the natural structure to be loaded with growth factor [56]. The macroporosity of alginate scaffolds enables the exchange between nutrition and metabolism waste. However, scaffolds that consist of only alginate have a limited role in endodontic regenerative therapy; therefore, its combination with other materials, such as bioactive polymers, is needed [52].

Hyaluronic acid (HA) is a biopolymer that can be modified and processed for biomedical applications, and it can be combined with other materials to increase its favorable

properties [60]. HA in dental pulp was found to decrease dental development in the odontogenesis process [52]. When applied to exposed pulp, HA can stimulate the production of reparative dentin. HA can be applied in 3D-sponge form to create a proper environment for blood vessel proliferation and stem cell differentiation [56]. HA is formed by d-glucuronic acid and N-acetyl-D-glucosamine and is commonly available in the form of liquid injection [45]. HA degradation products include pro-angiogenic growth factors, which represent the revascularization elements of dental regeneration tissue, although HA has the disadvantages of poor mechanical properties and can cause hypersensitivity reactions [52].

Chitosan is a widely used natural scaffold [62]. Chitosan is a cation polymer from chitin [55]. Chitosan has good biocompatibility, biodegradation, and other favorable biological properties, such as being antimicrobial, fungistatic, and noncarcinogenic, with hemostatic and protein fusion abilities, as well as being able to stimulate cell adhesion, proliferation, and differentiation [55,62]. However, the application of chitosan is difficult because of the complex gelation and degradation process due to unusual polycationics and a highly crystalline structure, which limits the application of this type of scaffold to the form of a natural injection [52]. The hydrogel form of chitosan can be injected into the dental pulp chamber [62]. Chitosan can be applied as an individual scaffold or in combination with polymers or other biomaterials to produce a large number of matrices for tissue engineering purposes. The addition of chitosan scaffolds into the blood for endodontic regeneration procedures can stimulate the formation of new soft tissue (as proven by histological regeneration) without the formation of mineralized tissue around the pulp canal wall [55]. Additional photo-biomodulation therapy could increase in vitro stem cell survival, proliferation, and migration from the root papilla [62].

When comparing several natural scaffolds, other studies have shown that human teeth can be applied as scaffolds for periodontal ligament and pulp regeneration [26]. Scaffolds from natural materials have higher biocompatibility and bioactivity properties when compared to synthetic scaffolds, whereas synthetic scaffolds have higher controlled degradation levels and mechanical properties [63]. The application of scaffolds that are not limited to the use of only one material, i.e., those that can be combined, can provide better endodontic regeneration therapy.

### 5.3.2. Scaffolds Made of Synthetic Polymers

The implantation of 3D scaffolds in the appropriate living cells that secrete their own extracellular matrix (ECM) can provide an acceptable environment. The adequate porosity and permeability of a polymeric scaffold are essential for guiding and supporting the cultured cells' ability to produce tissue. Synthesizing synthetic biodegradable polymers is challenging in tissue engineering applications [64,65].

The progenitor/stem cells should then be able to attach, travel through, proliferate, and organize themselves spatially in 3D space and differentiate into odontogenic, vasculogenic, and neurogenic lineages with the support of an adequate scaffold for dentin–pulp regeneration. Furthermore, the biocompatibility of the material is critical to avoid any negative reactions from the host tissue. Biodegradability that can be adjusted to match the rate of regeneration is critical for facilitating constructive remodeling. As a result of scaffold deterioration, a series of tissue responses occur, comprising the targeted tissue replacement of the scaffold, vascularization, differentiation, spatial structure, and cellular infiltration [66–68].

Metals, ceramics, and polymers are examples of materials that can be used to make scaffolds. Both dental and bone implants are frequently made of metallic alloys. When it comes to bone tissue engineering, ceramics with strong osteoconductivity have been used, although metals and ceramics have substantial disadvantages because metals do not biodegrade and do not serve as a matrix that mimics biological processes for the proliferation of cells and tissue creation. Additionally, due to brittleness, ceramics are difficult to convert into highly porous structures and have a limited capacity for biodegradation. In contrast,

polymers can be molecularly designed to have increased biodegradability and excellent processing flexibility. Therefore, for tissue engineering, polymers are the most common type of scaffolding material [31,68–70].

Biological recognition represents one potential benefit of naturally generated polymers, which may help to stabilize cell adherence and ensure proper function. The synthetic polymers used as scaffolding materials have been spurred on by the challenges associated with natural polymeric materials, such as their complex purification, structural composition, pathogen transmission, and immunogenicity. When compared to naturally occurring extracellular matrix (ECM) proteins, synthetic polymers offer better processing flexibility and no immunological issues. Functionalized scaffolds that combine the benefits of synthetic and natural polymeric materials can be made by adding bioactive molecules to synthetic polymers [69–71].

The advantages of synthetic polymers include nontoxicity, biodegradability, and the ability to precisely manipulate their physicochemical characteristics, such as degradation rate, structural rigidity, microstructure, and porosity [72–74]. Natural polymers are mostly broken down by enzymes, but synthetic polymers are typically broken down by simple hydrolysis. However, because of the relative acidity of the hydrolytically destroyed byproducts, synthetic polymers might cause localized pH reductions and a chronic or acute inflammatory host response [74–76].

Tissue engineering frequently uses poly (-hydroxy acids), such as poly (lactic acid), poly (l-lactic acid), poly (glycolic acid), polyethylene glycol, and their copolymers poly [(lactic acid)-co-(glycolic acid)] (PLGA) and poly-epsilon caprolactone (PCL), which appears to be the most synthetic polymeric material. These polymers have an established track record and have been approved by the FDA for specific human applications (e.g., sutures). Two of the synthetic polymer scaffolds that have been suggested for dental tissue engineering are PGA and PLA, which are biodegradable polyesters that can be produced from a range of renewable sources. When compared to PGA, PLA, which is an aliphatic polyester, is more hydrophobic [66,69,74,76–78].

The synthetic scaffold known as PGA, which has been used for cell transplantation, breaks down when the cells secrete an ECM. Several cell types, including cellular origins of dental pulp, pulpal fibroblasts, and ex vivo human pulp tissue cells, have been shown to be able to adhere and develop on PGA scaffolds. The copolymers of PGA and PLA that are sown with dental pulp progenitor cells have been shown in rabbit and mouse xenograft models to produce pulp-like tissue [66,69,74,75].

Since structural strength is vital in many applications, PLLA, an extremely strong polymer, has been used in several of them. Nanofibrous scaffolds have been created from it that resemble the structure of genuine collagen (a crucial element of ECM). It has been shown that nanofiber PLLA scaffolds promote cell attachment and differentiation. Previous studies demonstrated how PLLA scaffolds could stimulate the development of endothelial cells from dental pulp cells and odontoblasts [66,69,75]. This was demonstrated by utilizing PLGA as a scaffold from which dentin-like tissue could emerge and in which pulp-like tissue could be repaired over the course of 3 to 4 months. A 50:50 blend of PLGA degrades after around 8 weeks. PCL, a slowly disintegrating polymer, has been utilized in bone tissue engineering projects either by itself or in conjunction with hydroxyapatite [75].

A different type of polymer, polyethylene glycol, is utilized in tissue engineering techniques, such as pulp regeneration. Dental pulp progenitor cells have been transformed to create 3D-tissue constructs while being linked to electrospun polyethylene glycol scaffolds. These artificial polymer scaffolds have also been utilized to convey a range of substances, including anti-inflammatory drugs, growth hormones, and sticky proteins. Such scaffolds could not only support cell growth and proliferation but could also reduce pulpitis and aid in pulpal healing. Synthetic polymer scaffolds have better handling characteristics and a more straightforward manufacturing process, which improves their potential for endodontic regeneration. They do, nevertheless, differ significantly from the natural dental

pulp extracellular environment. As a result, ECM-based natural scaffolds that are closer to the microenvironment have been developed [66,74,79,80].

Planting human exfoliated deciduous teeth stem cells (SHED) on dentin disks with PLA resulted in the structure of odontoblast-like cells, new dentin, and vascularized pulp-like tissue. A study by Huang et al. illustrated that when implanted *in vivo* into an empty root canal area, the stem cell constructions made from the apical papilla (SCAPs) and L-lactide, poly-D, and glycoside were able to create soft tissue that resembles pulp, with the continual addition of new dentin to the surface. However, synthetic polymers have the potential to cause an immediate or long-lasting inflammatory response. Additionally, the locally decreased pH brought on by the hydrolytically degraded metabolites may impair its clinical use [66,75].

Several methods have been used to construct 3D scaffolds from poly (hydroxy acids). The inability of the poly (a-hydroxy acids) chains to allow functional groups, however, restricts the incorporation of biologically active moieties onto the scaffolding surface. In order to increase the functioning of these polymers and broaden their usage, significant efforts have been made in this direction; creating copolymers out of a-hydroxy acids with additional monomers that have functional pendant groups, including amino and carboxyl groups, is one technique. In one study, ring-opening polymerization was used to copolymerize (RS)-b-benzyl malate and L-lactide; then, the benzyl groups were removed to create (RS)-b-malic acid) poly (L-lactide) with connected carbonyl compounds [69,81,82].

In order to copolymerize this with L-lactide, benzyloxymethyl methyl glycolide and benzyloxymethyl glycolide are required, which have preserved hydroxyl groups. The matching hydroxylated PLLA copolymers were produced when the benzyloxymethyl groups were unprotected. Comparable carboxylic acid functionalized copolymers can be created using succinic anhydride [69,83].

The researchers created a poly [(L-lactic acid)-co-(L-lysine)] containing a useful lysine residue that they further linked to the RGD peptide. Even though the development of functional groups in random copolymers by lactide/glycolide copolymerization with additional monomers can be successful, this procedure frequently affects the physical characteristics of the starting homopolymers, such as crystallinity and mechanical strength. Numerous block and graft copolymers based on poly(a-hydroxy acid) have been developed and made as a result of this [69,84].

Polymer PEG, or poly (ethylene glycol), is the component that is most frequently used in (a-hydroxy acids). PL(G)A/PEG diblock, triblock, and multiblock copolymers could be made by the ring-opening of PEG and certain catalysts and the presence of glycolide/lactide polymers. However, the hydroxyl or carboxyl (functional groups) in the block copolymers containing PEG are only present at the end of each PEG segment, and the content in these block copolymers is very low, further restricting chemical alterations. Numerous block and graft copolymers made without PEG have been described [69,85].

Amphiphilic poly [hydroxyalkyl (meth) acrylate)] is a variety of biodegradable polymer. Copolymers of -graft-poly (L-lactic acid) (PHAA-gPLLA) with hanging hydroxyl groups were employed to successfully produce 3D-nanofibrous scaffolds. The further functionalization of these copolymers can result in biomimetic scaffolds that are more hydrophilic, degrade more quickly, and have uses in tissue engineering [69,86].

The fabrication of highly porous poly ( $\alpha$ -hydroxy acid) scaffolds can be used for tissue engineering based on star-shaped functional poly( $\epsilon$ -caprolactone). The functional groups were added to PCL chains using similar methods. Examples of these methods include the copolymerization of  $\epsilon$ -caprolactone and a-chloro- $\epsilon$ -caprolactone to produce functionalized PCL copolymers, and the subsequent addition of carboxyl, pendant hydroxyl, and epoxide groups via atom transfer radical addition. In order to produce the pendant hydroxyl groups in the PCL copolymers,  $\epsilon$ -caprolactone was copolymerized with another monomer, 5-ethyleneketal- $\epsilon$ -caprolactone, and the resulting molecule was subsequently deacetylated to convert the ketone groups into hydroxyl groups [69,87].



However, these deprotection processes (as well as the synthesis of these functional comonomers) are typically challenging and time-consuming. Aside from poly (3-hydroxybutyrate), polyurethanes, polycarbonate, poly (ortho ester), poly (propylene fumarate), and polyphosphazenes, other synthetic biodegradable polymers have also been used as scaffolding biomaterials. Comparatively, there are many fewer reports of the functionalization of these biomaterials (α-hydroxy acids), which include the creation of functionalized PC using synthetic methods [69,87,88].

Pendant amino groups were added to PC chains after polymerizing the cyclic carbonate monomer (2-oxo-[1,3]-dioxan-5-yl) carbamic acid benzyl ester and disposing of the protective benzyloxy carbonyl groups. The pendant amino groups' further functionalization was shown using RGD peptide grafting; synthetic efficiency should be considered, given the number of steps in this reaction cycle [69,89].

The five distinctive structural characteristics of these PAs are as follows: (1) an extended alkyl tail that contributes to the molecule's amphiphilic characteristic; (2) maintenance of the structure by possessing four consecutive cysteine residues that create disulfide bonds; (3) a flexible hydrophilic head group due to the three glycine residues in the linker region, which separates the hard cross-linked region; (4) phosphorylated serine residues that interact strongly with calcium ions to encourage mineralization; and (5) an effective RGD peptide [69].

The high electrostatic interaction between molecules causes the PAs to self-assemble into nanofibrous networks when the pH is changed or when divalent ions are added, as evidenced by this study. Additionally, the hydrophilic peptide signals can be displayed in a specific way on the surfaces of the produced nanostructures due to the molecule's amphiphilic characteristics. However, the creation of sufficient mechanical three-dimensional structures from these PAs must be addressed, as is true for several other hydrogel materials. Proteinase-sensitive motifs represent an inventive technique to make biomaterials react to cells [69,90].

As cell-ingrowth frameworks for tissue formation, Hubbell et al. presented a valuable example of how to build synthetic PEG-based hydrogels. The functionalization molecules for PEG chains in hydrogel networks, which also include pendant oligo peptides (RGDSP) for cell attachment, are matrix metalloproteinase (MMP)-sensitive peptides. The material's reaction to the MMPs secreted by cells is controlled by the MMP-sensitive binding agent. This hydrogel, with a PEG foundation, functions as a biomaterial and reacts to cells. The authors also showed that these gels could promote bone regeneration and are efficient delivery systems for recombinant human bone morphogenetic protein-2 (rhBMP-2) [49,69].

Many of the requirements for the dental pulp tissue engineering approach may be accommodated by self-assembling, adaptable, and customizable peptides. Due to the peptide chains' natural amino acid makeup, they can produce biodegradable products. The potential for uniform cell encapsulation, the rapid transport of nutrients and metabolites, and the characteristics of peptide hydrogel systems are affected by their viscoelastic properties, which are comparable to the properties of collagenous tissues such as dental pulp [66,91].

The term "bioceramic scaffolds" refers to a group of materials, including glass ceramics, bioactive glasses, and calcium/phosphate compounds. Calcium phosphate-based (CaP) ceramics are the biomaterials that are utilized most frequently. Due to their characteristics of osteoclast genesis, nontoxicity, antigenicity, osteoinduction, bone bonding, and similarity to mineralized tissues, CaP scaffolds, such as -TCP or HA, have been extensively explored for bone regeneration. Three-dimensional CaP porous granules have demonstrated their potential in the engineering of dental tissue by providing excellent 3D-substrate characteristics for hDPSC growth and odontogenic differentiation. Pure TCP scaffolds are doped with SiO<sub>2</sub> and ZnO to increase their mechanical stability and capacity for cellular proliferation. Glass ceramics made of SiO<sub>2</sub> Na<sub>2</sub>O CaO P<sub>2</sub>O<sub>5</sub> are bioactive and offer ideal crystallization conditions. The osteoblastic activity of the substance is increased by the release of dissolving products, such CaP [15,75].



Ceramic scaffolds can be altered to control the dissolving rate, provide the appropriate permeability, and control certain surface properties to promote cellular activity. The mechanical rigidity of the scaffold is influenced by variations in pore size and volume. Glass ceramics made of magnesium can increase mechanical strength and provide a high rate of bioactivity. Excellent hDPSC attachment, proliferation, and differentiation have been demonstrated by niobium-doped fluorapatite glass ceramics [75,92].

The several disadvantages of bioceramics include a longer creation time, the lack of an organic phase, nonhomogeneous particle size and form, huge grains, difficulty to shape, brittleness, slow degradation, and high density. Bioceramics are fragile and have little mechanical strength when individually utilized. This drawback can be remedied by combining them with polymer scaffolds [75,92]. Comparison of various types of scaffolds for tissue engineering can be seen in Table 1.

**Table 1.** Comparison of various types of scaffolds for tissue engineering.

Article (Author, Year)	Type Scaffold	Properties	Advantages	Disadvantages
Alaribe, 2016; Jang, 2020; Ducret, 2021 [50,61,93]	Fibrin	Biodegradation, protein natural blood clot, hydrogel base, stimulates the formation of odontoblast	High adhesion to surface, good cytocompatibility and biodegradability, nontoxic, easy to inject	Produced by the body after an injury
Alaribe, 2016; Palma, 2017; Moreira, 2021; Raddal, 2019 [52,55,62,93]	Chitosan	Easier to process, hydrogels, films, fibers or sponges, gel-forming abilities; chitosan hydrogels: low viscosity, high adsorption capability. Chitosan, which is the cationic polymer of chitin, has the attractive properties of biodegradability.	It has been used extensively, can support the differentiation of stem cells, noncytotoxicity, biocompatible, biodegradable, antitumor, antifungal, antibacterial activity, nonimmunogenicity, Easily processes, enhances proliferation and cell attachment, hemostatic, noncarcinogenic	Hard use; high crystalline structure: limited application
Amini, 2021; Erisken, 2015; Nosrat, 2019; Ayala-Ham, 2021; Raddal, 2019; Liu, 2022 [51,52,54,57,60,73]	Collagen	It lacks structural stability, good mechanical properties, and a material that is comparable to soft dental pulp's viscoelastic properties, more recommended in combination with a blood clot, hydrogel-based: mimics interactions between cells and ECM in vivo, type 1 collagen is most used.	Low antigenicity, high biocompatibility; biodegradability, bioactivity, and good cell adhesion, high mechanical strength, the ability to cross-link	Problems with controlling space and the rate of degradation, as well as difficulties with sterilization and processing, pathogen transmission low mechanical properties, irregular biodegradation, risks immunogenicity
Amini, 2021; Wu, 2021; Raddal, 2019; Yu, 2019; Nowicka, 2021 [45,52,53,56,73]	Alginate	Requires a multistep purification procedure to achieve extremely high purity, natural polymer from algae; alginate hydrogels: crosslinking polysaccharides and divalent cations, the mechanical properties can be adjusted (alginate hydrogels)	High biocompatibility and biodegradability, low toxicity, chelating properties, and non-antigenicity, cheap price, low toxicity optimal structure for exchange nutrition	Endotoxins, heavy metals, polyphenolic and protein compounds, as well as compounds derived from marine sources, are among the naturally occurring impurities; poor mechanical properties. It must be combined with other polymers.

Table 1. Cont.

Article (Author, Year)	Type Scaffold	Properties	Advantages	Disadvantages
Amini, 2021; Ayala, 2021; Raddal, 2019; Wu, 2021; Nowicka, 2021 [45,52,56,60,73]	Hyaluronic Acid	Nanofibrous scaffolds, water insolubility, modified biopolymer; in dental pulp, the amount decreases according to the process of odontogenesis, contains d-glucuronic acid and N-acetyl-D-glucosamine, available in liquid injection form.	Excellent biocompatibility, high water content, suitable viscoelastic properties for many tissue types, capacity to degrade into safe products, and the capability to join to the specific cell surface receptors, reparative dentin stimulation, 3D sponge shape suitable for blood vessel proliferation and stem cell differentiation	It is impossible for the cells to adhere to the surface, low mechanical properties, hypersensitivity reactions, and minor biodegradability
Amini, 2021; Farzamfar, 2017; Gathani KM, 2016; Dissanayaka WL, 2020 [66,73,75,94]	Poly (lactic acid) (PLA)	Good mechanical strength	Biocompatibility, processability, biodegradability; planting human exfoliated deciduous teeth stem cells (SHED) on dentin disks with PLA resulted in the structure of odontoblast-like cells, new dentin, and vascularized pulp-like tissue	Low impact toughness, hydrophobicity, and a slow rate of degradation
Amini, 2021; Gaaz, 2015; Gathani KM, 2016; Dissanayaka WL, 2020; Liu X, 2012 [66,69,73,75,95]	Poly (l-lactic acid) (PLLA)	Excellent porosity, a high surface-to-volume ratio, nanofibers, and a variety of pore-size distributions	Biodegradable, promotes cell attachment and differentiation, PLLA scaffolds encouraged the development of endothelial cells from dental pulp cells and odontoblasts	During degradation, hydrophilicity, biocompatibility, and mechanical properties are all poor
Zhai, 2015; Gathani KM, 2016; Dissanayaka WL, 2020; Liu X, 2012 [66,69,75,96]	Poly (glycolic acid) (PGA)	Highly crystalline and hydrophilic linear polyester, better solubility in water, degradation half-life is about 2 weeks	Help attachment cell	Degradation rate is too high
Barroca, 2018; Amini, 2021; Saini, 2016; Santoro M, 2016; Dissanayaka WL, 2020; Rizk A, 2013; Danhier F, 2012 [66,73,79,80,97,98]	Polyethylene glycol (PEG), Copolymer poly [(lactic acid)-co-(glycolic acid)] (PLGA),	Crystallinity, glass transition temperature, good mechanical Strength	Biodegradable, biocompatible, low toxicity/swelling; these artificial polymer scaffolds have also been utilized to convey a range of substances, including anti-inflammatory drugs, growth hormones, and sticky proteins, and support cell growth and proliferation, reduce pulpitis and aid in pulpal healing	The degradation pattern of PLGA is highly dependent on the sequence of monomers that make up its structure, which liberates acidic products
Mir M, 2017; Amini, 2021; Sisson, 2013; Gathani KM, 2016 [73,75,99,100]	Poly-epsilon caprolactone (PCL)	Good mechanical properties, high elasticity, high strength	Biocompatible, biodegradable, low toxicity, slowly disintegrating polymer, has been utilized in bone tissue engineering projects either by itself or in conjunction with hydroxyapatite	Hydrophobicity, slow degradation, lack of functional groups

Tissue engineering technology requires a scaffold as a porous structure that can assist in tissue regeneration. In addition to various scaffold properties with various advantages needed to provide mechanical support in the regeneration process, tortuosity is also an important parameter in developing the permeability of 3D scaffolds to be used in tissue engineering technology. This affects the occurrence of cell attachment, proliferation, differentiation, and cell migration in the process of tissue regeneration [101,102].

Research on tissue engineering technology has not been widely carried out in humans, so this study cannot discuss how far its success has been when applied to living tissue. Therefore, the application of various types of polymer scaffolds needs to be developed further.

## 6. Conclusions

Various types of scaffolds, both natural and synthetic, can be used to regenerate dental pulp by utilizing tissue engineering technology. Scaffolds made from natural materials have advantages in cell recognition and molecular signal adhesion, while synthetic scaffolds can be made in unlimited quantities. However, a better effect might be realized if the two types of scaffolds are combined to obtain good mechanical properties so that they can support pulp regeneration properly. In the future, it is hoped that more extensive research can be carried out on various types of scaffolds so that not only polymer-based scaffolds are described for the regeneration of dental pulp tissue.

**Funding:** This research was funded by Maranatha Christian University.

**Institutional Review Board Statement:** Not applicable.

**Data Availability Statement:** Data sharing not available.

**Acknowledgments:** The authors would like to thank the Faculty of Dentistry, Maranatha Christian University and the Faculty of Dentistry, Jenderal Achmad Yani University.

**Conflicts of Interest:** The authors declare no conflict of interest.

## References

1. Farges, J.C.; Alliot-Licht, B.; Renard, E.; Ducret, M.; Gaudin, A.; Smith, A.J.; Cooper, P.R. Dental Pulp Defence and Repair Mechanisms in Dental Caries. *Mediat. Inflamm.* **2015**, *2015*, 230251. [CrossRef] [PubMed]
2. Xie, Z.; Shen, Z.; Zhan, P.; Yang, J.; Huang, Q.; Huang, S.; Chen, L.; Lin, Z. Functional dental pulp regeneration: Basic research and clinical translation. *Int. J. Mol. Sci.* **2021**, *22*, 8991. [CrossRef] [PubMed]
3. Kwack, K.H.; Lee, H.W. Clinical Potential of Dental Pulp Stem Cells in Pulp Regeneration: Current Endodontic Progress and Future Perspectives. *Front. Cell Dev. Biol.* **2022**, *10*, 734. [CrossRef] [PubMed]
4. Srivastava, S. Current and future perspectives for dentin-pulp tissue engineering—An update. *S. Afr. Dent. J.* **2019**, *74*, 110–114. [CrossRef]
5. Sugiaman, V.K.; Djuanda, R.; Pranata, N.; Naliani, S.; Demolsky, W.L.; Jeffrey. Tissue Engineering with Stem Cell from Human Exfoliated Deciduous Teeth (SHED) and Collagen Matrix, Regulated by Growth Factor in Regenerating the Dental Pulp. *Polymers* **2022**, *14*, 3712. [CrossRef]
6. Retana-Lobo, C. Dental Pulp Regeneration: Insights from Biological Processes. *Odovtos-Int. J. Dent. Sci.* **2017**, *20*, 10–16. [CrossRef]
7. Zakrzewski, W.; Dobrzyński, M.; Szymonowicz, M.; Rybak, Z. Fuel Cells: Past, Present and Future. *IEEJ Trans. Fundam. Mater.* **2019**, *128*, 329–332. [CrossRef]
8. Ayavoo, T.; Murugesan, K.; Gnanasekaran, A. Roles and mechanisms of stem cell in wound healing. *Stem Cell Investig.* **2021**, *8*, 1–9. [CrossRef]
9. Kulebyakin, K.Y.; Nimiritsky, P.P.; Makarevich, P.I. Growth Factors in Regeneration and Regenerative Medicine: “The Cure and the Cause”. *Front. Endocrinol.* **2020**, *11*, 384. [CrossRef]
10. Li, Z.; Liu, L.; Wang, L.; Song, D. The effects and potential applications of concentrated growth factor in dentin–pulp complex regeneration. *Stem Cell Res. Ther.* **2021**, *12*, 357. [CrossRef]
11. Krupińska, A.M.; Skocekiewicz-Malinowska, K.; Staniowski, T. Different approaches to the regeneration of dental tissues in regenerative endodontics. *Appl. Sci.* **2021**, *11*, 1699. [CrossRef]
12. Park, Y.; Huh, K.M.; Kang, S.W. Applications of biomaterials in 3d cell culture and contributions of 3D cell culture to drug development and basic biomedical research. *Int. J. Mol. Sci.* **2021**, *22*, 2491. [CrossRef] [PubMed]
13. Jazayeri, H.E.; Lee, S.M.; Kuhn, L.; Fahimipour, F.; Tahriri, M.; Tayebi, L. Polymeric scaffolds for dental pulp tissue engineering: A review. *Dent. Mater.* **2020**, *36*, e47–e58. [CrossRef] [PubMed]
14. Dhivya, S.; Keshav Narayan, A.; Logith Kumar, R.; Viji Chandran, S.; Vairamani, M.; Selvamurugan, N. Proliferation and differentiation of mesenchymal stem cells on scaffolds containing chitosan, calcium polyphosphate and pigeonite for bone tissue engineering. *Cell Prolif.* **2018**, *51*, e12408. [CrossRef]
15. Sharma, S.; Srivastava, D.; Grover, S.; Sharma, V. Biomaterials in tooth tissue engineering: A review. *J. Clin. Diagn. Res.* **2014**, *8*, 309–315. [CrossRef]
16. Ricucci, D.; Loghin, S.; Lin, L.M.; Spångberg, L.S.W.; Tay, F.R. Is hard tissue formation in the dental pulp after the death of the primary odontoblasts a regenerative or a reparative process? *J. Dent.* **2014**, *42*, 1156–1170. [CrossRef]
17. Yang, J.; Yuan, G.; Chen, Z. Pulp regeneration: Current approaches and future challenges. *Front. Physiol.* **2016**, *7*, 58. [CrossRef]
18. Huang, C.; Narayanan, R.; Warshawsky, N. Dual ECM Biomimetic Scaffolds for Dental Pulp Regenerative Applications. *Front. Physiol.* **2018**, *9*, 495. [CrossRef]
19. Gaje, P.N.; Ceausu, R.A. Cell types of the dental pulp behind the odontoblast. *Res. Clin. Med.* **2020**, *4*, 16–18.

20. Erdek, Ö.; Bloch, W.; Rink-Notzon, S.; Roggendorf, H.C.; Uzun, S.; Meul, B.; Koch, M.; Neugebauer, J.; Deschner, J.; Korkmaz, Y. Inflammation of the Human Dental Pulp Induces Phosphorylation of eNOS at Thr495 in Blood Vessels. *Biomedicines* **2022**, *10*, 1586. [CrossRef]
21. Huang, X.; Li, Z.; Liu, A.; Liu, X.; Guo, H.; Wu, M.; Yang, X.; Han, B.; Xuan, K. Microenvironment Influences Odontogenic Mesenchymal Stem Cells Mediated Dental Pulp Regeneration. *Front. Physiol.* **2021**, *12*, 656588. [CrossRef]
22. Fawzy El-Sayed, K.M.; Jakusz, K.; Jochens, A.; Dörfer, C.; Schwendicke, F. Stem cell transplantation for pulpal regeneration: A systematic review. *Tissue Eng.-Part B Rev.* **2015**, *21*, 451–460. [CrossRef]
23. Kökten, T.; Bécavin, T.; Keller, L.; Weickert, J.L.; Kuchler-Bopp, S.; Lesot, H. Immunomodulation stimulates the innervation of engineered tooth organ. *PLoS ONE* **2014**, *9*, e86011. [CrossRef]
24. Goldberg, M.; Njeh, A.; Uzunoglu, E. Is Pulp Inflammation a Prerequisite for Pulp Healing and Regeneration? *Mediat. Inflamm.* **2015**, *2015*, 347649. [CrossRef]
25. Starnitz, S.; Klimczak, A. Bone Repair: From Research Perspectives to Clinical Practice. *Cells* **2021**, *10*, 1925. [CrossRef]
26. Kim, I.H.; Jeon, M.; Cheon, K.; Kim, S.H.; Jung, H.S.; Shin, Y.; Kang, C.M.; Kim, S.O.; Choi, H.J.; Lee, H.S.; et al. In vivo evaluation of decellularized human tooth scaffold for dental tissue regeneration. *Appl. Sci.* **2021**, *11*, 8472. [CrossRef]
27. Wei, X.; Yang, M.; Yue, L.; Huang, D.; Zhou, X.; Wang, X.; Zhang, Q.; Qiu, L.; Huang, Z.; Wang, H.; et al. Expert consensus on regenerative endodontic procedures. *Int. J. Oral Sci.* **2022**, *14*, 55. [CrossRef]
28. Colombo, J.S.; Moore, A.N.; Hartgerink, J.D.; D'Souza, R.N. Scaffolds to control inflammation and facilitate dental pulp regeneration. *J. Endod.* **2014**, *40*, S6–S12. [CrossRef] [PubMed]
29. Osman, Z.F.; Ahmad, A.; Noordin, K.B.A.A. Naturally derived scaffolds for dental pulp regeneration: A review. *Gulhane Med. J.* **2019**, *61*, 81–88. [CrossRef]
30. Smojver, I.; Katalinić, I.; Bjelica, R.; Gabrić, D.; Matišić, V.; Molnar, V.; Primorac, D. Mesenchymal Stem Cells Based Treatment in Dental Medicine: A Narrative Review. *Int. J. Mol. Sci.* **2022**, *23*, 1662. [CrossRef] [PubMed]
31. Olaru, M.; Sachelarie, L.; Calin, G. Hard dental tissues regeneration—Approaches and challenges. *Materials* **2021**, *14*, 2558. [CrossRef]
32. Sándor, G. Tissue engineering: Propagating the wave of change. *Ann. Maxillofac. Surg.* **2013**, *3*, 1–2. [CrossRef] [PubMed]
33. Samiei, M.; Fathi, M.; Barar, J.; Fathi, N.; Amiryaghoubi, N.; Omidi, Y. Bioactive hydrogel-based scaffolds for the regeneration of dental pulp tissue. *J. Drug Deliv. Sci. Technol.* **2021**, *64*, 102600. [CrossRef]
34. Dissanayaka, W.L.; Zhang, C. The Role of Vasculature Engineering in Dental Pulp Regeneration. *J. Endod.* **2017**, *43*, S102–S106. [CrossRef] [PubMed]
35. Sun, H.H.; Chen, B.; Zhu, Q.L.; Kong, H.; Li, Q.H.; Gao, L.N.; Xiao, M.; Chen, F.M.; Yu, Q. Investigation of dental pulp stem cells isolated from discarded human teeth extracted due to aggressive periodontitis. *Biomaterials* **2014**, *35*, 9459–9472. [CrossRef]
36. Yang, J.W.; Zhang, Y.F.; Sun, Z.Y.; Song, G.T.; Chen, Z. Dental pulp tissue engineering with bFGF-incorporated silk fibroin scaffolds. *J. Biomater. Appl.* **2015**, *30*, 221–229. [CrossRef]
37. Yang, J.W.; Zhang, Y.F.; Wan, C.Y.; Sun, Z.Y.; Nie, S.; Jian, S.J.; Zhang, L.; Song, G.T.; Chen, Z. Autophagy in SDF-1 $\alpha$ -mediated DPSC migration and pulp regeneration. *Biomaterials* **2015**, *44*, 11–23. [CrossRef]
38. Caraccappa, J.D.; Vincent, S. The future in dental medicine: Dental stem cells are a promising source for tooth and tissue engineering. *J. Stem Cell Res. Ther. Rev.* **2019**, *5*, 30–36. [CrossRef]
39. Staniewski, T.; Zawadzka-Knefel, A.; Skośkiewicz-Malinowska, K. Therapeutic potential of dental pulp stem cells according to different transplant types. *Molecules* **2021**, *26*, 7423. [CrossRef]
40. Morotomi, T.; Washio, A.; Kitamura, C. Current and future options for dental pulp therapy. *Jpn. Dent. Sci. Rev.* **2019**, *55*, 5–11. [CrossRef]
41. Dang, M.; Saunders, L.; Niu, X.; Fan, Y.; Ma, P.X. Biomimetic delivery of signals for bone tissue engineering. *Bone Res.* **2018**, *6*, 25. [CrossRef] [PubMed]
42. Moussa, D.G.; Aparicio, C. Present and future of tissue engineering scaffolds for dentin-pulp complex regeneration. *J. Tissue Eng. Regen. Med.* **2019**, *13*, 58–75. [CrossRef] [PubMed]
43. Suamte, L.; Tirkey, A.; Babu, P.J. Design of 3D smart scaffolds using natural, synthetic and hybrid derived polymers for skin regenerative applications. *Smart Mater. Med.* **2023**, *4*, 243–256. [CrossRef]
44. Tran, T.T.; Hamid, Z.A.; Cheong, K.Y. A Review of Mechanical Properties of Scaffold in Tissue Engineering: Aloe Vera Composites. *J. Phys. Conf. Ser.* **2018**, *1082*, 012080. [CrossRef]
45. Wu, D.T.; Munguia-Lopez, J.G.; Cho, Y.W.; Ma, X.; Song, V.; Zhu, Z.; Tran, S.D. Polymeric scaffolds for dental, oral, and craniofacial regenerative medicine. *Molecules* **2021**, *26*, 7043. [CrossRef] [PubMed]
46. Echeverria Molina, M.I.; Malollari, K.G.; Komvopoulos, K. Design Challenges in Polymeric Scaffolds for Tissue Engineering. *Front. Bioeng. Biotechnol.* **2021**, *9*, 617141. [CrossRef] [PubMed]
47. Putra, R.U.; Basri, H.; Prakoso, A.T.; Chandra, H.; Ammarullah, M.I.; Akbar, I.; Syahrom, A.; Kamarul, T. Level of Activity Changes Increases the Fatigue Life of the Porous Magnesium Scaffold, as Observed in Dynamic Immersion Tests, over Time. *Sustainability* **2023**, *15*, 823. [CrossRef]
48. Zhang, H.; Zhou, L.; Zhang, W. Control of scaffold degradation in tissue engineering: A review. *Tissue Eng.-Part B Rev.* **2014**, *20*, 492–502. [CrossRef]
49. Van Bochove, B.; Grijpma, D.W. Photo-crosslinked synthetic biodegradable polymer networks for biomedical applications. *J. Biomater. Sci. Polym. Ed.* **2019**, *30*, 77–106. [CrossRef]



50. Jang, J.H.; Moon, J.H.; Kim, S.G.; Kim, S.Y. Pulp regeneration with hemostatic matrices as a scaffold in an immature tooth minipig model. *Sci. Rep.* **2020**, *10*, 12536. [CrossRef]
51. Erisken, C.; Kalyon, D.M.; Zhou, J.; Kim, S.G.; Mao, J.J. Viscoelastic properties of dental pulp tissue and ramifications on biomaterial development for pulp regeneration. *J. Endod.* **2015**, *41*, 1711–1717. [CrossRef] [PubMed]
52. Raddall, G.; Mello, I.; Leung, B.M. Biomaterials and Scaffold Design Strategies for Regenerative Endodontic Therapy. *Front. Bioeng. Biotechnol.* **2019**, *7*, 317. [CrossRef]
53. Yu, H.; Zhang, X.; Song, W.; Pan, T.; Wang, H.; Ning, T.; Wei, Q.; Xu, H.H.K.; Wu, B.; Ma, D. Effects of 3-dimensional Bioprinting Alginate/Gelatin Hydrogel Scaffold Extract on Proliferation and Differentiation of Human Dental Pulp Stem Cells. *J. Endod.* **2019**, *45*, 706–715. [CrossRef] [PubMed]
54. Liu, H.; Lu, J.; Jiang, Q.; Haapasalo, M.; Qian, J.; Tay, F.R.; Shen, Y. Biomaterial scaffolds for clinical procedures in endodontic regeneration: Biomaterial scaffolds in endodontic regeneration. *Bioact. Mater.* **2022**, *12*, 257–277. [CrossRef]
55. Palma, P.J.; Ramos, J.C.; Martins, J.B.; Diogenes, A.; Figueiredo, M.H.; Ferreira, P.; Viegas, C.; Santos, J.M. Histologic Evaluation of Regenerative Endodontic Procedures with the Use of Chitosan Scaffolds in Immature Dog Teeth with Apical Periodontitis. *J. Endod.* **2017**, *43*, 1279–1287. [CrossRef]
56. Nowicka, A.; Miller-Burchacka, M.; Lichota, D.; Metlerska, J.; Gońda-Domin, M. Tissue engineering application in regenerative endodontics. *Pomeranian J. Life Sci.* **2021**, *67*, 10–17. [CrossRef]
57. Nosrat, A.; Kolahdouzan, A.; Khatibi, A.H.; Verma, P.; Jamshidi, D.; Nevins, A.J.; Torabinejad, M. Clinical, Radiographic, and Histologic Outcome of Regenerative Endodontic Treatment in Human Teeth Using a Novel Collagen-hydroxyapatite Scaffold. *J. Endod.* **2019**, *45*, 136–143. [CrossRef]
58. De Araújo, L.; Goulart, T.S.; Gil, A.C.K.; Schuldt, D.P.V.; Coelho, B.S.; Figueiredo, D.D.R.; Garcia, L.D.F.R.; De Almeida, J. Do alternative scaffolds used in regenerative endodontics promote better root development than that achieved with blood clots? *Braz. Dent. J.* **2022**, *33*, 22–32. [CrossRef] [PubMed]
59. Jung, C.; Kim, S.; Sun, T.; Cho, Y.B.; Song, M. Pulp-dentin regeneration: Current approaches and challenges. *J. Tissue Eng.* **2019**, *10*. [CrossRef] [PubMed]
60. Ayala-Ham, A.; López-Gutierrez, J.; Bermúdez, M.; Aguilar-Medina, M.; Sarmiento-Sánchez, J.I.; López-Camarillo, C.; Sanchez-Schmitz, G.; Ramos-Payan, R. Hydrogel-Based Scaffolds in Oral Tissue Engineering. *Front. Mater.* **2021**, *8*, 708945. [CrossRef]
61. Ducret, M.; Costantini, A.; Gobert, S.; Farges, J.C.; Bekhouche, M. Fibrin-based scaffolds for dental pulp regeneration: From biology to nanotherapeutics. *Eur. Cells Mater.* **2021**, *41*, 1–14. [CrossRef] [PubMed]
62. Moreira, M.S.; Sarra, G.; Carvalho, G.L.; Gonçalves, F.; Caballero-Flores, H.V.; Pedroni, A.C.F.; Lascala, C.A.; Catalani, L.H.; Marques, M.M. Physical and Biological Properties of a Chitosan Hydrogel Scaffold Associated to Photobiomodulation Therapy for Dental Pulp Regeneration: An in Vitro and in Vivo Study. *Biomed Res. Int.* **2021**, *2021*, 6684667. [CrossRef] [PubMed]
63. Sharma, S.; Mittal, N. A comparative evaluation of natural and artificial scaffolds in regenerative endodontics: A clinical study. *Saudi Endod. J.* **2016**, *6*, 9–15. [CrossRef]
64. Rojo, L.; Vazquez, B.; Roman, J.S. Synthetic Polymers for Tissue Engineering Scaffolds: Biological Design, Materials, and Fabrication Biomaterials for Scaffolds: Synthetic Polymers. In *Scaffolds for Tissue Engineering*; CRC Press: Boca Raton, FL, USA, 2014; pp. 263–300.
65. Nikolova, M.P.; Chavali, M.S. Recent advances in biomaterials for 3D scaffolds: A review. *Bioact. Mater.* **2019**, *4*, 271–292. [CrossRef] [PubMed]
66. Dissanayaka, W.L.; Zhang, C. Scaffold-based and Scaffold-free Strategies in Dental Pulp Regeneration. *J. Endod.* **2020**, *46*, S81–S89. [CrossRef] [PubMed]
67. Joshi, S.R.; Pendyala, G.S.; Shah, P.; Mopagar, V.P.; Padmawar, N.; Padubidri, M. Scaffolds-The Ground for Regeneration: A Narrative Review. *J. Int. Soc. Prev. Community Dent.* **2020**, *10*, 692–699. [CrossRef]
68. Azaman, F.A.; Zhou, K.; Del Blanes-Martínez, M.M.; Brennan Fournet, M.; Devine, D.M. Bioresorbable Chitosan-Based Bone Regeneration Scaffold Using Various Bioceramics and the Alteration of Photoinitiator Concentration in an Extended UV Photocrosslinking Reaction. *Gels* **2022**, *8*, 696. [CrossRef]
69. Liu, X.; Holzwarth, J.M.; Ma, P.X. Functionalized Synthetic Biodegradable Polymer Scaffolds for Tissue Engineering. *Macromol. Biosci.* **2012**, *12*, 911–919. [CrossRef]
70. Dos Santos Gomes, D.; De Sousa Victor, R.; De Sousa, B.V.; De Araújo Neves, G.; De Lima Santana, L.N.; Menezes, R.R. Ceramic Nanofiber Materials for Wound Healing and Bone Regeneration: A Brief Review. *Materials* **2022**, *15*, 3909. [CrossRef]
71. Nuge, T.; Liu, Z.; Liu, X.; Ang, B.C.; Andriyana, A.; Metselaar, H.S.C.; Hoque, M.E. Recent advances in scaffolding from natural-based polymers for volumetric muscle injury. *Molecules* **2021**, *26*, 699. [CrossRef]
72. Kim, S.G.; Zhou, J.; Ye, L.; Cho, S.; Suzuki, T.; Fu, S.Y.; Yang, R.; Zhou, X.; Mao, J.J. Regenerative Endodontics: Barriers and Strategies for Clinical Translation. *Dent. Clin. N. Am.* **2014**, *56*, 639–649. [CrossRef]
73. Amini, S.; Salehi, H.; Setayeshmehr, M.; Ghorbani, M. Natural and synthetic polymeric scaffolds used in peripheral nerve tissue engineering: Advantages and disadvantages. *Polym. Adv. Technol.* **2021**, *32*, 2267–2289. [CrossRef]
74. Reddy, M.S.B.; Ponnamma, D.; Choudhary, R.; Sadasivuni, K.K. A comparative review of natural and synthetic biopolymer composite scaffolds. *Polymers* **2021**, *13*, 1105. [CrossRef] [PubMed]
75. Gathani, K.M.; Raghavendra, S.S. Scaffolds in regenerative endodontics: A review. *Dent. Res. J.* **2016**, *13*, 379–386. [CrossRef]



76. Banerjee, A.; Chatterjee, K.; Madras, G. Enzymatic degradation of polymers: A brief review. *Mater. Sci. Technol.* **2014**, *30*, 567–573. [CrossRef]
77. Gentile, P.; Chiono, V.; Carmagnola, I.; Hatton, P.V. An overview of poly(lactic-co-glycolic) Acid (PLGA)-based biomaterials for bone tissue engineering. *Int. J. Mol. Sci.* **2014**, *15*, 3640–3659. [CrossRef]
78. Prakasam, M.; Silvain, J.F.; Largeteau, A. Innovative high-pressure fabrication processes for porous biomaterials—A review. *Bioengineering* **2021**, *8*, 170. [CrossRef]
79. Rizk, A.; Rabie, A.B.M. Human dental pulp stem cells expressing transforming growth factor  $\beta$ 3 transgene for cartilage-like tissue engineering. *Cytotherapy* **2013**, *15*, 712–725. [CrossRef]
80. Danhier, F.; Ansorena, E.; Silva, J.M.; Coco, R.; Le Breton, A.; Pr at, V. PLGA-based nanoparticles: An overview of biomedical applications. *J. Control. Release* **2012**, *161*, 505–522. [CrossRef]
81. Jammalamadaka, U.; Tappa, K. Recent advances in biomaterials for 3D printing and tissue engineering. *J. Funct. Biomater.* **2018**, *9*, 22. [CrossRef]
82. Bencherif, S.A.; Braschler, T.M.; Renaud, P. Advances in the design of macroporous polymer scaffolds for potential applications in dentistry. *J. Periodontal Implant Sci.* **2013**, *43*, 251–261. [CrossRef] [PubMed]
83. Zhang, B.; Bian, X.; Xiang, S.; Li, G.; Chen, X. Synthesis of PLLA-based block copolymers for improving melt strength and toughness of PLLA by in situ reactive blending. *Polym. Degrad. Stab.* **2017**, *136*, 58–70. [CrossRef]
84. Śmigi el-Gac, N.; Pamuła, E.; Krok-Borkowicz, M.; Smola-Dmochowska, A.; Dobrzyński, P. Synthesis and properties of bioresorbable block copolymers of l-lactide, glycolide, butyl succinate and butyl citrate. *Polymers* **2020**, *12*, 213. [CrossRef] [PubMed]
85. Haugen, H.J.; Basu, P.; Sukul, M.; Mano, J.F.; Reseland, J.E. Injectable biomaterials for dental tissue regeneration. *Int. J. Mol. Sci.* **2020**, *21*, 3442. [CrossRef]
86. Kaliva, M.; Georgopoulou, A.; Dragatogiannis, D.A.; Charitidis, C.A.; Chatzinikolaidou, M.; Vamvakaki, M. Biodegradable Chitosan-graft-Poly(l-lactide) Copolymers For Bone Tissue Engineering. *Polymers* **2020**, *12*, 316. [CrossRef]
87. Chocholata, P.; Kulda, V.; Babuska, V. Fabrication of scaffolds for bone-tissue regeneration. *Materials* **2019**, *12*, 568. [CrossRef]
88. Wei, S.; Ma, J.X.; Xu, L.; Gu, X.S.; Ma, X.L. Biodegradable materials for bone defect repair. *Mil. Med. Res.* **2020**, *7*, 54. [CrossRef]
89. Svobodova, J.; Proks, V.; Karabiyik,  .;  alıkođlu Koyuncu, A.C.; Torun K ose, G.; Rypacek, F.; Studenovska, H. Poly (Amino Acid)-Base fibrous scaffold modified with surface-pendant eptides for cartilage tissue engineering. *J. Tissue Eng. Regen. Med.* **2017**, *11*, 831–842. [CrossRef]
90. Li, T.; Lu, X.M.; Zhang, M.R.; Hu, K.; Li, Z. Peptide-based nanomaterials: Self-assembly, properties and applications. *Bioact. Mater.* **2022**, *11*, 268–282. [CrossRef]
91. Galler, K.M.; Hartgerink, J.D.; Cavender, A.C.; Schmalz, G.; D’Souza, R.N. A customized self-assembling peptide hydrogel for dental pulp tissue engineering. *Tissue Eng.-Part A* **2012**, *18*, 176–184. [CrossRef]
92. Khanna-Jain, R.; Mannerstr om, B.; Vuorinen, A.; Sandor, G.K.B.; Suuronen, R.; Miettinen, S. Osteogenic differentiation of human dental pulp stem cells on  $\beta$ -tricalcium phosphate/poly (l-lactic acid/caprolactone) three-dimensional scaffolds. *J. Tissue Eng.* **2012**, *3*, 2041731412467998. [CrossRef] [PubMed]
93. Alaribe, F.N.; Manoto, S.L.; Motaung, S.C.K.M. Scaffolds from biomaterials: Advantages and limitations in bone and tissue engineering. *Biologia* **2016**, *71*, 353–366. [CrossRef]
94. Farzamfar, S.; Esmailpour, F.; Rahmati, M.; Vaez, A.; Mirzaii, M.; Garmabi, B.; Shayannia, A.; Ebrahimi, E.; Vahedi, H.; Salehi, M. Poly-lactic Acid/Gelatin Nanofiber (PLA/GTNF) Conduits Containing Platelet-Rich Plasma for Peripheral Nerve Regeneration. *Int. J. Health Stud.* **2017**, *3*, 29–32. [CrossRef]
95. Gaaz, T.S.; Sulong, A.B.; Akhtar, M.N.; Kadhun, A.A.H.; Mohamad, A.B.; Al-amiery, A.A. Properties and Applications of Polyvinyl Alcohol, Halloysite Nanotubes and Their Nanocomposites. *Molecules* **2015**, *20*, 22833–22847. [CrossRef] [PubMed]
96. Zhai, H.; Wu, Y. Research and progress of cartilage tissue-engineering scaffold materials. *Discuss. Clin. Cases* **2015**, *2*, 51–54. [CrossRef]
97. Barroca, N.; Marote, A.; Vieira, S.I.; Almeida, A.; Fernandes, M.H.; Vilarinho, P.M.; Silva, O.A.D.C.E. Electrically polarized PLLA nanofibers as neural tissue engineering scaffolds with improved neuritogenesis. *Colloids Surf. B Biointerfaces* **2018**, *167*, 93–103. [CrossRef]
98. Saini, P.; Arora, M.; Kumar, M.N.V.R. Poly(lactic acid) Blends in Biomedical Applications. *Adv. Drug Deliv. Rev.* **2016**, *107*, 47–59. [CrossRef]
99. Sisson, A.L.; Ekinici, D.; Lendlein, A. The contemporary role of  $\epsilon$ -caprolactone chemistry to create advanced polymer architectures. *Polymer* **2015**, *54*, 4333–4350. [CrossRef]
100. Mir, M.; Ahmed, N.; Rehman, A. Recent Applications of Plga Based Nanostructures in Drug Delivery. *Colloids Surf. B Biointerfaces* **2017**, *159*, 217–231. [CrossRef]
101. Prakoso, A.T.; Basri, H.; Adanta, D.; Yani, I.; Ammarullah, M.I.; Akbar, I.; Ghazali, F.A.; Syahrom, A.; Kamarul, T. The Effect of Tortuosity on Permeability of Porous Scaffold. *Biomedicines* **2023**, *11*, 427. [CrossRef]
102. Guerreiro, R.; Pires, T.; Guedes, J.M.; Fernandes, P.R.; Castro, A.P.G. On the Tortuosity of TPMS Scaffolds for Tissue Engineering. *Symmetry* **2020**, *12*, 596. [CrossRef]

**Disclaimer/Publisher’s Note:** The statements, opinions and data contained in all publications are solely those of the individual author(s) and contributor(s) and not of MDPI and/or the editor(s). MDPI and/or the editor(s) disclaim responsibility for any injury to people or property resulting from any ideas, methods, instructions or products referred to in the content.



Review

# Polymers Use as Mulch Films in Agriculture—A Review of History, Problems and Current Trends

Zinnia Mansoor <sup>1,2</sup>, Fideline Tchuenbou-Magaia <sup>3</sup>, Marek Kowalczyk <sup>4</sup>, Grazyna Adamus <sup>4</sup>, Georgina Manning <sup>1</sup>, Mattia Parati <sup>1</sup>, Iza Radecka <sup>1,\*</sup> and Habib Khan <sup>1,\*</sup>

<sup>1</sup> School of Sciences, Faculty of Science and Engineering, University of Wolverhampton, Wolverhampton WV1 1LY, UK

<sup>2</sup> Department of Biotechnology, Virtual University of Pakistan, Lahore 54000, Pakistan

<sup>3</sup> Division of Chemical Engineering, School of Engineering, Computing and Mathematical Sciences, Faculty of Science and Engineering, University of Wolverhampton, Wolverhampton WV1 1LY, UK

<sup>4</sup> Centre of Polymer and Carbon Materials, Polish Academy of Sciences, M. Curie-Skłodowskiej 34, 41-819 Zabrze, Poland

\* Correspondence: i.radecka@wlv.ac.uk (I.R.); h.khan6@wlv.ac.uk (H.K.)

**Abstract:** The application of mulch films for preserving soil moisture and preventing weed growth has been a part of agricultural practice for decades. Different materials have been used as mulch films, but polyethylene plastic has been considered most effective due to its excellent mechanical strength, low cost and ability to act as a barrier for sunlight and water. However, its use carries a risk of plastic pollution and health hazards, hence new laws have been passed to replace it completely with other materials over the next few years. Research to find out about new biodegradable polymers for this purpose has gained impetus in the past few years, driven by regulations and the United Nations Organization's Sustainable Development Goals. The primary requisite for these polymers is biodegradability under natural climatic conditions without the production of any toxic residual compounds. Therefore, biodegradable polymers developed from fossil fuels, microorganisms, animals and plants are viable options for using as mulching material. However, the solution is not as simple since each polymer has different mechanical properties and a compromise has to be made in terms of strength, cost and biodegradability of the polymer for its use as mulch film. This review discusses the history of mulching materials, the gradual evolution in the choice of materials, the process of biodegradation of mulch films, the regulations passed regarding material to be used, types of polymers that can be explored as potential mulch films and the future prospects in the area.

**Keywords:** mulch films; biodegradability; biopolymers; SDGs; plastic pollution

**Citation:** Mansoor, Z.; Tchuenbou-Magaia, F.; Kowalczyk, M.; Adamus, G.; Manning, G.; Parati, M.; Radecka, I.; Khan, H. Polymers Use as Mulch Films in Agriculture—A Review of History, Problems and Current Trends. *Polymers* **2022**, *14*, 5062.

<https://doi.org/10.3390/polym14235062>

Academic Editor: Raffaella Striani

Received: 19 October 2022

Accepted: 17 November 2022

Published: 22 November 2022



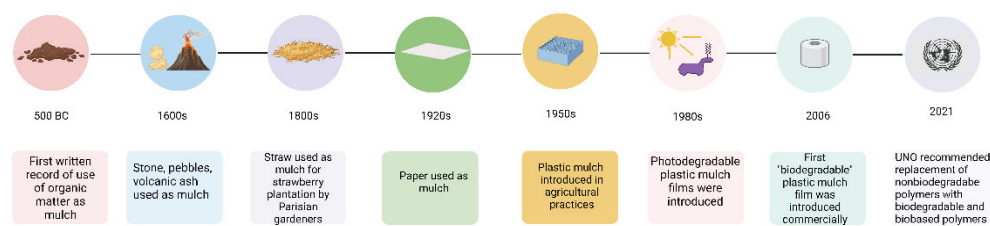
**Copyright:** © 2022 by the authors. Licensee MDPI, Basel, Switzerland. This article is an open access article distributed under the terms and conditions of the Creative Commons Attribution (CC BY) license (<https://creativecommons.org/licenses/by/4.0/>).

## 1. Introduction

The technique of mulching has been a part of agricultural practice for a long time. In simple terms, mulches are defined as materials that are applied directly onto the surface of soil for various purposes such as the protection of seedlings and young shoots through insulation, reduction of evaporation, control of weed growth and prevention of soil erosion [1]. They specifically protect delicate crop species from unfavourable abiotic and biotic stresses that may occur as a result of extreme weather conditions, insects, pests and weeds. Therefore, mulches are commonly used in agriculture to prevent loss of crop yield [2].

The history of using mulching to enhance crop production dates back to around 500 BCE, as shown in Figure 1. It is from that age that the first documented proof of the use of organic matter as a mulch film has been obtained [3]. The material used gradually changed to stones, pebbles and volcanic ash in the 1600s, although these were mostly used in arid regions. In the 1800s the Parisian market gardeners found that the use of straw as mulching material for strawberry production was beneficial. Thus, over a span of hundreds of years, different naturally available materials were tried and used for mulching

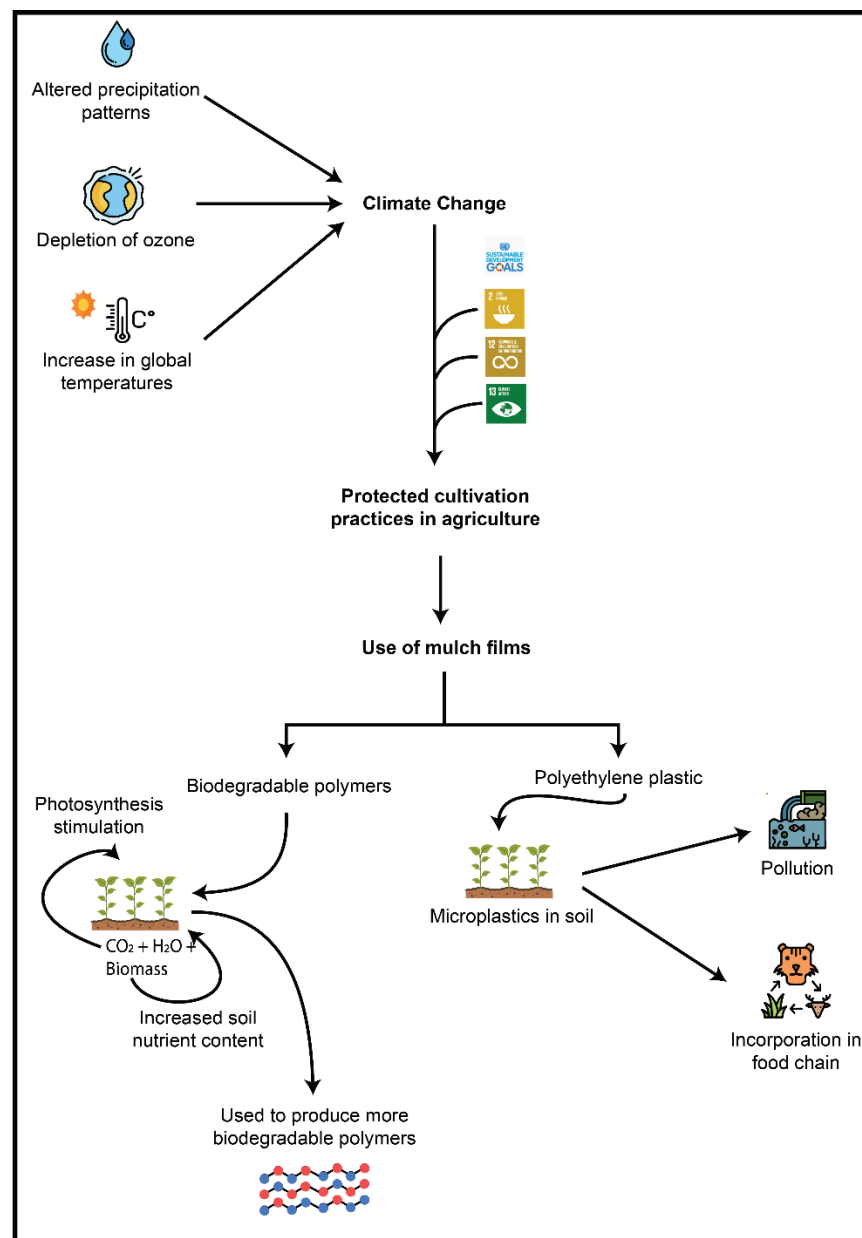
depending upon climatic conditions in different parts of the world [4]. As science advanced in the 20th century, mulching was also revolutionized. Paper sheets were introduced as mulch films in the 1920s, followed by the commercialization of plastic, specifically polyethylene films for mulching in the late 1950s. Plastic mulching gained popularity and proved to be very effective. However, the negative impact of plastic became evident within three decades and by the early 1980s photo-degradable and oxo-degradable plastics were introduced as an alternative to polyethylene based films. It soon became apparent that these polymers did not degrade in field conditions and generated microplastics [5]. Research was accelerated in this area and in 2006 the first biodegradable plastic mulch film was introduced in the market commercially. Following this, a number of biodegradable mulch films were manufactured by companies throughout the world. It was not until 2021, however, that the Food and Agriculture Organization, which is a part of the United Nations Organization, gave its recommendation to replace conventional and non-biodegradable polymers with bio-based and biodegradable materials for mulching practices [6].



**Figure 1.** The history and development of different mulching materials.

Various anthropogenic activities over the years have led to the production of greenhouse gases, which, in turn, have resulted in climate change. The emission and accumulation of these gases in the atmosphere has led to global warming, i.e., an increase in average temperatures and fluctuations that contribute to extreme weather conditions, as well as alterations in precipitation patterns throughout the world. Such changes in agricultural regions have an adverse impact on crop production, thus creating problems when providing adequate food supply for an increasing population in an efficient and sustainable manner [7]. The limited availability of arable land, depletion of water sources for irrigation, soil erosion, overexploitation of natural resources, pollution of ecosystems and climate change are some of the factors that restrict food crop production and yields [8].

In 2015, under the banner of the United Nations Organization, the international community developed a series of Sustainable Development Goals, known as SDGs, which include ensuring access to food for all, increasing agricultural productivity and achieving zero hunger by 2030 [9]. These goals not only imply the provision of food to achieve zero hunger on a global scale, but also aim to enhance agricultural productivity in a sustainable, manageable and efficient manner. The primary focus is to increase yields of food crops by adopting farming practices that are environmentally friendly and ecologically viable [10]. Mulching is already commonly used all over the world as a strategy to improve crop yield and prevent losses. The global mulch market is estimated at USD 3.5 billion in the year 2020, and is projected to amount to USD 5.1 billion by 2027 [11]. Considering the expansion of the market, it is pertinent to check that the practice is in line with the UN SDGs, specifically in terms of responsible production and consumption (Figure 2). Currently, the main material used for mulch films is polyethylene plastic, which is raising concerns. These mulch films do not degrade naturally and need to be removed from fields after harvesting. They cannot be recycled, and the debris left in soil contributes to soil pollution. A lack of disposal options for used plastic films adds to land and water pollution [12]. Therefore, there is an urgent need to explore other alternative polymers that may be used to replace plastic for mulching purposes [13].



**Figure 2.** The need for mulching as an agricultural practice and the materials available for use as mulch films.

Biodegradable polymers may be one solution, and have the potential to replace plastics for many applications. However, these polymers have certain limitations which are restricting their use on a commercial scale for the purpose of mulching. Factors that need to be considered before a polymer can be used include not only its physical and chemical properties but also the source and method of production. These polymers have different mechanical properties, which, in turn, affect their biodegradation in the environment [14]. Moreover, legislation and laws passed over the past few years have defined and strict criteria regarding biodegradation, chemical composition, deployment and toxicity for materials that may be used as a mulch film [15].

This review discusses the practice of mulching in agriculture, its benefits, the materials used as mulch films, and the alternate options that can be explored for sustainable agricultural practices. It also includes an overview of the biodegradation process that occurs in the soil for the breakdown of mulching materials, factors affecting this process, and a list of

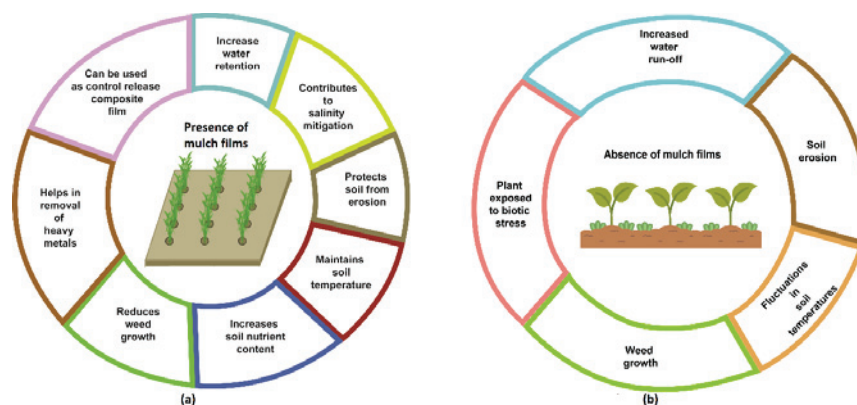


different commercially available mulches, highlighting the direction of further research in this area.

## 2. The Benefits of Mulch Films

The increasing food demand of a growing world population has driven the need to increase agricultural crop yields. Protected cultivation is one way to help optimize the yield of crops. This involves controlling the microclimate around the growing plant to protect it from harsh climatic conditions [16]. Mulching is based on the principle of protected cultivation and involves the application of a protective ground cover made of different materials that may be organic or synthetic, to improve the growth and yield of agricultural crops. The word mulch is derived from the German word 'molsch', which means 'easy to decay' [3].

The use of mulch films in agriculture has several benefits when compared to non-mulched crop production. These may be categorized as improvements in the soil microenvironment or economic advantages (Figure 3a). Soil moisture content is an important factor that affects the growth of plants. Winds, high temperature, adverse climatic conditions and particularly weed infestation can contribute to the reduction of soil moisture. Mulches have been reported to increase the percolation and water retention capacity of soil, to the extent that the use of mulching material can reduce the irrigation requirement of crop plants. This is attributed to their water retention ability, which reduces the runoff from the soil profile [17,18]. This can indirectly contribute to salinity mitigation, as well. Various studies have demonstrated that the application of mulch films reduces the impact of salt toxicity on plants and helps in soil reclamation [19]. Mulches are also associated with the protection of soil from wind and water erosion, as well as the reduction of the compaction of soil. It has been observed that crop growth is negatively affected due to erosion and soil compaction in the absence of mulch films (Figure 3b). Mulches protect the soil by breaking the speed of water, especially in slopes or hilly areas, thereby increasing the infiltration rate. Similarly, the presence of covering material in the form of mulch films prevents soil erosion by winds [20]. Mulch materials also reduce the impact of weathering and the beating action of heavy rain, and the weight of feet and tyres of heavy machinery, helping to overcome the problem of compaction in soil [21].



**Figure 3.** A comparison of the effect of mulch films on plant growth and soil—(a) in the presence of mulch films and (b) in the absence of mulch films.

It is important to control the temperature of soil, since temperature fluctuations adversely affect the development of roots [20]. Since the material used for mulching covers the soil surface entirely, it helps to maintain the optimal soil temperature required for plant growth. Studies have shown that the application of mulch films keeps the soil temperature warmer on chilly days, and cooler during hot spells [17,22]. Mulches also contribute to the soil nutrient content, since these are broken down or degraded by soil microorganisms into simpler compounds that become a part of the soil itself [23]. Weed control is one of the key benefits that mulching provides. When mulch is spread on the surface of the

soil, it acts as a barrier to the passage of sunlight, which reduces germination of weeds, especially small-seeded weed species. This phenomenon has been observed and widely used in nurseries as well as agricultural fields [24].

The presence of heavy metals in soil affects the growth of plants. Mulches can be used as a remediation strategy for the removal of these heavy metals from soil. Organic and plant-based mulch material forms complexes with heavy metals and converts them into a form that renders them non-toxic for plants [25]. Mulches can also be used as control release composite films, which are embedded with fertilizers, herbicides or pesticides. This strategy allows the gradual and slow release of these materials from the mulch films, ensuring that these are constantly available for use by the plant instead of being run off after the first application [26,27].

Generally, mulching decreases the stress level on plants, leading to better growth. This leads to enhanced crop yield and improved product quality. The crop may also be harvested earlier and tends to be more profitable [28]. All these facts confer economic advantages to the use of mulch films.

### 3. Types of Mulch Films

The use of mulch films dates back to ancient civilizations. The earliest mulch material comprised by-products from the agricultural and forestry industries, and included the trimmings of trees and shrubs, animal waste, stubble and residues of crop plants [20]. With time the material was modified, and now mulches can be categorized as organic or inorganic mulches. Organic mulches are made from materials found in nature and are usually broken down into simpler compounds by soil microorganisms. Inorganic mulches, on the other hand, are made of synthetic material that does not decompose easily [29]. The different types of materials used for mulching and their application in the field are shown in Figure 4.



**Figure 4.** Application of different mulch films in the field—(A): Compost, (B): Straw, (C): Bark, (D): Newspaper, (E): Woodchips, (F): Sawdust, (G): Plastic, (H): Black plastic, (I): LDPE. Adapted from [30].

The type of mulch used is governed by many factors, including the plant species, soil type and characteristics, the cost and availability of mulching material, as well as the regulations and law governing the region [31]. For instance, for vineyards or fruit orchards, the mulch film is generally thick and has a lifespan of years until it becomes

ineffective. For vegetable fields, on the other hand, thinner mulch films are used that last one growing season only [32]. Similarly, the effect of each mulching material is a combination of various factors including the amount of material applied, the carbon and nitrogen ratio of the material, its thickness, colour and other physical attributes, and the amount of toxic substances present [33]. Each material has certain advantages and disadvantages regarding its use for mulching, as summarized in Table 1 [34–72].

**Table 1.** Comparison of the sources, advantages and disadvantages of organic and synthetic mulch films.

Type of Mulch	Source	Advantages	Disadvantages
Organic	Compost	Adds nutrients to soil	Promotes pests and disease-causing organisms
	Straw and Husks	Inexpensive with long life	Harbours pests and weed seeds
	Sawdust	Readily available	Hardens over time and does not allow water to seep into the soil
	Grass clippings	Controls weeds effectively	Develops own root systems and competes with plant for nutrients
	Paper clippings	Decomposes easily	Rips and tears apart during application
	Bark chips and Pine needles	Retains soil moisture	Reduces soil pH
Inorganic	Glass pieces	Aesthetically appealing	Interferes with soil temperature and does not allow sunlight to penetrate
	Rubber clippings	Effective recycling	Hazard of fire and may promote zinc toxicity in plants
	Plastic	Retains moisture and controls weed growth	Labour intensive and contributes to plastic pollution
	PAC plastic	Retains moisture, controls weed growth and degrades in presence of UV light	Forms micro plastics in soil

### 3.1. Organic Mulches

Organic mulches mainly comprise animal or plant residues such as compost, manures, straws, husks, saw dust, grass and paper clippings, and wood/bark chips (Figure 4A–F). The application of compost and manure is an age-old practice in many regions of the world. The use of compost is as a way of recycling waste. It is cheap and readily available. Studies have exhibited that repeated use of compost for mulching over a number of years can increase the organic content of the soil and improve plant yield [34]. However, the use of compost as mulch has the added risk of phytotoxicity due to high nitrogen content. If applied near the stalks it absorbs moisture that promotes diseases and pests, leading to low crop yields [35]. Depending on the source of compost, it may contain heavy metals that accumulate in the soil as well as plants. While the presence of these heavy metals may not lead to toxicity in plants, it renders the crop unfit for human consumption. Compost is therefore not preferred anymore as a mulching material [36].

Other organic materials that can be used include straw and husks. These materials have a long life span when used for mulching and are effective for vegetables grown in winter months [37]. They are inexpensive, readily available and field trials have exhibited that they are good at preventing water loss via evaporation [38]. Both husk and straw mulches have the potential to increase crop yield and can significantly lower water losses from a well-irrigated system [39]. However, they often contaminate the soil with weed seeds and in addition harbour pests such as termites, snails, slugs and earwigs, leading to losses in crop yield, reducing their use for mulching [40].

Sawdust is readily available and has exhibited potential as a mulching material specifically for acid loving plants. It is very efficient in minimizing water runoff and soil erosion [41]. Studies have shown that it is not efficient in controlling the growth of weeds and also tends to harden over time, preventing water from reaching the deeper layers of the soil [42]. Another disadvantage is the low nitrogen content of sawdust, which means that it

uses up nitrogen from the soil as it decomposes. This has been seen in field trials where the use of sawdust mulch reduced the number of flowers produced and had an adverse impact on plant growth [43].

Grass clippings are very effective as a mulching material when applied as an appropriately thick layer. If the layer is too thick, it prevents air from penetrating, resulting in rotten and odorous clippings. If the layer is thin, the grass clippings decompose quickly, and need to be replenished frequently to maintain efficacy of the mulching material [44]. Fresh grass clippings also have the potential to develop their own root systems and offer growth competition to the crop plants. The use of these has also been shown to increase soil temperature and affect plant growth negatively in hot climates, limiting their application as mulching material [45].

Paper mulches are made up of cellulose fibres which can be decomposed naturally by most soil-borne microorganisms. Sheets of paper, mainly newspapers with black ink, can be used as mulch, as a part of a recycling strategy. The colour of paper used for mulching has an impact on the control of weed growth. Black paper mulching has shown promising results for decreasing the growth of weeds in lettuce and cantaloupe farming [46]. However, the main problem is that due to their light weight, these clippings are easily blown away by the wind. When applied as sheets, they tear apart easily when damp or wet, and are penetrated by weeds. Paper mulches degrade quickly so they cannot be used for long-term cultivation. These disadvantages limit the use of paper as a mulching material [40,47].

Wood and bark chips are preferred as mulching materials since these are very effective in retaining moisture in the soil. They also allow proper aeration and contribute to the organic content of the soil. Pine bark makes an attractive, usually dark-coloured mulch and may be used for ornamental plants. However, bark chips and pine needles have been reported to reduce the soil pH upon application and cause phytotoxicity [48]. The decomposition of woody material results in the release of phenolic acids which contribute to acidification of the soil, affecting plant growth. While this may be beneficial for crops that require an acidic pH for growth, it limits the large-scale use of woody material for mulching [49].

The main factors that limit the use of organic mulches are that they may not be available in adequate amounts throughout the year, have an inconsistent quality and are extremely labour intensive [50].

### 3.2. Synthetic Mulches

Inorganic or synthetic mulches are made up of materials such as glass, rubber sheets and plastic [51]. Glass mulches are usually made from chips of bottled glass as a method of recycling parts that cannot be separated from organic matter and other debris. These are exquisitely used to aesthetically modify a landscape while functioning as a mulch film [1]. However, the use of glass mulch films has become limited over the years because of their low efficiency in controlling weed growth. The ability of glass to reflect light reduces the sunlight that can reach the soil and has an impact on the soil temperature [52]. Moreover, the incorporation of non-recyclable glass into soil disturbs the physico-chemical characteristics of the soil, which subsequently impairs plant growth [53].

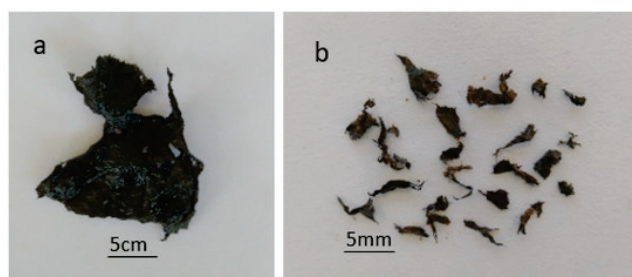
Rubber mulches are frequently made by shredding worn out tyres as a strategy of recycling. These shredded tyres include very fine particulate matter that can be inhaled, ingested or taken up transdermally, increasing health risks. The use of rubber mulches is also associated with the hazard of ignition since rubber catches fire quickly and is very difficult to extinguish [54]. Moreover, it has also been reported that rubber mulches are less effective in controlling weed growth compared to organic mulches [55]. In fact, high levels of zinc incorporated in tyres during manufacturing is released in the soil from the mulch and leads to zinc toxicity in plants, which adversely affects their growth [56].

Plastic mulch films (Figure 4G–I) have been used extensively since the 1950s and their global market has shown a continuous growth with a worth of USD 4.1 billion a year [57]. These are very effective in controlling weed growth and over time they have increased



global grain and cash crop yields by 15% and 40%, respectively [58]. Polyethylene plastic is the most popular and frequently used inorganic mulch throughout the world because of its efficacy and low price [59]. It is a low-density plastic that is highly resistant to weathering due to its chemical structure, which comprises saturated hydrocarbon chains [60]. These mulch films have low cost, low frequency of replacement, versatility and strength, and are therefore very effective in the field [61].

However, there are several problems associated with the use of plastic mulch films, including laborious and costly removal from the fields after use, lack of sustainable end-of-life management options and the addition of plastic waste to the environment [62]. At the end of the growing season, the mulch film is often contaminated with plant as well as soil debris which restricts its recycling. Therefore, these are categorized as single-use plastic films and are usually landfilled or incinerated, contributing significantly to plastic pollution [63]. Complete removal of polyethylene mulch films is often not possible from fields, which has led to considerable amounts of macro and microplastic debris in soils as shown in Figure 5 [54]. This accumulation of plastic residue in soil has a negative impact on crop production by affecting the plant growth-promoting bacteria (PGPB), damaging soil structure, retarding root growth and development, and altering the carbon concentration of the soil [65]. In some countries the lack of disposal options means that farmers simply stockpile these mulch films after use, which subsequently leads to the dispersion of the mulch fragments into the environment by water and wind erosion, causing pollution [66].



**Figure 5.** The debris of black plastic mulch films—(a): piece of plastic mulch film, (b): microplastics collected from soil after removal of mulch film. Adapted from [67].

Most countries in the world are now opting for sustainable practices and have banned single-use plastics to overcome plastic waste generation and pollution. This has necessitated the need to look for sustainable and eco-friendly alternatives that can be used as mulch films [68]. As a solution, pro-oxidant additive containing (PAC) plastics have been formulated. These are chemically similar to low density polyethylene plastics but contain a pro-oxidant additive that increases oxidation and degradation of the polymer in the presence of light [69]. This photo-oxidation reduces the molar mass and adds oxygenated groups that make the polymer more prone to breakdown by microorganisms under aerobic environments. These plastics are also referred to as ‘oxo-degradable’ plastics. An example is Oxo-PP or oxo-degradable polypropylene [70]. PAC plastic mulches have been reported to be as efficient as conventional plastic mulches in the field for controlling the growth of weeds. They also have no adverse impact on soil health [71].

However, these mulch films have low strength and can break down prematurely while being spread onto the field. This fragility and their lightweight nature makes the application very difficult. Moreover, the absence of UV light reduces degradation of these plastics once they are incorporated into the soil. Even if there is breakdown in the soil, it is never fully biodegraded. The mulch pieces persist in soil and watersheds, and form microplastics that have the ability to adsorb toxic pesticides, insecticides and herbicides, and carry them into the food chain [3]. Research reports suggest that while these mulch films are more expensive than polyethylene plastic films, they contribute equally to the generation of microplastics that pollute the soil [72]. Many countries in the European Union, including



France, have completely banned the use of PAC plastics, making it imperative to explore more sustainable, economical and environment friendly alternatives [66].

#### 4. Current Trends in Mulching Material

In recent years a lot of research has been carried out to produce mulch material that is both sustainable and eco-friendly. The material for a mulch film should ideally be bio-based and very prone to biodegradation [73]. To replace plastic, it should have similar mechanical properties including a high tensile strength and high percentage elongation. The European Union has set up the product standards for biodegradable mulch films that are to be used in the horticulture and agriculture sectors. The first and only standard (EN 17033) has specified values that must be met, in terms of biodegradability, deployment, chemical composition and eco-toxicity, for a material to be used as a mulch film [15]. The generally acceptable standard for biodegradability is that the material should completely breakdown to carbon dioxide, water, methane, inorganic compounds and biomass within a year of application without producing any visible, toxic residue [74].

The use of biodegradable material imparts the main advantage of being tilled into soil once used, so that it can be degraded by the action of soil microbiota, reducing the costs of labour and disposal [75]. To replace conventional polyethylene mulch, the material should have the ability to maintain the optimum microclimate for plant growth and degrade completely without producing any harmful toxic products. In terms of efficacy, it should possess high tensile strength, good water retention capacity and allow for easy application. The film should be readily available, especially in the cropping season, and be inexpensive so that farmers can use it. Any material that is to be used as mulch should meet the minimum design requirements according to EN17033 and ISO 23517:2021 [76,77]. The main attributes required in a material to be used as mulch film are shown in Figure 6.

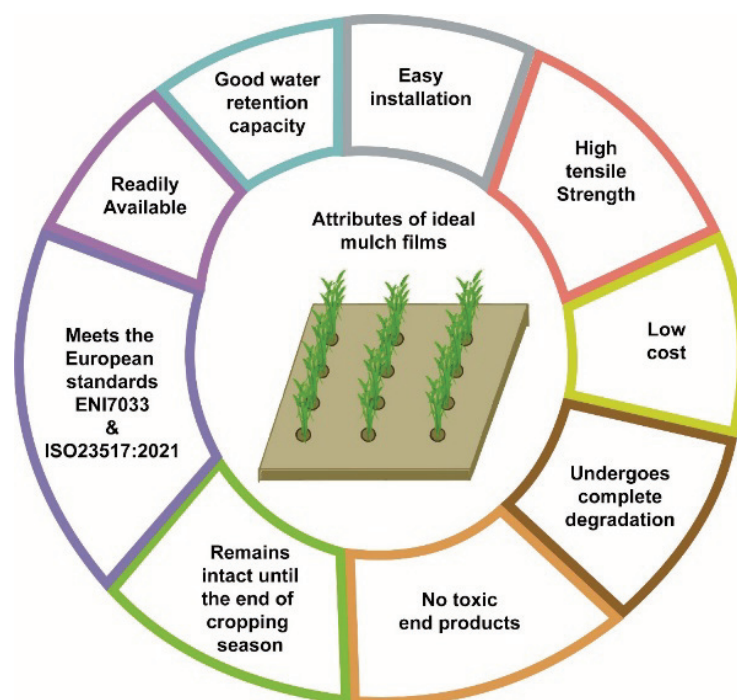
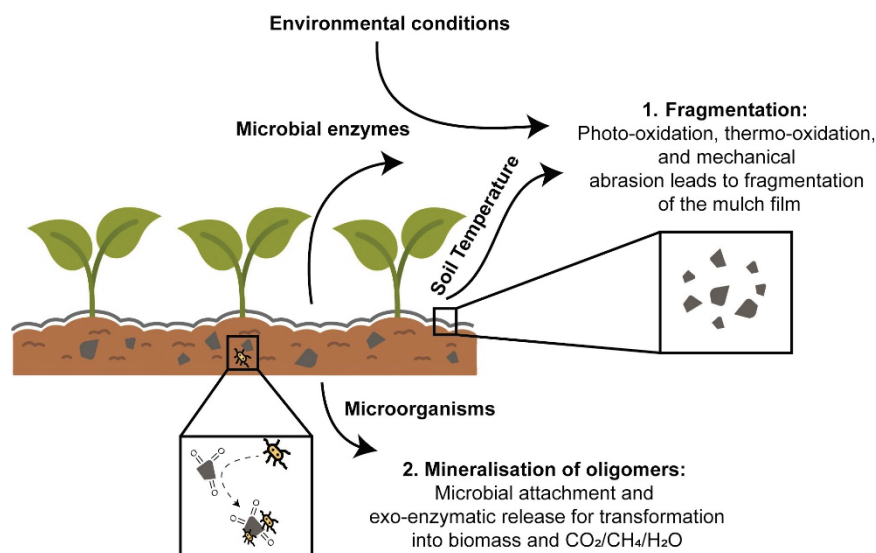


Figure 6. Properties of the ideal mulch film materials.

#### 5. Biodegradable Polymers for Mulch Films

The term biodegradation refers to the breakdown of macromolecules by the action of microorganisms. Molecular level studies have shown that it is a two-step process [78]. In the first step fragmentation occurs in which the high molecular weight polymer chain is broken down into smaller units that may be oligomeric units with polar chain ends or monomers with specific properties. Fragmentation may occur through hydrolysis, which

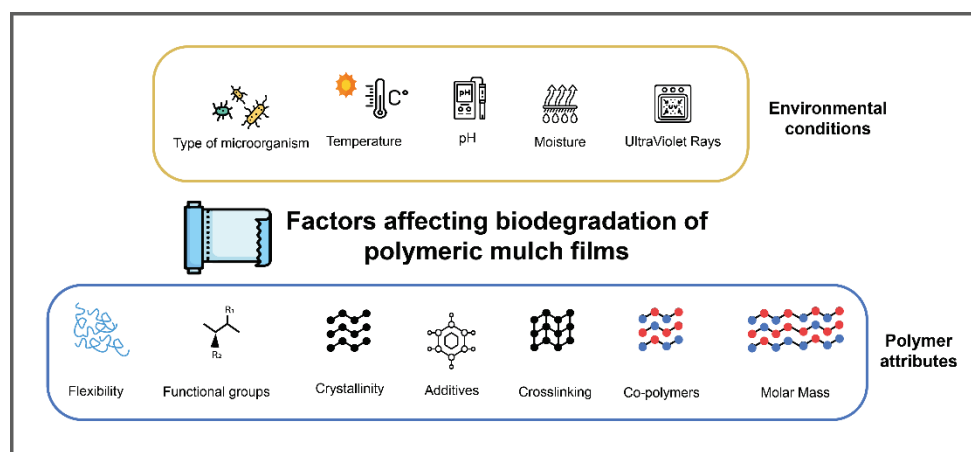
may or may not be enzyme-mediated, oxidation or other chemical reactions depending on the environment as well as the chemical structure of the polymers. In the second step, oligomers and monomers formed in the first step are mineralized by microorganisms to produce carbon dioxide, methane, water, and biomass. The products formed may vary slightly depending upon the microorganisms involved and the aerobic/anaerobic nature of the process [79]. The schematic diagram of the process of degradation is shown in Figure 7.



**Figure 7.** The two steps of biodegradation of mulch films.

Polymers may constitute aliphatic chains or aromatic groups. Generally aliphatic polymers are easily hydrolysable while aromatic polymers require harsh conditions for breakdown, such as extremely acidic environments at high temperatures. Most biodegradable polymers are therefore aliphatic, but some aliphatic-aromatic polymers that have a limited number of aromatic units may also be included in this category [80].

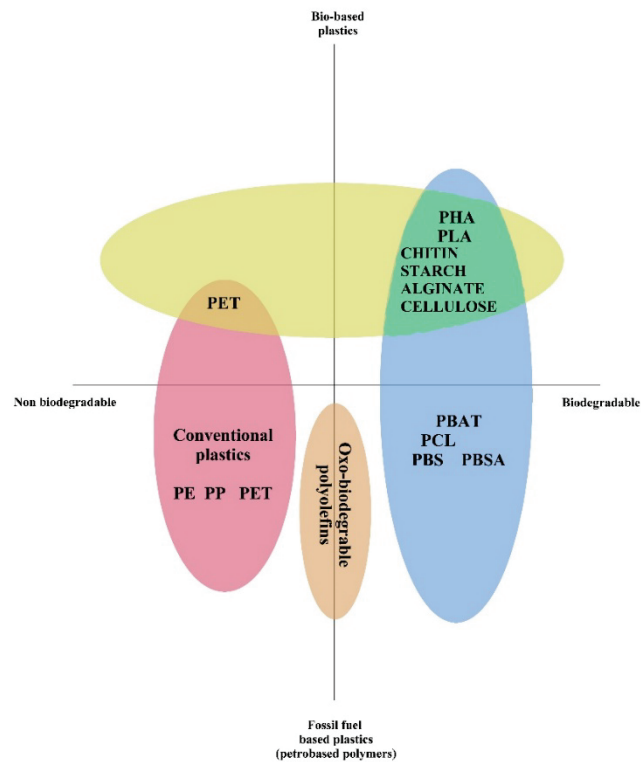
Many factors affect the biodegradation of a polymer, including environmental conditions and the characteristics of the polymer, as shown in Figure 8. Environmental conditions may further be categorized as abiotic or biotic factors [50]. Abiotic factors include temperature, moisture, pH, and the presence of UV radiation. It has been reported in numerous studies that the temperature of the soil has a significant effect on the initiation of the biodegradation process, and lower temperatures decrease the rate at which the polymer is broken down [81]. Soil moisture is important and may become a limiting factor when fragmentation proceeds through hydrolysis. It is less likely to slow down degradation during irrigation periods, but has a marked effect if the moisture content drops too low or increases to the extent of making the soil anoxic [74,82]. Soil pH has a marked effect on the metabolism of microorganisms which, in turn, has an impact on their ability to degrade mulch films. It has been observed that generally soils with a neutral pH show maximum biodegradation, although depending on the type of microorganisms present there may be exceptions [83]. Ultraviolet radiation has a direct impact on the breakdown of mulch films. Experiments have shown that UV radiation speeds up biodegradation two-fold [84]. Biotic factors that affect biodegradation include the type of microorganisms present, the enzymes produced by them, and their ability to colonize the surface of the mulch films to initiate biodegradation. Climate and soil characteristics define the type of microbial communities present indigenously. Whilst it is mostly bacteria that are involved in biodegradation, the presence of fungi may accelerate the process in some cases [85].



**Figure 8.** The factors that affect biodegradation of mulch films.

It is interesting to note that the biodegradability of a polymer is not linked to its source but is dependent on its physiochemical properties such as molar mass, cross-linking, functional groups, crystallinity, flexibility and the presence of co-polymers, additives or cross-linkers [86]. As a general rule, an increase in the molar mass leads to a decrease in degradation. This is also linked to the solubility of the polymer, since high molecular weight compounds have low solubility which makes them unfavourable for microbial attack [87]. Similarly, highly cross-linked polymers have slower degradation since the close mesh-like structure makes the polymer inaccessible to both microbes and water molecules. The polymer needs to be mechanically broken down into smaller pieces before biodegradation can occur [88]. The type of bonds and functional groups present in the polymer are directly linked to its degradation. The presence of hydrophobic and non-polar functional groups makes a polymer less prone to biodegradation [89]. The breakdown of a mulch film is dependent on the type of polymer present. The biodegradation mechanism becomes more complex if the film is made of more than one type of polymer. These co-polymer mulches or blends may be degraded at a slower or at times greater rate than single polymer mulches. For instance, it has been observed that PBAT blends degrade more slowly compared to PBAT mulches, whilst PLA blends show better degradation than mulches made of PLA alone [90,91]. Sometimes additives are included in polymer blends to increase the solubility or flexibility of the product. The presence of additives, specifically in co-polymers, may contribute to a reduction in its biodegradation. Depending on the type of additive, it may form cross-links with the polymer upon exposure to solar radiation. This cross-linking reduces accessibility to microbial enzymes and water, which leads to a decline in the degradation rate [92]. The degree of crystallinity of a polymer is one of the main factors that affect the biodegradation phenomenon. The more crystalline a polymer is, the denser the packing of molecules, which slows down the rate at which it can be broken down [93]. Although flexibility of a polymer seems more linked to its mechanical properties, it is surprising that it also has an impact on the rate of biodegradation. It has been observed that polymers with increased flexibility show enhanced biodegradation [94].

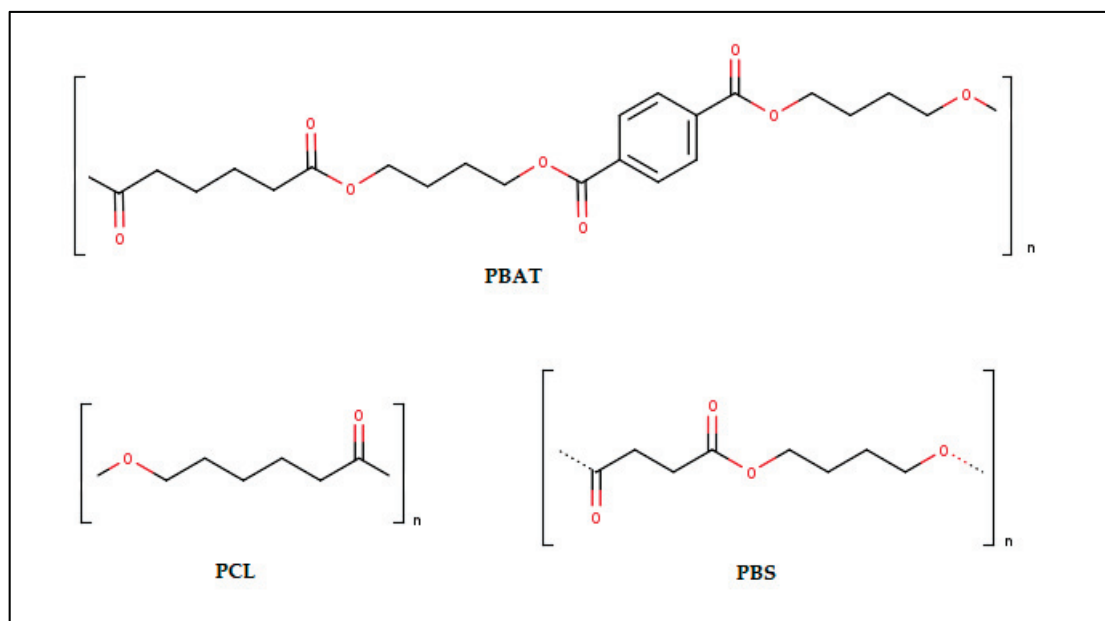
Biodegradable polymers may be derived from fossil fuels or renewable resources, or even a blend of both (Figure 9). They usually contain ester, amide and ether functional groups. Considering the already limited fossil fuel supplies, renewable resource-based materials or bio-based polymers are preferred over conventional petroleum based products due to easy availability and superior degradability [95].



**Figure 9.** A comparison of the diversity of plastics and bio-based polymers. Abbreviations include: PBAT—Polybutyrate Adipate Terephthalate, PCL—Polycaprolactone, PE—Polyethylene, PET—Polyethylene Terephthalate, PP—Polypropylene, PHA—Polyhydroxyalkanoate, PLA—Poly(Lactic Acid), PBS—Poly(Butylene Succinate), PBSA—Poly(Butylene Succinate Adipate). Adapted and modified from [96].

5.1. Fossil Fuel Based Biodegradable Polymers Used for Mulching

Biodegradable material made from synthetic polymers or derived from fossil fuels that have been used as mulch films includes polyurethanes such as polybutylene adipate terephthalate or PBAT, poly  $\epsilon$ -caprolactone or PCL, and polybutylene succinate PBS [97]. The chemical structures of fossil fuel based biodegradable polymers is shown in Figure 10.



**Figure 10.** The chemical structures of fossil fuel based biodegradable polymers [98–100].

### 5.1.1. Polybutylene Adipate Terephthalate

Polybutylene adipate terephthalate (PBAT) is a derivative of common petrochemicals and is considered to be fossil fuel based. It is a co-polymer of 1,4-butanediol, adipic acid and terephthalic acid. Therefore, it is an example of an aromatic–aliphatic polymer, with properties that are partially attributed to the aromatic group and partially to the aliphatic chain. It has a higher elongation break than most other polymers and is flexible [101]. PBAT also has good stretchability, impact resistance, extensibility and heat resistance, properties that are desirable for a material to be used as mulch film. The butylene adipate group imparts good soil biodegradability, making it a potential alternative to plastic mulches [102]. However, it is both expensive and highly sensitive to UV radiation. In field applications, PBAT undergoes severe crosslinking, which makes it brittle and reduces its efficacy, so it is generally recommended for short season crops only [103]. To overcome these limitations, blends of PBAT have been formulated with PLA, PPC, and/or starch. These co-polymers have exhibited increased durability and less brittleness. Additionally, they have a considerably lower cost of manufacturing since the blend is less expensive than the pure PBAT film. Now, many countries are producing PBAT-based mulch films commercially and their use is reported to have beneficial effects [104]. Blends of PBAT also have the property of functioning as controlled release systems via mulch films when fertilizers, fungicides, or herbicides are embedded into these films. The slow release of these compounds increases their efficiency and enhances crop production [2,24].

The degradability of these films may not be same in all types of soil. Studies have shown that the type of microorganisms present in the soil and the composition of soil structure influenced the extent of biodegradability of PBAT-based mulch films in field experiments [105], while more than 90% degradation of these blends under aerobic soil, within two years of application, has been documented. However, the persistence of fragments not converted to carbon dioxide or organic carbon within this time is not accounted for. There is a possibility that these micro-fragments and other chemical constituents will accumulate over time after repeated applications in the same field [106]. The degradation of PBAT under soil conditions results in the production of adipic acid and terephthalic acid, both of which are categorized as slight to moderate environmental toxins [107,108]. The presence of these compounds in the form of micro plastics has been detected in soils where PBAT-based mulch films were applied. Additionally, it was noticed that the presence of these micro plastics reduced the electrical conductivity and nitrate content in soil, which decreased the availability of water-soluble nutrients [109]. Studies have been carried out to compare the effect of mulch residues left in the soil. The results of these studies show that compared to LDPE plastic, PBAT mulch residues have a negative and harmful impact on soil bacterial community and plant growth. Further work and research need to be undertaken to ensure that PBAT-based mulch films are not hazardous to the environment, as well as the plants and microbial community of soil [110]. Since it is a petroleum-based polymer, long term use and availability of PBAT remains questionable [111].

### 5.1.2. Poly $\epsilon$ -Caprolactone

Poly  $\epsilon$ -caprolactone (PCL) is an aliphatic, synthetic, and thermoplastic polyester derived from petrochemical feedstocks. It is produced by ring-opening polymerization of  $\epsilon$ -caprolactone, which is obtained from crude oil. It has ester linkages and can be easily broken down by microorganisms that produce the enzymes lipase or esterase [112]. The chemical structure of PCL imparts it flexibility, low melting temperature and variable viscosity. It can be moulded easily, making it a potential candidate for mulching material [113]. However, PCL mulches have poor impact, weak tear strength behaviour and there are reports on film extrusion for these mulches. It is biodegradable, but the degradation rate is slow. Therefore, it is often mixed with starch to form blends with enhanced biodegradability. The application of these blends in the field has exhibited promising results. It has been observed that these films show better degradation compared to polyethylene mulches and have a positive impact on root growth and density, which is an important indicator of plant



growth [114]. Trials have also demonstrated that PCL-starch based mulch films can be degraded in most soil types and are effective in conserving soil moisture under various environmental conditions [74]. Many PCL-starch based blends are commercially available and being used as mulch films in many countries as an alternative to plastic mulches [99].

However, results of the field trials have indicated that these mulch films degrade in a shorter time if certain fungi and actinomycetes are present in the soil. In some conditions, these films degrade within a short span of 60 days, reducing their practical value and importance in agricultural practices [115]. With this in mind, this problem and the fact that the source of this polymer is non-renewable, concerns have been raised over its sustainability. Therefore, better alternatives are being searched for use in the agricultural sector [116].

### 5.1.3. Poly Butylene Succinate

Poly Butylene Succinate (PBS) is a thermoplastic polyester which has physico-chemical properties such as conventional non-biodegradable plastic. It is made up of 1,4-butanediol and succinic acid [117]. PBS is a synthetic, petroleum-based polymer with good thermal stability and desirable mechanical properties. Its melting point is higher than other synthetic polymers but lower compared to natural polymers, so it can be melted in a shorter time and blended with other materials to develop films [118].

PBS is synthesized through various processes including co-polycondensation and reactive and physical blending, all of which impart different physical characteristics to the product formed. The higher the degree of crystallinity in the polymer, the lower its potential to be degraded by enzymes or microorganisms [119]. To overcome this problem, amorphous domains are added to the polymer by making blends with other materials. These blends have adequate strength and are available commercially as mulch films [120]. Interestingly, these PBS-based mulch films function as controlled release systems and have shown efficacy when embedded with different beneficial chemical compounds such as fertilizers or herbicides [121].

PBS and its blends are broken down by microorganisms that produce esterases. It has been found that the degradation rate of a PBS-based mulch film is influenced by the presence of certain fungi in the soil, as well as the availability of nitrogen and carbon sources to these microorganisms [122]. This may be linked to the fact that microorganisms do not produce esterases under conditions of nitrogen limitation. Similarly, the availability of carbon source plays a role in the regulation of esterase production. Therefore, soil characteristics and the type of indigenous microorganisms present are decisive factors in biodegradation of PBS-based mulch films [86]. It is important to understand that while the formulation of blends seems to be the most plausible solution to altering the properties of the polymer, PBS-based blends are often immiscible, resulting in phase separation which leads to poor mechanical properties. An alternative approach is the use of cross linkers or compatibilizer compounds in the blend, which enhance the phase mixing properties. However, the addition of these compounds compromises the biodegradability of the end-product [123]. It has been found that, compared to laboratory conditions, the biodegradation of PBS and its blends under field conditions takes longer. Low degradation of PBS-based mulches, with less than 3% degradation in more than 100 days, has been reported [124,125]. The price of PBS compared to petrochemical-based plastics is higher due to the cost of production. The large-scale production and application of PBS blends as mulch films is limited because of slow degradation, high cost and the fact that the polymer is derived from fossil fuels which are non-renewable [126].

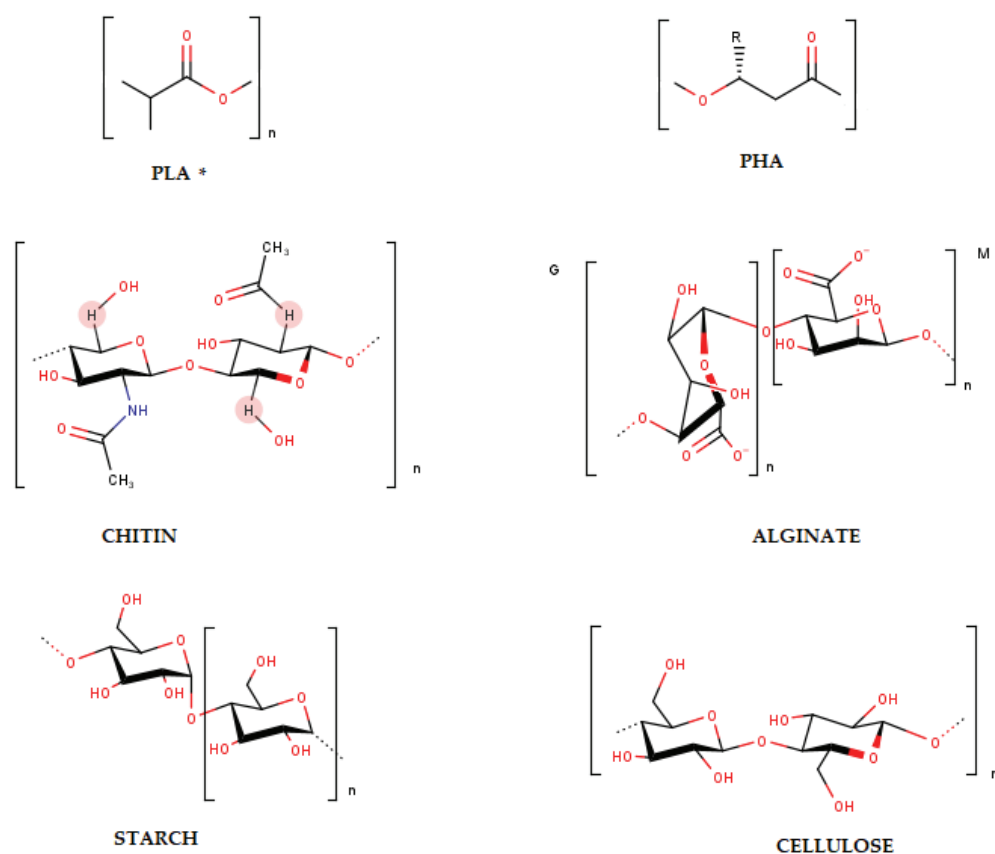
### 5.2. Bio-Based Polymers Used for Mulching

Bio-based polymers are defined as materials formed naturally by living organisms over many growth cycles. These include lipids, proteins, and carbohydrates. Lipids are hydrocarbons, chemically, and may exist as esters, acid polyesters or free acids. They include hydrogenated fats, oils, fatty acids, and waxes [127]. Although lipids can undergo

biodegradation, they are hydrophobic in nature and cannot be used as mulch films. The preparation and handling of films made of pure lipids is also very difficult, limiting their uses [128].

Proteins may be produced by microbial cells or extracted from plants and animals. These can be easily degraded in the environment by indigenous bacteria and fungi. Films made from soy protein, zein protein, wheat gluten, collagen and gelatine have been tried for mulching applications but have not been successful. The main problem associated with the use of protein-based mulches is their high-water sensitivity, which reduces the efficiency of these films [14].

The most abundant among these polymers are carbohydrates; mainly polysaccharides. These may be produced by the bacteria or exist naturally in plants and animals. Naturally occurring polysaccharides include chitin, alginate, starch, and cellulose (Figure 11). Chemically, all of these are made up of monosaccharides that are linked together by glycosidic bonds, but the presence of various functional groups and charges impart versatility [99]. The key advantages associated with the use of these materials for mulching are enhanced biodegradability, non-toxicity, availability and low cost [127]. Bacteria can utilize carbohydrates to synthesize polymers. Two such polymers are polylactic acid and polyhydroxyalkanoates, which are chemically polyesters that are synthesized from a carbohydrate base [129]. The chemical structures of PLA and PHAs are shown in Figure 11.



**Figure 11.** The chemical structures of bio-based biodegradable polymers (PLA\* is a synthetically produced bio-based polymer, whilst PHA, Chitin, Alginate, Starch and Cellulose are naturally produced bio-based polymers) [98–100].

### 5.2.1. Polylactic Acid

Poly(lactic acid) (PLA) was discovered in the 1930s and is produced by lactic acid forming microorganisms. It can be manufactured using renewable resources as the substrate for the microorganisms, such as corn, sugar beet starch and other agricultural products [129]. As suggested by the name, PLA is made from monomers of lactide which are synthesized

from lactic acid. Commercially available PLA is usually a co-polymer of poly L-lactic acid and poly D-lactic acid. The monomers are produced by bacteria but the polymer is made through a synthetic process usually involving ring opening polymerization and poly-condensation. The ratio of these two polymers influences the physical properties of PLA, including its melting temperature and crystallinity, as well as molecular weight [130]. Although the large-scale production of PLA is relatively inexpensive, the total cost of the polymer is high when compared to commercially available plastics [131]. PLA has good thermoplasticity, biocompatibility and processability which allows for a wide range of applications. However, as a mulch film, brittleness is its only drawback which reduces its efficiency [132].

To counter the problems of high cost and brittleness, blends of PLA are made with other polymers. A common blend is to mix PLA with starch, which has been shown to enhance the mechanical properties of PLA. Formulation of PLA-starch blend also reduces the cost of the mulch films, making it more economical for use [133]. Studies have shown that PLA blends as mulch films are effective, biodegradable and have good mechanical properties as well as higher water holding capacity [132,134]. Additionally, PLA-based mulch films can act as controlled release systems which allow for the release of chemical compounds embedded in the film over time, to enhance plant growth while preventing leaching of these compounds. Several studies have shown their efficacy as controlled release systems when PLA-based mulch films are embedded with herbicides [2,135,136].

However, the formation of these blends is challenging and difficult. The non-compatibility of composites is an area that is still under research. It has been found that formation of unstable bubbles in the film may occur after blending, leading to wrinkles and tears in the sheet. Similarly, electrostatic attraction may result in adhesion between these films, reducing the efficacy in agricultural applications [99,137]. To overcome this problem, plasticizers are added to the blends. Plasticizers are compounds used as additives, which are added to polymers to make them softer and more pliable. However, the addition of some plasticizers to these blends is not permitted due to the stringent requirements of manufacturing materials allowed for used in agriculture. These plasticizers are not biodegradable and are released into the environment once the mulch is applied and degraded [138]. Another problem related to the use of PLA based mulch films is the commercial production of PLA using genetically modified organisms. In many European countries, as well as the USA, there are strict restrictions on the use of GMOs for manufacturing agricultural products. For example, the National Organic Program rule in the USA states that any synthetic biodegradable mulch must be produced without involvement of any GMOs, restricting the use of such products on a large-scale [139].

### 5.2.2. Polyhydroxy Alkanoates

Polyhydroxy alkanoates (PHA) are a class of aliphatic polyesters that are produced by many bacterial species as distinct granules. Discovered in 1925, the polyesters are synthesized intracellularly and used as storage polymers for carbon sources in many prokaryotes [140]. PHA granules differ in their content and chain arrangement depending on the microorganism used for production. PHAs are polyesters of hydroxyalkanoates where the number of monomeric units may vary from as little as 600 to as many as 35,000. The presence of different functional groups on the monomeric units is used as a classification system for types of PHAs [141]. The carbon source utilized for production, constituents of the media, fermentation process and conditions, as well as the downstream processes used for purification are other factors that have an effect on the structure and composition of the polymer [142–144]. More than 150 different PHAs are known to date, based on the combination of the monomeric units that make up the chain. The most common and well-known PHAs are poly 3-hydroxybutyrate (PHB) and poly 3-hydroxybutyrate-co-3-hydroxyvalerate (PHBV). Both are short chain polymers and available commercially [145].

Generally, the mechanical properties of PHAs do not support their use as mulch films. However, blending different PHAs together or with other polymers improves their

mechanical strength. The main feature of PHAs that imparts an advantage is their ability to function as controlled release systems for agricultural chemicals. Studies have shown that PHB blends are particularly effective as mulch films for the slow and controlled release of pesticides and fungicides [146,147]. Blends of PHB with PLA have desirable mechanical properties such as polyethylene mulch films [91]. Biodegradation of PHB blends has been studied in a wide range of conditions including a controlled laboratory environment as well as natural habitats including different types of soil, river water, activated sludge, and compost. PHB is known to degrade rapidly in both aerobic and anaerobic environments, and thus can be disposed of easily without any negative impact on the environment [148,149].

The desirable characteristics such as structural variability, raw material availability, and biodegradability of PHB polymers make them an ideal candidate for replacing plastic as mulch films. Yet, despite the microbial source and versatility, the large-scale production of PHAs is restricted by the high cost of the manufacturing process [14]. Different production strategies, including the use of waste material as a carbon source, have been employed to decrease the cost of production. While these studies have shown positive results, the extraction of PHAs from bacterial cells still contributes significantly to the higher cost of the process. Extensive chemical extraction methods cause degradation of the polymer during the purification process. Therefore, efficient biological methods for extraction of PHAs are being investigated to decrease the cost of the production and to ensure that the useful properties of the polymer are not lost [150].

### 5.2.3. Chitin

Chitin is found naturally in the cell walls of fungi and yeast, and in the exoskeleton of arthropods. The most abundant crystalline form of the polymer is  $\alpha$ -chitin, which may be obtained from seafood waste in large quantities [151]. It is made up of D-glucosamine and N-acetyl-D-glucosamine residues which are linked together. The deacetylation of chitin forms chitosan. Chitosan readily dissolves in dilute acids but remains insoluble in water. It can also be moulded to form films. These two features make it a good choice for use as a material from which to make mulch films [152]. Chitosan is the second largest and abundant biological polysaccharide found in nature. However, films of pure chitosan may be brittle due to low fluidity of the linear chain. Plasticizers such as glycerol may be added to chitosan to enhance its flexibility and improve fluidity [153].

When used for mulching, chitosan has exhibited the potential to control weed growth much better compared to some herbicides [154]. It can also function effectively as a controlled release system and chitosan mulch films may be loaded with fungicides to protect plants against fungal diseases [155]. Chitosan is also considered to promote plant growth by contributing to soil nutrients, and many studies have shown that it enhances the growth rate, number of flowers and quality of vegetables when used as a mulch for various plant species [156–158]. However, it has been observed that the use of chitosan-based mulch affects soil temperature, increasing it during the day and lowering it at night, which has an adverse impact on plant growth [159]. Moreover, the production of chitosan from chitin is an expensive process. The interference in soil temperature and high cost mean that chitin and chitosan are usually not preferred as a mulching material [14,152].

### 5.2.4. Alginate

Alginate is an aliphatic, water-soluble polymer found in the cell wall of brown algae. It is chemically made up of  $\beta$ -D-mannuronic acid (monomer M), and  $\alpha$ -L-guluronic acid (Monomer G). The sequential arrangement and proportions of these two monomers in the alginate chain impart its different properties [160]. It can form three-dimensional mesh networks in the presence of cations, where the cation acts as a cross-linker that joins the alginate chains from the G residues. This property has been exploited for the production of gels or films from alginate, mainly with calcium ions, for the controlled release of active agents [161]. Alginate mulches have been produced as a solution of sodium alginate which

is sprayed on the soil, where it forms cross-linking with naturally occurring calcium ions. Once the water has evaporated, a thin layer of the polymer appears on the soil surface that functions as a mulch film [162]. Field trials have shown that these alginate mulches improve plant growth and have a positive impact on the population of soil microorganisms including fungi and actinomycetes. It also lowers soil temperature, making it a good option for use in hot climatic zones [163]. Alginate is known to act as a biostimulant and promotes plant growth, specifically through better root development and fruit quality, and it also improves the plant's ability to tolerate salt stress. Therefore, the use of alginate mulches may contribute in many ways to enhanced plant growth [164–166]. Moreover, alginate is non-toxic and biodegradable, and has good water holding capacity [167].

However, the main problem with the use of alginate-based mulch films is their dependency of synthesis on the presence of calcium ions in the soil, since the films cannot be produced in the absence of these ions. Furthermore, the stiff structure of sodium alginate and the rigidity of the resulting cross-linked film leads to rips and tears in the mulch film, which paves way for the growth of weeds [14]. A method to overcome this problem is the formation of blends including polyglycerol or hydroxyethylcellulose. While these blends have shown potential to be used as mulch films, the cost of production increases considerably, reducing the overall efficacy of the product [168].

#### 5.2.5. Starch

Starch is the main storage polysaccharide found in plants and is made up of the chains of amylose and amylopectin. Amylose is linear and consists of glucose units linked by  $\alpha$ -1, 4 glycosidic linkages, while amylopectin has branches that stem out of the main chain. The main chain is made up of glucose units joined by  $\alpha$ -1, 4 glycosidic linkages while the branch points have  $\alpha$ -1, 6 glycosidic linkages [169]. Starch is found in the form of granules in seeds, roots, and tubers. Depending upon the plant source, starch may consist of amylose, amylopectin and other compounds such as lipids, proteins and phosphate or ester groups in minor quantities. The proportion of amylose and amylopectin influences the properties of starch. High amylose starches produce stiffer gels and stronger films, while high amylopectin starches produce softer gels which are more stable over longer periods of time. The proportion of these components is the main factor that helps to choose the source of starch and its applicability [170]. Commercially, starch is extracted from corn, wheat, rice, sorghum and potato depending on the geographical regions and local availability [171].

Starch is one of the most abundant and cheap polymers that can be used to replace plastic. It can be easily processed without any stringent requirements and can be produced commercially using already installed plastic processing machinery/equipment [172]. Considering these attributes and the fact that it can be used easily to form a film through the process of gelatinization, it is a good choice for use as a mulching material [173]. However, it has poor water resistance or high hydrophilicity which leads to enhanced degradation. In fact, it has been observed that more than 33% of the starch mulch film degrades within 55 days of application as a mulching material [64]. Starch films also have low elastic strength and are brittle, which means that they often tear apart while being spread on the field [68]. One way to overcome these problems is to modify or blend starch with other materials such as glycol, chitosan, and PLA. Films synthesized in this manner have exhibited better elastic strength but are expensive to produce and are often sensitive to high humidity. Moreover, the mechanical properties of these films are still not comparable to plastic mulch films, limiting their potential use in agriculture [174,175].

#### 5.2.6. Cellulose

Cellulose is the main structural component of plant cell walls and is the most abundant polysaccharide in nature. It is a linear homopolymer made up of D-glucose units joined through  $\beta$ -1, 4 glycosidic bonds [176]. Cellulose is found in plants and can also be produced by a number of microorganisms including common soil-borne bacteria. Naturally occurring cellulose is found in two crystalline or allomorphic forms, I $\alpha$  and I $\beta$ , depending upon the



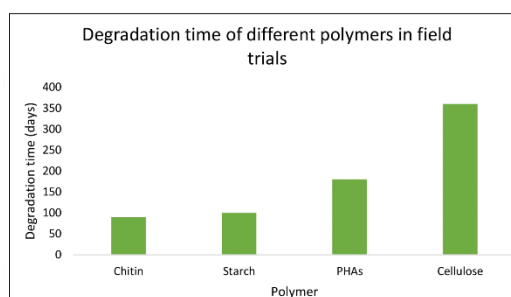
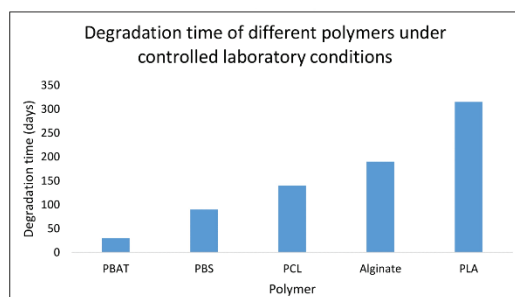
network of hydrogen bonds formed between the hydroxyl groups of cellulose chains.  $I\alpha$  is predominantly found in plants, while  $I\beta$  is the form of cellulose produced by bacteria [177]. These allomorphs vary in their solubility because of the hydrogen bonding pattern. Bacterial cellulose is preferred over plant cellulose due to relative abundance and ease of production and extraction [178]. Additionally, bacterial cellulose has good biodegradability, purity, water holding capacity, transparency, flexibility, and greater mechanical strength, making it an ideal material to replace plastic for mulch films [179]. Field trials have demonstrated that mulch films made of bacterial cellulose better retain soil moisture and are effective in providing a suitable microclimate for plant growth. Furthermore, these films can be modified as composite films to release nutrients by the addition of fertilizers [180,181].

The main challenge for the production of cellulose on a commercial scale is the higher cost of this process. Scientists are investigating the use of cheap waste material as a substrate for the bacteria to produce cellulose to decrease the cost of production [182,183]. Other aspects to reduce production costs include developing new strategies for agitated and static culturing and designing new, cost-effective fermentation vessels [184].

A comparison of the advantages and disadvantages of biodegradable polymers and their degradation times is given in Table 2 [103–184] and Figure 12, respectively [185–189].

**Table 2.** Comparison of the advantages and disadvantages of different synthetic and bio-based biodegradable mulch films.

Type of Biodegradable Polymer	Polymer	Advantages	Disadvantages
Synthetic	Polybutylene adipate terephthalate	Good impact resistance and extensibility	Produces microplastics
	Poly $\epsilon$ -caprolactone	Flexible material and effective in retaining soil moisture	Degrades very quickly and has to be replenished frequently
	Poly Butylene Succinate	Good thermal stability	Expensive with limited biodegradability
Bio-based	Polylactic acid	Good processibility and thermoplasticity	Brittle and expensive
	Polyhydroxyalkanoates	Can act as controlled release system	Expensive to produce and lacks mechanical strength
	Chitin	Controls weed growth	Alters soil temperature and expensive to produce
	Alginate	Acts as biostimulant and promotes plant growth	Rips after application
	Starch	Abundant and cheap	Brittle and low tensile strength so tears apart during application
	Cellulose	Flexible with good tensile strength	Expensive to produce on large-scale



(a)

(b)

**Figure 12.** The degradation time estimated for different biodegradable polymers (a) under controlled conditions and (b) in field trials.

## 6. Commercially Available Biodegradable Mulches—Current Trends and Challenges

Despite the challenges and problems related to production of biodegradable mulch films, consistent research efforts over a number of years have resulted in the development of some commercial mulching materials. All these mulch films are polysaccharide-based and are manufactured by blending two or more polymers [99].

The first biodegradable mulch film used in agriculture was Mater-Bi<sup>®</sup>, which was produced by Novamont, an Italian company. The mulch film is made of a blend of poly  $\epsilon$ -caprolactone and thermoplastic starch and possesses reasonable biodegradability and mechanical strength [82]. Its application in the field has demonstrated that the material can be used effectively for mulching purposes [190]. Other commercially available mulch films include Biomax<sup>®</sup> TPS, Biopar<sup>®</sup>, Bionelle, Biosafe<sup>™</sup>, Ingeo<sup>®</sup>, and WeedGuardPlus [65,191,192]. These films are manufactured by various companies in different countries and are being used in farming practices (Table 3).

**Table 3.** Some commercially available mulch films and the crops grown using them.

Commercial Mulch Film	Composition	Manufacturer	Crops Grown Using Mulch Films	Reference
Biomax <sup>®</sup> TPS	TPS + starch	DuPont	Corn	[193]
Bionolle	TPS + PLA + (PBS or PBSA)	Showa Denko Europe	Onion	[194]
Mater-Bi <sup>®</sup>	TPS + PCL	Novamont	Tomato	[195]
Eco-Flex <sup>®</sup>	Starch + PBAT	BASF	Strawberry, Tomato	[196,197]
Ecovio <sup>®</sup>	TPS + PBAT + PLA	BASF	Cucumber	[198]
EcoWorks	TPS + PBAT	Cortec Corporation	Bell Pepper	[199]
Ingeo <sup>®</sup>	Starch + PLA	Nature Works	Tomato	[200]
Naturecycle	Starch + polyester	Custom Bioplastics	Pumpkin	[106]
WeedGuardPlus	Cellulose	Sunshine Paper	Strawberry	[201]

Results obtained from field experiments have indicated that biodegradable mulch films are as effective as polyethylene mulch in controlling weed infestation and promoting plant growth. However, the increasing demand for food and cash crops has led to a continuous rise in the global consumption of plastic mulch film. Although there is a wide range of biodegradable material available on the market, the quantity is still not sufficient to completely replace non-degradable plastic mulch films [202]. The main challenge associated with the large-scale production of biodegradable mulch films is the economic viability of the production process. The profit and economic feasibility analysis of biodegradable mulches indicates that if these are to be used as alternatives to plastic mulches, governments need to provide subsidies to promote their use through extensive marketing [203–205].

## 7. Future Prospects of Biodegradable Mulch Films

Despite extensive research in the development of biodegradable mulch films commercially, the large-scale use of these materials is still limited. The biodegradable mulching material needs to be cost effective and easily accessible to the farmers for complete replacement of polyethylene in the field. Commercially available biodegradable mulch films are not preferred by most farmers because these are expensive, difficult to manage and require specialized equipment for application [206]. This means that although some alternatives to plastic mulches are available, they are not being used. Governments need to play a part in subsidising these mulch films and raising awareness about their benefits over plastic mulch films. For example, some regional authorities in Spain are giving incentives to farmers who use biodegradable mulch films to promote their use [204]. Such policies need to be adopted globally to encourage the use of biodegradable materials.

There is a need to develop polymers suitable for mulching in different climatic zones, with a wide range of temperatures and soil types, so that these can be utilized for the production of different crops [207]. It is currently a challenge to develop a material that fits the criteria of mulching products with good physical characteristics, durability, and

biodegradability. In this context, while there are standard testing methods for determination of mechanical strength, biodegradation analysis is still raising questions on many platforms. The biodegradability testing methods have several shortcomings, since these are mostly carried out in laboratory conditions and rely on indirect testing methods without taking soil characteristics into account. It is important to understand that the biodegradation process in the field is affected by many factors and the polymer may not exhibit the same rate of breakdown in lab and field conditions [208]. Even if the polymer degrades in soil, the long-term effects of any residual matter left after biodegradation of these polymers is yet to be investigated. Therefore, there is a dire need to develop testing methods that can estimate the biodegradation of the polymer in field conditions and allow for a close-to-reality simulation of the possible residual effects [139].

Among all polymers that may be used, cellulose offers potential for further research since the only problem associated with it is the cost of production. New processing methodologies such as 3D printing and electrospinning are also being considered for production of mulch material and can be used for lowering the cost of cellulose [209]. However, work in this area is still limited to laboratory trials, and field application still needs to be carried out to commercialize these products for further use [86].

## 8. Conclusions

This review provides a detailed account of the history of mulching, the concerns about the use of plastic mulch films and their impact on the environment. It also discusses the alternative biodegradable polymers with the potential to be used for mulching, including those produced naturally by microorganisms, animals and plants as well as some derived from fossil fuels, alongside their advantages and limitations. Most of the biodegradable polymers have characteristics that are a compromise in terms of parameters that need to be met for agricultural use in terms of maintaining the optimum microclimate for plant growth for the whole growth cycle and sufficient high tensile strength. For example, materials that exhibit good biodegradation often lack mechanical strength, and vice versa. The formation of blends or use of co-polymers appears to be a promising solution but presents a limitation of increasing the cost of production significantly. The future outlook for the development of biodegradable mulch films is nonetheless favourable. The cost of production can be reduced by adopting waste valorisation strategies wherever possible, and advanced scientific techniques can be used to improve the quality of the polymer produced so that it can meet the required standards. The discussion reflects the potential for research and development in the design of biodegradable mulch films. Further research in all domains of production, design, characterization, biodegradation analysis and commercialization needs to be carried out to encourage the use of biodegradable polymers for mulching to promote sustainable practices.

**Author Contributions:** This review article was written by Z.M., H.K. and I.R. were the main people involved in the planning of this review. M.K., G.A., M.P., G.M., F.T.-M. worked on the interpretation of the data. All authors were involved in the final editing of this article. All authors have read and agreed to the published version of the manuscript.

**Funding:** This research was funded by the University of Wolverhampton Research Investment Fund (RIF4) and the Commonwealth Scholarship Commission (CSC) UK (reference PKCS-2021-645).

**Institutional Review Board Statement:** Not applicable.

**Data Availability Statement:** Not applicable.

**Acknowledgments:** Many thanks to the University of Wolverhampton, School of Sciences for their financial support and the library at the University of Wolverhampton for provision of necessary sources. We gratefully acknowledge support through Commonwealth Scholarship PKCS-2021-645.

**Conflicts of Interest:** The authors declare no conflict of interest.

## References

- Chalker-Scott, L. Impact of mulches on landscape plants and the environment—A review. *J. Environ. Hortic.* **2007**, *25*, 239–249. [CrossRef]
- Khan, H.; Kaur, S.; Baldwin, T.C.; Radecka, I.; Jiang, G.; Bretz, I.; Duale, K.; Adamus, G.; Kowalczyk, M. Effective control against broadleaf weed species provided by biodegradable PBAT/PLA mulch film embedded with the herbicide 2-methyl-4-chlorophenoxyacetic acid (MCPA). *ACS Sustain. Chem. Eng.* **2020**, *8*, 5360–5370. [CrossRef] [PubMed]
- Lightfoot, D.R. Morphology and ecology of lithic-mulch agriculture. *Geogr. Rev.* **1994**, *84*, 172–185. [CrossRef]
- Ray, M.; Biswasi, S. Impact of mulching on crop production: A review. *Trends Biosci.* **2016**, *9*, 757–767.
- Steinmetz, Z.; Wollmann, C.; Schaefer, M.; Buchmann, C.; David, J.; Tröger, J.; Muñoz, K.; Frör, O.; Schaumann, G.E. Plastic mulching in agriculture. Trading short-term agronomic benefits for long-term soil degradation? *Sci. Total Environ.* **2016**, *550*, 690–705. [CrossRef] [PubMed]
- Moshood, T.D.; Nawadir, G.; Mahmud, F.; Mohamad, F.; Ahmad, M.H.; AbdulGhani, A. Sustainability of biodegradable plastics: New problem or solution to solve the global plastic pollution? *CRGSC* **2022**, *5*, 100273. [CrossRef]
- Leisner, C.P. Climate change impacts on food security-focus on perennial cropping systems and nutritional value. *Plant Sci.* **2020**, *293*, 1104112–1104120. [CrossRef] [PubMed]
- Campi, M.; Dueñas, M.; Fagiolo, G. Specialization in food production affects global food security and food systems sustainability. *World Dev.* **2021**, *141*, 105411. [CrossRef]
- United Nations Organization. Available online: <https://sdgs.un.org/goals> (accessed on 7 September 2022).
- Bizikova, L.; Jungcurt, S.; McDougal, K.; Tyler, S. How can agricultural interventions enhance contribution to food security and SDG 2.1. *Glob. Food Secur.* **2020**, *26*, 100450. [CrossRef]
- Li, K.; Jia, W.; Xu, L.; Zhang, M.; Huang, Y. The plastisphere of biodegradable and conventional microplastics from residues exhibit distinct microbial structure, network and function in plastic-mulching farmland. *J. Hazard. Mater.* **2023**, *442*, 130011. [CrossRef]
- Changrong, Y.; Wenqing, H.; Neil, C. Plastic-film mulch in Chinese agriculture: Importance and problems. *World Agric.* **2014**, *4*, 32–36.
- Dong, H.; Yang, G.; Zhang, Y.; Yang, Y.; Wang, D.; Zhou, C. Recycling, disposal, or biodegradable-alternative of polyethylene plastic film for agricultural mulching? A life cycle analysis of their environmental impacts. *J. Clean. Prod.* **2022**, *380*, 134950. [CrossRef]
- Yang, Y.; Li, P.; Jiao, J.; Yang, Z.; Lv, M.; Li, Y.; Zhou, C.; Wang, C.; He, Z.; Liu, Y.; et al. Renewable sourced biodegradable mulches and their environment impact. *Sci. Hortic.* **2020**, *268*, 109375. [CrossRef]
- Anunciado, M.B.; Hayes, D.G.; Astner, A.F.; Wadsworth, L.C.; Cowan-Banker, C.D.; Gonzalez, J.E.; DeBruyn, J.M. Effect of environmental weathering on biodegradation of biodegradable plastic mulch films under ambient soil and composting conditions. *J. Polym. Environ.* **2021**, *29*, 2916–2931. [CrossRef]
- Maitra, S.; Shankar, T.; Sairam, M.; Pine, S. Evaluation of gerbera (*Gerbera jamesonii* L.) cultivars for growth, yield and flower quality under protected cultivation. *Indian J. Nat. Sci.* **2020**, *10*, 20271–20276.
- Kader, M.A.; Singha, A.; Begum, M.A.; Jewel, A.; Khan, F.H.; Khan, N.I. Mulching as water-saving technique in dryland agriculture. *Bull. Natl. Res. Cent.* **2019**, *43*, 1–6. [CrossRef]
- Ahmad, S.; Raza, M.A.S.; Saleem, M.F.; Zaheer, M.S.; Iqbal, R.; Haider, I.; Aslam, M.U.; Ali, M.; Khan, I.H. Significance of partial root zone drying and mulches for water saving and weed suppression in wheat. *J. Anim. Plant Sci.* **2020**, *30*, 154–162. [CrossRef]
- Gan, J.; Zhu, Y.; Wilen, C.; Pittenger, D.; Crowley, D. Effect of planting covers on herbicide persistence in landscape soils. *Environ. Sci. Technol.* **2003**, *37*, 2775–2779. [CrossRef]
- Iqbal, R.; Raza, M.A.S.; Valipour, M.; Saleem, M.F.; Zaheer, M.S.; Ahmad, S.; Toleikiene, M.; Haider, I.; Aslam, M.U.; Nazar, M.A. Potential agricultural and environmental benefits of mulches—A review. *Bull. Natl. Res. Cent.* **2020**, *44*, 1–16. [CrossRef]
- Lalitha, M.; Thilagam, V.K.; Balakrishnan, N.; Mansour, M. Effect of plastic mulch on soil properties and crop growth—A review. *Agric. Rev.* **2010**, *31*, 145–149.
- Long, C.E.; Thorne, B.L.; Breisch, N.L.; Douglass, L.W. Effect of organic and inorganic landscape mulches on subterranean termite (*Isoptera: Rhinotermitidae*) foraging activity. *Environ. Entomol.* **2001**, *30*, 832–836. [CrossRef]
- Szwedo, J.; Maszczyk, M. Effects of straw-mulching of tree rows on some soil characteristics, mineral nutrient uptake and cropping of sour cherry trees. *J. Fruit Ornament. Plant Res.* **2000**, *8*, 147–153.
- Bhaskar, V.; Westbrook, A.S.; Bellinder, R.R.; DiTommaso, A. Integrated management of living mulches for weed control: A review. *Weed Technol.* **2021**, *35*, 856–868. [CrossRef]
- Abhijith, L.; Varghese, E.M. Removal of zinc and copper from contaminated soil by using adsorbents and mulches. In Proceedings of the International Conference on Energy and Environment, Jyothi Engineering College, Kerala, India, 10–11 April 2021.
- Sun, Y.; Mi, W.; Su, L.; Shan, Y.; Wu, L. Controlled-release fertilizer enhances rice grain yield and N recovery efficiency in continuous non-flooding plastic film mulching cultivation system. *Field Crops Res.* **2019**, *231*, 122–129. [CrossRef]
- Li, N.; Sun, C.; Jiang, J.; Wang, A.; Wang, C.; Shen, Y.; Huang, B.; An, C.; Cui, B.; Zhao, X.; et al. Advances in controlled-release pesticide formulations with improved efficacy and targetability. *J. Agric. Food Chem.* **2021**, *69*, 12579–12597. [CrossRef] [PubMed]
- Wang, K.; Sun, X.; Long, B.; Li, F.; Yang, C.; Chen, J.; Ma, C.; Xie, D.; Wei, Y. Green Production of Biodegradable Mulch Films for Effective Weed Control. *ACS Omega* **2021**, *6*, 32327–32333. [CrossRef] [PubMed]



29. Ranjan, P.; Patle, G.T.; Prem, M.; Solanke, K.R. Organic mulching—a water saving technique to increase the production of fruits and vegetables. *Curr. Agric. Res. J.* **2017**, *5*, 371–380. [CrossRef]
30. El-Beltagi, H.S.; Basit, A.; Mohamed, H.I.; Ali, I.; Ullah, S.; Kamel, E.A.; Shalaby, T.A.; Ramadan, K.M.; Alkhateeb, A.A.; Ghazzawy, H.S. Mulching as a Sustainable Water and Soil Saving Practice in Agriculture: A Review. *Agronomy* **2022**, *12*, 1881. [CrossRef]
31. Rathore, A.L.; Pal, A.R.; Sahu, K.K. Tillage and mulching effects on water use, root growth and yield of rainfed mustard and chickpea grown after lowland rice. *J. Sci. Food Agric.* **1998**, *78*, 149–161. [CrossRef]
32. Finkenstadt, V.L.; Tisserat, B. Poly (lactic acid) and Osage Orange wood fiber composites for agricultural mulch films. *Ind. Crops Prod.* **2010**, *31*, 316–320. [CrossRef]
33. Caspersen, S.; Svensson, B.; Håkansson, T.; Winter, C.; Khalil, S.; Asp, H. Blueberry—Soil interactions from an organic perspective. *Sci. Hortic.* **2016**, *208*, 78–91. [CrossRef]
34. Larco, H.; Strik, B.; Sullivan, D.M.; Bryla, D. Mulch effects on highbush blueberry under organic management. In Proceedings of the I International Symposium on Organic Matter Management and Compost Use in Horticulture, Adelaide, Australia, 4–7 April 2011.
35. Hunter, C.M.; Williamson, D.H.; Pearson, M.; Saikawa, E.; Gribble, M.O.; Kegler, M. Safe community gardening practices: Focus groups with garden leaders in Atlanta, Georgia. *Local Environ.* **2020**, *25*, 18–35. [CrossRef]
36. Pinamonti, F. Compost mulch effects on soil fertility, nutritional status and performance of grapevine. *Nutr. Cycl. Agroecosyst.* **1998**, *51*, 239–248. [CrossRef]
37. Zhao, H.; Liu, J.; Chen, X.; Wang, Z. Straw mulch as an alternative to plastic film mulch: Positive evidence from dryland wheat production on the Loess Plateau. *Sci. Total Environ.* **2019**, *676*, 782–791. [CrossRef]
38. Li, S.X.; Wang, Z.H.; Li, S.Q.; Gao, Y.J.; Tian, X.H. Effect of plastic sheet mulch, wheat straw mulch, and maize growth on water loss by evaporation in dryland areas of China. *Agric. Water Manag.* **2013**, *116*, 39–49. [CrossRef]
39. Tiwari, K.N.; Singh, A.; Mal, P.K. Effect of drip irrigation on yield of cabbage (*Brassica oleracea* L. var. *capitata*) under mulch and non-mulch conditions. *Agric. Water Manag.* **2003**, *58*, 19–28. [CrossRef]
40. Cirujeda, A.; Aibar, J.; Anzalone, Á.; Martín-Closas, L.; Meco, R.; Moreno, M.M.; Pardo, A.; Pelacho, A.M.; Rojo, F.; Royo-Esnal, A.; et al. Biodegradable mulch instead of polyethylene for weed control of processing tomato production. *Agron. Sustain. Dev.* **2012**, *32*, 889–897. [CrossRef]
41. Jourgholami, M.; Abari, M.E. Effectiveness of sawdust and straw mulching on postharvest runoff and soil erosion of a skid trail in a mixed forest. *Ecol. Eng.* **2017**, *109*, 15–24. [CrossRef]
42. Yimer, O. Different mulch material on growth, performance and yield of garlic: A review. *Int. J. Food Sci. Agric.* **2020**, *4*, 38–42. [CrossRef]
43. Wright, P.J.; Burge, G.K. Irrigation, sawdust mulch, and Enhance<sup>®</sup> biocide affects soft rot incidence, and flower and tuber production of calla. *N. Z. J. Crop Hortic. Sci.* **2000**, *28*, 225–231. [CrossRef]
44. Downer, J.; Hodel, D. The effects of mulching on establishment of *Syagrus romanzoffiana* (Cham.) Becc., *Washingtonia robusta* H. Wendl. and *Archontophoenix cunninghamiana* (H. Wendl.) H. Wendl. & Drude in the landscape. *Sci. Hortic.* **2001**, *87*, 85–92. [CrossRef]
45. Maitra, S.; Gaikwad, D.J.; Shankar, T. Mulching: Materials, Advantages and Crop Production. In *Protected Cultivation and Smart Agriculture*, 1st ed.; New Delhi Publishers: New Delhi, India, 2002; pp. 55–66.
46. Li, A.; Zhang, J.; Ren, S.; Zhang, Y.; Zhang, F. Research progress on preparation and field application of paper mulch. *Environ. Technol. Innov.* **2021**, *24*, 101949. [CrossRef]
47. Xu, A.; Buchanan, R.L.; Micallef, S.A. Impact of mulches and growing season on indicator bacteria survival during lettuce cultivation. *Int. J. Food Microbiol.* **2016**, *224*, 28–39. [CrossRef] [PubMed]
48. Patil Shirish, S.; Kelkar Tushar, S.; Bhalerao Satish, A. Mulching: A soil and water conservation practice. *Res. J. Agric. For. Sci.* **2013**, *1*, 26–29.
49. Ahn, I.; Kim, S.H.; Maeng, W.Y.; Lee, I.E.; Chang, K.W.; Lee, J.J. Effects of soil acidity and organic matter by application of organic materials and soil mulching with pine needles for soil surface management in blueberry eco-friendly farming. *Korean J. Soil. Sci. Fert.* **2013**, *46*, 556–562. [CrossRef]
50. Kasirajan, S.; Ngouajio, M. Polyethylene and biodegradable mulches for agricultural applications: A review. *Agron. Sustain. Dev.* **2012**, *32*, 501–529. [CrossRef]
51. Chopra, M.; Koul, B. Comparative assessment of different types of mulching in various crops: A review. *Plant Arch.* **2020**, *20*, 1620–1626.
52. Mejias Barrera, P. Effect of Crushed Glass, Used as a Reflective Mulch, on Pinot Noir Performance. Doctoral Dissertation, Lincoln University, Lincoln, New Zealand, 2012.
53. De Louvigny, N.; Dürr, C.; Fiès, J.C.; Bruckler, L. Emergence of sugar beet (*Beta vulgaris* L.) from seedbeds after glass waste deposition on soil. *Soil Tillage Res.* **2002**, *66*, 35–46. [CrossRef]
54. Steward, L.G.; Sydnor, T.D.; Bishop, B. The ease of ignition of 13 landscape mulches. *J. Arboric.* **2003**, *29*, 317–321. [CrossRef]
55. Stokes, V. Some biodegradable mulch materials provide effective weed control during establishment of ash (*Fraxinus excelsior* L.) on farm woodland sites. *Q. J. Forest.* **2012**, *106*, 257–268.
56. Benoit, G.; Demars, S. Evaluation of organic and inorganic compounds extractable by multiple methods from commercially available crumb rubber mulch. *Water Air Soil Pollut.* **2018**, *229*, 1–13. [CrossRef]



57. Hayes, D.G. Enhanced end-of-life performance for biodegradable plastic mulch films through improving standards and addressing research gaps. *Curr. Opin. Chem. Eng.* **2021**, *33*, 100695. [CrossRef]
58. Sun, D.; Li, H.; Wang, E.; He, W.; Hao, W.; Yan, C.; Li, Y.; Mei, X.; Zhang, Y.; Sun, Z.; et al. An overview of the use of plastic-film mulching in China to increase crop yield and water-use efficiency. *Natl. Sci. Rev.* **2020**, *7*, 1523–1526. [CrossRef] [PubMed]
59. Zhang, H.; Miles, C.; Gerdeman, B.; LaHue, D.G.; DeVetter, L. Plastic mulch use in perennial fruit cropping systems—A review. *Sci. Hortic.* **2021**, *281*, 109975. [CrossRef]
60. Crawford, C.B.; Quinn, B. *Microplastic Pollutants*, 1st ed.; Elsevier Limited: Amsterdam, The Netherlands, 2016; pp. 58–60.
61. Manzano, V.; García, N.L.; Ramírez, C.R.; D'Accorso, N.; Goyanes, S. Mulch plastic systems: Recent advances and applications. In *Polymers for Agri-Food Applications*, 1st ed.; Gutiérrez, T., Ed.; Springer: Cham, Switzerland, 2019; pp. 265–290.
62. Velandia, M.; Smith, A.; Wszelaki, A.; Galinato, S. The Economic Feasibility of Adopting Plastic Biodegradable Mulches in Pumpkin Production. 2019. Available online: <https://bit.ly/2UaqAYx> (accessed on 7 September 2022).
63. Goldberger, J.R.; Jones, R.E.; Miles, C.A.; Wallace, R.W.; Inglis, D.A. Barriers and bridges to the adoption of biodegradable plastic mulches for US specialty crop production. *Renew. Agric. Food Syst.* **2015**, *30*, 143–153. [CrossRef]
64. Sarkar, D.J.; Barman, M.; Bera, T.; De, M.; Chatterjee, D. Agriculture: Polymers in crop production mulch and fertilizer. In *Encyclopedia of Polymer Applications*, 1st ed.; Mishra, M., Ed.; CRC Press: Boca Raton, FL, USA, 2019; pp. 28–47.
65. Bai, J.; Wang, J.; Chen, X.; Luo, G.; Shi, H.; Li, L.; Li, J. Seasonal and inter-annual variations in carbon fluxes and evapotranspiration over cotton field under drip irrigation with plastic mulch in an arid region of Northwest China. *J. Arid Land* **2015**, *7*, 272–284. [CrossRef]
66. Hayes, D.G.; Anunciado, M.B.; DeBruyn, J.M.; Bandopadhyay, S.; Schaeffer, S.; English, M.; Ghimire, S.; Miles, C.; Flury, M.; Sintim, H.Y. Biodegradable plastic mulch films for sustainable specialty crop production. In *Polymers for Agri-Food Applications*, 1st ed.; Gutiérrez, T., Ed.; Springer: Cham, Switzerland, 2019; pp. 183–213.
67. Isari, E.A.; Papaioannou, D.; Kalavrouziotis, I.K.; Karapanagioti, H.K. Microplastics in agricultural soils: A case study in cultivation of watermelons and canning tomatoes. *Water* **2021**, *13*, 2168. [CrossRef]
68. Gao, H.; Yan, C.; Liu, Q.; Ding, W.; Chen, B.; Li, Z. Effects of plastic mulching and plastic residue on agricultural production: A meta-analysis. *Sci. Total Environ.* **2019**, *651*, 484–492. [CrossRef] [PubMed]
69. Selke, S.; Auras, R.; Nguyen, T.A.; Castro Aguirre, E.; Cheruvathur, R.; Liu, Y. Evaluation of biodegradation-promoting additives for plastics. *Environ. Sci. Technol.* **2015**, *49*, 3769–3777. [CrossRef] [PubMed]
70. Ahmed, T.; Shahid, M.; Azeem, F.; Rasul, I.; Shah, A.A.; Noman, M.; Hameed, A.; Manzoor, N.; Manzoor, I.; Muhammad, S. Biodegradation of plastics: Current scenario and future prospects for environmental safety. *Environ. Sci. Pollut. Res.* **2018**, *25*, 7287–7298. [CrossRef]
71. López-Tolentino, G.; Ibarra-Jiménez, L.; Méndez-Prieto, A.; Lozano-del Río, A.J.; Lira-Saldivar, R.H.; Valenzuela-Soto, J.H.; Lozano-Cavazos, C.J.; Torres-Olivar, V. Photosynthesis, growth, and fruit yield of cucumber in response to oxo-degradable plastic mulches. *Acta Agric. Scand. B* **2017**, *67*, 77–84. [CrossRef]
72. Yang, Y.; Li, Z.; Yan, C.; Chadwick, D.; Jones, D.L.; Liu, E.; Liu, Q.; Bai, R.; He, W. Kinetics of microplastic generation from different types of mulch films in agricultural soil. *Sci. Total Environ.* **2022**, *814*, 152572. [CrossRef] [PubMed]
73. Velandia, M.; DeLong, K.L.; Wszelaki, A.; Schexnayder, S.; Clark, C.; Jensen, K. Use of polyethylene and plastic biodegradable mulches among Tennessee fruit and vegetable growers. *HortTechnology* **2020**, *30*, 212–218. [CrossRef]
74. Borrowman, C.K.; Johnston, P.; Adhikari, R.; Saito, K.; Patti, A.F. Environmental degradation and efficacy of a sprayable, biodegradable polymeric mulch. *Polym. Degrad. Stab.* **2020**, *175*, 109126. [CrossRef]
75. Sintim, H.Y.; Flury, M. 2017. Is biodegradable plastic mulch the solution to agriculture's plastic problem? *Environ. Sci. Technol.* **2017**, *51*, 1068–1069. [CrossRef]
76. Miles, C.; Wallace, R.; Wszelaki, A.; Martin, J.; Cowan, J.; Walters, T.; Inglis, D. Deterioration of potentially biodegradable alternatives to black plastic mulch in three tomato production regions. *HortScience* **2012**, *47*, 1270–1277. [CrossRef]
77. Akhir, M.A.M.; Mustapha, M. Formulation of Biodegradable Plastic Mulch Film for Agriculture Crop Protection: A Review. *Polym. Rev.* **2022**, 1–29. [CrossRef]
78. Eskander, S.B.; Saleh, H.M. *Environmental Science and Engineering Vol. 8: Biodegradation and Bioremediation*, 1st ed.; Studium Press: Houston, TX, USA, 2017; pp. 1–3.
79. Agarwal, S. Biodegradable Polymers: Present Opportunities and Challenges in Providing a Microplastic-Free Environment. *Macromol. Chem. Phys.* **2020**, *221*, 2000017. [CrossRef]
80. Witt, U.; Einig, T.; Yamamoto, M.; Kleeberg, I.; Deckwer, W.D.; Müller, R.J. Biodegradation of aliphatic–aromatic copolyesters: Evaluation of the final biodegradability and ecotoxicological impact of degradation intermediates. *Chemosphere* **2001**, *44*, 289–299. [CrossRef]
81. Ruggero, F.; Carretti, E.; Gori, R.; Lotti, T.; Lubello, C. Monitoring of degradation of starch-based biopolymer film under different composting conditions, using TGA, FTIR and SEM analysis. *Chemosphere* **2020**, *246*, 125770. [CrossRef]
82. Sintim, H.Y.; Bary, A.I.; Hayes, D.G.; Wadsworth, L.C.; Anunciado, M.B.; English, M.E.; Bandopadhyay, S.; Schaeffer, S.M.; DeBruyn, J.M.; Miles, C.A.; et al. In situ degradation of biodegradable plastic mulch films in compost and agricultural soils. *Sci. Total Environ.* **2020**, *727*, 138668. [CrossRef]
83. Zhang, Y.; Gao, W.; Mo, A.; Jiang, J.; He, D. Degradation of polylactic acid/polybutylene adipate films in different ratios and the response of bacterial community in soil environments. *Environ. Pollut.* **2022**, *313*, 120167. [CrossRef] [PubMed]

84. Viljoen, S.J.; Brailsford, F.L.; Murphy, D.V.; Hoyle, F.C.; Chadwick, D.R.; Jones, D.L. Leaching of phthalate acid esters from plastic mulch films and their degradation in response to UV irradiation and contrasting soil conditions. *J. Hazard. Mater.* **2022**, *443*, 130256. [CrossRef] [PubMed]
85. Bandopadhyay, S.; Liquey y González, J.E.; Henderson, K.B.; Anunciado, M.B.; Hayes, D.G.; DeBruyn, J.M. Soil microbial communities associated with biodegradable plastic mulch films. *Front. Microbiol.* **2020**, *11*, 587074. [CrossRef]
86. Sander, M. Biodegradation of polymeric mulch films in agricultural soils: Concepts, knowledge gaps, and future research directions. *Environ. Sci. Technol.* **2019**, *53*, 2304–2315. [CrossRef] [PubMed]
87. Anunciado, M.B.; Hayes, D.G.; Wadsworth, L.C.; English, M.E.; Schaeffer, S.M.; Sintim, H.Y.; Flury, M. Impact of agricultural weathering on physicochemical properties of biodegradable plastic mulch films: Comparison of two diverse climates over four successive years. *J. Polym. Environ.* **2021**, *29*, 1–16. [CrossRef]
88. Kijchavengkul, T.; Auras, R. Compostability of polymers. *Polym. Int.* **2008**, *57*, 793–804. [CrossRef]
89. Hou, L.; Xi, J.; Chen, X.; Li, X.; Ma, W.; Lu, J.; Xu, J.; Lin, Y.B. Biodegradability and ecological impacts of polyethylene-based mulching film at agricultural environment. *J. Hazard. Mater.* **2019**, *378*, 120774. [CrossRef] [PubMed]
90. Rudnik, E.; Briassoulis, D. Degradation behaviour of poly (lactic acid) films and fibres in soil under Mediterranean field conditions and laboratory simulations testing. *Ind. Crops Prod.* **2011**, *33*, 648–658. [CrossRef]
91. Touchaleaume, F.; Martin-Closas, L.; Angellier-Coussy, H.; Chevillard, A.; Cesar, G.; Gontard, N.; Gastaldi, E. Performance and environmental impact of biodegradable polymers as agricultural mulching films. *Chemosphere* **2016**, *144*, 433–439. [CrossRef]
92. Hayes, D.G.; Wadsworth, L.C.; Sintim, H.Y.; Flury, M.; English, M.; Schaeffer, S.; Saxton, A.M. Effect of diverse weathering conditions on the physicochemical properties of biodegradable plastic mulches. *Polym. Test.* **2017**, *62*, 454–467. [CrossRef]
93. Pantani, R.; Sorrentino, A. Influence of crystallinity on the biodegradation rate of injection-moulded poly (lactic acid) samples in controlled composting conditions. *Polym. Degrad. Stab.* **2013**, *98*, 1089–1096. [CrossRef]
94. Kim, Y.D.; Kim, S.C. Effect of chemical structure on the biodegradation of polyurethanes under composting conditions. *Polym. Degrad. Stab.* **1998**, *62*, 343–352. [CrossRef]
95. Abrha, H.; Cabrera, J.; Dai, Y.; Irfan, M.; Toma, A.; Jiao, S.; Liu, X. Bio-Based Plastics Production, Impact and End of Life: A Literature Review and Content Analysis. *Sustainability* **2022**, *14*, 4855. [CrossRef]
96. Johnston, B.; Radecka, I.; Hill, D.; Chiellini, E.; Ilieva, V.I.; Sikorska, W.; Musioł, M.; Zięba, M.; Marek, A.A.; Keddie, D.; et al. The microbial production of polyhydroxyalkanoates from waste polystyrene fragments attained using oxidative degradation. *Polymers* **2018**, *10*, 957. [CrossRef] [PubMed]
97. Filiciotto, L.; Rothenberg, G. Biodegradable plastics: Standards, policies, and impacts. *ChemSusChem* **2021**, *14*, 56–72. [CrossRef] [PubMed]
98. Xu, J.; Manepalli, P.H.; Zhu, L.; Narayan-Sarathy, S.; Alavi, S. Morphological, barrier and mechanical properties of films from poly (butylene succinate) reinforced with nanocrystalline cellulose and chitin whiskers using melt extrusion. *J. Polym. Res.* **2019**, *26*, 1–10. [CrossRef]
99. Menossi, M.; Cisneros, M.; Alvarez, V.A.; Casalongué, C. Current and emerging biodegradable mulch films based on polysaccharide bio-composites. A review. *Agron. Sustain. Dev.* **2021**, *41*, 1–27. [CrossRef]
100. Suzuki, M.; Tachibana, Y.; Kasuya, K.I. Biodegradability of poly (3-hydroxyalkanoate) and poly ( $\epsilon$ -caprolactone) via biological carbon cycles in marine environments. *Polym. J.* **2021**, *53*, 47–66. [CrossRef]
101. Fukushima, K.; Wu, M.H.; Bocchini, S.; Rasyida, A.; Yang, M.C. PBAT based nanocomposites for medical and industrial applications. *Mater. Sci. Eng. C* **2012**, *32*, 1331–1351. [CrossRef]
102. Qu, P.; Guo, B.; Wang, H.; Zhao, Y. Degradation characteristics of PBAT mulch in maize field. *Trans. Chin. Soc. Agric. Eng.* **2017**, *33*, 194–199.
103. Kijchavengkul, T.; Auras, R.; Rubino, M.; Alvarado, E.; Montero, J.R.C.; Rosales, J.M. Atmospheric and soil degradation of aliphatic–aromatic polyester films. *Polym. Degrad. Stab.* **2010**, *95*, 99–107. [CrossRef]
104. Jian, J.; Xiangbin, Z.; Xianbo, H. An overview on synthesis, properties and applications of poly (butylene-adipate-co-terephthalate)–PBAT. *Adv. Ind. Engg. Polym. Res.* **2020**, *3*, 19–26. [CrossRef]
105. Zhang, M.; Jia, H.; Weng, Y.; Li, C. Biodegradable PLA/PBAT mulch on microbial community structure in different soils. *Int. Biodeterior. Biodegrad.* **2019**, *145*, 104817. [CrossRef]
106. Ghimire, S.; Wszelaki, A.L.; Moore, J.C.; Inglis, D.A.; Miles, C. The use of biodegradable mulches in pie pumpkin crop production in two diverse climates. *HortScience* **2018**, *53*, 288–294. [CrossRef]
107. Kim, M.N.; Lee, B.Y.; Lee, I.M.; Lee, H.S.; Yoon, J.S. Toxicity and biodegradation of products from polyester hydrolysis. *J. Environ. Sci. Health Part A* **2001**, *36*, 447–463. [CrossRef]
108. Kennedy, G.L., Jr. Toxicity of adipic acid. *Drug Chem. Toxicol.* **2002**, *25*, 191–202. [CrossRef] [PubMed]
109. Li, C.; Cui, Q.; Li, Y.; Zhang, K.; Lu, X.; Zhang, Y. Effect of LDPE and biodegradable PBAT primary microplastics on bacterial community after four months of soil incubation. *J. Hazard. Mater.* **2022**, *429*, 128353. [CrossRef] [PubMed]
110. Liu, L.; Zou, G.; Zuo, Q.; Li, C.; Gu, J.; Kang, L.; Ma, M.; Liang, K.; Liu, D.; Du, L. Soil bacterial community and metabolism showed a more sensitive response to PBAT biodegradable mulch residues than that of LDPE mulch residues. *J. Hazard. Mater.* **2022**, *438*, 129507. [CrossRef] [PubMed]
111. França, D.C.; Almeida, T.G.; Abels, G.; Canedo, E.L.; Carvalho, L.H.; Wellen, R.M.; Haag, K.; Koschek, K. Tailoring PBAT/PLA/Babassu films for suitability of agriculture mulch application. *J. Nat. Fibers* **2019**, *16*, 933–943. [CrossRef]

112. Nair, N.R.; Sekhar, V.C.; Nampoothiri, K.M.; Pandey, A. Biodegradation of biopolymers. In *Current Developments in Biotechnology and Bioengineering*, 1st ed.; Dubey, S.K., Pandey, A., Sangwan, R.S., Eds.; Elsevier Limited: Amsterdam, The Netherlands, 2017; pp. 739–755.
113. Bartnikowski, M.; Dargaville, T.R.; Ivanovski, S.; Hutmacher, D.W. Degradation mechanisms of polycaprolactone in the context of chemistry, geometry and environment. *Prog. Polym. Sci.* **2019**, *96*, 1–20. [CrossRef]
114. Gu, X.B.; Li, Y.N.; Du, Y.D. Biodegradable film mulching improves soil temperature, moisture and seed yield of winter oilseed rape (*Brassica napus* L.). *Soil Tillage Res.* **2017**, *171*, 42–50. [CrossRef]
115. Liu, M.; Huang, Z.B.; Yang, Y.J. Analysis of biodegradability of three biodegradable mulching films. *J. Polym. Environ.* **2010**, *18*, 148–154. [CrossRef]
116. Yang, N.; Sun, Z.X.; Feng, L.S.; Zheng, M.Z.; Chi, D.C.; Meng, W.Z.; Hou, Z.Y.; Bai, W.; Li, K.Y. Plastic film mulching for water-efficient agricultural applications and degradable films materials development research. *Mater. Manuf. Process.* **2015**, *30*, 143–154. [CrossRef]
117. Ayu, R.S.; Khalina, A.; Harmaen, A.S.; Zaman, K.; Mohd Nurrazi, N.; Isma, T.; Lee, C.H. Effect of empty fruit brunch reinforcement in polybutylene-succinate/modified tapioca starch blend for agricultural mulch films. *Sci. Rep.* **2020**, *10*, 1–7.
118. Zeng, J.B.; Li, Y.D.; Zhu, Q.Y.; Yang, K.K.; Wang, X.L.; Wang, Y.Z. A novel biodegradable multiblock poly (ester urethane) containing poly (L-lactic acid) and poly (butylene succinate) blocks. *Polymer* **2009**, *50*, 1178–1186. [CrossRef]
119. AL-Oqla, F.M.; Omari, M.A. Sustainable biocomposites: Challenges, potential and barriers for development. In *Green Biocomposites*, 1st ed.; Jawaid, M., Sapuan, S.M., Othman, A.Y., Eds.; Springer: Cham, Switzerland, 2017; pp. 13–19.
120. Hongsriphan, N.; Pinpueng, A. Properties of agricultural films prepared from biodegradable poly (butylene succinate) adding natural sorbent and fertilizer. *J. Polym. Environ.* **2019**, *27*, 434–443. [CrossRef]
121. Yamamoto-Tamura, K.; Hoshino, Y.T.; Tsuboi, S.; Huang, C.; Kishimoto-Mo, A.W.; Sameshima-Yamashita, Y.; Kitamoto, H. Fungal community dynamics during degradation of poly (butylene succinate-co-adipate) film in two cultivated soils in Japan. *Biosci. Biotechnol. Biochem.* **2020**, *84*, 1077–1087. [CrossRef] [PubMed]
122. Yamamoto-Tamura, K.; Hiradate, S.; Watanabe, T.; Koitabashi, M.; Sameshima-Yamashita, Y.; Yarimizu, T.; Kitamoto, H. Contribution of soil esterase to biodegradation of aliphatic polyester agricultural mulch film in cultivated soils. *AMB Express* **2015**, *5*, 1–8. [CrossRef] [PubMed]
123. Peñas, M.I.; Pérez-Camargo, R.A.; Hernández, R.; Müller, A.J. A Review on Current Strategies for the Modulation of Thermomechanical, Barrier, and Biodegradation Properties of Poly (Butylene Succinate) (PBS) and Its Random Copolymers. *Polymers* **2022**, *14*, 1025. [CrossRef] [PubMed]
124. Kim, H.S.; Yang, H.S.; Kim, H.J. Biodegradability and mechanical properties of agro-flour-filled polybutylene succinate biocomposites. *J. Appl. Polym. Sci.* **2005**, *97*, 1513–1521. [CrossRef]
125. Huang, Z.; Qian, L.; Yin, Q.; Yu, N.; Liu, T.; Tian, D. Biodegradability studies of poly (butylene succinate) composites filled with sugarcane rind fiber. *Polym. Test.* **2018**, *66*, 319–326. [CrossRef]
126. Rafiqah, S.A.; Khalina, A.; Harmaen, A.S.; Tawakkal, I.A.; Zaman, K.; Asim, M.; Nurrazi, M.N.; Lee, C.H. A review on properties and application of bio-based poly (butylene succinate). *Polymers* **2021**, *13*, 1436. [CrossRef]
127. Briassoulis, D. An overview on the mechanical behaviour of biodegradable agricultural films. *J. Polym. Environ.* **2004**, *12*, 65–81. [CrossRef]
128. Shogren, R.L.; Rousseau, R.J. Field testing of paper/polymerized vegetable oil mulches for enhancing growth of eastern cottonwood trees for pulp. *For. Ecol. Manag.* **2005**, *208*, 115–122. [CrossRef]
129. Drumright, R.E.; Gruber, P.R.; Henton, D.E. Polylactic acid technology. *Adv. Mater.* **2000**, *12*, 1841–1846. [CrossRef]
130. Carrasco, F.; Pagès, P.; Gámez-Pérez, J.; Santana, O.O.; MasPOCH, M.L. Processing of poly (lactic acid): Characterization of chemical structure, thermal stability and mechanical properties. *Polym. Degrad. Stab.* **2010**, *95*, 116–125. [CrossRef]
131. Jamshidian, M.; Tehrani, E.A.; Imran, M.; Jacquot, M.; Desobry, S. Poly-Lactic Acid: Production, applications, nanocomposites, and release studies. *Compr. Rev. Food Sci. Food Saf.* **2010**, *9*, 552–571. [CrossRef] [PubMed]
132. Parida, M.; Shajkumar, A.; Mohanty, S.; Biswal, M.; Nayak, S.K. Poly (lactic acid)(PLA)-based mulch films: Evaluation of mechanical, thermal, barrier properties and aerobic biodegradation characteristics in real-time environment. *Polym. Bull.* **2022**, *15*, 1–26. [CrossRef]
133. Koh, J.J.; Zhang, X.; He, C. Fully biodegradable Poly (lactic acid)/Starch blends: A review of toughening strategies. *Int. J. Biol. Macromol.* **2018**, *109*, 99–113. [CrossRef]
134. Jandas, P.J.; Mohanty, S.; Nayak, S.K. Sustainability, compostability, and specific microbial activity on agricultural mulch films prepared from poly (lactic acid). *Ind. Eng. Chem. Res.* **2013**, *52*, 17714–17724. [CrossRef]
135. de Souza, A.G.; Ferreira, R.R.; Harada, J.; Rosa, D.S. Field performance on lettuce crops of poly (butylene adipate-co-terephthalate)/polylactic acid as alternative biodegradable composites mulching films. *J. Appl. Polym. Sci.* **2021**, *138*, 50020. [CrossRef]
136. Wang, D.; Li, G.; Mo, Y.; Zhang, D.; Xu, X.; Wilkerson, C.J.; Hoogenboom, G. Evaluation of subsurface, mulched and non-mulched surface drip irrigation for maize production and economic benefits in northeast China. *Irrig. Sci.* **2021**, *39*, 159–171. [CrossRef]
137. Zeng, J.B.; Li, K.A.; Du, A.K. Compatibilization strategies in poly (lactic acid)-based blends. *RSC Adv.* **2015**, *5*, 32546–32565. [CrossRef]



138. Arrieta, M.P.; Perdiguero, M.; Fiori, S.; Kenny, J.M.; Peponi, L. Biodegradable electrospun PLA-PHB fibers plasticized with oligomeric lactic acid. *Polym. Degrad. Stab.* **2020**, *179*, 109226. [CrossRef]
139. Miles, C.; DeVetter, L.; Ghimire, S.; Hayes, D.G. Suitability of biodegradable plastic mulches for organic and sustainable agricultural production systems. *HortScience* **2017**, *52*, 10–15. [CrossRef]
140. Tan, G.Y.A.; Chen, C.L.; Li, L.; Ge, L.; Wang, L.; Razaad, I.M.N.; Li, Y.; Zhao, L.; Mo, Y.; Wang, J.Y. Start a research on biopolymer polyhydroxyalkanoate (PHA): A review. *Polymers* **2014**, *6*, 706–754. [CrossRef]
141. Sathya, A.B.; Sivasubramanian, V.; Santhiagu, A.; Sebastian, C.; Sivashankar, R. Production of polyhydroxyalkanoates from renewable sources using bacteria. *J. Polym. Environ.* **2018**, *26*, 3995–4012. [CrossRef]
142. Koller, M. Production, properties, and processing of microbial polyhydroxyalkanoate (PHA) biopolyesters. In *Microbial and Natural Macromolecules*, 1st ed.; Surajit, D., Hirak, R.D., Eds.; Academic Press: Cambridge, MA, USA, 2021; pp. 3–55.
143. Sindhu, R.; Madhavan, A.; Arun, K.B.; Pugazhendhi, A.; Reshmy, R.; Awasthi, M.K.; Sirohi, R.; Tarafdar, A.; Pandey, A.; Binod, P. Metabolic circuits and gene regulators in polyhydroxyalkanoate producing organisms: Intervention strategies for enhanced production. *Bioresour. Technol.* **2021**, *327*, 124791. [CrossRef] [PubMed]
144. Sirohi, R. Sustainable utilization of food waste: Production and characterization of polyhydroxybutyrate (PHB) from damaged wheat grains. *Environ. Technol. Innov.* **2021**, *23*, 101715. [CrossRef]
145. Meereboer, K.W.; Misra, M.; Mohanty, A.K. Review of recent advances in the biodegradability of polyhydroxyalkanoate (PHA) bioplastics and their composites. *Green Chem.* **2020**, *22*, 5519–5558. [CrossRef]
146. Volova, T.; Prudnikova, S.; Boyandin, A.; Zhila, N.; Kiselev, E.; Shumilova, A.; Baranovskiy, S.; Demidenko, A.; Shishatskaya, E.; Thomas, S. Constructing slow-release fungicide formulations based on poly (3-hydroxybutyrate) and natural materials as a degradable matrix. *J. Agric. Food Chem.* **2019**, *67*, 9220–9231. [CrossRef]
147. Chen, G.; Cao, L.; Cao, C.; Zhao, P.; Li, F.; Xu, B.; Huang, Q. Effective and sustained control of soil-borne plant diseases by biodegradable polyhydroxybutyrate mulch films embedded with fungicide of prothioconazole. *Molecules* **2021**, *26*, 762. [CrossRef] [PubMed]
148. Muhammadi, S.; Afzal, M.; Hameed, S. Bacterial polyhydroxyalkanoates-eco-friendly next generation plastic: Production, biocompatibility, biodegradation, physical properties and applications. *Green Chem. Lett. Rev.* **2015**, *8*, 56–77. [CrossRef]
149. Boey, J.Y.; Mohamad, L.; Khok, Y.S.; Tay, G.S.; Baidurah, S. A review of the applications and biodegradation of polyhydroxyalkanoates and poly (lactic acid) and its composites. *Polymers* **2021**, *13*, 1544. [CrossRef]
150. Chee, J.Y.; Lakshmanan, M.; Jeeperly, I.F.; Hairudin, N.H.M.; Sudesh, K. The potential application of *Cupriavidus necator* as polyhydroxyalkanoates producer and single cell protein: A review on scientific, cultural and religious perspectives. *Appl. Food Biotechnol.* **2019**, *6*, 19–34.
151. Herrera, N.; Roch, H.; Salaberria, A.M.; Pino-Orellana, M.A.; Labidi, J.; Fernandes, S.C.; Radic, D.; Leiva, A.; Oksman, K. Functionalized blown films of plasticized polylactic acid/chitin nanocomposite: Preparation and characterization. *Mater. Des.* **2016**, *92*, 846–852. [CrossRef]
152. Virtanen, S.; Chowreddy, R.R.; Irmak, S.; Honkapää, K.; Isom, L. Food industry co-streams: Potential raw materials for biodegradable mulch film applications. *J. Polym. Environ.* **2017**, *25*, 1110–1130. [CrossRef]
153. Ning, R.; Liang, J.; Sun, Z.; Liu, X.; Sun, W. Preparation and characterization of black biodegradable mulch films from multiple biomass materials. *Polym. Degrad. Stab.* **2021**, *183*, 109411. [CrossRef]
154. Giaccone, M.; Cirillo, C.; Scognamiglio, P.; Teobaldelli, M.; Mataffo, A.; Stinca, A.; Pannico, A.; Immirzi, B.; Santagata, G.; Malinconico, M.; et al. Biodegradable mulching spray for weed control in the cultivation of containerized ornamental shrubs. *Chem. Biol. Technol. Agric.* **2018**, *5*, 1–8. [CrossRef]
155. Liang, W.; Zhao, Y.; Xiao, D.; Cheng, J.; Zhao, J. A biodegradable water-triggered chitosan/hydroxypropyl methylcellulose pesticide mulch film for sustained control of *Phytophthora sojae* in soybean (*Glycine max* L. Merr.). *J. Clean. Prod.* **2020**, *245*, 118943. [CrossRef]
156. Mondal, M.M.; Malek, M.A.; Puteh, A.B.; Ismail, M.R.; Ashrafuzzaman, M.; Naher, L. Effect of foliar application of chitosan on growth and yield in okra. *Aust. J. Crop Sci.* **2012**, *6*, 918–921.
157. Mondal, M.M.A.; Malek, M.A.; Puteh, A.B.; Ismail, M.R. Foliar application of chitosan on growth and yield attributes of mungbean (*Vigna radiata* (L.) Wilczek). *Bangladesh J. Bot.* **2013**, *42*, 179–183. [CrossRef]
158. Al-Hassani, F.A.; Majid, B.H. Effect of arginine, chitosan and agryl mulching on the growth and yield of pepper plant under the conditions of unheated greenhouses. *Plant Arch.* **2019**, *19*, 256–262.
159. Anifantis, A.; Canzio, G.; Cristiano, G.; De Lucia, B.; Russo, G.; Vecchiotti, L.; Immirzi, B.; Malinconico, M.; Santagata, G. Influence of the use of drip irrigation systems and different mulching materials on ornamental sunflowers in greenhouse cultivation. In Proceedings of the International Symposium on Advanced Technologies and Management Towards Sustainable Greenhouse Ecosystems: Greensys2011, Neos Marmaras-Sithonia, Greece, 5–10 June 2011.
160. Gómez-Ordóñez, E.; Rupérez, P. FTIR-ATR spectroscopy as a tool for polysaccharide identification in edible brown and red seaweeds. *Food Hydrocoll.* **2011**, *25*, 1514–1520. [CrossRef]
161. Manivasagan, P.; Oh, J. Marine polysaccharide-based nanomaterials as a novel source of nanobiotechnological applications. *Int. J. Biol. Macromol.* **2016**, *82*, 315–327. [CrossRef]
162. Liling, G.; Di, Z.; Jiachao, X.; Xin, G.; Xiaoting, F.; Qing, Z. Effects of ionic crosslinking on physical and mechanical properties of alginate mulching films. *Carbohydr. Polym.* **2016**, *136*, 259–265. [CrossRef]

163. Merino, D.; Salcedo, M.F.; Mansilla, A.Y.; Casalongué, C.A.; Alvarez, V.A. Development of Sprayable Sodium Alginate-Seaweed Agricultural Mulches with Nutritional Benefits for Substrates and Plants. *Waste Biomass Valorization* **2021**, *12*, 6035–6043. [CrossRef]
164. Zhang, Y.; Yin, H.; Zhao, X.; Wang, W.; Du, Y.; He, A.; Sun, K. The promoting effects of alginate oligosaccharides on root development in *Oryza sativa* L. mediated by auxin signaling. *Carbohydr. Polym.* **2014**, *113*, 446–454. [CrossRef] [PubMed]
165. Battacharyya, D.; Babgohari, M.Z.; Rathor, P.; Prithiviraj, B. Seaweed extracts as biostimulants in horticulture. *Sci. Hortic.* **2015**, *196*, 39–48. [CrossRef]
166. Santos, N.L.; de Oliveira Ragazzo, G.; Cerri, B.C.; Soares, M.R.; Kieckbusch, T.G.; da Silva, M.A. Physico-chemical properties of konjac glucomannan/alginate films enriched with sugarcane vinasse intended for mulching applications. *Int. J. Biol. Macromol.* **2020**, *165*, 1717–1726. [CrossRef] [PubMed]
167. Vox, G.; Santagata, G.; Malinconico, M.; Immirzi, B.; Mugnozza, G.S.; Schettini, E. Biodegradable films and spray coatings as eco-friendly alternative to petro-chemical derived mulching films. *J. Agric. Eng.* **2013**, *44*, 221–225. [CrossRef]
168. Immirzi, B.; Santagata, G.; Vox, G.; Schettini, E. Preparation, characterisation and field-testing of a biodegradable sodium alginate-based spray mulch. *Biosyst. Eng.* **2009**, *102*, 461–472. [CrossRef]
169. Vamadevan, V.; Bertoft, E. Structure-function relationships of starch components. *Stärke* **2015**, *67*, 55–68. [CrossRef]
170. Agama-Acevedo, E.; Bello-Perez, L.A. Starch as an emulsions stability: The case of octenyl succinic anhydride (OSA) starch. *Curr. Opin. Food Sci.* **2017**, *13*, 78–83. [CrossRef]
171. Ojogbo, E.; Ogunsona, E.O.; Mekonnen, T.H. Chemical and physical modifications of starch for renewable polymeric materials. *Mater. Today Sustain.* **2020**, *7*, 100028. [CrossRef]
172. Kowalczyk, D.; Gustaw, W.; Zięba, E.; Lisiecki, S.; Stadnik, J.; Baraniak, B. Microstructure and functional properties of sorbitol-plasticized pea protein isolate emulsion films: Effect of lipid type and concentration. *Food Hydrocoll.* **2016**, *60*, 353–363. [CrossRef]
173. Rosseto, M.; Krein, D.D.; Balbé, N.P.; Dettmer, A. Starch–gelatin film as an alternative to the use of plastics in agriculture: A review. *J. Sci. Food Agric.* **2019**, *99*, 6671–6679. [CrossRef] [PubMed]
174. Fei, Z.; Huang, S.; Yin, J.; Xu, F.; Zhang, Y. Preparation and characterization of bio-based degradable plastic films composed of cellulose acetate and starch acetate. *J. Polym. Environ.* **2015**, *23*, 383–391. [CrossRef]
175. Dang, X.; Shan, Z.; Chen, H. The preparation and applications of one biodegradable liquid film mulching by oxidized corn starch-gelatin composite. *Appl. Biochem. Biotechnol.* **2016**, *180*, 917–929. [CrossRef]
176. Baharin, K.W.; Zakaria, S.; Ellis, A.V.; Talip, N.; Kaco, H.; Gan, S.; Zailan, F.D.; Hashim, S.N.A.S. Factors affecting cellulose dissolution of oil palm empty fruit bunch and kenaf pulp in NaOH/urea solvent. *Sains Malays.* **2018**, *47*, 377–386.
177. Zainul Armir, N.A.; Zulkifli, A.; Gunaseelan, S.; Palanivelu, S.D.; Salleh, K.M.; Che Othman, M.H.; Zakaria, S. Regenerated cellulose products for agricultural and their potential: A review. *Polymers* **2021**, *13*, 3586. [CrossRef]
178. Esa, F.; Tasirin, S.M.; Abd Rahman, N. Overview of bacterial cellulose production and application. *Agric. Agric. Sci. Procedia* **2014**, *2*, 113–119. [CrossRef]
179. Hussain, Z.; Sajjad, W.; Khan, T.; Wahid, F. Production of bacterial cellulose from industrial wastes: A review. *Cellulose* **2019**, *26*, 2895–2911. [CrossRef]
180. Cárcamo, L.; Sierra, S.; Osorio, M.; Velásquez-Cock, J.; Vélez-Acosta, L.; Gómez-Hoyos, C.; Castro, C.; Zuluaga, R.; Gañán, P. Bacterial Nanocellulose Mulch as a Potential Greener Alternative for Urban Gardening in the Small-Scale Food Production of Onion Plants. *Agric. Res.* **2021**, *10*, 66–71. [CrossRef]
181. Pinpru, N.; Charoonsuk, T.; Khaissat, S.; Sawanakarn, O.; Vittayakorn, N.; Woramongkolchai, S. Synthesis and preparation of bacterial cellulose/calcium hydrogen phosphate composite film for mulching film application. *Mater. Today Proc.* **2021**, *47*, 3529–3536. [CrossRef]
182. Lindström, T.; Aulin, C. Market and technical challenges and opportunities in the area of innovative new materials and composites based on nanocellulosics. *Scand. J. For. Res.* **2014**, *29*, 345–351. [CrossRef]
183. Fernandes, I.D.A.A.; Pedro, A.C.; Ribeiro, V.R.; Bortolini, D.G.; Ozaki, M.S.C.; Maciel, G.M.; Haminiuk, C.W.I. Bacterial cellulose: From production optimization to new applications. *Int. J. Biol. Macromol.* **2020**, *164*, 2598–2611. [CrossRef]
184. Blanco Parte, F.G.; Santoso, S.P.; Chou, C.C.; Verma, V.; Wang, H.T.; Ismadji, S.; Cheng, K.C. Current progress on the production, modification, and applications of bacterial cellulose. *Crit. Rev. Biotechnol.* **2020**, *40*, 397–414. [CrossRef]
185. Palsikowski, P.A.; Kuchnier, C.N.; Pinheiro, I.F.; Morales, A.R. Biodegradation in soil of PLA/PBAT blends compatibilized with chain extender. *J. Polym. Environ.* **2018**, *26*, 330–341. [CrossRef]
186. Liu, B.; Guan, T.; Wu, G.; Fu, Y.; Weng, Y. Biodegradation Behavior of Degradable Mulch with Poly (Butylene Adipate-co-Terephthalate) (PBAT) and Poly (Butylene Succinate) (PBS) in Simulation Marine Environment. *Polymers* **2022**, *14*, 1515. [CrossRef]
187. Dharmalingam, S.; Hayes, D.G.; Wadsworth, L.C.; Dunlap, R.N. Analysis of the time course of degradation for fully biobased nonwoven agricultural mulches in compost-enriched soil. *Text. Res. J.* **2016**, *86*, 1343–1355. [CrossRef]
188. Boyandin, A.N.; Rudnev, V.P.; Ivonin, V.N.; Prudnikova, S.V.; Korobikhina, K.I.; Filipenko, M.L.; Volova, T.G.; Sinskey, A.J. Biodegradation of polyhydroxyalkanoate films in natural environments. *Macromol. Symp.* **2012**, *320*, 38–42. [CrossRef]
189. Merino, D.; Mansilla, A.Y.; Casalongué, C.A.; Alvarez, V.A. Effect of nanoclay addition on the biodegradability and performance of starch-based nanocomposites as mulch films. *J. Polym. Environ.* **2019**, *27*, 1959–1970. [CrossRef]
190. Alvarez, V.A.; Ruseckaite, R.A.; Vazquez, A. Degradation of sisal fibre/Mater Bi-Y biocomposites buried in soil. *Polym. Degrad. Stab.* **2006**, *91*, 3156–3162. [CrossRef]



191. Cozzolino, E.; Giordano, M.; Fiorentino, N.; El-Nakhel, C.; Pannico, A.; Di Mola, I.; Mori, M.; Kyriacou, M.C.; Colla, G.; Roupael, Y. Appraisal of biodegradable mulching films and vegetal-derived biostimulant application as eco-sustainable practices for enhancing lettuce crop performance and nutritive value. *Agronomy* **2020**, *10*, 427. [CrossRef]
192. Hayes, D.G.; Dharmalingam, S.; Wadsworth, L.C.; Leonas, K.K.; Miles, C.; Inglis, D.A. Biodegradable agricultural mulches derived from biopolymers. In *Degradable Polymers and Materials: Principles and Practice*, 2nd ed.; Khemani, K., Scholz, C., Eds.; American Chemical Society: Washington, DC, USA, 2012; pp. 201–223.
193. Cowan, J.S.; Ghimire, S.; Miles, C.A. Biodegradable mulch films: Their constituents and suitability for organic agriculture. In Proceedings of the ASHS Annual Conference, Atlanta, GA, USA, 7–11 August 2016.
194. Kaya-Celiker, H.; Mallikarjunan, P.K. Agricultural Applications of Biodegradable Films. In *Edible Films and Coatings*, 1st ed.; García, M.P.M., Gómez-Guillén, M.C., López-Caballero, M.E., Barbosa-Cánovas, G.V., Eds.; CRC Press: Boca Raton, FL, USA, 2016; pp. 567–602.
195. Siwek, P.; Libik, A.; Zawiska, I. The impact of biodegradable nonwoven fabric covers on the yield and quality of overwintering onions. *Acta Sci. Pol. Hortorum Cultus* **2013**, *12*, 3–11.
196. Cowan, J.S.; Miles, C.A.; Andrews, P.K.; Inglis, D.A. Biodegradable mulch performed comparably to polyethylene in high tunnel tomato (*Solanum lycopersicum* L.) production. *J. Sci. Food Agric.* **2014**, *94*, 1854–1864. [CrossRef] [PubMed]
197. Bilck, A.P.; Grossmann, M.V.; Yamashita, F. Biodegradable mulch films for strawberry production. *Polym. Test.* **2010**, *29*, 471–476. [CrossRef]
198. Mendonça, S.R.; Ávila, M.C.R.; Vital, R.G.; Evangelista, Z.R.; de Carvalho Pontes, N.; dos Reis Nascimento, A. The effect of different mulching on tomato development and yield. *Sci. Hortic.* **2021**, *275*, 109657. [CrossRef]
199. Siegenthaler, K.O.; Künkel, A.; Skupin, G.; Yamamoto, M. Ecoflex<sup>®</sup> and Ecovio<sup>®</sup>: Biodegradable, performance-enabling plastics. In *Synthetic Biodegradable Polymers*; Rieger, B., Künkel, A., Coates, G., Reichardt, R., Dinjus, E., Zevaco, T., Eds.; Springer: Heidelberg, Germany, 2011; Volume 245, pp. 91–136.
200. Warner, J.; Zandstra, J.W. Biodegradable Polymer Mulches in Bell Pepper Production 2004. Available online: <https://atrium.lib.uoguelph.ca/xmlui/handle/10214/6419> (accessed on 6 September 2022).
201. Moore-Kucera, J.; Cox, S.B.; Peyron, M.; Bailes, G.; Kinloch, K.; Karich, K.; Miles, C.; Inglis, D.A.; Brodhagen, M. Native soil fungi associated with compostable plastics in three contrasting agricultural settings. *Appl. Microbiol. Biotechnol.* **2014**, *98*, 6467–6485. [CrossRef] [PubMed]
202. DeVetter, L.W.; Zhang, H.; Ghimire, S.; Watkinson, S.; Miles, C.A. Plastic biodegradable mulches reduce weeds and promote crop growth in day-neutral strawberry in western Washington. *HortScience* **2017**, *52*, 1700–1706. [CrossRef]
203. Briassoulis, D.; Giannoulis, A. Evaluation of the functionality of bio-based plastic mulching films. *Polym. Test.* **2018**, *67*, 99–109. [CrossRef]
204. Marí, A.I.; Pardo, G.; Cirujeda, A.; Martínez, Y. Economic evaluation of biodegradable plastic films and paper mulches used in open-air grown pepper (*Capsicum annum* L.) crop. *Agronomy* **2019**, *9*, 36. [CrossRef]
205. Abduwaiti, A.; Liu, X.; Yan, C.; Xue, Y.; Jin, T.; Wu, H.; He, P.; Bao, Z.; Liu, Q. Testing Biodegradable Films as Alternatives to Plastic-Film Mulching for Enhancing the Yield and Economic Benefits of Processed Tomato in Xinjiang Region. *Sustainability* **2021**, *13*, 3093. [CrossRef]
206. Warnick, J.P.; Chase, C.A.; Roskopf, E.N.; Simonne, E.H.; Scholberg, J.M.; Koenig, R.L.; Roe, N.E. Weed suppression with hydramulch, a biodegradable liquid paper mulch in development. *Renew. Agric. Food Syst.* **2006**, *21*, 216–223. [CrossRef]
207. Ravichandran, M.; Samiappan, S.C.; Pandiyan, R.; Velu, R.K. Improvement of crop and soil management practices through mulching for enhancement of soil fertility and environmental sustainability: A review. *J. Exp. Biol. Agric. Sci.* **2022**, *10*, 697–712. [CrossRef]
208. Kyrikou, I.; Briassoulis, D. Biodegradation of agricultural plastic films: A critical review. *J. Polym. Environ.* **2007**, *15*, 125–150. [CrossRef]
209. Haider, T.P.; Völker, C.; Kramm, J.; Landfester, K.; Wurm, F.R. Plastics of the future? The impact of biodegradable polymers on the environment and on society. *Angew. Chem. Int. Ed.* **2019**, *58*, 50–62. [CrossRef]



## Article

# Preparation and Characterization of Acrylonitrile Butadiene Rubber Reinforced with Bio-Hydroxyapatite from Fish Scale

Namthip Bureewong<sup>1,2</sup>, Preeyaporn Injorhor<sup>1,2</sup>, Saifa Krasaekun<sup>1,2</sup>, Pawida Munchan<sup>1,2</sup>, Oatsaraphan Waengdongbang<sup>1,2</sup>, Jatuporn Wittayakun<sup>3</sup>, Chaiwat Ruksakulpiwat<sup>1,2,\*</sup> and Yupaporn Ruksakulpiwat<sup>1,2,\*</sup>

<sup>1</sup> School of Polymer Engineering, Institute of Engineering, Suranaree University of Technology, Nakhon Ratchasima 30000, Thailand

<sup>2</sup> Research Center for Biocomposite Materials for Medical Industry and Agricultural and Food Industry, Suranaree University of Technology, Nakhon Ratchasima 30000, Thailand

<sup>3</sup> School of Chemistry, Institute of Science, Suranaree University of Technology, Nakhon Ratchasima 30000, Thailand

\* Correspondence: charuk@sut.ac.th (C.R.); yupa@sut.ac.th (Y.R.); Tel.: +66-44-22-4430 (C.R.); +66-44-22-3033 (Y.R.)

**Abstract:** This work aims to enhance the mechanical properties, oil resistance, and thermal properties of acrylonitrile butadiene rubber (NBR) by using the *Nile tilapia* fish scales as a filler and using bis(triethoxysilylpropyl)tetrasulfide (TESPT) as a coupling agent (CA). The prepared fish scale particles (FSp) are B-type hydroxyapatite and the particle shape is rod-like. The filled NBR with FSp at 10 phr increased tensile strength up to 180% ( $4.56 \pm 0.48$  MPa), reduced oil absorption up to 155%, and increased the decomposition temperature up to 4 °C, relative to the unfilled NBR. The addition of CA into filled NBR with FSp at 10 phr increased tensile strength up to 123% ( $5.62 \pm 0.42$  MPa) and percentage of elongation at break up to 122% relative to the filled NBR with FSp at 10 phr. This work demonstrated that the prepared FSp from the *Nile tilapia* fish scales can be used as a reinforcement filler to enhance the NBR properties for use in many high-performance applications.

**Citation:** Bureewong, N.; Injorhor, P.; Krasaekun, S.; Munchan, P.; Waengdongbang, O.; Wittayakun, J.; Ruksakulpiwat, C.; Ruksakulpiwat, Y. Preparation and Characterization of Acrylonitrile Butadiene Rubber Reinforced with Bio-Hydroxyapatite from Fish Scale. *Polymers* **2023**, *15*, 729. <https://doi.org/10.3390/polym15030729>

Academic Editor: Raffaella Striani

Received: 29 November 2022

Revised: 25 January 2023

Accepted: 28 January 2023

Published: 31 January 2023



**Copyright:** © 2023 by the authors. Licensee MDPI, Basel, Switzerland. This article is an open access article distributed under the terms and conditions of the Creative Commons Attribution (CC BY) license (<https://creativecommons.org/licenses/by/4.0/>).

**Keywords:** acrylonitrile butadiene rubber; fish scale; bis(triethoxysilylpropyl)tetrasulfide; composite; compatibilizer

## 1. Introduction

*Nile tilapia* is a freshwater fish that finds public favor in consumption, which makes it popular in aquaculture. About 140,000 tons of *Nile tilapia* fish were produced in Thailand, and 23% of those were processed into fillets. That left about 2% of the *Nile tilapia* fish scales as waste [1–3]. Generally, fish scales are considered discarded waste from the food processing industry and are often disposed of in landfills, which pollute both soil and water resources [4,5]. Therefore, the development of fish scales into functional materials is interesting because it could reduce the impact of environmental pollution and increase their value. Normally, the fish scales are rich in hydroxyapatite, collagen, polysaccharide, and chitin, which contain the mineral elements magnesium, calcium, fluoride, and phosphorus [6,7]. Recently, fish scales have been used to produce various products, such as fertilizer and fillers for plastic and rubber industrials. Additionally, it also has a wide use in tissue engineering for biomedical applications [3,4]. Hydroxyapatite from fish scales has gained the attention of many researchers. Majhool et al. [8] have prepared hydroxyapatite from tilapia fish scales. They expected that it can be used as a potential filler in polymers. Similar to Prasad et al. [9], they have used hydroxyapatite from fish scales as a filler in polylactic acid (PLA) composites for use as fixation devices. Their work revealed that hydroxyapatite can be improved the wettability and thermal stability of PLA/hydroxyapatite composites.

Acrylonitrile butadiene rubber (NBR) is a synthetic rubber that has excellent resistance to solvents and oils due to the presence of polar cyanide groups in the NBR backbone. In addition, NBR is convenient to use in various industrial applications because of its moderate cost, processability, and heat resistance. The majority of NBR applications are used in petroleum and automobile industrials, such as fuel hoses, gaskets, oil seals, radiator hoses, v-belts, etc. [10,11]. However, NBR has drawbacks in tensile strength, flexibility and flame resistance, etc., that restrict its potential to be used in many applications requiring high performance [10–15]. Several researchers have recently been fabricating elastic composites, especially NBR-based nanocomposites, not only to improve the mechanical properties of NBR but also to enhance the resistance to solvents, oils, and heat [13,16,17].

However, although the addition of nanofillers to NBR has several advantages, as mentioned, it also has some disadvantages, such as the ability to agglomerate due to the filler–filler interactions, which limits the potential of the filler to improve the performance of NBR vulcanizate. Therefore, the addition of coupling agents could be an alternative way to reduce these problems because it would reduce the filler–filler interactions and enhance the filler–rubber interactions, which would improve the overall polymer composite properties [18,19]. Normally, bis(triethoxysilylpropyl)tetrasulfide (TESPT) is typically the coupling agent (CA) that is widely used in the rubber industry due to its low cost, availability, and the simplicity of the process [20]. TESPT is a bifunctional compound which is composed of two functionally active end groups. It can act as a bridge between filler and rubber via chemical linkages in the sulfur vulcanization, so enhancing of the rubber–filler interaction occurred [21].

In this work, alkali heat treatment was used to prepare *Nile tilapia* fish scales as fish scale particles (FSp). The method was based on previous research [22]. The particle size of FSp was expected to decrease with increasing treatment time and can be used as a filler in NBR. The characteristics of FSp were characterized using an X-ray diffractometer (XRD), an energy dispersive X-ray spectrometer (EDS), Fourier transform infrared spectroscopy (FTIR), a nitrogen adsorption–desorption analyzer, and a field emission scanning electron microscope (FE-SEM). The effects on the cure characteristics, mechanical properties, morphological properties, oil resistance, and thermal properties of the filled NBR with FSp at different contents (0, 5, and 10 phr) were investigated. Furthermore, the effects of CA on NBR samples with optimal FSp content were compared. NBR composites filled with FSp were expected to provide the oil resistance properties. This is a novelty of the work.

## 2. Materials and Methods

### 2.1. Materials

*Nile tilapia* fresh fish scales of approximately 3 kg were collected from the local market in Nakhon Ratchasima, Thailand. Acrylonitrile butadiene rubber (NBR) with the trademark NANCAR<sup>®</sup> 3345 was supplied by NANTEX Industry Co., Ltd. (Kaohsiung, Taiwan). Bis(triethoxysilylpropyl)tetrasulfide (TESPT) with the product ID KBE-846 was supplied by Shin-Etsu Chemical Co., Ltd. (Tokyo, Japan). Hydrochloric acid (HCl) with AR grade and 37% purity was supplied by RCI Labscan Co., Ltd. (Bangkok, Thailand). Sodium hydroxide (NaOH) with RPE grade and 99% purity was supplied by Carlo Erba (Milan, Italy). Stearic acid (SA), zinc oxide (ZnO), Di(benzothiazol-2-yl)disulfide (MBTS), N-Cyclohexylbenzothiazole-2-sulfenamide (CBS), and sulfur (S) were supported by Chemical Innovation Co., Ltd. (Bangkok, Thailand).

### 2.2. Preparation of Fish Scale Particles (FSp) from Fresh Fish Scales

The method for preparing FSp was adapted from Kongsri et al. and Injorhor et al. [22,23]. The collected fresh fish scales were washed with tap water several times to remove dirt, and dried using a hot-air oven at 60 °C for 12 h to obtain the dried fish scales. The protein and fat on the surface of the dried fish scales were removed using HCl solution at 0.1 M under stirring for 2 h at room temperature. Then, the removed fish scales were filtered, washed with DI water until they reached pH = 7, and dried at 60 °C using a hot-air oven. The prior

removed fish scales were alkali heat treated with 50% (*w/v*) of NaOH solution at 70 °C for 7 h. Afterwards, the slurry of fish scales was filtered, washed with DI water until it reached pH = 7, and dried using a hot-air oven at 60 °C. The FSp were then obtained.

### 2.3. Characterizations of FSp

The crystalline phase compositions and diffraction lines of FSp were analyzed by an X-ray diffractometer (XRD, D2 PHASER, Bruker, Billerica, MA, USA) with Cu K $\alpha$  radiation source operated at 30 kV and current 10 mA. The 2 $\theta$  range carried out was between 10 and 60 degrees.

The elemental compositions of FSp were analyzed by an energy dispersive X-ray spectrometer (EDS, EDAX Genesis 2000, AMETEK, Inc., Berwyn, PA, USA) in a scanning electron microscope (SEM-EDS, JSM-6010LV, JEOL, Tokyo, Japan).

The functional groups of FSp were analyzed by Fourier transform infrared spectroscopy (FTIR, TENSOR 27, Bruker, Billerica, MA, USA). The sample was mixed with potassium bromide (KBr) using agate mortar and pressed into a disk to obtain the test specimen with a smooth surface for transmittance measurement. The wavenumber range of 4000 to 400 cm<sup>-1</sup> with resolution of 4 cm<sup>-1</sup> and number of scans of 64 were used to collect data.

The characteristics of FSp in terms of BET surface area, total pore volume and particle size were determined from nitrogen adsorption–desorption analysis, which was performed on BELSORP-mini II (MicrotracBEL, Osaka, Japan). The sample was degassed at 160 °C for 6 h before analysis. The microstructure of FSp was acquired using a field emission scanning electron microscope (FE-SEM, AURIGA, Carl Zeiss, Oberkochen, Germany) at 3 kV. The samples were sputtered with gold for 3 min at 10 mA beforehand.

### 2.4. Preparation of NBR/FSp and NBR/FSp/CA Composites

The NBR/FSp and NBR/FSp/CA composites were prepared by compounding using an internal mixer at 70 °C with roller speed at 40 rpm and vulcanizing using a compression molding machine at 160 °C with an optimal cure time of each compound that was determined using a moving die rheometer (MDR). First, the NBR was masticated for 4 min, followed by the addition of different FSp contents (0, 5, and 10 phr), CA, and vulcanizing agent for 2 min. Then, the accelerators and activators were added separately for 1 min. The sample codes and compositions of NBR/FSp and NBR/FSp/CA composites are listed in Table 1.

**Table 1.** Sample codes and compositions of NBR/FSp and NBR/FSp/CA composites.

Materials (phr *)	Unfilled NBR	NBR-5FSp	NBR-10FSp	NBR-10FSp-CA
NBR	100	100	100	100
SA	2	2	2	2
ZnO	5	5	5	5
MBTS	1.5	1.5	1.5	1.5
CBS	0.5	0.5	0.5	0.5
S	1.5	1.5	1.5	1.5
FSp	-	5	10	10
TESPT	-	-	-	2

\* phr = part per hundred of rubber.

### 2.5. Characterizations of NBR/FSp and NBR/FSp/CA Composites

The cure characteristics, such as minimum torque, maximum torque, scorch time, and optimal cure time of NBR/FSp and NBR/FSp/CA composites, were determined using an MDR (M-2000AN, GOTECH, Taichung, Taiwan) according to ASTM D2084 with a temperature at 160 °C. The cure rate index of NBR/FSp and NBR/FSp/CA composites were calculated by following the equation:

$$\text{Cure rate index} = 100 / (\text{optimal cure time} - \text{scorch time}) \quad (1)$$



The modulus at 100% elongation (M100), modulus at 300% elongation (M300), tensile strength, and percentage of elongation at break of NBR/FSp and NBR/FSp/CA composites were measured according to ASTM D412 using a universal testing machine (UTM, Model:5565, INSTRON, Norwood, MA, USA) with a load cell of 5 kN and crosshead speed of 500 mm/min.

The hardness of NBR/FSp and NBR/FSp/CA composites were measured according to ASTM D2240 using a hardness tester (HPE II, Bareiss, Stouffville, ON, Canada) with the Shore A test method.

The secondary electron images of NBR/FSp and NBR/FSp/CA composites were acquired using a field emission scanning electron microscope (FE-SEM, AURIGA, Carl Zeiss, Oberkochen, Germany). The tensile fracture surfaces of NBR/FSp and NBR/FSp/CA composites were coated with gold before the SEM observation.

The oil resistance in terms of change in mass percentage of NBR/FSp and NBR/FSp/CA composites were performed according to ASTM D471 by immersing the standard specimens in toluene for 22 h. The equation that was used to calculate the change in mass percentage of NBR/FSp and NBR/FSp/CA composites is:

$$\Delta M (\%) = [(M_2 - M_1)/M_1] \times 100 \quad (2)$$

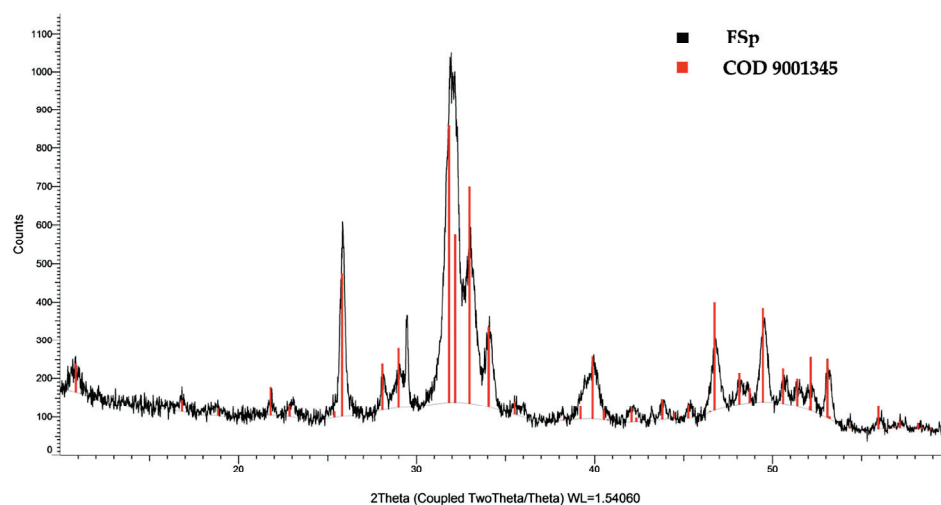
where  $\Delta M$  is the change in mass (%),  $M_1$  is the initial mass of the specimen in air (g), and  $M_2$  is the mass of specimen in air after immersion (g).

The thermogravimetric analyzer (TGA, TGA/DSC 1, METTLER TOLEDO, Greifensee, Switzerland) was used to analyze the thermal decompositions of NBR/FSp and NBR/FSp/CA composites. The specimens were placed in an alumina pan and heated from room temperature up to 650 °C under nitrogen with a heating rate of 10 °C/min and a gas flow rate of 20 mL/min.

### 3. Results and Discussion

#### 3.1. Characterizations of FSp

The XRD pattern of FSp is represented in Figure 1. The sample consisted entirely of the hydroxyapatite phase with defined peaks following the Crystallography Open Database (COD 9001345) and similar to the standard of JCDPS 00-009-0432 [24] without other phases. The characteristic peaks of the FSp are similar to the synthetic hydroxyapatite of Pon-On et al. [25] and the fish scale nano-hydroxyapatite of Kongsri et al. [23]. It was confirmed that the obtained FSp are a type of hydroxyapatite, which is a bio-material.



**Figure 1.** XRD pattern of FSp compared with COD 9001345.

The elemental compositions and EDS spectra of FSp are shown in Figure 2. It confirms that the major constituents are calcium (Ca), phosphorous (P), and oxygen (O). Moreover,

the typical presence of sodium (Na) and magnesium (Mg) are significant factors in bone and tooth growth [26]. However, the Ca/P of FSp is 1.86, which is higher than the stoichiometric ratio of 1.67 for stoichiometric hydroxyapatite because of the presence of carbonate ( $\text{CO}_3^{2-}$ ) ions that substitute phosphate ( $\text{PO}_4^{3-}$ ) in the hydroxyapatite structure (B-type hydroxyapatite) [25].

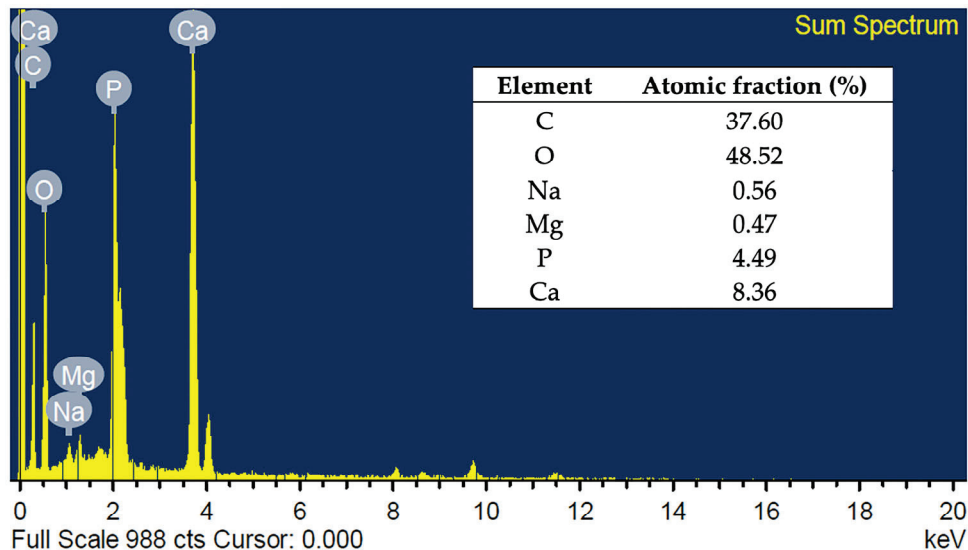


Figure 2. Elemental analysis by EDS of FSp.

The functional groups of FSp are shown in Figure 3. The broad band around  $3500\text{ cm}^{-1}$  corresponds to the  $\text{OH}^-$  stretching vibration of adsorbed water. The bands at  $1471$  and  $1415\text{ cm}^{-1}$  correspond to the asymmetric stretching vibration of the  $\text{CO}_3^{2-}$  band, and a band at  $873\text{ cm}^{-1}$  corresponds to the bending vibration of  $\text{CO}_3^{2-}$  [23,27]. The presence of  $\text{CO}_3^{2-}$  bands indicated that some  $\text{PO}_4^{3-}$  groups were replaced with  $\text{CO}_3^{2-}$  groups. These results confirmed the FSp are B-type hydroxyapatite, which corresponds to the EDS result and with Kongsri et al. [23]. In addition, the strong band at  $1043\text{ cm}^{-1}$  corresponds to the stretching vibration of  $\text{PO}_4^{3-}$ , and the sharp bands at  $601$  and  $563\text{ cm}^{-1}$  correspond to the degenerate bending vibrations of  $\text{PO}_4^{3-}$  in a hydroxyapatite structure.

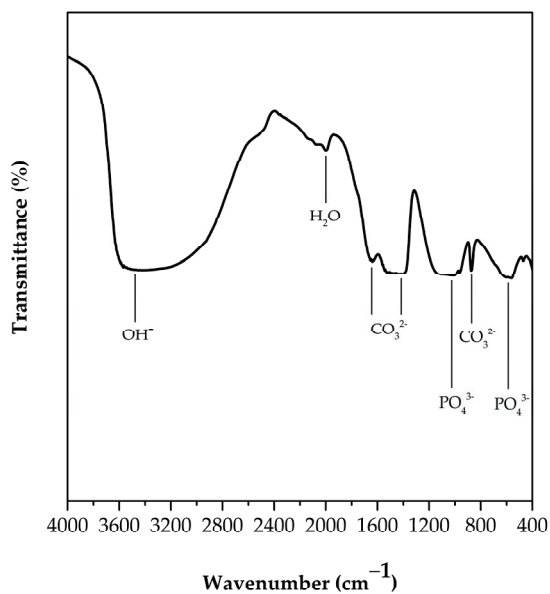


Figure 3. FTIR spectrum of FSp.

The adsorption–desorption isotherm of FSp is represented in Figure 4 and the information on FSp analysis in terms of BET surface area and total pore volume are listed in Table 2. The isotherm shape shows unrestricted monolayer–multilayer adsorption up to high  $P/P_0$  without the final saturation plateau. Therefore, the isotherm of FSp is fitted to the second (II) type of the IUPAC classification given by nonporous adsorbents [28,29]. The BET surface area of FSp shows a higher value as compared to the extracted hydroxyapatite from carp fish that was reported by Muhammad et al. [30]. In addition, the BET surface area of FSp shows a higher value than the commercial hydroxyapatite in these reports [23,30]. For use as filler in composite materials, the high surface area of FSp has an advantage in terms of greater interactions with the matrix. It was expected to be a bio-filler for improving NBR composites.

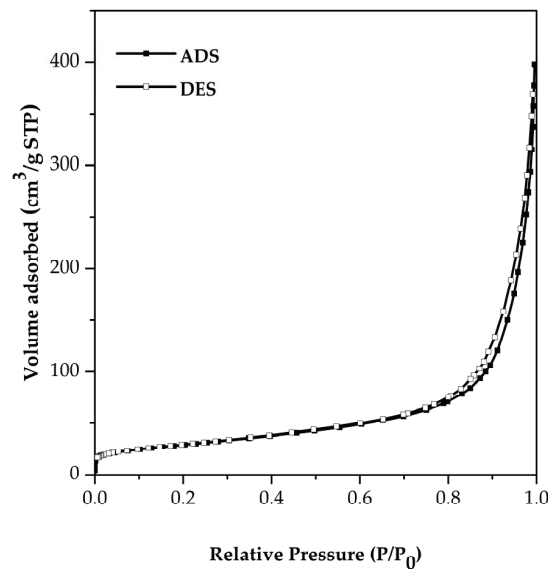


Figure 4. Physisorption isotherm of FSp.

Table 2. Information on FSp analysis.

Sample	BET Surface Area (m <sup>2</sup> /g)	Total Pore Volume (cm <sup>3</sup> /g)
FSp	104	0.50

The microstructure of FSp is shown in Figure 5. The FE-SEM images show the FSp in a rod-like shape with some agglomerates of FSp due to the static force between the FSp. However, the particle size of the FSp is in the range of the nanoscale.

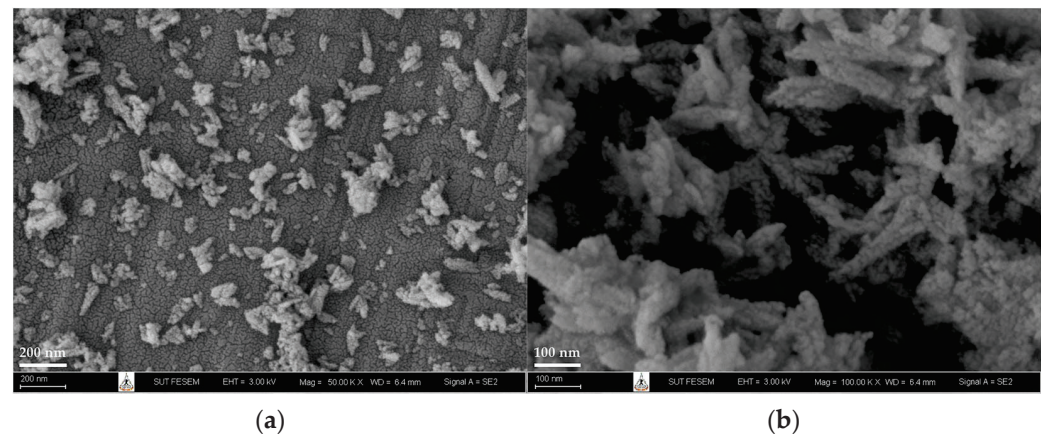


Figure 5. FE-SEM images of FSp at (a)  $\times 50,000$  and (b)  $\times 100,000$  magnification.

### 3.2. Characterizations of NBR/FSp and NBR/FSp/CA Composites

The cure characteristics such as minimum torque, maximum torque, scorch time, optimal cure time, and cure rate index of NBR/FSp and NBR/FSp/CA composites are listed in Table 3. Normally, the minimum torque is related to the viscosity of the rubber compound, while the maximum torque is related to the rigidity of the rubber vulcanizate. In the case of the addition of filler to rubber, these properties are also related to the nature of the filler. In addition, the scorch time is the time with no crosslinks in the rubber compound, which is an important parameter for the safe processing of rubber in molds. The optimal cure time is another important parameter that determines the time required to produce the rubber products [15,31–35]. The value of minimum torque of NBR-5FSp tends to increase as compared to unfilled NBR because the dispersion of FSp at 5 phr reduces the mobility of the macromolecular chains of NBR, which causes the viscosity of the compound to increase [15,32,34]. Meanwhile, the value of minimum torque of NBR-10FSp decreases as compared to unfilled NBR and NBR-5FSp because the addition of FSp at this amount has agglomerated in the NBR matrix. The values of maximum torque of the filled NBR with FSp are higher than unfilled NBR because the stiffness of the FSp increases the rigidity of composite vulcanizates. The values of scorch time and optimal cure time of filled NBR with FSp decrease as compared to unfilled NBR because the mineral content of FSp acts as an activator for composite vulcanizates [4,34]. Meanwhile, the NBR-10FSp slightly decreases the values of scorch time and optimal cure time as compared to NBR-5FSp because the system of filled NBR with increasing FSp content becomes more heated from the filler friction that affects the increased degree of curing. These results resemble the cure characteristics of filled rubbers with prepared hydroxyapatite that were reported by Nihmath and Ramesan [15,34]. Therefore, the use of FSp as a filler in NBR is an alternative idea for producing NBR composite because it can reduce the optimal cure time of NBR to obtain the product in a shorter time. However, the NBR-10FSp-CA shows the value of minimum torque decreasing as compared to filled NBR because the CA acts as a lubricant, which causes the viscosity of the compound to decrease. Moreover, the value of the optimal cure time of NBR-10FSp-CA tends to increase as compared to filled NBR because the CA coats on the surface of FSp, which reduces their activator activity, which causes the optimal cure time of the composite vulcanizate to increase.

**Table 3.** Cure characteristics of NBR/FSp and NBR/FSp/CA composites.

Samples	Minimum Torque (dNm)	Maximum Torque (dNm)	Scorch Time (min)	Cure Time (min)	Cure Rate Index (min <sup>-1</sup> )
Unfilled NBR	7.50	23.12	3:32	11:53	0.20
NBR-5FSp	7.86	30.25	1:32	2:38	1.52
NBR-10FSp	6.44	29.02	1:31	2:32	1.64
NBR-10FSp-CA	5.91	24.00	1:32	3:12	1.00

Figure 6 represents the mechanical properties of NBR/FSp and NBR/FSp/CA composites, and Table 4 shows the values of the mechanical properties of NBR/FSp and NBR/FSp/CA composites in terms of M100, M300, tensile strength, percentage of elongation at break, and hardness. It is well known that the characteristics and dispersion of filler are directly related to the properties of the polymer composite. Additionally, the area under the stress–strain curves is related to the toughness of the polymer. In general, the mechanical properties depend on the nature of the filler, dispersion, and the interaction between the filler and polymer matrix [4,15,34,36]. The modulus and tensile strength of filled NBR with FSp show increased values as compared to unfilled NBR because of the interactions between FSp and the NBR matrix, which improve the fracture resistance of NBR composites. However, the percentage of elongation at the break of filled NBR with FSp shows decreased values as compared to unfilled NBR because the addition of FSp restricts the molecular motions of the NBR matrix, which reduces the elasticity of NBR. When

compared to the filled NBR with FSp at 5 and 10 phr, the NBR-10FSp shows higher values of tensile strength and percentage of elongation at break that resemble the mechanical properties reported by Akbay et al. [4]. According to this research, the tensile strength and percentage of elongation at break of the rubber were increased by increasing the fish scale content, because the calcium oxide (CaO) content of fish scale acts as a vulcanizate activator that improved the mechanical strength and flexibility of the rubber composite. Meanwhile, the hardness values of filled NBR increase with increasing FSp content because the stiffness of FSp improves the resistance to indentation of NBR composite, which resembles the hardness results in these reports [15,34]. Moreover, the NBR-10FSp-CA shows increased values of tensile strength and percentage of elongation at break as compared to filled NBR because the CA enhances the chemical interaction between FSp and the NBR matrix, which assists the stress-transfer of NBR composite but has no effect on the modulus value. Figure 7a represents the schematic of NBR/FSp/CA interactions. The first step is CA hydrolysis, which generates the silanol groups (Si-OH) on the side chains of CA. The second step is that the Si-OH of CA and the Ca of FSp generate an ionic reaction together. In addition, the sulfur (S) of the CA and the carbon (C) on the NBR chains undergo a crosslinking reaction. Figure 7b represents a sketch of the interface interactions between FSp, CA, and NBR chains. These interactions are similar to these reports [19,37,38]. All results show that the modulus, tensile strength, and hardness of NBR are improved by adding the FSp with increasing contents. In addition, the tensile strength, percentage of elongation at break, and hardness of NBR composites are also improved by using a CA to obtain superior values.

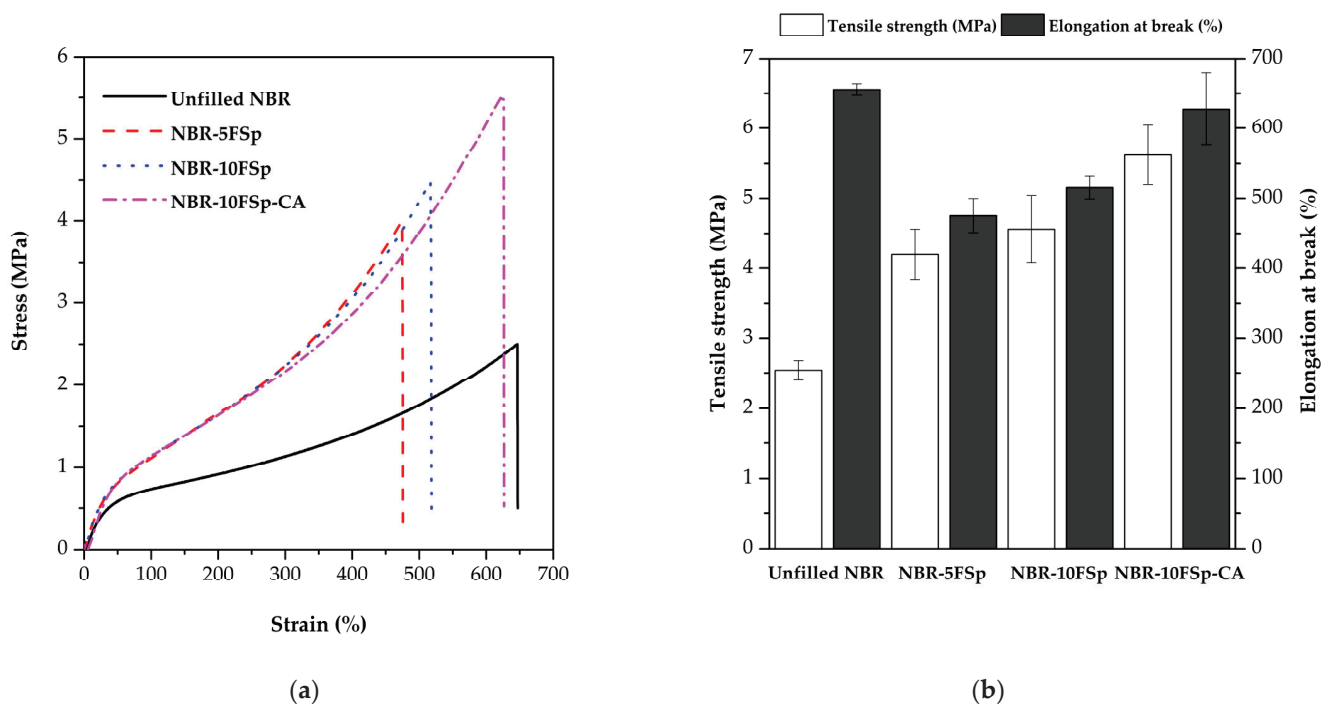
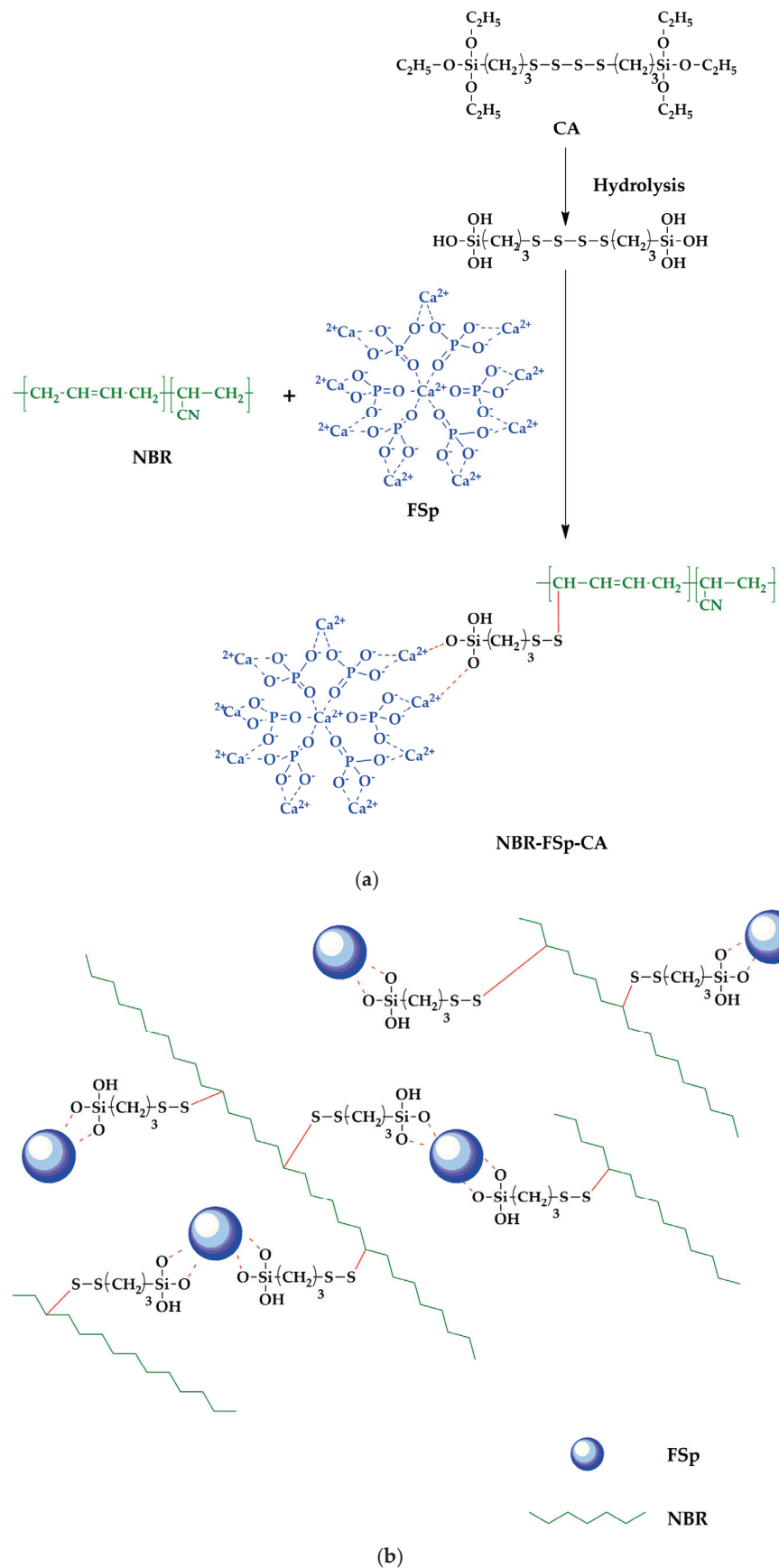


Figure 6. Mechanical properties of NBR/FSp and NBR/FSp/CA composites showing (a) Stress–strain curves and (b) Tensile strength and percentage of elongation at break.

Table 4. Mechanical properties of NBR/FSp and NBR/FSp/CA composites.

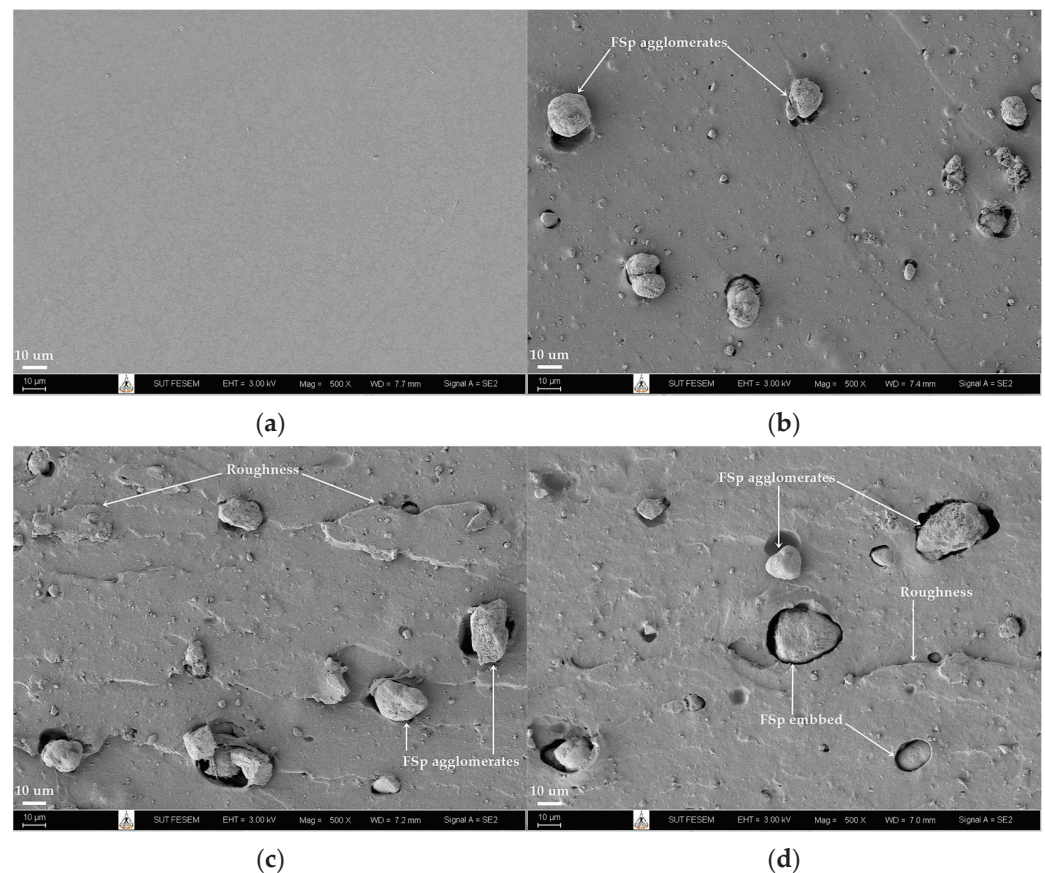
Samples	M100 (MPa)	M300 (MPa)	Tensile Strength (MPa)	Elongation at Break (%)	Hardness (Shore A)
Unfilled NBR	0.73 ± 0.02	1.14 ± 0.06	2.54 ± 0.14	655.35 ± 8.07	35.40 ± 0.25
NBR-5FSp	1.15 ± 0.04	2.39 ± 0.13	4.20 ± 0.36	475.21 ± 24.37	37.90 ± 0.30
NBR-10FSp	1.14 ± 0.02	2.21 ± 0.06	4.56 ± 0.48	515.81 ± 16.68	38.33 ± 0.25
NBR-10FSp-CA	1.13 ± 0.03	2.21 ± 0.08	5.62 ± 0.42	627.56 ± 51.10	41.40 ± 1.14





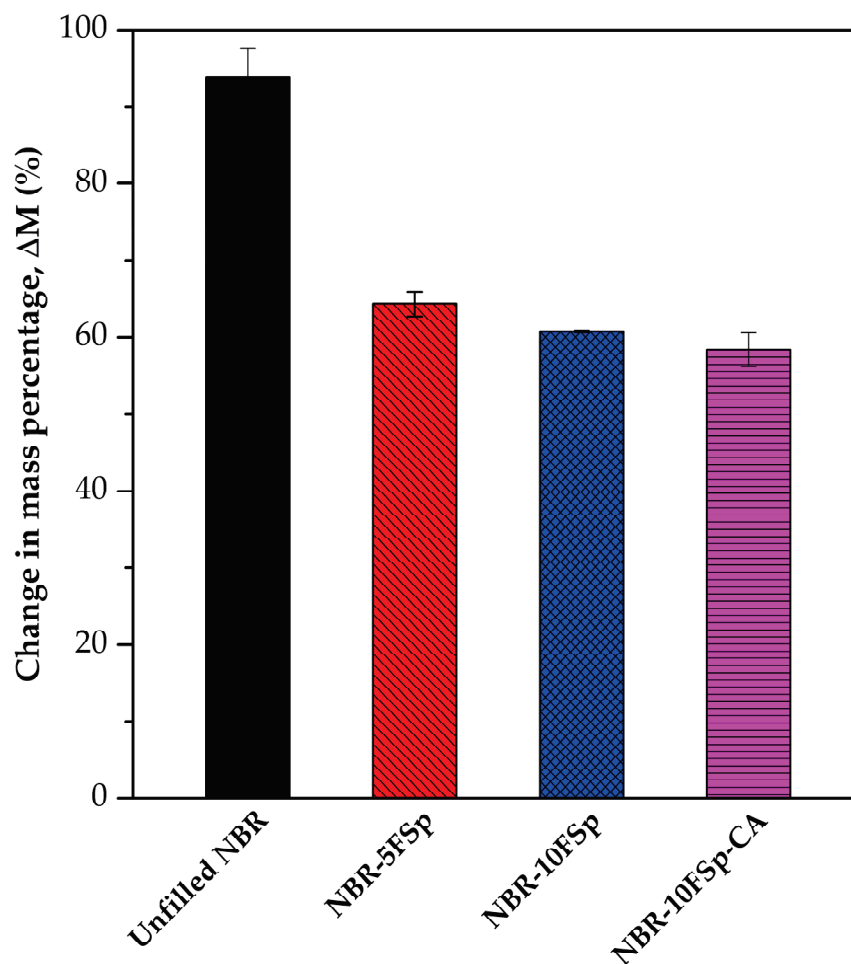
**Figure 7.** (a) Schematic representation of NBR/FSp/CA interactions and (b) Sketch of the interface interaction between FSp, CA, and NBR chains.

Figure 8 presents the FE-SEM images of tensile fracture surfaces of the NBR/FSp and NBR/FSp/CA composites. Generally, the morphological properties of the polymer composite are necessary to report in order to understand the dispersion, compatibility, and characteristics of the filler after the mixing and forming processes [13,32,39]. The unfilled NBR shows the smooth fracture surface without the particles on the surface (Figure 8a). On the other hand, the filled NBR with FSp shows the dispersion of FSp with some agglomerates on the rough fracture surface (Figure 8b,c). These characteristics tend to increase with increasing FSp content in NBR (Figure 8c). In general, the dispersion of the filler should be uniform with no agglomerates in a polymer composite. Nevertheless, the mechanical properties in terms of modulus, tensile strength, and hardness of filled NBR increase with increasing FSp content. This indicated that the FSp are effective reinforcement fillers for improving the mechanical properties of NBR, although the FSp exhibit non-uniform dispersion and have some agglomeration in the NBR matrix. Additionally, the roughness on the fracture surface indicates the resistance to fracture of the polymer composite due to the good mechanical interlocking between filler and matrix [32]. That corresponds to the results of tensile strength and percentage of elongation at break of filled NBR, which increase with increasing FSp content. In the case of the addition of CA, the NBR-10FSp-CA shows the image of fracture surface with similar characteristics as compared to the NBR-10FSp. However, the FSp on the fracture surface of NBR-10FSp-CA tend to be more embedded in the NBR matrix than the FSp on the fracture surface of NBR-10FSp (Figure 8d), which affects the increased tensile strength and the percentage of elongation at break of the NBR-10FSp-CA. This indicated that the CA increases the reinforcement efficiency of the FSp and NBR matrix.



**Figure 8.** FE-SEM images of (a) Unfilled NBR, (b) NBR-5FSp, (c) NBR-10FSp, and (d) NBR-10FSp-CA composites.

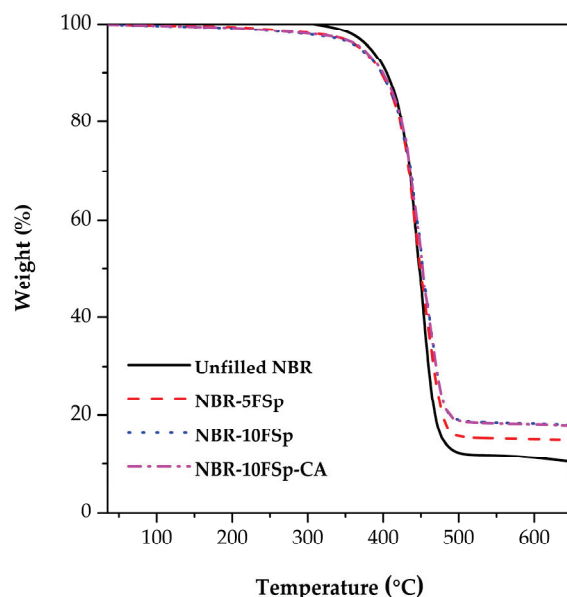
Figure 9 depicts the oil resistance of NBR/FSp and NBR/FSp/CA composites in terms of change in mass percentage. The oil resistance is an important parameter for polymer products that are used in petroleum applications. In general, the oil resistance depends on the interactions between solvent and polymer, crosslink density, and crystallinity of polymer [15,34]. The oil resistance of NBR is enhanced by adding the FSp, because the intermolecular forces between FSp and NBR increase the energy required to separate the NBR molecules for the penetration of oil molecules, which affects the decreased swelling percentages of filled NBR with FSp. In addition, this result also depends on the content of FSp added, which shows a decrease in the swelling percentage with increasing FSp content in NBR. Meanwhile, the value of the swelling percentage of NBR-10FSp-CA is no different when compared to NBR-10FSp, which indicates that the CA has no effect on this property. The values of the swelling percentage of unfilled NBR, NBR-5FSp, NBR-10FSp, NBR-10FSp-CA are 93.91%, 64.33%, 60.73%, and 58.41%, respectively. Therefore, although it is well known that NBR is a synthetic rubber that has excellent resistance to solvents and oils, the filled NBR with increasing FSp content increases the oil resistance efficiency.



**Figure 9.** Oil resistance of NBR/FSp and NBR/FSp/CA composites.

The TGA thermograms of NBR/FSp and NBR/FSp/CA composites are presented in Figure 10, and the thermal properties in terms of the initial degradation temperature ( $T_{\text{onset}}$ ), temperature at maximum weight loss level ( $T_{\text{max}}$ ), final degradation temperature ( $T_{\text{endset}}$ ), and residue percentages of NBR/FSp and NBR/FSp/CA composites are listed in Table 5, according to the TGA thermograms of NBR composites, which can divide the stages of weight loss into three stages: 35–350, 350–500, and 500–650 °C. The first stage shows a slightly decreased weight loss percentage in all samples, which is about 3% due to

the volatile water. Meanwhile, the decomposition of organic compounds from filler and polymer is the reason for the maximum weight loss in all samples that is shown in the second stage. However, the values of  $T_{\text{onset}}$  of NBR tend to increase with increasing FSp content, and the results of  $T_{\text{max}}$  and  $T_{\text{endset}}$  also show this tendency. The reason for these results is that the decomposition temperature of FSp is higher than the NBR matrix, so the FSp act as a heat barrier during the thermal decomposition process of NBR composites, which resembles the thermal properties reported in these reports [13,40,41]. According to these studies, the thermal stability of the polymer was increased by increasing the prepared hydroxyapatite content. Additionally, due to the incomplete decomposition of organic compounds in the second stage, all samples exhibit a slightly decreased weight loss percentage in the third stage. At a temperature of 650 °C, the values of residue percentage of NBR increased with increasing FSp content due to the remaining inorganic compounds from FSp in NBR composites. Nevertheless, the NBR-10FSp and NBR-10FSp-CA show similar results in their thermal properties. Therefore, the thermal properties of NBR are increased by adding FSp with increasing content, but the CA has no effect on these results.



**Figure 10.** TGA thermograms of NBR/FSp and NBR/FSp/CA composites.

**Table 5.** Thermal properties of NBR/FSp and NBR/FSp/CA composites.

Samples	$T_{\text{onset}}$ (°C)	$T_{\text{max}}$ (°C)	$T_{\text{endset}}$ (°C)	Residue (%)
Unfilled NBR	410	445	475	10.91
NBR-5FSp	411	446	482	14.04
NBR-10FSp	412	449	483	17.47
NBR-10FSp-CA	413	449	483	17.23

#### 4. Conclusions

FSp were successfully obtained from *Nile tilapia* fish scales biowaste and used to prepared NBR/FSp composites. The obtained FSp are B-type hydroxyapatite with a rod-like shape. The FSp were the effective reinforcement filler in the NBR matrix because it enhanced the tensile strength, oil resistance, and thermal properties of NBR. Moreover, the scorch time and optimal cure time of NBR also reduced with increasing FSp content, resulting in a shorter time to obtain the NBR product. The addition of CA gave the best properties, because the CA enhanced the tensile strength and percentage of elongation at break of NBR-10FSp. The obtained NBR composites filled with FSp are expected to be used



in sealing gadgets that can resist oil. In the future, the NBR composites will compare with other bio-fillers.

**Author Contributions:** Conceptualization, Y.R. and C.R.; methodology, N.B., Y.R. and C.R.; validation, J.W., Y.R. and C.R.; formal analysis, N.B., P.I., S.K., P.M. and O.W.; investigation, N.B., P.I., S.K., P.M. and O.W.; resources, Y.R. and C.R.; data curation, N.B., P.I., S.K., P.M. and O.W.; writing—original draft preparation, N.B. and P.I.; writing—review and editing, N.B., J.W., Y.R. and C.R.; visualization, Y.R. and C.R.; supervision, Y.R. and C.R.; project administration, Y.R. and C.R.; funding acquisition, Y.R. and C.R. All authors have read and agreed to the published version of the manuscript.

**Funding:** This research was funded by Thailand Science Research and Innovation (TSRI), Grant No. 160344.

**Data Availability Statement:** Not applicable.

**Acknowledgments:** The authors are grateful to Suranaree University of Technology (SUT), to Thailand Science Research and Innovation (TSRI), to the National Science, Research and Innovation Fund (NSRF), to the Research Center for Biocomposite Materials for Medical Industry and Agricultural and Food Industry for the financial support, and to the Chemical Innovation Co., Ltd. for supporting the chemicals.

**Conflicts of Interest:** The authors declare no conflict of interest.

## References

1. El-Sayed, A.-F.M. *Tilapia Culture*; CABI Publishing: Wallingford, UK, 2006.
2. Mohammad, A.W.; Kumar, A.G.; Basha, R.K. Optimization of enzymatic hydrolysis of tilapia (*Oreochromis Spp.*) scale gelatine. *Int. Aquat. Res.* **2015**, *7*, 27–39. [CrossRef]
3. Kittiphattanabawon, P.; Sriket, C.; Kishimura, H.; Benjakul, S. Characteristics of acid and pepsin solubilized collagens from Nile tilapia (*Oreochromis niloticus*) scale. *Emir. J. Food. Agric.* **2019**, *31*, 95–101. [CrossRef]
4. Akbay, İ.K.; Güngör, A.; Özdemir, T. Using fish scales (*Sardina pilchardus*) within ethylene-propylene-diene ter monomer rubber as bio-based filler. *J. Appl. Polym. Sci.* **2018**, *135*, 46698. [CrossRef]
5. Qin, D.; Bi, S.; You, X.; Wang, M.; Cong, X.; Yuan, C.; Yu, M.; Cheng, X.; Chen, X.-G. Development and application of fish scale wastes as versatile natural biomaterials. *Chem. Eng. J.* **2022**, *428*, 131102. [CrossRef]
6. Ikoma, T.; Kobayashi, H.; Tanaka, J.; Walsh, D.; Mann, S. Microstructure, mechanical, and biomimetic properties of fish scales from *Pagrus major*. *J. Struct. Biol.* **2003**, *142*, 327–333. [CrossRef]
7. Kim, S.-K.; Dewapriya, P. Biologically active compounds from seafood processing by-products. In *Biotransformation of Waste Biomass into High Value Biochemicals*; Springer: Berlin/Heidelberg, Germany, 2014; pp. 299–311.
8. Majhool, A.; Zainol, I.; Jaafar, C.; Jahil, M.; Ha, A.; Asaad, A.; Mezaal, F. Preparation of Fish Scales Hydroxyapatite (FshAp) for Potential Use as Fillers in Polymer. *J. Chem. Chem. Eng.* **2019**, *13*, 97–104.
9. Prasad, A.; Mohan Bhasney, S.; Sankar, M.R.; Katiyar, V. Fish Scale Derived Hydroxyapatite reinforced Poly (Lactic acid) Polymeric Bio-films: Possibilities for Sealing/locking the Internal Fixation Devices. *Mater. Today Proc.* **2017**, *4*, 1340–1349. [CrossRef]
10. Yasin, T.; Ahmed, S.; Yoshii, F.; Makuuchi, K. Effect of acrylonitrile content on physical properties of electron beam irradiated acrylonitrile-butadiene rubber. *React. Funct. Polym.* **2003**, *57*, 113–118. [CrossRef]
11. Degrange, J.-M.; Thomine, M.; Kapsa, P.; Pelletier, J.-M.; Chazeau, L.; Vigier, G.; Dudragne, G.; Guerbé, L. Influence of viscoelasticity on the tribological behaviour of carbon black filled nitrile rubber (NBR) for lip seal application. *Wear* **2005**, *259*, 684–692. [CrossRef]
12. Liu, J.; Li, X.; Xu, L.; Zhang, P. Investigation of aging behavior and mechanism of nitrile-butadiene rubber (NBR) in the accelerated thermal aging environment. *Polym. Test.* **2016**, *54*, 59–66. [CrossRef]
13. Nihmath, A.; Ramesan, M. Fabrication, characterization and dielectric studies of NBR/hydroxyapatite nanocomposites. *J. Inorg. Organomet. Polym. Mater.* **2017**, *27*, 481–489. [CrossRef]
14. Nihmath, A.; Ramesan, M. Synthesis, characterization, processability, mechanical properties, flame retardant, and oil resistance of chlorinated acrylonitrile butadiene rubber. *Polym. Adv. Technol.* **2018**, *29*, 2165–2173. [CrossRef]
15. Nihmath, A.; Ramesan, M. Hydroxyapatite as a potential nanofiller in technologically useful chlorinated acrylonitrile butadiene rubber. *Polym. Test.* **2020**, *91*, 106837. [CrossRef]
16. Hwang, W.G.; Wei, K.H.; Wu, C.M. Mechanical, thermal, and barrier properties of NBR/organosilicate nanocomposites. *Polym. Eng. Sci.* **2004**, *44*, 2117–2124. [CrossRef]
17. Shchegolkov, A.V.; Nachtane, M.; Stanishvskiy, Y.M.; Dodina, E.P.; Rejepov, D.T.; Vetcher, A.A. The Effect of Multi-Walled Carbon Nanotubes on the Heat-Release Properties of Elastic Nanocomposites. *J. Compos. Sci.* **2022**, *6*, 333. [CrossRef]
18. He, S.; Xue, Y.; Lin, J.; Zhang, L.; Du, X.; Chen, L. Effect of silane coupling agent on the structure and mechanical properties of nano-dispersed clay filled styrene butadiene rubber. *Polym. Compos.* **2016**, *37*, 890–896. [CrossRef]



19. Yangthong, H.; Pichaiyut, S.; Jumrat, S.; Wisunthorn, S.; Nakason, C. Mechanical, thermal, morphological, and curing properties of geopolymer filled natural rubber composites. *J. Appl. Polym. Sci.* **2019**, *136*, 47346. [CrossRef]
20. Kahavita, K.; Samarasekara, A.; Amarasinghe, D.; Karunanayake, L. Nanofibrillated cellulose reinforced polypropylene composites: Influence of silane (SI-69) surface modification. *Cellul. Chem. Technol.* **2020**, *54*, 789–797. [CrossRef]
21. Sae-oui, P.; Sirisinha, C.; Thepsuwan, U.; Hatthapanit, K. Roles of silane coupling agents on properties of silica-filled polychloroprene. *Eur. Polym. J.* **2006**, *42*, 479–486. [CrossRef]
22. Injorhor, P.; Trongsatitkul, T.; Wittayakun, J.; Ruksakulpiwat, C.; Ruksakulpiwat, Y. Nano– Hydroxyapatite from White Seabass Scales as a Bio– Filler in Polylactic Acid Biocomposite: Preparation and Characterization. *Polymers* **2022**, *14*, 4158. [CrossRef]
23. Kongsri, S.; Janpradit, K.; Buapa, K.; Techawongstien, S.; Chanthai, S. Nanocrystalline hydroxyapatite from fish scale waste: Preparation, characterization and application for selenium adsorption in aqueous solution. *Chem. Eng. J.* **2013**, *215*, 522–532. [CrossRef]
24. Deb, P.; Deoghare, A.B. Effect of Acid, Alkali and Alkali–Acid Treatment on Physicochemical and Bioactive Properties of Hydroxyapatite Derived from Catla catla Fish Scales. *Arab. J. Sci. Eng.* **2019**, *44*, 7479–7490. [CrossRef]
25. Pon-On, W.; Suntornsaratoon, P.; Charoenphandhu, N.; Thongbunchoo, J.; Krishnamra, N.; Tang, I.M. Hydroxyapatite from fish scale for potential use as bone scaffold or regenerative material. *Mater. Sci. Eng. C.* **2016**, *62*, 183–189. [CrossRef] [PubMed]
26. Sathiskumar, S.; Vanaraj, S.; Sabarinathan, D.; Bharath, S.; Sivarasan, G.; Arulmani, S.; Preethi, K.; Ponnusamy, V.K. Green synthesis of biocompatible nanostructured hydroxyapatite from Cirrhinus mrigala fish scale—A biowaste to biomaterial. *Ceram. Int.* **2019**, *45*, 7804–7810. [CrossRef]
27. Sricharoen, P.; Limchoowong, N.; Nuengmatcha, P.; Chanthai, S. Ultrasonic-assisted recycling of Nile tilapia fish scale biowaste into low-cost nano-hydroxyapatite: Ultrasonic-assisted adsorption for Hg<sup>2+</sup> removal from aqueous solution followed by “turn-off” fluorescent sensor based on Hg<sup>2+</sup>-graphene quantum dots. *Ultrason. Sonochem.* **2020**, *63*, 104966. [CrossRef]
28. Thommes, M.; Kaneko, K.; Neimark, A.V.; Olivier, J.P.; Rodriguez-Reinoso, F.; Rouquerol, J.; Sing, K.S. Physisorption of gases, with special reference to the evaluation of surface area and pore size distribution (IUPAC Technical Report). *Pure Appl. Chem.* **2015**, *87*, 1051–1069. [CrossRef]
29. Chen, K.; Zhang, T.; Chen, X.; He, Y.; Liang, X. Model construction of micro-pores in shale: A case study of Silurian Longmaxi Formation shale in Dianqianbei area, SW China. *Pet. Explor. Dev.* **2018**, *45*, 412–421. [CrossRef]
30. Muhammad, N.; Gao, Y.; Iqbal, F.; Ahmad, P.; Ge, R.; Nishan, U.; Rahim, A.; Gonfa, G.; Ullah, Z. Extraction of biocompatible hydroxyapatite from fish scales using novel approach of ionic liquid pretreatment. *Sep. Purif. Technol.* **2016**, *161*, 129–135. [CrossRef]
31. Rabiei, S.; Shojaei, A. Vulcanization kinetics and reversion behavior of natural rubber/styrene-butadiene rubber blend filled with nanodiamond—The role of sulfur curing system. *Eur. Polym. J.* **2016**, *81*, 98–113. [CrossRef]
32. Balan, A.K.; Mottakkunnu Parambil, S.; Vakyath, S.; Thulissery Velayudhan, J.; Naduparambath, S.; Etathil, P. Coconut shell powder reinforced thermoplastic polyurethane/natural rubber blend-composites: Effect of silane coupling agents on the mechanical and thermal properties of the composites. *J. Mater. Sci.* **2017**, *52*, 6712–6725. [CrossRef]
33. Srisuwan, L.; Jarukumjorn, K.; Suppakarn, N. Effect of silane treatment methods on physical properties of rice husk flour/natural rubber composites. *Adv. Mater. Sci. Eng.* **2018**, *2018*, 1–14. [CrossRef]
34. Nihmath, A.; Ramesan, M.T. Development of hydroxyapatite nanoparticles reinforced chlorinated acrylonitrile butadiene rubber/chlorinated ethylene propylene diene monomer rubber blends. *J. Appl. Polym. Sci.* **2021**, *138*, 50189. [CrossRef]
35. Inphonlek, S.; Bureewong, N.; Jarukumjorn, K.; Chumsamrong, P.; Ruksakulpiwat, C.; Ruksakulpiwat, Y. Preparation of Poly (Acrylic Acid-co-acrylamide)-Grafted Deproteinized Natural Rubber and Its Effect on the Properties of Natural Rubber/Silica Composites. *Polymers* **2022**, *14*, 4602. [CrossRef]
36. Keawkumay, C.; Jarukumjorn, K.; Wittayakun, J.; Suppakarn, N. Influences of surfactant content and type on physical properties of natural rubber/organoclay nanocomposites. *J. Polym. Res.* **2012**, *19*, 1–9. [CrossRef]
37. Wu, W.; Zuo, H. Used tire rubber powder/plant cellulose composites treated with coupling agent. *Cellulose.* **2016**, *23*, 1939–1947. [CrossRef]
38. Oprea, M.; Voicu, S.I. Recent advances in applications of cellulose derivatives-based composite membranes with hydroxyapatite. *Materials* **2020**, *13*, 2481. [CrossRef]
39. Nihmath, A.; Ramesan, M. Preparation, characterization, thermal, and electrical properties of chlorinated ethylene propylene diene monomer/hydroxyapatite nanocomposites. *Polym. Compos.* **2018**, *39*, 2093–2100. [CrossRef]
40. Rakmae, S.; Lorprayoon, C.; Ekgasit, S.; Suppakarn, N. Influence of heat-treated bovine bone-derived hydroxyapatite on physical properties and in vitro degradation behavior of poly (lactic acid) composites. *Polym. Plast. Technol. Eng.* **2013**, *52*, 1043–1053. [CrossRef]
41. Nihmath, A.; Ramesan, M. Fabrication, characterization, dielectric properties, thermal stability, flame retardancy and transport behavior of chlorinated nitrile rubber/hydroxyapatite nanocomposites. *Polym. Bull.* **2021**, *78*, 6999–7018. [CrossRef]

**Disclaimer/Publisher’s Note:** The statements, opinions and data contained in all publications are solely those of the individual author(s) and contributor(s) and not of MDPI and/or the editor(s). MDPI and/or the editor(s) disclaim responsibility for any injury to people or property resulting from any ideas, methods, instructions or products referred to in the content.

Review

# Role of Polymers in Microfluidic Devices

Laila A. Damiaty<sup>1,\*</sup>, Marwa El-Yaagoubi<sup>2</sup>, Safa A. Damiaty<sup>3</sup>, Rimantas Kodzius<sup>4,5</sup>, Farshid Sefat<sup>6,7</sup> and Samar Damiaty<sup>8,\*</sup><sup>1</sup> Department of Biology, Collage of Science, University of Jeddah, Jeddah 23890, Saudi Arabia<sup>2</sup> Department of Pure and Applied Chemistry, University of Strathclyde, 295 Cathedral Street, Glasgow G1 1XL, UK<sup>3</sup> Department of Pharmaceutics, Faculty of Pharmacy, King Abdulaziz University, Jeddah 21589, Saudi Arabia<sup>4</sup> Faculty of Medicine, Ludwig Maximilian University of Munich (LMU), 80539 Munich, Germany<sup>5</sup> Faculty of Medicine, Vilnius University, 03101 Vilnius, Lithuania<sup>6</sup> Interdisciplinary Research Centre in Polymer Science & Technology (Polymer IRC), University of Bradford, Bradford BD7 1DP, UK<sup>7</sup> Department of Biomedical and Electronics Engineering, School of Engineering, University of Bradford, Bradford, BD7 1DP, UK<sup>8</sup> Department of Chemistry, College of Sciences, University of Sharjah, Sharjah 27272, United Arab Emirates

\* Correspondence: ladamiati@uj.edu.sa (L.A.D.); sdamiati@sharjah.ac.ae (S.D.)

**Abstract:** Polymers are sustainable and renewable materials that are in high demand due to their excellent properties. Natural and synthetic polymers with high flexibility, good biocompatibility, good degradation rate, and stiffness are widely used for various applications, such as tissue engineering, drug delivery, and microfluidic chip fabrication. Indeed, recent advances in microfluidic technology allow the fabrication of polymeric matrix to construct microfluidic scaffolds for tissue engineering and to set up a well-controlled microenvironment for manipulating fluids and particles. In this review, polymers as materials for the fabrication of microfluidic chips have been highlighted. Successful models exploiting polymers in microfluidic devices to generate uniform particles as drug vehicles or artificial cells have been also discussed. Additionally, using polymers as bioink for 3D printing or as a matrix to functionalize the sensing surface in microfluidic devices has also been mentioned. The rapid progress made in the combination of polymers and microfluidics presents a low-cost, reproducible, and scalable approach for a promising future in the manufacturing of biomimetic scaffolds for tissue engineering.

**Citation:** Damiaty, L.A.; El-Yaagoubi, M.; Damiaty, S.A.; Kodzius, R.; Sefat, F.; Damiaty, S. Role of Polymers in Microfluidic Devices. *Polymers* **2022**, *14*, 5132. <https://doi.org/10.3390/polym14235132>

Academic Editor: Raffaella Striani

Received: 12 October 2022

Accepted: 22 November 2022

Published: 25 November 2022



**Copyright:** © 2022 by the authors. Licensee MDPI, Basel, Switzerland. This article is an open access article distributed under the terms and conditions of the Creative Commons Attribution (CC BY) license (<https://creativecommons.org/licenses/by/4.0/>).

**Keywords:** polymers; microfluidics; lab-on-chip; biomedical engineering; drug carrier; artificial cell; 3D bioprinting

## 1. Introduction

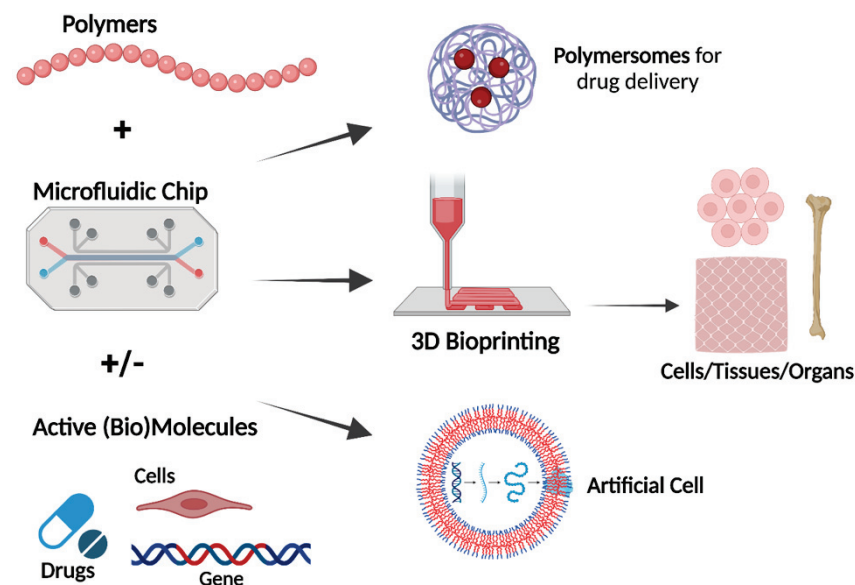
Polymeric biomaterials have been used to provide artificial matrices that can mimic the biological cell. This requires appropriate biophysical and biochemical properties, such as certain topography, stiffness, signaling, and growth factors [1]. Polymers are commonly used in tissue engineering scaffolds and wound dressing due to their ability to enhance cellular regeneration. Further, drugs are encapsulated in the polymeric particles to generate drug vehicles that can improve drug uptake into the disease sites and bioavailability. However, the physical and self-assembled properties of polymers, such as charges, composition, biodegradation, shape, size, and surface chemistry, play a dominant role in determining polymer behavior within biological environments [2]. Further, these interactions are directed by the physicochemical properties of the polymers in micro or nanostructures. The developed polymeric models are able to navigate the body, infect and transform cells, or repair damaged cells. The incorporation of cells into polymeric matrix can be performed by cell implantation into readily prepared polymer matrix. This strategy has a significant drawback, namely the lack of good integration between cells and polymer matrix. Another

alternative strategy relies on the fabrication the polymer matrix with encapsulated cells, which allows development of complex cellular microenvironments. New techniques, such as microfluidics, 3D printing, and electrospinning, enable direct cell integration into the matrix to mimic the matrix of desired tissue [1].

Microfluidics technology, also known as lab-on-chip technology, has been used as a platform for biomedical engineering applications [3]. Generally, a microfluidic chip is network of microchannels incorporated into the microenvironment by several holes throughout the chip. Microfluidics allow the integration of biological and chemical processes on a single platform. These microdevices allow controlling of the flow behavior of small volumes of fluids in micro-chambers in the range of tens to hundreds of micrometers. Microfluidics are widely used to synthesize polymeric particles for various applications involving drug carrier vehicles, as well as bioarchitecture models mimicking cell-like structures or extracellular matrix (ECM). Furthermore, recent studies have demonstrated the possibility of using microfluidic chips as an artificial cell chassis. Depending on the application, glass or polymer can be used to manufacture microfluidic devices and several parameters should be taken into consideration in the fabrication of a microfluidic chip, such as the compatibility of constructed materials with various solvents and channel geometries [4–7]. Polymer-based chips are usually selected due to their cost efficiency, suitable optical transparency, elasticity, and appropriate mechanical and chemical properties [8]. Several polymers, such as polydimethylsiloxane (PDMS) and poly(methyl methacrylate) (PMMA), are employed to fabricate microfluidic devices [3]. However, polymers have some limitations regarding their properties, including operation temperature range limitations, higher autofluorescence, and the limited availability of surface modification techniques [9]. The fabrication of polymer microfluidic devices is relatively simple, and hazardous etching reagents are not needed to create the polymer microstructure [10].

It is common to use natural polymers, such as polysaccharides and bacterial polyesters, to generate polymer-based therapeutics, while it is common to use synthetic polymers as building blocks for microfluidic devices. Figure 1 shows different applications of utilizing polymers and microfluidics. Biodegradable and bioreducible polymers that are used for polymeric drug/gene delivery systems are rapidly emerging in pharmaceutical fields. Combining therapeutic agents with polymers can improve their safety and efficacy by controlling the rate, time, and preferentially delivers the therapeutic agents to the target site in the body [11]. Combining microfluidic devices and polymers presents unique advantages for the development of efficient carriers of a wide range of drugs and genetic materials (e.g., polymersomes). Microfluidic technology enables the production of highly stable, uniform, monodispersed particles with higher encapsulation efficiency [5]. Furthermore, many studies showed the possibility of using polymer-based bioinks in 3D printing for applications in tissue engineering and regenerative medicine. There are several natural (e.g., alginate, collagen, agarose) and synthetic (e.g., Pluronic and poly(ethylene glycol) (PEG)) polymeric biomaterials that are used as bioinks for 3D printing based on their ability to support cell growth, mechanical properties, and printability. Combining of cells, biomedical polymers and biosignals is the basic requirement to develop 3D tissues or organ structures [12]. The fabrication of vessel-like microfluidic channels is an example of organ fabrication and thick tissue. Besides supporting the mechanical integrity, the printed 3D microfluidic network enables fluid transport. The microfluidic architecture allows media transport, including nutrients, oxygen, water, and removal of the waste in the same manner [13]. Recent developments in droplet microfluidics allowed the creation of versatile vesicles with a structure that resembles the biological membrane. These artificial cell-like structures with well-defined size enable the implementation of various biological reactions within a compartment separated by a membrane that mimics a natural cell membrane [3]. In this perspective, this review deals with polymers used to either fabricate microfluidic devices or create functional particle/matrix models using polymers and microfluidic chips. The review first provides an overview of the different types of polymers. Then, it highlights some of the recent advances in the design of microfluidics and polymers for various

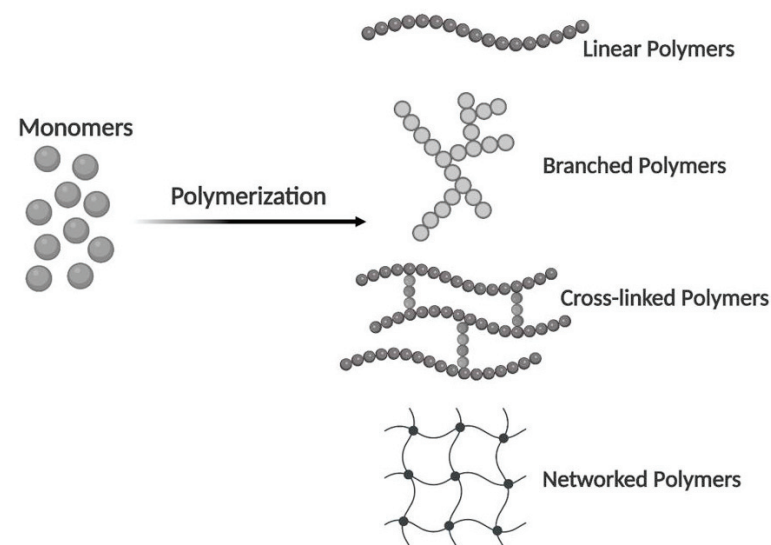
biomedical engineering applications, including drug delivery, 3D bioprinting, and artificial cell-like structures.



**Figure 1.** Utilizing of microfluidic chips and polymers for various applications (Created with Biorender.com, accessed on 12 October 2022).

## 2. Polymers Used in Microfluidic Devices

A single polymer unit may be composed of hundreds or millions of monomers. They have one of the four basic polymer structures: linear, branched, cross-linked, or networked (Figure 2). The two types of polymers are natural and synthetic. Natural polymers can be extracted from biological systems such as plants, algae, microorganisms, and animals, which have a similar ECM structure to native tissues. Synthetic polymers are similar to natural polymers, but they are much cheaper, can be produced at large scale, and have long shelf life compared with natural polymers. As such, generally, they present good cellular attachment, which improves the cellular behaviors and prevents immunological reactions [1,14].



**Figure 2.** From monomers to polymers. Linear, branched, cross-linked, and networked structures in polymers (Created with Biorender.com, accessed on 12 October 2022).



Choosing the right material is the first and most critical step in designing a successful microfluidic device. A wide range of constraints and requirements dictates the selection of the material for a specific component. The design of the device, the compatibility of the material with the chemicals, as well as the applied temperature and pressure are crucial considerations in material selection. Additionally, the final application of the device is an essential consideration. For example, devices intended for in vivo applications in tissue engineering must be nontoxic, exhibit a slow and predictable degradation rate, have nontoxic and safe degradation products, and potentially capable of mimicking certain physical and chemical properties of the native ECM or of supporting other agents that play such roles. The architecture of the device can also influence the choice of materials. For example, in devices that contain microfluidic systems, the materials have to be mechanically robust but have a controlled degree of flexibility [15,16]. The material also has to be compatible with microfabrication techniques, easily processed in mild conditions, and cheap to manufacture, among others [17]. Polymers are classified into two major groups: biodegradable and biostable polymers. These two types of polymers are commonly used as scaffolds or bioactive coatings in biomedical applications [8,15]. The next section focuses on these two classes of polymers for the manufacture of microfluidic devices and their biomedical applications.

### 2.1. Biodegradable Polymers

Sustainable polymers from various renewable resources can be directly obtained from biomass (proteins and polysaccharides), or through chemical modifications of natural polymers [18]. However, there are many sources of natural and synthetic biodegradable polymers. Natural polymers are derived from natural raw materials and available in large quantities while synthetic polymers are synthesized by the chemical polymerization of bio-monomers.

#### 2.1.1. Natural Biodegradable Polymers

In this section, we distinguish between natural polymers, which are produced outside the human body (xenobiotic polymers), and proteins, which are native to the human body, such as the ECM proteins. The use of natural biopolymers in microfluidics provides many advantages, such as surface chemistry biocompatibility and having the same mechanical properties of the native proteins of interest [16,19].

Natural polymers, such as chitosan, alginate, and gelatin, are also biologically derived and biodegradable polymers. They are used in the manufacturing of biodevices that are intended to interact with the biological systems of the human body. The crosslinking ability of these natural polymers, which is induced by physical and chemical stimuli, makes them ideal for the preparation of microgels for microfluidic devices. The two natural biopolymers, alginate and gelatin, were used as substrates to make two types of hydrogel-based microfluidics. Subsequently, the fabricated hydrogel microchannels can be used as platforms to provide 3D cell culture environments for mammalian cells: fibroblasts and vascular endothelial cells. The developed enclosed microchannel models are simple and reproducible and do not require complicated operations [16,19].

One class of natural biomaterials that is a good candidate for microfluidic devices is silk fibroin (SF) [20]. SF protein, originally found in the silkworm *Bombyx mori*, is a high-molecular-weight protein that primarily consists of hydrophobic residues. This protein is approved by Food and Drug Administration (FDA) for many medical applications, such as drug delivery and tissue engineering. SF can be easily processed to form hydrogels, films, and nanofiber mats under mild conditions [21]. In recent years, SF has also been used to fabricate microfluidic devices due to its excellent biocompatibility, robust mechanical properties, and slow proteolytic degradation rate [16,20]. The solubility and mechanical properties of SF materials are linked to its secondary structure. Whereas self-assembled  $\beta$ -sheet structures are responsible for the mechanical stability and water insolubility of SF, the amorphous regions, including random coil,  $\alpha$  helix, and  $\beta$  turn structures, contribute



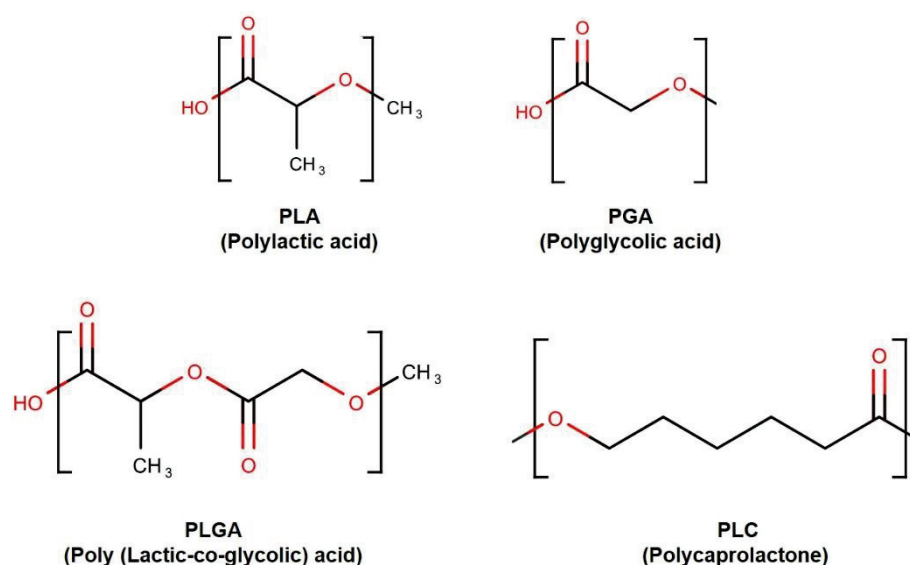
to the elasticity and solubility of the biomaterial. Thus, SF-based microfluidic fabrication strategies allow the rapid and scalable production of devices without the need for harsh processing conditions that require cytotoxic reagents. Mao et al. used SF and chitosan to construct porous SF–CS scaffolds with predefined microfluidic channels. The generated model showed structural properties suitable for seeding and growth of hepatic cells. Mass transport and uniform cell distribution within the 3D scaffold were successfully achieved [19].

In addition to all the above-mentioned advantages of natural polymers, the inclusion of natural ECM proteins into microfluidic devices allows the reproduction native cell–biomaterial interactions *in vitro* [22]. The use of ECM proteins is crucial in controlling cell function overall via other physicochemical mechanisms such as specific cell binding domain sequences. Proteins, such as fibronectin, vitronectin, and collagen I, contain the amino acid sequence of arginine–glycine–aspartic acid (RGD), which supports the adhesion of cells and to control stem cell differentiation. For example, Arik et al. reported the fabrication of a collagen-I-based membrane incorporated in an organ-on-chip device [23]. The membrane demonstrated permeability, as well as the adhesion of both endothelial and epithelial cells. Moreover, they characterized the degradation and remodeling of the basement membrane by a protease. Natural proteins offer an environment that more closely mimics that of the body and more realistically mimics the cell–ECM interactions, which are crucial for tissue engineering. However, these biomaterials have a complex structural composition that prevents complete control over their composition and other factors, such as molecular weight, immune response, degradation, and mechanical properties. As an alternative, scientists have focused on the development and use of synthetic polymers, which have more tunable properties [22].

### 2.1.2. Synthetic Biodegradable Polymers

Synthetic polymers were proposed as ideal candidates for the fabrication of biodegradable microstructures, including microfluidic biomaterials [16,24]. Poly(glycolic acid) (PGA), poly(lactic acid) (PLA), and their copolymer poly(lactic acid-co-glycolic acid) (PLGA), belong to the linear aliphatic polyesters family [25] (Figure 3). This polymer family is one of the most widely used in tissue engineering and drug delivery [25,26]. These polymers have several advantages, such as low cost, ease of processing, and well-characterized biological behavior. These polymers (PLA, PGA, and PLGAs) are among the few synthetic polymers approved by the U.S. FDA for certain human clinical applications [26]. These polymers degrade through the hydrolysis of the ester bonds [27]. Although PGA and PLA belong to the same family, they also display distinct properties. For instance, because of its very hydrophilic nature, PGA rapidly degrades in aqueous solutions. However, PGA and PLA show the same behavior *in vivo*: they lose mechanical integrity in a period between two and four weeks [28]. Conversely, PLA contains a methyl group, which renders the chains more hydrophobic and hence reduces the affinity to water, and displays a slower hydrolysis rate (months to years) [28]. This class of biodegradable polymers is suitable for microfluidics because of the wide range of tunable properties [27]. They can be modulated by adjusting the lactide-to-glycolide ratio. The physical properties of the copolymer PLGA are defined by the properties of both pure PGA and PLA [25]. The presence of PLA makes it more hydrophobic than PGA. Hence, lactide-rich PLGA copolymers are less hydrophilic and more slowly degrade. Additionally, PLA exhibits relatively a high glass transition temperature ( $T_g = 50\text{--}80\text{ }^\circ\text{C}$ ) and melting point ( $T_m = 173\text{--}178\text{ }^\circ\text{C}$ ). PLGA blends of various copolymer ratios exhibit a reduced phase transition temperature ( $T_g$ , PLGA75/25 =  $54\text{ }^\circ\text{C}$ ) and melting point ( $T_m$ , PLGA75/25 =  $80\text{ }^\circ\text{C}$ ) [29]. Poly(caprolactone) (PCL) is another example of an aliphatic polyester used in microfluidics. PCL demonstrates advantageous properties for replica molding strategies, such as a low melting point ( $T_m = 57\text{ }^\circ\text{C}$ ) and low glass-transition temperature ( $T_g = -62\text{ }^\circ\text{C}$ ) [30]. PCL can be degraded by micro-organisms as well as by the hydrolysis of its ester linkage in physiological conditions [31]. However, PCL materials have a substantially slower biodegradation rate than PLA and PGA, mak-

ing it suitable for the use in long-term implantable systems. Biodegradable cell-support scaffolds play an important role in the growth of engineered tissue and the delivery of biologically active agents. Therefore, the concept of biodegradable microfluidic devices formed by various biodegradable polymers has attracted considerable research attention. For example, microstructured PLGA films were used to construct a high-resolution and high-precision 3D device. The developed device allows diffusion distance reduction in cell-seeded scaffolds with convective transport [32]. PLA microchannels have been widely generated by 3D printing. Kadimisetty et al. developed a microfluidic immunoarray using PLA and a 3D printer. The fabricated device was low cost and could sensitively detect prostate cancer biomarker proteins [33].



**Figure 3.** Synthetic bio-degradable polymer structures.

Poly(1,3-diamino-2-hydroxypropane-co-polyol sebacate) (APS) is another biodegradable elastomeric polymer used to construct microfluidic scaffolds. The simple microchannel network design exhibited a very low degradation rate while retaining the elastomeric properties required for tissue scaffold applications [24].

## 2.2. Biostable Polymers

PDMS is a mineral–organic polymer structurally composed of silane–oxygen backbones covered with alkyl groups. Depending on the size of the monomer chain, non-cross-linked PDMS may be almost liquid (low amount of  $n$  monomer) or semi-solid (high amount of  $n$  monomer) [34]. The high level of viscoelasticity displayed by the polymer chain is due to the siloxane bonds in the polymer structure. After cross-linking with a curing agent, PDMS becomes a hydrophobic elastomer [34]. One of the main reasons for the success of PDMS in microfluidics is the ease of PDMS device fabrication, which also allows mass production. Among many other methods, PDMS microchips can be fabricated through microscale molding processes [35]. For example, a silicon wafer with patterns can be used as a mold master. Prepolymer PDMS is poured into the mold master. Then, cured PDMS is peeled off from the master to be pasted on a flat plate, i.e., PMMA, glass, etc. [34]. The flat support should be drilled in advance to provide access ports for the introduction of reagents and samples. PDMS can precisely replicate structures down to the submicron size [36]. Due to the favorable optical properties of PDMS (almost no absorbance in the visible wavelength range), fluorescent dyes are widely used for the detection and quantification of molecules in most biochemical analyses. In addition, PDMS is transparent, biocompatible, nontoxic, and displays high gas permittivity, so has been traditionally used as a biomaterial in catheters, insulation for pacemakers, and ear and nose implants [10].

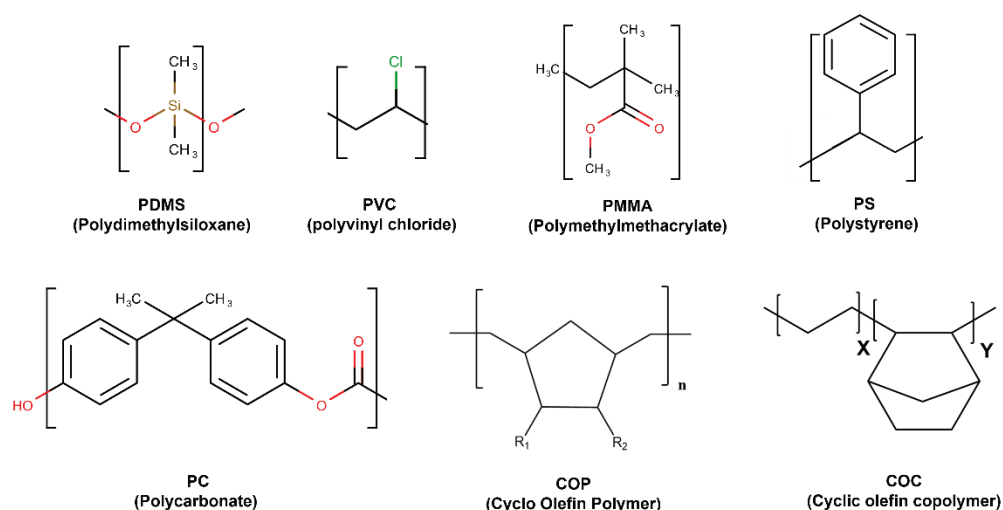
The combination of its elastic properties, easy processability, and the other properties mentioned above make PDMS an ideal candidate for use in microfluidic devices for biomedical and cell applications.

Many studies have been performed to further examine the compatibility of PDMS with both microfluidic technology and biomedical applications [37]. In terms of microfluidic technology, the effects of the structure and surface of PDMS in widely used microfluidics methods, such as spin coating and chemical immersion, on different liquid chemicals have been studied. Successful spin-coating of PDMS depends on the crosslinking ratio; increased amounts of crosslinker agent in the formulation decrease film thickness. Additionally, whereas chemical immersion (solvents such as alcohol, toluene, acetone, etc.) does not result in major changes in the surface hydrophilicity of PDMS, macrotecture distortion and destructions are observed with strong acids (hydrofluoric, nitric, sulfuric, and hydrofluoric acids) and bases (potassium hydroxide). For biomedical applications, the effect of oxygen plasma and sterilization and the exposure to tissue culture media was also explored. Oxygen plasma exposure increases PDMS surface hydrophilicity, whereas a following exposure to air leads to hydrophobic recovery. UV and alcohol sterilization do not affect the PDMS surface microtexture, element concentration, hydrophilicity, or mechanical properties. Finally, immersion in tissue culture media increases the surface concentration of oxygen relative to silicon [38].

Despite all these advantages, the use of PDMS is limited due to challenges encountered in microfluidics. For example, incomplete curing of PDMS leaves uncrosslinked oligomers within the material, which can leach out and contaminate the culture medium. Other problems, such as incompatibility with some organic solvents, water evaporation, channel deformation, and adsorption of biomolecules onto channel walls, present severe limitations to the use of PDMS for microfluidics applications [39].

### Thermoplastics

Thermoplastics are plastic polymer materials that have emerged as a commercially viable material. Their use has recently increased, being widely applied to fabricate microfluidics platforms for biomedical applications. The most commonly used thermoplastics are PMMA, polycarbonate (PC), polystyrene (PS), polyvinyl chloride (PVC), Cyclo-olefin-copolymer (COC), and Cyclo-olefinpolymer (COP) [39,40] (Figure 4).



**Figure 4.** Most used thermostable polymers structures for microfluidic chips.

Because of their linear structure, their thermoplastic rigidity resists temperature and pressure changes. The properties of the most common thermoplastics used for chips fabrication are summarized in Table 1. Thermoplastic-based materials have good physical and chemical characteristics, such as high chemical and mechanical stability; low water-

absorption capacity; acid/base resistivity; and are suitable for mass production at low cost. In term of fabrication, thermoplastics can be softened after exposure to heat at their transition temperature ( $T_g$ ), making them processable around this temperature. During cooling, the softened polymer hardens, and it takes the shape of the container or mold, without any chemical change. They can be reshaped multiple times by reheating, which is important for the molding and microfluidics fabrication process [41].

**Table 1.** Properties of the most used biocompatible thermoplastics in the microfluidic field.

Thermoplastics	Young's Modulus (Gpa)	$T_g$ ( $^{\circ}$ C)	$T_m$ ( $^{\circ}$ C)	Solubility Parameter $\delta$ (MPa) <sup>1/2</sup>	Water Adsorption (%)	O <sub>2</sub> Permeability ( $\times 10^{-13}$ cm <sup>3</sup> .cm cm <sup>-2</sup> s <sup>-1</sup> Pa <sup>-1</sup> )	Transparency	Auto-fluorescence	Study
Polymethylmethacrylate (PMMA)	2.4–3.4	105	250–260	20.1	0.1–0.4	0.1	Transparent	Low	[42]
Polyethylene terephthalate (PET)	2–2.7	70	255	20.5	0.16	0.03	Transparent	Medium	[43]
Polypropylene (PP)	1.5–2	–20	160	16.3	0.01–0.1	1.7	Both opaque and transparent	Medium	[41,44]
Polystyrene (PS)	3–3.5	95	240	18.7	0.02–0.15	2	Transparent	High	[45]
Polycarbonate (PC)	2.6	145	260–270	19.4	0.23	1	Transparent	High	[41]
Polyvinyl chloride (PVC)	2.4–4.1	80	100–260	19.4	0.04–0.4	0.04	Transparent	High	[46]
Polyamide (Nylon)	2.5	47–60	190–350	28	1.6–1.9	0.03	Transparent	High	[47]
Polytetrafluoroethylene (PTFE)	0.4	115	326	12.6	0.005–0.01	3	Transparent	High	[48]
Polyetheretherketone (PEEK)	4–24	143	343	21.9	0.1–0.5	0.1	Opaque	N/A	[49]

One of the first properties to consider in cell biology is biocompatibility. According to Table 1, most of the thermoplastics are biocompatible. However, for long-term applications, some of the materials can be problematic. For example, polycarbonates can be experience surface erosion during in vivo applications. In addition, bisphenol A (BPA), which is hazardous in food contact situations, might be released during hydrolysis.

PVC can release toxic gases during manufacturing, and nylon is a heat-sensitive material. Resistance to solvents is also a main criterion that must be considered for microdevice fabrication and biomedical applications (sterility). PS is widely used in molecular and cell biology studies due to its biocompatibility and its high resistivity to alcohols, polar solvents, and alkalis [50]. PMMA is affected by ethanol, isopropyl alcohol, acetone, and other important solvents used in microfabrication and sterilization [51]. When working with cell cultures, low water absorption is beneficial because the cells consume more oxygen from water, which can be limited by the absorption of water onto the polymer surface.

The optical properties of the selected material (e.g., transparency and autofluorescence) are crucial. Consequently, PMMA, polyethylene terephthalate (PET), and polypropylene (PP) are less suitable for applications that require further reactions inside the microfluidic devices under a microscope. Additionally, PC displays high autofluorescence, so PC is difficult to use when working with fluorescently labelled cells or materials. In contrast, PS has high transparency, and the surface of PS is suitable for long-term cell studies [41]. Table 2 highlights some studies that used polymers as a chassis or to functionalize sensing surface.

**Table 2.** Some studies using polymers for microfluidics devices for various biological applications.

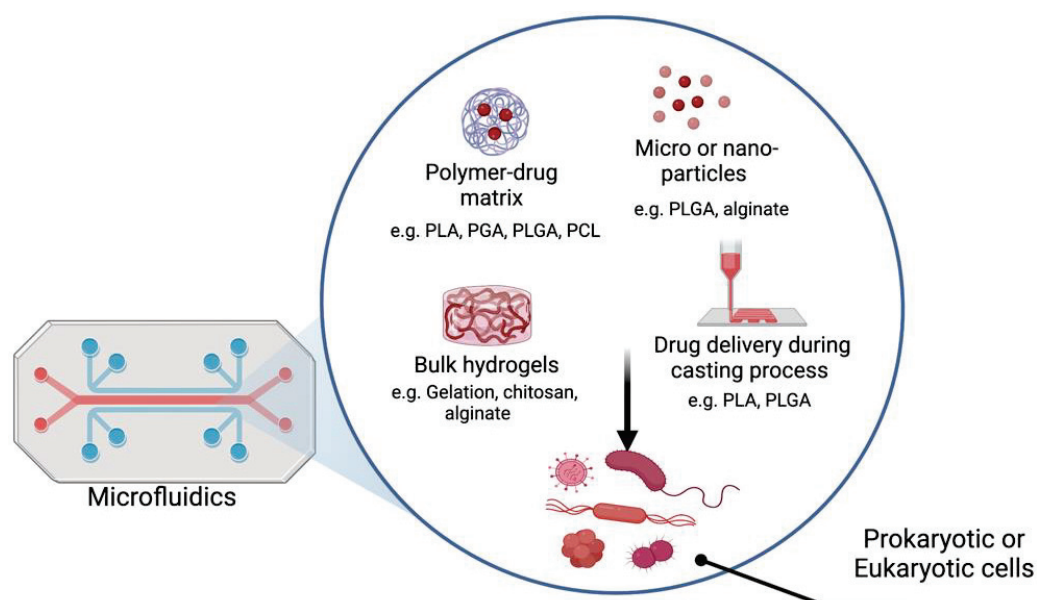
Polymer	Cell Type	Application	Study
Polydimethylsiloxane (PDMS)	Alveolar epithelial cells, Macrophages, <i>Mycobacterium tuberculosis</i>	Rapid and uncontrolled bacterial growth in the mammalian cells can cause a surfactant deficiency in the lung-on-chip infection model.	[52]
PDMS, Carboxymethylated cellulose nanofibrils (CNF)	HCT 116 colon cancer cell	The functionalized chip was able to capture the cancer cells from the whole blood with >97% efficiency which may use as rapid diagnostic tool.	[53]
PDMS, Dimethylallylamine (DMAA)	<i>Escherichia coli</i>	The encapsulated bacteria with a membrane with a selective permeability of tetracycline cultured on the PDMS composition and functionalized with DMAA inhibit the bacterial growth which can be used as a diagnostic tool to evaluate the bacterial resistance.	[54]
PDMS microchannel layer and PDMS membrane	Human mesenchymal stem cells (hMSCs)	The two layer-microfluidic chips with three different stretching modes (uniaxial, radial, and gradient) showed different cell responses which may enhance the study of cells on biomaterials under various stretching stimuli.	[55]
Combination between PDMS and polymer substrate using a PrimeCoat-Epoxy adhesive layer by selective stamp bonding	Human lung epithelial cells	The cells cultured inside the device showed a similar viability comparing to the conventional cell culture technique.	[56]
Rapidly Integrated Debubbler (RID) from PMMA	human umbilical vein endothelial cells	The RID module showed a potential method to prevent the bubble entry into the microfluidics which may lead to device delamination and cell damage.	[57]
PDMS chambers separated by thin layer of polyester (PE) membrane	Primary human small airway epithelial cells	The microfluidics airway system showed a highly controllable and readily accessible physiologic pulmonary environments tailored for lung epithelial cells.	[58]
Combination of PDMS hydrophilic surface treatment and vacuum filling system equipped with bubble trap.	Mouse pancreatic islets	The system showed normal cell viability and morphology, normal insulin secretion, and normal intracellular calcium signaling.	[59]
PDMS	Endothelial cells	The actin filaments alignments directions of the cells cultured in microfluidics channels was significantly higher comparing to the cells cultured in the static condition.	[60]
PDMS-glass	Human umbilical vein endothelial cells (VECs)	The synergistic effect of wall shear stress (WSS) and adenosinetriphosphate (ATP) signals played a vital role in the VEC Ca <sup>2+</sup> signal transduction on the microfluidic device.	[61]
Photopolymer and chitosan	Hepatic oval cells (HOCs)	Electrochemical sensor is developed to rare cancer cells. Photopolymer is used to construct a 3D-printed continuous flow system and a chitosan film is served as a scaffold for the immobilization of anti-OV6-antibodies.	[62]

### 3. Polymers as Drug Carriers

Generally, a drug is any bioactive molecule, including medicine, small molecules, and proteins, e.g., growth factors and nucleic acids [63]. Different polymers have been used in drug delivery approaches: i. a drug can be directly incorporated onto scaffolds throughout the casting process [64], ii. bulk hydrogels [65,66], iii. drug reversibly and covalently conjugated to the matrix [67], iv. micro- or nanodrug particles spread on the



surface [68–70]. However, all of these methods have advantages and disadvantages in terms of drug stability [63]. When manufacturing new drug delivery system, different factors should be taken into consideration for instance cost, efficacy, and properties differences. Advances in manufacturing techniques may produce more complex drug carrier designs to allow specific drug release targeted to a particular disease [71]. Using a microfluidic platform approach can allow generation of drug carriers that can meet the sophisticated requirements of biomedical applications [72] (Figure 5).



**Figure 5.** A scheme of different approaches of using polymer for drug delivery. Microfluidics control synthesis of various drug delivery systems. Subsequently, microfluidic chips can be used for cell culture and drug toxicity screening (Created with Biorender.com, accessed on 12 October 2022).

Drug delivery devices have potential to be used for various clinical applications, such as tissue regeneration, diabetes, oncology, and infectious diseases. Moradikhah et al. used a cross-junction microfluidic device to prepare alendronate-loaded chitosan nanoparticles. They showed that this system substantially enhanced the osteogenic differentiation of human adipose MSCs, so can be a suitable component of bone tissue engineering scaffolds [73]. Mora-Boza et al. illustrated that their fabricated hMSC-laden microcarriers based on in situ ionotropic gelation of water-soluble chitosan in a microfluidic device using antioxidant glycerolphytate and tripolyphosphate maintained cell viability over time and increased the secretion of paracrine factor [74]. An example of oral delivery drug was examined by Jaradat et al.; insulin was encapsulated into various PLGA nanoparticles prepared by the microfluidic technique. They found that the mucopenetrating heparin sulfate-conjugated PLGA nanoparticles enhance insulin permeability in a triple-cultured intestinal model compared with unmodified and free insulin nanoparticles [75]. Another model developed by Damiani et al. used PLGA to generate indomethacin-loaded PLGA microparticles employing a 3D flow-focusing microfluidic chip. This model not only successfully incorporates indomethacin, which is a poorly water-soluble drug and nonsteroidal anti-inflammatory drug, but the authors also developed an artificial neural network as in silico tool to predict size microparticles [76,77].

An example of using polymers in drug delivery in cancer is biodegradable polymeric nanocapsules. Oxaliplatin, irinotecan, and 5-fluorouracil chemotherapy drugs were encapsulated and carried on a coaxial glass capillary microfluidic device, which the potential for targeting tumors as the drug release could be controlled [78]. Hong et al. reported that the synthesized amphiphilic tri-chain tricarballylic acid-poly ( $\epsilon$ -caprolactone)-methoxypolyethylene glycol (Tri-CL-mPEG) and enzyme-targeted tetra-chain pentaerythritol-

poly ( $\epsilon$ -caprolactone)-polypeptide (PET-CL-P) using microfluidics continuous granulation technology improved the bioavailability and antitumor effects of curcumin in a mouse model [79]. A recent review by Salari et al. provides a comprehensive assessment of studies in the field of polymer-based drug delivery for anti-cancer therapy. In their study, 71 papers were investigated, and they conclude that the polymeric nanoparticles have influential roles in cancer treatment comparing to the conventional chemotherapy. Polymeric nanoparticles were able to reduce the cytotoxicity following chemotherapy drug administration, enhance therapeutic agents solubility, and inhibit tumor growth rate [80].

As bacterial infections are posing a major threat to human health, in addition to increasing antibiotic resistance, new methods for bacterial detection are necessary to reduce disease spread. Recently, advances in antibiotic treatment have focused on the targeted delivery of antibiotics, as well as antibiotics alternatives, such as antimicrobial polymers, peptides, nucleic acids, and bacteriophages [81]. Borro et al. reported that by using polymyxin B-alginate- $\text{Ca}^{2+}$  microgels prepared by 3D printing, the microfluidic mixer affected the charge contrast and composition of the microgel formation and the interaction with bacteria-mimicking liposomes at different ionic strengths [82]. Additionally, a P-based nanoparticles delivery system was used as therapy against bacterial biofilm infections. Huang et al. used PLGA-based nanoformations combined with carbon quantum dots (CQDs) using a microfluidic flow-focusing pattern to load different types of antibiotics, e.g., azithromycin and tobramycin. They found that the azithromycin-loaded CQD-PLGA hybrid nanoparticles showed synergistic chemo-photothermally antibiofilm effects against *Pseudomonas aeruginosa* [83]. Norries et al. illustrated that the hydrogel developed from the poly(2-hydroxyethyl methacrylate) (PHEMA) and coated with ciprofloxacin antibiotic reduced the biofilm production of *Pseudomonas aeruginosa* [84].

#### 4. Polymers as Bioink for 3D Printing

Three-dimensional (3D) printing is a development technique that has been used during the last decade to produce microfluidic devices. It has many advantages such as low cost, enabling the easy design of complex 3D structures and rapid prototyping. However, 3D printing has some limitations regarding the size of the microchannels and some final steps that are related to the laborious fabrication [85].

Different methods can be used to produce printed porous materials: i. curing a porous monolithic polymer sheet into the chosen pattern with photolithography, ii. screen-printing silica gel particles with gypsum, and iii. dispensing silica gel particles with polyvinyl acetate binder using a 3D printer. All three approaches can be successfully used in microfluidics [86].

Hydrophilic and hydrophobic polymers can be used to generate 3D-printed microfluidic droplets to prevent water-in-oil or oil-in-water droplets from sticking to the interior device surfaces. Warr et al. investigated two different approaches to avoid this issue: First, different resins were tested to evaluate their suitability for droplet formation and material properties. They found that the hexanediol diacrylate/lauryl acrylate resin forms the best hydrophobic solid polymer that prevents aqueous droplets from attaching to the device wall. Second, they formed a fully 3D microfluidic annular channel-in-channel geometry that forms droplets that do not contact channel walls. As such, this geometrical approach can be used with hydrophilic resins [87].

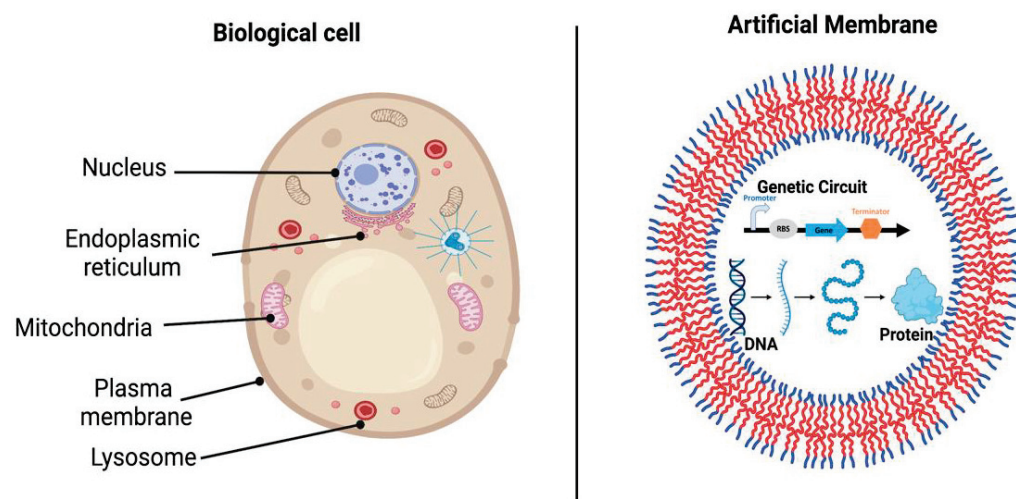
Distler et al. found that 3D-printed hydrogel is more electroactive and cytocompatible and enhances cell adhesion and proliferation compared with a 2D flat hydrogel. This kind of hydrogel formulation has shown promise in in vitro studies, cell therapy, and assisted tissue engineering electrical stimulation [88]. Wright et al. used a hydrogel composed of calcium crosslinked alginate (polypyrrole-alginate composite) as bioink for tissue engineering. They found that PC12 neural cells adhere and proliferate slightly better than alginate scaffold alone [89]. A compensation between metallic and polymer materials was used to fabricate a novel complex 3D structure. A soft polymer was cast and cured into a 3D-printed thin-shelled metallic mold, followed by metallic mold etching in an acidic

solvent, which did not affect the soft polymer. This approach provided various polymeric complex structures [90].

At present, organ failure is a worldwide issue, and allograft organ transplantations are seriously limited due to donor organ shortages, immune rejection, and ethical conflicts, so finding an alternative solution is crucial [91–93]. Several polymers have been used for bioartificial organ manufacturing with different types of cells, e.g., stem cells, various growth factors, and vascular and neural networks. However, 3D bioprinting technology is a challenging engineering approach. Cooperation is required between different fields, such as biomaterials, biology, medicine, physics, chemistry, bioinformatics, and engineering, to fulfill all the requirements from the molecular to organ levels. Further, 3D bioprinting of polymers needs to meet several basic requirements to be applied in clinical applications. These requirements include biocompatibility, biostability, good mechanical properties, bioprintability, biodegradability, suturable with host vascular and nerves, permeability for nutrients and gases, and sterilizability [93].

### 5. Polymers as Artificial Cells or Organs

Numerous researchers have been trying to reduce the gap between the structures that can be designed and produced in the laboratory and those found in biology. Biological cells provide multiple functions, such as synthesizing proteins and lipids, storing genetic materials, storing and harvesting energy, etc. [92,94] (Figure 6). Additionally, homogeneous cells organize into specific tissues, whereas heterogeneous cells aggregate into an organ with specific physiological functions [93]. As such, creating an artificial cell or organ that has the same compartmentalized, multifunctional architecture is a challenging task. Two fundamental approaches have been considered for artificial cell construction: top-down and bottom-up approaches. The top-down approach starts from living organisms, moving down the genome to the lowest number of genes that are essential for maintaining cell viability and functionality. The bottom-up approach starts from scratch by using biological and nonbiological molecules to build up a “living” artificial organelle or cell [95].



**Figure 6.** Architecture of typical biological cell and artificial cell. Left: Eukaryotic cell containing different types of organelles. Right: artificial “synthase” cell that mimic that structure of biological cell (Created with Biorender.com, accessed on 12 October 2022).

Several researchers have tried to mimic the natural cell or tissue function and reduce the gap between normal and artificial cells. In studies involving artificial cells, microfluidics provides a powerful tool to produce a large number of compartments with different size ranges [96,97]. For instance, a circular design PDMS microfluidic compartmentalized co-culture platform was developed by Park et al. In the fabricated model, neurons and oligodendrocytes are co-cultured in two separate compartments connected by arrays of

shallow axon-guiding microfluidic channels. The chip design offers physical and fluidic isolation between the soma and the axon/glia compartments [98]. In an attempt to mimic the structure of biological cells, alginate was used as a biomaterial in artificial systems, and four types of glass microfluidics with flow-focusing or co-flowing droplet generators were used to produce alginate droplets. The generated alginate microgels exhibited various architectures, including individual monodisperse or polydisperse beads, small clusters, and multicompartment systems [99]. For cell culture, microfluidic systems are mainly fabricated with silicon, PDMS, and borosilicate. These materials have been used to test the mammalian embryos within microfluidic systems [100]. Moreover, many microfluidic devices have been reported to enhance cell growth, differentiation, and micro-environmental changes in various perfusion system [101–104]. In 3D cellular environment, combining PDMS and hydrogel into hybrid device has been used to produce 3D-ECM of aligned for endothelial cell cultures [105]. A study by Leclerc et al. illustrated that the culture of fetal human hepatocytes (FHHs) microfluidic bioreactors is promising for liver tissue engineering. They found that the albumin production by FHHs was four times higher than in static culture which can be influenced to the potentiality of fetal liver cells maturation [106].

These fabricated models show the use of a variety of polymers as distinctive biomaterials and the ease of using microfluidic platforms, which can be used to construct simple mimics of cellular environments or cellular architectures, and thus offer a promising approach for synthesizing bioarchitectures. Table 3 summarizes some studies used polymers and microfluidics in applications described in this review.

**Table 3.** Summary of some studies used polymers and microfluidics for several applications include drug delivery, 3D printing, and artificial cells.

Polymers	Microfluidic Chip Type	Applications	Study
Alginate	Alginate-based bioinks with cartilage cells used to print hollow constructs	The vessels-like printable microfluidic channels were capable to transport nutrients, biomolecules, oxygen through the construct and can support cell growth.	[13]
PLGA	Quartz Droplet X-Junction Chip	insulin was encapsulated into PLGA nanoparticles and then appended with heparin sulfate for oral insulin delivery.	[75]
PDMS	Deep channels or single layer pattern using soft lithography method	High-throughput drug screening can perform using a single chip where enzymatic assays are in picolitre-scale droplets.	[107,108]
PLGA	3D flow-focusing microfluidic chip	Indomethacin was encapsulated into microparticles to develop in silico tool to predict size particles.	[77]
Collagen and alginate	PDMS microfluidic encapsulation device	3D microenvironment of human tumor developed by encapsulating MCF-7 cancer cells in the collagen core of microcapsules with an alginate hydrogel shell for miniaturized 3D culture. Then the cytotoxicity of doxorubicin hydrochloride was assessed.	[109]
Chitosan and alginate	Coaxial flow microfluidic chip	HepG2 cells encapsulated in the chitosan-alginate fibers to guide growth, alignment, and migration of encapsulated cells.	[110]
PDMS and graphene oxide (GO)	Nano-sized GO -modified nanopillars on microgroove hybrid polymer array (NMPA) were fabricated using sequential laser interference lithography and microcontact printing technique.	Mouse myoblast cells (C2C12) were significantly differentiated into skeletal muscle cells on the micro-sized line pattern with GO coating (<10 nm).	[111]

Table 3. Cont.

Polymers	Microfluidic Chip Type	Applications	Study
1,6-hexanediol diacrylate (HDDA), lauryl acrylate (LA), polyethylene glycol diacrylate (PEGDA)	3D-printed microfluidic droplet generator	the hydrophobic HDDA/LA 3D printing resin allows droplet formation in 3D-printed planar microfluidics for the basic geometries while hydrophilic PEGDA resin allows droplet formation in non-planar 3D geometry.	[87]
Elastin-like protein (ELP)	Two custom-designed chips: one with ready-made channel and another with sacrificial gel-made channel	ELP hydrogels with cell-adhesive RGD amino acid sequence was used as bioinks for constructing 3D in vitro models with on-chip vascular-like channels. The developed model was compatible with both single cell suspensions of neural progenitor cells (NPCs) and spheroid aggregates of breast cancer cells.	[112]
PDMS	Microfluidic-based droplet system	The high-throughput tree-branched microfluidic droplet system for multicellular spheroids formation showed a high protentional to mimic the in vivo solid tumor structure with heterogeneous cell types and for anti-cancer drug screening applications.	[113]
Alginate	Flow-focusing or co-flowing droplet generators	Generated alginate microgels exhibited various architectures, including individual monodisperse or polydisperse beads, small clusters, and multicompartement systems.	[99]
Au-PEG-PFPE diblock-copolymer surfactant	Microfluidic flow-focusing junction	Lipid vesicles (LUVs or GUVs) were encapsulated into copolymer-stabilized droplets. Generated synthetic cells were able to be loaded with biomolecules, such as FoF1-ATP synthase.	[114]

## 6. Conclusions

The combination of natural/synthetic polymers and new biofabrication techniques, such as microfluidics, offers promising approach for tissue engineering scaffolds. Polymers and microfluidics enable rapid prototyping, reliability, as well as easy and low-cost manufacturing in research laboratories and for commercialization. Currently, there are many polymer-based drug delivery systems approved by FDA that are available on the market. Further, for commercial mass production, thermoplastics are used to develop standard microfluidic devices. However, despite scientific progress in biofabrication technologies, we are still in the early stages of the development of microfluidic technology for tissue engineering applications. There are serious obstacles to be overcome in producing a functional, complex, and large-scale system.

**Author Contributions:** Conceptualization, L.A.D., M.E.-Y. and S.D.; writing—original draft preparation, L.A.D., M.E.-Y. and S.D.; review and editing, S.A.D., R.K. and F.S. All authors have read and agreed to the published version of the manuscript.

**Funding:** This research received no external funding.

**Institutional Review Board Statement:** Not applicable.



**Informed Consent Statement:** Not applicable.

**Data Availability Statement:** Not applicable.

**Conflicts of Interest:** The authors declare no conflict of interest.

## References

1. Puertas-Bartolomé, M.; Mora-Boza, A.; García-Fernández, L. Emerging Biofabrication Techniques: A Review on Natural Polymers for Biomedical Applications. *Polymers* **2021**, *13*, 1209. [CrossRef] [PubMed]
2. Pearce, A.K.; O'Reilly, R.K. Polymers for Biomedical Applications: The Importance of Hydrophobicity in Directing Biological Interactions and Application Efficacy. *Biomacromolecules* **2021**, *22*, 4459–4469. [CrossRef]
3. Damiati, L.A.; Damiati, S.A.; Damiati, S. Chapter 26—Developments in the use of microfluidics in synthetic biology. In *New Frontiers and Applications of Synthetic Biology*; Singh, V., Ed.; Academic Press: Cambridge, MA, USA, 2022; pp. 423–435. ISBN 978-0-12-824469-2.
4. Damiati, S. New opportunities for creating man-made bioarchitectures utilizing microfluidics. *Biomed. Microdevices* **2019**, *21*, 62. [CrossRef] [PubMed]
5. Damiati, S.; Kompella, U.B.; Damiati, S.A.; Kodzius, R. Microfluidic Devices for Drug Delivery Systems and Drug Screening. *Genes* **2018**, *9*, 103. [CrossRef]
6. Damiati, S.; Mhanna, R.; Kodzius, R.; Ehmoser, E.-K. Cell-Free Approaches in Synthetic Biology Utilizing Microfluidics. *Genes* **2018**, *9*, 144. [CrossRef] [PubMed]
7. Xiao, K.; Kodzius, R.; Wu, J. Selection of Easily Accessible PCR- and Bio-Compatible Materials for Microfluidic Chips. In *Microfluidic*; Nova Science Publishers, Inc.: Hauppauge, NY, USA, 2013.
8. Ferry, M.S.; Razinkov, I.A.; Hasty, J. Microfluidics for Synthetic Biology. In *Methods in Enzymology*; Voigt, C., Ed.; Elsevier: New York, NY, USA, 2011; Volume 497, pp. 295–372. [CrossRef]
9. Attia, U.M.; Marson, S.; Alcock, J.R. Micro-injection moulding of polymer microfluidic devices. *Microfluid. Nanofluidics* **2009**, *7*, 1–28. [CrossRef]
10. Tsao, C.-W. Polymer Microfluidics: Simple, Low-Cost Fabrication Process Bridging Academic Lab Research to Commercialized Production. *Micromachines* **2016**, *7*, 225. [CrossRef]
11. Sung, Y.K.; Kim, S.W. Recent advances in polymeric drug delivery systems. *Biomater. Res.* **2020**, *24*, 12. [CrossRef]
12. Gopinathan, J.; Noh, I. Recent trends in bioinks for 3D printing. *Biomater. Res.* **2018**, *22*, 11. [CrossRef]
13. Zhang, Y.; Yu, Y.; Chen, H.; Ozbolat, I.T. Characterization of printable cellular micro-fluidic channels for tissue engineering. *Biofabrication* **2013**, *5*, 025004. [CrossRef]
14. Damiati, L.A.; El-Messeiry, S. An Overview of RNA-Based Scaffolds for Osteogenesis. *Front. Mol. Biosci.* **2021**, *8*, 682581. [CrossRef] [PubMed]
15. Ma, J.; Wang, Y.; Liu, J. Biomaterials Meet Microfluidics: From Synthesis Technologies to Biological Applications. *Micromachines* **2017**, *8*, 255. [CrossRef]
16. Bettinger, C.J.; Borenstein, J.T. Biomaterials-based microfluidics for engineered tissue constructs. *Soft Matter* **2010**, *6*, 4999–5015. [CrossRef]
17. Niculescu, A.-G.; Chircov, C.; Bîrcă, A.C.; Grumezescu, A.M. Fabrication and Applications of Microfluidic Devices: A Review. *Int. J. Mol. Sci.* **2021**, *22*, 2011. [CrossRef]
18. Papageorgiou, G.Z. Thinking Green: Sustainable Polymers from Renewable Resources. *Polymers* **2018**, *10*, 952. [CrossRef]
19. Yajima, Y.; Yamada, M.; Yamada, E.; Iwase, M.; Seki, M. Facile fabrication processes for hydrogel-based microfluidic devices made of natural biopolymers. *Biomicrofluidics* **2014**, *8*, 024115. [CrossRef] [PubMed]
20. Bettinger, J.C.; Cyr, M.K.; Matsumoto, A.; Langer, R.; Borenstein, T.J.; Kaplan, L.D. Silk Fibroin Microfluidic Devices. *Gerontology* **2015**, *61*, 515–525. [CrossRef] [PubMed]
21. Gorenkova, N.; Maitz, M.F.; Böhme, G.; Alhadrami, H.A.; Jiffri, E.H.; Totten, J.D.; Werner, C.; Carswell, H.V.O.; Seib, F.P. The innate immune response of self-assembling silk fibroin hydrogels. *Biomater. Sci.* **2021**, *9*, 7194–7204. [CrossRef]
22. Joyce, K.; Fabra, G.T.; Bozkurt, Y.; Pandit, A. Bioactive potential of natural biomaterials: Identification, retention and assessment of biological properties. *Signal Transduct. Target. Ther.* **2021**, *6*, 122. [CrossRef]
23. Arık, Y.B.; Vivas, A.d.S.; Laarveld, D.; van Laar, N.; Gemser, J.; Visscher, T.; Berg, A.V.D.; Passier, R.; van der Meer, A.D. Collagen I Based Enzymatically Degradable Membranes for Organ-on-a-Chip Barrier Models. *ACS Biomater. Sci. Eng.* **2021**, *7*, 2998–3005. [CrossRef] [PubMed]
24. Wang, J.; Bettinger, C.J.; Langer, R.S.; Borenstein, J.T. Biodegradable microfluidic scaffolds for tissue engineering from amino alcohol-based poly(ester amide) elastomers. *Organogenesis* **2010**, *6*, 212–216. [CrossRef] [PubMed]
25. Hirenkumar, M.; Steven, S. Poly Lactic-co-Glycolic Acid (PLGA) as Biodegradable Controlled Drug Delivery Carrier. *Polymers* **2012**, *3*, 1377–1397. [CrossRef]
26. Chen, G.; Ushida, T.; Tateishi, T. Hybrid Biomaterials for Tissue Engineering: A Preparative Method for PLA or PLGA-Collagen Hybrid Sponges. *Adv. Mater.* **2000**, *12*, 455–457. [CrossRef]
27. Stefaniak, K.; Masek, A. Green Copolymers Based on Poly(Lactic Acid)—Short Review. *Materials* **2021**, *14*, 5254. [CrossRef] [PubMed]

28. Jain, R.A. The manufacturing techniques of various drug loaded biodegradable poly(lactide-co-glycolide) (PLGA) devices. *Biomaterials* **2000**, *21*, 2475–2490. [CrossRef] [PubMed]
29. Lan, P.; Zhang, Y.; Gao, Q.; Shao, H.; Hu, X. Studies on the synthesis and thermal properties of copoly(L-lactic acid/glycolic acid) by direct melt polycondensation. *J. Appl. Polym. Sci.* **2004**, *92*, 2163–2168. [CrossRef]
30. Armani, D.K.; Liu, C. Microfabrication technology for polycaprolactone, a biodegradable polymer. *J. Micromechanics Microengineering* **2000**, *10*, 80–84. [CrossRef]
31. Tokiwa, Y.; Calabia, B.P.; Ugwu, C.U.; Aiba, S. Biodegradability of Plastics. *Int. J. Mol. Sci.* **2009**, *10*, 3722–3742. [CrossRef]
32. King, K.R.; Wang, C.C.J.; Kaazempur-Mofrad, M.R.; Vacanti, J.P.; Borenstein, J.T. Biodegradable Microfluidics. *Adv. Mater.* **2004**, *16*, 2007–2012. [CrossRef]
33. Kadimisetty, K.; Mosa, I.M.; Malla, S.; Satterwhite-Warden, J.E.; Kuhns, T.M.; Faria, R.C.; Lee, N.H.; Rusling, J.F. 3D-printed supercapacitor-powered electrochemiluminescent protein immunoarray. *Biosens. Bioelectron.* **2016**, *77*, 188–193. [CrossRef] [PubMed]
34. Friend, J.; Yeo, L. Fabrication of microfluidic devices using polydimethylsiloxane. *Biomicrofluidics* **2010**, *4*, 026502. [CrossRef] [PubMed]
35. Fujii, T. PDMS-based microfluidic devices for biomedical applications. *Microelectron. Eng.* **2002**, *61–62*, 907–914. [CrossRef]
36. Choi, W.M.; Park, O.O. The fabrication of submicron patterns on curved substrates using a polydimethylsiloxane film mould. *Nanotechnology* **2004**, *15*, 1767–1770. [CrossRef]
37. Miranda, I.; Souza, A.; Sousa, P.; Ribeiro, J.; Castanheira, E.M.S.; Lima, R.; Minas, G. Properties and Applications of PDMS for Biomedical Engineering: A Review. *J. Funct. Biomater.* **2022**, *13*, 2. [CrossRef] [PubMed]
38. Mata, A.; Fleischman, A.J.; Roy, S. Characterization of Polydimethylsiloxane (PDMS) Properties for Biomedical Micro/Nanosystems. *Biomed. Microdevices* **2005**, *7*, 281–293. [CrossRef]
39. Ren, K.; Zhou, J.; Wu, H. Materials for Microfluidic Chip Fabrication. *Acc. Chem. Res.* **2013**, *46*, 2396–2406. [CrossRef]
40. Prada, J.; Cordes, C.; Harms, C.; Lang, W. Design and Manufacturing of a Disposable, Cyclo-Olefin Copolymer, Microfluidic Device for a Biosensor. *Sensors* **2019**, *19*, 1178. [CrossRef]
41. Gencturk, E.; Mutlu, S.; Ulgen, K.O. Advances in microfluidic devices made from thermoplastics used in cell biology and analyses. *Biomicrofluidics* **2017**, *11*, 051502. [CrossRef]
42. Ali, U.; Karim, K.J.B.A.; Buang, N.A. A Review of the Properties and Applications of Poly (Methyl Methacrylate) (PMMA). *Polym. Rev.* **2015**, *55*, 678–705. [CrossRef]
43. Crawford, C.B.; Quinn, B. (Eds.) Physicochemical properties and degradation. In *Microplastic Pollutants*; Elsevier: Amsterdam, The Netherlands, 2017; pp. 57–100. ISBN 978-0-12-809406-8.
44. Gülsoy, H.; Taşdemir, M. Physical and Mechanical Properties of Polypropylene Reinforced with Fe Particles. *Int. J. Polym. Mater. Polym. Biomater.* **2006**, *55*, 619–626. [CrossRef]
45. Sastri, V.R. (Ed.) Chapter 6—Commodity Thermoplastics: Polyvinyl Chloride, Polyolefins, and Polystyrene. In *Plastics Design Library*; William Andrew Publishing: Boston, MA, USA, 2010; pp. 73–119. ISBN 978-0-8155-2027-6.
46. Luzi, F.; Torre, L.; Kenny, J.M.; Puglia, D. Bio- and Fossil-Based Polymeric Blends and Nanocomposites for Packaging: Structure–Property Relationship. *Materials* **2019**, *12*, 471. [CrossRef]
47. Shindo, R.; Yamanaka, N.; Wakamatsu, T.; Nagai, K. Permeability of dried gases and gases dissolved in water through polyimide membranes modified by immersing in amino compound solutions. *Polym. Eng. Sci.* **2016**, *56*, 178–186. [CrossRef]
48. Wang, R.; Xu, G.; He, Y. Structure and properties of polytetrafluoroethylene (PTFE) fibers. *e-Polymers* **2017**, *17*, 215–220. [CrossRef]
49. Skirbutis, G.; Dzingutė, A.; Masiliūnaitė, V.; Šulcaitė, G.; Žilinskas, J. A review of PEEK polymer's properties and its use in prosthodontics. *Stomatologija* **2017**, *19*, 19–23. [PubMed]
50. Young, E.W.K.; Berthier, E.; Beebe, D.J. Assessment of Enhanced Autofluorescence and Impact on Cell Microscopy for Microfabricated Thermoplastic Devices. *Anal. Chem.* **2013**, *85*, 44–49. [CrossRef] [PubMed]
51. Trinh, K.T.L.; Thai, D.A.; Chae, W.R.; Lee, N.Y. Rapid Fabrication of Poly(methyl methacrylate) Devices for Lab-on-a-Chip Applications Using Acetic Acid and UV Treatment. *ACS Omega* **2020**, *5*, 17396–17404. [CrossRef] [PubMed]
52. Thacker, V.V.; Dhar, N.; Sharma, K.; Barrile, R.; Karalis, K.; McKinney, J.D. A lung-on-chip model of early Mycobacterium tuberculosis infection reveals an essential role for alveolar epithelial cells in controlling bacterial growth. *eLife* **2020**, *9*, e59961. [CrossRef] [PubMed]
53. Kumar, T.; Soares, R.R.G.; Dholey, L.A.; Ramachandraiah, H.; Aval, N.A.; Aljadi, Z.; Pettersson, T.; Russom, A. Multi-layer assembly of cellulose nanofibrils in a microfluidic device for the selective capture and release of viable tumor cells from whole blood. *Nanoscale* **2020**, *12*, 21788–21797. [CrossRef]
54. Manimaran, N.H.; Usman, H.; Kamga, K.L.; Davidson, S.-L.; Beckman, E.; Niepa, T.H.R. Developing a Functional Poly(dimethylsiloxane)-Based Microbial Nanoculture System Using Dimethylallylamine. *ACS Appl. Mater. Interfaces* **2020**, *12*, 50581–50591. [CrossRef]
55. He, Y.; Mao, T.; Gu, Y.; Yang, Y.; Ding, J. A simplified yet enhanced and versatile microfluidic platform for cyclic cell stretching on an elastic polymer. *Biofabrication* **2020**, *12*, 045032. [CrossRef] [PubMed]
56. Li, X.; Wu, N.; Rojanasakul, Y.; Liu, Y. Selective stamp bonding of PDMS microfluidic devices to polymer substrates for biological applications. *Sens. Actuators A Phys.* **2013**, *193*, 186–192. [CrossRef]

57. Williams, M.J.; Lee, N.K.; Mylott, J.A.; Mazzola, N.; Ahmed, A.; Abhyankar, V.V. A Low-Cost, Rapidly Integrated Debubbler (RID) Module for Microfluidic Cell Culture Applications. *Micromachines* **2019**, *10*, 360. [CrossRef] [PubMed]
58. Huh, D.; Fujioka, H.; Tung, Y.-C.; Futai, N.; Paine, R.; Grothberg, J.B.; Takayama, S. Acoustically detectable cellular-level lung injury induced by fluid mechanical stresses in microfluidic airway systems. *Proc. Natl. Acad. Sci. USA* **2007**, *104*, 18886–18891. [CrossRef]
59. Wang, Y.; Lee, D.; Zhang, L.; Jeon, H.; Mendoza-Elias, J.E.; Harvat, T.A.; Hassan, S.Z.; Zhou, A.; Eddington, D.T.; Oberholzer, J. Systematic prevention of bubble formation and accumulation for long-term culture of pancreatic islet cells in microfluidic device. *Biomed. Microdevices* **2012**, *14*, 419–426. [CrossRef] [PubMed]
60. Van Der Meer, A.D.; Poot, A.A.; Feijen, J.; Vermes, I. Analyzing shear stress-induced alignment of actin filaments in endothelial cells with a microfluidic assay. *Biomicrofluidics* **2010**, *4*, 011103. [CrossRef] [PubMed]
61. Chen, Z.-Z.; Yuan, W.-M.; Xiang, C.; Zeng, D.-P.; Liu, B.; Qin, K.-R. A microfluidic device with spatiotemporal wall shear stress and ATP signals to investigate the intracellular calcium dynamics in vascular endothelial cells. *Biomech. Model. Mechanobiol.* **2019**, *18*, 189–202. [CrossRef] [PubMed]
62. Damiati, S.; Peacock, M.; Leonhardt, S.; Damiati, L.; Baghdadi, M.A.; Becker, H.; Kodzius, R.; Schuster, B. Embedded Disposable Functionalized Electrochemical Biosensor with a 3D-Printed Flow Cell for Detection of Hepatic Oval Cells (HOCs). *Genes* **2018**, *9*, 89. [CrossRef] [PubMed]
63. Kohane, D.S.; Langer, R. Polymeric Biomaterials in Tissue Engineering. *Pediatr. Res.* **2008**, *63*, 487–491. [CrossRef]
64. Watts, P.J.; Davies, M.; Melia, C.D. Microencapsulation using emulsification/solvent evaporation: An overview of techniques and applications. *Crit. Rev. Ther. Drug Carr. Syst.* **1990**, *7*, 235–259.
65. Jia, X.; Colombo, G.; Padera, R.; Langer, R.; Kohane, D.S. Prolongation of sciatic nerve blockade by in situ cross-linked hyaluronic acid. *Biomaterials* **2004**, *25*, 4797–4804. [CrossRef] [PubMed]
66. Yeo, Y.; Adil, M.; Bellas, E.; Astashkina, A.; Chaudhary, N.; Kohane, D.S. Prevention of peritoneal adhesions with an in situ cross-linkable hyaluronan hydrogel delivering budesonide. *J. Control. Release* **2007**, *120*, 178–185. [CrossRef] [PubMed]
67. Ito, T.; Fraser, I.P.; Yeo, Y.; Highley, C.B.; Bellas, E.; Kohane, D.S. Anti-inflammatory function of an in situ cross-linkable conjugate hydrogel of hyaluronic acid and dexamethasone. *Biomaterials* **2007**, *28*, 1778–1786. [CrossRef] [PubMed]
68. Ashton, R.S.; Banerjee, A.; Punyani, S.; Schaffer, D.V.; Kane, R.S. Scaffolds based on degradable alginate hydrogels and poly(lactide-co-glycolide) microspheres for stem cell culture. *Biomaterials* **2007**, *28*, 5518–5525. [CrossRef]
69. Yeo, Y.; Ito, T.; Bellas, E.; Highley, C.B.; Marini, R.; Kohane, D.S. In Situ Cross-linkable Hyaluronan Hydrogels Containing Polymeric Nanoparticles for Preventing Postsurgical Adhesions. *Ann. Surg.* **2007**, *245*, 819–824. [CrossRef]
70. Damiati, L.A.; Tsimbouri, M.P.; Hernandez, V.-L.; Jayawarna, V.; Ginty, M.; Childs, P.; Xiao, Y.; Burgess, K.; Wells, J.; Sprott, M.R.; et al. Materials-driven fibronectin assembly on nanoscale topography enhances mesenchymal stem cell adhesion, protecting cells from bacterial virulence factors and preventing biofilm formation. *Biomaterials* **2021**, *280*, 121263. [CrossRef] [PubMed]
71. Stewart, S.A.; Domínguez-Robles, J.; Donnelly, R.F.; Larrañeta, E. Implantable Polymeric Drug Delivery Devices: Classification, Manufacture, Materials, and Clinical Applications. *Polymers* **2018**, *10*, 1379. [CrossRef]
72. Procopio, A.; Lagreca, E.; Jamaledin, R.; La Manna, S.; Corrado, B.; Di Natale, C.; Onesto, V. Recent Fabrication Methods to Produce Polymer-Based Drug Delivery Matrices (Experimental and In Silico Approaches). *Pharmaceutics* **2022**, *14*, 872. [CrossRef] [PubMed]
73. Moradikhah, F.; Doosti-Telgerd, M.; Shabani, I.; Soheili, S.; Dolatyar, B.; Seyedjafari, E. Microfluidic fabrication of alendronate-loaded chitosan nanoparticles for enhanced osteogenic differentiation of stem cells. *Life Sci.* **2020**, *254*, 117768. [CrossRef] [PubMed]
74. Mora-Boza, A.; Castro, L.M.M.; Schneider, R.S.; Han, W.M.; García, A.J.; Vázquez-Lasa, B.; Román, J.S. Microfluidics generation of chitosan microgels containing glycerylphosphate crosslinker for in situ human mesenchymal stem cells encapsulation. *Mater. Sci. Eng. C* **2021**, *120*, 111716. [CrossRef]
75. Jaradat, A.; Macedo, M.H.; Sousa, F.; Arkill, K.; Alexander, C.; Aylott, J.; Sarmento, B. Prediction of the enhanced insulin absorption across a triple co-cultured intestinal model using mucus penetrating PLGA nanoparticles. *Int. J. Pharm.* **2020**, *585*, 119516. [CrossRef]
76. Damiati, S.A.; Rossi, D.; Joensson, H.N.; Damiati, S. Artificial intelligence application for rapid fabrication of size-tunable PLGA microparticles in microfluidics. *Sci. Rep.* **2020**, *10*, 19517. [CrossRef]
77. Damiati, S.A.; Damiati, S. Microfluidic Synthesis of Indomethacin-Loaded PLGA Microparticles Optimized by Machine Learning. *Front. Mol. Biosci.* **2021**, *8*, 595. [CrossRef] [PubMed]
78. Xu, Y.; Hu, B.; Xu, J.; Wu, J.; Ye, B. Preparation of Biodegradable Polymeric Nanocapsules for Treatment of Malignant Tumor Using Coaxial Capillary Microfluidic Device. *Cancer Biother. Radiopharm.* **2020**, *35*, 570–580. [CrossRef] [PubMed]
79. Hong, W.; Gao, Y.; Lou, B.; Ying, S.; Wu, W.; Ji, X.; Yu, N.; Jiao, Y.; Wang, H.; Zhou, X.; et al. Curcumin-Loaded Hybrid Nanoparticles: Microchannel-Based Preparation and Antitumor Activity in a Mouse Model. *Int. J. Nanomed.* **2021**, *16*, 4147–4159. [CrossRef] [PubMed]
80. Salari, N.; Faraji, F.; Torghabeh, F.M.; Faraji, F.; Mansouri, K.; Abam, F.; Shohaimi, S.; Akbari, H.; Mohammadi, M. Polymer-based drug delivery systems for anticancer drugs: A systematic review. *Cancer Treat. Res. Commun.* **2022**, *32*, 100605. [CrossRef] [PubMed]



81. Deussenberg, C.; Wang, Y.; Shukla, A. Recent Innovations in Bacterial Infection Detection and Treatment. *ACS Infect. Dis.* **2021**, *7*, 695–720. [CrossRef] [PubMed]
82. Borro, B.C.; Toussaint, M.S.; Bucciarelli, S.; Malmsten, M. Effects of charge contrast and composition on microgel formation and interactions with bacteria-mimicking liposomes. *Biochim. Biophys. Acta (BBA) Gen. Subj.* **2020**, *1865*, 129485. [CrossRef]
83. Huang, Z.; Zhou, T.; Yuan, Y.; Kłodzińska, S.N.; Zheng, T.; Sternberg, C.; Nielsen, H.M.; Sun, Y.; Wan, F. Synthesis of carbon quantum dot-poly lactic-co-glycolic acid hybrid nanoparticles for chemo-photothermal therapy against bacterial biofilms. *J. Colloid Interface Sci.* **2020**, *577*, 66–74. [CrossRef] [PubMed]
84. Norris, P.; Noble, M.; Francolini, I.; Vinogradov, A.M.; Stewart, P.; Ratner, B.D.; Costerton, J.W.; Stoodley, P. Ultrasonically Controlled Release of Ciprofloxacin from Self-Assembled Coatings on Poly(2-Hydroxyethyl Methacrylate) Hydrogels for *Pseudomonas aeruginosa* Biofilm Prevention. *Antimicrob. Agents Chemother.* **2005**, *49*, 4272–4279. [CrossRef]
85. Scott, S.; Ali, Z. Fabrication Methods for Microfluidic Devices: An Overview. *Micromachines* **2021**, *12*, 319. [CrossRef]
86. Evard, H.; Priks, H.; Saar, I.; Aavola, H.; Tamm, T.; Leito, I. A New Direction in Microfluidics: Printed Porous Materials. *Micromachines* **2021**, *12*, 671. [CrossRef] [PubMed]
87. Warr, C.; Hinnen, H.; Avery, S.; Cate, R.; Pitt, W. 3D-Printed Microfluidic Droplet Generator with Hydrophilic and Hydrophobic Polymers. *Micromachines* **2021**, *12*, 91. [CrossRef]
88. Distler, T.; Polley, C.; Shi, F.; Schneidereit, D.; Ashton, M.D.; Friedrich, O.; Kolb, J.F.; Hardy, J.G.; Detsch, R.; Seitz, H.; et al. Electrically Conductive and 3D-Printable Oxidized Alginate-Gelatin Polypyrrole:PSS Hydrogels for Tissue Engineering. *Adv. Health Mater.* **2021**, *10*, e2001876. [CrossRef] [PubMed]
89. Wright, C.J.; Molino, B.Z.; Chung, J.H.Y.; Pannell, J.T.; Kuester, M.; Molino, P.J.; Hanks, T.W. Synthesis and 3D Printing of Conducting Alginate–Polypyrrole Ionomers. *Gels* **2020**, *6*, 13. [CrossRef]
90. Kamat, A.M.; Pei, Y.; Jayawardhana, B.; Kottapalli, A.G.P. Biomimetic Soft Polymer Microstructures and Piezoresistive Graphene MEMS Sensors Using Sacrificial Metal 3D Printing. *ACS Appl. Mater. Interfaces* **2021**, *13*, 1094–1104. [CrossRef] [PubMed]
91. Orive, G.; Hernández, R.M.; Gascón, A.R.; Calafiore, R.; Chang, T.M.S.; de Vos, P.; Hortelano, G.; Hunkeler, D.; Lacík, I.; Pedraz, J.L. History, challenges and perspectives of cell microencapsulation. *Trends Biotechnol.* **2004**, *22*, 87–92. [CrossRef] [PubMed]
92. Marguet, M.; Bonduelle, C.; Lecommandoux, S. Multicompartmentalized polymeric systems: Towards biomimetic cellular structure and function. *Chem. Soc. Rev.* **2012**, *42*, 512–529. [CrossRef] [PubMed]
93. Wang, X. Advanced Polymers for Three-Dimensional (3D) Organ Bioprinting. *Micromachines* **2019**, *10*, 814. [CrossRef]
94. Lu, A.X.; Oh, H.; Terrell, J.L.; Bentley, W.E.; Raghavan, S.R. A new design for an artificial cell: Polymer microcapsules with addressable inner compartments that can harbor biomolecules, colloids or microbial species. *Chem. Sci.* **2017**, *8*, 6893–6903. [CrossRef] [PubMed]
95. Xu, C.; Hu, S.; Chen, X. Artificial cells: From basic science to applications. *Physiol. Behav.* **2017**, *176*, 139–148. [CrossRef]
96. Sato, Y.; Takinoue, M. Creation of Artificial Cell-Like Structures Promoted by Microfluidics Technologies. *Micromachines* **2019**, *10*, 216. [CrossRef]
97. Young, A.T.; Rivera, K.R.; Erb, P.D.; Daniele, M.A. Monitoring of Microphysiological Systems: Integrating Sensors and Real-Time Data Analysis toward Autonomous Decision-Making. *ACS Sens.* **2019**, *4*, 1454–1464. [CrossRef]
98. Park, J.; Koito, H.; Li, J.; Han, A. Microfluidic compartmentalized co-culture platform for CNS axon myelination research. *Biomed. Microdevices* **2009**, *11*, 1145–1153. [CrossRef] [PubMed]
99. Damiati, S. In Situ Microfluidic Preparation and Solidification of Alginate Microgels. *Macromol. Res.* **2020**, *28*, 1046–1053. [CrossRef]
100. Kricka, L.J.; Nozaki, O.; Heyner, S.; Garside, W.T.; Wilding, P. Applications of a microfabricated device for evaluating sperm function. *Clin. Chem.* **1993**, *39*, 1944–1947. [CrossRef]
101. Leclerc, E.; Furukawa, K.; Miyata, F.; Sakai, Y.; Ushida, T.; Fujii, T. Fabrication of microstructures in photosensitive biodegradable polymers for tissue engineering applications. *Biomaterials* **2004**, *25*, 4683–4690. [CrossRef] [PubMed]
102. Taylor, A.M.; Rhee, S.W.; Tu, C.H.; Cribbs, D.H.; Cotman, C.W.; Jeon, N.L. Microfluidic Multicompartment Device for Neuroscience Research. *Langmuir* **2003**, *19*, 1551–1556. [CrossRef] [PubMed]
103. Leclerc, E.; Sakai, Y.; Fujii, T. Perfusion culture of fetal human hepatocytes in microfluidic environments. *Biochem. Eng. J.* **2004**, *20*, 143–148. [CrossRef]
104. Tan, W.; Desai, T.A. Layer-by-layer microfluidics for biomimetic three-dimensional structures. *Biomaterials* **2004**, *25*, 1355–1364. [CrossRef]
105. Lii, J.; Hsu, W.-J.; Parsa, H.; Das, A.; Rouse, R.; Sia, S.K. Real-Time Microfluidic System for Studying Mammalian Cells in 3D Microenvironments. *Anal. Chem.* **2008**, *80*, 3640–3647. [CrossRef] [PubMed]
106. Toh, Y.-C.; Zhang, C.; Zhang, J.; Khong, Y.M.; Chang, S.; Samper, V.D.; van Noort, D.; Hutmacher, D.W.; Yu, H. A novel 3D mammalian cell perfusion-culture system in microfluidic channels. *Lab Chip* **2007**, *7*, 302–309. [CrossRef] [PubMed]
107. Clausell-Tormos, J.; Lieber, D.; Baret, J.-C.; El-Harrak, A.; Miller, O.J.; Frenz, L.; Blouwolff, J.; Humphry, K.; Köster, S.; Duan, H.; et al. Droplet-Based Microfluidic Platforms for the Encapsulation and Screening of Mammalian Cells and Multicellular Organisms. *Chem. Biol.* **2008**, *15*, 427–437. [CrossRef] [PubMed]
108. Huebner, A.; Bratton, D.; Whyte, G.; Yang, M.; Demello, A.J.; Abell, C.; Hollfelder, F. Static microdroplet arrays: A microfluidic device for droplet trapping, incubation and release for enzymatic and cell-based assays. *Lab Chip* **2009**, *9*, 692–698. [CrossRef]

109. Agarwal, P.; Wang, H.; Sun, M.; Xu, J.; Zhao, S.; Liu, Z.; Gooch, K.J.; Zhao, Y.; Lu, X.; He, X. Microfluidics Enabled Bottom-Up Engineering of 3D Vascularized Tumor for Drug Discovery. *ACS Nano* **2017**, *11*, 6691–6702. [CrossRef]
110. Lee, B.R.; Lee, K.H.; Kang, E.; Kim, D.-S.; Lee, S.-H. Microfluidic wet spinning of chitosan-alginate microfibers and encapsulation of HepG2 cells in fibers. *Biomicrofluidics* **2011**, *5*, 022208. [CrossRef]
111. Choi, H.K.; Kim, C.-H.; Lee, S.N.; Kim, T.-H.; Oh, B.-K. Nano-sized graphene oxide coated nanopillars on microgroove polymer arrays that enhance skeletal muscle cell differentiation. *Nano Converg.* **2021**, *8*, 40. [CrossRef]
112. Campos, D.F.D.; Lindsay, C.D.; Roth, J.; LeSavage, B.L.; Seymour, A.J.; Krajina, B.A.; Ribeiro, R.; Costa, P.F.; Blaeser, A.; Heilshorn, S.C. Bioprinting Cell- and Spheroid-Laden Protein-Engineered Hydrogels as Tissue-on-Chip Platforms. *Front. Bioeng. Biotechnol.* **2020**, *8*, 374. [CrossRef] [PubMed]
113. Lee, S.I.; Choi, Y.Y.; Kang, S.G.; Kim, T.H.; Choi, J.W.; Kim, Y.J.; Kim, T.-H.; Kang, T.; Chung, B.G. 3D Multicellular Tumor Spheroids in a Microfluidic Droplet System for Investigation of Drug Resistance. *Polymers* **2022**, *14*, 3752. [CrossRef] [PubMed]
114. Weiss, M.; Frohnmayer, J.P.; Benk, L.T.; Haller, B.; Janiesch, J.-W.; Heitkamp, T.; Börsch, M.; Lira, R.B.; Dimova, R.; Lipowsky, R.; et al. Sequential bottom-up assembly of mechanically stabilized synthetic cells by microfluidics. *Nat. Mater.* **2018**, *17*, 89–96. [CrossRef] [PubMed]





## Article

# The Effect of Dual-Modification by Heat-Moisture Treatment and Octenylsuccinylation on Physicochemical and Pasting Properties of Arrowroot Starch

Herlina Marta <sup>1,\*</sup>, Ari Rismawati <sup>1</sup>, Giffary Pramafisi Soeherman <sup>2</sup>, Yana Cahyana <sup>1</sup>, Mohamad Djali <sup>1</sup>, Tri Yuliana <sup>1</sup> and Dewi Sondari <sup>3</sup>

<sup>1</sup> Department of Food Technology, Faculty of Agro-Industrial Technology, Universitas Padjadjaran, Bandung 45363, Indonesia; ari20001@mail.unpad.ac.id (A.R.); y.cahyana@unpad.ac.id (Y.C.); djali@unpad.ac.id (M.D.); t.yuliana@unpad.ac.id (T.Y.)

<sup>2</sup> Department of Agroindustry Technology, Lampung State Polytechnic, Lampung 35141, Indonesia; giffarypramafisi@polinela.ac.id

<sup>3</sup> Research Center for Biomass and Bioproducts, Cibinong Science Center, National Research and Innovation Agency, Cibinong 16911, Indonesia; dewi004@brin.go.id

\* Correspondence: herlina.marta@unpad.ac.id

**Abstract:** Starch is widely applied in various industrial sectors, including the food industry. Starch is used as a thickener, stabilizer, or emulsifier. However, arrowroot starch generally has weaknesses, such as unstable under heating and acidic conditions, which are generally applied to processing in the food industry. Modifications were applied to improve the characteristics of native arrowroot starch. In this study, arrowroot starch was modified by heat-moisture treatment (HMT), octenylsuccinylation (OSA), and dual modification between OSA and HMT in a different sequence—namely, HMT followed by OSA, and OSA followed by HMT. This study aims to determine the effect of different modification methods on the physicochemical and functional properties of native arrowroot starch. The result shows that both single HMT and dual modification caused damage to native starch granules, such as the formation of cracks and roughness. For single OSA treatment, especially, there is no significant change in granule morphology after modification. All modification treatments did not change the crystalline type of starch but reduced the RC of native starch. Both single HMT and dual modifications (HMT-OSA, OSA-HMT) increased pasting temperature and setback, but, conversely, decreased the peak and the breakdown viscosity of native starch, whereas single OSA had the opposite trend compared with the other modifications. HMT played a greater role in increasing the thermal stability and the retrogradation ability of arrowroot starch. Both single modifications (HMT and OSA) increased the hardness and gumminess of native starch, and the opposite was true for the dual modifications. HMT had a greater effect on color characteristics, where the lightness and whiteness index of native arrowroot starch decreased. Single OSA modification increased swelling volume higher than dual modification. Both single HMT and dual modifications increased water absorption capacity and decreased the oil absorption capacity of native arrowroot starch.

**Keywords:** arrowroot starch; heat-moisture treatment; octenylsuccinilation; dual-modification; physicochemical properties; functional properties

**Citation:** Marta, H.; Rismawati, A.; Soeherman, G.P.; Cahyana, Y.; Djali, M.; Yuliana, T.; Sondari, D. The Effect of Dual-Modification by Heat-Moisture Treatment and Octenylsuccinylation on Physicochemical and Pasting Properties of Arrowroot Starch. *Polymers* **2023**, *15*, 3215. <https://doi.org/10.3390/polym15153215>

Academic Editor: Raffaella Striani

Received: 12 June 2023

Revised: 24 July 2023

Accepted: 25 July 2023

Published: 28 July 2023



**Copyright:** © 2023 by the authors. Licensee MDPI, Basel, Switzerland. This article is an open access article distributed under the terms and conditions of the Creative Commons Attribution (CC BY) license (<https://creativecommons.org/licenses/by/4.0/>).

## 1. Introduction

Arrowroot (*Maranta arundinacea* L.) is a tuber plant with a rhizome root, which is elongated like an arrow. Arrowroot tubers have been considered inferior commodities and have not been utilized optimally. Arrowroot tuber is one of the commodity sources of carbohydrates, which can be processed into starch or flour. Starch can be utilized in many ways, such as a food thickener, stabilizer, and emulsifier [1]. Starches that are commonly found in the market are corn starch (maize) and cassava starch (tapioca). However, there

are still many potential plants that are potential sources of starch, and one of them is arrowroot tubers.

Native arrowroot starch, however, as with starches from other sources, has several limitations, such as low thermal stability and susceptibility to acidic conditions, which are generally used in processing in the food industry [2]. To improve the characteristics of native arrowroot starch, modifications were applied. One modification method that can be used to enhance thermal stability is the heat-moisture treatment (HMT) method [3,4]. However, several studies have shown that HMT increases starch syneresis [5,6]. Dual modification technology is an alternative to overcome the weakness of HMT starch by combining HMT modification treatment with other modification treatments, such as chemical modification. This study combined both modified treatments using heat-moisture treatment and octenylsuccinilation using octenyl-succinic anhydride (OSA). Modification of OSA has advantages because it can increase the hydrophobicity of starch [7,8]. Thus, OSA-modified starch can be applied as an emulsifier or used as a fat replacer in high-fat products, resulting in decreased fat products [8–10].

Information regarding the modification of arrowroot starch modified by two methods, HMT and OSA, is still limited. This current study aimed to determine the physicochemical and pasting properties of native and modified starches for both single and dual modifications using HMT and OSA in the reverse sequence. HMT and OSA-modified starch is expected to be an ingredient in the manufacture of a functional food because each single modification treatment has advantages from a health perspective. For example, HMT-modified starch has very slowly digested starch, making it suitable for diabetics [11], while single OSA modification can produce starch that can replace the role of fat and could thus be used to produce low-fat products [8].

## 2. Materials and Methods

### 2.1. Materials

Arrowroot tubers (*Maranta arundinacea* L.) cultivated in Pangandaran, West Java, Indonesia were used as the raw material for starch extraction. All chemicals used for the modification process were 2-octen-1-ylsuccinic anhydride (OSA) (Sigma-Aldrich, St. Louis, MO, USA), hydrochloric acid, sodium hydroxide, ethanol 95%, acetic acid, isopropanol, AgNO<sub>3</sub>, and phenolphthalein, with specification analytical grade.

### 2.2. Arrowroot Starch Isolation

Arrowroot starch isolation method was followed according to Marta et al. [11] with a slight modification. The tubers were peeled and cut into small pieces, and were then further soaked in water with a tuber/water ratio of 1:5. The tubers were crushed to form a pulp using a blender (Sharp EM-121-BK, Chiba, Japan) for 2 min. The resulting slurry was squeezed using a muslin cloth. The slurry was allowed to precipitate for 18 h and decanted to separate starch and supernatant. The resulting starch was washed and centrifugated using SL 16 Centrifuge, Thermo Scientific, Waltham, MA, USA at 5000 rpm for 2–3 min to precipitate the starch. Starch washing and centrifugation were repeated 3 times in order to obtain clean starch. The resulting starch was dried in a drying oven at 50 °C for 24 h, and was then dried and sieved using a 100-mesh sieve.

### 2.3. Heat-Moisture Treated (HMT) Starch Preparation

Preparation of HMT-starch refers to Marta et al. [12]. The moisture content of arrowroot starch was adjusted to 30% ( $\pm 2\%$ ) by adding distilled water, and it was then equilibrated at 4 °C for 24 h in the refrigerator. The starch was then transferred to a tightly-closed Teflon and heated at 100 °C for 8 h. The modified starch was dried in a drying oven at 50 °C for 24 h, and was then ground and sieved using a 100-mesh sieve.

#### 2.4. Octenylsuccinilated (OSA) Starch Preparation

Preparation of OSA-starch refers to Marta et al. [13] with a slight modification. The starch sample was first made into a 30% (*w/w*) starch suspension by dissolving the starch in distilled water. The pH of the starch suspension was then adjusted to pH 8 using 1 M NaOH before the addition of 3% OSA solution (*w/w*). The esterification was then carried out by stirring the solution for 3 h. During the modification process, the pH of the suspension was adjusted and maintained in the range of 8.0–8.5 using 1 M NaOH and 1 M HCl. After the reaction, the starch suspension was adjusted to pH 6.5 using 1 M HCl. Starch was centrifuged at 5000 rpm for 2–3 min. The precipitated starch was washed using distilled water and then centrifuged again, and this process was repeated 2–3 times. The starch was then dried in a drying oven at 50 °C for 24 h. The dried modified starch was ground and sieved (no. 100 mesh sieve).

#### 2.5. Dual Modification by HMT Followed by OSA (HMT-OSA)

The native starch of arrowroot was modified by HMT (as mentioned in Section 2.3) and followed by OSA modification, as mentioned in Section 2.4, and the obtained starch was named HMT-OSA starch.

#### 2.6. Dual Modification by OSA Followed by HMT (OSA-HMT)

The native starch of arrowroot was modified by OSA (as mentioned in Section 2.4) and then followed by HMT modification, as mentioned in Section 2.3, and the obtained starch was named OSA-HMT starch.

#### 2.7. Granule Morphology Observation Using Scanning Electron Microscopy (SEM)

The granular morphology of native and modified arrowroot starch was determined using scanning electron microscopy (SEM), a JEOL JSM-6360 LA at 15 kV (JEOL, Tokyo, Japan). Mounted starch samples were coated with gold/palladium at 8–10 mA for 10–15 min under low pressure (less than 10 tors). Representative digital images of native and modified starch granules were obtained at 5000 and 10,000 magnifications.

#### 2.8. Starch Crystallinity Using X-ray Diffractometer (XRD)

The crystallinity of native and modified arrowroot starch was measured using an X'Pert PRO series PW3040/60 X-ray diffractometer (Malvern Panalytical, Malvern, UK) that operated using Cu-K alpha radiation with a wavelength of 1.540 nm as an X-ray source at 40 kV and 30 mA. The diffraction angle ( $2\theta$ ) scanning was from 3.0° to 50.0° with a scanning rate time of 2.9 s. OriginLab Program was used to calculate the relative crystallinity of the starch samples.

#### 2.9. Thermal Properties Determination Using Differential Scanning Calorimetry (DSC)

Thermal properties of starch samples were measured using DSC-Q100, TA Instruments (New Castle, DE, USA). The parameters observed were onset temperature ( $T_o$ ), peak temperature ( $T_p$ ), conclusion temperature ( $T_c$ ), and enthalpy of gelatinization ( $\Delta H$ ). Starch was made into a slurry, with the ratio of water and starch being 3:1. The slurry was then hermetically sealed using a DuPont encapsulation press before weighing. The starch samples were heated at a rate of 5 °C/min from 20 to 100 °C.

#### 2.10. Pasting Properties Determination Using Rapid Visco Analyzer (RVA)

The pasting properties of arrowroot starch were determined using an RVA Starch-Master 2, Parten Instruments. A total of 3 g of starch samples were added with 25 mL of distilled water in the RVA canister tube, and stirred in an RVA canister at 960 rpm for 10 s. RVA was set with a temperature profile, initially held at 50 °C for 1 min; the heating was from 50 to 95 °C for 3.7 min; the temperature was held at 95 °C for 2.5 min; and cooling was then achieved at 50 °C in 3.8 min and then kept at 50 °C for 2 min. The gel was then maintained at 50 °C for 2 min with constant paddle rotational speed (160 rpm) used

throughout the analysis, and the total analysis time was 12 min. The pasting properties included the following parameters: pasting temperature (PT), peak viscosity (PV), hold viscosity (HV), final viscosity (FV), breakdown (BD), and setback (SB).

#### 2.11. Texture Properties Evaluation Using Texture Analyzer (TA)

The texture properties of starch gels were evaluated on a TA-XT express enhanced Stable Micro System (Surrey, UK). Exponent Lite Express software was used to collect and calculate the data obtained. The gelatinized starch in the canister after the RVA measurement was poured into cylindrical plastic tubes (20 mm diameter, 40 mm deep) and then kept at 4 °C for 24 h to form a solid gel. Each gel sample in the tube was penetrated with a cylindrical probe (P36/R) at a speed of 5 mm/s to a distance of 10 mm for two penetration cycles. The texture profile curves were used to calculate hardness, adhesiveness, springiness, cohesiveness, and gumminess.

#### 2.12. Functional Properties

Swelling volume and solubility of arrowroot starch were measured referring to Marta et al. [13]. A total of 0.35 g (db) of starch sample was mixed with 10 mL distilled water and put into a centrifuge tube. It was then mixed using a vortex mixer for 20 s, and the sample was then heated in a water bath at 92.5 °C for 30 min and stirred regularly. The starch sample was cooled for 1 min in ice water and centrifuged at 3500 rpm for 15 min, and then the supernatant was separated and the volume was measured. Swelling volume was calculated using the equation:

$$\text{Swelling volume (mL/g)} = \frac{\text{total volume} - \text{supernatant volume}}{\text{weight of sample (db)}} \quad (1)$$

After being separated, the supernatant was dried in a drying oven for 24 h. Solubility was calculated using the equation:

$$\text{Solubility (\%)} = \frac{\text{weight of dried supernatant}}{\text{weight of sample (db)}} \times 100\% \quad (2)$$

Water absorption capacity (WAC) and oil absorption capacity (OAC) were measured referring to Marta et al. [13]. One gram (db) of the starch sample was added with 10 mL of distilled water or oil into a centrifuge tube, and then mixed using a vortex for 20 s. Samples were stored at room temperature for 1 h and then centrifuged at 3500 rpm for 30 min. The volume of the supernatant (water or oil) was measured and separated. WAC and OAC are calculated using the following equation:

$$\text{WAC (g/g)} = \frac{\text{volume of water absorbed}}{\text{weight sample (db)}} \quad (3)$$

$$\text{OAC (g/g)} = \frac{\text{volume of oil absorbed}}{\text{weight sample (db)}} \quad (4)$$

Freeze-thaw stability or syneresis was determined by a previous method [12] with a slight modification. An aqueous starch suspension (5%) was prepared and heated at 95 °C for 30 min with constant light stirring, then cooled to room temperature in an ice water bath. A total of 20 g of aliquots of the paste was then taken and put into a centrifuge tube, and a freeze-thaw cycle was then carried out with storage at 4 °C for 24 h, frozen at −15 °C for 48 h, and then thawed at 25 °C for 3 h. The samples were then centrifuged at 3500 rpm for 15 min. The supernatant was separated from the gel. The syneresis was calculated using the following equation:

$$\text{Syneresis (\%)} = \frac{\text{weight of separated water}}{\text{weight of starch paste}} \times 100\% \quad (5)$$



### 2.13. Color Analysis Using CM-5 Spectrophotometer

The starch color was measured using a CM-5 Spectrophotometer (Konica Minolta Co., Osaka, Japan) with SpectraMagic NX version 3.0 Software. The samples were placed in a glass cell and above the light source. After that, measurements were taken at room temperature. The parameters measured were CIE-lab namely, the  $L^*$ ,  $a^*$ , and  $b^*$  values in each sample.  $L^*$  value indicates the lightness (whiteness/darkness), representing dark (0) to light (100);  $a^*$  value indicates the degree of red-green color ((+) redness/(-) greenness); and  $b^*$  value indicates the degree of the yellow-blue color ((+) yellowness/(-) blueness). The whiteness index for native and modified starches was determined using the following equation [14]:

$$\text{Whiteness Index} = 100 - \sqrt{(100 - L^*)^2 + a^{*2} + b^{*2}} \quad (6)$$

Total color differences between starch samples were calculated using the following equation [15]:

$$\Delta E = \sqrt{(L^* - L_n^*)^2 + (a^* - a_n^*)^2 + (b^* - b_n^*)^2} \quad (7)$$

$L^*$ ,  $a^*$ , and  $b^*$  were parameters for modified starch, and  $L_n^*$ ,  $a_n^*$ , and  $b_n^*$  were parameters for native starch.

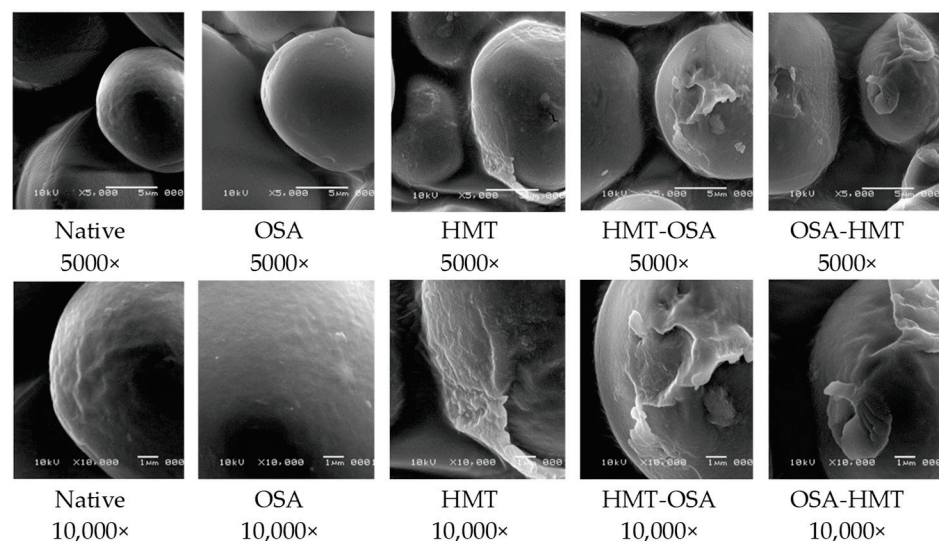
### 2.14. Statistical Analysis

Data are displayed as the mean  $\pm$  SD. Experiments were all performed in triplicate. One-way analysis of variance (ANOVA) was used to analyze all of the data, and the Duncan test was used to compare the sample mean at a significance level of 5% ( $p < 0.05$ ). The statistical software program IBM SPSS Statistics version 25 was used to examine all of the data.

## 3. Results

### 3.1. Granule Morphology

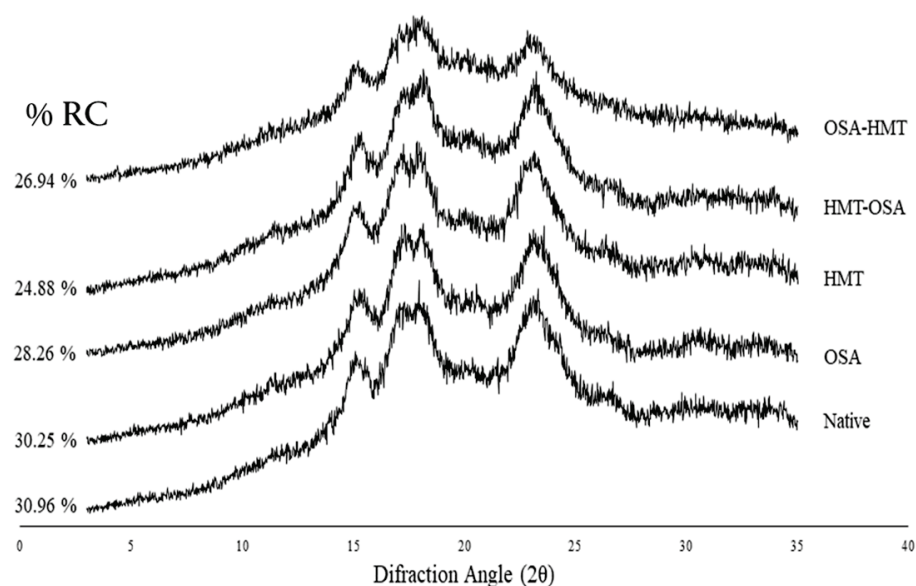
The granule morphology of native and modified arrowroot starches is presented in Figure 1. The granules of arrowroot starch are spherical and ellipsoid to oval-shaped. There was no damage on the surface of starch granules after OSA treatment. In HMT-modified starch, in both single and dual modifications (HMT, HMT-OSA, and OSA-HMT), the damage occurred on the surface of the granules, where the surface became rougher due to the formation of fine cracks.



**Figure 1.** Granule morphology of native and modified arrowroot starches with 5000 $\times$  and 10,000 $\times$  magnification. OSA = octenyl-succinic anhydride treatment; HMT = heat-moisture treatment; HMT-OSA = HMT followed by OSA treatment; OSA-HMT = OSA followed by HMT treatment.

### 3.2. Starch Crystallinity

The crystallinity properties of native and modified arrowroot starch are presented in Figure 2. According to the diffractograms, both native and modified arrowroot starch possessed an A-type crystalline pattern, which was indicated by several diffraction peaks at  $15^\circ$ ,  $17^\circ$ ,  $18^\circ$ ,  $23^\circ$ , and  $26^\circ$  ( $2\theta$ ), showing that all of the treatments did not alter the crystalline pattern of the arrowroot starches. However, in terms of relative crystallinity (RC), the modified starches have lower RC compared to the native starch. The native arrowroot starch has an RC value of 30.96%, while OSA, HMT, HMT-OSA, and OSA-HMT starches have 30.25%, 28.26%, 24.88%, and 26.94% RC values, respectively. Additionally, HMT-modified starch in both single and dual modifications (HMT, HMT-OSA, and OSA-HMT) has a greater effect on RC than single OSA modification.



**Figure 2.** X-ray diffractograms of native and modified arrowroot starches. OSA = octenyl-succinic anhydride treatment; HMT = heat-moisture treatment; HMT-OSA = HMT followed by OSA treatment; OSA-HMT = OSA followed by HMT treatment.

### 3.3. Thermal Properties

DSC is used for thermal analysis in order to determine the transition of starch crystallinity caused by heating with the following parameters: (1)  $T_o$ , or temperature onset, is the temperature at which gelatinization begins, and is also defined as the melting temperature of the weakest crystals in starch granules; (2)  $T_p$ , or peak temperature, represents the the endothermic peak on the DSC thermogram; (3)  $T_c$ , or conclusion temperature, is the final temperature at which the sample is wholly gelatinized, and is sometimes known as the crystalline melting temperature (high-perfection crystalline); and (4)  $\Delta H$  or enthalpy (J/g) is calculated based on the DSC endotherm, expressing the energy required to break the double helix structure during starch gelatinization [12,16].

The thermal properties of native and modified arrowroot starches are presented in Table 1. All modified starch has a lower  $T_o$  than native starch, except for HMT starch.  $T_p$  native starch decreased after modification from  $50.46^\circ\text{C}$  to  $39.83\text{--}44.36^\circ\text{C}$ . Both single methods (OSA and HMT) decreased  $T_c$ , but, conversely, both dual modification methods increased the  $T_c$  of native starch. The temperature range ( $T_c - T_o$ ) of modified starches was higher than native starch, except for HMT-starch, whereas the enthalpy of modified starch decreased significantly from  $1117.08$  (J/g) to  $936.44\text{--}647.30$  (J/g).

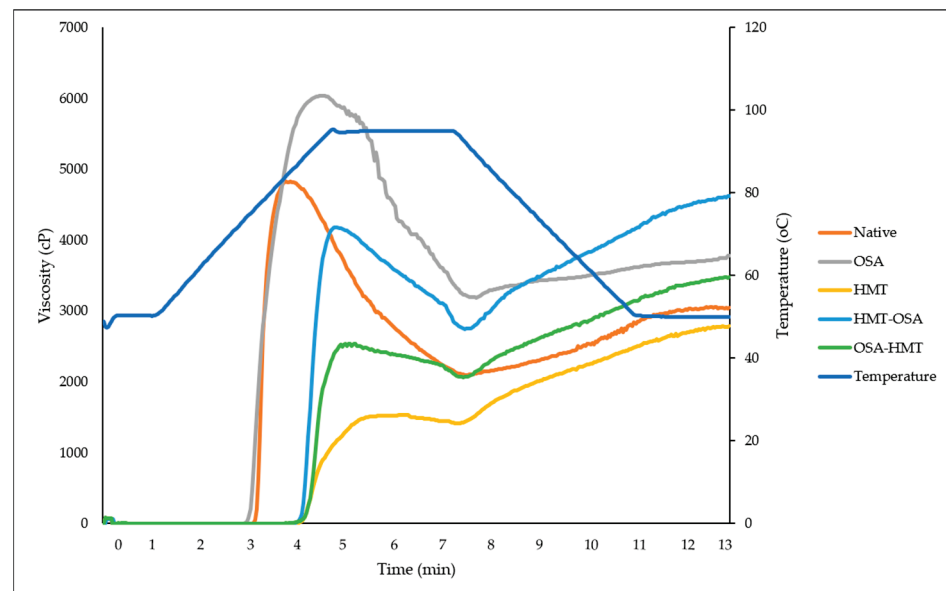
**Table 1.** Thermal properties of native and modified arrowroot starches.

Treatment	T <sub>0</sub> (°C)	T <sub>p</sub> (°C)	T <sub>c</sub> (°C)	T <sub>c</sub> -T <sub>0</sub> (°C)	ΔH (J/g)
Native	21.70 ± 3.86 <sup>a</sup>	50.46 ± 5.89 <sup>a</sup>	62.29 ± 3.60 <sup>b</sup>	40.60 ± 7.21 <sup>bc</sup>	1117.08 ± 56.09 <sup>a</sup>
OSA	14.39 ± 0.69 <sup>b</sup>	39.83 ± 3.96 <sup>b</sup>	58.99 ± 6.67 <sup>bc</sup>	44.60 ± 7.08 <sup>b</sup>	647.30 ± 45.86 <sup>d</sup>
HMT	20.43 ± 2.60 <sup>a</sup>	44.36 ± 2.60 <sup>ab</sup>	53.75 ± 1.65 <sup>c</sup>	33.32 ± 2.55 <sup>c</sup>	936.44 ± 35.08 <sup>b</sup>
HMT-OSA	10.89 ± 3.01 <sup>b</sup>	42.98 ± 3.62 <sup>ab</sup>	85.76 ± 1.11 <sup>a</sup>	74.87 ± 2.44 <sup>a</sup>	781.64 ± 30.73 <sup>c</sup>
OSA-HMT	11.38 ± 2.21 <sup>b</sup>	39.98 ± 5.51 <sup>b</sup>	83.96 ± 1.70 <sup>a</sup>	72.58 ± 1.32 <sup>a</sup>	902.26 ± 87.22 <sup>b</sup>

Means marked with different letters are significantly different ( $p < 0.05$ ). OSA = octenyl-succinic anhydride treatment; HMT = heat-moisture treatment; HMT-OSA = HMT followed by OSA treatment; OSA-HMT = OSA followed by HMT treatment.

### 3.4. Pasting Properties

The viscoamylograph and pasting properties parameters of native and modified arrowroot starches are presented in Figure 3 and Table 2, respectively. Both single HMT and dual modifications (HMT-OSA, OSA-HMT) increased PT and SB of native starch, but, conversely, decreased PV and BD viscosity of native starch, whereas single OSA has the opposite trend compared with the other modification treatments.



**Figure 3.** Viscoamylograph of native and modified arrowroot starches. OSA = octenyl-succinic anhydride treatment; HMT = heat-moisture treatment; HMT-OSA = HMT followed by OSA treatment; OSA-HMT = OSA followed by HMT treatment.

**Table 2.** Pasting properties of native and modified arrowroot starches.

Treatment	Pasting Temperature (°C)	Peak Viscosity (cP)	Hold Viscosity (cP)	Final Viscosity (cP)	Breakdown (cP)	Setback (cP)
Native	75.74 ± 0.26 <sup>a</sup>	4857 ± 42.52 <sup>d</sup>	2119 ± 37.58 <sup>bc</sup>	3087 ± 41.15 <sup>a</sup>	2738 ± 7.00 <sup>d</sup>	967 ± 15.50 <sup>a</sup>
OSA	73.02 ± 0.08 <sup>a</sup>	6094 ± 60.86 <sup>e</sup>	3033 ± 157.88 <sup>d</sup>	3956 ± 167.62 <sup>c</sup>	3060 ± 216.75 <sup>e</sup>	923 ± 316.74 <sup>a</sup>
HMT	86.91 ± 0.42 <sup>c</sup>	1604 ± 57.50 <sup>a</sup>	1486 ± 60.00 <sup>a</sup>	2860 ± 61.49 <sup>a</sup>	118 ± 3.61 <sup>a</sup>	1373 ± 9.50 <sup>b</sup>
HMT-OSA	86.78 ± 0.46 <sup>c</sup>	3111 ± 263.28 <sup>c</sup>	2261 ± 79.00 <sup>c</sup>	4081 ± 221.72 <sup>c</sup>	850 ± 188.80 <sup>c</sup>	1787 ± 122.11 <sup>c</sup>
OSA-HMT	83.21 ± 4.03 <sup>b</sup>	2544 ± 63.58 <sup>b</sup>	2063 ± 99.00 <sup>b</sup>	3621 ± 242.31 <sup>b</sup>	481 ± 35.59 <sup>b</sup>	1557 ± 166.08 <sup>bc</sup>

Means marked with different letters are significantly different ( $p < 0.05$ ). OSA = octenyl-succinic anhydride treatment; HMT = heat-moisture treatment; HMT-OSA = HMT followed by OSA treatment; OSA-HMT = OSA followed by HMT treatment.

### 3.5. Texture Properties

Texture properties parameters of native and modified arrowroot starches are presented in Table 3. Both single modifications, OSA and HMT alone, increased the gel hardness of native arrowroot starch, and the converse effect was seen for the dual modifications. All modified starches have higher adhesiveness and lower springiness and cohesiveness than native starch. Both dual modifications, HMT-OSA and OSA-HMT, decreased the gumminess of native arrowroot starch from 208.95 to 29.21–59.60.

**Table 3.** Texture profile of native and modified arrowroot starches.

Treatment	Hardness (gF)	Adhesiveness	Springiness	Cohesiveness	Gumminess
Native	244.51 ± 36.93 <sup>b</sup>	−3.10 ± 2.74 <sup>c</sup>	1.58 ± 1.02 <sup>a</sup>	0.86 ± 0.02 <sup>c</sup>	208.95 ± 27.82 <sup>b</sup>
OSA	485.03 ± 35.65 <sup>d</sup>	−34.20 ± 0.85 <sup>b</sup>	0.90 ± 0.01 <sup>a</sup>	0.76 ± 0.01 <sup>b</sup>	368.29 ± 21.10 <sup>d</sup>
HMT	406.78 ± 36.95 <sup>c</sup>	−47.50 ± 24.71 <sup>b</sup>	0.90 ± 0.04 <sup>a</sup>	0.68 ± 0.05 <sup>a</sup>	274.39 ± 21.43 <sup>c</sup>
HMT-OSA	43.68 ± 5.89 <sup>a</sup>	−54.14 ± 6.61 <sup>b</sup>	0.83 ± 0.00 <sup>a</sup>	0.60 ± 0.02 <sup>a</sup>	29.21 ± 3.49 <sup>a</sup>
OSA-HMT	76.95 ± 14.88 <sup>a</sup>	−103.14 ± 6.12 <sup>a</sup>	0.86 ± 0.02 <sup>a</sup>	0.64 ± 0.06 <sup>a</sup>	59.59 ± 10.38 <sup>a</sup>

Means marked with different letters are significantly different ( $p < 0.05$ ). OSA = octenyl-succinic anhydride treatment; HMT = heat-moisture treatment; HMT-OSA = HMT followed by OSA treatment; OSA-HMT = OSA followed by HMT treatment.

### 3.6. Functional Properties

OSA modification, for both single OSA and dual HMT-OSA, significantly increased the SV of native starch, but we saw a converse trend for OSA-HMT. All modified starch has lower solubility and higher syneresis than native starch (Table 4). HMT starch, for both single HMT and dual modifications (HMT-OSA, OSA-HMT), increased the water absorption capacity (WAC) and decreased the oil absorption capacity (OAC) of native starch. All modification treatments increased the syneresis of native starch.

**Table 4.** Functional properties of native and modified arrowroot starches.

Treatment	Swelling Volume (mL/g db)	Solubility (%)	WAC (g/g db)	OAC (g/g db)	Syneresis (%)
Native	16.27 ± 0.12 <sup>c</sup>	9.33 ± 0.14 <sup>c</sup>	1.13 ± 0.20 <sup>b</sup>	2.33 ± 0.03 <sup>b</sup>	7.02 ± 0.06 <sup>a</sup>
OSA	25.84 ± 0.56 <sup>e</sup>	9.13 ± 0.21 <sup>b</sup>	0.83 ± 0.10 <sup>a</sup>	2.31 ± 0.07 <sup>b</sup>	18.71 ± 0.96 <sup>b</sup>
HMT	11.46 ± 0.54 <sup>a</sup>	8.92 ± 0.14 <sup>a</sup>	1.35 ± 0.05 <sup>c</sup>	2.15 ± 0.12 <sup>a</sup>	38.76 ± 0.49 <sup>c</sup>
HMT-OSA	17.66 ± 0.17 <sup>d</sup>	9.08 ± 0.09 <sup>b</sup>	1.41 ± 0.07 <sup>c</sup>	2.21 ± 0.09 <sup>a</sup>	59.06 ± 2.27 <sup>d</sup>
OSA-HMT	14.31 ± 0.34 <sup>b</sup>	8.90 ± 0.04 <sup>a</sup>	1.60 ± 0.06 <sup>d</sup>	2.20 ± 0.04 <sup>a</sup>	65.80 ± 3.54 <sup>e</sup>

Means marked with different letters are significantly different ( $p < 0.05$ ). OSA = octenyl-succinic anhydride treatment; HMT = heat-moisture treatment; HMT-OSA = HMT followed by OSA treatment; OSA-HMT = OSA followed by HMT treatment.

WAC describes the amount of water available for gelatinization [12]. WAC of native and modified arrowroot starches ranges from 0.83–1.60 g/g (db). The WAC of native arrowroot starch is 1.13 g/g db, which is smaller than in the previous study, where it was 1.81 g/g db [17]. Meanwhile, the ability of starch to absorb oil is called OAC, which could also represent the emulsifying properties of the starch [18]. The OAC of native and modified arrowroot starches range from 2.15–2.33 g/g db. All of the modification methods, except for OSA, decreased the OAC of native starch from 2.33 g/g db to 2.15–2.21 g/g db.

### 3.7. Color Characteristics

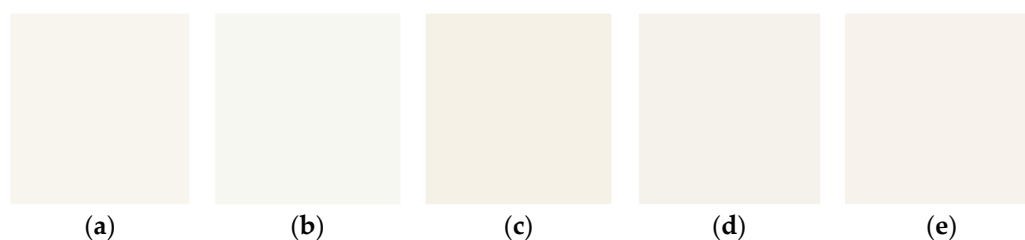
The color parameters of native and modified arrowroot starches are  $L^*$ ,  $a^*$ , and  $b^*$ , whiteness index, and  $\Delta E$  (Table 5). HMT modification of both single HMT and dual modifications (HMT-OSA and OSA-HMT) significantly decreased the  $L^*$  value of native arrowroot starch. Single OSA did not alter the  $a^*$  value, whereas HMT modification of both single and dual had a different effect on the  $a^*$  value of native arrowroot starch. Native and OSA-modified arrowroot starches have a negative value of  $a^*$ , which indicates that the

color tends towards greenness, whereas all HMT modifications have a positive value of  $a^*$ , which indicates that the color tends towards redness. All modified starch has a lower whiteness index than native starch, except for OSA starch. OSA starch has the highest whiteness index among all of the samples.  $\Delta E$  is a value indicating the total color difference between a modified starch and the native starch. The  $\Delta E$  of modified starch ranged from 0.64 to 1.61. The higher the  $\Delta E$ , the greater the color differences between modified and native starches, whereas the HMT starch has the highest  $\Delta E$  among other modified starches. The color images of native and modified arrowroot starches which were captured from Spectrophotometer CM-5 are presented in Figure 4.

**Table 5.** Color parameters of native and modified arrowroot starches.

Treatment	$L^*$	$a^*$	$b^*$	Whiteness Index	$\Delta E$
Native	$96.26 \pm 0.03^d$	$-0.25 \pm 0.01^a$	$3.18 \pm 0.03^c$	$95.09 \pm 0.01^d$	-
OSA	$96.39 \pm 0.19^d$	$-0.29 \pm 0.01^a$	$2.13 \pm 0.10^a$	$95.80 \pm 0.11^e$	$1.08 \pm 0.11$
HMT	$94.96 \pm 0.12^a$	$0.09 \pm 0.00^b$	$4.07 \pm 0.01^d$	$93.52 \pm 0.09^a$	$1.61 \pm 0.09$
HMT-OSA	$95.44 \pm 0.24^b$	$0.05 \pm 0.03^b$	$3.07 \pm 0.23^{bc}$	$94.51 \pm 0.33^b$	$0.92 \pm 0.13$
OSA-HMT	$95.80 \pm 0.09^c$	$0.07 \pm 0.07^b$	$2.97 \pm 0.25^b$	$94.86 \pm 0.22^c$	$0.64 \pm 0.09$

Means marked with different letters are significantly different ( $p < 0.05$ ). OSA = octenyl-succinic anhydride treatment; HMT = heat-moisture treatment; HMT-OSA = HMT followed by OSA treatment; OSA-HMT = OSA followed by HMT treatment.



**Figure 4.** The color of arrowroot starch (a) native, (b) OSA, (c) HMT, (d) HMT-OSA, and (e) OSA-HMT. The color images were captured from Spectrophotometer CM-5.

## 4. Discussion

### 4.1. Granule Morphology

Native arrowroot starch has a round, oval shape with a granular surface that is slightly textured without cracks, and this is in line with some of the previous studies [1,19]. The morphology of OSA starch granules did not show significant changes compared to native starch granules. This result was consistent with the study of OSA-modified Japonica rice starch [20] and OSA-modified sago starch [13], whereas the HMT caused damage to the starch granules, with cracks forming and the surface of the granules becoming rougher. Some of the previous studies also reported granule surface deformation after HMT [5,6,12], and this is due to the thermal strength, which changes the morphology of the arrowroot starch [11]. Both dual-modified starch granules (OSA-HMT and HMT-OSA) showed similar surface characteristics to the HMT starch. The surface of the granules became rougher, and there were also indentations. This indicated that thermal treatment significantly dominates the alteration of granule morphology of dual-modified arrowroot starch.

### 4.2. Crystallinity

X-ray Diffraction (XRD) is a method for assessing and quantifying long-range crystalline order in starch [21]. Figure 2 shows that native and modified starches have a similar crystallinity pattern, i.e., an A-type crystalline pattern, as indicated by several diffraction peaks at  $2\theta$   $15^\circ$ ,  $17^\circ$ ,  $18^\circ$ ,  $23^\circ$ , and  $26^\circ$  [22], which indicated that all of the modification treatments did not significantly affect the crystalline type of native arrowroot starch. Several studies have reported that native arrowroot starch has an A-type crystalline pattern [1,23].



However, this is not in agreement with another study by Nogueira et al. [24], which reported that arrowroot starch has a C-type crystalline pattern, indicating a mixture of polymorphs types A and B. The HMT showed no change in the crystalline pattern, similar to the study of Marta et al. [11] on banana starch, and a similar trend has been seen on OSA-sago starch [13].

Relative crystallinity (RC) was calculated based on the ratio of the diffraction peak area (crystalline area) to the total diffraction area [25]. Arrowroot native starch has an RC of 30.96%, which was in range with the other studies (52.84% [26] and 28.8–30.2%) [27]. All modification treatments, however, decreased the RC of native starch—that is, from 30.96% for native arrowroot starch to 30.25% for OSA-treated starch, 28.26% for HMT-treated starch, 28.88% for HMT-OSA, and 26.94% for OSA-HMT. Several studies have reported that HMT decreased the RC, such as in sago starch [13], banana starch [11,13]; mango kernel starch [28], breadfruit starch [6], rice, cassava, and pinhão starches [29]. Decreased RC in hydrothermally modified starches, both for single HMT and dual modifications (HMT, HMT-OSA, and OSA-HMT), can be associated with changes in the crystalline phase (amylopectin) of starch, where dehydration and double helix movements can disrupt starch crystallinities and change the crystal orientation of the semi-crystalline fraction to the amorphous phase [30–32] or possibly partial gelatinization [4,33]. The RC of OSA starches, for both single and dual modified starches (OSA, OSA-HMT, and HMT-OSA), was lower than its native counterpart, which was in line with some of the previous studies [13,34,35]. These results indicated that OSA esterification occurs in the amorphous region of starch granules and slightly changes the starch crystal structure.

#### 4.3. Thermal Properties

Esterification using OSA on arrowroot starch causes a decrease in  $T_o$ ,  $T_p$ , and  $\Delta H$  compared to native starch, which is in agreement with some of the previous studies [36,37]. The introduction of OSA molecules changes the degree of hydrogen bonding, which tends to weaken the interactions between the starch macromolecules, allowing the granules to swell and melt at lower temperatures [7,38], whereas heat-moisture treatment could weaken the interaction between amylose-amylose, amylose-amylopectin, and amylose-lipid, which leads to imperfect crystal formation. This phenomenon could cause a decrease of  $T_c$  and  $\Delta H$  in HMT-treated starch [39]. Some previous studies have reported that HMT-modified starch showed higher gelatinization parameters ( $T_o$ ,  $T_p$ ,  $T_c$ ) than native starch [12,30,40,41], whereas in this study,  $T_o$  and  $T_p$  of HMT starch were not significantly different to native starch. Both dual-modified starch HMT-OSA and OSA-HMT starches tend to have thermal characteristics that are almost similar, where the  $T_o$ ,  $T_p$ ,  $T_c$ , and  $T_c - T_o$  are not significantly different from each other, whereas  $\Delta H$  of OSA-HMT starch is significantly higher than HMT-OSA starch.

#### 4.4. Pasting Properties

The increase in PT and the decrease in PV on HMT starch, both for single HMT and dual modifications (HMT-OSA and OSA-HMT), could be due to the partial breakage of the ordered chain structure and the rearranging of the broken molecules, facilitated by the high temperature (100 °C) and limited moisture content (30%) during HMT. As a result, the forces of the intra-granular bonds would be augmented, and the linkages between starch chains would be strengthened. The HMT-treated starch samples needed greater heat for structural breakdown and paste production, resulting in a lower paste viscosity [4]. On the other hand, an increase in PV was observed in single OSA-treated starch. According to Bajaj et al. [8], substituting bulky octenyl groups could decrease the inter- and intramolecular bond between starch granules, resulting in limited incorporation of water into starch molecules. When OSA groups are substituted, the starch granule is destroyed, which enhances swelling and raises PV. The hydrophobic properties of OSA also increased the viscosity of starch. This characteristic was discovered advantageous for making mayonnaise with improved emulsion stability [8].

The significant difference in PV between HMT-OSA and OSA-HMT-treated starch is because HMT facilitated this OSA particle to attack more of the –OH group in starch. According to Park et al. [42], HMT before cross-linking could increase the phosphate content of the starch, showing that the HMT facilitates the incorporation of the cross-linking agent to react more with starch granules. This occurred in the octenyl group as well. The OSA modification increased the BD, which was in line with some of the previous studies [8,43], whereas the other modifications significantly decreased the BD of the native starches. The lower BD indicated the higher thermal stability of starch. All HMT modifications, both single and dual modifications, have a higher SB than native and single OSA starch, which indicates that HMT increases the ability of starch to retrograde.

From the industrial point of view, the modification of arrowroot starch could give arrowroot more value, as the starch could be used more in the food industry. HMT and dual-modified starches (OSA-HMT and HMT-OSA starch) have a higher thermal stability than native starch, as shown by the lower breakdown viscosity of the starches. Starch with good thermal stability could be used as a thickening agent for food products that need to be sterilized, e.g., sauce, paste, etc. [39], whereas OSA starch has a lower ability to retrograde, which indicates that the starch may be used as an ingredient in baby food and baked goods (as it can inhibit staling on bread).

#### 4.5. Texture Properties

Texture parameters in starch have an important role because starch can be a texturizer agent, such as a thickening and gelling agent. TPA (texture profile analysis) is used to observe texture parameters, such as hardness, adhesiveness, springiness, cohesiveness, and gumminess [44]. Gel hardness or hardness is related to the strength of the gel network, and changes in hardness are related to the effect of swelling granules and amylose content [44,45], and hardness increases with increasing amylose content. The hardness of HMT and OSA-modified starches were higher than native starch, whereas the amylose content of native starch was lower than both HMT and OSA starch. The amylose content for native, HMT, and OSA starches are 29.15%db, 36.01%db, and 33.44%db, respectively. The gel network structure depends on the quantity and intensity of hydrogen bonds formed between the amylose chains [46]. Conversely, the hardness of dual-modified starch (OSA-HMT and HMT-OSA starch) decreased very sharply compared to native starch, and it was not in line with the amylose content of the dual-modified starches, where the hardness decreased with increasing amylose content. The amylose content of HMT-OSA and OSA-HMT starches was 35.32%db and 36.36%db, respectively. This indicated that hardness is not only affected by amylose content. The adhesiveness of native starch was higher than all of the modified starches, which is in line with the other studies [47,48]. All modification treatments did not significantly affect the springiness of starch gel, but they decreased the cohesiveness, which may be due to the degradation of starch molecules, resulting in a weaker starch network structure [49]. In terms of gumminess, dual-modified starches tend to have lower values compared to both native and single-modified starch. The low level of elasticity in the dual-modified starch is influenced by its low hardness and low cohesive strength compared to single-modified starch (OSA and HMT).

#### 4.6. Functional Properties

Swelling volume (SV) measures the hydration capacity of starch molecules due to the presence of water trapped in granules [50]. SV is related to amylose leaching or the solubility of starch [51]. Solubility indicates the amount of amylose leaching, which dissociates and diffuses out of the starch granules during the gelatinization process, resulting in starch swelling [10].

The SV of HMT starch decreased when compared to native starch, which is in line with other studies [2,12,52]. Furthermore, the decrease might be due to the rearrangement of starch molecules, increased intramolecular forces [52], and amylose-amylose, amylopectin-amylose, and amylopectin-amylopectin interactions, which become stronger where the

starch granules become more rigid [11]. Among other modified starches, OSA starch has the highest SV. Furthermore, Park et al. [51] reported that the SV of OSA arrowroot starch was significantly higher than its native starch. This increase in swelling strength is associated with an increase in the ability of water to percolate into starch granules [53]. HMT-OSA-modified starch had a higher SV than OSA-HMT starch. It was presumed that the HMT process resulted in cracks and porous starch granules. When the OSA treatment was applied, the presence of succinate groups could weaken the internal bonds in the starch granules and increase the percolation of water so that the SV of HMT-OSA starch became higher [53,54].

All modified starches have lower solubility than native starch, and this is caused by amylose leaching during the starch gelatinization process. Amylose is in the crystalline region and is relatively small in size and linear shape, making it easier to leach out from the starch granules [25]. However, another study [24] reported that HMT on corn starch increased its solubility, which was influenced by the treatment time: the longer the treatment time, the more solubility [2].

Among the modified starches, OSA starch has the lowest WAC (0.83 g/g db). The reduced WAC on OSA starch was due to the presence of a hydrophobic substituent group from OSA that replaces the hydroxyl group on starch granules, which causes an increase in the hydrophobicity of starch [55], whereas HMT starch increased WAC (1.35 g/g db), which is in agreement with some of the previous studies [51,56]. The increased WAC of HMT starch was caused by the breaking of hydrogen bonds in the crystalline and amorphous regions, resulting in the expansion of the amorphous areas, which increased the hydrophilic properties of the starch [18,57]. The presence of pores on the surface of starch granules can also increase WAC because it will be easier for water to diffuse into the granules [12]. The increased WAC in dual-modified starch (HMT-OSA and OSA-HMT) was significantly influenced by the second modification treatment applied because HMT-OSA starch showed a lower WAC than OSA-HMT starch. OSA treatment after HMT was suspected to reduce starch hydrophilicity and increase its hydrophobicity due to the presence of OSA groups, which decreased WAC.

The esterification process with OSA increased starch's hydrophobicity, thereby increasing the OAC [7]. On the other hand, the OAC is related to the degree of substitution (DS), where the oil absorption capacity increases with the degree of substitution of OSA [58].

Freeze-thaw stability was determined as syneresis (%). Syneresis releases water from gel or starch paste during cooling, storage, and freeze-thawing [59]. High syneresis indicates low stability at low-temperature storage [12]. Native arrowroot starch has the lowest syneresis among other starches, and this is in agreement with some of the previous studies on arrowroot starch [19,60]. All modifications applied in this study tend to increase syneresis. However, when compared with modified starches, OSA starch has higher stability, which indicates that OSA starch is more stable at low-temperature storage conditions. A previous study reported that the modification of starch into succinate derivatives (OSA starch) can improve the freeze-thaw stability (FTS) of corn and amaranth starch [50]. This is associated with a steric effect on the OSA group, which can prevent starch chain alignment when stored at low temperatures [7], whereas in this study, OSA modification cannot improve the FTS of native arrowroot starch. Increased syneresis in HMT starch might be due to the resulting random interactions reducing the water-holding capacity of the starch gel [61]. The intensity of syneresis depends on various factors, such as the composition of the amylose fraction, the length of the amylopectin chains, and the degree of polymerization of amylose and amylopectin [57].

HMT and OSA-HMT decrease SV and SOL and increase the WAC of native starch, which indicates that HMT and OSA-HMT starches can be applied in pasta and noodle formulations. Marta et al. [62] have reported that HMT banana starch can be used as an ingredient in noodle production. All modified starches have higher syneresis, so they cannot be applied in frozen foods.

#### 4.7. Color Analysis

Color is a characteristic that has an important role in determining the quality and the level of consumer acceptance in selecting a product. In flour or starch products, consumers generally prefer products that are white or bright in color. To determine the color of both native and modified arrowroot starch objectively, color analysis was performed. Color testing of products, mainly arrowroot starch, can be carried out using a stand-alone, top-port color measuring instrument, which was the Spectrophotometer CM-5 in this research. The color of each starch sample was then interpreted by referring to the CIELAB systems through the  $L^*$ ,  $a^*$ , and  $b^*$  values [63].

The highest lightness ( $L^*$ ) was shown by OSA starch (96.39), while HMT starch showed the lowest lightness (94.96). There was a significant difference in lightness, especially for HMT-modified starch. This is presumably because thermal treatment can cause the degradation of color pigments in starch. The redness ( $a^*$ ) in arrowroot starch with a negative value is indicated by both native and OSA starches, which indicated a tendency to be green in color [64]. Meanwhile, the positive values for HMT starches, both single HMT and dual modified starches (HMT-OSA and OSA-HMT starches), indicated that these starches tended to be red. The color shift to red was caused by the application of thermal treatment. The level of yellowness ( $b^*$ ) in all arrowroot starch (native and modified) has a positive value, indicating that all starch leads to a yellow color. The highest  $b^*$  value was shown by HMT starch (4.07), while the lowest was indicated by OSA starch (2.13). This means that HMT starch is more yellow than OSA starch (Figure 3).

The whiteness index (WI) is based on a scale of 0–100, with the highest value described as the highest level of lightness. The WI value is positively correlated with the  $L^*$  value; the higher the WI, the higher the  $L^*$  value. HMT-modified starch, for both the single HMT and dual-modified starches, had low WI. The HMT modification process that was carried out reduced the lightness level of starch. Total color difference ( $\Delta E$ ) is a parameter used to assess how much change or difference can be seen in the  $Lab^*$  value results in ingredients or food after specific treatments [65]. Dual modification, especially OSA-HMT starch, has the smallest  $\Delta E$  value, which indicates that the color produced between native and OSA-HMT starch is not much different, whereas HMT starch showed the highest  $\Delta E$  value, in which there was a significant difference/change in starch color compared to native starch.

#### 5. Conclusions

All modification treatments, both for the single and dual modifications, had significant effects on granule morphology, crystallinity, thermal, pasting, and functional properties, texture, and color characteristics of native arrowroot starch. The granules of arrowroot starch are spherical and ellipsoid to oval shaped. There was no damage on the surface of the starch granules after OSA. In HMT-modified starch, both for single and dual modifications (HMT, HMT-OSA, and OSA-HMT), the damage occurred on the surface of the granules. Native and modified starches have a similar crystallinity pattern, which was an A-type crystalline pattern. All modification treatments decreased the RC of native starch, where HMT has a greater effect on RC than OSA. Both single HMT and dual modification (HMT-OSA, OSA-HMT) increased PT and SB, and, conversely, decreased PV and BD viscosity of native starch. All HMT treatments, both for single and dual modifications, can improve the thermal stability of native starch, especially the HMT single treatment, whereas OSA single treatment has the opposite trend compared with the other modification treatments. OSA starch has a firm texture characteristic, which is indicated by the high value of hardness and gumminess. Both single OSA treatment and HMT-OSA significantly increased the SV of native starch, but, conversely, trend for the OSA-HMT. All modified starches have lower solubility and higher syneresis than native starch. Both single HMT modification and dual modifications (HMT-OSA, OSA-HMT) increase WAC and decrease the OAC of native starch. HMT starch for both single and dual modifications have low  $L^*$  and WI values, while OSA starch has the brightest color among other starches. Based on pasting and functional properties, both HMT and OSA-HMT starch can be applied in pasta and



noodle formulation and also as a thickening agent, whereas OSA starch can be used as an ingredient in baby food and bakeries because it has a low ability to retrograde.

**Author Contributions:** Conceptualization, H.M. and M.D.; methodology, H.M. and D.S.; software, A.R.; validation, H.M., Y.C. and M.D.; formal analysis, A.R. and G.P.S.; investigation, H.M. and T.Y.; data curation, D.S., A.R. and G.P.S.; writing—original draft preparation, H.M., A.R. and G.P.S.; writing—review and editing, Y.C., M.D. and T.Y.; visualization, A.R. and G.P.S.; supervision, H.M., Y.C. and M.D.; funding acquisition, H.M. and Y.C. All authors have read and agreed to the published version of the manuscript.

**Funding:** This research was funded by Grant of Ministry of Education, Culture, Research, and Technology (MoECRT), Republic of Indonesia [grant number: 2393/UN6.3.1/PT.00/2022] and The APC was funded by Universitas Padjadjaran.

**Data Availability Statement:** Not applicable.

**Acknowledgments:** The authors acknowledge the facilities, scientific and technical support from Advanced Characterization Laboratories Cibinong—Integrated Laboratory of Bioproduct, National Research and Innovation Agency through E-Layanan Sains, Badan Riset dan Inovasi Nasional.

**Conflicts of Interest:** The authors declare no conflict of interest.

## References

1. Tarique, J.; Sapuan, S.M.; Khalina, A.; Sherwani, S.F.K.; Yusuf, J.; Ilyas, R.A. Recent Developments in Sustainable Arrowroot (*Maranta arundinacea* Linn) Starch Biopolymers, Fibres, Biopolymer Composites and Their Potential Industrial Applications: A Review. *J. Mater. Res. Technol.* **2021**, *13*, 1191–1219. [CrossRef]
2. Pepe, L.S.; Moraes, J.; Albano, K.M.; Telis, V.R.; Franco, C.M. Effect of Heat-Moisture Treatment on the Structural, Physicochemical, and Rheological Characteristics of Arrowroot Starch. *Food Sci. Technol. Int.* **2016**, *22*, 256–265. [CrossRef]
3. Polesi, L.F.; Sarmiento, S.B.S. Structural and Physicochemical Characterization of Rs Prepared Using Hydrolysis and Heat Treatments of Chickpea Starch. *Starch Stärke* **2011**, *63*, 226–235. [CrossRef]
4. Zavareze, E.d.R.; Dias, A.R.G. Impact of Heat-Moisture Treatment and Annealing in Starches: A Review. *Carbohydr. Polym.* **2011**, *83*, 317–328. [CrossRef]
5. Cahyana, Y.; Wijaya, E.; Halimah, T.S.; Marta, H.; Suryadi, E.; Kurniati, D. The Effect of Different Thermal Modifications on Slowly Digestible Starch and Physicochemical Properties of Green Banana Flour (*Musa acuminata* colla). *Food Chem.* **2019**, *274*, 274–280. [CrossRef]
6. Marta, H.; Cahyana, Y.; Arifin, H.R.; Khairani, L. Comparing the Effect of Four Different Thermal Modifications on Physicochemical and Pasting Properties of Breadfruit (*Artocarpus altilis*) Starch. *Int. Food Res. J.* **2019**, *26*, 269–276.
7. Sweedman, M.C.; Tizzotti, M.J.; Schäfer, C.; Gilbert, R.G. Structure and Physicochemical Properties of Octenyl Succinic Anhydride Modified Starches: A Review. *Carbohydr. Polym.* **2013**, *92*, 905–920. [CrossRef]
8. Bajaj, R.; Singh, N.; Kaur, A. Properties of Octenyl Succinic Anhydride (OSA) Modified Starches and Their Application in Low Fat Mayonnaise. *Int. J. Biol. Macromol.* **2019**, *131*, 147–157. [CrossRef]
9. Chen, X.; He, X.; Huang, Q. Effects of Hydrothermal Pretreatment on Subsequent Octenylsuccinic Anhydride (OSA) Modification of Cornstarch. *Carbohydr. Polym.* **2014**, *101*, 493–498. [CrossRef] [PubMed]
10. Segura-Campos, M.; Chel-Guerrero, L.; Betancur-Ancona, D. Synthesis and Partial Characterization of Octenylsuccinic Starch from Phaseolus Lunatus. *Food Hydrocoll.* **2008**, *22*, 1467–1474. [CrossRef]
11. Marta, H.; Cahyana, Y.; Djali, M. Densely Packed-Matrices of Heat Moisture Treated-Starch Determine the Digestion Rate Constant as Revealed by Logarithm of Slope Plots. *J. Food Sci. Technol.* **2021**, *58*, 2237–2245. [CrossRef] [PubMed]
12. Marta, H.; Cahyana, Y.; Bintang, S.; Soeherman, G.P.; Djali, M. Physicochemical and Pasting Properties of Corn Starch as Affected by Hydrothermal Modification by Various Methods. *Int. J. Food Prop.* **2022**, *25*, 792–812. [CrossRef]
13. Marta, H.; Hasya, H.N.; Lestari, Z.I.; Cahyana, Y.; Arifin, H.R.; Nurhasanah, S. Study of Changes in Crystallinity and Functional Properties of Modified Sago Starch (*Metroxylon* sp.) Using Physical and Chemical Treatment. *Polymers* **2022**, *14*, 4845. [CrossRef] [PubMed]
14. Yang, Z.; Wang, W.; Wang, H.; Ye, Q. Effects of a Highly Resistant Rice Starch and Pre-Incubation Temperatures on the Physicochemical Properties of Surimi Gel from Grass Carp (*Ctenopharynxodon Idellus*). *Food Chem.* **2014**, *145*, 212–219. [CrossRef]
15. Ačkar, Đ.; Babić, J.; Šubarić, D.; Kopjar, M.; Miličević, B. Isolation of Starch from Two Wheat Varieties and Their Modification with Epichlorohydrin. *Carbohydr. Polym.* **2010**, *81*, 76–82. [CrossRef]
16. Luo, Z.; Fu, X.; He, X.; Luo, F.; Gao, Q.; Yu, S. Effect of Ultrasonic Treatment on the Physicochemical Properties of Maize Starches Differing in Amylose Content. *Starch Stärke* **2008**, *60*, 646–653. [CrossRef]
17. Jyothi, A.N.; Sheriff, J.T.; Sajeev, M.S. Physical and Functional Properties of Arrowroot Starch Extrudates. *J. Food Sci.* **2009**, *74*, E97–E104. [CrossRef]



18. Adebowale, K.O.; Olu-Owolabi, B.I.; Olawumi, E.k.; Lawal, O.S. Functional Properties of Native, Physically and Chemically Modified Breadfruit (*Artocarpus artilis*) Starch. *Ind. Crops Prod.* **2005**, *21*, 343–351. [CrossRef]
19. Charles, A.L.; Cato, K.; Huang, T.-C.; Chang, Y.-H.; Ciou, J.-Y.; Chang, J.-S.; Lin, H.-H. Functional Properties of Arrowroot Starch in Cassava and Sweet Potato Composite Starches. *Food Hydrocoll.* **2016**, *53*, 187–191. [CrossRef]
20. Zhang, W.; Cheng, B.; Li, J.; Shu, Z.; Wang, P.; Zeng, X. Structure and Properties of Octenyl Succinic Anhydride-Modified High-Amylose Japonica Rice Starches. *Polymers* **2021**, *13*, 1325. [CrossRef]
21. Warren, F.; Gidley, M.; Flanagan, B. Infrared Spectroscopy as a Tool to Characterise Starch Ordered Structure—A Joint FTIR-ATR, NMR, XRD and DSC Study. *Carbohydr. Polym.* **2015**, *139*, 35–42. [CrossRef] [PubMed]
22. Lopez-Rubio, A.; Flanagan, B.M.; Gilbert, E.P.; Gidley, M.J. A Novel Approach for Calculating Starch Crystallinity and Its Correlation with Double Helix Content: A Combined Xrd and Nmr Study. *Biopolymers* **2008**, *89*, 761–768. [CrossRef] [PubMed]
23. Villas-Boas, F.; Franco, C.M.L. Effect of Bacterial  $\beta$ -Amylase and Fungal  $\alpha$ -Amylase on the Digestibility and Structural Characteristics of Potato and Arrowroot Starches. *Food Hydrocoll.* **2016**, *52*, 795–803. [CrossRef]
24. Nogueira, G.F.; Fakhouri, F.M.; de Oliveira, R.A. Extraction and Characterization of Arrowroot (*Maranta arundinaceae* L.) Starch and Its Application in Edible Films. *Carbohydr. Polym.* **2018**, *186*, 64–72. [CrossRef]
25. Marta, H.; Cahyana, Y.; Djali, M.; Arcot, J.; Tensiska, T. A Comparative Study on the Physicochemical and Pasting Properties of Starch and Flour from Different Banana (*Musa* spp.) Cultivars Grown in Indonesia. *Int. J. Food Prop.* **2019**, *22*, 1562–1575. [CrossRef]
26. Handarini, K.; Hamdani, J.S.; Cahyana, Y.; Setiasih, I.S. Gaseous Ozonation at Low Concentration Modifies Functional, Pasting, and Thermal Properties of Arrowroot Starch (*Maranta arundinaceae*). *Starch Stärke* **2020**, *72*, 1900106. [CrossRef]
27. Barroso, A.G.; del Mastro, N.L. Physicochemical Characterization of Irradiated Arrowroot Starch. *Radiat. Phys. Chem.* **2019**, *158*, 194–198. [CrossRef]
28. Bharti, I.; Singh, S.; Saxena, D.C. Exploring the Influence of Heat Moisture Treatment on Physicochemical, Pasting, Structural and Morphological Properties of Mango Kernel Starches from Indian Cultivars. *LWT Food Sci. Technol.* **2019**, *110*, 197–206. [CrossRef]
29. Klein, B.; Pinto, V.Z.; Vanier, N.L.; Zavareze, E.d.R.; Colussi, R.; Evangelho, J.A.d.; Gutkoski, L.C.; Dias, A.R.G. Effect of Single and Dual Heat–Moisture Treatments on Properties of Rice, Cassava, and Pinhao Starches. *Carbohydr. Polym.* **2013**, *98*, 1578–1584. [CrossRef]
30. Chen, Y.; Yang, Q.; Xu, X.; Qi, L.; Dong, Z.; Luo, Z.; Lu, X.; Peng, X. Structural Changes of Waxy and Normal Maize Starches Modified by Heat Moisture Treatment and Their Relationship with Starch Digestibility. *Carbohydr. Polym.* **2017**, *177*, 232–240. [CrossRef]
31. Li, H.; Wang, R.; Liu, J.; Zhang, Q.; Li, G.; Shan, Y.; Ding, S. Effects of Heat-Moisture and Acid Treatments on the Structural, Physicochemical, and in Vitro Digestibility Properties of Lily Starch. *Int. J. Biol. Macromol.* **2020**, *148*, 956–968. [CrossRef] [PubMed]
32. Hoover, R. The Impact of Heat-Moisture Treatment on Molecular Structures and Properties of Starches Isolated from Different Botanical Sources. *Crit. Rev. Food Sci. Nutr.* **2010**, *50*, 835–847. [CrossRef] [PubMed]
33. Rafiq, S.I.; Singh, S.; Saxena, D.C. Effect of Heat-Moisture and Acid Treatment on Physicochemical, Pasting, Thermal and Morphological Properties of Horse Chestnut (*Aesculus indica*) Starch. *Food Hydrocoll.* **2016**, *57*, 103–113. [CrossRef]
34. He, G.-Q.; Song, X.-Y.; Ruan, H.; Chen, F. Octenyl Succinic Anhydride Modified Early Indica Rice Starches Differing in Amylose Content. *J. Agric. Food Chem.* **2006**, *54*, 2775–2779. [CrossRef] [PubMed]
35. Zhang, C.; Ma, M.; Xu, Y.; Xu, Z.; Sui, Z.; Corke, H. Octenyl Succinic Anhydride Modification Alters Blending Effects of Waxy Potato and Waxy Rice Starches. *Int. J. Biol. Macromol.* **2021**, *190*, 1–10. [CrossRef] [PubMed]
36. Xu, J.; Zhou, C.-W.; Wang, R.-Z.; Yang, L.; Du, S.-S.; Wang, F.-P.; Ruan, H.; He, G.-Q. Lipase-Coupling Esterification of Starch with Octenyl Succinic Anhydride. *Carbohydr. Polym.* **2012**, *87*, 2137–2144. [CrossRef]
37. Bhosale, R.; Singhal, R. Effect of Octenylsuccinylation on Physicochemical and Functional Properties of Waxy Maize and Amaranth Starches. *Carbohydr. Polym.* **2007**, *68*, 447–456. [CrossRef]
38. Abiddin, N.F.Z.; Yusoff, A.; Ahmad, N. Effect of Octenylsuccinylation on Physicochemical, Thermal, Morphological and Stability of Octenyl Succinic Anhydride (OSA) Modified Sago Starch. *Food Hydrocoll.* **2018**, *75*, 138–146. [CrossRef]
39. Schafranski, K.; Ito, V.C.; Lacerda, L.G. Impacts and Potential Applications: A Review of the Modification of Starches by Heat-Moisture Treatment (HMT). *Food Hydrocoll.* **2021**, *117*, 106690. [CrossRef]
40. Na, J.H.; Kim, H.R.; Kim, Y.; Lee, J.S.; Park, H.J.; Moon, T.W.; Lee, C.J. Structural Characteristics of Low-Digestible Sweet Potato Starch Prepared by Heat-Moisture Treatment. *Int. J. Biol. Macromol.* **2020**, *151*, 1049–1057. [CrossRef] [PubMed]
41. Sui, Z.; Yao, T.; Zhao, Y.; Ye, X.; Kong, X.; Ai, L. Effects of Heat–Moisture Treatment Reaction Conditions on the Physicochemical and Structural Properties of Maize Starch: Moisture and Length of Heating. *Food Chem.* **2015**, *173*, 1125–1132. [CrossRef]
42. Park, E.Y.; Ma, J.-G.; Kim, J.; Lee, D.H.; Kim, S.Y.; Kwon, D.-J.; Kim, J.-Y. Effect of Dual Modification of HMT and Crosslinking on Physicochemical Properties and Digestibility of Waxy Maize Starch. *Food Hydrocoll.* **2018**, *75*, 33–40. [CrossRef]
43. No, J.; Mun, S.; Shin, M. Properties and Digestibility of Octenyl Succinic Anhydride-Modified Japonica-Type Waxy and Non-Waxy Rice Starches. *Molecules* **2019**, *24*, 765. [CrossRef] [PubMed]
44. Molavi, H.; Razavi, S.M.A. Dynamic Rheological and Textural Properties of Acorn (*Quercus brantii* Lindle.) Starch: Effect of Single and Dual Hydrothermal Modifications. *Starch Stärke* **2018**, *70*, 1800086. [CrossRef]

45. Kaur, L.; Singh, J.; McCarthy, O.; Singh, H. Physico-Chemical, Rheological and Structural Properties of Fractionated Potato Starches. *J. Food Eng.* **2007**, *82*, 383–394. [CrossRef]
46. Cao, M.; Gao, Q. Effect of Dual Modification with Ultrasonic and Electric Field on Potato Starch. *Int. J. Biol. Macromol.* **2020**, *150*, 637–643. [CrossRef]
47. Abedi, E.; Pourmohammadi, K.; Abbasi, S. Dual-Frequency Ultrasound for Ultrasonic-Assisted Esterification. *Food Sci. Nutr.* **2019**, *7*, 2613–2624. [CrossRef]
48. Colussi, R.; Halal, S.; Zanella Pinto, V.; Bartz, J.; Gutkoski, L.; Zavareze, E.; Dias, A. Acetylation of Rice Starch in an Aqueous Medium for Use in Food. *Lebensm. Wiss. Technol.* **2015**, *1*, 1. [CrossRef]
49. Majzoobi, M.; Kaveh, Z.; Blanchard, C.L.; Farahnaky, A. Physical Properties of Pregelatinized and Granular Cold Water Swelling Maize Starches in Presence of Acetic Acid. *Food Hydrocoll.* **2015**, *51*, 375–382. [CrossRef]
50. Bhandari, P.N.; Singhal, R.S. Effect of Succinylation on the Corn and Amaranth Starch Pastes. *Carbohydr. Polym.* **2002**, *48*, 233–240. [CrossRef]
51. Park, J.J.; Olawuyi, I.F.; Lee, W.Y. Characteristics of Low-Fat Mayonnaise Using Different Modified Arrowroot Starches as Fat Replacer. *Int. J. Biol. Macromol.* **2020**, *153*, 215–223. [CrossRef] [PubMed]
52. Jyothi, A.N.; Sajeev, M.S.; Sreekumar, J.N. Hydrothermal Modifications of Tropical Tuber Starches. Effect of Heat-Moisture Treatment on the Physicochemical, Rheological and Gelatinization Characteristics. *Starch Stärke* **2010**, *62*, 28–40. [CrossRef]
53. Shogren, R.L.; Viswanathan, A.; Felker, F.; Gross, R.A. Distribution of Octenyl Succinate Groups in Octenyl Succinic Anhydride Modified Waxy Maize Starch. *Starch Stärke* **2000**, *52*, 196–204. [CrossRef]
54. Ačkar, Đ.; Babić, J.; Jozinović, A.; Miličević, B.; Jokić, S.; Miličević, R.; Rajič, M.; Šubarić, D. Starch Modification by Organic Acids and Their Derivatives: A Review. *Molecules* **2015**, *20*, 19554–19570. [CrossRef]
55. Mehboob, S.; Ali, T.M.; Alam, F.; Hasnain, A. Dual Modification of Native White Sorghum (*Sorghum bicolor*) Starch Via Acid Hydrolysis and Succinylation. *LWT Food Sci. Technol.* **2015**, *64*, 459–467. [CrossRef]
56. Biliaderis, C.G. Chapter 8—Structural Transitions and Related Physical Properties of Starch. In *Starch*, 3rd ed.; BeMiller, J., Whistler, R., Eds.; Academic Press: San Diego, CA, USA, 2009; pp. 293–372.
57. Sindhu, R.; Devi, A.; Khatkar, B. Physicochemical, Thermal and Structural Properties of Heat Moisture Treated Common Buckwheat Starches. *J. Food Sci. Technol.* **2019**, *56*, 2480–2489. [CrossRef]
58. Sharma, M.; Singh, A.K.; Yadav, D.N.; Arora, S.; Vishwakarma, R.K. Impact of Octenyl Succinylation on Rheological, Pasting, Thermal and Physicochemical Properties of Pearl Millet (*Pennisetum typhoides*) Starch. *LWT Food Sci. Technol.* **2016**, *73*, 52–59. [CrossRef]
59. Chen, Y.-F.; Kaur, L.; Singh, J. Chapter 7—Chemical Modification of Starch. In *Starch in Food*, 2nd ed.; Sjöo, M., Nilsson, L., Eds.; Woodhead Publishing: Sawston, UK, 2018; pp. 283–321.
60. Pérez, E.; Lares, M. Chemical Composition, Mineral Profile, and Functional Properties of Canna (*Canna edulis*) and Arrowroot (*Maranta* spp.) Starches. *Plant Foods Human Nutr.* **2005**, *60*, 113–116. [CrossRef]
61. Yadav, B.S.; Guleria, P.; Yadav, R.B. Hydrothermal Modification of Indian Water Chestnut Starch: Influence of Heat-Moisture Treatment and Annealing on the Physicochemical, Gelatinization and Pasting Characteristics. *LWT Food Sci. Technol.* **2013**, *53*, 211–217. [CrossRef]
62. Marta, H.; Cahyana, Y.; Djali, M.; Pramafisi, G. The Properties, Modification, and Application of Banana Starch. *Polymers* **2022**, *14*, 3092. [CrossRef]
63. Daudt, R.M.; Küllkamp-Guerreiro, I.C.; Cladera-Olivera, F.; Thys, R.C.S.; Marczak, L.D.F. Determination of Properties of Pinhão Starch: Analysis of Its Applicability as Pharmaceutical Excipient. *Ind. Crops Prod.* **2014**, *52*, 420–429. [CrossRef]
64. Leon-Bejarano, M.; Durmus, Y.; Ovando-Martínez, M.; Simsek, S. Physical, Barrier, Mechanical, and Biodegradability Properties of Modified Starch Films with Nut by-Products Extracts. *Foods* **2020**, *9*, 226. [CrossRef] [PubMed]
65. Kutlu, N.; Pandiselvam, R.; Kamiloglu, A.; Saka, I.; Sruthi, N.U.; Kothakota, A.; Socol, C.T.; Maerescu, C.M. Impact of Ultrasonication Applications on Color Profile of Foods. *Ultrason. Sonochem.* **2022**, *89*, 106109. [CrossRef]

**Disclaimer/Publisher’s Note:** The statements, opinions and data contained in all publications are solely those of the individual author(s) and contributor(s) and not of MDPI and/or the editor(s). MDPI and/or the editor(s) disclaim responsibility for any injury to people or property resulting from any ideas, methods, instructions or products referred to in the content.

## Article

# Toward a Circular Bioeconomy: Development of Pineapple Stem Starch Composite as a Plastic-Sheet Substitute for Single-Use Applications

Chanaporn Thongphang<sup>1</sup>, Atitiya Namphonsane<sup>1</sup>, Sombat Thanawan<sup>2</sup>, Chin Hua Chia<sup>3</sup>,  
Rungtiwa Wongsagonsup<sup>4,5</sup>, Siwaporn Meejoo Smith<sup>1</sup> and Taweechai Amornsakchai<sup>1,\*</sup>

<sup>1</sup> Center of Sustainable Energy and Green Materials, Faculty of Science, Mahidol University, Phuttamonthon 4 Road, Salaya, Nakhon Pathom 73170, Thailand; siwaporn.smi@mahidol.ac.th (S.M.S.)

<sup>2</sup> Rubber Technology Research Center, Faculty of Science, Mahidol University, Phuttamonthon 4 Road, Salaya, Nakhon Pathom 73170, Thailand; sombat.tha@mahidol.ac.th

<sup>3</sup> Department of Applied Physics, Faculty of Science and Technology, Universiti Kebangsaan Malaysia, Bangi 43600, Selangor, Malaysia; chia@ukm.edu.my

<sup>4</sup> Division of Food Technology, Kanchanaburi Campus, Mahidol University, Kanchanaburi 71150, Thailand; rungtiwa.won@mahidol.ac.th

<sup>5</sup> Food and Nutrition Academic and Research Cluster, Institute of Nutrition, Mahidol University, Nakhon Pathom 73170, Thailand

\* Correspondence: taweechai.amo@mahidol.ac.th

**Abstract:** Plastic waste poses a significant challenge for the environment, particularly smaller plastic products that are often difficult to recycle or collect. In this study, we developed a fully biodegradable composite material from pineapple field waste that is suitable for small-sized plastic products that are difficult to recycle, such as bread clips. We utilized starch from waste pineapple stems, which is high in amylose content, as the matrix, and added glycerol and calcium carbonate as the plasticizer and filler, respectively, to improve the material's moldability and hardness. We varied the amounts of glycerol (20–50% by weight) and calcium carbonate (0–30 wt.%) to produce composite samples with a wide range of mechanical properties. The tensile moduli were in the range of 45–1100 MPa, with tensile strengths of 2–17 MPa and an elongation at break of 10–50%. The resulting materials exhibited good water resistance and had lower water absorption (~30–60%) than other types of starch-based materials. Soil burial tests showed that the material completely disintegrated into particles smaller than 1 mm within 14 days. We also created a bread clip prototype to test the material's ability to hold a filled bag tightly. The obtained results demonstrate the potential of using pineapple stem starch as a sustainable alternative to petroleum-based and biobased synthetic materials in small-sized plastic products while promoting a circular bioeconomy.

**Keywords:** biodegradable plastic; starch; circular economy; pineapple; tensile strength

**Citation:** Thongphang, C.; Namphonsane, A.; Thanawan, S.; Chia, C.H.; Wongsagonsup, R.; Smith, S.M.; Amornsakchai, T. Toward a Circular Bioeconomy: Development of Pineapple Stem Starch Composite as a Plastic-Sheet Substitute for Single-Use Applications. *Polymers* **2023**, *15*, 2388. <https://doi.org/10.3390/polym15102388>

Academic Editor: Raffaella Striani

Received: 26 April 2023

Revised: 15 May 2023

Accepted: 17 May 2023

Published: 19 May 2023



**Copyright:** © 2023 by the authors. Licensee MDPI, Basel, Switzerland. This article is an open access article distributed under the terms and conditions of the Creative Commons Attribution (CC BY) license (<https://creativecommons.org/licenses/by/4.0/>).

## 1. Introduction

In recent years, there has been growing concern about the environmental impact of plastics, which are known to persist in the environment and harm living organisms [1]. To address this issue, a variety of solutions have been proposed, including the use of biodegradable polymers in single-use applications and outright bans on plastic use in some countries [2]. Biodegradable polymers are available in a variety of forms, including fully biobased polylactic acid (PLA), partially biobased polybutylene succinate (PBS), fully synthetic polybutylene adipate terephthalate (PBAT), and natural polymers such as starch, polyhydroxyalkanoates (PHAs), and polyhydroxybutyrate (PHB). However, not all biodegradable polymers are created equal, and it is important to understand the specific properties and limitations of each type. For example, polylactic acid (PLA), polybutylene

adipate terephthalate (PBAT), and polybutylene succinate (PBS) are widely used biodegradable polymers, but they do not easily biodegrade in natural environments. Instead, they require specific conditions, such as controlled humidity and temperature, which are typically only found in industrial composting facilities [3,4]. Therefore, it is still crucial to ensure that these biodegradable materials are properly disposed of and collected in such facilities to ensure their complete degradation. On the other hand, starch-based materials, polyhydroxyalkanoates (PHAs), and polyhydroxybutyrates (PHBs) are fully biodegradable in natural environments and may be a more appropriate choice for certain applications where collection and recycling are not easy or economical, such as small and lightweight objects or products. These materials can biodegrade completely without requiring specialized industrial composting facilities and may, therefore, offer a more practical and environmentally friendly solution for certain types of waste.

Considering the availability, cost of production, and other environmental impacts, starch may be the material of choice to make bioplastics and, indeed, there are many reviews available [5–7]. However, unmodified starch has poor properties, especially low mechanical strength and poor water resistance. Thus, it requires modification or blending with other polymers to make it more useful [8–11]. Unfortunately, most starches are used for human consumption. Using them for materials would certainly interrupt food supply chains and limit access to food for vulnerable groups, making it unsustainable. Researchers have investigated various nonconventional or nonfood starches for use in material applications [12–18]. However, the availability of these alternative starch sources is relatively limited. As a result, much of the research on starch-based materials has focused on modifying traditional food-grade starch to improve its properties. One of the main challenges of using starch as a material is its poor water resistance and low mechanical strength. To address these limitations, researchers have developed a range of modification methods. Initially, modification was achieved through a single method, but the resulting products still had limitations. Over time, researchers developed more advanced modification techniques, such as dual modifications [19–22] or combining starch with various fillers [23–25]. This not only adds complexity to the process but also produces products with higher intensity in terms of material and energy, leading to a higher carbon footprint. Therefore, finding starch that does not require modification or requires very little modification would make it more sustainable.

Recently, our group started investigating pineapple stem starch (PSS) as a promising material for a variety of applications. This is because the PSS has a relatively high amylose content and can be obtained from pineapple field waste, which is abundantly available in Thailand [26–28]. We reported that the PSS film exhibits good properties, such as high water resistance, low water absorption, and good mechanical strength, while still being readily biodegradable [29]. As a result, the PSS film has been proposed for use in single-use or disposable applications.

This study aims to extend the potential applications of PSS by developing a biodegradable composite suitable for single-use purposes. The high amylose content of PSS is expected to confer good water-resistant properties to the composite. The matrix material used for the composite was unmodified and raw PSS. The mechanical properties of the material were enhanced by adding glycerol and calcium carbonate as modifiers. By exploring the range of mechanical properties achievable through these modifications, we can identify suitable applications for our composite material. This knowledge is critical for developing sustainable alternatives to conventional plastics and reducing the environmental impact of single-use products.

Glycerol was chosen as the primary plasticizer in this study due to its widespread use and effectiveness in previous research [5,30,31] and its availability as a byproduct from the biodiesel industry [32–34]. Similarly, calcium carbonate was chosen as the primary filler due to its wide use in plastic manufacturing and its availability from natural sources, such as the Earth's crust [35,36], or byproducts from food industries, such as eggshells and seashells [37,38]. Notably, the use of PSS, a nonconventional food-grade starch, in



this research ensures that it does not pose a threat to food security. This approach not only makes use of waste or byproducts but also supports the principles of a circular economy and sustainability. The use of renewable resources such as PSS, glycerol, and calcium carbonate in the development of biodegradable composites can significantly reduce reliance on nonrenewable resources and mitigate the environmental impact associated with conventional plastics.

## 2. Materials and Methods

### 2.1. Raw Material and Chemicals

Pineapple stem waste, a byproduct of a proprietary bromelain extraction process, was obtained from Hong Mao Biochemicals Co., Ltd., (Rayong, Thailand). In general, the process involves crushing peeled pineapple stems to disrupt the cell structure and extract liquid by centrifugation [28]. The remaining solid material was dried under the sun for a few days and further ground into a powder using a grinder. The stem powder was collected by sieving (80 mesh) to separate the coarse fibers, cell wall, and other solid contaminants, which constitute about 56% of the whole mass. The powder was used as obtained without further washing. The extractive constituents make up about 15% of the dry powder. The characteristics of the powder are similar to that obtained by the wet milling process reported previously [27]. Commercial-grade glycerol was obtained from local stores and the uncoated-grade calcium carbonate was produced by Surint Omya Chemicals (Kok Toom, Thailand) Co., Ltd., (Lopburi, Thailand).

### 2.2. Preparation of Starch Paste and Composites

A starch paste was prepared by mixing a predetermined amount of PSS, water, and glycerol in a glass beaker. The amount of glycerol was varied at 20, 30, 40, and 50% based on the weight of the PSS. For all formulations, the amount of water was fixed at the same weight as PSS. The mixture was left for at least 60 min at ambient condition before being gelatinized in a household microwave (Toshiba, model ER-G33SC(S), Toshiba Thailand Co., Ltd., Nonthaburi, Thailand) set at 50% of maximum power (1100 W) for 90 s. The gelatinized PSS was left to cool down to room temperature. A predetermined amount of calcium carbonate (0, 20, and 30% wt. of PSS) was then added into the paste on a laboratory 2-roll mill until a homogeneous mixture was obtained. The mixing time was approximately 15 min. After mixing, the mixture was sheeted out to a thickness of approximately 1 mm. The sheet was then dried in a hot-air oven at 80 °C for 6 h. The samples were then left in an ambient environment to gain equilibrium moisture content at least 7 days before any measurements were made. The sample code is represented as GXCaY, where X and Y are the amounts of glycerol and calcium carbonate, respectively.

### 2.3. Characterization of PSS Composites

#### 2.3.1. Fourier-Transform Infrared Spectroscopy (FTIR)

The FTIR spectra of the materials were recorded with a spectrophotometer (Frontier, Perkin Elmer, Waltham, MA, USA) in the attenuated total reflection (ATR) mode using a diamond crystal. The measurements were performed at room temperature over a range of 4000 to 400  $\text{cm}^{-1}$  with 16 scans and a resolution of 4  $\text{cm}^{-1}$ .

#### 2.3.2. X-ray Diffraction (XRD)

The X-ray diffraction patterns of the materials were obtained from a benchtop X-ray powder diffractometer (D2 Phaser, Bruker AXS GmbH, Karlsruhe, Germany) using an X-ray wavelength of 1.54 Å with a step scan of 15 s/point over the 2θ of 5–40 degrees. The percentage of crystallinity of each PSS composite sample was determined using the following equation:

$$\text{Crystallinity (\%)} = A_c / (A_c + A_a) \times 100 \quad (1)$$

where  $A_c$  = the area of crystalline region and  $A_a$  = the area of amorphous region. The peaks belonging to calcium carbonate were excluded from the calculation.



### 2.3.3. Mechanical Properties

**Tensile test:** Specimens were punched out from a 1 mm sheet with a cutter (ISO 37 type 2 dumbbell die). Tensile tests were carried out on a universal testing machine (Instron 5569, Instron, High Wycombe, UK) according to ISO 527-3 with a long-travel, contact-type extensometer. A crosshead speed of 50 mm/min was used. The secant modulus at 1% and the tensile strength and elongation at break were obtained as average values from five specimens.

**Hardness and density:** The hardness of the material was determined according to the durometer method or Shore hardness of ISO 7619-1 (Zwick Model 7206.07, Zwick, Ulm, Germany). The density of the material was determined following Archimedes' principle with a density kit on a laboratory balance (XS105, Mettler Toledo, Greifensee, Switzerland) according to method A of ISO 1183. The specimen was weighed in air and then weighed when immersed in distilled water using a sinker and wire to hold the specimen completely submerged. The measurement was carried out at 25 °C and the density was calculated using the below equation. The water density for the calculation was set at 1.00 g/cm<sup>3</sup>.

$$\text{Density} = W_{\text{air}} / (W_{\text{air}} - W_{\text{water}}) \quad (2)$$

where

$W_{\text{air}}$  = weight of the sample in air.

$W_{\text{water}}$  = weight of the sample in water.

### 2.3.4. Morphology

The fractured surfaces of the specimens obtained from the tensile tests were observed with a scanning electron microscope (SEM) (JSM-IT500, JEOL, Tokyo, Japan). The samples were coated with platinum before the observation.

### 2.3.5. Water Solubility and Absorption

A piece of specimen was immersed in distilled water for 24 h and its weights (wet and dried) were monitored. The amount of water absorbed was determined following ISO 62 at 25 °C. The water resistance was determined qualitatively by observing the uptake of water by the sheet samples. The water solubility and absorption of the sheets were determined from the following equations:

$$\text{Water solubility} = ((w_i - w_{fd}) / w_i) \times 100 \quad (3)$$

$$\text{Water absorption} = ((w_f - w_i) / w_i) \times 100 \quad (4)$$

where

$w_{fd}$  is the weight of the dried PSS sheet after being immersed in distilled water.

$w_f$  is the weight of the wet PSS sheet after being immersed in distilled water.

$w_i$  is the initial weight of the PSS sheet.

### 2.3.6. Soil Burial Test

This test can be used to determine the biodegradability of starch-based materials by microorganisms [39]. The test was slightly modified from a protocol reported previously [39]. Specimens of size 4.0 × 4.0 cm<sup>2</sup> were cut and put in envelopes made from a high-density polyethylene net for easy recovery. The envelopes were buried at the edge of a garden of the department building, about 10 cm beneath the surface. The pH of the soil was measured to be 7.5. The area was under the shade of trees and was watered every week. No attempt was made to regulate the moisture content and temperature of the area to obtain a natural environment. The envelopes were taken out for the observation of samples after different periods of time. The state of biodegradation was evaluated visually.

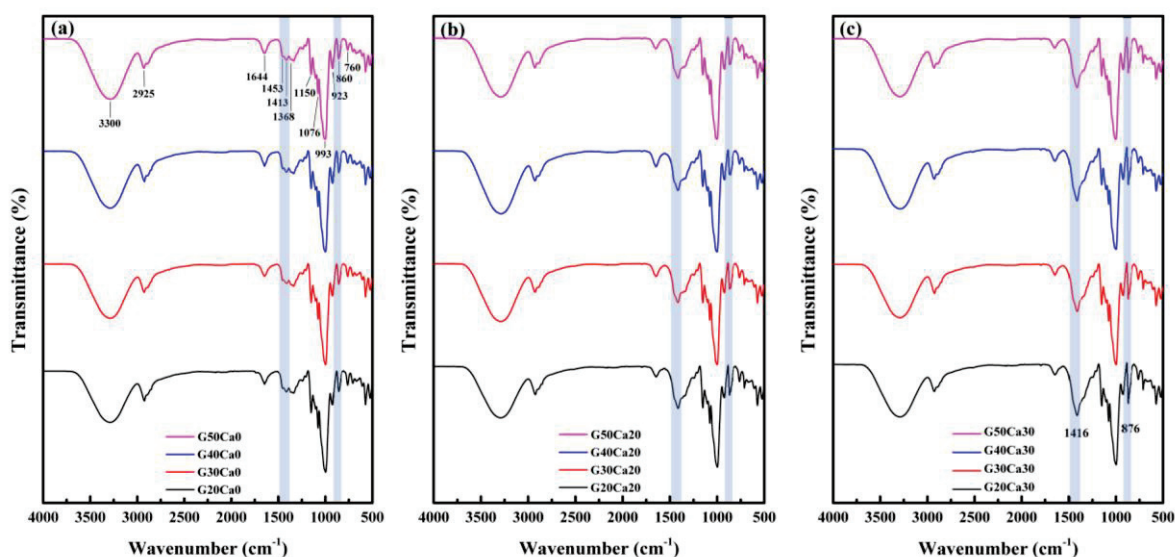
## 2.4. Statistical Analysis

Statistical analysis was performed using analysis of variance (ANOVA) with the Data Analysis tool in the Microsoft Excel (Office16) program. The *t*-test method, with two-sample assuming unequal variances, was performed to analyze differences among the means at a confidence level of 95%.

## 3. Results and Discussion

### 3.1. Fourier-Transform Infrared Spectroscopy (FTIR)

Figure 1 displays the FTIR spectra of the PSS composites containing different amounts of glycerol and calcium carbonate. In the controlled system without calcium carbonate, the amount of glycerol did not significantly affect the FTIR spectra of the composites. The FTIR spectra of the PSS with only glycerol were very similar to that of other starches that have been well understood and documented [40,41]. The peak positions and their corresponding functional group vibrations are listed in Table 1. When calcium carbonate was added, obvious changes were noticed at two positions (shaded area in Figure 1) belonging to calcium carbonate, i.e., the asymmetric stretching peak at  $1416\text{ cm}^{-1}$  and out-of-plane bending at  $876\text{ cm}^{-1}$  [42]. The intensity of these peaks increased on increasing the amount of calcium carbonate.



**Figure 1.** FTIR spectra of PSS composites containing different amounts of glycerol and calcium carbonate: (a) no calcium carbonate, (b) 20% calcium carbonate, and (c) 30% calcium carbonate.

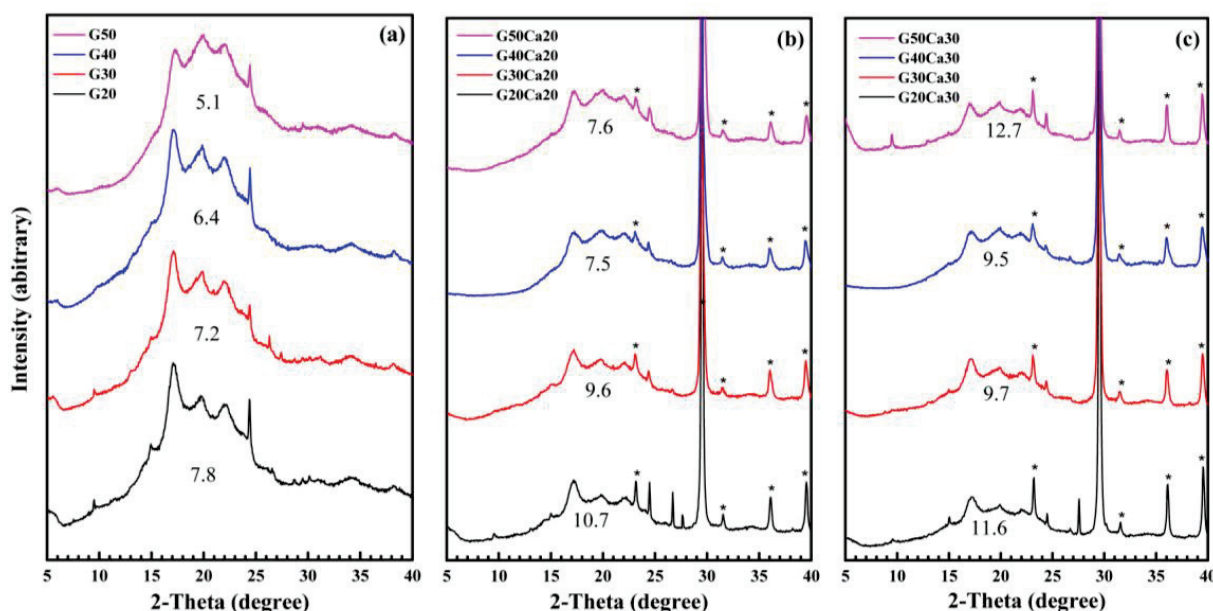
**Table 1.** FTIR peak positions and corresponding functional group vibrations.

No.	Observed Position ( $\text{cm}^{-1}$ )	Functional Group
1	3300	O-H stretching
2	2925	C-H stretching
3	1644	C-O bending (associate with OH group)
4	1453	$\text{CH}_2$ symmetric deformation
5	1413	$\text{CH}_2$ symmetric scissoring
6	1368	C-H symmetric bending
7	1150	C-O-C asymmetric stretching
8	1076, 993	C-O stretching
9	923, 860, 760	C-O-C ring vibration of carbohydrate

### 3.2. X-ray Diffraction (XRD)

Figure 2 displays the XRD patterns of the PSS composites containing different amounts of glycerol and calcium carbonate. All PSS composites have a certain degree of crystallinity.

The crystalline structure is different from that of the original PSS, which has an A-type structure, similar to other types of starches as shown previously [27]. The appearance is similar to that of PSS film prepared by solution casting [29] and that of ozonated cassava starch films [11]. These crystalline peaks are attributed to the spontaneous recrystallization of amylose molecules during film drying [43,44] or retrogradation. It was stated that retrograded starch is always B-type regardless of the starch type [11,45]. The crystallinity index decreased on increasing the amount of glycerol added. In systems containing calcium carbonate, five new peaks appeared, which were characteristics of calcium carbonate. The patterns were simply a combination of the PSS matrix and calcium carbonate. The diffraction intensity of PSS dropped significantly but still displayed crystallinity. The drop in intensity is due to the lesser amount of PSS within the measurement volume of XRD. Again, for each set of calcium carbonate contents, the crystallinity index decreased on increasing the amount of glycerol. It is worth noting that most reported thermoplastic starches do not exhibit such a distinct crystalline structure as is observed here [20,25,46]. This is presumably due to the high amylose content of PSS as it is the component that undergoes rapid reordering to form double helices and crystallites [47,48].

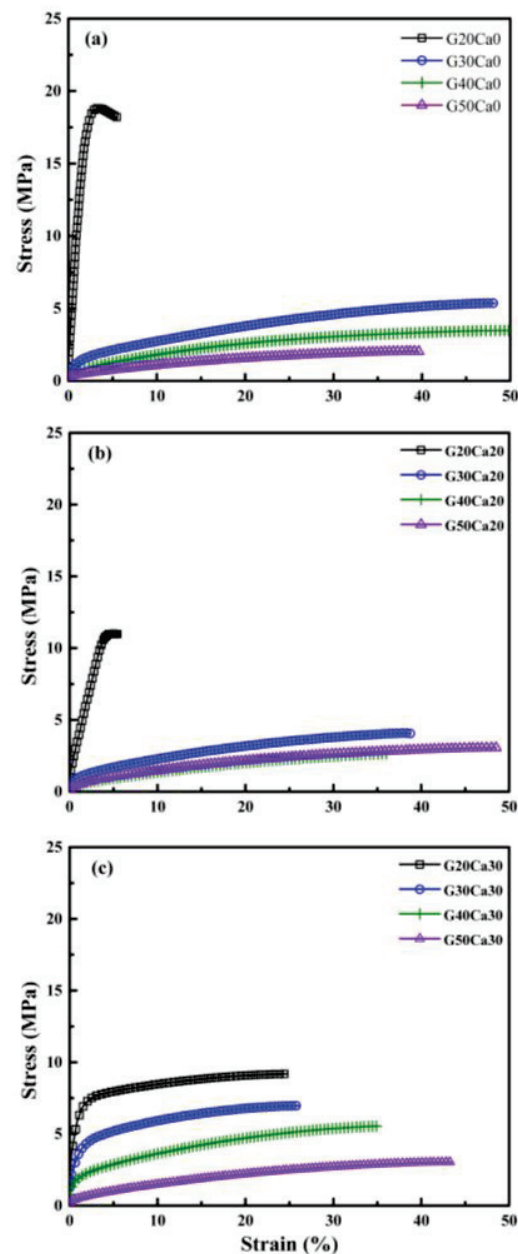


**Figure 2.** X-ray diffraction patterns of PSS composites containing different amounts of glycerol and calcium carbonate: (a) no calcium carbonate, (b) 20% calcium carbonate, and (c) 30% calcium carbonate. The number on each pattern indicates the crystallinity of the starch matrix. \* indicate calcium carbonate diffraction peaks.

### 3.3. Mechanical Properties

Figure 3 displays the stress–strain curves of the PSS composites containing different amounts of glycerol and calcium carbonate. For the system without calcium carbonate (Ca0), that with 20% glycerol displayed a sharp rise in stress as it was extended, and the stress reached a maximum point and then dropped slightly and broke at about 5% strain. When the glycerol content increased to 30, 40, and 50%, the stress dropped significantly, but the material could still be extended to a strain of about 50%. The maximum stress decreased with increasing glycerol content. When 20% calcium carbonate was added, the stress dropped from that without calcium carbonate but still broke at a strain of about 5%. On increasing the glycerol content to 30% and beyond, a similar pattern was observed, i.e., the stress dropped sharply and further decreased with increasing glycerol content and failure strains increased to about 40–50%. For the last set with 30% calcium carbonate, a very different pattern of behavior was seen. The composite with a glycerol content of 20% displayed a sharp rise in stress and then leveled off and failed at much a greater strain

of about 25%. On increasing the glycerol content to 30, 40, and 50%, the stress dropped in steps while the failure strain also increased in steps, reaching a value of about 45%. Average values for the moduli, tensile strength, and elongation at break are shown in Figure 4. The range of moduli obtained was about 45–1120 MPa, and the tensile strength was about 3.0–17.4 MPa. It should be noted that the modulus and tensile strength of the PSS sheet with glycerol content of 20 wt.% were much greater than that of other starches with similar glycerol content, which were about 95.0–529.0 MPa and 5.7–12.0 MPa, respectively [49,50].



**Figure 3.** Stress–strain curves of PSS composites containing different amounts of glycerol and calcium carbonate: (a) no calcium carbonate, (b) 20% calcium carbonate, and (c) 30% calcium carbonate.

Figure 5 displays the hardness of the PSS composites containing different amounts of glycerol and calcium carbonate. At the lowest glycerol content of 20%, the hardness of the composite was about 90–95 Shore A, and the hardness decreased with increasing glycerol content. The lowest hardness obtained was about 63 Shore A for PSS with 50% glycerol without calcium carbonate. For each glycerol content, the hardness increased with increasing calcium carbonate content.

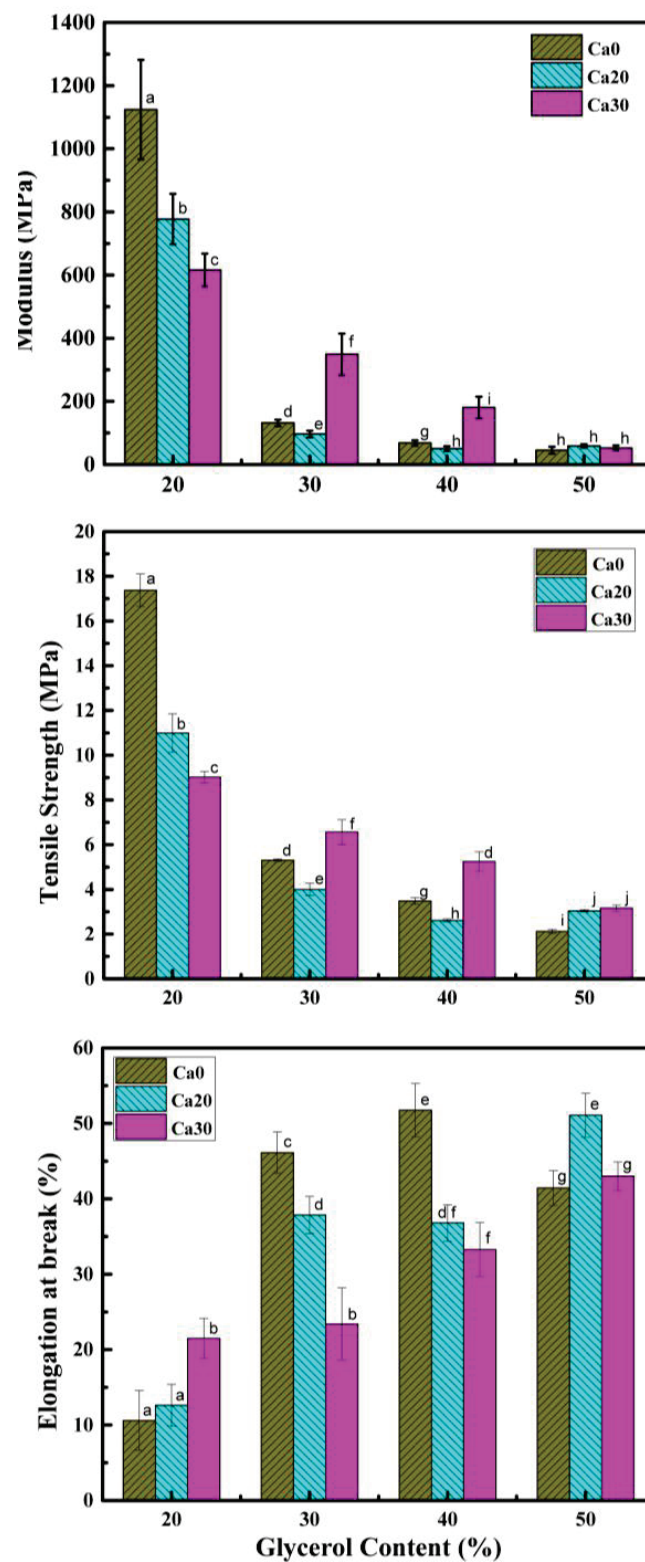
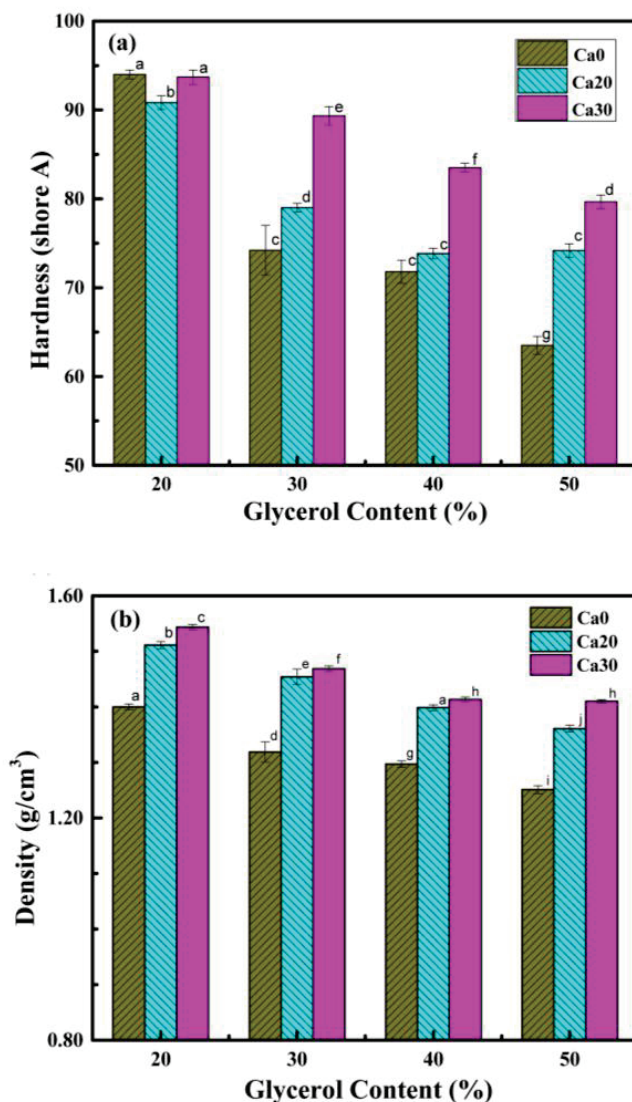


Figure 4. Modulus, tensile strength, and elongation at break of PSS composites containing different amounts of glycerol and calcium carbonate. Different letters on each bar indicate statistically significant differences in the means.

The densities of the PSS composites containing different amounts of glycerol and calcium carbonate are shown in Figure 5b. A trend similar to that for hardness was observed here. For each set of calcium carbonate contents, the density decreased with



increasing glycerol content, and for each glycerol content, the density increased with increasing calcium carbonate. These results are to be expected as calcium carbonate has a density of 2.65 g/cm<sup>3</sup> [35] while that of thermoplastic starch with 35 wt.% glycerol is about 1.4 g/cm<sup>3</sup> [51]. By assuming these values, the observed densities of the PSS composite sheets fit well with the calculated values.

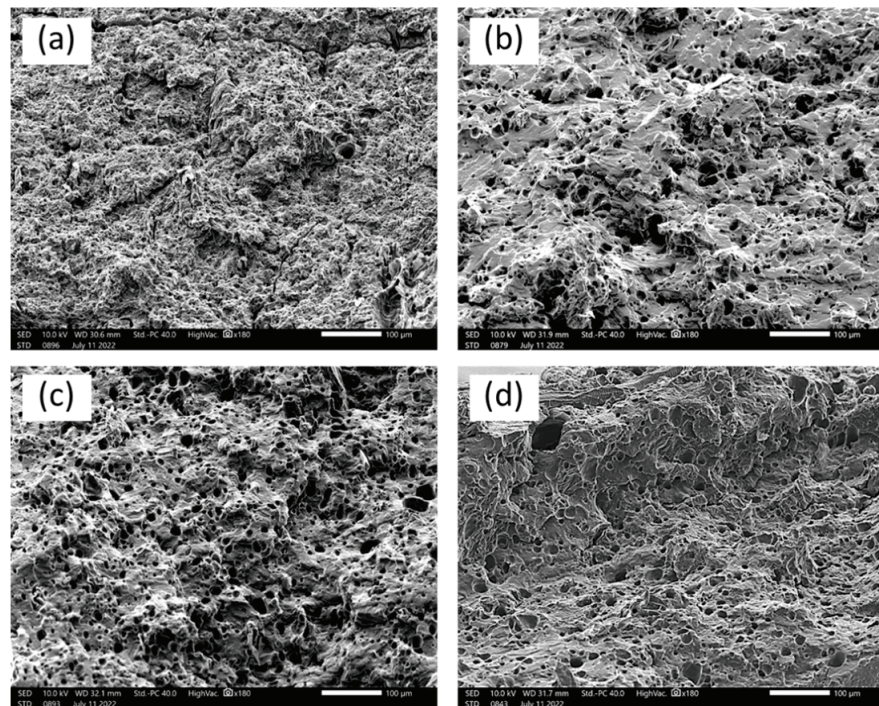


**Figure 5.** Hardness (a) and density (b) of PSS composites containing different amounts of glycerol and calcium carbonate. Different letters on each bar indicate statistically significant differences in the means.

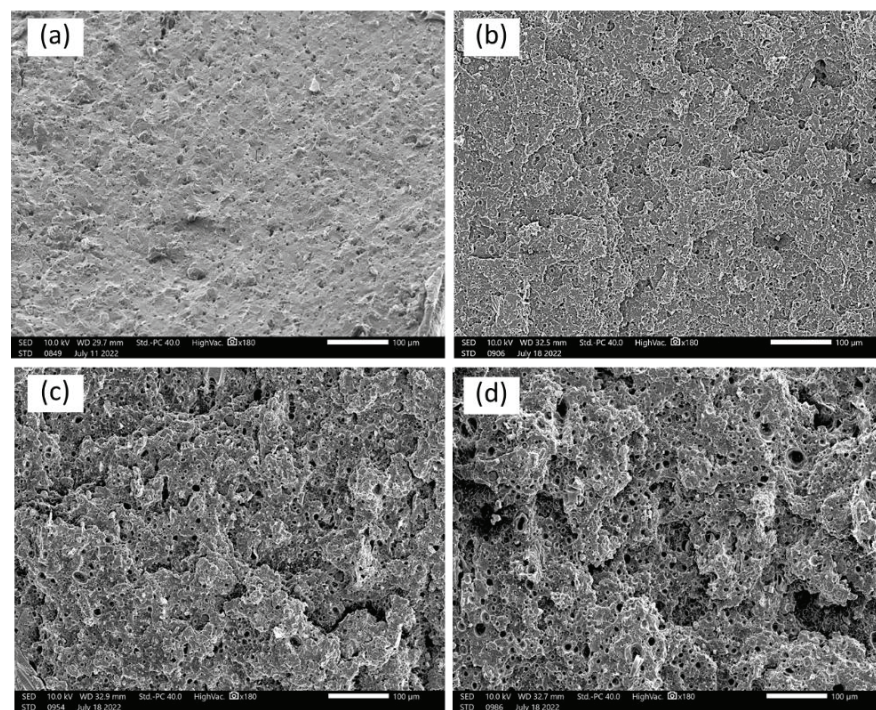
### 3.4. Morphology

Figures 6–8 display the scanning electron micrographs of tensile-fractured specimens of G20Ca0, G30Ca0, G40Ca0, and G50Ca0. It is apparent that all specimens contained numerous voids. Presumably these voids occurred because of syneresis process in which water is expelled from the starch network due to retrogradation [52] and then evaporates away in the drying stage. The presence of voids agrees well with the decrease in density with increasing glycerol content observed in Figure 5b. This observation can further support the decrease in tensile modulus and tensile strength of the films with increasing glycerol content. For specimens without calcium carbonate (Figure 6), the fracture surface displayed a very rough morphology. It seems that as the amount of glycerol increases, the size of

the voids increases. With calcium carbonate added, the fracture surface showed brittle behavior and no other feature was seen.

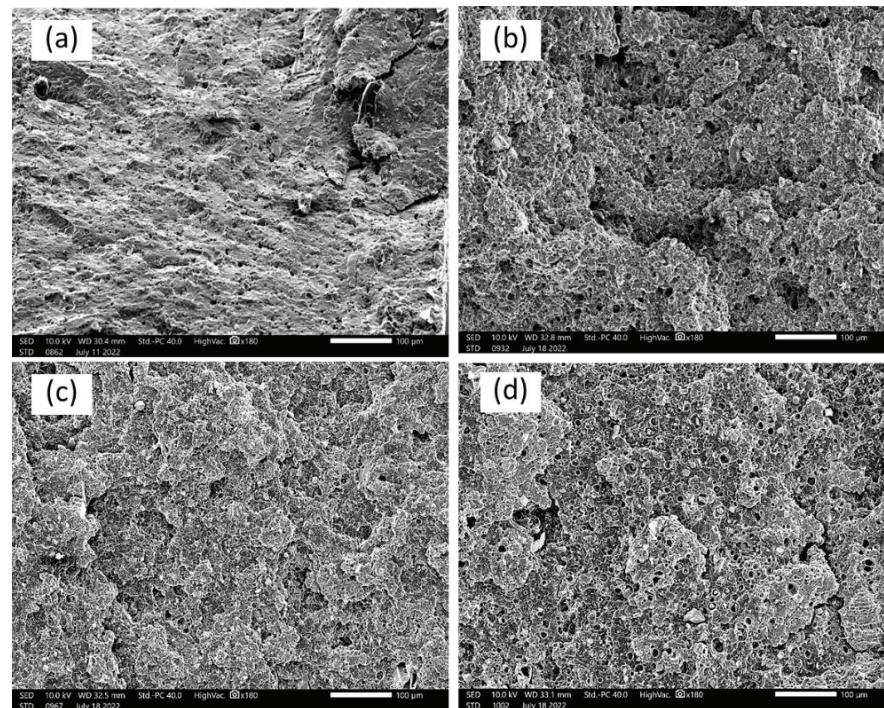


**Figure 6.** SEM micrographs of tensile-fractured surface of (a) G20Ca0, (b) G30Ca0, (c) G40Ca0, and (d) G50Ca0 specimens (scale bar = 100 µm).



**Figure 7.** SEM micrographs of the tensile-fractured surface of (a) G20Ca20, (b) G30Ca20, (c) G40Ca20, (d) G50Ca20 specimens (scale bar = 100 µm).

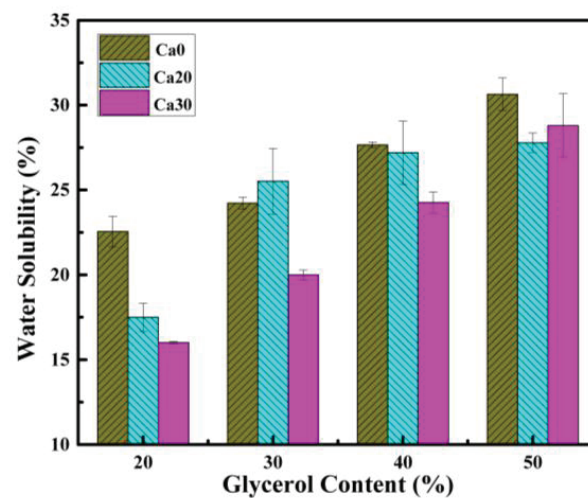




**Figure 8.** SEM micrographs of the tensile-fractured surface of (a) G20Ca30, (b) G30Ca30, (c) G40Ca30, (d) G50Ca30 (scale bar = 100  $\mu\text{m}$ ).

### 3.5. Water Solubility and Absorption

Figure 9 displays the water solubility of different PSS composite sheets. Solubility increases with increasing glycerol content indicating more material is leached out. Since both starch and glycerol are water soluble, it follows that the leached material could be both. With the addition of calcium carbonate, the water solubility decreased but still increased with increasing glycerol content. This is to be expected as calcium carbonate is not water soluble. Considering that glycerol molecules are small and readily soluble in water and the water solubility is close to but less than the amount of glycerol added, it is likely that some glycerol could still be trapped inside the composites.



**Figure 9.** Water solubility of PSS composites containing different amounts of glycerol and calcium carbonate.

Figure 10 displays the water absorption of the PSS composite sheets. For all composites, it is seen that the water absorption increased with increasing immersion time and then leveled off after a certain period of time. The points where the water absorption starts to level off seem to change with the calcium carbonate content, i.e., it increased with increasing calcium carbonate content. In addition, the maximum water absorption for each set of calcium carbonate content depends on the glycerol content. For specimens without calcium carbonate, maximum water absorption decreased with increasing glycerol content. These data should not be treated as evidence for actual lower water absorption since glycerol leaching did occur as will be shown in the next section, and more discussion will follow.

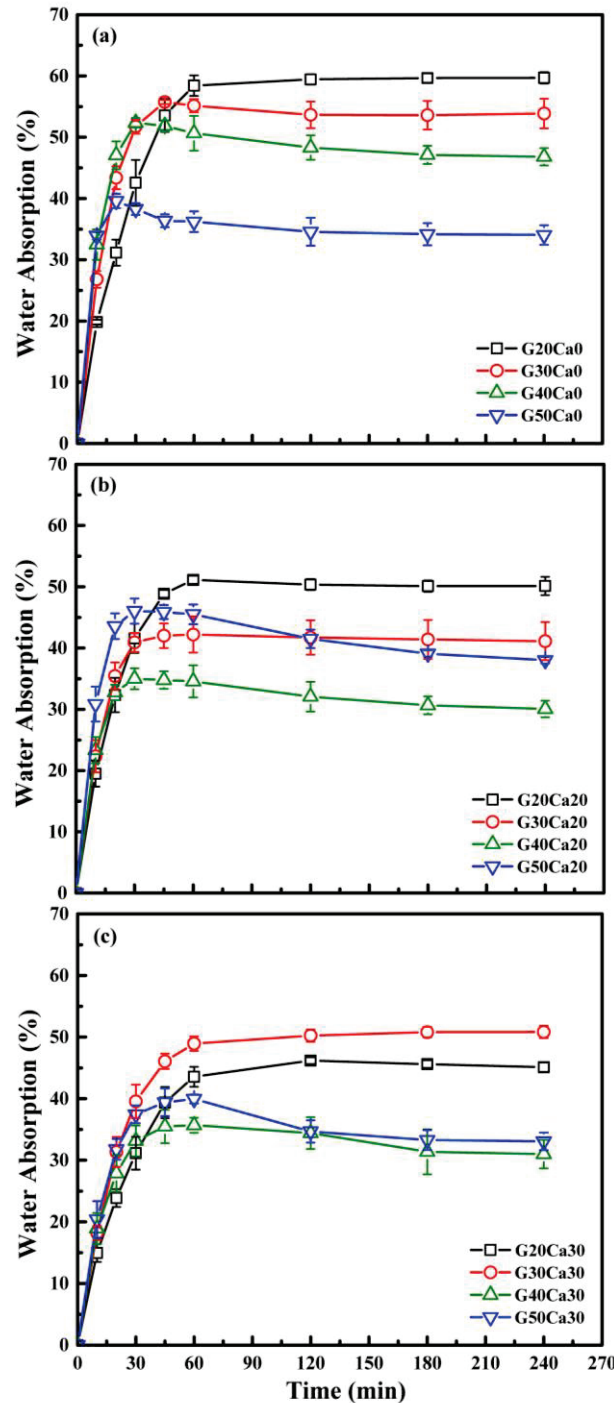
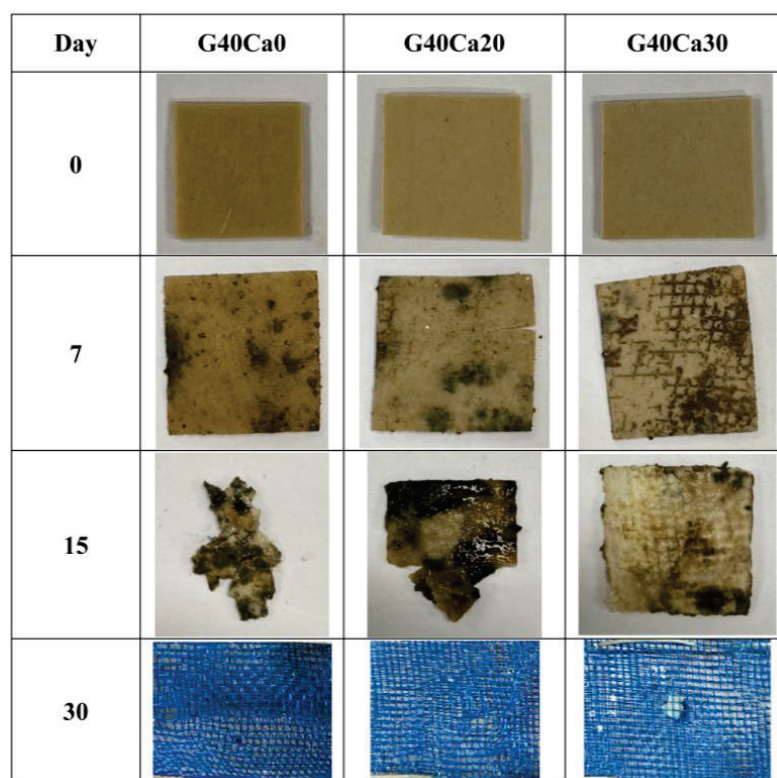


Figure 10. Water absorption of PSS composites containing different amounts of glycerol and calcium carbonate of 0 (a), 20 (b) and 30 (c) wt.%.

For composites with calcium carbonate, Figure 10b,c, the maximum water absorption decreased, and similar trend was seen that maximum water absorption decreased with increasing glycerol content, but the change was not regularly spaced as in the system without calcium carbonate. This could suggest complex interactions within the structure of the composites. To clearly understand the behavior, further work would be needed, and this will be reported in future correspondence.

### 3.6. Soil Burial Test

Figure 11 displays photographs of some selected composite samples before and after the burial test. All composite samples clearly deteriorated in the burial test but at different rates. It appears that, after 7 days, the composites became moldy but still maintained their original shape. After 15 days, composites with little or no  $\text{CaCO}_3$  were broken into small pieces, while those with a higher content largely retained their shape. After 30 days, all composites completely disintegrated, and nothing could be recovered.



**Figure 11.** Photographs of some PSS composite specimens before and after burial in the soil for different periods of time.

## 4. Discussion and Potential Applications

It has been shown that composites with a wide range of properties can be prepared from pineapple stem waste, an abundant agricultural waste in Thailand and many other countries. A wide range of properties were obtained from the inherent property of PSS, which has a high amylose content, due to its ability to accept a large amount of plasticizer and filler. The material is completely biodegradable in a natural environment. Thus, properties can be adjusted or tailored to suit different applications. It can be used to replace synthetic plastics in applications where collection for recycling is difficult or not economical and the plastic is likely to leak into the environment, such as bread clips, cotton buds, or golf tees. Compostable versions of these types of products are being offered, such as cardboard bread clips [53]. To demonstrate potential applications of the PSS composite sheet, simple bread clips were cut from a sheet using a manual punching tool, and their photographs are shown in Figure 12. The bread clip was chosen as an example as its function is just to carry



some information (related to the product in the packaging) and allow re-closure of a bag with very little stress on the clip. Some composite formulations were found to be too hard and broke during punching, while some gave a good cut. The clips were found to be able to close a sample plastic bag nicely as shown in Figure 12. The clip in the figure was cut from G40Ca0 (without calcium carbonate).



**Figure 12.** Photographs of simple bread clips made from PSS composites compared with a commercial clip (left) and its use for closing a plastic bag (right).

In summary, our study demonstrated the potential of using pineapple stem starch, glycerol, and calcium carbonate for the production of biodegradable composites. The utilization of waste, byproducts, and renewable sources for these materials offers numerous advantages, including a reduction in the energy required for raw material production, lower carbon dioxide emissions, and a reduced need for land and water resources, compared to the use of edible starch. Furthermore, the use of pineapple stem starch, which is not conventionally used as food, does not pose a threat to food security, and edible starches can be reserved for food production. We have also shown that a range of composite formulations can be achieved with varying mechanical and water-resistant properties, making them suitable for various applications. For instance, our proposed application of using the composite as bread clips is a practical example of how it can be used to replace single-use plastics in everyday items that are too small for people to collect for recycling. Moreover, the observed range of properties could serve as a starting point for future research, where other sustainable materials can be incorporated to obtain specific properties tailored to various applications. Overall, our findings hold great potential for advancing sustainable materials and circular economy, reducing plastic waste, and mitigating the environmental impact of plastic production and disposal. With the increasing concern over climate change and resource depletion, our study offers a promising solution toward a more sustainable future.

## 5. Conclusions

Biodegradable plastic sheets with a wide range of mechanical properties were successfully developed from PSS. The high amylose content allows a sufficient degree of crystallinity to impart a good starting point. The use of simple chemicals, such as glycerol as plasticizer and calcium carbonate as reinforcement, provides an opportunity to alter the mechanical properties to suit various applications. The material is specifically useful for applications where strength is not so critical and collection back for recycling is difficult. Since it is starch-based, the material is readily biodegradable within a short period of time and should leave no microplastics and other contaminants behind. In addition, the rate at which the composite deteriorates can be controlled via the filler or other additive contents.

**Author Contributions:** Conceptualization, T.A. and C.H.C.; methodology, C.T., A.N. and T.A.; validation, and data curation, C.T. and A.N.; writing—original draft preparation, T.A.; writing—review and editing, T.A., S.T., C.H.C., R.W. and S.M.S.; funding acquisition, T.A. All authors have read and agreed to the published version of the manuscript.

**Funding:** This research was funded by Mahidol University (Basic Research Fund: fiscal year 2022; grant No. BRF1-046/2565).

**Institutional Review Board Statement:** Not applicable.

**Data Availability Statement:** The data presented in this study are available on request from the corresponding author.

**Acknowledgments:** We thank Mahidol University Frontier Research Facility (MU-FRF) for instrument support and the MU-FRF scientists, Nawapol Udpuay, Chawalit Takoon, and Suwilai Chaveanghong, for their kind assistance in the operation of SEM.

**Conflicts of Interest:** The authors declare no conflict of interest.

## References

- Andrady, A.L. Microplastics in the marine environment. *Mar. Pollut. Bull.* **2011**, *62*, 1596–1605. [CrossRef] [PubMed]
- Buchholz, K. The Countries Banning Plastic Bags. Available online: <https://www.statista.com/chart/14120/the-countries-banning-plastic-bags/> (accessed on 25 April 2023).
- Muniyasamy, S.; Ofosu, O.; John, M.J.; Anandjiwala, R.D. Mineralization of poly(lactic acid) (PLA), Poly(3-hydroxybutyrate-co-valerate) (PHBV) and PLA/PHBV blend in compost and soil environments. *J. Renew. Mater.* **2016**, *4*, 133–145. [CrossRef]
- Jia, M.Z. Biodegradable Plastics: Breaking Down the Facts, Greenpeace East Asia. 2020. Available online: <https://www.greenpeace.org/static/planet4-eastasia-stateless/84075f56-biodegradable-plastics-report.pdf> (accessed on 11 April 2023).
- Wang, B.; Yu, B.; Yuan, C.; Guo, L.; Liu, P.; Gao, W.; Li, D.; Cui, B.; Abd El-Aty, A.M. An overview on plasticized biodegradable corn starch-based films: The physicochemical properties and gelatinization process. *Crit. Rev. Food. Sci.* **2022**, *62*, 2569–2579. [CrossRef] [PubMed]
- Carvalho, A.J.F. Starch: Major sources, properties and applications as thermoplastic materials. In *Monomers, Polymers and Composites from Renewable Resources*; Belgacem, M.N., Gandini, A., Eds.; Elsevier: Amsterdam, The Netherlands, 2008; pp. 321–342.
- Niranjana Prabhu, T.; Prashantha, K. A review on present status and future challenges of starch based polymer films and their composites in food packaging applications. *Polym. Compos.* **2018**, *39*, 2499–2522. [CrossRef]
- Arvanitoyannis, I.; Biliaderis, C.G.; Ogawa, H.; Kawasaki, N. Biodegradable films made from low-density polyethylene (LDPE), rice starch and potato starch for food packaging applications: Part 1. *Carbohydr. Polym.* **1998**, *36*, 89–104. [CrossRef]
- Kaur, H.; Banipal, T.S.; Thakur, S.; Bakshi, M.S.; Kaur, G.; Singh, N. Novel Biodegradable Films with Extraordinary Tensile Strength and Flexibility Provided by Nanoparticles. *ACS Sustain. Chem. Eng.* **2012**, *1*, 127–136. [CrossRef]
- Leal, I.L.; da Silva Rosa, Y.C.; da Silva Penha, J.; Cruz Correia, P.R.; da Silva Melo, P.; Guimarães, D.H.; Barbosa, J.D.V.; Druzian, J.I.; Machado, B.A.S. Development and application starch films: PBAT with additives for evaluating the shelf life of Tommy Atkins mango in the fresh-cut state. *J. Appl. Polym. Sci.* **2019**, *136*, 48150. [CrossRef]
- La Fuente, C.I.A.; de Souza, A.T.; Tadini, C.C.; Augusto, P.E.D. Ozonation of cassava starch to produce biodegradable films. *Int. J. Biol. Macromol.* **2019**, *141*, 713–720. [CrossRef]
- Tagliapietra, B.L.; Felisberto, M.H.F.; Sanches, E.A.; Campelo, P.H.; Clerici, M.T.P.S. Non-conventional starch sources. *Curr. Opin. Food. Sci.* **2021**, *39*, 93–102. [CrossRef]
- Henning, F.G.; Ito, V.C.; Demiate, I.M.; Lacerda, L.G. Non-conventional starches for biodegradable films: A review focussing on characterisation and recent applications in food. *Carbohydr. Polym. Tech. Appl.* **2021**, *4*, 100157. [CrossRef]
- González-Soto, R.A.; Sánchez-Hernández, L.; Solorza-Feria, J.; Núñez-Santiago, C.; Flores-Huicochea, E.; Bello-Pérez, L.A. Resistant starch production from non-conventional starch sources by extrusion. *Food. Sci. Tech. Int.* **2006**, *12*, 5–11. [CrossRef]
- Souza, C.O.; Silva, L.T.; Silva, J.R.; López, J.A.; Veiga-Santos, P.; Druzian, J.I. Mango and acerola pulps as antioxidant additives in cassava starch bio-based film. *J. Agr. Food. Chem.* **2011**, *59*, 2248–2254. [CrossRef]
- Nawab, A.; Alam, F.; Haq, M.A.; Hasnain, A. Biodegradable film from mango kernel starch: Effect of plasticizers on physical, barrier, and mechanical properties. *Starch Stärke* **2016**, *68*, 919–928. [CrossRef]
- Alimi, B.A.; Workneh, T.S.; Zubair, B.A. Microstructural and physicochemical properties of biodegradable films developed from false banana (*Ensete ventricosum*) starch. *Heliyon* **2022**, *8*, e09148. [CrossRef]
- Maniglia, B.C.; Tessaro, L.; Lucas, A.A.; Tapia-Blácido, D.R. Bioactive films based on babassu mesocarp flour and starch. *Food Hydrocoll.* **2017**, *70*, 383–391. [CrossRef]
- Tanetrungroj, Y.; Prachayawarakorn, J. Effect of dual modification on properties of biodegradable crosslinked-oxidized starch and oxidized-crosslinked starch films. *Int. J. Biol. Macromol.* **2018**, *120*, 1240–1246. [CrossRef]
- Prachayawarakorn, J.; Kansanthia, P. Characterization and properties of singly and dually modified hydrogen peroxide oxidized and glutaraldehyde crosslinked biodegradable starch films. *Int. J. Biol. Macromol.* **2022**, *194*, 331–337. [CrossRef] [PubMed]

21. González-Soto, R.A.; Núñez-Santiago, M.C.; Bello-Pérez, L.A. Preparation and partial characterization of films made with dual-modified (acetylation and crosslinking) potato starch. *J. Sci. Food Agr.* **2019**, *99*, 3134–3141. [CrossRef]
22. Woggum, T.; Sirivongpaisal, P.; Wittaya, T. Properties and characteristics of dual-modified rice starch based biodegradable films. *Int. J. Biol. Macromol.* **2014**, *67*, 490–502. [CrossRef]
23. Shanmathy, M.; Mohanta, M.; Thirugnanam, A. Development of biodegradable bioplastic films from Taro starch reinforced with bentonite. *Carbohydr. Polym. Technol. Appl.* **2021**, *2*, 100173. [CrossRef]
24. Gutiérrez, T.J.; Alvarez, V.A. Cellulosic materials as natural fillers in starch-containing matrix-based films: A review. *Polym. Bull.* **2017**, *74*, 2401–2430. [CrossRef]
25. Pongsuwan, C.; Boonsuk, P.; Sermwittayawong, D.; Aiemcharoen, P.; Mayakun, J.; Kaewtatip, K. Banana inflorescence waste fiber: An effective filler for starch-based bioplastics. *Ind. Crop. Prod.* **2022**, *180*, 114731. [CrossRef]
26. Chen, Y.M.; Liu, H.Y. Studies on stem bromelain and stem starch from pineapple plants. *Taiwania* **1972**, *17*, 266–276.
27. Nakthong, N.; Wongsagonsup, R.; Amornsakchai, T. Characteristics and potential utilizations of starch from pineapple stem waste. *Ind. Crop. Prod.* **2017**, *105*, 74–82. [CrossRef]
28. Rinju, R.; Harikumarán-Thampi, B.-S. Characteristics of Starch Extracted from the Stem of Pineapple Plant (*Ananas comosus*)—An Agro Waste from Pineapple Farms. *Braz. Arch. Biol. Tech.* **2021**, *64*, e21190276. [CrossRef]
29. Namphonsane, A.; Suwannachat, P.; Chia, C.H.; Wongsagonsup, R.; Smith, S.M.; Amornsakchai, T. Toward a Circular Bioeconomy: Exploring Pineapple Stem Starch Film as a Plastic Substitute in Single Use Applications. *Membranes* **2023**, *13*, 458. [CrossRef]
30. Mali, S.; Grossmann, M.V.E.; García, M.A.; Martino, M.N.; Zartitzky, N.E. Effects of controlled storage on thermal, mechanical and barrier properties of plasticized films from different starch sources. *J. Food Eng.* **2006**, *75*, 453–460. [CrossRef]
31. Mohd Nizam, N.H.; Mohammad Rawi, N.F.; Ramle, S.F.M.; Abd Aziz, A.; Abdullah, C.K.; Rashedi, A.; Mohamad Kassim, M.H. Physical, thermal, mechanical, antimicrobial and physicochemical properties of starch based film containing aloe vera: A review. *J. Mater. Res. Technol.* **2021**, *15*, 1572–1589. [CrossRef]
32. Yang, F.; Hanna, M.A.; Sun, R. Value-added uses for crude glycerol—A byproduct of biodiesel production. *Biotechnol. Biofuels.* **2012**, *5*, 13. [CrossRef]
33. Zhu, C.; Chiu, S.; Nakas, J.P.; Nomura, C.T. Bioplastics from waste glycerol derived from biodiesel industry. *J. Appl. Polym. Sci.* **2013**, *130*, 1–13. [CrossRef]
34. Bilck, A.P.; Olivera Müller, C.M.; Olivato, J.B.; Mali, S.; Grossmann, M.V.E.; Yamashita, F. Using glycerol produced from biodiesel as a plasticiser in extruded biodegradable films. *Polimeros* **2015**, *25*, 331–335. [CrossRef]
35. Mallick, P.K. 2.09—Particulate and Short Fiber Reinforced Polymer Composites. *Compr. Compos. Mater.* **2000**, *2*, 291–331.
36. Rothon, R.; Paynter, C. Calcium carbonate fillers. In *Fillers for Polymer Applications*; Rothon, R., Ed.; Springer: Cham, Switzerland, 2017; pp. 149–160.
37. Barros, M.C.; Bello, P.M.; Bao, M.; Torrado, J.J. From waste to commodity: Transforming shells into high purity calcium carbonate. *J. Clean. Prod.* **2009**, *17*, 400–407. [CrossRef]
38. Oliveira, D.A.; Benelli, P.; Amante, E.R. A literature review on adding value to solid residues: Egg shells. *J. Clean. Prod.* **2013**, *46*, 42–47. [CrossRef]
39. Seligra, P.G.; Jaramillo, C.M.; Famá, L.; Goyanes, S. Biodegradable and non-retrogradable eco-films based on starch-glycerol with citric acid as crosslinking agent. *Carbohydr. Polym.* **2016**, *138*, 66–74. [CrossRef]
40. Warren, F.J.; Gidley, M.J.; Flanagan, B.M. Infrared spectroscopy as a tool to characterise starch ordered structure—A joint FTIR-ATR, NMR, XRD and DSC study. *Carbohydr. Polym.* **2016**, *139*, 35–42. [CrossRef] [PubMed]
41. Abdullah, A.H.D.; Chalimah, S.; Primadona, I.; Hanantyo, M.H.G. Physical and chemical properties of corn, cassava, and potato starches. *IOP Conf. Ser. Earth Environ. Sci.* **2018**, *160*, 012003. [CrossRef]
42. Falini, G.; Manara, S.; Fermani, S.; Roveri, N.; Goisis, M.; Manganelli, G.; Cassar, L. Polymeric admixtures effects on calcium carbonate crystallization: Relevance to cement industries and biomineralization. *CrystEngComm* **2007**, *9*, 1162–1170. [CrossRef]
43. Myllärinen, P.; Buleon, A.; Lahtinen, R.; Forsell, P. The crystallinity of amylose and amylopectin films. *Carbohydr. Polym.* **2002**, *48*, 41–48. [CrossRef]
44. Rindlav-Westling, A.; Stading, M.; Hermansson, A.M.; Gatenholm, P. Structure, mechanical and barrier properties of amylose and amylopectin films. *Carbohydr. Polym.* **1998**, *36*, 217–224. [CrossRef]
45. Sarko, A.; Wu, H.-C.H. The Crystal Structures of A-, B- and C-Polymorphs of Amylose and Starch. *Starch Stärke* **1978**, *30*, 73–78. [CrossRef]
46. Mendes, J.F.; Paschoalin, R.T.; Carmona, V.B.; Sena Neto, A.R.; Marques, A.C.P.; Marconcini, J.M.; Mattoso, L.H.C.; Medeiros, E.S.; Oliveira, J.E. Biodegradable polymer blends based on corn starch and thermoplastic chitosan processed by extrusion. *Carbohydr. Polym.* **2016**, *137*, 452–458. [CrossRef] [PubMed]
47. Ottenhof, M.-A.; Farhat, I.A. Starch retrogradation. *Biotechnol. Genet. Eng. Rev.* **2004**, *21*, 215–228. [CrossRef] [PubMed]
48. Yamaguchi, Y.; Okawa, Y.; Ninomiya, K.; Kumagai, H.; Kumagai, H. Evaluation and suppression of retrogradation of gelatinized rice starch. *J. Nutr. Sci. Vitaminol.* **2019**, *65*, S134–S138. [CrossRef] [PubMed]
49. Fourati, Y.; Tarrés, Q.; Mutjé, P.; Boufi, S. PBAT/thermoplastic starch blends: Effect of compatibilizers on the rheological, mechanical and morphological properties. *Carbohydr. Polym.* **2018**, *199*, 51–57. [CrossRef]
50. Andretta, R.; Luchese, C.L.; Tessaro, I.C.; Spada, J.C. Development and characterization of pH-indicator films based on cassava starch and blueberry residue by thermocompression. *Food Hydrocoll.* **2019**, *93*, 317–324. [CrossRef]

51. Mazerolles, T.; Heuzey, M.-C.; Soliman, M.; Martens, H.; Kleppinger, R.; Huneault, M.A. Development of multilayer barrier films of thermoplastic starch and low-density polyethylene. *J. Polym. Res.* **2020**, *27*, 44. [CrossRef]
52. Wang, S.; Li, C.; Copeland, L.; Niu, Q.; Wang, S. Starch Retrogradation: A Comprehensive Review. *Compr. Rev. Food Sci. Food Saf.* **2015**, *14*, 568–585. [CrossRef]
53. KLR Launches Sustainable Bag Clip. Available online: <https://www.bakersjournal.com/klr-launches-sustainable-bag-clip-7854/> (accessed on 24 April 2023).

**Disclaimer/Publisher’s Note:** The statements, opinions and data contained in all publications are solely those of the individual author(s) and contributor(s) and not of MDPI and/or the editor(s). MDPI and/or the editor(s) disclaim responsibility for any injury to people or property resulting from any ideas, methods, instructions or products referred to in the content.





MDPI  
St. Alban-Anlage 66  
4052 Basel  
Switzerland  
[www.mdpi.com](http://www.mdpi.com)

*Polymers* Editorial Office  
E-mail: [polymers@mdpi.com](mailto:polymers@mdpi.com)  
[www.mdpi.com/journal/polymers](http://www.mdpi.com/journal/polymers)



Disclaimer/Publisher's Note: The statements, opinions and data contained in all publications are solely those of the individual author(s) and contributor(s) and not of MDPI and/or the editor(s). MDPI and/or the editor(s) disclaim responsibility for any injury to people or property resulting from any ideas, methods, instructions or products referred to in the content.





Academic Open  
Access Publishing

[mdpi.com](http://mdpi.com)

ISBN 978-3-0365-9536-8